Diplôme d'Habilitation à Diriger des Recherches

FORMATION ET EVOLUTION DE LA MATIERE ORGANIQUE COMETAIRE ET DES PETITS CORPS DU SYSTEME SOLAIRE

Hervé COTTIN

Maître de conférences

Université Paris 12

LISA

Septembre 2008

SOMMAIRE

INTRODUCTION

Ce document présente mes activités de recherche en **astrochimie** et **exobiologie** depuis la soutenance de ma thèse en Novembre 1999. Il regroupe les travaux que j'ai conduit en tant qu'Attaché Temporaire d'Enseignement et de Recherche (ATER) à l'université Paris 12 au Laboratoire Interuniversitaire des Systèmes Atmosphériques (LISA – Universités Paris 12 et Paris 7, UMR 7583 CNRS) en 2000, puis comme NRC Research Associate au Cosmic Ice Laboratory du NASA Goddard Space Flight Center (Greenbelt, MD, USA) en 2001, et enfin consécutivement à ma nomination sur un poste de maître de conférences de l'université Paris 12, au LISA, le 1er Février 2002.

Astrochimie

Chimiste de formation, j'ai été recruté en section CNU n°34 (Astronomie et Astrophysique), pour intégrer le Groupe de Physico Chimie Organique Spatiale (GPCOS) du LISA. Depuis le début de ma thèse, mes activités ont toujours été menées à l'interface de la chimie (essentiellement des expériences de photochimie en laboratoire) et de l'astronomie (interprétation de données observationnelles, préparation d'expériences spatiales). Alors que l'étude des structures moléculaires dans les environnements extraterrestres est majoritairement menée par des astrophysiciens, j'ai pu sentir au cours de mon début de carrière de chercheur l'émergence d'une communauté d'astrochimistes, se revendiquant comme tels, avec une implication croissante de chimistes de formation. Le LISA, sous l'impulsion de François Raulin, a joué un rôle moteur dans ce basculement en France, en assurant la formation de nombreux thésards et post-doctorants dans le champ de l'astrochimie, après un cursus universitaire à dominante chimie. Plusieurs chercheurs formés au GPCOS/LISA ont d'ailleurs intégré comme permanents d'autres équipes Françaises[1] de planétologie, ou commencé à développer cette thématique dans d'autres laboratoires. Ce besoin nouveau, très récent, motivé très probablement par la complexité croissante des molécules organiques détectées dans les différents environnements astrophysiques, et la complexification des instruments spatiaux dédiés à leur analyse, transparaît dans les profils de postes récents publiés et les recrutements associés. Par exemple, en 2006 pour un poste de maître de conférences « en astrochimie » au Laboratoire de Physique et Chimie de l'Environnement de l'université d'Orléans, il n'y a pas eu de candidat possédant déjà une expérience en astrochimie acquise en thèse ou après ; Christelle Briois qui a été recrutée sur ce poste avait en revanche une très bonne formation de chimie de l'atmosphère terrestre. Par contre, en 2008, pour un autre poste de maître de conférences en astrochimie ouvert à l'Institut d'Astrophysique Spatiale de l'université Paris 11, 7 candidats ont été

[1] Parmi les thèses soutenues au GPCOS et post-doctorants depuis 2000, ont été recruté en tant que permanents : Cyril Szopa au Service d'Aéronomie (Université Paris 6), Véronique Vuitton au Laboratoire de Planétologie de Grenoble, Claude Rodier à l'université de Poitier, Arnaud Buch à l'école centrale de Paris et Donia Baklouti à l'Institut d'Astrophysique Spatiale de l'université Paris 11 (avant son post-doctorat au LISA Donia Baklouti avait effectué sa thèse au LPG de Grenoble).

auditionnés, tous ayant un profil d'astrochimie. La candidate recrutée (Donia Baklouti) avait obtenue sa thèse au Laboratoire de Planétologie de Grenoble avant d'effectuer un post-doc au LISA. Les autres candidats avaient effectués leur thèse au LISA (2 d'entre eux), à Rennes, Montpellier, Marseille et Catane (Italie). Cet exemple illustre bien à mes yeux l'implication récente des chimistes dans le champ de l'astronomie, et l'effort de formation associé. Cette discipline est par conséquent en évolution rapide en France, mais aussi à l'étranger comme l'illustre la multiplication de congrès ou sessions d'astrochimie organisés dans le monde.

Exobiologie et Origines

L'origine de la matière organique, son évolution et sa distribution dans les environnements extraterrestres, sont intrinsèquement liés au domaine de l'exobiologie[2]. D'ailleurs, les limites entre ce qui relèverait purement de l'astrochimie et ce qui aurait en plus un « label » exobiologique sont assez floues. Telle qu'elle est définie par le Groupe de Recherche en Exobiologie du CNRS : « l'exobiologie a pour objet l'étude de la vie dans l'univers. Plus précisément, elle inclut l'étude des conditions et des processus qui ont permis l'émergence du vivant sur notre planète, et ont pu ou pourraient le permettre ailleurs, **l'étude de l'évolution de la matière organique vers des structures complexes dans l'univers**, et les recherches qui concernent la distribution de la vie sous toutes les formes qu'elle pourrait revêtir, et son évolution ». Ainsi, ce seraient les processus de complexification de la matière organique qui donnent une coloration exobiologique à certaines études astrochimiques. Mais le terme « complexe » a des limites dans ce contexte : la matière organique insoluble des météorites carbonées est composée de molécules organiques de haut poids moléculaire dont la composition élémentaire est proche de celle des kérogènes terrestres. Sa structure chimique est bien plus complexe que celle des acides aminés, et pourtant c'est la détection de ces derniers, avec d'autres composés organiques relativement simples (bases azotés, sucres, acides gras) dans certaines météorites qui a généré tout l'intérêt exobiologique de l'étude des chondrites carbonées.

De plus, si l'étude de la formation d'un composé dans un environnement est primordiale, il ne faut pas qu'elle occulte le fait que les environnements extraterrestres sont rarement à l'équilibre thermodynamique, mais le plus souvent dans un état cinétique stationnaire, résultant de la somme des cinétiques des voies d'apparition et de disparition du composé. Ainsi, montrer que telle ou telle molécule d'intérêt exobiologique est produite au cours d'une simulation de laboratoire ou d'un calcul théorique, et affirmer qu'elle est forcément présente dans l'environnement étudié, sans prendre en compte les mécanismes de destruction, ou au contraire, mesurer une vitesse de disparition sans prendre en compte les voies de formation, et affirmer que la molécule ne peut être présente car détruite rapidement, peut conduire à une interprétation erronée. Sources et puits doivent être étudiés sur un pied d'égalité.

[2] Le terme « astrobiologie » est strictement synonyme de celui d'exobiologie. J'utiliserai ce dernier terme dans ce document car il est employé par la majorité de la communauté française : GDR exobiologie, Ecoles thématiques d'Exobiologie de Propriano, future société savante d'exobiologie, etc.

Il ne faut donc pas voir de l'exobiologie dans chaque molécule organique détectée en laboratoire, prédite par des calculs théoriques, ou observée dans le système solaire, ou le milieu interstellaire. La détection très controversée de la glycine dans le milieu interstellaire (Cunningham et al. 2007, Kuan et al. 2003), même si elle est un jour avérée, n'a strictement aucun intérêt exobiologique tant qu'elle n'est pas placée dans un contexte où la possibilité de transport de ces molécules du milieu interstellaire vers une planète n'est évoquée. Hors un tel transport est loin d'être évident, ce qui n'empêche pas Kuan et al. d'écrire dans leur abstract : «*The discovery of interstellar glycine strengthens the thesis that interstellar organic molecules could have played a pivotal role in the prebiotic chemistry of the early Earth*» avant de tempérer ces propos dans la conclusion de leur article : *« However, the crucial '' link '' that connects amino acids in space to prebiotic chemistry in the solar system, and perhaps to the emergence of life elsewhere in the Galaxy, is still missing. The discovery of interstellar glycine is only a first step toward answering this question* ». Précaution d'autant plus pertinente qu'il a été montré que le temps de vie photochimique des acides aminés soumis à un rayonnement UV inférieur à 200 nm est extrêmement limité (Ehrenfreund et al. 2001) (voir aussi plus loin dans ce document). Il n'existe pour l'instant pas de données cinétiques quantitatives concernant la formation d'acides aminés dans des environnements astrophysique. La pertinence exobiologique de la détection éventuelle d'acides aminés (ou autres biomolécules[3]) dans le milieu interstellaire est donc loin d'être avérée, alors que la détection des mêmes composés dans une météorite revêt une toute autre importance du fait qu'il est prouvé que ces molécules ont pu ensemencer les océans primitifs terrestres et initier l'évolution chimique qui aurait pu conduite à terme à l'émergence de la vie sur notre planète, et par extrapolation sur une autre planète possédant de l'eau liquide à sa surface.

Mais l'intérêt de l'étude de la chimie organique dans le système solaire dépasse largement le cadre de l'exobiologie, tout en restant lié à la problématique des origines. La chimie organique est l'une des clés de compréhension de la formation et de l'évolution de notre Système Solaire. Hors de tout questionnement lié aux origines de la vie, la détection d'une molécule organique dans un environnement extraterrestre peut nous apporter des informations sur son histoire, et dans le cas des petits corps non différenciés du système solaire (comètes, astéroïdes carbonés), nous permettre

[3] On peut trouver cette définition de ce qu'est une biomolécule sur Wikipédia : *Une biomolécule est une molécule qui participe au processus métabolique et à l'entretien d'un organisme vivant, par exemple les glucides, les lipides, les acides aminés, les acides nucléiques et même l'eau. On parle aussi de biomolécules pour des molécules identiques à celles trouvées dans le vivant, mais obtenues par d'autres moyens, par exemple dans les conditions qui prévalent dans l'espace ou dans des processus purement géophysiques*. Mais « une biomolécule » n'a pas forcément un intérêt exobiologique suivant le lieu où elle est détectée. Ce terme est donc à employer avec précaution, car il est malgré tout très connoté. Il ne viendrait à personne l'idée de dire que puisque la molécule d'eau est omniprésente dans l'univers la vie doit y être abondante, alors que ce pas a été déjà maintes fois franchi à l'occasion de la détection supposée de la glycine dans le milieu interstellaire, ou suite à la détection d'acides aminés après l'hydrolyse de résidus organiques obtenus après photolyse d'analogues de glaces cométaires ou interstellaire. Il faut noter que la référence à l'espace n'est d'ailleurs pas retrouvée dans la définition anglaise sur Wikipédia, ou dans d'autres ouvrages de biologie.

de remonter aux conditions qui régnaient dans notre Système Solaire au moment de sa formation, il y a 4,56 milliards d'années. Une molécule organique, lorsqu'elle est détectée, peut nous apporter de nombreuses informations sur l'objet astrophysique qui la contient. Elle est produite à la suite de réactions chimiques, sous certaines conditions. Ces dernières seraient-elles différentes (température, type de rayonnement), qu'un autre produit pourrait avoir été formé à sa place. Nous savons encore assez mal « lire » l'histoire de notre Système Solaire à la lumière de ce que nous enseignent les molécules organiques qui s'y trouvent. Les travaux que je présente dans ce document, principalement consacrés à la chimie des comètes, peuvent paraître encore assez parcellaires sur ce plan. La raison principale à cela est la dispersion de l'ensemble des moyens expérimentaux qui seraient nécessaires pour mener à bien un tel projet. Certains laboratoires étant spécialisés dans l'étude des voies de production de molécules organiques complexes, et d'autres dans les processus de dégradation de ces dernières. Par exemple, je disposais des outils pour l'étude de la formation de composés organiques complexes dans les glaces interstellaires et cométaire au Goddard Space Flight Center, alors que j'ai pu étudier au LISA leur dégradation thermique et photolytique. Les projets en cours de développement au LISA, et notamment l'expérience OREGOC, devraient nous permettre d'avoir une vision plus large de l'évolution chimique au sein des comètes, et être prêt à tirer tout le bénéfice des mesures des instruments de ROSETTA et PHILAE auxquels le LISA est associé : COSAC et COSIMA.

Après une brève présentation de mes activités de recherche et d'encadrement depuis 2000, j'exposerai plus en détail le cadre et le contexte scientifique, ainsi que les objectifs de mes travaux. Je décrirai ensuite les résultats obtenus et les projets en cours en les illustrant de façons approfondie au travers des articles publiés. Une dernière partie de document d'habilitation est consacré à la liste de mes principales collaborations, contrats de recherches, ainsi qu'un curriculum détaillé. Mes articles et chapitres d'ouvrages sont rassemblés en fin de document afin d'en faciliter la lecture.

RESUME DE MES ACTIVITES DE RECHERCHE

J'ai ma effectué thèse dans le Groupe de Physico Chimie Organique Spatiale (GPCOS) du Laboratoire Interuniversitaire des Systèmes Atmosphériques (LISA, Universités Paris 12 et Paris 7, UMR 7583 CNRS) sous la direction de François Raulin et Marie-Claire Gazeau. Intitulée « *Chimie organique de l'environnement cométaire : étude expérimentale de la contribution de la composante organique réfractaire à la phase gazeuse* », je l'ai soutenue le 10 Novembre 1999 à l'université Paris 12. Ce travail avait consisté à montrer que la présence de polyoxyméthylène ($-(CH_2-O-)_n-$ POM) dans les comètes pouvait expliquer la source distribuée de formaldéhyde observée dans la comète de Halley. Il s'agissait d'un travail essentiellement expérimental (étude de la dégradation thermique et photochimique du POM), où je ne faisais qu'ébaucher l'approche théorique permettant d'appliquer mes mesures cinétiques à l'environnement cométaire. En 2000, bénéficiant d'un demi-support d'Attaché Temporaire d'Enseignement et de Recherche à l'université Paris 12 qui m'a permis de poursuivre mes travaux au LISA, j'ai poursuivi le travail initié en approfondissant l'aspect modélisation avec Yves Bénilan. A la fin de ma thèse, le modèle ne prenait en compte que des grains composés entièrement de POM, alors que suite à cette année d'ATER nous modélisions des grains hétérogènes. En parallèle, j'ai encadré avec Marie-Claire Gazeau le stage de DEA de Souleyman Bachir consacré à l'étude de la photodégradation de l'hexaméthylènetétramine ($C_6N_4H_{12}$ – HMT). Nous avons montré à cette occasion que cette molécule est très stable photochimiquement et thermiquement, et n'était donc probablement pas à l'origine des sources distribuées de CN observées dans plusieurs comètes.

A partir du 1er Février 2001, j'ai bénéficié d'une bourse du National Research Council (NRC) et intégré l'équipe du Cosmic Ice Laboratory (dirigée par Marla H. Moore) de la branche d'astrochimie du NASA Goddard Space Flight Center (GSFC) en tant que Research Associate. Je me suis alors plus particulièrement intéressé aux synthèses organiques de molécules complexes dans des analogues de glaces interstellaires et cométaires, et à la photolyse de petites molécules telles que CO, CO_2, NH_3, etc. En parallèle, j'ai poursuivi mon travail de modélisation des sources distribuées cométaire en collaboration avec Yves Bénilan, pour aboutir à une nouvelle version de notre modèle prenant cette fois-ci en compte toute une population de grains de tailles, vitesses, et températures différentes, toujours pour le cas de la comète de Halley.

En Février 2002, j'ai été recruté en tant que maître de conférences au LISA. Depuis lors je développe des programmes d'étude de l'évolution de la matière organique dans le système solaire, mêlant des approches expérimentales, théoriques et observationnelles. Mes travaux ont été en grande partie consacrés à l'étude des comètes, mais aussi plus récemment à d'autres objets du système solaire comme Mars, Titan, ou les astéroïdes carbonés. Ceci m'a conduit à proposer de nombreux stages en maitrise de chimie option environnement de l'université Paris 12 (puis en troisième année de licence sciences de la matière, L3 parcours chimie), et en DEA de chimie de la pollution atmosphérique et physique de l'environnement (puis en seconde année de Master Science et Génie de l'Environnement, M2 SGE parcours Atmosphère et Qualité de l'Air recherche). Mes travaux s'articulent principalement autour de deux grands axes : la caractérisation de la matière

organique cométaire d'une part, et l'évolution photochimique de la matière organique dans le système solaire d'autre part.

MATIERE ORGANIQUE COMETAIRE

En ce qui concerne les comètes, dès mon retour au LISA, j'ai participé à l'encadrement de la thèse en cours de Nicolas Fray (*Etude expérimentale et théorique de la contribution de la composante organique réfractaire à la phase gazeuse dans l'environnement cométaire,* direction de la thèse : Marie-Claire Gazeau et Yves Bénilan) qui a permis d'étendre le travail de modélisation des sources distribuées, appliqué jusqu'alors uniquement au cas de la comète de Halley, à la comète Hale-Bopp. Ce travail a été mené avec l'équipe comètes de l'observatoire de Meudon avec laquelle nous collaborons régulièrement depuis (Nicolas Biver, Dominique Bockelée Morvan et Jacques Crovisier). Cette thèse, soutenue en 2004, a aussi permis d'initier un travail expérimental concernant la dégradation thermique et photochimique des polymères de HCN. A l'époque, nous ne disposions que d'une quantité réduite d'échantillons fournis par Robert Minard (Pennstate University, USA), ce qui m'a conduit en 2007-2008 à encadrer avec Nicolas Fray[4] un stage de M2 consacré à l'étude de synthèse de polymères de HCN, et à la mesure de leur cinétique de dégradation thermique (Léna Le Roy – Synthèse et étude de la dégradation thermique des polymères de HCN : Application aux sources distribuées de CN dans les comètes). Ce travail de synthèse a été mené avec succès, et nous travaillons à la caractérisation de ces solides avec Eric Quirico (LPG, Grenoble). Edith Hadamcik (Service d'Aéronomie) mesurera très prochainement leurs propriétés de polarisation dans le cadre de la collaboration que nous avons initiée avec l'équipe d'Annie-Chantal Levasseur-Regourd. En effet, au-delà des observations de sources distribuées cométaires, nous nous sommes aperçus que la dégradation de composés organiques de hauts poids moléculaires pouvait être à l'origine des modifications de propriétés de polarisation de grains interplanétaires lorsqu'ils s'approchent du Soleil.

J'ai aussi cherché à approfondir notre connaissance de la structure chimique du POM et son influence sur sa cinétique de dégradation thermique en encadrant en 2003-2004 le stage de DEA de Sébastien Desrutin : *Dégradation thermique du polyoxyméthylène en fonction de sa structure et application à l'étude des sources étendues de formaldéhyde dans les comètes*. Dans le même temps, sur une problématique annexe, j'ai proposé deux stages consacrés à l'étude de l'hydrolyse du HMT et du POM afin d'évaluer dans quelle mesure l'apport de ces molécules sur Terre via les comètes pourrait avoir eu rôle dans la formation de molécules d'intérêt prébiotique (2003 - stage de Maîtrise de Nacima Siad - *Hydrolyse de l'hexaméthylènetétramine à la recherche d'acides aminés*, 2004-2005 – Stage de DEA de Cyril Duval - *Etude de l'hydrolyse de molécules organiques cométaires d'intérêt prébiotique. Cas de l'hexaméthylènetétramine et d'un mélange d'hexaméthylènetétramine et de polyoxyméthylène*).

[4] Recruté sur un poste de Maître de Conférences au LISA le 1er Septembre 2006.

Enfin, après être devenu Co Invistigator (CoI) de l'expérience COSIMA en Janvier 2005, j'ai commencé à travailler avec Laurent Thirkell (LPCE, Orléans) et Cécile Engrand (CSMSM, Paris 11), rejoints à partir de Septembre 2006 par Christelle Briois (LPCE, Orléans), à la préparation de l'interprétation des spectres de masses de matière organique qui seront mesurés à partir de 2014 lorsque ROSETTA arrivera à sa destination : la comète 67P/Churyumov-Gerasimenko. Ce travail a été l'occasion de deux stages de L3 (2006 – Léna Le Roy et Audrey Noblet – *Elaboration d'un protocole de dépôt de molécules organiques en vue d'une analyse par spectrométrie de masse à temps de vol dans le cadre de la mission Rosetta* ; 2007 – Karen Habib et Guillaume Valette – *Préparation d'une bibliothèque de spectres de masse TOF-SIMS pour des molécules organiques d'intérêt cométaire : application à la mission ROSETTA*). Ces travaux préliminaires nous ont conduits à proposer un projet de thèse au CNES et à la région Centre (cofinancement) pour un travail dans le prolongement de ces deux sujets : *Caractérisation de la matière organique cométaire par simulation expérimentale et par spectrométrie de masse (applications à l'instrument COSIMA)*. Ce sujet en partenariat entre le LPCE et le LISA a été retenu, et Léna Le Roy commencera ce travail en Octobre 2008 (Directeur de Thèse : Gilles Poulet-LPCE, Co-directeur : Hervé Cottin-LISA). Cette collaboration autour de l'analyse de la matière organique cométaire a également récemment débouché sur une proposition d'instrumentation pour la mission Marco Polo d'exploration d'un astéroïde carboné géocroiseur avec retour d'échantillon. L'instrument ILMA (Ion Laser Mass Analyzer), dont je suis le Principal Investigator (PI), est un spectromètre de masse haute résolution construit autour d'une trappe ionique. Une équipe internationale de 23 scientifiques, appartenant à 16 institutions des 5 pays européens est réunie autour de ce projet d'exploration in-situ. J'ai aussi participé à la proposition de mission de retour d'échantillon cométaire Triple F dans le cadre de l'appel d'offre Cosmic Vision de l'ESA. Cette mission n'a pas été retenue.

Actuellement, je développe avec Nicolas Fray un nouveau projet appelé OREGOC (ORigine et Evolution des Glaces et de la matière Organique Cométaire), qui permettra de suivre au sein d'un même dispositif l'évolution de la matière organique depuis sa synthèse dans les glaces cométaires jusqu'à sa dégradation lorsqu'elle est éjectée dans l'atmosphère cométaire et dégradée sous l'action du rayonnement ultraviolet et de la chaleur. Ce dispositif est unique puisqu'il combine une expérience semblable à celle que j'ai pu utiliser au GSFC et que l'on retrouve dans d'autres laboratoires pour étudier les glaces interstellaires et cométaire (IAS, Leiden, AMES, Catane…) avec les programmes expérimentaux dédiés aux sources distribuées qui sont développés au LISA depuis le début de ma thèse.

EVOLUTION PHOTOCHIMIQUE DE LA MATIERE ORGANIQUE DANS LE SYSTEME SOLAIRE

Depuis Avril 2005, je suis le PI de deux expériences de photochimie en orbite terrestre, l'une placée à l'extérieur de la Station Spatiale Internationale, sur le module européen Columbus (expérience PROCESS – LISA/Centre de Biophysique Moléculaire (CBM-Orléans)/Service d'Aéronomie, 2007-2009) et l'autre à l'extérieur d'une capsule russe FOTON (Expérience UVolution – LISA/SA – Septembre 2007). A partir de Janvier 2007, j'ai pris la succession d'André Brack en tant que

PI de l'expérience AMINO (LISA/CBM/SA/Institut Jacques Monod/INRA) qui sera exposée à l'extérieur du module Russe Zarya fin 2008 pour deux années. La préparation de ces projets a été l'objet d'un stage de maîtrise en 2005 (Jonathan Danjean et Europe Mortier, *Elaboration d'un protocole de dépôt de molécules organiques sur les fenêtres d'exposition spatiale*), puis d'un stage de seconde année de Master (SGE) en 2005-2006 (Yuan Yong Guan - *Photochimie expérimentale en orbite terrestre : élaboration d'un protocole de dépôt de films de molécules organiques*). Yuan Yong Guan a ensuite poursuivi son travail en thèse sous la direction de François Raulin et moi-même. Les résultats de UVolution sont déjà disponibles au retour de 12 jours d'exposition en orbite au mois de Septembre 2007, et l'expérience a été un succès. L'une des originalités de ces expériences a été de développer des cellules d'exposition fermées étanches, permettant l'exposition de mélanges gazeux. Cette étude a été menée en partenariat avec le CNES, la COMAT (industriel basé à Toulouse) et la direction des techniques avancées d'Air Liquide (Toulouse). Les molécules exposées dans le cadre de ces expériences ne relèvent pas toutes de l'étude des comètes, mais aussi de la chimie de l'atmosphère de Titan, ou encore de la stabilité de molécules organiques à la surface de Mars. J'ai ainsi été amené à participer à l'encadrement de la thèse de Fabien Stalport (2004-2007, *Recherche d'indices de vie sur Mars : détermination de signatures spécifiques de biominéraux et étude expérimentale de l'évolution de molécules organiques dans des conditions environnementales martiennes*, direction : Patrice Coll et Cyril Szopa).

Dans la continuité de ces expériences d'exposition, j'ai proposé au CNES en réponse à son appel à idée en 2008, un projet d'instrument d'exposition appelé VITRINE (Test for Remotely controlled INstrument for Exobiology) pour des expositions longue durée (à l'extérieur de la station spatiale ou d'un autre engin spatial, voire à la surface de la Lune), permettant l'analyse in-situ de l'évolution des échantillons par spectroscopie. Ce projet regroupe pour l'instant six laboratoires français et fait l'objet d'une activité de Recherche et Développement soutenue par la CNES.

AUTRES ACTIVITES DE RECHERCHE ET DE FORMATION

Sur des aspects annexes à ces deux thématiques dominantes, j'ai encadré en 2004 un stage de Maitrise de chimie avec Yves Bénilan concernant la synthèse et la caractérisation spectrale en infrarouge de la molécule d'acide isocyanique (HNCO) (Alexandra Fursy et Cécilia Reis – Synthèse de l'acide isocyanique et étude de son spectre infrarouge), faisant bénéficier mes collègues spectroscopistes des méthodes de synthèses « propres » auxquelles j'avais été formé pendant mon année au GSFC. J'ai aussi « importé » des Etats-Unis un nouveau protocole de synthèse de l'acide cyanhydrique (HCN) qui a été largement utilisé dans le cadre des activités de mesures VUV sur le synchrotron de Bessy par mes collègues Yves Bénilan, Nicolas Fray et Marie-Claire Gazeau.

Je participe aussi à un groupe de réflexion animé par Alain Léger de l'IAS consacré à la recherche de biosignatures et biosignatures-technologiques dans les atmosphères d'exoplanètes. C'est à ce titre que j'ai rejoint l'équipe proposante DARWIN dans le cadre de l'appel COSMIC VISION de l'ESA.

De plus, outre mes activités d'enseignement dispensées à Paris 12, je me suis impliqué dans la formation doctorale et post-doctorale en organisant depuis 2007 avec Muriel Gargaud (Observatoire de Bordeaux) les Rencontres Exobiologiques pour Doctorants (RED'07 et '08 ; '09 à venir), école interdisciplinaire annuelle pour doctorants sur des thématiques relevant de l'exobiologie (voir programme sur le site web des écoles). J'ai aussi participé à l'organisation de l'école thématique CNRS d'exobiologie qui s'est tenue en septembre 2007 à Propriano (avec Muriel Gargaud et Franck Selsis de l'observatoire de Bordeaux). L'une des grandes originalités de ces écoles et que les cours sont filmés et disponibles en ligne[5]. J'ai aussi participé en 2005 et 2007 avec François Raulin à l'organisation en France d'un programme européen de cours en exobiologie initié par Gerda Horneck (Cologne, DLR) et financé par l'ESA, intitulé ABCnet. Ces cours sont eux aussi disponibles en ligne.

L'ensemble de ces travaux à pour l'instant conduit à 22 publications dans des revues à comité de lecture, dont 11 en premier auteur, 5 chapitres d'ouvrages à comité de lecture, et plus de 50 présentations dans des congrès internationaux, dont 7 présentations invitées en tant que premier auteur.

[5] Sites des écoles : RED'07 - http://www.u-bordeaux1.fr/red07/ ; RED'08 - http://www.u-bordeaux1.fr/red07/ ; Propriano - http://www.u-bordeaux1.fr/exobio07/ ;
ABCnet - http://streamiss.spaceflight.esa.int/?pg=production&dm=1&PID=abcnet0708)

I. CADRE ET OBJECTIFS DE RECHERCHE

L'étude d'environnements extraterrestres actuelle fait partie des thématiques principales du LISA depuis sa création. Ce thème y a trouvé naturellement sa place car il fait appel aux mêmes types d'outils tant théoriques qu'expérimentaux que ceux employés pour le développement des thématiques terrestres. Le Groupe de Physico Chimie Organique Spatiale (GPCOS) auquel j'appartiens, dirigé par François Raulin, développe des programmes expérimentaux, théoriques et observationnels, dont le but ultime est de mieux comprendre les lois qui régissent l'évolution de la matière organique dans le système solaire.

Ces études sont menées en relation directe avec l'exobiologie, qui est l'une des six grandes thématiques du laboratoire. Ce domaine interdisciplinaire couvre l'ensemble des recherches relatives à l'étude des origines, de la distribution et de l'évolution de la vie dans l'univers, mais aussi des structures (y compris au niveau moléculaires) et des processus (y compris organiques) liées à la vie et à son apparition. L'Exobiologie est actuellement en pleine expansion au niveau national, sous l'impulsion en particulier du CNES et du GDR CNRS « Exobio » dont le LISA a assuré la direction (François Raulin) de sa création en 1999 jusqu'à fin 2006. J'ai ensuite assuré la codirection du GDR (avec Frances Westall – Directrice, et Daniel Prieur – codirecteur) lors de son troisième renouvellement pour les années 2007 et 2008. La mise en place du nouveau programme interdisciplinaire du CNRS « Origines des Planètes et de la Vie (PID OPV), démarrant le 1er janvier 2007, montre bien l'importance qui est aujourd'hui accordée à cette thématique. Ce domaine est aussi en pleine expansion au niveau international, avec en particulier les activités du NASA Astrobiology Institute (auquel le GDR Exobio est affilié) et la création en 2002 de l'European Astrobiology Network Association (EANA). Le LISA a été l'un des coordinateurs principaux de cette discipline au niveau national, et a largement contribué à la création du GDR Exobio, ainsi qu'à la création de l'EANA.

L'une des particularités du GPCOS du LISA dans les domaines de l'astrochimie est qu'il est constitué en grande partie de chimistes et physico-chimiste de formation. Les activités du groupe s'articulent principalement autours de l'étude de Titan, des comètes et de Mars. Ce choix s'explique par l'importance exobiologique de ces objets et par la perspective de missions spatiales susceptibles de nous apporter, à court et moyen terme des données essentielles au sujet de ces corps célestes. Parmi elles figurait la mission Cassini-Huygens dans laquelle le LISA est très fortement investi. Le groupe est maintenant particulièrement mobilisé autour de la mission cométaire ROSETTA et des futures missions Martiennes (Rovers NASA et ESA).

Les activités du GPCOS s'articulent plus précisément autour de deux grands volets :

1. L'étude de processus chimiques et plus précisément les études de réactivité et d'évolution moléculaire, afin de mieux comprendre quels sont et comment interviennent les mécanismes de formation et d'évolution de la matière organique dans des milieux extraterrestres.

2. La recherche de structures moléculaires dans ces environnements, afin de contraindre les modèles théoriques et expérimentaux, en s'appuyant sur les données de laboratoire et sur les missions d'observation, au sol ou en orbite terrestre, ou encore portées par des missions d'exploration spatiales.

Cette articulation se retrouve aussi au sein de mes recherches : mes travaux autour des sources distribuées cométaires et la photochimie se rattachant au premier volet, alors que mes activités relevant de l'instrumentation spatiale et la spectrométrie de masse relèvent du second volet. Les programmes que j'ai développés au LISA se situent à l'interface de la chimie, la physicochimie, la planétologie et l'exobiologie. Ils gravitent principalement autour de l'étude des petits corps du système solaire, en particulier les comètes. Ils consistent à chercher à comprendre ce que les petits corps peuvent nous apprendre sur la formation du système solaire, et à évaluer leur contribution éventuelle en tant que source exogène de matière organique ayant pu initier la chimique prébiotique sur Terre, et éventuellement Mars.

I-1. LES PETITS CORPS ET LA FORMATION DU SYSTEME SOLAIRE

Tous les corps de notre Système Solaire se sont formés il y a environ 4,56 milliards d'années, suite à l'effondrement sur lui même d'une partie d'un nuage moléculaire. De ce même matériau, probablement uniformément mélangé à l'origine, sont nés des objets aussi différents que le Soleil, les planètes telluriques, les planètes géantes ainsi que leurs satellites, et les petits corps (astéroïdes et comètes).

Les comètes ont été stockées dans les régions les plus reculées et donc les plus froides du système solaire (ceinture de Kuiper et nuage d'Oort), ces planétésimaux glacés n'ont pas subi de processus de différentiation du fait de leur petite taille. Ils devraient donc avoir gardé leur composition initiale, témoignant des conditions physico-chimiques qui régnaient là où ils se sont formés, voire même de la composition de notre nuage moléculaire natal. Les comètes sont donc considérées comme les archives les plus anciennes du système solaire.

Les nuages moléculaires que l'on peut observer actuellement dans la galaxie présentent très probablement de fortes analogies avec la composition de notre nuage natal. Leur observation par télédétection a montré que ce sont des environnements où la chimie organique est très active aussi bien en phase gazeuse que solide (glaces interstellaires) (Ehrenfreund & Charnley 2000). Des molécules comme HCN, HC_3N ou HCHO, dont l'intérêt prébiotique est indéniable[6], y ont été détectées. De plus, l'existence de molécules organiques beaucoup plus complexes y est prédite si l'on se fie aux résultats d'expériences de laboratoire simulant la chimie se déroulant dans les glaces des nuages interstellaires lorsqu'elles sont soumises à des irradiations (par des photons ou des particules chargées) ou à des cycles thermiques. Ainsi, une grande partie de la matière organique présente dans

[6] Voir à ce sujet : Cottin H., Basic prebiotic chemistry. In Complete course in astrobiology (ed. P. Rettberg and G. Horneck), pp. 55-83. Wiley-VCH, 2007

les nuages moléculaires serait gelée autour de noyaux de condensation composés de silicates (Figure 1). Suite à une perturbation gravitationnelle, notre nuage moléculaire natal (ou une partie) s'est effondré sur lui même pour donner naissance au Soleil et à son système planétaire.

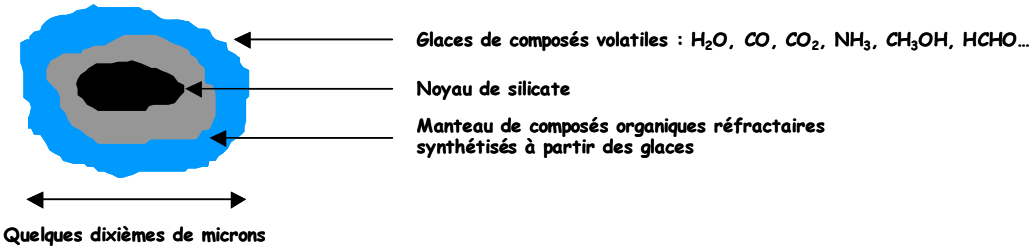

Figure 1. Modèle de grain interstellaire. Un noyau de silicate autour duquel se condensent des molécules volatiles dans les nuages moléculaires. La chimie entre celles-ci conduit à la synthèse de composés plus complexes. Notre système solaire s'est formé par accrétion de ce matériau de base. Certaines comètes pourraient avoir conservé ces grains intacts.

De façon simplifiée, on peut considérer que la composition originelle des grains interstellaires a été perdue car soit ils ont été incorporés au Soleil ou aux planètes, soit ils ont été pyrolysés au voisinage du Soleil, soit encore les glaces interstellaires ont été sublimées dans les régions les plus chaudes de la nébuleuse (les plus proches du Soleil) dans lesquelles elles ont été amenées à séjourner du fait de la turbulence qui a conduit à homogénéiser la nébuleuse solaire (Figure 2). L'extension de cette région turbulente dans la nébuleuse va déterminer la possibilité de conserver la matière interstellaire intacte au sein des comètes. A l'intérieur de cette région, un brassage vigoureux de la matière aura conduit les grains interstellaires au voisinage du Soleil, leur faisant ainsi perdre leur composition d'origine. Suivant les modèles, la région turbulente de la nébuleuse peut s'étendre jusqu'à environ 30 UA (Bockelée-Morvan et al. 2002, Hersant et al. 2001). Au delà, les grains auront toujours séjourné dans un environnement froid, et auront ainsi probablement pu conserver leur composition interstellaire. De là découlent plusieurs modèles dans lesquels la matière organique interstellaire subit différents degrés de transformation avant d'être stockée dans les comètes. Elles sont parfois considérées comme de simples agrégats de grains interstellaires n'ayant subi aucune transformation (Greenberg 1982), ou bien comme composées de matière complètement transformée ne témoignant plus que de la chimie interne à la nébuleuse solaire (Prinn & Fegley 1989). D'autres modèles envisagent des solutions intermédiaires (Iro et al. 2003, Lunine et al. 1991) probablement plus réalistes. Mais quoiqu'il en soit, si l'on met de coté les débats encore non tranchés concernant l'origine de la matière cométaire, les observations témoignent pour ces objets d'une richesse indéniable en composés organiques, et qu'elles soient d'origine interstellaire ou interne à la nébuleuse, des molécules telles que HCN, HCHO ou HC_3N que nous avons déjà évoquées, et qui ont été détectées dans plusieurs comètes, gardent le même intérêt d'un point de vue exobiologique. De plus, des observations in situ réalisées au voisinage de la comète P/Halley (en 1986) ou après retour d'échantillons prélevés dans l'atmosphère de la comète 81P/Wild 2 en 2004, attestent de la présence de structures encore plus complexes qui du fait de leur masse moléculaire élevée restent sous forme solide sur les grains éjectés du noyau. L'absence d'eau liquide sur les comètes pendant de longues périodes ne permet pas d'envisager la présence de vie sur leur noyau (même si de courts épisodes de fonte des glaces sont envisagés peu après la formation des

comètes à cause de la décroissance radioactive de radioéléments tels que ^{26}Al (Podolak & Prialnik 1997)). Par contre, les molécules déjà détectées, auxquelles s'ajoutent un nombre plus important encore de composés organiques complexes suspectés (grâce aux simulations en laboratoire) d'être présents sur les noyaux, font des comètes des objets d'un grand intérêt exobiologique en tant que sources exogènes de molécules prébiotiques.

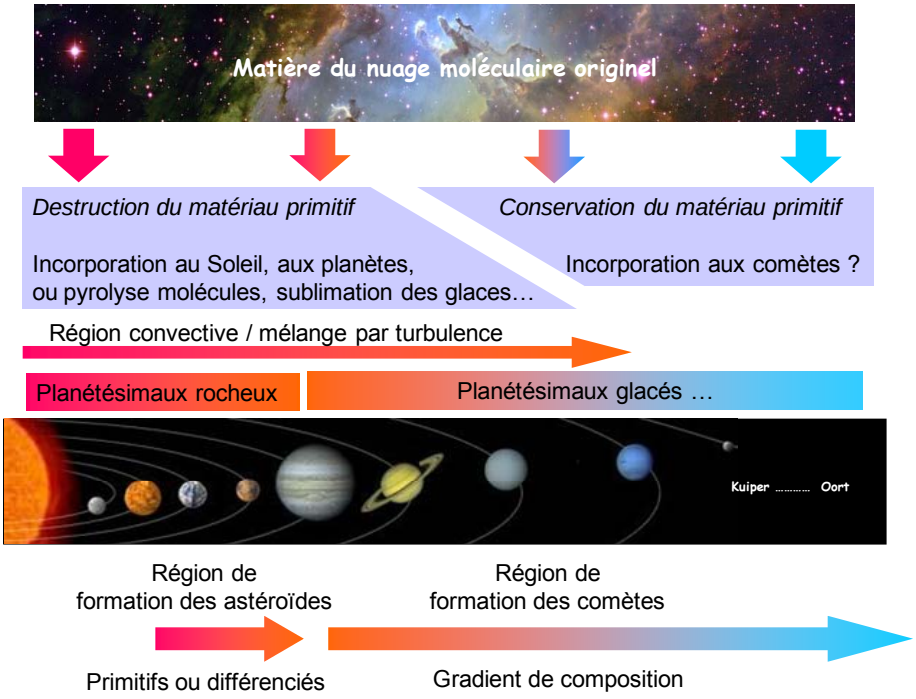

Figure 2. Evolution de la matière entre le nuage moléculaire originel, la nébuleuse solaire et l'incorporation aux différents corps du système solaire.

Une fois synthétisées dans le milieu interstellaire ou dans la nébuleuse solaire, les molécules d'intérêt prébiotique peuvent toutefois être détruites par les mêmes apports d'énergie qui ont conduit à leur synthèse (UV, particules chargées, chaleur). Des expériences menées dans l'espace, sur la station MIR ou encore les capsules spatiales FOTON, ont montré que des acides aminés peuvent survivre à l'exposition aux UV solaires dans la mesure où ils sont protégés par une matrice minérale (sur des grains cométaires par exemple, mais aussi dans des météorites) (Barbier et al. 1998, Barbier et al. 2002, Boillot et al. 2002). Les expériences d'exposition en orbite que je coordonne sont dans la lignée de ces travaux. Ensuite, après avoir survécu à un séjour prolongé dans l'espace, ces molécules doivent résister à la violence des impacts cométaires ou météoritiques avec la Terre. Des travaux théoriques (Chyba et al. 1990) et expérimentaux (Blank et al. 2001) ont permis de montrer que des acides aminés peuvent effectivement survivre à de telles collisions.

I-2. L'EXOBIOLOGIE DANS LE SYSTEME SOLAIRE

La vie telle que nous la connaissons est basée sur des processus chimiques extrêmement complexes, mettant en jeu des molécules telles que les protéines ou les acides ribo- et désoxyribo-nucléiques. Des structures aussi élaborées n'apparaissent pas spontanément et résultent d'une évolution complexe dont le point de départ est un mélange de molécules organiques très simples, courantes dans le milieu interstellaire, les atmosphères de certaines planètes et satellites, et des objets comme les comètes et les astéroïdes carbonés. A un certain point, lorsque la matière atteint un stade de complexité et d'organisation encore non défini à ce jour, la chimie devient biologie, et la vie apparaît. On décrit traditionnellement cette étape comme étant celle où une structure acquiert la propriété de pouvoir catalyser la formation de copies d'elle-même, tout en laissant une certaine marge à l'évolution en commettant parfois une légère erreur dans sa réplication. L'évolution chimique conduisant à l'origine de la vie est similaire à l'évolution biologique décrite par Darwin.

Ainsi, à partir du même matériau de départ, incorporé au système solaire depuis notre nuage moléculaire natal, l'évolution physico-chimique a permis l'apparition de la vie au moins sur la Terre, et peut être aussi sur Mars ou encore de façon plus spéculative sur Europe. Grâce à l'exploration spatiale, nous cherchons à comprendre ce qui fait de la Terre cet objet si particulier qu'il est le seul à notre connaissance à abriter la vie, et ainsi dans quelle mesure la vie aurait pu apparaître ailleurs. Deux facteurs semblent essentiels à ce jour: une source de molécules organiques et la présence d'eau à l'état liquide, solvant nécessaire pour atteindre un stade avancé de complexité chimique, préalable à l'apparition de la vie. Ainsi, les missions spatiales traitant de questions exobiologiques s'articulent autour de ces deux axes :

- Quelles sont l'origine et la répartition de la matière organique dans le Système Solaire ?
- L'eau existe-t-elle, ou a-t-elle existé, sous forme liquide sur d'autres planètes ?

La figure 3 schématise l'évolution de la matière depuis notre nuage moléculaire natal, vers les différents objets du système solaire. Elle fait apparaître pour chaque objet les paramètres que l'on estime favorables ou défavorables à l'apparition de la vie sur ces corps. Tout commence avec la matière d'un nuage moléculaire que l'on pourrait appeler LUC (Last Universal Cloud) par analogie avec LUCA (Last Universal Common Ancestor) (Forterre 2001) l'ancêtre commun de tous les organismes vivant sur Terre, et LUCY qui a longtemps été la plus lointaine aïeule connue de l'espèce humaine.

Voir à ce sujet :

Article 1 – p.48

COTTIN H. *(2007) Basic prebiotic chemistry. In Complete course in astrobiology (eds. P. Rettberg and G. Horneck), pp. 55-83. Wiley-VCH.*

Article 2 – p.78

BÉNILAN Y. and ***COTTIN H.*** *(2007) Comets, Titan and Mars: Astrobiology and space projects. In Lectures in Astrobiology (eds. M. Gargaud, P. Claeys and H. Martin), pp. 347-428. Springer Verlag.*

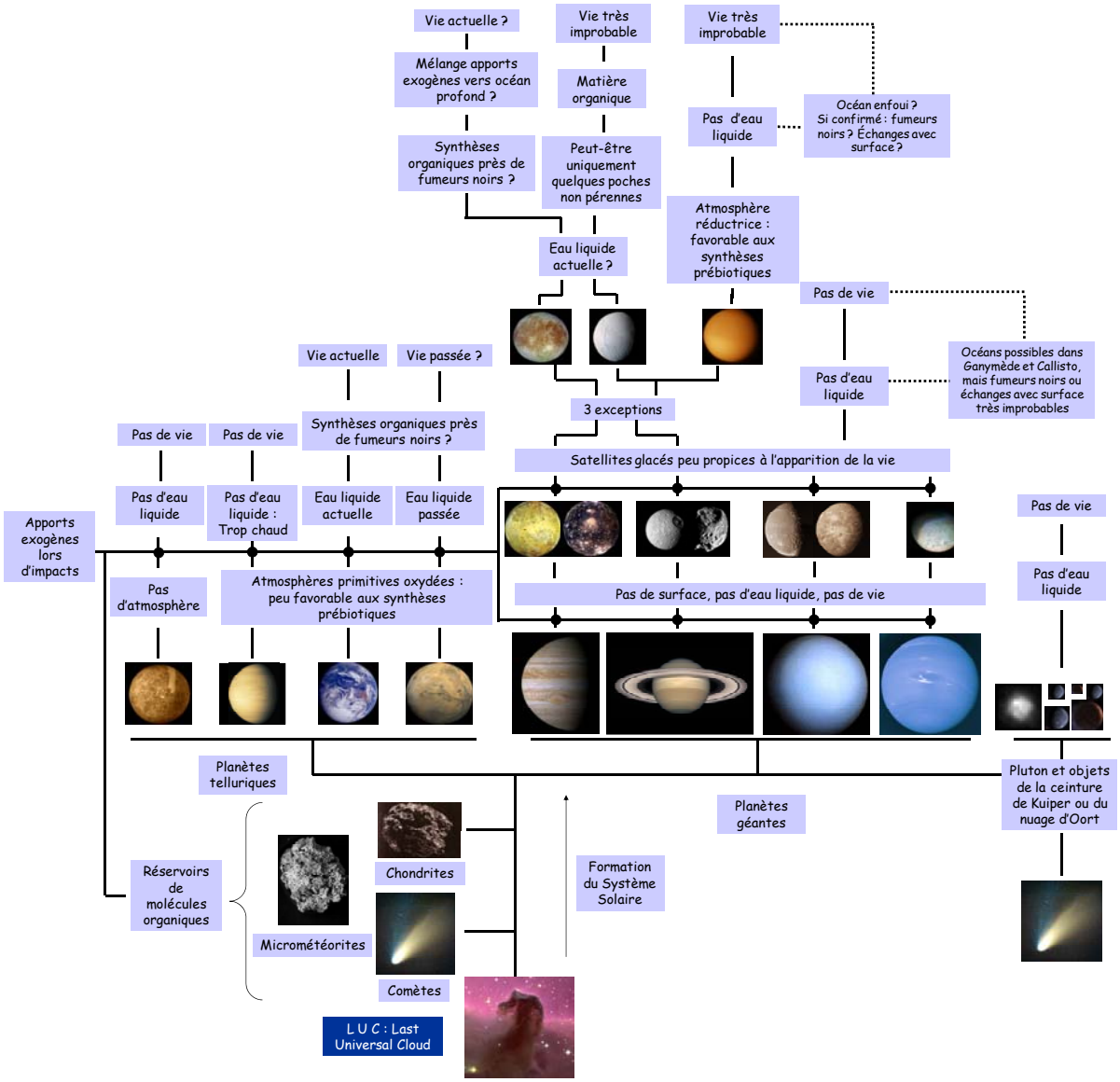

Figure 3. : Arbre exobiologique du système solaire : évolution de la matière (voir aussi Figure 2) et intérêt exobiologique des différents corps du système solaire. Avec de bas en haut, et de gauche à droite : La nébuleuse de la tête de cheval, la comète C/1995 O1 (Hale-Bopp), une micrométéorite collectée à la base antarctique de Concordia, la météorite d'Orgueil, Mercure, Vénus, La Terre, Mars, Jupiter, Saturne, Uranus, Neptune, Pluton et objets de la ceinture de Kuiper et du Nuage d'Oort, Io, Callisto, Mimas, Phoebe, Ariel, Obéron, Triton, Europe, Encelade et Titan.

I-3. METHODOLOGIE

L'étude et la compréhension des processus chimiques qui régissent l'évolution de la matière organique dans les environnements astrophysiques, ainsi que les tentatives d'identification de structures moléculaires qui y sont associées, se déclinent sous trois modes différents : des approches observationnelles, la construction de modèles numériques, et enfin la mise en œuvre d'expériences de laboratoires. Ces trois grandes familles d'approches sont bien sûr complémentaires et l'une des grandes chances de travailler sur des thématiques aussi récentes que la planétologie et l'exobiologie est de pouvoir mener des activités qui relèvent de ces trois grandes familles d'approches en parallèle.

La Figure 4 reprend un schéma synthétique de ces trois grandes catégories d'approches que j'avais déjà présenté dans mon manuscrit de thèse. Elle détaille en particulier les trois grandes familles de simulation expérimentales :

- Les simulations **globales** : à partir d'observations, elles testent la validité d'hypothèses concernant une évolution générale, et permettent de prédire la présence de composés nouveaux : « L'atmosphère primitive terrestre était composée de tel et tel constituants, voyons l'évolution d'un tel mélange lors d'un apport d'énergie », «Les atmosphères cométaires sont dominées par un certain mélange de composés volatiles, quel est l'évolution d'un mélange analogue, condensé à 10K, lorsqu'il est soumis à un apport d'énergie simulant les processus de photolyse ou irradiation que les glaces cométaires rencontrent au cours de leur histoire ?». Les informations que les simulations globales procurent restent qualitatives et les résultats ne peuvent que rarement être incorporés à des modèles.

- Les simulations **spécifiques** : elles tendent à déterminer un paramètre physico-chimique bien précis, qui doit être incorporé à un modèle. Par exemple, le rendement quantique de production de formaldéhyde à partir du POM à 122 nm, la cinétique de production de HCN à partir de polymère de HCN en fonction de la température, ou encore la vitesse de photolyse de la glycine à 1 unité astronomique. C'est seulement avec un grand nombre de ces données cinétiques (ou thermodynamiques) que l'on peut faire fonctionner un modèle numérique permettant de faire des prédictions ou d'interpréter des observations. Mais dans ces modèles ne se forment que les molécules que l'on a prévues, d'où la nécessité du premier type de simulations.

- Les simulations **restreintes** : elles tendent à tester et affiner une partie d'un modèle global, en ne mettant en jeu qu'un nombre restreint de composé. Par exemple, chercher à comprendre le mécanisme de production du POM ou du HMT dans les glaces interstellaires et cométaires en faisant varier la composition d'un nombre limité de constituant d'un mélange initial de glaces, ou encore tester la sensibilité d'un même mélange au type d'apport d'énergie auquel il est soumis (photons UV *Vs*. particules chargées).

Une étroite interaction entre tous ces aspects doit être entretenue. Il n'est malheureusement pas caricatural d'évoquer un modélisateur interprétant une divergence entre ses

résultats et une mesure expérimentale comme étant due à des effets de parois, alors que l'expérimentateur prétextera que le schéma chimique du modèle de son collègue est incomplet. Il est de plus, à mon avis, important que les travaux menés au laboratoire, qu'ils soient théoriques ou expérimentaux, puissent se rattacher à une donnée observationnelle. Par exemple, tous les travaux expérimentaux que j'ai entrepris autour de la dégradation thermique et photochimique de composés organiques complexes dans les atmosphères cométaires sont liés grâces aux modèles que nous avons développés aux observations de sources distribuées. La présence de POM, HMT, ou polymères de HCN sur lesquels j'ai travaillé pourra j'espère à terme être confirmée ou infirmée par des mesures in situ (par exemple grâce à l'instrument COSIMA dont je suis un CoI). La Figure 5 illustre mon implication autour des différents pôles de recherche que je viens de définir. On remarque que je n'ai pour l'instant pas directement abordé ma problématique au travers des simulations globales. Nous verrons par la suite, que dans le cadre du projet OREGOC, que je développe avec Nicolas Fray, nous réaliserons des simulations globales de la matière organique cométaires afin d'obtenir des analogues de matière organique réfractaire, susceptible d'être présente sur les grains qui seront analysés par l'instrument COSIMA. Ces expériences nous permettront de calibrer l'instrument et nous préparer à l'interprétation de spectres de masse complexes.

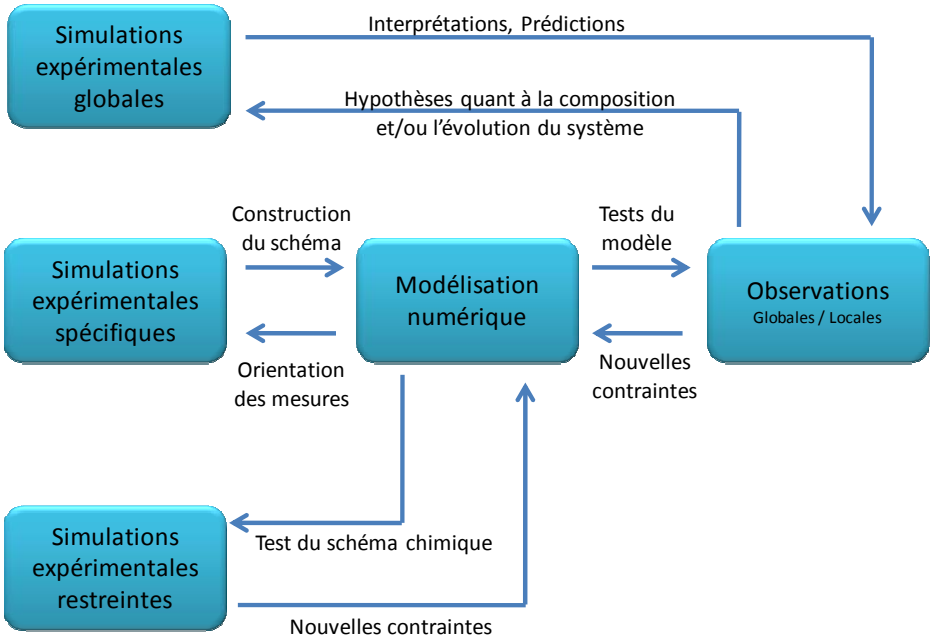

Figure 4. Couplage entre les simulations expérimentales, les modèles numériques et les observations. Deux types d'observations sont distinguées car certaines permettent de couvrir une vaste région ou la totalité de l'objet étudier (observations depuis le sol ou d'un orbiter), tandis que d'autres ne sondent qu'une région géographiquement très limitée (lander, rover).

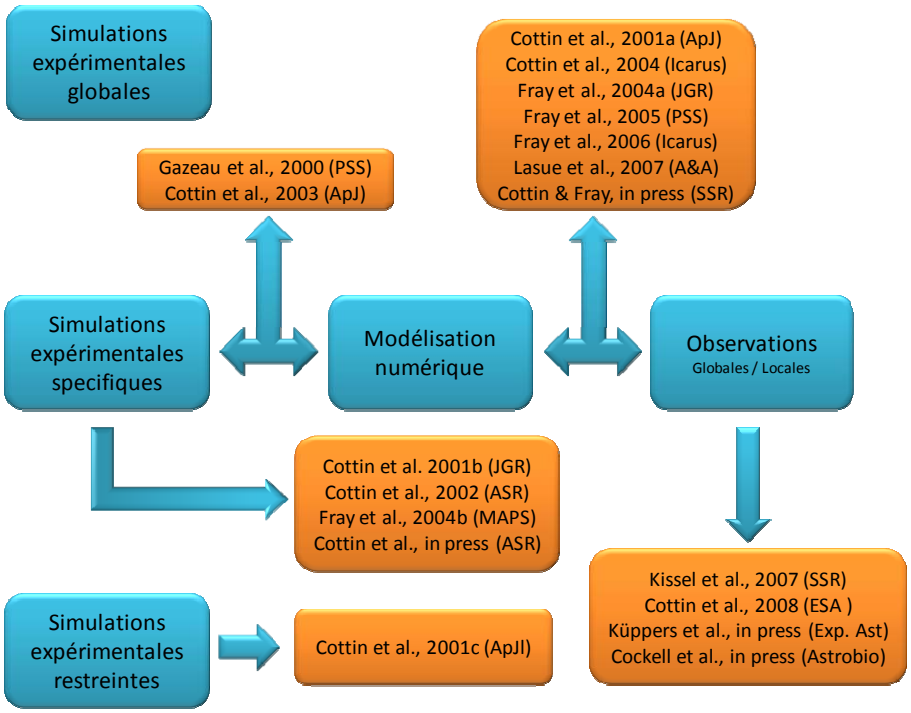

Figure 5. Insertion de mes activités de recherche autour des trois axes d'études que sont les simulations expérimentales, les modélisations numérique et les observations.

Dans la suite de ce document j'ai divisé l'exposition détaillée de mes activités de recherches en deux grandes parties :

1 L'étude de la matière organique cométaire (et par extension des petits corps du système solaire), principalement au travers de mon travail autour des sources distribuées.

2 L'étude de la formation et de l'évolution de la matière organique dans le système solaire, notamment au travers d'expériences de photochimie d'analogues de glaces cométaires et interstellaires, ou encore des expériences d'exposition de matière organique en orbite terrestre. Même si les comètes sont encore au cœur de cette partie, les expériences présentées dans cette seconde partie sont applicables de façon plus générale à d'autres objets du système solaire et au milieu interstellaire.

II. PROGRAMMES DE RECHERCHES ET PROJETS

II-1. LA CHIMIE ORGANIQUE DES COMETES ET L'ETUDE DES SOURCES DISTRIBUEES

Comme nous l'avons déjà vu, les comètes, tout comme les planètes, se sont formées à partir de la matière du nuage moléculaire qui s'est effondré pour donner naissance à notre Système Solaire. Stockés dans les régions les plus reculées et donc les plus froides du Système Solaire (ceinture de Kuiper et nuage d'Oort), ces planétésimaux glacés n'ont pas subi de processus de

différentiation du fait de leur petite taille. Ils devraient donc avoir gardé leur composition initiale, témoignant des conditions physico-chimiques qui régnaient là où ils se sont formés, voire même de la composition de notre nuage moléculaire natal. Les comètes sont donc considérées comme les archives les plus anciennes de notre Système Solaire. A ce jour, une vingtaine de molécules en phase gazeuse ont pu être détectées par télédétection depuis le sol (principalement H_2O, mais aussi CO, CO_2, CH_3OH, H_2CO, NH_3, HCN, CH_4, etc…). Des informations minéralogiques ont aussi été obtenues par les mêmes méthodes. Néanmoins, des analyses in-situ dans les atmosphères cométaires (missions spatiales Giotto, Véga et Stardust) sont requises afin de mettre en évidence la présence de composés organiques plus complexes dans les grains éjectés des noyaux. Cette détection a été confirmée grâce à l'analyse en laboratoire des grains cométaires collectés lors de la mission Stardust et qui ont été rapportés sur Terre très récemment. Cependant, la nature chimique de ces composés organiques complexes n'est connue que de manière très parcellaire et il n'existe à ce jour que très peu d'informations directes concernant la composition moléculaire du noyau des comètes. La diversité des molécules organiques détectées en phase gazeuse dans les comètes et le degré de complexité que la chimie semble y avoir atteint, font des comètes des objets d'intérêt pour l'exobiologie puisqu'elles ont potentiellement importé sur Terre des composés qui ont pu jouer un rôle clé dans les premières étapes de l'évolution chimique qui a conduit à l'apparition de la vie sur Terre.

Voir à ce sujet :

Article 3 – p.135

DESPOIS D. and ***COTTIN H.*** *(2005) Comets: potential sources of prebiotic molecules for the early Earth. In Lectures in Astrobiology, (eds. M.Gargaud, B.Barbier, H. Martin and J.Reisse), pp. 289-352. Springer Verlag.*

L'objectif du programme S.E.M.A.Ph.Or.E. Cométaire (Simulation Expérimentale et Modélisation Appliquée aux PHénomènes Organiques dans l'Environnement Cométaire), développé au LISA depuis le début de ma thèse en 1997 avec Marie-Claire Gazeau et François Raulin, est de mieux comprendre la chimie organique de l'environnement cométaire, et plus particulièrement la production d'espèces gazeuses par dégradation des molécules organiques solides présents dans les grains cométaires. Ces études nous permettent de préciser, de manière indirecte, la nature chimique de ces composés organiques réfractaires. La distribution spatiale dans la coma de certaines espèces gazeuses montre que celles-ci ne sont pas produites directement à partir du noyau ou par photolyse d'une espèce gazeuse connue. Ces espèces doivent être produites directement dans l'environnement cométaire. Ce phénomène est donc appelé 'source distribuée' et est observé principalement pour H_2CO, CO et CN. S'appuyant sur des expériences en laboratoire et la construction de modèles numériques, le programme S.E.M.A.Ph.Or.E. Cométaire cherche à expliquer l'origine de ces espèces gazeuses en prenant en compte la dégradation des molécules organiques solides. Ces recherches nous permettent de proposer des corrélations entre certaines espèces gazeuses observées dans l'atmosphère cométaire et la composition moléculaire des noyaux cométaires. Il s'agit par ailleurs de

préparer l'interprétation des données de la mission ROSETTA, entre ce qui sera mesuré sur le noyau par le lander, et en phase gazeuse par l'orbiteur. A partir de fin 1999, Yves Bénilan a travaillé avec nous pour le développement des aspects de modélisation. En 2001, Nicolas Fray à débuté une thèse dans la continuité du travail que j'avais commencé. Nous avons initié avec lui le travail sur l'origine de la source distribuée de CN et approfondi nos capacités de modélisation. Afin de préparer l'application de nos futurs résultats expérimentaux consacrés à l'étude de l'origine de la source distribuée du radical CN, nous avons compilé et calibré toutes les observations disponibles dans la littérature relatives à la distribution spatiale et au taux de production du radical CN dans de nombreuses comètes. Ce travail nous a permis de montrer que la dégradation thermique et/ou photochimique d'un composé solide ou la présence de C_2N_2 pouvaient être à l'origine de la source distribuée observée pour ce radical.

Depuis le recrutement de Nicolas Fray au LISA en tant que maître de conférences, lui et moi coordonnons les recherches sur les sources distribuées. Nous avons proposé en 2008 un cadrage de la définition de ce phénomène dans une revue exhaustive de la question. Nous somme aussi en train de développer la suite du programme S.E.M.A.Ph.Or.E. Cométaire : le projet OREGOC, qui sera présenté plus loin dans ce document.

Voir à ce sujet :

Article 4 – p.200

*FRAY N., BÉNILAN Y., **COTTIN H.**, GAZEAU M.-C. and CROVISIER J. (2005) The origin of the CN radical in comets : A review from observations and models. Planetary and Space Science 53(12), 1243-1262.*

Article 5 – p.221

***COTTIN H**. and FRAY N. (In Press) Distributed Sources in Comets. Space Science Reviews.*

A. ETUDES DES SOURCES DISTRIBUEES : SEMAPHORE COMETAIRE - EXPERIMENTATION

J'ai débuté mes études sur les sources distribuées au LISA à l'aide d'une enceinte expérimentale permettant l'étude de la photodégradation de composés organiques solides à trois longueurs d'onde dans l'UV lointain (122 nm, 147 nm ou 193 nm), ainsi que l'étude de la stabilité thermique de ces mêmes composés entre 250 et 340 K. Ce dispositif a nettement évolué, puisqu'une nouvelle enceinte réactionnelle a été construite pour étudier la dégradation thermique de matière organique réfractaire jusqu'à des températures pouvant atteindre 600 K (température que certains grains peuvent atteindre dans l'atmosphère des comètes à 1 UA) et permettre des analyses in-situ d'espèces radicalaires par couplage avec le dispositif SETUP.

Nos mesures se sont d'abord concentrées autour de la dégradation du polyoxyméthylène, avec extension de la plage de température d'étude par rapport à mon travail en thèse, et étude de la sensibilité de la vitesse de dégradation à la structure initiale du polymère.

Voir à ce sujet :

> ***Article 6 – p.241***
>
> ***COTTIN H.**, GAZEAU M. C., CHAQUIN P., BÉNILAN Y. and RAULIN F. (2001) Experimental and theoretical studies on the gas/solid/gas transformation cycle in extraterrestrial environments. Journal of Geophysical Research (Planets) 106(E12), 33,325-33,332.*

> ***Article 7 – p.250***
>
> *FRAY N., BÉNILAN Y., **COTTIN H.** and GAZEAU M.-C. (2004) New experimental results on the degradation of polyoxymethylene. Application to the origin of the formaldehyde extended source in comets. Journal of Geophysical Research (Planets) 109, E07S12.*

Nous avons aussi diversifié nos cibles expérimentales, et mené une étude de la photodégradation de l'héxaméthylènetétramine (HMT), et avons étudié les dégradations thermique et photolytique de polymères de HCN dans le cadre de l'étude des sources distribuées de CN. Nous avons montré que le HMT ne se dégrade pas sous l'effet de la chaleur, en effet ce composé se sublime lors d'une augmentation de température. D'autre part, nous avons montré que les polymères de HCN ne commencent à se dégrader thermiquement qu'à partir d'environ 450 K en produisant principalement NH_3 et HCN, et que les rendements quantiques de production d'espèces gazeuses (HCN, CH_4,..) lors de la photolyse de ces polymères sont extrêmement faibles. Un long travail de recherche a été effectué afin de tenter de mettre en évidence une production de radicaux CN lors de la dégradation thermique des polymères de HCN. Ces études ont été effectuées en couplant les dispositifs expérimentaux des programmes 'S.E.M.A.Ph.Or.E. Cométaire' et 'S.E.T.U.P.'. Néanmoins, nous ne sommes pas encore en mesure de conclure quant à la production directe de CN.

Nous avons été très limités dans nos études sur les polymères de HCN car nous ne disposions que d'une quantité assez faible d'échantillons fournis par Robert Minard (Pennstate University). Suite au stage de M2 de Léna Le Roy en 2008, nous avons mis au point au LISA un protocole pour synthétiser ces polymères et approfondir nos travaux.

Voir à ce sujet :

> ***Article 8 – p.258***
>
> ***COTTIN H.**, BACHIR S., RAULIN F. and GAZEAU M. C. (2002) Photodegradation of Hexamethylenetetramine by VUV and its relevance for CN and HCN extended sources in comets. Advances in Space Research 30(6), 1481-1488.*

> ***Article 9 – p.267***
>
> *FRAY N., BÉNILAN Y., **COTTIN H.**, GAZEAU M.-C., MINARD R. D. and RAULIN F. (2004) Experimental study of the degradation of polymers. Application to the origin of extended sources in cometary atmospheres. Meteoritics and planetary science 39(4).*

B. ETUDES DES SOURCES DISTRIBUEES : SEMAPHORE COMETAIRE – MODELISATION

Depuis les premières bases posées au cours de ma thèse, nous avons considérablement amélioré nos modèles numériques permettant de simuler la chimie hétérogène dans l'atmosphère cométaire. Partis d'un système très simple dans lequel nous simulions la dégradation de grains purs de POM, pour une taille, une vitesse et une température données, en fonction de la distance au noyau, nous sommes maintenant en mesure de modéliser le comportement d'une population de grains hétérogènes (mélange minéraux/organiques) avec pour chaque classe de taille de grains une vitesse et une température calculées à partir de paramètres physiques (dégazage du noyau, porosité des grains, etc…), non seulement en fonction de la distance au noyau, mais aussi de la distance de la comète au Soleil. Il nous a été possible de montrer que la présence de POM (quelques pourcents en masse) dans les grains cométaires permet d'expliquer la variation de la densité de formaldéhyde en fonction de la distance au noyau telle qu'elle a été mesurée par la sonde Giotto dans la comète Halley en 1986, et ceci pour différentes natures de POM. Nous avons aussi montré que la même abondance de POM, par dégradation thermique de ce composé dans la comète Hale-Bopp, permet d'expliquer l'évolution héliocentrique particulièrement rapide du taux de production de H_2CO mesuré dans cette comète entre 0.9 et 4 UA. Ce dernier travail a été mené en collaboration étroite avec les membres de l'équipe 'comète' du LESIA (observatoire de Meudon) qui avaient au préalable réalisé les mesures de taux de production dans la comète Hale-Bopp.

Voir à ce sujet :

Article 10 – p.275

***COTTIN H.**, GAZEAU M. C., BÉNILAN Y. and RAULIN F. (2001) Polyoxymethylene as parent molecule for the formaldehyde extended source in comet Halley. The Astrophysical Journal 556(1), 417-420.*

Article 11 – p.280

***COTTIN H.**, BÉNILAN Y., GAZEAU M.-C. and RAULIN F. (2004) Origin of cometary extended sources from degradation of refractory organics on grains: polyoxymethylene as formaldehyde parent molecule. Icarus 167, 397–416.*

Article 12 – p.301

*FRAY N., BÉNILAN Y., BIVER N., BOCKELÉE-MORVAN D., **COTTIN H.**, CROVISIER J. and GAZEAU M.-C. (2006) Heliocentric evolution of the degradation of polyoxylmethylene. Application to the origin of the formaldehyde (H2CO) extended source in comet C/1995 O1 (Hale-Bopp). Icarus 184(1), 239-254.*

Très récemment, avec Annie-Chantal Levasseur-Regourd et Jérémie Lasue du Service d'Aéronomie, nous avons commencé à réfléchir aux implications de nos travaux sur l'étude de la dégradation de la matière organique non plus dans les comètes, mais dans les grains interplanétaires dont les observations de polarisation montrent qu'ils contiennent probablement de la matière organique qui évolue lorsqu'ils s'approchent du Soleil.

Voir à ce sujet :

Article 13 – p.318

*LASUE J., LEVASSEUR-REGOURD A. C., FRAY N. and **COTTIN H.** (2007) Inferring the interplanetary dust properties from remote observations and simulations. Astronomy & Astrophysics 473, 641–649.*

C. MISSIONS SPATIALES – MESURES IN-SITU PAR SPECTROMETRIE DE MASSE

La mission ROSETTA a été lancée avec succès le 26 février 2004 à destination de la comète 67P/Churyumov-Gerasimenko. Il comporte un vaisseau qui suivra pendant plusieurs mois la comète, en effectuant des mesures physiques et chimiques de son environnement et un module de surface (Philae) qui se posera à la surface du noyau cométaire, en 2014. Le LISA est impliqué, en tant que Co-Investigateur dans les instruments COSAC et COSIMA de cette mission. Je suis personnellement investi dans cette dernière expérience dont je suis l'un des CoI depuis Janvier 2005.

COSIMA (COmetary Secondary Ion MAss spectrometer) est un spectromètre de masse à temps de vol dont l'objectif est l'analyse de la composition chimique (élémentaire, moléculaire et isotopique) de grains qui seront capturés dans l'atmosphère de la comète Churyumov-Gerasimenko. Après nous êtres cantonnés pendant plusieurs années à un rôle consultatif concernant les apports de l'instrument à l'étude des aspects exobiologiques des comètes, j'ai commencé à partir de 2006 à collaborer de façon étroite avec le LPCE d'Orléans (qui dispose d'un spectromètre de masse dont les caractéristiques sont voisines de celles de l'instrument de vol), et le MPI Lindau (laboratoire du PI de COSIMA où se trouve un modèle sol de l'instrument identique à celui embarqué sur ROSETTA). Le travail a pour l'instant consisté à élaborer et optimiser des protocoles de dépôts de molécules organiques en vue d'analyse par les instruments sol, et étudier l'influence du mode de préparation de l'échantillon sur le spectre obtenu. L'objectif est de constituer à terme une bibliothèque de spectres étalons utiles à l'interprétation des résultats qui seront collectés à partir de 2014 dans l'environnement cométaire. Je co-encadre d'ailleurs sur cette thématique la thèse de Léna Le Roy en partenariat entre le LPCE d'Orléans et le LISA depuis septembre 2008. Ce travail sera développé en parallèle avec le projet OREGOC dont l'un des objectifs est de produire des analogues de matière organique cométaire qui serviront à préparer l'interprétation des spectres de masses de grains cométaires qui seront mesurés par COSIMA en 2014.

Voir à ce sujet :

Article 14 – p.328

*KISSEL J., ALTWEGG K., CLARK B. C., COLANGELI L., **COTTIN H.**, CZEMPIEL S., EIBEL J., ENGRAND C., FEHRINGER H. M., FEUERBACHER B., FOMENKOVA M., GLASMACHERS A., GREENBERG J. M., GRÜN E., HAERENDEL G., HENKEL H., HILCHENBACH M., HOERNER H. V., HÖFNER H., HORNUNG K., JESSBERGER E. K., KOCH A., KRÜGER H., LANGEVIN Y., PARIGGER P., RAULIN F., RÜDENAUER F., RYNÖ J., SCHMID E. R., SCHULZ R., SILEN J., STEIGER W., STEPHAN T., THIRKELL L., THOMAS R., TORKAR K., UTTERBACK N. G., VARMUZA K., WANCZEK K. P., WERTHER W. and ZSCHEEG H. (2007) COSIMA, a High Resolution Time of Flight Spectrometer for Secondary Ion Mass Spectroscopy of Cometary Dust Particles. Space Science Reviews Volume 128(1-4), 823-867.*

Après ROSETTA, l'avenir de l'exploration cométaire résidera dans un retour d'échantillon du noyau. C'était l'objet de la proposition TRIPLE F coordonnée par M. Küppers en réponse à l'appel COSMIC VISION auquel j'ai participé. Ce projet n'a malheureusement pas été retenu.

Voir à ce sujet :

Article 15 – p.352

KÜPPERS M., KELLER H. U., KÜHRT E., A'HEARN M. F., ALTWEGG K., BERTRAND R., BUSEMANN H., CAPRIA M. T., COLANGELI L., DAVIDSSON B., EHRENFREUND P., KNOLLENBERG J., MOTTOLA S., RATHKE A., WEISS P., ZOLENSKY M., AKIM E., BASILEVSKIJ A., GALIMOV E., GERASIMOV M., KORABLEV O., LOMAKIN I., MAROV M., MARTYNOV M., NAZAROV M., ZAKHAROV A., ZELENYI L., ARONICA A., BALL A. J., BARBIERI C., BAR-NUN A., BENKHOFF J., BIELE J., BIVER N., BLUM J., BOCKELÉE-MORVAN D., BOTTA O., BREDEHÖFT J.-H., CAPACCIONI F., CHARNLEY S., CLOUTIS E., ***COTTIN H.****, CREMONESE G., CROVISIER J., CROWTHER S., EPIFANI E. M., ESPOSITO F., FERRARI A. C., FERRI F., FULLE M., GILMOUR J., GOESMANN F., GORTSAS N., GRADY M., GREEN S. F., GROUSSIN O., GRÜN E., GUTIÉRREZ P. J., HARTOGH P., HENKEL T., HILCHENBACH M., HO T.-M., HORNECK G., HVIID S. F., IP W.-H., JÄCKEL A., JESSBERGER E., KALLENBACH R., KARGL G., KÖMLE N. I., KORTH A., KOSSACKI K., KRAUSE C., KRÜGER H., LI Z.-Y., LICANDRO J., LOPEZ-MORENO J. J., LOWRY S. C., LYON I., MAGNI G., MALL U., MANN I., MARKIEWICZ W., MARTINS Z., MAURETTE M., MEIERHENRICH U., MENNELLA V., NG T. C., NITTLER L., PALUMBO P., PÄTZOLD M., PRIALNIK D., RENGEL M., RICKMAN H., RODRIGUEZ J., ROLL R., ROST D., ROTUNDI A., SANDFORD S., SCHOENBAECHLER M., et al. (In press) Triple F - A Comet Nucleus Sample Return Mission. Experimental Astronomy.*

Dans le prolongement du travail en cours sur COSIMA, je coordonne en tant que Principal Investigator un instrument proposé pour être intégré à la charge utile de MARCO POLO, mission d'exploration avec retour d'échantillon d'un astéroïde carboné géocroiseur. ILMA (Ion Laser Mass Analyzer) est un spectromètre de masse haute résolution de nouvelle génération, construit autour d'une trappe ionique. Son objectif est de caractériser la composition chimique élémentaire, moléculaire et isotopique de la surface de l'objet géocroiseur qui sera sélectionné comme cible de la mission. ILMA sera un instrument clé pour contribuer aux principaux objectifs de MARCO POLO : mieux comprendre les origines et l'évolution du système solaire, de la Terre et de la vie. Une équipe internationale de 23 scientifiques, appartenant à 16 institutions des 5 pays européens est réunie autour de ce projet d'exploration in-situ.

Voir à ce sujet :

> ***Article 16[7] - p.373***
>
> ***COTTIN H.****, BRIOIS C., ENGRAND C., THIRKELL L., GRAND N., TAJMAR M., GLASMACHERS A., ALIMAN M. and ILMA-TEAM (2008) ILMA (Ion Laser Mass Analyser). In Declaration of interest in science instrumentation for the MARCO POLO Cosmic Vision mission candidate.*

II.2- FORMATION ET EVOLUTION DE LA MATIERE ORGANIQUE DANS LE SYSTEME SOLAIRE

A. GLACES INTERSTELLAIRES ET COMETAIRES : LE PROJET OREGOC

Comme nous l'avons déjà vu, on suppose que les comètes n'ont quasiment pas évolué depuis leur formation. Celles qui se sont formées dans les régions les plus reculées du système solaire pourraient même avoir pu conserver la composition des grains interstellaires du nuage moléculaire qui s'est effondré pour donner naissance à notre Système Solaire.

Le polyoxymethylène est le produit majoritaire qui se forme lors du réchauffement d'un mélange de H_2O, CO, NH_3, CH_3OH, entre 10 et 300 K (Schutte et al. 1993). Par contre, ce même type de glace, lorsqu'il est photolysé à 10 K, conduit à la formation majoritaire de l'Hexaméthylènetétramine (Bernstein et al. 1995). Ainsi, ce composé était considéré comme une signature potentielle de processus photochimiques s'il venait à être détecté dans les glaces interstellaires ou les comètes. Au cours de ma période passée au GSFC, j'ai pu confirmer que l'Hexaméthylènetétramine est bien synthétisé par photolyse, mais j'ai aussi montré qu'il était aussi majoritairement produit dans le même type de glaces irradiées par des protons. Le HMT doit donc maintenant être plus généralement considéré comme la signature d'une glace dont l'histoire à été dominée par des irradiations UV et protons. Ces récents travaux augmentent nettement la probabilité de présence de cette molécule dans les glaces interstellaires et les comètes, et insistent sur la nécessité de calibrer les instruments de la mission Rosetta en vue de sa détection. En effet, si les photons sont absorbés en quelques dizaines de microns, des particules énergétiques comme les protons du vent solaire ou des rayons cosmiques peuvent pénétrer les glaces sur plusieurs mètres de profondeur. Ils sont donc beaucoup plus efficaces que les photons.

Voir à ce sujet :

[7] Aucun article n'étant encore soumis sur ce sujet, la réponse à l'appel à déclaration d'intérêt en instrumentation de l'ESA pour MARCO POLO est proposée pour illustrer ce volet de mes activités de recherche.

Article 17 – p.399

***COTTIN H.**, SZOPA C. and MOORE M. H. (2001) Production of hexamethylenetetramine in photolyzed and irradiated interstellar cometary ice analogs. The Astrophysical Journal Letters 561(1), L139-L142.*

Ces études de traçabilité de l'histoire des glaces interstellaires et cométaires en fonction de leur composition initiale et des processus d'apport d'énergie qui ont dominé leur histoire pourront être poursuivies dans le cadre du projet OREGOC (Origine et Evolution des Glaces et des composés Organiques Cométaires) (Figure 6). En effet, ce projet qui s'inscrit naturellement dans le prolongement du programme SEMAPHORE Cométaire, nous permettra aussi de synthétiser des molécules organiques complexes par photolyse UV ou processus thermiques appliqués à des mélanges de glaces simples dans le cadre d'expériences de simulations restreintes ou globales. Dans le cas des simulations restreintes, nous pourrons déterminer s'il existe des molécules organiques formées dans ces glaces qui seraient des signatures de processus thermiques ou photochimiques, ou de telle ou telle composition initiale du mélange. Dans le cas des simulations globales, nous aurons accès à des échantillons représentatifs de la matière organique contenue dans les noyaux cométaires. Ces échantillons pourront être utilisés pour des tests et la calibration d'un instrument comme COSIMA.

L'objectif principal d'OREGOC est d'étudier l'ensemble des processus hétérogènes (solide → gaz) de production des espèces gazeuses observées dans les noyaux et l'environnement cométaires (Figure 7). L'originalité de ce dispositif est de pouvoir étudier au sein d'un même système la continuité des processus physico-chimiques cométaires aussi bien à basse température (~10 K – glaces du noyau) qu'à haute température (~600 K – température des grains éjectés dans l'atmosphère cométaire). Le dispositif expérimental que nous sommes en train de mettre en place à l'aide de financements du PID OPV et du GDR exobiologie nous permettra d'étudier la production d'espèces gazeuses non seulement lors de la dégradation de composés organiques solides présents dans les grains cométaires mais aussi lors de la sublimation des glaces contenues dans les noyaux. Comme dans le cadre du programme SEMAPHORE Cométaire les résultats expérimentaux seront inclus dans des modèles théoriques permettant d'interpréter les observations astronomiques. L'ensemble de ces travaux nous permettra de contraindre la nature physico-chimique des glaces et des composés organiques contenus dans les noyaux cométaires.

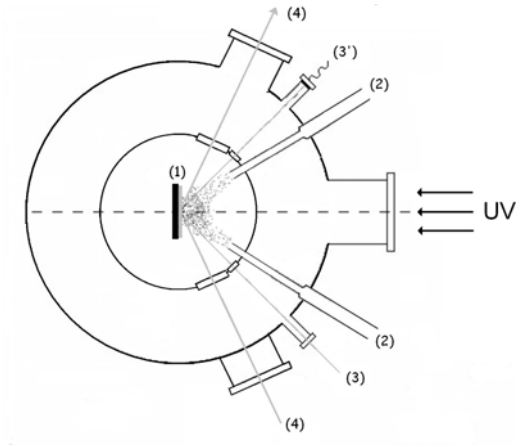

Figure 6. Schéma de principe du dispositif expérimental. L'échantillon solide (1) est situé au centre de ce dispositif. La présence d'une double paroi permettra l'étude de l'ensemble des mécanismes hétérogènes solides – gaz. L'échantillon de glace (1) est déposé par injection de gaz (2) sur un substrat connecté au doigt froid du cryothermostat. En termes d'apport d'énergie, cet échantillon pourra être irradié par un rayonnement UV ou soumis à un simple réchauffement. Son épaisseur sera contrôlée par un dispositif interférentiel (3 – Laser He-Ne et 3' – Photodiode). La nature de l'échantillon solide sera analysée par spectroscopie infrarouge (4) alors que celle des gaz le sera par spectrométrie de masse (non représentée sur ce schéma de principe).

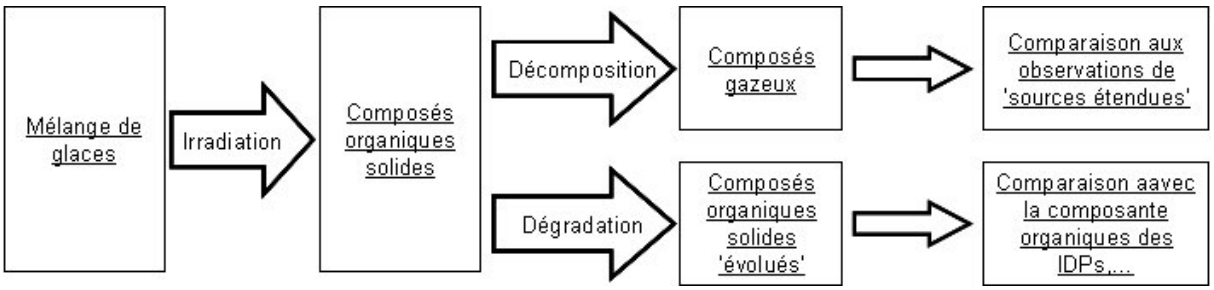

Figure 7. Processus physico-chimiques qui seront étudiés dans le cadre d'OREGOC et 'observations' auxquelles seront comparés les résultats expérimentaux.

B. PHOTOLYSE DANS LE SYSTEME SOLAIRE : UV-OLUTION, PROCESS, AMINO

Au cours de mon année passée au GSFC, j'ai aussi mesuré les sections efficaces de photodestruction des principales molécules détectées dans le milieu interstellaire. Ces données quantitatives sont indispensables à la construction de modèles photochimiques des glaces interstellaires et cométaires. J'ai étudié l'influence de la composition de mélanges binaires sur ces vitesses de photolyse. Ces mesures permettent d'estimer les temps de demi-vie de ces molécules dans le milieu interstellaire diffus et les nuages moléculaires. Ce travail entrait dans le cadre du projet SARA (Space Astrophysics Research and Analysis) de la NASA, dont le but est de constituer une base de données quantitatives concernant la chimie des glaces interstellaires en préparation des missions SPITZER et SOFIA (Stratospheric Observatory For Infrared Astronomy – observations depuis un avion stratosphérique à partir de 2011). J'ai aussi au cours de cette période proposé une méthode de mesure de constantes de photolyses dans des glaces optiquement épaisses dans le domaine de longueur d'onde qui les irradie.

Voir à ce sujet :

Article 18 – p.404

***COTTIN H.**, MOORE M. H. and BÉNILAN Y. (2003) Photodestruction of relevant interstellar molecules in ice mixtures. The Astrophysical Journal 590, 874-881.*

Ce travail a en quelques sorte été préliminaire aux expériences en orbite terrestre dont j'ai la responsabilité au LISA depuis 2005. En effet, à l'heure actuelle, le LISA coordonne la préparation de trois expériences spatialisées de photochimie de molécules d'intérêt exobiologique et planétologique. Ces expériences se sont déroulées ou se déroulent soit dans le module BIOPAN de la capsule automatique russe FOTON (expérience UVolution – septembre 2007), soit dans les deux instruments EXPOSE (E et R) qui ont été ou seront prochainement implantés sur la Station Spatiale Internationale (expériences PROCESS et AMINO). Je suis le PI de ces trois expériences (André BRACK, PI historique de l'expérience AMINO, m'a confié la responsabilité de son expérience début 2007).

UVolution, PROCESS et AMINO consistent à exposer aux rayonnements ultraviolets solaires des molécules solides ou des mélanges gazeux d'intérêt : (1) cométaire dans le cadre de nos études sur l'origine des sources distribuées (POM, HMT, polymères de HCN, de C_3O_2,), (2) météoritique (acides aminés, bases azotées), (3) concernant la chimie organique de l'atmosphère de Titan (tholins, mélanges gazeux représentatifs de l'atmosphère), (4) la stabilité photochimique de molécules organiques dans l'environnement Martien (glycine, hopanes, lipides, kérogènes…). Le calendrier de ces expériences est présenté dans la Table 1. L'analyse des résultats de ces expériences, à leur retour sur Terre, est effectuée principalement par spectroscopie infrarouge et chromatographie en phase gazeuse. Les résultats sont comparés à des mesures de photolyse réalisées avec les moyens « classiques » dont nous disposons au laboratoire.

Voir à ce sujet :

Article 19 – p.413

***COTTIN H.**, COLL P., COSCIA D., FRAY N., GUAN Y. Y., MACARI F., RAULIN F., RIVRON C., STALPORT F., SZOPA C., CHAPUT D., VISO M., BERTRAND M., CHABIN A., THIRKELL L., WESTALL F. and BRACK A. (In Press) Heterogeneous solid/gas chemistry of organic compounds related to comets, meteorites, Titan and Mars: in laboratory and in lower Earth orbit experiments. Advances in Space Research.*

Table 1. Calendrier des expériences en orbite terrestre du LISA

Expérience	Support	Lancement	Durée d'exposition
UV-olution	BIOPAN (capsule FOTON) EXPOSE-Eutef	Septembre 2007	12 jours
PROCESS	Station Spatiale Internationale Module Européen EXPOSE-R	Février 2008	15 mois
AMINO	Station Spatiale Internationale Module Russe	Novembre 2008	15 +/- 3 mois

Les résultats de l'expérience UVolution, de retour au LISA depuis Octobre 2007, sont encore en cours d'exploitation. Au moment de la rédaction de ce document, ils ne sont pas encore publiés sous forme d'article et sont donc présentés partiellement sous forme résumée ci-dessous.

L'expérience UVolution, comportait 60 échantillons de matière organique. Elle a été placée en orbite terrestre (à environ 300 km d'altitude) dans le module BIOPAN en septembre 2007 pendant 12 jours. Au cours de cette période, la durée effective d'exposition au rayonnement UV solaire a été d'environ 24 heures. Au retour des échantillons au LISA, toutes les cellules étaient intactes, et les cellules fermées étaient encore remplies de gaz (temps d'exposition suffisamment court pour que les fuites soient négligeables).

La durée d'exposition n'a pas été suffisante pour mettre en évidence une photolyse dans les mélanges gazeux et pour certaines des molécules déposées sous forme de films solides. Les résultats ont par contre été concluants pour plusieurs molécules comme la glycine (Figure 8).

Certains des résultats préliminaires (qui sont toujours en cours de traitement) sont présentés dans la Table 2. Le résultat le plus étonnant (encore très préliminaire) est la différence entre les mesures effectuées en orbites, et celles que nous effectuons à l'aide de notre système de photolyse (lampe à hydrogène utilisée dans de nombreux laboratoires pour simuler le rayonnement UV solaire <200 nm) (Table 3). Il est encore trop tôt pour que nous ayons pu interpréter de telles différences. Il est possible que le flux des lampes lors des expériences en laboratoire soit très mal estimé (mais il s'agirait dans ce cas d'une erreur systématique avec un rapport constant entre les différentes molécules), que les films déposés soient trop épais pour qu'ils soient irradiés de façon homogène (mais dans ce cas nous obtiendrions un résultat faux, mais identique dans le cas des expériences spatiales ou de laboratoire), ou plus probablement que les lampes UV de laboratoire sont de très mauvais simulateurs solaires.

Table 2. Vitesse de photolyse et temps de vie mesurés au cours de l'expérience UVolution pour quelques molécules. Les valeurs sont les moyennes entre les deux échantillons exposés. J est la constante de photolyse. Le temps de vie à 1 UA est donné, ainsi qu'une extrapolation pour le milieu interstellaire et les nuages moléculaires.

Molecule	Method	J(s-1)	Half Life at 1 AU (d)	Half Life in ISM* (yr)	Half Life in DC* (yr)
Glycine	1	1,9E-06	4,3	1803	1,8E+08
Xanthine	1	9,6E-07	8,3	3499	3,5E+08
Urea	1	3,0E-07	27,1	11342	1,1E+09
HCN polymer	1	4,0E-06	2,0	847	8,5E+07
Adenine	2	9,4E-07	8,6	3597	3,6E+08
Guanine	2	2,7E-06	3,0	1260	1,3E+08
				*Interstellar Medium	*Dark Clouds

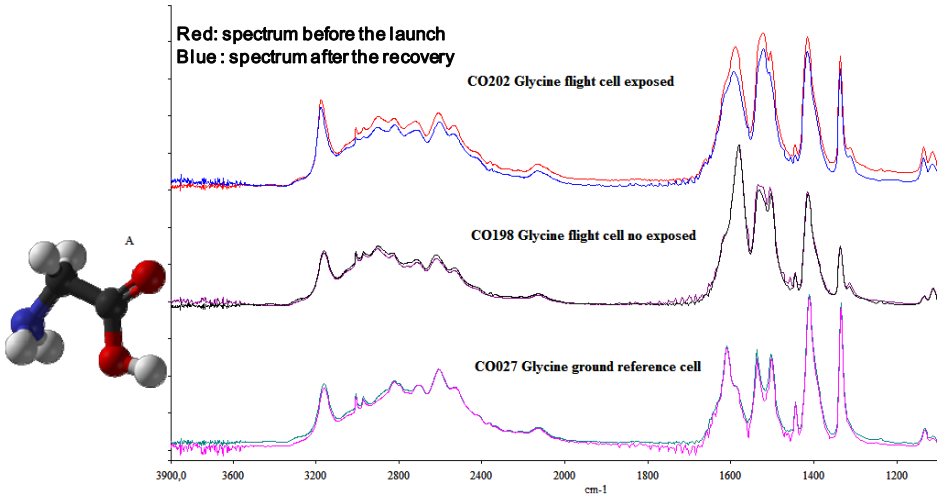

GLYCINE CELL N°	expo,/non expos,	Area before flight	Area after flight	Variation (%)
CO202	EXPOSED	32,25	28,74	-11%
CO208	EXPOSED	25,45	22,72	-11%
CO198	NOT EXPOSED	46,07	47,20	0%
CO199	NOT EXPOSED	25,08	28,18	0%
CO027	Laboratory Ref.	28,22	28,32	0%
CO026	Laboratory Ref.	31,40	30,78	-2%

Figure 8. Spectres infrarouges de films de glycine. Haut : cellule ouverte exposée avant et après le vol. Milieu : Cellule de contrôle en vol (non exposée) avant et après le vol. Bas : Cellule de contrôle conservée au sol. Chaque expérience étant doublée, le tableau indique les résultats pour l'ensemble des cellules contenant de la glycine.

Table 3. Comparaison des sections efficaces de destruction (σ en cm²) intégrées sur tout rayonnement solaire (= J/flux UV solaire au cours de l'expérience) mesurées en orbite avec des mesures similaires obtenues en laboratoire.

MOLECULE	σ (orbit)	σ (lab's simulation)	Ratio ($\sigma_{orbit}/\sigma_{lab}$)
XANTHINE	6,3E-20	1,08+/-1,40(E-22)	580
GUANINE	1,7E-19	<7,55E-23	>2300
ADENINE	6,1E-20	7,55+/-9,45(E-23)	810
GLYCINE	1,2E-19	5,26+/-2,93(E-21)	23

C. LE PROJET VITRINE

Les outils présentés ci-dessus présentent toutefois des limitations qui restreignent significativement leur champ d'application :

1) il s'agit de modules placés passivement à l'extérieur de modules spatiaux en orbite, et la durée intégrée d'exposition au rayonnement solaire est relativement faible par rapport au temps effectif passé en orbite (Biopan : ~ 24 heures pour 12 jours en orbite, EXPOSE : 10 jours prévus pour une année en orbite),

2) il n'est pas possible d'avoir un suivi cinétique de l'évolution de l'échantillon au cours de l'exposition, seuls deux points de données sont disponibles : la composition de l'échantillon avant le lancement, et la composition après le retour,

3) la température des échantillons n'est pas contrôlée, ce qui limite le choix des molécules étudiées (si certaines molécules ne sont pas suffisamment réfractaires, elles se sublimeront si les échantillons sont portés à trop haute température). D'autre part, il est à l'heure actuelle impossible d'effectuer des expériences d'exposition sur des échantillons maintenus à basse température (glaces simples ou mélanges à 10 ou 77 K). Ce type d'expériences est pourtant très répandu en laboratoire pour mieux comprendre la chimie des glaces interstellaires et cométaires, et celle des surfaces des satellites glacés des planètes géantes.

En conséquence, j'ai coordonné en 2008 en réponse à l'appel à idées du CNES, le développement d'un instrument spatial qui permettrait de réaliser des expériences de photochimie de molécules organiques en phase solide (molécules réfractaires ou glaces) ou en phase gazeuse, pendant de longues périodes (plusieurs années). Il s'agit du projet VITRINE ((ValidIty Test for Remotely controlled INstrument for Exobiology). Cet instrument pourrait être placé sur un satellite automatique en orbite basse, sur la Station Spatiale Internationale, à la surface de la Lune, ou à l'extérieur de sondes spatiales d'exploration du Système Solaire pour être utilisé durant la phase de croisière, en général peu productive scientifiquement. Ce projet est proposé conjointement par le LISA, le CBM (Orléans), l'IAS (Orsay), le SA (Paris 6), et le PIIM (Marseille).

Puisqu'il n'existe pour l'instant aucune publication à ce sujet, le projet est rapidement décrit ci-dessous.

Avantages d'un tel instrument sur les expériences en laboratoires :

Le flux d'une lampe UV classique de laboratoire est de l'ordre de 10^{15} photon.cm^{-2}.s^{-1} pour λ<200 nm. Dans la même gamme de longueur d'onde, le flux solaire est de l'ordre de 2.10^{13} photon.cm^{-2}.s^{-1}. Ainsi, à priori il pourrait sembler que les expériences en laboratoire sont bien plus efficaces car elles sont 50 fois plus rapides qu'en orbite. Cependant, pour des raisons pratiques, il est difficile de photolyser un même échantillon plus de 24 h dans le cas d'échantillons condensés à basse température (pollution des glaces par les contaminations résiduelles du dispositif expérimental à ~10^{-8} mb). Ce paramètre est moins gênant dans le cas de mélanges de gaz ou de composés réfractaires, mais la stabilité de la lampe est un facteur limitant les expériences trop longues. Ce facteur peut par contre être largement compensé par la possibilité de réaliser de multiples expériences simultanées. Plusieurs centaines d'échantillons peuvent êtres exposés en orbite en même temps, dans les mêmes conditions, alors que du fait de la géométrie des lampes, les dispositifs de laboratoire ne permettent l'exposition simultanée que d'un nombre limité d'échantillons.

L'intérêt majeur du dispositif proposé est toutefois de réaliser les expériences avec le spectre solaire tel qu'il est réellement, et non plus avec des simulateurs approximatifs du rayonnement solaire. Les récents résultats de l'expérience UVolution à bord du module BIOPAN en 2007 ont montré qu'il existe des différences significatives entre les temps de vie

photochimiques de composés organiques quand ils sont mesurés en orbite, et ceux mesurés en laboratoire (facteur 20 à 500 selon la molécule étudiée). Les lampes à hydrogène utilisées classiquement en laboratoire semblent donc être pour l'instant de mauvais simulateurs solaires. Les expériences en orbite permettent de plus une exposition simultanée à l'ensemble des conditions spatiales : rayonnement UV et rayonnement cosmique. Ce dernier est très peu pris en considération dans les expériences en laboratoire : difficile à simuler, et d'autre part difficile à coupler à un dispositif UV.

Ainsi, sans minimiser l'importance du travail mené en laboratoire qui doit continuer, une approche complémentaire réalisée dans l'espace semble nécessaire.

Avantages d'un tel instrument sur les expériences en orbite précédentes :

Il devra être équipé d'un dispositif dynamique de pointage des échantillons vers le Soleil (ou un équivalent type héliostat) afin d'optimiser le temps d'exposition des échantillons quelque soit la position de l'instrument sur son porteur. L'absence d'un tel dispositif pour les instruments EXPOSE sur la Station Spatiale Internationale (alors qu'il était prévu lors de sa conception puis éliminé pour des raisons de budget) conduit au fait qu'il est prévu qu'une année passée sur l'ISS ne corresponde qu'à 10 jours d'exposition au rayonnement solaire.

Il sera équipé de dispositifs de suivi de l'évolution des échantillons : spectroscopie infrarouge et UV, éventuellement chromatographie en phase gazeuse et spectrométrie de masse. Les expériences menées en son sein ne nécessiteront plus un retour des échantillons sur Terre pour analyse : étape coûteuse et risquée. Les analyses non destructives par spectroscopie IR et UV permettront un suivi cinétique de l'évolution des échantillons. A l'heure actuelle, les résultats sont extrapolés à partir de deux points de mesure : la composition avant le lancement et celle au retour. Les analyses par chromatographie et/ou spectrométrie de masse sont des analyses destructives, mais sont plus sensibles. Certains échantillons pourraient être remplacés après analyse pour répéter l'expérience (mélanges des gaz stockés dans des réservoirs, puis condensés sur un point froid avant exposition sous forme de glace, ou injectés dans une cellule d'exposition pour gaz).

L'exposition d'échantillons directement au rayonnement solaire, c'est-à-dire sans passer par le filtre d'une fenêtre (type MgF_2), doit être considérée. A l'heure actuelle, tout photon <120 nm est filtré.

L'instrument sera aussi équipé de capteurs permettant la mesure du flux solaire jusque dans l'UV lointain, ainsi que d'un dispositif de mesure du rayonnement cosmique.

Exemples d'applications scientifiques :

Production et évolution de la matière organique à basse température dans les comètes, à la surface des satellites glacés des planètes géantes et des objets

transneptuniens, dans les nuages moléculaires, et dans le milieu interstellaire diffus : irradiations de mélanges de glaces composées de H_2O, CO, CH_3OH, NH_3, H_2CO…

Origine des sources distribuées dans les comètes : exposition à 300 K de molécules solides telles que le polyoxyméthylène, les polymères de HCN ou de C_3O_2 et analyse des gaz produits par photodégradation de ces composés pour étudier l'origine des sources distribuées de H_2CO, CN, CO dans les atmosphères cométaires.

Etude de la stabilité photochimique de molécules organiques réfractaires dans un contexte météoritique et/ou cométaire : composés aromatiques polycycliques, acides aminés, bases azotées, et autres composés prébiotiques exposés pur, ou mélangés à des phases minérales.

Formation des aérosols de Titan à partir de mélanges représentatifs de l'atmosphère du satellite de Saturne.

Evolution des aérosols de Titan par exposition d'analogues synthétisés en laboratoire, ou synthétisés préalablement en orbite à partir de mélanges gazeux.

Etude de l'évolution de la matière carbonée à la surface d'astéroïdes (qui ne nécessitent pas de températures très basses). Ces objets commencent à être accessibles à la spectroscopie de réflexion en IR depuis le sol, au moyen de grands télescopes (VLT) et des comparaisons spectrales directes sont envisageables, en particulier pour comprendre certains aspects (couleur rouge) observés dans la réflectance des surfaces

Etude de la stabilité photochimique de la matière organique à la surface de Mars et de Phobos, cas d'autant plus intéressant que des échantillons de Phobos sont susceptibles de devenir disponibles dans un délai assez bref de quelques années : acides aminés, composés aromatiques polycycliques, acide mellitique (apports exogènes via comètes et météorites ou bio-indices). Dans le cas des échantillons analysés dans un contexte martien, le rayonnement solaire dont λ est inférieur à 200 nm est filtré.

Des études d'évolution de minéraux (carbonates, argiles, etc.) peuvent aussi être envisagées dans un contexte d'étude des petits corps ou de la surface martienne. Des expériences d'évolution de silicates par exemple, en laboratoire, donnent des résultats potentiellement importants pour les surfaces lunaires et astéroïdales, résultats jusqu'ici appliqués uniquement au milieu interstellaire et protoplanétaire.

CONCLUSION

L'exobiologie, et l'astrochimie de façon plus générale, sont des sciences encore en plein essor, et la communauté française dans ces domaines suit cette tendance. Le CNES a joué un rôle particulièrement moteur dans ce développement en soutenant non seulement les projets spatiaux, mais aussi les recherches plus fondamentales au sol. Ces approches sont intimement liées. Les projets auxquels je propose de participer au cours des prochaines années (à différents niveaux d'implication) s'inscrivent dans cette démarche : OREGOC pourra en effet servir d'accompagnement sol VITRINE, et d'outil de calibration pour COSIMA et ILMA.

Rien à ce jour ne nous permet d'imaginer quand nous aurons enfin une réponse à la question de savoir si la Terre est la seule planète à abriter la vie dans l'univers (si tant est que nous puissions un jour obtenir une réponse à cette question). Pourtant l'exobiologie a parcouru un long chemin depuis les toutes premières expériences de Miller en 1950, et son questionnement croisé à celui de l'astrochimie nourrit depuis l'exploration de notre Système Solaire. La réponse est peut être déjà à notre portée, au détour d'une roche qui sera analysée par un rover martien, ou plus lointaine sous quelques kilomètres de banquise dans la banlieue de Jupiter… Peut être est-elle même au-delà avec les ambitieux projets d'observations des planètes extrasolaires (TPF, Darwin). C'est dans ce dernier cadre, à un niveau presque anecdotique comparé au reste de mes travaux, que je participe à un groupe de travail animé par Alain Léger autour de biosignatures et biosignatures-technologiques dans les atmosphères d'exoplanètes. C'est à ce titre que j'ai rejoint l'équipe proposante de DARWIN dans le cadre l'appel COSMIC VISION de l'ESA.

Voir à ce sujet :

Article 20 – p.431

COCKELL C. S., LEGER A., FRIDLUND M., HERBST T., KALTENEGGER L., ABSIL O., BEICHMAN C., BENZ W., BLANC M., BRACK A., CHELLI A., COLANGELI L., ***COTTIN H.****, COUDE DU FORESTO V., DANCHI W., DEFRERE D., DEN HERDER J.-W., EIROA C., GREAVES J., HENNING T., JOHNSTON K., JONES H., LABADIE L., LAMMER H., LAUNHARDT R., LAWSON P., LAY O. P., LEDUIGOU J.-M., LISEAU R., MALBET F., MARTIN S. R., MAWET D., MOURARD D., MOUTOU C., MUGNIER L., PARESCE F., QUIRRENBACH A., RABBIA Y., RAVEN J. A., ROTTGERING H. J. A., ROUAN D., SANTOS N., SELSIS F., SERABYN E., SHIBAI H., TAMURA M., THIEBAUT E., WESTALL F., WHITE and GLENN J. (In Press) DARWIN - A Mission to Detect, and Search for Life on, Extrasolar Planets. Astrobiology.*

BIBLIOGRAPHIE

Barbier, B., Chabin, A., Chaput, D., & Brack, A. 1998, Planetary and Space Science, 46, 391-398

Barbier, B., Henin, O., Boillot, F., Chabin, A., Chaput, D., & Brack, A. 2002, Planetary and Space Science, 50, 353-359

Bernstein, M. P., Sandford, S. A., Allamandola, L. J., Chang, S., & Scharberg, M. A. 1995, The Astrophysical Journal, 454, 327-344

Blank, J. G., Miller, G. H., Ahrens, M. J., & Winans, R. E. 2001, Origins of Life and Evolution of the Biosphere, 31, 15-51

Bockelée-Morvan, D., Gautier, D., Hersant, F., Huré, J.-M., & Robert, F. 2002, Astronomy and Astrophysics, 384, 1107-1118

Boillot, F., Chabin, A., Buré, C., Venet, M., Belsky, A., Bertrand-Urbaniak, M., Delmas, A., Brack, A., & Barbier, B. 2002, Origins of Life and Evolution of the Biosphere, 32, 359-385

Chyba, C. F., Thomas, P. J., Brookshaw, L., & Sagan, C. 1990, Science, 249, 249-373

Cunningham, M. R., Jones, P. A., Godfrey, P. D., Cragg, D. M., Bains, I., Burton, M. G., Calisse, P., Crighton, N. H. M., Curran, S. J., Davis, T. M., Dempsey, J. T., Fulton, B., Hidas, M. G., Hill, T., Kedziora-Chudczer, L., Minier, V., Pracy, M. B., Purcell, C., Shobbrook, J., & Travouillon, T. 2007, Monthly Notices of the Royal Astronomical Society, 376, 1201-1210

Ehrenfreund, P., Bernstein, M. P., Dworkin, J. P., Sandford, S. A., & Allamandola, L. J. 2001, The Astrophysical Journal, 550, L95-L99

Ehrenfreund, P., & Charnley, S. B. 2000, Annual Review of Astronomy & Astrophysics, 38, 427-483

Forterre, P. 2001, A la recherche des formes de vie terrestre les plus "primitives" : impasses et progrès, ed. M. Gargaud, D. Despois, & J.-P. Parisot (Presses Universitaires de Bordeaux, Bordeaux), 399-416

Greenberg, J. M. 1982, What are comets made of ? A model based on interstellar dust, ed. L. L. Wilkening (University of Arizona Press, Tucson), 131-163

Hersant, F., Gautier, D., & Huré, J.-M. 2001, Astrophysical Journal, 554, 391-407

Iro, N., Gautier, D., Hersant, F., Bockelée-Morvan, D., & Lunine, J. I. 2003, Icarus, 161, 511-532

Kuan, Y.-J., Charnley, S. B., Huang, H.-C., Tseng, W.-L., & Kisiel, Z. 2003, Astrophysical Journal, 593, 848-867

Lunine, J. I., Engel, S., Bashar, R., & Horanyi, M. 1991, Icarus, 94, 333-344

Podolak, M., & Prialnik, D. 1997, 26-Al and Liquid Water Environments in Comets, ed. P. J. Thomas, C. F. Chyba, & C. P. McKay (Springer, New York),

Prinn, R. G., & Fegley, B. J. 1989, Solar Nebula Chemistry: Origin of planetary, satellite and cometary volatiles, ed. S. K. Atreya, J. B. Pollack, & M. Matthews (Univ. Of Arizona Press., 78-136

Schutte, W. A., Allamandola, L. J., & Sandford, S. A. 1993, Science, 259, 1143-1145

CONTRATS DE RECHERCHES

2003

Programme chimie prébiotique HMT. *Financement GDR Exobiologie.* *3 k€*

2004

Programme EXPOSE/BIOPAN. *Financement CNES.* *16.3 k€*

Programme chimie prébiotique HMT. *Financement GDR Exobiologie.* *3 k€*

2005

Programme EXPOSE/BIOPAN. *Financement CNES.* *31 k€*

Programme COSIMA. *Financement CNES.* *4 k€*

Programme chimie prébiotique HMT. *Financement GDR Exobiologie.* *2 k€*

2006

Programme EXPOSE/BIOPAN. *Financement CNES.* *15 k€*
AO interne LISA *5 k€*

Programme COSIMA. *Financement CNES.* *6 k€*

2007

Programme EXPOSE/BIOPAN. *Financement CNES.* *20.5 k€*

Programme COSIMA. *Financement CNES.* *8 k€*

Programme OREGOC *Financement BQR P12* *20 k€*
AO interne LISA *12 k€*
PID OPV *35 k€*

2008

Programme EXPOSE/BIOPAN. *Financement CNES.* *20 k€*

Programme COSIMA. *Financement CNES.* *8 k€*

Programme OREGOC. *Financement GDR Exobio* *6 k€*

A venir : Contrat CNES R&T Vitrine.
R&T ILMA gérée par le LPCE

CURRICULUM VITAE DETAILLE

Hervé COTTIN
Né le 6 Juillet 1972 (36 ans)

Maître de Conférences
Université Paris 12, Val de Marne
Section 34

Laboratoire **I**nteruniversitaire des **S**ystèmes **A**tmosphériques (*LISA*)
Universités Paris XII - Paris VII / UMR 7583 CNRS
Tel : 33-(0)1 45 17 15 63
Fax : 33-(0)1 45 17 15 64
cottin@lisa.univ-paris12.fr

Domaine de compétence : ASTROCHIMIE/EXOBIOLOGIE

Outils : Chimie en phase gazeuse et solide / Photochimie expérimentale / Cinétique chimique / Spectroscopie / Spectrométrie de masse
Objets : Planétologie / Exobiologie / Chimie du milieu interstellaire / Comètes / Astéroïdes carbonés

Situations antérieures et formation universitaire

Février 2001 - Janvier 2002 : National Research Council (NRC) Associate
NASA - Goddard Space Flight Center, Astrochemistry Branch (code 691) - Cosmic Ice Laboratory, Greenbelt, MD, 20771, USA

Octobre 1999 – Octobre 2000 : ATER (Chimie), Université Paris 12, LISA

Novembre 1999 : Soutenance de Thèse :
Chimie organique de l'environnement cométaire : étude expérimentale de la contribution de la composante organique réfractaire à la phase gazeuse
Directeurs de thèse : François Raulin, Marie-Claire Gazeau
(Bourse MENESR / Moniteur Chimie Paris 12) – Thèse obtenue avec mention très honorable et les félicitations du jury

1994-1995 : D.E.A. de Chimie de la Pollution et Physique de l'Environnement
Sujet : Etude de la Formation de HCN dans l'atmosphère de Neptune.
Universités Paris VII - Paris XII – Orléans – Grenoble – Chambéry
Mention TB - Major de promotion

Formations complémentaires

Ecole CNRS d'Exobiologie (Sept. 2003, 2005 et 2007) / Propriano
E.R.C.A. (European Resarch Course on the Atmosphere) (Jan-Fev 1997) / Grenoble
Ecole de Planétologie Comparée (Sept 1996) / Hendaye

Organisation d'écoles

Ecole CNRS d'Exobiologie, Septembre 2007 / Propriano (Avec Muriel Gargaud et Franck Selsis)
Rencontres Exobiologiques pour Doctorants, RED'07 & '08 ('09 à venir), Février 2007-2008(-2009), Parc Ornithologique du Teich (Avec Muriel Gargaud).

Animation de la recherche et activités d'intérêt général au sein du laboratoire et d'autres organismes

Depuis Janvier 2005 : Membre élu du conseil de laboratoire du LISA
Depuis Janvier 2004 : Membre du groupe de travail astro/exobiologie du CNES
Depuis Juin 2003 : Collaborateur étranger au Goddard Center for Astrobiology
Depuis Janvier 2003 : Membre du conseil de groupement du GDR exobiologie
Depuis Janvier 2007 : Directeur adjoint du GDR exobiologie
Depuis Octobre 1999 : Webmaster de la page du GDR Exobio (http://www.exobio.cnrs.fr/)
Depuis Juin 1997 : Webmaster de la page du GPCOS du LISA (http://www.lisa.univ-paris12.fr/)
Depuis Mars 2007 : Membre externe de la CSE de Paris 11 (Section 34)

Referee pour plusieurs articles soumis à *The Astrophysical Journal*, *Icarus, Advances in Space Research* notamment.

Activités pédagogiques

Enseignement en Chimie (60 %) et Sciences de l'Univers (Astronomie, Planétologie, Exobiologie) (40%)
Depuis ma nomination j'ai effectué chaque année l'intégralité de mon temps de service (192 h eq TD) avec actuellement une répartition de 30 % Cours, 40 % TD, 30 % TP, à tous les niveau entre le L1 et le M2.
Responsable pédagogique du plateau technique de Chimie à la faculté des sciences de Paris 12.
Responsable (création) de deux nouveaux modules d'enseignement en L : « Astrophysique, Astrochimie et Astrobiologie » (Faculté des Sciences P12), « De l'origine de l'univers à l'origine de la vie » (Module libre Université P12) (30h chacun)

Responsable pour P12 de deux modules dans le cadre du Master Sciences et Génie de l'Environnement (P7, P12, ENPC) : « Environnements planétaires et exobiologie » (M1 – 30h), « Physique et Chimie des atmosphères planétaires » (M2 – 30h)

Coresponsable de l'organisation d'un atelier consacré à l'enseignement de l'exobiologie en France. 10-11 Avril 2006. CNES, Paris. (www.exobio.cnrs.fr)

Encadrement pédagogique :

2008-… : Léna Le Roy, Thèse CNES (codirecteur, direction Gilles Poulet)
2007-2008 : Léna Le Roy, Master Sciences et Génie de l'Environnement -M2
2007 : Karen Habib, Guillaume Valette – L3 – Parcours chimie[1]
2006-… : Yuan Yong Guan, Thèse P12 (codirecteur, direction François Raulin)
2006 : Audrey Noblet, Léna Le Roy – L3 – Parcours chimie[1]
2005-2006 : Yuan Yong Guan – Master Sciences et Génie de l'Environnement -M2
2005 : Europe Mortier, Jonathan Danjean – Maîtrise de chimie[1]
2004-2007 : Fabien Stalport - Thèse P7 (Participation à l'encadrement)[2]
2004-2005 : Cyril Duval – Master Sciences et Génie de l'Environnement – M2
2004 : Cécilia Reis, Alexandra Fursy – Maîtrise de Chimie[1]
2001-2004 : Nicolas Fray – Thèse P12 (Participation à l'encadrement)[3]
2003-2004 : Sébastien Desrutin – DEA Chimie de la Pollution Atmosphérique
2003 : Nacima Siad – Maîtrise de Chimie[1]
1999-2000 : Souleyman Bachir – DEA Chimie de la Pollution Atmosphérique
1999 : Souleyman Bachir, Rodolphe Mulette – Maîtrise Chimie[1]
1998 : Nelson Martin, Frédéric Moindrot – Maîtrise Chimie[1]

[1] : stage de recherche pendant deux mois en laboratoire
[2] : direction de la thèse : Patrice Coll, François Raulin
[3] : direction de la thèse : Marie Claire Gazeau et Yves Bénillan

Projets Spatiaux

Depuis Février 2008 : **Principal Investigator** (PI) de l'instrument ILMA (spectromètre de masse haute résolution pour la mission MARCO POLO) proposé à l'ESA.
Depuis Janvier 2007 : **PI** de l'expérience AMINO (photochimie de molécules organiques par les UV solaires) sur la Station Spatiale Internationale. Succession d'A. Brack.
Depuis Avril 2005 : **PI** des expériences UVolution et PROCESS (photochimie de molécules organiques par les UV solaires) sur la capsule automatique Foton et sur la Station Spatiale Internationale (ISS).
Depuis Janvier 2005 : CoInvestigator (CoI) expérience COSIMA (analyse de grains cométaires) TOF SIMS sur la sonde ROSETTA. PI : M. Hilchenbach.
Depuis Janvier 2003 : CoI expérience AMINO. PI : A. Brack.

Membre de sociétés savantes

COSPAR, ISSOL, EANA

Publications dans des revues à comité de lecture

22. Cottin H. and Fray N. (In Press) Distributed Sources in Comets. Space Science Reviews.

21. Cockell C. S., Leger A., Fridlund M., Herbst T., Kaltenegger L., Absil O., Beichman C., Benz W., Blanc M., Brack A., Chelli A., Colangeli L., **Cottin H.**, Coude du Foresto V., Danchi W., Defrere D., den Herder J.-W., Eiroa C., Greaves J., Henning T., Johnston K., Jones H., Labadie L., Lammer H., Launhardt R., Lawson P., Lay O. P., LeDuigou J.-M., Liseau R., Malbet F., Martin S. R., Mawet D., Mourard D., Moutou C., Mugnier L., Paresce F., Quirrenbach A., Rabbia Y., Raven J. A., Rottgering H. J. A., Rouan D., Santos N., Selsis F., Serabyn E., Shibai H., Tamura M., Thiebaut E., Westall F., White, and Glenn J. (In Press) DARWIN - A Mission to Detect, and Search for Life on, Extrasolar Planets. Astrobiology.

20. Küppers M., Keller H. U., Kührt E., A'Hearn M. F., Altwegg K., Bertrand R., Busemann H., Capria M. T., Colangeli L., Davidsson B., Ehrenfreund P., Knollenberg J., Mottola S., Rathke A., Weiss P., Zolensky M., Akim E., Basilevskij A., Galimov E., Gerasimov M., Korablev O., Lomakin I., Marov M., Martynov M., Nazarov M., Zakharov A., Zelenyi L., Aronica A., Ball A. J., Barbieri C., Bar-Nun A., Benkhoff J., Biele J., Biver N., Blum J., Bockelée-Morvan D., Botta O., Bredehöft J.-H., Capaccioni F., Charnley S., Cloutis E., **Cottin H.**, Cremonese G., Crovisier J., Crowther S., Epifani E. M., Esposito F., Ferrari A. C., Ferri F., Fulle M., Gilmour J., Goesmann F., Gortsas N., Grady M., Green S. F., Groussin O., Grün E., Gutiérrez P. J., Hartogh P., Henkel T., Hilchenbach M., Ho T.-M., Horneck G., Hviid S. F., Ip W.-H., Jäckel A., Jessberger E., Kallenbach R., Kargl G., Kömle N. I., Korth A., Kossacki K., Krause C., Krüger H., Li Z.-Y., Licandro J., Lopez-Moreno J. J., Lowry S. C., Lyon I., Magni G., Mall U., Mann I., Markiewicz W., Martins Z., Maurette M., Meierhenrich U., Mennella V., Ng T. C., Nittler L., Palumbo P., Pätzold M., Prialnik D., Rengel M., Rickman H., Rodriguez J., Roll R., Rost D., Rotundi A., Sandford S., Schoenbaechler M., et al. (In Press) Triple F - A Comet Nucleus Sample Return Mission. Experimental Astronomy.

19. Cottin H., P. Coll, D. Coscia, N. Fray, Y. Y. Guan, F. Macari, F. Raulin, C. Rivron, F. Stalport, C. Szopa, D. Chaput, M. Viso, M. Bertrand, A. Chabin, L. Thirkell, F. Westall, and A. Brack (In Press) Heterogeneous solid/gas chemistry of organic compounds related to comets, meteorites, Titan and Mars: in laboratory and in lower Earth orbit experiments. Advances in Space Research.

18. Lasue J., A. C. Levasseur-Regourd, N. Fray, and **H. Cottin** (2007) Inferring the interplanetary dust properties from remote observations and simulations. Astronomy

& Astrophysics 473, 641–649.

17. Kissel J., Altwegg K., Clark B. C., Colangeli L., **Cottin H.**, Czempiel S., Eibel J., Engrand C., Fehringer H. M., Feuerbacher B., Fomenkova M., Glasmachers A., Greenberg J. M., Grün E., Haerendel G., Henkel H., Hilchenbach M., Hoerner H. v., Höfner H., Hornung K., Jessberger E. K., Koch A., Krüger H., Langevin Y., Parigger P., Raulin F., Rüdenauer F., Rynö J., Schmid E. R., Schulz R., Silen J., Steiger W., Stephan T., Thirkell L., Thomas R., Torkar K., Utterback N. G., Varmuza K., Wanczek K. P., Werther; W., and Zscheeg H. (2007) COSIMA, a High Resolution Time of Flight Spectrometer for Secondary Ion Mass Spectroscopy of Cometary Dust Particles. Space Science Reviews Volume 128(1-4), 823-867.

16. Fray N., Bénilan Y., Biver N., Bockelée-Morvan D., **Cottin H.**, Crovisier J., and Gazeau M.-C. (2006), Heliocentric evolution of the degradation of polyoxylmethylene. Application to the origin of the formaldehyde (H_2CO) extended source in comet C/1995 O1 (Hale-Bopp). Icarus 184(1), 239-254.

15. Fray N., Bénilan Y., **Cottin H.**, Gazeau M.-C., and Crovisier J. (2005) The origin of the CN radical in comets: A review from observations and models. *Planetary and Space Science* **53**(12), 1243-1262.

14. Fray, N., Bénilan, Y., **Cottin, H.**, Gazeau, M.-C., Minard, R. D., and Raulin, F. (2004). Experimental study of the degradation of polymers. Application to the origin of extended sources in cometary atmospheres. Meteoritics and planetary science 39(4), 581-587.

13. Cottin, H., Y. Bénilan, M.-C. Gazeau, and F. Raulin (2004) Origin of cometary extended sources from degradation of refractory organics on grains: polyoxymethylene as formaldehyde parent molecule. Icarus 167, 397–416.

12. Fray, N., Bénilan, Y., **Cottin, H.**, and Gazeau, M.-C. (2004). New experimental results on the degradation of polyoxymethylene. Application to the origin of the formaldehyde extended source in comets. Journal of Geophysical Research (Planets) 109, E07S12

11. Cottin H., Moore M. H., and Bénilan Y. (2003) Photodestruction of relevant interstellar molecules in ice mixtures. The Astrophysical Journal 590, 874-881.

10. Cottin H., Bachir S., Raulin F., and Gazeau M. C. (2002) Photodegradation of Hexamethylenetetramine by VUV and its relevance for CN and HCN extended sources in comets. Advances in Space Research 30 (6), 1481-1488

9. Cottin H., Gazeau M. C., Chaquin P., Bénilan Y., and Raulin F. (2001) Experimental and theoretical studies on the gas/solid/gas transformation cycle in extraterrestrial environments. Journal of Geophysical Research (Planets) 106 (E12), 33,325-33,332.

8. Cottin H., Szopa C., and Moore M. H. (2001) Production of hexamethylenetetramine in photolyzed and irradiated interstellar cometary ice analogs. The Astrophysical Journal Letters 561 (1), L139-L142.

7. Cottin H., M.C. Gazeau, Y. Bénilan, and F. Raulin (2001) Polyoxymethylene as parent

molecule for the formaldehyde extended source in comet Halley, The Astrophysical Journal 556 (1), 417-420.

6. Gazeau M. C., **Cottin H.**, Vuitton V., Smith N. and Raulin F. (2000) Experimental and theoretical photochemistry : application to the cometary environment and Titan's atmosphere. Planetary and Space Science 48, 437-445.

5. Cottin H., Gazeau M. C., Doussin J. F., and Raulin F. (2000) An experimental study of the photodegradation of polyoxymethylene at 122, 147 and 193 nm. Journal of photochemistry and photobiology (A : Chemistry) 135, 53-64.

4. Szopa C., Sternberg R., Coscia D., **Cottin H.**, Raulin F., Goesmann F., and Rosenbauer H. (1999) Gas chromatography for in situ analysis of cometary nucleus: I. Characterization and optimization of diphenyl/dimethyl polysiloxane stationary phase using coupled experimental/computer modelling approaches. Journal of Chromatography 863, 157-169.

3. Cottin H., M.C. Gazeau, and F. Raulin, (1999) Cometary organic chemistry : a review from observations, numerical and experimental simulations, Planetary and Space Science 47 , 1141-1162.

2. Cottin H., M.C. Gazeau, J.F. Doussin, and F. Raulin (1999) S.E.M.A.Ph.Or.E COMETAIRE, a tool for the study of the photochemical decomposition of probable cometary large organic molecules. First application: Polyoxymethylene, Physic and Chemistry of the Earth 24 (5), 597-602.

1. Gazeau M.C., **H. Cottin**, L. Guez, P. Bruston, and F. Raulin (1997) HCN formation under electron impact: experimental studies and application to Neptune's atmosphere, Advances in Space Research 19 (7), 1135-1144.

Chapitres dans des ouvrages à comité de lecture

5. Cottin H. and D. Despois (In Press) Comets and astrobiology. In Prebiotic Evolution and Astrobiology (ed. J. T.-F. Wong and A. Lazcano). Landes Bioscience of Texas.

4. Cottin H. (2007) Basic prebiotic chemistry. In Complete course in astrobiology (ed. P. Rettberg and G. Horneck), pp. 55-83. Wiley-VCH.

3. Cottin H. and Bénilan Y. (2005) Les comètes, Titan et Mars : exobiologie et projets spatiaux. In *Des atomes aux planètes habitables* (ed. M. Gargaud, P. Claeys, and H. Martin), pp. 185-236. Presses Universitaires de Bordeaux.

2. Bénilan, Y., and **H. Cottin**, Comets, Titan and Mars: Astrobiology and space projects, in Lectures in Astrobiology, vol 2,, edited by M.Gargaud, B.Barbier, H. Martin, and J.Reisse, Springer Verlag, sous presse.

1. Despois, D., and **Cottin, H.**, Comets : potential sources of prebiotic molecules for the early Earth, in Lectures in Astrobiology, vol 1, edited by M.Gargaud, B.Barbier, H. Martin, and J.Reisse, pp. 289-352, Springer Verlag, 2005.

Communications orales les plus significatives

Cottin H., Coll P., Coscia D., Guan Y. Y., Raulin F., Rivron C., Stalport F., Szopa C., Bertrand M., Chabin A., Westall F., and Brack A. (2006) Solid/gas heterogeneous chemistry of organic compounds related to comets, Titan and Mars, through experiments in the laboratory and in Earth orbit. 36th assembly of Committee on Space Research (COSPAR), Beijing, Chine. (*Invité)*

Cottin H., Bénilan Y., Fray N., Gazeau M.-C., Raulin F., Sternberg R., Szopa C., Thirkell L., and Thomas R. (2006) Laboratory work on cometary organic matter in support of space missions. 36th assembly of Committee on Space Research (COSPAR) , Beijing, Chine. (*Invité)*

Cottin H., Coll P., Coscia D., Szopa C., Raulin F., and Brack A. (2005), AMINO, PROCESS and UV-olution: investigation of the solid/gas heterogeneous chemistry of organic compounds in space via FOTON and the Space Station. 5th EUROPEAN WORKSHOP ON ASTROBIOLOGY, Budapest, Hungary.

Cottin, H., S. Desrutin, C. Engrand, L. d'Hendecourt, and M.H. Moore (2004), Production of HMT and POM in interstellar and cometary ices, in 35th assembly of Committee on Space Research (COSPAR), Paris, France.

Cottin, H., Y. Bénilan, N. Fray, M.-C. Gazeau, F. Raulin, and R. Sternberg (2004), Cometary organic chemistry : understanding the history of their ice from their composition, and potential astrobiology interest, in Biannual Conference on Chemistry, Chem 03, Cairo, Egypt. (*Invité)*

Cottin H., Lowenthal M. S., Khanna R., Hudson R. L., and Moore M. H. (2002) The stability of the cyanate ion and production of urea in interstellar ices. 34th assembly of Committee on Space Research (COSPAR), Houston, USA.

Cottin H., Gazeau M. C., Bénilan Y., and Raulin F. (2001) The degradation of refractory organic material as a source of volatile molecules : the extended sources in comets. American Chemical Society Meeting, San Diego, USA. (*Invité)*

Sur un total de plus de 50 présentations depuis 1998, dont 7 invitées en premier auteur

PUBLICATIONS INTEGRALES CITEES DANS LE DOCUMENT

Article 1

COTTIN H. (2007) Basic prebiotic chemistry. In Complete course in astrobiology (eds. P. Rettberg and G. Horneck), pp. 55-83. Wiley-VCH.

3
Basic Prebiotic Chemistry

Hervé Cottin

This chapter is devoted to the study of prebiotic chemistry. It focuses on the abiotic synthesis of key prebiotic compounds – amino acids, purine and pyrimidine bases, and sugars – from simple molecules, such as methane (CH_4), hydrogen cyanide (HCN), and formaldehyde (H_2CO), thereby filling the gap between chemistry and biology. In the first section living systems are dismantled into more elemental fragments: organic molecules. To address the origin of life, the next question is how those fragments can be synthesized in an abiotic manner. After a short historical review, different tracks of prebiotic chemical evolution are explored: an endogenous production of the molecules of life within early Earth's atmosphere or in the depths of primitive oceans, or an exogenous source of prebiotic molecules through space delivery via meteorites and comets. The last section describes chemical pathways of the synthesis of the building blocks of life.

3.1
Key Molecules of Life

Life as we know it is based on a complex chemistry involving highly sophisticated biological molecules such as proteins, ribonucleic acids (RNA), or deoxyribonucleic acids (DNA). Such elaborated structures result from a complex chemical evolution, starting with the simplest organic compounds. At some point, at an as yet undefined stage of complexity and organization of matter, an important step is made and chemistry turns into biology.

Complete Course in Astrobiology. Edited by Gerda Horneck and Petra Rettberg

ISBN: 978-3-527-40660-9

3.1.1
Dismantling the Robots

In Chapter 1 André Brack compares the premises of an emerging life to parts of "chemical robots," which make copies of themselves and are capable of evolution through "mistakes" during reproduction. Following this idea, life could be considered as any type of structure (at a molecular or cellular level or any other form) with some complexity that bears information to make the robot work and that makes copies of itself. From time to time, the copy would not be the exact image of its original. This modified copy could be either more adapted to the environment than its original or less adapted, and therefore either more or less favored to survive. Then it would make more copies of its new model with either more or less efficiency.

Whereas it is quite difficult to find a proper general definition of life (see Chapter 1), it is much easier to answer the question "What is life made of?" The answer turns out to be surprisingly simple. If one considers all living systems on Earth, from unicellular systems such as bacteria to multicellular systems such as plants and animals, they are all built from the same basic components.

Each living system is made of at least one cell. A cell can in turn be broken down into more elemental parts: proteins, RNA, and DNA molecules embedded within the membrane of the cell. These biomolecules are made of mainly the following elements: carbon (C), hydrogen (H), oxygen (O), and nitrogen (N). The membrane is built from long organic amphiphile chains. These chains possess a polar head, which makes them soluble in water (hydrophilic part of the molecule), and an apolar tail, which is insoluble in water (hydrophobic part of the molecule). Such molecules are called amphiphiles (amphi = both), because they consist of both a hydrophobic and a hydrophilic part. These amphiphile structures may self-organize into vesicles (Fig. 3.1).

Inside the cell, which is surrounded by the membrane, a complex molecular engine is working (Fig. 3.2). But, from a simplified chemical point of view, the interior of the cell turns out to be made of mainly proteins and nucleic acids, such as DNA and RNA. Of course, there is a wide range of proteins that play various key

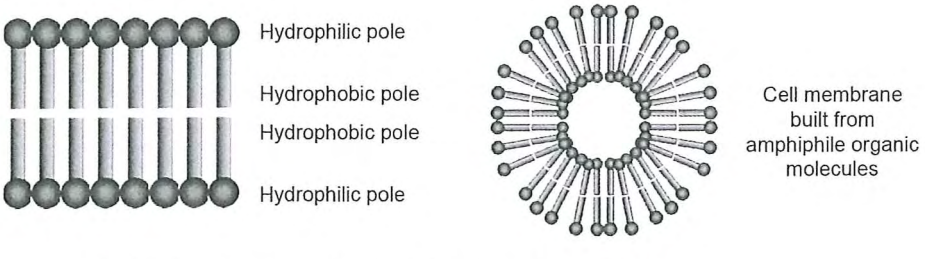

Fig. 3.1 Long organic amphiphile chains with a polar head that makes them soluble in water and a water-insoluble apolar tail (left), which may self-organize into vesicles (right).

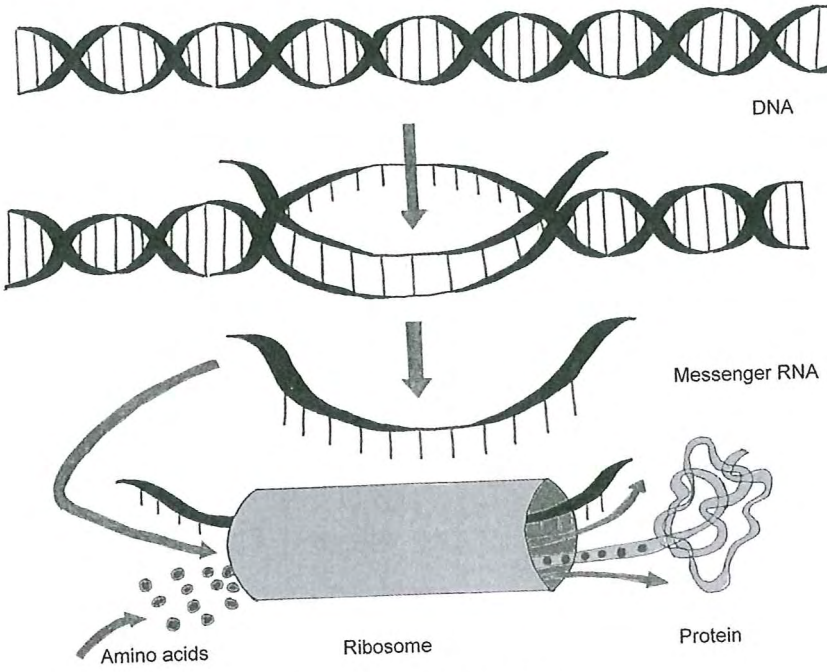

Fig. 3.2 Basic cellular components (DNA, RNA, and proteins) and functions (storage and transfer of information and protein synthesis in the ribosomes).

roles in metabolism and an enormous diversity of DNA and RNA molecules, which is reflected by the large diversity of living forms on Earth. But this diversity results from a combination of 28 molecules only. Every known living organism could be compared with a Lego construction with 28 different kinds of bricks: 20 amino acids to build the proteins, five purine or pyrimidine bases, two sugars, and one phosphate bridge to build DNA and RNA. The following main functions can be attributed to the three families of molecules:

- DNA stores information,
- RNA transmits information, and
- proteins act as catalysts.

Table 3.1 shows the basic composition of a cell exemplified by the bacterium *Escherichia coli*.

Table 3.1 Composition of a bacterial cell as exemplified by *Escherichia coli*.

Component	Percentage of total cellular weight	Molecular mass (g mol^{-1})[a]
Water	70	18
Proteins	15	40 000
RNA	6	~ 10^6
DNA	1	2.5×10^9
Carbohydrates and precursors[b]	3	150
Lipids and precursors[b]	2	750
Amino acids and precursors	0.4	120
Nucleotides and precursors	0.4	300
Others[c]	2	–

a Averaged in a mixture
b Parts of the cell membrane
c Other small molecules and inorganic ions

3.1.2 Proteins and Amino Acids

Proteins are organic compounds built from a succession of amino acids linked together by peptide bonds. Proteins can play different roles: some are of importance at a structural level in the cells, while others are enzymes that act as catalysts for chemical reactions. Their properties result from their chemical formula and from their spatial conformation (how the amino acid chain organizes itself in space).

An amino acid is a molecule that contains both an amino group (-NH_2) and a carboxylic acid (-COOH) function (Fig. 3.3). If the carbon that bears the amino

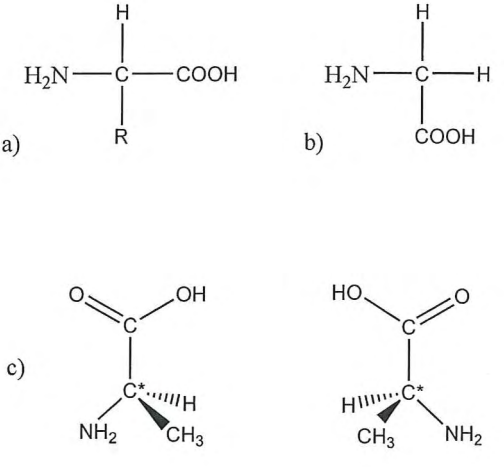

Fig. 3.3 (a) General formula of an α-amino acid; R represents different side chains; (b) glycine; (c) 3-dimensional presentation of an α-amino acid (alanine) with an asymmetric carbon (marked with a star). Note that these molecules, which have an identical molecular formula, cannot be superimposed one over the other.

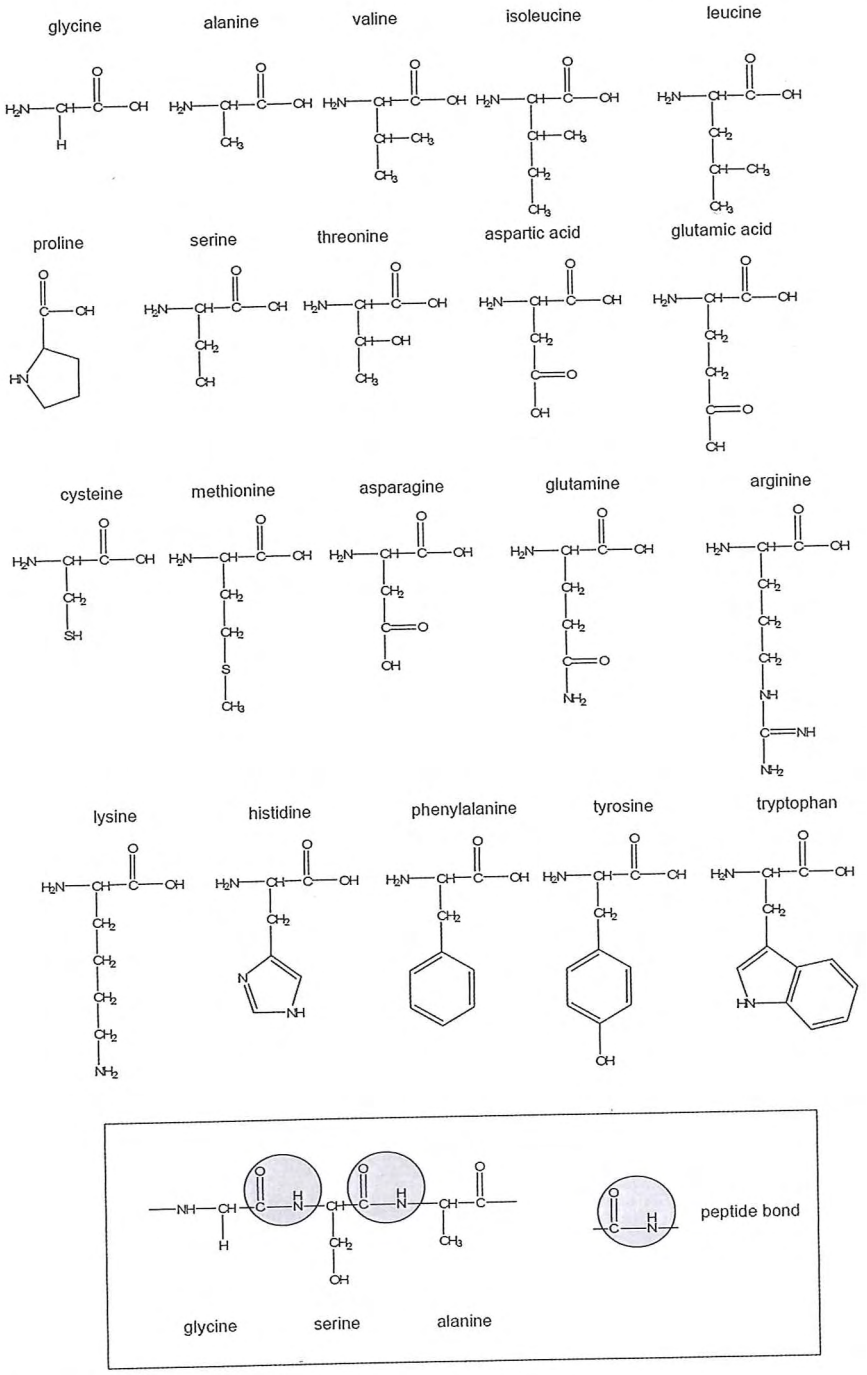

Fig. 3.4 The 20 biological amino acids; association of several amino acids through peptide bonds produces a polypeptide.

group is the same as the one bearing the carboxylic function, then the amino acid is called an α-amino acid. If the amino group is linked to a carbon that is one C away from the carbon bearing the carboxylic function, then the amino acid is called a β-amino acid, and so forth.

The general structure of an α-amino acid is shown in Fig. 3.3 a. R represents a side chain specific to each amino acid. In only the simplest amino acid, glycine, is the R-group hydrogen (Fig. 3.3 b). For all other α-amino acids, R is different from H. In that case the central carbon atom has four different substituents and is then called an asymmetrical carbon. As shown in Fig. 3.3 c, two spatial arrangements (configurations) of these substituents are possible, resulting in two different molecules (called enantiomers) that are mirror images of each other. Molecules with an asymmetric or chiral C atom affect the orientation of polarized light when it passes through a sample of molecules of one configuration. Configuration 1 shifts the orientation of polarized light to the right (dextrorotary), while configuration 2 would shift it to the left (levorotary). These two configurations of amino acids are called L or D (L-compounds rotate the plane of polarized light to the left, D-compounds to the right). A mixture of equal quantities of both configurations is called a racemic mixture. It neutralizes the effect, and polarized light passes unchanged. This property toward polarized light has no direct effect on life, but the configuration of amino acid (D or L) is extremely important for the spatial orientation (conformation) of long chains of amino acids: the proteins. The properties of proteins are directly linked to their conformation, and they have different characteristics if built from L-amino acids, D-amino acids, or a mixture of both (see also Chapter 1).

As mentioned above, in the proteins the amino acids are linked by peptide bonds. Peptide bond formation is a condensation reaction leading to the polymerization of amino acids into peptides and proteins with the concomitant elimination of water (Fig. 3.4). Peptides are small, consisting of a few amino acids. Proteins are polypeptides of greatly divergent length.

To build the proteins, life uses a combination of only 20 amino acids (Fig. 3.4), all of which appear in one enantiomer: the L-form. Why L-enantiomers were selected over D-enantiomers remains unknown, but this is a property shared by all living systems (with a few exceptions in the bacterial domain; see Chapter 5).

3.1.3 DNA, RNA, and Their Building Blocks

DNA (deoxyribonucleic acid) and RNA (ribonucleic acid) are long-chained organic molecules that contain genetic code information (see Chapter 4). From a chemical point of view, in terms of building blocks of life, their composition and structure can be quite simply explained.

The backbone of DNA and RNA is a succession of sugars (deoxyribose for DNA, ribose for RNA) linked by phosphate bridges (PO_4^{2-}) (Fig. 3.5). The "letters" of the genetic code, which are connected to each sugar molecule, are the purine bases adenine (A) and guanine (G) and the pyrimidine bases cytosine (C), thymine (T) (T in DNA only), and uracil (U) (in RNA only) (Fig. 3.6). The association of the sugar

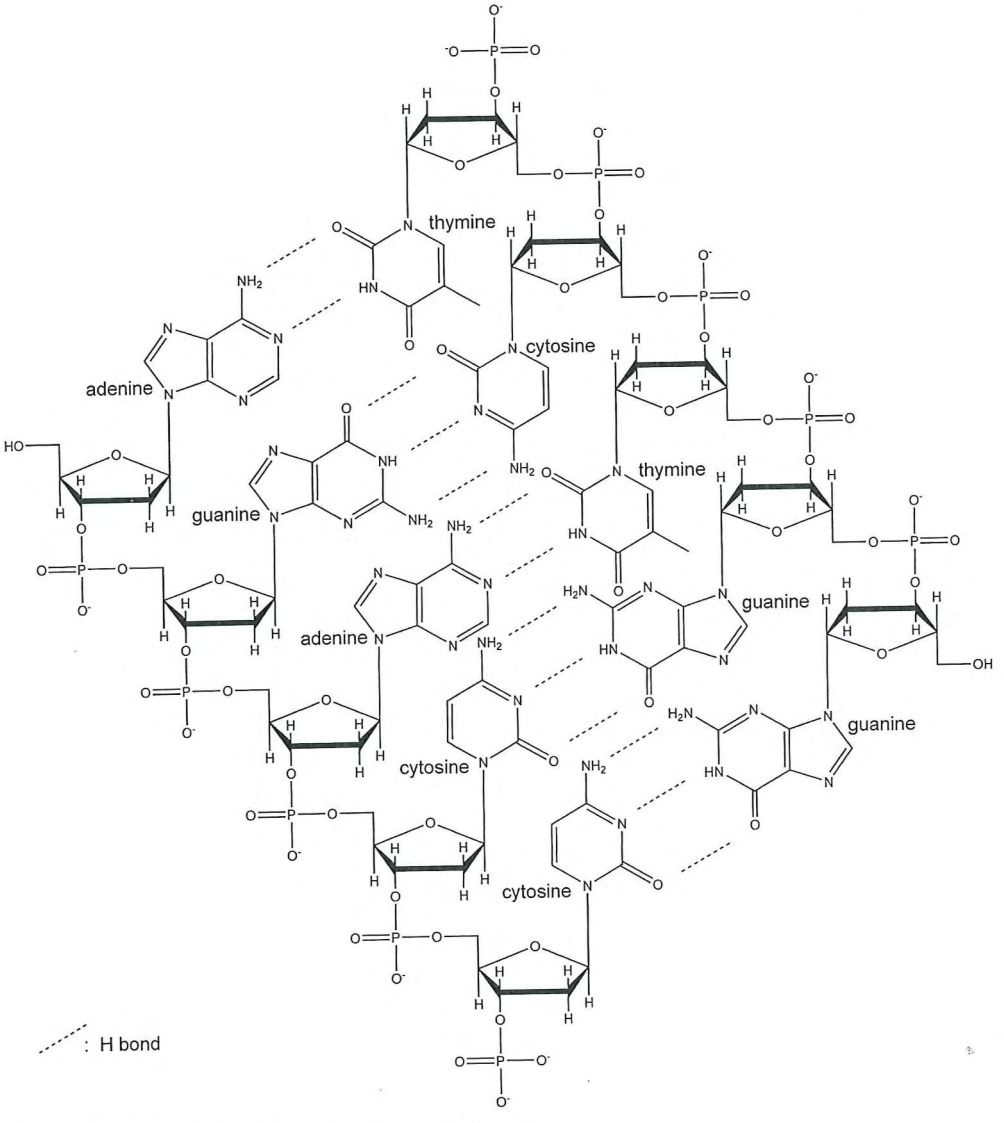

Fig. 3.5 Structure of DNA. DNA and RNA are linked chains of nucleotides, each consisting of a sugar, a phosphate, and one of the five nucleobases (purine bases: adenine and guanine; pyrimidine bases: cytosine and thymine in DNA or cytosine and uracil in RNA)

with one of the bases is called a nucleoside. If a phosphate is linked to a nucleoside, the resulting structure is called a nucleotide. The polynucleotide is named according to the sugar in its structure: DNA if the sugar is a deoxyribose, and RNA if the sugar is a ribose.

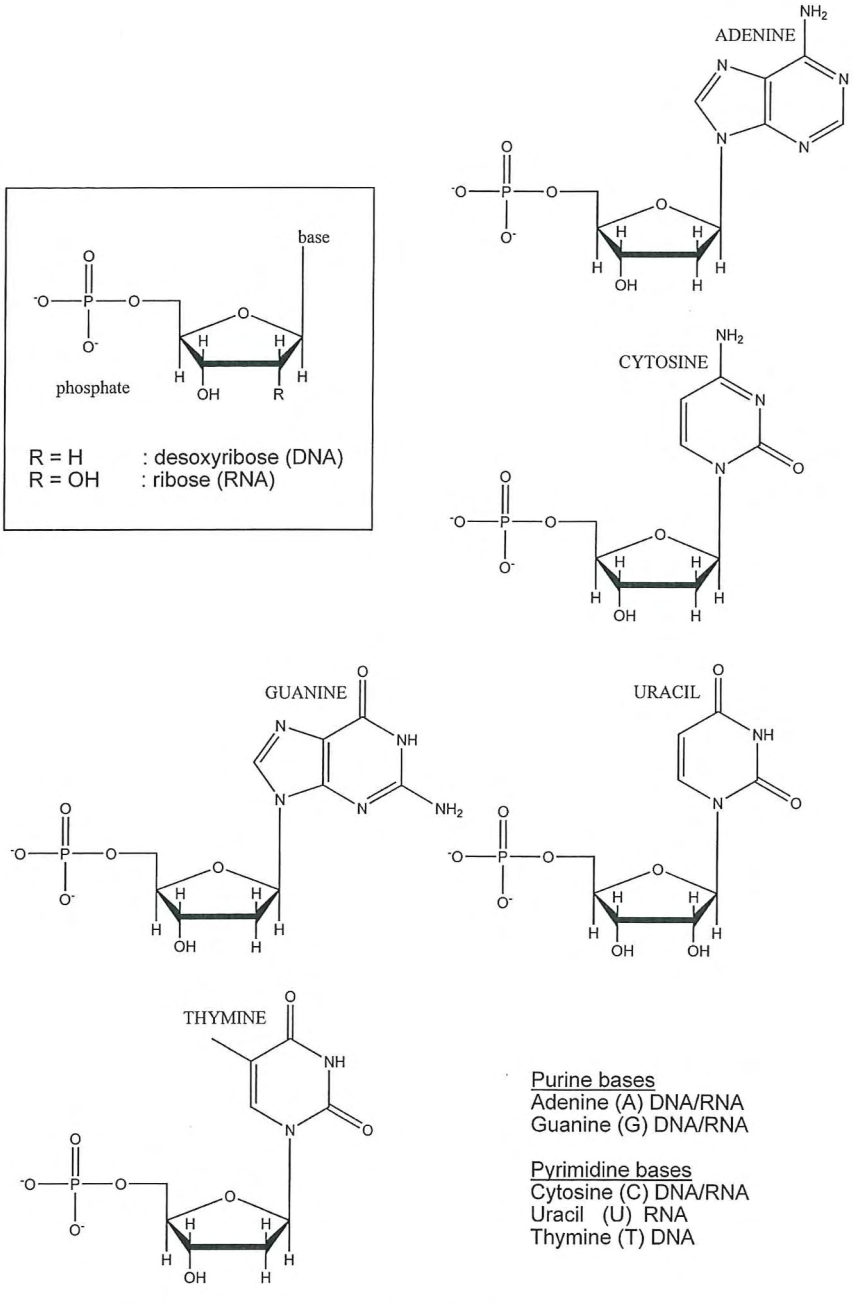

Fig. 3.6 Chemical structure of DNA and RNA nucleotides. The difference between the two types of molecules is the substitution of one H (DNA) by OH (RNA) on the sugar and thymine (DNA) by uracil (RNA).

The genetic code is encrypted in the specific succession of purine and pyrimidine bases. It contains information about which succession of amino acids is to be built in which proteins (see Chapter 4). This information is transferred to the ribosomes, the "proteins factory," via RNA (Fig. 3.2). Ribosomes are composed of RNA and proteins.

All living systems function according to this very same mechanism. What makes a mouse different from an elephant or a mushroom is the number and succession of the "letters" in the DNA molecules.

DNA and RNA are usually seen as carriers of genetic information. This picture has changed with the discovery of the self-splicing of certain RNAs. These observations laid the foundation for the concept of catalytic RNA, the ribozymes (see Chapter 4). This catalytic capacity of RNA led to the idea of the *RNA world* that might have preceded life as we know it today: a simplified cellular biochemical machinery in which RNA plays all roles that are essential for life; it carries and transmits information, and it catalyzes the reactions.

3.1.4
First "Prebiotic Robot"

For building the first "prebiotic robot," and then the first living system, the following compounds must be available:

- long organic amphiphile chains for building membranes;
- amino acids for building proteins;
- phosphate for the backbone of nucleic acids;
- purine and pyrimidine bases as "letters" for the genetic code in DNA and/or RNA; and
- sugars for the nucleic acids (ribose in the RNA world scenario).

These molecules need to be synthesized under prebiotic conditions, either on early Earth or in space. Of course, the presence of the building blocks for life is not sufficient to make the first prebiotic robot; however, they are prerequisites in the scenario of the origin of life.

3.2
Historical Milestones

The building blocks of life have been discovered and characterized since the early 19th century (Table 3.2). In these early times, the question of the abiotic synthesis of such molecules in the test tube seemed far beyond the scope of most of the chemists' capabilities. Moreover, it was not even considered as a question of interest. It was the generally accepted opinion that *organic* molecules are the result of the activity of *organized*, i.e., living, systems, and are associated with a mysterious "vital energy." In 1827, the Swedish chemist Jöns Jacob Berzelius (Fig. 3.7) wrote, "Art cannot combine the elements of inorganic matter in the manner of living

nature." (Berzelius also invented the words "polymerization," "catalysis," "electronegative," and "electropositive" and discovered the elements selenium [Se], silicon [Si], and titanium [Ti]). At that time, there was no way known to synthesize organic molecules in the laboratory, and no reason to look for such ways.

Table 3.2 Milestones in the discovery and characterization of important biochemical monomers or polymers.

Year	Discoverer	Monomer/polymer
1810	W.H. Wollatson	Cystine[a]
1819	J.L. Proust	Leucine[a]
1823	M. E. Chevreul	Fatty acids
1838	J.J. Berzelius	Proteins
1869	F. Miescher	DNA
1882	A. Kossel	Guanine
1883	A. Kossel and A. Neumann	Thymine
1886	A. Kossel and A. Neumann	Adenine
1894	A. Kossel and A. Neumann	Cytosine
1900	A. Ascoli	Uracil
1909	P.T. Levene and W. A. Javok	Desoxyribose
1906–1936	P.T. Levene et al.	Ribose, ribonucleotides

Source: Adapted from Miller and Lazcano 2002.
a Amino acid

A firm denial to this theory was brought in 1828 by Berzelius' friend and former student Friedrich Wöhler (Fig. 3.7). This German chemist succeeded in the first abiotic synthesis of an organic molecule, urea (NH_2-CO-NH_2), "without the need of an animal kidney," as he said at the time, by simple heating of ammonium cyanate (NH_4OCN). From then on, a breach was made in the "vital energy" theory, and, slowly, organic chemistry became the chemistry of carbon-based molecules.

Fig. 3.7 Famous chemists of the 19th century. From left to right: Jöns Jacob Berzelius (1779–1848), Friedrich Wöhler (1800–1882), Adolph Strecker (1822–1871), and Alexandr Butlerov (1828–1886).

Soon after this pioneering finding, the synthesis of other organic compounds was realized. Regarding the synthesis of molecules of prime interest to the origin of life, two major achievements shall be pointed out. In 1850, Adolf Strecker (Fig. 3.7) succeeded in the first laboratory synthesis of an amino acid: alanine from a mixture of acetaldehyde (CH_3CHO), ammonia (NH_3), and hydrogen cyanide (HCN). A few years later, in 1861, Alexandr Butlerov (Fig. 3.7) performed the first laboratory synthesis of sugar mixtures (also known as the *formose reaction*) from formaldehyde (HCHO) using a strong alkaline catalyst (NaOH) (see Section 3.4.3).

Although these discoveries were very interesting, they were not linked to the origin-of-life problem. Hence, little progress was made in finding a scientific description of the origin of life. One had to wait until 1924 for the publication of the book *Origin of Life* by Aleksandr Ivanovich Oparin (1894–1980). Oparin introduced the concept of chemical evolution, which could be seen as the roots of the Darwinian tree of evolution. In this concept, life was the result of a succession of spontaneous chemical reactions that produce increasingly complex chemical structures. In the first edition of his book (1924) he suggested that such chemical evolution would take place within an oxidizing atmosphere of the primitive Earth (it was the generally accepted view at that time that the early Earth had an oxidizing atmosphere). In the second edition (1938) he changed the early atmosphere to a highly reducing environment. Similar ideas were simultaneously developed by the English biologist John Haldane, who was the first to mention the concept of a "prebiotic soup" where chemical evolution took place, a term that became quite popular in the scientific community studying the origins of life.

Some paragraphs of Oparin's book *Origin of Life* from 1924 show its actuality:

> *At first we found carbon scattered in the form of separate atoms, in the red hot stellar atmospheres. We then found it as a component of hydrocarbons which appeared on the surface of the Earth. ...In the waters of the primitive ocean these substance formed more complex compounds. Proteins and similar substance appeared ....[They]...acquired a more and more complex and improved structure and were finally transformed into primary living beings – the forbears of all life on Earth.*

He concluded quite optimistically, bearing promises of spectacular breakthroughs in the field within a few years:

> *We have every reason to believe that sooner or later we shall be able practically to demonstrate that life is nothing else but a special form of existence of matter. The successes scored recently by Soviet biology hold out the promise that the artificial creation of the simplest living beings is not only possible, but that it will be achieved in the not too distant future.*

Facing the hard reality of facts, he did temper his optimism and wrote as a conclusion of the second edition of his book in 1934:

We are faced with a colossal problem of investigating each separate stage of the evolutionary process as it was sketched here. ...The road ahead of us is hard and long but without doubt it leads to the ultimate knowledge of the nature of life. The artificial building or synthesis of living things is a very remote, but not an unattainable goal along this road.

As elegant as Oparin and Haldane's ideas appeared to be, they were expressed at a theoretical level only. The experimental confirmation of the theory of chemical evolution was provided in 1953 by Stanley Miller, a graduate student in the laboratory of the Nobel Prize laureate Harold Clayton Urey. They conceived and built an experiment to simulate a putative primitive Earth environment (Fig. 3.8).

In this experiment a gaseous mixture of hydrogen (H_2), methane (CH_4), ammonia (NH_3), and water (H_2O) was exposed to an electric discharge that simulated that of storm lightning. The mixture was connected to a bulb filled with liquid water that could be heated. This experiment resulted in the production of a large amount of organic molecules, including several amino acids. Those measurements were experimental proof of the theory of chemical evolution. They showed that the chemistry between simple molecules, which were abundant in the atmosphere of

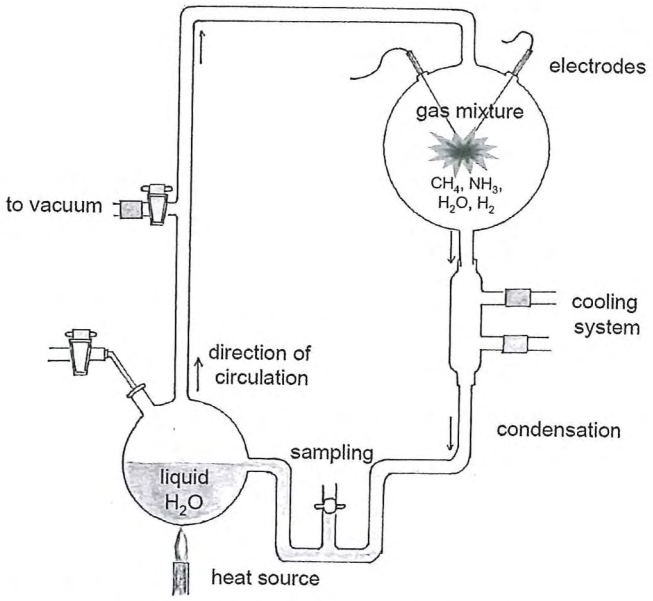

Fig. 3.8 Miller–Urey experiment, which simulates in the laboratory the coupled chemistry between the primitive Earth atmosphere (upper right bulb) and warm oceans (lower left bulb). In the first version, an atmosphere made of CH_4, NH_3, H_2O, and H_2 was considered. A spark discharge simulated storm lightning.

the primitive Earth, led to the synthesis of key compounds that in turn might have led to the forms of life as we know it on Earth.

The choice of a reducing atmosphere with C as CH_4 and N as NH_3 (Table 3.3) was motivated by the following considerations:

- CH_4, NH_3, H_2O, and H_2 had been detected in the atmosphere of giant planets since the 1930 s.
- All the primitive atmospheres of planets were identical, captured from the Solar Nebula.
- Giant planets, cold and distant from the Sun, have kept their original composition.

Therefore, Urey and Miller concluded that the current composition of the atmosphere of giant planets of the Solar System was a good proxy for the composition of the atmosphere of the primitive Earth.

Table 3.3 Classification of planetary atmospheres, in terms of their redox potential, as a function of their composition.

Redox state of the atmosphere	Composition
Reducing	CH_4, NH_3, H_2O, H_2
	CO_2, N_2, H_2O, H_2
	CO_2, H_2, H_2O
Neutral	CO_2/CO, N_2, H_2O
Oxidizing	CO_2/CO, N_2, H_2O, O_2

However, several recent findings disprove this argumentation. First, it is now quite well established that telluric planets do not have sufficient mass to capture the Solar Nebula gas like the giant planets did. To do this, a minimum mass of 10 to 15 Earth masses is required. Only then can a forming planet efficiently trap the volatile elements of the nebula to form its atmosphere. In addition, recent observations have supported the conception that at a distance of one astronomical unit (AU) from the Sun – that is where the Earth accreted – the gaseous component of the Solar Nebula was probably dominated by CO_2 and N_2. Second, Earth, like Venus and Mars, has a secondary atmosphere built from volatile compounds that outgassed from the mantle on one hand or were imported via meteorites and comets on the other hand. Third, the composition of the primitive Earth atmosphere was most probably dominated by CO_2 and N_2, in which organic syntheses are not as efficient as in a reducing atmosphere (see Section 3.3).

Even if the Miller–Urey experiment is not as conclusive as thought at first glance, it was a great achievement because it showed that important prebiotic compounds can be abiotically synthesized in environments simulating "natural" conditions. In Section 3.3 different kinds of such "natural" environments are presented that allow an interesting "prebiotic" chemistry.

Table 3.4 Organic molecules synthesized in Miller-type experiments as a function of the composition of the starting mixture, after electron impact or photolysis as energetic inputs. Compounds in the solid-phase residues are usually detected after acid hydrolysis.

Gaseous mixture	Redox state	Related planetary atmosphere	Families of synthesized organic products	
			Electric discharge	Photolysis
$CH_4 + NH_3 + H_2O$ (+ H_2)	Reducing	Giant planets	RH (saturated and unsaturated) HCN and other nitriles (saturated) RCO_2H H_2CO, other aldehydes Ketones and alcohols Solid: Amino acids and nitrogenated heterocycles after hydrolysis	RH (mostly saturated) HCN RCN (saturated) if N/C <1 RNH_2 if N/C >1 H_2CO, other aldehydes Ketones and alcohols Solid: Amino acids after hydrolysis
$CH_4 + N_2$ (+ H_2O)	Reducing	Titan, Triton	RH (saturated and unsaturated) HCN and other nitriles (saturated and unsaturated) including HC_3N and C_2N_2 H_2CO, other aldehydes Ketones and alcohols Solid: Amino acids and nitrogenated heterocycles after hydrolysis	RH (saturated & unsaturated) H_2CO & other aldehydes with low yields Solid: Carboxylic acids
$CO + NH_3 + H_2O$	Reducing		HCN, oxygenated organic compounds Solid: Amino acids after hydrolysis	HCN, oxygenated organic compounds Solid: Amino acids after hydrolysis
$CO_2 + N_2 + H_2O + CO/H_2$	Neutral	Primitive Earth?	RH (mostly saturated) HCN, other nitriles (saturated) H_2CO, other aldehydes, ketones Solid: Amino acids after hydrolysis	RH (mostly saturated) HCN, other nitriles (saturated) H_2CO, other aldehydes, ketones Solid: Amino acids after hydrolysis
$CO_2 + N_2 + H_2O$	Neutral	Primitive Earth? Venus, Mars	No synthesis	No synthesis

Source: Adapted from Raulin 2001.
RH = hydrocarbons

3.3
Sources of Prebiotic Organic Molecules

3.3.1
Endogenous Sources of Organic Molecules

3.3.1.1 Atmospheric Syntheses

Miller and Urey thought that the first building blocks of life were synthesized in Earth's primitive atmosphere. For the reasons discussed above, the gaseous mixture they chose is no longer considered to be representative of Earth's early atmosphere. Table 3.4 shows some results obtained in different "Miller-type" experiments, using different gaseous mixtures and energy sources.

Energy inputs through electric discharges represent lightning or electron inputs in the atmosphere. For example, in the case of Saturn's moon Titan, electrons trapped in the magnetosphere of Saturn cascade down into Titan's atmosphere (see Chapter 9). Photolysis experiments simulate the energetic inputs of the Sun via energetic UV photons that initiate chemical reactions. Using different energy sources but the same atmosphere led to minor differences in the resulting products.

In contrast, a high sensitivity of the resulting syntheses to the starting gaseous mixture was observed. Reducing gaseous mixtures, such as the one chosen by Miller and Urey, are the most efficient ones in the formation of complex organic structures. However, current models of the primitive atmosphere of Earth suggest a rather neutral atmosphere, and such environments are not as efficient in initiating chemical evolution as reducing ones. Figure 3.9 shows the yield in amino acids (percentage of initial C) as a function of the composition of the simulated atmosphere when performing Miller-type experiments. In a reducing atmosphere, if carbon is in a reduced state (in the form of CH_4), a large diversity of amino acids is synthesized in a rather efficient way. On the other hand, if carbon is in an oxidized

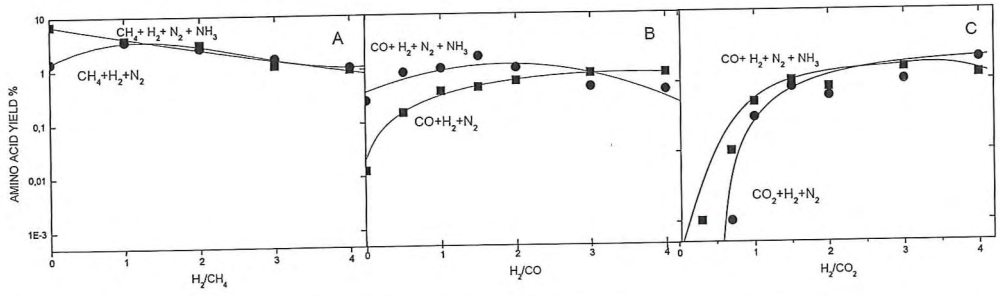

Fig. 3.9 Amino acid yield (percentage of initial C) as a function of the simulated atmosphere composition in Miller-type experiments, performed at room temperature and in the presence of liquid water. Results were obtained after 2 days of electric discharge experiments. Partial pressure of N_2, CO, or CO_2 was 100 Torr (131 hPa). (A) A great diversity of amino acids was produced. (B, C) Glycine predominated; little else was produced except a small amount of alanine (adapted from Miller and Lazcano 2002).

state (CO or CO_2), the amino acid glycine predominates, and the reaction yields are much lower than those using CH_4. Moreover, in the absence of CH_4, the yield of amino acids drops significantly if the atmosphere is depleted in H_2 and becomes more and more neutral.

Therefore, if the Earth mantle was less oxidized 3.8 billion years ago than today, an important amount of CH_4 could have been emitted through volcanism. In this case, endogenous Miller-type syntheses are possible. It has been estimated that depending on the redox state of the atmosphere, the endogenous production could vary by several orders of magnitude, leading to a steady-state concentration of organics in primitive oceans ranging from 0.4 10^{-3} g L^{-1} to 0.4 g L^{-1}. However, it must be stressed that to date the actual amount of reduced gas in Earth's primitive atmosphere is not known.

3.3.1.2 Hydrothermal Vents

The synthesis of organic compounds at the bottom of the ocean in hydrothermal vents (also known as black smokers; Fig. 3.10) has to be considered as another endogenous source of prebiotic molecules. Where oceanic plates drift apart, seawater circulating through the ocean crust is heated up, and it dissolves and exchanges chemicals with the rock. At some places it springs back to the ocean from black smokers at a high temperature, enriched in gas, ions, and minerals. Catalytic clays and minerals interact with the aqueous reducing environment rich in H_2, H_2S, CO, CO_2, and CH_4 (and possibly HCN and NH_3). When exhausted from the vent, the dramatic drop in temperature, from 350 °C to about 2 °C, favors chemical reactions and polymerizations.

It has been shown experimentally that amino acids can be synthesized in such conditions (high temperature and pressure, reduced environment, and rich in minerals, which can act as catalyst). But one has to take into account that molecules synthesized in the vicinity of black smokers can also be destroyed because of the high temperature. Nowadays, a volume equivalent to the world's entire ocean

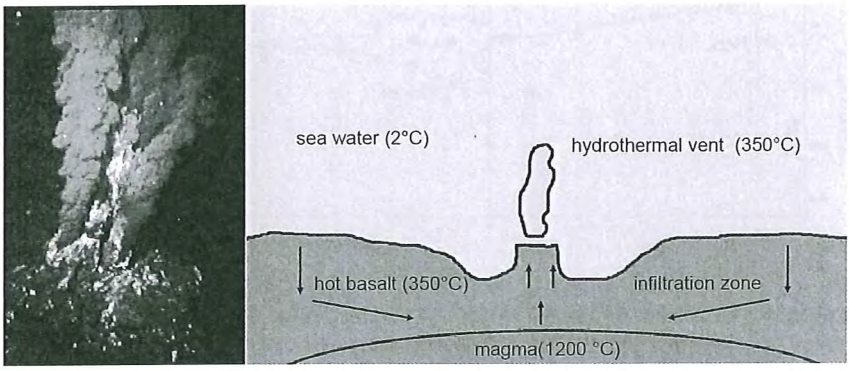

Fig. 3.10 Hydrothermal vents (photograph on the left courtesy of NOAA).

system circulates through hydrothermal vents every 10 million years. Their presence would have fixed an upper limit on the concentration of organics in the primitive ocean. More experimental data and field measurements are required to assess the feasibility of this mechanism.

3.3.2 Exogenous Delivery of Organic Molecules

Remote sensing observations have given evidence that organic chemistry is very active in interstellar molecular clouds, as much in the gaseous phase as in the solid phase (interstellar ices) (see Chapter 2). HCN, HC_3N, and HCHO have been detected. Such molecules are of great astrobiological interest, as will be discussed in Section 3.4. Our Solar System is thought to be the result of the collapse of such a cloud.

Laboratory experiments simulating the conditions in the molecular clouds predict the existence of molecules that are much more complex than the ones already detected by remote sensing. These experiments aim to reproduce the chemistry occurring in interstellar ices. For this, gaseous mixtures consisting of simple volatile compounds (H_2O, CO, CO_2, CH_4, NH_3, CH_3OH, H_2CO, and others), which have been detected in interstellar environments, are introduced into a cryostat. These molecules then condense onto a cold finger where they form an icy mixture. If exposed to irradiations (either photons or charged particles) or to thermal cycles, chemical reactions between these simple compounds, which the ice is made of, lead to the formation of much more elaborated organic structures, which remain solid at room temperature. This refractory residue was called "yellow stuff" by Mayo Greenberg, the astrophysicist who conceived these laboratory experiments in the late 1970 s. From those simulations, one can infer that in molecular clouds a large amount of organic matter should be frozen on condensation nuclei made of silicates (Fig. 3.11).

3.3.2.1 Comets

It is generally accepted that during the formation of our Solar System the original composition of interstellar grains was lost, because they were either incorporated in the Sun or planets or pyrolyzed in locations close to the Sun. Turbulent radial

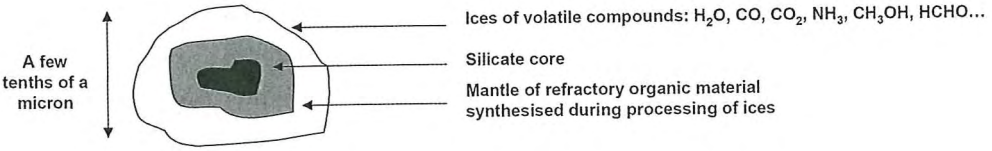

Fig. 3.11 Interstellar grain model: silicate core embedded in a mixture of complex refractory molecules, coated with ice of volatile compounds.

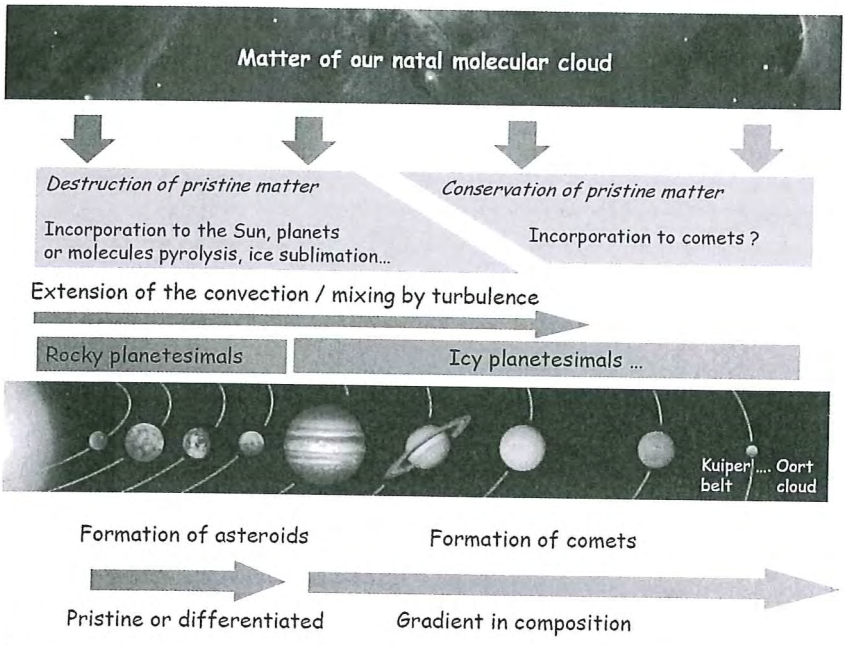

Fig. 3.12 Scheme of the evolution of matter in our Solar System: from a natal molecular cloud, the Solar Nebula, until its incorporation into Solar System bodies (Molecular cloud background courtesy of NASA, Solar System background courtesy of ESA).

mixing in the Solar Nebula can bring interstellar ices to the warmest parts of the nebula where they would sublimate (Fig. 3.12). Inside the turbulent region, radial mixing brings interstellar grains close to the Sun, resulting in a loss of their initial composition. According to models, this turbulent region of the Solar Nebula might have extended up to the orbit of Neptune (about 30 AU). Beyond this region, grains might have remained in a cold environment and thus might have kept an unaltered interstellar composition. Hence, the extension of the turbulent region determines the chances of keeping pristine interstellar matter in small, undifferentiated icy bodies: the comets.

Cometary models consider that interstellar organic matter undergoes different levels of transformation before it will be stored in comets. In some models, comets are considered to be aggregates composed of unaltered interstellar grains. From a rather different point of view, comets are considered to be made of matter completely reprocessed in the Solar Nebula. Other models consider an intermediate scenario, which is probably the more realistic one.

Putting aside the discussion about the origin of cometary matter, observations show an undeniable abundance of a large variety of organic compounds in comets. Molecules such as HCN, HCHO, or HC_3N, which have been detected in several comets, might have an origin in the interstellar medium or might have been

produced inside the Solar Nebula. In either case, they are of the same astrobiological interest.

In 1961, John Oro calculated the amount of organic molecules that could have been delivered to the Earth via comets as follows: if one considers a typical cometary nucleus with a density of 1 g cm^{-3}, a comet 1 km in diameter would contain about 2×10^{11} moles of HCN. This amount is equivalent to about 40 nmoles cm^{-2} of HCN distributed over Earth's surface. It corresponds to an amount comparable to the yearly production of HCN by electric discharge in a CH_4-rich reducing atmosphere.

As predicted in laboratory simulation experiments, *in situ* measurements in close vicinity to the comets 1P/Halley (in 1986) and 81P/Wild 2 (in 2004) bear witness to the existence of more-complex structures that – because of their high molecular mass – remain in the solid phase on dust grains when ejected from the cometary nucleus. It must be stressed that the lack of liquid water in comet nuclei over long periods of time excludes the possibility of the existence of life in or on comets – even if short periods of ice melting occur after nucleus formation caused by the decay of radioactive elements.

Summing up, comets are considered to be exogenous sources of prebiotic molecules of great astrobiological potential. This has been inferred from measurements in space as well as from laboratory simulation experiments. Therefore, comets are the target of several past, current, and future space missions, such as NASA's *Stardust* (http://stardust.jpl.nasa.gov/) and *Deep Impact* missions (http://deepimpact.jpl.nasa.gov/) and ESA's *Rosetta* mission (http://rosetta.esa.int/).

3.3.2.2 Meteorites

By definition, meteorites are celestial bodies that reach the surface of the Earth. Meteorites – more specifically, those belonging to the carbonaceous chondrite family (the most famous among them are the Murchison, Murray, and Orgueil) – are another exogenous source of organic molecules. Unlike comets, for which no direct analysis of the nucleus composition has ever been made, a large number of meteorites have been studied with the most sensitive laboratory instruments.

The current flux of meteorites is estimated to be about 10 tons per year and was probably higher on the primitive Earth. A great number of organic molecules have been detected in meteorites, such as hydrocarbons; alcohols; carboxylic acids; amines; amides; heterocycles including uracil, adenine, and guanine; and more than 70 amino acids in the Murchison meteorite. Recently, diamino acids have been found in the same object. This shows that molecules once synthesized in space are able to survive a meteorite impact.

Enantiomeric excess at the level of a few percent has been measured for some amino acids in the Murchison and Murray meteorites. This could give us a key to understanding the origin of homochirality in living organisms on Earth. Unlike comets, the parent bodies of meteorites might have gone through periods with liquid water, which might have led to more advanced stages of chemical evolution. It is interesting to note that some organic compounds extracted from carbonaceous

chondrites would spontaneously organize to form vesicles. They can be considered as a type of primitive membrane that might have been used by the very first organisms.

No space mission is currently scheduled to analyze the composition of carbonaceous asteroids, which are probably the parent bodies of chondrites. However, projects to explore a carbonaceous asteroid could certainly be planned in the years to come, and this will provide important information about the evolutionary stage of those bodies and the origin of their organic components.

3.3.2.3 Micrometeorites

Micrometeorites are another vector for exogenous delivery of organic molecules. With an asteroidal or cometary origin, their current flux is estimated to be about 20 000 tons per year. They slowly sediment in the terrestrial atmosphere and thus undergo little warming that could destroy their organic content. Amino acids have been detected in micrometeorites collected in Antarctica. Therefore, they could also have played an important role in the origin-of-life process.

3.3.3 Relative Contribution of the Different Sources

The three different types of exogenous delivery of organic matter to the early Earth, i.e., by comets, meteorites, or micrometeorites, occurred not only on the Earth but also throughout the Solar System. However, in order to reach an increased level of complexity that could have led to life, those ingredients require liquid water.

Unlike endogenous sources of organics, as inferred by Miller-type experiments and the hypothesis of black smoker syntheses, which are still at an experimental and conceptual level, exogenous deliveries are actually observed even nowadays. The contribution of the atmosphere as an endogenous source of organics is still model dependent, and the contribution of hydrothermal vents to produce and destroy organics lacks experimental data, whereas the exogenous delivery of organics is an ongoing process.

A clear distinction of the relative contribution of each source cannot be established and seems to be out of reach as long as no other life forms are detected on another planet that would be deprived of one or two of these factors. Only then could it be said that one source is not essential. On the other hand, non-detection of life on a planet with liquid water and at least one of the three factors could lead to the conclusion that one specific source of organics is not sufficient for the origin of life. But from an Earthling point of view, we can say that too many cooks can't spoil the prebiotic soup and that the processes leading from the rather simple building blocks of life discussed in this section to more elaborated structures are more interesting.

3.4
From Simple to Slightly More Complex Compounds

In this section, the chemical pathways to synthesize the building blocks of life in a test tube are described. Some of the mechanisms presented here are already familiar to students of chemistry or biology, although they generally are not presented from an astrobiological perspective. Students in other fields should not be afraid of the reactions presented here and should retain that simple mechanisms explain the production of most of the molecules considered essential to life.

3.4.1
Synthesis of Amino Acids

The synthesis of amino acids has been known since 1850 and was discovered by Adolf Strecker. The mechanism is now well established (Fig. 3.13) and proceeds in liquid water as follows:

- In the first step, the addition of ammonia to aldehyde produces an imine.
- In the second step, the addition of HCN onto the imine produces an α-aminonitrile.
- In the final step, the hydrolysis of the -CN function (nitrile) into $-CO_2H$ (carboxylic acid) leads to the production of an amino acid.

In works published after the release of his first results in 1953, Stanley Miller showed that the production of amino acids during his experiments followed the

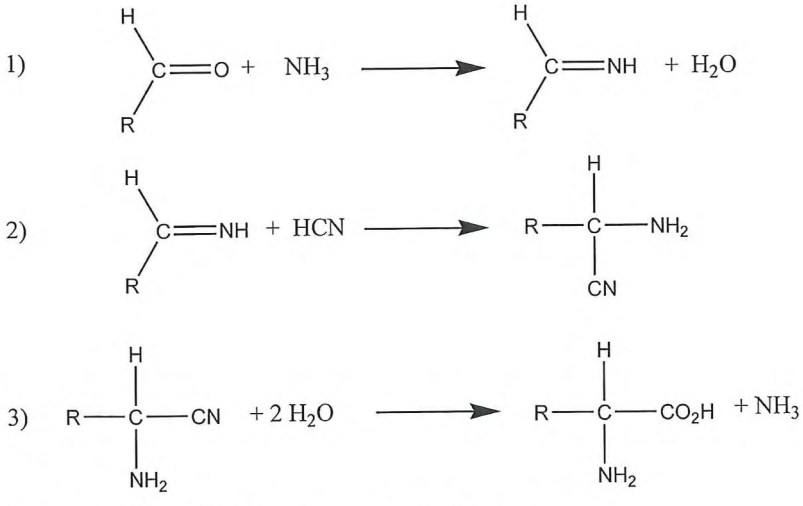

Fig. 3.13 Synthesis of an amino acid through Strecker synthesis, with H_2CO, NH_3, and HCN.

same synthesis processes (see Fig. 3.13). Other pathways are also possible, because it has been shown that an acid hydrolysis of HCN polymers results in the production of various amino acids.

3.4.2 Synthesis of Purine and Pyrimidine Bases

Synthesis of the purine base adenine follows a spectacular prebiotic synthesis pathway that proceeds by oligomerization of HCN in aqueous solution under the influence of photons of 350 nm. This process was discovered by James P. Ferris and Leslie Orgel in 1966 (Fig. 3.14). It proceeds as follows:

- In the first step, the addition of four HCN compounds results in the formation of diaminomaleonitrile (DAMN).
- In the second step, a first-photon-step rearrangement of DAMN results in the formation of diaminofumaronitrile and then a second one in the formation of aminoimidazole carbonitrile.
- In the last step, the addition of a fifth HCN molecule leads to the production of adenine.

It is quite stunning to imagine that one of the most poisonous organic compounds, HCN, reacting with itself may result in the formation of one of the "letters" of the genetic code, i.e., adenine, which is essential for life. Such are the ways of chemistry.

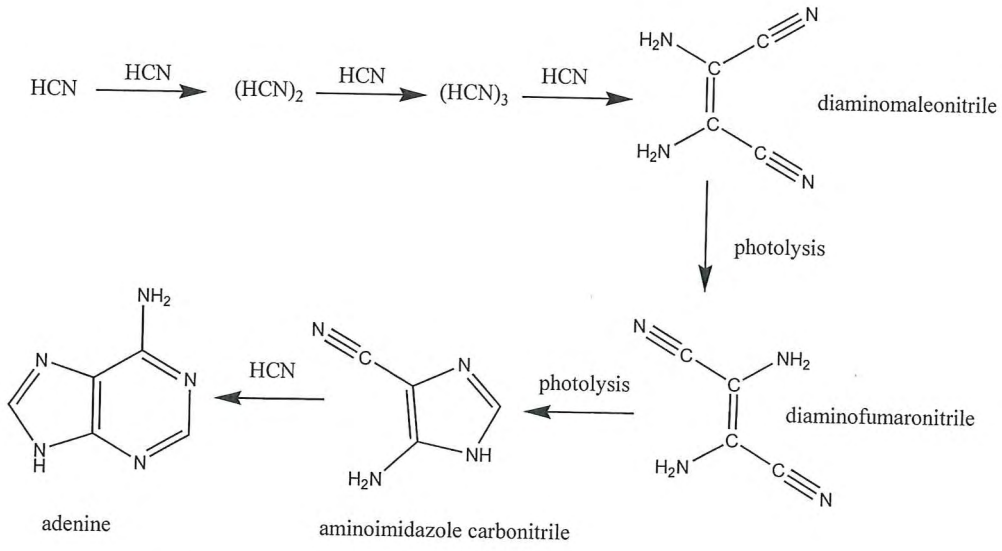

Fig. 3.14 Synthesis of adenine from HCN.

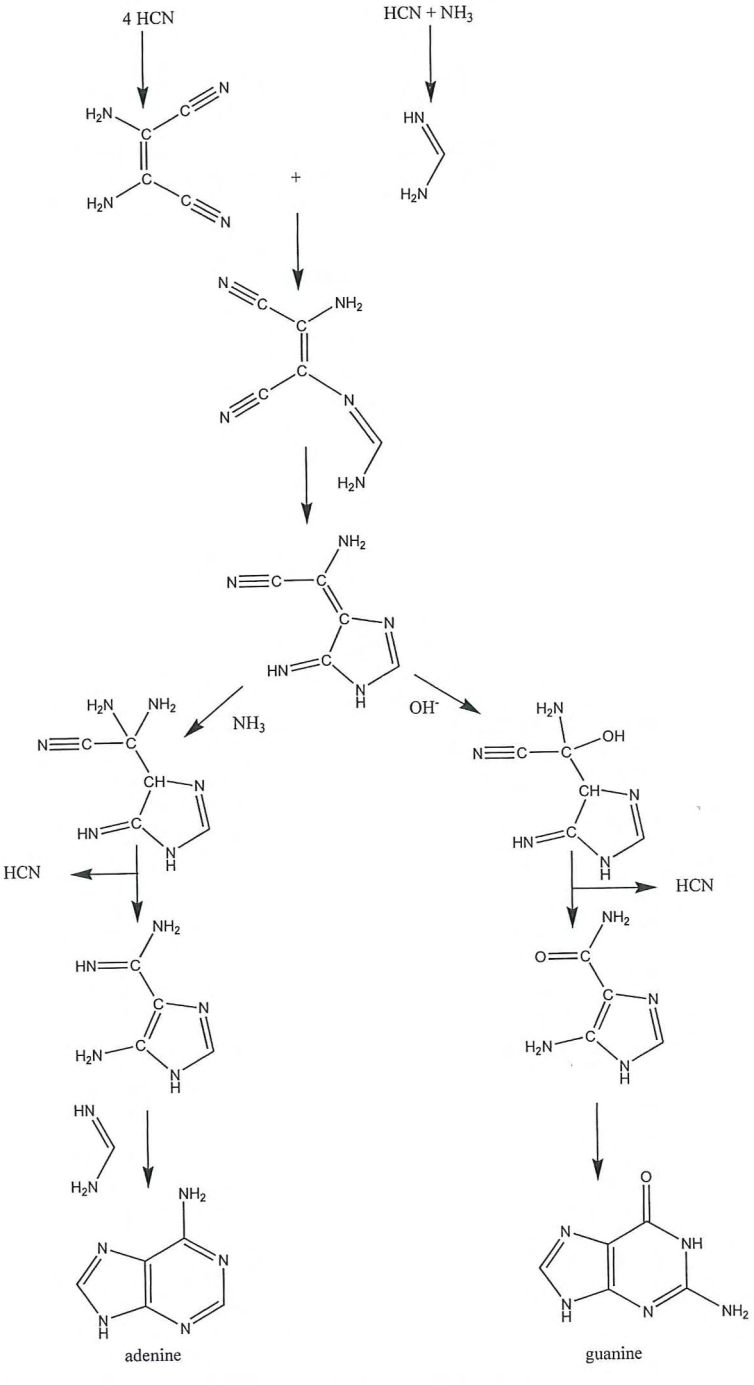

Fig. 3.15 Synthesis of adenine and guanine from HCN and NH_3.

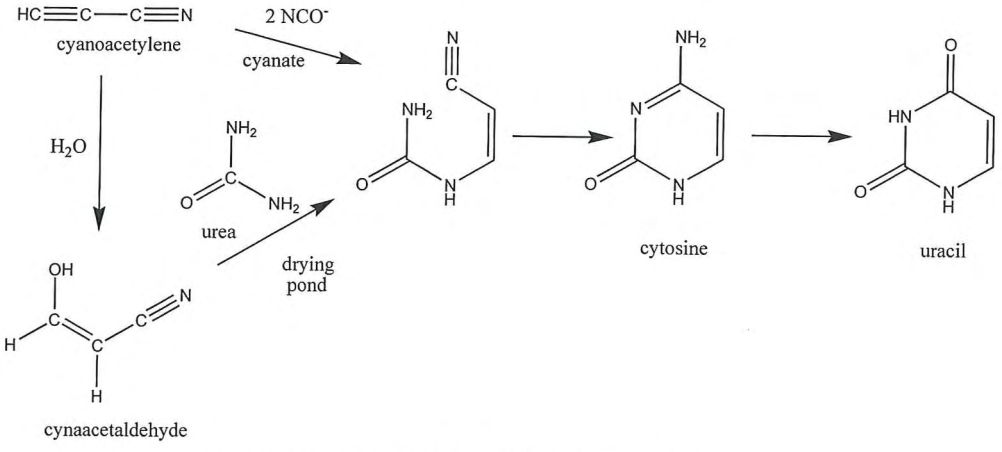

Fig. 3.16 Synthesis of cytosine and uracil from cyanoacetylene (HC_2CN) and cyanate (NCO^-).

Other pathways leading to the synthesis of purine bases are now known, such as the ones presented in Fig. 3.15. In this example, a mixture of HCN and NH_3 leads to the production of adenine and guanine.

Prebiotic pathways leading to the formation of pyrimidine bases have also been investigated, such as the ones presented in Fig. 3.16. It is interesting to note that cyanoacetylene (HC_3N), the main reactant of the synthesis, is a compound detected in the interstellar medium and comets and is also efficiently produced by the action of spark discharges in CH_4/N_2 mixtures.

The direct reaction of HC_3N with cyanate (NCO^-) gives quite low yields of pyrimidine products, or it requires a quite large concentration of cyanate (>0.1 M) for higher yields. In 1995, Robertson and Miller showed that after hydrolysis and formation of cyanoacetaldehyde, the reaction with urea in an evaporating solution (simulating primitive drying lagoons on Earth) forms a noticeable amount of cytosine.

These are only a few illustrations of reactions that lead to the production of purine and pyrimidine bases in prebiotic conditions. It is quite reasonable to believe that not all the pathways have been discovered yet, but the synthesis of these important compounds is not yet considered a problem for the chemists studying the origin of life.

3.4.3 Synthesis of Sugars

Synthesis of the sugars required for the backbone of RNA and DNA molecules is more difficult than that of the previously discussed compounds. Actually, it is not complicated to abiotically produce sugars. Butlerov found a simple way to obtain sugars as early as in 1861. This reaction is now known as the "formose reaction"

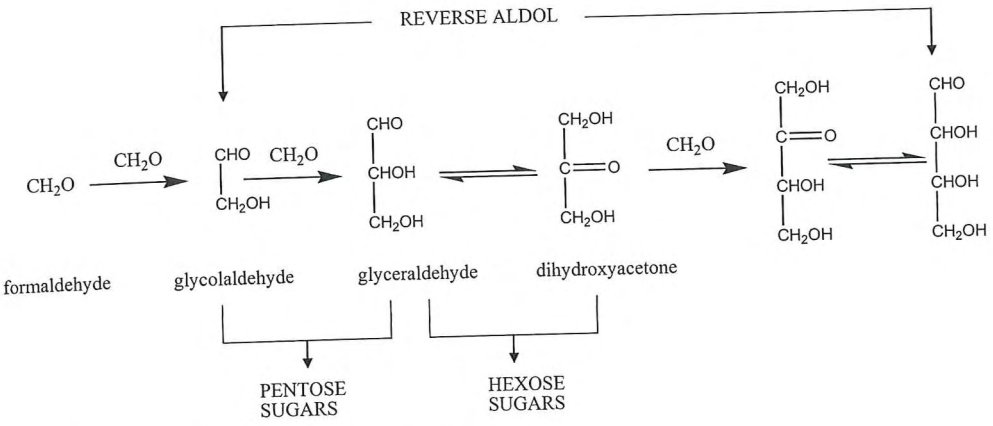

Fig. 3.17 Synthesis of sugars through the formose reaction from H_2CO.

(Fig. 3.17). It requires a concentrated formaldehyde solution and a suitable catalyst, such as calcium hydroxide $Ca(OH)_2$, calcium carbonate $CaCO_3$, or clay minerals.

The formose reaction results in a mixture of many kinds of sugars (more than 40 species), in which ribose is present at only a very low level. Hence, the formose reaction, although highly efficient, leads to an unspecific production of sugars.

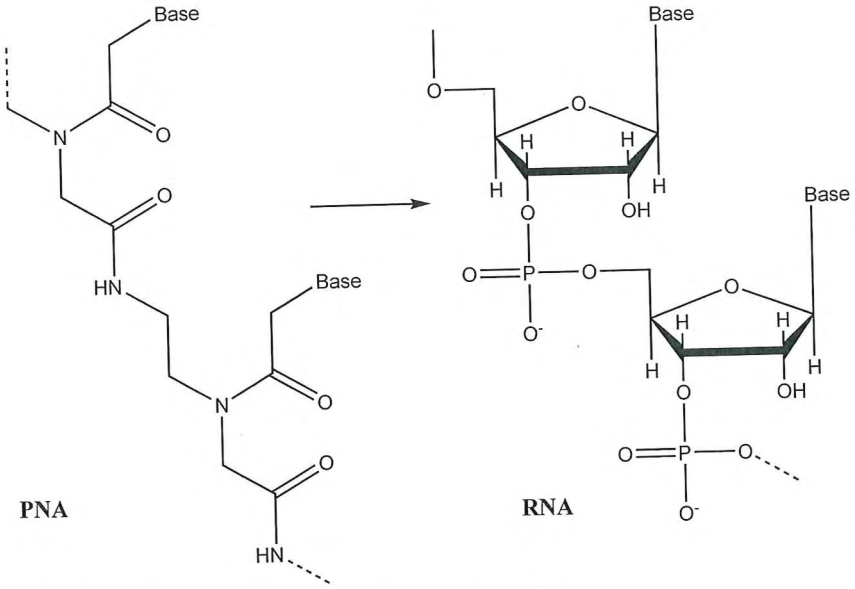

Fig. 3.18 Structure of PNA, a hypothetical information-bearing molecule based on peptides, and of RNA.

This makes it less interesting from an astrobiological point of view. Moreover, the formose reaction needs a concentrated solution of formaldehyde, which is not very relevant for the conditions of the primitive Earth. However, with the use of a proper catalyst, e.g., the clay mineral kaolin, sugars including ribose can be obtained from lower concentrations (0.01 M) of formaldehyde.

Therefore, in the frame of the RNA world hypothesis (see Chapter 4), the question of why ribose among other sugars has been selected remains open. Because it is so complicated to find a suitable pathway for the prebiotic selective synthesis of ribose and to understand how ribose was selected among other sugars, alternative solutions have been suggested, such as a pre-RNA world. This could be based, for example, on peptide analogues of nucleic acids, which are called "peptide nucleic acids" (PNAs) (Fig. 3.18), in which the sugar would be replaced by amino acids. In this scenario, ribose would be incorporated into the structure of life's informational molecule at a later stage.

3.4.4 Synthesis of Polymers

It has been shown in the previous sections that chemistry is not without solutions to explain how the building constituents of life could have been synthesized abiotically. The next step would be to associate the prebiotic elements into complex biochemical material such as polypeptides (proteins) and polynucleotides (RNA and DNA). Here, prebiotic chemistry faces a further challenge.

The linkage of amino acids to peptides is not favored from an energetic point of view. The free enthalpy for the association of alanine (Ala) with glycine (Gly) is $\Delta G^\circ = 4.13$ kcal mol^{-1}. This means that the equilibrium is displaced to left and the dissociation of the di-peptide:

$$\text{H-Ala-OH} + \text{H-Gly-OH} \rightleftharpoons \text{H-Ala-Gly-OH} + H_2O \qquad (3.1)$$

$$\Delta G^\circ = 4.13 \text{ kcal mol}^{-1}$$

$$37\,^\circ\text{C, pH} = 7$$

Reaction 3.1 shows that peptide bond formation is energetically not favored. The reaction occurs in water and the equilibrium tends to be displaced to the left, because a water molecule is released during peptide bond formation.

A thought experiment might illustrate this point. If one considers starting peptide bond formation from a molar solution (1 mol L^{-1}) of 20 natural amino acids, thermodynamics says that a resulting protein of about 100 monomer units would have a concentration equal to 10^{-99} mol L^{-1}. This means that 50 times the volume of the Earth is required to get at least one protein!

Other promising ways of polypeptide formation include catalytic synthesis on mineral surfaces or evaporation–hydration cycle processes with activated amino acids, e.g., with compounds, in which the acid function of the amino acid is

replaced by an ester function. However, these pathways are still under investigation.

The abiotic production of polynucleotides is even more complicated than that of polypeptides. The reaction of a purine base with ribose in the solid state at 100 °C results in their association into a nucleoside with a yield of about 3 %. But in this case, the base is not linked to the sugar at its "natural" place (Fig. 3.6). Moreover, nucleoside synthesis with a pyrimidine base has not yet been accomplished.

As the next step, the reaction of the nucleoside with a phosphate needs to be considered. Phosphorus is present in igneous rocks as fluorapatite ($Ca_5(PO_4)_3F$) and in meteorites as chlorapatite ($Ca_5(PO_4)_3Cl$). Heating at temperatures above 100 °C leads to the association of the compounds into a nucleotide, but, again, the linkage of the phosphate does not occur specifically at the "natural" place. To date, the polymerization of nucleotides from their building blocks has not been achieved under prebiotic conditions.

3.5 Conclusions

In this chapter, the basic building blocks of life on Earth and simple ways to synthesize them under prebiotic conditions have been discussed. But, having the blocks of life does not give a living system. Jacques Reisse, a Belgian chemist working on the origin of life, says that at the present stage trying to understand the chemistry of the origin of life is like considering building a cathedral (life) but having only a pile of bricks (amino acids, sugars, purine and pyrimidine bases). Getting from the bricks to the cathedral, without a plan, an architect, or any workers (for the stones have to spontaneously combine themselves), is the challenge chemists are facing. Even if the road is tricky, many chemists have decided to devote their studies to that complicated task. Year after year new discoveries are made, but it is difficult to know how long it will take before, somewhere in a laboratory, an organic molecule synthesized under prebiotic conditions will behave like a "robot," spontaneously making copies of itself and capable of evolution. To date, it is not even possible to say if such an achievement will ever be made. What does it take to turn chemistry into biology? Many tracks have to be investigated, and crucial breakthroughs may not come from the laboratory studies but rather from the observation of other bodies in our Solar System. For example, how far does the chemistry go on Mars, Saturn's moon Titan, or the Jovian moon Europa? What does it tell us about the origin of life on Earth? These are a few of the many fascinating questions that need to be addressed in future studies.

3.6 Further Reading

3.6.1 Books or Articles in Books

Cronin, J., Reisse, J. Chirality and the origin of homochirality, in: M. Gargaud, B. Barbier, H. Martin, J. Reisse (Eds.) *Lectures in Astrobiology*, Vol. 1, pp. 473–515, Springer, Berlin, Heidelberg, New York, 2005.

Despois, D., Cottin, H. Comets: Potential sources of prebiotic molecules for the early Earth. In: M. Gargaud, B. Barbier, H. Martin, J. Reisse (Eds.) *Lectures in Astrobiology*, Vol. 1, pp. 289–352, Springer, Berlin, Heidelberg, New York, 2005.

Greenberg, J. M. What are comets made of? A model based on interstellar dust, in: L. L. Wilkening (Ed.) *Comets*, pp. 131–163, University of Arizona Press, 1982.

Maturana, H., Varela, F. J. *Autopoiesis and Cognition: The Realization of the Living*, Reidel, Boston, 1980.

Miller, S., Lazcano, A. Formation of the building blocks of life, in J. W. Schopf (Ed.) *Life's Origin*, pp. 78–112, University of California Press, 2002.

Oparin, A. I. *The Origin of Life*, Foreign languages publishing house, 1924.

Oparin, A. I. *Origin of Life*, Dover publication, 1938.

Oro, J., Cosmovici, C. B. Comets and life on the primitive Earth, in: C. B. Cosmovici, S. Bowyer, D. Werthimer (Eds.) *Astronomical and Biochemical Origins and the Search for Life in the Universe, Proceedings of the 5th International Conference on Bioastronomy* pp. 97–120, Editrice Compositori, Bologna, 1997.

Raulin, F. Chimie prébiotique: expériences de simulation en laboratoire et "vérité terrain," in: M. Gargaud, D. Despois, J.-P. Parisot (Eds.) *L'environnement de la Terre Primitive*, pp. 343–360, Presses Universitaires de Bordeaux, 2001.

Raulin, F., Coll, P., Navarro-Gonzalez, R. Prebiotic Chemistry: Laboratory Experiments and Planetary Observations, in: M. Gargaud, B. Barbier, H. Martin, J. Reisse (Eds.) *Lectures in Astrobiology*, Vol. 1, pp. 449–471, Springer, Berlin, Heidelberg, New York, 2005.

Schopf, J. W. *Life's Origin, the Beginnings of Biological Evolution*, University of California Press, 2002.

3.6.2 Articles in Journals

Botta, O., Bada, J. L. Extraterrestrial organic compounds in meteorites. *Surveys in Geophysics* **2002**, *23*, 411–467.

Cottin, H., Gazeau, M. C., Raulin, F. Cometary organic chemistry: a review from observations, numerical and experimental simulations. *Planet. Space Sci.* **1999**, *47*, 1141–1162.

Ferris, J. P., Hagan j., W. J. HCN and chemical evolution: The possible role of cyano compounds in prebiotic synthesis. Tetrahedron **1984**, *40*, 1093–1120.

Hennet, R. J.-C., Holm, N. G., Engel, M. H. Abiotic synthesis of amino acids under hydrothermal conditions and the origin of life: a perpetual phenomenon. Naturwissenschaften **1992**, *79*, 361–365.

Miller, S. L. The production of amino acids under possible primitive Earth conditions, *Science* **1953**, *117*, *528–529*.

Pascal, R., Boiteau, L., Commeyras, A. From the prebiotic synthesis of á-amino acids towards a primitive translation apparatus for the synthesis of peptides, *Top. Curr. Chem.* **2005**, *259, 69–122*.

Shapiro, R. Prebiotic ribose synthesis: a critical analysis. *Orig. Life Evol. Biosphere* **1988**, *18*, 71–85.

3.7
Questions for Students

3.7.1
Basic-level Questions

Question 3.1

Describe the Miller–Urey experiment. What did we learn from its results? What are its limitations?

Question 3.2

What are the main sources of organic compounds that are currently considered for understanding the first steps of chemical evolution towards the origin of life? Could they be the same on Jupiter's moon Europa? Why or why not?

3.7.2
Advanced-level Questions

Question 3.3

Draw a scheme describing an experiment attempting to simulate the chemistry of interstellar ices.

Question 3.4

Describe the history of a C atom, from its synthesis in a star to its incorporation into a living system on an imaginary planet harboring life.

Question 3.5

Describe the extent to which RNA molecules could be considered living systems.

Article 2

Bénilan Y. and Cottin H. (2007) Comets, Titan and Mars: Astrobiology and space projects. In Lectures in Astrobiology (eds. M. Gargaud, P. Claeys and H. Martin), pp. 347-428. Springer Verlag.

Comets, Titan and Mars: Astrobiology and space projects

Yves Bénilan and Hervé Cottin

Introduction

All the Solar System bodies were formed about 4.6 billions years ago, when a molecular cloud collapsed. The Sun, the telluric planets, the giant planets as well as their satellites, and the small bodies (asteroids and comets), were born from this material, which was probably quite homogeneously mixed in the beginning. From then, the physico-chemical evolution yielded life at least on the Earth, and also maybe on Mars or more speculatively on Europa. Thanks to space exploration, from an astrobiological point of view, we try to figure out what makes the Earth such a peculiar object that it is the only one known to harbor life, and therefore, the extent to which life may have arisen somewhere else in the universe. To date, two factors appear to be of prime importance: a source of organic molecules and liquid water, the only solvent in which advanced molecular complexity appears to be possible to achieve, a preliminary condition for life. Henceforth, space missions dealing with astrobiology questions are conceived to answer these questions:

- **What are the origin and the distribution of the organic matter in the Solar System?**
- **Does water exist or did water exist in the liquid form on other objects?**

The goal of this chapter is to briefly review space exploration dealing with three bodies with great astrobiological interest in our Solar System: comets, Titan and Mars. Each of them is located at a specific level of understanding the origin of life on the Earth, and the possibility life could arise somewhere else. Comets as exogenous sources for prebiotic molecules, Titan as a model of an atmosphere in which endogenous syntheses of such molecules are very efficient, and finally Mars, the Earth "twin-sister planet" more than 3 billions years ago, on which it is now established that liquid water once flowed, and thus which might have once harboured life.

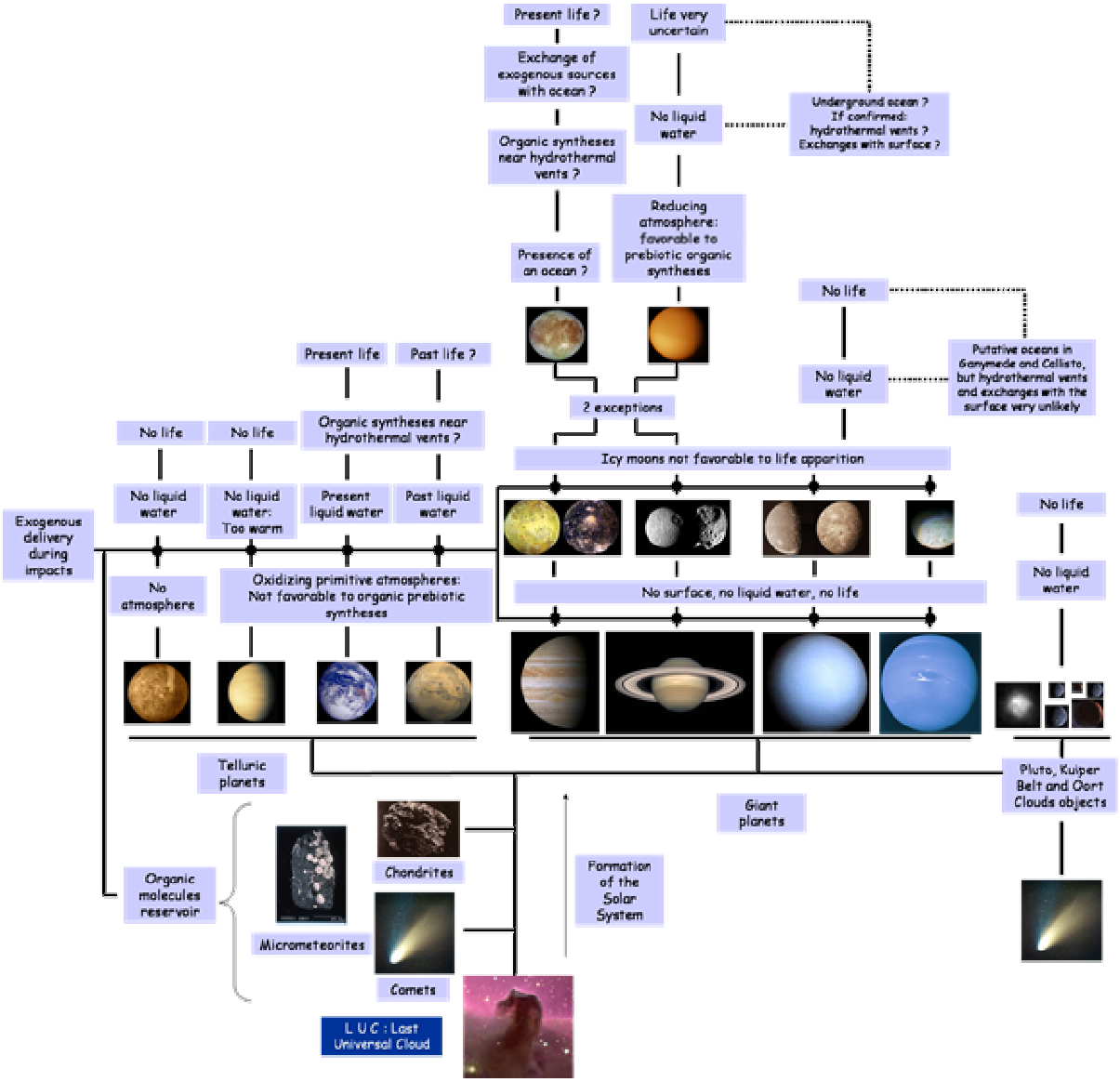

Figure 1: Astrobiological tree of the Solar System. The evolution of matter (see also Figure 3) and astrobiological relevance of Solar System objects.

1. An astrobiological look on the Solar System

1.1 The origin of the organic matter

1.1.1 The exogenous track

Figure 1 is a scheme the evolution of the matter from our natal molecular cloud, to the different objects of the Solar System. It shows, for each of them, the critical parameters that one considers to be favourable or unfavourable for life to appear on those bodies. Everything starts with the matter of a molecular cloud (Figure 1), which one might call LUC (Last Universal Cloud) as an analogy with LUCA (Last Universal Common Ancestor) the common ancestor to all living organisms on the Earth, and LUCY who once was the oldest found human ancestor. Most certainly, the molecular clouds that we are now able to observe in our galaxy show strong analogies with the composition of our natal cloud LUC. Remote sensing observations have shown that organic chemistry is very active and advanced in such clouds, as well in the gaseous phase than in the solid phase (interstellar ices) (Ehrenfreund and

Charnley, 2000). HCN, HC_3N or HCHO have been detected, and such molecules are of great astrobiological interest (Brack, 2003; Oro and Cosmovici, 1997)[1]. Moreover, a large number of experimental simulations in the laboratory predict that one might expect the existence of molecules much more complex than the ones already detected. Such experiments are simulating the chemistry occurring in interstellar ices, when submitted to irradiations (with photons or charged particles) or thermal cycles (Despois and Cottin, In press). Then, in molecular clouds, a large amount of organic matter would be frozen on condensation nuclei made of silicates (Figure 2). Some gravitational perturbation probably leads the cloud to collapse on itself, which resulted in the birth of our Sun and our planetary system.

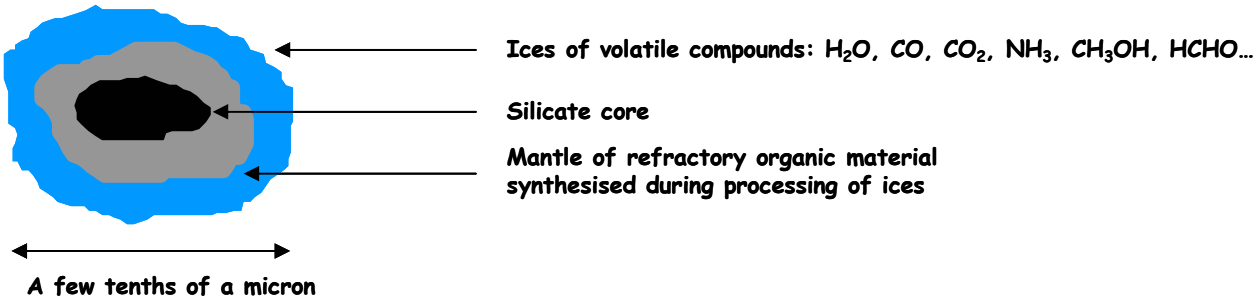

Figure 2: Interstellar grain model. A silicate core on which volatile molecules condense in molecular clouds. The chemistry between those molecules leads to the synthesis of other compounds, with enhanced complexity. Our Solar System formed with the accretion of such material. Some comets might have kept intact some of those grains.

A schematic view is to consider that the original composition of interstellar grains was lost since they have been either incorporated to the Sun or planets, or pyrolysed in the vicinity of the Sun, or interstellar ices did sublimate in the warmest parts of the nebula in which they would have been brought by turbulent radial mixing in the nebula (Figure 3). However, the extension of the turbulent region determines chances to keep pristine interstellar matter in comets. Inside the turbulent region, radial mixing brought interstellar grains close to the Sun, resulting in a loss of their initial composition. According to models, the turbulent region of the nebula can extend up to 30 AU (Bockelée-Morvan et al., 2002; Hersant et al., 2001). Beyond, grains might have always remained in a cold environment, and thus have kept an unaltered interstellar composition. Several models derive from these considerations, in which the interstellar organic matter undergoes different levels of transformation before it is stored in comets. They are sometimes considered as simple unaltered interstellar grains aggregates (Greenberg, 1982), or from a rather different point of view, as made of matter completely reprocessed in the Solar Nebula (Prinn and Fegley, 1989). Other models consider an intermediate scenario (Lunine et al., 1991), (Iro et al., 2003), which are probably more realistic (see (Despois and Cottin, In press) for more details on this topic). But however, putting aside any discussion about the origin of the cometary matter, observations of these objects shows an undeniable abundance of a large variety of organic compounds. Molecules such as HCN, HCHO or HC_3N, which have already been mentioned in this chapter, and that have been detected in several comets, keep the same astrobiological interest. Moreover, in-situ measurements in the close vicinity of comets 1P/Halley (in 1986) and 81P/Wild 2 (in 2004) bear witness to the existence of more complex structures, which remain in the solid phase on dust grains when ejected from the nucleus, due to their high molecular mass (Huebner, 1987; Kissel and Krueger, 1987; Kissel et al., 2004; Mitchell et al., 1992). The lack

[1] In liquid water HCN chemistry leads to the synthesis of amino acids and puric bases (adenine and guanine), whereas HC_3N chemistry produce pyrimidic bases, and HCHO chemistry results in sugars or amino acids (when coupled with HCN).

of liquid water flowing in the nuclei over long period of time does not allow to seriously considering the possibility of life on comets (even if short events of ice melting are possible for brief periods after the nucleus formation due to the radioactive decay of radioelements such as ^{26}Al (Podolak and Prialnik, 1997)). However, detected molecules, to which the complex molecules inferred from laboratory experimental simulations can be added, turn comets into objects with great astrobiological potential as endogenous sources for prebiotic molecules. Comets are the target of several past, current and future space missions, on which we focus later in this chapter.

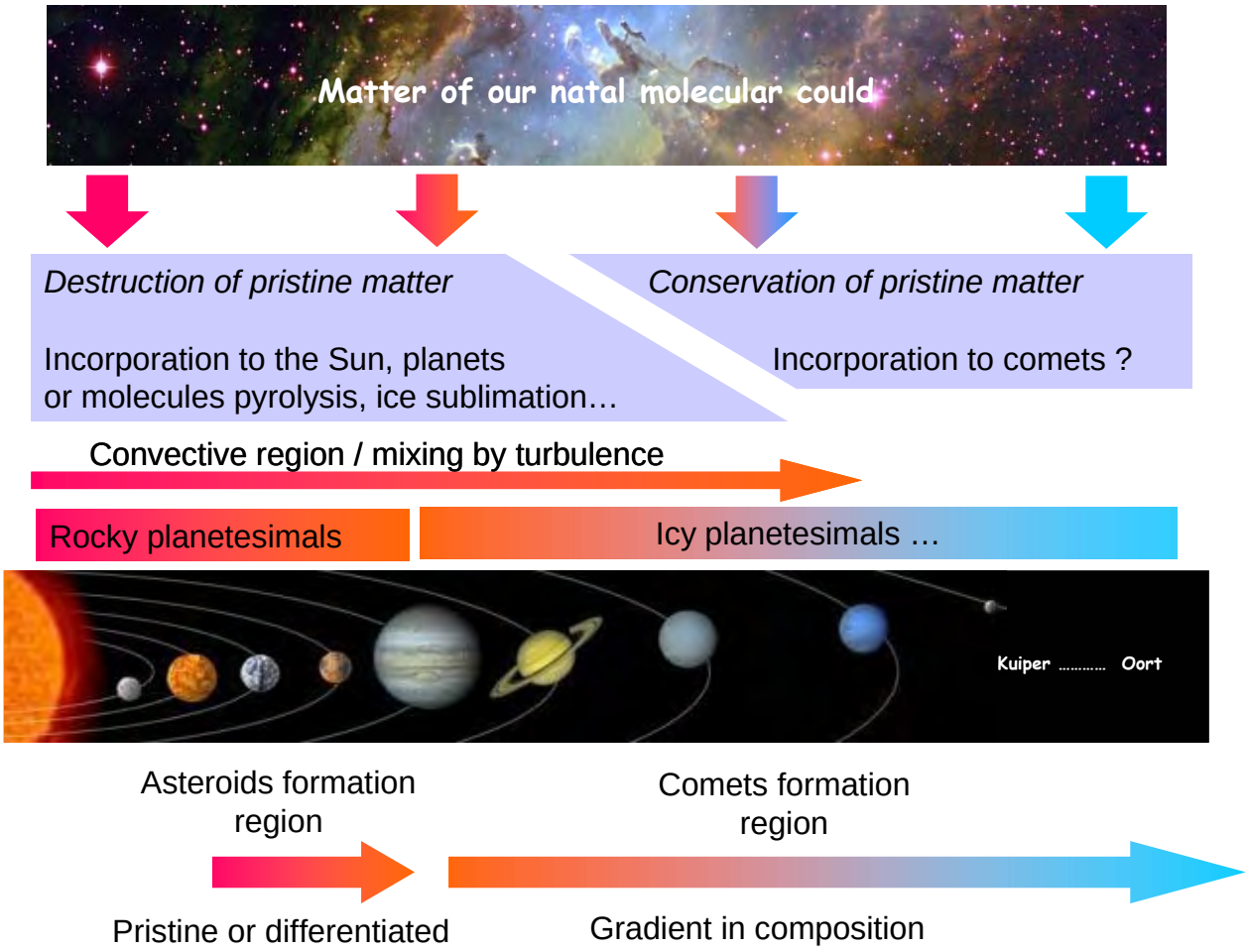

Figure 3: Evolution of the matter between our natal molecular cloud, solar nebula and incorporation to the Solar System bodies.

Nevertheless, molecules of astrobiological interest can be destroyed by the same processes that lead to their formation once synthesized in the interstellar medium or in the solar nebula (UV, charged particles, or thermal cycles). Experiments conducted in space, onboard the MIR station, or space capsules FOTON, have shown that amino acids can survive exposition to solar UVs if they are embedded in a mineral matrix (on cometary grains for example, but also in meteorites) (Barbier et al., 1998; Barbier et al., 2002; Boillot et al., 2002). After surviving a long stay in space, those molecules have to endure the energy release when comets and meteorites impact the Earth. Theoretical (Chyba et al., 1990) and laboratory (Blank et al., 2001) works have shown that amino acid can survive such collisions.

Meteorites and more specifically those belonging to the carbonaceous chondrite family are another exogenous source for organic molecules. Unlike comets, for which no direct analysis of the nucleus composition has ever been made to date, a large number of meteorites have been studied with the most sensitive instruments in Earth laboratories since by definition meteorites are bodies reaching Earth surface (the most famous among them being Murchison, Murray and Orgueil). The current flux of meteorites is estimated to be about 10 tons/year (Bland et al., 1996), and was probably higher on the primitive Earth. A great amount of organic molecules have been detected in comets (hydrocarbons, alcohols, carboxylic acids, amines, amides, heterocycles including uracile, adenine ang guanine guanine (Stoks and Schwartz, 1979; Stoks and Schwartz, 1981), more than 70 amino acids for Murchison meteorite, and recently di-amino acids in the same object (Meierhenrich et al., 2004). Those detections are evidences that molecules once synthesized in space are able to survive impacts. Enantiomeric excess at the level of a few percents have been measured for some amino acids in meteorites Murchison and Murray (Cronin and Pizzarello, 1997; Pizzarello and Cronin, 2000). This could give us a key to understand the origin of homochirality in living organisms on Earth. Unlike comets, it is clear that parent bodies of meteorites have known events with liquid water, which might have lead chemistry to reach more advanced stages of evolution. No space mission is currently developed to analyse the composition of carbonaceous asteroids, which are probably the parent bodies of chondrites. Therefore it is not in the frame of this chapter to discuss further about those objects. Our point is simply to underline the astrobiological importance of meteorites as exogenous source of complex organic material. A very detailed review dealing with organic molecules in meteorites can be found in (Botta and Bada, 2002). However, a project for space exploration of a carbonaceous asteroid will certainly be selected in the years to come, and this will give us important information about the evolution stage of those bodies and the origin of their organic component.

Micrometeorites are a last vector for exogenous delivery of organic molecules. With an asteroidal or cometary origin, their current flux is estimated to be in the order of 10 000 tons a year. They slowly sediment in the terrestrial atmosphere and thus undergo little warming that could destroy their organic content. Amino acids have been detected in micrometeorites collected in Antarctica (Maurette, 1998). Therefore, they could also have played an important role in the origin of life process.

These three different kinds of exogenous delivery (comets, meteorites and micrometeorites) did occur not only on the Earth, but also throughout the Solar System (Figure 1). However, those ingredients require liquid water to reach an increased level of complexity that could have lead to life.

1.1.2 The endogenous track

During the 50's, for the first time, Stanley Miller implements an experiment that consists in simulating the chemistry coupled between a model of the primitive Earth atmosphere and oceans. He submits a gaseous mixture made of H_2, CH_4, NH_3 and H_2O to an electric discharge that simulates storm lightning's, this mixture being connected with a warm liquid water bulb. This experiment results in the detection of a large amount of organic molecules, including several amino acids (Miller, 1953). Those measurements are the basis of the chemical evolution theory, showing that the chemistry between simple and abundant molecules (in planetary atmosphere in the case of Miller's experiment) synthesizes key compounds implied in biological process for life as we know it on Earth. The choice of a reduced atmosphere (C as CH_4 and N as NH_3) was motivated by the observations of the giant planets (detection of H_2, CH_4 and NH_3), which are supposed to have not evolved since their formation, and were therefore considered by Miller as good models for the primitive

atmosphere of the telluric planets. But it is now considered that Earth primitive atmosphere was dominated by CO_2 and N_2, just like Venus and Mars. That kind of composition does not allow syntheses of complex organic molecules, as shown in Table 1. However, if Earth mantle was less oxidized 3.8 billions years ago than today, an important amount of methane would have been emitted through volcanism (Kasting, 1993; Selsis and Parisot, 2001). In this case, endogenous "Miller kind syntheses" were possible. But to date, we don't have any indication of the amount of reduced gas in Earth primitive atmosphere. Unlike exogenous deliveries that are still observed nowadays, there's no evidence that atmospheric endogenous syntheses actually occur in Earth prebiotic environment.

However, unlike the Earth, Titan, the largest of Saturn, has an atmosphere made of nitrogen and a noticeable fraction of methane. As shown in Table 1, organic syntheses are very efficient in that kind of environment, which is confirmed by observations since the surface of Titan is hidden by a thick layer of organic aerosols resulting from N_2/CH_4 complex chemistry. Yet, the temperature of the satellite does not allow liquid water at its surface. Therefore Titan can be considered as a laboratory at the planetary scale in which we can study the level of complexity that chemical evolution can reach without any water in the liquid phase, without serious reason to consider that life might have arisen. Nevertheless, the presence of oceans is considered under a deep ice layer (Fortes, 2000), but transport between surface organics and underground liquid water is still an open issue. Titan is the goal of the European probe Huygens, which will be later developed in this chapter.

Table 1:: Organic molecules synthesized during "Miller-like" experiments as a function of the composition of the starting mixture (From (Raulin, 2001)). Compounds measured is solid phase residues are usually detected after an acid hydroysis.

Gaseous Mixture	Related planetary atmosphere	Organic products	
		Electruc discharge	Photolysis
$CH_4 + NH_3 + H_2O$ (+ H_2)	Giant planter	RH (saturated & unsaturated) HCN & other nitriles (saturated) RCO_2H H_2CO, other aldehydes Ketones & alcohols *Solid:* Amino acids & nitrogated heterocycle after hydrolysis	RH (mostly sat) HCN RCN (saturated) if N/C <1 RNH_2 if N/C >1 H_2CO, other aldehydes Ketones & alcohols *Solid*: Amino acids after hydrolysis
$CH_4 + N_2$ (+ H_2O)	Titan, Triton	RH (saturated & unsaturated) HCN & other nitriles (saturated & unsaturated) including HC_3N and C_2N_2 H_2CO, other aldehydes Ketones & alcohols *Solid:* Amino acids & nitrogated heterocycle after hydrolysis	RH (saturated & unsaturated) H_2CO & other aldehydes with low yields *Solides* : Carboxylic acids
$CO + NH_3 + H_2O$		HCN, oxygenated organic compounds *Solid*: Amino acids after hydrolysis	
$CO_2 + N_2 + H_2O + CO/H_2$	Primitive Earth ?	RH (mostly saturated) HCN, other nitriles (saturated) H_2CO, other aldehydes, ketones *Solid*: Amino acids after hydrolysis	
$CO_2 + N_2 + H_2O$	Primitive Earth ? Vénus, Mars	No synthesis	

At last, another kind of endogenous source of organic compounds has to be considered: a synthesis at the bottom of the oceans, in hydrothermal vents (also known as black smokers) (Corliss et al., 1981). Where oceanic plates are drifting apart, water infiltrates the crust and springs from black smokers at high temperature, enriched in gas (H_2, N_2, CH_4, H_2S…) and minerals. It has been shown experimentally that amino acids are synthesized in such conditions (high temperature and pressure, reduced environment, and minerals which can act as catalyst) (Hennet et al., 1992; Yanagawa and Kobayashi, 1992). But the production of such molecules is in competition with their destruction due to the very high temperatures in those environments. More experimental data and field measurements are required to asses the feasibility of this mechanism.

1.2. Follow the water

Water in the liquid state seems to be the most favourable solvent to allow molecules with an exogenous or endogenous origin to reach more evolved structures, and thus makes possible the life apparition. If the H_2O molecule is ubiquitous in the Solar System and the galaxy, it is most of the time in the gaseous phase (Venus, Mars, giant planets, interstellar medium) or the solid phase (giant planets icy moons, comets, interstellar ices). To date, the presence of water in the liquid state has only been established on the Earth. Yet, two Solar System objects are of prime interest.

1.2.1 Mars

NASA's current strategy for the Martian exploration is summarized in the expression: "Follow the water". Even if nowadays there is no evidence of liquid water on the surface of the red planet, the record of past aqueous flows can be read in the landscapes morphology, and in the composition of some minerals or rocks, which can only be formed in the presence of liquid water. A large number of space missions to Mars slowly lift the veil on its past. As we will see later in this chapter, it is now quite well established that an abundant amount of water once flowed on Mars (rivers, or even an ocean covering almost the whole northern hemisphere), and this, at a time period during which life had already appeared on Earth. Thus, a source of organic molecules (Mars primitive atmosphere being probably similar to the Earth's, the exogenous source hypothesis is the most likely) combined with liquid water, could have induced life apparition just like on Earth. However, attempts to detect organic molecules on Mars have not yet been successful. Today, these molecules and possible liquid water pockets if any, could be buried underground, and future space missions have to dig the oxidized soil of the planet to add a new dimension to our knowledge of Mars. If life developed on Mars, independently from the Earth[2], this could mean that the jump from chemistry to biology is written in the laws of organic matter "natural" evolution each time the requirements "organic matter + liquid water" are fulfilled.

1.2.2 Europa and the icy moons of the giant planets

Observations of the jovian satellite Europa from the space probe Galileo lead to an accumulation of data that converge to the hypothesis of the presence of an ocean buried under

[2] It is also possible that life appeared on only one of the two planets, and then was exported to the other (Martian meteorites have indeed been collected on Earth showing that such a travel is feasible, one of these meteorites contains very controversial hints of past microbial activity: ALH 84001). Experiments implemented in space have shown that some microorganisms can survive such interplanetary journey.

its icy surface (morphological clues (Carr et al., 1998), detection of a magnetic field (Kivelson et al., 2000), and hydrated salts at the surface (McCord et al., 1999)). The ocean would be created by the heating of the planet due to Jupiter gravity field, which puts Europe out of shape and induce important stresses in ices. It could be a hundred of kilometres deep and would be covered with an icy layer of 10 to 50 km thick (Figure 4) (Sotin et al., 2002), which casts the feasibility of a submarine exploration mission into rather distant future. Nevertheless, an external exploration mission is currently considered to confirm the presence of an ocean under the ices of Europa: JIMO (Jupiter Icy Moons Orbiter). In case of selection by NASA, it should not be launched before 2012[3].

But the association between this liquid water and a source of organic molecules is still problematic on Europa. According to the thickness of the ice layer, exchanges between exogenous deliveries at the surface and the ocean are possible but could be very limited (Pierazzo and Chyba, 2002; Schenk, 2002). Concerning endogenous sources, in the absence of an atmosphere, organic syntheses in the black smokers' vicinity could be the only way to synthesise prebiotic compounds. Indeed, theoretical models have shown that the putative ocean of Europa could be in contact with the silicate mantle of the planet. If an inner source of heat from inside the satellite does exist, hydrothermal vents could be presents at the bottom of the ocean, even if these considerations are still very speculative. Thus, a conjunction of those favourable conditions could make out of Europa another object of the Solar System currently harbouring life.

The presence of oceans is also considered inside Ganymede (McCord et al., 2001) and Callisto (Zimmer et al., 2000). However, in both cases, they would be embedded at larger depths than on Europa, and trapped between two ice layers, which do not makes possible the presence of hydrothermal vents. Ganymede and Callisto are also targets of the JIMO mission.

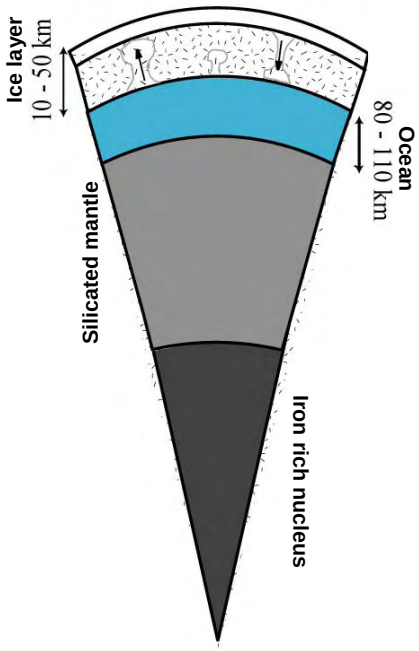

Figure 4: A representation of the internal structure of Europa (Sotin et al., 2002)

[3] For more information about JIMO : : http://www.jpl.nasa.gov/jimo/

2. The space exploration of comets

2.1. A few general considerations

As already mentioned in this chapter, comets, such as planets, are made of the matter of a molecular cloud which collapsed to give birth to our Solar System. Those icy planetesimals have not been through differentiation processes thanks to their small size. And they have been stored in the outermost, hence coldest, regions of the Solar System (Kuiper Belt and Oort Cloud). Therefore they should have kept unchanged their initial composition and thus bear testimony of the physico-chemical environment prevailing in the solar nebula region in which they accreted, or even more, some might have kept the same composition than our natal molecular cloud (Figure 3). Therefore comets are considered as the oldest archives of planetary system, as if samples of pristine matter were stored in a freezer to be preserved. A gravitational perturbation or a collision can eject a cometary nucleus out of its reservoir and place it on an elliptical orbit which will lead it near the Sun. This approach triggers the sublimation of the ices (first CO, then H_2O and other volatile compounds which are frozen far from the Sun) which lead to the formation of the cometary atmosphere (the coma) and the tails that can sometimes be seen in the naked eyes from the Earth (Figure 5) (much more about comets can be found in (Despois and Cottin, In press)).

Most of the currently available data about the composition of comets are derived from observations by teledetection methods from Earth. To date, about twenty molecules have been detected in the gaseous phase (mainly H_2O, but also CO, CO_2, CH_3OH, NH_3, HCN, CH_4, etc… (Bockelée-Morvan et al., In press) and (Despois and Cottin, In press)), but there is no direct information about the molecular composition of cometary nuclei. Those observations are the starting point for a large number of laboratory experiments, which consist in simulating the behaviour of ices made of molecules detected in the coma. Those ices are submitted to different kind of energy sources (UV photons, charged particles, thermal cycles) simulating the conditions they encountered during their history (which history can go back to long before being incorporated into comets, maybe even to the interstellar medium). Those experiments yield the production of molecules much more complex than the starting material, and are a sign of a great complexity of the nucleus in term of organic composition (Table 2). Space missions are a necessary complement to observation from the Earth and laboratory experimental simulations.

Finally, since the nucleus is hidden behind the coma, it is impossible to be observed from the Earth. If the comet is not active, the nucleus is much too far and too dark to be observed. Thus, we have the pictures of only three cometary nucleus, which have been taken from space probes (Figure 6).

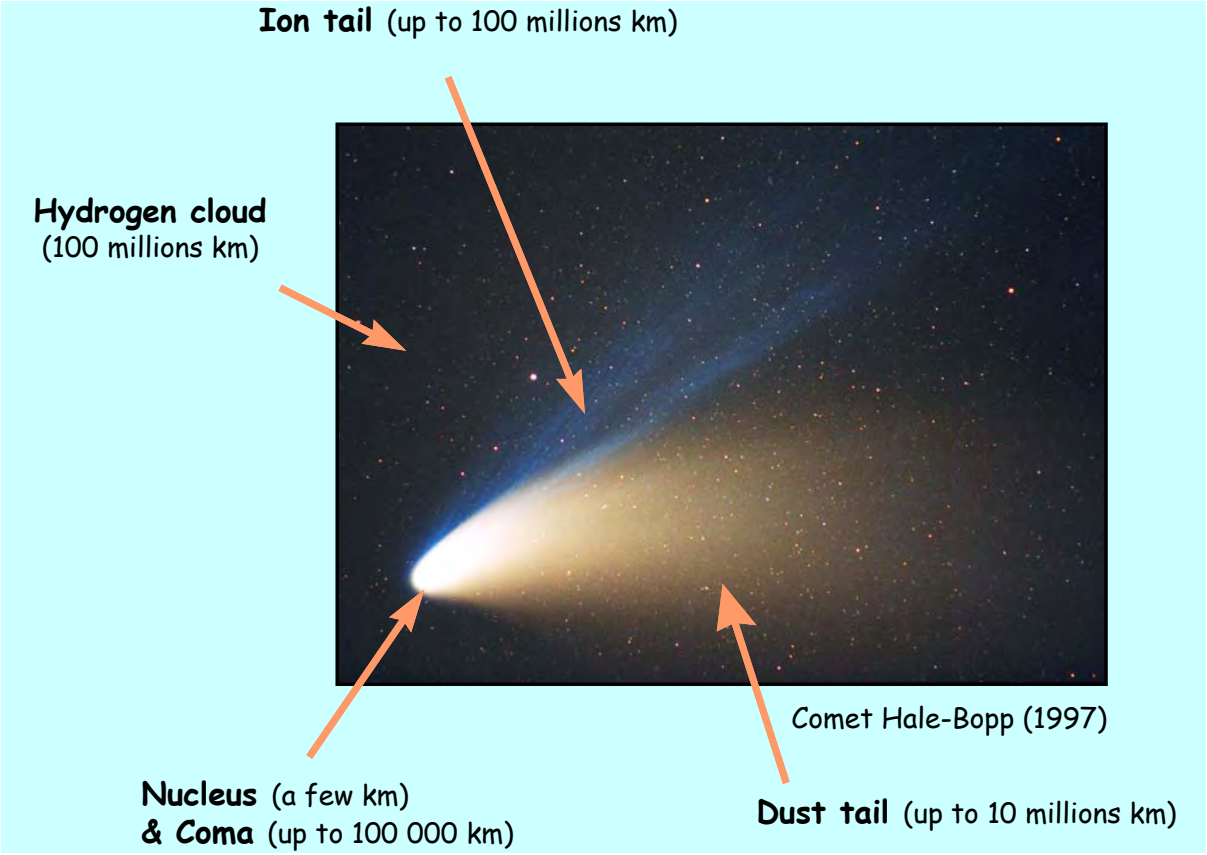

Figure 5: Structure of a comet at about 1 AU from the Sun.

Table 2: Molecules detected during experimental simulations of cometary and interstellar ice analogs. Italic letters refer to molecules actually detected in comets. (t) means tentative detection only in the analogs. Amino acids (alanine, AIB … except glycine) were detected after acid hydrolysis of the room temperature residue. Updated from Cottin *et al.* 1999.

Hydrocarbons:
CH_4
C_2H_2, C_2H_4, *C_2H_6*
C_3H_8, C_4H_{10}
C_5H_{10}, C_5H_{12}
C_6H_{12}, C_6H_{14}
C_7H_{16}

Amides:
NH_2CHO
CH_3CONH_2
$HOCH_2CONH_2$
$NH_2(CO)_2NH_2$
$HOCH_2CH(OH)CONH_2$

Amines:
$HOCH_2CH_2NH_2$
$HCNH(NH_2)$
Diaminopyrrole
Diaminofurane
Triaminopropane
$(CH_2)_6N_4$ (HMT)

Aldehydes:
H_2CO
CH_3OCH_2CHO (t)

Ketones:
CH_3COCH_3
$HOCH_2COCH_3$
$HOCH_2CH_2COCH_3$

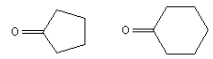

Carboxylic acids:
$HCOOH$
CH_3COOH (t)
$HOCH_2COOH$
$HOCH_2CH(OH)COOH$
$HOCH_2CH_2COOH$
$NH_2COCOOH$

Aromatic Compounds:

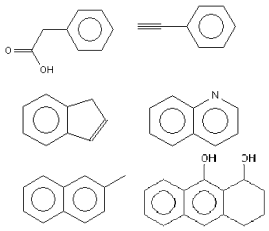

Ethers:
$CH_3OCH_2OCH_3$ (t)
$C_3H_6O_3$ (Trioxane) (t)
$(-CH_2-O-)_n$ (POM)

Alcohols:
CH_3OH
CH_3CH_2OH
$HOCH_2CH_2OH$
$HOCH_2CH(OH)CH_2OH$
$C_4H_8(OH)_2$
C_5H_9OH (t)
$C_5H_{11}OH$

Amino Acids:
NH_2CH_2COOH (Glycine)
$NH_2CH(CH_3)COOH$ (Alanine)
$CH_3CH_2CH(NH_2)COOH$ (α ABA)
$CH_3CH(NH_2)CH_2COOH$ (β ABA)
$(CH_2NH_2)(CH_3)CHCOOH$ (AIBA)
Sarcosine
Ethylglycine
Valine, Proline, Serine
Aspartic acid
Diaminopropanoic acid
Diaminobutyric acid
Diaminopentanoic acid
Diaminohexanoic acid

Esters:
$HCOOCH_3$
CH_3COOCH_3
$CH_3CH_2COOCH_3$

Others: *CO*, *CO_2*, C_3O_2, H_2O_2, H_2CO_3, N_2H_4, *HNCO*, NH_2CONH_2, $NH_2CONHCONH_2$

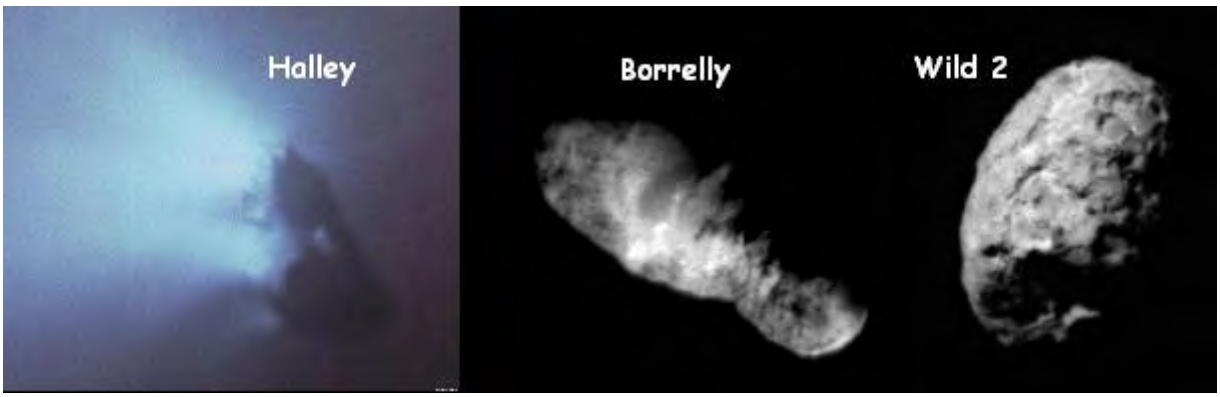

Figure 6: The three cometary nuclei observed to date: Halley from the Giotto spacecraft in 1986 (distance at picture time: ~700 km, nucleus: 4.1x4.2x8 km) © ESA/MPIfA; Borrelly from the Deep Space 1 spacecraft in 2001 (distance : 3417 km, nucleus : 3.2 x 8 km) ©NASA; and Wild 2 from Stardust in 2004 (distance : 500 km, nucleus : ~5 km) ©NASA

2.2. Past Missions

Past cometary space missions are presented in the Table 3 and Figure 7. It is not possible to summarize all the results obtained from those missions in the frame of this chapter; therefore we have chosen to focus most specifically on astrobiology related data.

Organic compounds with molecular weights higher than those observed by teledetection methods (from the Earth or from the instruments of space probes) have been detected by mass spectrometry, mainly with the PICCA instrument (part of RPA) onboard Giotto spacecraft, and PUMA instrument, onboard Vega-1. The first was dedicated to the analysis of the gaseous phase, whereas the latest was conceived to analyse the composition of cometary dust grains. The most fruitful related work have been reported in by Kissel and Krueger ((Kissel and Krueger, 1987; Krueger and Kissel, 1987). To interpret the PUMA's mass spectra, they considered that all sudden dissipation processes near solid surfaces after an impact are governed by the same rules of molecular ion formation. Such impacts occur when a dust particle hits the mass spectrometer's target. This hypothesis yields a good agreement between their predictions and other observations for small molecules (e.g.: HCN, CH_3CN). For larger molecules the problem is more complex, as they cannot survive the impact process without fragmentation. In addition to the difficulty of assembling correctly the fragments to reconstitute the original molecule, the nature of the fragments themselves is uncertain, several fragments having the same mass (to the resolution of the spectrometer). Thus the identification by these authors of purines and adenine, for example, should be considered as very tentative. However, what is clearly shown by PUMA mass spectra is that compounds with complex structure and large molecular masses (at least with m/z up to 160 $g.mol^{-1}$) are present on grains, which goes the same direction than results from laboratory experimental simulations.

On the other hand, first interpretations of the heavy-ion mass spectra from the PICCA instrument led W.F. Huebner (1987) to conclude the presence of polyoxymethylene (a.k.a. POM, the formaldehyde polymer) in comet Halley. The alternation of patterns with a ratio m/z =14 et 16 is in good agreement with the succession of $-CH_2-$ (m=14) and -O- (m=16) that constitute the polymer (Figure 9). First, Huebner's hypothesis seems to be confirmed by laboratory studies that measure POM mass spectra which are in agreement with observations ((Möller and Jackson, 1990; Moore and Tanabe, 1990)). Later, however, (Mitchell et al., 1992) showed that the mass spectrum pattern which led Huebner to announce the detection of polyoxymethylene is only characteristic of a mixing of molecules composed of C, H, O and N atoms (CHON molecules). Therefore PICCA mass spectra do not imply the presence of POM, but only of a large diversity of CHON molecules, among which POM could be present. Moreover, measurements with the NMS (Neutral Mass Spectrometer) instrument, onboard Giotto, showed that the formaldehyde in comet Halley could be produced by an extended source[4] throughout the coma of comet Halley (Meier et al., 1993). It has recently been shown that such observations can be explained by the presence of POM on grains (a few percents in mass). The polymer would be slowly decomposed into H_2CO as it is heated and photolysed (Cottin et al., 2004). Without being a final evidence for the presence of POM in comets, this polymer is so far the best explanation to this extended source. Once it is imported to Earth primitive oceans, it could be an interesting source of concentrated formaldehyde, and play a

[4] H_2CO spatial distribution in the coma is not compatible with an emission from the nucleus only. This supports the hypothesis that there is an (at least one) additional source which produces formaldehyde as it spreads outwards from the nucleus. This is what is called an extended source.

key role in the synthesis of prebiotic sugars. Table 4 shows all the molecules detected with mass spectrometry in comet Halley vicinity. Those results, even if they are not always very specific, show that comets are extremely rich in term of organic composition, and thus are of prime interest for astrobiology studies. Current and future missions have to take up the challenge of formal identification of complex molecules in comets.

Table 3: Specifications and main results for past cometary space missions

Mission	Space agency	Dates	Description and objectives	Instruments	Mains results
ISEE-3/ICE Mass : 390 kg Nominal power: 173 W	NASA	08/12/1978: Launch 1981: End of nominal mission 09/11/1985: Fly through the ion tail of comet Giacobini-Zinner	The International Sun-Earth Explorer 3 was part of a program of three probes conceived to study interactions between the Sun and Earth magnetosphere The probe was then renamed International Cometary Explorer and headed toward comet Giacobini-Zinner. The probe will maybe be captured in August 2014 and then exposed in a space museum	Instruments for measurements of magnetic fields, plasma, ions, X and γ rays.	First confirmation that comets are made of ice and dust as predicted by (Whipple, 1950) Closest Giacobini-Zinner approach: 26 650 km
SAKIGAKE Mass: 138.1 kg Nominal power: 100 W Means « Pionnier » in japanese	ISAS (Japan)	01/07/1985: Launch 03/11/1986: Comet Halley flyby	This mission is the first space probe launched independently from USA and USSR. It was mainly consisting in a feasibility study for Suisei probe, both missions being devoted to comet Halley.	Mainly magnetic fields and solar wind measurement instruments.	Was used as a distant reference point for the interpretation of the results of other probes that got closer to the nucleus. Closest Halley approach: 7 10^6 km
SUISEI Mass: 139.5 kg Nominal power: 100 W Signifie « Comète » en japonais	ISAS	08/18/1985: Launch 03/08/1986: Comet Halley flyby	Twin probe of SAKIKAGE, except for the instrument. After Halley flyby, attempts to redirect the spacecraft towards comets Giacobini-Zinner and Temple-Tuttle failed because of lack of fuel.	Mainly a UV imagery camera and a solar wind measurement instrument	Study of the hydrogen cloud around the nucleus of comet Halley. Closest Halley approach: 152 400 km. Was hit by at least two cometary grains (about 1mm in diameter) at this distance.
VEGA 1 Mass: 4920 kg (including 1500 kg for the Venusian module) Vega is a contraction between Venera (name of the soviet Venusian missions) and Gallei (Halley in russian)	USSR	12/15/1984: Launch 06/11/1985: Arrival and release of the Venusian probe 03/06/1986: Comet Halley flyby	Twin probe of Vega 2, it had two goals: to release an entry probe in the atmosphere of Venus (atmospheric balloon), and the flyby of comet Halley. Concerning comets, it was conceived to measure the physical parameters of the nucleus (size, shape, temperature and surface properties), the structure and dynamic of the coma, the composition of gas and grains, and solar wind interactions.	1 – **TVS** : Television system, 2 – **TKS** : 3 channels spectrometer, 3 – **IKS** : Infrared spectrometer, 4 – **PUMA** : Mass spectrometer for dust grains, 5 – **SP-1 & 2** : Dust particles counter, 6 – **ING** : Mass spectrometer for neutral gas, 7 – **PLASMAG** : Plasma energy analysis, 8 – **TUNDE-M** : Energetic particles analysis, 9 – **MISCHA** : Magnetometer, 10 – **APV-N & V** : Waves and plasma analysis, 11 – **DUCMA** : Dust particles detector, 12 – **MSU-TASPD** : Energetic particles analysis	Vega 1 & 2 probes were the first to accomplish comet Halley flyby. Pictures taken at that time were used to refine the final approach of Giotto spacecraft. On Vega 1 pictures two bright regions could be distinguished, and were first interpreted as two distinct nuclei (whereas it was latter established that it was indeed more active regions on the nucleus). First detection of organic molecules on grains. Closest Halley approach: 8890 km Speed relative to nucleus: 78 km/s
VEGA 2	USSR	12/21/1984 : Lauch	See VEGA 1	See VEGA 1	

Mass: 4920 kg (including 1500 kg for the Venusian module)		15/06/1985 : Arrival and release of the Venusian probe 03/09/1986 : Comet Halley flyby			Closest Halley approach: 8030 km Speed relative to nucleus: 78 km/s
GIOTTO Mass: 582.7 kg Nominal power: 196 W The name Giotto was chosen because the artist painted a comet on one of his paintings.	ESA	07/02/1985: Launch 03/14/1986: Comet Halley flyby 07/10/1992 : Comet Grigg-Skjellerup flyby	First probe of the European Space Agency. Its main goals were: (1) to collect colour pictures of the nucleus, (2) to determine the molecular and isotopic abundances in the coma, (3) to characterise the physical and chemical processes in the coma and in the ionosphere, (4) to determine the molecular and isotopic composition of cometary grains, (5) to measure the gas and dust production, and, (7) to study comets/solar wind interactions. After Halley flyby, even if some instruments were damaged (including the camera), the probe was redirected towards comet Grigg-Skjellerup.	1 – **HMC** : Halley Multicolour Camera (nucleus pictures); 2 – **MAG**, Magnetometer, 3 – **DID** : dust impact detection system (dust flux and mass measurements), 4 – **RPA** : Retarding Plasma Analyser which consists in **ESSA** : electrostatic analysis + **PICCA** : Positive Ion Cluster Composition Analyser (mass spectrometer), 5 – **JPA** : Johnstone Plasma Analyser (two instruments devoted to the study of the solar wind and charged particles), 6 – **OPE** : Optical Probe Experiment (brightness of the coma), 7 – **EPA** : Energetic Particles (electrons, protons and α particles measurement), 8 – **GRE** : Giotto Radio Experiment (electronic environment), 9 – **PIA** : Particulate Impact Analyser, 10 – **NMS** : Neutral Mass Spectrometer, 11 – **IMS** : Ion Mass Spectrometer (9,10,11 : three mass spectrometers for the analysis of gas and grains compositions)	First picture of a cometary nucleus. With a very low albedo, comet Halley nucleus is one of the darkest objects of the Solar System. The probe detected complex organic matter on grains. Halley closest approach: 596 km (14 seconds before closest approach, a large impact interrupted transmissions during 32 minutes) Speed relative to nucleus: 68 km/s. After Halley flyby, the spacecraft was covered in at least 26 kg of dust. During the encounter with comet Grigg-Skjellerup (at less than 200 km from the nucleus), Giotto was able to measure surprising variations in the magnetic field, and gathered evidences that a second nucleus might be present in the coma..
DEEP SPACE 1 Mass: 374 kg Nominal power: 2500 W	NASA	10/24/1998 : Launch 07/29/1999 : Asteroid 9969 Braille flyby 09/22/2001 : Comet Borrelly flyby	Technological mission mainly devoted to testing ionic propulsion. First objective was the flyby of an asteroid. Then, the mission was extended to the flyby of two comets: Wilson-Harrington in January 2001 and Borrelly in September 2001. Due to a failure of the navigation system, only comet Borrelly encounter was feasible.	1- **MICAS** : Miniature Integrated Camera Spectrometer (UV, Visible, IR imager), 2 – **PEPE** : Plasma Experiment for Planetary Exploration, 3 – **FGM** : Fluxgate magnetometer	Second cometary nucleus to be photographed. No water ice detected at the surface. Asteroid Braille closest approach: 26 km, relative speed : 15.5 km/s Comet Borrelly closest approach: 2171 km, relative speed: 16.6 km/s
CONTOUR Mass: 328 kg	NASA	07/03/2002: Launch 08/15/2002: Contact lost	The goal of the mission was a detailed study of three comets: Encke, Schwassman-Wachmann 3, and comet d'Arrest or another one according to new detections during	1 - **CRISP** : CONTOUR Remote Imager/Spectrograph, (Visible and infrared imager) 2 – **CFI** :	*Mission lost*

			the mission. The contact with the probe was lost during the ignition of one of the engines. It is thought that the temperature increase caused the spacecraft destruction.	CONTOUR Forward Imager (Imager and navigation), 3 – **NGIMS** : Neutral Gas Ion Mass Spectrometer, 4 – **CIDA** : CONTOUR Dust Analyzer (Mass spectrometer for dust analysis)	
Missions not dedicated to comets, but with related opportunity results					
GALILEO Exploration of Jupiter an its moons	NASA	10/18/1990 : Launch 09/21/2003 : Impact with Jupiter	Direct observation of the collision between comet Shoemaker-Levy 9 and Jupiter (July 16 to 22, 1994), which took place on the other side of Jupiter when seen from the Earth		
ULYSSE Sun exploration and more specifically its poles (out of the ecliptic plane)	ESA	06/10/1990 : Launch 05/1996 : Encounter with comet Hyakutake tails	Crossed by chance the tails of comet Hyakutake, and showed that cometary tails were much longer than expected.		

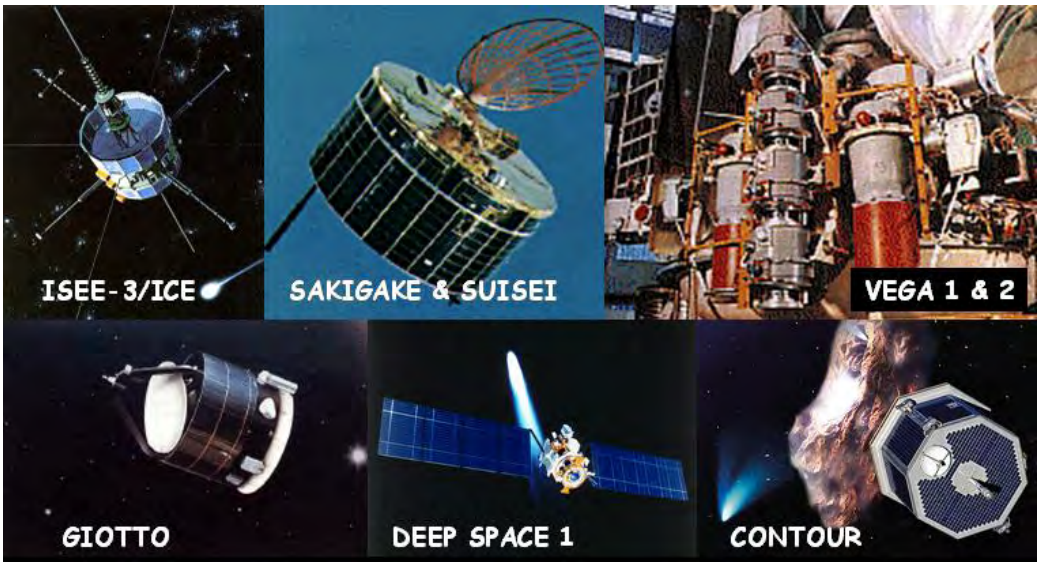

Figure 7: Past cometary missions

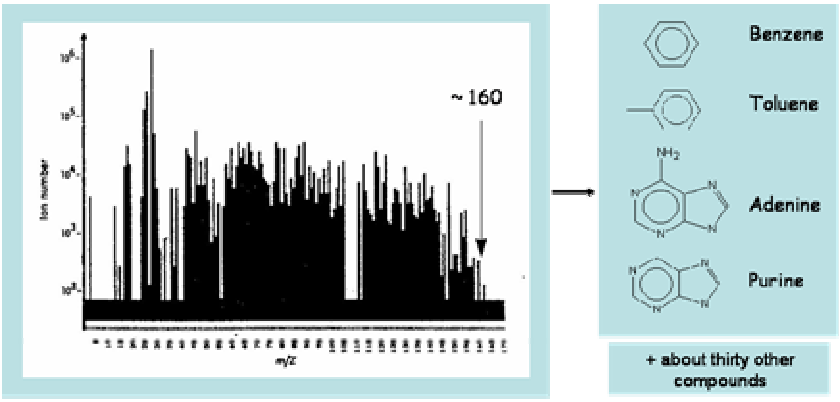

Figure 8: Cumulated mass spectra collected in comet Halley by instrument PUMA on board VEGA-1 spacecraft and tentative interpretation. Adapted from Kissel & Krueger (1987).

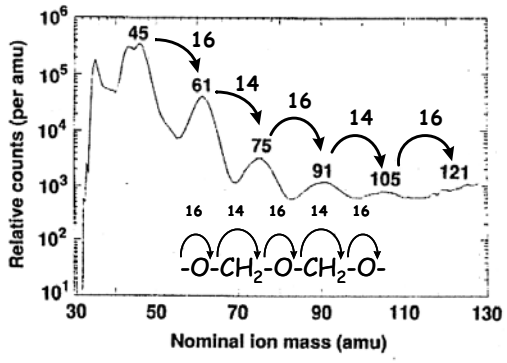

Figure 9: Mass spectrum obtained with PICCA instrument on board Giotto, Mars 14 1986. This a mean of spectra acquired between 8200 and 12600 km from the nucleus (Huebner, 1987)). Peaks near m/z=45 are saturated, and masses beyond 120 are dominated by the apparatus noise. Comparison of the results with POM structure.

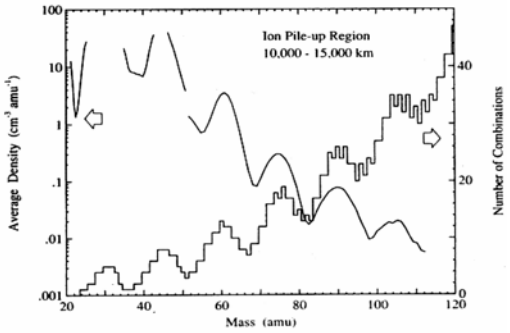

Figure 10: PICCA mass spectrum compared to the number of combinations between C, H, O, N atoms leading to a molecular ion that can be observed (Mitchell et al., 1992).

Table 4: Organic molecules inferred from mass spectra of gas and dust particles in comet Halley**.** The confidence levels of detections by MS are established as follows: - Confirmed: Molecule also detected by remote observations; - High: Molecule not detected by remote observations but present after laboratory irradiations of cometary ice analogs; - Medium: Molecule detected only by mass spectroscopy with a good confidence level according to the authors; Low: Molecule only inferred by mass spectroscopy with a low confidence level according to the authors.

Molecule	Family	Mass Spectrometer	Confidence Level	Reference
Hydrocyanic Acid	C-N-H	PUMA, PICCA	Confirmed	1, 2, 3
Methyl cyanide	C-N-H	IMS	Confirmed	7
Acetonitril	C-N-H	PUMA, PICCA	Confirmed	1, 2, 3
Methanol	C-O-H	NMS	Confirmed	6
Formaldehyde	C-O-H	PUMA, PICCA	Confirmed	3
Formic Acid	C-O-H	PUMA	Confirmed	1, 2
Acetaldehyde	C-O-H	PUMA, PICCA	Confirmed	1, 3
Ammonia	N-H	PUMA	Confirmed	2

Isocyanic acid	C-N-O-H	PUMA	Confirmed	1, 2
Ethane	C-H	NMS	Confirmed	8
Acetylene	C-H	NMS	Confirmed	8
Acetic acid	C-O-H	PUMA	High	1
Polyoxymethylene	C-O-H	PICCA	High (itself or derivatives)	4, 5
Ethene	C-H	NMS	High	8
Iminoethane	C-N-H	PUMA	Medium	1, 2
Aminoethene	C-N-H	PUMA	Medium	1, 2
Pyrroline	C-N-H	PUMA	Medium	1
Pyrrole	C-N-H	PUMA	Medium	1, 2
Imidazole	C-N-H	PUMA	Medium	1
Pyridine	C-N-H	PUMA	Medium	1, 2
Pyrimidine	C-N-H	PUMA	Medium	1, 2
Ethyl cyanide	C-N-H	IMS	Medium	7
Pentyne	C-H	PUMA	Low	1
Hexyne	C-H	PUMA	Low	1
Butadiene	C-H	PUMA	Low	1
Pentadiene	C-H	PUMA	Low	1
Cyclopentene	C-H	PUMA	Low	1
Cyclopentadiene	C-H	PUMA	Low	1
Clyclohexene	C-H	PUMA	Low	1
Cyclohexadiene	C-H	PUMA	Low	1
Benzene	C-H	PUMA	Low	1
Toluene	C-H	PUMA	Low	1
Propanenitrile	C-N-H	PUMA	Low	1
Iminomethane	C-N-H	PUMA	Low	1
Iminopropene	C-N-H	PUMA	Low	1
Purine	C-N-H	PUMA	Low	1, 2
Adenine	C-N-H	PUMA	Low	1, 2
Polyaminocyanomethylene	C-N-H	PICCA	Low	5
Methanolnitrile	C-N-O-H	PUMA	Low	1
Methanalimine	C-N-O-H	PUMA	Low	1
Aminomethanol	C-N-O-H	PUMA	Low	2
Aminomethanal	C-N-O-H	PUMA	Low	2
Oxyimidazole	C-N-O-H	PUMA	Low	1
Oxypyrimidine	C-N-O-H	PUMA	Low	1
Xanthine	C-N-O-H	PUMA	Low	1

1 (Kissel and Krueger, 1987); 2 (Krueger and Kissel, 1987); 3 (Krueger et al., 1991); 4 (Huebner, 1987); 5 (Huebner et al., 1989); 6 (Eberhardt and Krankowsky 1995); 7 (Geiss *et al.* 1999); 8 (Altwegg *et al.* 1999)

2.3. Current missions

In the infrared and radio wavelengths domain, simple organic molecules have very specific signatures, and thus, they can be detected from the Earth by remote sensing. It is not the case for complex compounds, for which low abundances and/or less specific spectroscopic signatures requires other investigation means that can be illustrated by the two current space missions dealing with comets: Stardust (sample return) and Rosetta (for which one of the instruments is a gas chromatograph).

Information about those two missions is presented in Table 5 and Figure 11. Stardust mission consists in two phases: collecting cometary dust grains with an aerogel, which is now completed, then the analysis of the grains in Earth laboratories after recovering the samples in January 2006. As far as the analysis of the molecular composition of grains and their astrobiological relevance are concerned, most of the science part will be done after the sample return. Yet, it is interesting to note that there are already evidences of the presence of complex organic material on grains thanks to mass spectroscopy measurements (CIDA instrument) (Kissel et al., 2004). However those analyses have been performed on grains that may have evolved since their release from the nucleus, and for the grains that will be analysed on Earth, one can't rule out some alteration when impacting the aerogel. Therefore measurements directly on the nucleus are necessary.

As for the Rosetta mission, it is made of two parts: one orbiter revolving around the nucleus, and a lander called Philae. The instruments onboard the orbiter will enable an unprecedented analysis of the composition of volatile and refractory compounds released from the nucleus. Three instruments (ROSINA, COSIMA and MIDAS) will collect and analyse gas and dust as close as 1 km from the surface of the nucleus, hopefully close enough to study almost unaltered matter compared to its release from the nucleus. But probably, the most fruitful information from an astrobiological point of view, will come from Philae. In this chapter, we have decided to emphasize the COSAC instrument since most of the new organic molecules should be detected thanks to this experiment.

The COSAC instrument is a gas chromatograph (GC) coupled with a mass spectrometer (MS, a linear time of flight spectrometer in this case). It consists in 8 chromatographic columns, each of them being connected to its own detector (TCD), but it is also possible to connect them to a mass spectrometer (Rosenbauer et al., 1999) (Figure 12). Previous results obtained thanks to direct mass spectrometry measurements with Puma, Giotto and Stardust spacecrafts, gave "only" the mass spectrum of the mixture of all the molecules at the same time. COSAC will carry out a preliminary separation by chromatography, which will achieve a quasi definite identification of the compounds since they will be recognised both from their retention time[5], and from their individual mass spectra. Samples will be collected after drilling the surface and heated at various temperatures before being injected into the analysis system. Pyrolysis (up to 600°C) is possible in order to degrade the most refractory component, and then enable gas phase analysis of the fragments. Out of the eight chromatographic columns, three are specifically devoted to the analysis of chiral molecules in order to distinguish enantiomers. The other five columns have been selected so that a maximum of molecules can be detected. Moreover, the simultaneous analysis of a single sample with several columns (up to four columns at the same time) will facilitate the data analysis by comparison, and thus increase the reliability of interpretation. Table 6 shows all the molecules that were considered for the selection of the chromatographic columns, and the ones that will be actually possible to detect. One can note that amino acids and other heavy compounds such as oxalic acid, urea, etc… are not detectable, since they are not volatile

[5] Time for a compound to be eluted from the chromatographic column, this time depends on the properties of both the molecules and the stationary phase of the column.

enough to be analysed in the gaseous phase. GC analysis of such compounds requires a preliminary stage called derivatization (chemical reaction which makes the targeted compound more volatile). This procedure is not feasible with the COSAC instrument, but work is in progress to include derivatization in future Martian exploration experiments (Rodier et al., 2001). Nucleus analyses by the COSAC instrument will be completed by CIVA (infrared analysis) and MODULUS (for isotopic measurements).

It is interesting to note that HMT, a molecule that is very often produced during laboratory simulations of cometary ices (Bernstein et al., 1995; Cottin et al., 2001; Muñoz Caro and Schutte, 2003), will be detected by the COSAC instrument if it is present on the nucleus. Indeed, even if this compound is easily synthesised in the conditions simulated in the laboratory, it still remains undetected in comets or interstellar medium. HMT could be a source of amino acids once imported to Earth, since its hydrolysis yield the formation of amino acids (Wolman et al., 1971). Its actual detection in comets would validate the contribution of laboratory experimental simulation to understanding the chemistry of cometary ices. On the other hand, COSAC won't be able to detect POM, another compound we already mentioned in this chapter, because it is readily degraded into formaldehyde when heated. Infrared measurements might be sufficient to detect it, but the spectroscopic signatures of this compound could be overlapped by the one of other high molecular weight organic molecules.

Thus, our knowledge in term of molecular composition of comets will do a great leap forward when Rosetta spacecraft arrive in the vicinity of comet Churuymov-Gerasimenko. According the newly detected molecules, we will be in a better position to evaluate the parameters necessary to their production, and then trace back the physico-chemical condition prevailing in the Solar System when the comet were accreted, or even more, to the composition of our natal molecular cloud. So, the astrobiology relevance of comet will be disproved or strengthened.

Table 5: Specifications and main results of current space missions

Mission	Space agency	Dates	Description and objectives	Instruments	Main results
STARDUST Mass : 300 kg Nominal Power : 330 W	NASA	02/07/1999 : Launch 2–5/2000 : 1st interstellar grains collection 7-12/2002 : 2nd interstellar grains collection 01/02/2004: Comet Wild 2 flyby and cometary grains collection 01/15/2006: Earth sample return	First mission with comet sample return: dust grains trapped in an aerogel during a comet flyby. Once brought back to Earth, their physical properties and chemical composition can be analysed with the most recent and sensitive instruments. The very low density of the aerogel should allow a progressive deceleration of dust grains, in order to minimize any alteration by heating, and pyrolysis of organic molecules. Comet Wild 2 is a relatively new comet in the inner Solar System, which passed only a few times in the sun vicinity.	1- Imagery camera, 2 – Aerogel for grains collection, 3 – **CIDA** : Cometary and Interstellar Dust Analyzer (mass spectrometer), 4 – **DFMI** : Dust Flux Monitor Instrument	Third cometary nucleus to be photographed, after Halley and Borrelly. Pictures haves shown a surprising topography: craters (probably due to the outgassing of the nucleus, which cause the surface to collapse), cliffs and pits. In-situ analysis of dust grains by mass spectrometry corroborate previous measurements on comet Halley grains, and confirm the presence of complex organics. Several thousands of grains have been collected and will be brought back to Earth early 2006. Wild 2 closest approach: 236 km

ROSETTA Mass : 1200 kg Nominal power: 850 W The name of the mission refers to the Rosetta stone that gave Champollion a crucial clue to understand Egyptian hieroglyphs. The lander was called Philae following the name of the island on which an obelisk was found. Its association with the Rosetta stone helped Champollion in his discovery. Comets are considered as the Rosetta stones that will help us in understanding the origin of the Solar System	ESA	03/02/2004: Launch 03/2005: 1st Earth gravity assist. 02/2007: Mars gravity assist. 11/2007: 2nd Earth gravity assist. 09/05/2008: Asteroid Steins flyby (distance: 1700 km). 11/2009: 3rd Earth gravity assist. 07/10/2010: Asteroid Lutetia flyby(distance 3000 km) 08/2014: orbital insertion with comet Churuymov-Gerasimenko 11/2014: Philae delivery	First mission which goal is to *land* on a cometary nucleus. It was first conceived to explore comet Wirtanen, but because of the failures of Ariane 5 launcher the mission was postponed and a new targer chosen: Churuymov-Gerasimenko. The science objectives of the mission are: (1) a global characterisation of the nucleus (dynamic properties, surface morphology and composition), (2) determination of the chemical, mineralogical and isotopic compositions of volatiles and refractories in a nucleus, as well the links between the gaseous and the solid phase, (3) study of the development of cometary activity and the processes in the surface layer of the nucleus and the inner coma (dust/gas interaction), (4) a global characterisation of asteroids (dynamic properties, surface morphology and composition)	**Instruments** **ROSETTA**: Observations: **OSIRIS**: Optical, Spectroscopic, and Infrared Remote Imaging System, **ALICE**: UV spectrometer, **VIRTIS**: Visible and InfraRed Thermal Imaging Spectrometer, **MIRO**: Microwave Instrument for the Rosetta Orbiter Composition analysis: **ROSINA**: Rosetta Orbiter Spectrometer for Ion and Neutral Analysis, **COSIMA**: COmetary Secondary Ion MAss spectrometer, **MIDAS**: Micro-Imaging Dust Analysis System Physical properties of the nucleus and the coma: **CONSERT**: COmet Nucleus Sounding ExperimenT, **GIADA**:Grain Impact Analyzer and Dust Accumulator, **RPC**: Rosetta orbiter Plasma Consortium, **RSI**: Radio Science **PHILAE** : **APX**: alpha-p-X rays spectrometer, **COSAC** : COmetary SAmpling and Composition experiment, **MODULUS** : Method Of Determining and Understanding Light elements from Unequivocal Stable isotope compositions, **CIVA/ROLIS** : Rosetta Lander Imaging System, **SESAME** : Surface Electrical, Seismic and Acoustic Monitoring Experiments, **MUPUS** : Multi-Purpose Sensor for surface and sub-surface science, **ROMAP** : Rosetta Magnetometer and Plasma monitor, **CONSERT** : Comet Nucleus Sounding

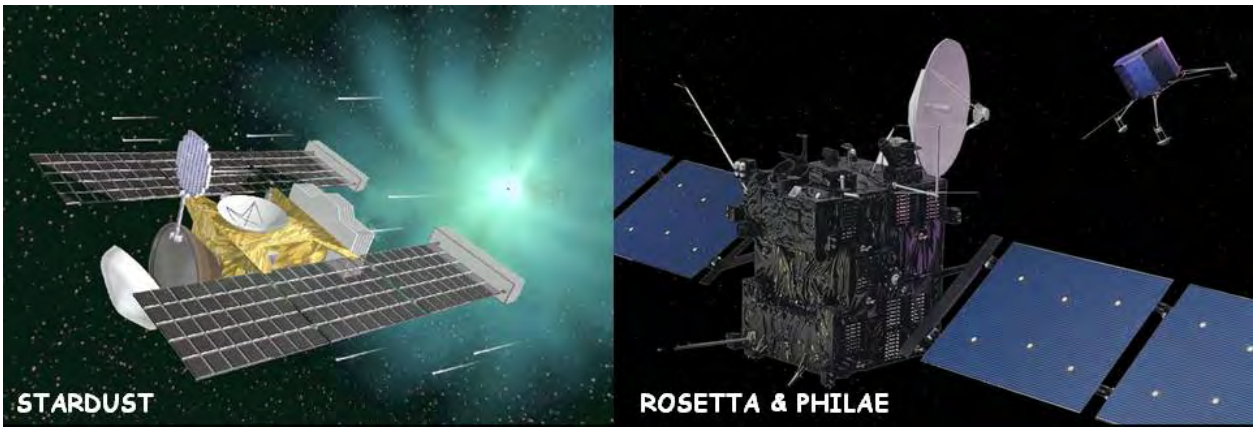

Figure 11: Current space missions

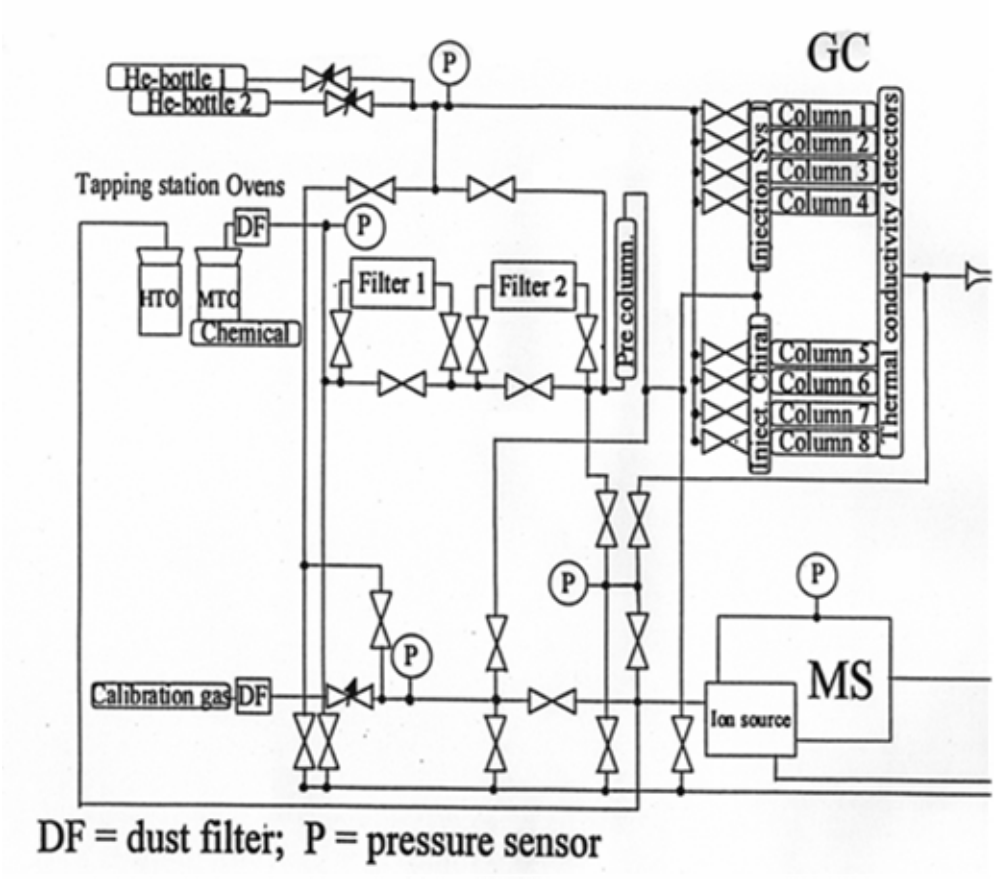

Figure 12: The COSAC experiment (Rosenbauer et al., 1999).

Tableau 6 : Organic molecules that might be detected in comets thanks to the COSAC instrument (Szopa et al., 2003).

List of the compounds considered for the study (Abbreviations: d: detected in comae; s: generated during experimental simulations; a: analysable by the COSAC GC subsystem within the space conditions; p: potentially; italic: compounds not vaporisable without decomposition)

Compounds	Formula	d	s	a
Hydrocarbons				
Methane	CH_4	x	x	x
Ethane	C_2H_6	x	x	x
Ethene	C_2H_4		x	x
Acetylene	C_2H_2	x	x	x
Allene	$H_2C_3H_2$		x	x
Propane	C_3H_8		x	x
Butane	C_4H_{10}		x	x
Pentane	C_5H_{12}		x	x
Cyclopentane	Cyclo-C_5H_{10}		x	x
3-Me-Pentane	$(C_2H_5)_2CHCH_3$		x	x
Hexane	C_6H_{14}		x	x
Heptane	C_7H_{16}		x	x
Octane	C_8H_{18}			x
Nonane	C_9H_{20}			x
Decane	$C_{10}H_{22}$			x
Aldehydes				
Formaldehyde	H_2CO	x	x	x
Acetaldehyde	CH_3CHO	x		x
Etheroxides				
Dimethylether	CH_3OCH_3		x	x
Diethylether	$C_2H_5OC_2H_5$		x	x
Dimethoxymethane	$CH_3OCH_2OCH_3$		x	x
Trioxane			p	x
Amides				
Formamide	$HCONH_2$	x	x	x
Acetamide	CH_3CONH_2		x	x
Urea	$(NH_2)_2CO$		x	
Biurea	$H_2NCONNCONH_2$		x	
Hydroxyacetamide	$HOCH_2CONH_2$		x	
Oxamide	$NH_2COCONH_2$		x	
Glyceramide	$HOCH_2CH(OH)CONH_2$		x	
Carboxylic acids				
Formic acid	HCOOH	x	x	x
Acetic acid	CH_3COOH		x	x
Oxamic acid	$H_2NCOCOOH$		x	
3-*Hydroxypropionic acid*	HOC_2H_4COOH		x	
Glycolic acid	$HOCH_2COOH$		x	
Glyceric acid	$HOCH_2CH(OH)COOH$		x	
Nitriles				
Cyanic acid	HCN	x		x
Isocyanic acid	HNC	x		
Acetonitrile	CH_3CN	x		x
Acrylonitrile	CH_2CHCN			x
Methacrylonitrile	$CH_2C(CH_3)CN$			x
Propanenitrile	C_2H_5CN	p		x
Butanenitrile	C_3H_6CN			x
Isobutanenitrile	$(CH_3)_2CHCN$			x

Compounds	Formula	d	s	a
Alcohols				
Methanol	CH_3OH	x	x	x
Ethanol	C_2H_5OH		x	x
Propan-2-ol	C_3H_7OH			x
2-Me-Propan-1-ol	$(CH_3)_2C_2H_3OH$		x	x
Butan-1-ol	C_4H_9OH			x
Pentan-1-ol	$C_5H_{11}OH$		x	x
1,4-Butanediol	HOC_4H_8OH		x	x
Ethylene glycol	HOC_2H_4OH		x	x
Glycerol	$(CH_2OH)_2CHOH$		x	x
Ketones				
Acetone	CH_3COCH_3		x	x
Hydroxypropanone	$HOCH_2COCH_3$		x	x
3-Hydroxybutan-2-one	$HOC_2H_4COCH_3$		x	
Cyclopentanone	Cyclo-C_4H_8CO		x	x
Cyclohexanone	Cyclo-$C_5H_{10}CO$		x	x
Esters				
Methyl formate	$HCOCH_3$	x	x	x
Methyl acetate	CH_3COCH_3		x	x
Methyl propionate	$C_2H_5COCH_3$		x	x
Ethyl acetate	$CH_3COC_2H_5$			x
Rare gases and inorganics				
Helium	He			
Neon	Ne			x
Argon	Ar	p		x
Krypton	Kr			x
Xenon	Xe			x
Carbon monoxide	CO	x	x	x
Carbon dioxide	CO_2	x	x	x
Ammonia	NH_3	x		x
Nitrogen	N_2	x		x
Amines				
Methanamine	CH_3NH_2			
Ethaneamine	$C_2H_5NH_2$			
2-Ethanolamine	$NH_2C_2H_4OH$		x	x
Formamidine	$HCNH(NH_2)$		x	
Pyridine	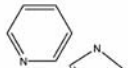	p		x
Imidazole		p		x
Pyrrole	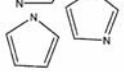	p		x
Sulfur species				
Disulfur	S_2	x		
Sulfur dioxide	SO_2	x		x
Hydrogensulfide	H_2S	x		x
Thioformaldehyde	HCHS	x		
Carbonylsulfide	OCS	x		x
Carbon disulfide	CS_2	x		x
Sulfurmonoxide	SO	x		

Compounds	Formula	d	s	a
Cis-crotonitrile	cis-$CH_3C_2H_2CN$			x
Trans-crotonitrile	trans-$CH_3C_2H_2CN$			x
Amino acids				
Glycine	NH_2CH_2COOH		x	
Alanine	$CH_3CH(NH_2)COOH$		x	
α-ABA	$C_2H_5CH(NH_2)COOH$		x	
β-ABA	$CH_3CH(NH_2)CH_2COOH$		x	
AIBA	$(CH_2NH_2)(CH_3)CHCOOH$		x	
Aromatics	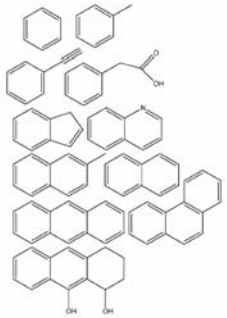			
Benzene		p		x
Toluene		p		x
Phenylacetylene			x	x
Benzeneacetic acid			x	x
Indene			x	x
Quinoline			x	x
2-Me-Naphthalene			x	x
Naphthalene				x
Anthracene				
Phenanthrene				
Dioltetrahydro--anthracene			x	

Compounds	Formula	d	s	a
Others				
Polyoxymethylene	$(-CH_2-O-)_n$	p	x	
Hydrazine	N_2H_4		x	
Carbonic acid	H_2CO_3		x	
Hydrogen Peroxide	H_2O_2		x	
Carbon suboxide	OC_3O		x	
Isocyanic acid	HNCO	x	x	
Water	H_2O	x		x
Hexamethylenetetramine			x	x

Some data about comet 67P/Churyumov-Gerasimenko:
Discovery: 1969, by Klim Churyumov et Svetlana Gerasimenko
Aphelion: 858 millions km, i.e. 5,73 astronomical units
Perihelion: 194 millions km, i.e. 1,3 UA
Mean nucleus diameter: 1 980 m

2.4. Future space missions

Only one launch of a cometary space mission is scheduled in the years to come: mission Deep Impact. However, its results will be known before Stardust sample return, and long before Rosetta reaches comet Churyumov-Gerasimenko. The main details about the mission are presented in Table 7 and Figure 13. This mission aims to gain access to the interior of a comet, and then observe what would be the most pristine matter of the Solar System ever, since cometary inside layers have been protected from irradiations and heating due to previous Sun approaches. A collision between an impactor and comet Temple 1 is planned, in order to excavate a large crater at the surface. New chemical species may be detected during the increase of outgassing after the impact, either with the onboard infrared instrument, or with other remote sensing instruments on Earth.

The next step of comets exploration will probably be a return of samples taken at the surface of a nucleus (and underneath). There is not yet such a mission under development, but proposals have already been submitted to NASA and nucleus sample return missions are to be expected to be accepted in the years to come.

As already mentioned earlier in this chapter, knowing the composition of one comet will not allow us to extrapolate the results to the whole families of comets as their composition should depend on the place they were formed (see Figure 3). Then, one shall vary our targets selections (from the Kuiper Belt, the Oort Cloud, few or many perihelion passages), before pretending to know these mysterious objects.

Tableau 7 : Futures missions spatiales

Mission	Space agency	Dates	Description and objectives	Instruments
DEEP IMPACT Mass : 650 kg + 370 kg (impactor) Nominal power: 92 W	NASA	12/30/2004: Launch 07/04/2005: Impact with comet Temple 1	The purpose of the mission is to know and characterize the inside of a comet. Its main feature is an impactor that will be launched toward comet Temple 1 and excavate a crater on its surface. During the impact the science objectives are: (1) observe how the crater forms, (2) measure its depth and diameter, (3) measure the composition of the interior of the crater and the ejectas, (4) determine the changes in outgassing after the impact. On impact, the crater produced is expected to range in size “from that of a house to that of a football stadium (~115 m), and two to fourteen stories deep (more than 30 m)”.	On spacecraft: 1 – **HRI**: High Resolution Instrument (visible and infrared) 2 – **MRI**: Medium Resolution Instrument (visible, mainly for navigation during the last 10 days of the approach) 3 – Impactor (370 kg, impact planned at about 10 km/s) On impactor: 4 – **ITS**: Impactor Targeting Sensor (Similar to MRI, visible imagery to direct the impactor and produce nucleus pictures just before the impact).
NUCLEUS SAMPLE RETURN ?	?	?	This mission would consist in landing a probe on a cometary nucleus, and then return samples for a complete analysis on Earth.	?

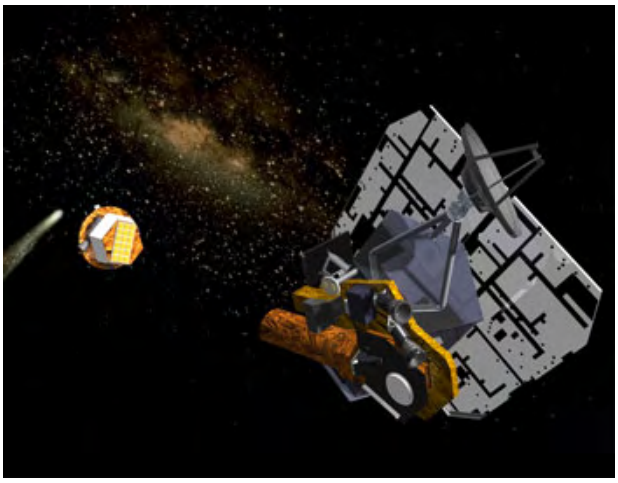

Figure 13: Deep Impact mission.

2. The space exploration of Titan

2.1. **Observations and models of Titan before space missions**

In the night of March 25th, 1655, using a refracting telescope having a focal of almost 4 meters and a magnifying power of 50, Christiaan Huygens observed for the first time a small star aligned with Saturn rings at a distance of 3 arc seconds[6]. During the following days, he makes new observations and notes the displacement of this object as compared to fixed stars and Saturn. This star follows Saturn course in the sky, and thus Huygens deduced that it has to be a satellite. He just discovered Titan.

In 1944, making spectroscopic measurements on Titan in the atmospheric window of 550 to 850 nm, Kuiper observed for the first time methane absorption bands (Figure 14). In 1965, Low (1965) made the first measurements of the flux emitted from Titan in the 10μm infrared atmospheric window. He determined a brightness temperature[7] of ~160 K. Nevertheless, it is only at the beginning of the 70's that the development of space missions and infrared detectors allow the discovery of the extraordinary rich organic chemistry occurring in the atmosphere of this satellite.

[6] Angular distance projected on the sky.
[7] Temperature of an object consider as a black body

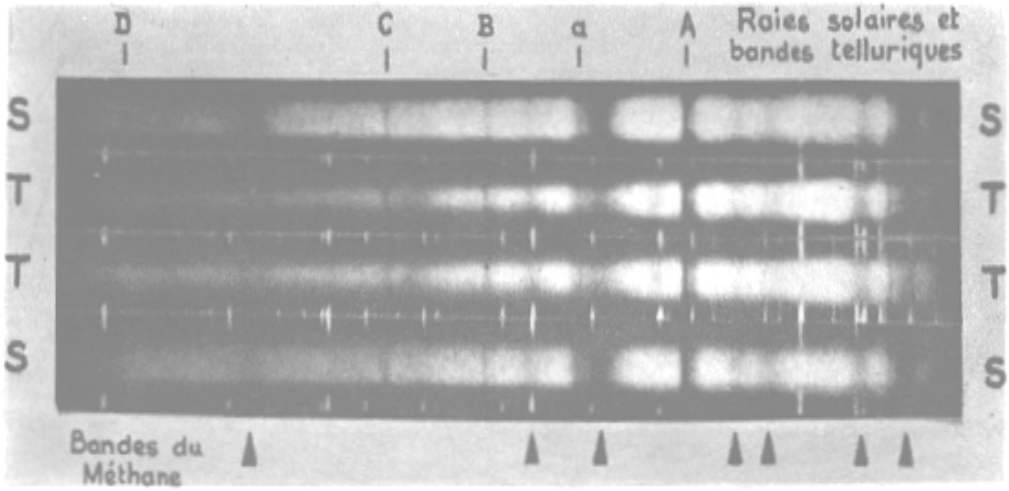

Band	Wavelenght (Å)	Origin
A	7594	O_2
a	7187	H_2O
B	6867	O_2
C	6563	Hα
D	5890,5896	Na

Figure 14 - Saturn (S) et Titan (T) spectra obtained by G. P. Kuiper, at the Mac-Donald observatory (1944) showing characteristic methane absorption bands between 5500 and 9000 Å. The wavelength calibration is given by the Fraunhofer[8] and telluric absorption bands.

From infrared observations obtained in the 8-14 μm window, Gillett et al. (1973 attributed the emissions bands to the ν_4 methane band and the ν_7 ethane band. At the same time, Trafton (1972a, b) detected traces of molecular hydrogen. On their side, Veverka (1973) and Zellner (1973) showed, analyzing polarimetric observational data, the presence of a dense and highly diffusive layer in the atmosphere. Finally, Caldwell (1975) using the OAO-2 (Orbital Astronomical Observatory) satellite, obtained photometric measurements in the ultraviolet wavelength range, around 260 nm. The albedo observed is very low, in the order of 0.05.

So, Titan's atmospheric models have to explain the high brightness temperature, a temperature inversion in the atmosphere that would explain that the infrared band of methane and ethane are in emission, the low ultraviolet albedo and the polarimetric measurements. A first kind of model, developed initially by Pollack (1973), includes a dense cloudy layer highly diffusive that would explain the visible spectrum and polarimetric data. Greenhouse effect produced by induced absorption of a 0.5 bar equimolar H_2 et CH_4 mixture, would explain the 160 K temperature. But, this model does not account for the low ultraviolet albedo and the temperature inversion. Consequently a second type of model had to be constructed. Since the Rayleigh diffusion (diffusion by the gas) cannot explain the low albedo, Danielson et al. (1973) proposed that small particles ("dust"), efficiently absorbing ultraviolet photons, are present in the high atmosphere. This hypothesis is supported by the

[8] Absorption lines visible in the solar spectra.

fact that at the same period Khare and Sagan (1973) produced in their simulation experiment (photon irradiation of a NH_3-CH_4-H_2 mixture) a brown polymer which seems to have the good optical properties to be the material composing the Danielson's dust. Thus, if such material were produce in the high atmosphere of Titan, these aerosol would have a very small size and could not reradiate efficiently the absorbed photons. Consequently, their temperature would increase until their emission equilibrates the absorbed energy. The temperature of the gas would then increase through collision with those aerosols up to the observed 160 K. In this model, the surface would have a black body temperature of 80 K.

The two models are very different one from the other but a compromise seems possible. Hunten (1978) proposed a model in which the low atmosphere is the one described by the first model and the high atmosphere corresponds to the second one. Taking into account the low gravity on Titan[9], the hydrogen amount proposed by Pollack (1973) is not realistic, it is therefore replaced by molecular nitrogen. The choice of N_2 comes from the studies on initial composition of Titan. Nitrogen could have been trapped in the ices in the form of ammonia that could then produce molecular nitrogen under photolysis. Atreya et al. (1978) calculated that, if Titan had an important greenhouse effect at the beginning of its history (T >150 K), NH_3 could have lead to the formation of 20 bars of N_2. The Hunten's model (1978) will include N_2 as main constituent (with 0.25% CH_4 and 0.5% H_2), a cloud with a highly diffusing upper part, and a high atmosphere containing dust. In this model, the tropopause is determined by the altitude where the optical depth (N_2 pressure induce absorption opacity plus cloud opacity) equals one. This region of the atmosphere is supposed to have a effective temperature of 77 K and a pressure of ~600 mbars. The surface pressure is then deduced from the adiabatic approximation from the tropopause down to the ground. This leads to a surface pressure of ~20 bars for a surface temperature of 200 K compatible with the one obtained from millimeter observations (Conklin et al., 1977). Nevertheless, radio observations in the centimeter domain where the atmosphere is supposed to be transparent, lead to brightness temperature of 100K. The main uncertainty on this measurement come from the poor angular resolution witch could lead to confusion between Titan and Saturn. Still, as pointed out by Hunten , its model could have a lower temperature: a 100K surface temperature would lead to a 2 bars surface pressure.

Finally, one can note that the photochemical model developed by Strobel (1974) with an atmosphere mainly composed of CH_4 and H_2 in same quantities (this model was initially developed for Jupiter with $CH_4/H_2<<1$), predict the production of C_2H_6, C_2H_2, and in smaller amount C_2H_4, and C_3H_4 as trace constituents. The presence of C_2H_2 and C_2H_4 has been latter confirmed by observational data obtained by Gillett (1975) in the 8 to 14 μm wavelength range. CH_3D has also been detected at the same time.

3.2. Voyager missions at Titan

Launched in 1977, the Voyager 1 et 2 spacecrafts arrived in the Saturn system three years later after a flyby of Jupiter in 1979, where they obtained a large amount of data. The Saturn encounter was planed so that the maximum information could be gathered on the rings, the satellites and the magnetosphere, and to allow the study of Saturn's and Titan's atmospheres. Titan studies focalized on several major goals: determine the diameter of the solid surface, the temperature and pressure profiles, the atmospheric composition and search for a magnetic field (Stone et Miner, 1981).

Voyager 1 spacecraft obtained the larger amount of data on Titan. In fact, its trajectory was determined so that it could approach the satellite as much as it could and its closest

[9] Low gravity favors light element such as hydrogen to escape from the atmosphere.

approach was at less than 7000 km from the center of Titan (Ness et al., 1981). A first deception came from the pictures obtained (Smith et al., 1981). In fact, even if the presence of aerosol was indubitable, some scientists were hopping that some hole in the haze would allow to observe the surface. It was not the case. A uniform orange haze hides entirely the surface. Nevertheless, the imagery data showed three distinct aerosol layers (Figure 15). The first one was observed around 200 km altitude. It was dense, optically thick in the visible and seemed to be made of particles having a ~0.3 μm radius at his top. A second layer detached from the first one (even if a small amount of aerosols was observed in between) was seen 100 km above and was about 50 km thick. The last layer was observed at a mean altitude of 400 km and was also observed by the ultraviolet occultation experiment. Finally, the observations showed a North-South asymmetry, the north being much darker than the southern hemisphere.

Figure 15 - Aerosol layers observed by Voyager 1.

The greatest advance in our knowledge of this satellite of Saturn came from radio and ultraviolet occultation measurements and from infrared and ultraviolet experiments. The radio occultation experiment (~3.6 et 13 cm) sounded the atmosphere (Tyler et al., 1981) down to the surface allowing to determine a radius of 2575.0 ± 0.5 km (Lindal et al., 1983). This type of sounding measure the variation of the refractive index of the atmosphere as a function of altitude. Since the refractivity is proportional to the density, this allows to determine the density profile of the atmosphere. Assuming hydrostatic equilibrium, the pressure profile can be deduced. And finally, the choice of a state equation allows to retrieve the ratio T/<m> as a function of altitude (T is the temperature and <m> mean molecular mass).

Making the assumption that the atmosphere is entirely composed of molecular nitrogen, Lindal et al. (1983) determined the density, pressure, and temperature profiles of Titan atmosphere. The temperature at the ground level is 94 K and the pressure 1495 mbars. The temperature decreases in the troposphere and the profile shows the presence of a tropopause with a temperature of 71.2 K at 40 km altitude (p~120 mbars). The temperature

then increases in the stratosphere to reach a temperature of ~170 K at 200 km (p~0.75 mbar) (see Figure 18). The choice of molecular nitrogen as the major constituent seems to be arbitrary since methane was the only abundant constituent detected. But it can be justified a posteriori by the results obtained with the infrared and ultraviolet instruments.

The ultraviolet spectroscopic experiment (UVS for UltraViolet Spectrometer) which did measurements in the 60 to 160 nm wavelength range, observed in addition to Lα emission due to atomic hydrogen, an intense emission around 100 nm (Broadfoot et al., 1981). This emission is similar to the one obtained in laboratory experiments when N_2 is excited by electronic impacts. The relative intensity of the bands allows determining a column density of $\sim 10^{15}$ cm^{-2}. Aside from that, the ultraviolet occultation experiment which measured the attenuation of the solar flux inside the atmosphere allowed to measure the atmospheric scale length[10] at an altitude of 1265 km (altitude where the optical depth[11] $\tau = 1$ for wavelengths lower than 80 nm), characteristics of nitrogen absorption : $H = 85 \pm 10$ km (Smith et al., 1982). Making the assumption that the atmosphere is entirely composed of nitrogen, this lead to a temperature $T = 176 \pm 20$ K. Furthermore, knowing the absorption coefficient of N_2 around 70 nm, one can determine the local density: $[N_2] = 2.7 \pm 0.2\ 10^8$ cm^{-3}. a change in the scale length is starting at an altitude of 1125 km and is attributed to methane. Smith et al. (1982) deduced from those measurements a mixing ratio $[CH_4]/[N_2] = 0.08 \pm 0.03$ (making the assumption of a constant temperature). They also determined a mixing ratio of acetylene of 1 to 2% above 825 km and less than 0.3% below 675 km. This would imply a high sink for this compound in this region of the atmosphere. The data also showed highly absorbing layers around 390 km and 760 km, with ~70 km thickness. The first layer seemed to be well correlated to the high altitude layer observed in the visible when the second one is not. Since in this region C_2H_2 abundance rapidly decreases one can think that in this region of the atmosphere, it could be efficiently photolysed, leading tout the formation of higher weight compounds that would efficiently absorb ultraviolet photons. A model of this emission spectrum leads to the determination of upper limits for the mixing ratio of H_2, Ar et Ne in the high atmosphere: $[H_2]/[N_2] \leq 0.06$, $[Ar]/[N_2] \leq 0.06$, $[Ne]/[N_2] \leq 0.01$ et $[CO]/[N_2] \leq 0.05$ (Strobel and Shemansky, 1982). As a conclusion, the UV data showed that nitrogen is the major compound in Titan atmosphere, so that this atmosphere should be the place for an active photochemistry involving nitrogen and methane. The confirmation came from the infrared spectroscopic experiment.

[10] The atmospheric scale length is the distance over which the pressure is divide by a factor *e* (2.718). It is proportional to temperature, et inversely proportional to mean molecular mass and gravity.

[11] The optical depth is the quantity which represents the opacity of a material. When it equals one, the light intensity is attenuated by a factor *e*.

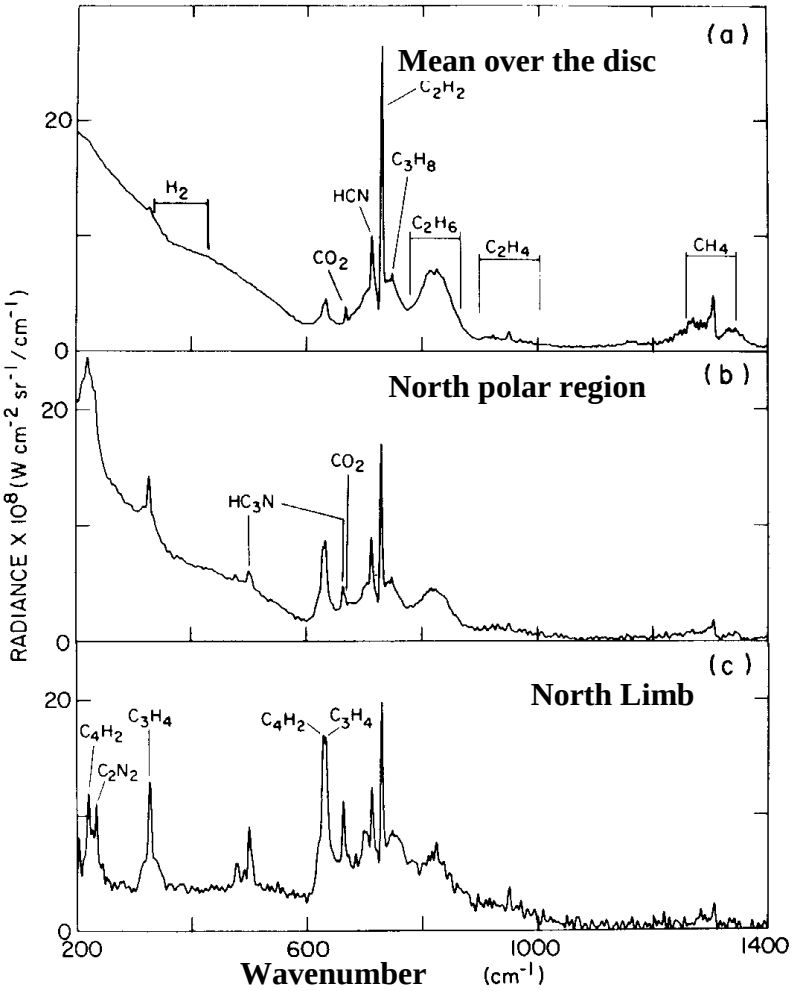

Figure 16 - Infrared spectra obtained at different latitudes (a and b) and at the limb (c) by the IRIS experiment of the Voyager 1 mission. The main compounds detected from those data are quoted on the figures. From Samuelson et al. [1983].

The infrared spectrometer (IRIS for **I**nfrared **R**adiometer and **I**nterferometer **S**pectrometer) onboard Voyager spacecraft was a Fourier transform spectrometer (resolution 4.3 cm^{-1}) covering the domain 180 to 2400 cm^{-1} (55 to 4.2 μm). The spectrometer of the Voyager 1 spacecraft took almost 3000 spectra during Titan flyby and a wide latitudinal-longitudinal geographical region was explored. The first analysis of the spectra obtained at the equator confirmed the presence of methane (CH_4), ethane (C_2H_6), acetylene (C_2H_2) but also the presence of ethylene (C_2H_4) and hydrogen cyanide (HCN) (Hanel et al., 1981). All these compounds are seen in emission showing that they are present in the relatively warm stratosphere of Titan. The study of Titan's North Pole will complete this list adding propane (C_3H_8), methyl acetylene (C_3H_4) (Maguire et al., 1981), diacetylene (C_4H_2), cyanoacetylene (HC_3N), and cyanogen (C_2N_2) (Kunde et al., 1981). The presence of all those compounds in the stratosphere confirm the complex and active chemistry that is occurring in the N_2 /CH_4 mixture which composes Titan's atmosphere.

A more careful study of the spectra obtained at different latitudes allowed Samuelson et

al. [1983] to put in light the presence of an oxygenated compound: CO_2 (Figure 16). In fact, even if its mole fraction is very low ~1.4 10^{-8}, its distribution is uniform over Titan disc which differentiate it from the other minor compounds. This will be the first detection of oxygenated compound in Titan atmosphere. It has been later confirmed by the detection of CO in near infrared (Lutz et al., 1983) and millimeter (Marten et al., 1988) observations.

Table 8: Past missions (Figure 17)

Mission	Space agency	Dates	Description and objectives	Instruments	Main results
PIONEER 11 Mass : 259 kg Nominal power : 165 W	NASA	04/05/1973: Launch 09/01/1979: Saturn Flyby 11/1995: end of the mission	Pioneer 11spacegraft was the second spatial vehicle to visit the external solar system but the first to explore Saturn.	Instruments to measure magnetic field, UV photometer, IR radiometer and imaging photopolarimeter	Confirmed the presence of submicronic aerosols having an increasing size with decreasing altitudes. Observed an hydrogen torus around Saturn.
VOYAGER 1 et 2 Mass : 722 kg Nominal power : 420 W	NASA	V1 05/09/1977 V2 20/08/1977: Launch V1 11/1980 V2 08/1981: Saturn Flyby	These two missions succeeded to study in a small time interval all the giant planets and their satellites. The trajectory of Voyager 1 was optimized to do a close flyby of Titan.	Imaging instruments, IR and UV spectrometry, magnetic and charge particles measurements.	Established that N_2 is the major gas. Measured the temperature and pressure profiles. Detections of numerous organics mainly hydrocarbons and nitriles. Colsest approached tot Titan: V1: 6490 km V2: 665960 km

Figure 17 : Pioneer 11 et Voyager spacecrafts.

3.3. **Similitude and differences between Titan and the Earth**

As we just saw, the results obtained from the data accumulated by Voyager missions have lead to a real breakthrough in our knowledge of Titan. One of the major results was the discovery of dense atmosphere mainly composed of nitrogen in which the very active coupled chemistry of nitrogen and methane leads to the formation of numerous organic compounds. This makes Titan a unique object in the solar system since it the only one, outside the Earth,

to have a dense atmosphere mainly made of nitrogen. Its atmosphere slightly reductive, in between the highly reductive atmospheres of the giant planets and the highly oxidant atmospheres of the telluric planets, make it a photochemical reactor which can lead to the production of complex organic compounds. With this unique characteristic, Titan can be considered as a planetary scale laboratory for the study of the evolution of organic mater in abiotic conditions.

Titan environment brings some elements to try do understand the primitive Earth and the chemical evolution which lead to the emergence of Life. The analogy between both object is underlined by several common aspects. Both have a dense atmosphere mainly composed of nitrogen and in which the temperature profiles present similar structures. Hence, if CO_2 is the major greenhouse gas in the terrestrial troposphere, in Titan, nitrogen, methane and hydrogen play this role through their pressure induced absorptions. The warming of Titan stratosphere is explained by ultraviolet absorption by small particles which cannot emit efficiently in the infrared, where on Earth, it is ultraviolet absorption by ozone that plays this role. The temperature in the terrestrial mesosphere is controlled by CO_2 infrared reemission where in Titan it is mainly HCN which plays this cooling role. And finally in the very high atmosphere the gas is heated by ionization. So the structures of both atmospheres are similar because controlled by similar physical processes. Only the chemical compounds implied in those processes changed between the two objects. We can also add to this the possible presence of clouds in the low atmosphere of Titan due to methane condensation which would be similar to our water clouds on Earth. And finally, it has been suggested the presence on Titan of liquid reservoir such as lakes or seas of methane and ethane.

Meanwhile, those similarities between Titan and the Earth should not mask the major existing differences. For example, the surface pressure surface pressure is approximately the same, a little bit higher in Titan, but the mean ground temperatures are very different on both objects: -180°C on Titan compared to 20°C on Earth. This leads to a density which is five times higher on Titan than on the Earth at the ground level. Another difference appears if we compare the compositions of both atmospheres: nitrogen is the major compound for both of them but methane (CH_4) is second in Titan whereas actually on Earth it is molecular oxygen and water and, furthermore, carbon is in its oxygenated state CO_2. Water certainly played an important role in the appearance of life. And, even if Coustenis et al. (1998) have detected traces of water vapor in the high atmosphere of Titan, using ISO satellite (Infrared Space Observatory), at the temperature of Titan surface, this water would be solid. Nevertheless, Thompson et Sagan (1991) showed that meteoritic impacts could have lead to ejecta containing water liquefied under the shock. In this model, large quantities of liquid water could have persisted on the surface for a total duration of several thousands years. But, were this sufficient for an aqueous organic chemistry to develop and produce prebiotic molecules? Finally, the presence of an underground ocean like in Europa open other exobiological perspectives (Fortes, 2000), but as we already said the question of the transport between this ocean and the surface would then be a major problem to solve.

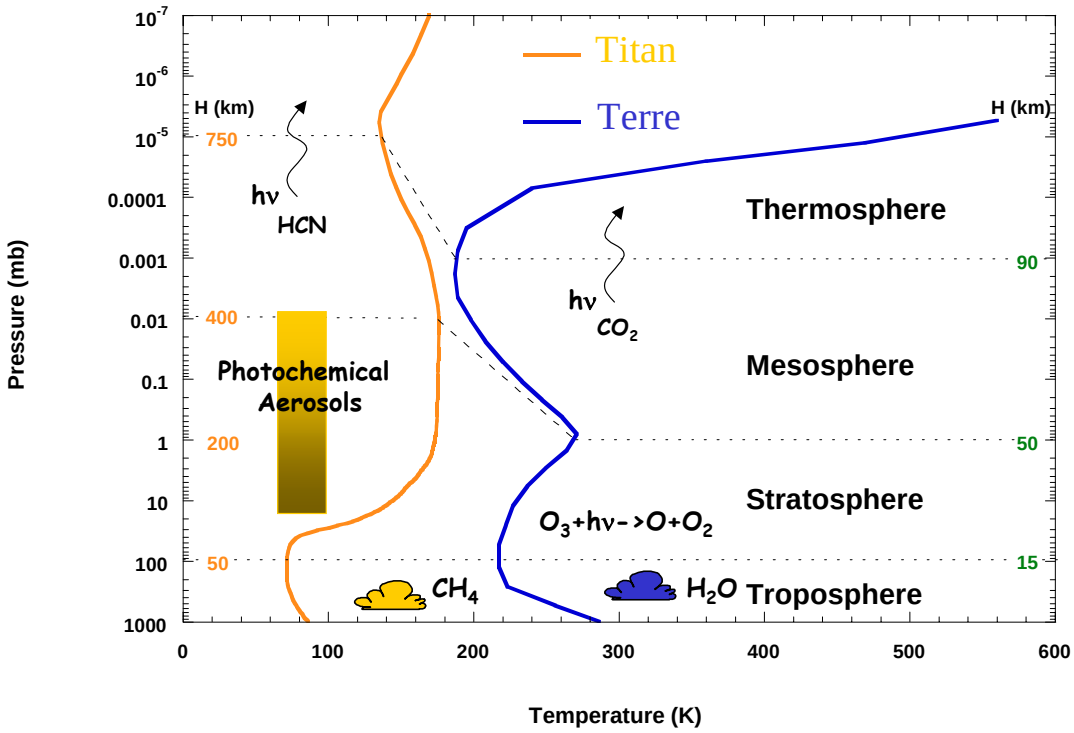

Figure 18 - Comparison between Earth's and Titan's atmospheric profiles.

In Titan a solid phase is also present as dust particles. Condensation of volatiles at their surface can transport gaseous compounds from the atmosphere to the surface and possibly into a methane/ethane liquid surface. So, Titan presents all the parts of what we can call a "geofluid" (Raulin, 1997). This underlines the importance of the study of this satellite for exobiology since it is the planetary body which is the closest to what could have been the Earth before the appearance of life. Of course, the major difference with the primitive Earth is certainly the very low temperature of Titan which implies the absence of liquid water. Nevertheless, the similitude between what could have been the primitive Earth and Titan, is one of the main reason that motivated the launch in of a probe called Huygens to do *in situ* measurements.

Finally, one will note that even if *in situ* measurements will bring data of primordial importance on the composition, structure and dynamic of the atmosphere, they will be done on a single trajectory of the space-time domain. So, they will have to be completed by teledetection measurements which allow studying phenomena at large scales with their time variations. This will be done by the instruments onboard Cassini spacecraft that has been put into orbit around Saturn in 2004 for a minimum period of time of four years.

3.4. Cassini-Huygens mission

Cassini-Huygens space mission is a joint mission from ESA and NASA (Figure 19). It is composed of an orbiter Cassini (NASA) and a descent probe Huygens (ESA). The whole set of instruments onboard is given in Table 9.

The main goal of the Huygens probe is to study the atmosphere and the surface of Titan. It will measure in situ the physical characteristics and chemical composition of the

atmosphere and the surface. It is equipped with six main instruments. After being released by the orbiter Cassini, it will enter Titan atmosphere on January 14, 2004 and will undergo a first deceleration protected by its thermal shield. Its first small parachute will be opened around 200 km and will cause the opening of a second much larger parachute (Lebreton et Matson, 1997). As soon as the main parachute is inflated the shield will dropped out. Thirty seconds later, measurements will start at a altitude around 150 km. The main parachute will be replaced by a smaller one after some time so that the probe reaches the ground after a descent that will last approximately 2,5hours. This time is fixed by the capacity of the batteries (1.8 kWh). With a maximum period of 153 minutes for the all mission, the probe should make measurements on the surface for at least 3 minutes. The data will be sent to the orbiter that will stay in contact for 3 hours.

One of the key objectives of the Huygens probe is to determine the chemical species present under gaseous, solid or liquid phase in the atmosphere and on the surface. But, further than simply obtaining quantities the main goal is to study the coupling between those different phases in order to try to understand the evolution that occurred on Titan since its formation. It is this approach that will allow bringing new elements to understand the prebiotic chemistry that could have occurred on Earth before the apparition of Life. In fact, if the "prebiotic chemist" is able to synthesize in the laboratory almost all biomacromolecules starting from hydrocarbons and nitriles observed on Titan, the question about what could happen on a planetary scale over geological time is still open. The questions that left over are (Raulin, 1997):

- What complexity could achieve organic synthesis in a reduced atmosphere where liquid water is absent?
- What could have the importance of multiphasic processes?
- What is the influence of the physical conditions: temperature, energetic deposition, and dynamics?

The study of Titan on which liquid water is absent, temperature very low, and energy sources diverse, can supply answers to those questions. The whole set of experiments on board the Huygens probe will contribute but in particular: the gas phase chromatograph coupled to a mass spectrometer (GCMS, Gas Chromatograph Mass Spectrometer), the collect and analysis of aerosols (ACP, Aerosol Collector Pyrolyser), the imager spectroradiometer (DISR, Descent Imager/Spectral Radiometer), the analysis of the surface (SSP, Surface Science Package) and the determination of the atmospheric structure (HASI, Huygens Atmospheric Structure Instrument). Each instrument has its specificities et will bring its answers.

GCMS (Niemann et al., 1997): the instrument is composed of a chromatographic system made of three columns coupled to a mass spectrometer: one column is devoted to the measure of permanent gases, one to light hydrocarbons (up to three carbons) and finally one is for the heavier compounds up to height nitrogen or carbons atoms. The atmosphere will be analyzed during all the descent by direct injection in the mass spectrometer (2-141 daltons). Nevertheless, during the first half hour a system will concentrate noble gases before their injection into the mass spectrometer. The chromatographic system itself will only be used on five different gaseous samples coming from five different altitudes. The first one will be taken just after the start up of the instruments around 150 km. Two samples will then be taken above 60 km altitude where the concentration of complex compounds is predicted to be the highest. The next analysis will be made on a sample coming for the pyrolysis of the aerosols collected by ACP (see below). At the minimum temperature of the tropopause, the analysis will devoted to the separation of N_2 et CO. And finally, if descent plan time is optimum a last sample will injected before impact. Then, if by chance the injector is correctly positioned, the

surface composition measurements will be done. The sensibility of the instrument should be very high on the order of ten parts per billions for most compounds.

ACP (Israel et al., 1997): Two regions of the atmosphere will be sounded by this instrument: the first one between 135 and 32 km and the second one between 22 and 17 km. The aerosols will be collected on a filter which can be placed a few millimeters outside the probe and then taken back inside the pyrolysis oven. The oven will allow warming the samples up to 600°C. Thus the following sequence is planned: 1) collect during the first hour of the descent then warming at ambient temperature, 250°C and 600°C , then transfer to GCMS ; 2) collect of a second sample above possible clouds then warming at the three temperatures and transfer to GCMS. The main goal of those measurements is to determine the composition of the condensation nuclei comparing the measurements obtained in Titan atmosphere with analogs produced in laboratory simulations. The relative composition of the condensates present at the aerosol surface should be obtained. And, finally, the possible abundance of adsorbed volatile like CO in the aerosols might be determined.

DISR (Tomasko et al., 1997): All over the descent, optical instrumentation of DISR (0,35-1,7 μm domain) will measure the upwelling and downwelling solar flux in order to determine the net flux. Then, the difference between two net fluxes taken at two different altitudes will allow to determine the energy deposited. This will then help to understand the thermal balance of the atmosphere. Measuring the diffusion properties, in two colors and two polarizations, together with the extinction of the aerosols will lead to the determination of the refractive index. This quantity is characteristic of a given material. Thus, this way it should be possible to constrain the chemical composition of Titan's aerosols. The optical instrumentation will allow to obtain the mixing ratio of methane as a function of altitude by measuring its absorption and will also help to constraint the nature of the surface determining its reflectivity. Those measurements will continue even in the last minutes of the descent when the probe will be closer and closer from the surface (where the atmosphere will become more and more opaque) thanks to a 20 W lamp that is attached to the instrument. DISR also includes two cameras that will allow to obtain images of the surface with a resolution going from a few hundred meters (like the orbiter) at the beginning of the descent to a few tenth of centimeters when approaching the surface.

HASI (Fulchignoni et al. 1997): The first goal of this instrumentation is to determine the density, pressure and temperature profiles all along the descent. But, this experiment also includes the possibility of measuring the electric field, the electric conductivity and even the sonic waves through a microphone. Thus, it should be possible to determine the electronic density in the atmosphere but also induce the presence of lightning storms if those are present in the atmosphere. The conductivity of the surface will also be measured after landing which will help to constrain the nature of the surface.

SSP (Zarnecki et al. 1997): this experiment is composed of nine different instruments. This set of instruments has been made to give indications on the solid or liquid surface. An accelerometer and a penetrometer will give the interesting information if the surface is solid: granularity, penetration resistance, and cohesion. An acoustic sounding device will give an idea of the topography of the surface. If the surface is liquid, the thermal conductivity, the density, the sound speed, the refracting index, and the permitivity will be determined. Other data will also be measured as for example the refractive index of aerosols collected during the descent. The sound speed, the temperature or the permitivity of the atmosphere will also be determined during the descent

The instruments of the orbiter will also contribute. In fact, those last one will allow to have a global view which is essential to interpret the probe data. The two major instruments that will furnish data concerning Titan atmospheric composition are:

CIRS (Flasar et al., 2004): this instrument is an infrared Fourier transform spectrometer that will acquire data in the range 10 to 1400 cm^{-1} (1 mm to 7 μm). This improved version of the IRIS spectrometers that were on Voyager spacecrafts (extension of the wavelength domain, of the resolution and of the sensitivity) will allow to map in three dimensions the chemical composition of Titan atmosphere but also the temperature.

UVIS (Esposito et al., 2003): this ultraviolet spectrometer is composed of two channels that will study the radiations that are coming from Titan between 56 and 190 nm. It will also give limb data with solar or stellar occultation. This should allow to determine the vertical profile of numerous species in the high atmosphere where a large amount of the energy is deposited.

The results that will be obtained by this space mission will certainly allow to make large breakthrough in the understanding of photochemical phenomena especially concerning organic processes which could lead to the emergence of life on a planet having a reductive atmosphere and liquid water. But, even if the Cassini-Huygens mission will bring a very large amount of data it will certainly not answer all the questions concerning the complexity of Titan. Especially, since the descent will be over one trajectory, it will not be possible to document the great complexity that already appears either on surface images or as a north-south asymmetry. In the future, it is possible and desirable that a new mission could be sent but this time with a mobile laboratory that will be able to study different regions of Titan surface and why not also different altitudes in the atmosphere [Lorentz , 2001].

Table 9: Ongoing missions

Mission	Space agency	Dates	Description and objectives	Instruments	Main results
Cassini Mass : 2523 kg Nominal power : 640 W **Huygens** Mass : 319 kg Nominal power : 250 W	NASA /ESA	10/15/1997 : Launch 07/01/2004 : Orbit insertion around Saturn. 01/14/2005 : Huygens descent in Titan atmosphere (2H30).	The first goal of the Cassini mission (NASA) is to transfer the descent probe Huygens (ESA) to Titan. Then it will stay in orbit around Saturn for a initial period of 4 years for a detail study of the rings, of the satellite surfaces including Titan, Saturn and Titan atmospheres including the spatial and temporal variability in terms of dynamic and chemical composition Huygens probe has the specific mission to determine the physical and chemical characteristics of Titan atmosphere and surface.	On board Cassini : Imaging system (ISS), magnetospheric imagery (MIMI), energy and charge of particles measurements (CAPS), magnetic field measurements (MAG), radio measurements (RPWS), cosmic dust analyzer (CDA), neutral and ionic mass spectrometer (INMS), radar, infrared spectrometer (CIRS), ultraviolet spectrometer (UVIS), visible/IR spectroimager (VIMS). On board Huygens : Atmospheric density, pressure and temperature profiles measurements (HASI), winds measurements (DWE), surface imaging and solar energy deposition in the atmosphere (DISR), Gas phase Chromatography coupled to mass spectrometry (GC-MS), collect et analysis of aerosols (ACP) and surface parameters measurements (SSP).	First results are being aquired and can be found on the site: http://saturn.jpl.nasa.gov/home/index.cfm.

Figure 19: Cassini-Huygens spacecraft arriving in the Saturn system and Huygens probe descent inside Titan atmosphere.

4. Mars exploration

4.1. Mars before space missions

Planet Mars, known since the prehistoric times (Egyptians were already talking about it in 4000 B.C.) has always attracted human beings. This is certainly partly due to its special trajectory in the sky, its aspect (its apparent diameter can vary by a factor greater than five), and its reddish color. It is on November, 28th 1659 that C. Huygens observed for the first time structures on the disk of Mars that are changing with time (Figure 20). From his observations, he will deduce a rotational period on itself of about 24 hours as on Earth. This will be the beginning of numerous phantasms that will tend to assimilate the Martian world to the terrestrial one.

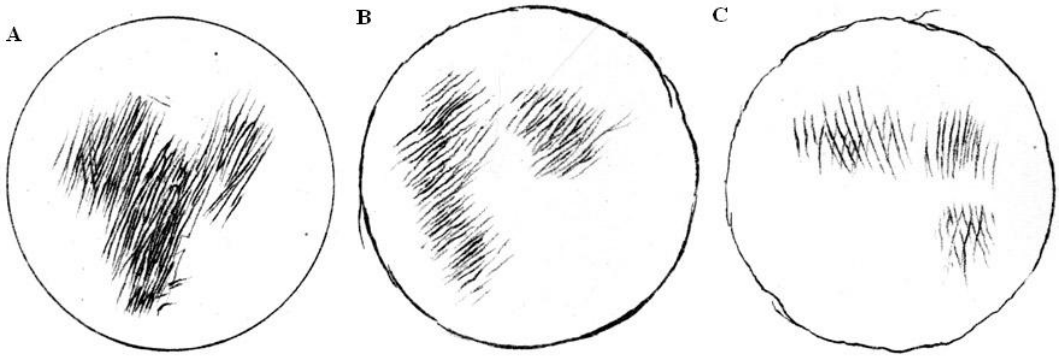

Figure 20: Three drawing made by par C. Huygens in 1659. The first one was drawn November, 28 at 7 pm (A), the second was done the same day but at 9.30 pm. (B). The last one was made three days later December, 1 at 6.30 pm (C).

The observations made in the following centuries will amplify those phantasms. Seas and "continents" will draw themselves at the surface of the red planet. Some, like P. Lowell at the end of the 19th century, imagined that a channel network irrigates Mars surface so that its occupant could survive. It has been necessary to wait for space exploration to definitively let down the idea that a life similar to one we know on Earth could be present.

Another problem that made cast a lot of ink is the one of the nature of the polar caps and the presence of water. Polar caps that were observed for the first time by J. B. Cassini have been followed through the centuries and the observer had noted their appearance and disappearance with seasons. The element that was supposed to compose them was water by analogy with the Earth but also because the measured temperatures was not sufficient to carbon dioxide to be present in condensed phase (Hess, 1948). Following this theory, water should have been observed in the atmosphere. But, it has been necessary to wait for the observation of Spinrad et al. (1963) for trace amount of water vapor to be finally detected. The observed quantities were very low, on the order of 10 μm. We had to wait for the first space missions to have a better idea of the water cycle on Mars.

Finally, the nature of the Martian atmosphere itself (pressure, composition, temperature) has been subject to discussions. In October 1947, G. P. Kuiper observed Mars in the wavelength region around 1,6 μm. Comparing this spectra with the one obtained from the moon that contain telluric carbon dioxide absorption lines, he shows that the absorption is greater in Martian spectra (Kuiper, 1952). Nevertheless, he could not deduce from his data the abundance of CO_2 because the bands were saturated. It has been necessary to wait for the very high resolution spectra, in the 870 nm domain were the bands are not saturated, for Kaplan et

al. (1964) to measure an abundance of 4 mbars of CO_2 at the surface. The total surface pressure is still unknown at this time. Nevertheless, using observations around 2 μm, Kuiper (1963) and Sinton (1963) deduced that the total pressure is between 10 and 40 mbars. So, for the first time, carbon dioxide appears as the main constituent of the Martian atmosphere.

4.2. The beginning of Martian exploration

Only eleven of the thirty or so missions sent to Mars effectively achieved their objectives. The lost missions have been reported in Table 12. As one can see the reasons of failure are various, they go from explosion at ignition to communication lost during Mars transfer or, more recently, communication lost during landing.

If the soviets were the first to fire, it is the US Mariner 4 spacecraft, launched November, 28 1964, which has been the first one to reach Mars on July, 14 1965. Thanks to its onboard camera it took the first pictures of Mars surface with a resolution of 4 km. The ground appears riddled with craters which lead to compare it with the moon, and seemed to indicate an age as old as the planet itself (Chapman et al., 1969). But, only 1% of the surface has been pictured. The greatest breakthrough was done thanks to the radio-occultation experiment which allowed to determine for the first time surface pressure and temperature. The pressure is on the order of 5 mbars (Kliore et al., 1965). Those measurements confirmed that carbon dioxide is the main element of a thin atmosphere.

The next mission burst to Mars with Mariner 6 et 7 in 1969, followed by Mariner 9 in 1971 and finally Viking probes in the mid 70's, allowed to reach a more and more precise idea of the martian environment using heavier and heavier equipment including more and more advanced technology (see Table 10).

Mariner 6 and 7 probes were equipped not only with a camera able to obtain images of 10% of the surface, but also an infrared spectrometer, a infrared radiometer and an ultraviolet spectrometer. This last one identified atomic hydrogen, atomic oxygen and carbon monoxide in the high atmosphere (Thomas, 1971). The infrared measurements allowed to identify carbonic ice as the major component of the South Pole (Herr et Pimentale, 1969).The radiometer measured a temperature at the South Pole of 148 K which led to confirm that it is composed of carbonic ice (Neugebauer et al., 1971). In fact, vapor pressure of CO_2 at this temperature is on the order of 6 mbars which is compatible with the measurements of Kliore et al. (1971). In the same conditions, the vapor pressure of water is only of 10^{-8} mbars. Finally, thanks to the UV spectrometer, ozone was observed for the first time.

Mariner 9 interplanetary probe has been put into orbit for a period of almost one terrestrial year. This allowed the cartography of almost all the Martian surface, the study of the atmospheric physico-chemistry and its temporal variations over a period ranging from the day to the month. Imagery experiment put in light an unsuspected diversity of the surface with the presence of volcanoes among which the highest, Olympus Mons, reach 26 km, or canyons deeper than 6 km like Valles Marineris. But, overall, valleys likely to come from erosion process appeared. Water vapor was detected for the first time in Martian orbit by the infrared Fourier transform spectrometer IRIS, (Hanel et al., 1972) during north summer. The condensation of this water vapor in the form of crystals will also be observed (Curan et al., 1973). All those results pushed forward for the sending of an *in situ* mission able to bring into light the possible traces of a biological activity on Mars.

Viking project included two vehicles, Viking 1 and Viking 2, each one composed of an orbiter and a probe able to land on Mars surface after a site selection. The main objectives of the Viking missions were the study of martian surface with high resolution imagery, the characterization of the structure and the composition of the atmosphere and the surface and also the search for possible life forms.

So, the orbiters will make maps of the entire Mars surface with a 200 meters resolution. In addition to the recurrent dust storms, they observed the variations of the surface pressure all along a Martian year. This evidenced the presence of a CO_2 cycle, related to the development and the retreat of the polar caps. The infrared spectrometer allowed to determine the water vapor content in Mars atmosphere (MAWD, Mars Atmospheric Water Detectors) and to follow the atmospheric humidity global variations during the seasons due to the seasonal cycle of the water transport between the two poles. Finally, the coupling with the radiometer (IRTM, Infrared Thermal Mappers) results permitted to demonstrate that, if the south pole was mainly composed of CO_2 ices, the residual north polar cap visible during the summer was mainly composed of water ice.

The Viking 1 lander made continuous measurements in the region of Chryse Planitia on Mars surface during six terrestrial years whereas Viking 2 lander operated during two martian years in Utopia Planitia (Figure 23). Each probe was carrying not only a set of experiment to detect possible life forms on Mars surface but also instruments to study the chemical, magnetic, apparent and physical properties of the surface and the atmosphere, and to achieve meteorological and seismic observations.

A small meteorological station was supported by a one meter mast. It put together three thermal sensors distributed along the height but also a pressure gauge and an anemometer allowing to measure the wind speed and direction. Those measurements acquired during more than three Martian years constituted a unique database for the study of Mars climate.

Inorganic chemical analysis of the surface were made by X fluorescence (XRFS). The obtained results were disconcerting. If, Mars seemed to be constituted mainly from silicon and oxygen like the Earth, iron and not aluminum was then the next most abundant element.

Each of the Viking landers was also equipped with a gas chromatograph coupled with a mass spectrometer (CPG-SM). They were designed to determine the molecular and isotopic atmospheric composition and to try to detect organic mater in the ground. The atmosphere could be either directly injected in the mass spectrometer. This allowed to determine the isotopic abundance of five constituents. Solid samples were first pyrolysed at 500°C and then the gaseous residues transferred to the chromatograph. No organic compounds have been identified down to the 1 part per billion threshold (Biemann et al., 1977). This result was surprising since even if no endogen source were present, the exogenous sources should have enriched the Martian soil in organic compounds. One explanation could be that organic mater was destructed by the combined action of radiation sources and oxidation.

Figure 21: One of the Viking landers with its mechanical arm deployed (Credit photo: NASA/JPL).

The exobiological experiment onboard Viking landers (Figure 21) was composed of three distinct experiments (Klein et al., 1972). The first one was the « Pyrolytic Release ». This experiment was made to detect carbonic gas assimilation (CO_2) by photosynthetic mechanisms or in the dark. Mars samples were submitted to an injection of a mixture of $^{14}CO_2$ and ^{14}CO (with a ratio 95:5). During a five days period, the sample could be lighted up by a Xenon lamp simulating the solar flux but filtered below 320 nm to suppress UV. After this period, the residual atmosphere was evacuated and the sample pyrolysed in an oven at 625°C. The organic mater was then extracted and the presence of ^{14}C determined. The procedure could be reproduced under the presence of water or in the dark. Obtained results were difficult to interpret. First, experiments were not reproducible: if the first experiment gave a positive result, the following one was negative. Furthermore, even if the sample was heated to high temperature (175 °C) the results would stay positive. The best explication would be that the positive experiment could come either from a chemical compound (for example, the formation of a polymer like carbon suboxyde (C_3O_2)), or from a physical process like the adsorption of CO_2 in the ground (Horowitz et al., 1977). The second experiment was the « Gas Exchange ». This experiment would help to detect different gases that organisms could reject after ingestion of nutriments. A nutriment solution was added to surface samples in contact with the Martian atmosphere. For the calibration, part of the sample was heated for sterilization. The determination of the gas composition present over the sample was done through GC-MS analysis. Here again, results were astonishing. First, a high oxygen degassing and a low release of CO_2 and nitrogen. The release of oxygen was very quick and a second introduction of nutriment did not liberate anymore oxygen. Furthermore, this degassing occurred even in the dark or with the sterilized sample. Those results could be explained if one suppose that martian soil contains very reactive oxidant molecules like superoxydes (Oyama et Berdahl, 1977). Finally, the third experiment was the « Labeled Release ». This experiment looks like the previous one except that the carbon atoms of each compound inside the nutriment were radioactive. One detector could identify the outgassing radioactive CO_2. A high outgassing of CO_2 was observed after the injection of nutriment. And this released was not observed with the sterilized samples. So, one could conclude on the presence of biological activity from this only experiment. Nevertheless, this last result can also be explained by non biological processes. For example, the action of hydrogen peroxyde (H_2O_2) could explain the

release of carbon dioxide from the oxidation of the organic mater present in the nutriment (Huguenin et al., 1979).

The results of those experiments constructed to detect biological activity are still today subject to controversy because one can hardly denied the positive results of the Label Release experiment (Levin et al., 1981). Nevertheless, if microorganisms were really present inside the samples, organic mater should have been detected by the GC-MS experiment (Klein et Harold, 1978). Consequently, most scientists agree to say that life is absent from the surface of Mars. Nevertheless, the question – Is there life on Mars? – is still an open issue since some niches could exist in the subsurface.

4.3. Current space missions.

Space missions currently in activity around Mars are resumed in Table 11. After the success of the 70's and notably the Viking probe experiences, a long inactivity of almost twenty years occurred for the Martian program. In 1988, the Russian Space Agency put in orbit around Mars its first probe: Phobos 2. But, one had to wait until the end of the 90's for the NASA to achieve the lander of its first rover: Pathfinder. The mission is a true technological achievement and it opens the way for a new Martian program. The missions that have followed since then had as a common objective to map Mars surface and atmosphere to try to answer the question: when has there been water on Mars, in what state and where is it today? In fact, one of the essential needs for life seems to be liquid water. Consequently, we hope that following the water on Mars will lead us to the sources of life.

Within this objective to follow the water on Mars, Mars Global Surveyor satellite brought its piece of the puzzle. The infrared imaging spectrometer allowed to map the minerals present on Mars surface. Chistensen et al. (2000) identified the presence of hematite concentrated in an unique region: Meridiani Planum (Figure 22). The presence of stagnant water in the past could have allowed precipitation of this iron oxyde in the past (Chistensen et al., 2004).

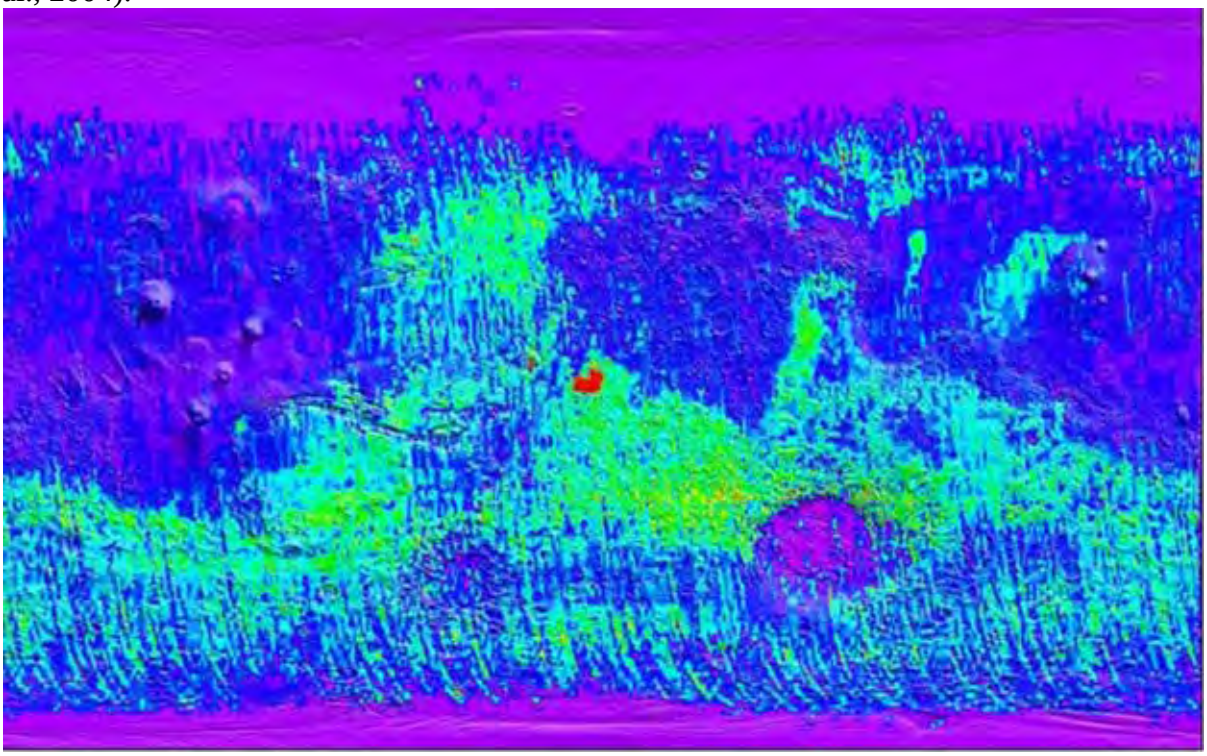

Figure 22: Hematite map on Mars obtained by TES of the MGS mission (Christensen, P.R. et al., 2000). Regions with high hematite concentration appear in red.

This observation led to the selection of this site for the landing of one of the Mars Explorating Rovers mission, MER B alias Opportunity. The other rover (MER A alias Spirit) landed in Gusev Crater (Figure 24). MER B confirmed the presence of hematite. This in concentrated small black spherules called « Blueberries » (Moore, 2004). The rover also found jarosite, an iron sulfate. In conditions where an atmosphere rich in carbon dioxide and sulfur dioxide is in contact with large water mass rich in iron, jarosite could form (Fairen et al., 2004). Such conditions would preclude the formation of carbonates which could explain their non detection until now at the Mars surface. The presence of sulfates in Meridiani Planum has been confirmed by Omega experiment onboard Mars Express mission (Gendrin et al., 2004). Furthermore, this experiment has allowed the identification of those minerals in and around Valles Marineris. The same instrument also put in light the presence of water ice at the south pole (Bibring et al. 2004).

The mapping of hydrogen present in the ground at less than one meter below the surface, either in the form of ice or in the form hydrated minerals, has been obtained thanks to the neutron detector and the gamma spectrometer of Mars Odyssey mission (Figure 24). A large concentration of ice appears at the poles and a low concentration at the equator except in two regions: Arabia Terra et Apollineris. In those region, the water could be in the form of ice present several tenth of centimeter below a dehydrated layer.

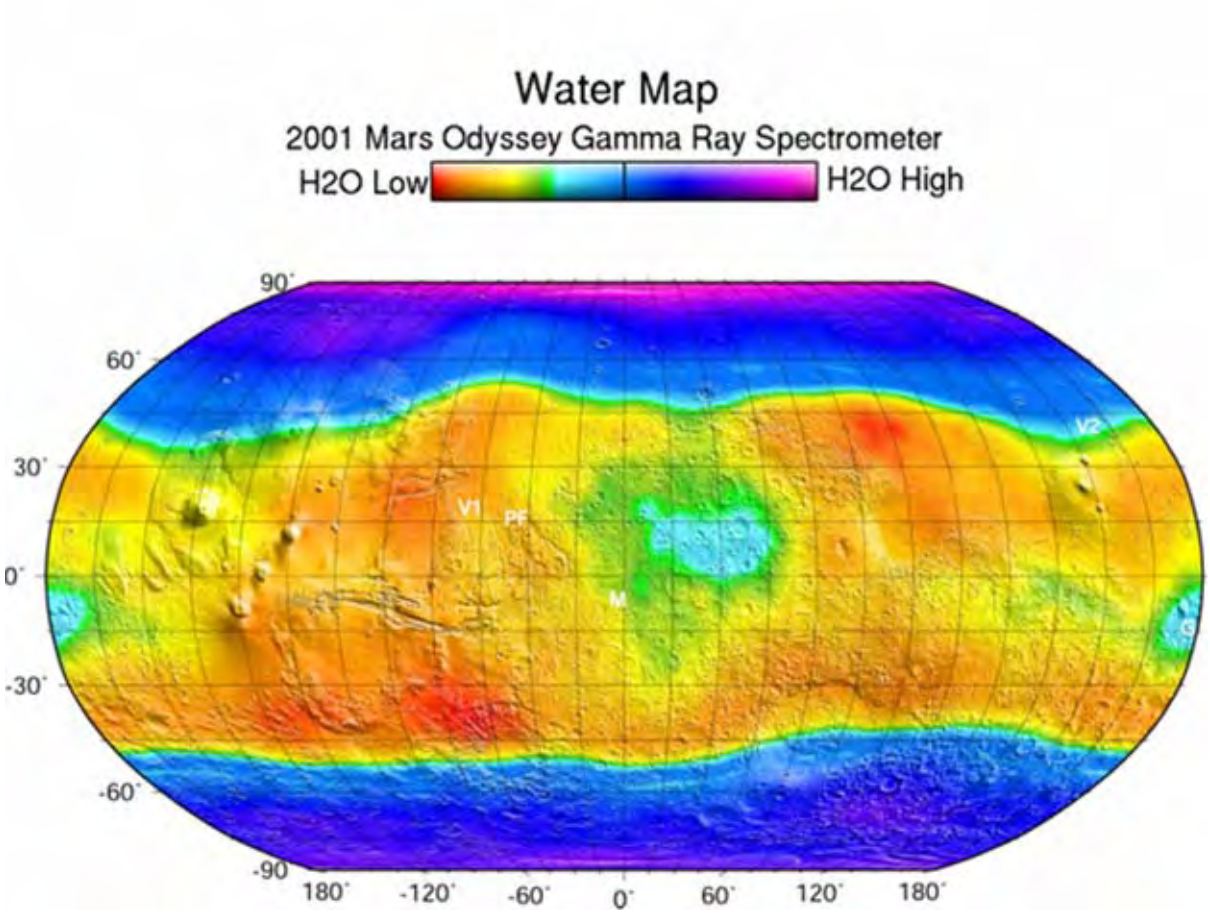

Figure 23 : Map done using the hydrogen measurements of the gamma spectrometer of the Mars Odyssey mission (Mitrofanov et al., 2002). If this hydrogen is really in the form of water, regions in blue/violet show the presence of more than 50% ice by volume in the ground. The significantly dryer equatorial regions show two sites more hydrated around

Arabia Terra (at center) and Apollineris (on the side). The localization of the lander missions are indicated: Viking 1 (VL1), Viking 2 (VL2), Pathfinder (PF), Spirit at Gusev (G), and Opportunity at Meridiani (M).

3.4. Future exobiological missions

If the results obtained by the exobiological experiment of Viking missions did not allow to definitely conclude on the presence of biological activity on Mars, they had the merit to exist in order to allow the criticism. This helps today to construct mission scenarios optimized for the search of life traces on Mars.

The first action on this way has begun, since as we saw in the previous paragraph, the present program consists to try to identify the places and the times where liquid water could exist on Mars. A second step will be to search for organic matter but to do that *in situ* measurements will be necessary. But, future missions will also have to go further. They will have to look not only at the martian surface but also to go deeper inside to explore the subsurface. The reason is that oxidation processes by molecules like hydrogen peroxide (H_2O_2) recently observed in the atmosphere (Clancy et al., 2004), or superoxydes certainly lead to the destruction of organic matter on the surface (Yen et al., 2000). The thickness of the oxidized regolite has lead to theoretical calculations but the uncertainties are such that this thickness can vary from one meter to several tenths of meters (Zent, 1998). Consequently, future missions will have to be able to drill at least down to one meter or even more.

The analytical system will then have to be able to extract organic mater from the rock and analyze it to determine its composition. The pyrolysis/GC-MS technique could be improved compared the one used on Viking mission. First, derivatisation could allow the analysis of refracting molecules that could appear in the degradation of the initial organic material. Then, the use of chiral chromatographic columns could allow the determination of the origin of molecules either biotic or abiotic (Cabane et al., 2004). Isotopic measurements could also complete such analysis of the organic matter because isotopic ratio can help to identify biotic process. For example, on Earth carbon fractionation ($^{12}C/^{13}C$) in favor of ^{12}C is of the order of 20 to 30 % in the biomass compared to inorganic carbon (Brack et al., 1999). One can think that such measurement set will be present on the future MSL mission (Mars Science Laboratory) planned in 2009 and for which the call for proposal as just been released (see Table 13).

Nevertheless, even with all the *in situ* detection effort of life traces, the sign of possible Martian life could be so subtle that the equipment necessary for its detection would be much too heavy and complex to be put on a space probe. The solution would then be to bring samples collected on Mars back to the Earth to study them in the laboratory. This type of mission initially planed for the end of 2000's year is actually not expected before the horizon 2015.

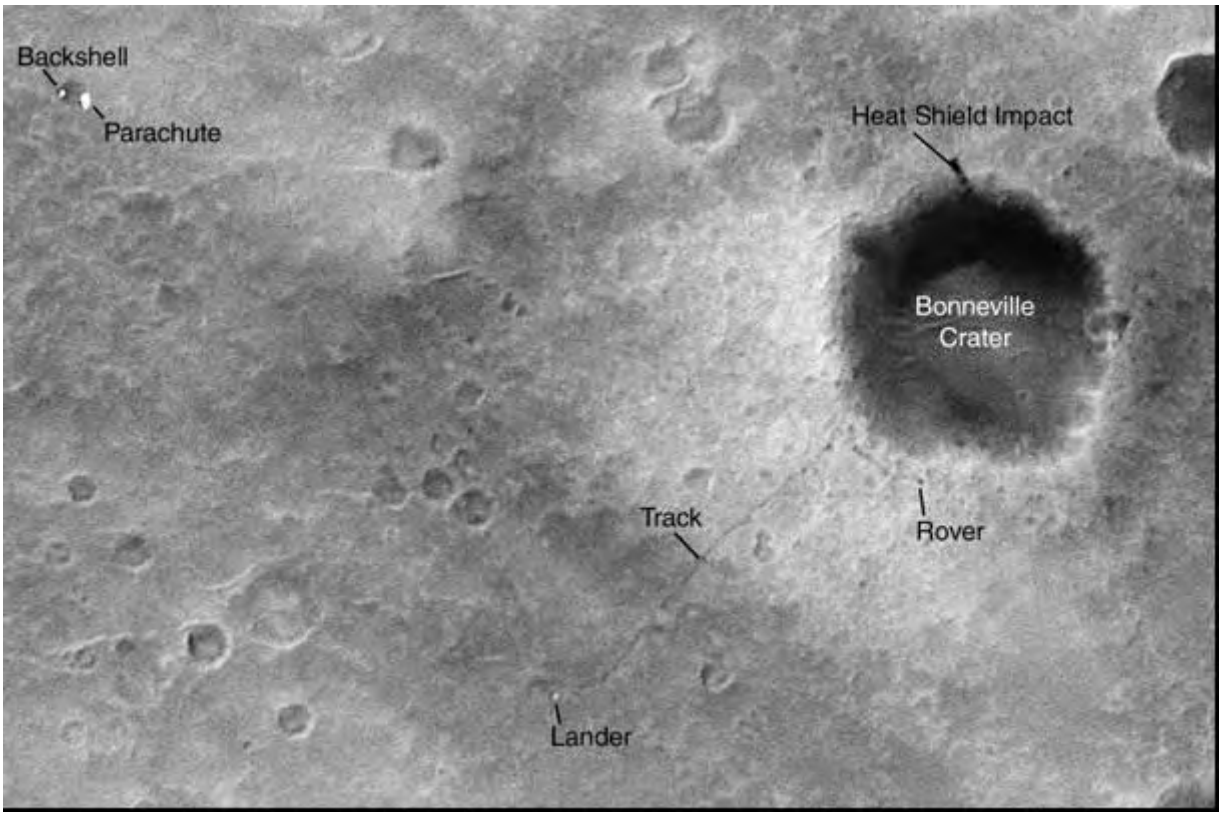

Figure 24: Image acquired on Mars, 30th 2004 by MOC of MGS (resolution 1,5x0,5 m/pixel). One can see the landing site of Spirit together with the track of the rover in direction of the Bonneville carter during 85-sol (Image Crédit: NASA/JPL/Malin Space Science Systems).

Table 10 : Past missions

Mission	Space agency	Dates	Description and objectives	Instruments	Main results
MARINER 4 Mass : 260,7 kg Nominal power : 170 W	NASA	11/28/1964 : Launch 07/14 /1965: Mars Flyby	**First space probe arrived at Mars.** Take surface images; obtain data on micrometeoritic impacts, magnetic field and solar wind.	Magnetometer, ion detector, radiometer, meteoritic particles detector and camera.	22 pictures were send to the Earth. Surface pressure was estimated between 4.1 and 7 mbars. No magnetic field observed.
MARINER 6 Mass : 411,8 kg Nominal power : 449 W	NASA	02/25/1969 : Launch	Study Mars surface and atmosphere to prepare future missions.	Wild field and long focal camera. Infrared spectrometer and radiometer. Ultraviolet spectrometer.	M 6 : 75 pictures M 7 : 125 pictures Surface pressure is estimated between 6 and 7 mbars. The south pole is covered with carbonic ice.
MARINER 7 Mass : 411,8 kg Nominal power : 449 W	NASA	03/27/1969 : Launch			
MARS 2 Mass : 2265 kg	USSR	05/19/1971 : Launch	**First orbiter and lander mission**. Study Mars surface and atmosphere to determine composition, temperature and topography. Serve as relay to the Earth for the landers.	Wild field and long focal camera. Infrared spectrometer and radiometer. Ultraviolet spectrometer. Surface modules.	Mars 2 lander was lost during atmospheric entry. Communication was lost with Mars 3 lander after 20 s. 60 pictures were obtain . Surface pressure is between 5 and 6 mbars. Atomic hydrogen and oxygen are detected in the high atmosphere.
MARS 3 Mass : 2265 kg	USSR	05/28/1971 : Launch			
MARINER 9 Mass : 997,9 kg Nominal power : 449 W	NASA	05/30/1971 : Launch	**First orbiter mission around Mars** To obtain surface map, study the atmosphere together with its spatial, diurnal and secular variations.	Camera, Infrared Fourier transform spectrometer. Ultraviolet spectrometer..	More than 7000 images. Determination of the wind field and the atmospheric dynamic. Determination of the water content of the atmosphere. Detection of water ice clouds.
MARS 5 Mass : 2270 kg	USSR	07/25/1973 : Launch	Composition, structure and properties of Mars surface and atmosphere.	Cameras, radiometer, visible and radio polarimeters, 5 photometers (study H at Lyα, ozone around 250 nm, visible albedo, H_2O and CO_2 in the infrared).	After a few days breakdown of the transmission system. Nevertheless, a high water concentration (100 μm) is measured close to Tharsis and an ozone layer is observed at high altitudes.
MARS 6 Mass : 635 kg	USSR	08/05/1973 : Launch	**First *in situ* probe.** Study *in situ* martian surface and atmosphere.	Telephotometer, temperature and pressure sensors, wind measurements, accelerometer and mass spectrometer.	Loose contact just before landing. Nevertheless, determination of the atmospheric profile below 25 km.
VIKING	NASA	08/20/1975 :	Orbiters : Thermal and visible map of Mars surface. Study	Orbiters : Camera, Infrared spectrometer	Orbiters : More than 50000

1 and 2 Mass : 997,9 kg Nominal power : 449 W		Launch V1 09/09/1975 : Launch V2	the water abundance in the atmosphere and its spatial, diurnal and secular variations. Landers : study the physical and chemical atmospheric parameters. Take pictures of the ground, obtain meteorological measurement on the surface, study the mineral and chemical, especially organic, composition of the surface, and search for the presence of life on Mars.	center on the water bands (MAWD), radiometer. Landers : Cameras, pressure and temperature sensors and and anemometer, gas phase chromatography couple to a mass spectrometer. X fluorescence spectrometer, biological activity measurement experiments.	images obtained covering 87% of the martian surface with a 200 m resolution Detrmination of the water content in the atmosphere and its annual variations. Detection of a residual north polar cap made of water. Landers : *in situ* determination of the temperature and pressure profiles during the entry phase. Meteorological measurements during 3 martian years. Measure of the chemical and isotopic composition of the atmosphere. Determination of the inorganic composition of the surface with the presence of ferrosilicates. No organic matter detected.
PHOBOS 2 Mass : 2600 kg	USSR	07/12/1988 : Launch	Characterization of the plasma environment around Mars. Study Mars atmosphere and the surface. Study Phobos surface.	Among others: plasma analyzer, particles detector, infrared spectrometer, mass spectrometer,…	Allowed to obtained the first mineralogical maps of Mars thanks to an infrared imaging spectrometer.
MARS PATHFINDER Mass : 895 kg Mass du Rover : 10 kg	NASA	12/04/1996 : Launch	**First rover on Mars**. Technological mission	Station : Imagers and meteorological station. Rover : X spectrometer and cameras	16500 pictures obtained by the station and 550 by the rover.

Tableau 11**: In progress missions**

Mission	Space agency	Dates	Description and objectives	Instruments	Main results
MARS GLOBAL SURVEYOR Mass : 1030.5 kg Nominal power : 667 W	NASA	11/07/1996 : Launch	Take images of the surface, study thermal emission an measure the topography, gravitational and magnetic field.	Camera (MOC), Infrared thermal spectrometer (TES), Laser altimeter (MOLA)	A complete map of the surface is achieve by MOC at a 1,5m resolution. The mineralogical composition is determine using TES and hematite is discovered. With MOLA, martian topography is determine with an absolute precision of 30 m. Still active to relay transmission from other missions like the rovers.
MARS ODYSSEY Mass : 376 kg	NASA	04/07/2001 : Launch	Measure radiations in martian environment to study potential risk for human explorer. Determine mineralogical composition and study the elemental composition and hydrogen content of the surface.	Radiation detector (MARIE), Camera imaging spectrometer (THEMIS), Gamma ray spectrometer (GRS) and neutron detectors and spectrometer (NS and HEND).	Map of the hydrogen content of the subsurface (> 1m). Seems to show the presence of water ice in high latitudes and the presence of hydrated minerals at lower latitudes. Still active to relay transmission from other missions like the rovers.
MARS EXPRESS Beagle 2 Mass : 666 kg Nominal power : 460W	ESA	06/02/2003 : Launch	Global geological map at high resolution (10 m). Mineralogical map. Atmospheric composition map. Study of the subsurface.	Stereo Imager (HRSC), Mineralogy imaging spectrometer (OMEGA), UV/IR spectrometer (SPICAM), IRTF spectrometer (PFS), Radar (MARSIS), High energy atoms and plasma analyzer (ASPERA).	First results being released. See the site: http://www.esa.int/SPECIALS/Mars_Express/index.html
MER A (Spirit) **MER B (Opportunity)**	NASA	06/10/2003 : Launch MER A 07/07/2003 : Launch MER B	Study mars surface to search for past water traces.	Camera, infrared spectrometer (mini-TES), Mossbauer, and X spectrometer (APX), microscope.	MER A : landed in Gusev Crater, has covered 3,5 km in 9 months. MER B : landed in Terra Meridiani, traveled only 1,5 km, but confirmed the presence of hematite.

Table 12: Lost missions :

Mission	Space agency	Dates	Description and objectives	Instruments	Main results
MARSNIK 1 Mass : 650 kg	USSR	10/10/1960 : Launch	**First known attempt of an interplanetary probe**. Study interplanetary space between Mars and Earth. Study Mars and take surface images. Test long distances radio transmissions.	Magnetometer, ions detector, radiometer, meteoritic particles detector, camera and spectroreflectrometer to study CH bands possibly indicative of life.	Lost during launch, the stage did not ignite.
MARSNIK 2 Mass : 650 kg	USSR	10/14/1960 : Launch	Second attempt of an interplanetary probe. Same objectives as MARSNIK 1	See Marsnik 1	Lost during launch
SPUTNIK 22 Mass : 893,5 kg	USSR	10/24/1962 : Launch	See Mars 1	See Mars 1	Explosion in Earth orbit.
MARS 1 Mass : 893,5 kg	USSR	11/01/1962 : Launch	Take surface images, obtain data on micrometeoritic impact and the magnetic field, determine the atmospheric structure and the possible presence of organic compounds.	Magnetometer, ions detector, radiometer, meteoritic particles detector, camera and spectroreflectrometer to study ozone band	Communications lost during transit to Mars.
SPUTNIK 24 Mass : 890 kg	USSR	11/04/1962 : Launch	**First attempt of a lander.**	?	Explosion during Mars transit.
MARINER 3 Mass : 260,8 kg	NASA	11/01/1964 : Launch	Take surface images, obtain data on micrometeoritic impact and the magnetic field, and the solar wind.	Magnetometer, ions detector, radiometer, meteoritic particles detector, and camera	Communications lost during transit to Mars.
ZOND 2 Mass : 893,5 kg	USSR	11/30/1964 : Launch	See Mars 1.	See Mars 1.	Communications lost during transit to Mars..
ZOND 3 Mass : 960 kg	USSR	07/18/1965 : Launch	See Mars 1.	See Mars 1.	Launch with a trajectory not compatible with Mars Flyby
MARS 1969A Mass : 4850 kg	USSR	03/27/1969 : Launch	**First attempt of a Mars orbiter.**	Camera, radiometer, water vapor detector, infrared, ultraviolet and gamma spectrometer, mass spectrometer.	Explosion during ignition of the third stage of the Proton launcher.
MARS 1969B Mass : 4850 kg	USSR	04/02/1969 : Launch			Problem with the ignition of one of the launcher motors lead to explosion.
MARINER 8 Mass :558,8 kg	NASA	05/09/1971 : Launch	Mars orbiter to measure temperature , pressure fields and the composition of the atmosphere and surface.	Ultraviolet and infrared spectrometer, radiometer, and camera.	Defect of ignition of the last launcher stage.
COSMOS 419 Mass : 4650 kg	USSR	05/10/1971 : Launch	Mars orbiter	See Mars 2.	Defect of ignition of the last launcher stage.
MARS 4 Mass : 2270 kg	USSR	07/21/1973 : Launch	See Mars 5.	See Mars 5.	Defect of ignition of the retrorocket during Mars orbit obit insertion.
MARS 7 Mass : 1200 kg	USSR	08/09/1973 : Launch	See Mars 6	See Mars 6	Le largage du module descente trop tôt conduira à rater Mars.
PHOBOS 1 Mass : 2600 kg	USSR	07/07/1988 : Launch	See Phobos 2	See Phobos 2	Communication lost during Mars transfer.

MARS OBSERVER Mass : 1018 kg	NASA	09/25/1992	Determine elemental and mineralogical composition of the surface. Topographic and gravitational and magnetic field measurements. Study of volatiles an dust together with their spatial and seasonal variations.	Camera, gamma spectrometer, laser altimeter, radiometer, thermal infrared spectrometer, magnetometer.	Communication lost during Mars transfer.
MARS 96 Mass : 3159 kg	RSA	11/16/1996	See Mars Express	See Mars Express	Reentry in Earth atmosphere for unknown reason.
NOZOMI Mass : 258 kg	ISAS	07/04/1998	Study the high atmosphere and its interactions with the solar wind.	Camera, neutral and ionic mass spectrometer, particles counter, VUV imaging spectrometer, wave plasma detector and low frequency analyzer.	In December 1998, Nozomi has problems with its propulsion system. The trajectory is then changed to save the mission. The trip will take four more years. But, the probe will flyby Mars December 14th 2003 without being able to be inserted into orbit.
MARS CLIMATE ORBITER Mass : 338 kg	NASA	12/11/1998	Everyday climate study including surface changes due to atmospheric events. Determination of temperature profiles. Follow the water vapor and dust atmospheric content..	Radiometer and cameras	Navigation error leading to the destruction of the probe during its orbit insertion on Mars.
MARS POLAR LANDER Mass : 290 kg	NASA	01/03/1999	Record meteorological conditions of the south pole. Analyze the surface deposit. Drill trench to search for seasonal layers. Determine surface composition.	Descent imager. Laser system (LIDAR) to study atmospheric aerosols. Meteorological station. Camera. Spectrometer to study volatiles after pyrolysis.	Communications never established after landing.
DEEP SPACE 2 Mass : 3,6 kg	NASA	01/09/1999	Impactor allowing to test the presence of water ice under the surface. Determine the properties of the subsurface. Measure temperature and pressure.	Accelerometer, water detector, conductivity measurement.	Communications never established after impact.
BEAGLE 2 Mass : 33 kg	ESA	06/02/2003	Geological, mineralogical, geochemical and climatological studies. Search for bio signatures.	Drilling system. Gas chromatography and mass spectrometry. Microscope, camera, X fluorescence spectrometer and Mossbauer .	Communications never established after landing.

Tableau 13 : Futures martian missions

Mission	Space agency	Dates	Description and objectives	Instruments	Main results
MARS RECONNAISSANCE ORBITER	NASA	Launch between August 10th and 30th 2005	Characterize surface, subsurface and atmosphere. Identify sites for future Identifier des sites for future *in situ* missions.	High resolution imaging, two wild field cameras, IR-visible imaging spectrometer, radiometer and radar.	Last year before launch. On going integration and tests.
PHOENIX	NASA	Launch in 2007	*In situ* studies of the north pole. Geological history of water. Search for potential habitable zone at the interface ground/ice.	Descent imager, camera, robotized arm, mass spectrometer, microscopes, chemical and meteorological measurements.	Low cost scout mission (heritage from Mars Polar Lander) being prepared.
MARS SCIENCE LABORATORY	NASA	Launch in 2009	Mobile laboratory on Mars surface.	Call for proposal being released.	Call for proposal being released.

Conclusion :

To date, there is nothing which could allow us to figure out if we shall ever know whether the Earth is the only inhabited planet in the universe. However, astrobiology has gone a long way since the very first experiments by Miller in 1950, and since then, its questioning feeds the exploration of our Solar System, and even beyond with ambitious programs for the observation of extrasolar planets (TPF, Darwin). The answer is maybe already at our hand, by a rock to be analysed with a Martian rover, our further away under a few kilometres ice layer in Jupiter neighbourhood… This chapter deals with the preliminary steps of the astrobiological exploration of the Solar System, the ones we are currently witnessing. We focussed on the search of organic matter and liquid water, but none of them is a clear indicator of past or present life. We did not discuss the next issue, concerning the question about knowing which measurement(s) (chemical, geological, spectroscopic) could allow us to claim we have finally detected life on another planet. This topic would need a whole chapter to be discussed, and even if the scientific debate about it is still at its very first stages, it opens the most fascinating prospects.

References :

Atreya, S.K., T.M. Donahue and W.R. Kuhn, Science, 201, 611-613, 1978.

Barbier, B., A. Chabin, D. Chaput, and A. Brack, Photochemical processing of amino acids in Earth orbit, Planetary and Space Science, 46 (4), 391-398, 1998.

Barbier, B., O. Henin, F. Boillot, A. Chabin, D. Chaput, and A. Brack, Exposure of amino acids and derivatives in the Earth orbit, Planetary and Space Science, 50, 353-359, 2002.

Bernstein, M.P., S.A. Sandford, L.J. Allamandola, S. Chang, and M.A. Scharberg, Organic Compounds Produced By Photolysis of Realistic Interstellar and Cometary Ice Analogs Containing Methanol, The Astrophysical Journal, 454, 327-344, 1995.

Bibring, Jean-Pierre; Langevin, Yves; Poulet, François; Gendrin, Aline; Gondet, Brigitte; Berthé, Michel; Soufflot, Alain; Drossart, Pierre; Combes, Michel; Bellucci, Giancarlo; Moroz, Vassili; Mangold, Nicolas; Schmitt, Bernard; and the OMEGA team. Perennial water ice identified in the south polar cap of Mars. Nature, Volume 428, Issue 6983, pp. 627-630, 2004.

Biemann, K.; Oro, J.; Toulmin, P., III; Orgel, L. E.; Nier, A. O.; Anderson, D. M.; Flory, D.; Diaz, A. V.; Rushneck, D. R.; Simmonds, P. G. The search for organic substances and

inorganic volatile compounds in the surface of Mars. Journal of Geophysical Research, vol. 82, Sept. 30, 1977, p. 4641-4658; 1977

Bland, P.A., T.B. Smith, A.J.T. Jull, F.J. Berry, A.W.R. Bevan, S. Cloudt, and C.T. Pillinger, The flux of meteorites to the Earth over the last 50,000 years, Monthly Notices of the Royal Astronomical Society, 283, 551, 1996.

Blank, J.G., G.H. Miller, M.J. Ahrens, and R.E. Winans, Experimental Shock Chemistry of Aqueous Amino Acid Solutions and the Cometary Delivery of Prebiotic Compounds, Origins of Life and Evolution of the Biosphere, 31, 15-51, 2001.

Bockelée-Morvan, D., D. Gautier, F. Hersant, J.-M. Huré, and F. Robert, Turbulent radial mixing in the solar nebula as the source of crystalline silicates in comets., Astronomy and Astrophysics, 384, 1107-1118, 2002.

Bockelée-Morvan, D., J. Crovisier, M.J. Mumma, and H.A. Weaver, The composition of cometary volatiles, in Comets II, edited by M. Festou, H.U. Keller, and H.A. Weaver, Univ. Arizona Press, Tucson, In press.

Boillot, F., A. Chabin, C. Buré, M. Venet, A. Belsky, M. Bertrand-Urbaniak, A. Delmas, A. Brack, and B. Barbier, The Perseus Exobiology Mission on MIR: Behaviour of Amino Acids and Peptides in Earth Orbit, Origins of Life and Evolution of the Biosphere, 32, 359-385, 2002.

Botta, O., and J.L. Bada, Extraterrestrial organic compounds in meteorites, Surveys in Geophysics, 23, 411-467, 2002.

Brack, A., La chimie de l'origine de la vie, in Les traces du vivant, edited by M. Gargaud, D. Despois, J.-P. Parisot, and J. Reisse, pp. 61-81, Presses universitaires de Bordeaux, Bordeaux, 2003.

Broadfoot, A.L., B.R. Sandel, D.E. Shemansky, J.B. Holberg, G.R. Smith, D.F. Strobel, J.C. McConnell, S. Kumar, D.M. Hunten, S.K. Atreya, T.M. Donahue, H.W. Moos, J.L. Bertaux, J.E. Blamont, R.B. Pomphrey and S. Linick, Science, 212, 206-211, 1981.

Cabane, M.; Coll, P.; Szopa, C.; Israël, G.; Raulin, F.; Sternberg, R.; Mahaffy, P.; Person, A.; Rodier, C.; Navarro-Gonzàlez, R.; Niemann, H.; Harpold, D.; Brinckerhoff, W. Did life exist on Mars? Search for organic and inorganic signatures, one of the goals for ``SAM'' (sample analysis at Mars). Advances in Space Research, Volume 33, Issue 12, p. 2240-2245. 2004.

Caldwell, J.J., Icarus, 25, 384-396, 1975.

Carr, M.H., M.J.S. Belton, C.R. Chapman, M.E. Davies, P. Geissler, R. Greenberg, A.S. McEwen, B.R. Tufts, R. Greeley, and R. Sullivan, Evidence for a subsurface ocean on Europa, Nature, 391, 363, 1998.

Christensen, P.R. et al., Detection of crystalline hematite mineralization on Mars by the Thermal Emission Spectrometer, J. Geophys. Res., 105, 9632-9642, 2000.

Christensen, Philip R.; Ruff, Steven W. Formation of the hematite-bearing unit in Meridiani Planum: Evidence for deposition in standing water. Journal of Geophysical Research, Volume 109, Issue E8, 2004.

Chyba, C.F., P.J. Thomas, L. Brookshaw, and C. Sagan, Cometary delivery of organic molecules to the early earth, Science, 249 (July), 249-373, 1990.

Clancy, R. T.; Sandor, B. J.; Moriarty-Schieven, G. H. A measurement of the 362 GHz absorption line of Mars atmospheric H_2O_2. Icarus, Volume 168, Issue 1, p. 116-121. 2004

Conklin, E.K., B.L. Ulich and J.R. Dickel, Bull. Amer. Astron. Soc., 9, 471, 1977.

Corliss, J.B., J.A. Baross, and S.E. Hoffman, An hypothesis concerning the relationship between submarine hot spring and the origin of life on Earth, Oceanologica Acta, N° SP (Proceedings of the 26th Geological Congress), 59-69, 1981.

Cottin, H., C. Szopa, and M.H. Moore, Production of hexamethylenetetramine in photolyzed and irradiated interstellar cometary ice analogs, The Astrophysical Journal Letters, 561 (1), L139-L142, 2001.

Cottin, H., Y. Bénilan, M.-C. Gazeau, and F. Raulin, Origin of cometary extended sources from degradation of refractory organics on grains: polyoxymethylene as formaldehyde parent molecule, Icarus, 167, 397–416, 2004.

Coustenis, A.; Salama, A.; Lellouch, E.; Encrenaz, Th.; Bjoraker, G. L.; Samuelson, R. E.; de Graauw, Th.; Feuchtgruber, H.; Kessler, M. F. A & A, 336, L85-L89, 1998.

Cronin, J.R., and S. Pizzarello, Enatiomeric Excesses in Meteoritic Amino Acids, Science, 275 (14 February), 951-955, 1997.

Curran, R.J., Conrath, B.J., Hanel, R.A., Kunde, V.G. and Pearl, J.C. Mars: Mariner 9 spectroscopic evidence for H_2O ice clouds. Science 175, pp. 381–383., 1973.

Danielson, R.E., J.J. Caldwell and D.R. Larach, Icarus, 20, 437-443, 1973.

Despois, D., and H. Cottin, Comets : potential sources of prebiotic molecules for the early Earth, in Lectures in Astrobiology, edited by M.Gargaud, B.Barbier, H. Martin, and J.Reisse, Springer Verlag, In press.

Ehrenfreund, P., and S.B. Charnley, Organic molecules in the interstellar medium, comets and meteorites: a voyage from dark clouds to the early earth, Annual Review of Astronomy & Astrophysics, 38, 427-483, 2000.

Esposito, L. W., C. A. Barth, J. E. Colwell, G. M. Lawrence, W. E. McClintock, A. I. F. Stewart, H. U. Keller, A. Korth, H. Lauche, M. C. Festou, A. L. Lane, C. J. Hansen, J. N. Maki, R. A. West, H. Jahn, R. Reulke, K. Warlich, D. E. Shemansky, and Y. L. YungThe Cassini Ultraviolet Imaging Spectrograph investigation. Space Sci. Rev. . In press 2004 (http://lasp.colorado.edu/cassini/archive/docs/pdf/ssr2.pdf).

Fairén, Alberto G.; Fernández-Remolar, David; Dohm, James M.; Baker, Victor R.; Amils, Ricardo. Inhibition of carbonate synthesis in acidic oceans on early Mars. Nature, Volume 431, Issue 7007, pp. 423-426 (2004).

Flasar, M. et al., ., Space Science Reviews , 2004.

Fortes, A.D., Exobiological Implications of a Possible Ammonia-Water Ocean inside Titan, Icarus, 146, 444-452, 2000.

Fulchignoni, M., F. Angrilli, G. Bianchini, A. Bar-Nun, M.A. Barucci, W. Borucki, M. Coradini, A. Coustenis, F. ferri, R.J. Grard, M. Hamelin, A.M. Harri, G.W. Leppelmeier, J.J. Lopez-Moreno, J.A.M. McDonnell, C. McKay, F.M. Neubauer, A. Pederson, G. Picardi, V. Pironello, R. Pirjola, R. Rodrigo, C. Sshwingenschuh, A. Seiff, H. Svedhem, E. Thrane, V. Vanzani, G. Visconti & J.C. Zarnecki., Huygens: Science, payload and Mission, ESA SP-1177, 163-195, 1997.

Gendrin, A., Bibring, J.-P., Gondet, B., Langevin, Y., Mangold, N., Mustard, J. F., Poulet, F. and C. Quantin. Identification of Sulfate Deposits on Mars by Omega/Mars Express. Second Conference on Early Mars, 11-15 Octobre 2004, Jackson Hole, USA.

Gillett, F.C., Astrophys. J., 201, L41-L43, 1975.

Gillett, F.C., W.J. Forrest and K.M. Merrill, Astrophys. J., 184, L93-L95, 1973.

Greenberg, J.M., What are comets made of ? A model based on interstellar dust, in Comets, edited by L.L. Wilkening, pp. 131-163, University of Arizona Press, Tucson, 1982.

Hanel, R., B. Conrath, F.M. Flasar, V. Kunde, W. Maguire, J. Pearl, J. Pirriglia, R. Samuelson, L. Herath, M. Allison, D. Cruikshank, D. Gautier, P. Gierasch, L. Horn, R. Koppany, and C. Ponnamperuma, Science, 212, 192-200, 1981.

Hanel, R., Conrath, B., Hovis, W., Kunde, V., Lowman, P., Maguire, W., Pearl, J., Pirraglia, J., Prabhakara, C. and Schlachman, B. Investigation of the Martian environment by infrared spectroscopy on Mariner 9. Icarus 17, pp. 423–442, 1972.

Hennet, R.J.-C., N.G. Holm, and M.H. Engel, Abiotic Synthesis of Amino Acids under Hydrothermal Conditions and the Origin of Life: a Perpetual Phenomenon, Naturwissenschaften, 79, 361-365, 1992.

Herr, K. C.; Pimental, G. C. Infrared absorptions near three microns recorded over the polar CAP of mars. Science, vol. 166, p. 496-499 (1969).

Hersant, F., D. Gautier, and J.-M. Huré, A Two-dimensional Model for the Primordial Nebula Constrained by D/H Measurements in the Solar System: Implications for the Formation of Giant Planets, Astrophysical Journal, 554, 391-407, 2001.

Horowitz, N. H.; Hobby, G. L.; Hubbard, J. S. Viking on Mars - The carbon assimilation experiments. Journal of Geophysical Research, vol. 82, Sept. 30, 1977, p. 4659-4662, 1977

Huebner, W.F., D.C. Boice, and A. Korth, Halley's polymeric organic molecules, Advances in Space Research, 9 (2), 29-34, 1989.

Huebner, W.F., First polymer in space identified in comet Halley, Science, 237 (August), 628-630, 1987.

Huguenin, R. L.; Miller, K. J.; Harwood, W. S. Frost-weathering on Mars - Experimental evidence for peroxide formation. Journal of Molecular Evolution, vol. 14, Dec. 1979, p. 103-132,1979

Hunten, D.M., The Saturn System (D.M. Hunten and D. Morison, eds.), NASA-CP 2068, pp. 113-126, 1978.

Iro, N., D. Gautier, F. Hersant, D. Bockelée-Morvan, and J.I. Lunine, An interpretation of the nitrogen deficiency in comets, Icarus, 161, 511-532, 2003.

Israel, G., Niemann, H., Raulin, F., Riedler, W., Atreya, S., Bauer, S., Cabane, M., Chassefière, E., Hauchecorne, A., Owen, T., Sablé, C., Samuelson, R., Torre, J. P., Vidal-Majar, C., Brun, J. F., Coscia, D., Ly, R., Tintignac, M., Steller, M., Gelas, C., Condé, E., and Millan, P. , Huygens: Science, payload and Mission, ESA SP-1177, 59-84, 1997.

Zarnecki, J.C., M. Banaszkiewicz, M. Bannister, W.V. Boynton, P. Challenor, B. Clark, P.M. Daniell, J. Delderfield, M.A. English, Fulchignoni, M., J.R.C. Garry, J.E. Geake, S.F. Green, B. Hathi, S. Jaroslawski, M.R. Leese, R.D. Lorenz, J.A.M. McDonnell, N. Merrywether-Clarke, C.S. Mill, R.J. Miller, G. Newton, D.J. Parker, P. Rabetts, H. Svedhem, R.F. Turner & M.J. Wright, Huygens: Science, payload and Mission, ESA SP-1177, 177-195, 1997.

Kasting, J.F., Earth's early atmosphere, Science, 259, 920-926, 1993.

Khare, B.N. and C. Sagan, Icarus, 19, 195-201, 1973.

Kissel, J., and F.R. Krueger, The organic component in dust from comet Halley as mesured by the PUMA mass spectrometer on board Vega 1, Nature, 326 (April), 755-760, 1987.

Kissel, J., F.R. Krueger, J. Silén, and B.C. Clark, The Cometary and Interstellar Dust Analyzer at Comet 81P/Wild 2, Science, 304, 1774-1776, 2004.

Kivelson, M.G., K.K. Khurana, C.T. Russell, M. Volwerk, R.J. Walker, and C. Zimmer, Galileo Magnetometer Measurements: A Stronger Case for a Subsurface Ocean at Europa, Science, 289, 1340-1343, 2000.

Klein, Harold P. The Viking biological experiments on Mars. Icarus, Volume 34, Issue 3, p. 666-674, 1978

Klein, Harold P.; Lederberg, Joshua; Rich, Alexander. Biological Experiments: The Viking Mars Lander. Icarus, vol. 16, p.139. 1972

Kliore, A., Cain, D. L., Levy, G. S., Eshleman, V. R., Fjeldbo, G. and Drake, F. D. Occultatio experiment – results of the first direct measurement of Mars's atmosphere and ionosphere. Science, vol. 149, pp.1243-1248, 1965.

Krueger, F.R., A. Korth, and J. Kissel, The organic matter of comet Halley as inferred by joint gas phase and solid phase analyses, Space Science Reviews, 56, 167-175, 1991.

Krueger, F.R., and J. Kissel, The chemical composition of the dust of comet P/Halley as measured by "Puma" on board Vega-1, Naturwissenschaften, 74, 312-316, 1987.

Kunde, V.G., A.C. Ainkin, R.A. Hanel, D.E. Jennings, W.C. Maguire, and R.E. Samuelson, Nature, 292, 686-688, 1981.

Lebreton et Matson, Huygens: Science, payload and Mission, ESA SP-1177, , 1997.

Levin, Gilbert V.; Straat, Patricia A. A search for a nonbiological explanation of the Viking Labeled Release life detection experiment. Icarus, Volume 45, Issue 2, p. 494-516,1981

Lindal, G.F., G.E. Wood, H.B. Hotz, D.N. Sweetnam, V.R. Eshleman and G.L. Tyler, Icarus, 53, 348-363, 1983.

Lorenz, Ralph D. Exo-/astro-biology. Proceedings of the First European Workshop, ESA SP-496, 215 – 218, 2001.

Low, F.J., Lowwell Obs Bull, 6(128), 184-187, 1965.

Lunine, J.I., S. Engel, R. Bashar, and M. Horanyi, Sublimation and reformation of icy grains in the primitive solar nebula, Icarus, 94, 333-344, 1991.

Lutz, B.L., C. de Bergh and T. Owen, Science, 220, 1374-1375, 1983.

Maguire, W.C., R.A. Hanel, D.E. Jennings, V.G. Kunde and R.E. Samuelson, Nature, 292, 683-686, 1981.

Marten, A., D. Gautier, L. Tanguy, A. Lecacheux, C. Rosolen and G. Paubert, Icarus, 76, 558-562, 1988.

Maurette, M., Carbonaceous Micrometeorites and the Origin of Life, Origins of Life and Evolution of the Biosphere, 28, 385-412, 1998.

McCord, T.B., G.B. Hansen, and C.A. Hibbitts, Hydrated Salt Minerals on Ganymede's Surface: Evidence of an Ocean Below, Science, 292, 1523-1525, 2001.

McCord, T.B., G.B. Hansen, D.L. Matson, T.V. Jonhson, J.K. Crowley, F.P. Fanale, R.W. Carlson, W.D. Smythe, P.D. Martin, C.A. Hibbitts, J.C. Granahan, and A. Ocampo, Hydrated salt minerals on Europa's surface from the Galileo near-infrared mapping spectrometer (NIMS) investigation, Journal of Geophysical Research, 104, 11827-11852, 1999.

Meier, R., P. Eberhardt, D. Krankowsky, and R.R. Hodges, The extended formaldehyde source in comet P/Halley, Astronomy and Astrophysics, 277, 677-691, 1993.

Meierhenrich, U.J., G.M.M. Caro, J.H. Bredehöft, E.K. Jessberger, and W.H.-P. Thiemann, Identification of diamino acids in the Murchison meteorite, Proceedings of the National Academy of Sciences, 101, 9182-9186, 2004.

Miller, S.L., The production of amino acids under possible primitive Earth conditions, Science, 117, 528-529, 1953.

Mitchell, D.L., R.P. Lin, C.W. Carlson, A. Korth, H. Rème, and D.A. Mendis, The origin of complex organic ions in the coma of comet Halley, Icarus, 98, 125-133, 1992.

Mitrofanov et al., Maps of Subsurface Hydrogen from the High Energy Neutron Detector, Mars Odyssey, Science, 297, 78-81, 2002.

Möller, G., and W.M. Jackson, Laboratory studies of polyoxymethylene : application to comets, Icarus, 86, 189-197, 1990.

Moore, M.H., and T. Tanabe, Mass spectra of sputtered polyoxymethylene : implications for comets, The Astrophysical Journal, 365, 1990.

Moore, Jeffrey M. Mars Blueberry fields for ever, Nature, Volume 428, Issue 6984, pp. 711-712 (2004).

Muñoz Caro, G.M., and W.A. Schutte, UV-photoprocessing of interstellar ice analogs: New infrared spectroscopic results, Astronomy and Astrophysics, 412, 121-132, 2003.

Ness, F.N., M.H. Acuña, R.P. Lepping, J.E.P. Connerney, K.W. Behannon, L.F. Burlaga and F.M. Neubaueur, Science, 212, 211-216, 1981.

Neugebauer, G., Miinch, G., Kieffer, H., Chase, S. C., & Miner, E. Mariner 1969 Infrared Radiometer Results: Temperatures and Thermal Properties of the Martian Surface. Astronomical Journal, Vol. 76, p. 719,1971

Niemann, H. et al., Huygens: Science, payload and Mission, ESA SP-1177, 85-107, 1997.

Oro, J., and C.B. Cosmovici, Comets and Life on the primitive Earth, in Astronomical and Biochemical Origins and the Search for Life in the Universe, edited by C.B. Cosmovici, S. Bowyer, and D. Werthimer, pp. 97-120, Proceedings of the 5th International Conference on Bioastronomy, Bologna, Italy, 1997.

Oyama, V. I.; Berdahl, B. J. The Viking gas exchange experiment results from Chryse and Utopia surface samples. Journal of Geophysical Research, vol. 82, Sept. 30, 1977, p. 4669-4676. 1977

Pierazzo, E., and C.F. Chyba, Cometary Delivery of Biogenic Elements to Europa, Icarus, 157, 120-127, 2002.

Pizzarello, S., and J.R. Cronin, Non-racemic amino acids in the Murray and Murchison meteorites, Geochimica et Cosmochimica Acta, 64, 329-338, 2000.

Podolak, M., and D. Prialnik, 26-Al and Liquid Water Environments in Comets, in Comets and the origin and evolution of life, edited by P.J. Thomas, C.F. Chyba, and C.P. McKay, Springer, New York, 1997.

Pollack, J.B., Icarus, 19, 43-58, 1973.

Prinn, R.G., and B.J. Fegley, Solar Nebula Chemistry: Origin of planetary, satellite and cometary volatiles, in Origin and Evolution of Planetary and Satellite Atmospheres, edited by S.K. Atreya, J.B. Pollack, and M. Matthews, pp. 78-136, Univ. Of Arizona Press., 1989.

Raulin, F. Huygens: Science, payload and Mission, ESA SP-1177, 219-229, 1997.

Raulin, F., Chimie prébiotique : expériences de simulation en laboratoire et "vérité terrain", in L'environnement de la Terre Primitive, edited by M. Gargaud, D. Despois, and J.-P. Parisot, pp. 343-360, Presses Universitaires de Bordeaux, Bordeaux, 2001.

Rodier, C., O. Vandenabeele-Trambouze, R. Sternberg, D. Coscia, P. Coll, C. Szopa, F. Raulin, C. Vidal-Madjar, M. Cabane, G. Israel, M.F. Grenier-Loustalot, M. Dobrijevic, and D. Despois, Detection of martian amino acids by chemical derivatization coupled to gas chromatography: in situ and laboratory analysis, Advances in Space Research, 27, 195-199, 2001.

Rosenbauer, H., S.A. Fuselier, A. Ghielmetti, J.M. Greenberg, F. Goesmann, S. Ulamec, G. Israel, S. Livi, J.A. MacDermott, T. Matsuo, C.T. Pillinger, F. Raulin, R. Roll, and W. Thiemann, The Cosac Experiment on the Lander of the Rosetta Mission, Advances in Space Research, 23 (333-340), 1999.

Samuelson, R.E., W.C. Maguire, R.A. Hanel, V.G. Kunde, D. Jennings, Y.L. Yung and A.C. Aikin, J. Geophys. Res., 88, 8709-8715, 1983.

Schenk, P.M., Thickness constraints on the icy shells of the galilean satellites from a comparison of crater shapes, Nature, 417, 419-421, 2002.

Selsis, F., and J.-P. Parisot, L'atmosphère primitive de la Terre et son évolution, in L'environnement de la Terre Primitive, edited by M. Gargaud, D. Despois, and J.-P. Parisot, pp. 217-233, Presses Universitaires de Bordeaux, Bordeaux, 2001.

Smith, B.A., J. Boyce, G. Briggs, A. Bunker, S.A. Collins, C.J. Hansen, T.V. Johnson, J.L. Mitchell, R.J. Terrile, M. Carr, A.F. Cook II, J. Cuzzi, J.M. Pollack, G.E. Danielson, A. Ingersoll, M.E. Davies, G.E. Hunt, H. Masursky, E. Shoemaker, D. Morrison, T. Owen, C. Sagan, J. Veverka, R. Strom and V.E. Suomi, Science, 212, 163-191, 1981.

Smith, G.R., D.F. Strobel, A.L. Bradfoot, B.L. Sandel, D.E. Shemansky and J.B. Holberg, J. Geophys. Res., 87, 1351-1359, 1982.

Sotin, C., J.W. Head, and G. Tobie, Europa: Tidal heating of upwelling thermal plumes and the origin of lenticulae and chaos melting, Geophysical Research Letters, 29, 74-1, 2002.

Stoks, P.G., and A.W. Schwartz, Nitrogen-heterocyclic compounds in meteorites - Significance and mechanisms of formation, Geochimica et Cosmochimica Acta, 45, 563-569, 1981.

Stoks, P.G., and A.W. Schwartz, Uracil in Carbonaceous Meteorites, Nature, 282, 709-710, 1979.

Stone, E.C. and E.D. Miner, Science, 212, 159-163, 1981.

Strobel, D.F. and D.E. Shemansky, J. Geophys. Res., 87, 1361-1368, 1982.

Strobel, D.F., Icarus, 21, 466-470, 1974.

Thomas, Gary E. Neutral Composition of the Upper Atmosphere of Mars as Determined from the Mariner UV Spectrometer Experiments. Journal of Atmospheric Sciences, vol. 28, Issue 6, pp.859-868, 1971.

Thompson , W.R., and C. Sagan, , Symposium on Titan, ESA SP, 167-176, 1991.

Tomasko, M. G. et al., Huygens: Science, payload and Mission, ESA SP-1177, 109-138 , 1997.

Trafton, L.M., Astrophys. J., 175, 285-293, 1972a.

Trafton, L.M., Astrophys. J., 175, 295-306, 1972b.

Tyler, G.L., V.R. Eshleman, J.D. Anderson, G.S. Levy, G.S. Lindal, G.E. Wood and T.A. Croft, Science, 212, 201-206, 1981.

Veverka, J., Icarus, 18, 657-660, 1973.

Whipple, F.L., A comet model. I. The acceleration of Comet Encke, Astrophys. J., 111, 375-394, 1950.

Wolman, Y., S.L. Miller, J. Ibanez, and J. Oro, Science, 174, 1039, 1971.

Yanagawa, H., and K. Kobayashi, An experimental approach to chemical evolution in submarine hydrothermal systems, Origins of Life and Evolution of the Biosphere, 22, 147-159, 1992.

Yen, A. S.; Kim, S. S.; Hecht, M. H.; Frant, M. S.; Murray, B. Evidence That the Reactivity of the Martian Soil Is Due to Superoxide Ions. Science, Volume 289, Issue 5486, pp. 1909-1912, 2000.

Zellner, B., Icarus, 18, 661-664, 1973.

Zent, Aaron P. On the thickness of the oxidized layer of the Martian regolith. Journal of Geophysical Research, Volume 103, Issue E13, p. 31491-31498.1998

Zimmer, C., K.K. Khurana, and M.G. Kivelson, Subsurface Oceans on Europa and Callisto: Constraints from Galileo Magnetometer Observations, Icarus, 147, 329-347, 2000.

Article 3

Despois D. and Cottin H. (2005) Comets: potential sources of prebiotic molecules for the early Earth. In Lectures in Astrobiology, (eds. M.Gargaud, B.Barbier, H. Martin and J.Reisse), pp. 289-352. Springer Verlag.

8 Comets: Potential Sources of Prebiotic Molecules for the Early Earth

Didier Despois, Hervé Cottin

"Of Ice and Men. . . "

Why should we be interested in comets when studying the origin of life on Earth? First, comets are rich in water and carbon, two essential constituents of terrestrial life; part of Earth's water and carbon might be of cometary origin. But comets might also have brought Earth one step further on the way to the emergence of life.

Early last century, Chamberlin and Chamberlin proposed that infalling carbonaceous chondrite meteorites could have been an important source of terrestrial organic compounds (Chamberlin and Chamberlin 1908). Oró was the first in 1961 to propose from observations of carbon- and nitrogen-containing radicals in cometary comae that comets may have played a similar role (Oró 1961):

> "I suggest that one of the important consequences of the interactions of comets with the Earth would be the accumulation on our planet of relatively large amounts of carbon compounds which are known to be transformed spontaneously into amino acids, purines and other biochemical compounds."

It is now quite obvious, from observations and laboratory experiments, that comets are important reservoirs of a wide variety of organic compounds.

Comets will be considered in this chapter mainly as potential reservoirs of carbon and organic molecules for the early Earth. We present first their general characteristics, then the chemical composition of cometary matter as deduced from observations and constrained by laboratory experiments, the origin and evolution of this matter – and of comets themselves – the various cometary contributions to the early Earth, and the main future of ground-based and space developments for comet science. We conclude with a list of important questions for which answers should and will be sought in the forthcoming years.

The book "Comets and the Origin and Evolution of Life", edited by Thomas et al. (1997), is a basic reference on the topic. Comets have been discussed as possible sources of prebiotic molecules by Delsemme (2000), Greenberg (e.g. 1982, 1993, 1998) and Chyba and Sagan (1997). Despois et al. (2002) and Crovisier (2004) have discussed recently the observed molecular content of comets in this perspective, while Whittet (1997) and Ehrenfreund et al. (2002) relate more generally astrochemistry to the origin of Life. Recent general reviews on cometary

science are Irvine et al. (2000), Festou et al. (1993a,b), and Bockelée-Morvan et al. (2004); the book Comets II (in press) edited by Festou, Keller and Weaver will present up-to-date information on many aspects of comets. In this book, Petit and Morbidelli (2004) survey the Solar System formation, and discuss the origin of water on Earth. Chapters of the French edition of this book (Gargaud et al., 2001, 2003), not included in this English edition, also contain much information on related topics only briefly alluded to here: build up and evolution of the Earth atmosphere (Marty; Selsis and Parisot), build up of the hydrosphere and D/H ratio (Robert), micrometeorites (Maurette). Recent related papers in English are Kasting (1993, 2003), Dauphas et al. (2000), Robert (2002), and Maurette (1998, 2000).

8.1 General Description of Comets

"Comets are small bodies of the Solar System, made of a mixture of ices and dust."

8.1.1 The Cometary Nucleus

The definition above describes in fact a specific part of comets, the cometary nucleus. Comets are most of the time far from the Sun and reduced to this nucleus, a solid body named a "dirty ice snow-ball" by Whipple (1950); it is only when comets get close enough to the Sun (less than a few UA) that they develop their other more spectacular and better known components – coma and tail – described below. Comet 1P/Halley[1] is the first of the only three comets whose nuclei have been closely observed by a space probe (the other two are 19P/Borrelly, observed from 3400 km by the Deep Space 1 spacecraft in September 2001, and P/Wild 2 observed by the Stardust spacecraft from 236 km in January 2004). In 1986, several probes were sent to observe comet Halley, among which the European Space Agency probe "Giotto" passed within approximately 500 km from the comet nucleus. The pictures taken by Giotto (Fig. 8.1) revealed an irregular-shaped body $8 \times 8 \times 16$ km by size, whose volume is roughly equivalent to a sphere of 10 km in diameter (see Newburn et al., 1991). The bright comet C/1996 B2 Hyakutake, which appeared in 1996 and passed rather close to the Earth (~ 0.1 AU), had a relatively small nucleus, about 3 km in diameter. Another comet, C1995 O1/Hale–Bopp, was detected for the first time during summer 1995 and became quite visible in spring 1997; although passing ten times further from the Earth, it has been more spectacular than Hyakutake due to its much larger diameter, approximately 45 km (see Weaver and Lamy 1999).

[1] 1P/Halley is the official complete name of the comet, according to the International Astronomical Union – see ref. CBAT for a description of the naming rules; the familiar names (e.g. "comet Halley") are also used in this chapter and should be considered as abbreviations.

Fig. 8.1. (**a**) The nucleus of comet Halley, as seen by the ESA probe Giotto in 1986. (© ESA and MPIfA) (**b**) the nucleus of comet P/Borrelly observed by NASA probe Deep Space 1 in 2001 (© NASA) (**c**) the nucleus of comet P/Wild 2 recently observed (Jan. 2004) with a resolution of 20 m by Stardust, the NASA probe that will return dust samples collected during the flyby (© NASA)

The density of cometary nuclei is difficult to measure precisely: some estimates are as low as $0.2\,g/cm^3$ or as high as $1.8\,g/cm^3$. However, most values are in the range $0.5–0.9\,g/cm^3$ (e.g. Ball et al., 2001). This is lower than the density of water ice, and would confirm the image of the "dirty snowball". Using this density, the mass of comet Halley is about 10^{18} g (1000 billion tonnes).

The cohesion of cometary nuclei is low at least in some cases, as shown by comet D/1993 F2 Shoemaker-Levy 9: when the comet passed near Jupiter, the tidal forces let the nucleus split up into a swarm of more than 20 major pieces, which later crashed onto the planet (see Noll et al., 1996). The fact

that cometary nuclei have irregular shapes shows that these bodies were never molten – otherwise they would be shaped according to the equilibrium figure of a liquid body: a sphere or, if the body rotates, an ellipsoid.

What are the ices and dust mentioned in the definition of a comet made of? Cometary ices are water ice mostly, mixed with smaller quantities of other species like methanol (CH_3OH), CO, CO_2, ... – the detailed composition is given below (Sect. 8.2.1 and Table 8.1). As for the dust grains, they are made of small particles of carbon, organic matter or silicates. The total mass of dust is roughly comparable to the mass of ices, within a factor of 10: some comets are "dusty", while other are "gaseous" (e.g. Rolfe and Battrick, 1987). Despite the presence of a large amount of ice inside the nucleus, the surface itself appears quite dark: for comet Halley, the proportion of reflected light (called *albedo*) is only 4%.

8.1.2 Comet Motion

Comets move around the Sun following orbits that are in most cases ellipses (the Sun being at one focus); in some cases the orbit may be parabolic or slightly hyperbolic (e.g. Festou et al., 1993a). The eccentricity is generally high, and often near 1 (parabola) or even slightly higher (hyperbola). For comparison, the eccentricity of a circle is zero, and that of the quasicircular orbit of the Earth is 0.017 (at present). The comet speed in the region of the Earth's orbit (i.e. at one AU from the Sun) is about 45 km/s (or 162 000 km/h). Combining (vectorially) this speed with Earth's own motion around the Sun ($\sim$ 30 km/s) leads to relative speeds ranging between 15 and 75 km/s. This confers a large kinetic energy to cometary particles entering the Earth's atmosphere and leads to dramatic effects when the nucleus itself impacts the Earth.

Comets are classified into various families according to their orbits. Long-period comets are defined as having an orbital period above 200 years. Among the long-period comets, one commonly calls "new comets" those for which aphelion (point of the trajectory furthest away from the Sun) is located beyond approximately 1000 AU and for which eccentricity is close to 1. This is not an official, well-defined, comet category; as these comets have periods above 10 000 years (and up to tens of Myr), no historical record of previous passages exists, and they appear "new" to us. Their orbits are very elongated ellipses, which, when they pass close to the Sun, look very much like parabolas. Comets with periods below 200 years are called short-period comets. Among those, one finds the *Halley family*, with periods from 20 to 200 years, and random inclinations of their orbital plane with respect to the ecliptic, and the *Jupiter family*, with periods of approximately 6 years, and small inclinations to the ecliptic.

8.1.3 Comet Reservoirs: Oort Cloud and Kuiper Belt

To explain the present number of observed comets (despite the rapid sublimation of the ice (see Sect. 8.1.5) and the origin of the various orbital families, the existence of two comet reservoirs is required.

The classical or *outer Oort cloud* (Oort, 1950) is a spherical reservoir situated between $\sim$ 20 000 and 100 000 AU; the inner radius is loosely defined (see below), whereas the outer radius corresponds to half the distance to the nearest stars, beyond which an object can no longer be considered gravitationnally linked to the Sun. Oort Cloud comets are thought to be icy planetesimals scattered by the giant planets, originating mostly from the Uranus–Neptune zone and to a lesser extent from the Jupiter–Saturn zone.

Due to stellar encounters, or to the effect of the gravitational potential of the Galaxy, some of these objects are regularly sent back towards the planet zone with nearly parabolic orbits ("new" comets). The possible quantitative importance of a more tightly bound *inner Oort cloud* (3000–20 000 AU), has been recently underlined (Fernandez, 1997, Levison et al. 2001) considering the very probable option that the Solar System and its Oort cloud formed in the dense stellar environment of a young open star cluster. Formation scenarios of the Oort cloud (e.g. Duncan et al., 1987) are still very uncertain, at least quantitatively. The total number of comets in the Oort cloud could be on the order of 10^{12}–10^{14} depending on the model and the size distribution, while the total mass estimate ranges from 1 to 250 M_{Earth}.

While the Oort cloud hypothesis explains quite well the long-period comet distribution, numerical simulations (Fernandez 1980) have stressed the importance of another reservoir, the *Kuiper Belt,* to explain the number of short-period comets. The existence of this belt was proposed first by Leonard (1930) and Edgeworth (1943), (the history of the concept, including the Kuiper (1950) paper and the later role of Cameron and Whipple, is discussed in Green 1999). The region has the shape of a thick torus and contains many small icy bodies beyond the orbit of Neptune. Since the discovery of the first Kuiper Belt object (KBO) by Jewitt and Luu in 1992, much observational and theoretical work has been undertaken (see Morbidelli and Brown (2004), Jewitt (2002) and de Bergh (2004) for recent reviews on the dynamical and physical properties of KBOs). Collisions in the Kuiper belt are thought to produce fragments, which are later scattered by Neptune and the other planets towards the inner Solar System, first as Centaurs, then as Jupiter Family comets. From the $\sim$ 800 objects now observed (summer 2003) a total population of 70 000 bodies larger than 100 km in diameter is estimated, and 1 to 10 billion bodies larger than 1 km. Several families, with probably different origin, are recognized in the Kuiper Belt (see Morbidelli and Brown 2002 and Jewitt 2002 for details). A subpopulation, the plutinos, is in a collision-avoiding resonant orbit with Neptune, and encompasses Pluto itself (and its satellite Charon). Pluto is considered as the largest KBO (with $D \sim 2500$ km), and several other large objects are known (Quaoar, $D \sim 1300$ km; Charon, $D \sim 1200$ km; Varuna, $D \sim 900$ km).

The formation of these reservoirs has been accompanied by substantial scattering of comets towards the zone of the terrestrial planets; these comets possibly supply carbon and organics to their surfaces (see Sect. 8.5) but probably make only a limited contribution to Earth's water (see Chap. 2, Part I by Petit and

Morbidelli). The composition of the comets coming from the two reservoirs is expected to differ more or less strongly according to the various formation models. Understanding the formation scenario of comets is vital for any considerations on the ubiquity (or scarcity) of terrestrial planets favourable to life development elsewhere in the Universe.

8.1.4 The Active Comet

When a comet approaches the Sun, it enters the active phase. A coma develops around the nucleus, which consists of a roughly spherical halo of neutral gas and dust particles. The radius of the coma depends on the chemical species, and ranges between less than a thousand to more than one million km (e.g. Crovisier and Encrenaz, 2000) (Fig. 8.2). What we call here "radius" is indeed a characteristic length describing the progressive decrease of the spatial density of particles. Beyond this coma, an atomic hydrogen cloud is produced by the photodissociation of a number of species, mainly H_2O and OH; this cloud can reach 1 to 10 million km. Starting from the nucleus and the coma, three types of cometary tails develop: a plasma tail, a dust tail, and a tail of neutral sodium

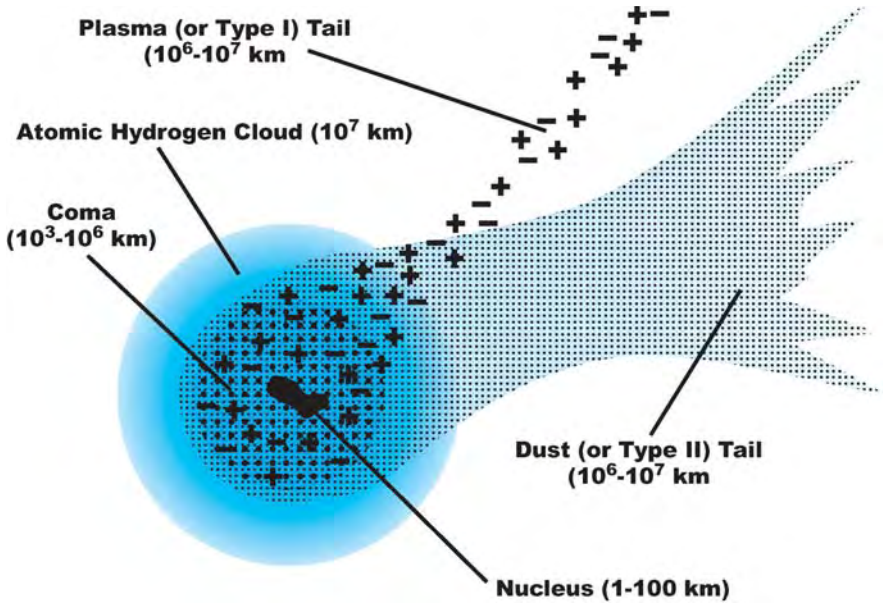

Fig. 8.2. Schematic view of an active comet. The Sun is (approximately) in the direction opposite to the ion tail, whose shape is due to the interaction with the rapid ($\sim 400-800$ km/s) charged particles of the solar wind. The dust particles that were previously released from the nucleus are slowly pushed away by the pressure of the solar photons, which, combined with the comet motion (here toward the left) explains the shape of the dust tail (see e.g. Festou et al., 1993b)

atoms – the latter clearly seen recently in observations of comet Hale–Bopp (Cremonese et al., 1997).

The plasma tail is made of (atomic and molecular) ions and electrons. It has a characteristic blue colour due to the CO^+ ions, a very rectilinear shape and is almost perfectly opposed to the Sun's direction. It is produced by the interaction of the solar wind – itself made of protons and charged particles – with the ions produced in the coma (Fig. 8.3). The yellow-white dust tail consists of small grains that have typically a diameter between 1 and 10 micrometres, and that reflect and scatter the light of the Sun. Its shape depends on the balance between the gravitational force from the Sun, and the radiation pressure due the photons of the solar radiation.

An antitail is seen in some comets, looking like a narwhal tusk pointing toward a direction opposite to the other tails. It is in fact always present, but not always visible. It reveals the presence of an accumulation of particles in the orbital plane of the comet. These particles are larger than those of the normal dust tail, and have thus been ejected at low speed from the cometary nucleus (they are less easily lifted by the gas flow) and are less sensitive to solar-radiation pressure (their mass/surface ratio is larger). By a projection effect, these particles appear as a spike at the head of the comet, when the Earth happens to cross the comet orbital plane. This feature usually appears only on the Sun side, but

Fig. 8.3. Image of a comet with well-developed tails (Hale–Bopp). The plasma tail (thin, rectilinear and bluish) is clearly recognized from the dust tail (diffuse, curved and white-yellow). (© Photo R. Lauqué)

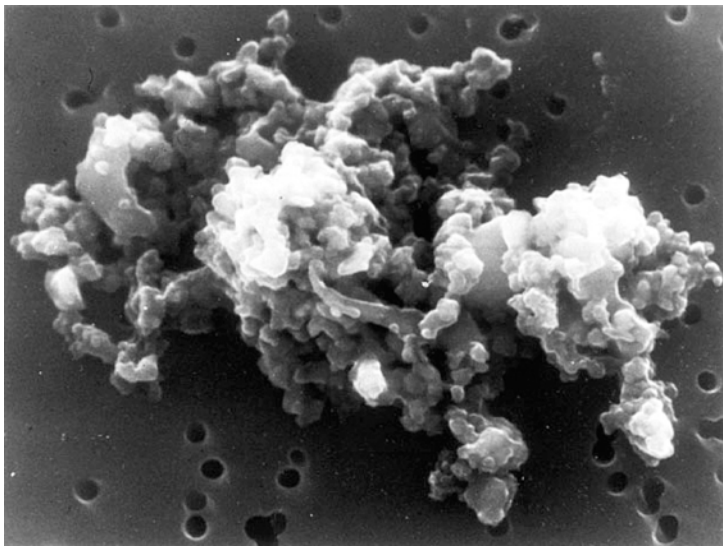

Fig. 8.4. Brownlee particle (interplanetary dust collected in the stratosphere). For the fluffiest of these particles, the origin is probably cometary

can sometimes also be distinguished as a thin line in the antisolar direction, superposed to the normal dust tail. The "neck-line" recently observed on comet P/Churyumov-Gerasimenko is an antitail (Weiler et al., 2004).

Cometary dust particles disperse more or less rapidly into the interplanetary space, according to their shape, nature and initial velocity. Some of them cross the path of the Earth; if large enough they produce meteors. One can get an idea of cometary dust particles by looking at particles collected in the Earth stratosphere ("Brownlee particles", or stratospheric interplanetary dust particles – SIDP). Many of these particles have a large surface to mass ratio and a very irregular, and somewhat fractal-like structure (Fig. 8.4). All collected particles are, however, not as irregular: one finds also among SIDPs more compact particles, similar to small blocks of clay. It is tempting – but perhaps too simplistic – to attribute to the most irregular particles a cometary origin, whereas the most compact ones would come from asteroids.

The third cometary tail, the sodium tail, made of neutral sodium atoms, was discovered for the first time in the Great Comet C/1910 A1, and reobserved more recently in comets C/1957 P1 (Mrkos) and Hale–Bopp. Sodium is pushed away in the antisolar direction by the radiation pressure, in a way similar to what happens for dust particles.

8.1.5 Gas and Dust Production

The weakest H_2O production rates currently detected in comets are of 10^{26} molecules/s (3 kg/s) when the comet is favourably situated. In comet Hale–Bopp

at perihelion, the production rate reached up to 10^{31} molecules/s, which corresponds to 300 tons/s. These rates imply that a bright comet typically loses a 1-m thick sheet at each perihelion passage. Thus for a nucleus of about a few tens km in diameter, one expects the comet to disappear after a few thousand passages close to the Sun. This implies that today short-period comets ($P < 200$ yr) cannot have occupied their present orbit since the beginning of the Solar System.

The expansion speed of most molecules in the coma is about 1 km/s. Photodissociation reactions take place, for example $H_2O \rightarrow H + OH$, followed by $OH \rightarrow O + H$. For the photodissociation fragments, the speeds can reach several km/s (8 and 21 km/s in the case of H produced from H_2O). The matter ejected by comets is almost equally distributed in mass between volatiles (mainly H_2O) and dust – within a factor 10. It is possible that the dispersion of the gas/dust ratio between comets represents a variation in the initial composition of the cometary nucleus; alternatively, it can also be an effect of evolution after many passages close to the Sun.

The dark surface observed on comet Halley's nucleus may consist of an accumulation of dust, and/or of complex refractory organic molecules. This crust may be broken by the explosion of gas pockets heated under the crust: this would enrich the coma in dust particles, and appear as an outburst of the comet.

8.1.6 Remote Activity, Outbursts and Split Comets

The activity of comets strongly depends on the distance to the Sun. It has long been thought that cometary activity developed only when the comet was closer than 4 AU from the Sun, because the "dirty snow ball" model of the nucleus suggested that water, the major volatile, controlled the emission of other molecules and of solid particles. The sublimation of H_2O ice is important only at heliocentric distances smaller than 4 AU and drives the coma development for such distances. However, a preperihelion cometary activity was detected in comet Hale–Bopp as far as 7 AU from the Sun. This activity has been attributed to the sublimation of carbon monoxide. CO is indeed present in large quantities with respect to H_2O, from 5% to above 20% – depending on the authors, the measurement techniques and the circumstances (type of comet, distance to the Sun). CO outgassing can, by a process similar to H_2O outgassing, lift dust particles and create a coma (Bockelée-Morvan and Rickman, 1999). After its passage at perihelion, comet Hale–Bopp was still outgassing CO as far as 14 AU.

Cometary matter is usually divided into two components: "refractories" and "volatiles"; the word "refractories" applies to species that do not sublimate. This classification is sometimes refined, introducing "hypervolatiles" (Ar, N_2, ...), and "semirefractories" (e.g. organic refractories, as opposed to more refractory species like silicates). Note here that water, traditionally ranking as the major volatile species in comets, behaves at 7 AU like a refractory.

A peculiar comet, 29P/Schwassmann-Wachmann 1, which follows an almost circular orbit at 6 AU from the Sun (i.e. somewhat beyond Jupiter), harbours intense and unpredictable outbursts; here also, CO is at the origin of this activity. Comet Halley showed an activity outburst after its perihelion passage, when it was already 14 AU from the Sun. Because of the lack of spectroscopic information, one does not know for sure if this outburst was also due to CO; on the pictures, only the development of a coma was noticed.

Breakup of cometary nuclei (see Boehnhardt 2002) is not uncommon. Some comets break into a few pieces (C/1975 v1 West), some into many pieces (57P/du Toit-Neujmin-Delporte in 2002), some even vanish (C/1999 S4 LINEAR). 90% of the Sun-grazing comets observed by the SOHO satellite belong to same orbital family: Kreutz family (Lamy and Biesecker 2002). They may have their origin in the splitting of one large comet. Depending on their size, the fragments have a lifetime between hours and years. The rate of splitting events of periodic comets has been evaluated to 0.01/yr/comet (Chen and Jewitt 1994). This makes splitting an important mass-loss factor, comparable to ordinary activity, and an important cause of comet death. While tidal forces close to Jupiter were clearly responsible for the breakup of Shoemaker-Levy 9, the other cases of splitting can occur at any place along the orbit, generally far from any planet. Other explanations (beside tidal forces – when applicable) involve thermal stress and gas explosions, possibly linked to runaway exothermic transformation of amorphous to crystalline ice, rotational breakup due to centrifugal force (Jewitt 2002) and fragmentation due to a collision with another small Solar System object.

Splitting events are an important source of information on the internal structure of comets. During the complete splitting of C/1999 S4 LINEAR, Bockelée-Morvan et al., (2001) detected no change in the relative molecular abundances, which pleads in favour of a rather homogeneous composition of the nucleus. Encounters with split cometary nuclei are a likely explanation for impact-crater chains seen on giant planet satellites, and that probably occurred on Earth too.

8.1.7 Nucleus Modelling: Outgassing and Internal Temperatures

Detailed modelling of the physical processes involved in nucleus formation, evolution and outgassing is a key tool to address important issues such as the pristine character of cometary matter, and the relation between abundances in the nucleus and those measured in the coma (see Sect. 8.2.1.4). Important phenomena and comet parameters include: ice sublimation; porosity of the cometary matter, which decreases from small to large objects, contributing to the density variation of icy bodies (from $\sim 0.5\,\mathrm{g/cm^3}$ for small comets to $2\,\mathrm{g/cm^3}$ for Pluto); heat transport by sublimated gases in the pores, which usually dominates solid thermal conductivity; radioactive heating by long-period elements like ^{235}U, ^{238}U, ^{40}K; disruptive and shattering collisions between comets; amorphous to crystalline ice transition, with possible release of trapped gas; surface

processing by solar and galactic photons and particles. In the formation phase, heat from the short-period element ^{26}Al and heat due to accretion itself may be critical, but their role and magnitude vary greatly from one model to another. The difference between the production rates of CO (highly volatile) and H_2O as a function of distance to the Sun is well reproduced by models (e.g. Prialnik 1999, 2002, Enzian 1999, Coradini et al., 1997a,b, Capria 2002, Benkhoff 1999, Huebner and Benkhoff 1999a); a review of those models is presented by Huebner et al., (1999b). However, several other phenomena take place that lead to the observed abundance in the coma; they make the link between nucleus and coma abundances for some species more complex (HNC, H_2CO, ...), whereas not preventing in other cases a simple connection, as shown by species whose release closely follows that of H_2O, without significant effects of differential sublimation (see Sect. 8.2.1.4 and Fig. 8.5).

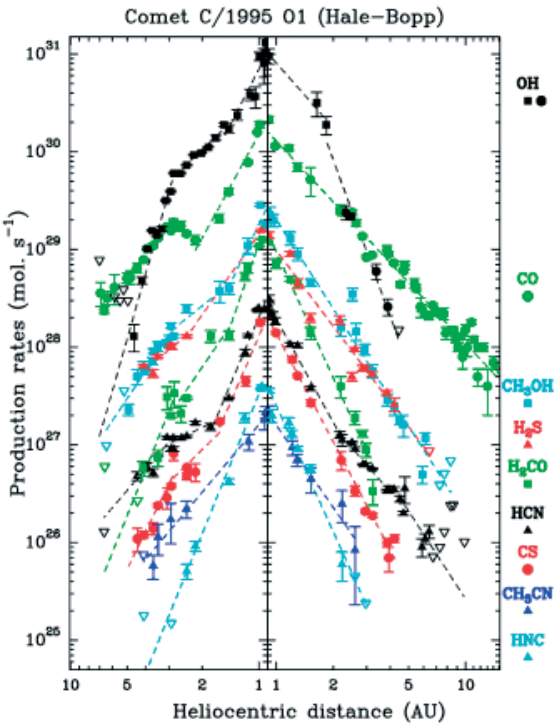

Fig. 8.5. This diagram displays the production rate Q_X of various cometary molecules as a function of heliocentric distance r_H (Biver et al. 2002). In this logarithmic scale Q_X shows, in general, a linear trend, corresponding to a power law in r_H. Whereas some species clearly depart from the mean behaviour (HNC, H_2CO, CO, CS – see discussion in text), the variation of the remaining species (e.g. CH_3OH, HCN, H_2S, CH_3CN) are roughly parallel ($\sim r_H^{-2}$), which sets a limit on the importance of differential sublimation effects for these species

8.1.8 Internal Temperature and the Case for Liquid Water

A crucial issue for prebiotic chemistry and exobiology is the maximum temperature reached by cometary matter during its history. Prialnik and Podolak (1999) consider that comets form rapidly, which leads to a key role of ^{26}Al decay in heating the interior of that comet. The maximal temperature reached somewhere in the nucleus ranges from low (35–90 K for a small 1-km radius comet with low/ high (0.1/0.9) porosity) to 270–210 K for a 100-km radius object. A very different situation is found in McKinnon (2002), who modelled the thermal history of large icy bodies in the outer solar nebula (Kuiper Belt). The accretion there is slow enough for ^{26}Al to have mostly decayed, and collisional accretion is the main heat source. The temperature remains below 100 K in most places for radii below 100 km, but reaches more than 250 K in the case of KBO Varuna ($R \sim 400$ km).

The prospect for high temperature inside the nucleus raises the question of possible liquid water inside comets or Kuiper Belt objects. Liquid water is a key parameter for chemical evolution toward prebiotic molecules, such as amino acids more complex than glycine. Therefore liquid water events on comets might allow the synthesis of more molecules than those one would expect in "dry" comets. From the model quoted above, liquid water seems excluded at present times in the bodies of modest size (< 100 km diameter) reaching the zone of terrestrial planets. Conditions were more favourable in the past but only a very limited parameter range would allow liquid water to be present for some time (Podolak and Prialnik 1997); in the case of KBOs, the body should be among the largest (Pluto?).

8.2 Chemical Composition of Comets as Deduced from Observations

8.2.1 Volatiles

8.2.1.1 Observations

Many observations and new discoveries concerning cometary volatiles were made recently, particularly thanks to the development of new instruments (large millimetre-wavelength radio telescopes, among which the IRAM 30-m dish on Pico Veleta and the Plateau de Bure interferometer have proven especially useful; infrared instruments, either ground-based or space-borne: Keck Telescope with NIRSPEC, and ISO satellite) and with the presence of very active comets: Hyakutake in 1996 and Hale–Bopp in 1997 (Bockelée-Morvan 1997, Despois 1999, Crovisier 1999, Bockelée-Morvan et al., 2000). Ten years before, the passage of comet Halley in 1985–86 had already brought considerable progress, from ground-based observations as well as from space probes, in particular Giotto and Vega 1 and 2 (Crovisier and Schloerb 1991, Encrenaz and Knacke 1991).

The majority of new detections of parent molecules (i.e. molecules coming directly from the nucleus) have been performed through radioastronomical observations. This technique provides very safe identifications of the molecular species through very high resolution study ($R = \lambda/\Delta\lambda \sim 10^7$ or better) of their rotational spectrum. Molecular abundances from radio data are usually considered to be accurate within 10–20% (calibration uncertainties), provided the excitation model for the molecule is correct. When comparing various techniques (UV, IR, radio), abundances agree usually well (within a factor of 2 at most). Among the species detected for the first time in Hale–Bopp, formamide (NH_2CHO) – a species already complex for astronomers! –already bears some resemblance to glycine NH_2-CH_2-COOH.

8.2.1.2 Molecular Abundances in Cometary Ices

Molecules detected in comets are given in Table 8.1; abundances – by molecule number – are expressed in per cent with respect to H_2O. The majority of the values are from Hale–Bopp observations. The next columns indicate, where available, the comet-to-comet variation range, and the number of comets observed (detected + undetected; Biver et al., 2002). The meaning of these abundances is discussed below (Sect. 8.2.1.4).

The most abundant species, with abundances around 10% of H_2O, are carbon monoxide CO (from 1 to 30%, see below), carbon dioxide CO_2 (5%) and methanol (1–5%). At the $\sim$ 1% level one finds the first sulfur-bearing species, H_2S, formaldehyde H_2CO (its exact abundance is hard to determine, due to the extended source problem discussed below), and the first nitrogen-bearing species: ammonia NH_3 (0.6%). Then, three hydrocarbons that are observable only in the infrared: methane CH_4 and ethane C_2H_6(0.6%) and acetylene C_2H_2 (0.1–0.5%). With 0.25%, ethylene glycol CH_2OHCH_2OH is the second alcohol. One also finds at these levels other sulfur species like SO_2 (0.1%), OCS and CS_2, and HCN (0.2%). SO (0.2–0.8%) is probably mostly a product of SO_2 photodissociation (estimated itself around 0.1%). The least abundant currently detectable species have a relative abundance of approximately 10^{-4}. Among them, isocyanic acid HNCO, formic acid HCOOH, the disulfur S_2, methylformate $HCOOCH_3$, HNC (see below), methyl cyanide CH_3CN and cyanoacetylene HC_3N (in comparable abundances), thioformaldehyde H_2CS and formamide NH_2CHO.

8.2.1.3 A Few Important Cases

• *Newly Found Species*

Bockelée-Morvan et al., (2000, note), and Bockelée-Morvan and Crovisier (2002) report the identification of acetaldehyde CH_3CHO, with an abundance of about 0.02% relative to H_2O from a reanalysis of comet Hale–Bopp data. Recently, CH_2OCH_2OH (ethylene glycol – commonly "antifreeze") has been identified

Table 8.1. Relative production rates of molecules in the coma, expressed by molecule number and in % relative to water ice (adapted from Despois et al., 2002). This rates are believed to be good tracers of molecular abundances in cometary ices, except for some species, like CO, H_2CO, HNC (see text). The values are for comet Hale–Bopp (Bockelée-Morvan et al., 2000, Crovisier et al., 2004a,b), except when indicated Hya. (Hyakutake) or I–Z (Ikeya–Zhang). When the molecule has been measured in several comets a range (Biver et al., 2002) is given

Molecule	Abundance (H_2O = 100)	Intercomet variation	Detected comets + upper limits	Notes
H_2O	100			
H_2O_2	< 0.03			
CO	23	$< 1.7 - 23$	$5 + 4$	Var.
CO_2	6 (various)			
CH_4	0.6			
C_2H_6	0.6			
C_2H_2	0.2			
C_4H_2	0.05?(I–Z)			Prelim.
CH_3C_2H	< 0.045			
CH_3OH	2.4	$< 0.9 - 6.2$	$15 + 2$	
H_2CO	1.1	$0.13 - 1.3$	$13 + 2$	Extend.
CH_2OHCH_2OH	0.25			
HCOOH	0.09			
$HCOOCH_3$	0.08			
CH_3CHO	0.025			
H_2CCO	< 0.032			
c-C_2H_4O	<0.20			
C_2H_5OH	< 0.10			
CH_2OHCHO	<0.04			
CH_3OCH_3	< 0.45			
CH_3COOH	< 0.06			
NH_3	0.7			
HCN	0.25	$0.08 - 0.25$	$24 + 0$	
HNCO	0.10			
HNC	0.04	$< 0.003 - 0.035$	$5 + 2$	Extend.
CH_3CN	0.02	$0.013 - 0.035$	$4 + 0$	
HC_3N	0.02			

Table 8.1. (continued)

Molecule	Abundance ($H_2O = 100$)	Intercomet variation	Detected comets + upper limits	Notes
NH_2CHO	0.015			
NH_2OH	< 0.25			
HCNO	< 0.0016			
CH_2NH	< 0.032			
NH_2CN	< 0.004			
N_2O	< 0.23			
Glycine I	< 0.15			
C_2H_5CN	< 0.010			
HC_5N	< 0.003			
H_2S	1.5	$0.12 - 1.5$	$11 + 3$	
OCS	0.4			Extend.
SO	0.3			Extend.
CS_2(from CS)	0.17	$0.05 - 0.17$	$9 + 0$	
SO_2	0.2			
H_2CS	0.02			
S_2	0.005 (Hya)			
CH_3SH	< 0.05			
NS	0.02			Parent?
PH_3	< 0.16			
NaOH	< 0.0003			
NaCl	< 0.0008			

Notes (see text for discussion):

- Extend.: extended source – in this case the abundance depends somewhat on the model adopted for the spatial distribution of the source
- Var.: CO shows large variability in a given comet along the orbit, and from comet to comet
- C_4H_2 values are preliminary
- NS is probably a photodissociation product from an unknown parent.
- CS_2 abundance indirectly deduced from CS abundance
- CO_2 measured to be 20% in Hale–Bopp at a distance of 2.9 UA by the ISO satellite
- Glycine is a compound with a very low volatility. Nondetection in the gaseous phase does not imply absence from the refractory component. Glycine I refers to one of the two most stable conformers of the molecule.

from the same archive spectra (Crovisier et al., 2004b); surprisingly, its abundance (0.25%) is higher than the upper limit for ethanol (0.1%), which may be an important constraint on the formation processes of cometary molecules. C_4H_2 has been possibly identified in the near infrared (NIR) spectrum of comet C/2002 C1(Ikeya–Zhang) (Magee–Sauer 2002). NS ($x \sim 0.02\%$), a radical, probably a dissociation product, has been detected in comet Hale–Bopp (Irvine et al., 2000b); its parent is not yet known: HNCS, HNSO, NH_4SH have been suggested.

• *Supervolatiles*

Very volatile ("supervolatile") species, like Ar, N_2, H_2, CO are important to set an upper limit to the highest temperature ever reached by the cometary nucleus and thus its degree of thermal processing. Bockelée-Morvan and Crovisier (2002) report doubts on the detection of Ar and N_2 (from N_2^+). H_2 appears to be a product of water dissociation, not a nuclear species. To date, the most volatile species are thus CO and CH_4.

• *Glycine Upper Limit in Volatiles*

Table 8.1 includes upper limits from radio observations of the coma (Bockelée-Morvan and Crovisier 2002). The limit ($x < 0.15\%$ or ~ 0.004 by weight or 6×10^{-5} mol/g) on glycine (the simplest amino acid, and one of the 20 that are the building blocks of proteins) is not very stringent, due to the intrinsic weakness of its radio lines. Furthermore, this limit concerns only the fraction of glycine molecules that could be released from the nucleus due to ice sublimation. Note that pure solid glycine itself is a refractory compound ($T_{\rm subl}$ is ~ 500K for 1 atm pressure) and that thermal destruction occurs at a similar temperature. In the CM carbonaceous chondrite meteorite Murchison, glycine abundance (here with respect to refractories) is about 10^{-7} mol/g (Cronin and Chang 1993).

8.2.1.4 Are Coma Abundances a True Image of Ice Composition in the Nucleus?

On a plot of their production rates according to the distance to the Sun (Fig. 8.5 "Christmas tree plot" Biver et al., 2002), a majority of individual molecules vary in a similar way, which suggests that most of the cometary material escapes as a whole, without strong differentiation between chemical species. A few species (most notably CO, H_2CO, and HNC) harbour, however, a peculiar behaviour, and require additional phenomena to be taken into account: differential sublimation, extended source, and coma chemistry.

• *Differential Sublimation*

The great volatility of CO induces an important variation of the CO/H_2O ratio with heliocentric distance. CO can not only move through the micropores present in the ice, but even through the structure of crystalline ice itself; as a result, the surface layers of the nucleus can, according to cases, be either depeleted or enriched in CO. This phenomenon has been modelled in detail (see Sect. 8.1.7).

• *Extended Sources*

Some coma molecules do not appear to be emitted directly from the nucleus, but are more probably secondary products of photo- or thermal degradation of larger species, or products of chemical reactions in the coma. Thus they appear to come from an extended source surrounding the nucleus. Bockelée-Morvan and Crovisier (2002) summarise different indicators of extended source (spatial distribution, line shape, production behaviour with distance to the Sun). The best established cases are H_2CO and CO. Recent observations indicate that SO, CS, OCS and HNC harbour extended source characteristics. Photodissociation is likely to explain the case of SO (from SO_2) and CS (from a yet uncertain parent, maybe CS_2). HNC may be partly chemically produced (see below). The origin of H_2CO is not only in the nucleus, but also in the coma, where it is released from a "carrier": maybe organic CHON grains, maybe polymers (polyoxymethylene – POM, which has been detected after experimental simulations of cometary ice analogs), maybe both. The degradation of polyoxymethylene (POM) has been studied in the laboratory and is found to be a possible source for H_2CO (Cottin et al., 2001, 2004). Various CN-bearing compounds including hexamethylenetetramine (HMT, see Fig. 8.13) and poly-HCN are possible sources of extended CN radical in the coma (Fray et al., submitted) in addition to the photodissociation of HCN.

• *Coma Chemistry*

HNC is a case for which coma reactions (other than photodissociation) can affect molecular abundances. The peculiar behaviour of the production rate of this species in comet Hale–Bopp, with its strong increase when the comet approached the sun, leads to the proposal of its production from HCN through chemical reactions in the coma as an explanation. Rodgers and Charnley (2001a) shows that reactions between HCN and high-speed ("suprathermal") hydrogen (from H_2O dissociation) could explain HNC production in comet Hale–Bopp. This process, however, is not efficient for smaller comets such as comet Hyakutake, for which the origin of HNC is still an open question (Irvine et al., 2003, Rodgers and Charnley 2001, Charnley et al., 2002a,b). It should be noted that in interstellar clouds, and thus perhaps also in protosolar nebulae, HNC and HCN are both present, and that HNC is stable in ice at sufficiently low temperature. Therefore, the presence of some HNC in the nucleus is not excluded.

Are some other minor species due to reactions in the coma? Rodgers and Charnley (2001b) show it cannot be the case for the detected species $HCOOCH_3$ and HCOOH, which are then expected to be directly released from the nucleus.

8.2.2 Grains

8.2.2.1 Nature of Grains

The chemical composition of the grains of comet Halley has been analyzed in situ by mass spectrometry (instrument PUMA on board the Vega 1&2 space-

craft, and instruments PICCA, IMS and NMS on board Giotto spacecraft – Altwegg et al., 1999). When grains are ejected from the nucleus, any embedded ice sublimes within the first few kilometres. Therefore, we will only consider the refractory (nonvolatile) component of grains in this section. Vega spacecraft have collected particles between 80 000 and 120 000 km from the nucleus. About 5000 particles were analyzed, with mass ranging from 5×10^{-17} to 5×10^{-12} g (which means a size ranging from 0.04 to 2 µm if one assumes a density equal to 1). The total mass that was analyzed was only a few nanograms. Their elemental composition shows that the particles are made of a mixture of silicates and organic material. In comet Halley's coma, when Giotto made its measurements, the ratio between silicates and organic matter was found to be between 1 and 2. When organic matter is very abundant, the grains are called "CHON" grains (i.e., compounds of C, H, O and N). According to some models, the small mineral particles might be embedded in a matrix of carbonaceous matter (Greenberg 1982); however, mass spectrometer measurements show the existence of pure silicate an d pure organic grains, beside grains of mixed composition (Fomenkova, 1999).

Figure 8.6 shows the production of grains in mass and number for comet Halley as derived by Crifo (Crifo 1995, Crifo and Rodionov 1997) from in situ measurements presented in McDonnell et al. (1991). It must be noted that data up to 1 mm are direct in situ measurements, whereas higher values are extrapolations (relevant within an order of magnitude of uncertainty).

The temperature of grains can be derived from observations, but the best estimations are reached through calculations based on hypotheses about their shape and composition (Crifo 1988). Two extreme temperatures for each grain

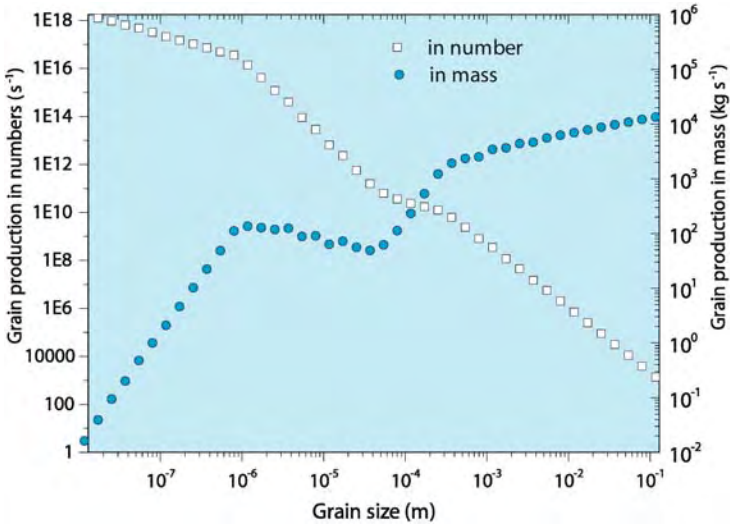

Fig. 8.6. Dust-grain production from comet Halley nucleus assuming a density of $1\,\mathrm{g\,cm^{-3}}$ (Cottin et al., 2004)

size are achieved, depending on whether the grain is made of olivine (low temperature) or amorphous carbon (high temperature). Olivine represents the silicate nucleus of grains with a very low absorbance in the visible; it is a lower temperature limit for grains. Amorphous carbon (aC) is representative of dark material, and stands as an upper limit for a strongly absorbing organic component of grains. As grain composition is poorly known, one cannot pretend to better constrain their temperature than between those two extremes. Grains temperatures are presented on Fig. 8.7 for a spherical shape; these temperatures are reached within the first few tens of kilometres from the nucleus (Crifo 1991). For porous or nonspherical grains the temperature tends to be higher.

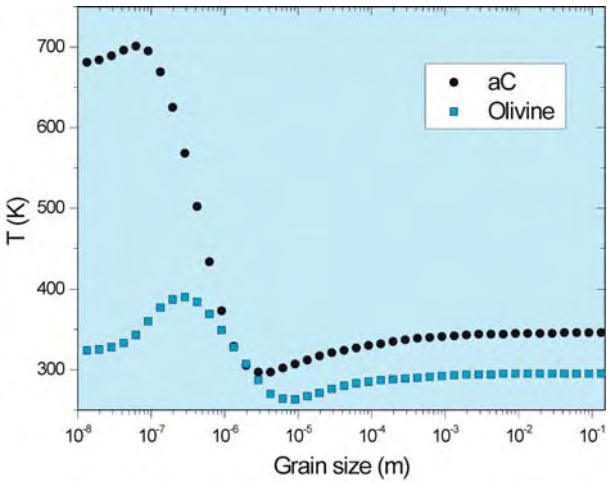

Fig. 8.7. Grain temperature as a function of size and composition (Cottin et al., 2004)

8.2.2.2 Organics in Grains

The most fruitful works related to the organic composition of grains have been reported in Kissel and Krueger 1987, and Krueger and Kissel 1987). To interpret the PUMA's mass spectra, they consider that all sudden dissipation processes near solid surfaces after an impact are governed by the same rules of molecular ion formation (Fig. 8.8). Such impacts occur when a dust particle hits the mass spectrometer's target. This hypothesis yields a good agreement between their predictions and other observations for small molecules (e.g. HCN, CH_3CN).

For larger molecules the problem is more complex, as they cannot survive the impact process without fragmentation. In addition to the difficulty of assembling correctly the fragments to reconstitute the original molecule, the nature of the fragments themselves is uncertain, several fragments having the same mass (to the resolution of the spectrometer). Thus the identification by these authors

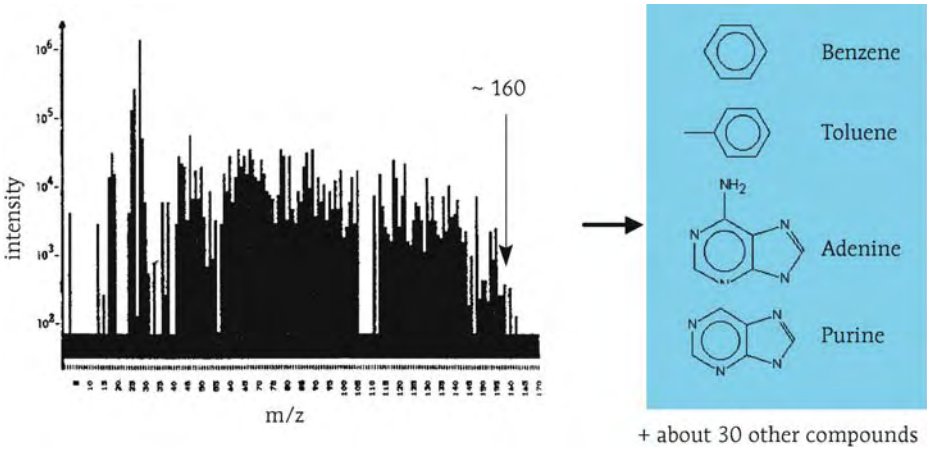

Fig. 8.8. Cumulated mass spectra collected in comet Halley by instrument PUMA on board VEGA-1 spacecraft and tentative interpretation. Adapted from Kissel and Krueger (1987)

of purines and adenine, for example, should be considered as very tentative. However, what is clearly shown by PUMA mass spectra is that compounds with complex structure and large molecular masses (at least with m/z up to $160\,\mathrm{g\,mol^{-1}}$) are present on grains.

First interpretations of the heavy-ion mass spectra from the PICCA instrument led Huebner (1987) to conclude the presence of polyoxymethylene (POM) in comet Halley. After further analyses, Huebner et al., (1989) discussed the presence of POM derivatives such as sulfur copolymers. As already stated in this chapter, the presence of POM in comets is coherent with the detection of extended sources of H_2CO in the coma. Indeed, this molecule could be the degradation product of POM. The authors also suggest the presence of HCN polymers such as polyaminocyanomethylene (PACM: $(NH_2–C–CN)_n$), even though these polymers are very difficult to detect because in the coma $HCN/H_2CO \sim 0.1$ and because from thermodynamic considerations N-containing polymers should be less volatile than O containing polymers (Krueger et al., 1991). The presence of HCN/H_2CO copolymers could also be suggested on comets because these two molecules polymerize very easily by themselves.

Later, however, Mitchell et al., (1992) showed that the mass spectrum pattern that led Huebner to announce the detection of polyoxymethylene is only characteristic of a mixing of molecules composed of C, H, O and N atoms (CHON molecules). Therefore PICCA mass spectra do not imply the presence of POM, but only of a large diversity of CHON molecules, among which POM could be present. The most we can say, if we consider laboratory simulation results presented latter in this chapter and the detection of an extended source of formaldehyde, is that the presence of POM on cometary nuclei is possible.

Beside polymers, heteropolymers and large CHON molecules, other compounds have been suggested: pure carbon grains, PAHs (polycyclic aromatic hydrocarbons, i.e. aromatic cycles linked together), very "branched" aliphatic hydrocarbons (Fomenkova 1999). PAH detection from in situ UV spectroscopy in Halley was announced (Moreels et al., 1994); PAHs were not seen in the ISO spectra of Hale–Bopp, possibly due to the lower temperature of the comet at the time of these observations (Crovisier 1999). A weak residual feature at 3.28 µm was, however, seen by Bockelée-Morvan et al., (1995) in various comets, and especially the dustier ones, which might be due to PAHs; this would correspond to a relative abundance to water 1.5 to 10×10^{-6}, at least 100 times below that deduced from UV data. A list of compounds probably and possibly detected in comet Halley grains by mass spectroscopy is reported in Table 8.2.

Table 8.2. Organic molecules inferred from mass spectra of gas and dust particles in comet Halley. The confidence levels of detections by MS are established as follows: – Confirmed: Molecule also detected by remote observations; – High: Molecule not detected by remote observations but present after laboratory irradiations of cometary ice analogs; – Medium: Molecule detected only by mass spectroscopy with a good confidence level according to the authors; Low: Molecule only inferred by mass spectroscopy with a low confidence level according to the authors

Molecule	Family	Mass spectrometer	Confidence level	Ref.
Hydrocyanic Acid	C–N–H	PUMA, PICCA	Confirmed	1, 2, 3
Methyl cyanide	C–N–H	IMS	Confirmed	7
Acetonitrile	C–N–H	PUMA, PICCA	Confirmed	1, 2, 3
Methanol	C–O–H	NMS	Confirmed	6
Formaldehyde	C–O–H	PUMA, PICCA	Confirmed	3
Formic acid	C–O–H	PUMA	Confirmed	1, 2
Acetaldehyde	C–O–H	PUMA, PICCA	Confirmed	1, 3
Ammonia	N–H	PUMA	Confirmed	2
Isocyanic acid	C–N–O–H	PUMA	Confirmed	1, 2
Ethane	C–H	NMS	Confirmed	8
Acetylene	C–H	NMS	Confirmed	8
Acetic acid	C–O–H	PUMA	High	1
Polyoxymethylene	C–O–H	PICCA	High (itself or derivatives)	4, 5
Ethene	C–H	NMS	High	8
Iminoethane	C–N–H	PUMA	Medium	1, 2
Aminoethene	C–N–H	PUMA	Medium	1, 2
Pyrroline	C–N–H	PUMA	Medium	1

Table 8.2. (continued)

Molecule	Family	Mass spectrometer	Confidence level	Ref.
Pyrrole	C–N–H	PUMA	Medium	1, 2
Imidazole	C–N–H	PUMA	Medium	1
Pyridine	C–N–H	PUMA	Medium	1, 2
Pyrimidine	C–N–H	PUMA	Medium	1, 2
Ethyl cyanide	C–N–H	IMS	Medium	7
Pentyne	C–H	PUMA	Low	1
Hexyne	C–H	PUMA	Low	1
Butadiene	C–H	PUMA	Low	1
Pentadiene	C–H	PUMA	Low	1
Cyclopentene	C–H	PUMA	Low	1
Cyclopentadiene	C–H	PUMA	Low	1
Clyclohexene	C–H	PUMA	Low	1
Cyclohexadiene	C–H	PUMA	Low	1
Benzene	C–H	PUMA	Low	1
Toluene	C–H	PUMA	Low	1
Propanenitrile	C–N–H	PUMA	Low	1
Iminomethane	C–N–H	PUMA	Low	1
Iminopropene	C–N–H	PUMA	Low	1
Purine	C–N–H	PUMA	Low	1, 2
Adenine	C–N–H	PUMA	Low	1, 2
Polyaminocyanomethylene	C–N–H	PICCA	Low	5
Methanolnitrile	C–N–O–H	PUMA	Low	1
Methanalimine	C–N–O–H	PUMA	Low	1
Aminomethanol	C–N–O–H	PUMA	Low	2
Aminomethanal	C–N–O–H	PUMA	Low	2
Oxyimidazole	C–N–O–H	PUMA	Low	1
Oxypyrimidine	C–N–O–H	PUMA	Low	1
Xanthine	C–N–O–H	PUMA	Low	1

1 (Kissel and Krueger 1987); 2 (Krueger and Kissel 1987); 3 (Krueger et al., 1991); 4 (Huebner 1987); 5 (Huebner et al., 1989); 6 (Eberhardt and Krankowsky 1995); 7 (Geiss et al., 1999); 8 (Altwegg et al., 1999)

8.2.2.3 Cometary Silicates

The nature of other refractory components is constrained by infrared observations of comets. Identification is achieved through a comparison of observations with laboratory spectra of different kinds of silicates and possibly carbonaceous

grains, and it should be noted that there is no unique solution to the fitting problem. It appears that grains are made of a mixture of crystalline and amorphous silicate (Brucato et al., 1999, Crovisier et al., 1997, Harker et al., 2002, Hayward and Hanner 1997, Nuth et al., 2002, Wooden et al., 2000).

Crystalline forsterite (a magnesium-rich olivine) has been detected thanks to the ISO infrared satellite (Crovisier et al., 1997). Ground-based telescopes have enabled a study of the infrared spectrum around 10 μm, and determined the ratio pyroxene/olivine. According to Harker et al., (2002) amorphous silicates make up about 70% (by mass) of the submicrometre-sized ($\leq 1\,\mu$m) silicate dust grains in Hale–Bopp's coma, and are distributed roughly equally between olivine and pyroxene composition, and between Fe-rich and Mg-rich species; the remaining 30% are predominantly Mg-rich crystalline silicates with a crystalline

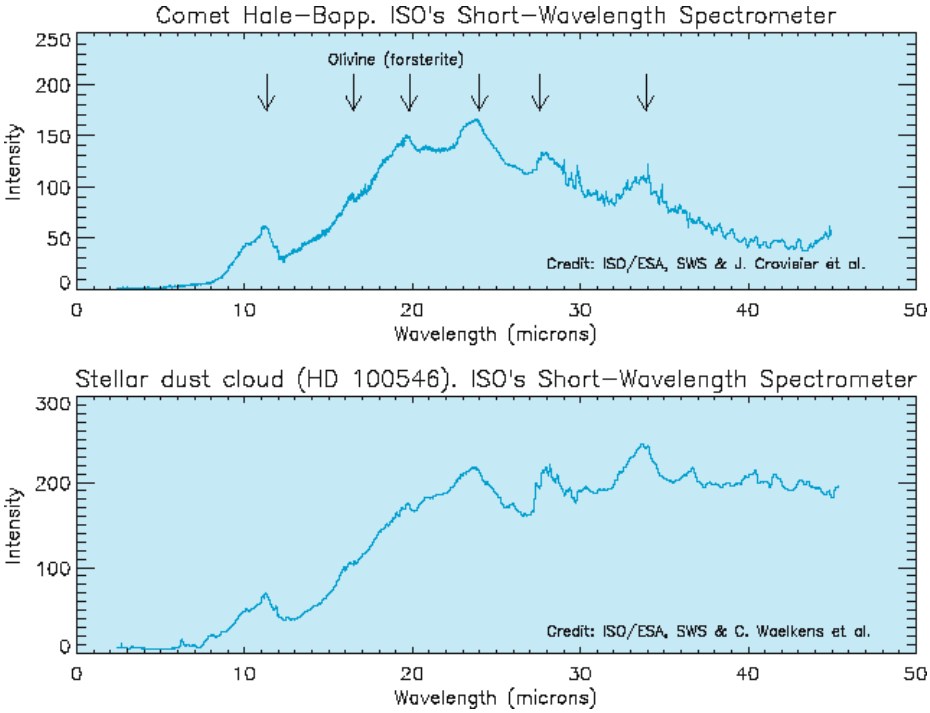

Fig. 8.9. Comparison of the infrared spectrum of Hale–Bopp obtained by ESA's Infrared Space Observatory ISO (Crovisier et al., 1997) with that of a young star of type AeBe (e.g. Malfait et al., 1998). The features in the comet spectrum lead to the identification of a crystalline silicate, fosterite, a magnesium-rich olivine. The AeBe stars are slightly more massive than the Sun, but the dust that surrounds them and that is responsible for this IR emission is considered to be similar to dust in the protosolar nebula. In HD100456, the similarity is even more striking and points towards a high crystalline mass fraction and small particle size ($< 10\,\mu$m) in both cases (Bouwman et al., 2003)

olivine:orthopyroxene ratio about 4 to 5 : 1 that seems to vary slightly with heliocentric distance. Figure 8.9 shows a comparison between the infrared spectrum of Hale–Bopp and circumstellar matter around a young star. However, data of such a high quality is only available for one comet (Hale–Bopp).

8.2.3 Elemental and Isotopic Composition

8.2.3.1 Elements

The composition in elements that can be deduced by combining dust and gas measurements (Geiss 1988) leads to abundances normalized to silicon close to solar abundances for carbon and oxygen. However, one notes a depletion (underabundance) of hydrogen of about 600, due to the high H_2 volatility and a depletion of 2 for nitrogen, which is explained in the same way by the fact that nitrogen is often in the form of N_2, a very volatile gas, too (Fig. 8.10). The

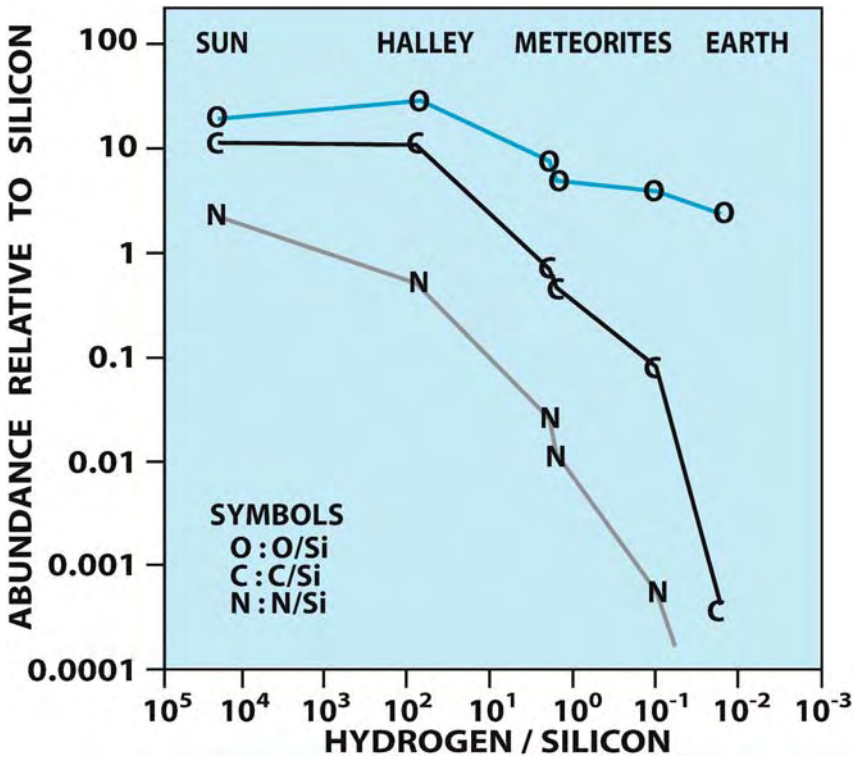

Fig. 8.10. Comparison of elemental abundances in the Sun, comet Halley, and (C1, C2) meteorites (Geiss 1988). The element abundance ratios in P/Halley are uncertain by a factor of about two (excluding the variability and uncertainty in the gas/dust ratio)

gas:dust ratio derived in the case of Halley is 1:2 in mass (Jessberger and Kissel 1991); note that the computation of the elemental composition for the whole comet uses this ratio and is quite sensitive to it.

In Fig. 8.10, the elemental composition of comets is also compared with that of carbonaceous chondrites (Geiss 1988). Elements of the series Mg–Al–Ca, as well as oxygen have comparable abundances within a factor of 2. On the other hand, in comet Halley, abundances of carbon, hydrogen, nitrogen and of any other element appearing mostly in volatile compounds are larger than in carbonaceous chondrites. This leads us to say that cometary matter is more "pristine" than that of carbonaceous chondrites, in the sense that it underwent less heating and thus was less processed.

8.2.3.2 Isotopic Abundances

Much of the information on the origin of cometary matter and on the importance of the cometary contribution to the Earth's water content derives from the study of isotopic abundances, which have been recently reviewed by Altwegg and Bockelée-Morvan (2003). The D/H ratio in particular is very important data to investigate the origin of cometary matter (e.g. Bockelée-Morvan et al., 1998, Mousis et al., 2000, Robert 2002) and its delivery to the Earth (Dauphas et al., 2000; see Sect. 8.5.3). It was measured for two species: HDO/H_2O ($D/H \sim 3 \times 10^{-4}$) and DCN/HCN ($D/H \sim 2.3 \times 10^{-3}$); upper limits on the order of 10^{-2} or below have also been set for deuterated formaldehyde, methanol, ammonia and H_2S. Molecules appear enriched in deuterium: as can be seen in Fig. 8.11, D/H in water for the 3 comets for which it has been measured is twice the ocean SMOW value, and an order of magnitude higher than the protosolar value of 2.5×10^{-5}. This enrichment is however not as high as in the interstellar gas (where multiply deuterated species like D_2CO and even ND_3 have been observed). Measurements of the O, C, N and S isotopes display, in general, abundances very close to solar abundances (e.g. Jewitt et al., 1997, Lecacheux et al., 2003), which confirms that the comets are Solar System objects. This does *not* contradict the assumption of an interstellar origin of the cometary matter discussed below. Indeed, the Sun and the Solar System as a whole were formed from a homogeneous clump of interstellar matter and it is from the same fragment of IS matter that the comets were made.

Some carbonaceous grains analyzed by in situ mass spectroscopy in Halley (Jessberger and Kissel 1991) showed a very high ratio $^{12}C/^{13}C$, rising up to 5000, whereas the normal ratio in Solar System objects is 89. These small grains would have been formed in the envelope of certain stars known as AGB stars (asymptotic giant branch) and would then have been injected into the interstellar medium. They thus would have been mixed with the interstellar cloud fragment that condensed to form the protosolar nebula, then later incorporated as such in the matter of forming comets. As this high departure from solar $^{12}C/^{13}C$ values is concentrated in very small grains, which do not represent a large quantity

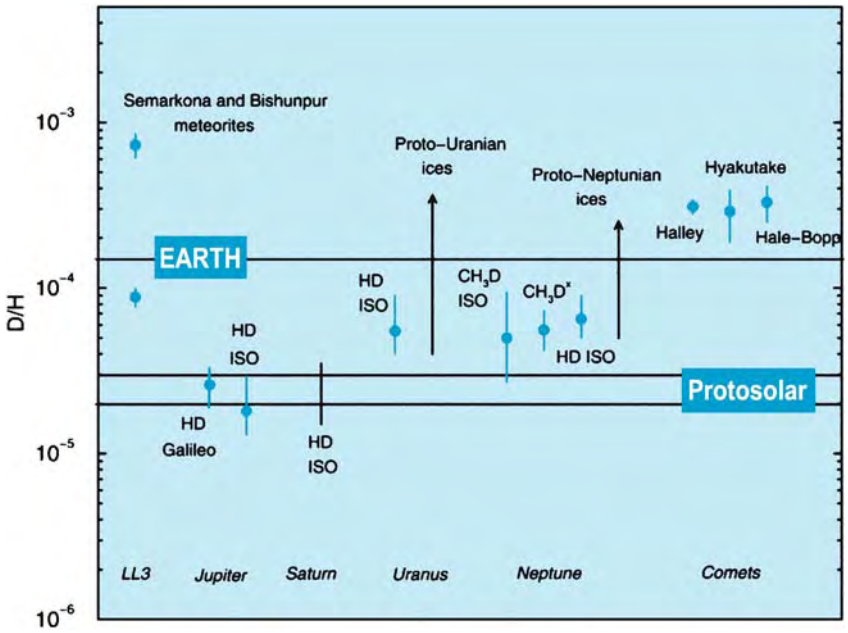

Fig. 8.11. D/H ratios in the Solar System. For comets, only measurements of D/H in water are shown (from Hersant et al., 2001)

of carbon, the average value of the cometary $^{12}C/^{13}C$ ratio remains close to the solar value, namely approximately 89. An intriguing measurement has been made in CN (Arpigny et al., 2003) suggesting the existence of parents of the CN radical other than HCN – possibly solid organic compounds – with strongly nonsolar N isotopic ratios.

8.2.4 Are All Comets Similar?

Abundance variations are observed from one comet to another, in particular for CO (from less than 1% to more than 30% according to comets and to the distance from the Sun) and CH_3OH (1 to 5%; e.g. Bockelée-Morvan 1997). This composition is deduced from gas abundances measured in the coma, making assumptions on the spatial distribution of the molecules, the limited chemistry in the coma, and the sublimation process.

That all comets are not similar already has observational evidence, as seen from dust content and daughter species C_2, CN (A'Hearn et al., 1995, Rolfe and Battrick 1987). Column 3 in Table 8.1 shows the range spanned by the observed molecular abundances in a sample of comets (Biver et al., 2002). Different compositions are expected, to some extent, between comets coming from the Oort cloud and the Kuiper Belt due to their different formation zone (respectively Jupiter–Neptune versus mostly transneptunian, see Sect. 8.4 and Morbidelli and

Table 8.3. Molecules detected during experimental simulations of cometary ice analogs. Italic letters refer to molecules actually detected in comets. (t) means tentative detection only in the analogs. Amino acids (alanine, AIB, ... except glycine) were detected after acid hydrolysis of the room temperature residue. Updated from Cottin et al., 1999

Hydrocarbons:
CH_4
C_2H_2, C_2H_4, *C_2H_6*
C_3H_8, C_4H_{10}
C_5H_{10}, C_5H_{12}
C_6H_{12}, C_6H_{14}
C_7H_{16}

Amides:
NH_2CHO
CH_3CONH_2
$HOCH_2CONH_2$
$NH_2(CO)_2NH_2$
$HOCH_2CH(OH)CONH_2$

Amines:
$HOCH_2CH_2NH_2$
$HCNH(NH_2)$
Diaminopyrrole
Diaminofurane
Triaminopropane
$(CH_2)_6N_4$ (HMT)

Aldehydes:
H_2CO
CH_3OCH_2CHO (t)

Ketones:
CH_3COCH_3
$HOCH_2COCH_3$
$HOCH_2CH_2COCH_3$

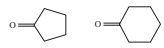

Carboxylic acids:
$HCOOH$
CH_3COOH (t)
$HOCH_2COOH$
$HOCH_2CH(OH)COOH$
$HOCH_2CH_2COOH$
$NH_2COCOOH$

Aromatic Compounds:

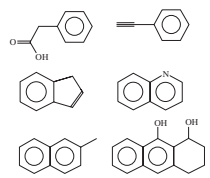

Ethers:
$CH_3OCH_2OCH_3$ (t)
$C_3H_6O_3$ (Trioxane) (t)
$(-CH_2-O-)_n$ (POM)

Alcohols:
CH_3OH
CH_3CH_2OH
$HOCH_2CH_2OH$
$HOCH_2CH(OH)CH_2OH$
$C_4H_8(OH)_2$
C_5H_9OH (t)
$C_5H_{11}OH$

Amino Acids:
NH_2CH_2COOH (Glycine)
$NH_2CH(CH_3)COOH$ (Alanine)
$CH_3CH_2CH(NH_2)COOH$ (α ABA)
$CH_3CH(NH_2)CH_2COOH$ (β ABA)
$(CH_2NH_2)(CH_3)CHCOOH$ (AIBA)
Sarcosine
Ethylglycine
Valine, Proline, Serine
Aspartic acid
Diaminopropanoic acid
Diaminobutyric acid
Diaminopentanoic acid
Diaminohexanoic acid

Esters:
$HCOOCH_3$
CH_3COOCH_3
$CH_3CH_2COOCH_3$

Others: *CO*, *CO_2*, C_3O_2, H_2O_2, H_2CO_3, N_2H_4, *$HNCO$*, NH_2CONH_2, $NH_2CONHCONH_2$

Brown 2004). Observational evidence has been claimed for variations in the C_2H_6/H_2O and CH_4/H_2O ratios (Mumma et al., 2002, and Gibb et al., 2003, respectively), but the statistics is still limited.

8.3 Laboratory Simulation of Cometary Matter

8.3.1 Experimental Simulations

Only volatile molecules have been detected so far in cometary atmospheres, as no direct cometary sample has ever been analyzed (except for IDPs, whose origin cannot, however, be uniquely assigned to comets). For a better insight into more complex, less volatile material, one has to turn to experimental laboratory work. The principle of such experiments is the following: from observations of the most abundant species in comas and in the interstellar medium, one can infer the

probable composition of the nucleus ices. A gaseous sample of the key species is deposited under vacuum on a cold substrate and irradiated during or after deposition by UV photons or charged particles. Condensed ices are sometimes simply warmed up slowly without irradiation. When the sample is warmed up for analysis a refractory organic residue remains on the substrate as the volatiles sublimate (Fig. 8.12). Greenberg has called this residue "yellow stuff". Bernstein et al., (1997) have shown that the organic residue is formed only when the initial mixture of ices contains polar molecules such as CH_3OH and NH_3.

The diversity of organic compounds synthesized is remarkable but their identification is seldom exhaustive. Table 8.3 is a simplified list of all the detected compounds. The simplest compounds such as CO, CO_2, H_2CO and CH_4 are

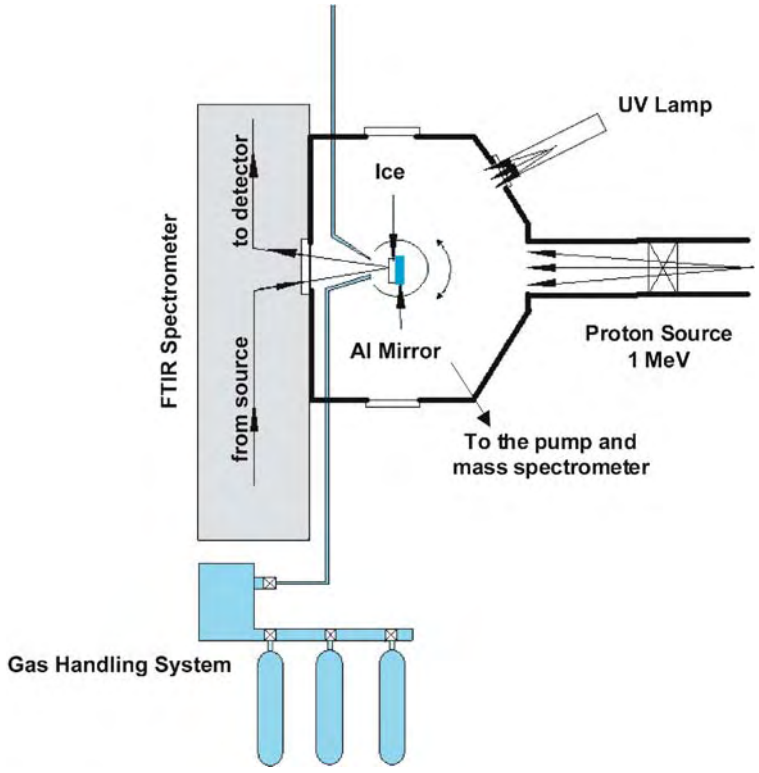

Fig. 8.12. A typical experimental setup allowing the irradiation (by UV and/or energetic protons) of cometary ice analogs made by deposition of a gas mixture on a rotating aluminium mirror cooled down to 10 K in a cryostat. The ice evolution can be analysed in situ by infrared reflection spectroscopy, and the volatiles released during warming, by mass spectrometry. The room-temperature residue can be collected for further analysis such as GC-MS (gas chromatography coupled to mass spectrometry), HPLC (high-performance liquid chromatography) and many others. From Hudson and Moore (1999)

detected in almost all the experiments, if the irradiated ice contains the appropriate elements. For more complex molecules, it depends on the ice composition and the nature of the energy source.

In addition to chemical transformations, it must be mentioned that experiments on the trapping of gases during ice condensation suggest that these processes play an important role in determining the composition of the ice and could lead to important enrichment or depletion between the gaseous and solid phases (Notesco and Bar-Nun 1996, Notesco and Bar-Nun 1997, Notesco et al., 1997).

8.3.2 Energy Deposition

Three kinds of energetic processing occur on icy coated dust grains in interstellar clouds (potentially precometary ices – see Sect. 8.4) or in the outer layers of comet ices in the Solar System:

In interstellar clouds, icy coated dust particles are subjected to processing by:

- *Charged particles*: Galactic cosmic rays.
- *UV-photons*: Lyman α photons from neighboring stars (in the diffuse outer regions of a cloud), or UV-photons induced by galactic cosmic rays (in the inner regions of dense clouds).
- *Thermal processes*: Cycling between the cold centre of a dense cloud and its warmer diffuse outer regions.

In the Solar System, the outer layers of comets undergo the same processes:

- *Charged particles*: Galactic cosmic rays, mainly in the Kuiper belt and the Oort cloud. This process has the largest effect on the outer few metres of the nucleus.
- *UV-photons*: Solar-UV, mainly in the inner Solar System when the comet is close to the Sun. This process would affect the outer few micrometres of the nucleus. Also during the Solar System formation, in the external layers of the disk, when solar UV luminosity was much higher than today.
- *Thermal processes*: During the formation of the Solar System (depending on the region in which the comet accretes), and in the inner Solar System (when the comet approaches perihelion).

Due to the diversity of environments involved, constraining the degrees to which different processes affect cosmic ices is a highly convoluted problem. Differences between the products synthesized during processing, according to the energy sources, could give information on the history of cometary matter and comets. Investigations are in progress to address this question.

8.3.2.1 UV Irradiation

UV irradiation is performed using a flowing-hydrogen discharge lamp (powered by a microwave cavity) delivering mainly Lyman α photons (122 nm) and a broad

band of photons centred at 160 nm (see Allamandola et al., 1988, and Cottin et al., 2003) for a detailed description). The irradiated ices comprise common cometary small molecules but the initial abundances of CH_3OH, NH_3 and/or CO relative to H_2O are usually higher than those deduced for present-day comets and displayed in Table 8.1. During these experiments a wide variety of organic compounds have been identified. From an initial mix of H_2O: CO: NH_3 (ratio = 5: 5: 1), glycine, the simplest amino acid, acetamide, glyceramide, and many other molecules have been detected by GC-MS (Briggs et al., 1992). Analysis by MS-MS on the organic residues formed, leads to the detection of heavier compounds: several cyclic molecules and PAHs (Greenberg and Mendoza-Gomez 1993). The composition of the heaviest part of the residue is still unknown but an elemental composition based on the overall structure of the mass spectra is given by Greenberg and Li (1998) (C: O: N: H = 1: 0.06: > 0.001: 1.1).

Among the molecules synthesized after such irradiations of ices, one of them is of great interest. Bernstein et al., (1995) have identified abundant hexamethylenetetramine (HMT – $C_6H_{12}N_4$) in the refractory residue. This compound has exobiological implications since its acid hydrolysis products are amino acids (Wolman et al., 1971). Typically, for an initial composition of H_2O: CH_3OH: CO: NH_3 (10: 5: 1: 1), the organic residue at 300 K contains HMT ($\sim$ 60%), ethers and POM-like polymers ($\sim$ 20%), ketones and amides ($\sim$ 20%). 1/5 of the carbon and 1/2 of the nitrogen from the initial ice composition remain in the refractory part (Bernstein et al. 1995). Thus a large fraction of HMT is formed (60% of the residue) whereas only 5% NH_3 is present in the ice before irradiation. A scheme of HMT production is shown in Fig. 8.13. Formaldehyde is produced by methanol UV oxidation. It then reacts with ammonia to produce methylimine and its trimer: hexahydro–1,3,5–triazine. Successive reactions with formaldehyde and ammonia result in the formation of HMT (Bernstein et al., 1995). Methanol plays a key role and it has been shown by ^{13}C isotopic substitution that it is the source of HMT's carbon. The production of HMT and some HMT family molecules has been studied in great detail by Muñoz Caro (2003).

HMT photolysis produce nitriles (HCN and RCN) and isonitriles (RNC) (Bernstein et al 1994, Cottin et al 2002). Knowing this, it is interesting to note that it has been shown that the CN radical might have an extended source in comet Halley (Klavetter and A'Hearn 1994). According to these authors, this source could be large molecules present on grains because the observed HCN cannot explain the amount of CN in comets. Other observed CN-containing compounds (HNC, CH_3CN, HC_3N) are only minor products and cannot explain the discrepancy. Thus having been produced in the interstellar ices, as we have just seen, HMT could act as a parent (HMT $\rightarrow$ CN) or "grandparent" (HMT $\rightarrow$ RCN $\rightarrow$ CN) molecule for the CN extended source. As yet, there has been no observation of HMT in comets. If present, its detection in the IR would be masked by the Si–O and C–O vibration bands that are in the same region as the strongest HMT infrared signatures. Direct detection of HMT should be

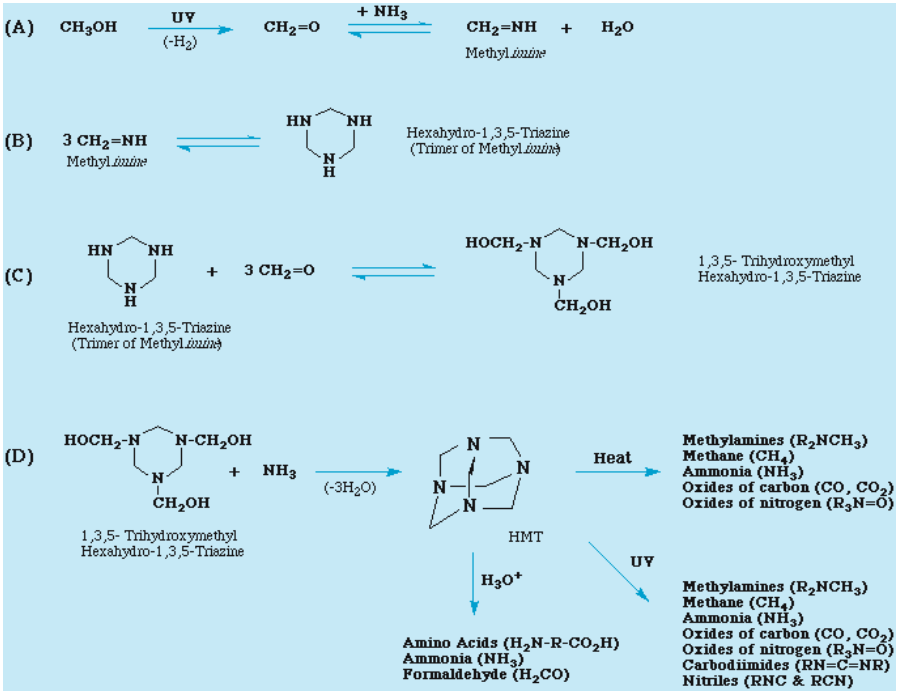

Fig. 8.13. Hexamethylenetetramine (HMT) chemistry. From (Bernstein et al., (1995))

feasible by in situ measurements with the GC-MS on board the lander of the Rosetta mission.

Bernstein et al (2002) and Muñoz Caro et al (2002) have detected a great number of amino acids (such as glycine, alanine, sarcosine, valine, proline, serine, etc.) in residues obtained after UV irradiation of ice mixtures made of H_2O: NH_3: CH_3OH: HCN and H_2O: CH_3OH: NH_3: CO: CO_2, respectively. Unhydrolyzed residues produce only a trace of glycine whose detection has already been reported by Briggs et al (1992) without any liquid water introduced to the analysis protocol. The detection of the other amino acids requires an acid hydrolysis of the residue in very strong conditions (HCl $\geq 6M$ and $T \geq 100$°C). Therefore it is not clear to date if 1) amino acids are present themselves in the laboratory residues, and henceforth in cometary ices, or if "only" amino acids precursors are synthesized, and 2) if the residues' processing (acid hydrolysis) is relevant to any chemistry that could have turned the amino acids' precursors imported by cometary impacts in the primitive oceans of the early Earth into actual amino acids. Note that the hydrolysis conditions would break a peptidic bond; some dipeptides have been found in the extraterrestrial organic matter of the Yamato-791198 and Murchison meteorites, but only glycine-glycine dimers and with a low (10^{-4}) abundance relative to glycine (Shimoyama and Ogasawara 2002).

8.3.2.2 Irradiation by Charged Particles

Important work concerning the particle bombardment of ices has been performed by Strazzulla's team in Catania and in Marla Moore's laboratory at NASA Goddard Space Flight Center. The particles used are H^+, He^+, N^+ or Ar. The bombardment of a large diversity of carbon-containing ices induces an evolution toward an amorphous material called Strazzulla "ion-produced hydrogenated amorphous carbon" (IPHAC) (Strazzulla 1997; Strazzulla and Baratta 1991; Strazzulla et al 1991).

The general results are the following: up to a dose of about 10 eV/C atom the ice is partially converted into a refractory material. From 10 to 25 eV/C atom, a massive loss of H is observed and the target evolves to an organic material made of chemical chains of different sizes. For stronger irradiations ($\geq$ 25 eV/C atom) IPHAC, the ultimate state of organic degradation, is formed (Strazzulla 1997). It has been shown by Jenniskens et al. (1993) that energetic UV (10 eV) irradiation of the organic residue of processed ices also leads to IPHAC formation, which then can be also called: "irradiation-produced hydrogenated amorphous carbon". Thus, after a typical lifetime in the interstellar medium, UV radiation and/or particles convert the organic mantle of interstellar dust into amorphous hydrogenated carbon.

A set of data comparing UV photolysis and ion irradiation of ices showed that the yield of major products was similar for a simple ice containing H_2O and CO_2 (Gerakines et al 2000), showing that the ice chemistry seems to be quite similar whether induced by photons or charged particles. Indeed, HMT production has been reported when interstellar ice analogs containing CH_3OH and NH_3 are irradiated with protons (Cottin et al., 2001), the same as with photons. The main difference is that UV photons (typically at 122 nm) only affect a few tenths of a micrometer in water-dominated ice, whereas protons can reach and alter the ice composition down to a few metres depth.

Chemical differentiation is more noticeable when molecules not dissociated by photons with a wavelength of 122 nm and above are involved in the chemical processes. This is the case for CO and N_2. Different results are obtained if pure CO is photolyzed or proton irradiated (Gerakines and Moore 2001). Likewise $N_3{}^+$ is detected when ices containing N_2 are proton irradiated, but not after photolysis (Hudson and Moore 2002). It seems that it is more the energy level than the way it is deposited (UV or charged particles) that matters for the chemistry.

We note that in these kinds of experiment, C_3O_2, which is sometimes evoked as an extended source of CO, has been detected after irradiation of ices containing CO or CO_2 (Brucato et al. 1997; Moore et al 1991). Kobayashi et al (1995) and Kasamatsu et al., (1997) were the first to report amino-acid production from irradiated ices. After an irradiation by 3-MeV protons of mixtures containing water, ammonia and a carbon-containing molecule (carbon monoxide, methane or propane), they detected by HPLC several amino acids: glycine, and for the first time in a cometary simulation, alanine, aminobutiric acid and aminoisobutiric

acid. These new detections were not made directly from the organic residue, but after an acid hydrolysis in water. Likewise for UV irradiation, only traces of glycine were found during the analysis of unhydrolyzed residues.

8.3.2.3 Thermal Processing of Ices

Polyoxymethylene and associated molecules and polymers have been detected when several mixtures containing formaldehyde, instead of being irradiated, were warmed slowly to room temperature (Schutte et al., 1993a, Schutte et al., 1993b).

There are many differences between the organics detected with or without UV processing of ices. Without irradiation, HMT is not detected, which is quite surprising as H_2CO and NH_3 readily react in the gaseous phase to form HMT (Bernstein et al., 1995; Walker 1964). Likewise, ketones, amides or esters, easily synthesized under irradiation, are quite rare in those thermal experiments. It seems that UV photons provide enough energy to surmount the energy barrier for formation of these molecules. Without UV, POM's production is favoured since it requires less energy.

8.3.3 Relevance and Importance of Laboratory Simulations

This section can not be concluded without discussing the relevance of experimental simulations. Of course, an irradiation of a few hours can not reproduce millions of years or more of slow evolution with complex heterogeneous chemistry in an interstellar environment that will never be completely reproduced in the laboratory. Nevertheless, in the 3.4-μm region, infrared spectra of methane and butane mixtures after a particle irradiation present a very good fit with the observations of dust particles in the diffuse interstellar medium (i.e. highly processed material), and even with spectra of residues from the Murchinson meteorite (Pendleton et al., 1994). The same results have been obtained with residues of H_2O: CO: NH_3: $CH_4/C_2H_2/CH_3OH$, which have been exposed to direct solar UV radiation on the EURECA space station (Greenberg and Li 1997, Greenberg et al., 1995). These are also highly processed materials. Thus Strazzulla's IPHAC appears to be similar to the refractory mantle of dust grains in the harsh conditions of the diffuse interstellar medium. The less-processed mantle formed in molecular clouds is almost certainly composed of the large range of molecules detected after experimental simulations, and the abundances of characteristic molecules like HMT or POM depends on the history of the grain and the relative contribution of the different energy sources: UV and proton irradiation lead to HMT, thermal processing to POM-like polymers. The importance of such simulations is underlined if one considers that data drawn from these simulations are necessary for the preparation of space missions to comets. A good illustration of this point is the selection and calibration of chromatographic columns for the COSAC experiment (ROSETTA mission – ESA) that requires an anticipation of the nature of the molecules to be searched for (see Sect. 8.6).

8.4 Origin and Evolution of Cometary Matter

8.4.1 Origin of Cometary Matter

We have already seen (Sect. 8.1.3) how icy planetesimals populated the two present comet reservoirs, the Oort cloud and the Kuiper Belt, in the early times of the Solar System. We address now the problem of the formation of these icy planetesimals, and the processes determining the composition of cometary matter. As underlined by Yamamoto (1991) these two steps are distinct: the chemical composition is probably fixed to a large extent early in the accretion process, well before km sized bodies are built.

Figure 8.14 summarizes the present view of Solar System formation. All the matter originates in an interstellar cloud composed of dust and gas. Close to the protosun, towards the centre of the nebula, only rocky material would condense, while volatile species remained in the gas phase. Rocky planetesimals – bodies of intermediate size, ranging between 1 m and a few km – were formed there. These rocky planetesimals represent a crucial stage in the process of planet formation; they present a great similarity with present-day asteroids. On the contrary, towards the outermost parts of the nebula, where the temperature was lower, dust and ices formed the material of icy planetesimals, similar to present-day comets.

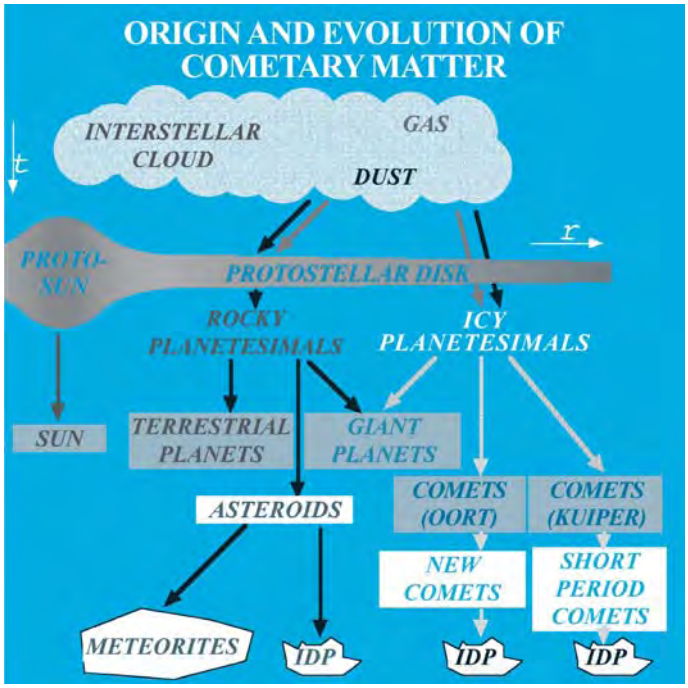

Fig. 8.14. Diagram showing the origin and the evolution of the cometary matter

These rocky and icy planetesimals intervened in very different proportions in the formation of planets. Rocky planetesimals played the major role for the formation of the Earth and other telluric planets (Mercury, Venus, Mars), while it was mostly the icy planetesimals that took part in the formation of the cores of the giant planets Jupiter, Saturn, Uranus and Neptune. Today comets are thought to be a subset of these ancient icy planetesimals, which survived until now with no or very little evolution.

This global picture, displayed in Fig. 8.14, presents in fact several simplifications. For example, there is also a small number of short-period comets that come from the Oort cloud. Moreover, the separation between rocky and icy planetesimals is not that clear, because bodies of intermediate composition and properties have been found (e.g. Phaeton, Chiron). In addition bipolar flows (see Chap. 1, Part I by T. Montmerle), which are produced in the vicinity of the protosun, may reinject a certain quantity of matter from the protosolar nebula into the collapsing protostellar envelope, allowing material highly processed in the vicinity of the Sun to be incorporated into comets at great heliocentric distances. A similar effect is obtained in the model by Shu et al. (1996) where grains are ejected from the vicinity of the protosun towards the outer parts of the disk.

8.4.2 Cometary Ices versus Interstellar Ices: the Facts

In cold dense interstellar clouds, interstellar grains are coated with ice mantles whose composition can be observed indirectly in a few regions where they evaporate: hot cores surrounding a massive star in formation inside an interstellar cloud, such as occur, for example, in the heart of the Orion Nebula, or shocked regions along bipolar flows (e.g. Kurtz et al., 2000, Bachiller et al., 2001). In the first case, the ice mantles of the grains of the collapsing envelope are thermally evaporated close to the young massive star in formation. In the second case, it is the shock wave created by the bipolar flow propagating through the interstellar medium surrounding the young star that leads to the destruction of the ice mantles and releases the molecules to the gas phase. The good correlation of molecular abundances between cometary and interstellar ices (Table 8.4 and Fig. 8.15) is one of the arguments that leads us to conclude that the matter of comets is very close to interstellar matter, suggesting similar conditions of formation, and even possibly a direct link (comets being then a frozen piece of interstellar matter).

A more straightforward comparison should arise from direct measurements of interstellar ices. Unfortunately, these measurements can only be performed in front of strong infrared sources (e.g. Ehrenfreund and Charnley 2000 and references therein). Furthermore, identification of a precise species and quantitative determination of its abundance from its IR vibrational bands are more difficult than in the case of millimetre-wave rotation spectra of gas-phase species. Table 8.4 lists the abundances in two sets of young stellar objects (YSO), respectively leading to low-mass ($< 2M_{\mathrm{Sun}}$) and high-mass stars. The former case,

Table 8.4. Cometary versus interstellar ices. Note their overall similarity. The agreement might be better in the case of ices surrounding low-mass protostars (a category to which the protosun belonged), but most of the present data are only upper limits, including NH_3 and CH_3OH. N_2, O_2, H_2 and rare gases are other important species whose ice abundances are not yet known. IS data are from Ehrenfreund and Charnley (2000); the range corresponds to 2 objects in each category (high-mass objects: W33A and N7538S; low-mass objects Elias16 and 29). Cometary data are from Table 8.1 (cometary volatiles); when no range is given, data refer to comet Hale–Bopp, except the O_2 limit, which comes from comet Halley. X-CN is the sum of various CN species (mainly the OCN^- ion in the case of IS ices)

Species	Interstellar ices high-mass YSO	Interstellar ices low-mass YSO	Cometary volatiles
H_2O	100	100	100
O_2	< 7	–	< 0.5 (*)
CO	9–16	6–25	1.7–23
CO_2	14–20	15–22	6
CH_4	2	< 1.6	0.6
C_2H_6	< 0.4	–	0.6
CH_3OH	5–22	< 4	0.9–6.2
H_2CO	1.7–7	–	0.13–1.3
HCOOH	0.4–3	–	0.09
NH_3	13–15	< 9	0.7
X-CN ($*$)	1–3	< 0.4	0.08–0.25
OCS, XCS	0.05–0.3	< 0.08	0.4

which corresponds to the Sun itself, is still very incomplete. O_2 and O_3, for which only upper limits have been measured, may contain a substantial fraction of atomic O. The very volatile species H_2 and N_2, and rare gases like Ar, may be present to an unknown extent in IS ices as well as in cometary ices.

Table 8.5 gives the list of the 137 interstellar and circumstellar molecules (not including isotopic variants) detected to date (January 2004) in the gas phase. Among them are ethanol C_2H_5OH, which has been long known, and glycolaldehyde CH_2OHCHO, whose detection has been recently claimed in the ISM (Hollis et al. 2000). Glycolaldehyde belongs to the family of molecules $C_n(H_2O)_n$, which for $n > 2$ are sugars or oses. In carbonaceous chondrites (the meteorites with composition closest to comets) Cooper et al. (2001) have detected several sugar molecules. If one also takes into account the presence of H_2CO, a sugar precursor at the per cent level in comets, that sugar molecules exist in comets is a likely hypothesis.

The heaviest known interstellar molecule to date is $HC_{11}N$, which belongs to the family of cyanopolyynes (a succession of acetylene molecules linked one

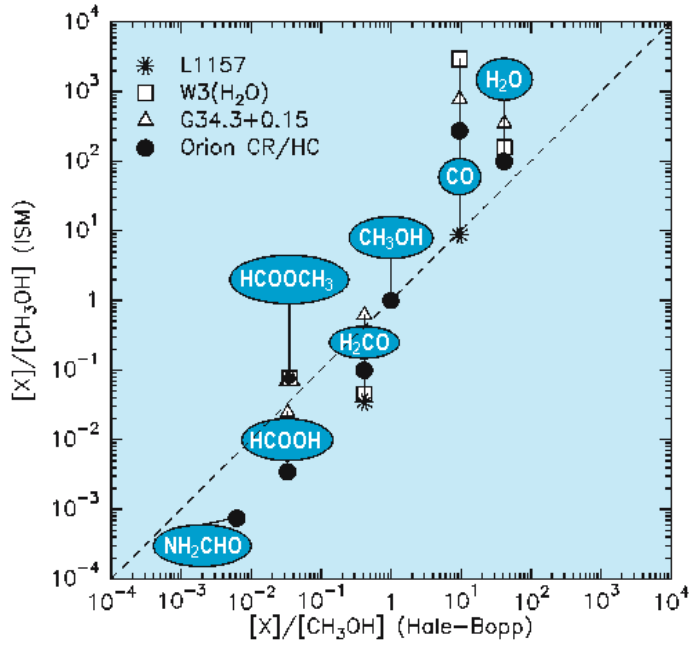

Fig. 8.15. Correlation of cometary (Hale–Bopp) and interstellar (ISM) gas-phase abundances (here for molecular species made of C, O, and H atoms; abundances are normalized to CH_3OH). The ISM regions selected for comparison are believed to release ice mantle molecules to the gas phase due to heat or shocks (Bockelée-Morvan et al., 2000)

to another to form a linear chain, and ending with a CN radical: $H(CC)_nCN$). The discovery of glycine NH_2–CH_2–COOH by Snyder et al., (e.g. 1997) in the ISM was not confirmed (Combes et al., 1996). Later searches by Ceccarelli et al., (2000) and Hollis et al., (2003) also led to upper limits. Recently, a detection has been published (Kuan et al., 2003) but it is also subject to debate. Due to the similarities between comets and the interstellar medium presented above, one can legitimately think that a number of these species exist also in comets; their detection is a challenge for new telescopes and space experiments (Sect. 8.6). In the interstellar medium grain surface chemistry also takes place. Charnley (1997) proposed a whole scheme of surface reactions to explain the formation of some complex compounds in the interstellar ices.

8.4.3 Models of Cometary Matter and Comet Nucleus Formation

According to some models, the rich IS chemistry may have been kept in comets, and thus be the ultimate source of some prebiotic compounds on Earth. This issue is especially important when discussing how common is prebiotic material

Table 8.5. List of the 137 molecules detected in the interstellar or circumstellar medium (April 2003), after Wootten (2003) and PCMI website (Boulanger and Gérin). The reality of some detections (followed by "?") is still under discussion, e.g. glycine NH_2CH_2COOH (see text)

Molecules with 2 atoms:	AlF, AlCl, C_2, CH, CH^+, CN, CO, CO^+, CP, CS, HCl, H_2, KCl, NH, NO, NS, NaCl, OH, PN, SO, SO^+, SiN, SiO, SiS, SiH, SiC, HF, SH, FeO?
Molecules with 3 atoms:	C_3, C_2H, C_2O, C_2S, CH_2, HCN, HCO, HCO^+, HCS^+, HOC^+, H_2O, H_2S, HNC, HNO, MgCN, MgNC, N_2H^+, N_2O, NaCN, OCS, SO_2, c-SiC_2, SiCN, CO_2, NH_2, $H_3{}^+$, AlNC
Molecules with 4 atoms:	C_4?, c-C_3H, l-C_3H, C_3N, C_3O, C_3S, C_2H_2, CH_3, CH_2D^+?, HCCN, $HCNH^+$, HNCO, HNCS, $HOCO^+$, H_2CO, H_2CN, H_2CS, H_3O^+, NH_3, c-SiC_3
Molecules with 5 atoms:	C_5, C_4H, C_4Si, l-C_3H_2, c-C_3H_2, C_2H_4, CH_2CN, CH_4, HC_3N, HC_2NC, HCOOH, H_2CHN, H_2C_2O H_2NCN, HNC_3, SiH_4, H_2COH^+
Molecules with 6 atoms:	C_5H, C_5O, C_5S, C_2H_4, CH_3CN, CH_3NC, CH_3OH, CH_3SH, HC_3NH^+, HC_2CHO, CH_2CHO, $HCONH_2$, l-H_2C_4, HC_4H, C_5N
Molecules with 7 atoms:	C_6H,CH_2CHCN, CH_3C_2H, HC_5N, $HCOCH_3$, NH_2CH_3 c-C_2H_4O, CH_2CHOH,
Molecules with 8 atoms:	CH_3C_3N,$HCOOCH_3$, CH_3COOH, C_7H, H_2C_6, HC_6H,CH_2OHCHO
Molecules with 9 atoms:	CH_3C_4H, CH_3CH_2CN, $(CH_3)_2O$, CH_3CH_2OH, HC_7N, C_8H
Molecules with 10 atoms:	CH_3C_5N?, $(CH_3)_2CO$, CH_2OHCH_2OH, NH_2CH_2COOH?
Molecules with 11 atoms:	HC_9N
Molecules with 12 atoms:	C_6H_6,$C_2H_5OCH_3$
Molecules with 13 atoms:	$HC_{11}N$

at the scale of our Galaxy, and the origin of chiral asymmetries (see Sect. 8.5.7 and the Chap. 3, Part II, by Cronin and Reisse). However, an important point is to realize that completely different and contradictory models are still proposed in this field, none of them being devoid of problems, although some are favoured by the present authors. A very detailed account of the pros and cons of each model can be found in Irvine et al., (2000a).

Following Yamamoto (1991) we distinguish the *formation of cometary matter* from the formation of comet nuclei: to a large extent, the size increase of the icy bodies in the protosolar nebula is decoupled from their chemical evolution.

8.4.3.1 Cometary Matter Formation

The beginning of the accretion process is the most critical step in fixing the composition of cometary matter, as the small ($\sim$ micrometre-sized) particles have the highest surface/volume ratio and maximize both surface reactions and gas-grain interactions. Furthermore, being small bodies ($\sim 1-10$ km), comets did not experience substantial heating (either internal, radioactive, or external, by collisions); these processes could, however, have affected the largest KBOs, a few 100 km in diameter (see Stern (2003) for a discussion of collisions in the Kuiper Belt, McKinnon 2002 and DeSanctis et al., (2001) for models of KBO thermal evolution). The three main categories of models for the first phase differ by the degree of reprocessing of the original material.

- In the *interstellar model* of comets, cometary matter is formed very early, with no or little further processing, by sticking together *interstellar grains*, and condensing to ice volatile molecules from the original interstellar gas phase to grain mantles. This is essentially the model proposed by Greenberg (1982, 1998) and retained by Irvine et al., (1980, 1996, 2000), Yamamoto (1983, 1985, 1991), Despois (1992), Bockelee-Morvan et al., (2000). In this model ice is mostly amorphous, except in the outer layer of the nucleus heated by the Sun when the comet approaches perihelion. The strong points in favour of this model are the coexistence of oxidized (CO_2, CO, SO_2) and reduced (H_2S, CH_4, H_2S) species, as observed in IS clouds, the rough overall abundances correlation (see previous section), including complex species like HC_3N, NH_2CHO, $HCOOCH_3$, and various indications of low-temperature processes (OPR, ortho:para ratios, in H_2O and other species, deuterium enrichment, presence of very volatile species like CO and CH_4). The syntheses occurred either in the interstellar cloud or during the protosolar phase, in the outer and cold part of the protosolar nebula, and bear testimony of ISM-like chemistry (low-temperature ion–molecule and surface reactions). Indeed the DCN/HCN and HDO/H_2O ratios would mean in this hypothesis a formation temperature around 30–50 K (Meier et al., 1998), coherent with the OPR and CO volatility. Furthermore, this model is predictive to some extent, as the list of IS molecules proved to be a very good guide for the detection of new cometary species. The main problems are the presence in comets of crystalline silicates, not seen at present in the IS medium, and the deuteration level that, although high enough to imply that interstellar processes played a role, are much lower than the record values in hot cores.
- in the *pure protosolar nebula model, or 'quenching' model* (e.g. Prinn and Fegley 1989, Fegley 1993), the chemical memory has been fully or largely

lost. This model is similar in many aspects to the successful models of the inner solar nebula (terrestrial planet zone). The comet-forming material is supposed to have experienced high temperatures in a hydrogen-rich nebula in thermochemical equilibrium (temperatures above ~ 500K), which favours CO over CH_4. The concept of "kinetic inhibition" of the CO to CH_4 conversion (Lewis and Prinn 1980, Prinn and Fegley 1981) leads to quenched thermochemistry: the hot-gas composition remains in chemical equilibrium when the gas cools down, until a quenching temperature below which reactions become too slow and the composition remains unchanged. This allows CO to be the major C-bearing volatile, despite the higher thermodynamical stability of CH_4 at low T. However, species predicted as abundant by the model are not observed (NH_4HCO_3, NH_4COONH_2), the observed complex species like $HCOOCH_3$ are not predicted, and explaining the cometary volatiles' chemical composition requires mixing contributions from IS gas, protosolar disk gas, and gas from the giant planet subnebulae in the right proportion (Prinn and Fegley 1989). Thus, an increasing complexity is required to explain even the gross features (e.g. oxidized/reduced species ratio) of the observed volatile composition.

- the *partially reprocessed IS matter model* is proposed by Lunine, Gautier and coworkers (e.g. Iro et al., 2003 and refs. therein). This aims at explaining several features of the Solar System besides cometary composition, such D/H ratios and rare-gas abundances in the giant planets. The solar nebula is initially rather hot (600K at 1AU) and cools down with the decrease of the disk accretion rate from 10^{-5} to $10^{-8} M_{\rm Sun}$/yr. The nebula is supposed to be already isolated from the parent cloud (protostellar envelope). A key feature is that a significant fraction (depending on the heliocentric distance) of ice mantles of infalling interstellar grains vaporize through an accretion shock before reaching the nebula; the molecules then recondense as crystalline ice (as in the preceding pure protosolar nebula models), which incorporates minor species as gas clathrates or stoichiometric hydrates. The chemical composition of the gas is supposed to be unaltered, whereas the deuteration is diminished by interaction with the H_2 of the nebula. Gas composition and clathrate/hydrate stoichiometry control the final composition of cometary ices (clathrates are a class of solids in which small gas molecules like CH_4, CO_2 or noble gases occupy "cages" made up of hydrogen-bonded water molecules; other species like NH_3 form solid hydrates with well-defined composition $(NH_3)\ (H_2O)_n$). Another essential feature is turbulence across the disk that can transport the silicate grains processed (crystallized) in the vicinity of the Sun to the cold regions where the ice forms.

8.4.3.2 The Building of the Nuclei

In the continuous accretion process leading from 0.1-μm grains to km-sized bodies, there is a scale level, probably close to 1–10m, after which the chemical com-

position of the matter is almost fixed (note, however, that very small molecules like CO could diffuse through the ice if warmed enough). At a larger size, most molecules are too deep inside to be affected by surface heating, energetic photons or particles (solar X or UV radiation, solar-wind particles and cosmic rays). Desorption processes and chemical reactions in the bulk of the ices, or on the probably large internal surface of this highly porous material, are limited, due to the very low temperature (a few tens of K to 150K at most). Occasionally, collisions occurring during the accretion process may heat locally the cometesimals. The accretion of particles to form comets (or icy planetesimals) has been thoroughly studied by Weidenschilling (1997); his simulations show the formation of comet-size bodies from micrometre-size grains up to bodies 80km in diameter in 2.5×10^5 yr.

8.4.4 Are Today's Comets Like Comets in the Early Solar System?

Were early comets similar to present ones? A given cometary nucleus is thought to have negligibly evolved since its formation, due to its low temperature. Exceptions may be a thin surface layer (due to particle and photon processing in the Oort cloud and the Kuiper Belt, and a few possible passages close to the Sun, see Mumma et al., 1993), and a slow volume loss of very volatile species (rare gases, CO). Occasional collisions may also have occurred in the Kuiper Belt and the Oort Cloud.

May chemistry inside the nucleus have altered the pristine composition of comets since their accretion? Navarro-Gonzalez et al., (1992) and Navarro-Gonzalez and Romero (1996) have studied theoretically the effect of ionizing radiation (cosmic rays and embedded radionuclides) on the cometary material and conclude that pristine organic compounds should not be altered except in the external layers of the comet. It is also predicted that an original enantiomeric excess of alanine would not be destroyed by radioracemisation during the decay of radionuclides. At the very most it should be attenuated, but comets could have contributed to the origin of chirality on Earth. The limitation of this work is that the kinetic data used in the calculations are for the liquid phase only, since no solid phase values are available; this may distort the result to some extent. The thermal racemization is a priori expected to be negligible at the comet low temperatures, but here also more theoretical and experimental work is required.

As stated before, the largest icy bodies (> 500km) in the Kuiper Belt might have for a limited time reached internally at some place conditions for melting to occur. This is, of course, a cause of chemical transformation.

If comets themselves are thought to have kept their original composition, their reservoirs have undergone at least a slow evolution in number and orbital parameters (e.g. Morbidelli et al., 2000). This affects directly the possibilities of delivery to the Earth.

8.5 Delivery to the Earth

8.5.1 Shooting Stars (Meteors)

When a comet passes close to the Sun, the gases that are produced by the sublimation of the ice drag along the dust particles and release them into the interplanetary medium. Comets are thus one of the two principal sources of interplanetary dust (interplanetary dust particles, IDPs, also called "meteoroids"). The other source of IDPs is the collisions between rocky objects: asteroids or asteroid fragments. The largest cometary dust particles remain confined in the vicinity of the comet orbit and spread progressively along this orbit, forming a ring-like swarm of particles. In fact, planetary perturbations deform the orbits, which are no longer closed but transform into a tightly packed set of successive turns. Due to small differences in ejection conditions, individual particles follow different orbits, which, however, are close one to another and form a long ribbon through the Solar System. When the Earth crosses such a swarm, we experience a shower of shooting stars: during the entry into the Earth's atmosphere, particles larger than a size of about 1 mm produce, through heating, combustion and ionization of the air, a trail visible to the naked eye.

8.5.2 Overall Picture of Matter Delivery to the Earth

Several kinds of objects of the Solar System are likely to bring matter to the Earth: large-size bodies (asteroids or comets) responsible for more or less devastating impacts, small-size bodies (smaller than 10 m) called meteoroids in general, and interplanetary dust for the smallest; if a fragment of these bodies reaches the ground, it is called a meteorite (or micrometeorite). This delivered material will affect the land, the oceans, the atmosphere and the terrestrial biosphere.

In Fig. 8.16 we present an overview of the different kinds of matter delivered to the Earth, displayed according to size. Around 0.1 micrometres are particles that are probably grains coming directly from the local interstellar medium surrounding the Sun. Above 10 micrometres the range of interplanetary particles starts. The smallest ones, around 10 micrometres, are decelerated and stopped in the stratosphere, where they can be collected by airplanes: these are the "stratospheric IDPs" previously mentioned. The slightly larger particles reach the ground and are thus called micrometeorites. If one considers the delivered mass (Fig. 8.17) and not the number of particles, the distribution presents a peak towards 100 micrometres. In the size range 10–100 micrometres these particles produce in the atmosphere ion trails detectable by radar echoes; when the size exceeds about 100 micrometres (the value depending on the velocity of the particle) they appear in the visible as "shooting stars". With even larger particles, ranging from centimetre to decametre, one enters the field of the traditional meteorites. A few tens of metres is roughly

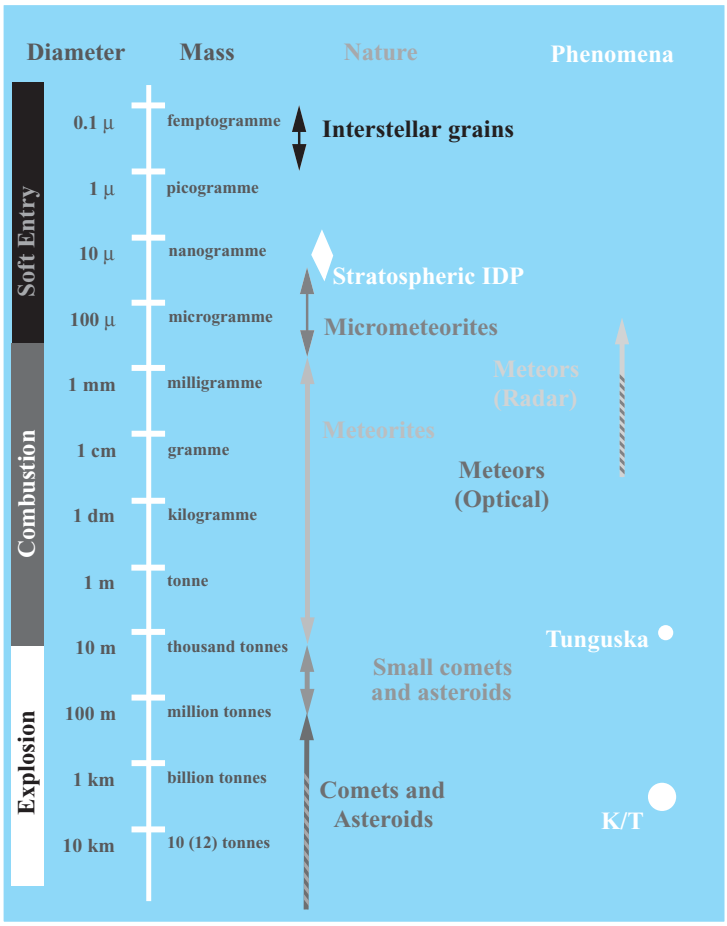

Fig. 8.16. Overview of particles delivered to Earth, displayed according to their size

the size of the bolide presumed to be responsible for the Tunguska explosion, which occurred in Siberia in June 1908, and blew down the forest over 2000 km^2; the nature of the object is still debated, see Shuvalov and Artemieva 2002, Jopek et al., 2002 for recent discussions. At around ten kilometres diameter lies the object (comet or asteroid – e.g. Jeffers et al., 2001 – recent data favours the latter hypothesis, e.g. Kyte 1998) which would have been responsible, 65 Myr ago, for producing the K-T sedimentary layer that marks in many places the boundary of the Cretaceous and the Tertiary geological periods, and of inducing massive species extinction, most notably that of dinosaurs (e.g. Frankel 1999; but the debate is still active, e.g. Stankel 2001, Facett et al., 2001, Le Loeuff and Laurent 2001). Such an impact occurs roughly every 100 Myr.

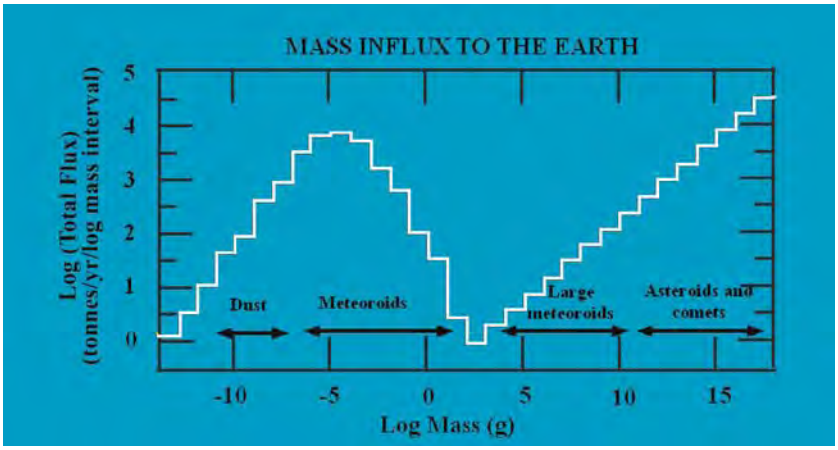

Fig. 8.17. Distribution in mass of the contributions to the Earth. The actual mean influx from the very largest objects is very uncertain. Rates are for present, and are believed to have been much higher in the first few 100 Myr of Earth's history (Steel 1996)

The micrometeorites represent a major contribution to the delivery of matter and especially of organic compounds and volatiles to the Earth; they may even be considered as a small prebiotic chemical reactor, as they contain many significant prebiotic compounds, including clays (catalyst), and insuring a natural confinement avoiding the dilution of the reactants (Maurette 1998, Maurette et al., 2000). The extrapolation of the micrometeoritic delivery in the past is highly uncertain, and ranges from conservative factors of 100 times the present rate to a high of 10^6 times.

8.5.3 Delivery of elements and Water

According to different estimations, extraterrestrial delivery to Earth over 4.5 billion years ranges from 10^{21} to 7×10^{23} kg. The lower limit of this amount that can be attributed to comets has been estimated to be 10% by Chyba et al., (1990).

- H_2O

It has been suggested that most of the water of the Earth oceans (1.4×10^9 km^3, roughly 10^6 times comet Halley mass) could have been imported by comet impacts during a period of heavy bombardment (e.g. Delsemme 2000). Recent dynamical models of the early Solar System (Morbidelli et al., 2000), and recent measurements of the D/H in cometary water (to be compared with D/H in the oceans (SMOW)) (Dauphas et al., 2000) both lead to a maximum of $\sim 10\%$ of

water of cometary origin; the latter argument assumes that the D/H ratio measured in 3 comets is typical of all comets. Petit and Morbidelli discuss further the delivery of water in their chapter. An even lower limit (1%) on cometary H_2O in ocean water has been recently presented, from indirect arguments on rare gases and metals (Dauphas and Marty 2002).

- *Carbon*

Carbon in comets is roughly 18% by mass. Chyba et al., (1990) estimated that the contribution of comets to the terrestrial carbon inventory ranges from 2×10^{19} to 10^{22} kg; while the total budget of carbon on Earth is about 9×10^{19} kg. Even if uncertainties linked to the total amount of comets impacting the Earth since its formation are not lifted, those estimations show that they brought a significant amount of carbonaceous material. The extent to which organic molecules can survive cometary impact is discussed in Sect. 8.5.5.

- *Other Elements*

The other elements required for a protocell formation are also present on comets. Phosphorus, which is involved in the synthesis of sugars, has been detected by mass spectroscopy ($m/e = 31$) in grains of comet Halley by the PUMA mass spectrometer on board Vega 1. But its abundance is very low and detection may have been affected by interference from ions such CH_2OH^+ (Kissel and Krueger 1987). However, analysis by laser probe mass spectroscopy of interplanetary dust particles (IDPs), whose cometary origin is probable, has led to the detection of PO_2 and PO_3 anions (Radicati-Di-Brozolo et al 1986). Ni and Fe have been detected in comet Ikeya-Seki and Halley.

8.5.4 Prebiotic Molecules from Comets?

Five families of compounds are considered to be the key prebiotic monomers required before starting a chemical evolution from which life would arise. These are amino acids (whose combinations lead to proteins), *purine bases* (adenine and guanine), *pyrimidines bases* (cytosine, uracil and thymine), *sugars* (whose association lead to RNA and DNA molecules), and *fatty acids* (cell walls). It is very interesting to note that, even if these compounds have not been detected in comets (maybe because of limitations in the sensitivity of telescopes, but also essentially because the synthesis of most of them requires liquid water), all but thymine can be easily produced in an early Earth environment from cometary precursors such as HCN, HC_3N, H_2CO and CO that have been firmly detected in cometary comae (Table 8.6).

Nevertheless, complex compounds of exobiological interest may also be present in comets. The only detection of adenine is a very tentative interpretation of PUMA's mass spectra of comet Halley's dust (Kissel and Krueger 1987). Such a molecule could be synthesized by HCN condensation without any

Table 8.6. Prebiotic syntheses from cometary molecules, from (Oró and Cosmovici 1997)

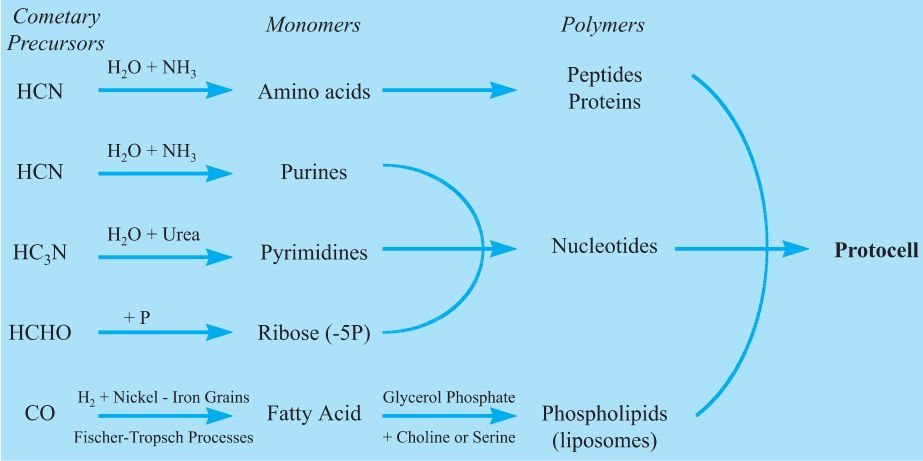

liquid water (Oro and Cosmovici 1997, Wakamutsu et al., 1966). Moreover, as already seen in this chapter, when ices relevant to the composition of interplanetary dust particles or comets are irradiated, complex molecules are formed, and among them, the simplest amino acid, glycine (Briggs et al., 1992). After an acid hydrolysis in water other amino acids, such as alanine, valine, proline and others, have also been identified (Bernstein et al., 2002; Kobayashi et al., 1995; Muñoz Caro et al., 2002).

8.5.5 Do Molecules Survive From Comets to the Earth?

Thus, comets may have imported prebiotic elements to early Earth, which, when mixed with liquid water, may have allowed the synthesis of all molecules thought to be necessary for the origin of life. To date, it is not clear as to whether the importation of such key compounds occurs at the simple stage of HCN, HC_3N, HCHO..., or more elaborate species such as amino acids, puric and pyrimidic acids and others. But before seeding the oceans, those compounds have to survive:

- if brought by small dust particles, they are subject in the interplanetary medium to the action of solar UV radiation, solar-wind particles and galactic cosmic rays; while the comet particle is slowed down and warmed up by the Earth's atmosphere, they must resist pyrolysis (destruction at very high temperature), and chemical reactions in the atmosphere. If they reach the ground, they should also survive the ensuing impact.
- alternatively, if the nucleus impacts directly the Earth, can the molecule survive the dramatic energy release?

Experiments conducted in space have shown that amino acids are quite unstable to solar UVs, but also that when somehow shielded in minerals, such as meteoritic powder, they can survive in space, and undergo no racemization (Barbier et al., 2002; Boillot et al., 2002).

The case of impacts of large bodies has been theoretically treated by Chyba et al (1990). It appears that organic compounds (even amino acids, if present) contained in cometary impactors of 100 to 200 m in size could survive a collision with Earth in a 10-bar CO_2 atmosphere thanks to an efficient aerobreaking. Comparisons with Venus and Mars lead us to think that it is the most probable composition of the primitive atmosphere. The authors note in their conclusion that "*It is intriguing that it is exactly these dense CO_2 atmospheres, where photochemical production of organic molecules should be the most difficult, in which intact cometary organics would be delivered in large amounts*". Indeed, organic syntheses are efficient in reduced atmospheres, and even in weakly reduced atmospheres such as that of Titan (N_2, CH_4), whereas they are very difficult in the oxidized environment that must have been the early Earth's atmosphere.

On the experimental scene, Blank et al (2001) conducted a series of shock experiments to assess the feasibility of the delivery of amino acids to the Earth via cometary impacts. It appears that a large fraction of the amino acids do survive impacts. It has also been shown that some chemistry occurs, which leads to the formation of peptide bonds and new compounds including amino-acid dimers.

8.5.6 Comparison of Comets with Other Likely Sources of Prebiotic Molecules

Figure 8.17 displays the total mass delivered to the Earth for each mass interval (note that these intervals are logarithmic). Two main contributions show up, which are very different in nature: while the small particles could more or less softly deliver molecules to the Earth atmosphere and surface, large-size impactors bring also large quantities of matter but of course in a very different – discontinuous and catastrophic – mode. The very high temperatures reached by gases allow the synthesis of some compounds, as well as leading to their destruction as discussed in the previous section.

In the so-called intermediate atmospheres (in which the main gases are e.g. CO_2, H_2O, N_2 instead of NH_3 and CH_4) extraterrestrial delivery plays a major role in the total budget of prebiotic molecules (Chyba and Sagan 1996, Jenniskens et al., 2000). Table 8.7 gives in kg/yr the quantity of these molecules brought by various processes in the case of reducing and neutral (or moderately oxidizing) atmospheres. The large difference between these two types of atmosphere is noticeable, in particular for the synthesis of molecules by the shock waves induced by impacts. It should be noted that if many experiments have been undertaken in the laboratory on the chemical syntheses induced by electric discharges or energetic photons, the experimental studies relevant to the entry of particles in the atmosphere are very difficult and are still in a much less elaborate stage. The direct observation of molecules deposited by the meteors in the

Table 8.7. Major sources of prebiotic organics for two candidate early Earth atmospheres. The intermediate atmosphere corresponds here to a ratio $H_2/CO_2 = 0.1$. Note the considerably larger synthesis efficiency in the case of reducing atmospheres, which are those used by Urey and Miller in their experiments. In the more probable case of an intermediate atmosphere, external delivery is a major source of organics, as 30% come from IDPs. After Chyba and Sagan (1996) for the atmospheric processes, and Ehrenfreund et al., (2002) for the hydrothermal vents and comet impact delivery estimations

Source	Reducing atmosphere (kg/yr)	Intermediate atmosphere (kg/yr)
UV photolysis	1×10^{12}	3×10^{8}
Electric discharge	3×10^{9}	3×10^{7}
IDPs	2×10^{8}	2×10^{8}
Shocks from impacts	2×10^{10}	4×10^{2}
Shocks from meteors	4×10^{9}	8×10^{1}
K/T extrapolation	2×10^{8}	2×10^{8}
Total (atmosphere)	1×10^{12}	7×10^{8}
Hydrothermal vents	1×10^{8}	1×10^{8}
Comet impact delivery	1×10^{11}	1×10^{11}

atmosphere has been attempted during the recent Leonid shower (CN: Rairden et al., 2000, HCN: Despois et al., 2000).

8.5.7 Chiral Molecules: from the Interstellar Medium to the Early Earth?

Among the most intriguing questions related to the origin of life on Earth is the origin of the chirality for some key molecules: amino acids (configuration L) and sugars (configuration D).

Even if the cometary contribution were modest in mass, it might still have played a remarkable role, allowing via cometary dust particles or impact to directly forward to the early Earth some interstellar molecules, which could have played an important part in the apparition of homochirality (e.g. Bonner et al., 1999 and references therein). Indeed, an enantiomeric excess has been measured for some nonbiological amino acids in meteorites (see Cronin and Reisse Chapt. 3, Part II). Therefore, it is conceivable that an excess was also present for the biological amino acids (for which analysis is much more difficult due to the risk of contamination by terrestrial biomolecules). Such an excess could have been transmitted to the early Earth, and constitute an initial asymmetry later amplified by prebiotic chemistry (see Commeyras et al., 2004). The possible importance of this scenario is the fact that abiotic mechanisms able to produce nonracemic mixtures are very rare.

Which physical or chemical mechanism could then have led to a non-racemic mixture in the meteorites? Bailey and collaborators highlighted conditions favourable for the buildup of chiral asymmetry in the interstellar medium, and more especially in regions of star formation (Bailey et al., 1998, Bailey 2001). They detected the presence of circularly polarized infrared radiation in vast regions, which could easily include a whole Solar System in formation. This suggests the possible existence in these same regions of circularly polarized ultraviolet radiation, which still has to be detected. This circularly polarized ultraviolet radiation could lead to a differential synthesis or destruction of one enantiomer with respect to the other. If conditions similar to those in Orion prevailed at the time of formation of our Solar System, and if these interstellar molecules could actually be preserved till their integration into the matter of the protosolar nebula, this could be a plausible and relatively natural scenario for L/D symmetry breaking between enantiomers. This scenario seems at least as probable as the assumption of a fortuitous encounter of the protosolar nebula with a neutron star (a pulsar), also suggested as a likely source of polarized light. In comets, the search for non-racemic mixtures will require in situ chemical analysis or laboratory analysis of returned samples.

8.6 Ground-based and Space Exploration of Comets: New Developments

In the Solar System, several major space missions relate to comets. ESA is preparing the ROSETTA probe that will reach comet 69P/Churyumov-Gerasimenko (the previous target, P/Wirtanen, had to be abandoned as the launch was delayed); after a ten-year cruise, it will meet the comet and follow it for almost two years, during which a lander will be deposited on the surface. On the lander, the COSAC experiment (e.g. Rosenbauer et al., 1999) will perform a chemical analysis of cometary volatiles by gas chromatography of samples taken after drilling down to 20 cm below the surface. With a detection limit of 10^{-5}–10^{-6} with respect to water, more than 100 cometary species might be detected (Szopa et al., (2003) and Crovisier (2004)). The use of chiral columns will allow the measurement of enantiomeric excess.

A US mission, STARDUST, aims to collect thousand of cometary grains and bring them back to Earth. Another probe, CONTOUR, intended to tour 3 cometary nuclei, seems unfortunately to have been definitively lost. Table 8.8 summarizes all the space efforts directed towards comets in the next few years. As for ground-based observers, they have to wait for a new bright comet, like the recent comets Hyakutake and Hale–Bopp. In the near future, large ground-based telescopes, like the Atacama Large Millimeter Array (64 antennas, 12 m in diameter, operating as an interferometer in a very good high altitude astronomical site in Chile), the Large Millimeter Telescope (50-m antenna), the Green Bank

Table 8.8. Recent, in progress and planned cometary missions (Nov. 2003)

Missions to comets	Launch	Dates	Events	Comet	Goal
DEEP SPACE 1 (NASA)	Oct. 24, 1998	Sept. 22, 2001	Flyby	P/Borrelly	Nucleus imaging, plasma
STARDUST (NASA)	Feb. 7, 1999	Jan. 2, 2004 Jan. 15, 2006	Flyby Return	P/Wild 2	Comet dust sample return
ROSETTA (ESA) (1)	Feb. 26, 2004	4/2014 11/2014 8/2015	Comet orbit Landing Perihelion	67P/Churyumov–Gerasimenko	Orbiter + lander Ice and dust in situ analysis
DEEP IMPACT (NASA)	Dec. 30, 2004	Jul. 4, 2005	Flyby + impact	P/Temple 1	500 kg projectile
CSSR (NASA) (2)	Aug. 2009	5/2017 3/2018 12/2018	Rendez-vous Comet depart Earth return	46P/Wirtanen	Comet surface sample return
Other Missions of interest	**Launch**	**Results**			**Comet-related science**
SIRTF (NASA)	Aug. 2003	2003→			Interplanetary dust disks (Exozodi)
COROT (CNES)	June 2006	2006→			Exocomets
HERSCHEL (ESA)	Feb. 2007	2007→			D/H in a variety of comets
NEW HORIZONS (NASA)	Jan. 2006	2015/2016 2017/2023	Pluto flyby KBO flyby		Pluto + Kuiper belt object imaging

(1) Rosetta Launch, foreseen 2003, has been rescheduled; previous target was 46 P/Wirtanen
(2) Project stage, not yet accepted; dates are indicative only.

Telescope (100 m antenna) will bring higher sensitivity and space resolution. Out of the Solar System, the Corot mission should make it possible to detect comets around other stars (Lecavelier des Etangs et al. 1999).

8.7 Conclusion

Comets can bring down to the Earth elements like carbon, as well as water (in an amount that remains to be determined). Moreover, they contain simple organic molecules, and it is probable that they contain more complex ones. Thus comets are likely candidates for early Earth enrichment in prebiotic molecules, either through the dust particles they release – some of which end up encountering the Earth atmosphere – or through the atmospheric chemical syntheses – and possibly also through direct delivery – taking place when cometary nuclei impact the Earth. The same impacts may also strongly affect the later development of life, either locally, or on the scale of the planet.

Many questions are central to the current debates, which we hope will find a response in coming years, and for which space missions can bring important results:

- Where and when were formed the cometary matter, and then the comets?
- How close is cometary matter to interstellar matter?
- Do comets contain amino acids and other bricks of life?
- Do these molecules present an enantiomeric excess, or are they in racemic mixture?
- What is the precise budget of the cometary contributions to the Earth (fraction of the water of the oceans; fraction of carbon; fraction of prebiotic molecules)?
  - What is the global effect of comets on life, its appearance and its development?

Out of the Solar System, is the presence of an Oort cloud or a Kuiper Belt an exceptional characteristic of our Solar System or a banal fact among main sequence stars? Given the crucial part potentially played by comets in the origin and the evolution of life on Earth, it appears fundamental to know the probability for a star with habitable planets to be also surrounded by comets. New research topics thus develop on these *exocomets* (comets orbiting around other stars). The properties of the spectra of a close star, β Pictoris – one of the rare main sequence stars around which a disc has been detected – are currently convincingly interpreted as due to a constant infall of "evaporating bodies" on this star (Lagrange et al., 2000, Karmann et al., 2001, 2003). Much is then to be expected from ambitious space experiments under development, like the Corot mission (Baglin 2003), which should make it possible to detect directly comets, as well as Earth-size planets around a wide range of other stars (Lecavelier des Etangs et al., 1999, Bordé et al., 2003).

Acknowledgement

We are very grateful for detailed reading, precious comments and many corrections on this text by W. Irvine, J. Crovisier, M. Gargaud, B. Barbier and J. Reisse.

References

A'Hearn, M. F., Millis, R. L., Schleicher, D. G., Osip, D. J., Birch, P. V. (1995). The ensemble properties of comets: Results from narrowband pghotometry of 85 comets, 1976–1992. *Icarus*, **118**, 223–270.

A'Hearn, M.F., Boehnhardt, H., Kidger, M., West, R.M. eds (1999). Proceedings of the first international conference on Comet Hale–Bopp. *Earth, Moon and Planets*, **77, 78** & **79.**

Allamandola, L. J., Sandford, S. A., Valero,G. J. (1988). Photochemical and thermal evolution of interstellar/precometary ice analogs. *Icarus*, **76**, 225–252.

Altwegg, K., Balsiger, H., Geiss, J. (1999). Composition of the Volatile Material in Halley's Coma from In Situ Measurements. *Space Science Reviews*, **90**, 3–18.

Altwegg, K., Bockelée-Morvan, D. (2003). Isotopic Abundances in Comets. *Space Science Reviews*, **106**, 139.

Arpigny, C., Jehin, E., Manfroid, J., Hutsemékers, D., Schulz, R., Stüwe, J. A., Zucconi, J., Ilyin, I. (2003). Anomalous Nitrogen Isotope Ratio in Comets, *Science*, **301**, 1522.

Bachiller, R., Pérez Gutiérrez, M., Kumar, M. S. N., Tafalla, M. (2001). Chemically active outflow L 1157, *Astronomy and Astrophysics*, **372**, 899.

Baglin, A. (2003). COROT: A minisat for pionnier science, asteroseismology and planets finding. *Advances in Space Research*, **31**, 345.

Bailey, J. (2001). Astronomical Sources of Circularly Polarized Light and the Origin of Homochirality. *Origins of Life and Evolution of the Biosphere*, **31**, 167.

Bailey, J., Chrysostomou, A., Hough, J. H., Gledhill, T. M., McCall, A., Clark, S., Menard, F., Tamura, M. (1998). Circular Polarization in Star-Formation Regions: Implications for Biomolecular Homochirality, *Science*, **281**, 672.

Ball, A. J., Gadomski, S., Banaszkiewicz, M., Spohn, T., Ahrens, T. J., Whyndham, M., Zarnecki, J. C. (2001) An instrument for in situ comet nucleus surface density profile measurement by gamma ray attenuation, *Planetary and Space Science*, **49**, 961.

Barbier, B., Henin, O., Boillot, F., Chabin, A., Chaput, D., Brack, A. (2002). Exposure of amino acids and derivatives in the Earth orbit. *Planet. Space Sci.*, **50**, 353–359.

Benkhoff, J. (1999). On the Flux of Water and Minor Volatiles from the Surface of Comet Nuclei, *Space Science Reviews*, **90**, 141.

Bernstein, M. P., Dworkin, J. P., Sandford, S. A., Cooper, G. W.,Allamandola, L. J. (2002). Racemic amino acids from the ultraviolet photolysis of interstellar ice analogues. *Nature*, **416**, 401–403.

Bernstein, M. P., Allamandola, L. J., Sandford, S. A. (1997). Complex organics in laboratory simulations of interstellar/cometary ices. *Adv. Space Res.*, **19**, 991–998.

Bernstein, M. P., Sandford, S. A., Allamandola, L. J., Chang, S. (1994). Infrared spectrum of matrix isolated Hexamethylenetetramine in Ar and H_2O at cryogenic temperatures. *J. Phys. Chem.*, **98**, 12 206–12 210.

Bernstein, M. P., Sandford, S. A., Allamandola, L. J., Chang, S., Scharberg, M. A. (1995). Organic Compounds Produced By Photolysis of Realistic Interstellar and Cometary Ice Analogs Containing Methanol. *Astrophys. J.*, **454**, 327–344.

Biver et al., (1999) Long-Term Evolution of the Outgassing of Comet Hale- Bopp from Radio Observations. *Earth, Moon and Planets*, **78**, 5–11.

Biver, N., Bockelée-Morvan, D., Crovisier, J., Colom, P., Henry, F., Moreno, R., Paubert, G., Despois, D., Lis, D. C. (2002a) Chemical Composition Diversity Among 24 Comets Observed At Radio Wavelengths. *Earth Moon and Planets*, **90(1)**, 323–333.

Biver, N., Bockelée-Morvan, D., Colom, P., Crovisier, J., Henry, F., Lellouch, E., Winnberg, A., Johansson, L. E. B., Gunnarsson, M., Rickman, H., Rantakyrö, F., Davies, J. K., Dent, W. R. F., Paubert, G., Moreno, R., Wink, J., Despois, D., Benford, D. J., Gardner, M., Lis, D. C., Mehringer, D., Phillips, T. G., Rauer, H. (2002b). The 1995–2002 Long-Term Monitoring of Comet C/1995 O1 (HALE-BOPP) at Radio Wavelength, *Earth Moon and Planets*, **90**, 5.

Blank, J. G., Miller, G. H., Ahrens, M. J., Winans, R. E. (2001). Experimental Shock Chemistry of Aqueous Amino Acid Solutions and the Cometary Delivery of Prebiotic Compounds. *Orig. Life*, **31**, 15–51.

Bockelée-Morvan, D. (1997). Cometary Volatiles: the status after comet C/1996 B2 Hyakutake. In *Molecules in Astrophysics: Probes and Processes*, IAU symposium 178, E.F. van Dishoeck ed., Kluwer, p. 219.

Bockelee-Morvan, D., Brooke, T.Y., Crovisier, J. (1995) On the origin of the 3.2 to 3.6-micrometre emission features in comets, *Icarus*, **116**, 18.

Bockelée-Morvan, D. Crovisier, J. (2002). Lessons of Comet Hale–Bopp for Coma Chemistry: *Observations and Theory. Earth Moon and Planets*, **89**, 53–71.

Bockelée-Morvan, D., Rickman, H. (1999). C/1995 O1 (Hale–Bopp): Gas Production Curves and Their Interpretation. *Earth Moon Plan.*, **79**, 55–77.

Bockelée-Morvan, D., Biver, N., Moreno, R., Colom, P., Crovisier, J., Gérard, E., Henry, F., Lism, D. C., Matthews, H., Weaver, H. A., Womack, M., Festou, M. C. (2001). Outgassing Behaviour and Composition of Comet C/1999 S4 (LINEAR) During Its Disruption. *Science*, **292**, 1339–1343.

Bockelée-Morvan, D., Gautier, D., Lis, D. C., Young, K., Keene, J., Phillips, T. G., Owen, T., Crovisier, J., Goldsmith, P. F., Bergin, E.A., Despois, D., Wootten, A. (1998). Deuterated Water in Comet C/1996 B2 (Hyakutake) and its Implications for the Origin of Comets. *Icarus*, **133**, 147–162.

Bockelée-Morvan D., Lis D. C., Wink J. E., Despois D., Crovisier J., Bachiller R., Benford D. J., Biver N., Colom P., Davies J. K., Gérard E., Germain B., Houde M., Mehringer D., Moreno R., Paubert G., Phillips T. G., Rauer H. (2000). New molecules found in comet C/1995 O1 (Hale–Bopp). Investigating the link between cometary and interstellar material., *Astronomy and Astrophysics*, **353**, 1101–1114.

Bockelée-Morvan, D., Crovisier, J., Mumma, M., Weaver, H. (2004, in press), The Composition of Cometary Volatiles, in *Comets II,* eds. M. Festou, U. Keller, H. Weaver, Univ. of Arizona Press.

Boehnhardt, H. (2002), Comet Splitting – Observations and Model Scenarios, *Earth Moon and Planets*, **89**, 91.

Boillot, F., Chabin, A., Buré, C., Venet, M., Belsky, A., Bertrand-Urbaniak, M., Delmas, A., Brack, A., Barbier, B. (2002). The Perseus Exobiology Mission on MIR: Behaviour of Amino Acids and Peptides in Earth Orbit. *Orig. Life*, **32**, 359–385.

Bonner, W. A., Mayo Greenberg, J., Rubenstein, E. (1999). The Extraterrestrial Origin of the Homochirality of Biomolecules – Rebuttal to a Critique, *Origins of Life and Evolution of the Biosphere*, **29**, 215.

Bordé, P., Rouan, D., Léger, A. (2003). Exoplanet detection capability of the COROT space mission, *Astronomy and Astrophysics*, **405**, 1137.

Boulanger, F., Gerin, M. *Interstellar and Circumstellar Molecules*, http://www.lra.ens.fr/∼pcmi/table-mol-an.html.

Bouwman, J., de Koter, A., Dominik, C., Waters, L.B.F.sM. (2003). The origin of crystalline silicates in the Herbig Be star HD 100546 and in comet Hale–Bopp. *Astronomy and Astrophysics*, **401**, 577.

Briggs, R., G. Ertem, J. P. Ferris, J. M. Greenberg, P. J. McCain, C. X. Mendoza-Gomez, W. Schutte (1992). Comet Halley as an aggregate of interstellar dust and further evidence for the photochemical formation of organics in the interstellar medium. *Orig. Life*, **22**, 287–307.

Brucato, J.R., Colangeli, L., Mennella, V., Palumbo, P., Bussoletti, E. (1999). Silicates in Hale–Bopp: hints from laboratory studies. *Planetary and Space Science*, **47**, 773–779.

Brucato, J.R., Castorina, A.C., Palumbo, M.E., Satorre, M.A., Strazzulla, G. (1997). Ion Irradiation and Extended CO Emission in Cometary Comae. *Planetary and Space Science*, **45**, 835–840.

Capria, M. T. (2002). Sublimation Mechanisms of Comet Nuclei, *Earth Moon and Planets*. **89**, 161.

CBAT. *Cometary Designation System*. http://cfa-www.harvard.edu/iau/lists/CometResolution.html.

Ceccarelli, C., Loinard, L., Castets, A., Faure, A., Lefloch, B. (2000). Search for glycine in the solar type protostar IRAS 16293-2422. *Astronomy and Astrophysics*, **362**, 1122–1126.

Chamberlin, T. C., Chamberlin, R. T. (1908). *Science*, **28**, 897.

Charnley, S.B. (1997). On the nature of interstellar organic chemistry. In Astronomical and Biochemical Origins and the Search for Life in the Universe, *5th Int. Conf. On Bioastronomy, IAU Coll. 161*, Cosmovici C.B., Bowyer S. Werthimer D. eds., pp 89–96.

Charnley, S.B., Rodgers, S.D., Butner, H. M., Ehrenfreund, P. (2002a). Chemical Processes in Cometary Comae, *Earth Moon and Planets*, **90**, 349.

Charnley, S.B., Rodgers, S.D., Kuan, Y.-J., Huang, H.-C. (2002b). Biomolecules in the interstellar medium and in comets, *Advances in Space Research*, **30**, 1419.

Chen, J., Jewitt, D. (1994). On the rate at which comets split, *Icarus*, **108**, 265.

Chyba, C., Sagan, C. (1997). Comets as a Source of Prebiotic Organic Molecules for the Early Earth, in *Comets and the Origin and Evolution of Life*, eds P.J. Thomas, C.F. Chyba, C.P. McKay, Springer.

Chyba, C.F., Thomas, P.J., Brookshaw, L., Sagan, C. (1990). Cometary delivery of organic molecules to the early earth. *Science*, **249**, 249–373.

Combes F., Q-Rieu N., Wlodarczak, G. (1996). Search for interstellar glycine. *Astronomy and Astrophysics,* **308**, 618–622.

Commeyras, A., Boiteau, L., Trambouze-Vandenabeele, O., Selsis, F. (2004). *Lectures in Astrobiology – Vol. I*, Eds. M. Gargaud, B. Barbier, H. Martin, J. Reisse, Springer Verlag, [this book]

Cooper et al., (2001). Carbonaceous meteorites as a source of sugar-related organic compounds for the early Earth, *Nature*, **414**, 879–883.

Coradini, A., Capaccioni, F., Capria, M. T., de Sanctis, M. C., Espinasse, S., Orosei, R., Salomone, M., Federico, C. (1997). Transition Elements between Comets and Asteroids, *Icarus*, **129**, 337.

Cottin, H. (1999). Chimie organique de l'environnement cométaire: étude expérimentale de la contribution de la composante organique réfractaire à la phase gazeuse. Thèse, Univ. Paris 12.

Cottin, H., Gazeau, M.C., Raulin, F. (1999). Cometary organic chemistry: a review from observations, numerical and experimental simulations. *Planet. Space Sci.*, **47**, 1141–1162.

Cottin, H., Gazeau, M. C., Bénilan, Y., Raulin, F. (2001). Polyoxymethylene as parent molecule for the formaldehyde extended source in comet Halley. *The Astrophysical Journal*, **556**, 417–420.

Cottin, H., Moore, M.H., Bénilan, Y. (2003). Photodestruction of relevant interstellar molecules in ice mixtures. *The Astrophysical Journal*, **590**, 874–881.

Cottin, H., Szopa, C., Moore, M.H. (2001). Production of hexamethylenetetramine in photolyzed and irradiated interstellar cometary ice analogs. *Astrophys. J. Lett.*, **561**, L139–L142.

Cottin, H., Bachir, S., Raulin, F., Gazeau, M.C. (2002). Photodegradation of Hexamethylenetetramine by VUV and its relevance for CN and HCN extended sources in comets. *Adv. Space Res.*, **30**, 1481–1488.

Cottin, H., Bénilan, Y., Gazeau, M.-C., Raulin, F. (2004). Origin of cometary extended sources from degradation of refractory organics on grains: polyoxymethylene as formaldehyde parent molecule. *Icarus*, **167**, 397–416.

Cremonese, G., Boehnhardt, H., Crovisier, J., Rauer, H., Fitzsimmons, A., Fulle, M., Licandro, J., Pollacco, D., Tozzi, G.P., West, R.M. (1997). Neutral Sodium from Comet Hale–Bopp: A Third Type of Tail. *Astrophysical Journal Letters*, **490**, L199.

Crifo, J.F. (1988). Cometary dust sizing: comparison between optical and in-situ sampling techniques. *Particle & Particle Systems Characterization*, **5**, 38–46.

Crifo, J.F. (1991). Hydrodynamic models of the collisional coma. In *Comets in the Post-Halley Era* (eds. R. L. Newburn, M. Neugebauer, J. Rahe), pp. 937–989. Kluwer.

Crifo, J.F. (1995). A general physicochemical model of the inner coma of active comets. I. Implications of spatially distributed gas and dust production. *The Astrophysical Journal*, **445**, 470–488.

Crifo, J.F., Rodionov, A.V. (1997). The Dependence of the Circumnuclear Coma Structure on the Properties of the Nucleus. I. Comparison between a homogeneous and an Inhomogeneous Spherical Nucleus, with Application to P/Wirtanen. *Icarus*, **127**, 319.

Cronin, J., Chang, S. (1993). Organic matter in meteorites: Molecular and isotopic analysis. In *The Chemistry of Life's origin*, Greenberg et al., eds., Kluwer, 209–258.

Crovisier, J. (1999) Infrared Observations Of Volatile Molecules In Comet Hale–Bopp. *Earth, Moon, and Planets*, **79**, 125–143.

Crovisier, J. (2004, in press) The molecular complexity of comets. *Astrobiology: Future Perspectives, ISSI,* Kluwer.

Crovisier, J., Bockelée-Morvan, D., Colom, P., Despois, D., Lis, D.C. et al., (submitted 2004a). The composition of ices in comet C/1995 O1 (Hale–Bopp) from radio spectroscopy: Further results and upper limits on undetected species. *Astron. Astrophys.*

Crovisier, J., Bockelée-Morvan, D., Biver, N., Colom, P., Despois, D., Lis, D.C. (submitted 2004b). Ethylene glycol in comet C/1995 O1. *Astron. Astrophys.*

Crovisier, J. Schloerb, F.P. (1991) The Study of Comets at Radio Wavelengths. In *Comets in the Post-Halley Era*, Newburn R.L. Jr., Neugebauer M. Rahe J. eds., Kluwer, pp 149–174.

Crovisier, J., Encrenaz, T. (2000). *Comet Science: The Study of Remnants From the Birth of the Solar System*, Cambridge University Press

Crovisier, J., Leech, K., Bockelée-Morvan, D., Brooke, T.Y., Hanner, M. S., Altieri B., Keller H. U., Lellouch E. (1997). The Spectrum of Comet Hale–Bopp (C/1995 O1) Observed with the Infrared Space Observatory at 2.9 Astronomical Units from the Sun. *Science*, **275**, 1904–1907.

Dauphas, N., Robert, F., Marty, B. (2000). The Late Asteroidal and Cometary Bombardment of Earth as Recorded in Water Deuterium to Protium Ratio, *Icarus*, **148**, 508–512.

Dauphas, N., Marty, B. (2002). Inference on the nature and the mass of Earth's late veneer from noble metals and gases, *Journal of Geophysical Research (Planets)*, **107**, E12, 5129

De Bergh, C. (2004, in press). Kuiper Belt: water and organics. *Astrobiology: Future Perspectives, ISSI,* Kluwer.

Delsemme, A. H. (2000). 1999 Kuiper Prize Lecture Cometary Origin of the Biosphere. *Icarus*, **146**, 313–325.

De Sanctis, M.C., Capria, M.T., Coradini, A. (2001). Thermal Evolution and Differentiation of Edgeworth-Kuiper Belt Objects, *Astronomical Journal*, **201**, 2792.

Despois, D. (1999). Radio line observations of molecular and isotopic species in comet C/1995 O1 (Hale–Bopp). *Earth Moon and Planets*, **79**, 103–124.

Despois, D., Ricaud, P., Lautié, N., Schneider, N., Jacq T., Biver, N., Lis, D.C., Chamberlin, R.A., Phillips, T.G., Miller, M., Jenniskens, P. (2000). Search for Extraterrestrial Origin of Atomic Trace Molecules – Radio Sub-mm Observations during the Leonids. *Earth, Moon and Planets*, **82–83**, 129–140.

Despois, D. (1992). Solar System – Interstellar Medium a Chemical Memory of the Origins(rp), IAU Symp. 150: *Astrochemistry of Cosmic Phenomena*, 451.

Despois, D., Crovisier, J., Bockelée-Morvan, D., Biver, N. (2002). Comets and prebiotic chemistry: the volatile component, ESA SP-518: *Exo-Astrobiology*, 123.

Despois, D., Crovisier, J., Bockelee-Morvan, D., Colom, P. (1992). Formation of Comets: Constraints from the Abundance of Hydrogen Sulfide and Other Sulfur Species, IAU Symp. 150: *Astrochemistry of Cosmic Phenomena*, 459.

Duncan, M., Quinn, T., Tremaine, S. (1997). The formation and extent of the solar system comet cloud, *Astronomical Journal*, **94**, 1330.

Eberhardt, P., Krankowsky, D. (1995). The electron temperature in the inner coma of comet P/Halley. *Astron. Astophys.*, **295**, 795.

Edgeworth, K.E. (1943). The evolution of our planetary system, *Journal of the British Astronomical Association*, **53**, 181–186.

Ehrenfreund, P., Charnley, S.B. (2000). Organic molecules in the interstellar medium, comets and meteorites: a voyage from dark clouds to the early earth. *Annual Review of Astronomy & Astrophysics*, **38**, 427–483.

Ehrenfreund, P., Irvine, W., Becker, L., Blank, J., Brucato, J. R., Colangeli, L., Derenne, S., Despois, D., Dutrey, A., Fraaije, H., Lazcano, A., Owen, T., Robert, F.

(2002). Astrophysical and astrochemical insights into the origin of life., *Reports of Progress in Physics*, **65**, 1427.

Encrenaz, T., Knacke, R. (1991). Infrared Spectroscopy of Cometary Parent Molecules. In *Comets in the Post-Halley Era*, Newburn R.L. Jr., Neugebauer M. Rahe J. eds., Kluwer, 149–174.

Enzian, A., Klinger, J., Schwehm, G., Weissman, P. R. (1999). Temperature and Gas Production Distributions on the Surface of a Spherical Model Comet Nucleus in the Orbit of 46P/Wirtanen, *Icarus*, **138**, 74.

Fassett, J.E., Lucas, S.G., Zielinski, R.A., Budahn, J.R. (2001). Compelling New Evidence for Paleocene Dinosaurs in the Ojo Alamo Sandstone San Juan Basin, New Mexico and Colorado, USA, *Proceedings of the 32nd Symposium on Celestial Mechanics*, 3139.

Fegley, B. Jr. (1993). Chemistry of the solar nebula, in *The Chemistry of Life's Origin*, eds J.M. Greenberg, C.X. Mendoza-Gomez, V. Pirronello, NATO ASI Series C, Kluwer, **416,** 75–147.

Fernandez, J.A. (1980). On the existence of a comet belt beyond Neptune, *Monthly Notices of the Royal Astronomical Society*, **192**, 481.

Fernandez, J.A. (1997). The Formation of the Oort Cloud and the Primitive Galactic Environment, *Icarus*, **129**, 106.

Festou, M.C., Rickman, H.West R. M. (1993a). Comets. 1: Concepts and observations. *Astronomy and Astrophysics Review*, **4**, 363–447.

Festou M.C., Rickman H.West R. M. (1993b). Comets. 2: Models, evolution, origin and outlook *Astronomy and Astrophysics Review*, **5**, 37–163.

Festou, M., Keller, U., Weaver, H. (2004, in press) eds, Comets II, Univ. of Arizona Press.

Fomenkova, M.N. (1999). On the Organic Refractory Component of Cometary Dust. *Space Science Reviews*, **90**, 109–114.

Frankel, Ch. (1999). *The End of the Dinosaurs: Chicxulub Crater and Mass Extinctions* Cambridge Univ. Press.

Fray, N., Bénilan, Y., Cottin, H., Gazeau, M.-C., Crovisier, J. (submitted). The origin of the CN radical in comets: A review from observations and models. *Planetary and Space Science*.

Gargaud, M., Despois, D., Parisot, J.-P. (2001). *L'environnement de la Terre Primitive*, Presses Universitaires de Bordeaux.

Gargaud, M., Despois, D., Parisot, J.-P., Reisse, J. (2003). *Les Traces du Vivant*, Presses Universitaires de Bordeaux.

Geiss, J. (1988). Composition in Halley's comet, *Reviews in Modern Astron.*, **1**, 1–27.

Geiss, J., Altwegg, K., Balsiger, H., Graf, S. (1999). Rare Atoms, Molecules and Radicals in the Coma of P/Halley. *Space Science Reviews*, **90**, 253–268. Gerakines, P. A. M. H. Moore (2001). Carbon suboxide in astrophysical ice analogs. *Icarus*, **154**, 372–380.

Gerakines, P.A., Moore, M.H., Hudson, R.L. (2000). Carbonic acid production in H_2O:CO_2 ices. UV photolysis vs. proton bombardment. *Astron. Astophys.*, **357**, 793–800.

Gibb, E.L., Mumma, M.J., dello Russo, N., Disanti, M.A., Magee-Sauer, K., (2003) Methane in Oort cloud comets, *Icarus*, **165**, 391.

Green, D.W.E. (1999). What is improper about the term "Kuiper belt"? (or, Why name a thing after a man who didn't believe its existence?) *International Comet Quarterly*, pp 44–46, January, 1999 and http://cfa-www.harvard.edu/icq/ICQpluto2.html.

Greenberg, J.M. (1982). What are comets made of ? A model based on interstellar dust. In *Comets* (ed. L. L. Wilkening), pp. 131–163. University of Arizona Press.

Greenberg, J.M., Li, A. (1997). Silicate core-organic refractory mantle particles as interstellar dust and as aggregated in comets and stellar disks. *Adv. Space Res.*, **19**, 981–990.

Greenberg, J.M., Li, A. (1998). From interstellar dust to comets: the extended CO source in comet Halley, *Astron. Astophys.*, **332**, 374–384.

Greenberg, J.M., Li, A., Mendoza-Gómez, C. X., Schutte, W. A., Gerakines, P. A., Groot, M. d. (1995). Approaching the Interstellar Grain Organic Refractory Component. *Astrophys. J.*, **455**, L177–L180.

Greenberg, J.M. (1998). Making a comet nucleus, *Astronomy and Astrophysics*, **330**, 375.

Greenberg, J.M. (1993). Physical and Chemical composition of Comets – From interstellar space to the Earth, in *The Chemistry of Life's Origin*, eds. J.M. Greenberg, C.X. Mendoza-Gomez, V. Pirronello, NATO ASI Series C, Kluwer, **416,** pp195–208.

Greenberg, J. M. C. X. Mendoza-Gomez (1993). Interstellar dust evolution: a reservoir of prebiotic molecules. In *The Chemistry of Life's Origins* (ed. Greenberg), 1–32. Kluwer Academic.

Harker, D.E., Wooden, D.H., Woodward, C.E., Lisse, C.M. (2002). Grain Properties of Comet C/1995 O1 (Hale–Bopp). *Astrophysical Journal*, **580**, 579–597.

Hayward, T.L. Hanner, M.S. (1997). Ground-Based Thermal Infrared Observations of Comet Hale–Bopp (C/1995 O1) During 1996. *Science,* **275**, 1907–1909.

Hersant, F., Gautier, D., Huré, J.-M. (2001). A Two-dimensional Model for the Primordial Nebula Constrained by D/H Measurements in the Solar System: Implications for the Formation of Giant Planets. *Astrophysical Journal*, **554**, 391–407.

Hollis, J.M., Lovas, F.J., Jewell, P.R. (2000). Interstellar Glycolaldehyde: The First Sugar. *Astrophys. Journal Lett.*, **540**, L107–L110.

Hollis, J.M., Pedelty, J.A., Snyder, L.E., Jewell, P.R., Lovas, F.J., Palmer, P., Liu, S.-Y. (2003). A Sensitive Very Large Array Search for Small-Scale Glycine Emission toward OMC-1, *Astrophysical Journal*, **588**, 353.

Hough, J.H., Bailey, J.A., Chrysostomou, A., Gledhill, T.M., Lucas, P. W., Tamura, M. Clark, S., Yates, J., Menard, F. (2001). Circular polarisation in star-forming regions: possible implications for homochirality, *Advances in Space Research*, **27**, 313.

Hudson, R. L., Moore, M. H. (1999). Laboratory Studies of the Formation of Methanol and Other Organic Molecules by Water+Carbon Monoxide Radiolysis: Relevance to Comets, Icy Satellites, and Interstellar Ices. *Icarus*, **140**, 451–461.

Hudson, R. L., Moore, M. H. (2002). The N_3 Radical as a Discriminator between ion irradiated and UV-photolyzed astronomical ices. *Astrophys. J.*, **568**, 1095–1099.

Huebner, W. F. (1987). First polymer in space identified in comet Halley. *Science*, **237**, 628–630.

Huebner, W. F., Boice D. C., Korth A. (1989). Halley's polymeric organic molecules. *Advances in Space Research,* **9**, 29–34.

Huebner, W. F., Benkhoff, J. (1999a). From Coma Abundances to Nucleus Composition, *Space Science Reviews*, **90**, 117.

Huebner, W. F., Benkhoff, J., Capria, M. T., Coradini, A., de Sanctis, M. C., Enzian, A., Orosei, R., Prialnik, D. (1999b). Results from the Comet Nucleus Model Team at the International Space Science Institute, Bern, Switzerland, *Advances in Space Research*, **23**, 1283.

Iro, N., Gautier, D., Hersant, F., Bockelée-Morvan, D., Lunine, J. I. (2003). An interpretation of the nitrogen deficiency in comets, *Icarus*, **161**, 511.

Irvine, W. M., Schloerb F. P., Crovisier J., Fegley B., Mumma M. J. (2000a). Comets: a link between interstellar and nebular chemistry. In *Protostar and Planets IV* (eds. V. Manning, A. Boss, S. Russel), pp. 1159. University of Arizona Press.

Irvine, W. M., Senay M., Lovell A. J., Matthews H. E., McGonagle D., Meier R. (2000b). Detection of Nitrogen Sulfide in Comet Hale–Bopp. *Icarus*, **143**, 412–414.

Irvine, W., Bockelee-Morvan, D., Lis, D. C., Matthews, H. E., Biver, N., Crovisier, J., Davies, J. K., Dent, W. R. F., Gautier, D., Godfrey, P. D., Keene, J., Lowell, A. J., Owen, T. C., Phillips, T. G., Rauer, H., Schloerb, F. P., Senay, M., Young, K (1996). Spectroscopic evidence for interstellar ices in Comet Hyakutake, *Nature*, **382**, 418.

Irvine, W. M., Bergman, P., Lowe, T. B., Matthews, H., McGonagle, D., Nummelin, A., Owen, T. (2003). HCN and HNC in Comets C/2000 Wm1 (Linear) and C/2002 C1 (Ikeya-Zhang), *Origins of Life and Evolution of the Biosphere*, **33**, 609.

Irvine, W. M., Leschine, S. B., Schloerb, F. P. (1980). Thermal History, Chemical Composition and Relationship of Comets to the Origin of Life, *Nature*, **283**, 748.

Jeffers, S. V., Manley, S. P., Bailey, M. E., Asher, D. J. (2001). Near-Earth object velocity distributions and consequences for the Chicxulub impactor, Monthly Notices of the Royal *Astronomical Society*, **327**, 126.

Jenniskens, P. (2001). Meteors as a delivery vehicle for organic matter to the early Earth, in *Meteoroids 2001 Conference*, ESA SP-495, 247–254

Jenniskens, P., Baratta, G. A., Kouchi, A. Groot, M. S. D., Greenberg, J. M., Strazzulla, G. (1993). Carbon dust formation on interstellar grains. *Astronomy and Astrophysics*, **273**, 583–600.

Jessberger, E. K., Kissel, J. (1991). Chemical properties of cometary dust and a note on carbon isotopes, *ASSL* Vol. 167: IAU Colloq. 116: *Comets in the Post-Halley Era*, 1075.

Jewitt, D. C., Matthews, H. E., Owen, T., Meier. R. (1997). Measurements of $^{12}C/^{13}C$, $^{14}N/^{15}N$, and $^{32}S/^{34}S$ Ratios in Comet Hale–Bopp (C/1995 O1). *Science,* **278**, 90–93.

Jewitt, D. (2002). From Kuiper Belt object to cometary nucleus, ESA SP-500: *Asteroids, Comets, and Meteors*, ACM 2002, 11.

Jewitt, D. C., Luu, J. X. (1993). Discovery of the Candidate Kuiper Belt Object 1992 QB1. *Nature*, **362**, 730–732.

Jopek, T. J., Gonczi, R., Froeschle', C., Michel, P., Longo, G., Foschini, L. (2002). A main belt asteroid: the most probable cause of the Tunguska event, Memorie della Societa *Astronomica Italiana*, **73**, 679.

Karmann, C., Beust, H., Klinger, J. (2003). The physico-chemical history of Falling Evaporating Bodies around beta Pictoris: The sublimation of refractory material, *Astronomy and Astrophysics*, **409**, 347.

Karmann, C., Beust, H., Klinger, J. (2001). The physico-chemical history of Falling Evaporating Bodies around beta Pictoris: investigating the presence of volatiles, *Astronomy and Astrophysics*, **372**, 616.

Kasamatsu, T., Kaneko, T., Saito, T., Kobayashi, K. (1997). Formation of organic compounds in simulated interstellar media with hich energy particles. *Bulletin of the Chemical Society of Japan*, **70**, 1021–1026.

Kasting, J. F (1993). Earth's early atmosphere, *Science*, **259**, 920–926.

Kasting, J. Catling, D. (2003). Evolution of a habitable planet, *Ann. Rev. Astron. Astrophys*, **41**, 429–63.

Kissel, J. Krueger, F. R. (1987). The organic component in dust from comet Halley as mesured by the PUMA mass spectrometer on board Vega 1. *Nature*, **326**, 755–760.

Kissel, J., Krueger, F.R. et Roessler, K. (1997). Organic Chemistry in Comets From Remote and In Situ Observations. In *Comets and the Origins and Evolution of Life*, Thomas P.J., Chyba C.P. McKay C.P. eds., Springer, 69–110.

Klavetter, J. J., A'Hearn, M. F. (1994). An extended source for CN jets in Comet P/Halley. *Icarus*, **107**, 322–334.

Kobayashi, K., Kasamatsu, T., Kaneko, T., Koike, J., Oshima, T., Saito, T., Yamamoto, T., Yanagawa, H. (1995). Formation of amino acid precursors in cometary ice environments by cosmic radiation. *Adv. Space Res.*, **16**, (2)21–(2)26.

Krueger, F. R. Kissel, J. (1987). The chemical composition of the dust of comet P/Halley as measured by "Puma" on board Vega-1. *Naturwissenschaften*, **74**, 312–316.

Krueger, F. R., Korth, A., Kissel, J. (1991). The organic matter of comet Halley as inferred by joint gas phase and solid phase analyses. *Space Science Reviews*, **56**, 167–175.

Kuan, Y., Charnley, S. B., Huang, H., Tseng, W., Kisiel, Z. (2003). Interstellar Glycine, *Astrophysical Journal*, **593**, 848.

Kuiper, G.P. (1951). in *Astrophysics: A Topical Symposium*, ed. J. A. Hynek (New York: McGraw-Hill), 400.

Kurtz, S., Cesaroni, R., Churchwell, E., Hofner, P., Walmsley, C. M. (2000). Hot Molecular Cores and the Earliest Phases of High-Mass Star Formation, *Protostars and Planets* **IV**, 299.

Kyte, F.T. (1998). A meteorite from the Cretaceous/Tertiary boundary. *Nature* **396**, 237–239.

Lagrange, A.-M., Backman, D. E., Artymowicz, P. (2000). Planetary Material around Main- Sequence Stars, *Protostars and Planets* **IV**, 639.

Lamy, P., Biesecker, D. (2002), The properties of Sun-grazing coments, 34th COSPAR meeting, Houston, p 3159

Le Loeuff, J., Laurent, Y. (2001). Biodiversity of Late Maastrichtian Dinosaurs, *Proceedings of the 32nd Symposium on Celestial Mechanics*, 3126.

Lecacheux, A., Biver, N., Crovisier, J., Bockelée-Morvan, D., Baron, P., Booth, R. S., Encrenaz, P., Floren, H.-G., Frisk, U., Hjalmarson, A., Kwok, S., Mattila, K., Nordh, L., Olberg, M., Olofsson, A. O. H., Rickman, H., Sandqvist, A., von Scheele, F., Serra, G., Torchinsky, S., Volk, K., Winnberg, A. (2003). Observations of water in comets with Odin, *Astronomy and Astrophysics*, **402**, L55.

Lecavelier Des Etangs, A., Vidal-Madjar, A., Ferlet, R. (1999). Photometric stellar variation due to extra-solar comets, *Astronomy and Astrophysics*, **343**, 916.

Leonard (1930). *Leaflet Astron. Soc. Pacific*, **30**, 21–124

Levasseur-Regourd, A. C., Hadamcik, E., Renard, J. B. (1996). Evidence for two classes of comets from their polarimetric properties at large phase angles. *Astronomy and Astrophysics*, **313**, 327.

Levison, H. F., Dones, L., Duncan, M. J. (2001). The Origin of Halley-Type Comets: Probing the Inner Oort Cloud. *The Astronomical Journal*, **121**, 2253–2267.

Lewis, J. S., Prinn, R. G. (1980). Kinetic inhibition of CO and N_2 reduction in the solar nebula, *Astrophysical Journal*, **238**, 357.

Magee-Sauer, K. (2002). CSHELL Observations of Comet C/2002 C1(Ikeya-Zhang) in the 3.0-Micron Region, DPS Meeting, *BAAS*, **34**, 16.05.

Malfait, K., Waelkens, C., Waters, L. B. F. M., Vandenbussche, B., Huygen, E., de Graauw, M. S. (1998). The spectrum of the young star HD 100546 observed with the Infrared Space Observatory. *Astronomy and Astrophysics*, **332**, L25.

Maurette M. (1998). Carbonaceous Micrometeorites and the Origin of Life, *Origins Life Evolution Biosphere*, **28**, 385–412.

Maurette, M., Duprat, J., Engrand, C., Gounelle, M., Kurat, G., Matrajt, G., Toppani, A. (2000). Accretion of neon, organics, CO_2, nitrogen and water from large interplanetary dust particles on the early Earth. *Planetary and Space Science*, **48**, 1117.

McDonnell, J. A. M., Lamy, P. L., Pankiewicz, G. S. (1991). Physical properties of cometary dust. In *Comets in the Post-Halley Era*, Vol. 2, pp. 1043–1073. Kluwer.

McKinnon, W. B. (2002). On the initial thermal evolution of Kuiper Belt objects, ESA SP-500: *Asteroids, Comets, and Meteors*: ACM 2002, 29.

Meier, R., Owen, T. C., Jewitt, D. C., Matthews, H. E., Senay, M., Biver, N., Bockelee–Morvan, D., Crovisier, J., Gautier, D. (1998). Deuterium in Comet C/1995 O1 (Hale–Bopp): Detection of DCN, *Science*, **279**, 1707.

Miller S.L. (1998). The endogenous synthesis of organic compounds, in *The Molecular Origin of Life: Assembling Pieces of the Puzzle*, A. Brack ed., Cambridge, 59–85.

Mitchell, D. L., Lin, R. P., Carlson, C. W., Korth, A., Rème, H., Mendis, D. A. (1992). The origin of complex organic ions in the coma of comet Halley. *Icarus*, **98**, 125–133.

Montmerle chapter this book.

Moore, M. H., R. Khanna, B. Donn (1991). Studies of Proton Irradiated H_2O+CO_2 and H_2O+CO Ices and Analysis of Synthesized Molecules. *J. Geophys. Res.*, **96**, 17541–17545.

Morbidelli, A. Brown, M.E. (2004, in press). The Kuiper belt and the primordial evolution of the Solar System in *Comets II*, eds. M. Festou, U. Keller, H. Weaver, Univ. of Arizona Press.

Morbidelli, A., Chambers, J., Lunine, J. I., Petit, J. M., Robert, F., Valsecchi, G. B., Cyr, K. E. (2000). Source regions and time scales for the delivery of water to Earth, *Meteoritics and Planetary Science*, **35**, 1309.

Moreels, G., Clairemidi, J., Hermine, P., Brechignac, P., Rousselot, P. (1994). Detection of a polycyclic aromatic molecule in comet P/Halley. *Astronomy and Astrophysics*, **282**, 643–656.

Moreno, R. (1998). Observations millimétriques et submillimétriques des planètes géantes. Etude de Jupiter après la chute de la comète SL9. PhD Thesis, Université de Paris VI.

Mousis, O., Gautier, D., Bockelée-Morvan, D., Robert, F., Dubrulle, B., Drouart, A. (2000). Constraints on the Formation of Comets from D/H Ratios Measured in H_2O and HCN, *Icarus*,, **148**, 513.

Mumma, M. J., Weissman, P. R., Stern, S. A. (1993). Comets and the Origin of the solar system: reading the Rosetta stone. In Protostars and Planets III, eds. E.H. Levy J. I. Lunine, Univ. of Arizona Press, pp 1177–1252.

Mumma, M. J., DiSanti, M. A., Dello Russo N., Magee-Sauer, K., Gibb, E., Novak, R. (2002), The organic volatile composition of Oort cloud comets: evidence for chemical diversity in the Giant-Planets nebular region., in *Asteroids Comets Meteors 2002*, ESA SP-500, 753.

Muñoz Caro, G. M. (2003). From photoprocessing of interstellar ice to amino acids and other organics. PhD Thesis, Leiden Observatory.

Muñoz Caro, G. M., Meierhenrich, U. J., Schutte, W. A., Barbier, B., Arcones Segovia, A., Rosenbauer, H., Thiemann, W. H.-P., Brack, A., Greenberg, J. M. (2002). Amino acids from ultraviolet irradiation of interstellar ice analogues. *Nature*, **416**, 403–406.

Navarro-Gonzalez, R. A. Romero (1996). On the Survivability of an Enantiomeric Excess of Amino Acids in Comet Nuclei During the Decay of 26 A1 and Other radionuclides. *Astrophys. Space Sci.*, **236**, 49–60.

Navarro-Gonzalez, R., Ponnamperuma, C., Khanna, R. K. (1992). Computational study of radiation chemical processing in comet nuclei. *Orig. Life*, **21**, 359–374.

Newburn, R. L.,Jr., Neugebauer, M. Rahe J. eds (1991). *Comets in the Post-Halley Era*, Kluwer

Noll, K.S., Weaver, H.A., Feldman, P.D. eds. (1996). *The Collision of Comet Shoemaker-Levy 9 and Jupiter*, Cambridge University Press.

Notesco, G., Bar-Nun, A. (1996). Enrichment of CO over N_2 by their Trapping in Amorphous Ice and Implications to Comet P/Halley. *Icarus*, **122**, 118–121.

Notesco, G., Bar-Nun, A. (1997). Trapping of Methanol, Hydrogen Cyanide, and n-Hexane in Water Ice, above Its Transformation Temperature to the Crystalline Form. *Icarus*, **126**, 336–341.

Notesco, G., Laufer, D., Bar-Nun, A. (1997). The Source of the High C_2H_6/CH_4 Ratio in Comet Hyakutake. *Icarus*, **125**, 471–473.

Nuth, J. A., III, Rietmeijer, F. J. M., Hill, H. G. M. (2002). Condensation processes in astrophysical environments: The composition and structure of cometary grains. *Meteoritics and Planetary Science*, **37**, 1579–1590.

Oort, J. H. (1950). The structure of the cloud of comets surrounding the Solar System and a hypothesis concerning its origin, *Bulletin of the Astronomical Institute of the Netherlands*, **11**, 91.

Oró, J. (1961). Comets and the formation of biochemical compounds on the primitive Earth. *Nature,* **190**, 389–390.

Oró, J. (2001). Cometary molecules and Life's origin, in *First Steps in the Origin of Life in the Universe*, Chela-Flores et al., eds., Kluwer, 113–120.

Oró, J. C. B. Cosmovici (1997). Comets and Life on the primitive Earth. In *Astronomical and Biochemical Origins and the Search for Life in the Universe* (eds. C. B. Cosmovici, S. Bowyer, D. Werthimer), 97–120.

Pendleton, Y. J., Sandford, S. A., Allamandola, L. J., Tielens, A. G. G., Sellgren, K. (1994). Near-Infrared Absorption spectroscopy of interstellar hydrocarbon grains. *Astrophys. J.*, **437**, 683–696.

Petit, J.-M., Morbidelli, A. (2004). *Lectures in Astrobiology – Vol. I*, eds. M. Gargaud, B. Barbier, H. Martin, J. Reisse, Springer Verlag, [this book].

Podolak, M., Prialnik, D. (1997). ^{26}*Al and Liquid Water Environment in Comets in Comets and the Origin and Evolution of Life*, Springer.

Prialnik, D. (2002). Modeling the Comet Nucleus Interior, *Earth Moon and Planets*, **89**, 27.

Prialnik, D. (1999). Modelling Gas and Dust Release from Comet Hale–Bopp, *Earth Moon and Planets,*, **77**, 223.

Prialnik, D., Podolak, M. (1999). Changes in the Structure of Comet Nuclei Due to Radioactive Heating, *Space Science Reviews*, **90**, 169.

Prinn, R. G., Fegley, B. (1981). Kinetic inhibition of CO and N_2 reduction in circumplanetary nebulae - Implications for satellite composition, *Astrophysical Journal*, **249**, 308.

Prinn, R. G. Fegley, B. Jr. (1989). Solar Nebula Chemistry: Origin of planetary, satellite and cometary volatiles. In *Origin and Evolution of Planetary and Satellite Atmospheres*, eds S.K. Atreya, J. B. Pollack, M. Matthews (1989) Univ. Of Arizona Press, pp 78–136.

Radicati-Di-Brozolo, F., Bunch, T. E., Chang, S. (1986). Laser microprobe study of carbon in interplanetary dust particles. *Orig. Life*, **16**, 236–237.

Rairden, R. L., Jenniskens, P., Laux, C. O. (2000). Search for Organic Matter in Leonid Meteoroids, *Earth Moon and Planets*, **82**, 71.

Robert, F. (2002). Water and organic matter D/H ratios in the solar system: a record of an early irradiation of the nebula? *Planetary and Space Science*, **50**, 1227–1234.

Rocchia, R. et Robin E. (2000) L'origine extraterrestre de la crise Crétacé-Tertiaire. Pour la Science (juillet 2000) La Valse des Espèces. Dossier Hors-Série, Belin, pp 100–111.

Rodgers, S. D., Charnley, S. B. (1998). HNC and HCN in Comets. *The Astrophysical Journal Letters*, **501**, L227–L230.

Rodgers, S. D., Charnley, S. B. (2001a). Organic synthesis in the coma of Comet Hale-Bopp? *Monthly Notices of the Royal Astronomical Society*, **320,** L61–64.

Rodgers, S. D., Charnley, S. B. (2001b). On the origin of HNC in Comet Lee, *Monthly Notices of the Royal Astronomical Society*, **323**, 84–92.

Rolfe, E., Battrick, B. eds. (1987). *Proceedings of the International Symposium on the Diversity and Similarity of Comets*, ESA SP-278

Rosenbauer, H., Fuselier, S. A., Ghielmetti, A., Greenberg, J. M., Goesmann, F., Ulamec, S., Israel, G., Livi, S., MacDermott, J. A., Matsuo, T., Pillinger, C. T., Raulin, F., Roll, R., Thiemann, W. (1999). The COSAC experiment on the lander of the ROSETTA mission, *Advances in Space Research*, **23**, 333.

Sankey, J. T. (2001). Late Cretaceous Theropod Dinosaur Diversity: Latitudinal Differences in North America and Implications for the K/T Extinctions, *Proceedings of the 32^{nd} Symposium on Celestial Mechanics*, 3148.

Shimoyama, A., Ogasawara, R. (2002). Dipeptides and Diketopiperazines in the Yamato-791198 and Murchison Carbonaceous Chondrites. *Origins of Life and the Biosphere*, **32**, 165.

Schutte, W. A., L. J. Allamandola, S. A. Sandford (1993a). Formaldehyde and organic molecule production in astrophysical ices at cryogenic temperatures. *Science*, **259**, 1143–1145.

Schutte, W. A., L. J. Allamandola, S. A. Sandford (1993b). An Experimental Study of the Organic Molecules Produced in Cometary and Interstellar Ice Analogs by Thermal Formaldehyde Reactions. *Icarus*, **104**, 118–137.

Shu, F. H., Shang, H., Lee, T. (1996). Toward an Astrophysical Theory of Chondrites, *Science*, **271**, 1545.

Shuvalov, V. V., Artemieva, N. A. (2002). Numerical modeling of Tunguska-like impacts, *Planetary and Space Science*, **50**, 181.

Snyder, L. E. (1997). The Search for Interstellar Glycine. *Origins of Life and Evolution of the Biosphere*, **27**, 115–133.
Steel, D. (1997). Cometary Impacts on the Biosphere. In *Comets and the Origins and Evolution of Life*, Thomas P.J., Chyba C.P. McKay C.P. eds, Springer, 209–242.
Stern, S. Alan (2003). The evolution of comets in the Oort cloud and Kuiper belt. *Nature*, **424**, 639.
Strazzulla, G. (1997). Ion irradiation: its relevance to the evolution of complex organics in the outer solar system. *Adv. Space Res.*, **19**, 1077–1084.
Strazzulla, G., Baratta, G. A. (1991). Laboratory study of the IR spectrum of ion-irradiated frozen benzene. *Astronomy and Astrophysics*, **241**, 310–316.
Strazzulla, G., Baratta, G. A., Johnson, R. E., Donn, B. (1991). Primordial comet mantle: irradiation production of a stable, organic crust. *Icarus*, **91**, 101–104.
Szopa, C., Sternberg, R., Raulin, F., Rosenbauer, H. (2003). What can we expect from the in situ chemical investigation of a cometary nucleus by gas chromatography: First results from laboratory studies. *Planetary and Space Science*, **51**, 863–877.
Thomas, P.J., Chyba, C.P., McKay, C.P. eds (1997). *Comets and the Origins and Evolution of Life*, Springer
Waelkens, C., Malfait K. Waters L.B.F.M. (1999) Comet Hale–Bopp, Circumstellar Dust, and the Interstellar Medium. *Earth, Moon and Planets*, **79**, 265–274.
Wakamutsu, H., Y. Yamada, T. Saito, I. Kumashiro, T. Takenishi (1966). Synthesis of Adenine by Oligomerization of Hydrogen Cyanide. *Journal of Organic Chemistry*, **31**, 2035–2036.
Walker, J. F. (1964). *Formaldehyde*. Reinhold.
Weaver, H. A., Lamy, P. L. (1999). Estimating the Size of Hale–Bopp's Nucleus, *Earth Moon and Planets*, **79**, 17.
Weidenschilling, S. J. (1997). The Origin of Comets in the Solar Nebula: A Unified Model, *Icarus*, **127**, 290.
Weiler, M., Rauer, H., Helbert, J. (2004). Optical observations of Comet 67P/ Churyumov-Gerasimenko (2004) *Astronomy and Astrophysics*, **414**, 749.
Whipple, F. L. (1950). A comet model. I. The acceleration of Comet Encke. *Astrophys. J.,* **111**, 375–394.
Whittet, D.C.B. ed., (1997). *Planetary and Interstellar Processes Relevant to the Origin of Life*, Kluwer.
Whittet, D. C. B. (1997). Is Extraterrestrial Organic Matter Relevant to the Origin of Life on Earth?, *Origins of Life and Evolution of the Biosphere*, **27**, 249.
Wolman, Y., S. L. Miller, J. Ibanez, J. Oro (1971). *Science*, **174**, 1039.
Wooden, D. H., Butner, H. M., Harker, D. E., Woodward, C. E. (2000). Mg-Rich Silicate Crystals in Comet Hale–Bopp: ISM Relics or Solar Nebula Condensates? *Icarus*, **143**, 126–137.
Wootten, H. A. (2003). http://www.cv.nrao.edu/awootten/allmols.html.
Yamamoto, T. (1991). Chemical theories on the origin of comets, ASSL Vol. 167: IAU Colloq. 116: *Comets in the Post-Halley Era*, 361.
Yamamoto, T. (1985). Formation environment of cometary nuclei in the primordial solar nebula, *Astronomy and Astrophysics*, **142**, 31–36.
Yamamoto, T., Nakagawa, N., Fukui, Y. (1983). The chemical composition and thermal history of the ice of a cometary nucleus, *Astronomy and Astrophysics*, **122**, 171.
Zahnle, K. (1998). Origins of Atmospheres, *ASP Conf. Ser. 148: Origins*, 364–391.

Article 4

Fray N., Bénilan Y., Cottin H., Gazeau M.-C. and Crovisier J. (2005) The origin of the CN radical in comets : A review from observations and models. Planetary and Space Science 53(12), 1243-1262.

Available online at www.sciencedirect.com
SCIENCE DIRECT®
Planetary and Space Science 53 (2005) 1243–1262
Planetary and Space Science
www.elsevier.com/locate/pss

The origin of the CN radical in comets: A review from observations and models

N. Fray[a,*], Y. Bénilan[a], H. Cottin[a], M.-C. Gazeau[a], J. Crovisier[b]

[a]*Laboratoire Interuniversitaire des Systèmes Atmosphériques (LISA), UMR 7583 du CNRS, Universités Paris 7 and Paris 12, C.M.C., 61 Avenue du Général de Gaulle, 94010 Créteil Cedex, France*
[b]*Observatoire de Paris-Meudon, 92195 Meudon, France*

Received 18 September 2003; received in revised form 30 May 2005; accepted 24 June 2005
Available online 15 August 2005

Abstract

The origin of CN radicals in comets is not completely understood so far. We present a study of CN and HCN production rates and CN Haser scale lengths showing that: (1) at heliocentric distances larger than 3 AU, CN radicals could be entirely produced by HCN photolysis; (2) closer to the Sun, for a fraction of comets CN production rates are higher than HCN ones whereas (3) in the others, CN distribution cannot be explained by the HCN photolysis although CN and HCN production rates seem to be similar. Thus, when the comets are closer than 3 AU to the Sun, an additional process to the HCN photolysis seems to be required to explain the CN density in some comets.

The photolysis of HC_3N or C_2N_2 could explain the CN origin. But the HC_3N production rate is probably too low to reproduce CN density profile, even if uncertainties on its photolysis leave the place for all possible conclusions. The presence of C_2N_2 in comets is a reliable hypothesis to explain the CN origin; thus, its detection is a challenging issue. Since C_2N_2 is very difficult to detect from ground-based observations, only in situ measurements or space observations could determine the contribution of this compound in the CN origin.

Another hypothesis is a direct production of CN radicals by the photo- or thermal degradation of complex refractory organic compounds present on cometary grains. This process could explain the spatial profile of CN inside jets and the discrepancy noted in the isotopic ratio $^{14}N/^{15}N$ between CN and HCN. Laboratory studies of the thermal and UV-induced degradation of solid nitrogenated compounds are required to model and validate this hypothesis.

Keywords: Astrochemistry; Comets; Molecules

1. Introduction

The CN radical was one of the first species, with the C_2 radical, to be detected in the cometary environment at the end of the XIXth century. The detection of HCN was first claimed by Huebner et al. (1974) in comet C/1973 E1 (Kohoutek). Whereas this detection is controversial, because of the low signal-to-noise ratio of the signal, it seemed to explain the origin of the CN radical since Combi and Delsemme (1980b) had shown that the Haser scale length of CN production was coherent with HCN photolysis. Subsequently, HCN has been securely detected in comet 1P/Halley by three independent teams (Despois et al., 1986; Schloerb et al., 1986; Winnberg et al., 1987).

Using a better value of the expansion velocity of the gas in the coma, Bockelée-Morvan et al. (1984) showed that the HCN production rates upper limits were smaller than the CN ones and that the CN parent Haser scale length could not be associated with the HCN photo-dissociation alone (Bockelée-Morvan and Crovisier, 1985). After this publication, the origin of the cometary

*Corresponding author. Tel.: +33 0 1 45 17 15 37; fax: +33 0 1 45 17 15 64.
E-mail address: fray@lisa.univ-paris12.fr (N. Fray).

0032-0633/$ - see front matter © 2005 Elsevier Ltd. All rights reserved.
doi:10.1016/j.pss.2005.06.005

CN radicals became highly debated and several gaseous molecules have been proposed as a second parent: C_2N_2 (Bockelée-Morvan and Crovisier, 1985; Festou et al., 1998), HC_3N (Bockelée-Morvan and Crovisier, 1985; Krasnopolsky, 1991) or even C_4N_2 (Krasnopolsky, 1991). Another hypothesis is that CN could be directly emitted from grains. This was first proposed in order to explain CN jets in comet 1P/Halley (A'Hearn et al., 1986a). Furthermore, comparative studies between comets supported the dust as CN source (Newburn and Spinrad, 1989; A'Hearn et al., 1995), since the CN and dust production rates seem to be correlated. Other authors, like Klavetter and A'Hearn (1994), proposed that CN could be produced by another extended source: a source other than the nucleus or a gaseous parent.

In this paper, we present a review about available data of CN radical observations and current interpretations in order to extract a global view of the recurrent problem: the origin of the cometary CN radical.

We first present a compilation of the published CN Haser scale lengths from which we derive an average value of CN parent scale length at 1 AU at minimum solar activity. This average value is compared to the photolysis data of several possible gaseous parent molecules. Then we compare the HCN and CN production rates in several comets and discuss the implications of the production rate uncertainties. Finally, we study the case of the CN jets.

2. CN scale lengths

In order to constrain the formation process(es) of CN radicals in comets, one can study its distribution in the coma. In a first approximation, one can consider that this distribution is directly related to the kinetics of the formation process(es). Thus, it can be compared with the destruction process of HCN and other CN-bearing molecules.

According to the Haser (1957) model, such a distribution can be modeled with two scale lengths: a "parent scale length" (l_p) and a "daughter scale length" (l_d). The hypotheses of this model are that: (1) the production rate is in steady state; (2) CN radicals are produced by the photodissociation of a single parent molecule and (3) the motion from the nucleus is radial for both parent and daughter molecules. Then, the density per unit volume follows the law

$$n(r) = \frac{Q_p}{4\pi r^2 V_{gas}} \frac{l_d}{l_p - l_d} (e^{-r/l_p} - e^{-r/l_d}), \quad (1)$$

where $n(r)$ is the density of CN radicals at a distance r from the nucleus, Q_p the production rate of the parent molecule and V_{gas} the expansion velocity of the daughter molecules in the coma. In this model, the parent scale length is the characteristic length of CN production and the daughter scale length is the characteristic length of CN dissociation. In a first approximation, one can consider that the parent scale length is related to the photodissociation rate of the parent molecule β_p through $l_p = V_{gas}/\beta_p$; but as we will see in Section 4, a better estimation is achieved with the model of Combi and Delsemme (1980a), which takes into account the excess energy acquired by the fragment during the photodissociation process.

As the photodissociation rates vary as R_H^2 (where R_H is the heliocentric distance in astronomical unit) and the expansion velocity as approximately as $R_H^{-0.5}$ (Cochran and Schleicher, 1993; Biver et al., 1999a), if we consider a pure Haser model, then the scale lengths should vary approximately as $R_H^{1.5}$. If we use the model of Combi and Delsemme (1980a), we find that the parent scale length should vary approximately as $R_H^{1.4}$ (see Section 4).

We have compiled all the CN Haser parent and daughter scale lengths that we have found in the literature. This allows us to constrain a mean value at 1 AU as well as the variation of these scale lengths as a function of the heliocentric distance of the parent and daughter scale lengths. The comparison with the observed distribution and photodissociation rates of the possible gaseous parent molecules is then discussed using the model of Combi and Delsemme (1980a).

2.1. Compilation of the CN scale lengths

We have compiled 104 values of CN Haser parent scale lengths (Combi, 1978; Combi and Delsemme, 1980b; Delsemme and Combi, 1983; Fink et al., 1991; Meredith et al., 1992; Newburn and Spinrad, 1984; Rauer et al., 2003; Umbach et al., 1998; Woodney et al., 2002). For each value, we have quoted the heliocentric distance (R_H) and the date of the observation. Fig. 1a shows the CN parent scale lengths as a function of the heliocentric distance. As one can see in this figure, there is a great dispersion between these values, which are indeed bracketed by the functions $6 \times 10^3 R_H^2$ and $5.2 \times 10^4 R_H^2$ km.

We have also compiled 38 values of the CN daughter scale lengths (Combi, 1978; Combi and Delsemme, 1980b; Fink et al., 1991; Meredith et al., 1992; Umbach et al., 1998; Woodney et al., 2002). As one can see in Fig. 2a, the CN daughter scale lengths as a function of the heliocentric distance also exhibit a great dispersion: they lie between $4 \times 10^4 R_H^{1.4}$ and 8.5×10^5 km$R_H^{1.4}$.

2.2. Reduction of the scale lengths to the minimum of solar flux

One possible source of the dispersion in the values of CN scale lengths could be the change of solar activity between the different periods of observations. Meredith et al. (1992) have shown that the measured values at

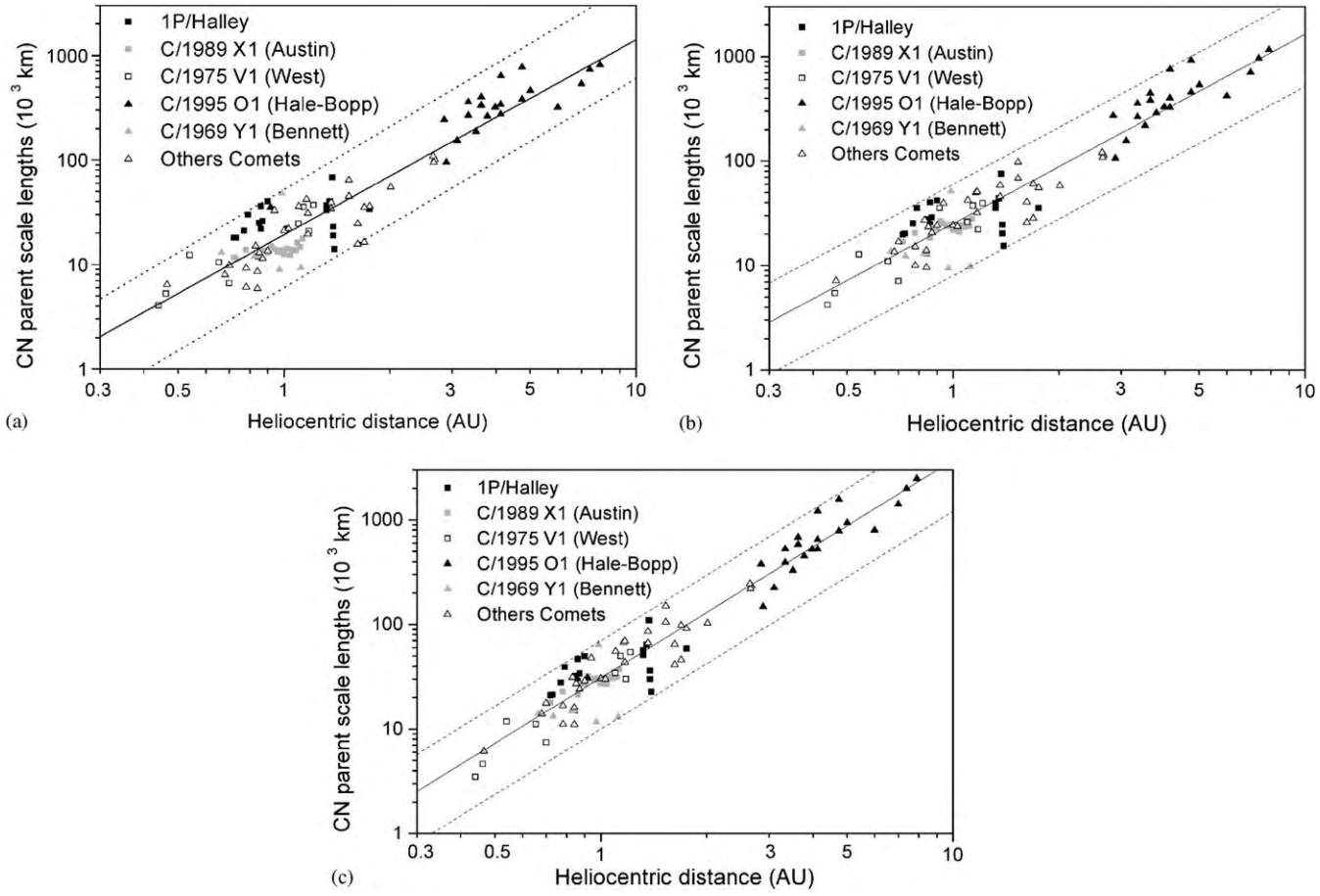

Fig. 1. (a) Original CN parent scale lengths as a function of the heliocentric distance R_H. The black line is the best fit ($1.93 \times 10^4 R_H^{1.86}$ km) and the dotted lines represent the functions $6 \times 10^3 R_H^2$ and $5.2 \times 10^4 R_H^2$ km. (b) CN parent scale lengths normalized to the minimum of solar flux as a function of the heliocentric distance R_H. The black line is the best fit ($2.5 \times 10^4 R_H^{1.8}$ km) and the dotted lines represent the functions $8 \times 10^3 R_H^{1.8}$ and $6 \times 10^4 R_H^{1.8}$ km. (c) CN parent scale lengths normalized to the minimum of solar flux and to an expansion velocity of 1 km s^{-1} (see text) as a function of the heliocentric distance R_H. The black line is the best fit ($3.1 \times 10^4 R_H^{2.1}$ km) and the dotted lines represent the functions $10^4 R_H^{2.1}$ and $7 \times 10^4 R_H^{2.1}$ km.

1 AU of parent scale lengths rise when the solar flux decreases.

So, in order to compare them with the photodissociation rates of parent molecules which are calculated for quiet Sun conditions, the CN parent scale lengths have been normalized to the minimum of solar activity.

We used the formula

$$l_{norm} = l_{orig}(F/F_{min}),$$

where l_{orig} is the original scale lengths, l_{norm} the "normalized" scale lengths, i.e., those which have been recalculated and F the flux at Lyman α at the date of the observation. We have used the Lyman α flux calculated by Woods et al. (2000), available on the site of the NOAA (ftp://ftp.ngdc.noaa.gov/STP/SOLAR_DATA/SOLAR_UV/SOLAR2000/Five_cycle_v1_23a.txt). As one can see in Fig. 1b, the dispersion of the parent scale lengths is not reduced by this operation, and at this stage, a similar result is found for the daughter scale lengths. However, the mean value of the normalized scale length are larger, because the solar flux F is larger than F_{min} (see Section 2.5).

2.3. Reduction of the scale lengths to an expansion velocity of 1 km s^{-1}

Another possible source of dispersion in the value of CN scale lengths could be the difference of the gas expansion velocity between more or less active comets (see Bockelée-Morvan et al., 1990; Combi, 2002). For example, the expansion velocity observed in the very active C/1995 O1 (Hale-Bopp) was greater than in any others comets observed up to now. So, we have reduced all the scale lengths to a gas expansion velocity of 1 km s^{-1}, considering that the expansion velocity in all comets was the one measured in 1P/Halley ($0.85 R_H^{-0.5}$ km s^{-1}; Cochran and Schleicher, 1993) except

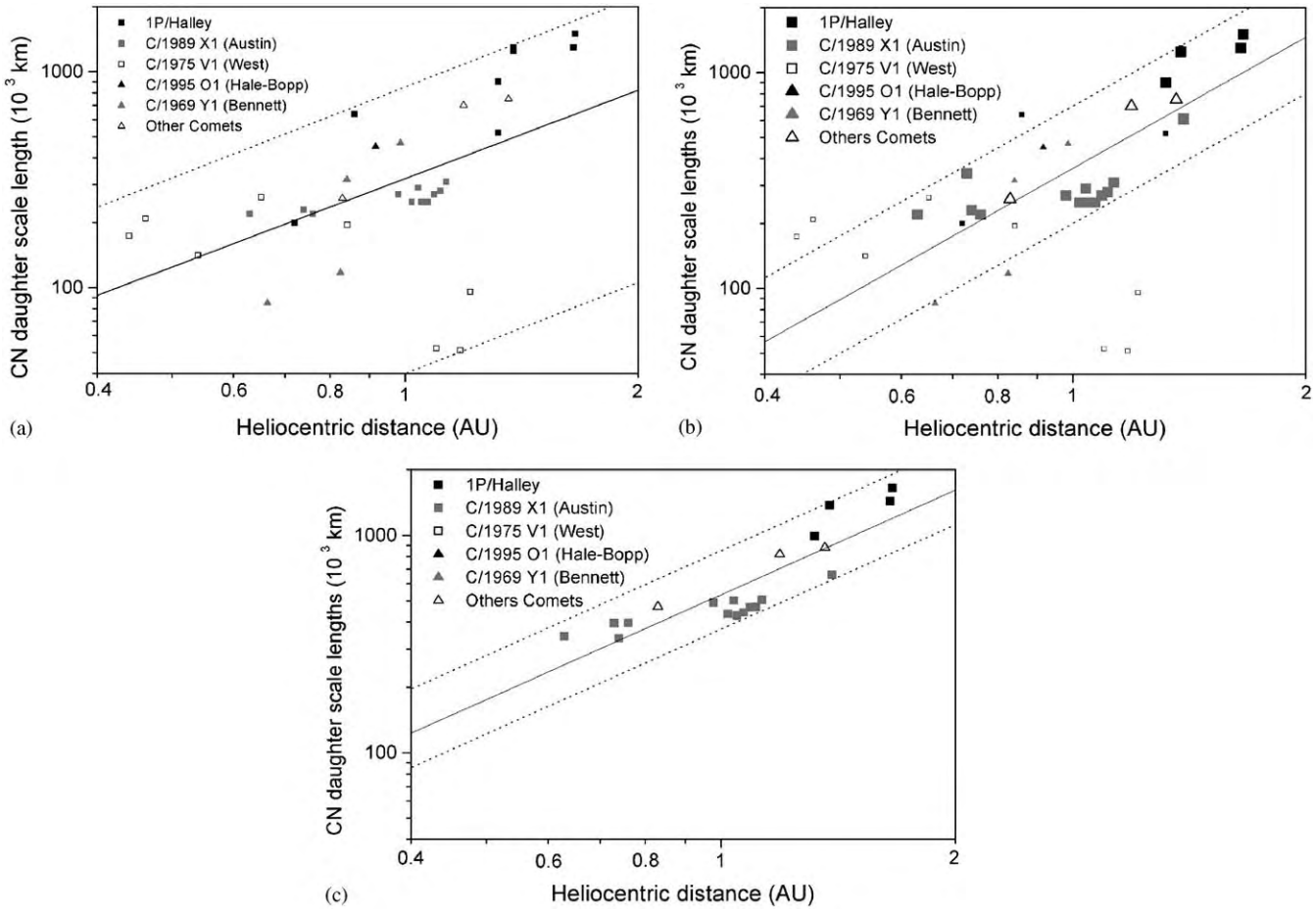

Fig. 2. (a) Original CN daughter scale lengths as a function of the heliocentric distance R_H. The black line is the best fit ($3.2\times10^5 R_H^{1.4}$ km) and the dotted lines represent the functions $4\times10^4 R_H^{1.4}$ and $8.5\times10^5 R_H^{1.4}$ km. (b) CN daughter scale lengths as a function of the heliocentric distance R_H. The bigger symbols represent the values that were obtained from a wide field of view, whereas the smaller symbols are daughter scale lengths obtained from profiles for which the extension of the measurements was smaller than the derived daughter scale lengths. This selection allows us to reduce the dispersion observed on the measured CN Haser daughter scale lengths. The black line is the best fit on the selected values ($3.6\times10^5 R_H^2$ km) and the dotted lines represent the functions $2\times10^5 R_H^2$ and $7\times10^5 R_H^2$ km. (c) Similar to (b), but the CN daughter scale lengths have been normalized to the minimum of solar flux. The black line is the best fit ($5.33\times10^5 R_H^{1.6}$ km) and the dotted lines represent the functions $3.7\times10^5 R_H^{1.6}$ and $8.5\times10^5 R_H^{1.6}$ km.

in C/1995 O1 (Hale-Bopp), where it was $1.12 R_H^{-0.42}$ km s^{-1} (Biver et al., 2002).

We have presented the parent scale lengths normalized to the minimum of solar flux and an expansion velocity of 1 km s^{-1} in Fig. 1c. The dispersion of the values is still not reduced by the operation.

2.4. Possible origin of the dispersion of the values of the CN Haser scale lengths

We have shown that the changes in the solar flux or in the expansion velocity between more or less productive comets are not responsible for the dispersion observed on the measured parent CN scale lengths. Thus, another explanation of such dispersion of the CN Haser scale lengths could be that an artifact is introduced by the Haser model. Indeed, most spatial measurements only yield to a family of solutions consisting of numerous parent and daughter scale length pairs that yield equally good fits with the Haser model.

In order to illustrate this fact, we studied two CN spatial profiles. The first one was published by Womack et al. (1994) and was acquired on comet 1P/Halley on December 14, 1985 at 1.28 AU from the Sun. The measurements extend from 8×10^3 to 5×10^5 km from the nucleus (Fig. 3a). The second one was published by Fink et al. (1991) and was measured on comet 1P/Halley on January 11, 1986 at 0.86 AU. It extends from 4×10^3 to 9×10^4 km from the nucleus (Fig. 4a). For both profiles, we have searched the best fit with a Haser model by χ^2 minimizing. Figs. 3b and 4b represent the χ^2 which is achieved for each pairs of parent and daughter scale lengths for both profiles.

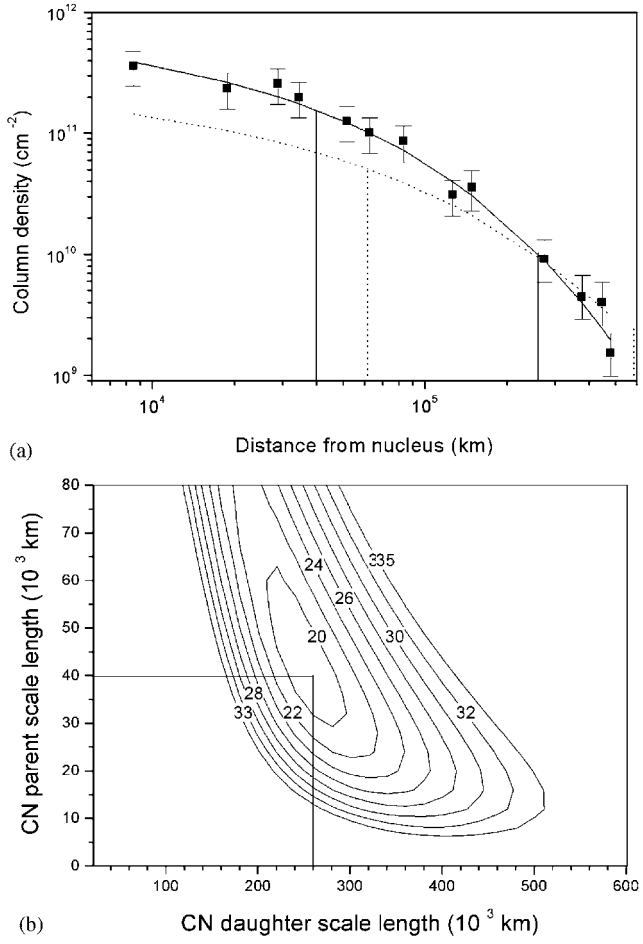

Fig. 3. (a) CN column density profile as a function of the projected distance from the nucleus observed by Womack et al. (1994) in comet Halley on December 14, 1985 at 1.28 UA from the Sun. The black line is the best fit with a Haser profile (the parent scale length is 40,000 km, the daughter scale length is 261,000 km; both these scale lengths have been represented as straight vertical lines). The χ^2 of this fit is 18.8 (see (b)). The dotted line is the best fit if we consider that HCN is the unique parent molecule of CN (the effective parent scale length is 6.22×10^4 km (see Fig. 11), the daughter scale length is 7.87×10^5 km (see (c) and Table 2); both these scale lengths have been represented as dotted vertical lines). The χ^2 of this second fit is 52.8. (b) The curves that are displayed correspond to the same value of the χ^2 which is achieved when we fit the profile presented in (a) with a Haser model as a function of the parent and daughter scale lengths. Best scale lengths to fit the profile presented in (a) with a Haser model are $l_p = 4 \times 10^4$ km and $l_d = 2.6 \times 10^5$ km (both these scale lengths are displayed as straight lines).

On the first set of measurements ($R_H = 1.28$ AU), the best fit is obtained for $l_p = 4 \times 10^4$ km and $l_d = 2.6 \times 10^5$ km, whereas for the second one ($R_H = 0.86$ AU), the best fit is achieved for $l_p = 3.8 \times 10^4$ km and $l_d = 2.1 \times 10^5$ km. Figs. 3a and 4a display both fits, respectively.

On the one hand, only couples of a small family (l_p, l_d) are solutions (Fig. 3b). Hence, the Haser scale lengths that are determined from this first profile, for which the extension of measurements (5×10^5 km) is greater than the derived daughter scale length (2.6×10^5 km), seem to be reliable. On the other hand, the second set of measurements can be fitted with a large number of parent and daughter scale lengths (Fig. 4b). Moreover, it allows us to point out the fact that the determination of the daughter Haser scale length with this second profile is not achievable with a good accuracy. Indeed, the extension of this second profile (up to 9×10^4 km from the nucleus) is smaller than the daughter scale length (about 3.2×10^5 km); hence, it could not be used to determine the daughter scale lengths.

These results show that only spatial profiles obtained with a telescope with a field of view extending further than the daughter scale length l_d allow one to determine parent and daughter scale lengths at the same time. That is the reason why, generally, when the extension of a spatial profile is shorter than the daughter scale length, a value of the daughter scale length is assumed in order to compute a parent scale length. So, if a wrong daughter value is assumed, then the resulting parent value is also likely incorrect.

2.5. *Fit of the CN daughter scale lengths as a function of the heliocentric distance*

Selecting only profiles taken with a wide enough field of view, we have kept 20 scale length values and rejected 18. This selection is presented in Fig. 2b (original scale lengths) and in Fig. 2c (scale lengths normalized to the minimum of solar flux).

This selection allows us to reduce the dispersion observed for the measurements on daughter scale lengths. The remaining dispersion could be due to short-term variation of the CN production rates. Indeed, some profiles that have an extension greater than 10^5 km from the nucleus exhibit some wavy structures characteristic of a time-dependent production rate related to the rotation of the nucleus (Combi and Fink, 1993; Combi et al., 1994). As the Haser model considers that the production rate is in steady state, these wavy structures could prevent a good determination of the scale lengths even if the extension of the profile is large.

Then, we have fitted the logarithm of the daughter scale length as a function of the logarithm of the heliocentric distance by a straight line. Three fits are presented in Fig. 2a, b and 2c, respectively, and the results are summarized in Table 2. For the original scale lengths, the best fit on the selected values is obtained for $l_d = 3.6 \times 10^5 R_H^2$ km (Fig. 2b). This mean value scaled at 1 AU and the heliocentric dependence are in accordance with the values previously published, which range from 2.1 to 4.2×10^5 km with an exponent of 2. On the other hand, the best fit obtained for the selected scale length normalized to the minimum of solar flux is

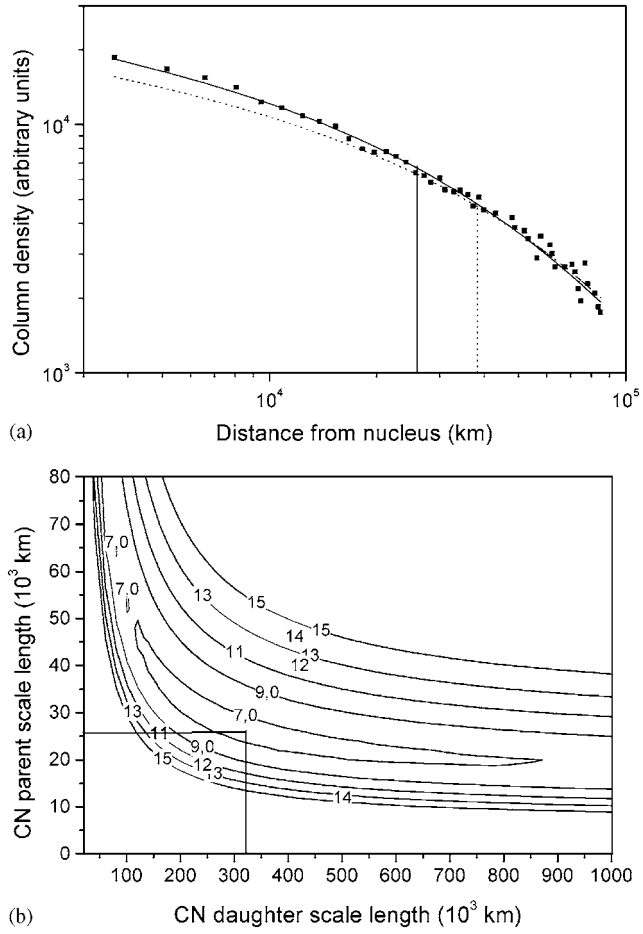

Fig. 4. (a) CN column density profile as a function of the projected distance from the nucleus observed by Fink et al. (1991) in comet Halley on January 11, 1986 at 0.86 UA from the Sun. The black line is the best fit with a Haser profile (the parent scale length is 2.6×10^4 km and displayed as a vertical straight line, the daughter scale length is 3.21×10^5 km and the χ^2 of this fit is 6.7). The dotted line is the best fit if we consider that HCN is the unique parent molecule of CN (the parent scale length is 3.8×10^4 km (see Fig. 11) and is displayed as a vertical dotted line, the daughter scale length is 2.65×10^5 km (see Fig. 2b and Table 2) and the χ^2 of this fit is 7.5). (b) The curves that are displayed correspond to the same value of the χ^2 which is achieved when we fit the profile presented in (a) with a Haser model as a function of the parent and daughter scale lengths. Best scale lengths to fit the profile presented in Fig. 3a with a Haser model are $l_p = 2.6 \times 10^4$ km and $l_d = 3.2 \times 10^5$ km (both these scale lengths are displayed as straight lines).

obtained with $l_d = 5.3 \times 10^5 R_H^{1.6}$ km. The mean value at 1 AU is almost double when the daughter scale lengths are normalized to the minimum of solar flux. Even if the daughter scale lengths are sensitive to the solar flux, changes of the latter cannot by itself explain their dispersion. Moreover, in the case of the corrected daughter scale lengths, we find a heliocentric dependence of 1.6 ± 0.2, which is in agreement with that expected from the Haser model.

2.6. Fit of the CN parent scale lengths as a function of heliocentric distance

Before we fit the parent scale length as a function of the heliocentric distance, we have tried to select some values in order to reduce the dispersion. We have searched correlations between the value of parent scale length and the value of daughter scale length which was assumed when fitting the spatial distribution, or with the activity of the comet (i.e., the gas expansion velocity). We found that no correlation and no selection could be achieved as we did for the daughter scale lengths. Thus, we have kept the complete set of 104 values of parent scale lengths.

We have fitted the parent scale length l_p as a function of the heliocentric distance R_H in a log–log plot; the same was done for the l_p values normalized to the minimum of solar flux and to 1 km s^{-1} expansion velocity. These three fits are presented in Fig. 1a–c, respectively, and results are summarized in Table 3, which also gives the correlation coefficient for each fit.

The correlation coefficients of the three fits are similar. Consequently, the corrections by the solar flux and the gas expansion velocity do not improve the fit as already noted. Our derived mean value scaled at 1 AU, and the heliocentric dependence (on original scale lengths) is in agreement with the values previously published (see Table 1). The results on the scale lengths normalized to the minimum of solar flux are similar except the mean values scaled at 1 AU, which are slightly higher. Depending on the case, we find a heliocentric dependence ranging from 1.8 to 2.1. This large value cannot be explained either by the Haser model or the model of Combi and Delsemme (1980a) (Tables 2 and 3).

3. Comparison of the production rates of CN and HCN

The quantum yield of CN production from HCN photodissociation is equal to 0.97 (Huebner et al., 1992). Because this yield is close to 1, if HCN is the only parent molecule of the CN radical, then the values of CN and HCN production rates should be close. Thus, we have compiled and compared published data in order to test the hypothesis of a single parent molecule for CN.

3.1. Compilation of the CN and HCN production rates

For CN radicals, we have chosen to compile only values that were obtained by narrow-band photometry with IHW filters, since the measurements performed by spectrophotometry with a narrow slit only view a small fraction of the coma. Therefore, among all CN production rates available in the literature, we have mainly considered the data of the team of D.G.

Table 1
Previous mean values of CN scale lengths published in the literature

Parent scale length of the CN radical in 10^3 km at 1 AU	Heliocentric dependence	Daughter scale length of the CN radical in 10^3 km at 1 AU	Heliocentric dependence	Reference
21.9 ± 0.7	1.8 ± 0.2	320		Combi and Delsemme (1980b)
12	2	300	2	Newburn and Spinrad (1984)
17	2	300	2	Cochran (1985)
16	1.5			Combi and Delsemme (1986)
18	2	420	2	Newburn and Spinrad (1989)
28 ± 14[a]	2	320^{+200}_{-100}	2	Fink et al. (1991)
23 ± 17[b]				
13	2	210	2	Randall et al. (1992), via A'Hearn et al. (1995)
54 ± 14[c]	1.3 ± 0.2			Rauer et al. (2003)
16 ± 2	1.5	300 ± 25	2	Lara et al. (2003)

[a]Average for the preperihelion period of comet Halley.
[b]Average for the postperihelion period of comet Halley.
[c]This value has been obtained from measurements on comet Hale-Bopp between 2.5 and 8 AU.

Table 2
Fits of the daughter scale lengths as a function of the heliocentric distance

	Mean value at 1 AU in 10^3 km	Heliocentric dependence	
Original scale lengths	320 ± 42	1.36 ± 0.37	$R = 0.53$
Selected original scale lengths	360 ± 34	2.02 ± 0.33	$R = 0.82$
Selected scale lengths normalized to the minimum of solar	533 ± 32	1.58 ± 0.21	$R = 0.87$

Note: The error bars are given at 1σ. R is the correlation coefficient of the fit.

Table 3
Results of the fits on the CN parent scale lengths

	Mean value at 1 AU in 10^3 km	Heliocentric dependence	
Original scale lengths	19.3 ± 1	1.86 ± 0.07	$R = 0.94$
Scale lengths normalized to the minimum of solar flux	25.3 ± 1.1	1.81 ± 0.06	$R = 0.95$
Scale lengths normalized to the minimum of solar flux and of an expansion velocity of 1 km s^{-1}	30.9 ± 1.3	2.08 ± 0.06	$R = 0.96$

Note: The error bars are given at 1σ. R is the correlation coefficient of the fit.

Schleicher and M.F. A'Hearn (see A'Hearn et al., 1995), who have published a consistent set of values for numerous comets. Indeed, it can be pointed out that production rates that have been obtained by different authors for the same comet at the same time could be different. Fink and Combi (2004) have shown that this difference is partly due to the use of different parameters to convert flux into production rates (parent and daughter scale lengths and fluorescence factors). Thus, we have gathered the observed fluxes and all the required parameters in order to perform our own consistent determination of CN production rates (heliocentric and geocentric distance, field of view and heliocentric velocity). This calculation has been made using formula (2) derived from the Haser model (O'Dell and Osterbrock, 1962; Boehnhardt et al., 1989):

$$N = \frac{Q_p}{V_{gas}} \rho \left(\frac{l_d}{l_d - l_p} \right) \left[\int_x^{\mu x} K_0(x)\,dx + \frac{1}{x}\left(1 - \frac{1}{\mu}\right) + K_1(\mu x) - K_1(x) \right], \quad (2)$$

where N is the total number of radicals within a circular aperture of radius ρ, Q_p the production rate in molecules s^{-1}, V_{gas} the expansion velocity of the gas in the coma, l_p and l_d the Haser parent and daughter scale lengths, $\mu = l_p/l_d$, $x = \rho/l_p$ and K_0 and K_1 are modified Bessel functions of the second kind of order 0 and 1. In

this calculation, we have used the values of CN scale lengths determined in Section 1 and the g-factors (fluorescence factors) from Tatum (1984) to convert measured fluxes into a number of radicals. This procedure allows us to reduce the dispersion between the CN production rate values as shown by Fink and Combi (2004) on comet 46P/Wirtanen.

Since the HCN production rates depend on the model, and especially on the assumed excitation scheme, we have chosen a consistent set of data derived from observations of numerous comets in the radio wavelengths by the Meudon team (composed of J. Crovisier, D. Bockelée-Morvan, N. Biver and coworkers). Whenever possible, we have used the re-evaluations performed by Biver (1997) with an excitation model which takes into account fluorescence as well as collisions with neutral molecules and electrons in the inner coma.

3.2. Comparison of the CN and HCN production rates for different comets

Below we present the details of our compilation for each studied comet.

3.2.1. C/1983 H1 (IRAS-Aracki-Alcock)

Bockelée-Morvan et al. (1984) have unsuccessfully searched the $J = 1-0$ HCN radio lines in this comet. They have determined a very low upper limit of 2.4×10^{25} molecules s^{-1} for the HCN production rate at 1 AU (on May 13, 1983). On the other hand, A'Hearn et al. (1983) measured a CN production rate of 5×10^{25} molecules s^{-1} on May 7, 1983. Thus, in this comet, the CN production rate is found to be at least two times greater than the HCN one. Therefore, Bockelée-Morvan et al. (1984) concluded that HCN should not be the only parent of the CN radical.

3.2.2. 21P/Giacobini-Zinner (1985 perihelion)

Bockelée-Morvan et al. (1987) have published an upper limit of 2.1×10^{25} molecules s^{-1} for the HCN production rate at $R_H = 1.03$ AU, whereas Schleicher et al. (1987) have published a CN production rate of 4×10^{25} molecules s^{-1} at the same heliocentric distance. Thus, as for IRAS-Aracki-Alcock, it seems that HCN is not the single parent of the CN radical.

3.2.3. C/1986 P1 (Wilson)

Crovisier et al. (1990) have unsuccessfully searched for HCN in this comet. When the comet was at 1.26 AU from the Sun, they have derived an upper limit for its production rate of 3×10^{25} molecules s^{-1}. At the same time, Schulz et al. (1993) have obtained narrow-band CCD images. Using a vectorial model, they have derived a production rate of about 2.3×10^{26} molecules s^{-1} at a heliocentric distance of 1.21 AU. Thus, CN production rates are 10 times larger than HCN ones. So, clearly for this comet, an additional process of CN production is required.

3.2.4. 1P/Halley

In comet Halley, HCN has always been observed through its $J = 1-0$ line and we found 22 values of HCN production rates in Bockelée-Morvan et al. (1987) and Schloerb et al. (1986) for heliocentric distances between 0.59 and 1.78 AU. At the same time, we have gathered 148 values of CN production rates for heliocentric distances between 0.67 and 2.41 AU (Schleicher et al., 1998; Catalano et al., 1986; Churyumov and Rosenbush, 1991).

Comet Halley appeared during the minimum of solar activity. In our recalculation of CN production rates (see Fig. 5), we have used our normalized CN scale lengths (i.e., $l_p = 2.5 \times 10^4 R_H^{1.8}$ km and $l_d = 5.3 \times 10^5 R_H^{1.6}$ km) and an expansion velocity of $0.85 R_H^{-0.5}$ km s^{-1} (Cochran and Schleicher, 1993).

However, even if our recalculation has reduced the dispersion, we find that the values of CN production rates, presented in Fig. 5, are still scattered. This dispersion might be due to short-term variations due to the rotation of the nucleus (Schleicher et al., 1990). This prevents us from deriving a clear conclusion from these data. But the lowest CN productions rates are approximately equal to the HCN ones, whereas the highest values are twice the HCN ones. So even if no definitive conclusion can be put forward, this suggests that the CN radical could have another source than the HCN photodissociation.

3.2.5. C/1989 X1 (Austin)

For comet Austin, six values of HCN production rates (Biver, 1997) are available for heliocentric

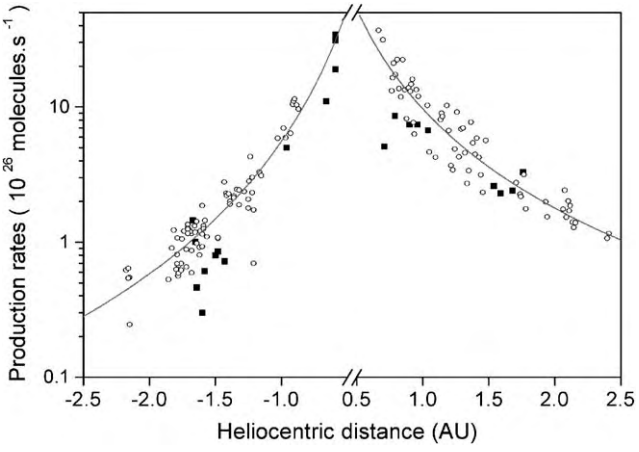

Fig. 5. CN and HCN production rates for comet 1P/Halley as a function of the heliocentric distance R_H. HCN production rates are represented as black squares and CN as open circles. The gray lines are fits by a power law of the CN production rates. To recalculate the CN production rates, we have used $l_p = 2.53 \times 10^4 R_H^{1.81}$ km, $l_d = 5.33 \times 10^5 R_H^{1.58}$ km and $V_{gas} = 0.85 R_H^{-0.5}$ km s^{-1}.

distances between 1.07 and 1.13 AU. These values are re-evaluations of those of Crovisier et al. (1993). For CN production rates, we have compiled 12 values (Waniak et al., 1994) ranging from 0.7 to 1.3 AU. All the observations were made during the postperihelion phase.

Comet Austin appeared during the maximum of solar activity; thus, for the re-evaluations of the CN production rates, we have used the scale lengths $l_p = 1.9 \times 10^4 R_H^{1.9}$ km and $l_d = 3.6 \times 10^5 R_H^2$ km (see Section 1). For the gas expansion velocity inside the coma, we have taken a value identical to the one measured on comet Halley: $0.85 R_H^{-0.5}$ km s^{-1}. HCN and CN production rates are presented as a function of the heliocentric distance in Fig. 6.

Again, HCN production rates near 1.1 AU are two times lower than the CN ones. So HCN cannot be the single parent molecules of the CN radical in comet Austin.

3.2.6. C/1990 K1 (Levy)

For comet Levy, we have found five values of HCN production rates (Biver, 1997) for heliocentric distances between 1.33 and 1.35 AU during the preperihelion phase. As for comet Austin, these values are re-evaluations of Crovisier et al. (1993). For the preperihelion phase, we found 48 values of CN production rates (Schleicher et al., 1991; Magdziarz et al., 1995). Comet Levy appeared during the maximum of the solar activity, so for the re-evaluation of CN production rates, we have used exactly the same parameters as for comet Austin. HCN and CN productions are presented as a function of the heliocentric distance in Fig. 7.

For comet Levy, HCN and CN productions are equal at a heliocentric distance of roughly 1.3 UA, suggesting that there is no additional source of CN radical.

3.2.7. C/1996 B2 (Hyakutake)

For comet Hyakutake, we have compiled 20 values of HCN production rates (Biver et al., 1999b) for heliocentric distances between 0.25 and 1.8 AU during the preperihelion phase. We can note that HCN has also been observed in the infrared near 3.3 μm (Magee-Sauer et al., 2002). The only derived production rate is about two times higher than that derived from millimeter observations at the same heliocentric distance. By Schleicher and Osip (2002) 108 values of CN production rates have been published. For the re-evaluations of the CN production rates, we have used the same values of scale lengths as for the comet Halley since comet Hyakutake appeared during the minimum of solar activity. For the expansion velocity, we have taken a value of $0.88 R_H^{-0.62}$ km s^{-1} measured in this comet (Biver et al., 1999b).

HCN and CN production rates as a function of the heliocentric distance are displayed in Fig. 8, except for the HCN production rate derived from infrared observation. Several outbursts occurred during the preperihelion phase of comet Hyakutake: a first one in March 20 (Schleicher and Osip, 2002) when the comet was at 1.16 AU from the Sun and a second one between April 13.9 and 15.7 at 0.56 AU (Biver et al., 1999b). After this second outburst, the production rates of all parent molecules (CO, H_2CO, CH_3OH, CS) have decreased. This fact is also true for HCN as seen in Fig. 8. The trend of the production rates in the

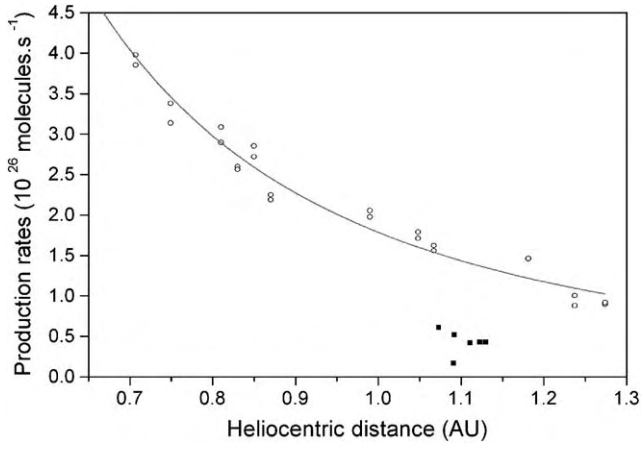

Fig. 6. CN and HCN production rates for comet C/1989 X1 (Austin) as a function of the heliocentric distance R_H. HCN production rates are represented as black squares and CN as open circles. The gray line is a fit by a power law of the CN production rates. To recalculate the CN production rates, we have used $l_p = 1.93 \times 10^4 R_H^{1.86}$ km, $l_d = 3.6 \times 10^5 R_H^{2.02}$ km and $V_{gas} = 0.85 R_H^{-0.5}$ km s^{-1}.

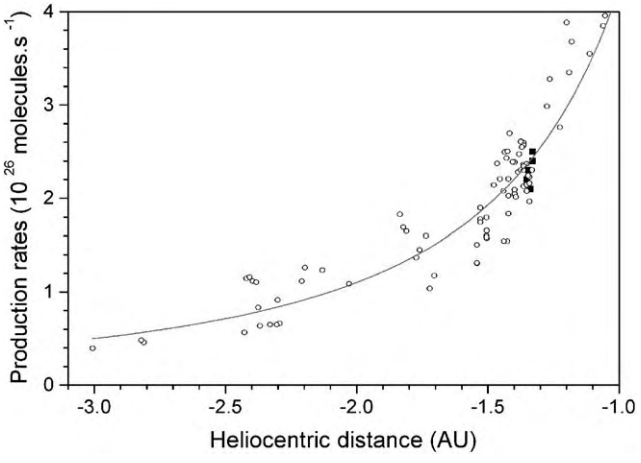

Fig. 7. CN and HCN production rates for comet C/1990 K1 (Levy) as a function of the heliocentric distance R_H. HCN production rates are represented as black squares and CN as open circles. The gray line is a fit by a power law of the CN production rates. To recalculate the CN production rates, we have used $l_p = 1.93 \times 10^4 R_H^{1.86}$ km, $l_d = 3.6 \times 10^5 R_H^{2.02}$ km and $V_{gas} = 0.85 R_H^{-0.5}$ km s^{-1}.

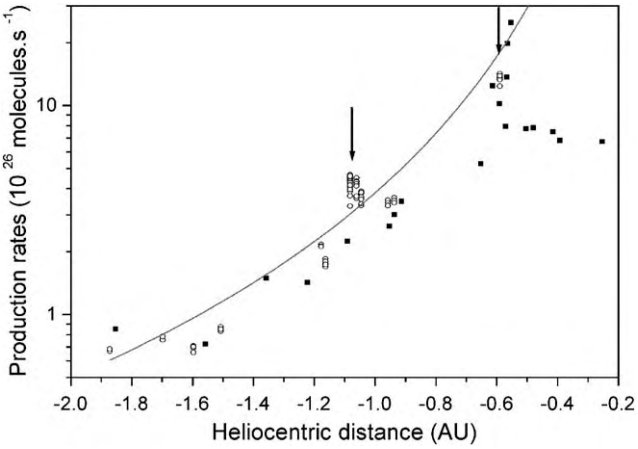

Fig. 8. CN and HCN production rates for comet C/1996 B2 (Hyakutake) as a function of the heliocentric distance R_H. HCN production rates are represented as black squares and CN as open circles. The gray line is a fit by a power law of the CN production rates. The arrows represent the location of both outbursts. To recalculate the CN production rates, we have used $l_p = 2.53 \times 10^4 R_H^{1.81}$ km, $l_d = 5.33 \times 10^5 R_H^{1.58}$ km and $V_{gas} = 0.88 R_H^{-0.63}$ km s^{-1}.

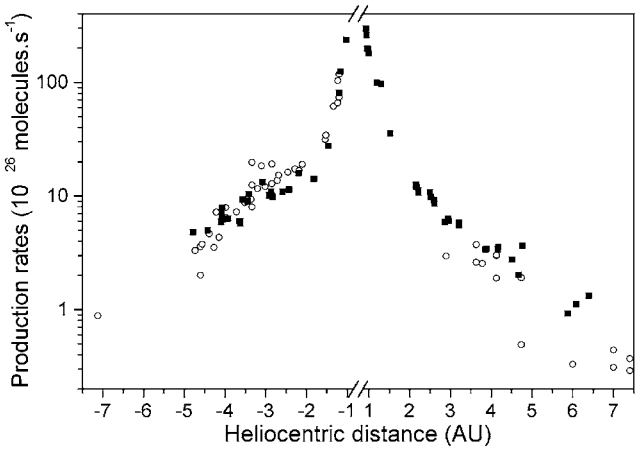

Fig. 9. CN and HCN production rates for comet C/1995 O1 (Hale-Bopp) as a function of the heliocentric distance R_H. HCN production rates are represented as black squares and CN as open circles.

preperihelion phase of comet Hyakutake is complex. Thus, it prevents us from giving a clear conclusion. However, one can note that for all the heliocentric distances, the HCN and CN production rates are approximately equal.

3.2.8. C/1995 O1 (Hale-Bopp)

For comet Hale-Bopp, we have gathered 49 values of HCN production rates (Biver, 1997; Biver et al., 1999a, 2002) for heliocentric distances between 0.92 and 6.39 AU. As for comet C/1996 B2 Hyakutake, HCN has also been observed in the infrared; the derived production rates are about two times higher than those derived from millimeter observations (Magee-Sauer et al., 1999). For the CN production rates, we have compiled 52 values (Rauer et al., 2003; Schleicher et al., 1997). Since flux values have not been published, we were not able to re-evaluate the CN production rates as we did for the previous comets. However, we have modified the values of Schleicher et al. (1997) using the velocity dependence of Biver et al. (1999a). We have chosen the values of Rauer et al. (2003) despite the fact that they have been obtained from spectrophotometry (no observations by narrow-band photometry have been published for heliocentric distances greater than 3 AU). Moreover, Rauer et al. (2003) have already made this comparison between HCN and CN production rates (see their Fig. 9) for comet Hale-Bopp. Our compilation is presented in Fig. 9. We have not represented the values of HCN production rates derived from infrared observations, as they extend to a very small range of heliocentric distances. Like Rauer et al. (2003), we conclude that the production rates of the two species are approximately equal for the whole range of heliocentric distances.

3.3. Discussion

The production rates are model dependent. The CN radical production rates depend on the g-factors and on the daughter and parent scale lengths, so we have studied the sensibility of each of these parameters on the resulting CN production rates. This study has been undertaken on the CN production rates that we have compiled on comet 1P/Halley since the details of the observations are available on a large range of heliocentric distances. The results are as follows:

1. If we use the g-factors of Schleicher et al. (1998) rather than those of Tatum (1984), the CN production rates increase up to 27%. Indeed, the g-factors of Schleicher et al. (1998) are slightly lower than those of Tatum (1984); then from the same value of flux, they lead to a greater number of radicals present in the field of view and then to a greater production rate.
2. If the daughter scale length is increased from $2.1 \times 10^5 R_H^{1.4}$ to $4.2 \times 10^5 R_H^{1.4}$ km (extreme values which have been published so far, see Table 1), the CN production rate decreases by 25%.
3. If the parent scale length is increased from $1.2 \times 10^4 R_H^{1.8}$ to $2.8 \times 10^4 R_H^{1.8}$ km (extreme values for heliocentric distances lower than 3 AU which have been published so far, see Table 1), the CN production rate increases by 93%.

This clearly shows that the most sensitive parameter for the calculation of the CN production rate with a Haser model is the parent scale length. Moreover, if one

considers all these parameters in the range of the previously published values, the resulting CN production rates vary as much as a factor of 2 as already noted by Fink and Combi (2004). These variations of CN production rates as a function of the values of parent and daughter scale lengths are illustrated in Fig. 10a and b. These figures present the minimal and maximal values which could be derived for comets Halley and Austin.

Comet Austin is an example for which the CN production rates are clearly higher than the HCN ones, whatever the values of scale lengths used (Fig. 10b). Then, for this comet, it is clear that at least half of CN radicals come from another source than the HCN photolysis. Comets IRAS-Aracki-Alcock, Giacobini-Zinner and Wilson also show higher CN production rates than the HCN ones, considering that only upper limits of HCN production rates have been published. In comet Halley, it seems that the CN ones are slightly higher than the HCN ones, when the comet is closer than 1.5 AU to the Sun. But comets Hale-Bopp, Levy and Hyakutake exhibit similar CN and HCN production rates.

In conclusion, whereas CN radicals could be almost entirely produced by HCN photolysis in some comets, an additional process of CN production is required in other ones.

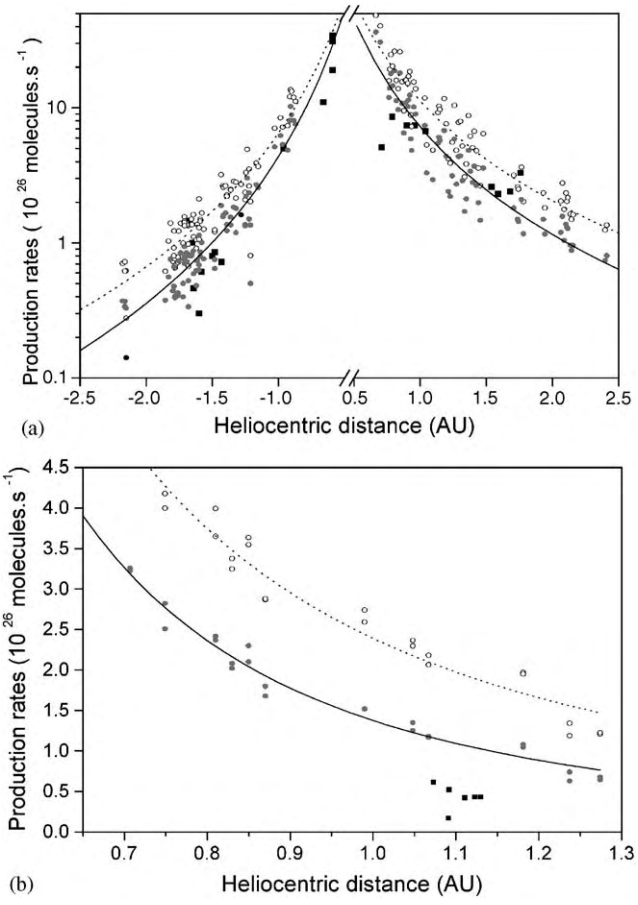

Fig. 10. (a) Sensitivity of the CN production rates of comet 1P/Halley to the values of the parent and daughter scale lengths. The open circles are the maximal CN production rates calculated with $l_p = 2.8 \times 10^4$ km and $l_d = 2.1 \times 10^5$ km, and the solid circles are the minimal values of CN production rates (calculated with $l_p = 1.2 \times 10^4$ km and $l_d = 5.3 \times 10^5$ km). The HCN production rates have also been displayed as black squares for comparison. (b) Similar to (a), but for comet C/1989 X1 (Austin).

4. Comparison of photochemical data of some CN-bearing molecules with the CN parent scale length

Since the origin of CN is difficult to constrain by the comparison between HCN and CN production rates alone, we have compared the CN parent scale length with the photodissociation rate of the possible gaseous parent molecules. After HCN, which is the major parent molecule, we have considered some others CN-bearing molecules, CH_3CN, HC_3N and HNC, that have already been detected in cometary atmospheres (Bockelée-Morvan et al., 1999) and also C_2N_2 and C_4N_2 that have been proposed as CN parent molecules (Festou et al., 1998; Krasnopolsky, 1991). Among the detected CN-bearing molecules (Bockelée-Morvan et al., 1999):

- HC_3N and CH_3CN have production rates about 1/10 that of HCN.
- HNC is observed with an HNC/HCN varying from 0.03 to 0.2, depending on the comet and on the heliocentric distance.

Thus, HCN is by far the most important progenitor for CN.

4.1. Model of Combi and Delsemme (1980a)

The photodissociation rate cannot be directly compared to the CN parent scale length determined by a Haser model. Since during the photodissociation process, the radical can receive an excess of energy and be released from the parent molecule in any direction, the Haser radial scale lengths have no immediate physical meaning and cannot be directly compared to the ratio of the expansion velocity to the photodissociation rate. Therefore, we have used the model of Combi and Delsemme (1980a) in order to compare the photodissociation rate to the CN parent scale length.

Using an average random walk model, Combi and Delsemme (1980a) have shown that, when the daughter scale length is much larger than the parent molecule one, which is the case for CN, the actual parent scale length

(defined as $l_p = V_{gas}/\beta_p$) and the observed Haser scale length l_{pH} are related by the simple formulae

$$l_{pH} = l_p \sin\delta \quad \text{with} \quad \tan\delta = V_{gas}/V_e, \tag{3}$$

where V_{gas} is the expansion velocity of the parent molecule, V_e the ejection velocity of the radical and β_p the photodissociation rate of the parent molecule. Finally, we have

$$l_{pH} = \frac{1}{\beta_p}\frac{V_{gas}^2}{[V_{gas}^2 + V_e^2]^{1/2}}. \tag{4}$$

This formula is valid if the quantum yield of CN production is equal to one. If it is not the case, we have to multiply the photodissociation rate of the parent molecule by the quantum yield of CN production. We call the scale lengths calculated with formula (4) "effective Haser scale length".

4.2. Photochemical data of the possible gaseous parent of the CN radical

In this section, we present the photodissociation properties of the possible gaseous parent molecules of the CN radical (HCN, CH_3CN, HC_3N, HNC, C_2N_2 and C_4N_2).

4.2.1. Hydrogen cyanide (or HCN)

HCN is mainly photodissociated by vacuum ultraviolet radiations into CN radical with a quantum yield equal to 0.97 (Huebner et al., 1992). In the solar radiation field, the published values of photodissociation rates at 1 AU and quiet Sun conditions range from 1.1×10^{-5} to $1.51\times10^{-5}\,s^{-1}$ (see Table 4), with a major contribution from Lyman α (122 nm). In this paper, we use a mean value of $1.3\times10^{-5}\,s^{-1}$. Jackson (1991) claimed that at this energy, CN radicals are produced in the $B^2\Sigma^+$, $A^2\Pi_I$ and $X^2\Sigma^+$ states. The excess velocity for these three different states has been calculated by Bockelée-Morvan and Crovisier (1985) (see Table 4). But more recent studies at 122 nm have shown that the CN radical is mainly produced in the $A^2\Pi_I$ state (Morley et al., 1992; Cook et al., 2000). At 157 nm, the available energy for disposal in the H and CN fragments is 1.32 ± 0.02 eV and the rotationnal and vibrationnal energies represent 25% of the excess energy (Guo et al., 2000). Hence, we can estimate that at Lyman α the excess energy, which could be converted into kinetic energy, is 2.72 eV. Using the conservation of energy and momentum, we can evaluate that CN radicals will have an excess velocity $V_{eHCN} = 0.864\pm0.006\,km\,s^{-1}$. This new value of the ejection velocity of the CN radical gives strong constraints on the comparison between the CN parent scale length and the photodissociation rate of HCN (see Section 4.3).

4.2.2. Methyl cyanide (or CH_3CN)

Bockelée-Morvan and Crovisier (1985) have calculated the photodestruction rate of CH_3CN in cometary conditions to be of $6.68\times10^{-6}\,s^{-1}$. But Halpern (1987) and Kanda et al. (1999) have shown that the CN production is a minor channel in the photodissociation of CH_3CN in the VUV region. The dominant pathway being the H elimination, the quantum yields of CN production could be lower than 0.02 (Kanda et al., 1999). Thus, the production rate of CN from CH_3CN photodissociation could be 100 times lower than that of HCN, with a value of about $10^{-7}\,s^{-1}$.

4.2.3. Cyanoacetylene (or HC_3N)

Considering that the CN production quantum yield is equal to 1, numerous values of HC_3N photodestruction rates have been published ranging from 2.8×10^{-5} to $7.7\times10^{-5}\,s^{-1}$ (see Table 4). The higher values take into account the electronic transition $^1\Delta - {}^1\Sigma_g$ (Bruston et al., 1989) around 190–230 nm (Crovisier, 1994). Then, at a first glance, those values seem to be more reliable for the total photodestruction rate of this molecule. But, the threshold for the CN production has been determined to be 185–200 nm (Clarke and Ferris, 1995). Thus, the lowest values of the HC_3N photodissociation rate should better correspond to the CN production rate from HC_3N photolysis. Hence, in the remainder of this article, we use a photodissociation rate of $3.4\times10^{-5}\,s^{-1}$ (Krasnopolsky, 1991). Furthermore, the quantum yield of CN production rate has never been directly measured in the VUV and Halpern et al. (1988) suggest that this quantum yield could be as low as 0.05 at 193 nm.

4.2.4. Cyanogen (or C_2N_2)

Jackson (1976) and Bockelée-Morvan and Crovisier (1985) have calculated the photodissociation rate of C_2N_2 (see Table 4) in cometary conditions. Both values are very different (9.1×10^{-5} and $3.08\times10^{-5}\,s^{-1}$). The quantum yield of CN production is also uncertain. Bockelée-Morvan and Crovisier (1985) proposed a value of 2, whereas Yung et al. (1984) used a value of 0.6. The state in which CN is formed is also not very well defined, but at 122 nm it could be produced in the $B^2\Sigma^+$ and $X^2\Sigma^+$ states (Bockelée-Morvan and Crovisier, 1985). In this case, the ejection velocity should be approximately equal to $2.07\,km\,s^{-1}$ for each radical (Bockelée-Morvan and Crovisier, 1985) (see Table 4).

4.2.5. Dicyanoacetylene (or C_4N_2)

Krasnopolsky (1991) has investigated the possibility that C_4N_2 could be a parent of the CN radicals and calculated its photodissociation rate. Depending on hypothesis on the threshold of CN production, the photodissociation rate of C_4N_2 range from 5×10^{-5} to $1.5\times10^{-4}\,s^{-1}$ (see Table 4).

Table 4
Photodissociation data of HCN, CH_3CN, HC_3N, C_2N_2 and C_4N_2

Molecules	Photodissociation rate (s^{-1})	Excess energy (eV)	Ejection velocity ($km\,s^{-1}$)	Remarks	References
HCN	1.3×10^{-5}				Huebner and Carpenter (1979)
	1.1×10^{-5}	3.8	1.02	$HCN\rightarrow H+CN(A^2\Pi_I)$	Combi and Delsemme (1980b)
				CN is formed in the state	
	1.51×10^{-5}	2.01	0.74	$B^2\Sigma^+$	Bockelée-Morvan and Crovisier
		4.08	1.06	$A^2\Pi_I$	(1985)
		5.21	1.19	$X^2\Sigma^+$	
	1.26×10^{-5}	3.82		$HCN\rightarrow H+CN(A^2\Pi_I)$	Huebner et al. (1992)
	4.51×10^{-7}	11.2		$HCN\rightarrow HCN^++e^-$	
		2.72	0.864	$HCN\rightarrow H+CN(A^2\Pi_I)$	This work
CH_3CN				CN is formed in the state	
	6.68×10^{-6}	2.56	2.63	$B^2\Sigma^+$	Bockelée-Morvan and Crovisier
		4.63	3.53	$A^2\Pi_i$	(1985)
		5.76	3.94	$X^2\Sigma^+$	
HC_3N	7.7×10^{-5}				Jackson (1976)
	2.8×10^{-5}				Huebner and Carpenter (1979)
				CN is formed in the state	
		0.79	1.69	$B^2\Sigma^+$	Bockelée-Morvan and Crovisier
		2.86	3.21	$A^2\Pi_i$	(1985)
		3.99	3.80	$X^2\Sigma^+$	
	3.4×10^{-5}		2.5 ± 0.5		Krasnopolsky (1991)
	3.92×10^{-5}	2.65			Huebner et al. (1992)
	6.6×10^{-5}				Crovisier (1994)
C_2N_2	9.1×10^{-5}				Jackson (1976)
	3.08×10^{-5}	1.16	2.07	$CN\ (X^2\Sigma^+)+CN\ (B^2\Sigma^+)$	Bockelée-Morvan and Crovisier
		2.10	2.78	$2\ CN\ (A^2\Pi_I)$	(1985)
		4.36	3.96	$2\ CN\ (X^2\Sigma^+)$	
	3×10^{-5}		2.5 ± 0.5		Krasnopolsky (1991)
C_4N_2	5×10^{-5}		3	For $\lambda<196$ nm	Krasnopolsky (1991)
	1.5×10^{-4}		1.5	For $\lambda<232$ nm	Krasnopolsky (1991)

4.2.6. *Hydrogen isocyanide (or HNC)*

No photodissociation rate in the solar radiation field has been reported for HNC. Millar et al. (1991) assume that the photodissociation rate of HNC is equal to the HCN one found in the ISM. So we have considered a photodissociation rate of HNC equal to the HCN one in the solar radiation field, i.e., $1.3\times10^{-5}\,s^{-1}$.

4.3. *Comparison of the CN parent scale length with the HCN photodissociation rate*

In order to compare the observed CN parent scale length to the photochemical data of HCN given for the minimum of solar activity, we have taken as a reference value the scale lengths that we have normalized to the minimum of solar flux. We have used Combi and Delsemme's model (1980a) in order to calculate the CN parent scale length from the HCN photodissociation rate. The results of this comparison are presented in Fig. 11. For this calculation, we have chosen a heliocentric dependence of the expansion velocity of $R_H^{-0.42}$ as measured in comet C/1995 O1 (Hale-Bopp) (Biver et al., 2002) and an averaged value of HCN photodissociation rate of $1.3\times10^{-5}\,s^{-1}$.

As one can see in Fig. 11, if one considers only HCN as a parent of the CN radical, the heliocentric evolution of the CN parent scale lengths is not well reproduced, except for $R_H>3$ AU, where the measured CN parent scale lengths are in agreement with the predicted ones. This is consistent with the observation of almost equal HCN and CN production rates for this range of heliocentric distances in comet C/1995 O1 (Hale-Bopp) (Rauer et al., 2003). For heliocentric distances lower than 3 AU, the measured CN parent scale lengths are shorter than the predicted ones. Indeed, the calculated effective HCN scale length at 1 UA is $5.8^{+3.0}_{-1.8}\times10^4$ km at 1 UA, whereas the observed CN parent one is about $2.5^{+2.5}_{-1.5}\times10^4$ km. This discrepancy could be explained in part by the acceleration of the gas in the inner coma (see Section 6). Nevertheless, the HCN photodissociation alone cannot explain the spatial distribution of CN for this range of heliocentric distances and an additional

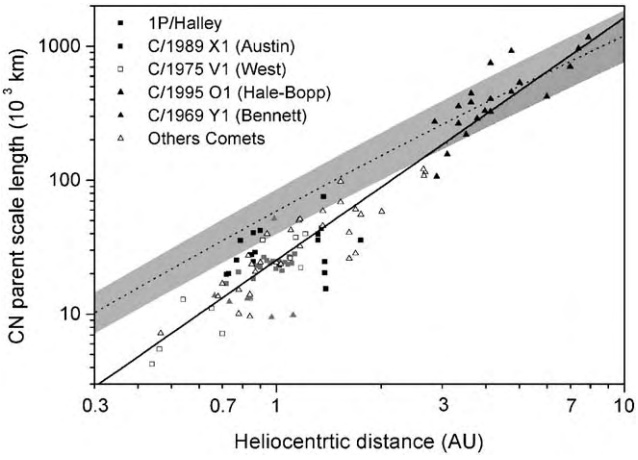

Fig. 11. Measured and effective CN parent scale lengths as a function of the heliocentric distance R_H. The points are the CN parent scale lengths normalized to the minimum of solar flux (see Section 1). The black line is the best fit ($2.53 \times 10^4 R_H^{1.81}$ km). The dashed line is the effective CN parent scale length with $\beta = 1.3 \times 10^{-5}\,s^{-1}$, $V_{gas} = 1R_H^{-0.42}\,km\,s^{-1}$ and $V_e = 0.864\,km\,s^{-1}$. The gray region represents the error on the effective CN parent scale lengths due to uncertainties on the photodissociation rate of HCN ($\pm 0.2 \times 10^{-5}\,s^{-1}$) and on the expansion velocity ($\pm 0.15\,km\,s^{-1}$). The heliocentric dependence of the expansion velocity $R_H^{-0.42}$ is from Biver et al. (2002).

parent is required, at least in some comets. The effective Haser scale length of this additional parent has to be smaller than 2.5×10^4 km at 1 AU.

4.4. Comparison of the CN parent scale length with the photochemical data of CH_3CN, HC_3N, HNC, C_2N_2 and C_4N_2

If another gaseous molecule could explain the difference between the measured and the effective Haser scale lengths from HCN photodissociation, its photodissociation rate has to be higher than the HCN one. This excludes CH_3CN and HNC, for which photodissociation rates are very close or lower than the HCN's one.

The case of HC_3N is more ambiguous. The absorption of one photon could produce the CN radical. But with a photodissociation rate of $3.4 \times 10^{-5}\,s^{-1}$ (Krasnopolsky, 1991), a CN quantum yield of production equal to 1, an ejection velocity of $2.5\,km\,s^{-1}$ (Krasnopolsky, 1991) and an expansion velocity of $1\,km\,s^{-1}$, the effective CN parent scale length could be about 1.1×10^4 km, i.e., shorter than the HCN one. So HC_3N could act as a second parent of the CN radicals as proposed by Krasnopolsky (1991). If we suppose that the CN profile is correctly modeled by a Haser profile with $l_p = 2.5 \times 10^4$ km, $l_d = 5.3 \times 10^5$ km and $V_{gas} = 1\,km\,s^{-1}$, that the photodissociation rate of HC_3N is about $3.4 \times 10^{-5}\,s^{-1}$ and that the quantum yield of CN production from HC_3N photolysis is equal to 1, then the HC_3N production rate has to be between 20% (for $\beta_{HCN} = 1.51 \times 10^{-5}\,s^{-1}$, $V_{eHCN} = 0.864\,km\,s^{-1}$ and $V_{eHC3N} = 4\,km\,s^{-1}$) and 70% (for $\beta_{HCN} = 1.1 \times 10^{-5}\,s^{-1}$, $V_{eHCN} = 0.864\,km\,s^{-1}$ and $V_{eHC3N} = 2\,km\,s^{-1}$) of the HCN one. These abundances are higher than the observed HC_3N production rate, which is only 10% of the HCN one (Bockelée-Morvan et al., 1999). Further experimental studies on the HC_3N photodissociation are needed to constraint the role of this compound in the origin of the cometary CN radical.

C_2N_2 was proposed as a parent molecule for the CN radicals by Bockelée-Morvan and Crovisier (1985) and Festou et al. (1998). We have calculated the effective CN parent Haser scale lengths for this molecule using a quantum yield of CN production equal to 2 (Bockelée-Morvan and Crovisier, 1985; Halpern and Yuhuia, 1997) and a photodissociation rate equal to $\beta = 3.1 \times 10^{-5}\,s^{-1}$ (Bockelée-Morvan and Crovisier, 1985; Krasnopolsky, 1991). In Fig. 12, we present the effective CN parent scale lengths from C_2N_2 photodissociation as a function of the ejection velocity at 1 AU and for three different expansion velocities. All the calculated Haser scale lengths are shorter than the measured one. Thus, a mixture of HCN and C_2N_2 could explain the observed radial profile of the CN radical. Then, we have calculated the fractions of CN radical which have to be produced from C_2N_2 and HCN photodissociation in order to reproduce a radial profile of CN. As for the study of HC_3N, we have supposed that the CN profiles are correctly modeled by a Haser profile with $l_p = 2.5 \times 10^4$ km, $l_d = 5.3 \times 10^5$ km and $V_{gas} = 1\,km\,s^{-1}$. We have found that the ratio of the C_2N_2 production rate to the HCN one has to be between 25% and 85%. Unfortunately, C_2N_2 has never been detected in comets and no upper limits have been published. The reason is that this molecule has no

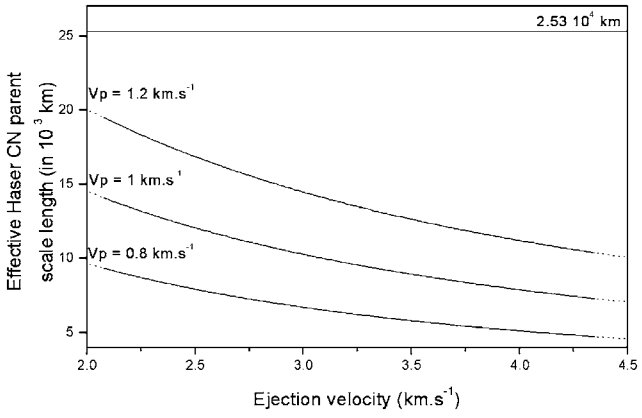

Fig. 12. Effective CN parent scale lengths from C_2N_2 photodissociation as a function of the ejection velocity of the CN radical (photodissociation rate $\beta = 3.1 \times 10^{-5}\,s^{-1}$). The three curves correspond to three different expansion velocities and the horizontal line represents the mean value of the CN parent scale lengths measured in comets and scaled to the minimum of the solar flux.

allowed rotational transitions, and its low vibrational band strengths do not lead to favorable excitation conditions in the infrared (Crovisier, 1987). In the same conditions and especially for the same production rate, the C_2N_2 vibrational band at 2157 cm^{-1} is 25 times less intense than the CO vibrational band at 2143 cm^{-1} (Crovisier, 1987). C_2N_2 is then almost undetectable in the 5 μm window. Despite the fact that C_2N_2 also has a vibrational band at 233 cm^{-1} (43 μm), it remains impossible to detect it by ground-based observations. Thus, even if the production rate of C_2N_2 is comparable to HCN one, this specie is quite difficult to detect by remote sensing. Indirect methods have been proposed by Petrie et al. (2003) consisting in trying to detect the $NCCNH^+$ ion or the polar isomer NCNC. As a matter of fact, C_2N_2 has never been detected in laboratory cometary ice analogs (Cottin et al., 1999), so its presence in comets has yet to be proven. The only astrophysical environment where this molecule has been detected is Titan's atmosphere in which it is produced by a specific chemistry dominated by N_2 and CH_4. The case for C_4N_2 is very similar to that for C_2N_2 except that its photochemistry is very badly known.

5. Observations of gaseous jets

Since the discovery of the CN jets in comet Halley by A'Hearn et al. (1986a), it has been proposed that the CN seen in the jets could be produced by the submicronic CHON grains discovered by Kissel et al. (1986). This hypothesis was proposed because no counterpart of this CN emission was visible in nearly simultaneous images taken in the diffused continuum (A'Hearn et al., 1986a).

In comet Halley, some C_2, C_3, OH and NH jets have also been detected and they have the same features as the CN jets (Cosmovici et al., 1988; Clairemidi et al., 1990a, b). Dust jets have also been observed, but it is not clear whether they are coincident or not with the gaseous jets. On the one hand, A'Hearn et al. (1986b) mentioned that the jets do not exist in the continuum images although it appears that one of the CN jets may come from the same area on the nucleus that produces most of the dust. On the other hand, the dust jets seen with the UV spectrometer of Vega 2 are co-spatial with all the gas jets (Goidet-Devel et al., 1997).

In comet Hale-Bopp, CN, C_2, C_3, OH and NH jets have also been observed (Lederer et al., 1999). This observation confirms the detection of CN jets by Larson et al. (1997) and Mueller et al. (1999). Near the perihelion, the CN images show a spiral pattern while the continuum shows some arcs confined to the sunward side (Mueller et al., 1999; Lederer et al., 1999). In these observations, dust jets coincided with the CN jets in the sunward direction, but not in the anti-sunward direction (Lederer and Campins, 2002).

Clairemidi et al. (1990a) have studied the radial intensity of a CN jet in comparison to a diffuse component (where no jets are present) called "valley". The CN spatial distributions in the jets and in the valley are quite similar up to 8000 km, but do not match anymore beyond this. It seems necessary to introduce a local production mechanism inside the jets to explain such a behavior. Klavetter and A'Hearn (1994) have performed a similar study. They have clearly shown that the CN radial profile of the diffuse component is different from that inside the jet. On the one hand, the profile of the diffuse component can be fitted with Haser or vectorial models, and thus is consistent with a simple photodissociation process. On the other hand, the jet profile cannot be explained by some simple process. Thus, using a numerical derivative of the profile, Klavetter and A'Hearn (1994) found that the CN production inside the jet occurs up to 15,000 km with a maximum approximately at 8000 km. This shift of the production peak from the nucleus to the coma is by definition an extended source. Klavetter and A'Hearn (1994) proposed that the CN is released from grains, the temperature of which increases with time, and therefore produce CN faster. Lederer and Campins (2002) have modeled the CN jets observed on comet Hale-Bopp with a 3-D time-dependent Monte-Carlo model considering that the daughter radicals are produced by photodissociation of parent gas and by an extended source. With this model, they have correctly reproduced the appearance of the CN jets, and also those of C_2 and OH. In one jet, 75% of the CN radicals seem to be produced by an extended source (Lederer and Campins, 2001).

From these three studies, we see that a large fraction of the CN that is present in the jets seems to be produced by an extended source whose productivity does not peak at the nucleus. Similar results have been obtained by Eberhardt et al. (1987) for the in situ measurements of CO by the Giotto neutral mass spectrometer (NMS). The measured density profile can only be explained if the CO production is maximum at 9000 km from the nucleus. The additional process cannot be the photodissociation of a gaseous parent, otherwise the peak production would be located at the nucleus surface where the density of the parent is maximal. The displacement of the production peak should rather be due to chemical reactions in the inner coma, release of gaseous parents during the fragmentation of grains, sublimation of icy grains or thermal degradation of large compounds present on grains. This will be discussed in Section 6.

6. Summary and discussion

We have compared CN and HCN production rates for eight comets (see Section 3). For four of them

(Austin, IRAS-Aracki-Alcock, Giacobini-Zinner and Wilson), the CN production rates are significantly higher than those of HCN. This leads to the conclusion that CN radicals cannot be produced only by the HCN photolysis and that an additional process is required. For comets Halley, Levy, Hyakutake and Hale-Bopp, CN and HCN production rates are quite similar. But for all comets, the CN parent scale lengths are lower than the scale length predicted from HCN photolysis for $R_H < 3$ UA, as we showed in Section 4. This fact has already been noted by Lara et al. (2003). But this result has to be taken with caution since the CN production rates are only known with a factor of 2 when taking into account all uncertainties (see Fig. 10a and b).

In order to convert the measured flux into CN production rates, one needs to know the parent scale length, which is the most sensitive parameter for this calculation. Since the CN parent scale lengths are lower than those corresponding to HCN photolysis and since production rates increase with parent scale lengths, the use of the effective scale length of HCN photodissociation leads to CN productions that are two times larger than the HCN production for all comets. Thus, only a fraction of CN radicals are effectively produced by the HCN photolysis and CN production rates should be calculated only with a model that takes into account the additional CN production mechanisms.

In Section 2, we have presented a compilation of the available parent and daughter CN Haser scale lengths. These CN Haser scale lengths present a large dispersion. We have shown that this dispersion is not due to the change of solar flux or variation of the gas expansion velocity from one comet to another. This dispersion derived certainly from the fact that most spatial measurements yield to a set of satisfying solutions: several parent and daughter scale length pairs lead to good fits between the Haser model and the spatial data. In order to correctly extract both parent and daughter scales lengths, the spatial distribution of CN has to extend far enough from the nucleus. Otherwise the CN daughter scale length (and consequently the parent scale length) cannot be adequately measured. Therefore, observations with a wide field of view telescope are necessary to constrain correctly the CN Haser scale lengths. We have also pointed out that short-term variations of the CN production rate, related to the rotation of the nucleus, could also be responsible in part for the dispersion observed in the values of CN Haser scale lengths, since the Haser model supposes a steady-state production rate.

Despite the dispersion of the CN Haser parent scale lengths, we have compared them with the photodissociation rate of HCN using the model of Combi and Delsemme (1980a) (Fig. 11). When the comet is located at heliocentric distances larger than 3 UA, the CN spatial distribution is consistent with HCN photolysis. Then, at these heliocentric distances, the CN radical could be entirely produced by HCN photodissociation as already shown by Rauer et al. (2003). Nevertheless, for heliocentric distances lower than 3 AU, the observed CN parent scale lengths are shorter than the predicted ones, as already shown by Bockelée-Morvan and Crovisier (1985), Krasnopolsky et al. (1991) and Lara et al. (2003). At 1 AU, the equivalent CN Haser scale length from HCN photolysis is equal to 5.9×10^4 km whereas the mean value of the observed ones is 2.5×10^4 km; then the spatial distribution of CN could not be explained so far by HCN photolysis alone. The acceleration of the gas in the inner coma could partly explain this difference. Indeed, between 10^2 and 10^4 km from the nucleus, the gas expansion velocity increases by a factor roughly equal to 1.5 (Combi, 1989; Combi et al., 1997). Whereas this factor could be higher in very productive comets such as C/1995 O1 (Hale-Bopp), it seems to be smaller than the ratio between the predicted and observed CN parent scale lengths. Surely, this acceleration could not fully explain this discrepancy. Nevertheless, no modeling of this effect on the CN spatial distribution has ever been performed so far.

To explain the discrepancy between the observed and predicted CN Haser parent scale lengths, another hypothesis can also be put forward: the presence of another CN production mechanism than HCN photolysis. This interpretation is supported by the observation of CN jets and particularly by the CN radial distribution inside jets which are not consistent with a production from a simple photodissociation process (Klavetter and A'Hearn, 1994). Moreover, from observations of CN in several comets, Arpigny et al. (2003), Jehin et al. (2004) and Manfroid et al. (2005) have derived an anomalously low $^{14}N/^{15}N$ isotopic ratio (about 130, compared with the terrestrial ratio of 280). This is quite different from $^{14}N/^{15}N$ isotopic ratio determined from the radio lines of HCN observed in comet Hale-Bopp, which is, in that case, close to the terrestrial ratio (Jewitt et al., 1997). This strongly suggests another source of CN, significantly enriched in ^{15}N as compared to HCN. Thus, HCN cannot be the unique source of CN radicals in comets. The different hypotheses for this additional source of cometary CN radicals are detailed below.

First, the CN spatial distribution could be explained by the photodissociation of another parent(s) molecule(s). In Section 4, we have studied the possible additional parents: CH_3CN, HNC, HC_3N, C_2N_2 and C_4N_2. CH_3CN and HNC, whose scale lengths are larger or of the same order than the one determined for CN parents, could not act as the second parent of the CN radical. HC_3N and C_2N_2 scale lengths could be consistent with the observed CN spatial profiles. The photodissociation of HC_3N, and particularly the quantum yields of CN production in cometary conditions, is not well known. Nevertheless, even if we suppose a

quantum yield of 1, the required production rate of HC_3N in order to explain the CN density profile would be higher than the measured one (Bockelée-Morvan et al., 1999). Thus, it seems improbable that HC_3N could explain the CN density profile. C_2N_2 has been proposed (Bockelée-Morvan and Crovisier, 1985; Festou et al., 1998) since its photodissociation leads to an effective scale length lower than the one measured for the CN parent (see Fig. 12). Unfortunately, C_2N_2 has no allowed rotational transition and its vibrational band strengths are very low (see Section 4); this leads to a very high detection limit for this compound. The hypothesis of this compound as a parent of the CN radical cannot be ruled out, but it will be hard to confirm since its detection is a very challenging issue.

Another possible mechanism is the production of CN radical by chemical reactions. Rodgers and Charnley (1998) have invoked such a process to explain the HNC extended source in comet Hale-Bopp. But it has been demonstrated that this process is not efficient enough to explain the HNC production in less productive comets such as Hyakutake or Lee (Rodgers and Charnley, 2001). It might also be the case for CN. But in order to confirm this statement, a specific model of CN production by chemical reactions has to be developed.

Finally, a mechanism where CN radical is produced directly from dust has been proposed by numerous authors. Such a mechanism was originally put forward to explain the presence of CN jets (A'Hearn et al., 1986a), since CN spatial profile inside the jets cannot be explained by the photodissociation of a gaseous molecule (Klavetter and A'Hearn, 1994). A'Hearn et al. (1995) and Newburn and Spinrad (1989) noticed that there is a correlation between the CN and dust production rates. Cottin et al. (2004) have recently demonstrated that H_2CO could be produced by the thermal degradation of polyoxymethylene (H_2CO polymer). This mechanism could then be responsible for the H_2CO extended source. A similar mechanism could be at the origin of the CN spatial distribution. Unfortunately, the model of Cottin et al. (2004) is, so far, not applicable to the CN extended source, because of the lack of chemical data concerning the degradation of high molecular weight nitrogenated compounds that could be present on cometary grains. Consequently, experimental studies on the measurements of CN production by heating and UV irradiation of nitrogenated compounds, such as HCN polymers or hexamethylenetetramine ($C_6H_{12}N_4$), have to be performed.

7. Conclusion

HCN photolysis is the major process in the production of CN in cometary atmospheres, but it cannot entirely explain the CN density profile and the CN production rates in most comets. Moreover, even if in some comets, the Haser CN production rates seem to be in agreement with those of HCN, the CN density profile can never be explained by HCN photolysis alone when the comet is closer than 3 AU from the Sun. The acceleration of gas in the inner coma could play a role, but further modeling of this effect is required. As a matter of fact, an additional production of CN is necessary to explain the spatial profile of CN inside the jets as well as the discrepancy between the $^{14}N/^{15}N$ isotopic ratio measured in CN and HCN.

A part of CN radicals could also be formed by HC_3N or C_2N_2 photolysis. But, even if the production of CN radicals from the HC_3N photolysis is poorly documented, HC_3N production rate seems to be too low to explain quantitatively the CN density profile. C_2N_2 is also a candidate to be the second parent of CN radicals. Unfortunately, no upper limit for its production rate has been published due to its difficult detection from ground-based observations. A challenging issue will be its in situ measurements by the Rosetta spacecraft or observations from space in the far infrared. Additionally, to get a better idea of the role of HC_3N and C_2N_2, further experimental studies of their photolysis should be performed, mainly at 121.6 nm (Lyman α).

At last, the hypothesis of the production of CN radical by photo- or thermal degradation of high molecular weight nitrogenated compounds present on cometary grains has to be explored. Modeling of this process should be done, but it requires to determine numerous chemical data concerning the degradation of adequate solid compounds. Thus, experimental measurements of the degradation of nitrogenated compounds, such as HCN polymers or hexamethylenetetramine ($C_6H_{12}N_4$), have to be performed in order to test this hypothesis.

Acknowledgements

We are very grateful to Dominique Bockelée-Morvan for the helpful discussion. We thank Nicolas Biver for his permission to use unpublished results from his thesis. We also thank our two referees, D.G. Schleicher and D. Despois for their corrections and help in improving this manuscript.

References

A'Hearn, M.F., Millis, R., Festou, M., Benvenuti, P., Cacciari, C., Cassatella, A., Talavera, A., Wamsteker, W., Green, D.W.E., Hale, A., Marsden, B.G., 1983. Comet IRAS-Araki-Alcock (1983d). IAU Circ., 3802.

A'Hearn, M.F., Hoban, S., Birch, P.V., Bowers, C., Martin, R., Klinglesmith, D.A., 1986a. Cyanogen jets in comet Halley. Nature 324, 649–651.

A'Hearn, M.F., Hoban, S., Birch, P.V., Bowers, C., Martin, R., Klinglesmith, D.A., 1986b. Gaseous jets in comet P/Halley. In: 20th ESLAB Symposium, ESA SP 250, Heidelberg, pp. 483–486.

A'Hearn, M.F., Millis, R.L., Schleicher, D.G., Osip, D.J., Birch, P.V., 1995. The ensemble properties of comets: results from narrowband photometry of 85 comets, 1976–1992. Icarus 118, 223–270.

Arpigny, C., Jehin, E., Manfroid, J., Hutsemekers, D., Schultz, R., Stuwe, J.A., Zucconi, J.-M., Ilyin, I., 2003. Anomalous nitrogen isotope ratio in comets. Science 301, 1522–1524.

Biver, N., 1997. Molécules mères cométaires: observations et modélisations. Ph.D. Thesis, Université de Paris 7.

Biver, N., Bockelée-Morvan, D., Colom, P., Crovisier, J., Germain, B., Lellouch, E., Davies, J.K., Dent, W.R.F., Moreno, R., Paubert, G., Wink, J., Despois, D., Lis, D.C., Mehringer, D., Benford, D., Gardner, M., Phillips, T.G., Gunnarsson, M., Rickman, H., Winnberg, A., Bergman, P., Johansson, L.E.B., Rauer, H., 1999a. Long-term evolution of the outgassing of comet Hale-Bopp from radio observations. Earth Moon Planets 78, 5–11.

Biver, N., Bockelée-Morvan, D., Crovisier, J., Davies, J.K., Matthews, H.E., Wink, J.E., Rauer, H., Colom, P., Dent, W.R.F., Despois, D., Moreno, R., Paubert, G., Jewitt, D., Senay, M., 1999b. Spectroscopic monitoring of comet C/1996 B2 (Hyakutake) with the JCMT and IRAM radio telescopes. Astron. J. 118, 1850–1872.

Biver, N., Bockelée-Morvan, D., Colom, P., Crovisier, J., Henry, F., Lellouch, E., Winnberg, A., Johansson, L.E.B., Gunnarsson, M., Rickman, H., Rantakyrö, F., Davies, J.K., Dent, W.R.F., Paubert, G., Moreno, R., Wink, J., Despois, D., Benford, D.J., Gardner, M., Lis, D.C., Mehringer, D., Phillips, T.G., Rauer, H., 2002. The 1995–2002 long-term monitoring of comet C/1995 O1 (Hale-Bopp) at radio wavelength. Earth Moon Planets 90, 5–14.

Bockelée-Morvan, D., Crovisier, J., 1985. Possible parents for the cometary CN radical: photochemistry and excitation conditions. Astron. Astrophys. 151, 90–100.

Bockelée-Morvan, D., Crovisier, J., Baudry, A., Despois, D., Perault, M., Irvine, W.M., Schloerb, F.P., Swade, D., 1984. Hydrogen cyanide in comets—excitation conditions and radio observations of comet IRAS-Araki-Alcock 1983d. Astron. Astrophys. 141, 411–418.

Bockelée-Morvan, D., Crovisier, J., Despois, D., Forveille, T., Gerard, E., Schraml, J., Thum, C., 1987. Molecular observations of comets P/Giacobini-Zinner 1984e and P/Halley 1982i at millimetre wavelengths. Astron. Astrophys. 180, 253–262.

Bockelée-Morvan, D., Crovisier, J., Gérard, E., 1990. Retrieving the coma gas expansion velocity in P/Halley, Wilson (1987 VII) and several other comets from the 18-cm OH line shapes. Astron. Astrophys. 238, 382–400.

Bockelée-Morvan, D., Lis, D.C., Wink, J.E., Despois, D., Crovisier, J., Bachiller, R., Benford, D.J., Biver, N., Colom, P., Davies, J.K., Gerard, E., Germain, B., Houde, M., Moreno, R., Paubert, G., Phillips, T.G., Rauer, H., 1999. New molecules found in comet C/1995 O1 (Hale-Bopp). Investigating the link between cometary and interstellar material. Astron. Astrophys. 353, 1101–1114.

Boehnhardt, H., Drechsel, H., Vanysek, V., Waha, L., 1989. Photometric investigation of comets Bradfield 1987S and P/Borelly. Astron. Astrophys. 220, 286–292.

Bruston, P., Poncet, H., Raulin, F., Cossart-Magos, C., Courtin, R., 1989. UV spectroscopy of Titan's atmosphere, planetary organic chemistry, and prebiological synthesis I. Absorption spectra of gaseous propynenitrile and 2-butynenitrile in the 185- to 250-nm region. Icarus 78, 38–53.

Catalano, F.A., Baratta, G.A., Lo Presti, C., Strazzulla, G., 1986. Pre-perihelion photometry of P/Halley (1982i) at Catania (Italy) Observatory. Astron. Astrophys. 168, 341–345.

Churyumov, K.I., Rosenbush, V.K., 1991. Peculiarities of gas and dust production rates in Comets P/Halley (1986 III), P/Giacobini-Zinner (1985 XIII), P/Hartley-Good (1985 XVII) and P/Thiele (1985 XIX). Astron. Nachr. 312, 385–391.

Clairemidi, J., Moreels, G., Krasnopolsky, V.A., 1990a. Gaseous CN, C2, and C3 jets in the inner coma of Comet P/Halley observed from the VEGA 2 spacecraft. Icarus 86, 115–128.

Clairemidi, J., Moreels, G., Krasnopolsky, V.A., 1990b. Spectro-imagery of P/Halley's inner coma in the OH and NH ultraviolet bands. Astron. Astrophys. 231, 235–240.

Clarke, D.W., Ferris, J.P., 1995. Photodissociation of cyanoacetylene: application to the atmospheric chemistry of Titan. Icarus 115, 119–125.

Cochran, A.L., 1985. A re-evaluation of the Haser model scale lengths for comets. Astron. J. 90, 2609–2614.

Cochran, A.L., Schleicher, D.G., 1993. Observational constraints on the lifetime of cometary H_2O. Icarus 105, 235–253.

Combi, M.R., 1978. Convolution of cometary brightness profiles by circular diaphragms. Astron. J. 83, 1459–1466.

Combi, M.R., 1989. The outflow speed of the coma of Halley's comet. Icarus 81, 41–50.

Combi, M., 2002. Hale-Bopp: what makes a big comet different? Coma dynamics: observations and theory. Earth Moon Planets 89, 73–90.

Combi, M.R., Delsemme, A.H., 1980a. Neutral cometary atmospheres. I—an average random walk model for photodissociation in comets. Astrophys. J. 237, 633–640.

Combi, M.R., Delsemme, A.H., 1980b. Neutral cometary atmospheres. II—the production of CN in comets. Astrophys. J. 237, 641–645.

Combi, M.R., Delsemme, A.H., 1986. Neutral cometary atmospheres v. C_2 and CN in comets. Astrophys. J. 308, 472–484.

Combi, M.R., Fink, U., 1993. P/Halley—effects of time-dependent production rates on spatial emission profiles. Astrophys. J. 409, 151–162.

Combi, M., Huang, B., Cochran, A., Fink, U., Schulz, R., 1994. Time-dependent analysis of 8 days of CN spatial profiles in comet P/Halley. Astrophys. J. 435, 870–873.

Combi, M.R., Kabin, K., DeZeeuw, D.L., Gombosi, T.I., Powell, K.G., 1997. Dust–gas interrelations in comets: observations and theory. Earth Moon Planets 79, 275–306.

Cook, P.A., Langford, S.R., Ashfold, M.N.R., Dixon, R.N., 2000. Angular resolved studies of the Lyman-photodissociation of HCN and DCN: new dynamical insights. J. Chem. Phys. 113, 994–1004.

Cosmovici, C.B., Schwartz, G., Ip, W., Mack, P., 1988. Gas and dust jets in the inner coma of comet Halley. Nature 332, 705–709.

Cottin, H., Gazeau, M.C., Raulin, F., 1999. Cometary organic chemistry: a review from observations, numerical and experimental simulations. Planet. Space Sci. 47, 1141–1162.

Cottin, H., Benilan, Y., Gazeau, M.-C., Raulin, F., 2004. Origin of cometary extended sources from degradation of refractory organics on grain: polyoxymethylene as formaldehyde parent molecule. Icarus 167, 397–416.

Crovisier, J., 1987. Rotational and vibrational synthetic spectra of linear parent molecules in comets. Astron. Astrophys. Suppl. 68, 223–258.

Crovisier, J., 1994. Photodestruction rates for cometary parent molecules. J. Geophys. Res. 99, 3777–3781.

Crovisier, J., Despois, D., Bockelée-Morvan, D., Gerard, E., Paubert, G., Johansson, L.E.B., Ekelund, L., Winnberg, A., Ge, W., Irvine, W.M., Kinzel, W.M., Schloerb, F.P., 1990. A search for the millimetre lines of HCN in Comets Wilson 1987 VII and Machholz 1988 XV. Astron. Astrophys. 234, 535–538.

Crovisier, J., Bockelée-Morvan, D., Colom, P., Despois, D., Paubert, G., 1993. A search for parent molecules at millimetre wavelengths in comets Austin 1990V and Levy 1990 XX: upper limits for undetected species. Astron. Astrophys. 269, 527–540.

Delsemme, A.H., Combi, M.R., 1983. Neutral cometary atmospheres. IV—brightness profiles in the inner coma of comet Kohoutek 1973 XII. Astrophys. J. 271, 388–397.

Despois, D., Crovisier, J., Bockelée-Morvan, D., Gerard, E., Schraml, J., 1986. Observations of hydrogen cyanide in comet Halley. Astron. Astrophys. 160, L11–L12.

Eberhardt, P., Krankowsky, D., Schulte, W., Dolder, U., Lammerzahl, P., Berthelier, J.J., Woweries, J., Stubbeman, U., Hodges, R.R., Hoffman, J.H., Illiano, J.M., 1987. The CO and N_2 abundance in comet P/Halley. Astron. Astrophys. 187, 481–484.

Festou, M.C., Barale, O., Davidge, T., Stern, S.A., Tozzi, G.P., Womack, M., Zucconi, J.M., 1998. Tentative identification of the parent of CN radicals in comets: C_2N_2. BAAS 30, 1089.

Fink, U., Combi, M.R., 2004. The effect of using different scale lengths on the production rates of Comet 46P/Wirtanen. Planet. Space Sci. 52, 573–580.

Fink, U., Combi, M.R., Disanti, M.A., 1991. Comet P/Halley—spatial distributions and scale lengths for C_2, CN, NH_2, and H_2O. Astrophys. J. 383, 356–371.

Goidet-Devel, B., Clairemidi, J., Rousselot, P., Moreels, G., 1997. Dust spatial distribution and radial profile in Halley's inner coma. Icarus 126, 78–106.

Guo, J., Eng, R., Carrington, T., Filseth, S., 2000. Photodissociation of HCN at 157 nm: energy disposal in the CN ($A^2\Pi$) fragment. J. Chem. Phys. 112, 8904–8909.

Halpern, J.B., 1987. The photochemistry of some possible cometary CN parent species. ESA SP-278, 159–162.

Halpern, J.B., Yuhuia, H., 1997. Radiative lifetimes, fluorescence quantum yields and photodissociation of the C_2N_2 ($A^1\Sigma_u$) and ($B^1\Delta_u$) states: evidence for sterically hindered, triplet mediated crossings to the ($X^1\Sigma_g$) ground state. Chem. Phys. 222, 71–86.

Halpern, J.B., Miller, G.E., Okabe, H., 1988. The UV photochemistry of cyanoacetylene. J. Photochem. Photobiol. 42, 63–72.

Haser, L., 1957. Distribution d'intensité dans la tête d'une comète. Bull. Acad. R. Belg. 43, 740–750.

Huebner, W.F., Carpenter, C.W., 1979. Solar photo rate coefficients. Los Alamos Sci. Lab. LA-8085-MS, 94.

Huebner, W.F., Buhl, D., Snyder, L.E., 1974. HCN radio emission from Comet Kohoutek 1973f. Icarus 23, 580–584.

Huebner, W.F., Keady, J.J., Lyon, S.P., 1992. Solar photo rates for planetary atmospheres and atmospheric pollutants. Astrophys. Space Sci. 195, 1–289.

Jackson, W.M., 1976. Laboratory observations of the photochemistry of parent molecules: a review. In: Donn, B., Mumma, M., Jackson, W., A'Hearn, M.A., Harrington, R. (Eds.), The Study of Comets. NASA Spec. Publ. SP-393, pp. 679–704.

Jackson, W.M., 1991. Recent laboratory photochemical studies and their relationship to the photochemical formation of cometary radicals. In: Newburn, Jr., R.L., et al. (Eds.), Comets in the Post-Halley Era. Kluwer Academic Publishers, Dordrecht, pp. 313–332.

Jehin, E., Manfroid, J., Cochran, A.L., Arpigny, C., Zucconi, J.-M., Hutsemékers, D., Cochran, W.D., Endl, M., Schulz, R., 2004. The anomalous 14N/15N ratio in comets 122/P 1995 S1 (De Vico) and 153P/2002 C1 (Ikeya-Zhang). Astrophys. J. 613, L161–L164.

Jewitt, D.C., Matthews, H.E., Owen, T.C., Meier, R., 1997. Measurements of $^{12}C/^{13}C$, $^{14}N/^{15}N$ and $^{32}S/^{34}S$ in comet Hale-Bopp (C/1995 O1). Science 278, 90–93.

Kanda, K., Nagata, T., Ibuki, T., 1999. Photodissociation of some simple nitriles in the extreme vacuum ultraviolet region. Chem. Phys. 243, 89–96.

Kissel, J., Sagdeev, R.Z., Bertaux, J.L., Angarov, V.N., Audouze, J., Blamont, J.E., Buchler, K., Evlanov, E.N., Fechtig, H., Fomenkova, M.N., VonHoerner, H., Inogamov, N.A., Khromov, V.N., Knabe, W., Krueger, F.R., Langevin, Y., Leonas, V.B., Levasseur-Regourd, A.C., Managadze, G.G., Podkolzin, S.N., Shapiro, V.D., Tabaldyev, S.R., Zubkov, B.V., 1986. Composition of comet Halley dust particles from Vega observations. Nature 321, 280–282.

Klavetter, J.J., A'Hearn, M.F., 1994. An extended source for CN jets in comet P/Halley. Icarus 107, 322–334.

Krasnopolsky, V.A., 1991. C_3 and CN parents in comet P/Halley. Astron. Astrophys. 245, 310–315.

Krasnopolsky, V.A., Tkachuk, A.Y., Korablev, O.I., 1991. CN and C_3 distributions in comet P/Halley measured by the Vega 2 spectrometer TKS. Astron. Astrophys. 245, 662–668.

Lara, L.-M., Licandro, J., Oscoz, A., Motta, V., 2003. Behaviour of comet 21P/Giacobini-Zinner during the 1998 perihelion. Astron. Astrophys. 399, 763–772.

Larson, S.M., Hergenrother, C.W., Randt, J.C., 1997. The spatial and temporal distribution of CO^+ and CN in C/1995 O1 (Hale-Bopp). BAAS, 1036.

Lederer, S.M., Campins, H., 2001. Modeling coma gas jets in comet Hale-Bopp. In: 32nd Annual Lunar and Planetary Science Conference, March 12–16, 2001, Houston, TX, Abstract No. 1421.

Lederer, S.M., Campins, H., 2002. Evidence for chemical heterogeneity in the nucleus of C/1995 O1 Hale-Bopp. Earth Moon Planets 90, 381–389.

Lederer, S.M., Campins, H., Osip, D.J., Schleicher, D.G., 1999. Gaseous jets in comet Hale-Bopp (1995 O1). Earth Moon Planets 78, 131–136.

Magdziarz, P., Winiarski, M., Waniak, W., 1995. CN photometry of comet Levy 1900XX. Icarus 116, 40–45.

Magee-Sauer, K., Mumma, M.J., DiSanti, M.A., Dello Russo, N.D., Rettig, T.W., 1999. Infrared spectroscopy of the ν_3 band of hydrogen cyanide in comet C/1995 O1 Hale-Bopp. Icarus 142, 498–508.

Magee-Sauer, K., Mumma, M.J., DiSanti, M.A., Dello Russo, N.D., 2002. Hydrogen cyanide in comet C/1996/B2 Hyakutake. JGR (Planets) 107, E11 6-1.

Manfroid, J., Jehin, E., Hutsemékers, D., Cochran, A., Zucconi, J.-M., Arpigny, C., Schulz, R., Stüwe, J.A., 2005. Isotopic abundance of nitrogen and carbon in distant comets. Astron. Astrophys. 432, L5–L8.

Meredith, N.P., Wallis, M.K., Rees, D., 1992. Narrow-band IPD images of cometary CN and C_2—the effect of solar activity on coma scales. Mon. Not. R. Astron. Soc. 254, 693–704.

Millar, T.J., Rawlings, J.M.C., Bennet, A., Brown, P.D., Charnley, S.B., 1991. Gas phase reactions and rate coefficients for use in astrochemistry. The UMIST ratefile. Astron. Astrophys. Suppl. Ser. 87, 585–619.

Morley, G.P., Lambert, I.R., Ashfold, M.N.R., Rosser, K.N., Western, C.M., 1992. Dissociation dynamics of HCN(DCN) following photoexcitation at 121.6 nm. J. Chem. Phys. 97, 3157–3165.

Mueller, B.E.A., Samarasinha, N.H., Belton, M.J.S., 1999. Imaging the structure and evolution of the coma morphology of comet C/1995 O1 (Hale-Bopp). Earth Moon Planets 77, 181–188.

Newburn, R.L., Spinrad, H., 1984. Spectrophotometry of 17 comets. I—the emission features. Astron. J. 89, 289–309.

Newburn, R.L., Spinrad, H., 1989. Spectrophotometry of 25 comets—post-Halley updates for 17 comets plus new observations for eight additional comets. Astron. J. 97, 552–569.

O'Dell, C.R., Osterbrock, D.E., 1962. Emission-band and continuum photometry of comet Seki (1961f). Astrophys. J. 136, 559–566.

Petrie, S., Millar, T.J., Markwick, A.J., 2003. NCCN in TMC-1 and IRC+10216. Mon. Not. R. Astron. Soc. 341, 609–616.

Randall, C.E., Schleicher, D.G., Ballou, R.G., Osip, D.J., 1992. Observational constraints on molecular scalelengths and lifetimes in comets. BAAS 24, 1002.

Rauer, H., Helbert, J., Arpigny, C., Benkhoff, J., Bockelée-Morvan, D., Boehnhardt, H., Colas, F., Crovisier, J., Hainaut, O., Jorda, L., Kueppers, M., Manfroid, J., Thomas, N., 2003. Long-term optical

spectrophotometric monitoring of comet C/1995 O1 (Hale-Bopp). Astron. Astrophys. 397, 1109–1122.
Rodgers, S.D., Charnley, S.B., 1998. HNC and HCN in comets. Astrophys. J. 501, L227–L230.
Rodgers, S.D., Charnley, S.B., 2001. On the origin of HNC in comet Lee. Mon. Not. R. Astron. Soc. 323, 84–92.
Schleicher, D.G., Osip, D.J., 2002. Long- and short-term photometric behavior of comet Hyakutake (1996 B2). Icarus 159, 210–233.
Schleicher, D.G., Millis, R.L., Birch, P.V., 1987. Photometric observations of comet P/Giacobini-Zinner. Astron. Astrophys. 187, 531–538.
Schleicher, D.G., Millis, R.L., Thompson, D.T., Birch, P.V., Martin, R., Tholen, D.J., Piscitelli, J.R., Lark, N.L., Hammel, H.B., 1990. Periodic variations in the activity of comet P/Halley during the 1985/1986 apparition. Astron. J. 100, 896–912.
Schleicher, D.G., Millis, R.L., Osip, D.J., Birch, P.V., 1991. Comet Levy (1990c)—groundbased photometric results. Icarus 94, 511–523.
Schleicher, D.G., Lederer, S.M., Millis, R.L., Farnham, T.L., 1997. Photometric behavior of comet Hale-Bopp (C/1995 O1) before perihelion. Science 275, 1913–1915.
Schleicher, D.G., Millis, R.L., Birch, P.V., 1998. Narrowband photometry of comet P/Halley: variation with heliocentric distance, season, and solar phase angle. Icarus 132, 397–417.
Schloerb, F.P., Kinzel, W.M., Swade, D.A., Irvine, W.M., 1986. HCN production from comet Halley. Astrophys. J. 310, 55–60.
Schulz, R., A'Hearn, M.F., Birch, P.V., Bowers, C., Kempin, M., Martin, R., 1993. CCD imaging of Comet Wilson (1987VII)—a quantitative coma analysis. Icarus 104, 206–225.
Tatum, J.B., 1984. Cyanogen radiance/column-density ratio for comets calculated from the Swings effect. Astron. Astrophys. 135, 183–187.
Umbach, R., Jockers, K., Geyer, E.H., 1998. Spatial distribution of neutral and ionic constituents in comet P/Halley. Astron. Astrophys. Suppl. 127, 479–495.
Waniak, W., Magdziarz, P., Winiarski, M., 1994. Narrowband photometry of comet Austin 1990V. Icarus 108, 92–102.
Winnberg, A., Ekelund, E., Ekelund, A., 1987. Detection of HCN in comet 1P/Halley. Astron. Astrophys. 172, 335–341.
Womack, M., Lutz, B.L., Wagner, R.M., 1994. Pre- and post-perihelon abundances of gas and dust in comet Halley. Astrophys. J. 433, 886–894.
Woodney, L.M., A'Hearn, M.F., Schleicher, D.G., Farnham, T.L., McMullin, J.P., Wright, M.C.H., Veal, J.M., Snyder, L.E., Pater, I.D., Forster, J.R., Palmer, P., Kuan, Y.J., Williams, W.R., Cheung, C.C., Smith, B.R., 2002. Morphology of HCN and CN in comet Hale-Bopp (1995 O1). Icarus 157, 193–204.
Woods, T.N., Tobiska, W.K., Rottman, G.J., Worden, J.R., 2000. Improved solar lyman alpha irradiance modeling from 1947 through 1999 based on UARS observations. J. Geophys. Res. 105, 27195–27216.
Yung, Y.L., Allen, M., Pinto, J.P., 1984. Photochemistry of the atmosphere of Titan: comparison between model and observations. Astrophys. J. Suppl. Ser. 55, 465.

Article 5

Cottin H. and Fray N. (In Press) Distributed Sources in Comets. Space Science Reviews.

Space Sci Rev
DOI 10.1007/s11214-008-9399-z

Distributed Sources in Comets

Hervé Cottin · Nicolas Fray

Received: 8 April 2007 / Accepted: 5 June 2008

Abstract The distribution of some molecules and radicals (H_2CO, CO, HNC, CN, ...) in the atmosphere of several comets cannot be explained only by a direct sublimation from the nucleus, or by gas phase processes in the coma. Such molecules are in part the result of a distributed source in the coma, which could be the photo and thermal degradation of dust. We present a review of the degradation processes and discuss possible interpretations of the observations in which the degradation of solid complex organic material in dust particles seems to play a major role. The knowledge of such gas production mechanisms provides important clues on the chemical nature of the refractory organic material contained in comet nuclei.

Keywords Comets · Distributed source · Extended source · Composition · Organic chemistry · Modelling

Introduction

Our current knowledge of the composition of the comet nuclei derives from observations made in their atmospheres, and from our understanding of the physico-chemical processes governing the emission of material into the atmosphere (sublimation of ices contained in the nucleus releasing gaseous molecules and dragging along solid particles), and its evolution once out-gassed or lifted. Recently, Stardust spacecraft captured cometary grains in the atmosphere of Comet 81P/Wild 2. Those grains were brought back to Earth in 2006 and were analysed in the laboratory where it has been shown they were made of a complex mineral and organic mixture (Brownlee et al. 2006). The grains collected during this mission are representative of the most refractory component of comets, emitted from the nucleus, that survived the collection process. Until the *Rosetta* mission succeeds in landing the *Philae* probe at the surface of Comet 67P/Churyumov–Gerasimenko in 2014, the only way to study

H. Cottin (✉) · N. Fray
Laboratoire Interuniversitaire des Systèmes Atmosphériques, Universités Paris 12 et Paris 7,
UMR CNRS 7583, 61 Av. du Général de Gaulle, Créteil 94010, France
e-mail: cottin@lisa.univ-paris12.fr

the whole unaltered molecular composition of cometary nuclei will be in an indirect way, reconstructing the composition of the nuclei from what we can probe in their atmospheres.

The simplest way to describe chemistry within cometary atmospheres is the application of Haser's model which supposes that 'parent molecules' are released only by the nucleus ices sublimating and that 'daughter molecules' are produced solely by the photodissociation of a single gaseous species. Moreover, this simple model requires many hypotheses: radial expansion of molecules at constant velocity, stationary state of the gas production, spherical symmetry around the nucleus, and destruction of the 'parent' species by photodissociation (Haser 1957). More advanced hypothesis have to be introduced into models to take into account a chemistry more elaborated than simple photolysis (proton transfer, dissociative recombination, etc.), and more elaborated physics than radial transport at constant velocity (hydrodynamic models, magnetohydrodynamic & Monte Carlo models (Rodgers et al. 2004; Ip 2004; Combi et al. 2004)). However, approaching the distribution of parent molecules in comets via a Haser distribution is usually sufficient, while the study of species formed in the coma requires the other kind of modelling.

The present paper focuses specifically on distributed sources, also called sometimes 'extended' sources in the literature. Properly speaking, this term could apply to any compound formed in the coma from a parent molecule by any kind of process (photolysis, electron impact, charge exchange reactions, dissociative electron recombination . . .). However, such mechanisms are considered as normal coma chemistry, and do not require the introduction of an additional term. In common cometary terminology, the use of "distributed sources" or "extended sources" can be confusing as it is not really associated to a clear and self consistent definition. It often refers to the production of a molecule in the coma through an unknown process, with no associated known parent. In the book Comets II (Festou et al. 2004), the following definition is given in the glossary:

> Extended source – Most stable molecular species (as opposed to radicals, atoms and ions) appear to be emitted directly from the nucleus. Some stable molecular species appear to have at least one component that is produced in the coma from another source. Processes that have been suggested are sublimation from grains or large polymerized molecules, photon-induced desorption or photo-sputtering from grains or large molecules, gas-phase chemistry in the coma, or photodissociation of other parent molecules. Well known examples in comets are extended source components of H_2CO and CO. The term "distributed source" is also often used.

We do not endorse this definition as it excludes radicals while CN, C_2 and C_3 radicals are also often associated with a distributed source, and including these species in the present definition would also include any compound produced in the coma through the mechanisms mentioned above. Moreover, the term "extended source" is rather ambiguous as it is also used to describe the extended nature of the gas and dust release across the nucleus surface (for example in Thomas et al. 1988). This problem is clarified by using the word *distributed*. It also makes sense to favour this term since it is the common mathematical word used to describe inhomogeneous terms in differential equations, e.g., the right-hand-sides of the conservation equations presented later in this paper. Therefore, using the word *distributed* causes less confusion and is more consistent with common science/mathematics usage.

Taking into account the previous discussion, we propose the following definition:
A *distributed source* is an additional source of a gaseous species being produced in the coma from the grains. It is an exchange of mass between the dust and the gas inventory of the coma. Henceforth, we restrict the expression "distributed source" to the production of gaseous species in the coma from solid materials. In this usage, mechanisms that simply

change one gaseous molecule to another, keeping the mass budget unchanged, are understood as chemistry, and not distributed sources. We propose the use of the term "secondary source" in this case as opposed to distributed to avoid any confusion and the use of "additional source" to cover both distributed and secondary sources. The present definition of the distributed sources seems rather consistent, for future use and with its historical use in the literature. Of course, it may not be known from observations alone whether an enhancement in the density of a species in the coma is due to a dust (distributed) source, but such a situation can't be avoided at present.

To date, the origins of observed species tagged as "distributed" are unknown or at least uncertain. The first section of this paper is a review of the observations of distributed species while interpretations of these observations are discussed in the second section.

1 Observations

The best way to reveal the origin of the production of a gaseous species detected in the atmosphere of a comet, and whether it is directly released from the nucleus, produced by chemistry in the gas phase, or by a distributed source, is to determine its radial distribution in the coma. Moreover, to make a distinction between a production by chemistry or a distributed source, the spatial distributions have to be carefully analysed. In some cases, densities of gaseous species as a function of the distance from the nucleus were measured in-situ by mass spectroscopy. This technique has revealed for the first time the existence of distributed sources in the coma of Comet 1P/Halley (Meier et al. 1993). Nevertheless, the spatial distribution of gas species is generally determined by long-slit spectroscopy at infrared, visible and ultraviolet wavelengths as well as by coarse mapping or interferometry at millimeter wavelengths (Bockelée-Morvan et al. 2004).

Others observational clues on the existence of distributed sources can be found. Indeed generally, the heliocentric evolution of the production rates of molecules produced by a distributed source is steeper than the one of molecules produced from the nucleus (Bockelée-Morvan and Rickman 1997). Moreover, the line shape at millimeter wavelengths, which is characteristic of the motion of gas species in the coma, could give clues on the production mechanism (Gunnarsson et al. 2002; Womack et al. 1997).

In this chapter, we review the observational evidences for some of the distributed source for H_2CO, CO, HNC, CN and some sulfur compounds. Concerning C_2 and C_3 radicals, for which the nature of the parents is uncertain, some information can be found in Combi and Fink (1997), Festou (1999) and Helbert et al. (2005).

1.1 Distributed Source for H_2CO

The radial distribution of H_2CO in the coma of 1P/Halley has been deduced from in-situ measurements by the Neutral Mass Spectrometer (NMS) onboard the Giotto spacecraft (Meier et al. 1993; Eberhardt 1999). It has been shown that its density profile cannot be reconciled with its only source in the nucleus. The additional source for the H_2CO production has been confirmed by coarse mapping at radio wavelengths in Comets C/1990 K1 (Levy), C/1989 X1 (Austin) (Colom et al. 1992) and C/1996 B2 (Hyakutake) (Biver et al. 1999). In Comet C/1995 O1 (Hale-Bopp), interferometric observations have also shown that H_2CO had an additional source (Wink et al. 1997; Bockelée-Morvan and Crovisier 2000; Milam et al. 2006). All these observations suggest that the production scale length for H_2CO is about 7000 km at 1 AU, which does not fit with the photodissociation of any known

possible gaseous parent (see Sect. 2). These observations have been performed for heliocentric distances lower than 1.5 AU. Moreover, the H_2CO production rates measured in C/1995 O1 (Hale-Bopp) present a very steep heliocentric evolution which suggests that the origin of some H_2CO is distributed out to 4 AU (in and outbound) (Biver et al. 2002a; Bockelée-Morvan and Rickman 1997).

1.2 Distributed Source for CO

In a similar manner than for H_2CO, an additional and potentially distributed source for CO has been discovered in the coma of 1P/Halley thanks to in situ measurements by mass-spectrometry (Eberhardt et al. 1987; Eberhardt 1999). These measurements indicate that approximately one third of the total CO is produced directly from the nucleus, while the remainder of CO comes from an additional source located in the innermost 25 000 km of the coma (Eberhardt 1999). Determination of the CO spatial distribution by infrared long-slit spectroscopy has confirmed the existence of a CO additional source in Comet C/1996 B2 (Hyakutake) (DiSanti et al. 2003). This observation suggests a parent scale length of about 1000 km and a release rate from nucleus that accounts for about 80% of total observed CO. A coarse map of the CO spatial distribution has also been obtained at millimetre wavelengths in this comet (Biver et al. 1999). Both observations are compatible with most of the CO being released from the nucleus, at least within the innermost 1000 km in the coma. As these observations do not extend farther than 7000 km in the coma, they are not sensitive to other sources with a scale length as large as the one observed in Comet 1P/Halley. In Comet C/1995 O1 (Hale-Bopp), the spatial distribution of CO has been determined by infrared long slit spectroscopy by numerous authors (Brooke et al. 2003; Disanti et al. 2001, 1999; Weaver et al. 1997) for heliocentric distances smaller than 2 AU. These observations suggest that the production of additional CO reaches its terminal value at a distance of about 7000 km from the nucleus at 1.49 AU and 5000 km at 1.06 AU (Brooke et al. 2003; Disanti et al. 2001). The ratio of nucleus to additional sources release rates determined from these infrared observations remains controversial. Indeed, according to different authors, the release of CO from additional source could represent 50% (Disanti et al. 2001) or 90% (Brooke et al. 2003) of the total. Beyond 2 AU from the Sun, only the nucleus source was seen by infrared long slit spectroscopy (Disanti et al. 2001). Nevertheless, this observation seems to be contradictory with the ones performed in the radio domain, which probe larger fractions of the coma than the infrared observations. The radio observations show that at large heliocentric distances, the profiles of the CO radio lines in Comet C/1995 O1 (Hale-Bopp) could be fitted assuming a production by a distributed source (Gunnarsson et al. 2003). Interferometric maps of the CO spatial distribution have been obtained when the comet was close to perihelion (Henry et al. 2002). They show strong deviations from those expected for an isotropic distribution of CO, probably caused by the existence of CO jets. One may also note that the heliocentric evolution of the CO production rates in Comet C/1995 O1 (Hale-Bopp) is not as steep as for H_2CO, HNC or CS (Biver et al. 2002a) as one might expect from distributed sources. First coarse mapping at millimeter wavelengths of CO in Comet 29P/Schwassmann–Wachmann 1 at 6.2 AU seems to reveal a strong additional source at such heliocentric distances (Gunnarsson et al. 2002). Nevertheless, new observations and analysis of the CO line profile indicate that the additional source, if present, is very weak (Gunnarsson et al. 2008). Since the observations seem to be inconsistent, a summary of them is given in Table 1.

Table 1 Summary of the observations of the CO additional source

Comet	References	Observational method	R_H (AU)	Remarks
1P/Halley	Eberhardt et al. 1987	(1)	0.9	• Production of CO at $\rho < 20\,000$ km
	Eberhardt 1999	(1)	0.9	• $Q_{nucleus}(CO)/Q_{nucleus}(H_2O) = 3.5\%$ • $Q_{total}(CO)/Q_{nucleus}(H_2O) = 11\%$ • Production of CO at $\rho < 25\,000$ km
C/1996 O2 (Hyakutake)	DiSanti et al. 2003	(2)	0.64–1.06	• $Q_{nucleus}(CO) = 14.9\%$ • $Q_{total}(CO) = 19.1\%$ • Production of CO at $\rho < 10^3$ km for $R_H = 0.64$ AU • Production of CO at $\rho < 2$–$3 \cdot 10^3$ km for $R_H = 1.06$ AU
	Biver et al. 1999	(4)	1.24	• $Q_{nucleus}(CO) \approx Q_{total}(CO)$ • $L_P \approx 400$ km (*)
C/1995 O1 (Hale-Bopp)	Weaver et al. 1997	(2)	1.1	• Detection of a CO distributed source
	Disanti et al. 1999 and 2001	(2)	0.93–4.11	• Detection of a CO distributed source only for $R_H < 2$ AU • $Q_{nucleus}(CO)/Q_{total}(CO) \approx 50\%$ for $R_H < 2$ AU • Production of CO at $\rho < 6$–$7 \cdot 10^3$ km for $R_H = 1.49$ AU and at $\rho < 5 \cdot 10^3$ km for $R_H = 1.06$ AU
	Brooke et al. 2003	(2)	1.02–1.05	• Detection of a CO distributed source • $Q_{nucleus}(CO)/Q_{total}(CO) \approx 10\%$ • $L_P \approx 5000$ km (*)
	Gunnarsson et al. 2003	(3)	3.7–10.8	• Detection of a CO distributed source • $Q_{nucleus}(CO)/Q_{total}(CO) \approx$ 10–60%
	Henry et al. 2002	(5)		• Presence of a spiral CO jet
	Biver et al. 2002a	(6)		• No steep heliocentric evolution of Q(CO)

(1) In-situ mass spectrometry
(2) Long slit spectroscopy at infrared wavelengths
(3) Analysis of the radio line profile
(4) Coarse mapping at radio wavelengths
(5) Interferometry at radio wavelengths
(6) Determination of the production rates at radio wavelengths
(*) L_p: production scale length of the distributed molecule. See precisions in Sect. 2.1

1.3 Distributed Source for HNC

HNC, which is an isomeric form of HCN, was detected for the first time in Comet C/1996 B2 (Hyakutake) (Irvine et al. 1996) at millimeter wavelengths. It was then observed in C/1995

O1 (Hale-Bopp) (Biver et al. 2002a; Irvine et al. 1998a) and in other comets (Biver et al. 2002b, 2006). In Comet C/1995 O1 (Hale-Bopp), interferometric observations made it possible to measure the HNC spatial distribution (Wink et al. 1997), which deviates from that of HCN in the innermost coma, and indicates production of HNC in the coma. Nevertheless, the main indication of an HNC distributed source is the heliocentric dependence of the HNC/HCN ratio. Indeed, as for the H_2CO production rates, this ratio increases with decreasing heliocentric distance in Comet C/1995 O1 (Hale-Bopp) (Biver et al. 2002a), C/2002 C1 (Ikeya-Zhang) (Irvine et al. 2003) as well as for other comets (Biver et al. 2006).

1.4 Distributed Source for CN

Reviews about the existence of the CN additional source have already been published (Festou 1999; Fray et al. 2005). It is clear that at least some of the CN radicals are produced in the coma through HCN photodissociation. Nevertheless, it is not clear if this mechanism could solely explain the abundance of CN. Indeed CN and HCN production rates have the same order of magnitude in most of the comets and considering the uncertainties in their production rates, we cannot conclude if HCN is the only parent molecule of CN or not in most of the comets. In comets, the $^{14}N/^{15}N$ isotopic ratios in CN is about two times lower than on Earth (Hutsemékers et al. 2005). First measurements of the $^{14}N/^{15}N$ in HCN (Jewitt et al. 1997; Ziurys et al. 1999) lead to values close to the terrestrial one. This was a major indication that HCN could not be the unique parent molecule of CN radicals until new measurements in comet 17P/Holmes and reanalysis of the older observations show that the $^{14}N/^{15}N$ isotopic ratio in CN and HCN are about the same (Bockelée-Morvan et al. 2008). Nevertheless, from this new result, we cannot exclude that CN has other major progenitors, than HCN, sharing the same low $^{14}N/^{15}N$ isotopic ratio (Bockelée-Morvan et al. 2008). The spatial distribution of CN has been measured in numerous comets by long-slit spectroscopy at UV wavelengths. From these observations, it seems that CN radicals could be entirely produced by the HCN photodissociation for heliocentric distances greater than 3 AU. Nevertheless, closer to the Sun, the CN spatial distribution is too narrow to be explained only by this process (Bockelee-Morvan and Crovisier 1985; Fray et al. 2005). Indeed for heliocentric distance less than 3 AU, the CN parent scale length is lower than the HCN photodissociation scale lengths (see Fig. 1).

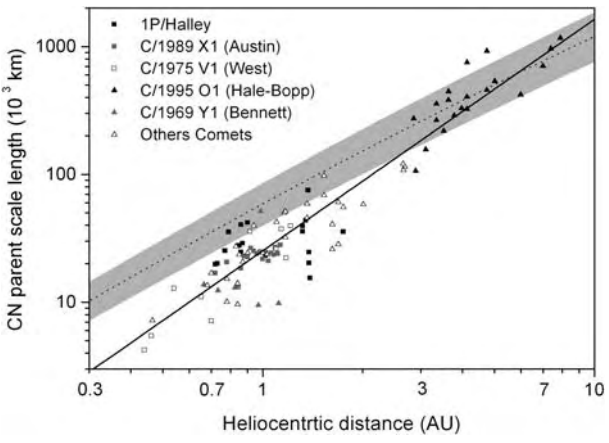

Fig. 1 Measured CN parent scale lengths as a function of the heliocentric distance. The CN parent scale lengths have been normalized to the minimum of solar flux and the *black line* is the best fit to these data. The *dashed line* is the effective CN parent scale length assuming that CN is produced exclusively by photodissociation of HCN. The *grey region* represents the error on the effective CN parent scale lengths due to uncertainties in the photodissociation rate of HCN and in the expansion velocity (figure from Fray et al. 2005)

1.5 Distributed Sources for Other Species

The radial distribution of OCS has been determined in Comet C/1995 O1 (Hale-Bopp) at about 1 AU from the Sun by infrared long-slit spectroscopy (Dello Russo et al. 1998). This observation suggests that about 70% of the total production of OCS comes from an additional source having a parent scale length of 3000–3500 km. The fact that most sulfur is contained in the refractory CHON grains suggests that OCS may be derived from refractory grains by a distributed source. However, as the mechanism for a distributed source for OCS is unknown, an additional contribution from other gaseous species cannot be ruled out.

CS has been observed in different comets at millimeter and ultraviolet wavelengths. The CS/HCN and CS/H_2O production rate ratios increase with decreasing heliocentric distance in all the comets for which CS has been observed (Biver et al. 2000, 2002a, 2006). The spatial distribution of CS has been determined thanks to coarse mapping at millimeter wavelengths in Comet C/1996 B2 (Hyakutake) at 0.7 AU (Biver et al. 1999) suggesting a parent scale length of about 1200 km. Whereas this value is roughly in agreement with the photodissociation scale length of CS_2, which has been tentatively detected in Comet P/122 de Vico (Jackson et al. 2004), the increase of CS abundance with decreasing heliocentric distance suggests that CS is also produced by an additional mechanism (Biver et al. 2006).

In Comet C/1995 O1 (Hale-Bopp), the SO spatial distribution has been measured by interferometry at millimeter wavelengths (Wink et al. 1997). This observation shows clearly that SO is a daughter species. SO is at least produced in part by the photodissociation of SO_2. Nevertheless, its production rate is greater than the one of SO_2, suggesting an additional production mechanism of SO (Bockelée-Morvan et al. 2000; Boissier et al. 2007).

First detection of radical NS is reported in Comet C/1995 O1 (Hale-Bopp) (Irvine et al. 2000). In their paper, the authors state that whether NS itself is present in the nucleus or has a distributed source in the coma is unknown.

2 Interpretations

2.1 General Discussion

Understanding the chemistry of comets is quite a difficult task. The additional sources, including distributed and secondary sources, do not have an origin based on the same mechanism. Some physical and chemical mechanisms which could explain the origin of secondary and distributed (i.e. additional) sources are summarized in Fig. 2. Some production of gaseous species may result from the dissociation (photolysis or other chemical processes including electron impact (Helbert et al. 2005)) of several gaseous parents (among which some may not have been detected to date) or chemistry between two gaseous compounds in the innermost coma. Distributed sources include sublimation of icy grains in the coma or the production of gaseous compounds during the degradation of solid organic material contained in cometary dust particles.

Indeed, it is now established that the organic content of comets is more complex than what is seen in the gaseous phase alone. Most of the detections presented in the above section are all remote sensing observations, probing the gaseous phase of comets, leading to the detection of about 20 stable gaseous molecules (Bockelée-Morvan et al. 2004). However in 1986, Vega 1 & 2 and Giotto spacecrafts probed the atmospheres of Comet 1P/Halley. Molecular analyses of solid particles in the coma were conducted by mass spectrometry and resulted in the detection of solid organic compounds much more complex than the gaseous

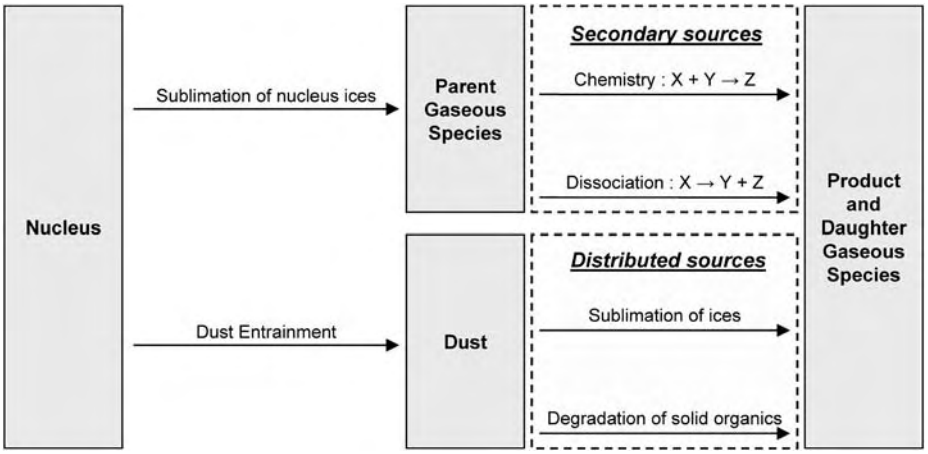

Fig. 2 Chemical mechanisms of production of the gaseous species in the cometary environment. The 'secondary' and 'distributed' sources have been clearly distinguished

ones securely detected from the Earth. It showed that more organic material is present, in the solid state, and that its molecular mass can reach value above 150 amu (Kissel and Krueger 1987; Mitchell et al. 1992). In-situ results from the Stardust mission (with the CIDA mass spectrometer) have confirmed these observations (Kissel et al. 2004). Recently, the analysis of grains captured from Comet 81P/Wild 2 by the Stardust spacecraft has also enabled the detection of complex organic material made of aliphatic and aromatic hydrocarbons, and molecules bearing a large range of organic functions (hydroxyl, carbonyl, amide, nitrile . . .) with high molecular weight (up to 300 amu) (Keller et al. 2006; Sandford et al. 2006).

For an even better insight into the most complex and less volatile material, one can turn to experimental laboratory work. The principle of such experiments is the following: from observations of the most abundant species in comae and in the interstellar medium, one can infer probable compositions of the nucleus ices. A gaseous sample of the key species is condensed under near vacuum conditions on a cold substrate and irradiated by UV photons or charged particles. Sometimes, condensed ices are also simply warmed up slowly without irradiation. These processes are similar to the ones precometary ices may have encountered in the Solar Nebula or in the interstellar medium and they allow the synthesis of complex organic compounds from the initial simple ice. When the sample is warmed up for analysis, a refractory organic residue remains on the substrate at ambient temperature. The diversity of organic compounds synthesized during those experiments is remarkable (Greenberg 1982; Colangeli et al. 2004; Despois and Cottin 2005), and this mixture of molecules can be considered as an analogue of the solid organic component of comets.

In the frame of the study of distributed sources, a new generation of cometary laboratory experiments has been developed. Proceeding in an opposite direction than the 'classical' ice experiments, they study the production of gaseous compounds during the photo-degradation (induced by the solar UV flux) and the thermal-degradation (induced by dust particles heating) of complex solid molecules suspected to be present in cometary dust particles, once they are ejected in the coma. Such experiments are described in Cottin et al. (2000), Fray et al. (2004a, 2004b) and an example is given in Fig. 3.

These experiments are not actually meant to *simulate* the cometary environment, but rather to measure physico-chemical data, such as production quantum yields (photo-

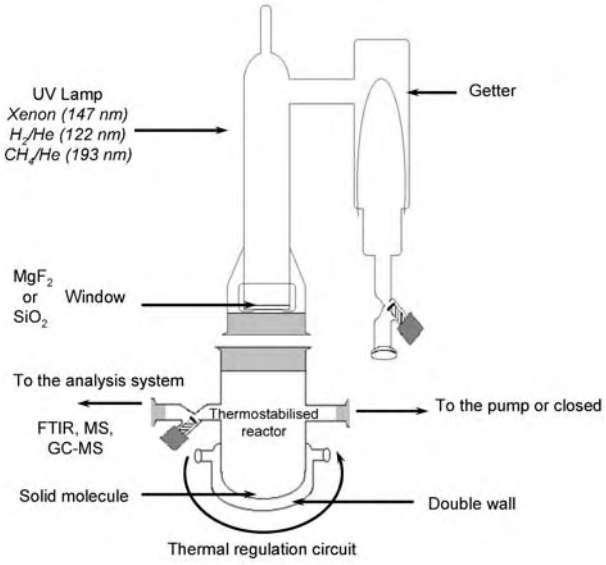

Fig. 3 Experimental setup dedicated to the study of the degradation of solid organic material into gaseous fragments. The solid organic molecule is deposited at the bottom of a Pyrex reactor where it can be heated with a thermal regulation circuit or photolyzed (at different wavelengths) with a UV lamp located at the top of the reactor. Gaseous degradation products can then be analyzed by infrared spectroscopy, direct mass spectrometry or gas chromatography coupled with a mass spectrometer (more details in Cottin et al. 1999, 2000)

degradation), Arrhenius constants and activation energies (thermal-degradation), characteristic of the gaseous production resulting from the decomposition of some specific targeted solid material. Results obtained after that kind of experiments, which were not necessarily conducted in a cometary context, are summarized in Table 2.

These quantitative data are then included into numerical models simulating the production of gaseous species during the degradation of solid compounds ejected in the cometary atmosphere on dust particles. The purpose of these models is to calculate the spatial distribution of the gaseous species produced by these mechanisms. With hypotheses similar to the classical Haser's approach, these models are based on the equation of conservation.

If a gaseous species is produced solely by the photodissociation of a unique parent molecule, then the conservation equation can be written:

$$\frac{\partial n_D}{\partial t} + div(n_D.v_{gas}) = \beta_P.n_P - \beta_D.n_D. \quad (1)$$

Here n_P and n_D are the number density (m^{-3}) of the parent and daughter molecules respectively, β_P and β_D the photodissociation rates (s^{-1}) of the parent and daughter molecules and v_{gas} the gas expansion velocity in the coma ($m\,s^{-1}$) assumed to be constant. In the frame of the Haser's model, the parent (l_P) and daughter (l_D) scale lengths are defined as the product of the gas expansion and the photo-lifetime (reciprocal of the photodissociation rate). The distribution of daughter molecules produced by the photo processes of a single gaseous parent is shown in (2), where Q_P and Q_D are the spherically symmetric production rates of parent and daughter molecules (s^{-1}).

$$n_D(r) = \frac{1}{r^2}\left(\frac{Q_P}{4\pi v_{gas}}\frac{l_D}{l_P - l_D}(e^{-r/l_P} - e^{-r/l_D}) + \frac{Q_D}{4\pi v_{gas}}e^{-r/l_D}\right). \quad (2)$$

In most cases, the parent and daughter scale lengths are measured by adjustment of the observations with (2). This parent scale length is then compared to the photodestruction rate of a candidate parent molecule. This comparison gives important clues on the nature

Table 2 Summary of data available on the degradation of potential precursors of distributed sources

	Photodegradation			Thermal degradation		
POM	Products and production quantum yields for various wavelength from Cottin et al. (2000)			H_2CO is the only product. Kinetic parameters for its production as a parameters for its production as a function of T (Arrhenius law) for two different POM polymers are given below. From Fray et al. (2004a).		
	λ (nm)	122	147	193		Ea ($J\,mol^{-1}$)	A ($molec\,g^{-1}\,s^{-1}$)
	H_2CO	0.75 ± 0.21	0.96 ± 0.19	<0.16	POM 1	81×10^3 ±0.76%	1.2×10^{30} +28%/−22%
	HCOOH	0.13 ± 0.05	0.26 ± 0.10	ε			
	CO	NE	~ 1	ε	POM 2	99×10^3 ±2.3%	7.2×10^{32} +140%/−60%
	CO_2	NE	~ 0.3	ε			
	CH_3OH	~ 0.05	~ 0.05	ε			
	NE : Present but not estimated						
HMT	Some HCN detected at 147 nm but at level too low to be quantified (Cottin et al. 2002)			No thermal degradation. HMT sublimates when heated under vacuum (Fray 2004)		
HCN polymer	Some HCN, CH_4 and C_2H_2 are produced with quantum yields lower than 0.03 at 122 and 147 nm (Fray 2004; Fray et al. 2004b)			NH_3 and HCN are the major products of the thermal degradation (Fray et al. 2004b). The production kinetics have been measured for $T > 420$ K (Fray 2004). Nevertheless, for lower T, the production declines to very low value (unpublished results)		
C_3O_2 polymer	No data available			For $T > 400$ K: release of CO_2 For $T > 500$ K: increased efficiency in the degradation, with release of CO_2 and CO. CO/CO_2 ratio increases with T. From Blake and Hyde (1964) and Smith et al. (1963)		

of the gaseous parent molecule. Nevertheless, one should keep in mind that the ejection velocity acquired by the daughter species during the photolysis of the parent is neglected. This actually changes the physical meaning of the parent scale length (Combi and Delsemme 1980), but as a first approximation this results in estimations usually sufficient to suggest a possible parent.

In the case of a production from the degradation of solid material in cometary dust particles, the conservation equation is:

$$\frac{\partial n_D(r)}{\partial t} + div(n_D(r) \cdot v_{gaz}) = \left(n_{grain}(r) \cdot \sigma_\alpha(r) \cdot C_D\right) + \left(n_{grain}(r) \cdot m_\alpha(r) \cdot k_D(T)\right) - \left(\beta_D \cdot n_D(r)\right). \quad (3)$$

In the right side of this equation, the first two terms are the production of the considered gaseous species by the photo- and the thermal-degradation of the solid material. In this equation, n_{grain} is the grain density in the coma (m^{-3}), σ_α the surface of material exposed to the

Solar flux and C_D the production rate of gaseous species by photo-degradation ($m^{-2}\,s^{-1}$), m_α the mass of solid material in each particles and k_D the production rate of the gaseous species by thermal-degradation ($kg^{-1}\,s^{-1}$).

With classical Haser's hypotheses regarding the dynamics in the coma, two scale lengths related respectively to the thermal- (l_T) and photo-degradation (l_P) can be defined (Cottin et al. 2004; Fray et al. 2006) and (3) is integrable analytically. Then, n_D can be written:

$$n_D(r) = \frac{1}{4\pi r^2 v_{gas}} \left\{ \begin{array}{l} \frac{3Q_{grain}\beta^3 m_\alpha}{m_D l_T X} \left[\begin{array}{l} l_D(1-X)(1-e^{-\frac{r}{l_D}}) \\ +\frac{(3X-2)(1+1/\beta)}{(1/l_D-1/l_T)}(e^{-\frac{r}{l_T}}-e^{-\frac{r}{l_D}}) \\ +\frac{(1-3X)(1+1/\beta)^2}{(1/l_D-2/l_T)}(e^{-\frac{2r}{l_T}}-e^{-\frac{r}{l_D}}) \\ +\frac{X(1+1/\beta)^3}{(1/l_D-3/l_T)}(e^{-\frac{3r}{l_T}}-e^{-\frac{r}{l_D}}) \end{array} \right] \\ +Q_D\, e^{-\frac{r}{l_D}} \end{array} \right\}. \quad (4)$$

Where Q_{grain} is the production of grains of a specific size and composition, β is the ratio l_T/l_P, m_D the mass of the daughter molecule, X is related to the photoproduction of the daughter compound, and Q_D the contribution from the nucleus to the production of the molecule (more details can be found in Cottin et al. (2004)).

Even if this equation can be simplified in the case that either thermal or photo degradation is not relevant (one being negligible compared to the other), (4) has to be integrated over the whole size distribution of dust particles, taking into account the velocity and temperature for each size range. Moreover, the scale lengths related to the degradation of solid material depend on the initial composition of the cometary dust particles: they are not characteristic for a specific solid material. Therefore, parent scale length, as the one used with gaseous parents (2) has no direct equivalent here and a discussion about this parameter is useless for identifying a parent compound in the solid phase. As an example, measuring the scale length of the parent of formaldehyde, which is about 7000 km at 1 AU as mentioned in Sect. 1.1, is purely formal and unfortunately of no help in assessing the nature of the parent if it is in the solid phase.

2.2 Origin of H_2CO

Adjusting the spatial distribution of formaldehyde in Comet 1P/Halley would be quite simple considering the photodissociation of CH_3OH. If H_2CO is considered as the main CH_3OH photoproduct (for rate coefficients see Huebner et al. 1992), methanol would have to be produced from the nucleus at a level of 16% relative to water to obtain a good fit to measurements (Cottin et al. 2004). But methanol is only produced in amounts ranging from ~ 1 to 6% in comets (Bockelée-Morvan et al. 2004). Moreover, as discussed in Bockelée-Morvan et al. (1994), formaldehyde is not the main dissociation product of methanol, but rather the CH_3O methoxy radical. Thus, the additional source of cometary H_2CO is not consistent with a production from the CH_3OH photodissociation.

Formaldehyde is known to polymerize into long linear molecules (–$(CH_2$–O$)_n$–) called polyoxymethylene (POM) (Fig. 4). This polymer was invoked in the cometary context to interpret a mass spectrum obtained with the PICCA instrument on board the Giotto spacecraft, between 8200 and 12600 km from the nucleus of Comet 1P/Halley. Indeed, Huebner (1987) suggested that the alternation of patterns with $\Delta m/z = 14$ and 16 shown in the PICCA spectrum is consistent with a sequence of –CH_2– ($m = 14$) and –O– ($m = 16$). But few years later, Mitchell et al. (1992) showed that the PICCA mass spectrum is not

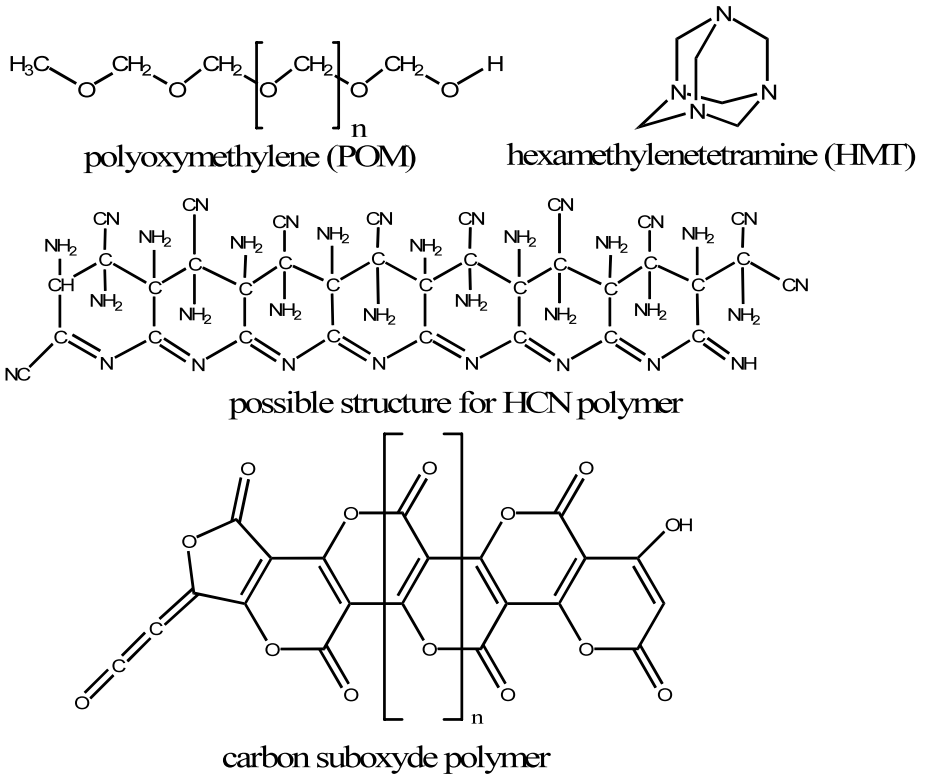

Fig. 4 Molecular structures of molecules evoked in this paper as possible parents for observed distributed sources. Structure of HCN polymer is one possible among others (see Minard et al. 1998 for more structures). Structure of carbon suboxide polymers proposed by Ballauff et al. (2004)

specifically characteristic of POM: the regular pattern observed is only the signature of a mixture of organic molecules composed of C, H, O, N atoms. Thus, even if the observed spectrum is not sufficient to establish its presence definitively, the presence of POM in cometary nucleus and dust particles cannot be ruled out at this stage. Furthermore, its production is possible under certain conditions in laboratory simulated interstellar and precometary ices (Schutte et al. 1993). Therefore, polyoxymethylene has often been suggested as the H_2CO distributed source (see, e.g. Boice et al. 1989, 1990; Meier et al. 1993; Eberhardt 1999). Boice et al. (1990) tried to estimate the production of formaldehyde from POM, but with the hypothesis that short polymer chains are emitted from dust particles and photodissociated in the gas phase. Because of the lack of experimental data, photodissociation rates were estimated from formaldehyde and related molecular bond strengths, without any direct laboratory measurement. Meier et al. (1993) showed that this does not fit the *Giotto* measurements.

First quantitative data considering the production of gaseous H_2CO by photo- and thermal-degradation of solid polyoxymethylene have been measured with the experimental setup shown Fig. 3 and described by Cottin et al. (2000) and Fray et al. (2004a). It has been shown that the major gaseous species produced by the photo-degradation of POM at 122 and 147 nm was H_2CO and CO and their production quantum yields have been measured (Cottin et al. 2000 and Table 2). Moreover, H_2CO is the sole gaseous species produced

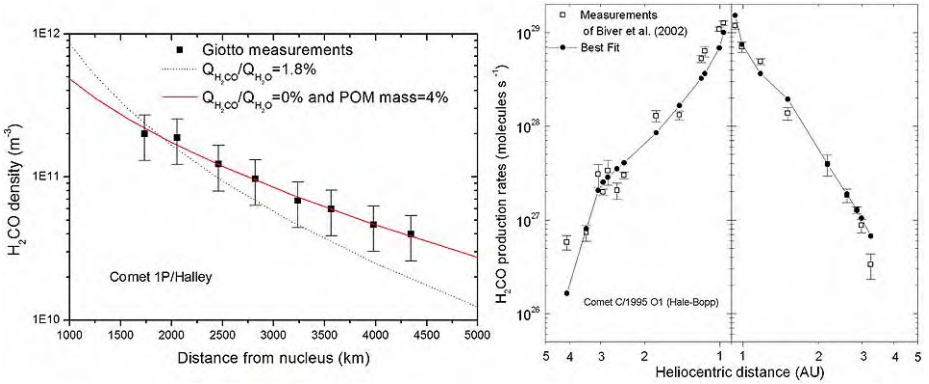

Fig. 5 *On the left*: H_2CO density profile in Comet 1P/Halley: measured by Giotto spacecraft (*squares*), and calculated considering a distributed source from solid polyoxymethylene (*continuous line*). This fit is obtained if POM represents 4% in mass of dust particles and H_2CO is not released from the nucleus. *Dotted line* is the best fit with no distributed source, obtained if 1.8% of H_2CO (relative to H_2O) is released from the nucleus. *On the right*: H_2CO production rates as a function of heliocentric distance in Comet C/1995 O1 (Hale-Bopp). The measurements of H_2CO are represented as open squares and the computed values as *black circles*. The latter have been obtained considering a POM mass fraction in the dust particles of 3.1% and H_2CO production at the surface of the nucleus equal to 3% of HCN production (i.e. $Q(H_2CO)/Q(H_2O) = 0.0075\%$)

by the thermal-degradation of POM. Its production kinetics follows an Arrhenius law and the Arrhenius constants and activation energies have been measured (Fray et al. 2004a and Table 2).

The production of gaseous formaldehyde in the coma from solid polyoxymethylene has been modelled using these quantitative data. If we consider that a few percent in mass of POM is present on dust particles when they are ejected from the nucleus, the spatial distribution of H_2CO in 1P/Halley as well as the steep heliocentric evolution of the H_2CO production rates in Comet C/1995 O1 (Hale-Bopp) are quite well reproduced (Cottin et al. 2004; Fray et al. 2006) (Fig. 5).

The fact that POM can account for the distributed source of formaldehyde in two comets, within the same abundance range, and for observations as a function of the nucleus distance and also as a function of the heliocentric distance, strengthens the probability of its presence without being an actual detection of the polymer in comets. The presence of POM (or POM-like polymers) in the solid state on cometary dust particles is to date the best interpretation of observations.

2.3 Origin of CO

The case of the additional source for CO is more controversial than for H_2CO. As shown in Sect. 1.2, not all the observations are consistent. The photodissociation of several gaseous molecules (C_3O_2, H_2CO and CO_2) have been proposed to explain the origin of CO in the coma.

In Comet 1P/Halley, it has been proposed that gaseous carbon suboxide (C_3O_2) could be a precursor for CO by photodissociation (Huntress et al. 1991). If present in the atmosphere of comets, C_3O_2 would be photodissociated into CO and C_2O, C_2O being photodissociated into CO and C, and be a parent molecule at least for some CO (Crovisier 1994). Nevertheless, its upper limit in this comet ($< 0.1\%$) is far from the amount required to produce the CO from secondary sources (7.5%) (Crovisier et al. 1991). Thus,

photodissociation of gaseous C_3O_2 cannot alone explain the formation of CO, even if it has been shown in the laboratory that it can be present in cometary ices (Brucato et al. 1997; Gerakines and Moore 2001). Looking for another gaseous parent, Meier et al. (1993) suggests that H_2CO is a precursor of 2/3 of the CO from an additional source, while later reanalysis of the data led to the conclusion that distributed formaldehyde produced from degradation of polyoxymethylene could fully explain all of the additional CO under certain assumptions such as the kinetics of POM degradation which were not known at that time (Eberhardt 1999). A comprehensive modelling with current knowledge of POM properties has yet to be done to settle this question for Comet 1P/Halley. If one considers CO_2 as a parent for CO, the CO Cameron system in the UV wavelength domain would be expected. It has been observed in several comets (Biermann 1976; Weaver et al. 1994; Bockelée-Morvan et al. 2004). This structure is thought to be produced mainly by prompt emission following the photodissociation of CO_2. Therefore it is clear that the photodissociation of CO_2 also contributes to the CO production in the coma. Nevertheless, as the photodissociation rate of CO_2 is very low ($\beta_{CO_2} = 2 \cdot 10^{-6}$ s^{-1}) (Huebner et al. 1992), this mechanism cannot explain the observed scale length of the CO distributed source. In Comet 1P/Halley, it is not yet settled whether a mechanisms different than the photodissociation of other gaseous molecules has to be considered to explain the CO additional source.

In Comet C/1995 O1 (Hale-Bopp), the additional source of the CO in the atmosphere seems to be triggered at 2 AU (Disanti et al. 2001). The photolysis of a gaseous parent would not result in the same kind of observation, which suggests some thermal threshold from which a solid precursor might start to decompose and release CO in the gas phase. Looking for a solid precursor leads one to consider if POM could also be the origin of the additional CO. But even if photo-degradation of POM yields a small amount of CO (about the same order of magnitude than for H_2CO (Cottin et al. 2000), no CO is produced by thermal-degradation, which is the dominant degradation mechanism of POM for most of dust particles. Also, if CO from distributed sources in C/1995 O1 (Hale–Bopp) originated from POM degradation, then one should expect H_2CO production from distributed sources to at least equal that for CO, and more probably be larger by perhaps as much as one or two orders of magnitude. This would result in more H_2CO than CO in the coma, which is not the case. Thus, POM cannot be the main precursor for carbon monoxide.

As we already discussed in this section, gaseous carbon suboxide is not sufficient to produce the observed amount of CO from additional sources. But its polymer (carbon suboxide polymer, shown in Fig. 4) is known to decompose into CO_2 and CO when pyrolysed. The polymer starts to release some gas (CO_2) at about 400 K, but only due to structural changes, the mass loss is low. Above 500 K the polymer degrades with increased efficiency as the temperature rises and with an additional production of CO. The CO/CO_2 ratio tends to 1/1 above 700 K and with increasing time (Blake and Hyde 1964; Smith et al. 1963). These studies show that if the same kind of polymers is present in comets, a distributed CO_2 source should also be observed, which, to date, is not the case. But laboratory synthesised polymer are extremely unstable as the compound is extremely hygroscopic (Schmedt auf der Günne et al. 2005). Exposed to air, it takes up atmospheric water within seconds and undergoes chemical modifications. Therefore, before reaching final conclusions about the relevance of this molecule in the cometary environment, new laboratory measurements have to be undertaken in controlled environment. Furthermore, no data about the photo-degradation of C_3O_2 polymers in VUV are currently available.

In Comet 29P/Schwassmann–Wachmann, located at large heliocentric distance , the temperature of the grains is so low that the distribution of CO in the coma can be explained by the slow sublimation of CO frozen on grains ejected from the nucleus (Gunnarsson et al. 2002, 2008). In this case, sublimation of the CO ice is a distributed source.

Because of the potential for multiple precursors, understanding the origin of CO from secondary and/or distributed sources requires probably a complete modelling work taking into account several gaseous and solid parents. Different compositions between comets, resulting in comets enriched or depleted in one or several precursors, and the use of different measurement methods probing different regions of the coma at different scales, could be an explanation for the contradictory observations.

2.4 Origin of HNC

In Comet C/1995 O1 (Hale-Bopp), Rodgers and Charnley (1998, 2005) and Irvine et al. (1998a, 1998b) show that the additional source for HNC could be accounted for by superthermal chemistry driven by fast hydrogen atoms ($HCN + H_f \rightarrow HNC + H$, with H_f = fast H). This would then be a secondary source. But this mechanism is only efficient in the relatively dense environment of Comet C/1995 O1 (Hale-Bopp), and due to the failure of such superthermal reactions to produce efficiently HNC in less active comets (Irvine et al. 2003; Rodgers and Charnley 2001, 2005), it seems more reasonable to look for other processes for the origin of HNC from additional sources.

Therefore, these authors propose the degradation of an unknown solid organic parent as the origin for the HNC from distributed sources. Candidates are the same as the ones presented and discussed in the next section for the parents of CN from distributed sources. However, quantitative and even qualitative data about its production by thermal or photo-degradation of refractory parents are rather difficult to obtain, since HNC is not easy to detect because of its rapid isomerisation into HCN in laboratory.

2.5 Origin of CN

The CN radicals may be produced by HCN photodissociation and another unknown mechanism. As the observed spatial distribution of CN is less distributed than the predicted distribution of CN produced solely by HCN photodissociation (Fig. 1), the scale length of the unknown production process has to be shorter than the observed production scale lengths (Fray et al. 2005). If the unknown mechanism is the photodissociation of a gaseous molecule, its lifetime has to be shorter than that of HCN. This is the case for HC_3N and C_2N_2. Nevertheless, the HC_3N production rate measured in Comet C/1995 O1 (Hale-Bopp) does not seem to be sufficient to explain the CN distribution and C_2N_2 has never been detected in comets (Fray et al. 2005). Another hypothesis is a direct production of CN radical by degradation of complex refractory organic compounds present on cometary dust particles. This hypothesis has originally been proposed by A'Hearn et al. (1986) and Lamy and Perrin (1988). Hexamethylenetetramine (HMT) could be a candidate since it is easily synthesized from H_2CO and NH_3 during laboratory simulations of interstellar and precometary ices (Bernstein et al. 1995; Cottin et al. 2001; Muñoz Caro et al. 2004). But it has been shown that this compound is quite stable when photolyzed (Cottin et al. 2002) and no degradation has been observed when heated (HMT sublimates when heated) (Fray 2004). Thus HMT is surely not the parent molecule of CN. It has also been shown that HCN polymers, which have been proposed to be present in cometary nuclei (Rettig et al. 1992), produce HCN and NH_3 when heated (Fray et al. 2004b). Under certain circumstances, such polymers can be synthesized in interstellar or precometary ices (Gerakines et al. 2004). If one turns to other candidates, it must be noted that thermal-degradation of polyacrylonitrile leads to the formation of HCN, NH_3 and CH_4 (Xue et al. 1997) and that thermal-degradation of numerous synthetic nitrogen polymers also leads to

the formation of HCN (Michal 1982). As numerous nitrogenated compounds can produce HCN by thermal-degradation, more experiments have to be implemented to measure quantitative data needed for proper modelling.

Nevertheless, one should keep in mind that since CN parent scale length is shorter than the HCN photodissociation scale length (Fig. 1), CN has to be directly produced from the dust particles without HCN as an intermediary species (Fray et al. 2005). So far, all the experimental studies investigating the volatile compounds produced during photo- or thermal-degradation of nitrogenated organic matter have been performed in conditions in which CN radicals were not detectable, even if it was produced. Indeed, in laboratory conditions CN radicals are very reactive species turning very rapidly into HCN.

2.6 Origin of Sulfur Compounds

A recent analysis of SO interferometric observations in Comet C/1995 O1 (Hale-Bopp) concludes that the discrepancy between measured and computed values of the SO photodissociation rate may indicate that SO_2 is not the sole parent of SO, or that SO_2 is itself created by an additional source in the coma (Boissier et al. 2007). Whether this results from coma chemistry or a distributed source remains unknown.

Concerning NS detection in the same comet, Canaves et al. (2002, 2007), have published a detailed modelling of the chemistry of NS in cometary comae. Their most recent results conclude that the amount of detected NS in Comet C/1995 O1 (Hale-Bopp) can be explained by gas phase chemistry in the atmosphere. They call it a distributed source, but it would rather be a secondary source if we stick to the definitions proposed in the present paper.

Very limited interpretation can be given for distributed sources of sulfur bearing species. Indeed, except the recent references given hereabove, the literature lacks discussion about the origin of these species. If, much work remains to be done in the laboratory for C, H, O, N molecules, almost everything has to be done for C, H, S (and possibly O and N) molecules.

3 Conclusions

We are far from being able to understand the origin of distributed sources in comets. They are for sure a signature of complex chemistry in both gaseous and solid phases, but we still lack crucial data characterizing the physico-chemical properties of candidate parent compounds to reach final interpretations. More laboratory work is needed, mostly to measure how the complex refractory organic component of comets behaves on dust particles (photo- and thermal-degradation).

The discussions developed in the present paper should not leave the impression that all the distributed sources could be explained evoking the convenient degradation of some unknown solid material. If this process seems to be quite adapted to the case of formaldehyde, it is possible that it actually hides our current ignorance of some other chemical processes in the atmosphere of comets. Work remains before a conclusion can be formed. However, as our knowledge of the composition of the nucleus of comets derives from what we observe in their atmosphere, distributed sources are precious, though tangled, Ariadne's threads to follow.

Acknowledgements The authors wish to thanks the two referees for their extensive work on the paper. Their valuable reviews greatly help to improve its clarity as well for the English than for its science content.

References

M.F. A'Hearn, S. Hoban, P.V. Birch, C. Bowers, R. Martin, D.A. Klinglesmith, Nature **324**, 649–651 (1986). doi:10.1038/324649a0

M. Ballauff, S. Rosenfeldt, N. Dingenouts, J. Beck, P. Krieger-Beck, Angew. Chem. Int. Ed. **43**(43), 5843–5846 (2004). doi:10.1002/anie.200460263

M.P. Bernstein, S.A. Sandford, L.J. Allamandola, S. Chang, M.A. Scharberg, Astrophys. J. **454**, 327–344 (1995). doi:10.1086/176485

L. Biermann, NASA STI/Recon technical report N 77, 22023 (1976)

N. Biver, D. Bockelée-Morvan, J. Crovisier, J.K. Davies, H.E. Matthews, J.E. Wink et al., Astron. J. **118**, 1850–1872 (1999). doi:10.1086/301033

N. Biver, D. Bockelée-Morvan, J. Crovisier, F. Henry, J.K. Davies, H.E. Matthews et al., Astron. J. **120**, 1554–1570 (2000). doi:10.1086/301529

N. Biver, D. Bockelée-Morvan, P. Colom, J. Crovisier, F. Henry, E. Lellouch et al., Earth Moon Planets **90**, 5–14 (2002a). doi:10.1023/A:1021599915018

N. Biver, D. Bockelée-Morvan, J. Crovisier, P. Colom, F. Henry, R. Moreno et al., Earth Moon Planets **90**, 323–333 (2002b). doi:10.1023/A:1021530316352

N. Biver, D. Bockelée-Morvan, J. Crovisier, D.C. Lis, R. Moreno, P. Colom et al., Astron. Astrophys. **449**, 1255–1270 (2006). doi:10.1051/0004-6361:20053849

A.R. Blake, A.F. Hyde, Trans. Faraday Soc. **60**, 1775–1782 (1964). doi:10.1039/tf9646001775

D. Bockelee-Morvan, J. Crovisier, Astron. Astrophys. **151**, 90–100 (1985)

D. Bockelée-Morvan, J. Crovisier, P. Colom, D. Despois, Astron. Astrophys. **287**(2), 647–665 (1994)

D. Bockelée-Morvan, H. Rickman, Earth Moon Planets **79**, 55–77 (1997). doi:10.1023/A:1006225030955

D. Bockelée-Morvan, J. Crovisier, Earth Moon Planets **89**, 53–71 (2000). doi:10.1023/A:1021530016410

D. Bockelée-Morvan, D.C. Lis, J.E. Wink, D. Despois, J. Crovisier et al., Astron. Astrophys. **353**, 1101–1114 (2000)

D. Bockelée-Morvan, J. Crovisier, M.J. Mumma, H.A. Weaver, in *Comets II*, ed. by M. Festou, H.U. Keller, H.A. Weaver (University of Arizona Press, Tucson, 2004), p. 391

D. Bockelée-Morvan, N. Biver, E. Jehin, A.L. Cochran, H. Wiesemeyer, J. Manfroid et al., Astrophys. J. **679**, L49–L52 (2008). doi:10.1086/588781

D.C. Boice, D.W. Naegeli, W.F. Huebner, Physics and mechanics of cometary materials. ESA SP **302**, 83–88 (1989)

D.C. Boice, W.F. Huebner, M.J. Sablik, I. Konno, Geophys. Res. Lett. **17**, 1813–1816 (1990). doi:10.1029/GL017i011p01813

J. Boissier, D. Bockelee-Morvan, N. Biver, J. Crovisier, D. Despois, B.G. Marsden et al., Astron. Astrophys. **475**, 1131–1144 (2007). doi:10.1051/0004-6361:20078380

T.Y. Brooke, H.A. Weaver, G. Chin, D. Bockelée-Morvan, S.J. Kim, L.H. Xu, Icarus **166**, 167–187 (2003). doi:10.1016/j.icarus.2003.08.008

D. Brownlee, P. Tsou, Aléon et al., Science **314**, 1711–1716 (2006). doi:10.1126/science.1135840 Medline

J.R. Brucato, A.C. Castorina, M.E. Palumbo, M.A. Satorre, G. Strazzulla, Planet. Space Sci. **45**(7), 835–840 (1997). doi:10.1016/S0032-0633(97)00071-8

M.V. Canaves, A.A. De Almeida, D.C. Boice, G.C. Sanzovo, Earth Moon Planets **90**, 335–347 (2002). doi:10.1023/A:1021582300423

M.V. Canaves, A.A. de Almeida, D.C. Boice, G.C. Sanzovo, Adv. Space Res. **39**, 451–457 (2007). doi:10.1016/j.asr.2006.09.040

L. Colangeli, J.R. Brucato, A. Bar-Nun, R.L. Hudson, M.H. Moore, in *Comets II*, ed. by M. Festou, H.U. Keller, H.A. Weaver (University of Arizona Press, Tucson, 2004), pp. 695–717

P. Colom, J. Crovisier, D. Bockelee-Morvan, D. Despois, G. Paubert, Astron. Astrophys. **264**, 270–281 (1992)

M.R. Combi, A.H. Delsemme, Astrophys. J. **237**, 633–640 (1980). doi:10.1086/157909

M.R. Combi, U. Fink, Astrophys. J. **484**, 879–890 (1997). doi:10.1086/304349

M.R. Combi, W.M. Harris, W.H. Smyth, in *Comets II*, ed. by M. Festou, H.U. Keller, H.A. Weaver (University of Arizona Press, Tucson, 2004), pp. 523–552

H. Cottin, M.C. Gazeau, J.F. Doussin, F. Raulin, Phys. Chem. Earth **24**, 597–602 (1999)

H. Cottin, M.-C. Gazeau, J.-F. Doussin, F. Raulin, J. Photochem. Photobiol. Chem. **135**(1), 53–64 (2000). doi:10.1016/S1010-6030(00)00274-4

H. Cottin, C. Szopa, M.H. Moore, Astrophys. J. Lett. **561**(1), L139–L142 (2001). doi:10.1086/324575

H. Cottin, S. Bachir, F. Raulin, M.C. Gazeau, Adv. Space Res. **30**(6), 1481–1488 (2002). doi:10.1016/S0273-1177(02)00508-2

H. Cottin, Y. Bénilan, M.-C. Gazeau, F. Raulin, Icarus **167**, 397–416 (2004). doi:10.1016/j.icarus.2003.10.009

J. Crovisier, T. Encrenaz, M. Combes, Nature **353**, 610 (1991). doi:10.1038/353610a0 Medline
J. Crovisier, J. Geophys. Res. **99**(E2), 3777–3781 (1994). doi:10.1029/93JE02088
N. Dello Russo, M.A. Disanti, M.J. Mumma, K. Magee-Sauer, T.W. Rettig, Icarus **135**, 377–388 (1998). doi:10.1006/icar.1998.5990
D. Despois, H. Cottin, in *Lectures in Astrobiology*, ed. by M. Gargaud, B. Barbier, H. Martin, J. Reisse (Springer, Berlin, 2005), pp. 289–352
M.A. Disanti, M.J. Mumma, N. dello Russo, K. Magee-Sauer, R. Novak, T.W. Rettig, Nature **399**, 662 (1999). doi:10.1038/21378 Medline
M.A. Disanti, M.J. Mumma, N. Dello Russo, K. Magee-Sauer, Icarus **153**, 361–390 (2001). doi:10.1006/icar.2001.6695
M.A. DiSanti, M.J. Mumma, N. Dello Russo, K. Magee-Sauer, D.M. Griep, J. Geophys. Res. Planets **108f**, 15–11 (2003)
P. Eberhardt, D. Krankowsky, Schulte et al., Astron. Astrophys. **187**, 481–484 (1987)
P. Eberhardt, Space Sci. Rev. **90**(1/2), 45–52 (1999). doi:10.1023/A:1005221309219
M.C. Festou, Space Sci. Rev. **90**, 53–67 (1999). doi:10.1023/A:1005225426057
M.C. Festou, H.U. Keller, H.A. Weaver, *Comets II* (University of Arizona Press, Tucson, 2004)
N. Fray, PhD thesis. Université Paris 12 (2004)
N. Fray, Y. Bénilan, H. Cottin, M.-C. Gazeau, J. Geophys. Res. Planets **109**, E07S12 (2004a). doi:10.1029/2003JE002191
N. Fray, Y. Bénilan, H. Cottin, M.-C. Gazeau, R.D. Minard, F. Raulin, Meteorit. Planet. Sci. **39**, 4 (2004b)
N. Fray, Y. Bénilan, H. Cottin, M.C. Gazeau, J. Crovisier, Planet. Space Sci. **53**, 1243–1262 (2005). doi:10.1016/j.pss.2005.06.005
N. Fray, Y. Bénilan, N. Biver, D. Bockelée-Morvan, H. Cottin, J. Crovisier et al., Icarus **184**(1), 239–254 (2006). doi:10.1016/j.icarus.2006.04.014
P.A. Gerakines, M.H. Moore, Icarus **154**(2), 372–380 (2001). doi:10.1006/icar.2001.6711
P.A. Gerakines, M.H. Moore, R.L. Hudson, Icarus **170**, 202–213 (2004). doi:10.1016/j.icarus.2004.02.005
J.M. Greenberg, in *Comets*, ed. by L.L. Wilkening (University of Arizona Press, Tuscon, 1982), pp. 131–163
M. Gunnarsson, H. Rickman, M.C. Festou, A. Winnberg, G. Tancredi, Icarus **157**, 309–322 (2002). doi:10.1006/icar.2002.6839
M. Gunnarsson, D. Bockelée-Morvan, A. Winnberg et al., Astron. Astrophys. **402**, 383–393 (2003) doi:10.1051/0004-6361:20030178
M. Gunnarsson, D. Bockelée-Morvan, N. Biver, J. Crovisier, H. Rickman, Astron. Astrophys. **484**, 537–546 (2008)
L. Haser, Bulletin de l'académie royale de Belgique **43**, 740–750 (1957)
J. Helbert, H. Rauer, D.C. Boice, W.F. Huebner, Astron. Astrophys. **442**, 1107–1120 (2005). doi:10.1051/0004-6361:20041571
F. Henry, D. Bockelée-Morvan, J. Crovisier, J. Wink, Earth Moon Planets **90**, 57–60 (2002). doi:10.1023/A:1021508216836
W.F. Huebner, Science **237**(August), 628–630 (1987). doi:10.1126/science.237.4815.628 Medline
W.F. Huebner, J.J. Keady, S.P. Lyon, Astrophys. Space Sci. **195**, 1–294 (1992). doi:10.1007/BF00644558
W.T. Huntress Jr., M. Allen, M. Delitsky, Nature **352**, 316–318 (1991). doi:10.1038/352316a0
D. Hutsemékers, J. Manfroid, E. Jehin, C. Arpigny, A. Cochran, R. Schulz et al., Astron. Astrophys. **440**, L21–L24 (2005). doi:10.1051/0004-6361:200500160
W.H. Ip, in *Comets II*, ed. by M. Festou, H.U. Keller, H.A. Weaver (University of Arizona Press, Tucson, 2004), pp. 605–629
W. Irvine, D. Bockelee-Morvan, Lis et al., Nature **382**, 418–420 (1996). doi:10.1038/383418a0
W.M. Irvine, E.A. Bergin, J.E. Dickens, D. Jewitt, A.J. Lovell, H.E. Matthews et al., Nature **393**, 547 (1998a). doi:10.1038/31171 Medline
W.M. Irvine, J.E. Dickens, A.J. Lovell, F.P. Schloerb, M. Senay, E.A. Bergin et al., Faraday Discuss. **109**, 475–492 (1998b). doi:10.1039/a709289j Medline
W.M. Irvine, M. Senay, A.J. Lovell, H.E. Matthews, D. McGonagle, R. Meier, Icarus **143**(2), 412–414 (2000). doi:10.1006/icar.1999.6281 Medline
W.M. Irvine, P. Bergman, T.B. Lowe, H. Matthews, D. McGonagle, A. Nummelin et al., Orig. Life Evol. Biosph. **33**, 609–619 (2003). doi:10.1023/A:1025791101127 Medline
W.M. Jackson, A. Scodinu, D. Xu, A.L. Cochran, Astrophys. J. **607**, L139–L141 (2004). doi:10.1086/421995
D.C. Jewitt, H.E. Matthews, T. Owen, R. Meier, Science **278**, 90–93 (1997). doi:10.1126/science.278.5335.90 Medline
L.P. Keller, S. Bajt, G.A. Baratta et al., Science **314**, 1728–1731 (2006). doi:10.1126/science.1135796 Medline
J. Kissel, F.R. Krueger, J. Silén, B.C. Clark, Science **304**, 1774–1776 (2004). doi:10.1126/science.1098836 Medline

J. Kissel, F.R. Krueger, Nature **326**, 755–760 (1987). doi:10.1038/326755a0
P.L. Lamy, J.-M. Perrin, Icarus **76**, 100–109 (1988). doi:10.1016/0019-1035(88)90142-X
R. Meier, P. Eberhardt, D. Krankowsky, R.R. Hodges, Astron. Astrophys. **277**, 677–690 (1993)
J. Michal, Fire Mater. **6**(1), 13–15 (1982). doi:10.1002/fam.810060105
S.N. Milam, A.J. Remijan, Womack et al., Astrophys. J. **649**, 1169–1177 (2006). doi:10.1086/506501
R.D. Minard, P.G. Hatcher, R.C. Gourley, C.N. Matthews, Orig. Life Evol. Biosph. **28**, 461–473 (1998). doi:10.1023/A:1006566125815 Medline
D.L. Mitchell, R.P. Lin, C.W. Carlson, A. Korth, H. Reme, D.A. Mendis, Icarus **98**, 125–133 (1992). doi:10.1016/0019-1035(92)90213-Q
G.M. Muñoz Caro, U. Meierhenrich, W.A. Schutte, W.H.-P. Thiemann, J.M. Greenberg, Astron. Astrophys. **413**, 209–216 (2004). doi:10.1051/0004-6361:20031447
T.W. Rettig, S.C. Tegler, D.J. Pasto, M.J. Mumma, Astrophys. J. **398**, 293–298 (1992). doi:10.1086/171857
S.D. Rodgers, S.B. Charnley, Astrophysical J. Lett. **501**(2), L227–L230 (1998). doi:10.1086/311459
S.D. Rodgers, S.B. Charnley, Mon. Not. R. Astron. Soc. **323**(1), 84–92 (2001). doi:10.1046/j.1365-8711.2001.04099.x
S.D. Rodgers, S.B. Charnley, W.F. Huebner, D.C. Boice, in *Comets II*, ed. by M. Festou, H.U. Keller, H.A. Weaver (University of Arizona Press, Tucson, 2004), pp. 505–522
S.D. Rodgers, S.B. Charnley, Mon. Not. R. Astron. Soc. **356**(4), 1542–1548 (2005). doi:10.1111/j.1365-2966.2004.08606.x
S.A. Sandford, J. Aléon, C.M.O.D. Alexander et al., Science **314**, 1720 (2006)
J. Schmedt auf der Günne, J. Beck, W. Hoffbauer, P. Krieger-Beck, Chem. Eur. J. **11**, 4429–4440 (2005). doi:10.1002/chem.200401133
W.A. Schutte, L.J. Allamandola, S.A. Sandford, Icarus **104**, 118–137 (1993). doi:10.1006/icar.1993.1087 Medline
R.N. Smith, D.A. Young, E.N. Smith, C.C. Carter, Inorg. Chem. **2**(4), 829–838 (1963). doi:10.1021/ic50008a041
N. Thomas, D.C. Boice, W.F. Huebner, H.U. Keller, Intensity profiles of dust near extended sources on comet Halley. Nature **332**(6159), 51–52 (1988) doi:10.1038/332051a0
H.A. Weaver, P.D. Feldman, J.B. McPhate, M.F. A'Hearn, C. Arpigny, T.A. Smith, Astrophys. J. **422**, 374–380 (1994). doi:10.1086/173732
H.A. Weaver, T.Y. Brooke, G. Chin, S.J. Kim, D. Bockelée-Morvan, J.K. Davies, Earth Moon Planets **78**, 71–80 (1997). doi:10.1023/A:1006227530238
J. Wink, D. Bockelée-Morvan, D. Despois, P. Colom, N. Biver, J. Crovisier et al., Earth Moon Planets **78**, 63–63 (1997). doi:10.1023/A:1006263026604
M. Womack, M.C. Festou, S.A. Stern, Astron. J. **114**, 2789–2796 (1997). doi:10.1086/118687
T.J. Xue, M.A. McKinney, C.A. Wilkie, Polym. Degrad. Stabil. **58**(1–2), 193–202 (1997). doi:10.1016/S0141-3910(97)00048-7
L.M. Ziurys, C. Savage, M.A. Brewster, A.J. Apponi, T.C. Pesch, Wyckoff, Astrophys. J. Lett. **527**(1), L67–L71 (1999). doi:10.1086/312388

Article 6

COTTIN H., GAZEAU M. C., CHAQUIN P., BÉNILAN Y. and RAULIN F. (2001) Experimental and theoretical studies on the gas/solid/gas transformation cycle in extraterrestrial environments. Journal of Geophysical Research (Planets) 106(E12), 33,325-33,332.

JOURNAL OF GEOPHYSICAL RESEARCH, VOL. 106, NO. E12, PAGES 33,325–33,332, DECEMBER 25, 2001

Experimental and theoretical studies on the gas/solid/gas transformation cycle in extraterrestrial environments

Hervé Cottin[1] and Marie-Claire Gazeau

Laboratoire Interuniversitaire des Systèmes Atmosphériques, Universités Paris VII-Paris XII, Créteil, France

Patrick Chaquin

Laboratoire de Chimie Théorique, Université Paris VI, Paris, France

François Raulin and Yves Bénilan

Laboratoire Interuniversitaire des Systèmes Atmosphériques, Universités Paris VII-Paris XII, Créteil, France

Abstract. The ubiquity of molecular material in the universe, from hydrogen to complex organic matter, is the result of intermixed physicochemical processes that have occurred throughout history. In particular, the gas/solid/gas phase transformation cycle plays a key role in chemical evolution of organic matter from the interstellar medium to planetary systems. This paper focuses on two examples that are representative of the diversity of environments where such transformations occur in the Solar System: (1) the photolytic evolution from gaseous to solid material in methane containing planetary atmospheres and (2) the degradation of high molecular weight compounds into gas phase molecules in comets. We are currently developing two programs which couple experimental and theoretical studies. The aim of this research is to provide data necessary to build models in order to better understand (1) the photochemical evolution of Titan's atmosphere, through a laboratory program to determine quantitative spectroscopic data on long carbon chain molecules (polyynes) obtained in the SCOOP program (French acronym for Spectroscopy of Organic Compounds Oriented for Planetology), and (2) the extended sources in comets, through a laboratory program of quantitative studies of photochemical and thermal degradation processes on relevant polymers (e.g., Polyoxymethylene) by the SEMAPhOrE Cometaire program (French acronym for Experimental Simulation and Modeling Applied to Organic Chemistry in Cometary Environment).

1. Introduction

A better knowledge of the organic chemistry involved in diverse environments such as the interstellar medium, planetary, and cometary atmospheres can be reached by combining observations, laboratory experiments, and theoretical modeling. However, reduction, analysis, and interpretation of pure observational results often require a large set of laboratory data. Many of these data are totally unknown, especially when one considers the extreme physical conditions of the corresponding environment. Furthermore, relevant laboratory simulations of extraterrestrial environments cannot easily be done. This implies a strong needs for realistic theoretical modeling. Improvement of our knowledge of processes occurring in the studied environment can be achieved by iteration between results of numerical models and observations. However, this methodology makes sense only if the theoretical descriptions of both physical and chemical phenomena are accurate. The aim of our work is to point out specific gaps in chemical schemes used in theoretical models to date and then do our best to measure part of the missing data. Indeed, by performing laboratory experiments, we should be able to reduce two major sources of uncertainty of theoretical models. The first one concerns laboratory determinations of the values of fundamental parameters: absorption cross sections, quantum yields, and rate constants. Many of those available are limited by great error bars or, even worse, have never been determined under appropriate temperature and pressure conditions. The second one is the possibility that models fail owing to systematic calculation errors when critical reaction pathways are not correctly described or are totally missing from the schemes.

In this paper, we present two programs developed at the Laboratoire Interuniversitaire des Systèmes Atmospheriques (LISA) at Créteil, near Paris: SCOOP (French acronym for Spectroscopy of Organic Compounds Oriented for Planetology) and SEMAPhOrE Cometaire (French acronym for Experimental Simulation and Modeling Applied to Organic Chemistry in Cometary Environment), which are dedicated studying particular species or processes in order to highlight their contribution to the gas/solid/gas transformation cycle in different Solar System environments.

The SCOOP program is establishing a spectroscopic data bank (both in the infrared and in the ultraviolet spectral range)

[1] Now at Astrochemistry Branch, NASA Goddard Space Flight Center, Greenbelt, USA

Paper number 2000JE001319.
0148-0227/01/2000JE001319$09.00

of molecules under adequate physical conditions of the studied environments (mainly low temperatures). In this paper we report on studies of polyynes (linear molecules with conjugated triple bonds with the general formula $C_{2n}H_2$), and explain how, using experimental and theoretical approaches, we plan to predict the spectral characteristics of longer carbon chain compounds which are unstable under the laboratory conditions. Studying those compounds is of prime importance because very recently polyynes (C_4H_2 and C_6H_2) have been observed in the circumstellar medium [*Cernicharo*, 2000] where they may be key molecules in the formation of higher molecular weight compounds like PAHs. Furthermore, C_4H_2 has been observed in planetary atmospheres and is thought to lead, via a complex photochemistry starting from methane, to the formation of solid particles (called "tholins" in experiments simulating the evolution of planetary atmospheres). The S.C.O.O.P. program coupling experimental and theoretical studies will determine the spectroscopic data of those compounds strongly needed to interpret observations and to develop photochemical models to explain the transformation of gases into complex organics.

In turn, through different processes, such as thermal- and photo-degradation, high-molecular weight molecules in the solid phase can release volatile products, which may be different than their original precursors and thus act as parent molecules for various compounds in the solar system and as new pathways for the production of interstellar species. Our interest focuses on the study of such processes in the cometary environment; these processes could be responsible for the extended source phenomenon. On the basis of their density profile in the coma as a function of the nucleus distance, some molecules (H_2CO [*Biver et al.*, 1999; *Meier et al.*, 1993], CO [*DiSanti et al.*, 1999]) are thought to have an origin other than direct sublimation from the nucleus. It could be the degradation of a parent molecule present on grains in the coma. The SEMAPhOrE Cometaire program consists specifically of the study of the degradation of high-molecular weight compounds (in the solid phase) leading to the formation of smaller gaseous compounds. The aim of this program is to bring a better understanding of the chemical mechanisms involved during those transformations and to provide physicochemical data such as the production quantum yield of gaseous molecules from the solid parent molecule as a function of the UV wavelength or the kinetics of its thermal degradation. Such data are not available for the interpretation and modeling of observations. We report here the results of studies on polyoxymethylene [POM: $(-CH_2-O-)_n$] degradation processes to determine if the presence of POM is relevant as an explanation for the formaldehyde extended sources observed in several comets.

2. SCOOP Program: From Volatile to Complex Molecules

2.1. Organic Matter in Methane Containing Atmospheres

Titan's atmosphere is mainly composed of molecular nitrogen with methane as the second major constituent having an abundance of a few percent. Several higher hydrocarbons (C2-C4) have also been detected during the Voyager fly-by [*Hanel et al.*, 1981; *Kunde et al.*, 1981] and more recently from Infrared Space Observatory (ISO) observations [*Coustenis et al.*, 1998]. Their mixing ratios range from a few ppm (C_2H_6, C_2H_2, C_3H_8) to a few ppb (C_2H_4, C_3H_4, C_4H_2) [*Coustenis and Bézard*, 1995]. The recent detection of butadiyne (also called diacetylene, C_4H_2), also in Saturn's atmosphere using ISO [*de Graauw et al.*, 1997], confirmed the predicted production of polyynes in methane containing atmospheres [*Yung et al.*, 1984]. The general mechanism invoked for the production of polyynes is:

$$C_{2n}H_2 \xrightarrow{h\nu} C_{2n}H + H$$

$$C_{2n}H + C_2H_2 \longrightarrow C_{2n+2}H_2 + H$$

$$\text{net}: C_{2n}H_2 + C_2H_2 \longrightarrow C_{2n+2}H_2 + 2H.$$

This chemical scheme for the production of long carbon chains has a special importance in the photochemical models of Titan's atmosphere since long chain molecules are supposed to be the main link between the gas phase and the solid phase particulates visible as haze at high altitude. Furthermore, acetylene and higher polyynes are supposed to control the abundance of atomic hydrogen by the competitive mechanism of molecular hydrogen dissociation and H recombination [*Gladstone et al.*,1996]. Polyynes are also involved in the methane catalytic dissociation via the radicals formed by their photolysis in the stratosphere [*Yung et al.*, 1984].

2.2. The SCOOP Program: From Volatile to Complex Molecules

One needs the absorption coefficient of a molecule, measured under physical conditions as close as possible to those of the extraterrestrial environment, to calculate its dissociation coefficient. Since the solar flux decreases rapidly with decreasing wavelength in the ultraviolet and apart from the Ly α (1216 Å) which does not penetrate below 600 km on Titan, the midultraviolet (mid-UV) wavelength range (λ>180 nm) is the most important for the determination of dissociation coefficients. Furthermore, the mid-UV range is also the most important wavelength range for observations since atmospheric opacity increases with decreasing wavelength.

For the detection and abundance determination of molecules present in the atmosphere by remote observations, the infrared wavelength range is complementary to the ultraviolet range. Indeed, they probe a different level in the atmosphere: IR radiation comes from thermal emission by the troposphere and lower stratosphere; observed UV radiation results from solar UV photons backscattered by the major gases and aerosols in the high stratosphere.

Band positions and absolute intensities of polyynes are required to be able to analyze observational data. Unfortunately, spectroscopic laboratory data are only partially available in the literature for polyynes. Thus we have started a specific program in the midultraviolet and infrared range to determine quantitative spectra of polyynes.

The description of the experimental setup for the determination of infrared and midultraviolet absorption coefficients is only briefly mentioned here. The ultraviolet absorption coefficient is presented for each molecule. Infrared results are also presented and compared with ab initio calculations.

2.3. Experimental Results

2.3.1. Ultraviolet spectra. Spectra in the 185-300 nm range were obtained with the SCOOP experimental setup

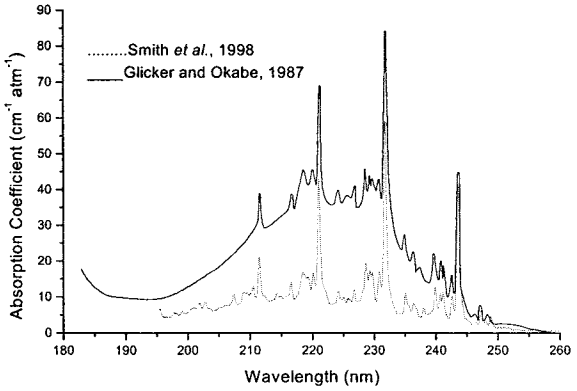

Figure 1. Comparison between the absorption spectrum obtained with our apparatus [*Smith et al.*, 1998] and that previously available in the literature for C_4H_2 [*Glicker and Okabe*, 1987]. The difference indicates the presence of impurity C_4H_3Cl, used in preparing C_4H_2.

[*Bruston et al.*, 1991; *Bénilan et al.*, 1994]. For spectra recorded below 200 nm, the monochromater was flushed with dry N_2 to remove, as much as possible, absorptions due to H_2O and O_2. The pressure regulation system, which used the sample vapor pressure, allows us to check the purity of the sample and detect the possible presence of trace impurities. As an example, we present in Figure 1 a comparison between our C_4H_2 spectrum and that obtained by *Glicker and Okabe* [1987]. The difference between the two seen as a continuum shift corresponds to absorption due to C_4H_3Cl, a by-product in the synthesis of C_4H_2 [*Smith et al.*, 1998]. The same kind of impurity was also observed in C_6H_2 samples [*Benilan et al.*, 1995].

A compilation of the polyyne spectra (n= 1 to 4) measured at room temperature, together with spectra available from the literature for wavelengths below 185 nm, is presented in Figure 2 from 150 to 300 nm. The C_8H_2 absolute absorption coefficient is presented for the first time. It was obtained at vapor pressure of a few 10^{-3} mb. The uncertainty associated with this measurement is around 20%, mainly owing to uncertainties in sample purity. In the 150-300 nm region, polyyne absorption can vary over 5 orders of magnitude. This results from the fact that allowed and forbidden transitions both occur in this wavelength range. For C_8H_2, the absorption coefficient corresponding to the forbidden transition cannot be measured because it requires study at high pressures where the sample starts to polymerize. It is clear, looking at figure 2 that polyyne absorption shifts to longer wavelengths as the length of the carbon chain increases. These results are in good agreement with previous measurements [*Kloster-Jensen et al.*, 1974]. However, we also find that the allowed transition oscillator strength, proportional to the integrated absorption coefficient, increases with the number of triple bonds. This has several important consequences for chemical evolution and for the possible detection of polyynes in planetary atmospheres as discussed in section 2.4.

2.3.2. Infrared spectra. IR spectra were obtained on a Perkin-Elmer 1710 FTIR spectrometer. Spectra were recorded at 4 cm^{-1} resolution between 250 and 4300 cm^{-1}. Typically, 50 scans were coadded to give a 0.3% noise in transmission. The gas was contained in a 10 cm path length cell equipped with CsI windows. Spectra were recorded at several pressures. N_2 gas at an approximate partial pressure of 700 mb was added to the cell to broaden the bands. All spectra were recorded at room temperature. The entire optical path in the spectrometer was flushed with dry N_2 to remove, as much as possible, absorptions due to H_2O and CO_2.

Infrared spectra were measured for polyynes with n=2, 3, and 4. However, absolute intensities have been obtained only for the first two molecules [*Khlifi et al.*, 1995; *Delpech et al.*, 1994] because of the small cell size which limits measurements to pressures ranging over only a few to tenths of millibars. For C_8H_2, as soon as the pressure increases to the millibar level, it spontaneously polymerizes onto the wall of the cell. Great caution has to be taken with this compound, since when the cold solid sample is allowed to warm up to room temperature, it quickly polymerizes and explodes violently.

For the study of cold planetary atmospheres, the region below 700 cm^{-1} is of particular interest. This is where the thermal emission flux is significant, being maximum at 300 cm^{-1} for a radiating black body at 150 K. However, many of the lower energy vibrational bands are out of our scope since our spectrometer is limited to 250 cm^{-1}. Thus we will concentrate here on the CCH bending mode of polyynes, which occurs in the 650-600 cm^{-1} range.

In Figure 3 we present spectra of this CCH band at 4 cm^{-1} resolution, with the absorbance normalized to the maximum value, for the three polyynes: C_4H_2, C_6H_2, and C_8H_2. As one can see, the band position shifts to lower energy as the length of the carbon chain increases. The intense Q branch starts to be less and less separated from R and P branches for higher polyynes. Since the moment of inertia increases with the length of the molecule, the separation between the P and R branches will decrease for higher polyynes because the separation varies as the square root of the rotational constant, itself proportional to the inverse of the moment of inertia.

A plot of the band position verses the number of triple bonds for each molecule is illustrated by Figure 4. The variation of the band position can be modeled by an empirical law varying as $1/n^4$, where n is the number of triple bonds in the molecule. This leads to an extrapolated position of 621 cm^{-1} for an infinite length polyyne. The convergence observed experimentally has been tested against ab initio calculations. Details of those calculations will be published elsewhere. The

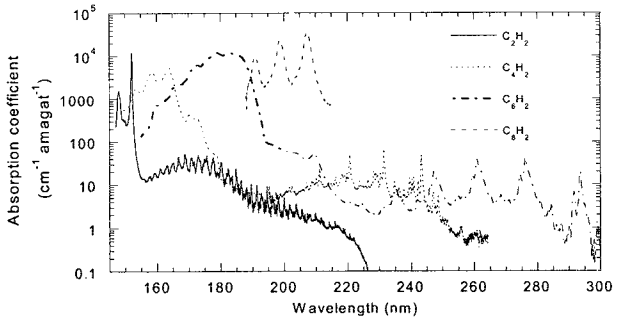

Figure 2. Absorption coefficient at ambiant temperature (T=293 K) of acetylene and polyynes ($C_{2n}H_2$, n=2-4) between 150 and 300 nm. Values below 185 nm are from the literature. C_2H_2 is from *Smith et al.* [1991]; C_4H_2 is from *Fahr and Nayak* [1994]; C_6H_2 is from *Kloster-Jensen et al.* [1974] normalized by *Benilan et al.* [1995], and C_8H_2 is from this work.

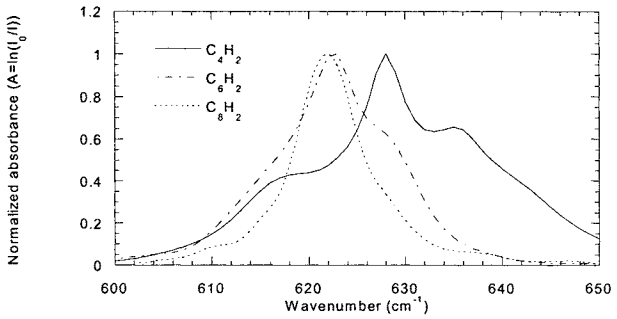

Figure 3. Spectra at 4 cm^{-1} resolution, broadened with 700 mb of N_2, of C_4H_2, C_6H_2, and C_8H_2, in the CCH bending region 600-650 cm^{-1}.

main result is that a theoretical approach leads to the same conclusions concerning the convergence of the band position as a function of the length of the molecule. Nevertheless, the theoretical data had to be scaled by a factor 1.05, which is the mean value of the ratio between experimental and theoretical results for 2-4 triple bond molecules. A discrepancy can still be observed since the theoretical positions converge less rapidly ($1/n^{2.5}$) than the experimental values.

2.4. Implications for Models and Observations of Planetary Atmospheres

We have reviewed the absolute absorption coefficient of polyynes in the 150-300 nm range. These results are essential for the development of photochemical models and for the interpretation of mid-UV spectra of planetary atmospheres in which these compounds are likely to be present. The wavelength shift of the allowed transitions of polyynes in the 150-220 nm wavelength range is almost linear with conjugated triple bonds. This agrees with measurements performed on higher polyynes trapped in a rare gas matrix [*Grutter et al*, 1998]. However, we also found that the intensity of the allowed transition increases almost linearly with the length of the molecule as well. Since the solar flux is also increasing with wavelength in the ultraviolet region, the dissociation coefficient of polyynes, proportional to the integrated product over wavelength of the solar flux times the absorption cross section, will increase very quickly with the size of the molecule. This leads to the conclusion that solar radiation could quickly polymerize the polyynes into solid material as inferred by the chemical mechanism if the second step of the chemical scheme is efficient. An important implication would be that these polyyne molecules (especially the longer ones) should not be observable in the atmosphere. Unfortunately, the recombinaizon of $C_{2n}H$ radicals with acetylene is largely unknown and experimentally difficult to measure. Ab initio calculations are underway to study those reactions. Nevertheless, a second conclusion can be drawn from our ultraviolet studies: higher polyynes might be more easily detectable from UV observations than lighter ones since the allowed transition shifts to longer wavelength as the size of the molecule increases. This is especially true in Titan's atmosphere for C_8H_2 as compared to C_6H_2 because the photon flux drops very quickly below 200 nm due to both the decrease of solar photons and the increase of opacity.

Infrared results also have several implications concerning the possible observation of polyynes in methane containing planetary atmospheres. First, since the position of the CCH bending mode converges to a fixed value for the higher polyynes, very high-resolution observations able to resolve rotational band structure would be needed to identify the different compounds. This is not expected in the near future. Composite Infrared Spectrometer (CIRS) onboard the Cassini mission will observed Jupiter in December 2000 and will be in orbit around Saturn in 2004. This will have a maximum apodized resolution of 0.5 cm^{-1}, insufficient for this purpose. Thus polyynes will have to be preferentially searched for in the far-IR using their emission bands below 250 cm^{-1}, corresponding to their CCC bending modes. Second, since the absolute intensity of the infrared band studied here is predicted to be almost constant for all polyynes, the upper limit that could be determined around 621 cm^{-1} will be characteristic of C_6H_2 and C_8H_2 because the emission from higher polyynes would be negligible if their abundance decreases rapidly as stated above. This leads again to the conclusion that infrared observations will have to concentrate on the low energy part of the spectrum to derive information on the amount of polyynes in the atmosphere of Jupiter, Saturn, and Titan.

3. The SEMAPhOrE Cometaire Program: From Complex Molecules to Volatiles

3.1. Cometary Investigations, Review of Previous Work

Our current knowledge about the cometary environment comes from (1) remote sensing through spectroscopic techniques from the UV to the submillimeter range, (2) in situ measurements using mainly mass spectrometry during the Halley encounter by Vega and Giotto spacecraft in 1986, and (3) laboratory simulation experiments [see *Cottin et al.*, 1999, and references therein]. The knowledge of the molecular composition of comets is of prime importance since these objects are generally considered to be accreted during the birth of our planetary system: they have been held in a cold environment and may have been unaltered by chemical evolution. Thus comets may have kept the primordial solar system chemical composition, offering a unique link to the interstellar medium. Comets are composed of a mixture of silicate minerals, ices, and complex refractory organic molecules. Until now, only the coma's composition has been analyzed by in situ measurements or remote observations, which has led to the detection of ~ 25 stable small molecules. Among them, formaldehyde (H_2CO) [*Biver et al.*, 1999; *Meier*

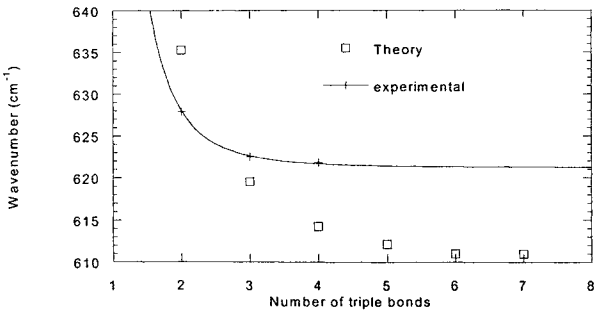

Figure 4. Comparison of the measured IR band position of the CCH bending mode of polyynes with ab initio calculations. The solid curve fits the experimental data with the equation: $\nu=621.2+107.9/n^4$.

et al., 1993] and carbon monoxide (CO) [*DiSanti et al.*, 1999] present an extended source which could be due to the degradation of a refractory parent molecule in the coma. However, there is no direct information about the molecular composition of the nucleus. Indeed, the abundance of compounds detected in the coma may not be directly representative of the molecular composition of the cometary nucleus because thermal differentiation processes may occur in the nucleus, and many products may have vapor pressures or abundances too low to be detected in the gaseous phase. This is the reason why experimental simulations have been carried out. The aim of these experiments is to understand the physical and chemical processes likely to occur in the interstellar medium or in comets, and to infer the organic composition of interstellar and cometary grains. These experiments consist of irradiating ices whose compositions are relevant to the interstellar medium or comets. After irradiating and subsequent warming to room temperature, a refractory mantle made of organic molecules remains. The resulting sample, supposed to mimic the interstellar or cometary organic refractory component, is analyzed by different techniques. A review of those experiments and their results are given in *Cottin et al.*, [1999]. Laboratory simulations on ice analogs can be classified into three different groups considering the source of energy deposition: ice analogs can be processed (1) thermally [*Schutte et al.*, 1993], (2) by UV lamps, specifically hydrogen discharge lamp (Leiden's observatory, Netherland: [*Briggs et al.*, 1992; *Gerakines et al.*, 1996]; NASA-Ames Research Center, Moffett Field, California, [*Bernstein et al.*, 1995]) or (3) by high energy particles (1-1000 keV): H, He ions and heavier nuclei generated by a Van de Graff accelerator (Catania, Italy: [*Strazzulla et al.*, 1991]; Yokohama, Japan, [*Kobayashi et al.*, 1995]; NASA-Goddard Space Flight Center, Maryland, [*Moore and Hudson*, 1998]). Generally, these experiments have been carried out at 10 K, representative of the interstellar medium or of the cometary environment in the outer solar system. These laboratory studies strongly suggest that many more compounds exist in the cometary environment than those that have been firmly detected by remote sensing up to now. Indeed, more than 100 compounds belonging to a wide range of chemical families, from the simplest hydrocarbons to amino acids or even more complex molecules such as HMT (hexamethylenetetramine, $C_6H_{12}N_4$) or POM (polyoxymethylene, $(-CH_2-O-)_n$) have been found in laboratory simulation experiments on processed ices. One has to note that the resulting information is often qualitative and few quantitative data have been obtained so far.

3.2. A Complementary Approach: The SEMAPhOrE Cometaire Program

The contribution of our team to the study of cometary chemistry concerns the processes that can be responsible for the evolution of material in a cometary environment, and in particular, the chemical mechanism involved in transformation from the solid to gaseous phase. Our interest focuses on the study of photo- and thermo-degradation of solid molecules present on grains ejected from the nucleus. Such mechanisms could be responsible of the observed extended sources. The SEMAPhOrE Cometaire experimental program has started with the test of the hypothesis that POM is a possible parent molecule for the formaldehyde extended source. This polymer has been tentatively detected in comet Halley by *Huebner*, [1987], and has been identified in simulation experiments [*Bernstein et al.*, 1995; *Schutte et al.*, 1993]. Abundances, rate, and quantum yields of formation of the dominant products resulting from POM degradation can be derived from our experiments. Kinetic parameters of its thermal degradation are also determined. Providing such fundamental data is necessary to model the cometary environment and to determine if POM may be a parent molecule of H_2CO or not.

Quantitative analysis of the molecular composition of the resulting gaseous phase gives the "signature" of any high molecular weight compound. In other words, the purpose of this experiment is to determine to what extent the refractory organic component of comets could contribute to the gaseous phase.

3.3. Experiment

The experimental set up has already been described by *Cottin* [1999] and *Cottin et al.* [2000]. The reactor, made of Pyrex, allows a thermal regulation of the sample that is necessary to discriminate thermal from irradiation effects. The compound is simply deposited at the bottom of the reactor, whose temperature is set at a level allowing to neglect thermal degradation compare to photodegradation (typically 10 C). POM is irradiated with UV photons. The lamp is filled with an appropriate gas or gas mixture depending on the desired wavelength for processing: 5.5 mb H_2 (2%) in He (> 99.99% - Linde - France) for a 122 nm emission (Lyman α), 0.3 mb Xe (99.99% - Linde - France) for 147 nm, and 0.5 mb CH_4 (1%) in He (> 99.99% - Linde - France) for 193 nm. Discharge in the lamp is initiated with a Tesla coil, and the gas is excited by a microwave generator (Somelec - France) with a power of 200 W at 2450 MHz. The pressure of the gas in the lamp is set at a level allowing maintaining a stable discharge. Window of MgF_2 transmits 122 and 147 nm UV, and SiO_2 transmits 193 nm (both thickness, 2 mm; Φ, 25 mm; Sorem; France). The SiO_2 window absorbs UV below 170 nm and thus filters the other atomic lines of C atom at 166 and 156 nm [*Okabe*, 1978]. For each wavelength, the UV lamp flux is measured by chemical actinometry. Actinometers have been chosen to be relevant for the irradiation conditions, each has a significant cross section at the studied wavelength and a simple photochemistry.

The reactor can be directly connected to an IR spectrometer (optical length settled at 96 or 288 m, resolution 0.5 cm^{-1}). Then, as the gaseous photodegradation products diffuse into the chamber, they are continuously analyzed. Analysis has also included direct mass spectrometry or gas chromatography coupled with mass spectrometry (GC-MS).

Concerning thermal degradation, the polymer is set at a constant temperature in the reactor and its H_2CO production is measured through the pressure augmentation as H_2CO which is the only thermal degradation product of POM. In this paper, we summarize results that have been presented in more detail by *Cottin et al.* [2000] for the photodegradation of POM and focus on results of interest for the planetary community. Thermal degradation results for POM are presented here for the first time.

3.4. Results

3.4.1. Photodegradation. The infrared spectrum of the gas phase products resulting from 7 hours of POM irradiation at

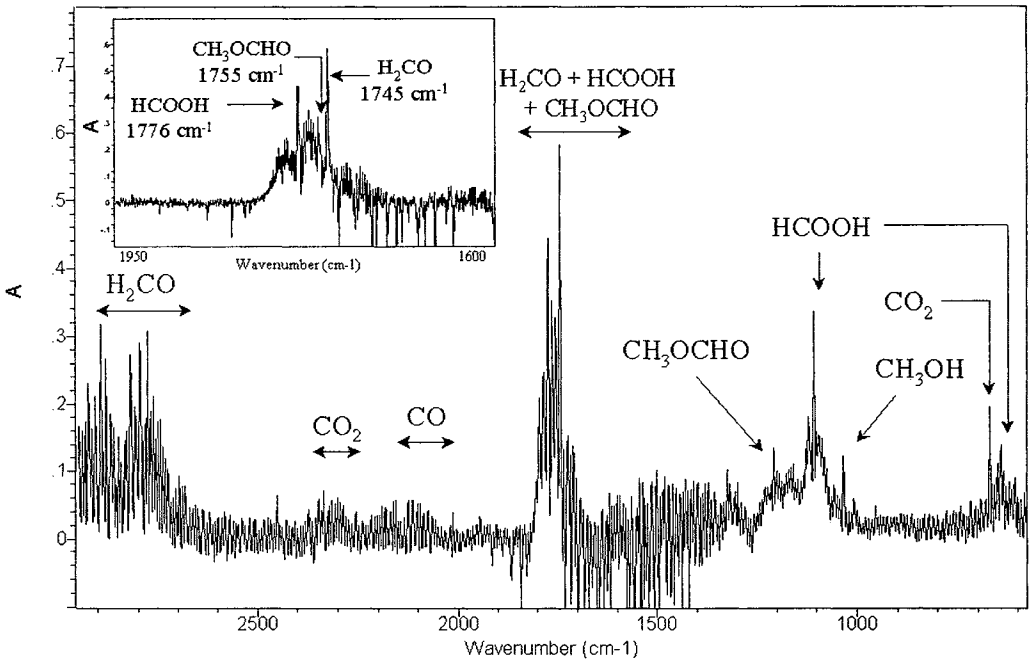

Figure 5. Infrared spectrum of the gas produced after 7 hours of POM irradiation at 122 nm. Optical path, 288 m; Resolution, 0.5 cm^{-1}; Polymer temperature, 288 K.

122 nm is presented in Figure 5. Calculation of the time required for molecules to diffuse from the photolysis reactor to the infrared cell, where they are no longer exposed to the UV flux, are reported by *Cottin et al.* [2000]. It shows that detected molecules are primary photodegradation products and that gaseous phase photochemistry during transport to the analysis system yields only a small amount of secondary products, which have been taken into account for quantum yields determination. Formaldehyde is the major product, clearly identified by its signatures at 1746, 2765, 2801, and 2897 cm^{-1}. Other molecules detected are CO, CO_2, HCOOH, CH_3OH, CH_3OCHO. These molecules have already been detected in comets. Knowing the lamp's flux, the production quantum yield as a function of the wavelength has been derived for H_2CO, HCOOH, CO, CO_2, and CH_3OH.

Quantum yields measured in this study are the result of a complex competition between initiation, production, and termination reactions, rather than a simple reaction such as one photon produces one molecule [*Rabek*, 1995]. The quantum yields of products as a function of the irradiating wavelength are reported in Table 1. We propose to interpolate those data for H_2CO and HCOOH and adopt the production profiles presented in Figure 6.

The analysis by GC-MS has led to the detection of other molecules, dimethoxymethane ($CH_3OCH_2OCH_3$) and trioxane (cyclic derivative compound of formaldehyde, $C_3H_6O_3$). Neither of these molecules has been detected in comets.

Table 1. Production Quantum Yield from POM Measured as a Function of Irradiation Wavelength.

Molecule/λ, nm	122	147	193
H_2CO	0.75±0.21	0.96±0.19	<0.16
HCOOH	0.13±0.05	0.26±0.10	ε
CO	not estimated	~1	ε
CO_2	not estimated	~0.3	ε
CH_3OH	~0.05	~0.05	ε

ε: below detection limit

3.4.2. Thermodegradation. The thermal degradation of POM has also to be considered. Indeed, the polymer is in equilibrium with formaldehyde (POM ⇔ n H_2CO) [*Dainton et al.*, 1959]. We have studied the reaction at different temperatures (278, 283, 288, 293, and 295.5 K):

$$POM_{solid} \xrightarrow{\Delta} H_2CO_{gas}.$$

The production rate of formaldehyde is a function of the amount of polymer. During an experiment, the mass loss of the polymer is negligible, thus we can consider a pseudo zero-order reaction and write its kinetics as

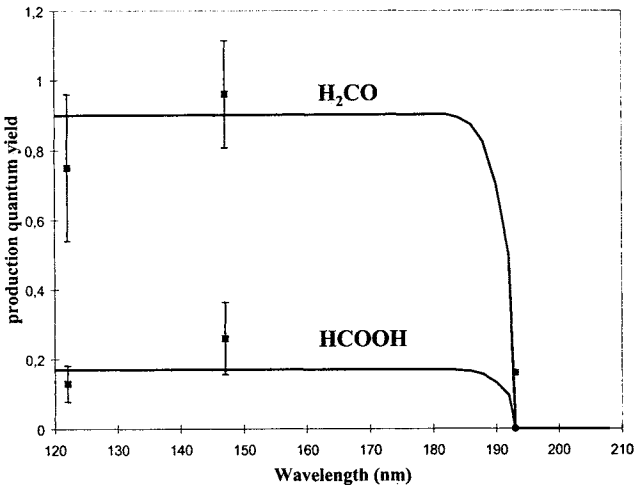

Figure 6. Quantum yield profiles as a function of irradiation wavelength for H_2CO and HCOOH under experimental conditions.

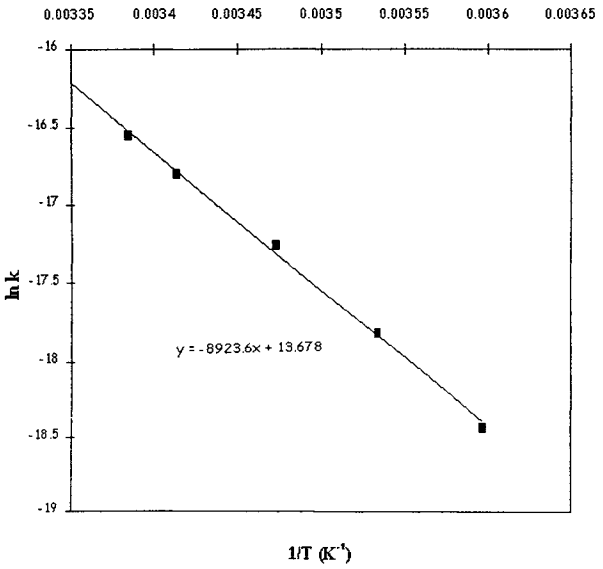

Figure 7. Arrhenius law for the production rate of formaldehyde from POM as a function of $1/T$.

$$\frac{dH_2CO}{dt} = km_{\mathrm{POM}} = K$$

From Arrhenius law, we write $k = A\, e^{-Ea/RT}$. Ea is the activation barrier, and A is the frequency factor. This law can also be written

$$\ln k = -\frac{Ea}{RT} + \ln A.$$

Figure 7 presents ln k as a function of $1/T$.
From those results, using a linear least-square regression fit, we derive Ea = 74.2 kJ mole^{-1} ± 10 % and A = 8.71 10^5 mole g^{-1} s^{-1} (the $\pm^{120\%}_{60\%}$ estimated uncertainty for ln A is 20% but is amplified in a nonsymmetric way due to the ln function). The relative uncertainty of these results applied to a typical cometary grain temperature of 300 K is ~20%. The Ea value is quite important and means that the production of H_2CO from POM is highly sensitive to temperature.

3.5. Discussion

SEMAPhOrE Cometaire is an experimental set up dedicated to the study of the degradation of high-molecular weight species likely to be present in the cometary nucleus. The first quantitative study of the photodegradation products of POM has been carried out. We have measured the quantum yield of formation of the different photoproducts as a function of wavelength and the kinetic parameters to calculate the thermal production of formaldehyde as a function of temperature. Using different sensitive analytical methods, we have been able to detect many products from POM irradiation. These are quite important results since most of these compounds have already been detected in comets with two exceptions, dimethoxymethane and trioxane. Thus observational programs should look for these molecules since their detection could be an indication of the presence of polyoxymethylene on the cometary nucleus. Both photo- and thermo-degradation mechanisms are quite efficient and could be responsible for formaldehyde in cometary comae. Moreover CO, which is a photodegradation product of POM, presents an extended source in several comets. Thus polyoxymethylene could also be involved in its production. We have provided here new quantitative data for understanding the origin of extended sources. The next step of this work will be to introduce these data into numerical models to interpret observations. This work is in progress [*Cottin et al.*, 2001].

Another experimental complement will be to repeat our experiments in the presence of water vapor in order to study the interaction of water photofragments with those from solid POM. Similar processes may occur in the inner coma.

To conclude, this experiment brings new insight into the chemistry of possible cometary environments. It appears that solid phase molecules can contribute directly to gas phase species, and thus these contributions have to be taken into account when one studies the chemical evolution of the coma.

4. Conclusion

The aim of both programs is to provide accurate experimental data (1) for models built in order to describe the photochemical evolution of Titan's atmosphere and other methane containing atmospheres and the extended source phenomenon in the cometary environment and (2) for the interpretation of observation.

In the highly complex chemical evolution of the studied planetary objects, there is a competition between formation of solid material starting from gases and degradation of solids leading to the production of gases. In order to study these transformations, both the SEMAPhOrE Cometaire and SCOOP programs are using the same methodological approach. It consists of complementary theoretical and experimental studies and proceeds step-by-step with an increasing complexity of the studied compounds or mechanisms.

The SCOOP program will continue to study long carbon chain molecules. Cyanopolyynes are of special interest since (1) HC_3N has already been observed by Voyager in Titan's atmosphere and (2) HC_5N has recently been observed in simulation experiments [*de Vanssay et al.*, 1995]. These compounds might be a new route to the formation of solids in the atmosphere. It can be noted that these compounds have also been observed for a long time in the interstellar medium. Dicyanopolyynes are also good candidates since C_2N_2 and C_4N_2 have been observed during the Voyager fly-by of Titan's atmosphere. C_4N_2 was observed in solid phase, which implies that other polyyne-like compounds could also be observed as ices. Future experimental efforts should include these species.

The SEMAPhOrE Cometaire program will be extended to other molecules. Studies on hexamethylenetetramine ($C_6H_{12}N_4$), HCN polymer, tholins, PAHs, and amino acids are in progress or planned. Investigation of the interaction mechanism between those molecules and water photofragments may also have implications on our knowledge of the chemistry of comets. Moreover, photo- and thermo-degradation of refractory organic material could also play an important role in interstellar clouds. Such mechanisms could be an efficient complementary pathway for the production of small compounds. From our point of view, generalizations of our results will allow us to clarify many aspects of the gas/solid/gas transformation cycle occurring in other extraterrestrial environments.

Acknowledgments. The authors are very grateful to the referees for their careful reading, comments, and English corrections, which were helpful in improving the manuscript. We thank Souleyman Bachir and Rodolphe Mulette for their participation in the experimental part of the work. SEMAPhOrE Cometaire and SCOOP programs are supported by grants from CNES (Centre National d'Etudes Spatiales) and PNP (Programme National de Planétologie, Institut National des Sciences de l'Univers, CNRS).

References

Bénilan, Y., P. Bruston, F. Raulin, C. Cossart-Magos and J.-C. Guillemin, Mid-UV spectroscopy of propynenitrile at low temperature: Consequences on expected results from observations of Titan's atmosphere, *J. Geophys. Res. 99*, 17,069-17,074, 1994.

Bénilan Y., P. Bruston, F. Raulin, R. Courtin, and J.-C. Guillemin, Absolute absorption coefficient of C_6H_2 in the mid-UV range at low temperature: implications for the interpretation of Titan atmospheric spectra, *Planet. Space Sci., 43*, 83-89, 1995.

Bernstein, M.P., S.A. Sandford, L.J. Allamandola, S. Chang, and M.A. Scharberg, Organic compounds produced by photolysis of realistic interstellar and cometary ice analogs containing methanol, *Astrophys. J., 454*, 327-344, 1995.

Biver, N., et al., Spectroscopic monitoring of Comet C/1996 B2 (Hyakutake) with the JCMT and IRAM Radio Telescopes, *Astron. J., 118*(4), 1850-1872, 1999.

Briggs, R., G. Ertem, J.P. Ferris, J.M. Greenberg, P.J. McCain, C.X. Mendoza-Gomez, and W. Schutte, Comet Halley as an aggregate of interstellar dust and further evidence for the photochemical formation of organics in the interstellar medium, *Origins Life Evol. Biosphere, 22*, 287-307, 1992.

Bruston, P., F. Raulin, and H. Poncet, A laboratory facility for mid-UV absorption spectroscopy of molecular compounds for planetary atmospheres, *J. Geophys. Res. 96*(17), 513-517, 1991.

Cernicharo, J., New molecular species discovered by ISO in the interstellar and circumstellar media, in *ISO beyond the Peaks: Proceedings of the Second ISO Workshop on Analytical Spectroscopy*, edited by A. Salama et al., Eur. Space Agency, Noordwijk, Netherland, 81-87, 2000.

Cottin, H., Chimie organique de l'environnement cométaire: Etude expérimentale de la contribution de la composante organique réfractaire à la phase gazeuse, Ph.D. thesis, Université Paris XII, Créteil, 1999. (Available as: http://www.lisa.univ-paris12.fr/GPCOS/Hc/H1t.htm)

Cottin, H., M.C. Gazeau, and F. Raulin, Cometary organic chemistry: a review from observations, numerical and experimental simulations, *Planet. Space Sci., 47*(8-9), 1141-1162, 1999.

Cottin, H., M.C. Gazeau, J.F. Doussin, and F. Raulin, An experimental study of the photodegradation of polyoxymethylene at 122, 147 and 193 nm, *J. Photochem. Photobiology*, Ser. A, *135*, 53-64, 2000.

Cottin H., M.C. Gazeau, Y. Bénilan, and F. Raulin, Polyoxymethylene as parent molecule for the formaldehyde extended source in comet Halley, *Astrophys. J.*, in press, 2001.

Coustenis, A., and B. Bezard, Titan's atmosphere from Voyager infrared observations, 4, Latitudinal variations of temperature and composition, *Icarus, 115*, 126-140, 1995.

Coustenis, A., et al., Titan's atmosphere from ISO observations: Temperature, composition and detection of water vapor, *Bull. Am. Astron. Soc., 30*(3), 1060, 1998.

Dainton, F.S., K.J. Ivin, and D.A.G. Walmsley, The equilibrium between gaseous formaldehyde and solid polyoxymethylene, *Trans. Faraday. Soc., 55*, 61-64, 1959.

de Graauw, T., et al., First results of ISO-SWS observations of Saturn: Detection of CO_2, CH_3C_2H, C_4H_2 and tropospheric H_2O, *Astron. Astrophys., 321*, L13-L16, 1997.

Delpech, C., J.C. Guillemin, P. Paillous, M. Khlifi, P. Bruston, and F. Raulin, Infrared spectra of triacetylene in the 4000-200 cm-1 region: absolute band intensity and implications for the atmosphere of Titan, *Spectrochim. Acta, 50A*(6), 1095-1100, 1994.

de Vanssay E., M.C. Gazeau, J.C. Guillemin, and F. Raulin Experimental simulation of Titan's organic chemistry at low temperature, *Planet. Space Sci., 43*, 25-31, 1995.

DiSanti, M.A., M.J. Mumma, N. DelloRusso, K. Magee-Sauer, R. Novak, and T.W. Rettig, Identification of two sources of carbon monoxide in comet Hale-Bopp, *Nature, 399*, 662-665, 1999.

Fahr, A., and A.K. Nayak, Temperature dependent ultraviolet absorption cross sections of 1,3-butadiene and butadiyne, *Chem. Phys, 189*(3), 725-731, 1994.

Gerakines, P.A., W.A. Schutte, and P. Ehrenfreund, Ultraviolet processing of interstellar ice analogs. I. Pure ices, *Astron. Astrophys., 312*, 289-305, 1996.

Gladstone, G. R., M. Allen and Y.L. Yung, Hydrocarbon chemistry in the upper atmosphere of Jupiter, *Icarus, 119*, 1-52, 1996.

Glicker, S. and H. Okabe, Photochemistry of diacetylene, *J. Phys. Chem, 91*(2), 437-440, 1987.

Grutter, M., M. Wyss, J. Fulara, and J.P Maier, Electronic absorption spectra of the polyacetylene chains $HC_{2n}H$, $HC_{2n}H^-$, and $HC_{2n-1}N^-$ (n = 6-12) in Neon matrixes, *J. Phys. Chem. A, 102*, 9785-9790, 1998.

Hanel, R., et al., Infrared observation of the Saturnian system from Voyager 1, *Science, 212*, 192-200, 1981.

Huebner, W.F., First polymer in space identified in comet Halley, *Science, 237*, 628-630, 1987.

Khlifi, M., P. Paillous, C. Delpech, M. Nishio, P. Bruston, and F. Raulin, Absolute IR band intensities of diacetylene in the 250-4300 cm-1 region: Implications for Titan's atmosphere, *J. Mol. Spectrosc., 174*, 116-122, 1995.

Kloster-Jensen, E., H-J. Haink, and H. Christen, The electronic spectra of unsubstitued mono- to penta-acetylene in the gas phase and in solution in the range 1100 to 4000 Å, *Helv. Chim. Acta, 57*, 1731-1744, 1974.

Kobayashi, K., T. Kasamatsu, T. Kaneko, J. Koike, T. Oshima, T. Saito, T. Yamamoto, and H. Yanagawa, Formation of amino acid precursors in cometary ice environments by cosmic radiation, *Adv. Space Res., 16*(2), 21-26, 1995.

Kunde, V.G., A.C. Ainkin, R.A. Hanel, D.E. Jennings, W.C. Maguire, and R.E. Samuelson, C_4H_2, HC_3N, C_2N_2 in Titan's atmosphere, *Nature, 292*, 686-688, 1981.

Meier, R., P. Eberhardt, D. Krankowsky, and R.R. Hodges, The extended formaldehyde source in comet P/Halley, *Astron. Astrophys., 277*, 677-691, 1993.

Moore, M.R., and R.L. Hudson, Infrared Study of Ion-Irradiated Water-Ice Mixtures with Hydrocarbons Relevant to Comets, *Icarus, 135*, 518-527, 1998.

Okabe, H., *Photochemistry of Small Molecules*, Wiley-Interscience, New York, 1978.

Rabek, J.F., *Polymer Photodegradation: Mechanisms and Experimental Methods*, Chapman & Hall, New York, 1995.

Schutte, W.A., L.J. Allamandola, and S.A. Sandford, An experimental study of the organic molecules produced in cometary and interstellar ice analogs by thermal formaldehyde reactions, *Icarus, 104*, 118-137, 1993.

Smith N., Y. Bénilan, and P. Bruston. The temperature dependent absorption cross-sections of C_4H_2 at mid ultraviolet wavelengths, *Planet. Space Sci., 46*(9/10), 1215-1220, 1998.

Smith, P. L., K. Yoshino, W.H. Parkinson, K. Ito, and G. Stark, High resolution VUV (147-201nm) photoabsorption cross sections for C_2H_2 at 195 and 295K, *J. Geophys. Res., 96*, 17,529-17,533, 1991.

Strazzulla, G., G. Leto, G.A. Baratta, and F. Spinella, Ion irradiation experiment relevant to cometary physics, *J. Geophys. Res., 96*, 17,547-17,552, 1991.

Yung, Y. L., M. Allen, and J. P. Pinto, Photochemistry of the atmosphere of Titan: comparison between model and observations, *Astrophys. J. Suppl., 55*, 465-506, 1984.

Y. Bénilan, M.-C. Gazeau, and F. Raulin, Laboratoire Interuniversitaire des Systèmes Atmospheriques, UMR CNRS 7583, Universités Paris VII-Paris XII, 94010 Créteil Cedex, France. (Benilan@lisa.univ-paris12.fr, Gazeau@lisa.univ-paris12.fr, Raulin@lisa.univ-paris12.fr).

P. Chaquin, Laboratoire de Chimie Théorique, Université Paris VI, Place Jussieu, 75005 Paris, France.

H. Cottin, Astrochemistry Branch, Code 691, NASA Goddard Space Flight Center, Greenbelt, MD 20770, USA. (hcottin@lepvax.gsfc.nasa.gov).

(Received July 11, 2000; revised April 10, 2001;
accepted April 25, 2001.)

Article 7

FRAY N., BÉNILAN Y., COTTIN H. and GAZEAU M.-C. (2004) New experimental results on the degradation of polyoxymethylene. Application to the origin of the formaldehyde extended source in comets. Journal of Geophysical Research (Planets) 109, E07S12.

New experimental results on the degradation of polyoxymethylene: Application to the origin of the formaldehyde extended source in comets

N. Fray, Y. Bénilan, H. Cottin, and M.-C. Gazeau

Laboratoire Interuniversitaire des Systèmes Atmosphériques (LISA), UMR 7583 du CNRS, Universités Paris 7 and Paris 12, C. M. C., Créteil, France

Received 2 October 2003; revised 3 December 2003; accepted 15 December 2003; published 3 June 2004.

[1] The formaldehyde (H_2CO) observed in cometary atmospheres presents a so-called "extended source," meaning that its distribution in the coma cannot be explained by sublimation from the nucleus alone; a production inside the coma has to be included. Polyoxymethylene (formaldehyde polymers: $(-CH_2-O-)_n$, also called POM) is sometimes evoked as a parent molecule for this extended source. This solid polymer on cometary grains could release gaseous formaldehyde through thermal and photolytic degradation. We have developed an experimental program in order to study the chemical reactions of degradation of POM by UV photolysis and heating. It provides identification of the degradation products and the determination of the photo degradation quantum yields or the thermal degradation kinetics. In this paper we present the improvements of our experimental setup and new measurements on the kinetics of gaseous formaldehyde production by thermal degradation of two types of commercial POM on a greater temperature range than the previous ones. These new data are then included in a model of the outer coma in order to interpret observations. This model takes into account the production of gaseous molecules from solid material present on grains and leads to a very good agreement with Giotto observations of comet 1P/Halley, if we assume that the cometary grains contain 1–16% of POM by mass. Thus, without being final evidence of this polymer presence on comets, we conclude that the degradation of solid POM-like polymers on cometary grains is to date the best explanation of the H_2CO extended source. *INDEX TERMS:* 6005 Planetology: Comets and Small Bodies: Atmospheres—composition and chemistry; 6008 Planetology: Comets and Small Bodies: Composition; *KEYWORDS:* comet, experimental simulation, extended source

Citation: Fray, N., Y. Bénilan, H. Cottin, and M.-C. Gazeau (2004), New experimental results on the degradation of polyoxymethylene: Application to the origin of the formaldehyde extended source in comets, *J. Geophys. Res.*, *109*, E07S12, doi:10.1029/2003JE002191.

1. Introduction

[2] Most of the molecules observed in the cometary environment are directly produced by sublimation from the nucleus or by the sublimation of ice coating grains within the first few kilometers after they are ejected from the nucleus. However, the radial distribution of some molecules (e.g., CO, H_2CO, HNC) cannot be totally explained with such simple processes. These molecules present a so-called extended source, i.e., a production throughout the coma and not only at or near the surface nucleus. This phenomenon prevents the direct extrapolation from the abundance of these gaseous molecules in the coma to their abundance in the nucleus. Nevertheless, the study of the extended source phenomenon could constrain the chemical composition of solid organics present on cometary grains.

[3] In this paper we study the origin of the formaldehyde (H_2CO) extended source. Its density profile has been derived in comet 1P/Halley from the Giotto Neutral Mass Spectrometer (NMS) measurements [*Meier et al.*, 1993]. This observation demonstrates that H_2CO is not produced only by nucleus sublimation. Moreover, it has been confirmed that H_2CO is produced by an extended source in comet Hyakutake [*Lis et al.*, 1997; *Biver et al.*, 1999] and also in comet Hale-Bopp [*Wink et al.*, 1999].

[4] As H_2CO cannot be produced by photodissociation of another gaseous molecule, polyoxymethylene (formaldehyde polymer: $(-CH_2-O-)_n$, also called POM) has been proposed to interpret the H_2CO extended source [*Meier et al.*, 1993; *Eberhardt*, 1999]. Indeed if POM is present on cometary grains, it may produce gaseous H_2CO by UV photolysis or thermal processing. This polymer of H_2CO has been tentatively detected on the grains of comet

0148-0227/04/2003JE002191$09.00

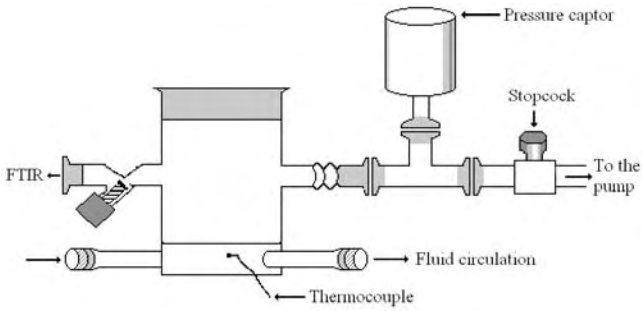

Figure 1. Experimental setup. The Pyrex reactor has a double wall for circulation of a thermostated liquid. The temperature is measured with a K-type thermocouple on the wall of the reactor. It is equipped with a vacuum stopcock leading to the analysis system and another connection to a vacuum pump.

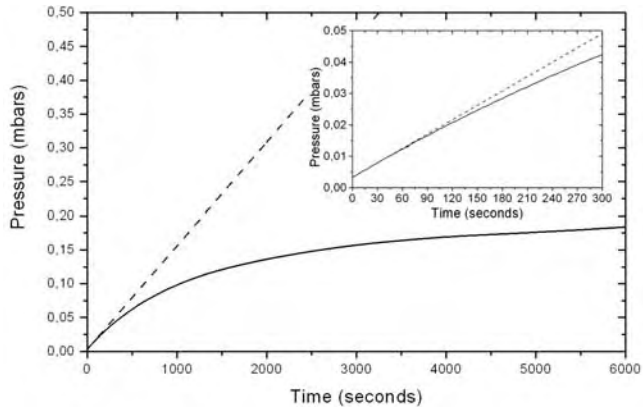

Figure 2. Pressure in the reactor as a function of time in an experiment at 274 K. The black line represents the pressure measurements, whereas the dotted line is a fit on the 20 first seconds of the pressure measurements as shown in the zoom.

Halley by the PICCA mass spectrometer [*Huebner*, 1987]. Nevertheless, this detection is controversial since it has been shown that the feature attributed to POM in the PICCA mass spectrum could be merely the signature of the presence of organic material [*Mitchell et al.*, 1992]. But POM has been surely detected in laboratory analogs of interstellar or cometary ices. It is synthesized by thermal processing of ices containing H_2O, H_2CO, NH_3 [*Schutte et al.*, 1993] or during UV photolysis of ices containing H_2O, CH_3OH, CO and NH_3 [*Bernstein et al.*, 1995]. Thus the presence of POM in cometary ices is possible.

[5] Recently, we have performed an experimental study of the POM degradation by UV photolysis and thermal processing [*Cottin et al.*, 2000, 2001b]. *Cottin et al.* [2000] have shown that several oxygenated compounds (H_2CO, HCOOH, CO, CO_2 and CH_3OH) are produced by UV photolysis of POM at 122, 147 and 193 nm. The quantum yield of H_2CO production is roughly 1 up to 180 nm but decreases at longer wavelengths. On heating, POM produces only gaseous H_2CO since the polymer is in equilibrium with gaseous formaldehyde (POM $\leftrightarrow$ n H_2CO) [*Dainton et al.*, 1959]. The production of gaseous molecules has been measured at several temperatures between 278 and 300 K by *Cottin et al.* [2001b]. The H_2CO kinetics has been shown to follow the Arrhenius law according to

$$\frac{dH_2CO}{dt} = k(T).m_{POM} \text{ where } k(T) = Ae^{-Ea/k_BT}. \quad (1)$$

Here k(T) is the number of gaseous formaldehyde molecules which are produced per gram of POM and per second, A is the frequency factor in molecule.g^{-1}.s^{-1} and Ea is the activation barrier in Joule.$molecule^{-1}$. These experimental data have been included in a model of the coma [*Cottin et al.*, 2001a, 2004]. The required fraction of POM on cometary grains in order to reproduce the observed density profile of H_2CO has been determined. A last version of the model [*Cottin et al.*, 2004] has been built more recently taking into account of the whole distribution size of cometary grains. Measurements of the Giotto spacecraft are very well reproduced, if we suppose that the cometary grains contain less than 10% of POM by mass [*Cottin et al.*, 2001a, 2004]. A second issue of this study is that the production of gaseous H_2CO by thermal degradation of POM is predominant over photo degradation when the comet Halley is at 0.9 AU from the Sun.

[6] The chemical parameters used to model the thermal degradation of POM were very uncertain as the measurements were performed only on a small range of temperature (between 273 and 298 K), whereas the temperature of cometary grains at 1 AU is approximately ranging from 300 to 700 K [*Greenberg and Li*, 1998]. Moreover, when

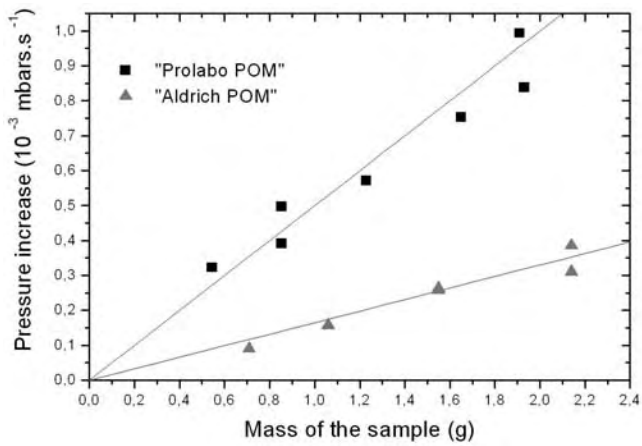

Figure 3. Pressure increase inside the reactor as a function of the mass of the sample of POM. All these measurements have been performed at 289 K. The black squares represent the measurements performed on the "Prolabo POM," whereas the gray triangles are for the "Aldrich POM." For both types of POM, the pressure increase is proportional to the mass of the sample; thus the kinetics of H_2CO production by thermal degradation is proportional to the mass sample at a given temperature.

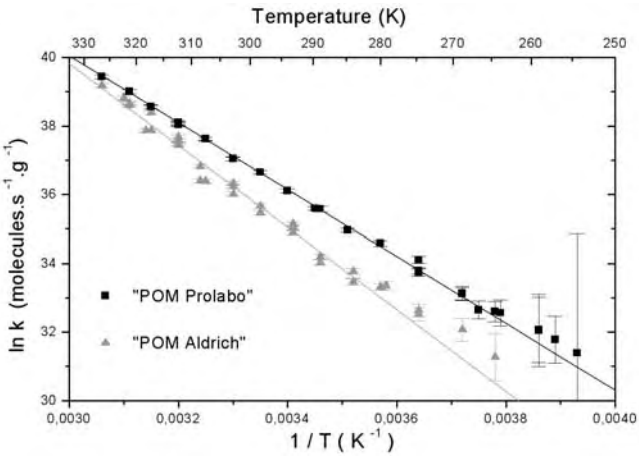

Figure 4. Logarithm of the formaldehyde production rates as a function of the inverse of the temperature. The black squares represent the measurement on the ''Prolabo POM,'' and the gray triangles represent the measurement on the ''Aldrich POM.'' The black and gray lines are fits on the measurements. They allow us to determine Ea (the activation barrier) and A (the frequency factor).

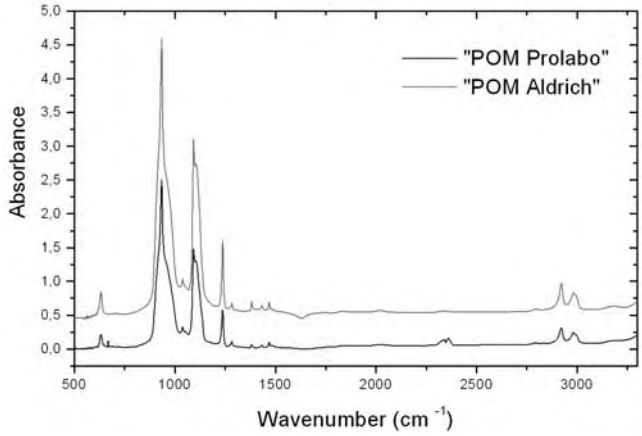

Figure 5. Infrared spectra of solid POMs in KBr pellets. The resolution is 4 cm^{-1}. The spectrum of ''POM Aldrich'' has been shifted.

the comet is close to the Sun, thermal processing is predominant over the photolysis. Therefore, in order to improve the theoretical description of the thermal degradation of POM, we have performed a new experimental study with a new experimental setup allowing a more accurate determination of the H_2CO production kinetics from POM and over a greater temperature range (from 255 to 325 K). Moreover, two commercial types of POM have been studied to test the influence of different polymers on the thermal degradation kinetics. All new results are presented in this paper.

2. Experimental Study

[7] Thermal degradation of two commercial polyoxymethylenes (>99.5%, Prolabo and >95%, Aldrich) has been studied in a Pyrex reactor (Figure 1) with a double wall allowing the circulation of a thermostated fluid necessary to operate at a constant temperature. The temperature is measured with a K-type thermocouple on the wall of the reactor and is recorded during the whole time duration of the experiment with a digital thermometer. The reactor is equipped with a vacuum stopcock leading to the analysis system and another connection to a secondary vacuum pump which allows it to reach a vacuum better than 10^{-6} mbars. A cryothermostat (LAUDA, RUL 80) filled with silicon oil (polydimethylsiloxane) allowing a thermal regulation between 210 and 350 K is used. The pressure inside the reactor is measured with a Baratron gauge (range 10^{-4}-1 mbars) and the pressure is recorded with a timescale of one second.

[8] The polymer is deposited at the bottom of the reactor. Then the temperature of the thermostated fluid is set at its minimal value. Several days are necessary to get rid of residual gas trapped between POM grains. After this step, the temperature was increase up to the required value.

[9] First, we have verified using infrared spectroscopy that formaldehyde (H_2CO) is the single product of thermal degradation for both types of POM. In this case, the kinetics of H_2CO production is directly related to the pressure increase. Figure 2 represents the pressure as a function of time during an experiment at 278 K. The pressure increases and tends toward the equilibrium pressure [*Dainton et al.*, 1959]. Thus the production of gaseous formaldehyde under vacuum is proportional to the pressure increase measured on the 20 first seconds (which can be accurately fitted by a straight line in all the experiments (Figure 2)). Assuming the Ideal Gas Law, the kinetics of formaldehyde production (in number of molecules per second) is directly proportional to the pressure increase. Moreover, if we suppose that this production is

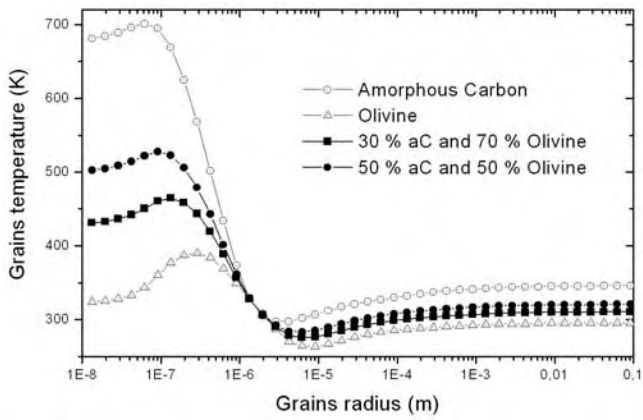

Figure 6. Grain temperature as a function of their radius and composition at 0.9 AU from the Sun. The gray circles and triangles are for pure grains of amorphous carbon and olivine. They represent the upper and lower limits for the grain temperature. The black squares are for grains made of a mixture of 30% amorphous carbon and 70% olivine. The black circles are for grains made of a mixture of 50% amorphous carbon and 50% olivine.

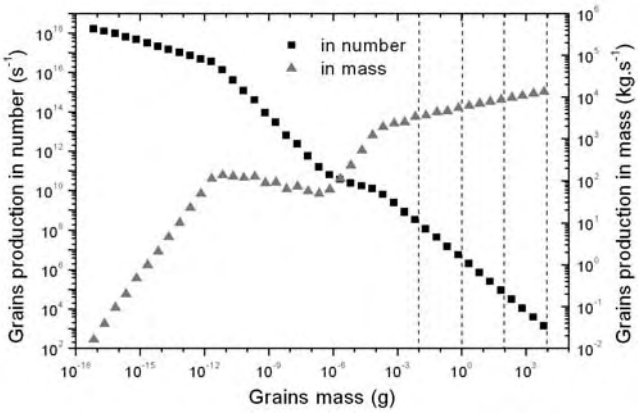

Figure 7. Dust grain production from the comet Halley nucleus as a function of the grain mass. This distribution has been presented by *Crifo and Rodionov* [1997] and is derived from in situ measurements. The data for grains up to 1 mg are direct in situ measurements, whereas higher values are extrapolation. The dashed lines represent the cutoffs which have been used in the modeling (10^{-2}, 1, 10^{+2} or 10^{+4}g).

proportional to the mass sample, the production of H_2CO in number of molecules per second and per gram of polymer is

$$k(T) = \frac{dn}{dt} \cdot \frac{1}{m_{POM}} = \frac{dP}{dt} \cdot \frac{V_{reactor}}{k_B \cdot T \cdot m_{POM}}, \qquad (2)$$

where $V_{reactor}$ is the total volume of the reactor including the volume of the connection of the pressure captor ($V_{reactor}$ = 195 ± 1 cm^3) and k_B is the Boltzmann constant.

[10] In order to check that the production of formaldehyde is proportional to the mass sample, we have studied the pressure increase as a function of the mass of POM in the reactor at 289 K. As shown in Figure 3, the pressure increase is proportional to the mass sample. Thus equation (2) can be used to determine the kinetics of formaldehyde production from the pressure increase. Moreover, the linear relationship shows that the thermal degradation of POM takes place in the whole volume of the sample, and not only at the surface like for the UV photolysis. This result has important implications for the modeling in the cometary grains. We also note that the "Prolabo POM" is more productive than the "Aldrich POM" at a temperature of 289 K.

[11] We have measured H_2CO production for both kinds of POM between 250 and 330 K. The results are presented in Figure 4. The errors bars on each point take into account the uncertainties of the slope of pressure increase, on the mass sample and of the total volume of the reactor. These measurements are well fitted by the Arrhenius law (see equation (1)). These fits allow us to determine Ea, the activation barrier and A the frequency factor:

[12] • Ea = 81 10^3 ± 0.76% J.mole^{-1} and A = 1.2 $10^{30+28\%}_{-22\%}$ molecules.g^{-1}.s^{-1} for the "Prolabo POM".

[13] • Ea = 99 10^3 ± 2.3% J.mole^{-1} and A = 7.2 $10^{32+140\%}_{-60\%}$ molecules.g^{-1}.s^{-1} for the "Aldrich POM."

[14] The non symmetric errors bars on A are due to the logarithm function (ln A is calculated with a symmetric error bar). The value of the activation barrier is quite important; it shows that the production of H_2CO from POM is highly sensitive to the temperature. But, the kinetics of formaldehyde production is different for the two kinds of POM. In order to understand the origin of this discrepancy, we have performed infrared spectroscopy of both types of POM in KBr pellets. These spectra are displayed in Figure 5 (the resolution is 4 cm^{-1}). The minor difference in the spectra at 668 and around 2350 cm^{-1} are due to the presence of CO_2 (due to incomplete purge of the spectrometer) and the one around 1630 cm^{-1} to H_2O. However, these spectra are roughly identical. It suggests that the POM structures are very similar so that the difference in the kinetics of thermal degradation could rather be due to the length of the chain of polymers or the impurities in the sample. Work focused on the differences between different kinds of POMs is currently in progress.

[15] In conclusion, we have determined new values of the activation barrier Ea and the frequency factor A that differ from [*Cottin et al.*, 2001b] ones (Ea = 74.2 10^3 ± 10% J.mole^{-1} and A = 8.7 $10^{27+120\%}_{-60\%}$ molecules.g^{-1}.s^{-1}) which were obtained on "Prolabo POM" between 273 and 298 K. These new results are considered to be more reliable as they have been retrieved with an optimized experimental setup. Indeed we are now able to record the pressure inside the reactor with a timescale of one second whereas previously it was manually recorded. Then we are now able to derive the pressure increase from the first 20 second of the experiments (see Figure 2) and therefore we are not affected by the equilibrium between gaseous

Table 1a. Results of the Fits Performed With the Kinetics Data Acquired on "POM Aldrich"[a]

	Grains Made of 30% Amorphous Carbon and 70% Olivine				Grains Made of 50% Amorphous Carbon and 50% Olivine			
Mass of the bigger grains, g	10^{-2}	1	10^{+2}	10^{+4}	10^{-2}	1	10^{+2}	10^{+4}
Q_{POM}, %	20	15.5	4	1.5	20	6.2	2.3	1
Q_{H2CO}/Q_{H2O}, %	1.8	0.8	0.7	0.35	1.3	0.65	0.15	0
σ, %	21.8	6.9	6.6	6.1	11.2	6.6	6	10.8

[a] Q_{POM} (%) is the percentage of POM by mass present in grains, Q_{H2CO} is the production rate of formaldehyde produced by the nucleus sublimation (in molecules.s^{-1}), and Q_{H2O} is the production rate of water (in molecules.s^{-1}) which has been taken equal to 6 10^{29} molecules.s^{-1} [*Fink and DiSanti*, 1990]; σ is the standard deviation of the fit.

Table 1b. Results of the Fits Performed With the Kinetics Data Acquired on "POM Prolabo"[a]

	Grains Made of 30% Amorphous Carbon and 70% Olivine				Grains Made of 50% Amorphous Carbon and 50% Olivine			
Mass of the bigger grains (g)	10^{-2}	1	10^{+2}	10^{+4}	10^{-2}	1	10^{+2}	10^{+4}
Q_{POM} (%)	20	9.3	2.8	1.3	19.9	5	2	0.9
Q_{H2CO}/Q_{H2O} (%)	1.65	0.75	0.55	0	0.8	0.5	0	0
σ (%)	16.6	6.8	6.4	6	6.8	6.3	6.3	14.1

[a] Q_{POM} (%) is the percentage of POM by mass present in grains, Q_{H2CO} is the production rate of formaldehyde produced by the nucleus sublimation (in molecules.s^{-1}), and Q_{H2O} is the production rate of water (in molecules.s^{-1}) which has been taken equal to 6 10^{29} molecules.s^{-1} [*Fink and DiSanti*, 1990]; σ is the standard deviation of the fit.

H_2CO and POM. These new results are then more reliable than the previous ones.

3. Modeling of the Cometary Environment

[16] We [*Cottin et al.*, 2001a, 2004] have derived new equations assuming the hypotheses of *Haser* [1957] (e.g., spherical symmetry of the coma, steady state in the production of gas and dust) in order to model the production of gaseous molecules from solid materials present on grains. This model takes into account the photo and thermal processes in order to reproduce the production of gaseous formaldehyde by an extended source but it takes also account of the possible production of formaldehyde by sublimation from nucleus. It allows us to fit the formaldehyde density profiles which have been obtained from Giotto NMS measurements [*Meier et al.*, 1993]. For the present study, we have used the last version of the model [*Cottin et al.*, 2004], which takes into account a grain size distribution. The free parameters of this model are the percentage of POM by mass percent in grains (Q_{POM}) and the production rate of parent formaldehyde (i.e., the formaldehyde produced directly at the nucleus surface, Q_{H2CO}). Other important parameters of this model are the temperature, the velocity and the size distribution of the grains. The grain temperature is calculated at 0.9 AU from the Sun using Mie theory considering spherical grains made of a mixture of amorphous carbon and olivine. Amorphous carbon is representative of black matter, and stands as an upper limit for a strongly absorbing organic component of grains. Olivine stands for the silicate component of grains with a very low absorption in the visible. Then pure grains of amorphous carbon stand for an upper limit of grain temperature whereas pure grains of olivine represent a lower limit. The grain temperature as a function of their radius for different composition is presented in Figure 6. A similar figure has already been presented in *Cottin et al.* [2004]. The velocity of each grain is calculated as a function of the grain size using the formula given by *Crifo* [1995]. We have used the grains distribution which is presented by *Crifo and Rodionov* [1997] (Figure 7). It is derived from in situ measurements presented in *McDonnell et al.* [1991]. Nevertheless, it must be noted that data for grains up to 1 mg are direct in-situ measurements, whereas higher values are extrapolation.

[17] The temperature of grains as well as the mass of the bigger ones which can be lifted by the nucleus are not well constrained. Therefore we have performed several fits with grains containing 30 or 50% of amorphous carbon to simulate different temperatures and for different mass of the bigger grains. This mass of the bigger grains is arbitrary set at 10^{-2}, 1, 10^{+2} or 10^{+4} g. For comparison, the grains distribution leading to the best fit of *Cottin et al.* [2004] corresponds to the same size distribution and a cutoff at 1 g. Moreover, we have used both kinetics data derived from "POM Prolabo" and "POM Aldrich." Results are presented in Tables 1a and 1b, which display both free parameters (Q_{POM} and Q_{H2CO}/Q_{H2O}) and σ, which is the standard deviation of the fit. Two examples of fits are presented in Figures 8a and 8b.

[18] As it has already been shown by *Cottin et al.* [2001a, 2004], we find that, at the heliocentric distance of the Giotto encounter with comet Halley, the thermal degradation of POM is predominant over the photo degradation. The required fraction of POM is from 1.2 to 1.7 times higher if we consider the kinetic data of the "Aldrich POM" rather than the ones of "Prolabo POM" (see Tables 1a and 1b). Indeed, most of the gaseous formaldehyde are produced by the bigger grains [*Cottin et al.*, 2004] for which the temperature is about 320 K. At this temperature, the kinetic of gaseous formaldehyde production is roughly 1.4 times higher for the "Prolabo POM" than for the "Aldrich

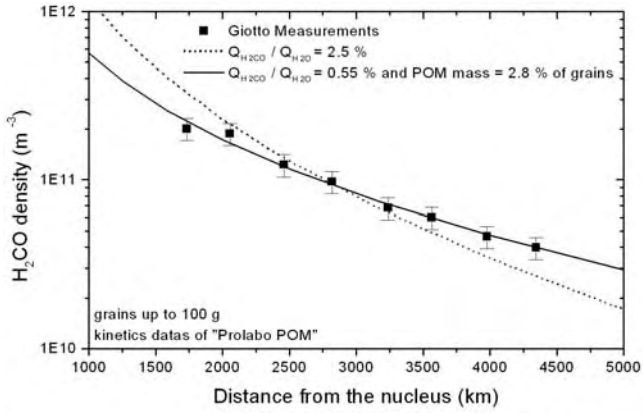

Figure 8a. H_2CO density as a function of the distance from the nucleus. The solid line represents the fit obtained with our model, whereas the dotted line is the fit obtained with a simple Haser model (production only at the nucleus surface). This fit has been obtained with the kinetics data of the "Prolabo POM," with grains made of 30% amorphous carbon and 70% olivine. The mass of the bigger grains is 100 g.

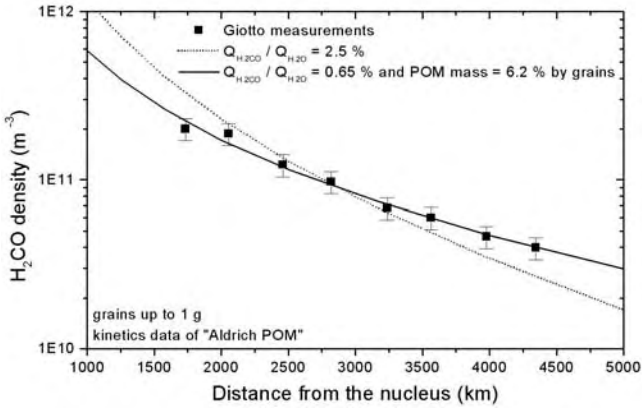

Figure 8b. H_2CO density as a function of the distance from the nucleus. The solid line represents the fit obtained with our model, whereas the dotted line is the fit obtained with a simple Haser model (production only at the nucleus surface). This fit has been obtained with the kinetics data of the "Aldrich POM," with grains made of 50% amorphous carbon and 50% of olivine. The mass of the bigger grains is 1 g.

POM." Thus the required fraction of POM in cometary grains is directly related to the kinetics data which are used.

[19] For some fits, the standard deviation is relatively high. Indeed, no relevant results are obtained with a mass of the bigger grains equal to 10^{-2} gram. In this case, the grains are not abundant enough to fit measurements. Nor are relevant results obtained if we consider high temperature grain (grains containing 50% of amorphous carbon) with a mass of the bigger grains equal to 10 grams. In this case, too much gaseous formaldehyde is produced from POM degradation. If we exclude these extreme cases, the best fits are obtained with a standard deviation ranging from 6 to 7%. For all these adjustments, the production of parent formaldehyde from the nucleus is ranging from 0 to and 0.8%, and the fraction of POM by mass from 1.3 to 15.5%.

[20] *Greenberg* [1998] has estimated that complex organic molecules dominated by carbon represent about 47% of the mass of the refractory materials present in cometary nucleus. Moreover, *Bernstein et al.* [1995] has measured that POM-related compounds represent 20% by mass of the organic material remaining after photolysis and heating at room temperature of laboratory ice analogs. We can derive from these data that values up to 9% in mass of POM-like polymers can be reached in comets. Thus the required fraction of POM to fit the H_2CO density profile is consistent with this latter value. Moreover, this result is not dependent on the type of POM used in the model. Therefore the production of gaseous formaldehyde from POM degradation is a quantitative explanation of the formaldehyde extended source and the presence of POM-like polymers in cometary nucleus is highly probable.

4. Conclusion

[21] It has been shown that the degradation by UV photolysis or heating of POM could explain the H_2CO extended source [*Cottin et al.*, 2001a, 2004]. We have presented in this paper new experimental measurements of the thermal degradation of this polymer on a greater temperature range than the previous ones. The kinetics of gaseous formaldehyde production has been derived for two types of POM. The results are quite different. This discrepancy is not completely understood so far, but it could be due difference of the length of the chains of the polymers. New studies are in progress to understand the origin of this difference.

[22] Nevertheless, these kinetics data have been included into a model of the coma, which takes into account the production of gaseous molecules from solid materials present on cometary grains. The data on both type of POM allow us to reproduce with a good accuracy the measurements of the H_2CO density acquired by the Giotto spacecraft inside the coma of comet Halley, and are leading to similar results at this heliocentric distance. Since the production of gaseous H_2CO depends of the type of polymer that we consider, we are now currently studying the H_2CO extended source as a function of the heliocentric distance in comet C/1995 O1 (Hale-Bopp) to test the influence of a variation of grain temperature.

[23] The required fraction of POM by mass on grains in order to fit the Giotto observations has been found to range from 1.3 to 15.5% for different parameters of grains. These values are quite consistent with previous estimates based on observations and laboratory works. Thus, without being final evidence of the presence of the polymer on comets, we conclude that POM-like polymers in the solid state on cometary grains are to date the best interpretation of the H_2CO extended source.

References

Bernstein, M. P., S. A. Sandford, L. J. Allamandola, S. Chang, and M. A. Scharberg (1995), Organic compounds produced by photolysis of realistic interstellar and cometary ice analogs containing methanol, *Astrophys. J.*, *454*, 327–344.

Biver, N., et al. (1999), Spectroscopic monitoring of comet C/1996 B2 (Hyakutake) with the JCMT and IRAM radio telescopes, *Astron. J.*, *118*(4), 1850–1872.

Cottin, H., M. C. Gazeau, J. F. Doussin, and F. Raulin (2000), An experimental study of the photodegradation of polyoxymethylene at 122, 147 and 193 nm, *J. Photochem. Photobiol. A: Chem.*, *135*, 53–64.

Cottin, H., M. C. Gazeau, Y. Bénilan, and F. Raulin (2001a), Polyoxymethylene as parent molecule for the formaldehyde extended source in comet Halley, *Astrophys. J.*, *556*, 417–420.

Cottin, H., M.-C. Gazeau, P. Chaquin, F. Raulin, and Y. Bénilan (2001b), Experimental and theoretical studies on the gas/solid/gas transformation cycle in extraterrestrial environments, *J. Geophys. Res.*, *106*(E12), 33,325–33,332.

Cottin, H., Y. Benilan, M.-C. Gazeau, and F. Raulin (2004), Origin of cometary extended sources from degradation of refractory organics on grain: Polyoxymethylene as formaldehyde parent molecule, *Icarus*, *167*(2), 397–416.

Crifo, J. F. (1995), A general physicochemical model of the inner coma of active comets. 1: Implications of spatially distributed gas and dust production, *Astrophys. J.*, *445*, 470–488.

Crifo, J. F., and A. V. Rodionov (1997), The dependence of the circumnuclear coma structure on the properties of the nucleus. I. Comparison between a homogeneous and an inhomogeneous spherical nucleus, with application to P/Wirtanen, *Icarus*, *127*(2), 319–353.

Dainton, F. S., K. J. Ivin, and D. A. G. Walmsley (1959), The equilibrium between gaseous formaldehyde and solid polyoxymethylene, *Trans. Faraday. Soc.*, *55*, 61–64.

Eberhardt, P. (1999), Comet Halley's gas composition and extended sources: Results from the neutral mass spectrometer on Giotto, *Space Sci. Rev.*, *90*, 45–52.

Fink, U., and M. A. DiSanti (1990), The production rate and spatial distribution of H_2O for comet P/Halley, *Astrophys. J.*, *364*, 687–698.

Greenberg, J. M. (1998), Making a comet nucleus, *Astron. Astrophys.*, *330*, 375–380.

Greenberg, J. M., and A. Li (1998), From interstellar dust to comets: The extended CO source in comet Halley, *Astron. Astrophys.*, *332*, 374–384.

Haser, L. (1957), Distribution d'intensité dans la tête d'une comète, *Bull Acad. R. Belg.*, *43*, 740–750.

Huebner, W. F. (1987), First polymer in space identified in comet Halley, *Science*, *237*, 628–630.

Lis, D. C., J. Keene, K. Young, T. G. Phillips, D. Bockelée-Morvan, J. Crovisier, P. Schilke, P. F. Goldsmith, and E. A. Bergin (1997), Spectroscopic observations of comet C/1996 B2 (Hyakutake) with the Caltech Submillimeter Observatory, *Icarus*, *130*(2), 355–372.

McDonnell, J. A. M., P. L. Lamy, and G. S. Pankiewicz (1991), Physical properties of cometary dust, in *Comets in the Post-Halley Era*, pp. 1043–1073, Kluwer Acad., Norwell, Mass.

Meier, R., P. Eberhardt, D. Krankowsky, and R. R. Hodges (1993), The extended formaldehyde source in comet P/Halley, *Astron. Astrophys.*, *277*, 677–691.

Mitchell, D. L., R. P. Lin, C. W. Carlson, A. Korth, H. Rème, and D. A. Mendis (1992), The origin of complex organic ions in the coma of comet Halley, *Icarus*, *98*, 125–133.

Schutte, W. A., L. J. Allamandola, and S. A. Sandford (1993), An experimental study of the organic molecules produced in cometary and interstellar ice analogs by thermal formaldehyde reactions, *Icarus*, *104*, 118–137.

Wink, J., et al. (1999), Evidence for extended sources and temporal modulations in molecular observations of C/1995 O1 (Hale-Bopp) at the IRAM interferometer, *Earth Moon Planets*, *78*(1), 63, 1997.

Y. Bénilan, H. Cottin, N. Fray, and M.-C. Gazeau, Laboratoire Interuniversitaire des Systèmes Atmosphériques (LISA), UMR 7583 du CNRS, Universités Paris 7 and Paris 12, C. M. C., 61 Avenue du Général de Gaulle, 94010 Créteil Cedex, France. (fray@lisa.univ-paris12.fr)

Article 8

COTTIN H., BACHIR S., RAULIN F. and GAZEAU M. C. (2002) Photodegradation of Hexamethylenetetramine by VUV and its relevance for CN and HCN extended sources in comets. Advances in Space Research 30(6), 1481-1488.

Pergamon
www.elsevier.com/locate/asr

Adv. Space Res. Vol. 30, No. 6, pp. 1481–1488, 2002

Printed in Great Britain
0273-1177/02 $22.00 + 0.00

PII: S0273-1177(02)00508-2

PHOTODEGRADATION OF HEXAMETHYLENETETRAMINE BY VUV AND ITS RELEVANCE FOR CN AND HCN EXTENDED SOURCES IN COMETS

Hervé Cottin, Souleyman Bachir, François Raulin and Marie-Claire Gazeau

Laboratoire Interuniversitaire des Systèmes Atmosphériques (LISA), UMR 7583 CNRS, Université Paris 7 and Paris 12, C.M.C., 61 Avenue du Général de Gaulle, 94010 Créteil Cedex, France

ABSTRACT

This paper presents our first experimental results on the photodegradation at 147 and 122 nm of hexamethylenetetramine (HMT). This molecule, suspected to be present on cometary grains, could be responsible for extended sources of CN and HCN in comets. We show that if HMT is quite resistant to direct photolysis under vacuum, interactions with water vapor photoproducts, which could happen in inner comae, lead to a much more efficient degradation with formation of HCN, NH_3 and other N bearing molecules. Thus HMT could act as a parent or grand parent molecule for observed extended sources. However, additional source with greater degradation efficiency is certainly required to account observations in outer comae.

INTRODUCTION

The nature of organic components of interstellar dust and comets is critical to understanding the chemical evolution of materials from the interstellar medium to the solar system. A classical laboratory approach to this problem is to start with various ice mixtures at temperature of 10 K and to photolyze with vacuum ultraviolet or irradiate with charged particles, or simply warm the ices, simulating the processing of ice-mantled dust in molecular clouds. When warmed to room temperature, these processed mixtures leave a residue which is called « yellow stuff » and which is generally presumed to be a close analog of the organic mantles of dust in molecular clouds (see for instance : (Allamandola et al., 1988; Briggs et al., 1992), or (Cottin et al., 1999) for a review on that subject).

Among the complex organic refractory molecules that have been synthesized during cometary and interstellar ice analog experiments, polyoxymethylene (POM - $(CH_2\text{-}O)_n$) and hexamethylenetetramine (HMT - $C_6H_{12}N_4$) (see Figure 1) seem to be of prime interest. POM and polymers of the same family have been detected when ice mixtures with formaldehyde and ammonia are slowly warmed to room temperature, without any photolysis or ion irradiation processing (Schutte et al., 1993a; Schutte et al., 1993b). After UV photolysis of mixtures such as H_2O : CH_3OH : CO : NH_3 (10 : 5 : 1 : 1), POM-like polymers have also been detected, but HMT represents ~60 % of the organic residue at 300 K (Bernstein et al., 1995). Thus, its looks like the presence of an important amount of POM is a good indicator for thermal processing of ices, while HMT plays the same role concerning UV photolysis. HMT is of particular interest since it forms amino acids when acid-hydrolyzed (Wolman et al., 1971).

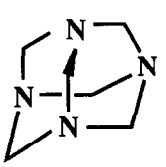

Fig. 1: Hexamethylenetetramine

Based on the interstellar dust model of comets as consisting of more or less reprocessed aggregated interstellar silicate grains with organic mantles, it was predicted that the comet dust would not only be rocky material (silicates), but have a significant fraction in the form of refractory organics; i.e. organics which are non-volatile with respect to the ices (Greenberg,

1982). This prediction was supported by the mass spectrometry analysis performed on the VEGA 1&2 and GIOTTO spacecraft, sent to fly by Comet Halley (Kissel and Krueger, 1987; Mitchell et al., 1992). However, even with this basic confirmation of the idea of organic mantles, one puzzling feature of comet dust is the source of the distributed CO (DiSanti et al., 1999; DiSanti et al., 1997; Eberhardt et al., 1987), H_2CO (Biver et al., 1999; Bockelée-Morvan et al., 1998; Lis et al., 1997; Meier et al., 1993), CN (Woodney et al., 1998) and HCN (Veal et al., 2000) in cometary comae. It is likely that their formation results from the thermal and/or photodegradation of refractory material on the outflowing dust. It has been shown that the thermal and photodegradation of polyoxymethylene on cometary grains could be a good explanation of formaldehyde in comet Halley (Cottin, 1999; Cottin et al., 2001). Since HMT synthesis is favored in photolyzed ice mixtures, its presence is likely on cometary grains, and its degradation could be a source of N bearing molecules, and thus may be a source for HCN and CN in comae.

CN and HCN extended sources in comets, and relevance of HMT as potential parent molecule

An extended source of CN radical has been detected in comet Halley, and could have for origin the degradation of larger molecules on grains (Klavetter and A'Hearn, 1994). Moreover, in most comets, the observed HCN is not enough to account for CN (Crovisier and Schloerb, 1991). Hale-Bopp observation at important heliocentric distances (> 2.9 AU) did not show any evidence for such a process (Rauer et al., 1997), but that far from the sun, the organic component of grains might be too cold or not irradiated enough to release CN. On the other hand, for smaller heliocentric distance, HCN and CN distribution maps are not compatible, which implies another parent molecule for the radical (Woodney et al., 1998). The abundance of the other detected potential parent molecules (HNC, CH_3CN, HC_3N) is not sufficient to solve this problem.

Concerning HCN, (Veal et al., 2000) have shown that its distribution in the coma of Hale-Bopp presents discrepancies with the one that would result from a direct sublimation from nucleus. The authors propose that a release of HCN from icy grains could explain observation. But in this case, we think that most of the other detected volatile molecules, subliming with the water, would present the same phenomenon, which has not been yet proved. Therefore, the process responsible of the extended source phenomenon is certainly a slow degradation of the refractory organic component of grains.

HMT could be such a parent molecule. Indeed, photolysis of HMT in water and argon matrices at ~ 12 K have already been performed (Bernstein et al., 1994). It leads to the production of nitriles (RCN), isonitriles (RNC), and other N bearing compounds. In this paper, we present results concerning HMT photodegradation at room temperature, and more precisely the study of gaseous molecules released during degradation. This process simulates the action of solar UV on cometary grains, in order to conclude if HMT can be at the origin of HCN and CN extended sources. HMT has been photolyzed under vacuum, and with water vapor to simulate the photochemical environment in comae.

EXPERIMENTAL

Photochemical Reactor

The experimental set-up has been described in details in (Cottin et al., 2000). It mainly consists in a pyrex reactor topped by a UV lamp (Fig. 2). The reactor is equipped with a vacuum stopcock leading to the analysis system (or to a cold trap), and another connection to a secondary vacuum pump (Turbomolecular pump, Balzers). A vacuum better than 10^{-4} mb can be reached during pumping. The photochemical reactor has a double wall for circulation of a thermostated liquid necessary to operate at a constant temperature.

The UV irradiation system is composed of a lamp filled with an appropriate gas or gas mixture according to the emitted wavelength: 5.5 mb H_2 (2%) in He (> 99.99 % - Linde - France) for a 122 nm emission (Lyman α), and 0.3 mb Xe (99.99 % - Linde - France) for 147 nm. Discharge in the lamp is initiated with a Tesla coil and the gas is excited by a microwave generator (Somelec - France) with a power of 200 W at 2450 MHz. The pressure of the gas in the lamp is set at a level allowing to maintain a stable discharge. Titanium wires heated by an electric current can be used as efficient getters to purify Xenon during 147 nm experiments. The window between the lamp and the reactor is made of MgF_2. The photon flux of the two lamps determined by chemical actinometry are $f_{122nm} \sim 2\ 10^{15}$ *photons.s*$^{-1}$ and $f_{147nm} \sim 10^{16}$ *photons.s*$^{-1}$.

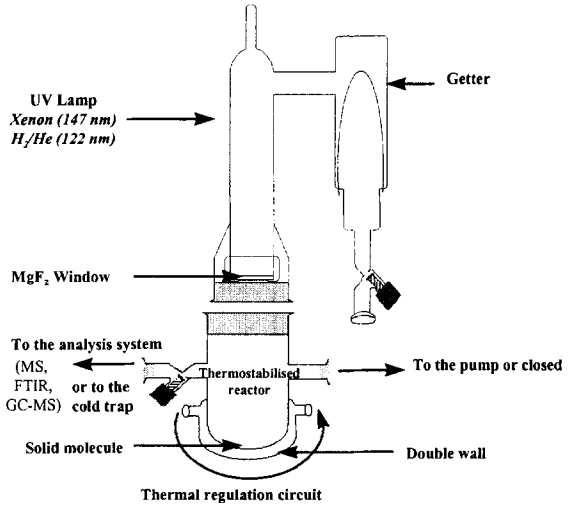

Fig. 2: Photochemical reactor and UV lamp

Chemical

We have used commercial hexamethylenetetramine (>99.5 %, Fluka). The molecule is deposited at the bottom of the reactor and irradiated at different wavelengths after several days of pumping. Irradiation experiments have been performed at room temperature. HMT vapor pressure is negligible and no spontaneous thermal degradation has been observed.
Two kinds of experiments have been performed : HMT photolysis under vacuum, and photolysis of HMT with 0.1 mb of water vapor.

Analysis

Preliminary chemical analysis of the gaseous mixture resulting from the photolyzed HMT has been carried out using a mass spectrometer (Leybold Inficon - Transpector). MS experiments have been performed at 5.10^{-5} mb, between 1 and 200 AMU with a resolution of 1 AMU. This technique is very sensitive, but since there is no separation of the different products before analysis, it can only give hints of the presence of a compound if one refers to the major ions detected. MS analysis can only be performed when HMT is irradiated under vacuum : presence of water vapor (0.1 mb) would saturate the MS detector (quadripole), which is usable for pressure < 10^{-4} mb.

The photodegradation products can also be concentrated in a cold trap at ~70 K (liquid nitrogen). The concentration is carried *during* irradiation when HMT is degraded under vacuum, or *after* irradiation in the presence of water vapor. When the trap is warmed up at room temperature, the resulting gaseous sample can be analyzed by FTIR (Perkin Elmer, 1710), or injected into a GC (Varian 3400), through a column MXT-1701 (Restek, 40°C, head pressure : 15 psi). The detector is a ion trap mass spectrometer (Finnigan - Varian) ranging from 1 to 650 amu, with a resolution of 1 AMU.

RESULTS

HMT irradiation under vacuum

MS analysis

Irradiations have been performed at 122 and 147 nm. No production of gaseous fragment have been detected during irradiation, including the 26 amu fragment that would suggest a production of CN radical resulting from HMT photodegradation.

FTIR analysis

In order to obtain a better detection, a cold trap has been used to concentrate photofragments for an FTIR analysis. Two hours irradiations have been performed at 147 nm.

Fig. 3 shows HCN detection by its signature at 713 cm^{-1}. Its amount is too low to be quantified. Some CO_2 is also detected by its signature centered at 668 cm^{-1}, and its band at 720 cm^{-1}. Its presence is due to an atmospheric contamination in the spectroscopic compartment and also to impurities in the industrial N_2 that is used to adjust the total pressure in the analysis cell at about 800 mb (an augmentation of the total pressure in the analysis cell broadens the IR bands of most compounds, and allows a better detection sensitivity).

No photofragment has been detected at 122 nm, probably because the lamp flux is significantly lower than for the 147 nm lamp.

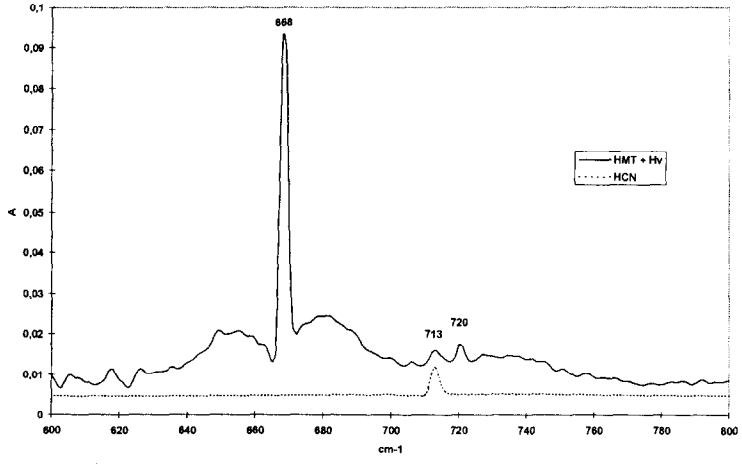

Fig. 3: *Continuous line* : Infrared spectrum of the gaseous phase resulting from HMT photodegradation, after 2 hours of concentration at 147 nm, between 600 and 800 cm^{-1}. *Dotted line* : HCN infrared spectrum. For both spectra : optical path : 10 cm ; resolution : 2 cm^{-1}. Pressure completed at 800 mb with nitrogen.

HMT + H_2O vapor irradiation

FTIR analysis

6 hours irradiations of HMT at 147 nm have been performed with 0.1 mb of water vapor. This pressure is not relevant of cometary environment, which is about 10^{-4} mb near the nucleus. Our aim is not to simulate the coma, but to study a chemical mechanism. The pressure has been chosen in order (1) that most of the UV flux reaches the HMT (~99%), and (2) obtain a process efficient enough (i.e. enough water) to allow detection of photoproducts. A resulting IR spectrum is presented on Figure 4. Again, HCN is detected by its signature at 713 cm^{-1}. NH_3 is also identified by its signatures at 967 and 929 cm^{-1}. Amounts of HCN and NH_3 detected decrease from an experiment to the other. This is due to a decrease of the lamp flux induced by the formation, on the window of the lamp, of an organic polymer, which absorbs the UV photons. Therefore, our experiments are not reproducible because the photonic flux cannot be controlled. No compound have been detected for irradiation at 122 nm.

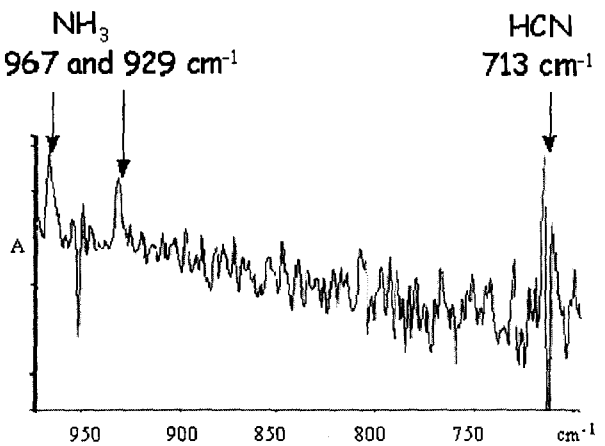

Fig. 4: Infrared spectrum of the gaseous phase resulting from HMT photodegradation, after 6 hours of irradiation at 147 nm, between 700 and 1000 cm^{-1}. Optical path : 10 cm ; resolution : 2 cm^{-1}. Pressure completed at 800 mb with nitrogen.

A rough estimation of the production quantum yields for both detected compounds can be achieved (how many molecules are produced for one photon in our photochemical system : HMT + H_2O). Considering the first experiment, for which the lamp flux is assumed at its highest level (measurement by chemical actinometry before irradiations), one can write :

$$\frac{d[HCN]}{dt} = \Sigma sources - \Sigma sinks = \frac{Flux * \Phi_{HCN}}{V} - (J_{HCN} * [HCN])$$

With :
[HCN] :concentration measured by FTIR, and calculated from a calibration performed at the same partial pressure and resolution. ($3.65\ 10^{14}\ molec.cm^{-3}$)
Flux : lamp flux before experiment ($f_{147nm} \sim 10^{16}\ photons.s^{-1}$)
Φ_{HCN} : quantum yield we want to estimate
V : reactor's volume ($300\ cm^3$)
J_{HCN} : photolysis constant calculated from (Okabe, 1978) ($1.6\ 10^{-2}\ s^{-1}$).
If a photostationary state is assumed $\frac{d[HCN]}{dt} = 0$, then $\Phi_{HCN} \sim 0.2$.

The same calculation can be achieved for NH_3, with $[NH_3] = 1.58\ 10^{15}$ molec.cm^{-3} and $J_{NH3}=3.2\ 10^{-3}\ s^{-1}$. Then $\Phi_{NH3} \sim 0.1$.
Considering our hypothesis of a photostationnary state, if this equilibrium is not achieved in the reactor, the concentration of the studied product has not reached its stationary level and [X] < [X]eq. Then our estimation is a lower limit.
Considering our second hypothesis, that the lamp flux is at its maximum during the irradiation, whereas it is decreasing because of the formation of a polymer on the window, we can derive that our estimation for the quantum yield is again a lower limit.

GC-MS analysis

GC-MS analysis after 6 hours irradiations of HMT at 147 nm is presented on Figure 5. Six products are detected. Compound 1 is not visible on the total mass plot (Figure 5-a), but it has been clearly identified to be CH_3CN from a specific

scan at 41 amu (Figure 5-b), its mass spectrum (Fig. 6 - Compound n°1), and its retention time measured after injection of the pure compound.

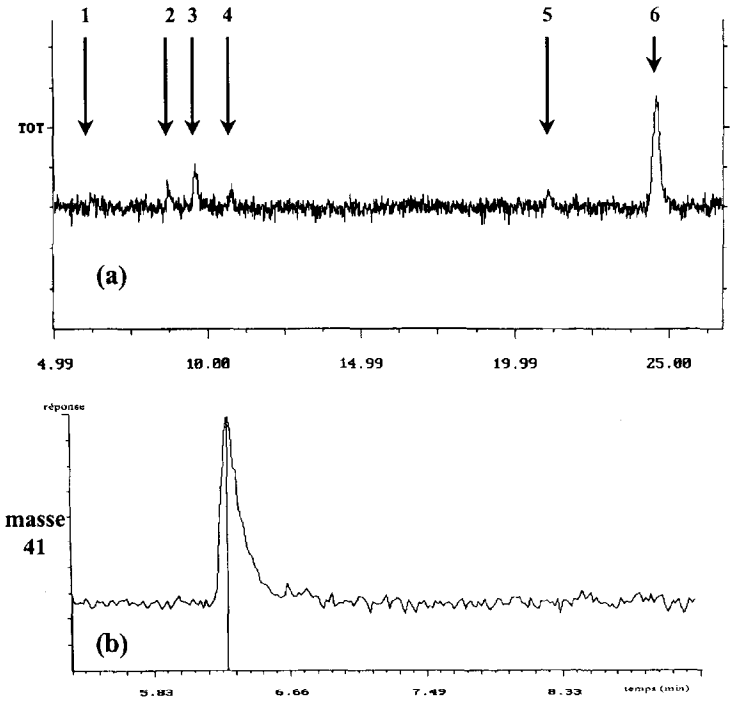

Figure 5: (a) Analysis of HMT 147 nm photodegradation products by GC-MS. Fig (b) is the specific chromatogram at mass 41 that lead to detection of CH_3CN, which is hidden in the noise of the total mass plot.

For compounds 2 to 6, tentative identifications are proposed based on standard mass spectra from the NIST data base, or based on hypothesis concerning combinations between C, H, N and O atoms, and derived structures compatible with spectra. Our results are presented in table 1. Experiments have also been performed at 122 nm: only compounds 1 and 6 have been detected. This is certainly due to the low hydrogen lamp flux.

Table 1: Interpretation of chromatograms and mass spectra obtained after HMT + H_2O photolysis. (t) refers to a tentative detection.

n°	Formula	Identification	147 nm	122 nm
1	CH_3CN	Retention Time	X	X
2 (t)	$CH_3COOCH_2CH_3$ Ethylacetate	NIST Mass Spectrum	X	
3 (t)	$CH_3CH_2CH(CH_3)CH_2CH_2CH_3$ 3 Methyl, Hexane	NIST Mass Spectrum	X	
4 (t)	N≡C-CH=CH-C≡N 2, Butenedinitrile	78 : $(NCCHCHCN)^+$ 52 : $(NCCHCH)^+$ 39 : $(NCCHCHCN)^{2+}$	X	
5 (t)	Not identified	Not identified	X	
6 (t)	N≡C-NH-C≡C-C≡N	91 : $(NCNHCCCN)^+$ 65 : $(HNCCCN)^+$ 51 : $(HCCCN)^+$	X	X

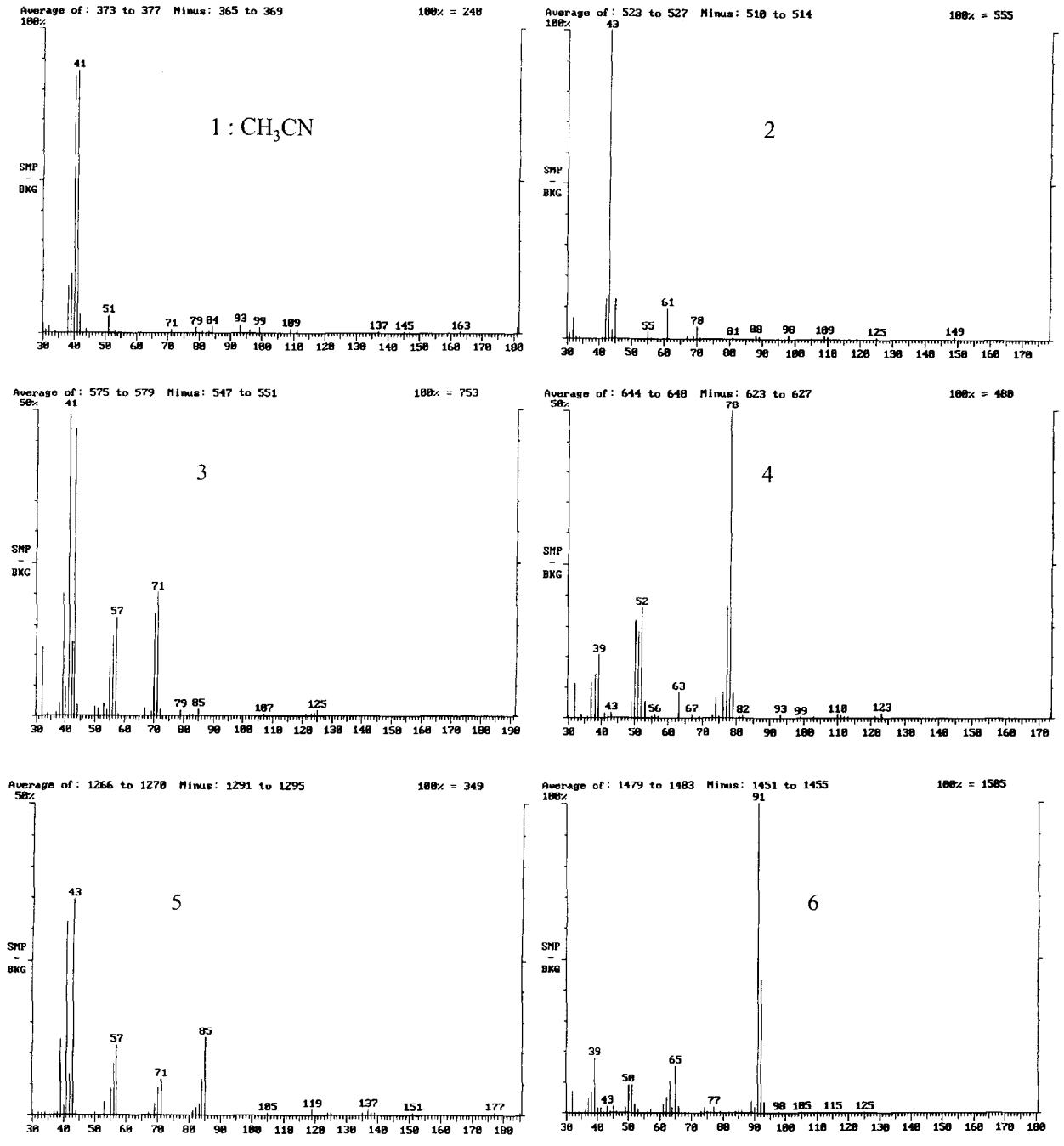

Fig. 6: Mass spectra of compounds 1 to 6. Higher fragments than the parent ion are due to molecular recombinations in the ion trap.

DISCUSSION

Further analyses are required to confirm the detection of tentatively identified compounds, and to better constrain our quantitative data. This is a difficult task, mainly because of the « darkening » of the MgF_2 window during irradiation, which shortens the possible duration of our experiments, and complicate achievement of quantitative results.

Nevertheless, those results show that the degradation of HMT is much more efficient in presence of water vapor: it yields more products, and induces quantum yield of about 0.2 and 0.1 for HCN and NH_3 production, whereas it has been impossible to quantify HCN produced during photolysis under vacuum. It seems that the degradation process is activated by the photolysis products of water : OH°, H°. Those radicals may react with HMT and lead to its degradation. After breaking of the molecule,

fragments may recombine. Dehydration of resulting compounds may lead to the formation of unsaturations observed in some of our resulting molecules.

Like (Bernstein et al., 1994), we detect nitriles and other N bearing molecules. But according to their results, a direct photolysis of HMT should be more efficient than we obtain. Indeed, they have shown a photodegradation of matrix-isolated HMT in Ar ice. Argon first ionization energy being of about 15 eV (i.e. $\lambda \sim 82$ nm), HMT degradation in that matrix should be similar to our photolysis under vacuum as Ar is not involved in the degradation mechanism. Water traces in the argon matrix may be an explanation for this discrepancy.

Those data cannot yet be directly used in numerical models to interpret observation, because they have been obtained with a water pressure much higher than it can be encountered in cometary environment. A pressure dependence study is necessary to model the process, but it is likely that the use of lower water pressure will induce lower quantum yields. Nevertheless those preliminary results show that to understand the chemistry of comae, one have to consider the release of molecules into the gaseous phase from refractory material on grains.

Thus, if we think that a direct photodegradation of HMT on cometary grains cannot be a good explanation for observed CN and HCN extended sources, in the inner coma, interactions between water photoproducts, and outflowing grains, may generate an additional source for these molecules: whether a direct production of HCN, or a production of volatile nitriles that should be photodissociated to produce the observed CN. In this latter case, HMT would act as a grandparent molecule. For large scale extended sources, far from the nucleus, in regions where the density becomes too low to allow an efficient gas-grain interaction, a different molecule is required, which would released CN and HCN with a high yield by direct photodegradation under vacuum, or by thermal degradation. HCN polymers will soon be studied with our experimental set-up to address this question.

REFERENCES

Allamandola, L.J., S.A. Sandford, and G.J. Valero, Photochemical and thermal evolution of interstellar/precometary ice analogs, *Icarus*, **76**, 225-252, 1988.

Bernstein, M.P., S.A. Sandford, L.J. Allamandola, and S. Chang, Infrared spectrum of matrix isolated Hexamethylenetetramine in Ar and H2O at cryogenic temperatures., *Journal of Physical Chemistry*, **98**, 12206-12210, 1994.

Bernstein, M.P., S.A. Sandford, L.J. Allamandola, S. Chang, and M.A. Scharberg, Organic Compounds Produced By Photolysis of Realistic Interstellar and Cometary Ice Analogs Containing Methanol, *The Astrophysical Journal*, **454**, 327-344, 1995.

Biver, N., D. Bockelée-Morvan, J. Crovisier, J.K. Davies, H.E. Matthews, J.E. Wink, H. Rauer, P. Colom, W.R.F. Dent, D. Despois, R. Moreno, G. Paubert, D. Jewitt, and M. Senay, Spectroscopic Monitoring of Comet C/1996 B2 (Hyakutake) with the JCMT and IRAM Radio Telescopes, *The Astronomical Journal*, **118** (4), 1850-1872, 1999.

Bockelée-Morvan, D., J. Wink, D. Despois, N. Biver, P. Colom, J. Crovisier, E. Gerard, E. Lellouch, and L. Jorda, Interferometric imaging of molecular lines in comet Hale-Bopp, *Bulletin of the American Astronomical Society*, **30** (3), 31.02, 1998.

Briggs, R., G. Ertem, J.P. Ferris, J.M. Greenberg, P.J. McCain, C.X. Mendoza-Gomez, and W. Schutte, Comet Halley as an aggregate of interstellar dust and further evidence for the photochemical formation of organics in the interstellar medium, *Origins of life and evolution of the biosphere*, **22**, 287-307, 1992.

Cottin, H., Chimie organique de l'environnement cométaire : étude expérimentale de la contribution de la composante organique réfractaire à la phase gazeuse, Doctorat thesis, Université Paris XII, Créteil, 1999. Available at: http://www.lisa.univ-paris12.fr/GPCOS/Hc/H1t.htm

Cottin, H., M.C. Gazeau, Y. Bénilan, and F. Raulin, Polyoxymethylene as parent molecule for the formaldehyde extended source in comet Halley, *The Astrophysical Journal*, **556** (1), 417-420, 2001.

Cottin, H., M.C. Gazeau, J.F. Doussin, and F. Raulin, An experimental study of the photodegradation of polyoxymethylene at 122, 147 and 193 nm, *Journal of photochemistry and photobiology*, **135** (A : Chemistry), 53-64, 2000.

Cottin, H., M.C. Gazeau, and F. Raulin, Cometary organic chemistry : a review from observations, numerical and experimental simulations, *Planetary and Space Science*, **47** (8-9), 1141-1162, 1999.

Crovisier, J., and F.P. Schloerb, The study of comets at radio wavelengths, in *Comets in the Post-Halley Era*, edited by R.L.N.J.e. al., pp. 149-173, Kluwer, Dordrecht, 1991.

DiSanti, M.A., M.J. Mumma, N. DelloRusso, K. Magee-Sauer, R. Novak, and T.W. Rettig, Identification of two sources of carbon monoxide in comet Hale-Bopp, *Nature*, **399**, 662-665, 1999.

DiSanti, M.A., M.J. Mumma, N.R.D. Russo, K. Magee-Sauer, R. Novak, T.W. Rettig, and M.N. Fomenkova, CO Emission in Comets C/1995 O1 (Hale-Bopp) and C/1996 B2 (Hyakutake): Evidence for a Distributed Source, *Bulletin of the American Astronomical Society*, **29**, 34.02, 1997.

Eberhardt, P., D. Krankowsky, W. Schulte, U. Dolder, P. Lammerzahl, J.J. Berthelier, J. Woweries, U. Stubbeman, R.R. Hodges, J.H. Hoffman, and J.M. Illiano, The CO and N2 abundance in comet P/Halley, *Astronomy and Astrophysic*, **187**, 481-484, 1987.

Greenberg, J.M., What are comets made of ? A model based on interstellar dust, in *Comets*, edited by L.L. Wilkening, pp. 131-163, University of Arizona Press, Tucson, 1982.

Kissel, J., and F.R. Krueger, The organic component in dust from comet Halley as mesured by the PUMA mass spectrometer on board Vega 1, *Nature*, **326**, 755-760, 1987.

Klavetter, J.J., and M.F. A'Hearn, An extended source for CN jets in Comet P/Halley, *Icarus*, **107** (2), 322-334, 1994.

Lis, D.C., J. Keene, K. Young, T.G. Phillips, D. Bockelée-Morvan, J. Crovisier, P. Schilke, P.F. Goldsmith, and E.A. Bergin, Spectroscopic Observations of Comet C/1996 B2 (Hyakutake) with the Caltech Submillimeter Observatory, *Icarus*, **130** (2), 355-372, 1997.

Meier, R., P. Eberhardt, D. Krankowsky, and R.R. Hodges, The extended formaldehyde source in comet P/Halley, *Astronomy and Astrophysics*, **277**, 677-691, 1993.

Mitchell, D.L., R.P. Lin, C.W. Carlson, A. Korth, H. Rème, and D.A. Mendis, The origin of complex organic ions in the coma of comet Halley, *Icarus*, **98**, 125-133, 1992.

Okabe, H., *Photochemistry of small molecules*, Wiley-Interscience Publication, 1978.

Rauer, H., C. Arpigny, H. Boehnhardt, F. Colas, J. Crovisier, L. Jorda, M. Küppers, J. Manfroid, K. Rembor, and N. Thomas, Optical Observations of Comet Hale-Bopp (C/1995 O1) at Large Heliocentric Distances Before Perihelion, *Science*, **275**, 1909-1912, 1997.

Schutte, W.A., L.J. Allamandola, and S.A. Sandford, An Experimental Study of the Organic Molecules Produced in Cometary and Interstellar Ice Analogs by Thermal Formaldehyde Reactions, *Icarus*, **104**, 118-137, 1993a.

Schutte, W.A., L.J. Allamandola, and S.A. Sandford, Formaldehyde and organic molecule production in astrophysical ices at cryogenic temperatures, *Science*, **259**, 1143-1145, 1993b.

Veal, J.M., L.E. Snyder, M. Wrigth, L.M. Woodney, P. Palmer, J.R. Forster, I.d. Pater, M.F. A'Hearn, and Y.J. Kuan, An Interferometric Study of HCN in Comet Hale-Bopp (C/1995 O1), *The Astronomical Journal*, **119** (3), 1498-1511, 2000.

Wolman, Y., S.L. Miller, J. Ibanez, and J. Oro, *Science*, **174**, 1039, 1971.

Woodney, L.M., M.F. A'Hearn, D.D. Wellnitz, D.G. Schleicher, T.L. Farnham, T.C. Cheung, J.P. McMullin, J.M. Veal, L.E. Snyder, I.D. Pater, J.R. Forster, M.C.H. Wright, P. Palmer, Y.J. Kuan, and N.H. Samarasinha, Morphology of HCN and CN in Comet Hale-Bopp, *Bulletin of the American Astronomical Society*, **30**, 31.03, 1998.

Article 9

FRAY N., BÉNILAN Y., COTTIN H., GAZEAU M.-C., MINARD R. D. and RAULIN F. (2004) Experimental study of the degradation of polymers. Application to the origin of extended sources in cometary atmospheres. Meteoritics and planetary science 39(4).

Meteoritics & Planetary Science 39, Nr 4, 581–587 (2004)
Abstract available online at http://meteoritics.org

Experimental study of the degradation of polymers: Application to the origin of extended sources in cometary atmospheres

N. FRAY,[1*] Y. BÉNILAN,[1] H. COTTIN,[1] M.-C. GAZEAU,[1] R. D. MINARD,[2] and F. RAULIN[1]

[1]Laboratoire Interuniversitaire des Systèmes Atmosphériques (LISA), UMR 7583, Universités Paris 7 and Paris 12, C. M. C., 61 Avenue du Général de Gaulle, 94010 Créteil Cedex, France
[2]Chemistry Department, Penn State University, 152 Davey Lab, University Park, Pennsylvania 16802, USA
*Corresponding author. E-mail: fray@lisa.univ-paris12.fr

(Received 27 November 2002; revision accepted 30 January 2004)

Abstract–This paper presents some preliminary results concerning the degradation of refractory nitrogenated polymers, which could be responsible for the CN extended source in comets. We are studying hexamethylenetetramine (HMT) and HCN polymers. Both compounds have been irradiated or heated to simulate the degradation processes they undergo in the cometary atmosphere. We show that, even if both compounds are quite stable under photolysis, the heating leads to a much more efficient degradation with the formation of HCN, NH_3, and other heavier compounds. Moreover, the thermal degradation of HCN polymers appears to be more efficient than that of HMT. Thus, the HCN polymers seem to be better candidates for the CN extended source. We are now developing a new reactor to quantify the production of gaseous molecules and to detect in situ CN radicals.

INTRODUCTION

Most of the gaseous material present in the coma of comets is directly released by the sublimation of the nucleus, and the main fraction of the observed radicals results from the photodissociation of gaseous "parent" molecules. However, some of these species have spatial distributions different from those expected for molecules directly ejected from the nucleus, which cannot be explained by these processes. They appear to arise from a "distributed source" or "extended source" in the coma, as observed for the spatial distribution of CO (Eberhardt et al. 1987) and H_2CO (Meier et al. 1993) measured in situ by the Giotto neutral gas mass spectrometer (NMS). Other molecules (OCS [DelloRusso et al. 1998], HNC [Irvine et al. 1998]), as well as radicals (CN [Fray Forthcoming; Klavetter and A'Hearn 1994], C_2, and C_3 radicals [Festou 1999]) also represent an extended source in different comets. The origin of these extended sources is not fully understood.

Knowledge of the physical and chemical processes involved in the origin of these extended sources is one of the challenging issues of cometary science because the study of these processes is a way to derive the molecular composition of the nucleus from the chemical composition observed in the coma. Several mechanisms have been proposed to explain these puzzling observations. Gaseous molecules may be released during the fragmentation of grains ejected from the nucleus. Another viable hypothesis is the degradation of high molecular weight organics coating the grains. This degradation can be due to photolysis by solar UV and/or pyrolysis caused by solar heating of the grains as they are released from the nucleus. Unfortunately, the lack of both qualitative and quantitative experimental data makes it impossible to model gas production from grains in the cometary environment by any of these mechanisms. To address this problem, we are developing experimental methods to measure the chemical parameters necessary to model these solid-gas processes. We have begun to study the photo and thermal degradation of solid and macromolecular organic materials to determine the yields of gaseous products formed, the quantum yields for photolysis, and the kinetics of the thermal degradation.

Astronomical observations and laboratory simulations have shown that polyoxymethylene—a polymer of formaldehyde $(-CH_2-O-)_n$, also called POM—could be present on cometary grains (Huebner et al. 1988; Schutte et al. 1993). POM is often proposed to explain the formaldehyde (H_2CO) extended source (Meier et al. 1993; Eberhardt et al. 1999) because solid POM is known to readily produce formaldehyde when heated as it is in equilibrium with gaseous formaldehyde (Dainton et al. 1959). We have measured the kinetic parameters of the POM degradation, and these new experimental data have been incorporated into a physico-chemical model of the coma. This model simulates the production of gaseous H_2CO via multiphase chemistry—POM in the solid state on cometary grains is slowly degraded

by solar photons and heat to produce gaseous H_2CO—and is in good agreement with the Giotto spacecraft observations if we assume that the cometary grains contain a few percent POM by mass (Cottin et al. 2001a, 2004). The results indicate that thermal degradation of POM is a more important process than photodegradation at 0.9 AU from the sun. This study demonstrates that the production of gaseous molecules from the solid phase should be taken into account in coma models to fully understand the origin of extended sources.

We are now investigating the degradation of some nitrogen-containing compounds to explain the CN extended source. In this article, we present the preliminary qualitative results of this new study. The primary goal is to determine which solid compounds can be decomposed into smaller gaseous molecules and at what temperature. This information should help us better assess which compounds may be responsible for the CN extended source.

THE TARGET MOLECULES

We are studying two nitrogen-containing materials, HCN polymer and hexamethylenetetramine (HMT, $C_6H_{12}N_4$), as possible contributors to the CN extended source.

Hexamethylenetetramine (HMT)

Hexamethylenetetramine, or HMT (Fig. 1), has been detected (Bernstein et al. 1995) after an irradiation at 122 nm of interstellar ice analogues containing H_2O, CH_3OH, CO, and NH_3 at low temperatures. It was found that HMT represented up to 60% of the solid residue remaining after warming of the photolysis products to room temperature (Bernstein et al. 1995). Moreover, Cottin et al. (2001c) have shown that HMT can also be produced by proton irradiation of the same starting ice mixture composition. Although HMT has not been detected in the cometary environment so far, since it is present in interstellar ice analogues, its presence in comets seems reasonable. Because of this and its chemical structure, HMT was investigated as a possible candidate for an extended source parent of the CN radicals.

A few studies have already focused on the degradation of HMT by photolysis or heating. For example, Bernstein et al. (1994) have studied the photolysis of HMT in an argon matrix and in frozen water and detected CH_4, NH_3, CO, CO_2, and some methylamines (R_2-N-CH_3), nitriles (R-CN), and isonitriles (R-NC). Iwakami et al. (1968) have studied the thermal degradation of HMT and have detected ammonia (NH3), methane (CH_4), acetonitrile (CH_3-CN), and some amines (R-NH_2). Unfortunately, none of these experiments was designed to detect CN radicals.

HCN Polymer

The presence of HCN polymers in cometary nuclei was first suggested by Matthews and Ludicky (1986). Since then, a number of investigators have lent support to this idea. From the mass spectrum obtained with the PICCA instrument on the Giotto spacecraft, Huebner et al. (1989) proposed that HCN polymers could fit the observed data. Combes et al. (1988) have also reported the detection of a weak 4.45 μm emission band in the infrared spectra of Halley acquired by IKS on Vega 1 and tentatively identified as a CN stretch. Cruikshank et al. (1991) inferred the presence of CN groups containing molecules on the dust of some comets through spectroscopic detection of the 2.2 μm overtone of the CN stretching fundamental mode. Cruikshank et al. (1991) suggested that these 2.2 and 4.45 μm bands were possibly due to HCN polymers. But if HCN polymers are present on cometary nuclei, a production process has to be found within the nucleus or precometary ices.

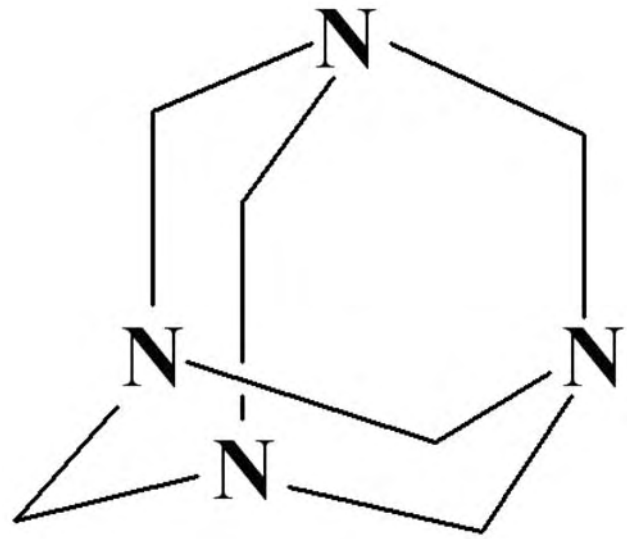

Fig. 1. Structure of hexamethylenetetramine.

In the laboratory, liquid HCN polymerizes spontaneously in non-aqueous solvents or in water (Völker 1960). Hydrogen cyanide polymers—heterogeneous solids ranging in mass from the tetramer to macromolecules containing at least 30 HCN units and ranging in color from yellow to orange to brown to black—are readily hydrolyzed to yield α-amino acids and nitrogen heterocycles, including purines and pyrimidines found in nucleic acids today. In spite of extensive efforts by Miller, Ferris, Matthews, Minard, and others, a complete structural understanding of HCN polymer eludes us. Several hypothetical models have been proposed (Minard et al 1998) but will not be given or discussed here. HCN polymer is also formed when methane and ammonia mixtures are converted to hydrogen cyanide by electric discharges (Matthews and Ludicky 1992). Thus, HCN polymers could be formed in cometary nuclei by interactions between hydrogen cyanide, methane, and ammonia with energetic particles and UV photons. Moreover, Rettig et al. (1992) have shown that HCN polymerization can be initiated in the cometary nucleus by HCN photoexcitation or heating. In spite of the fact that

there is no direct proof that HCN polymer is present on cometary nuclei, this hypothesis cannot be ruled out.

These polymers have indeed been proposed as a source for the observed CN, NH_2, and C_2 jets (Huebner et al. 1989; Schulz and A'Hearn 1995). Calculations of the required energy for photodissociation have shown that the production of CN and NH_2 may be easier from these polymers than from HCN and NH_3 (Rettig et al. 1992). Similar to HMT, the HCN polymer appears to be a good candidate for the source of CN radicals in comets. To date, no study had been performed to investigate the decomposition of these compounds under cometary conditions.

Since HMT and HCN polymer could be readily formed under astrophysical conditions and can be easily degraded by photolysis or heating, we studied the degradation of these solids to better understand their possible contribution to the CN extended source phenomenon. Initial results are presented in this paper.

DEGRADATION EXPERIMENTS

SEMAPhOrE Cometaire (French acronym for Experimental Simulation and Modelling Applied to Organic Chemistry in Cometary Environments), a program developed in our laboratory, is dedicated to the study of photo and thermal degradation of polymers and, generally, of any kind of solid molecules under temperature and pressure conditions relevant to the cometary environment. In this section, we present our experimental setup protocol.

Chemicals

We used commercial HMT (>99.5%, Fluka) for all experiments. R. Minard synthesized HCN polymer. HCN polymerization is catalyzed by traces of various bases such as ammonia or triethylamine and occurs in a variety of organic solvents, in water, or without solvent. The polymer used in the experiments was prepared by adding 50 μL of triethylamine base catalyst to 1 g of neat liquid HCN (no solvent) to initiate polymerization, which occurred at room temperature over 2 to 3 days to give a black solid, $(HCN)_x$. For both samples, the vapor pressure is negligible, and we detected no spontaneous degradation at ambient temperature.

Photodegradation

The experimental setup for the photodegradation study consists of a UV lamp and a temperature-controlled photochemical reactor as shown in Fig. 2. The photochemical reactor, in which solid materials are irradiated, is equipped with two vacuum stopcocks: one leads to the analysis system, and the other one leads to a pumping system (TSH 065 D, Pfeiffer) consisting of a membrane pump (MZ 2T) and a turbomolecular pump (TMH 065). The reactor has a glass jacket to allow temperature regulation. Generally, during an irradiation, the temperature is set at 300 K. The pressure inside the reactor is measured by a Baratron sensor (MKS 627A-01TDC) ranging from 10^{-4} to 1 mbar. A vacuum better than 10^{-4} mbar is achieved in the reactor after one night of pumping.

The UV lamp is filled with an appropriate gas or gas mixture according to the wavelength(s) desired (H_2/He: 122 nm, Xe: 147 nm, and CH_4/He: 193 nm). A microwave discharge inside the lamp is initiated with a Tesla coil. Titanium wires within the lamp can be heated to purify xenon during emission at 147 nm. The lamp could be equipped with two different windows (diameter of 19 mm): MgF_2 for transmission of 122 and 147 nm lines and SiO_2 for selective transmission of the 193 nm line of CH_4. For each wavelength, the UV flux measured by chemical actinometries is given in Fig. 2.

The reactor is connected directly to an analysis system to detect the gaseous molecules produced during the irradiation, or to a liquid nitrogen cold trap to concentrate the resulting gas mixture before analysis, and to permit a more efficient detection of minor compounds.

Thermodegradation

As HMT and HCN polymers are stable at room temperature, we have used a pyrolyser (SGE pyrojector II), which can reach 1000 °C (Fig. 3), to study their thermal degradation, rather than the experimental setup, which had been used for the study of POM (Cottin et al. 2001a, 2004). The solid sample is placed into a small quartz tube, which is attached at the end of an injection syringe. The syringe is attached to the injector, and the plunger is depressed to move the sample tube to a quartz-lined furnace. The temperature of the furnace is constant during an experiment, and it is measured with a thermocouple inside the furnace. The gaseous products of the pyrolysis are swept by nitrogen through a transfer tube and into the analysis system. The pressure of nitrogen inside the furnace is slightly higher than 1 bar to prevent contamination by the atmosphere. Unfortunately, the diffusion of the gaseous products inside the quartz tube appears to vary widely. So, at this point, we can only identify the nature of the degradation products and cannot determine the kinetics of the reaction. While rapid heating and high nitrogen pressures are undoubtedly not relevant to the cometary environment, the qualitative results we can derive from these experiments are a necessary step toward further investigations.

Analysis

The degradation products are analysed with three different and complementary systems: a mass spectrometer (MS), a gas chromatograph coupled with a mass spectrometer (GC-MS), and a Fourier transform infrared spectrometer (FTIR).

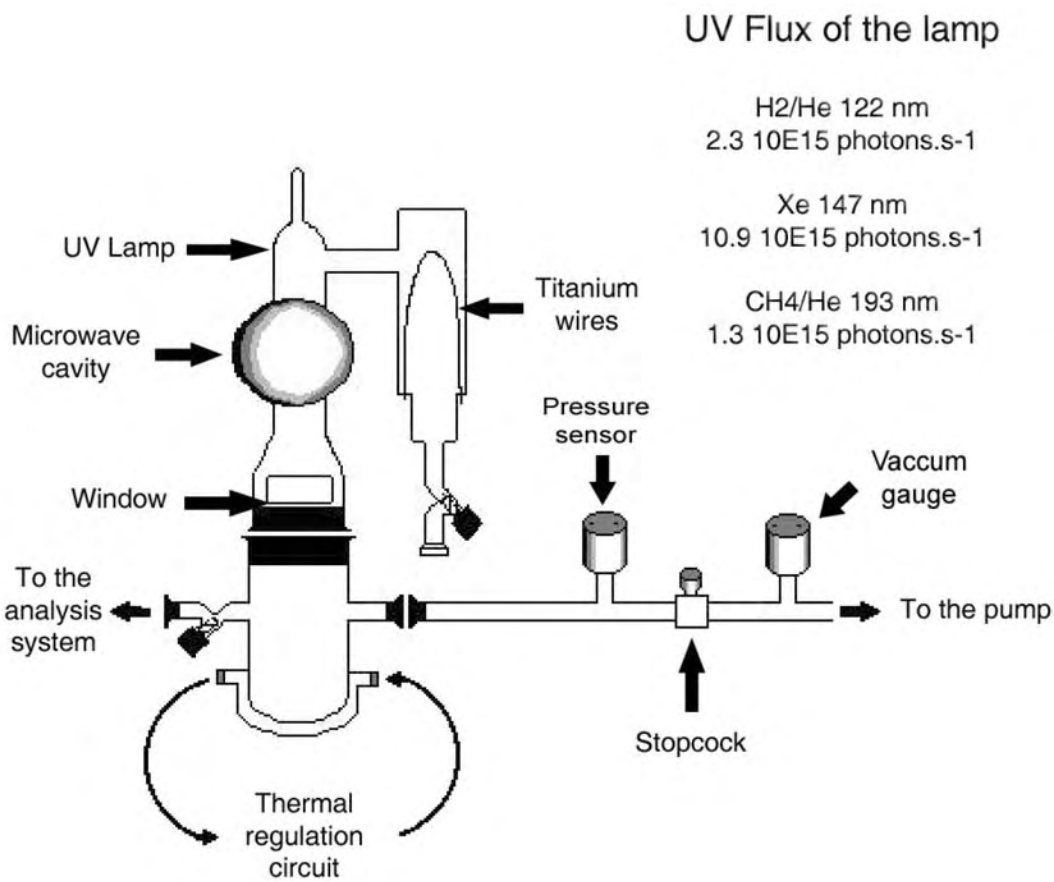

Fig. 2. Photodegradation experimental setup organization.

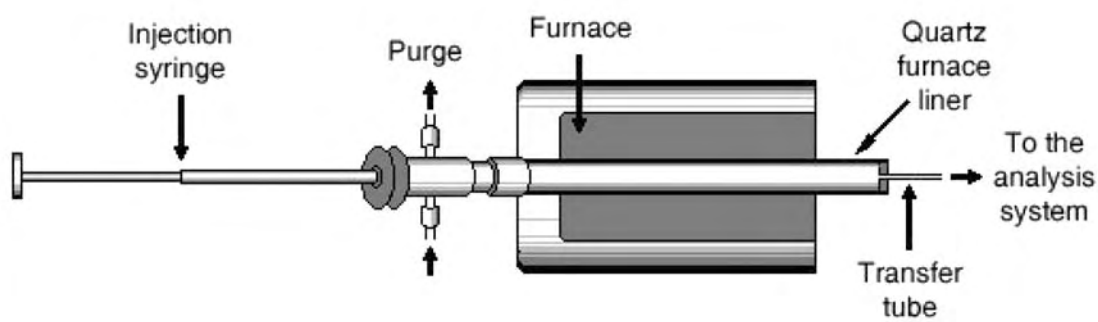

Fig. 3. The pyrolyser.

The mass spectrometer (Leybold, Transpector) has a mass range of m/z 1 to 200 with a resolution of 1 amu and is directly connected to the reactor through a vacuum line. This technique is very sensitive, but since there is no separation of the different products before analysis, the presence of a product is inferred from the presence of key fragments observed that are somewhat unique to that product.

We have also used a GC (Varian 3400) equipped with an apolar column (MXT-1/Restek: 0.18 mm internal diameter; 30 m long; 0.6 μm film thickness). The detector is an ion trap mass spectrometer (Finnigan-Varian) with a scan range of m/z 1 to 650 at a resolution of 1 amu. The pyrolyser can be directly connected to this GC through a septum, but, in the case of irradiation experiments, concentration of the gaseous products in a cold trap is required. This kind of analysis allows us to identify all the degradation products but does not allow kinetics studies of the degradation process.

The infrared spectrometer is a Brüker Equinox 55 with a

wavenumber range of 350 to 7000 cm^{-1} and a resolution of 0.5 cm^{-1}. It is equipped with a multireflection cell (2.6 liters) with an optical path ranging from 2.1 to 10.6 m. The reactor and the pyrolyser can be directly connected to this cell.

RESULTS

HMT

HMT has been irradiated under vacuum at 122 and 147 nm at reactor pressures of less than 10^{-4} mbars. During irradiation, no products were detected by directly coupled MS analysis. To reach a better detection limit, a liquid nitrogen cold trap was used to concentrate the products and produced a lower detection limit by FTIR spectrometry than by MS analysis. After two hours of irradiation performed at 147 nm, HCN is detected by FTIR analysis. Unfortunately, its amount is too low to be quantified (Cottin et al. 2002). At 122 nm, no products have been detected, probably because the lamp flux is lower at this wavelength than at 147 nm. These results are different from those obtained by Bernstein et al. (1994) in frozen water or argon matrix, which produced CH_4, NH_3, and heavier compounds such as CH_3NH_2. When we performed irradiation at 147 nm with 0.1 mbar of water vapor for 6 hr, we detected HCN by its signature at 713 cm^{-1} and NH_3 by its signature at 967 and 929 cm^{-1}. GC-MS analysis indicated some heavier compounds were produced, and one of these was tentatively identified as CH_3CN (Cottin et al. 2002).

In the pyrolysis of HMT, no products were detected by FTIR and GC-MS analysis at temperatures lower than 300 °C. At 350 °C, several compounds are identified by FTIR analysis: HCN, NH_3, and CO_2 (Fig. 4). CO_2 is not a degradation product of HMT. The CO_2 could arise from the incomplete purge of the FTIR spectrometer or from desorption of this gas that had been adsorbed on the sample from the exposure to the atmosphere. A complex feature between 2300 and 2220 cm^{-1} could not be readily interpreted, but it is probably attributable to a nitrile (R-CN) or isonitrile (R-NC). GC-MS analysis shows that some heavy compounds are produced by the heating of HMT at 350 °C (Fig. 5), and several components were identified from their mass spectra observed at a given retention time. The mass spectrum of the second chromatographic peak is presented in Fig. 6 and matches that of triazine ($C_3H_3N_3$). The last peak has been attributed to HMT that was vaporized at this temperature.

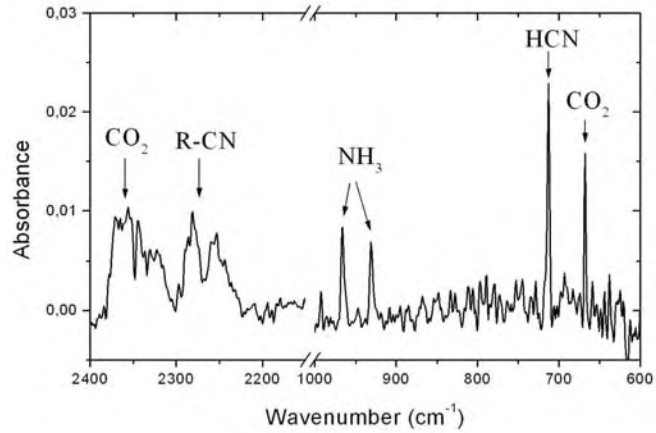

Fig. 4. FTIR spectrum of the thermal degradation products of the HMT at 350 °C. The resolution of the spectrum is 2 cm^{-1}.

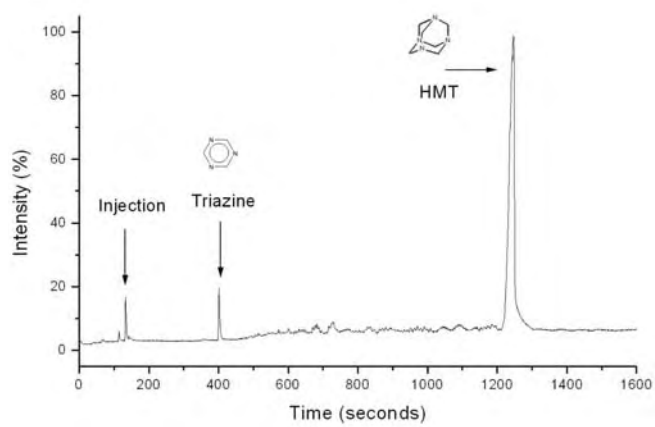

Fig. 5. Chromatogram of the thermal degradation products of HMT after pyrolysis at 350 °C.

HCN Polymer

We have irradiated the HCN polymers at 147 and 193 nm. After eight hours of irradiation at 147 nm, HCN (by its signature at 713 cm^{-1}) and C_2H_2 (by its signature at 730 cm^{-1}) are detected in very low amounts. No products are detected during an irradiation at 193 nm, either because the lamp flux is significantly lower than for the 147 nm lamp or because the quantum yield decreases for longer wavelengths.

No product of HCN polymer thermal degradation is detected by FTIR or GC-MS analysis for temperatures lower than 200 °C. Above 200 °C, we observe the signature of several compounds: HCN, NH_3, CO_2, and traces of triethylamine used as the base catalyst for the polymerization (Fig. 7). As mentioned earlier, the detected CO_2 is certainly due either to an incomplete purge of the spectrometer or to desorption of this molecule previously adsorbed on the sample. Thus, HCN and NH_3 seem to be the main products produced by the thermal degradation of HCN polymer.

Discussion

These preliminary results show that hexamethylenetetramine and HCN polymers seem to be quite stable to direct photolysis since photodegradation products are detected at very low amounts. A comparison of the present

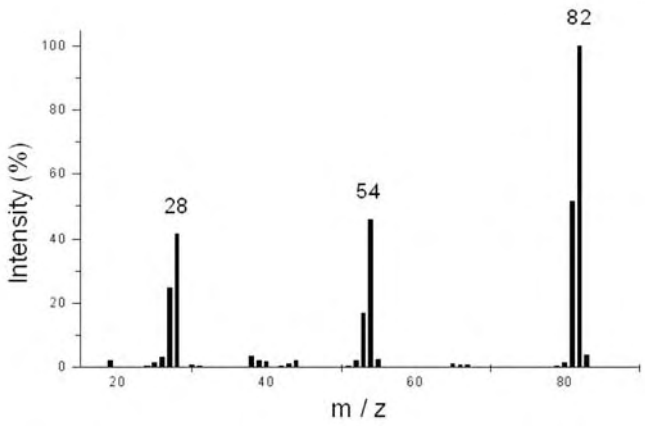

Fig. 6. Mass spectrum corresponding at the second peak of the chromatogram, triazine.

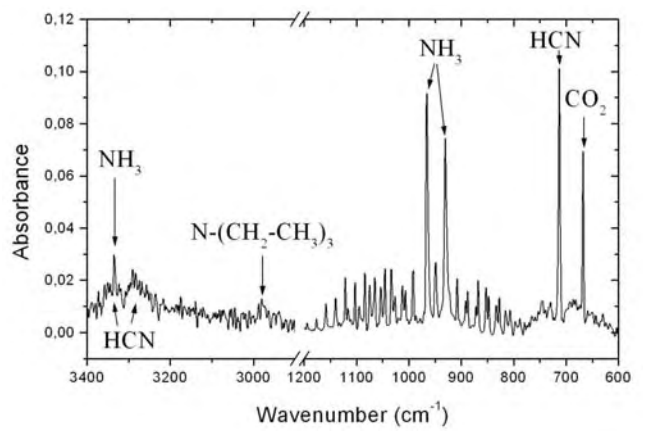

Fig. 7. FTIR spectrum of the degradation products of HCN polymers at 200 °C. The resolution of the spectrum is 2 cm^{-1}.

study and the previous one performed on POM (Cottin et al. 2000) with the same apparatus leads to an estimate of the quantum yields for HCN and NH_3 production from HMT and HCN polymer being lower than 0.1. As in Bernstein et al. (1994), we detect nitriles and other N-bearing molecules. But, according to their results, photolysis of HMT should be more efficient than what we obtain. We think that the detection of most degradation products reported by Bernstein et al. (1995) when HMT is irradiated in an Argon matrix could be due to the trace amount of water evoked by the authors. Perhaps the degradation is enhanced by the presence of water ice or water vapor. HMT is more easily degraded by energetic H atoms or OH radicals produced from the photodissociation of water (Cottin et al. 2002).

The thermal degradation of HCN polymer seems to be more efficient than the one of HMT. Products are detected at lower temperature than for the HMT thermal degradation. Thus, HCN polymer seems to be a better candidate than HMT as the origin of the CN extended source in comets.

Although the temperature of degradation of these compounds is high, it is relevant to the cometary environment since small grains, which are present in the coma, can reach temperatures higher than 300 °C at 1 AU from the sun (Lamy and Perrin 1988; Greenberg and Li 1998).

A question still remains: are HCN and NH_3 directly produced from HCN polymer and HMT or are these compounds a recombination of radicals we are not yet able to detect? This is a key question in the frame of the study of CN extended sources. We are currently developing a new reactor to be able to slowly heat solid compounds under a vacuum. Moreover, this reactor will be equipped with windows to be able to detect radicals in situ by LIF (laser induce fluorescence) or CRDS (cavity ring-down spectroscopy). It will also allow us to measure the kinetics of thermal degradation of solid compounds into gaseous molecules.

CONCLUSION

In conclusion, just as previous studies have shown that thermal degradation of cometary grains containing a few percent POM can explain the extended source of H_2CO, this preliminary study has shown that thermal degradation of nitrogen-containing organic molecules or macromolecules has to be considered to understand the origin of extended CN sources.

Initial results indicate that HMT and HCN polymer are quite resistant to direct photolysis and that thermal degradation seems to be more efficient. Moreover, it appears that the degradation of HCN polymer is easier than that of HMT. Thus, HCN polymer seems to be a better candidate as a parent molecule for CN extended sources.

Due to a range of temperatures different than those used to study POM degradation, our present experimental setup does not allow us to quantify the production of gaseous products of thermal degradation. Moreover, to relate our experimental results to the cometary environment, it would be desirable to detect CN radicals. Thus, we are now developing a new reactor that will be dedicated to the study of thermal degradation of solid compounds at high temperature and be able to detect in situ the CN radical by LIF (laser induce fluorescence) or CRDS (cavity ring-down spectroscopy). This should provide the quantitative kinetic and product distribution data required to model the production of the CN extended sources from the degradation of HMT and/or HCN polymer.

Editorial Handling—Dr. Scott Sandford

REFERENCES

Bernstein M. P., Sandford S. A., Allamandola L. J., and Chang S. 1994. Infrared spectrum of matrix isolated hexamethylenetetramine in Ar and H_2O at cryogenic temperatures. *Journal of Physical Chemistry* 98:12206–12210.

Bernstein M. P., Sandford S. A., Allamandola L. J., Chang S., and Scharberg M. A. 1995. Organic compounds produced by photolysis of realistic interstellar and cometary ice analogs containing methanol. *The Astrophysical Journal* 454:327–344.

Combes M., Moroz V. I., Crosivier J., Encrenaz T., Bibring J. P., Grigoriev A. V., Sanko N. F., Coron N., Crifo J. F., Gispert R., Bockelée-Morvan D., Nikolsky Y. V., Krasnopolsky V. A., Owen T., Emerich C., Lamarre J. M., and Rocard F. 1988. The 2.5–12 μm spectrum of comet Halley from the IKS-VEGA experiment. *Icarus* 76:404–436.

Cottin H., Gazeau M. C., Doussin J. F., and Raulin F. 1999. S.E.M.A.Ph.Or.E COMETAIRE, a tool for the study of the photochemical decomposition of probable cometary large organic molecules. First application: Polyoxymethylene. *Physics and Chemistry of the Earth* 24:597–602.

Cottin H., Gazeau M. C., Doussin J. F., and Raulin F. 2000. An experimental study of the photodegradation of polyoxymethylene at 122, 147, and 193 nm. *Journal of Photochemistry and Photobiology A: Chemistry* 135:53–64.

Cottin H., Gazeau M. C., Bénilan Y., and Raulin F. 2001a. Polyoxymethylene as parent molecule for the formaldehyde extended source in comet Halley. *The Astrophysical Journal Letters* 556:417–420.

Cottin H., Gazeau M.-C., Chaquin P., Raulin F., and Bénilan Y. 2001b. Experimental and theoretical studies on the gas/solid/gas transformation cycle in extraterrestrial environments. *Journal of Geophysical Reserach* 106:33325–33332.

Cottin H., Szopa C., and Moore M. H. 2001c. Production of HMT in photolysed and irradiated interstellar cometary ices analogs. *The Astrophysical Journal* 561:L139–L142.

Cottin H., Souleyman B., Raulin F., and Gazeau M.-C. 2002. Photodegradation of hexamethylenetetramine by VUV and its relevance for CN and HCN extended sources in comets. *Advances in Space Research* 30:1481–1488.

Cottin H., Benilan Y., Gazeau M.-C., and Raulin F. 2004. Origin of cometary extended sources from degradation of refractory organics on grain: Polyoxymethylene as formaldehyde parent molecule. *Icarus* 167:397–416.

Cruikshank D. P., Allamandola L. J., Hartmann W. K., Tholen D. J., Brown R. H., Matthews C. N., and Bell J. F. 1991. Solid CN bearing material on outer solar system bodies. *Icarus* 94:345–353.

Dainton F. S., Ivin K. J., and Walsmey D. A. G. 1959. The equilibrium between gaseous formaldehyde and solid polyoxymethylene. *Transactions of the Faraday Society* 55:61–64

DelloRusso N., DiSanti M. A., Mumma M. J., Magee-Sauer K., and Rettig T. W. 1998. Carbonyl sulfide in comets Csolar1996 B2 (Hyakutake) and Csolar1995 O1 (Hale-Bopp): Evidence for an extended source in Hale-Bopp. *Icarus* 135:377–388.

Eberhardt P., Krankowsky D., Schulte W., Dolder U., Lammerzahl P., Berthelier J. J., Woweries J., Stubbeman U., Hodges R. R., Hoffman J. H., and Illiano J. M. 1987. The CO and N_2 abundance in comet P/Halley. *Astronomy and Astrophysic* 187:481–484.

Eberhardt P. 1999. Comet Halley's gas composition and extended sources: Results from the neutral mass spectrometer on Giotto. *Space Science Reviews* 90:45–52.

Festou M. C. 1999. On the existence of distributed sources in comet comae. *Space Science Reviews* 90:53–67.

Fray N. Forthcoming. CN extended source: A review of observations and modelisations. *Planetary and Space Science*.

Greenberg J.M. and Li A. 1998. From interstellar dust to comets: The extended CO source in comet Halley. *Astronomy and Astrophysics* 332:374–384.

Huebner W. F. 1987. First polymer in space identified in comet Halley. *Science* 237:628–630.

Huebner W. F., Boice D. C., and Korth A. 1988. Halley's polymeric organic molecules. *Advances in Space Research* 9:29–34.

Irvine W. M., Bergin E. A., Dickens J. E., Jewitt D., Lovell A. J., Matthews H. E., Schloerb F. P., and Senay M. 1998. Chemical processing in the coma as the source of cometary HNC. *Nature* 393:547–550.

Iwakami Y., Takazono M., and Tsuchiya T. 1968. Thermal decomposition of hexamethylene tetramine. *Bulletin of the Chemical Society of Japan* 41:813–817.

Klavetter J. J. and A'Hearn M. F. 1994. An extended source for CN jets in comet P/Halley. *Icarus* 107:322–334.

Lamy L. P. and Perrin J. -M. 1988. Optical properties of organic grains: Implications for interplanetary and cometary dust. *Icarus* 76:100–109.

Matthews C. N. and Ludicky R. 1992. Hydrogen cyanide polymers on comets. *Advances in Space Research* 12:21–32.

Matthews C. N. and Ludicky R. 1986. The dark nucleus of comet Halley: Hydrogen cyanide polymers. Proceedings, 20th ESLAB Symposium on the Exploration of Halley's Comet. ESA Special Paper 250. pp. 273–277.

Meier R., Eberhardt P., Krankowsky D., and Hodges R. R. 1993. The extended formaldehyde source in comet P/Halley. *Astronomy and Astrophysics* 277:677–691.

Minard R. D., Hatcher P. G., Gourley R. C., and Matthews C. N. 1998. Structural investigations of hydrogen cyanide polymers: New insights using TMAH thermochemolysis/GC-MS. *Origins of Life and Evolution of the Biosphere* 28:461–473.

Mitchell D. L., Lin R. P., Carlson C. W., Korth A., Rème H., and Mendis D. A. 1992. The origin of complex organic ions in the coma of comet Halley. *Icarus* 98:125–133.

Rettig T. W., Tegler S. C., Pasto D. J., and Mumma M. J. 1992. Comet outbursts and polymers of HCN. *The Astrophysical Journal* 398:293–298.

Rodgers S. D. and Charnley S. B. 2001. On the origin of HNC in comet Lee. *Monthly Notices of the Royal Astronomical Society* 323:84–92.

Schutte W. A., Allamandolla L. J., and Sandford S. A. 1993. An experimental study of the organic molecules produced in cometary and interstellar ice analogs by thermal formaldehyde reactions. *Icarus* 104:118–137.

Schulz R. and A'Hearn M. F. 1995. Shells in the C2 coma of comet P/Halley. *Icarus* 115:191–198.

Völker T. H. 1960. Polymeric hydrogen cyanide. *Angewandte Chemie* 7:384.

Article 10

COTTIN H., GAZEAU M. C., BÉNILAN Y. and RAULIN F. (2001) Polyoxymethylene as parent molecule for the formaldehyde extended source in comet Halley. The Astrophysical Journal 556(1), 417-420.

THE ASTROPHYSICAL JOURNAL, 556:417–420, 2001 July 20

POLYOXYMETHYLENE AS PARENT MOLECULE FOR THE FORMALDEHYDE EXTENDED SOURCE IN COMET HALLEY

H. COTTIN,[1] M. C. GAZEAU, Y. BENILAN, AND F. RAULIN
Laboratoire Interuniversitaire des Systèmes Atmosphériques, UMR 7583 CNRS, Universités Paris VII-Paris XII, 94010 Créteil CEDEX, France;
Cottin@lisa.univ-paris12.fr, Gazeau@lisa.univ-paris12.fr, Benilan@lisa.univ-paris12.fr, Raulin@lisa.univ-paris12.fr
Received 2000 November 14; accepted 2001 March 20

ABSTRACT

Among unsolved questions raised by observations of comets is the origin of extended sources, i.e., the distribution of molecules in the coma which cannot be explained by a direct sublimation from the nucleus. Polyoxymethylene [formaldehyde polymer: $(-CH_2\text{-}O-)_n$, also called POM] is sometimes invoked as a potential parent compound, the degradation of which could produce the required amount of H_2CO across the coma, but no quantitative study has ever been undertaken with relevant parameters. From new experimental data, we are now able to consider multiphase chemistry: POM in the solid state on cometary grains slowly degrades by solar photons and heat and produces H_2CO in the gaseous phase. This is a new approach to cometary organic chemistry. We show, by considering simple assumptions about the cometary environment, that the hypothesis of POM on grains leads to a very good agreement with *Giotto* observations if we assume that the cometary grains are ~7% POM by mass at a temperature of 330 K.

Subject headings: comets: general — comets: individual (Halley) — molecular processes

1. INTRODUCTION

Formaldehyde density profiles in comet Halley have been derived from *Giotto* NMS (Neutral Mass Spectrometer) measurements between 1740 and 4400 km from the nucleus (Meier et al. 1993). It cannot be interpreted by a direct sublimation of H_2CO from the nucleus, and no interpretation relevant to cometary conditions has ever been proposed. Indeed, none of the gaseous parent molecules already detected have a lifetime compatible with formaldehyde observations (Biver et al. 1999). This is also the case for comets Hyakutake (Biver et al. 1999) and Hale-Bopp (Wink et al. 1999).

Polyoxymethylene has been tentatively detected in the coma of comet Halley by the Positive Ion Cluster Composition Analyzer (PICCA) mass spectrometer instrument onboard the *Giotto* spacecraft (Huebner 1987). This detection is very uncertain since it has been shown that the mass pattern attributed to POM in the PICCA mass spectrum is only a signature of the presence of complex organic material made of C, H, O, and N atoms (Mitchell et al. 1992). Nevertheless, POM has been detected after experimental simulations of energetic processes on cometary or interstellar ice analogs. It is synthesized in ices containing H_2O, H_2CO, CH_3OH, CO, and NH_3, during UV photolysis or thermal processing (Bernstein et al. 1995; Schutte et al. 1993). The latter mechanism seems to be the more efficient; therefore, the presence of an important amount of POM in comets could be an indicator of an ice history dominated by thermal transformation rather than UV photolysis or energetic particle bombardment (Cottin et al. 1999). Thus, the presence of POM is still an open and important issue.

Recently, we have performed an experimental study that has provided physicochemical data that were missing to model the production of formaldehyde from solid polyoxymethylene: its production quantum yield from photolysis as a function of wavelength (Cottin et al. 2000) as well as its thermal production rate as a function of temperature (Arrhenius constant and activation barrier) (Cottin et al. 2001). If formaldehyde is the one and only molecule produced by thermal degradation of POM, its photodegradation leads to the production of other molecules, mainly CO, CO_2, HCOOH, CH_3OH, CH_3OCHO, already detected in comets (Bockelée-Morvan et al. 2000). We have developed a mathematical model describing the degradation of polyoxymethylene present in the solid state on grains. This model is applied to *Giotto* measurements in comet Halley. Our work differs from previous studies on this subject (Boice et al. 1990; Meier et al. 1993), where POM photochemistry was modeled in the gaseous phase with estimated rate coefficients and no parameters for H_2CO thermal production were included.

2. MODEL

We consider that polyoxymethylene is ejected from the nucleus as single spherical grains of pure POM. Discussions of our results show that our conclusions can be extended to a production from grains with heterogeneous compositions and sizes.

A decrease of the grain size (caused by loss of material by POM degradation) as a function of the distance from the nucleus is described by equations (1) and (2):

$$\frac{dm}{dr} = 4\mu\pi R^2 \frac{dR}{dr}, \tag{1}$$

where m is the grain mass, r the distance from nucleus, $\mu = 1.46 \times 10^3$ kg m^{-3} the density of POM, and R the radius of the grain:

$$\frac{dm}{dt} = -\sigma C - L_T . \tag{2}$$

The photodegradation of the grain is described by σ C, with $\sigma = \pi R^2$, the effective absorbing surface (see Fig. 1), and C the grain mass loss by photodegradation per second

[1] Presently at NASA GSFC, Code 691, Greenbelt MD 20771.

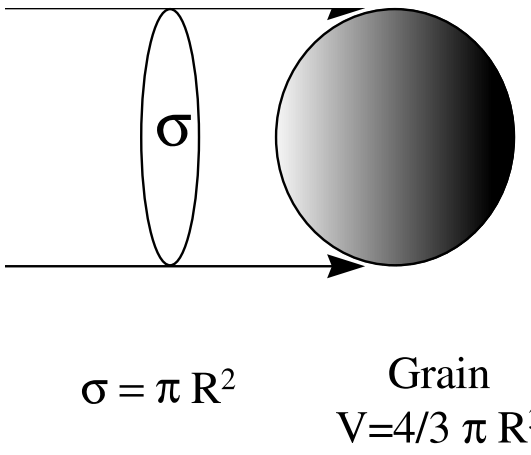

FIG. 1.—Spherical grain (radius = R) lit up by a parallel photon flux. Photons reaching the grain surface are in a σ section cylinder.

given by

$$C = \sum_X \left(m_X \int_\lambda f_\lambda \Phi_\lambda^X \, d\lambda \right). \quad (3)$$

The molecular mass of the main photodegradation products of POM is $m_X (X = H_2CO, CO, CO_2, HCOOH)$, f_λ is the solar flux at the wavelength λ (Mount & Rottman 1981), and the production quantum yield profile as a function of wavelength proposed in Cottin et al. (2000) (i.e., for H_2CO, roughly 0.9 from 120 to 190 nm and 0 for higher wavelength) is adopted.

We consider that the grain rotates on itself, so that its mass loss by photodegradation is uniform over its surface, and calculate $C = 6.76 \times 10^{-9}$ kg m^{-2} s^{-1}.

L_T describes the polymer's thermal degradation. We assume a homogeneous grain temperature and the fact that formaldehyde is not only produced from the grain surface but that the polymer is porous enough to allow a production and diffusion of H_2CO throughout its volume and thereby contribute to the extended source. Then $L_T = M_{H_2CO}\, k\, m$, with M_{H_2CO} the molar mass of formaldehyde and k the kinetic constant for the thermal degradation reaction calculated from the Arrhenius law: $k = A \exp(-Ea/RT)$, where the Arrhenius constant $A = 8.7 \times 10^8$ mol kg^{-1} s^{-1} $\pm 60\%$; the activation barrier $Ea = 74.2$ kJ mol^{-1} $\pm$ 10%; $R = 8.32$ J mol^{-1} K^{-1}, and T is the grain temperature (Cottin et al. 2001).

Equations (1) and (2) lead to an expression for the grain radius as a function of its distance from the nucleus:

$$R = -\frac{D}{B} + \left(R_0 + \frac{D}{B} \right) e^{-Br}, \quad (4)$$

with R_0 the initial radius of the grains, $B = k\, M_{H_2CO}/3v_p$ and $D = C/(4\mu v_p)$.

The grain velocity is v_p, calculated from Crifo (1995) using the initial radius for the grains, and assumed constant (the acceleration occurs in the first kilometers from nucleus, where $R = R_0$ can be assumed).

Since the dynamics of the coma are complex, we make simplifying assumptions in order to describe the density profile of a particle (gaseous molecule or solid grain) around the nucleus. We use Haser's model (Haser 1957), which assumes the following points:

1. Spherical symmetry around the nucleus: uniform emission from the nucleus at surface, or the mixing of emitted particles within the first few kilometers,
2. Stationary state: the nuclear production is constant on the timescale of the modeled processes, and
3. Radial expansion occurs at a constant rate.

The formaldehyde density profile in the coma as a function of the distance r from the nucleus can be described, according to the Haser model, by the following equation of conservation (H_2CO production and loss is from POM degradation and H_2CO photochemistry, respectively):

$$\frac{v}{r^2} \frac{dnr^2}{dr} = \left(\frac{dn}{dt} \right)_g - Jn, \quad (5)$$

where v is the mean gas velocity in the studied region (780 m s^{-1}; Meier et al. 1993), n is the formaldehyde density (m^{-3}), and J is the formaldehyde photodissociation rate (2.00×10^{-4} s^{-1}; Crovisier 1994).

The formaldehyde production rate by photo and thermal degradation of POM is

$$\left(\frac{dn}{dt} \right)_g = \frac{Q_p C'}{4v_p} \frac{R^2}{r^2} + \frac{Q_p N \mu k}{3v_p} \frac{R^3}{r^2}, \quad (6)$$

where Q_p is the grain production from nucleus, $C' = \int_\lambda f_\lambda \Phi_\lambda^{H_2CO} \, d\lambda = 5.07 \times 10^{16}$ m^{-2} s^{-1} is the formaldehyde photoproduction calculated from Mount & Rottman (1981) and Cottin et al. (2000), and N is the Avogadro number (6.02×10^{23}).

The solution of former equations (4), (5), and (6) leads to

$$\begin{aligned} n_{H_2CO} = \frac{1}{r^2} \Bigg\{ & \left[\frac{MH}{(1/l) - 3B} \left(\exp^{-3Br} - \exp^{-r/l} \right) \right] \\ & + \left[\frac{EL - MI}{(1/l) - 2B} \left(\exp^{-2Br} - \exp^{-r/l} \right) \right] \\ & + \left[\frac{MJ - FL}{(1/l) - B} \left(\exp^{-Br} - \exp^{-r/l} \right) \right] \\ & + \left[(lG^2 L - lG^3 M) \cdot (1 - \exp^{-r/l}) \right] \\ & + \left(\frac{Q_{H_2CO}}{4\pi v} \exp^{-r/l} \right) \Bigg\} \end{aligned} \quad (7)$$

with Q_{H_2CO}, the direct production rate of formaldehyde as a parent molecule from the nucleus (s^{-1}), l the formaldehyde scale length (v/J), $G = D/B$, $E = (G + R_0)^2$, $F = 2(G^2 + GR_0)$, $H = (G + R_0)^3$, $I = 3(G^3 + 2G^2 R_0 + GR_0^2)$, $J = 3(G^3 + G^2 R_0)$, $L = Q_p C'/4v_p v$, and $M = Q_p N \mu k/3v_p v$. Q_{H_2CO}, Q_p, R_0, and T are the free parameters adjusted to fit the *Giotto* formaldehyde measurements within ranges relevant to known cometary environments.

3. RESULTS AND DISCUSSION

The best fit to *Giotto* NMS measurements with our model is presented in Figure 2. Such a result is obtained for $Q_{H_2CO} = 5 \times 10^{27}$ s^{-1}, $Q_p = 1.2 \times 10^{14}$ s^{-1}, $R_0 = 10$ μm, $T = 330$ K. Since $Q_{H_2O} = 3 \times 10^{29}$ s^{-1}, and the grain production from Halley near perihelion was $\sim 10^4$ kg s^{-1} (Arpigny 1994), we can conclude that the direct H_2CO production from the nucleus (i.e., as a monomer) is 1.7% relative to water and that POM grains with $R_0 = 10$ μm are

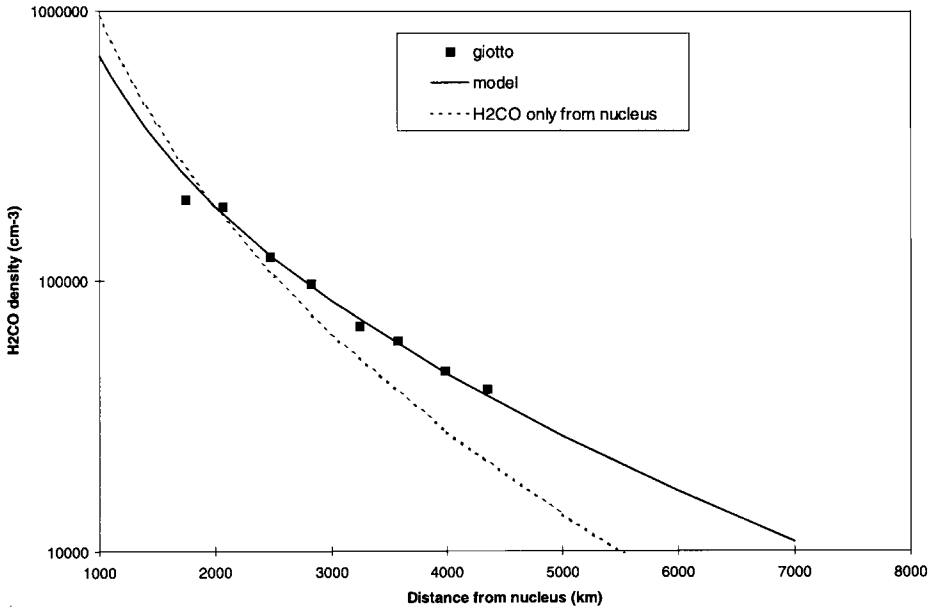

FIG. 2.—Formaldehyde density profile in comet Halley measured by *Giotto* (*squares*) and calculated with (*continuous line*) or without (*dotted line*) extended source production. The density profile without POM is calculated with $Q_{H_2CO} = 1.2 \times 10^{28}$ (i.e., ~4% relative to water production).

~7% of the total dust mass. From equation (4), we can check that the grain lifetime is consistent with our results: at 330 K, an initial POM grain radius of 10 micrometers ($vp = 0.2$ km s^{-1} calculated from Crifo 1995) is reduced ~30% at 5000 km, thus grains can contribute to the extended source throughout all the studied part of the coma.

A good production can also be achieved without any photodegradation for 330 K grains with the same POM amount, whereas considering only photodegradation requires a POM grain production from the nucleus at a level more than 10 times above the total grain production. We conclude that the main process responsible for H_2CO production is the thermal degradation of POM.

Only the porosity, which is not parameterized here, is an important factor that could change our results because some H_2CO diffusing within the grain might be trapped. But if we assume that grain temperature is the only influential parameter controlling a H_2CO production rate proportional to the mass of POM, the geometry, composition, and size of grains would not influence our results, which can then be extended to heterogeneous grains made of refractory material, including a certain amount of POM-emitting formaldehyde throughout its volume as previously described in this paper.

Our model leads to the same fit for the same relative mass of POM (~7%) for any grain size between 0.1 and 10 micrometers with T ranging from 340 to 320 K. Concerning the other free parameters of our model, Q_{H_2CO} can vary from 0% to 3% compensated by small variation of T ($\pm$10 K). Such a formaldehyde production is consistent with measurements in Halley ranging from 1.5% to 4.5% (Mumma & Reuter 1989; Snyder et al. 1989; Combes et al. 1988) but cannot be better constrained. We have presented here the best production for the most relevant conditions. Indeed, Greenberg (1998) has estimated from observations and laboratory investigations that a cometary nucleus is made (by mass) of 26% silicates, 23% refractory organic molecules, 9% polycyclic aromatic hydrocarbons, and a mixture of volatile molecules dominated by water as the remainder. Thus, refractory organic molecules would represent 40% of the nonvolatile component of comets. On the other hand, a laboratory photolyzed H_2O:CH_3OH:CO:NH_3 ice mixture (ratio 10:5:1:1) leads to the formation of a refractory material containing 20% ethers and POM-like polymers (Bernstein et al. 1995), i.e., 8% of the cometary nucleus and grains refractory component. Moreover, we already underlined that POM production is more efficient in ices containing H_2CO and NH_3 when they are submitted to a simple warming process (Schutte et al. 1993), which could result in a mass fraction higher than 8%. Good production can also be achieved for higher amounts of POM and lower T, but the more polymer that is required, the less realistic is the simulation. Thus, the POM abundance derived from our model is consistent with the observations and experimental investigations of comets. Nevertheless, this abundance is low enough to originate either from UV or thermal processing of the initial ice mixture; we cannot conclude which is the dominant process at this point.

The temperature of cometary grains is a parameter that is not well constrained in the literature because it depends mainly on the nature of refractory material, which is poorly known. However, 320–340 K are typical temperatures that can be reached by grains in comae (Crifo 1991; Greenberg & Li 1998). Further improvements of our model should allow us to physically constrain the temperature, which is here a free parameter.

Carbon monoxide is another molecule that presents an extended source in comets (Eberhardt et al. 1987; DiSanti et al. 1999). The total amount of CO (nucleus + extended) is 24% in Hale-Bopp: about one half is produced by an extended source and the other half is from nucleus (DiSanti et al. 1999). CO can be produced by POM photodegradation at about the same quantum yield as H_2CO (Cottin et al. 2000) but not by thermal degradation. This latter mechanism contributes more than 99.9% to the extended formaldehyde profile for 330 K grains. Thus, if extended CO in Hale-Bopp originated from POM photodegradation, then one should expect a formaldehyde pro-

duction at least a thousand times more elevated because of its thermal production. This would result in more H_2CO than CO in the coma. Bockelée-Morvan et al. (2000) have calculated a formaldehyde molecular abundance of 1% in the coma of Hale-Bopp, assuming an extended source. POM clearly cannot be the main precursor for carbon monoxide. An experimental study of CO release by photodegradation or thermal degradation of refractory material obtained after energetic processing of ice mixtures should be undertaken in order to determine if a CO extended source can also originate from the slow degradation in the coma of other high molecular weight molecules.

Clearly thermal degradation of polyoxymethylene is a very efficient way to produce formaldehyde in cometary comae, and our model shows for the first time a realistic interpretation of the *Giotto* measurements in comet Halley. Other molecules could also permit a good fit to observation, but to date none of those have been detected after experimental simulation on cometary ice analogs. Without being a final evidence of the polymer presence on comets, we conclude that POM-like polymers in the solid state on cometary grains is to date the best interpretation of observations that have remained puzzling for a long time. A next step toward POM identification, apart from an in situ analysis during a space mission like *Rosetta*, would be to either directly detect its signature from near-infrared observation or to observe as extended sources its other photodegradation products: CO_2, HCOOH, CH_3OH, and CH_3OCHO. But, as we have shown, photodegradation is not the main degradation mechanism, and production efficiencies of those molecules are low compared to that for H_2CO. An extended source for methanol has already been reported by Womack et al. (1997) but with a signal-to-noise ratio so low that this detection remains very tentative. Achieving detection sensitivity and spatial resolution high enough to study such processes will be the future challenge.

The experimental part of this work has been supported by CNES and PNP (Programme National de Planétologie) and could not have been achieved without help of J. F. Doussin, R. Durand-Jolibois, B. Picquet, and P. Carlier. The theoretical part has benefitted from help and discussion with J. Crovisier, D. Bockelée-Morvan, M. Greenberg, and J. F. Crifo. The authors wish to thank Marla Moore for her help in improving the English of the manuscript and the referee of the paper for his comments. This paper has been written while H. C. held a Société de Secours des Amis des Sciences associateship.

REFERENCES

Arpigny, C. 1994, in AIP Conf. Proc. 312, Molecules and Grains in Space, ed. I. Nenner (New York: AIP), 205
Bernstein, M. P., Sandford, S. A., Allamandola, L. J., Chang, S., & Scharberg, M. A. 1995, ApJ, 454, 327
Biver, N., et al. 1999, AJ, 118, 1850
Bockelée-Morvan, D., et al. 2000, A&A, 353, 1101
Boice, D. C., Huebner, W. F., Sablik, M. J., & Konno, I. 1990, Geophys. Res. Lett., 17, 1813
Combes, M., et al. 1988, Icarus, 76, 404
Cottin, H., Gazeau, M. C., Chaquin, P., Bénilan, Y., & Raulin, F. 2001, J. Geophys. Res., in press
Cottin, H., Gazeau, M. C., Doussin, J. F. & Raulin, F. 2000, J. Photochem. & Photobiol., 135, 53
Cottin, H., Gazeau, M. C., & Raulin, F. 1999, Planet. Space Sci., 47, 1141
Crifo, J. F. 1991, in Comets in the Post-Halley Era, ed. R. L. Newburn, M. Neugebauer, & J. Rahe (Dordrecht: Kluwer), 937
Crifo, J. F. 1995, ApJ, 445, 470
Crovisier, J. 1994, J. Geophys. Res., 99, 3777
DiSanti, M. A., Mumma, M. J., Dello Russo, N., Magee-Sauer, K., Novak, R., & Rettig, T. W. 1999, Nature, 399, 662
Eberhardt, P., Krankowsky, D., Schulte, W., Dolder, U., Lammerzahl, P., Berthelier, J. J., Woweries, J., Stubbeman, U., Hodges, R. R., Hoffman, J. H., & Illiano, J. M. 1987, A&A, 187, 481
Greenberg, J. M. 1998, A&A, 330, 375
Greenberg, J. M., & Li, A. 1998, A&A, 332, 374
Haser, L. 1957, Bull. Acad. Roy. Belgique, 43, 740
Huebner, W. F. 1987, Science, 237, 628
Meier, R., Eberhardt, P., Krankowsky, D., & Hodges, R. R. 1993, A&A, 277, 677
Mitchell, D. L., Lin, R. P., Carlson, C. W., Korth, A., Rème, H., & Mendis, D. A. 1992, Icarus, 98, 125
Mount, G. H., & Rottman, G. J. 1981, J. Geophys. Res., 86, 9193
Mumma, M. J., & Reuter, D. C. 1989, ApJ, 344, 940
Schutte, W. A., Allamandola, L. J., & Sandford, S. A. 1993, Icarus, 104, 118
Snyder, L. E., Palmer, P., & Pater, I. 1989, AJ, 97, 246
Wink, J., et al. 1999, Earth Moon Planets, 78, 1997
Womack, M., Festou, M. C., & Stern, S. A. 1997, AJ, 114, 2789

Article 11

COTTIN H., BÉNILAN Y., GAZEAU M.-C. and RAULIN F. (2004) Origin of cometary extended sources from degradation of refractory organics on grains: polyoxymethylene as formaldehyde parent molecule. Icarus 167, 397–416.

Available online at www.sciencedirect.com
SCIENCE DIRECT®
Icarus 167 (2004) 397–416
ICARUS
www.elsevier.com/locate/icarus

Origin of cometary extended sources from degradation of refractory organics on grains: polyoxymethylene as formaldehyde parent molecule

Hervé Cottin,* Yves Bénilan, Marie-Claire Gazeau, and François Raulin

Laboratoire Interuniversitaire des Systèmes Atmosphériques, UMR 7583 CNRS, Universités Paris VII–Paris XII, 94010 Créteil Cedex, France

Received 20 January 2003; revised 2 September 2003

Abstract

The radial distribution of some molecules (CO, H_2CO, HNC, ...) observed in the coma of some comets cannot be explained only by a direct sublimation from the nucleus, or by the photolysis of a detected parent compound. Such molecules present a so-called extended source in comae. We show in this paper that extended sources can be explained by refractory organic material slowly releasing gas from grains ejected from the cometary nucleus, due to solar UV photons or heat. The degradation products are produced throughout the coma and therefore are presenting an extended distribution. To model this multiphase chemistry we derive new equations, which are applied to Comet 1P/Halley for the case of the production of formaldehyde from polyoxymethylene (POM), the polymer of formaldehyde $(–CH_2–O–)_n$. We show that the presence of a few percent of POM on cometary grains (a nominal value of $\sim 4\%$ in mass of grains is derived from our calculations) is in good agreement with the observed distribution, which so far were not interpreted by the presence of any gaseous parent molecule.

Keywords: Comets, composition; Organic chemistry

1. Introduction

To date, about 25 molecules (excluding ions and radicals) have been detected in the atmosphere of comets (coma) (Crovisier and Bockelée-Morvan, 1999). Most of them are considered as parent compounds, i.e., they are ejected into the gaseous phase either directly from the cometary nucleus ices or within the first kilometers during the sublimation of ice coated grains. The abundance of such compounds relative to water is likely to be the same in the nucleus and in the coma. Parent compounds can be dissociated in the coma by solar photons and produce daughter fragments. The density of both gaseous parent and daughter species as a function of the distance from the nucleus are calculated as distributions consistent with Haser's hypotheses (those hypotheses are presented and discussed later in this paper) (Haser, 1957). However, some detected compounds present strong discrepancies with Haser's distribution and other mechanisms have been evoked.

(1) Gas phase reactions between species in the coma, as seems to be the case for HNC produced by the reaction $HCN + H \rightarrow HNC + H$ in Comet C/1995 O1 (Hale–Bopp) (Irvine et al., 1998b; Rodgers and Charnley, 1998).
(2) Production from an unknown parent compound for the origin of H_2CO and for the origin of HNC in Comets C/1996 B2 (Hyakutake) and C/1999 H1 (Lee) (Meier et al., 1993; Irvine et al., 1996; Rodgers and Charnley, 1998, 2001; Biver et al., 1999, 2000).

The difficulty of that latter approach is the identification of a relevant unknown parent whereas most of the abundant compounds in coma in the gaseous phase are probably now detected. From in-situ measurements (Kissel and Krueger, 1987), and from laboratory work on cometary and interstellar ice analogs (see for instance: Greenberg (1982), Allamandola et al. (1988) or Cottin et al. (1999a) for reviews), we know that cometary grains are rich in complex refractory organic material. So far, their potential degradation, and contribution to the gaseous phase, has never been quantitatively investigated. First and foremost, intrinsic degradation data (kinetics, products) for potential candidates are miss-

* Corresponding author.
E-mail address: cottin@lisa.univ-paris12.fr (H. Cottin).

0019-1035/$ – see front matter
doi:10.1016/j.icarus.2003.10.009

ing. Candidate refractory parent compounds can potentially be established from results obtained on laboratory-irradiated interstellar and cometary ice analogs leading to the detection of large molecules likely to be present on comets. Second, new equations, different than those proposed by Haser, have to be developed. As a matter of fact, the production of gaseous daughter molecules from a solid parent compound involves mechanisms quite different than those usually included in models. In comets, a refractory molecule present on grains can be submitted to photodegradation, thermal degradation, or both, and release small gaseous molecules, whose spatial distributions cannot be described by a purely native source, nor solely to gas phase reactions in the coma.

In this paper, we propose to develop a new approach: the degradation of refractory organic material on cometary grains, and production of smaller gaseous molecules. To illustrate this process, the example of the production of H_2CO in Comet 1P/Halley from solid polyoxymethylene is chosen. Indeed, new quantitative data about the degradation of this polymer are now available (Cottin et al., 2000, 2001c). The first section of this paper is a review of the possible presence of polyoxymethylene in comets, and thus the validity of our study. Then we describe the classical Haser approach of cometary chemistry, and show that gaseous compounds cannot account for the observation of formaldehyde in Comet Halley. Then we present our new equations for three cases: photodegradation, thermal degradation, and a coupled modeling of both processes. Even if only the last and most complete approach is relevant in the case of POM, we chose to develop the three of them in the present paper, since any of the three cases might be the most adapted for specific molecules other than POM to interpret existing or future observations. Thus they are presented here and made available for any future work. In the last section we present a complete modeling of formaldehyde production from POM, with a relevant Halley-like dust distribution, and we discuss the extent to which our results are to be considered.

2. Why study polyoxymethylene?

2.1. Review of POM history in comets

The presence of polyoxymethylene in the interstellar medium was evoked for the first time in the middle 1970's by Bessel and Wickramasinghe (1975), and by Cooke and Wickramasinghe (1977). This hypothesis was put forward because of H_2CO detection in the gaseous phase (first detection reported by Snyder et al. (1969)), and because of good agreement between POM optical properties and observation (polarization spectra). Concerning comets, Vanysek and Wickramasinghe (1975) discuss the point that infrared signatures of silicates are similar to those of POM, and that detected silicates may in fact be formaldehyde polymers. Nevertheless, by calculating that POM formation in ISM environment is not favorable, Goldanskii (1977) showed that the claim of the presence of POM in space has to be taken with caution, although it cannot be excluded. But our knowledge of interstellar chemistry has improved since that time, and his conclusions should be reconsidered. He was dealing with formation of 1000 monomer units at 4 K, whereas we presently know that the interstellar environment presents a wide range of temperatures, and experimental simulations show that POM formation occurs after thermal processes (Schutte et al., 1993b) and photolysis (Bernstein et al., 1995) of interstellar ice analogs. Moreover, shorter polymer molecules also have to be considered, and the study of 1000-unit molecules was an arbitrary choice. Woon (1999) has recently published ab initio calculations about H_2CO/NH_3 mixtures in water, which yield a production of small amine-terminated ($–NH_2$) POM-chains at temperatures as low as 40 K. The production of larger-chain polymers has not yet been theoretically explained, and might require higher temperatures.

Ten years after this first tentative detection, the presence of POM in comets was invoked again to interpret a mass spectrum obtained with the PICCA instrument on board the Giotto spacecraft, between 8200 and 12600 km from the nucleus of Comet Halley. Indeed, Huebner (1987) suggested that the alternation of patterns with $\Delta m/z = 14$ and 16 is consistent with a sequence of $–CH_2–$ ($m = 14$) and –O– ($m = 16$), which comprises the polymer (Huebner, 1987; Huebner et al., 1987).

Huebner's hypothesis seems to be confirmed by Möller and Jackson (1990) and Moore and Tanabé (1990) who have performed POM mass spectra that fit observation. However, these conclusions have been reconsidered. Mitchell et al. (1992) have shown that the PICCA mass spectrum is not specifically characteristic of POM: the regular pattern observed is only the signature of a mixture of organic molecules composed of C, H, O, N atoms. Thus, even if the presence of POM cannot be ruled out, the observed spectrum is not sufficient to established its presence definitively. Nevertheless, Mitchell's conclusion strengthens the idea that high molecular weight organic molecules are present in comets.

In addition to the PICCA observations, polyoxymethylene has been synthesized in experimental simulation of energetic processes on cometary or interstellar ice analogs. It is synthesized in ices containing H_2O, H_2CO, CH_3OH, CO, and NH_3 submitted to UV photolysis or thermal processing (Bernstein et al., 1995; Schutte et al., 1993a, 1993b). The latter mechanism seems to be the most efficient. Therefore, the presence of a significant amount of POM in comets could indicate a history of domination by thermal transformation rather than by UV or energetic particle bombardment (see Cottin et al. (1999a) for a review of experimental simulation on ice analogs). Thus, the presence of POM in comets is still an open and important question.

2.2. H_2CO extended source

Cometary formaldehyde was detected for the first time in 1986 in Comet Halley with the infrared instrument IKS

Table 1
Molecules with extended sources in comets (ions and radicals have been excluded)

Molecule with extended source	Comet	Reference
H_2CO	Halley	(Meier et al., 1993)
	Hyakutake	(Lis et al., 1997)
	Hale–Bopp	(Bockelée-Morvan et al., 1998; Wink et al., 1999)
CO	Halley	(Eberhardt et al., 1987)
	Hyakutake	(DiSanti et al., 2003)
	Hale–Bopp	(DiSanti et al., 1999)
OCS	Hale–Bopp	(Dello Russo et al., 1998)
SO	Hale–Bopp	(Bockelée-Morvan et al., 1998)
HNC	Hale–Bopp	(Irvine et al., 1998a; Rodgers and Charnley, 1998)

on board Vega 1. Its production rate from nucleus was then estimated to be 4% relative to water (Combes et al., 1988; Mumma and Reuter, 1989), whereas observations at radio wavelengths led to an estimate of about 1.5% (Mumma and Reuter, 1989; Snyder et al., 1989).

Meier et al. (1993) studied measurements performed from 1740 to 4400 km from nucleus with the NMS mass spectrometer on board Giotto. They show that the formaldehyde density profile, as a function of cometocentric distance, cannot be explained by direct release of formaldehyde from the nucleus, expanding with spherical symmetry and photolyzed by solar UV. On the contrary, it looks like its production rate increases with the distance. Since these measurements were made within about one hour, native production (from the nucleus) would have had to increase by a factor three during that time period to account for observation, whereas the production rates of molecules like H_2S and CH_3OH were constant within an uncertainty of $\pm 20\%$. Moreover, it cannot be explained by inhomogeneous emission, since all the gaseous molecules are well mixed within the first kilometers of the coma.

This implies the presence of an *extended source* (or additional source) of formaldehyde in Comet Halley. It does not seem to be a direct H_2CO emission from cometary grains, because ices coating them sublimate within the first few kilometers from the nucleus. Moreover, if it were a consistent explanation, such a phenomenon should be observed for the other detected gaseous molecules, whereas it is only seen for few (Table 1). Therefore it is likely that the refractory organic component of comets might be involved in this process, through its degradation.

It must be noted that an extended source of formaldehyde has also been detected in Comets Hyakutake (Biver et al., 1999; Lis et al., 1997) and Hale–Bopp (Bockelée-Morvan et al., 1998; Wink et al., 1999). So that phenomenon is common to all comets that have been observed with sensitivity sufficient to detect it, yet there is no quantitative explanation to interpret it.

A fraction of the carbon monoxide extended source is associated to H_2CO, because the photochemistry of this molecule produces CO. But the difference in abundance between these two molecules (about ten times less H_2CO than CO) demonstrates that the extended source of CO in Comet Hale–Bopp (50% of the total observed CO within 1.5 AU from the Sun (DiSanti et al., 1999)) cannot originate exclusively from formaldehyde chemistry.

Considering the points we discussed in the previous section of this paper, polyoxymethylene is often pushed forward to provide the H_2CO extended source (see, e.g., Boice et al., 1990; Meier et al., 1993; Biver, 1997; Greenberg and Li, 1998; Eberhardt, 1999). We now show that this idea is consistent with what was known about the physico-chemistry of the polymer, but until very recently important quantitative data were missing to allow a discerning analysis of that hypothesis.

2.3. POM photodegradation and radiolysis: previous works and latest results

Polyoxymethylene is commonly used as a source of pure formaldehyde by simple heating. Indeed, commercial H_2CO contains some methanol to avoid its polymerization. Thus pure thermal degradation of POM is one mechanism to consider for formaldehyde production in comets. Another mechanism is the degradation of the polymer by photons: photodegradation.

There are few data relevant to the cometary environment, related to POM photodegradation. Most studies have dealt with oxidative photodegradation of POM, i.e., in the presence of molecular oxygen. Chemical mechanisms, products and reaction yields should be very different from those that could be obtained without O_2 (Rabek, 1995). Irradiation of POM under vacuum and for wavelengths below 200 nm were first reported by Roessler et al. (1992). This work concludes with the detection of CO and H_2CO in the gas phase (identified by direct MS), while an infrared analysis of the solid irradiated residue reveals the presence of ester functions. Unfortunately, this study remains qualitative, and has not been pursued further to our knowledge. More is known about POM radiolysis, i.e., irradiation with particles with energy high enough to ionize the molecule (gamma rays, electrons, and photons below 100 nm). Under vacuum, the polymer irradiated by 1 MeV electrons produces several gaseous compounds such as H_2, CH_4, CO, H_2CO, CH_3CHO, CH_3OCHO, $CH_3OCH_2OCH_3$, CH_3OCH_2OCHO, and H_2O. The production yield of formaldehyde from the polymer is $G_{H_2CO} = 4 \pm 1$ (Fischer and Langbein, 1967; Dole, 1973; Shalaby, 1979) (note: G-value is defined as the number of molecules produced per 100 eV of energy absorbed from ionizing radiation).

Recently, we have performed a quantitative experimental study of polyoxymethylene degradation:

- Photodegradation: we have identified the main gaseous photodegradation products of polyoxymethylene:

H_2CO, CO, HCOOH, CO_2, CH_3OH, CH_3OCHO, $CH_3OCH_3OCH_3$, and $C_3H_6O_3$ (trioxane). We have determined the production quantum yields for formaldehyde ($\phi_{122\,nm} = 0.75 \pm 0.21$, $\phi_{147\,nm} = 0.96 \pm 0.19$) and formic acid ($\phi_{122\,nm} = 0.13 \pm 0.05$, $\phi_{147\,nm} = 0.26 \pm 0.10$), and roughly estimated the yields for the other compounds (Cottin et al., 1999b, 2000).
- Concerning thermal degradation, we have verified that H_2CO is the only product, and determined the variation of its production rate as a function of temperature (based on $A = 8.7 \times 10^5$ mol g^{-1} s^{-1} ± 60% and $Ea = 74.2$ kJ mol^{-1} ± 10%, for the Arrhenius constant and the activation barrier, respectively; see Cottin et al. (2001c)).

We expect these results (ϕ's for photodegradation and A, Ea for thermal degradation) to be useful for interpreting cometary observations, as well as for further theoretical studies such the one we present below.

Polyoxymethylene seems to be a good candidate as a parent molecule for extended H_2CO based on the following:

- it is produced during experimental simulations performed with cometary and interstellar ice analogs;
- its detection in Comet Halley is controversial but cannot be ruled out;
- its degradation due to heating as well as photon and charged particle bombardment leads to the production of formaldehyde.

This polymer (POM) is therefore appropriate for studying the contribution of the solid organic phase of cometary grains to the gas phase composition of the coma.

3. Haser's model

A brief description of the model and its preliminary results have already been presented in Cottin et al. (2001a). We propose here to describe the algebraic approach we develop concerning the production of gaseous molecules from the solid phase. Equations involved to describe such heterogeneous chemistry derive but are different from the ones usually used for cometary gas phase chemistry. Our work differs from previous studies on this subject (Boice et al., 1990; Meier et al., 1993), where the POM photochemistry was modeled in the gaseous phase with estimated rate coefficients, with no parameterization for H_2CO thermal production.

First, the classical approach that describes density profiles for parent and daughter *gaseous* molecules in comets is recalled in detail. On this basis, we present extensions of those equations to the production of gaseous molecules from compounds in the *solid* phase. Three cases are developed below:

- photodegradation;
- thermal degradation;
- combined photo and thermal degradation.

Each model will be illustrated with solid POM producing gaseous H_2CO. Although only the last case will be used in this paper with a 'Halley-like' dust distribution (this appears to be the most relevant for the POM polymer case), we think it is worthwhile to describe each mechanism in this paper. All three cases can be more or less adapted according to the solid molecule considered. Therefore this detailed treatment might be useful for future studies of extended sources and/or precursors.

The complexity of comae dynamics leads to making simplifying hypotheses to describe the density profile of a particle (gaseous molecule or solid grain) in the inner coma. The most commonly used model is the one described by Haser (1957), and assumes the following:

(1) spherically-symmetric outflow from the nucleus: the emission is uniform from all the nucleus surface, or the emitted particles are well mixed within the first kilometers;
(2) steady state: the nucleus production is constant over the time-scale of the modeled process;
(3) radial expansion at a constant velocity, which means no collisions, no excess velocities during photodissociation;
(4) molecules and radicals are only destroyed by photochemistry with constant rate coefficients and without chemical reaction between two compounds.

Hypothesis (3) (constant outflow speed v) frees us from the dynamic equation. Only the budget of mass has to be considered, which is written under its Eulerian form:

$$\frac{\partial n}{\partial t} + \operatorname{div}(nv) = \sum_i S_i, \tag{1}$$

where n (cm^{-3}) is the number density of the considered particle, and the S_i represent its sources and sinks.

In a simple case, with particles ejected from the nucleus and not being destroyed, one can write:

$$\frac{\partial n}{\partial t} + \operatorname{div}(nv) = 0 \tag{2}$$

with $\partial n/\partial t = 0$, because of steady state (hypothesis (2)).

For particles undergoing spherically symmetric flow, with v being constant (hypothesis (3)), we obtain the density at a distance r from the nucleus in the absence of particle destruction:

$$n(r) = \frac{Q}{4\pi r^2 v}. \tag{3}$$

Where Q is the production rate of particles from the nucleus (s^{-1}). This allows to determine the density of grains as a function of the distance from the nucleus.

3.1. Parent compound

A first step in complexity can then be achieved: molecule M is emitted from the nucleus with a production rate Q_M, and is photodissociated by solar UV. The sink of this molecule can be written as a function of its number density n_M:

$$\frac{dn_M}{dt} = -Jn_M \tag{4}$$

with J being the photolysis rate (s^{-1}):

$$J = \int_\lambda \sigma I \Phi \, d\lambda. \tag{5}$$

In Eq. (5), σ is the photon–molecule cross section (cm^2), I is the solar irradiance (photon s^{-1} cm^{-2} nm^{-1}), and Φ represents the quantum yield.

With constant v, and assuming $r \ll l_M$ ($l_M = v/J$ being the scale length of M) we obtain by integration of Eq. (1):

$$n_M(r) = \frac{Q_M}{4\pi r^2 v} e^{-r/l_M}. \tag{6}$$

This expression is used to determine the density profile of H_2CO as a parent molecule, as shown in Fig. 4 (dotted line).

3.2. Daughter fragments

Molecules observed in the coma are not necessarily directly emitted from the nucleus. Photodissociation of a parent compound can produce new species, or an additional source for another parent molecule. Those photolysis products are called daughter species.

We now calculate the density profile $n_D(r)$ for such a molecule, photolyzed at a rate J_D, and emitted from a parent compound, whose production and photodestruction rates are respectively Q_M and J_M. Parent and daughter species are assumed to expand with a spherical symmetry and at the same velocity v (which is an approximation: photodissociation products receive an excess of kinetic energy compared to the parent molecule (Crifo, 1994), and in this case an equivalent scale length can be used (Combi and Delsemme, 1980)).

Thus we have:

$$\frac{\partial n_D}{\partial t} + \operatorname{div}(n_D v) = J_M n_M - J_D n_D, \tag{7}$$

$$\Leftrightarrow \quad \frac{dn_D r^2}{dr} + \frac{J_D}{v} n_D r^2 = \frac{J_M}{v} n_M r^2. \tag{8}$$

From Eq. (6) and since $l = v/J$, we obtain:

$$\frac{dn_D r^2}{dr} + \frac{n_D r^2}{l_D} = \frac{n_M r^2}{l_M} = f(r) \tag{9}$$

with

$$f(r) = \frac{Q_M}{4\pi v l_M} e^{-r/l_M}. \tag{10}$$

A general solution for Eq. (9) can be written as:

$$n_D r^2 = \frac{Q_M}{4\pi v} \frac{l_D}{l_M - l_D} e^{-r/l_M} + K e^{-r/l_D}, \tag{11}$$

K is an integration constant calculated from boundary conditions: $r \ll l_M$ and $r \ll l_D$, for which exponential terms tend towards 1 so that

$$n_D r^2 \to \frac{Q_M}{4\pi v} \frac{l_D}{(l_M - l_D)} + K.$$

Then we have two possibilities:

- The daughter molecule has no direct source from the nucleus. Then as a boundary condition: $n_D r^2 = 0$ and we get:

$$n_D(r) = \frac{Q_M}{4\pi r^2 v} \frac{l_D}{l_M - l_D} \left(e^{-r/l_M} - e^{-r/l_D}\right). \tag{12}$$

- The daughter molecule has also a direct source Q_D from the nucleus (which appears to be the case for H_2CO in some comets; see, e.g., DiSanti et al., 2002a, 2002b).

Then as a boundary condition, $n_D r^2 = Q_D/(4\pi v)$ and we get:

$$n_D(r) = \frac{1}{r^2}\left(\frac{Q_M}{4\pi v} \frac{l_D}{l_M - l_D}\left(e^{-r/l_M} - e^{-r/l_D}\right) + \frac{Q_D}{4\pi v} e^{-r/l_D}\right). \tag{13}$$

In order to discuss the relevance of a gaseous parent of formaldehyde, Fig. 1 and Table 2 present three fits of the previous equation to the Giotto measurements of formaldehyde in Comet Halley published by Meier et al. (1993). The absolute error of their measurements is reported to be less than 35%. To first order, this absolute error is a systematic error caused by uncertainties on reactions rates used to calculate the H_2CO density from in-situ MS measurements of the 31 amu e^{-1} peak dominated by H_3CO^+. These errors shift the density scale up or down. Nevertheless, the error on the slope of the curve is quite insensitive to these reaction rates, and the random error on each measurement can be estimated from the scatter of the date at the few percent level. Taking this discussion into consideration, Giotto measurements are plotted with 15% error bars in the figures of this paper. A detailed discussion about the adjustment of our

Table 2
Parameters for the calculation of the best fits to Giotto measurements of formaldehyde when considering a gaseous parent molecule (see also Fig. 1)

	J_{Biver}	J_{Meier}	J_{CH_3OH}
Q_{H_2CO} (s^{-1})	4.5×10^{27}	2.0×10^{27}	7.0×10^{27}
Q_M (s^{-1})	1.9×10^{28}	2.0×10^{28}	1.0×10^{29}
v (km/s)	7.8×10^{-1}	7.8×10^{-1}	7.8×10^{-1}
L_{H_2CO} (km)	3.9×10^3	3.9×10^3	3.9×10^3
L_M (km)	6.0×10^3	4.6×10^3	6.0×10^4

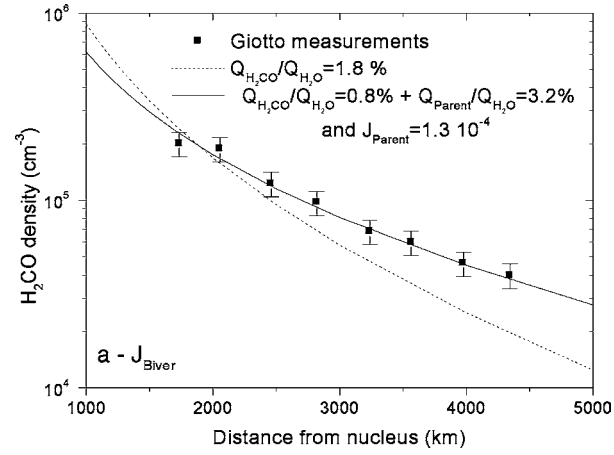

(a)

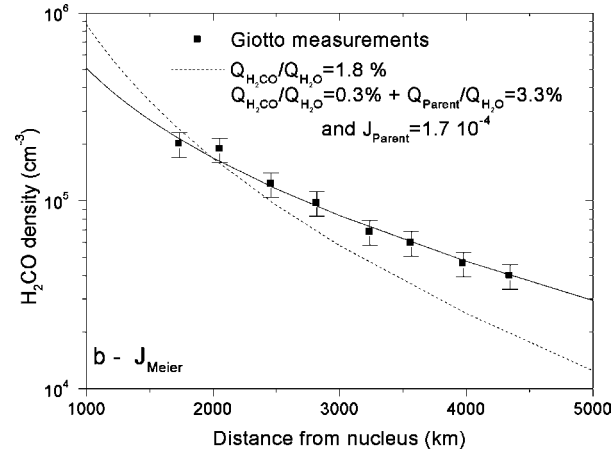

(b)

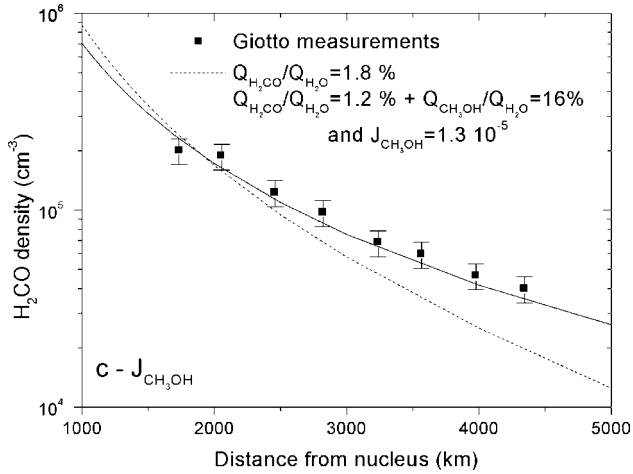

(c)

Fig. 1. Formaldehyde density profile in Comet Halley: measured by Giotto (squares), and calculated with (continuous line) or without (dotted line) extended source production. Several fits are presented (see text). The density profile without extended source is calculated with $Q_{H_2CO} = 1.1 \times 10^{28}$ s^{-1} (i.e., $\sim 1.8\%$ relative to water production).

calculations to measurements will be given in the last section of the paper for a specific case. The coma expansion velocity has been set to 780 m s^{-1}, which is the mean value in the measurement zone (Meier et al., 1993). In the first case (a), J_M is set to the value proposed by Biver (1997) and Biver et al. (1999) from estimates of the H_2CO parent scale-length in comets Hyakutake, Austin, Levy, and Swift-Tuttle: $J_M = 1.3 \times 10^{-4}$ s^{-1}. The best fit presented is achieved for a direct formaldehyde production of about 0.8% from the nucleus (relative to $Q_{H_2O} = 6 \times 10^{29}$ s^{-1} from Fink and DiSanti (1990), for heliocentric distance = 0.9 AU, when the Giotto measurements were achieved) and 3.8% for the parent molecule. We use $J_{H_2CO} = 2 \times 10^{-4}$ s^{-1} throughout this paper (Crovisier, 1994).

Other solutions fitting Giotto measurements can be achieved by adjusting the free parameters of the model: Q_{H_2CO}, Q_M, and J_M. Graph (b) is obtained for $J_M = 1.7 \times 10^{-4}$, which is the nominal value proposed by Meier et al. (1993) "*We find that the lifetime of the parent is restricted to the range of* 0.8 *to* 1.5 *times the lifetime of* H_2CO *with the best fit obtained for a factor of* 1.2," i.e., $J_M = J_{H_2CO}/1.2$. This results in a production rate for the parent compound of $Q_M = 3.3\%$, and agrees with measurements with 0.3% of native formaldehyde.

None of these solutions corresponds to the photodissociation rate of an observed parent molecule likely to produce formaldehyde. Methanol, actually detected in Comet Halley, might be a relevant candidate. But if H_2CO is considered as the main CH_3OH photoproduct (Huebner et al., 1992), and adopting $J_{CH_3OH} = 1.3 \times 10^{-5}$ s^{-1} (Crovisier, 1994), methanol should be produced at a level of 16% from nucleus relative to water (with $\sim 1\%$ of H_2CO) to obtain a good fit to measurements (c). But methanol is only produced in amounts ranging from ~ 1 to 6% in comets (Biver et al., 2002). Moreover, as discussed in Bockelée-Morvan et al. (1994), formaldehyde is not the main dissociation product of methanol, but rather the $CH_3O°$ methoxy radical. Therefore 16% is a lower limit for the amount of CH_3OH required.

Thus, the extended source of cometary H_2CO is not consistent with a CH_3OH parent.

4. POM grain model and its extension

Thanks to the new experimental data about POM degradation, we now establish a new set of equations that model the contribution of solid POM particles to the gaseous phase, through its photo and thermal degradation. Boice et al. (1990) tried to estimate the formaldehyde production from POM, but with the hypothesis that short polymer chains are emitted from grains and photodissociated in the gas phase. Because of the lack of experimental data, photodissociation rates were estimated from formaldehyde and related molecular bond strengths, without any direct laboratory measurement. Meier et al. (1993) showed that those data did not fit the Giotto measurements. On the other hand, as underlined by those authors, and as we have verified experimentally, thermal degradation of solid POM produces only formaldehyde. The presence of short polymer chains in the gas phase would then remain marginal.

Formaldehyde production from solid grains is a function of several unknown parameters: the matrix in which it is imbedded, the geometry of the grains, the chemical structure of the polymer, and its temperature. Here, we can only pretend to simulate the behavior of grains made of a polymer similar to the one studied in laboratory as a model of a high molecular weight compound self-degrading because of solar UV and heat.

As a first approach, we apply Haser's model to pure spherical POM particles uniformly emitted from the nucleus. Such hypotheses are certainly far from the reality and complexity of the cometary environment, but we shall keep in mind that our goal is to show whether there is a mechanism that can explain observation, for realistic abundances of the parent compound. First we will present the case of photodegradation and thermal degradation separately, before presenting a coupled model with both processes. Then we will use a "Halley-like" heterogeneous grain distribution to gain a better insight into our model results.

4.1. Photodegradation

4.1.1. Grain lifetime

Let us consider a spherical grain made of POM, with a radius R, exposed to solar UV. This grain will produce different gas-phase compounds in the gaseous phase (H_2CO, CO, HCOOH, CO_2, CH_3OH, CH_3OCHO, $CH_3OCH_2OCH_3$, and $C_3H_6O_3$). If we assume that the grain rotates randomly, loss of mass will occur uniformly over its surface.

The grain being spherical, the equivalent cross-section exposed to solar UV is $\sigma = \pi R^2$.

The production rate of a molecule $[M]$ by photodegradation can then be written:

$$\frac{d[M]}{dt} = \sigma \int_{\lambda} f_\lambda \Phi_\lambda \, d\lambda, \tag{14}$$

where f_λ is the solar irradiance photon $\mathrm{cm^{-2}\,s^{-1}\,nm^{-1}}$ and ϕ_λ is the production quantum yield of M from the grain surface at wavelength λ. We also consider the grain to be sufficiently thick that each photon is absorbed. If not, we obtain an upper limit for the production rate of the parent.

If μ is the mass density of POM ($\mu = 1.46 \times 10^3$ $\mathrm{kg\,m^{-3}}$—specification *Prolabo*-France), r is the cometocentric distance of the grain outflowing with velocity v_p calculated from Crifo (1995).[1] Then, the mass lost from the grain can be written:

$$\frac{dm}{dr} = 4\pi\mu R^2 \frac{dR}{dr}. \tag{15}$$

We take v_p to be constant (acceleration should occur within the first 100 or so km of the nucleus), and R_0 to be the initial radius of the grain.

[1] Equations to calculate the grain velocity are displayed latter in this paper (Eqs. (49)–(51)) with further comments, in order to not overload this section, which is devoted to the calculation of the density profile.

As mentioned earlier in the paper, H_2CO, CO, HCOOH, and CO_2 are the dominant products of POM photodegradation. Then:

$$\begin{aligned}\frac{dm}{dt} = -\sigma C = -\sigma \Bigg(& \left((m_{H_2CO} + m_{CO}) \int_{\lambda} f_\lambda \Phi_\lambda^{H_2CO} \, d\lambda \right) \\ & + \left(m_{HCOOH} \int_{\lambda} f_\lambda \Phi_\lambda^{HCOOH} \, d\lambda \right) \\ & + \left(m_{CO_2} \int_{\lambda} f_\lambda \Phi_\lambda^{CO_2} \, d\lambda \right) \Bigg)\end{aligned} \tag{16}$$

with m_x representing masses of the molecules.

The Φ^X are from Cottin et al. (2000), and through lack of accurate data concerning CO we have assumed that its production quantum yield profile is identical to H_2CO. We have neglected production of CH_3OH, $CH_3OCH_2OCH_3$, and $C_3H_6O_3$.

The quantity C has been estimated using Cottin et al. (2000) and the solar spectrum published by Mount and Rottman (1981). Those measurements were made near solar maximum, in order to model photodegradation at its maximum efficiency:

$$C = 6.76 \times 10^{-9}\ \mathrm{kg\,m^{-2}\,s^{-1}},$$

v_p, which is reached in the first few kilometers from the nucleus (Crifo, 1995) is supposed to be constant at our scale, thus $v_p\,dt = dr$. We can also assume that all the solar UV flux reaches up to 5–50 km from the nucleus depending on the comet (Crifo, private communication). We can then consider that a grain starts being photodegraded as soon it is emitted, thus:

$$\frac{dm}{dr} = -\frac{\sigma C}{v_p}. \tag{17}$$

Comparing Eqs. (15) and (17), we get:

$$4\pi\mu R^2 \frac{dR}{dr} = -\frac{\sigma C}{v_p}. \tag{18}$$

Integration with $\sigma = \pi R^2$ and $R = R_0$ at $r = 0$, we obtain after integration:

$$R = R_0 - \frac{C}{4\mu v_p} r \quad \text{for } r \leqslant \frac{4\mu v_p}{C} R_0. \tag{19}$$

If we set:

$$l^p = \frac{4\mu v_p R_0}{C} = \frac{3 M_0 v_p}{\pi R_0^2 C} \tag{20}$$

as the POM scale length and M_0 the initial mass of an individual POM grain then:

$$R = R_0 \left(1 - \frac{r}{l^p} \right) \quad \text{for } r < l^p. \tag{21}$$

According to Lisse et al. (1998), a typical size range of most cometary grains is between 0.1 and 10 μm. We can then calculate l_{POM} (for which $R = 0$) of POM grains in the coma (Table 3).

Table 3
Photodegradation scale length as a function of the grain size

R_0 (μm)	10	1	0.1
v_p (m s^{-1})	250	480	680
Grain lifetime (days)	100	10	1
l_p (km)	2.2×10^6	4.1×10^5	5.9×10^4

v_p is calculated using Eqs. (49) to (51).

The photodegradation rate of grain is low enough for its influence to be observed at the scale of observation in Halley's coma.

4.1.2. H_2CO density

Grain density n_p, as a function of the nucleus distance r, can be described by an equation similar to Eq. (7) if we assume uniform emission of particles Q_p and radial expansion with constant velocity v_p:

$$n_p = \frac{Q_p}{4\pi r^2 v_p}, \tag{22}$$

v_p is calculated according to the grain size. We consider here a single size grain population whose radius R decreases following Eq. (21). The formaldehyde production rate (calculated as a density number) from these POM grains at a distance r from the nucleus can be written:

$$\left(\frac{d\mathrm{H_2CO}}{dt}\right)_p = n_p \sigma(r) \underbrace{\int_\lambda f_\lambda \Phi_\lambda^{\mathrm{H_2CO}}\, d\lambda}_{C'} \tag{23}$$

$$\left(\frac{d\mathrm{H_2CO}}{dt}\right)_p = \frac{Q_p}{4r^2 v_p} C' \left(R_0 - \frac{C}{4\mu v_p} r\right)^2. \tag{24}$$

The mass budget equation is then:

$$\frac{\partial n_{\mathrm{H_2CO}}}{\partial t} + \mathrm{div}(n_{\mathrm{H_2CO}} v) = \left(\frac{d\mathrm{H_2CO}}{dt}\right)_p - J_{\mathrm{H_2CO}} n_{\mathrm{H_2CO}}. \tag{25}$$

(Note: both v: gas velocity and v_p: grain velocity are used in the following equations.)

With Haser's model hypotheses we get an equivalent of Eq. (9):

$$\frac{dn_{\mathrm{H_2CO}} r^2}{dr} + \frac{n_{\mathrm{H_2CO}} r^2}{l_{\mathrm{H_2CO}}} = \frac{r^2}{v}\left(\frac{d\mathrm{H_2CO}}{dt}\right)_p = f(r) \tag{26}$$

with

$$f(r) = \frac{Q_p}{4\pi v_p l^p_{\mathrm{H_2CO}}}\left(1 - \frac{r}{l^p}\right)^2 \tag{27}$$

and the two scale lengths of grain destruction l^p and of H_2CO production from grains $l^p_{\mathrm{H_2CO}}$

$$l^p = \frac{4\mu v_p R_0}{C} = \frac{3 m_0 v_p}{\pi R_0^2 C} \quad \text{and} \quad l^p_{\mathrm{H_2CO}} = \frac{v}{\pi R_0^2 C'}.$$

The general solution for Eq. (26) is:

$$n_{\mathrm{H_2CO}} r^2 = \frac{Q_p}{4\pi v_p} \frac{l_{\mathrm{H_2CO}}}{l^p_{\mathrm{H_2CO}}} \left[\left(1 + \frac{(l_{\mathrm{H_2CO}} - r)}{l^p}\right)^2 + \left(\frac{l_{\mathrm{H_2CO}}}{l^p}\right)^2\right] + K e^{-r/l_{\mathrm{H_2CO}}}, \tag{28}$$

where K is an integration constant set by boundary conditions. If we set for $r \to 0$, $n_{\mathrm{H_2CO}} \times r^2 = Q_{\mathrm{H_2CO}}/(4\pi v)$, we finally get:

$$n_{\mathrm{H_2CO}} = \frac{Q_p}{4\pi r^2 v_p} \frac{l_{\mathrm{H_2CO}}}{l^p_{\mathrm{H_2CO}}} \left[\left[1 + 2\frac{l_{\mathrm{H_2CO}}}{l^p}\left(1 + \frac{l_{\mathrm{H_2CO}}}{l^p}\right)\right] \times \left(1 - e^{-r/l_{\mathrm{H_2CO}}}\right) - \frac{r}{l^p}\left(2 + 2\frac{l_{\mathrm{H_2CO}}}{l^p} - \frac{r}{l^p}\right)\right] + \frac{Q_{\mathrm{H_2CO}}}{4\pi r^2 v} e^{-r/l_{\mathrm{H_2CO}}}. \tag{29}$$

4.1.3. Results and discussion

Figure 2a and Table 4 presents one of the best fits to Giotto measurements that can be achieved from Eq. (29).

The result seems to be very good for 1 μm grains, but the amount of POM emitted from the nucleus (3.48×10^4 kg s^{-1}) is more than the average grain production estimated for Comet Halley ($\sim 10^4$ kg s^{-1} (Arpigny, 1994)). Thus, to explain the observations, it seems as though even if all grains were POM, the yield would still be too small by a factor of ~ 3.5.

This demonstrates that POM photodegradation by itself cannot account for the observed formaldehyde. Let us now consider thermal degradation of the polymer.

Table 4
Parameters for the calculation of the best fits to Giotto measurements of formaldehyde when considering the degradation of polyoxymethylene (see also Fig. 2)

	Photodegradation	Thermal degradation	Coupled model
$Q_{\mathrm{H_2CO}}$ (s^{-1})	6.50×10^{27}	3.30×10^{27}	3.30×10^{27}
Q_p (s^{-1})	5.70×10^{18}	1.10×10^{17}	1.10×10^{14}
v (km s^{-1})	7.80×10^{-1}	7.80×10^{-1}	7.80×10^{-1}
v_p (km s^{-1})	4.80×10^{-1}	4.80×10^{-1}	2.50×10^{-1}
$L_{\mathrm{H_2CO}}$ (km)	3.90×10^3	3.90×10^3	3.90×10^3
μ (g km^{-3})	1.46×10^{15}	1.46×10^{15}	1.46×10^{15}
R_0 (km)	1.00×10^{-9}	1.00×10^{-9}	1.00×10^{-8}
T (K)	–	345	336
k (g^{-1} s^{-1})	–	3.55×10^{-6}	1.90×10^{-6}
$l^p/l^T/l^T$ (km)	4.15×10^5	6.39×10^3	1.34×10^4
$l^p_{\mathrm{H_2CO}}/l^T_{\mathrm{H_2CO}}/l^p$ (km)	4.90×10^{-6}	4.90×10^{-6}	2.16×10^6
Emitted mass (kg s^{-1})	3.48×10^4	6.72×10^2	7.34×10^2

T and R_0 are free parameters. They are adjusted to obtain the best fit to measurements. This is the reason why T and R_0 may vary from one process to another.

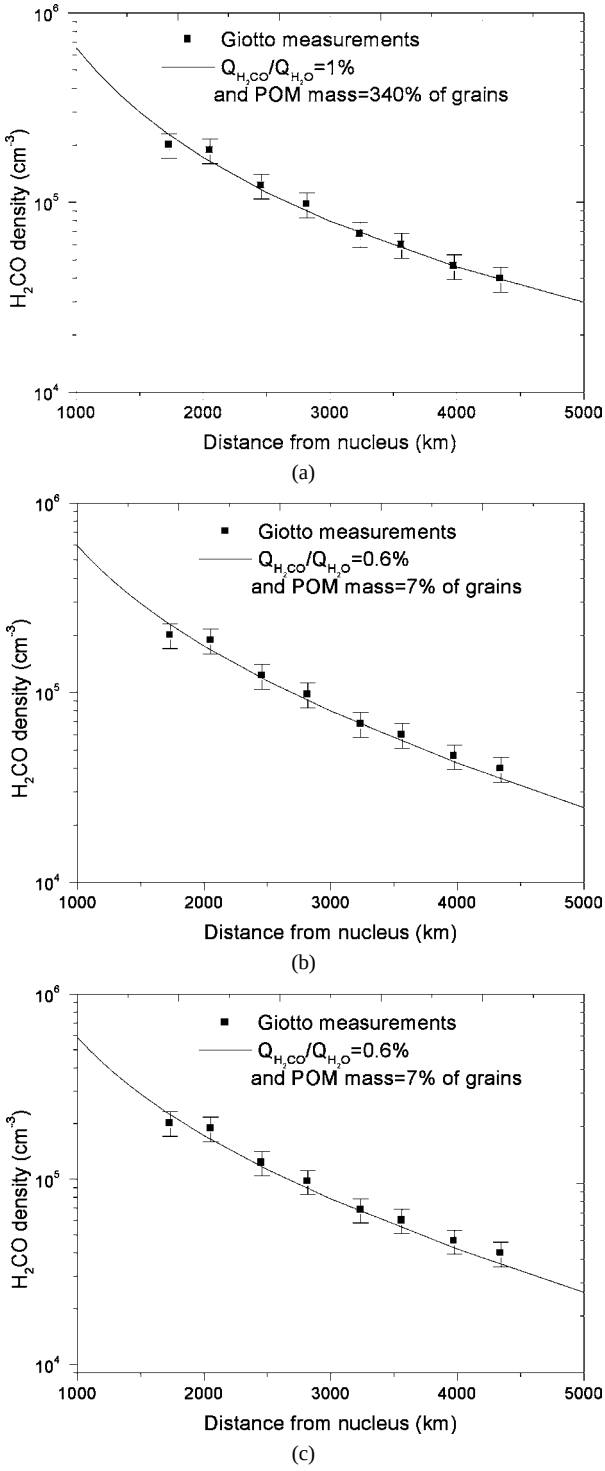

Fig. 2. Formaldehyde density profile in Comet Halley: measured by Giotto (squares), and calculated with an extended source from polyoxymethylene (continuous line) if the degradation of the polymer is (a) photodegradation, (b) thermal degradation or (c) both.

4.2. Thermal degradation

We are now going to describe the thermal production of a gaseous compound from a solid precursor, in the case of H_2CO production from solid POM.

4.2.1. Grain lifetime

Let us consider a spherical grain made of POM, with radius R, mass m, and temperature T.

The H_2CO production rate (mol s^{-1}) can be written:

$$\frac{d\mathrm{H_2CO}}{dt} = km \tag{30}$$

with k given by the Arrhenius law:

$$k = Ae^{-Ea/(RT)}, \tag{31}$$

where $R = 8.314\ \mathrm{J\,mol^{-1}\,K^{-1}}$.

As already mentioned in this paper, the Arrhenius constant $A = 8.7 \times 10^5\ \mathrm{mol\,g^{-1}\,s^{-1}} \pm 60\%$ and the activation barrier $Ea = 74.2\ \mathrm{kJ\,mol^{-1}} \pm 10\%$ (Cottin et al., 2001c).

Then we have:

$$\frac{dm}{dt} = -M_{\mathrm{H_2CO}}km. \tag{32}$$

As v_p is assumed constant we can write with $M_{\mathrm{H_2CO}}$ being the mass of H_2CO per mol:

$$\frac{dm}{dr} = -\frac{M_{\mathrm{H_2CO}}}{v_p}km \tag{33}$$

comparing with Eq. (15) leads to:

$$\frac{dR}{dr} = -\frac{R}{3}\frac{M_{\mathrm{H_2CO}}}{v_p}k \tag{34}$$

with $l^T = 3v_p/(M_{\mathrm{H_2CO}}k)$ representing the thermal degradation scale length. The previous equation can be written as follows:

$$\frac{dR}{dr} = -\frac{R}{l^T}. \tag{35}$$

By integration and again with boundary condition $R = R_0$ for $r = 0$:

$$R = R_0e^{-r/l^T}. \tag{36}$$

The grain lifetime depends only on T and v_p. The scale length l^T is the distance at which R_0 is decreased by the factor $1/e$. As shown in Table 5, thermal degradation of grains is very sensitive to temperature and is very efficient for $T > 300$ K.

Table 5
Thermal degradation scale length as a function of the grain size and temperature

	l^T (km)		
Temperature (K)	R_0 (μm)		
	10	1	0.1
250	8.9×10^7	1.7×10^8	2.4×10^8
300	2.3×10^5	4.5×10^5	6.3×10^5
350	3.3×10^3	6.4×10^3	9.1×10^3
400	1.4×10^2	2.7×10^2	3.8×10^2

v_p is the same than in Table 3 for each grain size and is calculated using Eqs. (49) to (51).

4.2.2. H_2CO density

The mass budget equation in this case is the same as Eq. (26):

$$\frac{dn_{\mathrm{H_2CO}}r^2}{dr} + \frac{n_{\mathrm{H_2CO}}r^2}{l_{\mathrm{H_2CO}}} = \frac{r^2}{v}\left(\frac{d\mathrm{H_2CO}}{dt}\right)_p = f(r). \tag{37}$$

The formaldehyde production from POM grains can be written:

$$\left(\frac{d\mathrm{H_2CO}}{dt}\right)_p = Nkm, \tag{38}$$

where N is the Avogadro number ($N = 6.02 \times 10^{23}\,\mathrm{mol}^{-1}$), and m the total mass of POM per unit volume unit in the coma at a distance r from the nucleus (i.e., in our case the POM grain mass density).

$$m = \frac{4}{3}\pi R^3 \mu n_p = \frac{4}{3}\pi R^3 \mu \frac{Q_p}{4\pi r^2 v_p} = \frac{R^3}{3}\frac{\mu Q_p}{r^2 v_p}. \tag{39}$$

Then we have:

$$f(r) = \frac{Q_p}{4\pi v_p}\frac{1}{l^T_{\mathrm{H_2CO}}}e^{-3r/l^T}, \tag{40}$$

where the H_2CO production scale length by thermal process and the initial mass of the grain are given by

$$l^T_{\mathrm{H_2CO}} = \frac{v}{Nm^0_g k} \quad \text{and} \quad m^0_g = \frac{4}{3}\pi R_0^3 \mu,$$

respectively. We can then solve the differential equation (Eq. (37)):

$$\begin{aligned} A &= \int_r f(r)e^{r/l_{\mathrm{H_2CO}}}\,dr \\ &= \frac{Q_p}{4\pi v_p}\frac{1}{l^T_{\mathrm{H_2CO}}}\int_r e^{\frac{r}{l_{\mathrm{H_2CO}}}(1-3l_{\mathrm{H_2CO}}/l^T)}\,dr. \end{aligned} \tag{41}$$

Then:

$$\begin{aligned} n_{\mathrm{H_2CO}}r^2 = {} & \frac{Q_p}{4\pi v_p}\frac{l^T}{l^T_{\mathrm{H_2CO}}}\left(\frac{l_{\mathrm{H_2CO}}}{l^T - 3l_{\mathrm{H_2CO}}}\right)e^{-3r/l^T} \\ & + Ke^{-r/l_{\mathrm{H_2CO}}} \end{aligned} \tag{42}$$

if $r \ll l_{\mathrm{H_2CO}}$ and $r \ll l^T$:

$$n_{\mathrm{H_2CO}}r^2 = \frac{Q_{\mathrm{H_2CO}}}{4\pi v} = \frac{Q_p}{4\pi v_p}\frac{l^T}{l^T_{\mathrm{H_2CO}}}\left(\frac{l_{\mathrm{H_2CO}}}{l^T - 3l_{\mathrm{H_2CO}}}\right) + K \tag{43}$$

and we finally obtain:

$$\begin{aligned} n_{\mathrm{H_2CO}} = {} & \frac{Q_p}{4\pi r^2 v_p}\frac{l^T}{l^T_{\mathrm{H_2CO}}}\left(\frac{l_{\mathrm{H_2CO}}}{l^T - 3l_{\mathrm{H_2CO}}}\right) \\ & \times \left(e^{-3r/l^T} - e^{-r/l_{\mathrm{H_2CO}}}\right) + \frac{Q_{\mathrm{H_2CO}}}{4\pi r^2 v}e^{-r/l_{\mathrm{H_2CO}}}. \end{aligned} \tag{44}$$

4.2.3. Results and discussion

Figure 2b and Table 4 present one of the best fits to Giotto measurements that can be achieved from Eq. (44) for 1 μm grains.

For thermal degradation, POM production is about 7% of the total dust amount emitted from Comet Halley if one consider a 345 K/1 μm grain population. For larger grains (10 μm for example), with a smaller radial velocity in the coma, an equivalent fit can be achieved with $T \sim 335$ K. For smaller grains (0.1 μm), with a larger radial velocity in the coma, the same fit is achieved with a higher grain temperature ($T \sim 350$ K). The formaldehyde production directly from nucleus as parent molecule can be increased up to 2% relative to water of compensated by small decrease of T (−5 K) for a result similar to the one presented Fig. 2b. Such a formaldehyde production rate is consistent with measurement in Halley ranging from 1.5 to 4.5% (Combes et al., 1988; Mumma and Reuter, 1989; Snyder et al., 1989), but it cannot be better constrained here.

Thus, the thermal degradation of POM is much more efficient than photodegradation. Moreover the amount of POM required to account for the Giotto NMS measurements is realistic, compared to what might be expected in cometary comae. Indeed Greenberg (1998) has estimated from observations and laboratory investigations that a cometary nucleus is made (by mass) of 26% silicates, 23% refractory organic molecules, 9% polycyclic aromatic hydrocarbons, and a mixture of volatiles (dominated by water) as the remainder. The refractory organic molecules would then represent about 40% of the non-volatile component of comets. On the other hand, a laboratory photolyzed H_2O:CH_3OH:CO:NH_3 ice mixture (ratio 10:5:1:1) leads to the formation of a refractory organic residue containing 20% ethers and POM-like polymers (Bernstein et al., 1995), i.e., 8% of the cometary nucleus and refractory component of grains (20% of the 40% of organics in the non-volatile component of comets = 8% of ethers and POM-like polymers). As already noted, POM production is more efficient in ices containing H_2CO and NH_3 when they are submitted to a simple warming process (Schutte et al., 1993b); in this case they could reach a mass fraction higher than 8%. Good fits to observations can also be achieved for higher amounts of POM and lower T, but we assume that the more polymer is required, the less realistic the results of our calculations.

Finally, we can extend our conclusions concerning thermal degradation of POM to heterogeneous grains. Cometary grains themselves are usually considered porous aggregates, where organic refractory molecules like POM are expected to be synthesized on the outer layers. The porosity, which is not parameterized here, is an important factor that could change our results, because some H_2CO diffusing within the grain might be trapped. But if we assume that the grain temperature is the only influential parameter controlling a H_2CO production rate proportional to the mass of POM, the geometry, composition and size of grains would not influence our results. This reasoning can then be extended to heteroge-

neous grains made of refractory material including a certain amount of POM emitting formaldehyde throughout its volume, as described in this paper. Then we can assume that our results can be extended to cometary grains made of about 7% of POM.

4.3. Coupled model

Let us now consider the production of formaldehyde from combined photo- and thermal-degradation of polyoxymethylene. In the next section of this paper, we use our modeling with a 'Halley-like' grain distribution. For such a study, even if thermal degradation remains the dominant mechanism for most grains, this may not be the case for all of them. Some are slower, colder, and have different photodegradation cross sections exposed to solar UV, which could then be the major process. Our model therefore has to take into account both mechanisms.

Preliminary results of this model have been presented in Cottin et al. (2001b), but we present here in further detail the calculations to obtain the density equation, and we extend our model to the 'Halley-like' grain distribution.

4.3.1. Grain's lifetime

Considering a spherical grain made of a fraction α of POM by mass, with radius R, mass m, density μ, and temperature T. The grain is supposed to be an homogeneous mixture of POM and other materials, rather than consisting of a silicon core coated with a POM layer.

With $m_\alpha = \alpha m$ the mass of POM in the grain, r the distance from nucleus, and μ' the POM density (1.46×10^3 kg m^{-3}-*Prolabo*), assuming Haser's model hypotheses, the mass loss by photo- and thermo-degradation can be written:

$$\frac{dm_\alpha}{dr} = -\frac{1}{v_p}(\sigma C + M_{\mathrm{H_2CO}} k m_\alpha). \tag{45}$$

Where σ is defined Section 4.1.1, C in Eq. (16) and k Eq. (31). In this section we still consider virtual pure POM grains, i.e., $\mu = \mu'$ and $\alpha = 1$, but we develop the general equation that will be used in our Halley-like dust case in the next section, with

$$m_\alpha = \frac{4}{3}\pi R_\alpha^3 \mu' = \alpha m \;\Rightarrow\; R_\alpha = \left(\alpha \frac{\mu}{\mu'}\right)^{1/3} R$$

so

$$\sigma = \pi R_\alpha^2 = \left(\alpha \frac{\mu}{\mu'}\right)^{2/3} \pi R^2$$

since

$$\frac{dm_\alpha}{dr} = 4\pi \mu' R_\alpha^2 \frac{dR_\alpha}{dr}.$$

With $l^T = 3v_p/(k M_{\mathrm{H_2CO}})$ and $l^p = 4\mu' R_\alpha^0 v_p / C$, representing the thermal and photo degradation scale lengths respectively, the previous equation can be written as follows:

$$\frac{dR_\alpha}{dr} + \frac{R_\alpha}{l^T} = -\frac{R_\alpha^0}{l^p}. \tag{46}$$

Table 6
Photo/thermo degradation scale length as a function of the grain size and temperature

Distance at which R_0 is divided by e (km)			
Temperature (K)	R_0 (μm)		
	10	1	0.1
250	1.4×10^6	2.6×10^5	3.7×10^4
300	1.9×10^5	1.6×10^5	3.5×10^4
350	3.3×10^3	6.2×10^3	7.1×10^3
400	1.4×10^2	2.6×10^2	3.7×10^2

v_p is the same than in Tables 3 and 5 for each grain size and is calculated using Eqs. (49) to (51).

By integration with boundary condition $R_\alpha = R_\alpha^0$ for $r = 0$:

$$R_\alpha = R_\alpha^0\left[-\beta + (1+\beta)e^{-r/l^T}\right] \tag{47}$$

with $\beta = l^T/l^p$.

As previously, we can calculate the lifetime for the grains as a function of the size and temperature of grains (Table 6). Since over 300 K thermal degradation dominates, the results for realistic coma temperatures are very similar to those presented in the previous section, for thermal degradation only.

4.3.2. H_2CO density

The mass budget equation take the same form as Eqs. (26) and (37) and the H_2CO production from grains is the sum of photo- and thermo-production (Eqs. (23) and (30)). To solve the differential equation we proceed with the same integration method as used previously, obtaining:

$$\begin{aligned} n_{\mathrm{H_2CO}}(r) = \frac{1}{4\pi r^2 v}\Bigg\{ & \frac{3Q_p\beta^3 m_\alpha}{m_{\mathrm{H_2CO}} l^T X} \\ & \times \Bigg[l_{\mathrm{H_2CO}}(1-X)\left(1-e^{-r/l_{\mathrm{H_2CO}}}\right) \\ & + \frac{(3X-2)(1+1/\beta)}{(1/l_{\mathrm{H_2CO}} - 1/l^T)}\left(e^{-r/l^T} - e^{-r/l_{\mathrm{H_2CO}}}\right) \\ & + \frac{(1-3X)(1+1/\beta)^2}{(1/l_{\mathrm{H_2CO}} - 2/l^T)}\left(e^{-2r/l^T} - e^{-r/l_{\mathrm{H_2CO}}}\right) \\ & + \frac{X(1+1/\beta)^3}{(1/l_{\mathrm{H_2CO}} - 3/l^T)}\left(e^{-3r/l^T} - e^{-r/l_{\mathrm{H_2CO}}}\right)\Bigg] \\ & + Q_{\mathrm{H_2CO}} e^{-r/l_{\mathrm{H_2CO}}}\Bigg\}, \end{aligned} \tag{48}$$

where $X = C/m_{\mathrm{H_2CO}} C'$ is the inverse of the relative photoproduction of H_2CO from POM grains.

This is the general equation for a daughter molecule emitted from refractory organic material on grains. Its structure differs from Eq. (13), which describes emission of a daughter species from *gas phase* photochemistry. There is no direct equivalent to the scale length as with Eq. (13), therefore a discussion about this parameter is useless for identifying a parent compound in the solid phase. Here, the free parameters are $Q_{\mathrm{H_2CO}}$, Q_p, R_0, and T, and these can vary from grain to grain according to its size and composition.

4.3.3. Results and discussion

Figure 2c and Table 4 present one of the best fits to Giotto measurements obtained from Eq. (48). It is achieved with 10 µm grains.

This result is similar to the one presented and discussed in Cottin et al. (2001b). A small difference with previously published results is due to the fact we adopted smaller error bars on Giotto measurements in this paper (15% instead of 35%). The amounts of required parent H_2CO and POM are similar to the one obtained in the previous section with $T = 336$ K. Since $Q_{H_2O} \sim 6 \times 10^{29}$ s^{-1}, and the grain production from Halley near perihelion was $\sim 10^4$ kg s^{-1} (Arpigny, 1994), we conclude that the direct H_2CO production from the nucleus (i.e., as a monomer) was $\sim 0.6\%$ relative to water, and that assuming a grain size of $R_0 = 10$ µm POM grains amount $\sim 7\%$ of the total dust mass. From Eq. (48) we can verify that the grain lifetime is consistent with our results at 336 K. An initial POM grain radius of 10 µm (assuming $v_p = 0.25$ km s^{-1} (Crifo, 1995)) is reduced by $\sim 40\%$ at 5000 km, thus grains can contribute to the extended source throughout all the studied part of the coma. Our model leads to the same fit for the same relative mass of POM ($\sim 7\%$) for any grain size between 0.1 and 10 µm with T ranging from 320 to 336 K. Concerning the other free parameters in our model, Q_{H_2CO} variation from 0 to 1.5% relatively to water can be compensated simply by small variation in T (± 5 K). Less native formaldehyde requires warmer grains, whereas more native formaldehyde requires colder grains.

As discussed in the thermal degradation section, these conclusions also apply to heterogeneous grains.

5. Halley-like dust model

We now extend our model to a 'Halley-like' dust distribution. Figure 3 presents the dust production calculated from Crifo and Rodionov (1997) (see Table II in this paper), assuming a density of 1 g cm^{-3} for grains. Those data are derived from in-situ measurements presented in McDonnell et al. (1991).

It must be noted that data for grains up to 1 mg (i.e., ~ 6 cm in size, points 1 to 29 in Fig. 3) are direct in-situ measurements, whereas higher values are extrapolation relevant within an order of magnitude uncertainty (Crifo, private communication).

The grain velocity is calculated with the following equations from Crifo (1995):

$$v_p(X) = \frac{W}{(0.9 + 0.45X^{0.615/2} + 0.275X^{0.615})}, \tag{49}$$

$$W = \sqrt{\left(\frac{\gamma+1}{\gamma-1}\right)\left(\frac{\gamma k T_g}{m_g}\right)}, \tag{50}$$

$$X = \frac{2\pi R \mu W r_n}{m_g Q_g} \tag{51}$$

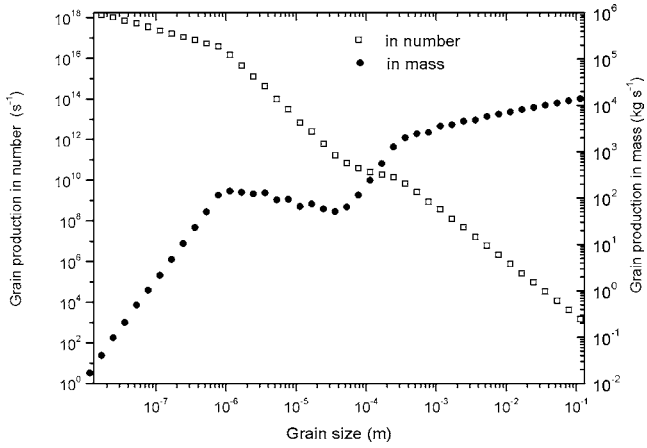

Fig. 3. Dust grain production from Comet Halley nucleus.

with (according to the same reference) $\gamma = 4/3$ (specific heats ratio), k the Boltzman constant, $Tg = 162$ K (gas kinetic temperature), $m_g = 3 \times 10^{-26}$ kg (molecular mass of the gas, assumed to be equal to the mass of the water molecule), $Q_g = 6 \times 10^{29}$ s^{-1} (native gas production), R is the grain radius, $\mu = 1000$ kg m^{-3} (grain density), $r_n = 3.8$ km (nucleus radius). Figure 10 in Crifo (1995) shows that this velocity is achieved between 10 and 100 km from the nucleus surface.

The temperature of grains can be calculated from an assumption about their shape (spherical) and composition (Crifo, 1988). Two extreme temperatures for each grain size are achieved according to whether the grain is made of olivine (low temperature) or amorphous carbon (high temperature). Olivine stands for the silicate nucleus of grains with a very low absorption in the visible; it is a temperature lower limit for grains. Amorphous carbon (aC) is representative of black matter, and stands as an upper limit for a strongly absorbing organic component of grains. As grain composition is poorly known, one cannot pretend to better constrain their temperature than between those two extremes.

Grain temperatures are presented on Table 7 and Fig. 4 (data from Crifo, private communication), those temperatures are reached in the first few tens of kilometers from nucleus and can be assumed constant (Crifo, 1991).

We have calculated the best fits to Giotto measurements, taking into account the grain distribution, their velocities and their temperatures in the following cases:

- temperature lower limit (olivine case);
- temperature upper limit (aC case);
- intermediate temperature (mixture of olivine and organics), considering grains made of 30% of aC and 70% of olivine.

For each case we have considered both the first 29 i labels (actual measurements in the coma up to 1 mg) and the all 43 labels (representing extrapolation up to 10 kg, see Table 7).

Table 7
Halley-like dust model—temperature

i	m_i (g)	T (K) olivine	T (K) aC
1	1.00×10^{-17}	324	681
2	3.16×10^{-17}	325	684
3	1.00×10^{-16}	328	689
4	3.16×10^{-16}	333	696
5	1.00×10^{-15}	343	701
6	3.16×10^{-15}	360	695
7	1.00×10^{-14}	377	669
8	3.16×10^{-14}	387	625
9	1.00×10^{-13}	390	568
10	3.16×10^{-13}	384	502
11	1.00×10^{-12}	369	434
12	3.16×10^{-12}	349	373
13	1.00×10^{-11}	328	329
14	3.16×10^{-11}	307	305
15	1.00×10^{-10}	287	297
16	3.16×10^{-10}	270	297
17	1.00×10^{-9}	264	302
18	3.16×10^{-9}	263	307
19	1.00×10^{-8}	267	312
20	3.16×10^{-8}	271	317
21	1.00×10^{-7}	276	321
22	3.16×10^{-7}	280	324
23	1.00×10^{-6}	283	327
24	3.16×10^{-6}	285	330
25	1.00×10^{-5}	287	332
26	3.16×10^{-5}	288	335
27	1.00×10^{-4}	289	337
28	3.16×10^{-4}	290	339
29	1.00×10^{-3}	291	340
30	3.16×10^{-3}	292	341
31	1.00×10^{-2}	293	342
32	3.16×10^{-2}	294	343
33	1.00×10^{-1}	294	344
34	3.16×10^{-1}	294	344
35	1.00×10^{0}	295	344
36	3.16×10^{0}	295	345
37	1.00×10^{1}	295	345
38	3.16×10^{1}	295	345
39	1.00×10^{2}	295	345
40	3.16×10^{2}	295	346
41	1.00×10^{3}	295	346
42	3.16×10^{3}	295	346
43	1.00×10^{4}	295	346

Temperature of grains for olivine and amorphous carbon (aC) composition. The index i labels the grain mass m_i.

For the last case (intermediate temperature), we have also considered an intermediate solution with grains up to 1 g.

The free parameters are:

- Q_{H_2CO} parent (s^{-1}).
- Q_{POM} on grains (% in mass of grains). An arbitrary upper limit of 20% is set on Q_{POM}. Considering laboratory experiments on cometary and interstellar ice analogs (Cottin et al., 1999a) and the complexity of residues after photolysis or irradiation, we consider that it is quite unrealistic to assume that a single molecule may represent more than 20% of the amount of complex organics by itself.

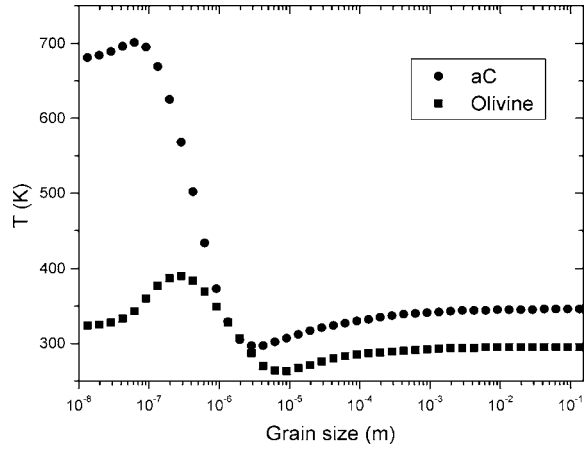

Fig. 4. Grain temperature as a function of size and composition.

As discussed previously in this paper, we consider both thermal degradation and photodegradation. For any distance from the nucleus, if the whole initial amount of POM has already been degraded, the grain is no longer taken into account.

The best fit is calculated by minimizing

$$S=\sqrt{\frac{\sum\left(\frac{\text{Giotto measurement}-\text{calculation}}{\text{Giotto measurements}}\right)^2}{n}},$$

n being the number of Giotto measurements available ($n=8$). E is an average value of the difference between Giotto and our calculation. We have chosen to display only results with $S<25\%$, and as discussed earlier in this paper, we consider that only results with $S<15\%$ are consistent with Giotto measurements.

5.1. Low temperature model

Results are shown in Table 8 and Figs. 5a and 5b. For the first case, with only the grains measured in the coma of Comet Halley, the upper limit of 20% of POM is reached. Best fits may be obtained with more POM, but are not presented here since they do not appear relevant to us. Best results, in terms of POM amount and adjustment to data, are achieved with the whole grain distribution considered (classes 1 to 43): $S=7\%$. Thus, in the present temperature hypothesis the distribution of formaldehyde can be interpreted with a rather large amount of grains, no parent formaldehyde, and with about a percent of POM in mass on grains.

5.2. High temperature model

Results are shown in Table 8 and Fig. 5c. For the calculation including all the grains (classes 1 to 43) we do not obtain any consistent solution to display. With a smaller

Table 8
Best fits with different temperature hypotheses

Grains	Low temperature		High temperature		Intermediate temperature (%org = 30)		
	$i = 1$–29	$i = 1$–43	$i = 1$–29	$i = 1$–43	$i = 1$–29	$i = 1$–35	$i = 1$–43
Q_{H_2CO} (s^{-1})	1.1×10^{28}	0	0	–	7.14×10^{27}	0	0
% H_2CO	1.8	0	0	–	1.19	0	0
Q_{POM} (%)	20.0	1.15	11	–	20	4	0.79
S	22%	7%	22%	> 35%	11%	6%	19%

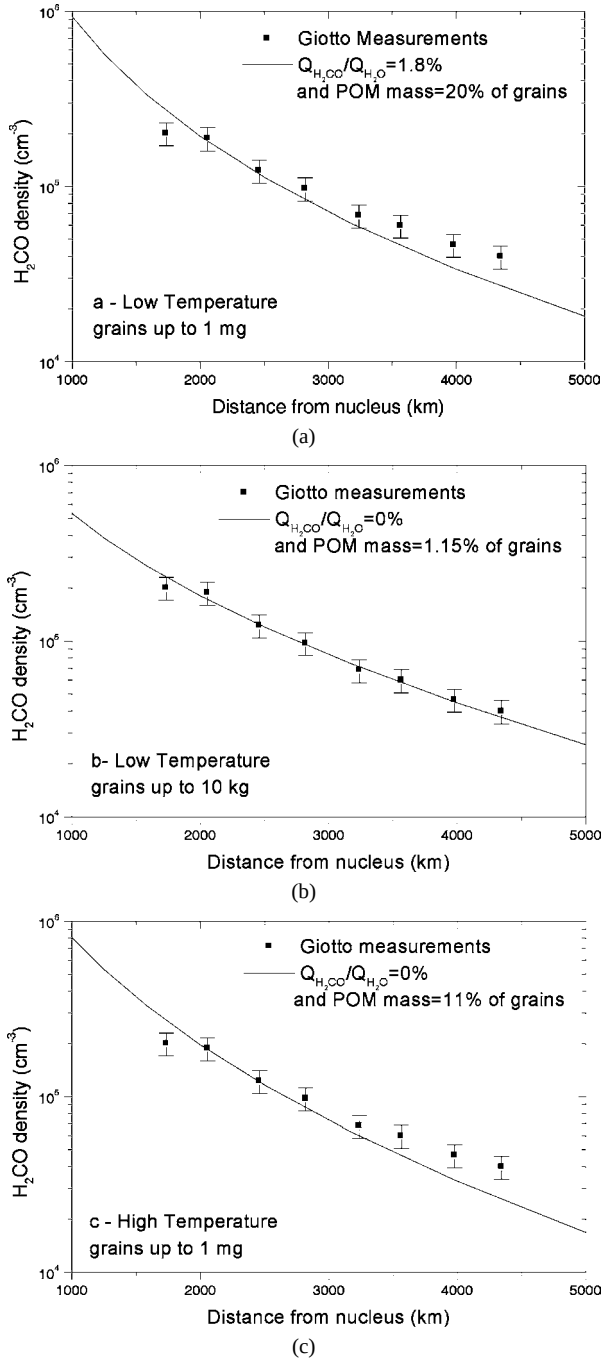

Fig. 5. Best fits for (a) $i = 1$–29 and (b) $i = 1$–43 with the low temperature model, and for (c) $i = 1$–29 with the high temperature model.

mass range for grains (classes 1 to 29), and as T_{grains} increases, the amount of POM estimated to obtain the best fit is less than for the low temperature case: 11% compared to 20%. This time, the best solution does not require any parent formaldehyde, but still, the fit to Giotto measurements is not really satisfying $S = 22\%$.

5.3. Intermediate model

Grain temperatures are actually between the two extremes previously presented. We propose now to discuss in further detail results obtained with our model for intermediate temperatures. Grain temperature depends not only on the amount of organic matter (which is the heating material), but also on the way it is mixed with silicates. We then consider three hypotheses:

(1) Silicates and organics are entirely separated and there are pure organic grains. Then we can just consider the high temperature model, which is quite unrealistic.
(2) Silicates and organics are homogeneously mixed. Then the temperature is an average of extreme values, dependent upon the relative amounts of both components. This assumption might be a better one, but still is far from being realistic.
(3) Grains are a heterogeneous mixture of both components (organics may be a link between silicates to keep them together, they may wrap silicate cores, etc.). In this case the temperature of the organic component of grains is between cases (1) and (2).

Nevertheless those considerations are only speculations in comparison with what is known vs. assumptions. Despite all our attempts to reduce complexity of grains in order to calculate T in the model, one shall keep in mind that the temperature of *real* cometary grains may vary, *from grain to grain, even within the same size category*, between the two extremes.

Our intermediate model simulates case (2) above. With regard to our previous reservations and assumptions about temperature modeling, results should be interpreted as follows:

- We chose to run the model with 30% of amorphous carbon on grains. This is a lower limit of organic material required to heat the grain. Indeed, amorphous carbon,

whose properties are used to calculate T, is absorbing more solar photons than any organic compound that would actually be present on grains. Then, probably a higher organic content than 30% of aC is needed to reach the calculated temperature. Nothing more precise than only "more than 30% in mass of organics is needed" can legitimately be said about it. Greenberg (1998) estimates that about 40% of cometary grains are made of organics, consistent with our conclusion here.

- Taking into account that the mixture between silicates and organics is certainly not homogeneous; again more organics are needed to reach the temperature achieved by the model. This goes in the same direction as the previous point.
- Those assumptions do not affect the other free parameters of the model: Q_{H_2CO}, Q_{POM}.

Results are shown in Table 8 and Fig. 6. According to this model: $0 < Q_{H_2CO} < 7.14 \times 10^{27}$ s^{-1}, $0.79\% < Q_{POM} < 20\%$. The best fit to Giotto measurement in all our simulations ($S = 6\%$) is achieved for this intermediate temperature model when only grains up to 1 g are incorporated into our calculations. One can consider this assumption as an attempt to take into account that the total amount of grains is not well constrained for grains above 10 mg, and that production of H_2CO from the bulk of large grains is probably limited by diffusion throughout the surface of the large grains.

5.4. Discussion

Results obtained with the Halley-like dust model are summarized in Fig. 7. Our knowledge of the total amount of grains, and their composition (and hence their temperature), provides only a range of results between extreme cases, rather than a firm conclusion. No relevant result is obtained at high temperature with the full range of grains, those ones being too hot and too abundant to fit observations. Three other cases are slightly out of the limits we set ($S < 15\%$), those are the cases including the small range of grains at low and high temperatures, and the one with the full range of grains for intermediate temperature. Removing these cases, production of parent formaldehyde from the nucleus is estimated to be between 0 and 1.2%, and the amount of POM between 0.8 and 20% relative to the total mass of grains. This large range reflects our lack of strong constraints on grain parameters. In terms of the low amount of POM, and good fit to Giotto measurements, the best results are obtained if we consider a lot of cold grains ($Q_{POM} = 1\%$ and $S = 7\%$) and for the middle case with intermediate T and intermediate amount of grains ($Q_{POM} = 4\%$ and $S = 6\%$). This last result is probably the most realistic since it is obtained with "average" cometary grain conditions. We choose this case to discuss in further detail the contribution of grains to the overall coma composition. Figure 8 presents the percentage of POM lost from grains as a function of their size (i.e., temperature) and their distance from the nucleus. It shows

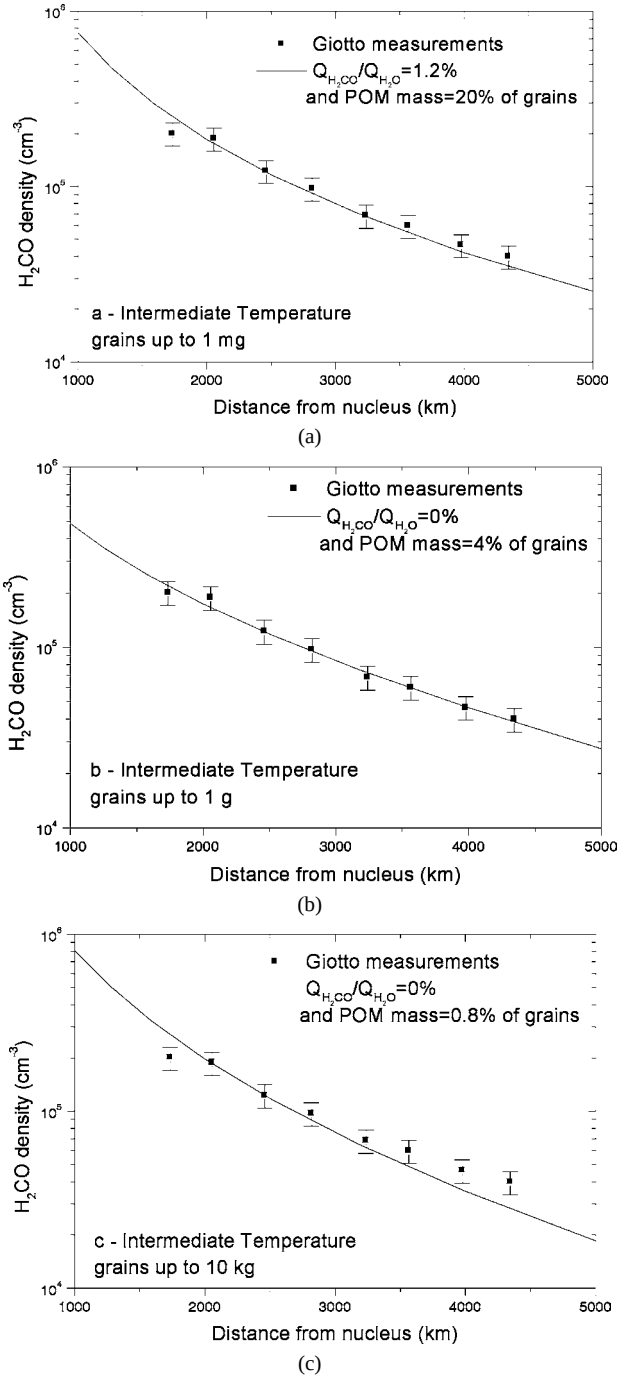

Fig. 6. Best fits for (a) $i = 1$–29, (b) $i = 1$–35, and (c) $i = 1$–43 with the intermediate temperature model.

that if POM is released entirely from small and large grains within 10^3 km, grains with a size of order 10 μm (the coldest ones) can contribute to an extended source of POM up to 10^5 km from the nucleus. Figure 9 shows the contribution of grain size to the extended formaldehyde. No contribution for grains below 1 μm is shown, because all polyoxymethylene is released before 1000 km from the nucleus, because the temperature of these grains is larger than for bigger grains. Their contribution is not displayed on the figures due to scale

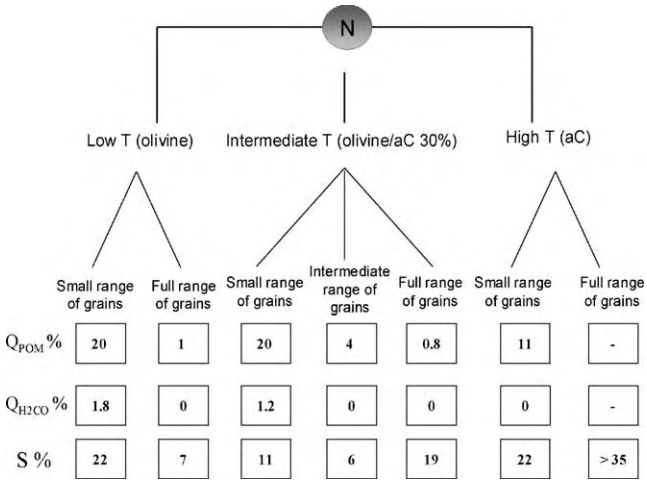

Fig. 7. Summary of results calculated with our model including both photo- and thermal-degradations of POM. From the nucleus (N) 3 grain temperature hypotheses are considered (aC: amorphous carbon). Grains incorporated into our calculations are: up to 1 mg for the small range ($i = 1$–29), up to 1 g for the intermediate range ($i = 1$–35), up to 10 kg for the full range ($i = 1$–43). Results for the best fit obtained are displayed below each case. Q_{POM} is the percentage in mass of POM in the refractory component of grains, $Q_{\mathrm{H_2CO}}$ is the ratio to water of parent formaldehyde, and σ is the divergence between our results and Giotto measurements estimated with a 35 percent error bars.

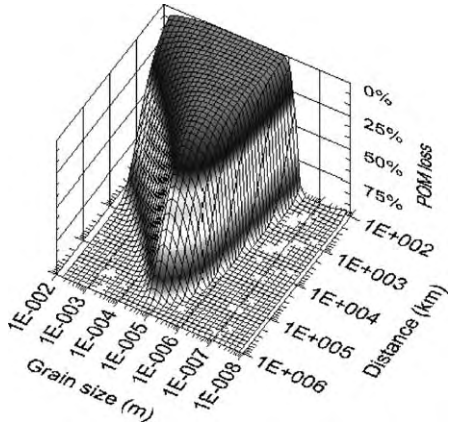

Fig. 8. Intermediate temperature and intermediate range of grains. Fraction of the total amount of POM lost by degradation as a function of grain size and distance from the nucleus.

factors, and for better clarity of the 3D graphs. For such small grains, one can see (Fig. 10) that the thermo degradation scale length is less than 100 km.

Figure 10 also shows that thermal degradation dominates the whole grain size distribution except on a range between 1 to 10 microns. For this last population the degradation is dominated by photolysis up to distances larger than 10^5 km from the nucleus. In the region covered by the Giotto measurements (1500 to 4500 km for nucleus), the production of the extended source of H_2CO is dominated by the thermal degradation of POM on the larger grains.

Figure 11 shows the discrepancy between our model and Giotto measurements (measured as a function of S) vs.

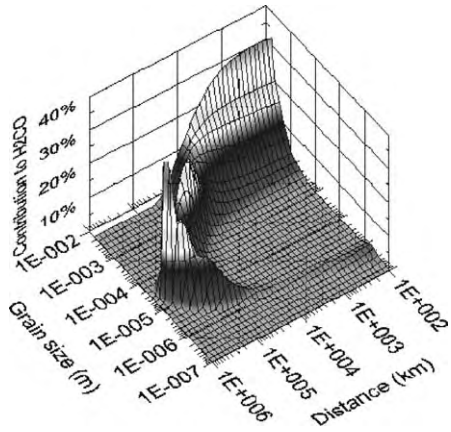

Fig. 9. Intermediate temperature and intermediate range of grains. Contribution to the production of extended formaldehyde in the coma as a function of grain size and distance from the nucleus.

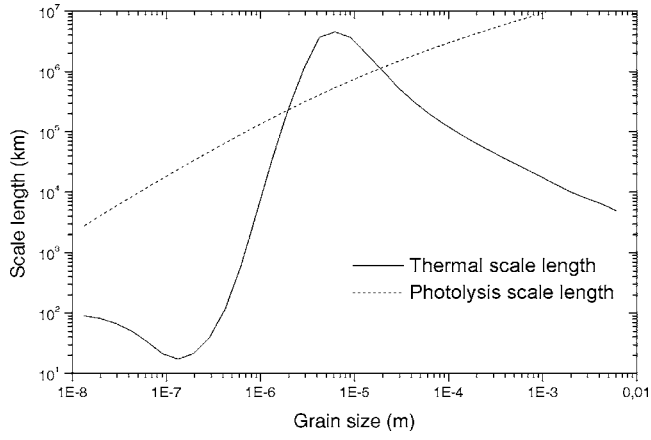

Fig. 10. Scale lengths for photo- and thermal-degradation of POM (l_p and l_t) as a function of the grain size.

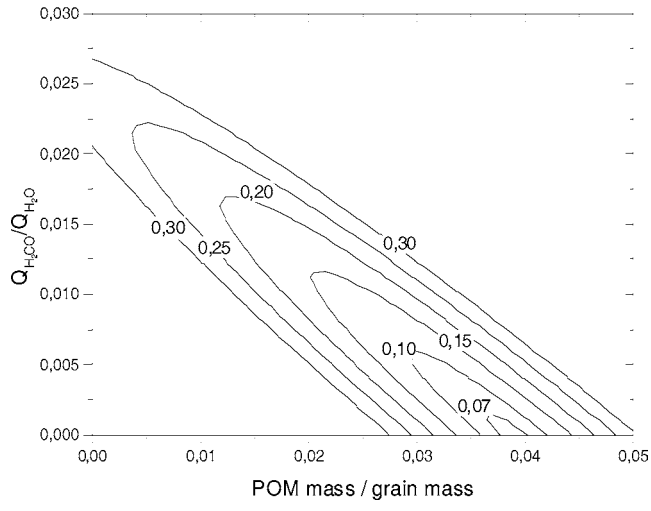

Fig. 11. Intermediate temperature and intermediate range of grains. Projected difference between model and Giotto observations (S) as a function of Q_{POM} (% POM in grains) and $Q_{\mathrm{H_2CO}}$ (% $Q_{\mathrm{H_2CO}}/Q_{\mathrm{H_2O}}$). Only solutions with $S < 30\%$ are displayed.

Q_{POM} (% POM in grains) and $Q_{\mathrm{H_2CO}}$ (% $Q_{\mathrm{H_2CO}}/Q_{\mathrm{H_2O}}$). The best solution (already presented above) is shown at the bottom and on the right of the figure: no parent formaldehyde and 4% of POM. However, the graph shows that the range of solutions for which $S < 15\%$ is rather well constrained regarding the amount of POM: $3.5\% \lesssim Q_{\mathrm{POM}} \lesssim 4.5\%$. It also shows that some parent formaldehyde $0\% < Q_{\mathrm{H_2CO}} < 1.2\%$ can be emitted from the nucleus. We think unlikely for H_2CO not to be present at all as a parent molecule. This compound has been detected in the interstellar medium in the gas phase (Snyder et al., 1969) as well as in the solid phase (Keane et al., 2001), moreover it is easily synthesized when ice mixtures containing H_2O + CO or CH_3OH are photolyzed (Allamandola et al., 1988; Bernstein et al., 1995) or irradiated with protons (Moore et al., 1991, 1996; Hudson and Moore, 1999). H_2O, CO, and CH_3OH are among the most abundant molecules detected in comets, and are known to be parent molecules (at least partially, in the case of CO (DiSanti et al., 1999)). Native formaldehyde has also been detected in comets through high resolution near-IR spectroscopy (see for example the case of 153P/Ikeya Zhang, C/1999 H1 (Lee) and C/2001 A2 (Linear) (DiSanti et al., 2002a, 2002b)). In Comet Hale–Bopp, formaldehyde molecular abundance is estimated to be 1.1% in the coma assuming an extended source (Bockelée-Morvan et al., 2000), with a contribution of the nucleus not exceeding 6% (Wink et al., 1999). This implies that the parent H_2CO is present at a level of at most $\sim 0.1\%$. Therefore, even if Halley and Hale–Bopp abundances are not necessarily similar, we think that a more realistic solution for our model is to consider a fraction of a percent for parent H_2CO, and less than 4% in mass of POM. For example, in Fig. 11, we can see that $S \sim 10\%$ with $Q_{\mathrm{H_2CO}} = 0.5\%$ and $Q_{\mathrm{POM}} \sim 3\%$. As mentioned earlier in this paper, from Bernstein et al. (1995) and Greenberg (1998), values up to 8% in mass of POM-like polymers can be reached in comets through irradiation of ice mixtures. Higher values may also be reached when ices containing H_2CO and NH_3 are submitted to thermal processes. Hence, our estimate of the amount of POM is quite consistent with previous estimates based on observations and laboratory work.

6. Conclusion

The distribution of formaldehyde in Comet Halley, as reported in Meier et al. (1993), has not been satisfactorily explained, either as a parent molecule released from the nucleus, or as a daughter product of any known parent gaseous cometary compound. Based on in-situ measurements and laboratory work on cometary ice analogs, it is now established that cometary grains are probably composed of a mixture of inorganic (silicates) and organic (high molecular weight molecules) material. We propose that refractory organic molecules can be slowly degraded by solar UV photons and/or heat and that they release volatile fragments in the coma.

We present new equations to model the distribution of daughter molecules as a function of distance from nucleus, when such compounds are released from a parent in the solid phase on grains: by photodegradation, thermal degradation, or a combination of both processes. Based on quantitative measurements of the production of formaldehyde from polyoxymethylene, we show that the degradation of this polymer is so far the best interpretation for formaldehyde measurements in Comet Halley. Because of the large number of uncertain parameters (mostly grains distribution and temperature) we cannot derive a sharp estimate of the amount of POM on cometary grains. Nevertheless, according to our different hypotheses, $1\% \lesssim Q_{\mathrm{POM}} \lesssim 20\%$ in mass of grains, with a nominal value of about 3 to 4%, and a related mixing ratio for parent formaldehyde between 0 to 1.2%, with a nominal value of a few tenths of a percent. Both nominal values are quite realistic if one refers to previous estimates based on observations and laboratory work (Bernstein et al., 1995; Greenberg, 1998; Bockelée-Morvan et al., 2000). Without being a definitive evidence for the presence polymers in comets, we conclude that the presence of POM-like polymers in the solid state on cometary grains is to date the best interpretation of observations that have remained puzzling for a long time.

This study will be extended to new measurements on Comet Hale–Bopp, in order to validate our hypothesis. This future work will require further theoretical developments of our approach and is in progress. (For Comet Hale–Bopp we deal with ground based observations, and we can both study the distribution of formaldehyde in the coma and its production as a function of heliocentric distance.) New laboratory work is also in progress to minimize the uncertainty in the kinetic constants for the degradation of the POM we use for the experimental part of this study. New quantitative measurements will also be undertaken with different kinds of POM-like polymers, different structures, synthesis procedures, etc. The sensitivity of our results to those new data will have to be checked. But the final step towards the identification of the parent molecule of formaldehyde in comets will be its in-situ detection, probably thanks to the Rosetta mission.

A main conclusion of this study is that we can no longer neglect the contribution of the refractory organic component of cometary grains to the composition of the gaseous coma. Other molecules or radicals present unexplained extended sources in comets, for example: CN (Klavetter and A'Hearn, 1994), HNC (Irvine et al., 1998a; Rodgers and Charnley, 1998, 2001), and CO (DiSanti et al., 1999). There are a few candidates to explain the origin of CN or HNC: hexamethylenetetramine ($C_6H_{12}N_4$), HCN polymers, but only a few preliminary experimental results have been published so far (Cottin et al., 2002; Fray et al., Experimental study of the degradation of polymers. Application to the origin of extended sources in cometary atmospheres, sub-

mitted for publication). More laboratory work is needed to include their degradation parameters in our model to conclude whether they are good candidates or not. Coma chemistry involving volatiles can also be evoked to explain the production of HNC in some cases (Irvine et al., 1998a, 1998b). CO is a more complex case. The total amount of CO (nucleus + extended) is 24% in Hale–Bopp: about one half is produced by an extended source and the other half is from nucleus (DiSanti et al., 1999). So far no mechanism can account such a production in the coma. Even if photodegradation of POM yields a small amount of CO (about the same order of magnitude than for H_2CO (Cottin et al., 2000)), no CO is produced by thermal degradation, which is the dominant degradation mechanism of POM for most of grains. Also, if extended CO in Hale–Bopp originated from POM photodegradation, then one should expect extended formaldehyde production to at least equal that for CO, and more probably be larger by perhaps as much as one or two orders of magnitude. This would result in more H_2CO than CO in the coma, which is not the case. This suggest that POM cannot be the main precursor for carbon monoxide. An experimental study of CO release by photodegradation or thermal degradation of refractory material obtained after energetic processing of ice mixtures should be undertaken in order to determine if a CO extended source can also originate from the slow degradation in the coma of other high molecular weight molecules. The diversity of the molecular composition of comets has been established. Henceforth, complex processes are likely to occur in the coma and multiphase chemistry (solid/gas) has to be included in our attempts to model its chemistry. The case of the extended source of formaldehyde and polyoxymethylene is certainly only one example among others, and its generalization requires new experimental developments. The approach presented in this paper offers a new insight to try to unravel the nature of the complex organic components of comets, which is critical to understand the chemical evolution of material from the interstellar medium to the Solar System.

Acknowledgments

The experimental part of this work has been supported by the French space agency CNES (Centre National d'Etudes Spatiales) and PNP (Programme National de Planétologie), and could not have been achieved without help of J.F. Doussin, R. Durand-Jolibois, B. Picquet, Nicolas Fray, and P. Carlier. The theoretical part has benefit from help and discussion with J. Crovisier, D. Bockelée-Morvan, M. Greenberg, and J.F. Crifo. This paper has partly been written while H.C. held a Société de Secours des Amis des Sciences associateship at LISA. We warmly thank our two referees, M.A. DiSanti and R. Meier for their corrections and help to improve this manuscript.

References

Allamandola, L.J., Sandford, S.A., Valero, G.J., 1988. Photochemical and thermal evolution of interstellar/precometary ice analogs. Icarus 76, 225–252.

Arpigny, C., 1994. Physical chemistry of comets: models, uncertainties, data needs. AIP Conf. Proc. 312, 205–238.

Bernstein, M.P., Sandford, S.A., Allamandola, L.J., Chang, S., Scharberg, M.A., 1995. Organic compounds produced by photolysis of realistic interstellar and cometary ice analogs containing methanol. Astrophys. J. 454, 327–344.

Bessel, M.S., Wickramasinghe, N.C., 1975. Polyoxymethylene polymers as interstellar grains. Mon. Not. R. Astron. Soc. 170, 11P–16P.

Biver, N., 1997. Molécules mères cométaires : observations et modélisations. Thesis. Université Paris VII, France.

Biver, N., Bockelée-Morvan, D., Crovisier, J., Colom, P., Henry, F., Moreno, R., Paubert, G., Despois, D., Lis, D.C., 2002. Chemical composition diversity among 24 comets observed at radio wavelengths. Earth Moon Planets 90, 323–333.

Biver, N., 13 colleagues, 1999. Spectroscopic monitoring of Comet C/1996 B2 (Hyakutake) with the JCMT and IRAM radio telescopes. Astron. J. 118, 1850–1872.

Biver, N., 12 colleagues, 2000. Spectroscopic observations of Comet C/1999 H1 (Lee) with the SEST, JCMT, CSO, IRAM, and Nançay radio telescopes. Astron. J. 120, 1554–1570.

Bockelée-Morvan, D., Crovisier, J., Colom, P., Despois, D., 1994. The rotational lines of methanol in Comets Austin 1990 V and Levy 1990 XX. Astron. Astrophys. 287, 647–665.

Bockelée-Morvan, D., Wink, J., Despois, D., Biver, N., Colom, P., Crovisier, J., Gerard, E., Lellouch, E., Jorda, L., 1998. Interferometric imaging of molecular lines in Comet Hale–Bopp. Bull. Am. Astron. Soc. 30, 31.02.

Bockelée-Morvan, D., 17 colleagues, 2000. New molecules found in Comet C/1995 O1 (Hale–Bopp). Investigating the link between cometary and interstellar material. Astron. Astophys. 353, 1101–1114.

Boice, D.C., Huebner, W.F., Sablik, M.J., Konno, I., 1990. Distributed coma sources and the CH_4/CO ratio in Comet Halley. Geophys. Res. Lett. 17, 1813–1816.

Combes, M., 16 colleagues, 1988. The 2.5–12 μm spectrum of Comet Halley from the IKS–VEGA experiment. Icarus 76, 404–436.

Combi, M.R., Delsemme, A.H., 1980. Neutral cometary atmospheres. I. An average random walk model for photodissociation in comets. Astrophys. J. 237, 633–640.

Cooke, A., Wickramasinghe, N.C., 1977. Polyoxymethylene co-polymers on grains. Astrophys. Space Sci. 50, 43–53.

Cottin, H., Gazeau, M.C., Raulin, F., 1999a. Cometary organic chemistry: a review from observations, numerical and experimental simulations. Planet. Space Sci. 47, 1141–1162.

Cottin, H., Gazeau, M.C., Doussin, J.F., Raulin, F., 1999b. S.E.M.A.Ph.Or.E COMETAIRE, a tool for the study of the photochemical decomposition of probable cometary large organic molecules. First application: polyoxymethylene. Phys. Chem. Earth C 24, 597–602.

Cottin, H., Gazeau, M.C., Doussin, J.F., Raulin, F., 2000. An experimental study of the photodegradation of polyoxymethylene at 122, 147 and 193 nm. J. Photochem. Photobiol. 135, 53–64.

Cottin, H., Szopa, C., Moore, M.H., 2001a. Production of hexamethylenetetramine in photolyzed and irradiated interstellar cometary ice analogs. Astrophys. J. Lett. 561, L139–L142.

Cottin, H., Gazeau, M.C., Bénilan, Y., Raulin, F., 2001b. Polyoxymethylene as parent molecule for the formaldehyde extended source in Comet Halley. Astrophys. J. 556, 417–420.

Cottin, H., Gazeau, M.C., Chaquin, P., Bénilan, Y., Raulin, F., 2001c. Experimental and theoretical studies on the gas/solid/gas transformation cycle in extraterrestrial environments. J. Geophys. Res. (Planets) 106, 33325–33332.

Cottin, H., Bachir, S., Raulin, F., Gazeau, M.C., 2002. Photodegradation of hexamethylenetetramine by VUV and its relevance for CN and HCN extended sources in comets. Adv. Space Res. 30, 1481–1488.

Crifo, J.F., 1988. Cometary dust sizing: comparison between optical and in-situ sampling techniques. Part. Part. Syst. Char. 5, 38–46.

Crifo, J.F., 1991. Hydrodynamic models of the collisional coma. In: Newburn, R.L., Neugebauer, M., Rahe, J. (Eds.), Comets in the Post-Halley Era. Kluwer, Dordrecht, pp. 937–989.

Crifo, J.F., 1994. Elements of cometary aeronomy. Current Science 66, 583–602.

Crifo, J.F., 1995. A general physicochemical model of the inner coma of active comets. I. Implications of spatially distributed gas and dust production. Astrophys. J. 445, 470–488.

Crifo, J.F., Rodionov, A.V., 1997. The dependence of the circumnuclear coma structure on the properties of the nucleus. I. Comparison between a homogeneous and an inhomogeneous spherical nucleus, with application to P/Wirtanen. Icarus 127, 319–353.

Crovisier, J., 1994. Photodestruction rates for cometary parent molecules. J. Geophys. Res. 99, 3777–3781.

Crovisier, J., Bockelée-Morvan, D., 1999. Remote observations of the composition of cometary volatiles. Space Sci. Rev. 90, 19–32.

Dello Russo, N., DiSanti, M.A., Mumma, M.J., Magee-Sauer, K., Rettig, T.W., 1998. Carbonyl sulfide in Comets Csolar1996 B2 (Hyakutake) and Csolar1995 O1 (Hale–Bopp): evidence for an extended source in Hale–Bopp. Icarus 135, 377–388.

DiSanti, M.A., Mumma, M.J., Dello Russo, N., Magee-Sauer, K., Novak, R., Rettig, T.W., 1999. Identification of two sources of carbon monoxide in Comet Hale–Bopp. Nature 399, 662–665.

DiSanti, M.A., Dello Russo, N., Magee-Sauer, K., Gibb, E.L., Reuter, D.C., Mumma, M.J., 2002a. CO, H_2CO, and CH_3OH in Comet 2002 C1 Ikeya–Zhang. In: Proceedings of Asteroids, Comets, Meteors—ACM 2002, International Conference. In: ESA SP, vol. 500, pp. 571–574.

DiSanti, M.A., Dello Russo, N., Magee-Sauer, K., Gibb, E.L., Reuter, D.C., Xu, L.-H., Mumma, M.J., 2002b. A comparison of the volatile carbon–oxygen chemistry in several Oort cloud comets. Bull. Am. Astron. Soc. 34, 855.

DiSanti, M.A., Mumma, M.J., Dello Russo, N., Magee-Sauer, K., Griep, D.M., 2003. Evidence for a dominant native source of carbon monoxide in Comet C/1996 B2 (Hyakutake). J. Geophys. Res. (Planets) 108, 15.

Dole, M., 1973. Polyoxymethylene. In: Dole, M. (Ed.), The Radiation Chemistry of Macromolecules, Vol. II. Academic Press, pp. 187–194.

Eberhardt, P., 1999. Comet Halley's gas composition and extended sources: results from the neutral mass spectrometer on Giotto. Space Sci. Rev. 90, 45–52.

Eberhardt, P., 10 colleagues, 1987. The CO and N_2 abundance in Comet P/Halley. Astron. Astrophys. 187, 481–484.

Fink, U., DiSanti, M.A., 1990. The production rate and spatial distribution of H_2O for Comet P/Halley. Astrophys. J. 364, 687–698.

Fischer, V.H., Langbein, W., 1967. Strahlungsinduzierte Reaktionen in Polyoxymethylen. Kolloid Z. Z. Polym. 216–217, 329–336.

Goldanskii, V.I., 1977. Mechanism for formaldehyde polymer formation in interstellar space. Nature 268, 612–613.

Greenberg, J.M., 1982. What are comets made of? A model based on interstellar dust. In: Wilkening, L.L. (Ed.), Comets. Univ. of Arizona Press, Tucson, pp. 131–163.

Greenberg, J.M., 1998. Making a comet nucleus. Astron. Astophys. 330, 375–380.

Greenberg, J.M., Li, A., 1998. From interstellar dust to comets: the extended CO source in Comet Halley. Astron. Astophys. 332, 374–384.

Haser, L., 1957. Distribution d'intensité dans la tête d'une comète. Bull. Acad. Roy. Belgique 43, 740–750.

Hudson, R.L., Moore, M.H., 1999. Laboratory studies of the formation of methanol and other organic molecules by water + carbon monoxide radiolysis: relevance to comets, icy satellites, and interstellar ices. Icarus 140, 451–461.

Huebner, W.F., 1987. First polymer in space identified in Comet Halley. Science 237, 628–630.

Huebner, W.F., Boice, D.C., Sharp, C.M., 1987. Polyoxymethylene in Comet Halley. Astrophys. J. Lett. 320, 149–152.

Huebner, W.F., Keady, J.J., Lyon, S.P., 1992. Solar photo rates for planetary atmospheres and atmospheric pollutants. Astrophys. Space Sci. 195, 1–294.

Irvine, W.M., 16 colleagues, 1996. Spectroscopic evidence for interstellar ices in Comet Hyakutake. Nature 383, 418–420.

Irvine, W.M., Bergin, E.A., Dickens, J.E., Jewitt, D., Lovell, A.J., Matthews, H.E., Schloerb, F.P., Senay, M., 1998a. Chemical processing in the coma as the source of cometary HNC. Nature 393, 547–550.

Irvine, W.M., Dickens, J.E., Lovell, A.J., Schloerb, F.P., Senay, M., Bergin, E.A., Jewitt, D., Matthews, H.E., 1998b. Chemistry in cometary comae. Faraday Discussion 109, 475–492.

Keane, J.V., Tielens, A.G.G.M., Boogert, A.C.A., Schutte, W.A., Whittet, D.C.B., 2001. Ice absorption features in the 5–8 μm region toward embedded protostars. Astron. Astophys. 376, 254–270.

Kissel, J., Krueger, F.R., 1987. The organic component in dust from Comet Halley as measured by the PUMA mass spectrometer on board Vega 1. Nature 326, 755–760.

Klavetter, J.J., A'Hearn, M.F., 1994. An extended source for CN jets in Comet P/Halley. Icarus 107, 322–334.

Lis, D.C., Keene, J., Young, K., Phillips, T.G., Bockelée-Morvan, D., Crovisier, J., Schilke, P., Goldsmith, P.F., Bergin, E.A., 1997. Spectroscopic observations of Comet C/1996 B2 (Hyakutake) with the Caltech Submillimeter Observatory. Icarus 130, 355–372.

Lisse, C.M., A'Hearn, M.F., Hauser, M.G., Kelsall, T., Lien, D.J., Moseley, S.H., Reach, W.T., Silverberg, R.F., 1998. Infrared observations of comets by COBE. Astrophys. J. 496, 971.

McDonnell, J.A.M., Lamy, P.L., Pankiewicz, G.S., 1991. Physical properties of cometary dust. In: Comets in the Post-Halley Era, Vol. 2. Kluwer, Dordrecht, pp. 1043–1073.

Meier, R., Eberhardt, P., Krankowsky, D., Hodges, R.R., 1993. The extended formaldehyde source in Comet P/Halley. Astron. Astophys. 277, 677–691.

Mitchell, D.L., Lin, R.P., Carlson, C.W., Korth, A., Rème, H., Mendis, D.A., 1992. The origin of complex organic ions in the coma of Comet Halley. Icarus 98, 125–133.

Möller, G., Jackson, W.M., 1990. Laboratory studies of polyoxymethylene: application to comets. Icarus 86, 189–197.

Moore, M.H., Tanabé, T., 1990. Mass spectra of sputtered polyoxymethylene: implications for comets. Astrophys. J. 365.

Moore, M.H., Khanna, R., Donn, B., 1991. Studies of proton irradiated $H_2O + CO_2$ and $H_2O + CO$ ices and analysis of synthesized molecules. J. Geophys. Res. 96, 17541–17545.

Moore, M.H., Ferrante, R.F., Nuth, J.A.I., 1996. Infrared spectra of proton irradiated ices containing methanol. Planet. Space Sci. 44, 927–935.

Mount, G.H., Rottman, G.J., 1981. The solar spectral irradiance 1200–3184 A near solar maximum. J. Geophys. Res. 86, 9188–9193.

Mumma, M.J., Reuter, D.C., 1989. On the identification of formaldehyde in Halley's comet. Astrophys. J. 344, 940–948.

Rabek, J.F., 1995. Polymer Photodegradation: Mechanisms and Experimental Methods. Chapman & Hall, London.

Rodgers, S.D., Charnley, S.B., 1998. HNC and HCN in comets. Astrophys. J. Lett. 501, L227–L230.

Rodgers, S.D., Charnley, S.B., 2001. On the origin of HNC in Comet Lee. Mon. Not. R. Astron. Soc. 323, 84–92.

Roessler, K., Sauer, M., Schulz, R., 1992. Gaseous products from VUV photolysis of cometary solids. Ann. Geophys. 10, 226–231.

Schutte, W.A., Allamandola, L.J., Sandford, S.A., 1993a. Formaldehyde and organic molecule production in astrophysical ices at cryogenic temperatures. Science 259, 1143–1145.

Schutte, W.A., Allamandola, L.J., Sandford, S.A., 1993b. An experimental study of the organic molecules produced in cometary and interstellar ice analogs by thermal formaldehyde reactions. Icarus 104, 118–137.

Shalaby, S.W., 1979. Radiative degradation of synthetic polymers: chemical physical, environmental, and technological considerations. J. Polymer Sci.: Macromol. Rev. 14, 419–458.

Snyder, L.E., Buhl, D., Zuckerman, B., Palmer, P., 1969. Microwave detection of interstellar formaldehyde. Phys. Rev. Lett. 22, 679.

Snyder, L.E., Palmer, P., Pater, I.d., 1989. Radio detection of formaldehyde emission from Comet Halley. Astron. J. 97, 246–253.

Vanysek, V., Wickramasinghe, N.C., 1975. Formaldehyde polymers in comets. Astrophys. Space Sci. 33, L19–L28.

Wink, J., 10 colleagues, 1999. Evidence for extended sources and temporal modulations in molecular observations of C/1995 O1 (Hale–Bopp) at the IRAM interferometer. Earth Moon Planets 78, 63.

Woon, D.E., 1999. Ab initio quantum chemical studies of reactions in astrophysical ices 1. Aminolysis, hydrolysis, and polymerization in $H_2CO/NH_3/H_2O$ ices. Icarus 142, 550–556.

Article 12

FRAY N., BÉNILAN Y., BIVER N., BOCKELÉE-MORVAN D., COTTIN H., CROVISIER J. and GAZEAU M.-C. (2006) Heliocentric evolution of the degradation of polyoxylmethylene. Application to the origin of the formaldehyde (H2CO) extended source in comet C/1995 O1 (Hale-Bopp). Icarus 184(1), 239-254.

Available online at www.sciencedirect.com
ScienceDirect
Icarus 184 (2006) 239–254
ICARUS
www.elsevier.com/locate/icarus

Heliocentric evolution of the degradation of polyoxymethylene: Application to the origin of the formaldehyde (H_2CO) extended source in Comet C/1995 O1 (Hale–Bopp)

Nicolas Fray [a,*], Yves Bénilan [a], Nicolas Biver [b], Dominique Bockelée-Morvan [b], Hervé Cottin [a], Jacques Crovisier [b], Marie-Claire Gazeau [a]

[a] *Laboratoire Interuniversitaire des Systèmes Atmosphériques, UMR 7583 du CNRS, Universités Paris VII–Paris XII, 61 Av. du Général de Gaulle, 94010 Créteil Cedex, France*

[b] *Observatoire de Paris-Meudon, 5 Place Jules Janssen, 92195 Meudon, France*

Received 22 September 2005; revised 27 April 2006

Available online 30 June 2006

Communicated by Combi

Abstract

The H_2CO production rates measured in Comet C/1995 O1 (Hale–Bopp) from radio wavelength observations [Biver, N., and 22 colleagues, 2002a. Earth Moon Planets 90, 5–14] showed a steep increase with decreasing heliocentric distance. We studied the heliocentric evolution of the degradation of polyoxymethylene (formaldehyde polymers: $(–CH_2–O–)_n$, also called POM) into gaseous H_2CO. POM decomposition can indeed explain the H_2CO density profile measured in situ by *Giotto* spacecraft in the coma of Comet 1P/Halley, which is not compatible with direct release from the nucleus [Cottin, H., Bénilan, Y., Gazeau, M.-C., Raulin, F., 2004. Icarus 167, 397–416]. We show that the H_2CO production curve measured in Comet C/1995 O1 (Hale–Bopp) can be accurately reproduced by this mechanism with a few percents by mass of solid POM in grains. The steep heliocentric evolution is explained by the thermal degradation of POM at distances less than 3.5 AU. This study demonstrates that refractory organics present in cometary dust can significantly contribute to the composition of the gaseous coma. POM, or POM-like polymers, might be present in cometary grains. Other molecules, like CO and HNC, might also be produced by a similar process.

Keywords: Comets, composition; Organic chemistry

1. Introduction

To date, about two dozen molecules (excluding ions and radicals) have been detected in cometary environments (Bockelée-Morvan et al., 2005). Most of them are directly produced by sublimation from the nucleus or from ice-coated grains within the first few kilometers after their ejection from the nucleus. However, for certain comets, the radial distribution of some molecules such as CO (Eberhardt et al., 1987; DiSanti et al., 2001) and H_2CO (Meier et al., 1993; Wink et al., 1999; Biver et al., 1999) cannot be entirely explained by such simple processes. These molecules present a so-called "extended source," i.e., involving production throughout the coma and not only at or near the surface of the nucleus. Such behavior could result from other mechanisms such as chemical reactions in the inner coma (Rodgers and Charnley, 1998) or degradation of high molecular weight organic compounds present in cometary grains (Cottin et al., 2004). As these molecules are not produced only by sublimation of the nucleus, their abundance in the gas phase cannot be directly related to their abundance in the nucleus. Nevertheless, the understanding of their production mechanism is of great interest to constrain the composition of the nucleus. In this paper, we focus on the steep heliocentric evolution of H_2CO production rates observed at radio wavelengths for Comet C/1995 O1 (Hale–Bopp) by Biver et al. (2002a).

* Corresponding author. Fax: +33 1 45 17 15 64.
E-mail address: fray@lisa.univ-paris12.fr (N. Fray).

0019-1035/$ – see front matter
doi:10.1016/j.icarus.2006.04.014

Formaldehyde is an important cometary molecule which has been observed through its radio rotational lines in more than 15 comets. With a production rate relative to water of about 1% (Bockelée-Morvan et al., 2005), it is the most abundant CHO cometary molecule after methanol. An even higher abundance (3.8%) was derived from the mass spectroscopic observations of Comet 1P/Halley by *Giotto* (Meier et al., 1993). This relative abundance is observed to vary from comet to comet (from 0.13 to 1.3% according to radio observations, Biver et al., 2002b).

Among comets for which the spatial distribution of H_2CO has been studied, all observations, except for those concerning Comet C/2002 C1 (Ikeya–Zhang) (DiSanti et al., 2002), suggest that formaldehyde does not come from sublimation of the pristine ices in the nucleus, but rather from an extended source within the coma. This was suggested by the analysis of the H_2CO density profiles of 1P/Halley measured by the Giotto Neutral Mass Spectrometer (NMS) (Meier et al., 1993). Maps of the spatial distribution of H_2CO at radio wavelengths in Comets C/1989 X1 (Austin) and C/1990 K1 (Levy) (Colom et al., 1992) and in C/1996 B2 (Hyakutake) (Biver et al., 1999) also show that H_2CO is produced by an extended source. Finally, radio-interferometric observations have shown an H_2CO extended source in Comet C/1995 O1 (Hale–Bopp) (Wink et al., 1999). All these observations show that H_2CO is produced with a scale length of about $6800 R_H^{1.4}$ km (Biver, 1997), where R_H is the heliocentric distance in AU. Given that the spatial distribution of H_2CO cannot be explained by the photodissociation of another gaseous parent, it has been proposed that H_2CO could be produced by the decomposition of solid polymers such as polyoxymethylene (H_2CO polymers: $(–CH_2–O–)_n$, also called POM) (Cottin et al., 2004).

POM has been detected in laboratory analogs of interstellar or cometary ices. It is synthesized by thermal processing of ices containing H_2O, H_2CO and NH_3 (Schutte et al., 1993a, 1993b). POM or POM-like polymers are also produced when ices containing some CH_3OH and NH_3, but no H_2CO in the initial mixture, are irradiated by UVs (Bernstein et al., 1995; Muñoz-Caro and Schutte, 2003). Moreover, this polymer was detected in Comet 1P/Halley by the PICCA mass spectrometer on board the *Giotto* spacecraft (Huebner, 1987), however this is controversial since it has been shown that the feature attributed to POM in the mass spectrum could be merely the signature of a mixture of organic material made of C, H, O and N atoms (Mitchell et al., 1992). POM is thus likely to be present in cometary grains among other refractory organic components and may produce gaseous H_2CO by photo-degradation (UV photolysis) and/or thermal-degradation (heating of the grains after their release from the nucleus).

To test this hypothesis, we have performed an experimental study of POM degradation. Subject to UV irradiation at 122 and 147 nm, POM produces several oxygenated compounds such as H_2CO, CO, HCOOH and CO_2 (Cottin et al., 2000). The H_2CO production quantum yield is about 1 at both wavelengths. Once heated, POM produces only gaseous H_2CO and the polymer is in equilibrium with gaseous H_2CO (POM $\leftrightarrow n H_2CO$) (Dainton et al., 1959). The production kinetics have been measured at several temperatures in the 250–330 K range (Cottin et al., 2001; Fray et al., 2004a). The H_2CO kinetics have been shown to follow the Arrhenius law according to:

$$\frac{\mathrm{d}H_2CO}{\mathrm{d}t} = k(T) m_{\mathrm{POM}}, \quad \text{where } k(T) = A e^{-E_a/k_B T},$$

where $k(T)$ is the number of gaseous formaldehyde molecules produced per gram of POM per second, A the frequency factor (molecules $\mathrm{g}^{-1}\,\mathrm{s}^{-1}$) and E_a the activation barrier ($\mathrm{J\,molecule}^{-1}$). These quantitative data have been included in a model of the cometary environment taking into account the production of gaseous compounds from photo- and thermal-degradation of solid organic compounds present in cometary grains. In this way, *Giotto* measurements of the H_2CO density were properly fitted assuming that cometary grains contain about 4% of POM by mass. This work has also allowed us to point out that, at 0.9 AU from the Sun, the thermal-degradation process is dominant with regard to the photolytic one (Cottin et al., 2004; Fray et al., 2004a). Nevertheless, this result is valid only for a heliocentric distance of 0.9 AU and for Comet 1P/Halley.

We have developed a new version of the model to study the effect of the heliocentric distance on H_2CO production from POM degradation. This time, we compare the H_2CO production rates observed at radio wavelengths using the JCMT, CSO, SEST and IRAM radio telescopes during the long term monitoring of Comet C/1995 O1 (Hale–Bopp), as described in Biver et al. (2002a), with our theoretical expectations. Observations, which have been performed from 4 AU pre-perihelion to 3.5 AU post-perihelion, have shown a steeper heliocentric evolution for H_2CO productions rates than for those of other species of similar volatility, such as HCN (Biver et al., 2002a). During the pre-perihelion phase, the H_2CO production rate varies with $R_H^{-3.6}$ while that of HCN varies with $R_H^{-2.6}$. During the post-perihelion phase, the H_2CO production rate varies with $R_H^{-4.2}$ while that of HCN varies with $R_H^{-2.8}$.

In Section 2 we describe a general model applicable to any species and new equations that allow us to study the influence of the considered mechanisms (photo- and thermal-degradation of POM) on the total H_2CO production. Then in Section 3 we discuss the parameters (such as gas and dust production rates), and their heliocentric dependence, which are required to calculate H_2CO production from POM degradation. Results are presented in Section 4 and we discuss their implications in the last section of this paper.

2. Description of the model

The model presented in this section is an extension of the Haser model (Haser, 1957). We assume that (1) the production rates of gas and dust are in steady state and that (2) the motion from the nucleus is radial and at constant velocity with respect to the nucleocentric distance. We consider that a gaseous species can be produced by three different mechanisms: (1) photo-degradation, (2) thermal-degradation of the solid organic component of grains and (3) direct sublimation from the nucleus. This model has already been partially presented in Cottin et al. (2004). Here, we will first describe the

model in detail and present new equations that are applicable to the production of any gaseous species from the degradation of the solid component of grains. They will allow us to evaluate the production of a gaseous species from photo- and thermal-degradation independently. Then we will apply the model to the case of H_2CO production from POM degradation with the aim of reproducing the steep heliocentric evolution of H_2CO production observed in Comet C/1995 O1 (Hale–Bopp) by Biver et al. (2002a).

2.1. Evolution of solid organic mass on grains

Let us now consider a spherical grain including a mass fraction α of solid polymer, with radius R, mass m and density μ. If m_α is the mass of the polymer and μ' its density, we can define the radius R_α of an equivalent grain made of pure solid polymer:

$$m_\alpha = \alpha m = \alpha\left(\frac{4}{3}\pi R^3 \mu\right) = \frac{4}{3}\pi R_\alpha^3 \mu'. \quad (1)$$

Assuming that photo-degradation takes place only at the surface of the grains and that thermal-degradation occurs throughout the highly porous material of the grains, the mass loss of this "pure polymer grain" can then be written:

$$\frac{\mathrm{d}m_\alpha(r)}{\mathrm{d}t} = -\big(\sigma_\alpha(r) C_{\text{grain}} + m_\alpha(r) k_{\text{grain}}\big). \quad (2)$$

In this equation:

- C_{grain} ($\mathrm{kg\,m^{-2}\,s^{-1}}$) represents the mass lost by photo-degradation of the polymer. It is calculated taking into account the production of all gaseous species produced by UV irradiation of the solid polymer. We can therefore write $C_{\text{grain}} = \sum_i m_i \int_\lambda f_\lambda \Phi_\lambda^i \,\mathrm{d}\lambda$, where m_i is the mass of the molecule i produced with a quantum yield Φ_λ^i and f_λ is the solar irradiance (photons $\mathrm{m^{-2}\,s^{-1}\,nm^{-1}}$). In Eq. (2), $\sigma_\alpha(r)$ is the area of polymer submitted to solar irradiation and is considered to be equal to $\pi R_\alpha^2(r)$.
- k_{grain} (molecules $\mathrm{s^{-1}}$) represents the mass lost per second by thermal-degradation of the polymer. k_{grain} is calculated taking into account the production of all gaseous species produced by thermal-degradation of the solid polymer. Generally, the production of gaseous species by this mechanism follows the Arrhenius law (Cottin et al., 2001; Fray et al., 2004a). Therefore we can write $k_{\text{grain}} = \sum_i m_i (A_i e^{-E_{ai}/kT})$, where m_i, A_i and E_{ai} are respectively the mass, frequency factor (molecules $\mathrm{kg^{-1}\,s^{-1}}$) and activation energy (J $\mathrm{molecule^{-1}}$) of the molecule i and k is the Boltzmann constant.

We consider that the dust expansion velocity and dust temperature do not vary with the distance from the nucleus. Note that, as we are modeling the degradation of refractory organics contained in grains, the grains will shrink leading to an increase in their temperature. Nevertheless, as we will see in the conclusions, this effect can be neglected given that the mass of disappearing organics represents only a few percent of the initial grain mass. Therefore, under these assumptions, we can integrate Eq. (2). The evolution of R_α with the nucleocentric distance is:

$$R_\alpha(r) = R_\alpha^0 \beta\big[-1 + Z e^{-r/L_T}\big]. \quad (3)$$

In this equation:

- R_α^0 is the radius of the equivalent "pure polymer grain" when ejected from the nucleus.
- $\beta = \frac{L_T}{L_P}$ and $Z = 1 + \frac{1}{\beta}$, where:
  - $L_T = \frac{3V_{\text{grain}}}{k_{\text{grain}}}$ is the "thermal-degradation scale length," i.e., at a distance L_T from the nucleus, R_α is decreased by a factor $1/e$ if only thermal-degradation occurs (Cottin et al., 2004).
  - $L_P = \frac{4\mu' R_\alpha^0 V_{\text{grain}}}{C_{\text{grain}}}$ is the "photo-degradation scale length." At a distance L_P from the nucleus, $R_\alpha = 0$ (i.e., the polymer initially present in the grains is totally degraded into gaseous species) if only photo-degradation occurs (Cottin et al., 2004).

Since these scale lengths have no direct physical meaning if photo- and thermal-degradation are both responsible of the production of gas, we define $r_C = L_T \times \ln(\frac{L_T + L_P}{L_T})$, called hereafter the 'critical distance,' which is the distance from the nucleus at which all the polymer initially present in the grains is totally degraded into gaseous species.

2.2. Production of gaseous species from grains

We will call M the gaseous species produced by degradation of the solid organic component of grains that we want to study. To calculate $n_M(r)$, the density of M, we use the mass budget equation:

$$\frac{\partial n_M(r)}{\partial t} + \mathrm{div}\big[n_M(r) v_{\text{gas}}\big] = \left(\frac{\mathrm{d}M}{\mathrm{d}t}\right)_P - \left(\frac{\mathrm{d}M}{\mathrm{d}t}\right)_D, \quad (4)$$

where:

- v_{gas} is the gas expansion velocity ($\mathrm{m\,s^{-1}}$).
- $\left(\frac{\mathrm{d}M}{\mathrm{d}t}\right)_D$ represents the destruction of the gaseous species M by photolysis. Therefore $\left(\frac{\mathrm{d}M}{\mathrm{d}t}\right)_D = \beta_M n_M(r)$.
- $\left(\frac{\mathrm{d}M}{\mathrm{d}t}\right)_P$ represents the production of the gaseous species M from solid polymer degradation. We can write:

$$\left(\frac{\mathrm{d}M}{\mathrm{d}t}\right)_P = n_{\text{grain}}(r)\big[\sigma_\alpha(r) C_M + m_\alpha(r) k_M(T_{\text{grain}})\big]. \quad (5)$$

In this equation,

- $n_{\text{grain}}(r)$ is the grain density in the coma (grains $\mathrm{m^{-3}}$) as a function of the distance from the nucleus. We consider $n_{\text{grain}}(r) = \frac{Q_{\text{grain}}}{4\pi v_{\text{grain}} r^2}$ where Q_{grain} is the grain production rate (grains $\mathrm{s^{-1}}$) and v_{grain} the grain velocity ($\mathrm{m\,s^{-1}}$). As Q_{grain} and v_{grain} depend on grain size, a grain size distribution is used to calculate the total production of M (sum of the contributions of each size of grains).

- C_M is the production rate of M (molecules $m^{-2}\,s^{-1}$) from photo-degradation of solid polymer. Therefore, $C_M = \int_\lambda f_\lambda \Phi_\lambda^M \,d\lambda$ where f_λ is the solar irradiance (photons $m^{-2}\,s^{-1}\,nm^{-1}$) and Φ_λ^M the production quantum yield of M from solid polymer.
- $k_M(T_{grain})$ is the production rate of M (molecules $kg^{-1}\,s^{-1}$) from thermal-degradation of solid polymer at a temperature T_{grain} and is taken to be equal to $k_M(T) = A_M e^{-E_{aM}/kT}$.

Considering a radial gas expansion velocity independent of the distance from the nucleus and an ejection velocity of M from grains equal to the gas expansion velocity, Eq. (4) can be integrated analytically:

$$n_M(r) = \frac{Y}{r^2}\left[\left[l_M(1-X)\left(1-e^{-r/l_M}\right)\right] + \left[\frac{(3X-2)Z}{(1/l_M-1/l_T)}\left(e^{-r/l_T}-e^{-r/l_M}\right)\right] + \left[\frac{(1-3X)Z^2}{(1/l_M-2/l_T)}\left(e^{-2r/l_T}-e^{-r/l_M}\right)\right] + \left[\frac{XZ^3}{(1/l_M-3/l_T)}\left(e^{-3r/l_T}-e^{-r/l_M}\right)\right]\right], \quad (6)$$

where:

- $Y = \dfrac{Q_{grain} C_M R_\alpha^{0^2} \beta^2}{4 V_{grain} V_{Gas}}$;
- $X = \dfrac{C_{grain}}{C_M}\dfrac{k_M}{k_{grain}}$;
- and $l_M = v_{gas}/\beta_M$ is the photo-dissociation scale length of the gaseous species M.

If M is produced only by solid polymer thermal-degradation, Eq. (4) can be modified and $n_M^T(r)$, the density of M (molecules m^{-3}) produced only by the thermal-degradation of solid polymer, can be written:

$$n_M^T(r) = \frac{Y}{r^2}\left[\left[-Xl_M\left(1-e^{-r/l_M}\right)\right] + \left[\frac{3XZ}{(1/l_M-1/l_T)}\left(e^{-r/l_T}-e^{-r/l_M}\right)\right] + \left[\frac{-3XZ^2}{(1/l_M-2/l_T)}\left(e^{-2r/l_T}-e^{-r/l_M}\right)\right] + \left[\frac{XZ^3}{(1/l_M-3/l_T)}\left(e^{-3r/l_T}-e^{-r/l_M}\right)\right]\right]. \quad (7)$$

Similarly, if M is only produced by photo-degradation of solid polymer, $n_M^P(r)$, the density of M (molecules m^{-3}) produced only by the photo-degradation of solid polymer, can be written:

$$n_M^P(r) = \frac{Y}{r^2}\left[\left[l_M\left(1-e^{-r/l_M}\right)\right] + \left[\frac{-2.Z}{(1/l_M-1/l_T)}\left(e^{-r/l_T}-e^{-r/l_M}\right)\right] + \left[\frac{Z^2}{(1/l_M-2/l_T)}\left(e^{-2r/l_T}-e^{-r/l_M}\right)\right]\right]. \quad (8)$$

As would be expected, $n_M(r)$ is calculated from Eq. (7) and Eq. (8): $n_M(r) = n_M^T(r) + n_M^P(r)$. Therefore Eq. (7) and Eq. (8) can be used to calculate the production of any gaseous species from photo- and thermal-degradation of the solid component of grains.

To calculate $n_M(r)$, we need to know the dust mass production rate (Q_{grain} in $kg\,s^{-1}$), grain size distribution, grain temperatures (T_{grain}) and grain velocities (V_{grain}). The calculations of these parameters as a function of heliocentric distance are presented in Section 3.

2.3. Production of gaseous species from sublimation of the nucleus

Equation (6) only takes into account the production of gaseous species from solid polymer degradation on grains, whereas a fraction of M could also be produced by direct sublimation of nucleus ices. The density of the native M produced at (or near) the surface of the nucleus is modeled using the equation established for a "parent molecule" by Haser (1957):

$$n_M^{nucleus}(r) = \frac{Q_M^{nucleus}}{4\pi v_{gas} r^2} e^{-r/l_M}, \quad (9)$$

where $Q_M^{nucleus}$ is the production rate of the native M.

2.4. Application of the model to H_2CO production from POM

To calculate the H_2CO density (molecules m^{-3}) produced from POM degradation, we have to determine the coefficients C_{grain}, C_{H_2CO}, k_{grain} and k_{H_2CO}. This can be done using the experimental data of Cottin et al. (2000) and Fray et al. (2004a) who have studied respectively the photo- and thermal-degradation of POM. Cottin et al. (2000) have shown that the dominant products of POM photo-degradation at 122 and 147 nm are H_2CO, CO, HCOOH and CO_2. Using the measured production quantum yields of each product and the solar flux published by Mount and Rottman (1981), we estimate that $C_{grain} = 6.76 \times 10^{-9}$ kg $m^{-2}\,s^{-1}$ and $C_{H_2CO} = 5.07 \times 10^{16}$ molecules $m^{-2}\,s^{-1}$ at 1 AU. Note that H_2CO production from POM photo-degradation accounts for only 37% of the total mass loss of the grains by this process. The remaining 63% contribute to production of CO, HCOOH and CO_2 (Cottin et al., 2000). Concerning thermal-degradation, two types of POM have been investigated between 250 and 330 K (Fray et al., 2004a); hereafter we will call "POM1" the POM supplied by the "Aldrich" company and "POM2" the POM supplied by the "Prolabo" company. The two polymers may slightly differ in chain lengths. It has been shown that, for both types of POM, H_2CO is the only gaseous species produced by thermal-degradation of POM and that the production kinetics follow the Arrhenius law (Fray et al., 2004a). We have determined $E_{a1} = 99 \times 10^3$ J mol^{-1} and $A_1 = 7.2 \times 10^{32}$ molecules $g^{-1}\,s^{-1}$ for "POM1" and $E_{a2} = 81 \times 10^3$ J mol^{-1} and $A_2 = 1.2 \times 10^{30}$ molecules $g^{-1}\,s^{-1}$ for

Table 1
H_2CO production kinetics from thermal-degradation of "POM1" and "POM2" for typical grain temperatures

Temperature (K)	$k(T)$ for POM1 (molecules g^{-1} s^{-1})	$k(T)$ for POM2 (molecules g^{-1} s^{-1})	Ratio of $k(T)$ for POM1 to $k(T)$ for POM2
200	9.7×10^{6}	8.2×10^{8}	0.012
250	1.5×10^{12}	1.4×10^{13}	0.10
300	4.1×10^{15}	9.3×10^{15}	0.44
350	1.2×10^{18}	9.6×10^{17}	1.23
400	8.4×10^{19}	3.1×10^{19}	2.67
450	2.3×10^{21}	4.7×10^{20}	4.87
500	3.2×10^{22}	4.1×10^{21}	7.88
550	2.8×10^{23}	2.4×10^{22}	11.68
600	1.7×10^{24}	1.1×10^{23}	16.22

"POM2." Note that the pre-exponential factors differ by a factor of 600. Despite this difference, H_2CO production kinetics of "POM1" and "POM2" are equal for $T = 339$ K and differ by a factor of between 0.012 and 16.2 for temperatures ranging from 200 to 600 K (see Table 1). As the temperature of grains depends on their size, these factors are attenuated when we consider the entire size distribution. Therefore, as we will see in Section 4.2.1, H_2CO production rates are not very sensitive to the type of POM we consider. Moreover, we have used a POM density of 1.46×10^3 kg m^{-3} (Prolabo).

To calculate the H_2CO density (molecules m^{-3}) produced by nucleus sublimation, we assume that the production rate of native H_2CO is proportional to that of HCN (see Fig. 1). Indeed the sublimation temperatures of H_2CO and HCN are quite close ($T_{H_2CO} = 64$ K and $T_{HCN} = 95$ K, Crovisier, 1997). Moreover, Magee-Sauer et al. (1999, 2002) have shown, from spectral observations of the ν_3 band of HCN and analysis of the spatial distribution of HCN for Comets C/1996 B2 (Hyakutake) and C/1995 O1 (Hale–Bopp), that HCN is predominantly released at the surface of the nucleus, while a small contribution from an extended source cannot be ruled out. A similar conclusion has been derived from single-field interferometric observations at radio wavelength for Comet C/1995 O1 (Hale–Bopp) (Snyder et al., 2001). The use of HCN as an indicator of native H_2CO rather than H_2O, the most abundant component of cometary ices, is also justified by the fact that HCN and H_2CO production rates were measured simultaneously with the same radio techniques, whereas H_2O production is obtained from sparse infrared observations or from indirect indicators. Moreover we use a H_2CO photo-dissociation rate of 2×10^{-4} s^{-1} (Crovisier, 1994).

Our objective is to compare the results of this model to the H_2CO production rates observed at radio wavelengths during the long-term monitoring of Comet C/1995 O1 Hale–Bopp (Biver et al., 2002a). Therefore the total H_2CO density (molecules m^{-3}) is integrated on the line of sight to calculate the H_2CO column density (molecules m^{-2}), which is afterwards integrated over the field of view of the radio telescope to derive the total number of H_2CO molecules observed during an observation. We assume an antenna beam size of 12″ (the real size varied from 10.6″ to 13.6″ depending on the observation) introducing a 10% uncertainty. Finally, the calculated total number of H_2CO molecules in the antenna beam is converted into H_2CO production rates (molecules s^{-1}) using the Haser model and assuming that H_2CO behaves as a "daughter species," i.e., a "parent scale length" of $6800 R_H^{1.4}$ km (Biver, 1997) and a "daughter scale length" of $l_{H_2CO} = v_{gas}/\beta_{H_2CO}$. This procedure is as close as possible to the one used by Biver et al. (2002a) to convert the observed flux of the H_2CO lines into production rates and can therefore be used to compare the equivalent H_2CO production rate of our model to those of Biver et al. (2002a).

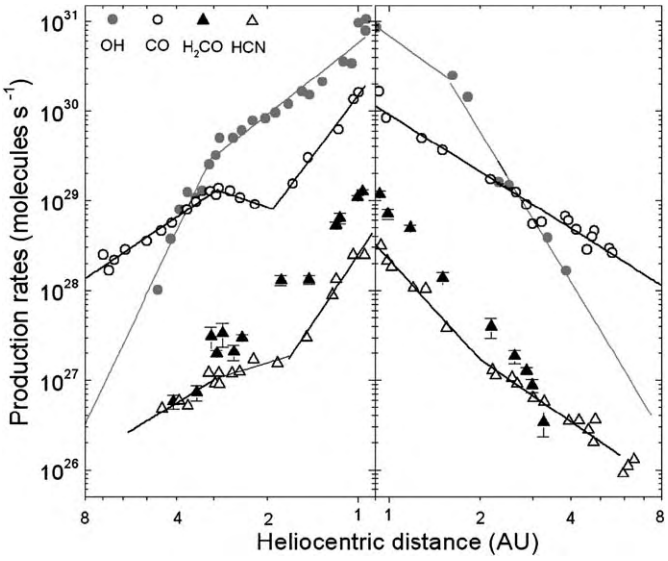

Fig. 1. OH, CO, H_2CO and HCN production rates measured by Colom et al. (1999) and Biver et al. (2002a) in Comet C/1995 O1 (Hale–Bopp) as a function of heliocentric distance. Note that the heliocentric evolution of the production rate of H_2CO is steeper than that of HCN. During the pre-perihelion phase, the H_2CO production rate varies with $R_H^{-3.6}$ while that of HCN varies with $R_H^{-2.6}$ and during the post-perihelion phase, the H_2CO production rate varies with $R_H^{-4.2}$ while that of HCN varies with $R_H^{-2.8}$. Note that the heliocentric evolution characteristics given here have been averaged over the whole range of heliocentric distances for which measurements have been performed, whereas more accurate fits, represented as solid lines, have been used to calculated the production rates in the model.

3. The dust model for Comet C/1995 O1 (Hale–Bopp)

As shown in Section 2, the calculation of the production rates (molecules s^{-1}) of gaseous species including solid organic compound degradation requires values for Q_{grain}, i.e., the dust mass production rate (kg s^{-1}) and its grain size distribution, the grain temperature T_{grain}, as well as V_{grain} and V_{gas}, the grain and gas expansion velocities. Finally, the total gas production rate is needed in order to estimate the dust-to-gas ratio and the grain velocities (as well as the HCN production rate to derive the native H_2CO density). The determination of these parameters as a function of heliocentric distance is presented in this section.

3.1. Gas production rates and velocity

The aim of the present study is to test if POM degradation is responsible for the steep heliocentric evolution of the H_2CO production rates observed at radio wavelengths in Comet C/

1995 O1 (Hale–Bopp) (Biver et al., 2002a). These observations were made for heliocentric distances ranging from 4.1 AU (June 1996, pre-perihelion) to 3.2 AU (October 1997, post-perihelion). Thus, our study concerns conditions ranging from the CO-dominated coma (at distances greater than 4 AU) to the H_2O dominated coma (between 3 AU and perihelion). The total gas production rate is taken as the sum of the CO and H_2O production rates. The latter are derived from the radio observations of Colom et al. (1999), whereas CO and HCN production rates are from Biver et al. (2002a). The OH, CO, H_2CO and HCN production rates are displayed in Fig. 1.

The assumed gas expansion velocity values are those derived from the analysis of radio line shapes (Biver et al., 2002a), i.e., $v_{\text{gas}} = 1.125 R_H^{-0.42}$ km s^{-1} (see Fig. 5).

3.2. Dust distribution

3.2.1. Shape of the distribution

The grain size distribution in the coma of Comet C/1995 O1 (Hale–Bopp) is assumed to be identical to the that measured in situ in Comet 1P/Halley. It has been derived by Crifo and Rodionov (1997) from the data acquired by the *Giotto* spacecraft (McDonnell et al., 1991) assuming spherical grains with a density of 1000 kg m^{-3}. This distribution is plotted in Fig. 2. Data for masses between 10^{-18} and 10^{-6} kg (i.e., for grain sizes between 6×10^{-8} and 6×10^{-4} m) are derived from in situ measurements, whereas data for grains lighter than 10^{-18} kg and heavier than 10^{-6} kg are estimated from a linear extrapolation of the measurements (Crifo and Rodionov, 1997). Most of the mass lies in the largest grains and two changes of slope can be observed at approximately 10^{-9} and 10^{-7} kg (i.e., 3×10^{-4} and 6×10^{-5} m). A similar distribution was recently measured in Comet 81P/Wild 2 by the *Stardust* spacecraft (Tuzzolino et al., 2004; Green et al., 2004). Therefore, such a distribution could apply more generally to all comets.

This distribution is then adapted to make it relevant to our study of the heliocentric evolution of production rates of gaseous species. First, we take into account the change of size of the largest grains lifted from the nucleus with the heliocentric distance, since the total gas production rate varies. Secondly, the total dust production rate (kg s^{-1}) is adjusted using the measurements performed on Comet C/1995 O1 (Hale–Bopp).

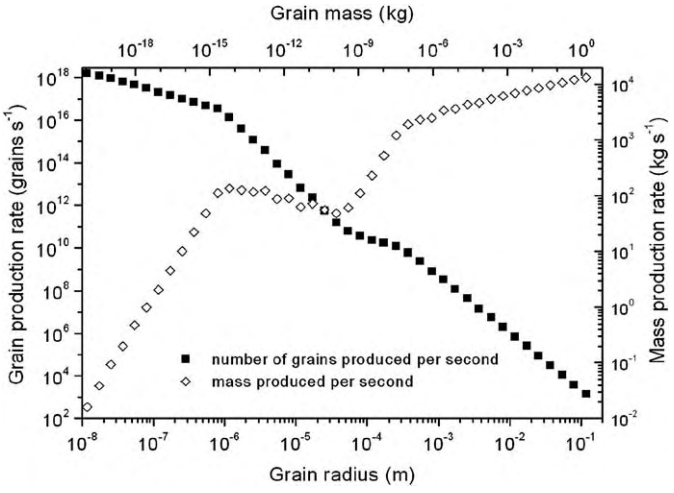

Fig. 2. Production rates in terms of number and mass of grains as a function of grain radius measured in Comet 1P/Halley by the *Giotto* spacecraft. (McDonnell et al., 1991; Crifo and Rodionov, 1997).

3.2.2. Size of the largest grains lifted from the nucleus of Comet C/1995 O1 (Hale–Bopp)

The balance between the gravitational force of the nucleus and the drag force due to the expansion of the gas influences the size of the largest grains, a_{Max}, lifted from the nucleus. Crifo and Rodionov (1997) have shown that a_{Max} can be written:

$$a_{\text{Max}} = \frac{3}{\pi}\frac{m_{\text{gas}}(1-A)c_{\Theta}}{G\rho_{\text{grain}}\rho_n R_n L_s}\sqrt{\frac{kT^0_{\text{gas}}}{2\pi m_{\text{gas}}}}\frac{f\cos(z)}{R_H^2}. \tag{10}$$

We use the same equation where:

- m_{gas} is the mean molecular mass taken to be equal to: $m_{\text{gas}} = (m_{\text{CO}}Q_{\text{CO}} + m_{\text{H}_2\text{O}}Q_{\text{H}_2\text{O}})/(Q_{\text{CO}} + Q_{\text{H}_2\text{O}})$ where Q_i are the production rates.
- A is the albedo of the grain taken to be equal to that measured for the 1P/Halley nucleus: 0.04 (Keller et al., 1987).
- ρ_{grain} is the grain density taken to be equal to 1000 kg m^{-3} (Crifo and Rodionov, 1997)
- ρ_n is the nucleus density taken arbitrary to be equal to 500 kg m^{-3}
- R_n is the radius of the nucleus considered to be 30 km. Note that values for the radius of the nucleus of Comet C/1995 O1 (Hale–Bopp), measured with different methods, range from 22 km (Altenhoff et al., 1999) to 35 km (Sekanina, 1999; Weaver and Lamy, 1999).
- L_s is the latent heat of sublimation of water ice (L_s = 2660 kJ kg^{-1} = 7.95×10^{-20} J molecule^{-1}, Kührt, 1999).
- T^0_{gas} is the gas temperature at the surface of the nucleus calculated using the analytical formula given by Crifo and Rodionov (1997) (Eq. (11) of Appendix B).
- f is the icy area fraction taken to be equal to 0.2.
- z is the zenith angle, as this equation is valid for a specific area on the surface of the nucleus. To determine the maximum possible radius, we have considered $\cos z = 1$.
- c_{Θ} is the solar constant ($c_{\Theta} = 1367.6$ W m^{-2})

The size of the largest grain that can be lifted from the nucleus is found to be 0.07 cm at 4 AU and 1.24 cm at 1 AU (see Fig. 4) with a heliocentric variation close to R_H^{-2}. These results are close to those of Weiler et al. (2003) and agree well with radar observations of centimetric grains in several comets near 1 AU (Harmon et al., 1999).

3.2.3. Dust production rates in Comet C/1995 O1 (Hale–Bopp)

A compilation of the dust production rates measured in Comet C/1995 O1 (Hale–Bopp) is used to assess the grain size distribution. As a very broad dust distribution is concerned, we use measurements performed over different wavelength ranges, each being more sensitive to a given grain size. Submillimeter

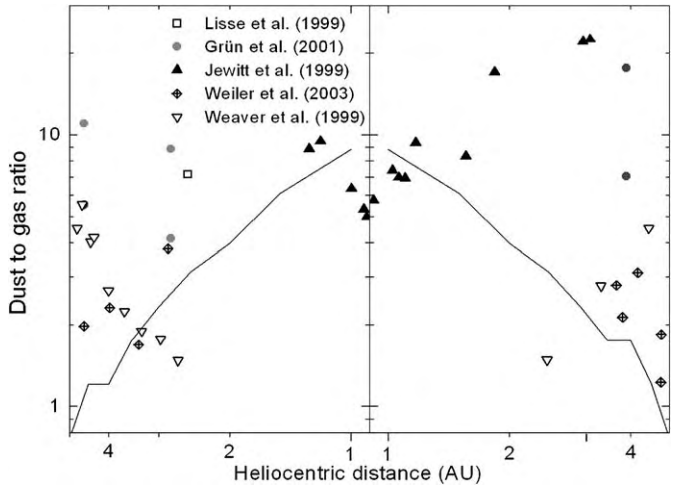

Fig. 3. Dust-to-gas ratio in Comet C/1995 O1 (Hale–Bopp) as a function of heliocentric distance, from measurements by various authors. The curve shows the nominal dust-to-gas ratio used in our model to calculate H_2CO production from POM degradation.

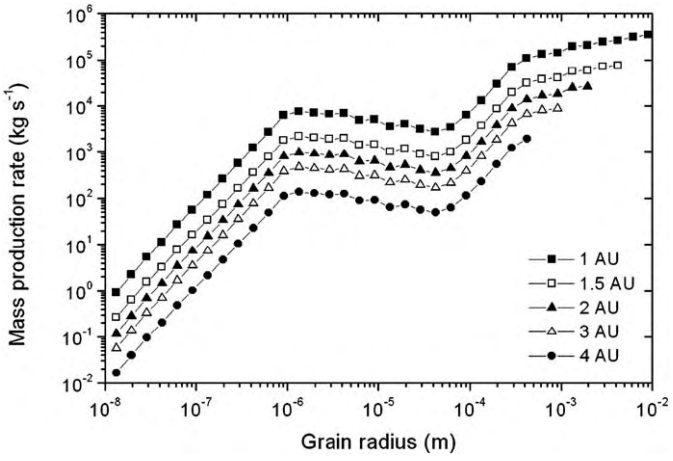

Fig. 4. Mass production rate as a function of grain radius for various heliocentric distances. These grain distributions were used to calculate H_2CO production from POM degradation.

(Jewitt and Matthews, 1999) as well as ultraviolet observations (Weaver et al., 1999) are therefore taken into account. Finally, we consider the dust production rates published by Jewitt and Matthews (1999), Weaver et al. (1999), Lisse et al. (1999), Grün et al. (2001) and Weiler et al. (2003). The related dust-to-gas ratios are derived using the total gas production rate, considered to be equal to the sum of the CO and H_2O production rates (see Fig. 1), varying with $R_H^{-2.8}$ and $R_H^{-3.4}$ during the pre- and post-perihelion phase, respectively. These values are plotted in Fig. 3. Depending on the authors, different dust-to-gas ratio trends with respect to the heliocentric distance have been proposed, which could be due to different assumptions on the size distribution and on the heliocentric evolution of the grain velocities (Weiler et al., 2003).

To calculate the grain size distribution, we have assumed (1) that the number of grains of a given size varies with the heliocentric distance in the same manner as the total gas production rate and (2) that the dust-to-gas ratio at 1 AU is equal to 8.8. This value corresponds to the measurements performed by Jewitt and Matthews (1999) at submillimeter wavelengths, which are more relevant to our study as they are sensitive to the larger grains. The grain distribution can then be calculated taking into account the variation of the size of the largest grains ($a_{\max}$) with the heliocentric distance. The resulting distributions for different heliocentric distances are presented in Fig. 4. As the comet approaches the Sun, the size of the largest grains increases, thereby increasing the dust-to-gas ratio. Therefore, the dust-to-gas ratio of our distribution varies with $R_H^{-1.3}$.

3.3. Dust velocities

In the cometary environment, grains are accelerated in the inner coma, due to the drag force of the gas. At a given distance from the nucleus, collisions between gas and grains become negligible and no longer influence grain velocities, which then reach a constant value. The latter can be calculated using an analytical formula given by Crifo (1995). It is a function of the grain radius a and the heliocentric distance via the gas production rate Q_{gas}:

$$v_{\text{grain}}(a, Q_{\text{gaz}}, \ldots) = \frac{W}{(0.9 + 0.45X^{0.615/2} + 0.275X^{0.615})}, \tag{11}$$

where:

$$W = \sqrt{\left(\frac{\gamma+1}{\gamma-1}\right)\left(\frac{\gamma k T_{\text{gas}}^0}{m_{\text{gas}}}\right)} \tag{12}$$

and

$$X = \frac{2\pi a \rho_{\text{grain}} W R_n}{m_{\text{gas}} Q_{\text{gas}}}. \tag{13}$$

In these equations:

- γ is the ratio between the specific heat at constant pressure and volume and is taken to be equal to 4/3 as for a polyatomic gas.
- T_{gas}^0 is the gas temperature at the surface of the nucleus and is calculated using the analytical formula given by Crifo and Rodionov (1997).
- m_{gas} is the mean molecular mass and is assumed to be equal to $m_{\text{gas}} = (m_{\text{CO}} Q_{\text{CO}} + m_{\text{H}_2\text{O}} Q_{\text{H}_2\text{O}})/(Q_{\text{CO}} + Q_{\text{H}_2\text{O}})$ where Q_i are the production rates.
- Q_{gas} is the total gas production rate (in molecules s^{-1}) and is taken to be equal to $Q_{\text{gas}} = Q_{\text{H}_2\text{O}} + Q_{\text{CO}}$.
- ρ_{grain} is the grain density and is taken to be equal to 1000 kg m^{-3} (Crifo and Rodionov, 1997).
- k is the Boltzmann constant.

Fig. 5 shows the resulting velocities as a function of heliocentric distance and for different grain sizes ($a = 10^{-4}$, 10^{-6} and 10^{-8} m). Results of our calculation can be compared to the projected velocities determined from the apparent motion of structures (jets, arcs,...) observed at infrared and visible wavelengths in the coma of Comet C/1995 O1 (Hale–Bopp) by Braunstein et al. (1997), Warell et al. (1999), Kidger et al.

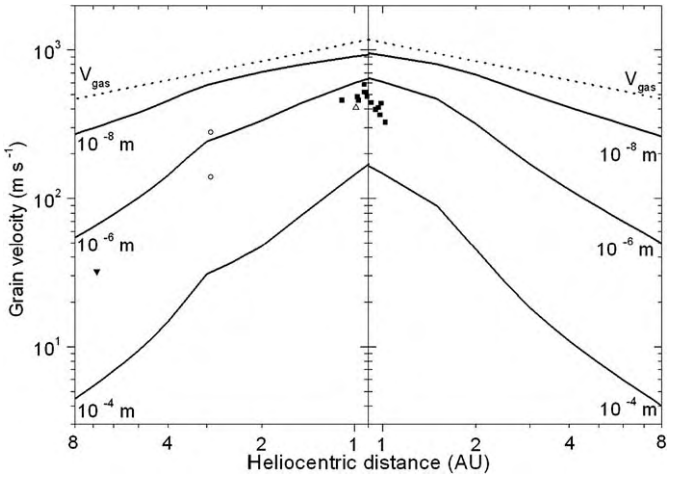

Fig. 5. Computed terminal grain velocities as a function of heliocentric distance for different grain radii ($a = 10^{-8}$, 10^{-6} and 10^{-4} m). For comparison, the dotted line shows the gas expansion velocity measured by Biver et al. (2002a) and the plotted points show the projected grain velocities derived from the apparent motion of dust structures (jets, arc, etc.). The data used to plot these points have been taken from Braunstein et al. (1997) (black squares), Warell et al. (1999) (empty triangle), Kidger et al. (1996) (black triangle) and Tozzi et al. (1997) (empty circles).

(1996) and Tozzi et al. (1997). These values can be considered as lower limits for the terminal velocity of micrometric grains. Our calculated velocities are consistent with these observations. At perihelion, the velocity of the smaller grains is 80% that of the gas.

3.4. Dust temperatures

To calculate the production of gaseous species from solid polymer thermal-degradation, the key factor is the grain temperature T_{grain}, which is derived from the balance between the energy received from the Sun and the infrared energy re-radiated by the grain.

The balance equation is given by:

$$\int_0^\infty Q_a(\lambda, a) S(\lambda)\, \mathrm{d}\lambda = 4\pi \int_0^\infty Q_a(\lambda, a) B(T_{\text{grain}}, \lambda)\, \mathrm{d}\lambda. \qquad (14)$$

Here a is the grain radius, $S(\lambda)$ the solar flux at the considered heliocentric distance and $B(T_{\text{grain}}, \lambda)$ the Planck function. $Q_a(\lambda, a)$ is the absorption efficiency of the grain which depends on the wavelength and the size and physical and chemical properties of the grain. To calculate $Q_a(\lambda)$, Mie theory has been used for compact and pure spherical grains with a refractive index m_p of the grain component and the size parameter $X = 2\pi a/\lambda$.

The temperature for porous grains composed of a mixture of silicates and organics has been calculated by successively applying the models of Greenberg and Hage (1990) and Hage and Greenberg (1990), as already done by Gunnarsson (2003) in his study of the CO extended source in 29P/Schwassmann–Wachmann 1.

The model of Greenberg and Hage (1990) makes it possible to calculate an equivalent refractive index, $m_{\text{core–mantle}}$, for a

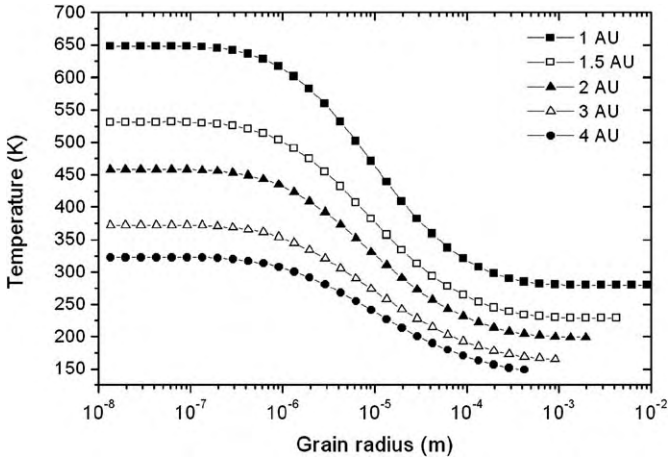

Fig. 6. Grain temperature as a function of grain radius for various heliocentric distances. The grains are assumed to have 60% organic mass and a porosity of 0.95.

"core–mantle" grain, i.e., a grain composed of a core of silicates covered by a mantle of organics.

$$(m_{\text{core–mantle}})^2 = m_{\text{mantle}}^2 \left\{ 1 + 3q^2 \left(\frac{m_{\text{core}}^2 - m_{\text{mantle}}^2}{m_{\text{core}}^2 + 2m_{\text{mantle}}^2} \right) \times \left[1 - q^3 \left(\frac{m_{\text{core}}^2 - m_{\text{mantle}}^2}{m_{\text{core}}^2 + 2m_{\text{mantle}}^2} \right) \right]^{-1} \right\}, \qquad (15)$$

where q is the fractional radius of the silicate core, and m_{core} and m_{mantle} are the refractive indices of the component of the core and of the mantle respectively. We use the refractive indices of pyroxene ($Mg_{0.6}Fe_{0.4}SiO_3$; Dorschner et al., 1995) and graphite (Jäger et al., 1998). Graphite is representative of black organic matter, and provides an upper limit for a strongly absorbing organic component of the grains, whereas pyroxene represents the silicate component of grains with very low absorption in the visible range. We assume that organics represent 60% of the mass of grains (Greenberg, 1998). In this case, the fractional radius, q, of the core, is about 0.74.

The model of Hage and Greenberg (1990) is used to calculate the equivalent refractive index (m_{porous}) of aggregates assumed to be made of the "core–mantle" grains, for which the refractive index $m_{\text{core–mantle}}$ has already been determined.

$$m_{\text{porous}}^2 = 1 + \frac{3(1-P)(m_{\text{core–mantle}}^2 - 1)/(m_{\text{core–mantle}}^2 + 2)}{1 - (1-P)(m_{\text{core–mantle}}^2 - 1)/(m_{\text{core–mantle}}^2 + 2)}, \qquad (16)$$

where P is the porosity of the aggregates, taken to be equal to 0.95 (Greenberg and Li, 1998).

The resulting temperature, for grains composed of 60% organics in terms of mass and a porosity equal to 0.95, is displayed in Fig. 6 as a function of the grain radius for different heliocentric distances.

The temperature of the grains larger than 10^{-3} m is always very close to the temperature of a black body for every considered heliocentric distance, whereas micrometric grains could

reach higher temperatures (see Fig. 6). Moreover for a given grain size, the temperature varies approximately with $R_H^{-0.5}$.

4. Results

With the parameters presented in the previous section, we are now able to calculate the H_2CO production rates taking into account POM degradation. They have to be compared with the production rates actually observed at radio wavelengths during the long-term monitoring of Comet C/1995 O1 (Hale–Bopp), as described by Biver et al. (2002a). H_2CO was monitored from June 1996 (at $R_H = 4.1$ AU pre-perihelion) to October 1997 (at $R_H = 3.2$ AU post-perihelion). We attempted to obtain the best fit of our model to the observations by adjusting the free parameters:

1) $\alpha(\%)$ the mass fraction of POM present in each grain.
2) $Q_{H_2CO}^{nucleus}/Q_{HCN}(\%)$ the native H_2CO production rate relative to HCN.

These parameters control the H_2CO fraction produced respectively by the degradation of POM and the sublimation of nucleus ices.

The best fit is determined by minimizing the chi-square root

$$\sigma = \sqrt{\sum_i \left[\left(\frac{Q_{H_2CO,obs.} - Q_{H_2CO,mod.}}{Q_{H_2CO,obs.}}\right)\frac{1}{e}\right]^2 \Big/ \left(\sum_i \left(\frac{1}{e}\right)^2\right) n}, \quad (17)$$

which takes into account the relative uncertainty e of each measurement of Q_{H_2CO} (n is the total number of measurements, $n = 22$).

4.1. Best fit

With the experimental data for 'POM1' and the grain distribution presented in Fig. 4, the best fit is found for $\alpha = 3.1\%$ and $Q_{H_2CO}^{nucleus}/Q_{HCN} = 3\%$. The derived H_2CO production rates are consistent with observations (see Fig. 7) for all heliocentric distances. For instance, during the pre-perihelion phase, both the calculated and observed H_2CO production rates vary with $R_H^{-3.6}$. During the post-perihelion phase, H_2CO calculated production rates vary with $R_H^{-4.1}$ while the observed rates vary with $R_H^{-4.2}$. However, although the results of the model well match the heliocentric evolution for H_2CO production rates, some points fall outside the errors bars determined from observations. This difference is partly due to day-to-day variations of the production rates, which are superimposed on the global evolution and which are not taken into account in this model.

To reproduce the H_2CO production rates in Comet C/1995 O1 (Hale–Bopp), we must consider that grains contain about a 3% mass fraction of POM. This value is close to the POM mass fraction upper limit of 3% derived from in situ measurements performed in the coma of 81P/Wild 2 by mass spectrometry (Kissel et al., 2004). Our value is therefore realistic. Moreover, it is also very close to the nominal value (4%) found to reproduce the spatial distribution of H_2CO in Comet

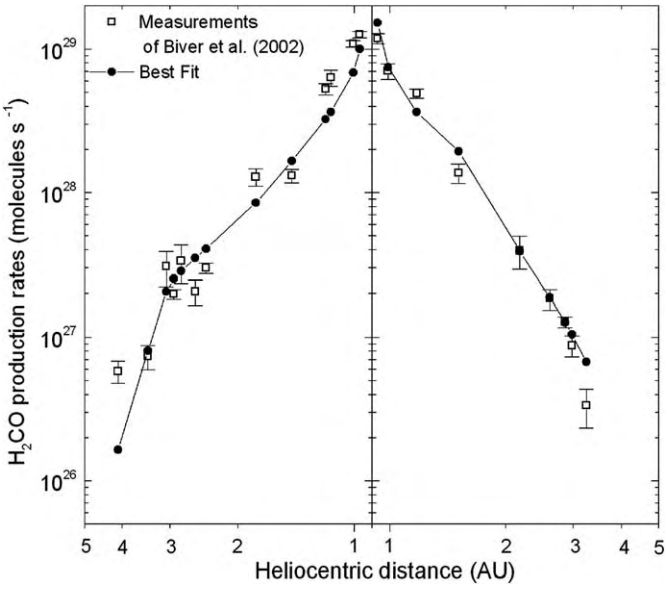

Fig. 7. H_2CO production rates as a function of heliocentric distance. The measurements of Biver et al. (2002a) are represented as open squares and the computed values as black circles. The latter have been obtained using the experimental data of "POM1" and assuming a POM mass fraction in the grains of 3.1% and H_2CO production at the surface of the nucleus equal to 3% of HCN production.

1P/Halley (Cottin et al., 2004). On the other hand, although no native H_2CO is required to reproduce observations between perihelion and 3.5 AU, a small fraction of H_2CO produced directly at the surface of the nucleus must be assumed to fit the data obtained for larger heliocentric distances. This production rate of native H_2CO could be as low as 3% of the HCN production rate ($Q_{H_2CO}^{nucleus}/Q_{HCN} = 3\%$).

We calculated independently H_2CO production rates related to the three H_2CO production mechanisms (photo- and thermal-degradation of POM and nucleus sublimation) using Eqs. (7), (8) and (9) (see Fig. 8).

At 1 AU, POM thermal-degradation represents more than 90% of total H_2CO production and this mechanism dominates until 3.5 AU (see Fig. 8). These results are consistent with those of Cottin et al. (2004), who have already shown that POM thermal-degradation is predominant at 0.9 AU. The steep heliocentric evolution of H_2CO production rates is due to the predominance of thermal-degradation. For heliocentric distances greater than 3.5 AU, due to the cooling of the grains, POM thermal-degradation becomes less efficient than POM photo-degradation. Furthermore, at these large heliocentric distances, the data derived from observations are reproduced by the model only under the assumption that a fraction of H_2CO is produced directly at the surface of the nucleus. At 1 AU from the Sun, this production of native H_2CO could represent less than a few percent of the total production of H_2CO. Nevertheless, the production rates of native H_2CO are not well constrained by our model as they depend on assumptions made on the grain distribution and on the few observations obtained at very large heliocentric distances. Therefore it cannot be ruled out that all H_2CO is produced from degradation of POM.

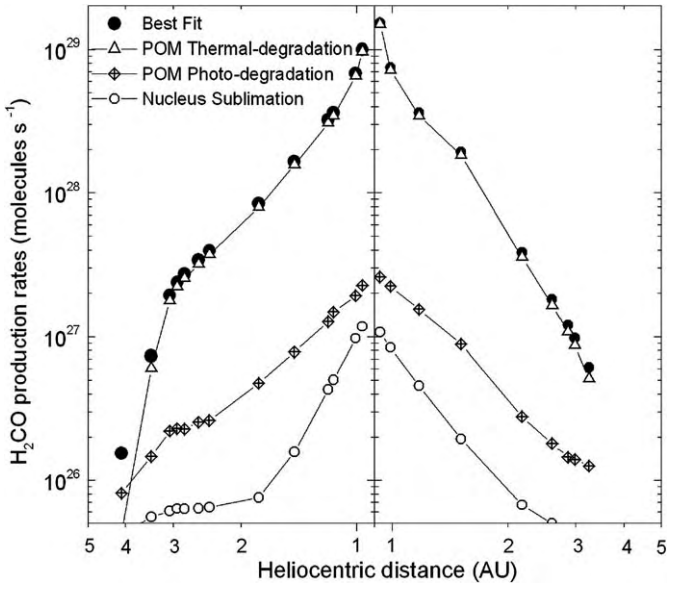

Fig. 8. H_2CO production rates as a function of heliocentric distance computed using the experimental data of "POM1." The different symbols represent different H_2CO production mechanisms: POM thermal-degradation (empty triangles), POM photo-degradation (crossed diamonds) and nucleus sublimation (empty circles). The black circles represent the total H_2CO production rates.

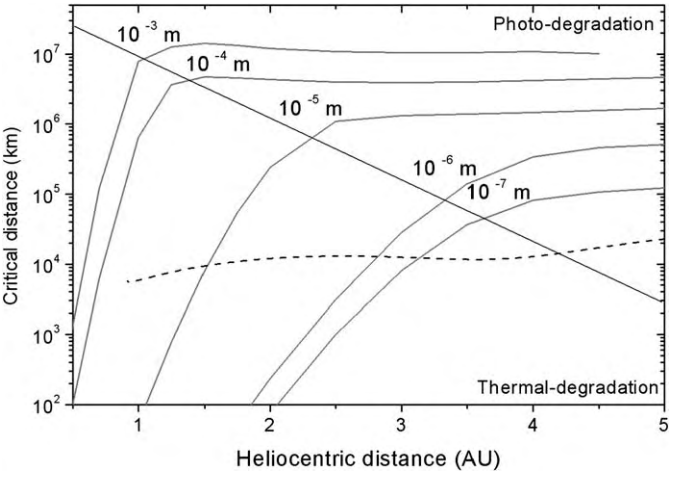

Fig. 9. Critical distance as a function of the heliocentric distance for different grain sizes. The "critical distance" is the distance from the nucleus at which POM initially present in the grains is completely degraded into gaseous species. It depends on the relative efficiency of photo- and thermal-degradation at a given heliocentric distance. This figure can be divided into two areas separated by the diagonal line. In the area situated on the right of the diagonal line, photo-degradation dominates, whereas in the other area it is negligible with respect to thermal-degradation. The dotted line shows the field of view radius assuming a beam width at half power of 12″ for the radio observations of Comet C/1995 O1 (Hale–Bopp) before perihelion.

The relative influence of thermal and photo-degradation of POM for different heliocentric distances can be understood by studying the kinetics of H_2CO production. Fig. 9 represents the critical distance (i.e., the distance from the nucleus at which POM initially present in grains is completely degraded into gaseous species) as a function of the heliocentric distance for different grains sizes.

As thermal-degradation depends heavily on grain temperature, photo-degradation dominates thermal-degradation for heliocentric distances greater than 4 AU, whatever the grains. On the other hand, for heliocentric distances less than 1 AU, thermal-degradation dominates for all grain sizes. Between 1 and 4 AU, thermal-degradation is the dominating process for the hot smaller grains, whereas photo-degradation dominates for the cold larger grains.

The heliocentric evolution of H_2CO production rates observed in Comet C/1995 O1 (Hale–Bopp) can be understood by comparing the critical distance to the size of the field of view of the H_2CO observations. At heliocentric distances larger than 4 AU, photo-degradation takes place up to distances larger than the field of view (see Fig. 9). Therefore, although POM is degraded, gaseous H_2CO cannot be observed by measurements such as those of Biver et al. (2002a). Between 4 and 3 AU, thermal-degradation becomes the predominant process as the critical distance for smaller grains decreases due to their heating. For these heliocentric distances, the critical distance for the smaller grains becomes less than the size of the field of view (see Fig. 9). Thus, POM present in the smaller grains is completely degraded into gaseous H_2CO inside the field of view. This explains the very steep increase of H_2CO production rates calculated between 4 and 3 AU (see Fig. 8). Finally, as the comet approaches the Sun, POM is completely degraded by thermal processes inside the field of view for larger and larger grains. This explains the steep heliocentric evolution of the H_2CO production rates measured by Biver et al. (2002a).

So, comparing the critical distance to the size of the field of view, it can be seen that at large heliocentric distances, extended H_2CO production is dominated by photo-degradation of the smallest grains, whereas inside 1.5 AU it is dominated by thermal-degradation of the largest grains.

4.2. Sensitivity of the results

In this sub-section, we study the sensitivity of H_2CO production rates to the different parameters used in the computation: chemical type of POM and grain velocity, temperature and distribution.

4.2.1. Sensitivity to the type of POM used for experimental studies

We have studied experimentally the thermal-degradation of two chemical types of POM. As this mechanism is predominant over a large range of heliocentric distances, the parameters A and E_a could influence H_2CO production rates. We calculate H_2CO production rates considering the experimental data of "POM2" (i.e., $A = 1.2 \times 10^{30}$ molecules $g^{-1}\,s^{-1}$ and $E_a = 8.1 \times 10^4\ J\,mol^{-1}$). We have kept all the parameters presented in Section 3 and $\alpha = 3.1\%$ and $Q^{\text{nucleus}}_{H_2CO}/Q_{HCN} = 3\%$ as already used in order to compare the results obtained for "POM1" and "POM 2." The corresponding H_2CO production rates are displayed in Fig. 10.

Close to 1 AU, the H_2CO production rates are greater for "POM2" than for "POM1" experimental data. At this heliocentric distance, most of the gaseous H_2CO is produced by

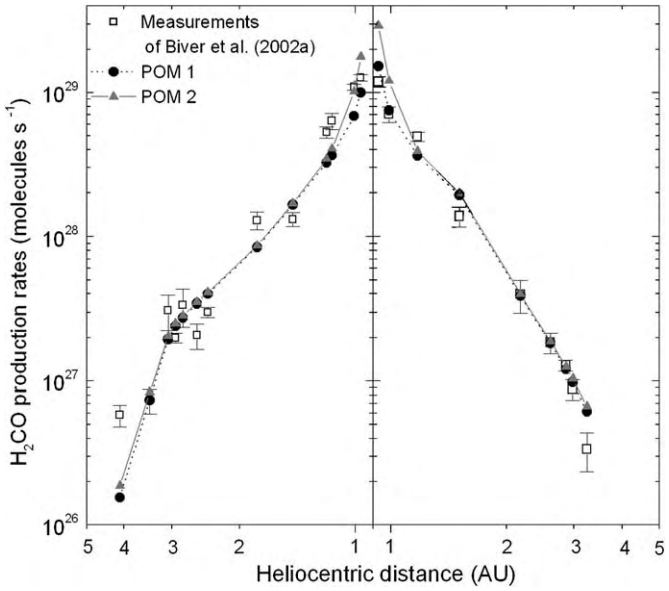

Fig. 10. H_2CO production rates as a function of the heliocentric distance. The measurements of Biver et al. (2002a) are represented as open squares, the values computed using the experimental data of "POM1" as black circles and the values computed using the experimental data of "POM2" as gray triangles. The latter have been obtained assuming a POM mass fraction in the grains of 3.1% and H_2CO production at the surface of the nucleus equal to 3% of HCN production.

thermal-degradation of POM present in the largest grains with temperatures at about 300 K, and at this temperature H_2CO production kinetics are faster for "POM2" than for "POM1" (see Fig. 4 in Fray et al., 2004a). For heliocentric distances greater than 1.5 AU, H_2CO production rates are only slightly affected by changes in parameters A and E_a. In summary, H_2CO production rates are only sensitive to the chemical type of POM when thermal-degradation of larger grains takes place inside the field of view.

4.2.2. Sensitivity to grain velocity

As already stated, the velocity of the smaller grains at 1 AU is 80% the gas velocity. The influence of an increase in grain velocity was first studied by multiplying grain velocities by a factor of 1.25 (the velocity of the smallest grains is then equal to the gas velocity). In this case, all parameters being identical to those used in Section 4.1, a decrease in H_2CO production rates ranging from 1 to 8% is noted depending on the heliocentric distance. Multiplying the grain velocity by a factor of 0.8, the H_2CO production rates increase by 1 to 12%. These variations are not surprising. Indeed, as their velocity decreases, more grains are present inside the field of view and H_2CO is produced closer to the nucleus, therefore enhancing the H_2CO production rates. However the most important points are that (1) the heliocentric evolution of H_2CO production rates is not significantly modified and (2) the H_2CO production rates are only slightly affected by grain velocity variations.

4.2.3. Sensitivity to grain temperature

POM thermal-degradation depends heavily on grain temperature as it follows the Arrhenius law. Grain temperature

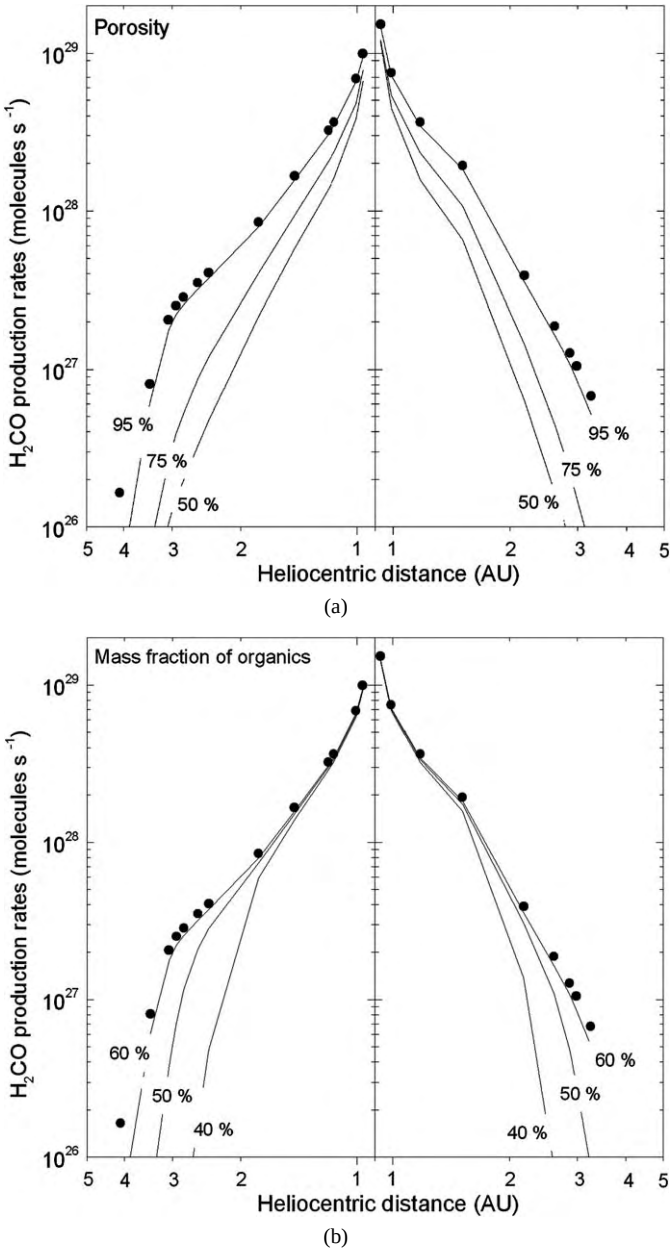

Fig. 11. (a) Sensitivity of the H_2CO production to the porosity of the grains, i.e., to their temperature, as a function of the heliocentric distance. The black circles represent the total H_2CO production rates found with the data of the "POM1" (see Fig. 7). The three black lines represent the H_2CO production rates from POM thermal-degradation for different grains porosities. Their heliocentric evolution increases when the porosity, i.e., the temperature of the micronic grains, increases. (b) Sensitivity of H_2CO production rates to the organic content of the grains, i.e., to their temperature, as a function of the heliocentric distance. The black circles represent the total H_2CO production rates calculated with the data of "POM1" (see Fig. 7). The three black lines represent H_2CO production rates from POM thermal-degradation for different grain organic contents. Production rates tend to increase with organic content, i.e., with grain temperature, particularly for heliocentric distances greater than 1 AU.

is controlled by two parameters: (1) porosity and (2) organic versus mineral content of the grains. As organics are more absorbent in visible wavelengths than silicates; grain temperature increases with organic content. Moreover, grain temperature also increases with porosity (Greenberg and Li, 1998). Using

the parameters presented in Section 3.4, we investigated the sensitivity of H_2CO production rates from POM degradation to the organic content and porosity of grains. Figs. 11a and 11b present the heliocentric evolution of H_2CO production rates for different values of these two parameters.

As expected, H_2CO production rates depend on grain temperature (see Figs. 11a and 11b), with higher grain temperatures leading to higher production rates. Moreover, higher porosity and organic content of the grains, i.e., higher grain temperatures, lead to a flatter evolution of the H_2CO production rates with the heliocentric distance. Therefore, considering a given heliocentric evolution of the dust-to-gas ratio, reproduction of the measurements of Biver et al. (2002a) could be achieved only for certain pairs of values of porosity and organics content of grains (see Figs. 11a and 11b).

4.2.4. Sensitivity to the dust-to-gas ratio

The dust-to-gas ratios measured in Comet C/1995 O1 (Hale–Bopp) are highly scattered and different trends with respect to the heliocentric distance can be observed (see Section 3.2). For the fit computed in the previous sections, we use a grain distribution presenting an increasing dust-to-gas ratio as the comet approaches the Sun (see Fig. 3).

First, in order to study the influence of the value of the dust-to-gas ratio (without a change its heliocentric evolution), we consider three grains distributions: (1) the distribution presented in Section 3.2 (case 'b'), (2) a distribution with a dust-to-gas ratio 2 times lower (case 'a') and (3) a distribution with a dust-to-gas ratio 2 times higher (case 'c'). The results, for the best fits to the H_2CO production rates measured by Biver et al. (2002a) are displayed in Table 2 for each distribution. In each case, observed values are still well fitted with reasonable POM content and negligible H_2CO production from nucleus sublimation with respect to POM degradation. The fraction of POM present in grains required to fit the observed values is approximately inversely proportional to the considered dust-to-gas ratio. This means that the POM production rate ($kg\,s^{-1}$) is constant whatever the value of the dust-to-gas ratio (see Table 2). In conclusion, the POM production rate ($kg\,s^{-1}$) is constant and more constrained than the POM mass fraction in grains. Consequently, it would be more meaningful to consider POM production rate ($kg\,s^{-1}$) than POM mass fraction in grains. This POM production rate is about $6.6 \times 10^4\ kg\,s^{-1}$ at 1 AU (see Table 2).

Secondly, the influence of the heliocentric dependence on the dust-to-gas ratio has also been studied. We have constructed a new grain size distribution (case 'd') which presents a constant dust-to-gas ratio equal to 5. This distribution presents the same cut-off for larger grains as was used above (see Fig. 4). The parameters leading to the best fit using this distribution, all others parameters being equal to those presented in Section 3, are reported in Table 2. Note in Table 2 that the standard deviation (σ) increases by a factor 2 compared to the previous cases. Indeed the computed heliocentric evolution of H_2CO production rates is flatter than for the case with an increasing dust-to-gas ratio as the comet approaches the Sun. Nevertheless, the observed values can be well reproduced if the grains are colder than previously, i.e., if the organic content is decreased from 60 to 40% (see Fig. 12 and Table 2). Indeed, even though the dust-to-gas is now constant with respect to the heliocentric distance, a decrease in the organic content of the grains (i.e., a decrease in their temperature) leads to steeper heliocentric evolution of H_2CO production rates. Thus, the effect of the heliocentric evolution of the dust-to-gas ratio is compensated by a decrease in the grain temperature. Therefore, considering a constant dust-to-gas ratio equal to 5, an organic mass content of the grains of 40%, $\alpha = 7\%$ and $Q_{H_2CO}^{nucleus}/Q_{HCN} = 0\%$, the calculated H_2CO production rates vary with $R_H^{-4.0}$ during the pre-perihelion phase and with $R_H^{-4.7}$ during the post-perihelion phase (see Fig. 12). Thus, the steep heliocentric evolution of H_2CO production rates could be reproduced irrespective of the heliocentric evolution of the dust-to-gas ratio.

4.2.5. Summary

The grain velocities and chemical type of POM only slightly affect the heliocentric evolution of the H_2CO production rate. In fact, it depends mainly on the grain temperature and the he-

Table 2
Parameters used to reproduce the H_2CO production rates measured by Biver et al. (2002a) for different grain size distributions

Grain distribution	(a)	(b)	(c)	(d)	(d)
Dust-to-gas ratio at 1 AU	4.4	8.8	17.6	5	5
Mass fraction of organics in grains assumed for the calculation of grain temperatures	60	60	60	60	40
POM mass in grains (%)	6.1	3.1	1.5	1.7	7
POM production rate at 1 AU ($10^3\ kg\,s^{-1}$)	65.2	66.3	68.4	20.6	84.8
$Q_{H_2CO}^{nucleus}/Q_{HCN}$ (%)	6	3	6	32	0
σ (%)	6.6	6.6	6.7	13.1	8.0
Relative production (%) of H_2CO from thermal-degradation of POM at 1 AU	94.9	95.8	93.6	63	97.6
Relative production (%) of H_2CO from photo-degradation of POM at 1 AU	2.2	2.8	3.5	2.3	2.4
Relative production (%) of H_2CO from nucleus sublimation at 1 AU	2.9	1.4	2.9	34.7	0

Distribution (b) is the distribution presented in Fig. 4. The distributions (a), (b) and (c) present the same heliocentric evolution of the dust-to-gas ratio as the one presented in Fig. 3; only the value of the dust-to-gas ratio varies. The dust-to-gas ratio of distribution (d) is equal to 5 and is constant with heliocentric distance. Two different grain temperatures have been used with this distribution.

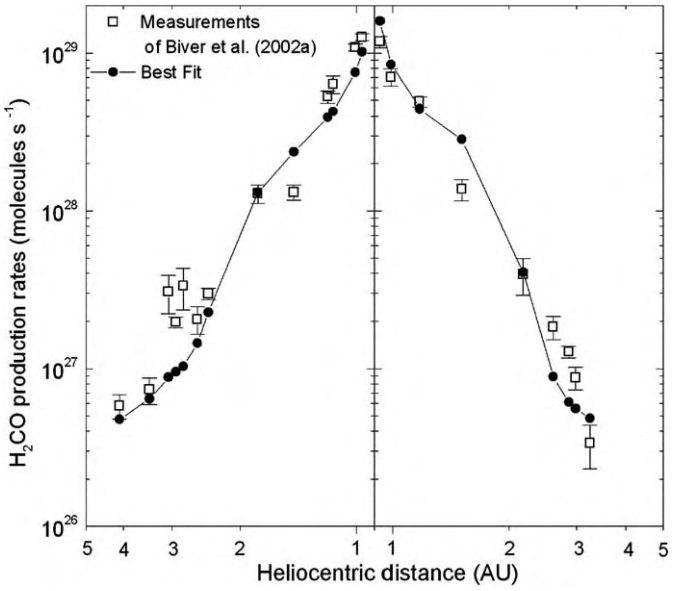

Fig. 12. H_2CO production rates as a function of the heliocentric distance. The measurements of Biver et al. (2002a) are plotted as open squares and the computed values as black circles. The latter are calculated using a grain distribution with a dust-to-gas ratio equal to 5 and constant for all heliocentric distances. To calculate these H_2CO production rates, we have assumed an organic mass content of the grains of 40%, $\alpha = 7\%$ and $Q^{\text{nucleus}}_{H_2CO}/Q_{HCN} = 0\%$. In this case, the calculated H_2CO production rate varies with $R_H^{-4.0}$ during the pre-perihelion phase and with $R_H^{-4.7}$ during the post-perihelion phase.

liocentric dependence of the dust-to-gas ratio. Nevertheless the effect of the heliocentric evolution of the dust-to-gas ratio can be compensated by the effect of the grain temperature. Thus, whatever the heliocentric dependence of the dust-to-gas ratio, there are some values of grain porosity and organic content that make it possible to reproduce the measurements of Biver et al. (2002a) taking into account POM degradation.

5. Conclusion

Abundant evidence based on observations indicates that the gaseous H_2CO observed in the cometary environment is not produced only by sublimation from the surface of the nucleus, but also directly in the coma (Meier et al., 1993; Wink et al., 1999). It has been proposed that gaseous H_2CO could be released by the degradation of polyoxymethylene (H_2CO polymers, also called POM) which could be present in grains (Huebner, 1987). To check this hypothesis, we experimentally studied the photo- and thermal-degradation of POM (Cottin et al., 2000, 2001; Fray et al., 2004a) and developed a model of the cometary environment taking into account gas production by the degradation of the refractory organic component present in grains (Cottin et al., 2004). We have shown that the H_2CO spatial distribution measured by the *Giotto* spacecraft in the coma of Comet 1P/Halley can be explained if we consider that the grains contain a few mass percent of POM. In the present article, we have shown that the very steep heliocentric evolution of H_2CO production measured at radio wavelengths by Biver et al. (2002a) in Comet C/1995 O1 (Hale–Bopp) between 4 AU pre-perihelion and 3 AU post-perihelion is also reproducible by considering that POM is present in grains and that it is degraded into gaseous H_2CO by solar UV photons and/or heating (see Fig. 7). Our studies have been focused on the H_2CO extended source and we have demonstrated that solid POM is a possible parent for gaseous H_2CO.

According to our different assumption, the grains of Comet C/1995 O1 (Hale–Bopp) could contain a few mass percent of POM, with a nominal value of 3.1%. The mass fraction of POM depends on the assumed dust-to-gas-ratio as shown in Section 4.2, whereas the production rate of POM (in kg s^{-1}) does not depend on this ratio. Concerning H_2CO production at the surface of the nucleus, it could represent less than 2% of total H_2CO production at 1 AU (see Table 2) and could remain negligible up to 3 AU. Moreover our calculations cannot be used to rule out the possibility that all H_2CO is produced from degradation of POM.

Moreover, we have shown that POM thermal-degradation could be the predominant H_2CO production mechanism at heliocentric distances up to 3.5 AU. It could account for about 95% of the total H_2CO production rate at 1 AU (see Table 2). Moreover the predominance of this H_2CO production mechanism as well as the heliocentric evolution of the dust-to-gas ratio could be responsible for the steep heliocentric evolution of the H_2CO production rates.

This work, combining experimental and model studies, has two important implications:

1) The contribution of the refractory organic component of cometary grains to the composition of the gaseous coma can no longer be considered negligible. Such a mechanism could then explain the production of other species possibly produced by an extended source such as HNC, CN and CO.
2) The presence of POM or POM-like polymers in cometary grains and nuclei is highly probable. Then, direct detection of POM in cometary environment is a major goal for future in situ studies.

Given that gaseous H_2CO may be produced by degradation of solid POM present in grains, this mechanism could explain the production of others species. As for H_2CO, the heliocentric evolution of HNC production rates measured by Biver et al. (2002a) is very steep. Irvine et al. (1998) and Rodgers and Charnley (1998) have suggested the formation of HNC through gas phase reactions in the coma. Nevertheless, this mechanism is not efficient enough to reproduce the observed levels of HNC in Comet C/1999 H1 (Lee) and Comet C/2002 C1 (Ikeya–Zhang) (Rodgers and Charnley, 2001; Rodgers et al., 2003). Consequently, Rodgers et al. (2003) propose that HNC could be injected into the coma through the destruction of an unknown precursor. The latter could be HCN polymers or hexamethylenetetramine ($C_6H_{12}N_4$, also called HMT), compounds which have already been proposed as parent molecules of CN radicals (Rettig et al., 1992; Bernstein et al., 1995). We have therefore undertaken an experimental analysis of the photo- and thermal-degradation of both compounds. Some preliminary results have already been published (Fray et al., 2004b), but more laboratory work is required to include their degradation para-

meters in our model and conclude as to whether or not they are good candidates to explain the origin of HNC and/or CN.

The in situ measurements of the *Giotto* spacecraft inside the coma of 1P/Halley have shown that CO is not entirely produced by nucleus sublimation (Eberhardt et al., 1987). Moreover DiSanti et al. (2001) have measured, from observations at infrared wavelengths, the spatial distribution of CO in Comet C/1995 O1 (Hale–Bopp). Between 2 and 1.5 AU, they observed a change in the CO spatial distribution, which becomes more extended, as well as a relatively abrupt increase of CO production rates. These facts suggest a thermal threshold like the one observed for H_2CO at 3–4 AU. Therefore, as already proposed by Greenberg and Li (1998), some CO could originate from the grains. As for HNC and CN, probing this hypothesis requires a complete experimental study of CO production from the degradation of complex organics starting from an appropriate refractory parent candidate. Note that our experimental study shows that CO is not produced by thermal-degradation of POM and therefore this mechanism cannot be used to explain the CO extended source (Cottin et al., 2004; Fray et al., 2004a).

The combination of experimental work and modeling is an effective tool that can be used to infer the presence and amount of organic compounds in the nucleus of comets. So far, from independent measurements in Comet 1P/Halley (Cottin et al., 2004; Fray et al., 2004a) and Comet C/1995 O1 (Hale–Bopp), we have shown that the presence of POM with a mass percent of about 3% in the cometary nucleus and grains is highly probable. Note that no attempt has yet been made to directly detect POM or POM-like polymers in cometary environments. Direct detection of POM in cometary grains or at the surface of the nucleus should therefore be made a major goal of future studies. The COSAC instrument, on board the surface landing probe of the *Rosetta* spacecraft, mainly composed of a GC-MS (gas chromatograph coupled with mass spectrometer), is devoted to the identification of complex organic molecules. However laboratory experiments, carried out with a setup that reproduces the flight configuration and simulates the in situ operating conditions, have shown that POM will be difficult to detect due to its degradation into H_2CO inside the heated columns of the chromatograph (Szopa et al., 2004). Therefore, COSAC will likely not make it possible to distinguish between H_2CO ices and POM, whereas some others organic compounds, like HCN polymers, will easily be detected if present. The COSIMA instrument, which is a secondary ion mass spectrometer, could provide insight on the presence of POM although it cannot separate all the different compounds present on cometary grains. POM has three intense vibration bands near 10 μm (8.1, 9.5 and 10.7 μm, see Schutte et al., 1993a; Fray et al., 2004a). Unfortunately these bands overlap with the 10 μm silicate band. POM has also two less intense bands at 3.35 and 3.43 μm (Fray et al., 2004a). However, interpretation of the emission features observed in comets between 3.2 and 3.6 μm is very complex due to the contribution of CH-stretching bands of methanol and other species (Bockelée-Morvan et al., 1995). Therefore, the direct detection of POM in cometary grains and/or nuclei will not be easy to achieve and new methods will have to be developed.

Another prospect is the study of the H_2CO extended source in a large number of comets to measure the POM production rate ($kg\,s^{-1}$) and compare it with other species such as CH_3OH for example. It appears that there is a correlation between CH_3OH and H_2CO production rates in different comets (Biver et al., 2002b) and it has already been shown that POM or POM-like polymers are easily synthesized in cometary ice analogs containing CH_3OH even if H_2CO is missing in the initial mixture (Muñoz-Caro and Schutte, 2003; Bernstein et al., 1995). POM production rates ($kg\,s^{-1}$) could be derived by studying the spatial distribution of H_2CO in the coma, as already done by Cottin et al. (2004). Such distributions have already been measured for C/1989 X1 (Austin) and C/1990 K1 (Levy) (Colom et al., 1992) and for C/1996 B2 (Hyakutake) (Biver et al., 1999) by cross-mapping at radio wavelengths. Such observations will provide new constraints on H_2CO production for a larger sample of comets, allowing us to compare the production rates of POM with those of others species.

Acknowledgments

The experimental part of this work was supported by the French space agency CNES (Centre national d'études spatiales) and PNP (Programme national de planétologie). N.F. thanks C. Szopa for fruitful discussions on the operation of COSAC and its ability to detect POM. We also thank N. Dello Russo and an anonymous referee for their corrections and help in improving this manuscript as well as H. Harder for his help in revising the English.

References

Altenhoff, W.J., and 20 colleagues, 1999. Coordinated radio continuum observations of Comets Hyakutake and Hale–Bopp from 22 to 860 GHz. Astron. Astrophys. 348, 1020–1034.

Bernstein, M.P., Sandford, S.A., Allamandola, L.J., Chang, S., Scharberg, M.A., 1995. Organic compounds produced by photolysis of realistic interstellar and cometary ice analogs containing methanol. Astrophys. J. 454, 327–344.

Biver, N., 1997. Molécules mères cométaires: Observations et modélisations. Thesis. Université Paris VII, France. 289 pp.

Biver, N., and 13 colleagues, 1999. Spectroscopic monitoring of Comet C/1996 B2 (Hyakutake) with the JCMT and IRAM radio telescopes. Astron. J. 118, 1850–1872.

Biver, N., and 22 colleagues, 2002a. The 1995–2002 long-term monitoring of Comet C/1995 O1 (Hale–Bopp) at radio wavelength. Earth Moon Planets 90, 5–14.

Biver, N., Bockelée-Morvan, D., Crovisier, J., Colom, P., Henry, F., Moreno, R., Paubert, G., Despois, D., Lis, D.C., 2002b. Chemical composition diversity among 24 comets observed at radio wavelengths. Earth Moon Planets 90, 323–333.

Bockelée-Morvan, D., Brooke, T.Y., Crovisier, J., 1995. On the origin of the 3.2–3.6 μm emission features in comets. Icarus 116, 18–39.

Bockelée-Morvan, D., Crovisier, J., Mumma, M.J., Weaver, H.A., 2005. The composition of cometary volatiles. In: Festou, M., Keller, H.U., Weaver, H.A. (Eds.), Comets II. Univ. of Arizona Press, Tucson, pp. 391–423.

Braunstein, M., and 14 colleagues, 1997. A ccd image archive of Comet C/1995 O1 (Hale–Bopp): Dust expansion velocities. Earth Moon Planets 78, 219–227.

Colom, P., Crovisier, J., Bockelée-Morvan, D., 1992. Formaldehyde in comets. I. Microwave observations of P/Brorsen–Metcalf (1989 X), Austin (1990 V) and Levy (1990 XX). Astron. Atrophys. 264, 270–281.

Colom, P., Gérard, E., Crovisier, J., Bockelé-Morvan, D., Biver, N., Rauer, H., 1999. Observations of the OH radical in Comet C/1995 O1 (Hale–Bopp) with the Nançay radio telescope. Earth Moon Planets 78, 37–43.

Cottin, H., Gazeau, M.-C., Doussin, J.-F., Raulin, F., 2000. An experimental study of the photo-degradation of polyoxymethylene at 122, 147 and 193 nm. J. Photochem. Photobiol. 135, 53–64.

Cottin, H., Gazeau, M.-C., Chaquin, P., Raulin, F., Bénilan, Y., 2001. Experimental and theoretical studies on the gas/solid/gas transformation cycle in extraterrestrial environments. J. Geophys. Res. 106, 33325–33332.

Cottin, H., Bénilan, Y., Gazeau, M.-C., Raulin, F., 2004. Origin of cometary extended sources from degradation of refractory organics on grain: Polyoxymethylene as formaldehyde parent molecule. Icarus 167, 397–416.

Crifo, J.-F., 1995. A general physicochemical model of the inner coma of active comets. 1. Implications of spatially distributed gas and dust production. Astrophys. J. 445, 470–488.

Crifo, J.-F., Rodionov, A.V., 1997. The dependence of the circumnuclear coma structure on the properties of the nucleus. I. Comparison between a homogeneous and an inhomogeneous spherical nucleus, with application to P/Wirtanen. Icarus 127, 319–353.

Crovisier, J., 1994. Photo-destruction rates for cometary parent molecules. J. Geophys. Res. 99, 3777–3781.

Crovisier, J., 1997. Solids and volatiles in comets: From cometary nuclei to cometary atmospheres. In: Greenberg, J.M., Li, A. (Eds.), Formation and Evolution of Solids in Space. In: NATO Science Series, vol. 523. Kluwer Academic, Dordrecht, pp. 389–426.

Dainton, F.S., Ivin, K.J., Walmsley, D.A.G., 1959. The equilibrium between gaseous formaldehyde and solid polyoxymethylene. Trans. Faraday Soc. 55, 61–64.

DiSanti, M.A., Mumma, J.M., Russo, N.D., Magee-Sauer, K., 2001. Carbon monoxide production and excitation in Comet C/1995 O1 (Hale–Bopp): Isolation of native and distributed CO sources. Icarus 153, 361–390.

DiSanti, M.A., Dello Russo, N., Magee-Sauer, K., Gibb, E.L., Reuter, D.C., and Mumma, M.J., 2002. CO, H_2CO, and CH_3OH in Comet C/2002 C1 Ikeya–Zhang. In: Proceedings of Asteroids, Comets, Meteors—ACM2002, International Conference, ESA SP, vol. 500, pp. 571–574.

Dorschner, J., Begemann, B., Henning, T., Jaeger, C., Mutschke, H., 1995. Steps toward interstellar silicate mineralogy. II. Study of Mg–Fe-silicate glasses of variable composition. Astron. Astrophys. 300, 503–520.

Eberhardt, P., and 10 colleagues, 1987. The CO and N_2 abundance in Comet P/Halley. Astron. Astrophys. 187, 481–484.

Fray, N., Bénilan, Y., Cottin, H., Gazeau, M.-C., 2004a. New experimental results on the degradation of polyoxymethylene: Application to the origin of the formaldehyde extended source in comets. J. Geophys. Res. 109. E07S12.

Fray, N., Cottin, H., Gazeau, M.C., Minard, R.D., Raulin, F., Bénilan, Y., 2004b. Experimental study of the degradation of polymers: Application to the origin of extended sources in cometary atmospheres. Meteor. Planet. Sci. 39, 581–587.

Green, S.F., McDonnell, J.A.M., McBride, N., Colwell, M.T.S.H., Tuzzolino, A.J., Economou, T.E., Tsou, P., Clark, B.C., Brownlee, D.E., 2004. The dust mass distribution of Comet 81P/Wild 2. J. Geophys. Res. 109. E12S04.

Greenberg, J.M., Hage, J.I., 1990. From interstellar dust to comets—A unification of observational constraints. Astrophys. J. 361, 260–274.

Greenberg, J.M., 1998. Making a comet nucleus. Astron. Astrophys. 330, 375–380.

Greenberg, J.M., Li, A., 1998. From interstellar dust to comets: The extended CO source in Comet Halley. Astron. Astrophys. 332, 374–384.

Grün, E., and 23 colleagues, 2001. Broadband infrared photometry of Comet Hale–Bopp with ISOPHOT. Astron. Astrophys. 377, 1098–1118.

Gunnarsson, M., 2003. Icy grains as a source of CO in Comet 29P/Schwassmann–Wachmann 1. Astron. Astrophys. 398, 353–361.

Hage, J.I., Greenberg, J.M., 1990. A model for the optical properties of porous grains. Astrophys. J. 361, 251–259.

Harmon, J.K., Campbell, D.B., Ostro, S.J., Nolan, M.C., 1999. Radar observations of comets. Planet. Space Sci. 47, 1409–1422.

Haser, L., 1957. Distribution d'intensité dans la tête d'une comète. Bull. Acad. R. Belg. 43, 740–750.

Huebner, W.F., 1987. First polymer in space identified in Comet Halley. Science 237, 628–630.

Irvine, W.M., Bergin, E.A., Dickens, J.E., Jewitt, D., Lovell, A.J., Matthews, H.E., Schloerb, F.P., Senay, M., 1998. Chemical processing in the coma as the source of cometary HNC. Nature 393, 547–550.

Jäger, C., Mutschke, H., Henning, T., 1998. Optical properties of carbonaceous dust analogues. Astron. Astrophys. 332, 291–299.

Jewitt, D., Matthews, H.E., 1999. Particulate mass loss from Comet Hale–Bopp. Astron. J. 117, 1056–1062.

Keller, H.U., Delamere, W.A., Reitsema, H.J., Huebner, W.F., Schmidt, H.U., 1987. Comet P/Halley's nucleus and its activity. Astron. Astrophys. 187, 807–823.

Kidger, M.R., Serra-Ricart, M., Bellot Rubio, L.R., Casas, R., 1996. Evolution of a spiral jet in the inner coma of Comet Hale–Bopp (1995 O1). Astrophys. J. 461, L119–L122.

Kissel, J., Krueger, F.R., Silen, J., Clark, B.C., 2004. The cometary and interstellar dust analyzer at Comet 81P/Wild 2. Science 304, 1774–1776.

Kührt, E., 1999. H_2O-activity of Comet Hale–Bopp. Space Sci. Rev. 90, 75–82.

Lisse, C.M., and 14 colleagues, 1999. Infrared observations of dust emission from Comet Hale–Bopp. Earth Moon Planets 78, 251–257.

Magee-Sauer, K., Mumma, M.J., DiSanti, M.A., Dello Russo, N.D., Rettig, T.W., 1999. Infrared spectroscopy of the ν_3 band of hydrogen cyanide in Comet C/1995 O1 Hale–Bopp. Icarus 142, 498–508.

Magee-Sauer, K., Mumma, M.J., DiSanti, M.A., Dello Russo, N., 2002. Hydrogen cyanide in Comet C/1996 B2 Hyakutake. J. Geophys. Res. 107 (E11). 5096.

McDonnell, J.A.M., Lamy, P.L., Pankiewicz, G.S., 1991. Physical properties of cometary dust. In: Comets in the Post-Halley Era, vol. 2. Kluwer, Dordrecht, pp. 1043–1073.

Meier, R., Eberhardt, P., Krankowsky, D., Hodges, R.R., 1993. The extended formaldehyde source in Comet P/Halley. Astron. Astrophys. 277, 677–691.

Mitchell, D.L., Lin, R.P., Carlson, C.W., Korth, A., Rème, H., Mendis, D.A., 1992. The origin of complex organic ions in the coma of Comet Halley. Icarus 98, 125–133.

Mount, G.H., Rottman, G.J., 1981. The solar spectral irradiance 1200-3184 A near solar maximum. J. Geophys. Res. 86, 9188–9193.

Muñoz-Caro, G.M., Schutte, W.A., 2003. UV-photo-processing of interstellar ice analogs: New infrared spectroscopic results. Astron. Astrophys. 413, 209–216.

Rettig, T.W., Tegler, S.C., Pasto, D.J., Mumma, M.J., 1992. Comet outbursts and polymers of HCN. Astrophys. J. 398, 293–298.

Rodgers, S.D., Charnley, S.B., 1998. HNC and HCN in comets. Astrophys. J. 501, L227–L230.

Rodgers, Charnley, 2001. On the origin of HNC in Comet Lee. Mon. Not. R. Astron. Soc. 323, 84–92.

Rodgers, S.D., Butner, H.M., Charnley, S.B., Ehrenfreund, P., 2003. The HNC/HCN ratio in comets: Observations of C/2002 C1 (Ikeya–Zhang). Adv. Space Res. 31, 2577–2582.

Schutte, W.A., Allamandola, L.J., Sandford, S.A., 1993a. An experimental study of the organic molecules produced in cometary and interstellar ice analogs by thermal formaldehyde reactions. Icarus 104, 118–137.

Schutte, W.A., Allamandola, L.J., Sandford, S.A., 1993b. Formaldehyde and organic molecule production in astrophysical ices at cryogenic temperatures. Science 259, 1143–1145.

Sekanina, Z., 1999. A determination of the nuclear size of Comet Hale–Bopp (C/1995 O1). Earth Moon Planets 77, 147–153.

Snyder, L.E., Veal, J.M., Woodney, L.M., Wright, M.C.H., Palmer, P., A'Hearn, M.F., Kuan, Y.-J., De Pater, I., Forster, J.R., 2001. BIMA array photodissociation measurements of HCN and CS in Comet Hale–Bopp (C/1995 O1). Astron. J. 121, 1147–1154.

Szopa, C., Sternberg, R., Raulin, F., Rosenbauer, H., 2004. What can we expect from the in situ chemical investigation of a cometary nucleus by gas chro-

matography: First results from laboratory studies. Planet. Space Sci. 51, 863–877.

Tozzi, G.P., Mannucci, F., Stanga, R., 1997. IR observations of an outburst in Comet Hale–Bopp (C/1995 O1). Earth Moon Planets 78, 279–284.

Tuzzolino, A.J., Economou, T.E., Clark, B.C., Tsou, P., Browlee, D.E., Green, S.F., McDonnell, J.A.M., McBride, N., Cowell, M.T.S.H., 2004. Dust measurements in the coma of Comet 81P/Wild2 by the dust flux monitor instrument. Science 304, 1776–1780.

Warell, J., Lagerkvist, C.-I., Lagerros, J.S.V., 1999. Dust continuum imaging of C/1995 O1 (Hale–Bopp): Rotation period and dust outflow velocity. Astron. Astrophys. Suppl. 136, 245–256.

Weaver, H.A., Feldman, P.D., A'Hearn, M.F., Arpigny, C., Brandt, J.C., Stern, S.A., 1999. Post-perihelion HST observations of Comet Hale–Bopp (C/1995 O1). Icarus 141, 1–12.

Weaver, H.A., Lamy, P.L., 1999. Estimating the size of Hale–Bopp's nucleus. Earth Moon Planets 79, 17–33.

Weiler, M., Rauer, H., Knollenberg, J., Jorda, L., Helbert, J., 2003. The dust activity of Comet C/1995 O1 (Hale–Bopp) between 3 AU and 13 AU from the Sun. Astron. Astrophys. 403, 313–322.

Wink, J., and 10 colleagues, 1999. Evidence for extended sources and temporal modulations in molecular observations of C/1995 O1 (Hale–Bopp) at the IRAM interferometer. Earth Moon Planets 78, 63.

Article 13

LASUE J., LEVASSEUR-REGOURD A. C., FRAY N. and COTTIN H. (2007) Inferring the interplanetary dust properties from remote observations and simulations. Astronomy & Astrophysics 473, 641–649.

A&A 473, 641–649 (2007)
DOI: 10.1051/0004-6361:20077623

Astronomy & Astrophysics

Inferring the interplanetary dust properties

from remote observations and simulations

J. Lasue[1], A. C. Levasseur-Regourd[1,2], N. Fray[3], and H. Cottin[3]

[1] Service d'aéronomie-IPSL-CNRS, UMR 7620, Route des Gâtines, BP 3, 91371 Verrières-le-Buisson, France
e-mail: jeremie.lasue@aerov.jussieu.fr
[2] Université Pierre et Marie Curie-Paris6, Service d'aéronomie UMR 7620, 75005 Paris, France
e-mail: chantal.levasseur-regourd@aerov.jussieu.fr
[3] Laboratoire Interuniversitaire des Systèmes Atmosphériques, UMR 7583, Universités Paris 7 et Paris 12, 61 Av. du Général de Gaulle, 94010 Créteil, France
e-mail: [fray;cottin]@lisa.univ-paris12.fr

Received 10 April 2007 / Accepted 25 June 2007

ABSTRACT

Context. Since in situ studies and interplanetary dust collections only provide a spatially limited amount of information about the interplanetary dust properties, it is of major importance to complete these studies with properties inferred from remote observations of scattered and emitted light, with interpretation through simulations.
Aims. Physical properties of the interplanetary dust in the near-ecliptic symmetry surface, such as the local polarization, temperature, and composition, together with their heliocentric variations, may be derived from scattered and emitted light observations, giving clues to the respective contribution of the particle sources.
Methods. A model of light scattering by a cloud of solid particles constituted by spheroidal grains and aggregates thereof is used to interpret the local light-scattering data. Equilibrium temperature of the same particles allows us to interpret the temperature heliocentric variations.
Results. A good fit of the local polarization phase curve, P_α, near 1.5 AU from the Sun is obtained for a mixture of silicates and more absorbing organic material (≈40% in mass) and for a realistic size distribution typical of the interplanetary dust in the 0.2 μm to 200 μm size range. The contribution of dust particles of cometary origin is at least 20% in mass. The same size distribution of particles gives a dependence of the temperature with the solar distance, R, in $R^{-0.45}$ that is different than the typical black body behavior. The heliocentric dependence of $P_{\alpha=90^\circ}$ is interpreted as a progressive disappearance of solid organic (such as HCN polymers or amorphous carbon) towards the Sun.
Conclusions.

Key words. interplanetary medium – polarization – radiation mechanisms: thermal – methods: numerical

1. Introduction

Describing the particles constituting the interplanetary dust cloud (IDC) in terms of morphology, porosity, size distribution, and complex refractive indices offers a clue to their origin and evolution. Information can be retrieved through (a few) in situ studies (see e.g. Jessberger et al. 2001) and through remote observations of the light-scattering properties (brightness and polarization of solar light scattered by the dust particles in the visible domain) and emissivity (in the infrared spectrum) of the dust cloud; see e.g. Levasseur-Regourd et al. (1999). Photometric measurements integrate all the local contributions emitted and scattered by the dust along the line of sight. Consequently, techniques of inversion, such as the "nodes of lesser uncertainty" method (see e.g. Dumont & Levasseur-Regourd 1988; Levasseur-Regourd et al. 2001, and references therein) are needed to retrieve the local properties. All the values given in the following text correspond to bulk values deduced from inversion methods over elementary volumes.

Light-scattering numerical simulations can be used to derive physical properties of clouds of dust particles, typically of comet origin (see e.g. Levasseur-Regourd et al. 2007, and references therein). Realistic light-scattering models for a distribution of particles constituted of a mixture of spheroidal grains and aggregates of small spheroids have already been used to derive information about the composition and size distribution (lower and upper cut-off, power law coefficient, proportion of absorbing and non-absorbing material, and proportion of aggregates) in the case of comet Hale-Bopp dust polarimetric observations (Lasue & Levasseur-Regourd 2006).

This study presents the results obtained by applying an irregular particle cloud model in the case of the interplanetary dust cloud observations to estimate the physical properties of the size distribution and the proportion of fluffy particles. It tentatively indicates the relative contribution of particles from cometary and asteroidal origins. In the next two sections, clues to the properties of the interplanetary dust cloud and source particles are reviewed. In the last two sections, the emitted light and local temperature properties of the cloud are analyzed through our model.

2. Local properties of the interplanetary dust cloud

2.1. Scattered light

The local albedo of the interplanetary dust cloud, A, approximately follows $A = (0.07 \pm 0.03)\, R^{-0.34\pm0.05}$ in the near-ecliptic

Article published by EDP Sciences and available at http://www.aanda.org or http://dx.doi.org/10.1051/0004-6361:20077623

symmetry surface as a function of the solar distance, R, between 1.5 and 0.5 AU, as deduced from the brightness observations in the visible (Dumont & Levasseur-Regourd 1988; Levasseur-Regourd et al. 2001).

The local polarization, P, cannot be estimated at all the phase angles and solar distances. With the "nodes of lesser uncertainty" method, two zones can be described. The radial node gives information on the polarization at 90° of phase angle with a varying solar distance, whereas the Martian node located at 1.5 AU from the Sun gives the variation in P with the phase angle (Dumont & Levasseur-Regourd 1988). The deduced phase curve presents a similar shape to the ones observed for comets and other dusty objects in the Solar System, with large error bars due to inversion methods at a single wavelength $\lambda = 550$ nm and with a shape typical of the interaction of light with irregular particles comparable in size to the wavelength (see e.g. Mann 1992; Lumme 2000; Levasseur-Regourd & Hadamcik 2003). The phase curve is smooth with a small negative branch below the inversion angle, $\alpha_0 \approx 15° \pm 2°$ and a large positive branch, with a value $P_{90°} \approx 30\% \pm 3\%$.

From the observational data, no significant variation in P with the wavelength, λ, can be noticed, as shown by Leinert et al. (1998); however, a heliocentric dependence of $P_{90°}$ between 1.5 and 0.5 AU can be pointed out (Lumme 2000; Levasseur-Regourd et al. 2001):

$$P_{90°} = (0.30 \pm 0.03)\, R^{0.5\pm0.1}. \quad (1)$$

This relation suggests that a change either in the physical properties or in the chemical composition of the particles is required to interpret the observed solar distance dependence of the IDC local polarization.

2.2. Temperature

Although the absolute temperature values may not be accurately determined, the variation in local temperature of the IDC with the solar distance is well-constrained. The dependence of T on R closely follows a power law, the exponent, t, (hereafter called temperature-distance factor), which is not as steep as the one expected from a black body (T proportional to $\frac{1}{\sqrt{R}}$):

$$T = (250 \pm 10\ \mathrm{K})\, R^{-0.36\pm0.03}. \quad (2)$$

This relation is approximately valid between 1.5 and 0.5 AU as deduced from the infrared observations (Dumont & Levasseur-Regourd 1988; Reach 1991; Renard et al. 1995; Levasseur-Regourd et al. 2001).

3. Clues to the properties of source particles

The IDC, as probed around 1 AU, originates from at least three different sources: fluffy and easily fragmenting particles of cometary origin (see e.g. Whipple 1951), asteroidal dust made of compact particles produced by asteroidal shattering (see e.g. Jessberger et al. 2001), and to a lesser extent elongated submicron interstellar grains passing through the solar system and a priori not directly linked to the primordial grains that formed the solar system and grains coming from the Jovian system (see e.g. Grün et al. 1993).

3.1. Sizes of the particles

The size distribution of compact or fluffy particles resulting from particle-particle collisions is expected to follow a power law, a^s, where the effective diameter, a, is the diameter of the sphere with a volume equivalent to the one of the irregular particle, and where s is equal to −3 from theoretical calculations (Hellyer 1970) and is between −3.5 and −3 from experimental simulations (see e.g. Mukai et al. 2001). Observations of the solid component of the cometary comæ have shown that such a coefficient is close to −3 (e.g. -3.1 ± 0.3 from Rosetta observations of comet 9P/Tempel 1 after the Deep Impact event by Jorda et al. 2007). In situ measurements within the IDC suggest s is around −3 for particles smaller than 20 μm and equal to −4.4 for larger particles (Grün et al. 2001).

So-called IDPs, i.e. interplanetary dust particles collected in the Earth's stratosphere, typical size ranges from 5 μm to 25 μm (Jessberger et al. 2001). For the IDPs presenting an aggregated structure and possibly originating from comets, the constituent grains have a mean size around 0.3 μm. Evidence of such a fluffy structure has also been shown from the study of the aluminium craters and aerogel penetration tracks from the Stardust samples (Hörz et al. 2006). The larger micrometeorites, collected in the polar regions or at the bottom of the oceans, have sizes ranging from 20 μm to 1 mm, and because of their large size, they are usually compact due to melting during their entry through the Earth's atmosphere (Engrand & Maurette 1998).

3.2. Optical constants of the particles

Studies of comets, IDPs, and micrometeorites have shown the predominance of silicates and "CHON" materials in the composition of extraterrestrial particles (Hanner & Bradley 2004). Precise spectroscopic studies of silicates have shown the presence of both amorphous and crystalline silicates consisting of olivine or pyroxene that could be explained by radial mixing of the elements in the early solar nebula (Bockelée-Morvan et al. 2002). Models of comets (Wooden et al. 1999; Hayward et al. 2000), as well as studies of fluffy IDPs (see e.g. Bradley et al. 1992), have shown that the main constituent of the silicates was actually Mg-rich pyroxene with a contribution between 60% and 90% and an absorption between 0.001 and 0.01 in the visible domain near 550 nm (as expressed in terms of the imaginary part, k, of the optical index $m = n+ik$, Dorschner et al. 1995). The recent mineralogical studies of the Stardust samples have also confirmed a variety of olivine and pyroxene silicates in various crystallization states as the main component (Zolensky et al. 2006). In the visible domain, the crystalline silicates present approximately the same optical indices as the amorphous, glassy silicates with an absorption $k \approx 0.0001$ (Jäger et al. 1998; Lucey 1998). It may thus be assumed that amorphous and crystalline silicates have similar optical indices in the visible. In this study, the complex index of silicates is assumed to be the one of Mg-rich pyroxene (typically $Mg_xFe_{1-x}SiO_3$ with $0.8 < x < 0.7$ as measured in laboratory by Dorschner et al. 1995), as it represents most of the observed silicates (see Sect. 4.1 for more details).

The "CHON", or the organic component of the particles, is a more absorbing material composed of lighter elements that could appear in cometary dust particles from the heavy radiation processing of ices and light elements deposited on the grains. Attempts to characterize the nature of the carbonaceous fraction in IDPs suggest that amorphous carbon is dominant (Keller et al. 1994). However, recent studies suggest that one half of the carbon contained in typical IDPs is present in the form of organic carbon (Flynn et al. 2004). Laboratory experiments of radiation processing of ices have been shown to produce absorbing organic material with a high real part of the optical index (close to 2) and imaginary part between 0.1 to 0.4, see e.g.

Jenniskens (1993) and Li & Greenberg (1997). Studies of deposited graphite gave optical index values in the visible on the order of 1.71 + i 0.1 (Papoular et al. 1993). The amorphous carbon presents a very high absorption with an optical index in the visible of 1.88 + i 0.71 (Edoh 1983). In this study, the complex index of organic material taken from Li & Greenberg (1997) is assumed to reproduce the behavior of irradiated cometary ices, and the complex index of amorphous carbon is taken from Edoh (1983).

The spectrum of the zodiacal light is similar to the solar spectrum (see e.g. Levasseur-Regourd et al. 2001), and it peaks around 550 nm. As a first approximation, for the calculations of light scattering, the complex index of the particles is taken around this particular wavelength. However, since equilibrium temperature calculations take the infrared emission of the particles into account, the variation in the complex index with the wavelength will be taken into account for these calculations.

3.3. Shapes of the particles

The IDC particles ejected by comets are probably very irregular with both compact and aggregated ones, as shown from light scattering studies (Lasue & Levasseur-Regourd 2006) and the study of foil craters and the aerogel penetration tracks of Stardust (Hörz et al. 2006). Following the "bird-nest" model proposed by Greenberg & Hage (1990), the aggregates are assumed to be built of spheroidal grains with an axis ratio around 2. Such grains might be expected to have a layered structure, such as a silicates-core covered by an organic-mantle, with a material ratio similar to what is expected from protosolar clouds models. These grains of interstellar origin may be used to model the IDC interstellar component.

The IDC particles resulting from asteroidal collisions are probably compact. They may be represented in a first approximation by prolate spheroids with an axis ratio less than 2 as estimated from IDPs collection analysis (Jessberger et al. 2001) and from the experimental simulations of collisions (Mukai et al. 2001). More specifically, the study of Na desorption on meteoroids by Kasuga et al. (2006) has shown that the meteoroids near 1 AU can be large, compact particles.

Finally, following the "bird-nest" model, the interstellar grains present in the interplanetary medium are assumed to be similar to the constituent grains of the aggregated particles described above.

4. Simulation of the scattered light

The variations in the local properties of the dust cloud with the solar distance point to spatial and temporal evolution of the particles, the small particles being ejected by radiation pressure and the largest ones spiralling slowly towards the Sun under the Poynting-Robertson effect (see e.g. Dermott et al. 2001). We now interpret the light scattered and emission results in terms of the properties of the particles through an IDC model using a mixture of fluffy and compact particles composed of silicates and (more absorbing) organic material and possibly amorphous carbon with a model of the IDC including fluffy as well as compact particles constituted from silicates and more absorbing organic material.

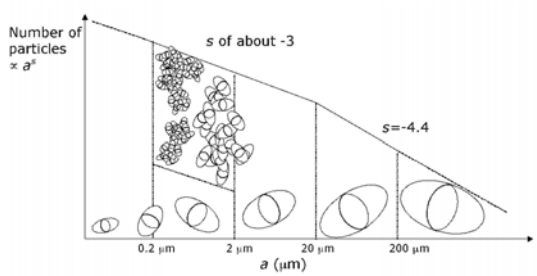

Fig. 1. Size distribution of prolate spheroids (from effective diameter a = 0.2 μm to 200 μm) and aggregates thereof (up to 256 spheroids from a = 0.2 μm to 2 μm).

4.1. Principle of the calculations

The light-scattering computations are performed for a size distribution of spheroids and aggregates there of following a size distribution similar to the one proposed by Grün et al. (2001) for the in situ measurements of the IDC particles, with two different slopes. The power-law coefficient, s, is around −3 for effective diameters, a, smaller than 20 μm and steeper (s = −4.4) for larger effective diameters.

Light scattering by prolate spheroids (axis ratio of 2) is calculated by a code adapted from T-matrix for small spheroids (a < 3.5 μm, Mishchenko & Travis 1998) and by ray tracing for large spheroids (a > 3.5 μm, Macke & Mishchenko 1996). Contribution of ballistic cluster-cluster aggregates and ballistic particle-cluster aggregates (BCCA and BPCA as defined in Meakin 1983) of up to 256 spheroidal grains calculated with the discrete dipole approximation (DDA) (Draine & Flatau 2000) is taken into account in the cloud for effective diameters of the aggregates, a, between 0.2 μm and 2 μm due to computation limitations. Figure 1 summarizes and illustrates such a size distribution with the mixture of particles.

The brightness, Z, and its two polarized components are calculated by integrating the incident light intensity $Z_{\rm inc}$ over the size distribution, $\Gamma(a)$, of the dust particles and their scattering cross section $\sigma_{\rm sca}(a, \alpha, \lambda)$ at a given phase angle α:

$$Z(\alpha, \lambda) = \frac{\int_0^\infty Z_{\rm inc}(\lambda)\sigma_{\rm sca}(a, \alpha, \lambda)\,\Gamma(a)\,{\rm d}a}{\int_0^\infty \sigma_{\rm sca}(a, \alpha, \lambda)\,\Gamma(a)\,{\rm d}a}\,. \quad (3)$$

Details of the calculations, together with results on comet Hale-Bopp coma composition, are given in Lasue & Levasseur-Regourd (2006). In that paper, the optical properties of particles with a silicates core surrounded by an organic mantle (with expected protosolar abundances) are shown to follow the ones of pure organic particles closely. Fitting the observational data in terms of silicates and organic particles mixture allows us to estimate the range of the carbonaceous material percentage in mass of the IDC, taking into account that organic particles can actually embed silicate material.

Since the light scattered by the particles reproduce the solar spectrum in the visible, for the following calculations we have taken only the complex index of the material near 550 nm as a first approximation of the complex index of the particles. The optical indices are taken to be those of Mg-rich pyroxene (1.62 + i 0.003 at λ = 550 nm, for $Mg_xFe_{1-x}SiO_3$ with 0.8 < x < 0.7, Dorschner et al. 1995) and refractive organic material obtained through radiation processing of light elements (≈1.88 + i 0.1 at λ = 550 nm, Li & Greenberg 1997).

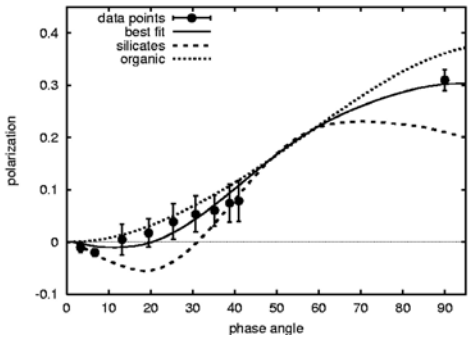

Fig. 2. Zodiacal dust polarization data (•) around 1.5 AU near the symmetry surface and phase curves calculated at 550 nm. Curves are plotted for a realistic interplanetary dust-size distribution of silicates (dashed line), organic (dotted line), and a mixture with ≈40% of organic in mass (thin solid line). Data points are adapted from Levasseur-Regourd et al. (2001) and references therein. The error bars are shown whenever greater than 0.5%.

4.2. Results for the scattered light

Figure 2 presents the phase curves calculated for the IDC size distribution described above. The phase curves obtained for silicates and (absorbing) organic particles are significantly different from each other and from the data points derived from the observations. The organic particles phase curve has a high value P_{90° around 38% and does not show any negative branch, in agreement with previous calculations for absorbing aggregates (Kimura 2001), whereas the silicate-particles phase curve presents a low value P_{90° around 20% and a value α_0 around 30°. Contribution of both absorbing and less-absorbing materials is thus expected to satisfactorily reproduce the IDC composition around 1.5 AU.

As shown in Fig. 2, a good fit of the data retrieved for the polarization phase curve of the IDC near 1.5 AU is obtained for the above-mentioned realistic size distribution with a small-particle power-law coefficient $s = -3.0$ ($s = -4.4$ for large particles as previously defined), effective diameter of 0.22 μm for the lower cutoff and 200 μm for the upper cutoff, and a silicate-organic mixture with about 50% of organic particles in mass. Taking the observational error bars into account, the mass of these organic particles actually comprises between 40% and 60%. When considering that the organic particles in the IDC might embed silicates cores, typically with the cosmic abundances considered in the Greenberg & Hage (1990) model, meaning that these particles actually contain less organic material than is visible, the total amount of organic material can be estimated to be comprised of between 20% and 60% in mass. The amount of aggregates (probably unfragmented particles of cometary origin) is about 20% in mass.

In Fig. 3 are plotted the root mean square values χ^2 of our model compared to the polarization data points, calculated following the equation

$$\chi^2_{\rm pol} = \sum_i \left| \frac{P_{\rm obs}(\alpha_i) - P_{\rm model}(\alpha_i)}{\sigma_P(\alpha_i)} \right|^2 . \quad (4)$$

The plots are shown as 2-dimensional maps as a function of the maximum organic percentage in mass of the cloud and the two other main parameters of the model (small grain size distribution coefficient and cutoff diameter). The first map shows that the size distribution coefficient for small grains (in the 0.2 to 20 μm diameter range) plays an important role for the shape of the phase curve, with a minimum located around -2.95 ± 0.15, thus confirming that a realistic size distribution of the particles should have a coefficient close to this value. The organic percentage in mass is around 50%. The second plot presents the dependence with the minimum diameter and the organic percentage in mass. This shows that the minimum is obtained for a lower cutoff around 0.22 μm. The high variation of the function towards higher values of the lower cutoff shows the predominance of the small particles in the final shape of the polarization phase curve. However too large a lower cutoff can be ruled out because IDPs studies have shown the importance of constituent grains in the 0.1 to 0.3 μm size range as building blocks for interplanetary dust particles. Upper cutoffs larger than 200 μm do not constrain the $\chi^2_{\rm pol}$, so that the larger particles of the size distribution do not influence the shape of the polarization phase curve significantly.

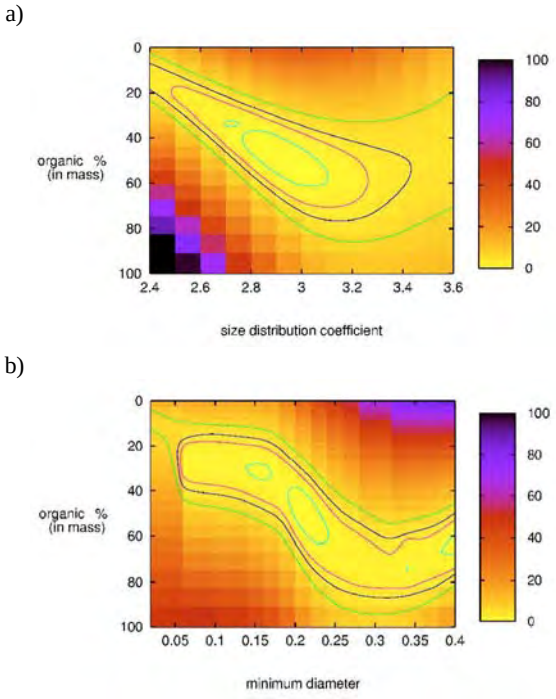

Fig. 3. χ^2 maps of the model compared to the polarization data. a) χ^2 as a function of the maximum organic mass ratio and the small grain size distribution coefficient for a lower diameter of 0.22 μm and b) χ^2 as a function of the maximum organic mass ratio and the small grains' lower diameter for a size distribution power law in $\Gamma(a) = a^{-3}$. The confidence levels curves for 70%, 90%, 95%, and 99% are represented.

In Fig. 4, the dependence of P_{90° on R deduced from the observations (Eq. (1)) is compared to the above model of particles with an organic material percentage varying with the distance to the Sun from 50–100% to 0% as indicated on the curve. The percentage corresponds to the quantity of organic material required to reproduce the variation in the observation's best fit (variation given by Eq. (1), which is more accurate near 1 AU than near 1.5 AU). For a given distance to the Sun the percent range corresponds to the possible existence of core-mantle particles (Lasue & Levasseur-Regourd 2006). A significant loss of organic is mandatory to explain the decrease in P_{90° in the 1.5 to 0.5 AU range. The decrease in P_{90° with R from 1.5 to 0.5 AU could thus be related to a change in the material ratio of the IDC. However, other parameters, such as the size distribution parameters (cutoff diameters or exponent s), could also change with the distance to the Sun when considering small distances to the Sun

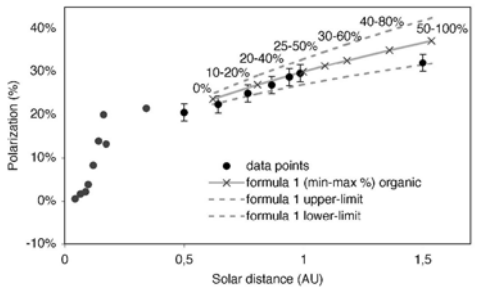

Fig. 4. Dependence of P_{90° on R. Data points (•) are compared to the previous IDC model with a silicate-organic composition expressed as percent of organic (×) varying with the distance to the Sun. Percentage values take the possible presence of core-mantle particles into account. Data points are adapted from Levasseur-Regourd et al. (2001) and references therein. The error bars are shown whenever greater than 0.5%.

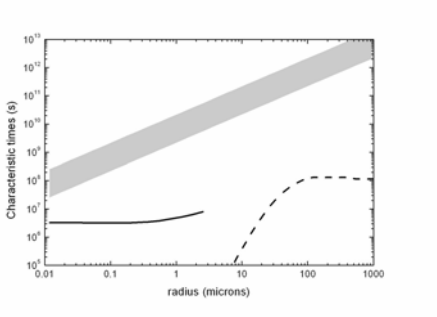

Fig. 5. Comparison between characteristic migration times and characteristic degradation times of spherical particles as a function of their radius. The gray zone corresponds to characteristic migration times of spherical particles submitted to the Poynting-Robertson effect with a density between 1000 kg m^{-3} (upper limit) and 100 kg m^{-3} (lower limit). The dashed and plain lines correspond to the degradation time of POM and poly-HCN particles respectively at 1 AU.

(in the 0.5 to 0 AU range), where a drastic change in polarization is observed.

4.3. Discussion

The light-scattering analysis (Fig. 2) indicates the presence of two types of material (typically non-absorbing silicates and more absorbing carbonaceous material), possibly mixed together in the IDC in the form of silicate-core, organic-mantle particles. It confirms previous studies showing that a significant part of the IDC is generated from cometary dust where these materials have been observed in large quantities (see e.g. Greenberg & Hage 1990). It also agrees with infrared observations showing silicates emission features (see e.g. Reach et al. 1996; Leinert et al. 2002), with the analysis of the IDPs collected in the stratosphere of the Earth and micrometeorites collected in ices (for a review, see Jessberger et al. 2001) and with recent analyses of Stardust samples (see e.g. Zolensky et al. 2006; Sandford et al. 2006). However, it does not rule out the existence of a significant contribution from dust resulting from asteroidal collisions.

Heliocentric dependence analysis (Fig. 4) also shows that a change in the composition of the IDC, with a decrease in the absorbing carbonaceous material percentage when the solar distance decreases, can explain the decrease in P_{90° from 1.5 to 0.5 AU. This interpretation is coherent with previous solar F-corona and zodiacal light data showing a probably wide extended zone of degradation of the carbonaceous material away from the Sun (Mann et al. 1994) reaching up to 1.8 AU (Mukai 1996). It also agrees with recent mid-infrared observations suggesting that the silicates emission feature decreases farther away from the Sun (Reach et al. 2003). It finally supports the decrease in the local albedo value of the particles farther away from the Sun deduced from the observations (Levasseur-Regourd et al. 2001).

This interpretation is also consistent with observations within cometary atmospheres. It has already been shown that solid organic material ejected from cometary nuclei on grains can be degraded when the temperature of the grains rises in the coma. The degradation of polyoxymethylene (formaldehyde polymers: (-CH_2-O-)n, also called POM) has been proposed as the origin of the formaldehyde extended source observed in comet Halley (Cottin et al. 2004). Such a mechanism is also consistent with the variation in the production of H_2CO in comet Hale-Bopp from 0.9 UA to 4 UA (Fray et al. 2006). However, POM is a rather fragile compound, and its degradation would only contribute to a variation in grain composition over a short period of time, inside the coma under thermal effect. From 1.5 to 0.5 AU, the characteristic time of POM disappearance is much lower than the one of migration towards the Sun under the Poynting-Robertson effect. As an example, considering a grain with an effective radius of 100 μm at 1 AU having a black body temperature near 280 K, 99% of POM presumably present in this grain would disappear in about 10^8 s (covering about 10^{-4} UA), whereas its migration time towards the Sun is about 10^{12} s, as can be seen in Fig. 5. Thus, POM cannot explain the dependence of P_{90° on R.

However, other organic compounds, such as HCN polymers (Rettig et al. 1992) have been proposed as part of the solid organic component of cometary grains. Their degradation could be responsible in part for the P_{90° variation. Preliminary results on the thermal degradation of HCN polymers have shown that this compound is much more resistant than POM (Fray et al. 2004) and that it starts to decompose only for temperatures higher than 450 K. Setting this triggering temperature implies that HCN polymer could survive closer to the Sun than POM. Other solid carbonaceous compounds should also be considered, such as amorphous carbon or carbon nitride, for which the onset decomposition temperature is comprised between 600 and 800 K (Zhang et al. 2002). The dependence of P_{90° on R could probably be explained by the degradation of a mixture of refractory compounds, for which degradation is triggered at different temperatures, depending on the grain size and the heliocentric distance.

Although the variation of polarization can be explained well in the 1.5 to 0.5 AU range with the composition change (see Fig. 4), it may be noticed that degradation processes may also change the size distribution but with a limited effect from 1 to 0.1 AU (see e.g. Kimura et al. 1998; Mann et al. 2004). However, other processes are mandatory for explaining the drastic variation of polarization further for R below 0.5 AU. Gail & Sedlmayr (1999) have shown that compounds such as enstatite and forsterite (typically Mg-rich pyroxene and olivine) have their stability limits under equilibrium conditions in the temperature region between 800 K and 1100 K. These temperatures should be reached for distances R to the Sun below 0.3 AU (see e.g. Kimura et al. 2002; Mann et al. 2004). The degradation of silicate minerals in this region could explain the observed variation in the polarization.

The amount of fluffy particles used in our model is about 20% in mass. This may be related to the unfragmented particles originating from comets constituting at least 20% of the IDC in mass. This is only a lower limit value since not all the cometary dust particles present a porous structure (Hörz et al. 2006). Such a result agrees reasonably with previous estimations of the asteroidal to cometary dust ratio deduced from collisional evolution of asteroids (at least 1/3 of IDC is of asteroidal origin, Dermott et al. 1996) and from lunar impact analysis (2/3 is of asteroidal origin, Fechtig et al. 2001).

5. Equilibrium temperature of the particles

The temperature, T, of dust particles in thermal equilibrium at a solar distance, R, typically between 1.5 and 0.5 AU, is computed by making incident and emitted energy equal over the ultraviolet, the visible, and infrared spectrum, from around 0.1 to 1000 μm,

$$\left(\frac{r}{R}\right)^2 \int_0^\infty B(\lambda, T_S) Q_{abs}(a, \lambda) d\lambda = \varsigma \int_0^\infty B(\lambda, T) Q_{abs}(a, \lambda) d\lambda \quad (5)$$

where r is the radius of the Sun, $B(\lambda, T)$ the Planck function, T_S the solar surface temperature, ς the ratio of the emitting surface over $\pi a^2/4$, and $Q_{abs}(a, \lambda)$ the absorption efficiency of a particle with a given optical index $m(\lambda)$ (Kolokolova et al. 2004).

Since the absolute value of T at 1 AU is not accurately known, we mainly discuss the variation of T with R and tentatively reproduce such a variation in the frame of the previous model. Calculations are performed for various shapes: core-mantle spheres, core-mantle prolate spheroids, and the typical fractal aggregates (BCCA and BPCA) of them. The optical indices are taken to be those of astronomical silicates (Draine & Lee 1984), Mg-rich pyroxene (as described in 4.1, Dorschner et al. 1995), refractive organic material (Li & Greenberg 1997), or amorphous carbon (Edoh 1983).

5.1. Results for the temperature of isolated dust particles

Figure 6 presents the variation in the equilibrium temperature with the heliocentric distance in logarithmic scale between 1.5 and 0.5 AU for spheres, spheroids, and 64 spheres BCCA-BPCA aggregates (of 1.5 μm equivalent volume sphere diameter meaning constituting spheres of 0.19 μm radius) made of astronomical silicates, Mg-rich pyroxene, organic, or amorphous carbon material. The curves are systematically compared to the IDC temperature variation (Eq. (2)) retrieved from the observations and the black body temperature. The absolute value of the temperature is approximated better by black body particles, low-absorbing materials (such as Mg-rich pyroxene), and the more compact particles amongst the aggregates. This agrees with previous works (see e.g. Reach et al. 2003; and Kasuga et al. 2006) showing that the particles near 1 AU are rather large and compact with behavior close to a black body. However, the temperature-distance factor, t, between 0.5 and 1.5 AU is approximately equal to −0.33 for organic, −0.35 for amorphous carbon that is significantly closer to the observations (Eq. (2)) than the values of −0.52 for astronomical silicates, and −0.5 for Mg-rich pyroxene. This suggests that absorbing materials constitute a non negligible component of the IDC between 0.5 and 1.5 AU.

The heliocentric power-law dependence of the temperature does not change significantly with the shape of the particle (spheres, spheroids, or BCCA-BPCA aggregates) and is instead

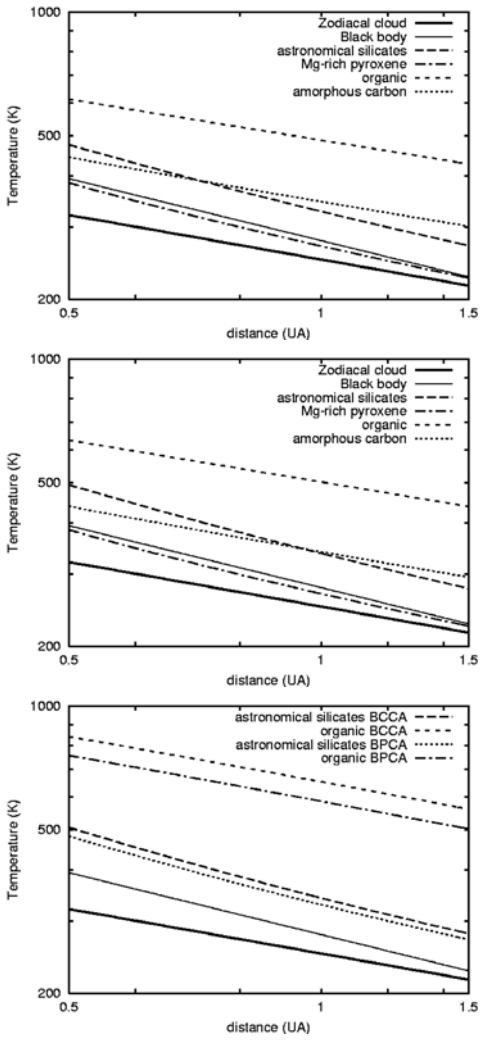

Fig. 6. Logarithmic plot of the dust temperature in the symmetry surface as a function of the solar distance. Temperature is inferred from observations (thick solid line), as compared to black body temperature (thin solid line) and temperature computed for spheres (*top*), spheroids (*middle*), and BCCA-BPCA aggregates (*bottom*) of an equivalent diameter 1.5 μm.

defined by the effective diameter and the material constituting the particle. The variation in t with the size of the particles is not accurately known, but should tend towards a black body law when the equivalent diameter of the particles increases.

Figure 7 shows the comparison between the temperature-distance factors retrieved from the observations (with the estimated error bar represented by a gray zone) and computed for spheres and spheroids as a function of the size of the particles. For an equivalent radius larger than 10 μm, the equilibrium temperature of these particles behaves like the one of a black body. For smaller sizes (<1 μm), the temperature-distance factor, t, of the astronomical silicates and pyroxene particles is around the black body value, whereas for the (more absorbing) organic and carbon material, t is equal to the temperature-distance factor retrieved from the observations within the error bars.

As illustrated in Fig. 6, the temperatures obtained for more absorbant materials (organic and amorphous carbon) are higher than those corresponding to less absorbant materials (astronomical silicates and Mg-rich pyroxene) for the same equivalent radius. This corresponds to the fact that organic or carbon particles

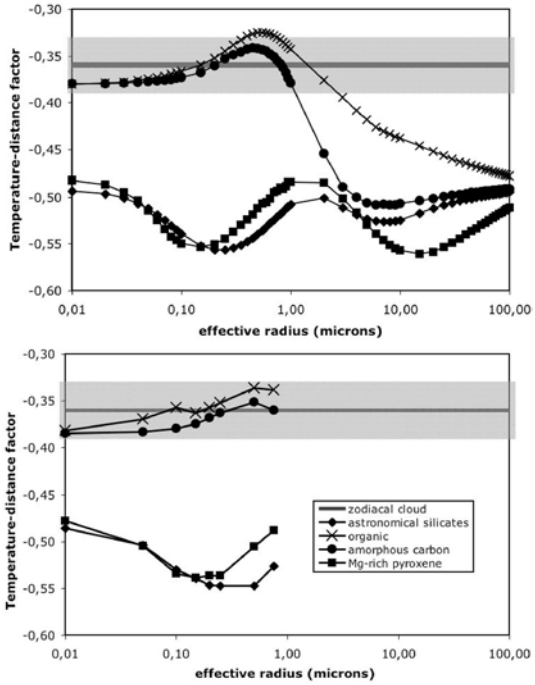

Fig. 7. Comparison between temperature-distance factors in the symmetry surface and between 0.5 and 1.5 AU, as inferred from observations (thick solid line surrounded by gray zone) and as calculated for spheres (top) and spheroids (bottom) as a function of their equivalent radius. Calculations are presented for astronomical silicates (♦), Mg-rich pyroxene (■), and absorbing material like organic (×), and amorphous carbon (●) material.

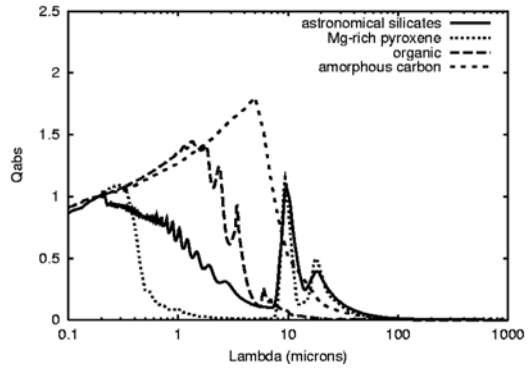

Fig. 8. Comparison of absorption efficiency, $Q_{\rm abs}$, for spheres made of different materials (astronomical silicates, Mg-rich pyroxene, organic, amorphous carbon) as a function of the wavelength for an equivalent radius of 0.75 μm.

absorb more than the silicates in the visible and the near infrared part of the spectrum, whereas they emit less in the infrared, as can be seen in Fig. 8 that shows the absorption efficiency of spherical particles of radius 0.75 μm.

Higher values of the temperature are obtained for fluffier particles: BCCA compared to BPCA aggregates, and aggregates compared to equal volume spheroids. This indicates the importance of the size and porosity of the particles for their equilibrium temperature and results from the fact that the more porous an aggregate is, the lower the contribution of the interaction between constituent particles, and the more prominent the properties of its individual, constituent particles (in agreement with Xing & Hanner 1997; and Kolokolova et al. 2007).

5.2. Equilibrium temperature of a cloud of spherical particles

5.2.1. Principles of the emissivity calculation of the particles

The emissivity, ε_λ, of a cloud of particles with different compositions at a given wavelength and distance to the Sun is obtained by summing the Planck function contribution of each particle (with a temperature, T, and an absorption efficiency, $Q_{\rm abs}$, depending on its size). These considerations are summed up in the following equation from Reach et al. (2003):

$$\varepsilon_\lambda = \sum_i \int \Gamma(a)^{(i)} B_\lambda \left(T^{(i)}(a)\right) \pi a^2 Q_{\rm abs}^{(i)}(a,\lambda) {\rm d}a, \quad (6)$$

where the sum over i corresponds to the sum over the different materials constituting the cloud, a is the equivalent diameter of the particles, and $B_\lambda \left(T^{(i)}(a)\right)$ is the value of the Planck function at a given temperature, $T^{(i)}(a)$, and a given wavelength, λ; and $\Gamma(a)$ is the same size distribution of particles than the one deduced from the polarization calculations in Part 4. To be able to compare the emissivity with Planck curves, the above integral is normalized:

$$\langle\varepsilon_\lambda\rangle = \sum_i \frac{\int \Gamma(a)^{(i)} B_\lambda \left(T^{(i)}(a)\right) \pi a^2 Q_{\rm abs}^{(i)}(a,\lambda) {\rm d}a}{\int \Gamma(a)^{(i)} \pi a^2 Q_{\rm abs}^{(i)}(a,\lambda) {\rm d}a}. \quad (7)$$

And $\langle\varepsilon_\lambda\rangle$ depends on the distance to the Sun, since the temperature of the particles varies with this parameter.

5.2.2. Heliocentric variation in the brightness temperature

The variation in the absorption efficiency with the wavelength implies that particles with a radius smaller than 0.1 μm absorb and emit very little, and thus do not contribute much to the emissivity function (see e.g. Reach 1988). Particles with a size less than 1 μm, generally have a much higher equilibrium temperature than the black body one as shown in Fig. 9, while particles with a radius larger than 10 μm have an emissivity close to the black body one.

This behavior, already perceptible in the behavior of the temperature-distance factor as a function of the particles radius (Fig. 7), is confirmed in Fig. 9, which shows the variation in the equilibrium temperature of the spheres as a function of their radius at a given solar distance (0.5, 1, and 1.5 AU). Particles with radius smaller than 1 μm have higher temperatures and particles with a radius larger than 10 μm have temperatures similar to a black body.

The approximation of the emissivity curve $\langle\varepsilon_\lambda\rangle$ by a Planck curve over the whole visible and infrared spectrum (from $\approx$0.1 μm to $\approx$1000 μm) gives the equivalent of the brightness temperature of the cloud of particles, which corresponds to the temperature of the black body that best fits the particles' cloud spectrum. This temperature calculated at different distances to the Sun gives the temperature-distance factor of the particle cloud. Temperatures and temperature-distance factors depending on the distance to the Sun are presented in the Tables 1 and 2.

The variation in the brightness temperature with the distance to the Sun depends strongly on the material. The calculations presented in Table 2 confirm that a cloud of silicate particles behave like a black body, whereas the temperature-distance factor has lower values for a cloud of particles constituted of more absorbing materials (organic and amorphous carbon).

The results of the brightness temperature obtained for a mixture of organic and astronomical silicates between 0.5 AU and

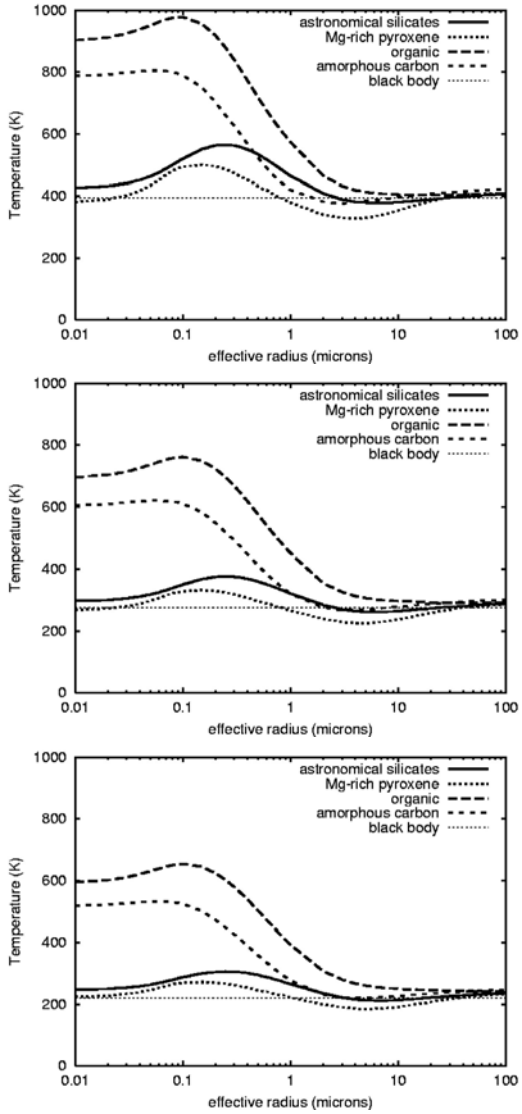

Fig. 9. Equilibrium temperature of spheres as a function of their radius and their constituent materials. The curves are computed for different solar distances: 0.5 AU (*top*), 1 AU (*middle*), 1.5 AU (*bottom*).

1.5 AU show that a mixture including approximately 50% of organic and 50% of astronomical silicates in mass as deduced from the previous light-scattering study can explain a significantly different behavior from a black body with a temperature-distance factor $t = -0.45$. The same temperature-distance factor would also be found if we considered only silicates material at 0.5 AU since the brightness temperature of the mixture of silicates and organic is close to the one of silicates at this distance (see Table 1). This result confirms the previous estimations of the composition of the IDC from the light-scattering observations.

5.3. Discussion

The temperature-distance factor retrieved from the light-scattering observations differs from the black body law. It is possible that the emitting particles may be small and irregular scatterers, for which the black body approximation cannot be used. Also, t does not change significantly with the shape of the particle (spheres, spheroids, or aggregates) and is mostly defined by the effective diameter and the material constituting the particle, in agreement with previous temperature calculations for amorphous carbon (Xing & Hanner 1997). The equilibrium temperature obtained for silicate particles decreases faster with R than for absorbing particles, as can be expected from the presence of silicate emission features in the infrared (Mann et al. 1994). This can also explain the lower temperature obtained for silicates as compared to more absorbing material in Fig. 6.

In agreement with Xing & Hanner (1997), the temperature obtained for an aggregate of grains is lower than one of its constituent grains but is higher than the temperature of the equivalent volume sphere. The temperature and polarization thus behave in opposite ways because a fluffy aggregate of small grains presents values of t close to the one of its equivalent volume sphere, whereas it scatters light in a similar way to one of its constituent grains as shown from numerical simulations (West 1991) and experimental simulations (Wurm et al. 2004).

The works of Reach et al. (1988, 2003) use different sphere size distributions (power law, interplanetary dust size distribution, Hanner cometary dust size distribution, etc.) and material similar to the ones we considered here (astronomical silicates, andesite, obsidian, amorphous and crystalline olivine, amorphous and crystalline pyroxene, carbon, etc.). Their study shows a best fit with the observations for a mixture of 10% carbon and 90% silicates and the interplanetary dust particles size distribution, which gives more weight to the particles in the 10 to 100 μm diameter. The conclusions presented in this work agree fairly with their model, but it has been developed specifically to try to interpret the peculiar variation in the temperature with the heliocentric distance.

6. Conclusions

The physical properties of the interplanetary dust cloud in the near ecliptic symmetry surface are tentatively derived from scattered and emitted light observations. Results for the composition of the dust cloud, the size distribution, and the shape of the particles are summarized below.

1. Both silicates and (more absorbing) organic materials are necessary to explain the local polarization and temperature values retrieved from observations, as well as their variation with the solar distance.
2. A good fit of the polarization phase curve available near 1.5 AU is obtained for a realistic particle size distribution (with a power law a^{-3} for particles with an equivalent diameter, a, between 0.22 μm and 20 μm and $a^{-4.4}$ for larger particles) and for a mixture of silicates and more absorbant organic materials (between 20% and 60% in mass).
3. The upper cutoff of the size distribution is not well-constrained with the above-mentioned size distribution, allowing the presence of rather large, compact particles.
4. The decrease in P_{90° with the solar distance between 1.5 and 0.5 AU is interpreted as a progressive disappearance of the solid carbonaceous compounds (such as HCN polymers or amorphous carbon) towards the Sun, probably linked with the presence of an extended zone of thermal degradation.
5. The drastic change in P_{90° closer to the Sun between 0.5 and 0 AU could be explained by other physical processes, such as the degradation of silicate materials or a change in the size distribution possibly favoring smaller particles towards the Sun.
6. Unfragmented aggregates of cometary origin that contribute to the interplanetary dust cloud are of at least 20% in mass around 1.5 AU.

Table 1. Brightness temperature as a function of the distance to the Sun, R, for a cloud of spherical particles with the size distribution obtained in Part 4.

R	Observations	Astronomical silicates	Mg-rich pyroxene	Organic	Amorphous carbon	50% silicates– –50% organic	Black body
0.5 AU	321 ± 20 K	414 K	371 K	524 K	471 K	408 K	394 K
1 AU	250 ± 10 K	295 K	255 K	388 K	351 K	298 K	279 K
1.5 AU	216 ± 11 K	243 K	210 K	327 K	299 K	249 K	228 K

Table 2. Brightness temperature-distance factor, t, for a cloud of spherical particles with the size distribution obtained in Part 4, where t is calculated over three domains (between 0.5 and 1.5 AU).

Domain (AU)	Observations	Astronomical silicates	Mg-rich pyroxene	Organic	Amorphous carbon	50% silicates– –50% organic	Black body
0.5–1	−0.36 ± 0.03	−0.49	−0.54	−0.43	−0.43	−0.45	−0.5
1–1.5	−0.36 ± 0.03	−0.48	−0.49	−0.42	−0.39	−0.44	−0.5
0.5–1.5	−0.36 ± 0.03	−0.48	−0.52	−0.43	−0.41	−0.45	−0.5

7. The size distribution retrieved from the polarization fit leads to a temperature variation in $R^{-0.45}$ different from the black body behavior and closer to the observations.
8. The variation in the temperature with the solar distance for absorbing materials is closer to the observations than the one of non absorbing materials. This behavior is mainly due to particles with a diameter smaller than 2 μm.

Acknowledgements. This research has been partially funded by the French space agency (CNES). The authors acknowledge fruitful discussions with J.-B. Renard and helpful comments from an anonymous referee.

References

Bockelée-Morvan, D., Gautier, D., Hersant, F., Huré, J.-M., & Robert, F. 2002, A&A, 384, 1107
Bradley, J. P., Humecki, H. J., & Germani, M. S. 1992, ApJ, 394, 643
Cottin, H., Bénilan, Y., Gazeau, M.-C., & Raulin, F. 2004, Icarus, 167, 397
Dermott, S. F., Grogan, K., Gustafson, B. A. S., et al. 1996, in Physics, Chemistry and Dynamics of Interplanetary Dust, ed. B. A. S. Gustafson, & M. S. Hanner, ASP Conf. Ser., 104, 143
Dermott, S. F., Grogan, K., Durda, D.D., et al. 2001, in Interplanetary dust, ed. E. Grün, B. A. S. Gustafson, S. Dermott, & H. Fechtig, 569
Dorschner, J., Begemann, B., Henning, Th., Jäger, C., & Mutschke, H. 1995, A&A 300, 503
Draine, B. T., & Lee, H. M. 1984, ApJ, 285, 89
Draine, B. T., & Flatau, P. J. 2000, http://arxiv.org/abs/astro-ph/0008151v4
Dumont, R., & Levasseur-Regourd, A. C. 1988, A&A, 191, 154
Edoh, O. 1983, Optical Properties of Carbon from the Far Infrared to the Far Ultraviolet, Ph.D. Thesis (University of Arizona Press)
Engrand, C., & Maurette, M. 1998, M&PS, 33, 565
Fechtig, H., Leinert, Ch., & Berg, O. E. 2001, in Interplanetary Dust, ed. E. Grün, B. A. S. Gustafson, S. Dermott, & H. Fechtig (Springer-Verlag), 1
Flynn, G. J., Keller, L. P., Jacobsen, C., & Wirick, S. 2004, Adv. Space Res., 33, 57
Fray, N., Bénilan, Y., Cottin, H., et al. 2004, M&PS, 39, 581
Fray, N., Bénilan, Y., Biver, N., et al. 2006, Icarus, 184, 239
Gail, H.-P., & Sedlmayr, E. 1999, A&A, 347, 594
Greenberg, J. M., & Hage, J. I. 1990, ApJ, 361, 260
Grün, E., Zook, H.A., Baguhl, M., et al. 1993, Nature, 362, 428
Grün, E., Baguhl, M., Svedhem, H., & Zook, H. A. 2001, in Interplanetary Dust, ed. E. Grün, B. A. S. Gustafson, S. Dermott, & H. Fechtig (Springer-Verlag), 295
Hanner, M. S., & Bradley, J. P. 2004, in Comets II, ed. M. C. Festou, H. U. Keller, & H. A. Weaver (University of Arizona Press), 555
Hanner, M. S., Veeder, G. J., & Tokunaga, A. T. 1992, AJ, 104, 386
Hayward, T. L., Hanner, M. S., & Sekanina, Z. 2000, ApJ, 538, 428
Hellyer, B. 1970, MNRAS, 148, 383
Hörz, F., Bastien, R., Borg, J., et al. 2006, Science, 314, 1716
Jäger, C., Molster, F. J., Dorschner, J., et al. 1998, A&A, 339, 904
Jenniskens, P. 1993, A&A, 274, 653
Jessberger, E. K., Stephan, T., Rost, D., et al. 2001, in Interplanetary Dust, ed. E. Grün, B. A. S. Gustafson, S. Dermott, & H. Fechtig (Springer-Verlag), 253
Jorda, L., Lamy, P., Faury, G., et al. 2007, Icarus, 187, 208
Kasuga, T., Yamamoto, T., Kimura, H., & Watanabe, J. 2006, A&A, 453, L17
Keller, L. P., Thomas, K. L., & McKay, D. S. 1994, in Analysis of Interplanetary Dust, ed. M. E. Zolensky, T. L. Wilson, F. J. M. Rietmeijer, & G. J. Flynn, AIP Conf. Proc., 310, 159
Kimura, H. 2001, JQSRT, 70, 581
Kimura, I., Mann, I., & Mukai, T. 1998, Planet. Space Sci., 46, 911
Kimura, I., Mann, I., Biesecker, D.A., & Jessberger, E.K. 2002, Icarus, 159, 529
Kolokolova, L., Hanner, M. S., Levasseur-Regourd, A. C., & Gustafson, B. A. S. 2004, in Comets II, ed. M. C. Festou, H. U. Keller, & H. A. Weaver (University of Arizona Press), 577
Kolokolova, L., Kimura, H., Kiselev, N., & Rosenbush, V. 2007, A&A 463, 1189
Lasue, J., & Levasseur-Regourd, A. C. 2006, JQSRT, 100, 220
Leinert, Ch., Bowyer, S., Haikala, L. K., et al. 1998, A&AS, 127, 1
Leinert, Ch., Ábrahám, P., Acosta-Pulido, J., Lemke, D., & Siebenmorgen, R. 2002, A&A, 393, 1073
Levasseur-Regourd A.C. 2003, Adv. Space Res., 31, 2599
Levasseur-Regourd, A. C., & Hadamcik, E. 2003, JQSRT, 79, 903
Levasseur-Regourd, A. C., Cabane, M., & Haudebourg, V. 1999, JQSRT, 63, 631
Levasseur-Regourd, A. C., Mann, I., Dumont, R., & Hanner, M. S. 2001, in Interplanetary Dust, ed. E. Grün, B. A. S. Gustafson, S. Dermott, & H. Fechtig (Springer-Verlag), 57
Levasseur-Regourd, A. C., Mukai, T., Lasue, J., & Okada, Y. 2007, Planet. Space Sci., 55, 1010
Li, A., & Greenberg, J. M. 1997, A&A, 323, 566
Lucey, P. G. 1998, JGR, 103, E1, 1703
Lumme, K. 2000, in Light scattering by non spherical particles, ed. M. I. Mishchenko, J. W. Hovenier, & L. D. Travis (San Diego: Academic Press), 555
Macke, A., & Mishchenko, M. I. 1996, App. Opt., 35, 4291
Mann, I. 1992, A&A, 261, 329
Mann, I., Okamoto, H., Mukai, T., Kimura, H., & Kitada, Y. 1994, A&A, 291, 1011
Mann, I., Kimura, I., Biesecker, D.A., et al. 2004, Space Sci. Rev., 110, 269
Meakin, P. 1983, Phys. Rev. Lett., 51, 1119
Mishchenko, M. I., & Travis, L. D. 1998, JQSRT, 60, 309
Mukai, T. 1996 in Physics, Chemistry and Dynamics of Interplanetary Dust, ed. B. A. S. Gustafson, & M. S. Hanner, ASP Conf. Ser., 104, 453
Mukai, T., Blum, J., Nakamura, A. M., Johnson, R. E., & Havnes, O. 2001, in Interplanetary Dust, ed. E. Grün, B. A. S. Gustafson, S. Dermott, & H. Fechtig (Springer-Verlag), 445
Papoular, R., Breton, J., Gensterblum, G., et al. 1993, A&A, 270, L5
Reach, W. T. 1988, ApJ, 335, 468
Reach, W. T. 1991, ApJ, 369, 529
Reach, W. T., Abergel, A., Boulanger, F., et al. 1996, A&A, 315, L381
Reach, W. T., Morris, P., Boulanger, F., & Okumura, K. 2003, Icarus, 164, 384
Renard, J. B., Levasseur-Regourd, A. C., & Dumont, R. 1995, A&A, 304, 602
Rettig, T. W., Tegler, S. C., Pasto, D.J., & Mumma, M. J. 1992, ApJ, 398, 293
Sandford, S. A., Aléon, J., Alexander, C. M. O'D., et al. 2006, Science, 314, 1720
West, R. A. 1991, App. Opt., 30, 5316
Whipple, F.L. 1951, ApJ, 113, 464
Wooden, D. H., Harker, D. E., Woodward, C. E., et al. 1999, ApJ, 517, 1034
Wurm, G., Relke, H., Dorschner, J., & Krauss, O. 2004, JQSRT, 89, 371
Xing, Z., & Hanner, M. 1997, A&A, 324, 805
Zhang, L. H., Gong, H., & Wang, J. P. 2002, J. Phys. Cond. Matter, 14, 1697
Zolensky, M. E., Zega, T. J., Yano, H., et al. 2006, Science, 314, 1735

Article 14

KISSEL J., ALTWEGG K., CLARK B. C., COLANGELI L., COTTIN H., CZEMPIEL S., EIBEL J., ENGRAND C., FEHRINGER H. M., FEUERBACHER B., FOMENKOVA M., GLASMACHERS A., GREENBERG J. M., GRÜN E., HAERENDEL G., HENKEL H., HILCHENBACH M., HOERNER H. V., HÖFNER H., HORNUNG K., JESSBERGER E. K., KOCH A., KRÜGER H., LANGEVIN Y., PARIGGER P., RAULIN F., RÜDENAUER F., RYNÖ J., SCHMID E. R., SCHULZ R., SILEN J., STEIGER W., STEPHAN T., THIRKELL L., THOMAS R., TORKAR K., UTTERBACK N. G., VARMUZA K., WANCZEK K. P., WERTHER W. and ZSCHEEG H. (2007) COSIMA, a High Resolution Time of Flight Spectrometer for Secondary Ion Mass Spectroscopy of Cometary Dust Particles. Space Science Reviews Volume 128(1-4), 823-867.

COSIMA – HIGH RESOLUTION TIME-OF-FLIGHT SECONDARY ION MASS SPECTROMETER FOR THE ANALYSIS OF COMETARY DUST PARTICLES ONBOARD ROSETTA

J. KISSEL[1], K. ALTWEGG[2], B. C. CLARK[3], L. COLANGELI[4], H. COTTIN[5], S. CZEMPIEL[6], J. EIBL[6], C. ENGRAND[7], H. M. FEHRINGER[8], B. FEUERBACHER[9], M. FOMENKOVA[10], A. GLASMACHERS[11], J. M. GREENBERG[12], E. GRÜN[13], G. HAERENDEL[6], H. HENKEL[14], M. HILCHENBACH[1], H. VON HOERNER[14], H. HÖFNER[8], K. HORNUNG[15], E. K. JESSBERGER[16], A. KOCH[14], H. KRÜGER[1], Y. LANGEVIN[17], P. PARIGGER[6], F. RAULIN[5], F. RÜDENAUER[18], J. RYNÖ[19], E. R. SCHMID[20], R. SCHULZ[8], J. SILÉN[19], W. STEIGER[21], T. STEPHAN[16], L. THIRKELL[22], R. THOMAS[22], K. TORKAR[23], N. G. UTTERBACK[24], K. VARMUZA[25], K. P. WANCZEK[26], W. WERTHER[20] and H. ZSCHEEG[27]

[1]*Max-Planck-Institut für Sonnensystemforschung, Max-Planck-Str. 2, 37191 Katlenburg-Lindau, Germany*

[2]*Physikalisches Institut, Universität Bern, Sidlerstr. 5, 3012 Bern, Switzerland*

[3]*Lockheed Martin Astronautics, Post Office Box 179, MS-B0560, Denver, CO 80201, USA*

[4]*Istituto Nazionale di Astrofisica – Osservatorio Astronomico di Capodimonte, Via Moiariello 15, 80131 Napoli, Italy*

[5]*LISA, Universites Paris 12 & Paris 7, Faculté des Sciences et Technologie, 61, Avenue du General de Gaulle, F-94010 Creteil Cedex, France*

[6]*Max-Planck-Institut für Extraterrestrische Physik, Giessenbachstrasse, 85740 Garching, Germany*

[7]*Centre de Spectrométrie Nucléaire et de Spectrométrie de Masse – CSNSM, Bat. 104, 91 405 Orsay, France*

[8]*ESA – ESTEC, Postbus 299, 2200AG Noordwijk, The Netherlands*

[9]*Deutsches Zentrum für Luft- und Raumfahrt e.V. (DLR) in der Helmholtzgemeinschaft, Institut für Raumsimulation, Linder Höhe, D-51147 Köln, Germany*

[10]*Center for Astrophysics and Space Sciences, University of California San Diego, La Jolla, CA 92093-0424, USA*

[11]*Universität Wuppertal, FB-E, Lehrstuhl für Messtechnik, Rainer-Gruenter-Str. 21, 42119 Wuppertal, Germany*

[12]*Raymond and Beverly Sackler Laboratory for Astrophysics, P.O. Box 9513, NL-2300 RA Leiden, The Netherlands, deceased Nov. 2001*

[13]*Max-Planck-Institut für Kernphysik, Saupfercheckweg 1, 69115 Heidelberg, Germany*

[14]*von Hoerner und Sulger GmbH, Schlossplatz 8, 68723 Schwetzingen, Germany*

[15]*Universität der Bundeswehr LRT-7, Werner Heisenberg Weg 39, 85577 Neubiberg, Germany*

[16]*Institut für Planetologie, Wilhelm-Klemm-Str. 10, 48149 Münster, Germany*

[17]*Institut d'Astrophysique, Batiment 121, Faculté des Sciences d'Orsay, 91405 Orsay, France*

[18]*Institut f. Physik, Forschungszentrum Seibersdorf, 2444 Seibersdorf, Austria*

[19]*Finnish Meteorological Institute, Department of Geophysics, rik Palménin aukio 1, FI-00560 Helsinki, Finland*

[20]*Department of Analytical and Food Chemistry, University of Vienna, Währingerstrasse 38, A-1090 Vienna, Austria*

[21]*ARC Seibersdorf Research GmbH Business Field Aerospace Technology, 2444 Seibersdorf, Austria*

[22]*Laboratoire de Phys.& Chim. de L'Environnement, 3 Av. de la Recherche Scientifique, 45071 Orléans, France*

Space Science Reviews (2007) 128: 823–867
DOI: 10.1007/s11214-006-9083-0

[23]*Institut für Weltraumforschung, Österreichische Akademie der Wissenschaften, Schmiedlstrasse 6, 8042 Graz, Austria*

[24]*Consultant, 93105 Sta. Barbara, CA, USA, deceased Nov. 2003*

[25]*Vienna University of Technology, Institute of Chemical Engineering, Getreidemarkt 9/166, A-1060 Vienna, Austria*

[26]*Institut für Anorganische und Physikalische Chemie, Universität Bremen, Haferwende 12, 28357 Bremen, Germany*

[27]*Abbott Laboratories Vascular Devices Ltd., Ampthauptstrasse, 8222 Beringen, Switzerland*

*(*Author for correspondence: E-mail: cometkissel@arcor.de)*

(Received 22 March 2006; Accepted in final form 11 October 2006)

Abstract. The ESA mission Rosetta, launched on March 2nd, 2004, carries an instrument suite to the comet 67P/Churyumov-Gerasimenko. The COmetary Secondary Ion Mass Anaylzer – COSIMA – is one of three cometary dust analyzing instruments onboard Rosetta. COSIMA is based on the analytic measurement method of secondary ion mass spectrometry (SIMS). The experiment's goal is in-situ analysis of the elemental composition (and isotopic composition of key elements) of cometary grains. The chemical characterization will include the main organic components, present homologous and functional groups, as well as the mineralogical and petrographical classification of the inorganic phases. All this analysis is closely related to the chemistry and history of the early solar system. COSIMA covers a mass range from 1 to 3500 amu with a mass resolution $m/\Delta m$ @ 50% of 2000 at mass 100 amu. Cometary dust is collected on special, metal covered, targets, which are handled by a target manipulation unit. Once exposed to the cometary dust environment, the collected dust grains are located on the target by a microscopic camera. A pulsed primary indium ion beam (among other entities) releases secondary ions from the dust grains. These ions, either positive or negative, are selected and accelerated by electrical fields and travel a well-defined distance through a drift tube and an ion reflector. A microsphere plate with dedicated amplifier is used to detect the ions. The arrival times of the ions are digitized, and the mass spectra of the secondary ions are calculated from these time-of-flight spectra. Through the instrument commissioning, COSIMA took the very first SIMS spectra of the targets in space. COSIMA will be the first instrument applying the SIMS technique in-situ to cometary grain analysis as Rosetta approaches the comet 67P/Churyumov-Gerasimenko, after a long journey of 10 years, in 2014.

1. Introduction

The *in situ* chemical analysis of solids in space is among the tasks that are technically most difficult. There are two main reasons for that: With a few exceptions, solids in space are not abundant, and, secondly, it is not easy to remove small samples from the solid into the vacuum for the analysis in a mass spectrometer.

For COSIMA, the objects of interest are cometary dust particles, which are abundant, indeed, in the neighborhood of the comet nucleus. It remains, however, to collect and bring the particles to the entrance of the spectrometer.

Most mass spectrometers need the parts of the sample to be analyzed, to carry an electric charge. The process of removing an ion from the specimen is then the critical feature of the method to be chosen.

The only mass spectrometric data on cometary dust particles available to date come from the dust impact mass spectrometers PIA, PUMA, and CIDA on the GIOTTO, VEGA, and Stardust spacecrafts, respectively. (Far more and more detailed mass spectra of IDPs of supposed cometary origin are available from laboratory measurements, and soon there will be results from the cometary dust particles retrieved from Stardust.) While other, remote, or indirect methods allow measurements of collective properties of the cometary dust, the mass spectrometers allowed the analysis of individual particles (cf. Kissel *et al.*, 1986a, b). Since then, we know unambiguously that each particle is an intimate mixture of a mineral component and simple as well as complex organic molecules. Since the impact velocity was large (>60 km/s), mostly atomic ions were formed and analyzed in the Halley case. In a first attempt, however, Kissel and Krueger (1987) found evidence for the chemical nature of the organic cometary material. It is clear that not only a few well known molecules constitute the cometary organics, but rather several chemical classes, with each being represented by a large number of individual substances. Indeed, it seems possible that all stable molecules compatible with the chemical environment are formed.

COSIMA therefore needed to be based on a method, which is readily available in laboratory, and which allows for tracing the ion directly to the molecular and structural form in which it was present in the solid. Since the size distribution of the dust particles is known (cf. Mazets *et al.*, 1987; McDonnell *et al.*, 1989), a reasonable ionizing beam focus should be achieved under the limitations of space instrumentation. Even though the method would be destructive, its sensitivity should be high enough to allow several analyses at different depths for one individual ~20 μm particle.

To satisfy all these requirements, we choose the method of Secondary Ion Mass Spectrometry (SIMS). A fast primary ion, in this case $^{115}In^{+}$ at 8 keV, impacts the sample and releases by desorption atoms and molecules of the sample, of which typically 0.1 to 10% are ionized, the so-called secondary ions. For sensitivity reasons, the analysis of a rather large mass range should be achieved simultaneously, which in turn leads to the type of a time-of-flight mass spectrometer. The mass resolution must be high enough to resolve isobaric ions, at least atomic from molecular ions. The mass range should at least cover 3500 amu. In total, the COSIMA instrument has the following main functional hardware elements:

- dust collector and target manipulator,
- COSISCOPE, a microscope for target inspection
- primary ion source, and
- mass spectrometer including the ion extraction optics and the ion detector.

Of course, for autonomous operation, the entire instrument is under microprocessor based software control.

It should be mentioned at this point that COSIMA did profit from but is not identical to the earlier development of the CoMA instrument for the NASA mission CRAF (Zscheeg, 1992), which was canceled in 1992.

The entire development of COSIMA was challenged by the complexity of especially the organic cometary material, which has to be expected. This has focused the goal of COSIMA on the identification of chemical classes and functional groups rather than the identification of individual substances. Consequently the system must have the capability to use the methods of chemometrics to compress the raw data on board, which helps to reduce the data volume without losing any of the chemical information.

There is also another important aspect for COSIMA, which comes from the rather long time the spacecraft travels from launch in 2004 until the core of the measurements takes place in 2014: Quite a large number of relevant results will be obtained from laboratory measurements with TOF-SIMS, potentially by the COSIMA team or in the published literature. In addition, NASA in its DISCOVERY program has several comet missions, which are expected to produce new, relevant data, before COSIMA enters its main analysis phase. Even if most of the flexibility is with the software involved, it is the hardware, which has to provide the resources necessary. Looking back at the fast development in the computer sector over the last ten years, this alone is a demanding task, even without the complexity of an up-to-date analysis instrument.

The overall parameters and resources describing COSIMA are:

- Atomic mass range 1 . . . 3500 amu
- Rel. atomic mass resolution $m/\Delta m$ (at $m = 100$ amu) >2000 at 50% peak width
- Indium ion pulse duration <3 ns
- Indium ion energy 8 keV
- Ion beam width about 50 μm FWHM
- Telemetry rate about 500 bit/sec
- Mass 19.8 kg
- Power consumption from 28 V DC 20.4 W

2. Functional Description

COSIMA is a time-of-flight secondary ion mass spectrometer. Like all such instruments, primary ions generate secondary ions from a target, which they hit. Those secondary ions are then accelerated to the same, constant kinetic energy, and their flight time to the ion detector is measured. This flight time follows the equation:

$$\text{time-of-flight} = a \times (\text{mass}/\text{abs(q)})^{0.5} + b; \quad (1)$$

with a is an instrumental constant depending on the length of the flight path and the electrical voltages applied, for COSIMA it is about 3.1 μs/(mass)$^{0.5}$; b is a constant for the offset of the time measurement; mass is the ion mass in amu; q is the ion charge state, in most cases $= -1$ or $+1$.

The schematic view of the COSIMA functional blocks is shown in Figure 1. COSIMA works pretty much like a laboratory instrument, with a somewhat reduced performance due to the limitations for a space instrument, but remotely operated in a 'distant lab'. The limitations come first of all from the mass and power available, but more pronounced from the limited capacity of data transfer to and from the instrument, combined with a reaction time (round trip time delay) of 32 minutes during the main operation time.

Consequently the individual steps for the analysis of a dust particle are:

(1) exposure of a collection substrate for a predetermined time
(2) optical search of the substrate for dust particles by the camera system COSIS-COPE
(3a) moving a dust particle in front of the spectrometer
(3b) either first clean the particle and surrounding by sputtering or
(3c) start the particle characterization
(4) decide if a detailed analysis is promising

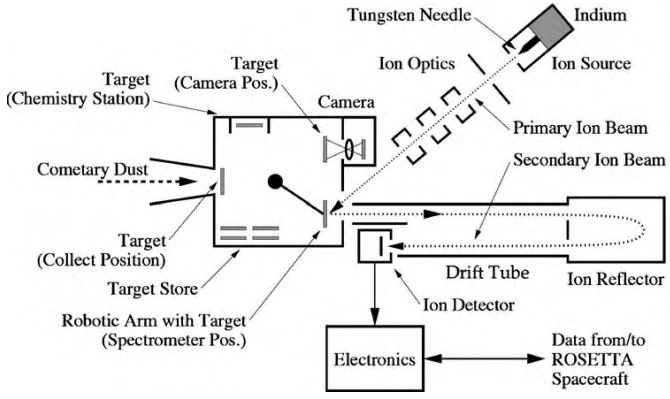

Figure 1. Schematic view of the COSIMA instrument: (1) Dust is collected on metal targets, (2) Positions of dust grains are determined by microscopic camera, (3) A pulsed primary ion beam sputters and partially ionizes the cometary material, (4) Secondary ions are accelerated by an electric field and travel through the time-of-flight section – a drift tube with an ion reflector, (5) Mass spectra data are extracted from the resulting time-of-flight spectra.

(5) if so, do a detailed analysis in both, the positive and negative, ion modes
(6) perform onboard chemistry
(7) do another detailed analysis in both, the positive and the negative, ion modes
(8) move to the next particle

In favor of clarity, the instrument's function is described in terms of the analysis steps above, while the more elaborate description of the subunits follows. See Figures 1 and 2 to locate the functional elements. As described in more detail below, COSIMA has dedicated surfaces for the collection of cometary dust particles. These

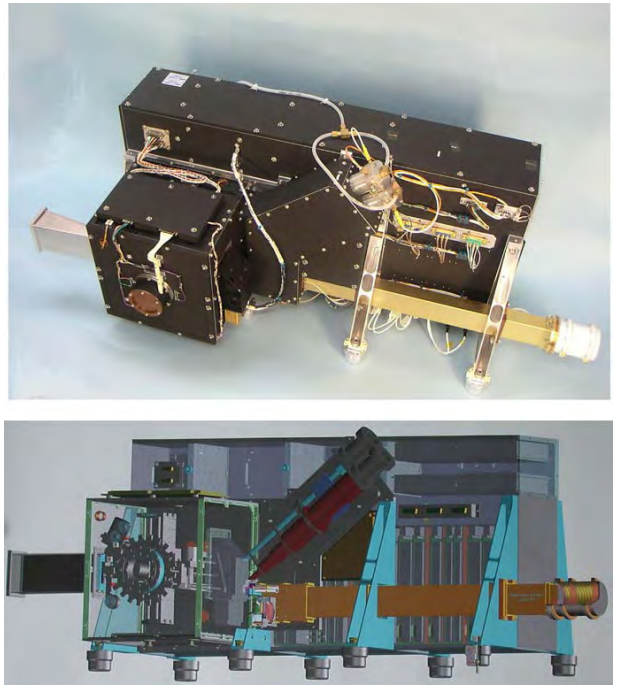

Figure 2. COSIMA instrument (flight model and 3D drawing). The COSIMA flight model consists of dust funnel, target manipulation unit (TMU), primary indium ion sources (PIS) with the primary ion beam subsystem (PIBS), the high-resolution mass spectrometer with ion detector, all mounted onto the COSIMA electronic box.

may impact with their release speed of the order of 100 m/s. Since SIMS is a very sensitive method, the collection surfaces need to be a material, which does not interfere with the type of materials expected in the dust. This excluded any kind of organic material. A study performed by Krueger (1988) identified metal blacks as suitable materials from the structural, and silver, palladium, gold, or platinum from the material properties point of view. The choice has turned out to be very sensible, as these blacks are also efficient pumps for contaminants unavoidable for a space instrument. Since the cometary particles can have a wide range of speeds depending on their size and on the gas activity of the nucleus, each unit of targets has three 1×1 cm^2 collection areas (substrates) and a separate 0.3×3 cm^2 strip as an unexposed reference area. Always an entire target assembly (see Figure 3) is exposed at a time.

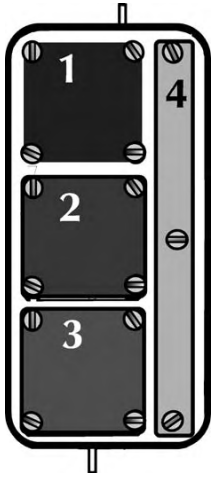

Figure 3. COSIMA Target Assembly. Three individually prepared and selected target plates for dust collection and a reference strip, which will not be exposed to dust make up a target assembly. Each target is numbered individually, and the coordinate system coincides with the S/C coordinate system in the COSISCOPE, ANALYZE, and CLEAN positions (see text). For each collection substrate the coordinate system starts at the lower left corner. Laser generated bright spots of 50 μm diameter (not shown) make it possible for COSISCOPE to identify the individual substrate, to define the position of the substrate in its field-of-view, and to determine of the relative positions of collected dust in the substrate reference frame. Specific dust grains can then be analyzed by moving them under spectrometer's primary beam using the TMU.

Manipulation of the target units is achieved with the Target Manipulator Unit (TMU), which was designed and added at a late state when a contributed system by our Italian partners did not materialize. As built by MPE and Cemec (Schwab, 1998) it is a semi-autonomous system, which provides access to the positions 'COLLECT', 'STORE', 'COSISCOPE', 'CLEAN', 'ANALYZE', and 'CHEMISTRY' upon simple (internal) commands.

The first inspection of the sample is done by COSISCOPE, a COSIMA internal camera. One of the 3 collection substrates is checked at a time. Light beams from two sets of LEDs left and right of the sample illuminate it. The images are checked for features like, e.g., shadows and interpreted as sites, the coordinates of which are transferred to the main instrument.

The next step is the decision if the target, or a part of it, needs cleaning by ion-sputtering. If so, it is moved in front of a DC ion beam at the 'CLEAN' position, else, it will be presented to the mass spectrometer. The primary ion source (PIBS) has a separate beam for cleaning, providing 10–100 μA on a 100 μm diameter spot equivalent to removing some 100 monolayers per second. The next step is to analyze a site, i.e., to take a mass spectrum. The target is put in front of the extraction lens of the spectrometer, with the selected site within 100 μm of the lens' center. Operational values are taken from the initial adjustment of the primary ion source. Trains of ion packages of 3 ns width at a rate of 1 kHz release secondary ions into the spectrometer. Its second order focusing design provides an inherent mass resolution of $m/\Delta m$ @ 50% peak height above 3000 (i.e., with 0-time spread of the primary beam). A typical primary ion package has 500 ions and releases 1 to 10 non-hydrogen secondary ions, depending on the material irradiated.

All secondary ions of the appropriate polarity are picked up by the electric field in front of the ion extraction lens. This field of about 1 kV/mm minimizes initial time-of-flight differences due to the acceleration process, which cannot be compensated later. The lens field also guides the ions into the time-of-flight section of the instrument reducing their drift energy to nominally 1 keV and focuses their arrival location on the detector into a 15 mm diameter area. As the ions travel down the drift tube, they pass the secondary deflection plates, which are needed to reposition the secondary ion package, should the analysis site be off center. It is also used to compensate the small changes in ion trajectories between the positive and negative secondary ions modes. At the end of the drift tube the ions enter the ion reflector, the device, which improves the intrinsic mass resolution of the spectrometer part by more than a factor of 100 (Mamyrin *et al.*, 1973). State-of-the-art would be a grid-less reflector (which we have studied) but which is very sensitive to the position of the ion entry and thereby on the perfect function of the secondary deflection plates. The actual design we have chosen uses several grids separating the drift section, the retarding section, and the reflecting section. As the ions enter under a small angle of 1°, they exit at a slightly different location but again into the same physical drift tube. At the end of this tube the ions hit the ion detector. The position and the orientation of the detector were carefully chosen,

as both are part of the system, which determines the mass resolution of COSIMA. Since we expect some of the organic ions to have high masses (well above 350 amu) the detector can be biased for a post-acceleration of the secondary ions by almost 9 kV (with the appropriate polarity for the respective ion type). The active element is a microsphere plate, which for its thickness of 1.4 mm provides a gain value well above 10^7. In order to decouple the signal from its high electrical potential (up to 14 kV in the case of negative secondary ions), the microsphere output is directed to an anode, which is one side of a capacitor, while the other side is connected to the input of a pulse amplifier. All arrival times and shot numbers are stored at 2 ns resolution. The differences between the modes for positive or negative secondary ions are reflected in the respective operational voltages. Besides the reversal of polarity, minor adjustments need to be applied to the voltages for the deflection plates of both, the primary beam and the secondary ion path. The safe switch-over from one ion type to the other will take a couple of minutes to allow the high voltages to decay, before the grounding of the power supplies is switched.

A total of 1000 (adjustable) secondary ion arrival times are accumulated into the time-bins of a time-of-flight spectrum. While the measurement is continued, a peak list is created from this set of data, which is then further pre-evaluated using mathematical tools like classifiers developed for chemometrics (see below). This procedure yields criteria, which characterize the site under analysis. Should these criteria suggest a high similarity with another site already analyzed, then this fact is documented and the instrument proceeds to the next site on the list. The degree of autonomy is assigned to the instrument by telecommand from ground. This type of operation is necessary, as the reaction time for normal operational procedures via ground loop may well be of the order of a week, while the efficient use of the resources of the instrument rather requires a full-time operation.

The individual, functional elements of COSIMA mentioned in this chapter are described in more detail below.

3. The Functional Elements of COSIMA

3.1. The Mechanical and Electrical Layout

The properties of a time-of-flight mass spectrometer are determined by its mechanical elements and their respective electrical potentials. The mechanical centerpiece is the target substrate, upon which the cometary dust particles are collected. For the analysis, their surface has to point towards the spectrometer. Dust cannot be collected in the same position even with the same orientation: the targets have to be mechanically moved. In addition, different target materials and/or surface configurations are needed. Therefore several target units are made available. These few requirements together necessitate that the target surfaces be best kept at 0 V instrument potential, which then is the potential from which the secondary ions start.

To produce these secondary ions, the primary ion source must point its beam to a spot in front of the secondary ion extraction lens. In order to minimize interference between the beams, the primary ion source is usually inclined. An angle of $45^\circ \pm 15^\circ$ in elevation is usually acceptable. In azimuth the angle is free to be chosen. Larger values lead to increasingly oblique impacts of the primary ions, increasing not only the spot size, but also the ion arrival time distribution and hence, the secondary ion emission time distribution. Smaller angles make the interface more complicated and increase the length necessary to assemble all the elements of the primary beam system. For COSIMA, an angle of 50° above the target plane (i.e., 40° from the target normal) was chosen.

The extraction lens is usually arranged co-axially with the center target normal. For COSIMA, it is tilted by 1° towards the ion detector to provide the necessary offset for the secondary ions to reach the ion detector (rather than to fly back to the target). The rest of the mechanical elements of the mass spectrometer are the first (or inbound) drift tube, the reflector, the second (or outbound) drift tube, and the ion detector. For COSIMA these elements are essentially placed again co-axially with the center target normal with the following modification: the detector is moved away from the target center to the degree that it can be placed entirely besides the target. The reflector is placed such that its center axis lies in the plane of the target normal and the detector normal at mid-angle, as shown schematically in Figure 1. The inbound and outbound drift tubes are combined into one, which is wide enough to cover the natural expansion of the secondary ion beam as well as the displacement between the target and the ion detector.

The electrical layout is straightforward: The target is at 0 V instrument potential, and by the secondary ion extraction lens, the ions are accelerated to the drift potential of $-/+1$ kV for positive or negative ions, respectively. The reflector, first introduced by Mamyrin *et al.*, (1973), has essentially the task to compensate for differences in total flight time, which occur as the ions start with different initial energies. Ions with higher kinetic energy penetrate deeper into the reflecting field and use more time to return from it. The best compensation occurs, when the ions spend about the same time in the reflector as they spend in the drift tubes. As the reflector is mechanically much shorter, it also helps to reduce the overall instrument length. For COSIMA, we chose a two stage reflector with a first retarding section, where the ions loose about 80% of their energy, and a second, reflecting section, where their direction of motion is reversed. The end of this section is formed by a grid, which should help to reduce background signals, caused by, e.g., neutral decay products from the secondary ions.

3.2. The Target Manipulator Unit

When COSIMA was proposed for ROSETTA, it included a dust collector subsystem, the design of which was inherited from the CoMA/CRAF instrument. Later,

the idea of a dedicated COSIMA target manipulation was followed up, relying on a higher degree of integration into COSIMA's mechanical and electronical subunits. This opened the chance for a redesign (Schwab 1998).

As will be described below, three individual target substrates (designed to collect dust) and a reference strip (not to be exposed to dust) are screwed down on a target holder and together make up the target assembly, which is to be manipulated. The new feature is that the target assemblies can now be moved individually, which includes the fact that they are released, once they are at their destination. This is achieved by the use of a grasping device working like a pair of tongs (see Figure 4). They are open when approaching the target assembly, and only, when they are tight

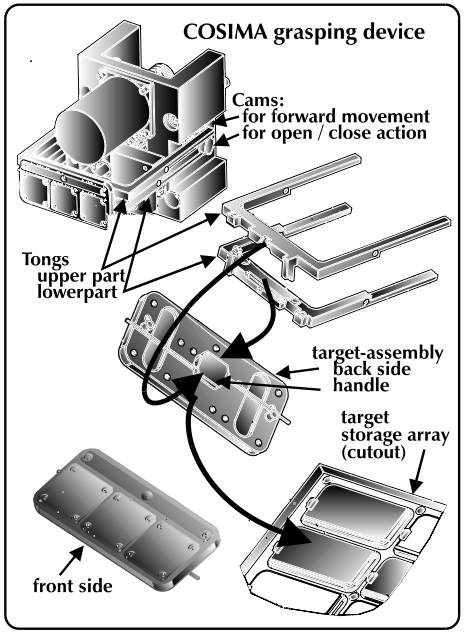

Figure 4. COSIMA Grasping Device. The COSIMA grasping device handles the internal transport of targets between individual stations. A single motor actuates the forward movement, the pick-up, deposit action and withdrawal with the help of two customized cams, controlling and synchronizing the movement. The device is mounted on an x-y-table (not shown).

enough not to let the object loose, they push on a spring, which latches the target assembly to the momentary position. When the object is firmly held, it is removed far enough to allow lateral and rotational motion. The motion in the forward and backward direction is actuated by a stepper motor, the opening and closing of the tongs is synchronized by a pair of cams. These cams have a specially designed shape. For one cam, the radial distance to its axis directly corresponds to the forward movement of the tongs. The other cam is fixed to the first, and its shape directly controls the opening action. The entire cycle of forward movement, opening/closing the tongs, and moving back takes less than one rotation of the axis. The sense of the axis rotation determines if a target assembly is picked up or deposited.

The housing of the Target Manipulator Unit is a rectangular box. In the center of the sides 1 and 6 (numbered as the sides of a dice) is a rotation axis, which carries an x-y table with the grasping device on top. In this way, targets can be reached on all remaining surfaces 2–5. These have the exact distance for the grasping device to properly pick up and place target assemblies. Let surface '2' be at the 'forward' end of COSIMA, where the position for the dust collection is, then the COSISCOPE, ANALYZE, and CLEAN positions are on surface '5'. Surface '3' is on the bottom of the box and carries the target storage area, where 24 target assemblies are stored in 6 rows of 4 positions each. This location is facing a radiator on the spacecraft skin, which allows the targets to be kept below about 30 °C even if the spacecraft interior is at 50 °C. On surface '4' is the chemistry station and on surface '1' is a docking structure, to which the grasping device will be locked during launch.

3.2.1. *Collection Substrates*

To meet its scientific requirements, COSIMA needs cometary dust particles for the analysis. Such dust particles are emitted by the cometary nucleus when its activity sets on under the influence of the solar heat input by radiation. The activity level of the comet depends on its position in the orbit, especially on the distance from the sun. Dust particles in the size range of 10 μm and above are expected to reach speeds of up to a few 100 m/s. To collect these particles, appropriate surfaces were designed. Within COSIMA the dust particles are trapped in metal black layers of a few 10 μm thickness, placed on top of square shaped 1×1 cm^2 metal plates of 0.5 mm thickness. Most of the substrates are made of gold and silver blacks, formed by evaporation of Au or Ag in a low pressure argon atmosphere. The Ar-atoms trigger the formation of nanometer-sized condensate particles, which deposit on the cold surface of the plates. They form a layer of loosely packed particles, sticking together and to the substrate by adhesive forces. The layer is thermally stable up to about 200°C. At higher temperatures, it collapses in a "sintering-like" process to a more dense structure, which looses its dark blackness to grey, but not its dust collection capability. The final configuration of this variant will be a multilayer structure, consisting of two "sintered" layers and one deep black on top of it, thus combining mechanical stability and blackness. A SEM image of an Ag-black layer is shown in Figure 5. Tests with SIMS showed that such blacks are not only optically

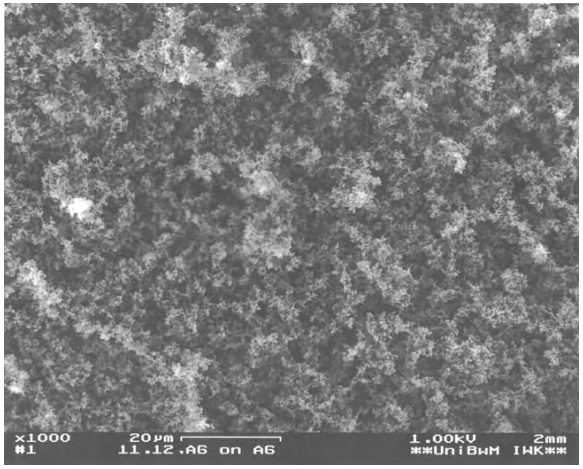

Figure 5. SEM image of an Ag-black layer. The COSIMA dust collection substrates are very evenly layers of Ag-black, which are soft enough to decelerate cometary dust and to keep it on their surface.

black, but also in the ion image, since the loose structure allows fewer secondary ions to reach the spectrometer.

Besides vapor deposited Au and Ag layers, some of the collection substrates are made from Pt and a few from Pd. Those types are manufactured by HERAEUS Noble Metal Techniques GmbH in Hanau/Germany, meeting the special needs for COSIMA. There are two types of platinum black substrates. One is made by anodic electro-deposition with subsequent sintering, which is needed for good mechanical contact to the backing as well as inner cohesion. As a result of the sintering process, the albedo of that substrate is not very low. The other is made by a proprietary method (patent pending) and produces a very black substrate with good mechanical connection to the backing. In either case, no residues from the production process were found by TOF-SIMS analysis. This was established after a long development procedure. Another substrate was palladium black on palladium foils, the production of which is difficult, due to the ultrahigh hydrogen pressure built up within the palladium bulk by the electro-deposition process. The mechanical properties of those three blacks differ from each other. Moreover, they are all harder than the vapor deposited blacks from gold or silver. A SEM picture of such a black is shown in Figure 6. It has a cauliflower-like structure and is mechanically much more firm

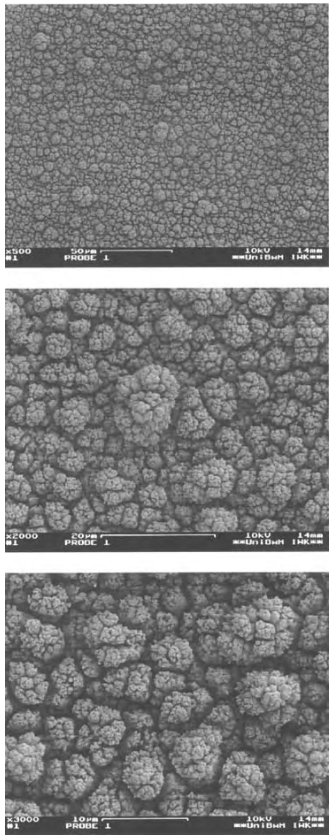

Figure 6. SEM picture of a liquid-deposited black. These collection substrates are thicker than those made by vapor deposition, and can be made from different materials. They usually show a 'cauliflower' like surface structure, in which smaller grains could be trapped and escape analysis.

than the vapor deposited blacks, which are thought to be used to trap very soft dust particles.

All blacks are marked directly after production at defined positions by pulse-laser generated test spots of about 50 μm size. These spots can be recognized optically

(COSISCOPE) and by SIMS as well, thus defining a precise local coordinate system for common reference. Moreover, they serve for in-flight tests, such as adjustment of the ion beam's focusing.

Collection efficiency was tested by a gasdynamic accelerator for dust particles. It consists of a small tube (2 mm diameter) filled with argon or xenon as well as a very small amount of dust. The fast opening of a valve to an attached vacuum vessel generates a rarefaction wave, which accelerates the gas and the dust to the vessel and to the target. Velocities were checked by Laser Doppler Anemometry to be in the 50–150 m/s range. A SIMS image of some SiO_2 particles, sitting on a vapor deposited gold black are shown in Figure 7 (the picture shows the spatial distribution of the Si-line).

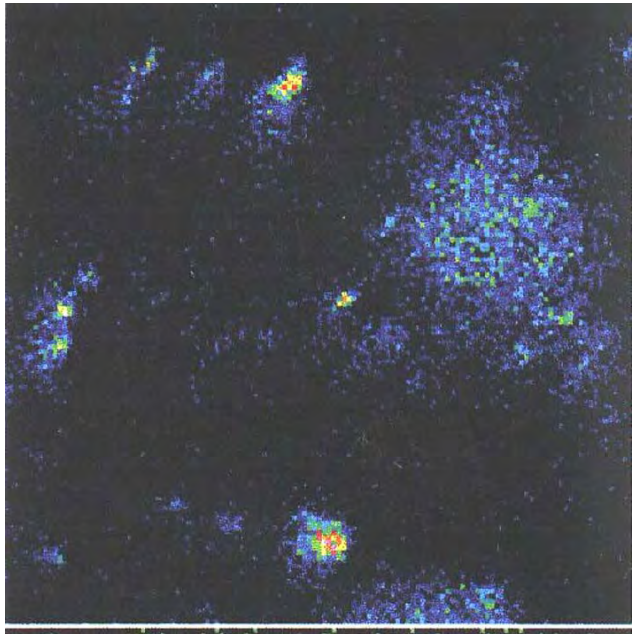

Figure 7. SIMS image of some SiO_2 particles, Si^+ spatial distribution. When particles are collected on the substrates, they can be found by COSIMA's primary ion source looking for indicative mass lines. Here is an example for silicate particles, detected by the Si^+-intensity-distribution.

3.2.2. *The Chemistry Station*

A 'chemistry station' is located opposite to the storage system. It is a heating place for one target assembly. When TOF-SIMS mass spectra have been taken from cometary dust collected upon a target assembly, there may be some open questions concerning the chemistry. One concerns the distribution of molecular weights of certain organic species of the dust. Heating the specimen causes the smaller molecules to evaporate faster according to their specific heat of evaporation. This depends not only on the molecular weights but also on the distribution of polar groups in the molecules (Krueger *et al.*, 1991). Another question is, whether oxygen found in the organic material is present as OH-groups (as in sugars), which would eliminate water by heating. To provide clues to answering those questions, the samples need to be heated to about 100–140 °C.

3.3. COSISCOPE

During the early close-encounter-phase of the mission, the number of collected grains is likely to be as low as 10 per day on the exposed target. The effective area over which the beam can be deflected while retaining adequate secondary ion collecting efficiencies is 200×200 μm^2, so that the complete exploration of the 10×10 mm^2 target by the primary ion beam would require 2500 displacements of the target and would consume a large percentage of the beam time. The target imaging device, COSISCOPE, will image an entire 14×14 mm^2 area holding one 10×10 mm^2 target with a magnifying power of 1 on its 1024×1024 pixels, which gives a pixel resolution of 13.7 μm. Each target will be imaged before and after exposure and will provide a list of coordinate positions where collected grains are most likely to be found. In addition, COSISCOPE is useful to monitor the evolution in time of targets coated with very fluffy material and to verify the accuracy and reproducibility of the target positioning by the Target Manipulator Unit.

COSISCOPE is contributed by the group at IAS, Orsay, France, and uses copies of the units developed for the ÇIVA camera system onboard the ROSETTA lander to save both, mass and volume. The CCD is part of a three-dimensionally integrated 'camera-head'. The processor unit is built around a DSP-21020 operating at 20 MHz with 6 Mbytes of RAM and two FPGAs for the interfaces. The command and data interface with the COSIMA CDPU is a pair of RS-422 serial lines, which can operate at up to 10 MHz. The total mass is 460 g including the mechanical structure and the optical elements.

Particle detection on metal black is difficult for two reasons: First, the albedo of the target surface is low, as is the expected albedo of a major fraction of cometary grains. Second, the targets have a surface roughness at scales comparable to the COSISCOPE resolution. Illumination by a red LED (650 nm) at a low incidence (5° to 10° above the surface) has proven to be effective to detect surface inhomogeneities. A second image, obtained by a LED from the opposite direction, improves the

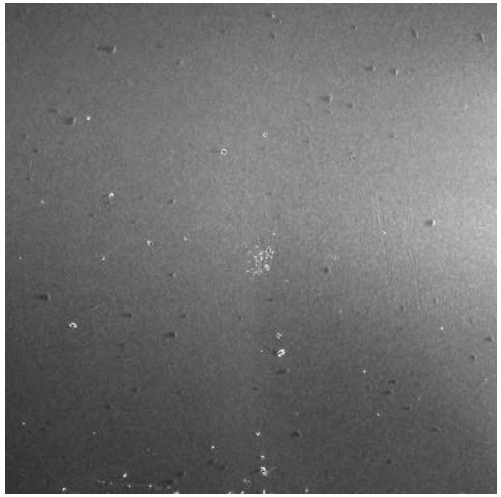

Figure 8. COSISCOPE image of a 2×2 mm^2 region on a collector substrate exposed to silicate dust. The low incidence light comes from the right. A cluster of silicate particles is visible in the center. Other dark 'low velocity' grains stick on the surface with long shadows extending to the left. The bright spots are scratches or blank metal particles from the (early) production process. The noise level from the substrate is acceptable even under shallow illumination.

detection quality. The grain detection algorithm takes advantage of the higher bidirectional reflection coefficient of the grain's side facing the LED when compared to the surface (even with the same low albedo), which provides a contrast with the shadow of the grain if it sticks out of the surface (see Figure 8 for an example). This approach is not so efficient for very fluffy aggregates, which are spread out over several pixels, but such features are still expected to provide a signature by increasing the local roughness. The output of the process is a series of messages to the COSIMA main processor with a list of features, each with its coordinates, size, and a quality index (based on a combination of criteria such as the observed contrast and the correlated detection with both LEDs). This list of features can be used on board and on the ground to define regions of interest to be analyzed.

The coordinates are calculated with reference to two pairs of 50μm sized reference dots at a distance of 5 mm on the calibration strip of the target holding assembly where the metal underneath the black has been exposed using laser blow-off (Figure 9). This allows COSISCOPE to monitor target positioning by the TMU

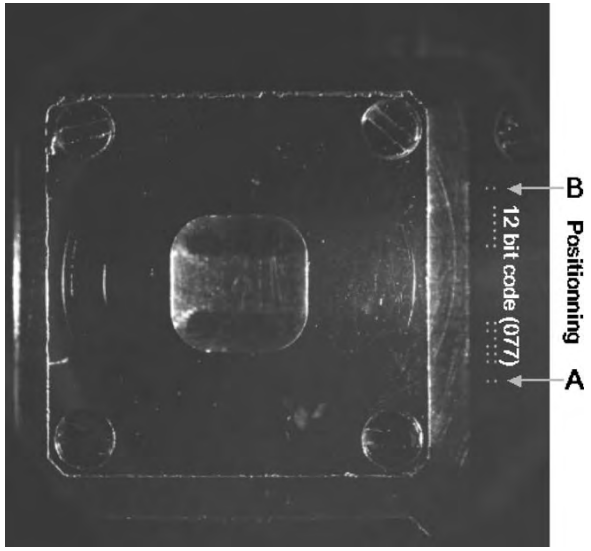

Figure 9. COSISCOPE image of a collector substrate obtained during the in-flight commissioning phase in September 2004. Two pairs of 50 μm dots with a 200 μm interval (A and B) on the calibration strip of the target assembly are separated by 5 mm. They are used by COSISCOPE to monitor the position of the target assembly in its field-of-view. After defining the target reference frame from the positioning pairs of dots, COSISCOPE checks the two groups of dots, which defines a 12 bits code (2 dots: 1; 1 dot: 0), here '000011101111' from top to bottom, or '077' in hexadecimal format.

with an accuracy of less than 10μm by comparing the nominal and observed position and angular orientation of the target in the COSISCOPE field of view. A 12 bit code constituted of two sets of six bits makes it possible for COSISCOPE to identify the target. The positioning and labeling information is sent to the ground together with the feature list, whether or not an image is transmitted, to monitor TMU operations.

The full COSISCOPE power cycle for one operation takes less than 20 s with a mean power of 4 W. A specific COSISCOPE calibration mode allows transmission of the actual image, compressed by a factor of 10, using a wavelet transform with tree-coding algorithm, as well as the associated list of features. COSISCOPE calibration sequences will be performed during in-flight instrument checkouts, at the beginning of the main encounter phase, and then upon request, e.g., every few

weeks to select the COSISCOPE operating parameters for the following measurement slot.

3.4. The Primary Ion Beam Subsystem (PIBS)

3.4.1. *Functional and Performance Requirements*

The PIBS, contributed by the group at the LPCE, Orléans, France, needs to perform to the following specifications to enable COSIMA to achieve its scientific objectives:

It has to provide a pulsed and focused beam of ions with the following properties:

- $^{115}In^{+}$ ions,
- at 8 keV,
- about 1000 ions per pulse,
- within an elliptical focal spot of less than 20 μm major axis,
- within 3 ns,
- to a location within 100 μm of the optical axis of the COSIMA extraction lens,
- at a repetition rate of up to 2000 ion pulses per second.

The ion emitters are provided by the Austrian Research Center in Seibersdorf, Austria, while the IWF in Graz, Austria, provides the emitter power supplies and control electronics.

3.4.2. *General Concept*

To achieve the above specifications, PIBS has a sophisticated ion optical concept, using fairly simple elements to keep the mechanics simple. It is shown in Figure 10 as schematic and in Figure 11 as picture. The ions are generated in one of two liquid metal ion sources, filled with isotopically clean ^{115}In (>99.9%) and accelerated into the ion optics by the same electrical field. Two separate emitters are implemented for a limited redundancy. During normal operation, one emitter is used for sample analysis, the other for target cleaning (by ion sputtering). Only one emitter can be operated at a time. Should one of the emitters fail or exhaust its indium reservoir, the backup mode can be chosen, in which the electrostatic switch allows transfer of the beam of either emitter to the respective other side.

On the analyze channel, a first lens LA1 (or LC1 in the backup configuration) gives an image of the emitter in the inlet plane of the chopper, then a second lens LA2 builds the final image on the target. The chopper consists of two pairs of short blades generating a transverse electrostatic field on the beam path between them in order to divert the beam to a screen. For analysis, the field is cut for 50 ns, and a beam packet is generated on the normal beam path. This packet is then compressed by a buncher into the short pulses required on the target. The actual buncher requires three stages due to the voltage limits imposed by the available electronic flight parts. In each buncher stage, a pulsed longitudinal electrostatic field is applied between

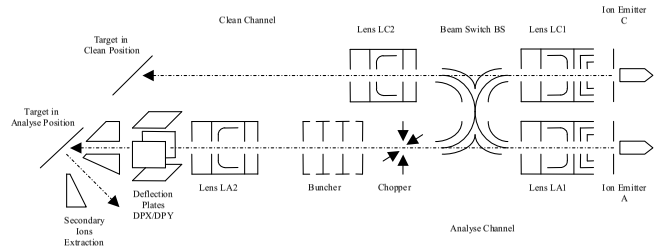

Figure 10. Schematic sketch of the Primary Ion Beam Subsystem design: Ions from two emitters at the right side can reach either of two positions: 'Analyze' or 'Clean', depending of the 'Beam Switch' in the center. The focusing elements are electrically shared, as only one beam can be active at any time. 'Chopper' and 'Bunchers' provide the pulsed beam for analysis, the deflection plates are used for steering the beam spot on the target.

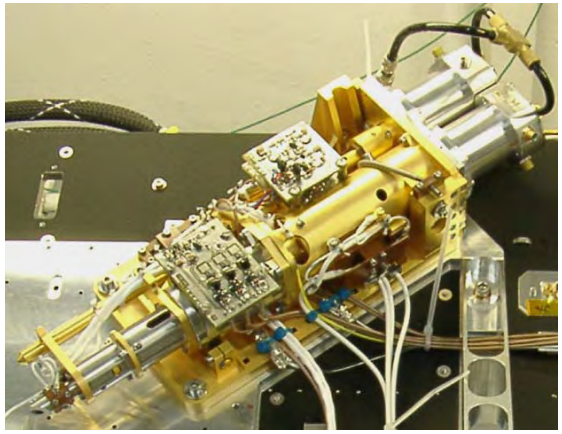

Figure 11. The COSIMA Primary Ion Beam Subsystem during integration at vH&S Schwetzingen, Germany (Photo vH&S): Note the amount of wiring to make the unit operational and yet keep it free from contamination.

two parallel electrodes at the time when the ion packet is completely between them. Typically, a potential of +250 V is applied to the upstream plate, once the ion packet has passed it. As a result, ions at the trailing end of the packet gain additional energy and ideally meet ions of the leading edge exactly at the target. Two orthogonal sets

of two parallel deflection plates are used to control the position of the beam on the target in both, horizontal and vertical directions. The horizontal deflection plane has been chosen to coincide with the deflection plane for the corresponding system for the secondary ions.

The other ion beam used for cleaning has a first lens LC1 (or LA1 in the backup configuration), which gives an image used by LC2 to build the final image on the target in the clean position. The ion beam for cleaning is not pulsed. This fact allows also a rapid sputtering of the sample (at about 1 monolayer/s) in order to make a measurement at a different depth (accepting the degree to which the sputtering does modify the sample).

The lenses LA1, LC1, LA2, and LC2 are three-electrode electrostatic lenses in the Einzel configuration. Their structure is chosen to minimize the spherical and chromatic aberrations. This is especially important for lenses LA1, LC1, and LA2, which are used in the analysis process. Since only one beam is active at any time, the lenses of groups '1' and '2' are connected in parallel.

3.5. The Spectrometer Ion Optics

The combination of SIMS and TOF methods places particular constraints and requirements on the ion optical system:

1. It is important to collect for analysis the maximum fraction of secondary sample ions produced by the primary ion impacts, which is normally achieved by using an electrostatic lens.
2. It is necessary to have low geometrical aberrations in the focusing lens so that the accelerated ions all hit the detector after passing through the drift region (small geometric aberration).
3. It is necessary that the ion optics does not add time dispersion to the ions' flight time due to the different electrical fields along the differing paths of the secondary ions during acceleration and focusing (small time dispersion).
4. The ion optical system must neutralize the effects of the initial energy distribution of the secondary ions, which adds time dispersion to the flight time and thereby limits the mass resolution (time compensation for initial energy).
5. As many of the ions as possible that enter the system should arrive at the detector (high transmission).

Design and optimization has been done by the CoI, N.G. Utterback, Santa Barbara, USA, using the SIMION software package (Dahl, 1997). The design was driven by the rule that as few elements as possible would be required. The extraction lens has an internal field stop and images the 100 μm source area onto the 30mm detector. No further lenses are implemented. The following sections will describe the COSIMA ion optical system as to how and how well these requirements have been met.

3.5.1. *Secondary Ion Extraction and Focusing Lens Elements*

The dust samples (cometary dust particles) are collected on electrically conducting surfaces. During analysis, as shown schematically in Figure 1, one of these targets with the dust sample on its surface is placed 3 mm from the extractor electrode entrance with an aperture of 2 mm in diameter. The target is maintained at ground (0 V) potential. The extractor electrode is maintained at -3000 or $+3000$ V (for positive or negative ions, respectively). The remainder of the ion optical system is biased to -1000 V or $+1000$ V to maintain an ion kinetic energy of 1000 eV in the drift region. The focusing lens elements follow the extraction aperture and consist of apertures producing two highly non-uniform, but radially-symmetric electric field regions. Between these regions is an aperture that limits the diameter of the beam at that point and has the effect of eliminating ions that have too high initial energies and angles. If not eliminated, these ions would follow large off-axis trajectories that would cause unacceptable geometric aberrations and time dispersion. The length of the lens elements from extractor surface to lens exit aperture is 15 mm. Immediately following the lens components is a deflection region with 2 sets of parallel plates, 25 mm long and set perpendicular, that are used to deflect the beam to compensate when the primary ion beam is scanning at an off-axis position. Without this compensating deflection, the lens magnification of the target region (lens object) would cause the secondary ion beam to miss the detector. The first drift region measures 540 mm from the lens exit aperture to the entrance grid of the ion reflector.

3.5.2. *Ion Reflector for the Compensation of Initial Ion Energies*

The distribution of the initial energy of the sample ions, resulting from the formation mechanism, causes ions of the same mass to arrive at a given distance at different times. This puts a limit on the mass resolution of TOF instruments. Without initial ion energy compensation, COSIMA would be limited to a mass resolution $m/\Delta m$ well below 100. Since the investigation needs a resolution $m/\Delta m$ of several thousands, initial ion energy compensation must be provided. Mamyrin *et al.*, (1973) have shown that a two stage reflectron has the capacity to achieve this. From their analysis it follows that the ion reflector must have two sections with different electric fields, one to retard the ions and a second one for the actual reflection. This allows compensation of the effects of the initial energy up to the second order in dE/E (initial energy/given energy). However, the appropriate drift path length, the retarding region path length, and electric field strengths depend on the magnitude of dE. Hence, the effectiveness of the initial ion energy compensation will depend on the initial ion energy distribution, and the parameters must be set for the best compromise for a given initial ion energy distribution. The COSIMA 2-stage reflector consists of the interior of a cylindrical region, 50 mm in diameter and 70 mm long. Three planar grids with 91% transmission and the solid end cap define the two electric field regions. The entrance grid defines the end of the first drift region. 20 mm beyond the entrance grid, the second 'retarding' grid defines the end of the

retarding region and the beginning of the reflection region. The third 'reflecting' grid another 40 mm beyond defines the end of the reflection region. The end cap 10 mm beyond is biased with respect to the third grid in order to trap any ions and electrons produced by impact of neutrals on the end cap. The uniform electric fields are produced by 14 cylindrical conducting rings, which are plated onto the inner surface of the cylindrical region. In the first deceleration region, the ions are slowed down from a kinetic energy of 1000 eV to 200 eV. A potential difference of about 290 V is placed between the grids defining the reflection region. This potential difference is varied to 'tune' the initial ion energy compensation so that ions of a given mass arrive at the detector with the minimum time dispersion possible. All these voltages can be modified by telecommand and an internal optimization routine, just to accommodate unexpected effects during flight.

After the reflected secondary ions exit the reflector, they travel in a field-free region for 510 mm before passing through the entrance grid of the ion detector. Discussions of the ion detector and electronic amplifiers and counters are covered elsewhere (see 3.6).

3.5.3. *Secondary Ion Optical System Design Properties and Results*

The design properties and results presented here are based on computer simulations, which are in turn based as closely as possible on the flight mechanical and electrical configurations, and the expected parameters for the physical processes involved. The computer simulation program was SIMION by Dahl (1997). The largest unknown in the simulations is the initial energy distribution of the secondary ions and their initial emission angular distributions. A further parameter, which is likely to be important, but is very hard to simulate accurately, is the effect of sample (collected dust particle) size and shape as it resides on the target surface. The simulation assumes that target and sample are co-planar and, hence, yields the best case in terms of time resolution. The actual finite sample size may degrade the time resolution, but only laboratory investigations can then show how and by how much. For the results presented here, a Maxwell-Boltzmann energy distribution with kT of 10 eV was assumed for the secondary ion initial energy distribution. A $\cos\vartheta$ angular distribution was assumed for the secondary ion emission angles. Other values for kT were also tried, as well as comparing a v^4-angular distribution, with results not markedly different in terms of COSIMA requirements. The primary beam is taken to have a Gaussian radial distribution with $\sigma = 10$ μm and strikes the target at 40°. Here the actual laboratory measurements and the SIMION results compare very well. The transmission of the secondary ion optical system for the flight configuration (limiting aperture in focus lens of 1.2 mm diameter) is found to be 21%. Transmission is defined as the number of secondary ions that reach the detector divided by the number of secondary ions produced at the target. It may be noted that 4 passages through 91% transmission grids already limits the transmission to 68%. The remainder of the ions lost strike the lens electrode outside the limiting aperture. The lens focusing quality is such that all ions strike the detector

within a circle with a diameter of 15 mm, which is well within the effective area of the detector. This includes the slight scattering due to the high field strengths near the grid wires, which is accurately simulated. The distribution of flight times for 25000 ions of mass 100 is approximately a Gaussian with σ of 1 ns, equivalent to 2.2 ns FWHM (full width at half maximum). There were no flight times outside a window of 5.5 ns. The distribution was centered at 31.037 microseconds. This corresponds to a value for $t/\Delta t$ of 14000, which yields a mass resolution $m/\Delta m$ of 7000 based on the FWHM criterion (it should be noted that $m/\Delta m$ is one half of the $t/\Delta t$ value). This flight time dispersion is due to the remaining uncompensated effects of the initial secondary ion energy as well as the different paths traversed through the high electric fields in the focusing lens. The latter effect is controlled by the limiting aperture within the focusing lens. In order to gain maximum transmission, the limiting aperture is chosen as large as possible without introducing unacceptable time dispersion. The flight time and spatial distributions widen slightly and the transmission decreases slightly when the primary ion beam is scanned off the lens axis at the target, but the effects are within about 15% for primary beam scanning up to 100 microns off the lens axis. It needs to be noted, that the mass resolution $m/\Delta m$ of 7000 is for the ion optical system only, and assumes that all secondary ions start at the same time (effectively achieved for high masses >3000). In reality, the primary ion pulses will have a time dependence which is roughly Gaussian with FWHM of order 3 ns. At mass 100 the actual $m/\Delta m$ is about 2000.

3.6. Ion Detection

Once the ions reach the end of the outgoing drift tube, they need to be detected with high time resolution. For this purpose a detection unit with high gain for single ion detection, a time resolution of about 1 ns, and an active area of about 5 cm^2 is required. Proven solutions are built on microchannel plates (MCP) or more recently on microsphere plates (MSP). We decided to use a MSP from EMUL because of its greater mechanical robustness and its higher gain, which leads to a single element solution with a 1.4 mm plate. The detector design is shown in Figure 12. Its elements are from top to bottom: the entrance grid at drift-tube potential, the intermediate grid to apply the post acceleration potential, the microsphere plate, the anode plate with capacitive coupling to the board with the trigger electronics. As the COSIMA target is always at ground potential, the potentials within the ion detector also refer to ground. Their values differ for positive or negative ions, they are not symmetrical to ground, and range up to more than 12 kV (see Figure 12 for details). This demonstrates the insulation needs associated especially with the negative ion case, which had to be solved within the very small volume available. The capacitive coupling of the detector output signal is an elegant and effective way to keep the associated detector electronics at ground potential. It actually represents two high quality coupling capacitors: C1 for the coupling to the trigger circuit and C2 for

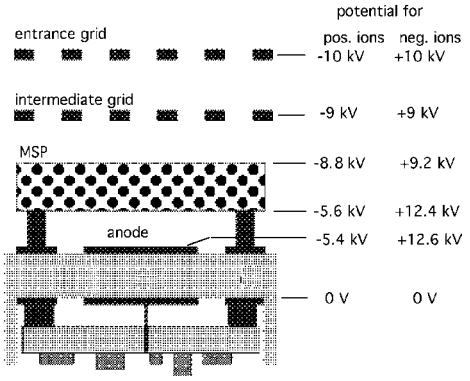

Figure 12. The COSIMA ion detector unit. The COSIMA ion detector is a complex arrangement with many grids and different high voltage values within a small space. An amplifier is integrated for low noise and high signal.

the signal return path. Due to the low parasitic inductance of the design, the fast output pulses are without significant ringing. The typical pulse height distribution of this detector is well determined and shows a typical gain of 10^7 for a MSP supply voltage of 3200 V. The shape of a typical MSP output pulse is shown in Figure 13. It was measured with an oscilloscope of 1 GHz bandwidth. The FWHM of about 1 ns and the signal rise time of less than 0.8 ns are quite adequate for COSIMA. The MSP output is coupled directly into the detector electronics through the capacitor, which also provides high voltage insulation. The electronics has to discriminate the output signals above a given threshold against noise background below this threshold. The pulse height distribution shows a distinct level for this threshold. Any change due to, e.g., aging of the MSP can be adjusted by changing the operational voltage applied to the MSP. The electronic pulses need to be standardized in both, amplitude and pulse width. As the rise time of the MSP pulse is less than 1 ns, a leading edge threshold trigger with a fixed threshold is sufficient to process the signal. The maximum principal time error caused by different pulse amplitudes is then also less than 1 ns. For a supply voltage of 3.2 kV a threshold charge of 2 to 5 pC is appropriate to separate ion signals from noise. For pulses with a width of about 1 ns, this results in peak currents in the range 2 to 5 mA. The direct coupling of the electronics avoids signal ringing due to, e.g., unmatched lines. The output feeds a 50 Ω terminated coaxial line with 200 mV amplitude and 5 ns pulse width. The length can be chosen within reasonable limits. The circuit is supplied with a single supply voltage of nominally -5 V and a worst-case power consumption of $P_{\max} = 75$ mW. Laboratory tests suggest that changes of the supply voltages

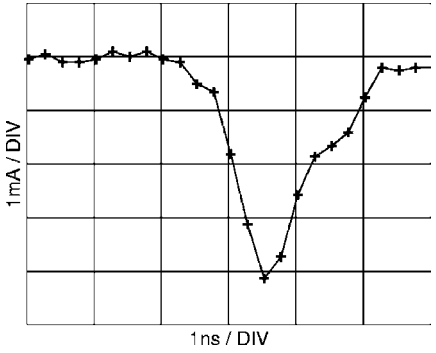

Figure 13. MSP output pulse. A typical output pulse from the microsphere plate shows the good signal quality and trigger properties achieved. The pulses are fast enough for the COSIMA timing requirements.

could be compensated with an adjustment of the MSP gain through its operational voltage, while temperature changes of several 10 K do not matter.

3.7. Electronics

The COSIMA electronics contains all necessary elements to control and operate COSIMA. It is also home to those components contributed by other groups. All electronics are housed in the electronics box with the exception of a few fast switching circuits of PIBS. This is done to prevent any outgassing products to directly interfere with the high sensitivity TOF-SIMS instrument. An overall block diagram of the COSIMA experiment is shown in Figure 14.

3.7.1. *Power Supply Electronics*

The COSIMA experiment operates from a single power line of nominally +28 V from the ROSETTA S/C power subsystem. A low-voltage supply unit within COSIMA, built from a set of switching DC/DC converters and a linear regulator, provides the main low voltages +15 V, +5 V, −5 V, and −15 V for supply of the experiment subsystems. The output power lines for the TMU, the COSISCOPE, and all HVCs are routed through a low-voltage switching unit. This unit allows some power management as the power budget of COSIMA does not allow simultaneous operation or even idling of all of its components. Switching is executed under software control through the experiment processor system. An optoelectronic device senses the power line from the spacecraft. Once it drops below a certain value, an interrupt is generated and the processor system will save the current settings of the

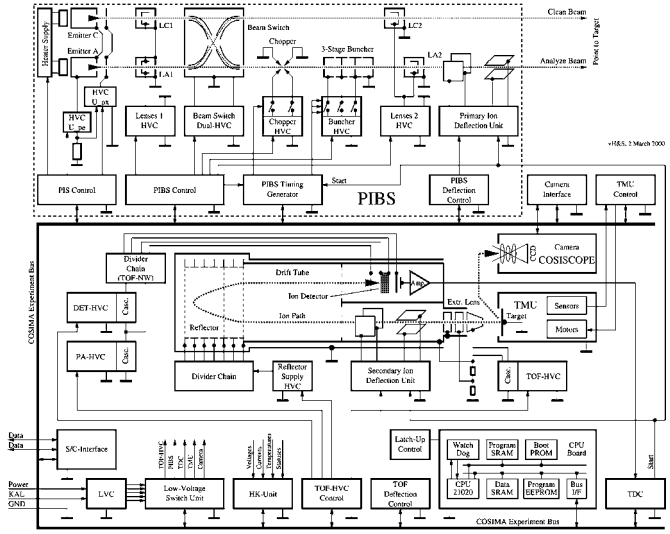

Figure 14. COSIMA block diagram. This full block diagram of COSIMA demonstrates the complexity and the predominance of the high voltage power supplies, which ultimately make COSIMA a very versatile instrument.

COSIMA operational parameters and try to shut down the instrument orderly, as long as secondary power lasts.

The multitude of ion optical elements of COSIMA requires a large number of high voltages, five for PIBS, two for the indium emitter, and five for the spectrometer, with their voltages being individually controlled through the instrument processor. Most of these voltages must be stable to 10^{-4} with respect to temperature and time, and must have a similarly low ripple. Otherwise the spectra would be badly affected and the mass resolution and mass identification would be lost. Therefore, a set of high voltage converters were designed based on a concept used for the CoMA/CRAF and the CIDA/STARDUST instruments. The converters are of 'Royer' type, optimized for precision and low power consumption. They are synchronized to subharmonics of a quartz oscillator frequency, so that their low EMC radiation is within fixed frequency bands specified by the project. Their feedback is achieved by pulse width modulation. The first high voltage stage is built from a step-up transformer, whereas the full voltage is generated through high voltage cascades.

3.7.2. *Time-of-Flight Measurement*

The total flight time, which is the time from the formation to the detection of an individual secondary ion, is the basis for the TOF spectrum, and, hence, the mass spectrum. For COSIMA, the start time for all time measurements is the chopper pulse for the primary ion beam. The time interval due to the flight time of the primary ions from the chopper to the target is an unavoidable offset to the flight time of the secondary ions. Each detector pulse is the 'STOP' signal for the flight time interval of an individual ion. The required mass resolution and total mass range necessitate a time resolution of about 2 ns and a measurement range of 250 μs. An additional requirement is a short dead time, i.e. the time interval during which two 'STOP' signals cannot be processed. The number of secondary ions per primary ion pulse can vary over a wide range, but 1000 has been accepted as a reasonable upper limit. Each of these time intervals has to be converted to a digital number. The time-to-digital converter (TDC) satisfying these requirements is designed in a completely digital form, for which most of the parts are included in a high reliability Field Programmable Gate Array (FPGA) from ACTEL.

The TDC has a 13 bit clock counter fed by the master clock with a period of $T_{\text{clock}} = 31.25$ ns, which gives a total measurement range of 256 μs. Within each clock period, a 16 stage interpolation leads to an overall resolution of about 1.95 ns. This interpolation is done by a time-to-position transformation using a 'tapped delay line', which is actually set up by 16 non-inverting CMOS buffers. Of course, the total propagation delay of the delay line has to be equal to one clock period. As the master oscillator is used for the PIBS timing too, the start signal is synchronous avoiding additional errors in the time measurement. The propagation delay is then the only critical parameter. It has to be adjusted to match exactly the length of one clock period. This is effected through the supply voltage. To do this, a simple calibration routine is run under processor control. The result is subjected to a statistical analysis of the times of randomly generated pulses. This way no precision calibration pulses need to be generated. Once all time bins are filled equally the adjustment is correct. In flight the calibration routine is selfcalibrating to compensate temperature induced drifts of the elctronics.

Figure 15 shows a simplified block diagram of the TDC. The input signals from the detector unit are fed into the delay line. The taps are sampled with the rising edge of the master clock. If a 'STOP' pulse is detected within the sampled bit pattern the 16 tap signals and the value of the clock counter C_{clock} are stored into a fast first-in-first-out memory (FIFO), which can hold about 3000 'STOP' entries. The experiment processor reads the data from the FIFO memory asynchronous at a lower speed.

The principle of the time-to-position transformation is shown in the Figure 16. An incoming 'STOP' pulse propagates through the delay line with a speed of one tap per 1.95 ns. All taps are sampled simultaneously at the edge of the master clock, i.e., at the time $C_{\text{clock}} * T_{\text{clock}}$. For a leading edge of a 'STOP' pulse at position P within the sampled bit pattern the time of arrival can be calculated to be

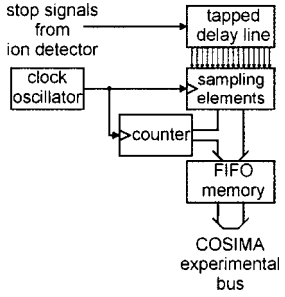

Figure 15. TDC Block diagram of the COSIMA time-to-digital Converter: The data from the tapped delay line and the master clock counter are added and stored in a hardware device until the instrument's processor can pick up the data.

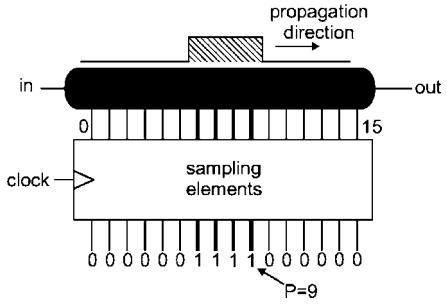

Figure 16. Time-to-position principle. The pulse from the detector amplifier moves from left to right through the delay line and, at a given time, is detected by several elements. The '1's are later interpreted by the software to derive the exact time of the event.

$t_{\text{arrival}} = C_{\text{clock}} * T_{\text{clock}} - P * 1.95$ ns. Once the position of the leading edge has been determined by the software, it can be decoded to a 4 bit number. Together with the 13 bit counter value, there are 17 bits corresponding to $2^{17} = 131072$ time bins. More than one 'STOP' pulse may occur within 32 ns and be inside the delay line at the same clock cycle. Such a case defines the dead time as the minimal distance between the two leading edges. It turned out, that for the proper function of the delay line the pulse width had to be increased to 5 ns, which results in a dead time of about 10 ns.

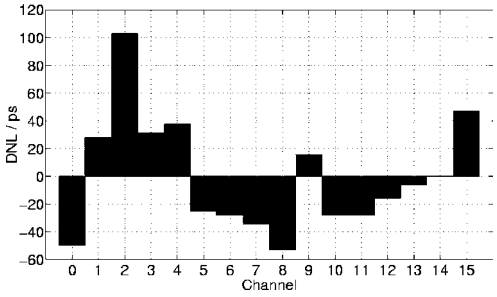

Figure 17. Differential linearity of TDC. The measured differential non-linearity of the system is an order of magnitude smaller than the COSIMA time-of-flight resolution.

The accuracy of the 2 ns delay steps is well defined and can be measured onboard using the calibration. Figure 17 shows the differential non linearity (DNA), which was measured for the 16 interpolation channels. The DNA is the deviation of the step width of one channel and is better than 120 ps for any channel which is much better than the nominal 0.5 LSB (Least Significant Bit) DNA. Thus all 17 bits are valid for the analysis of flight times.

3.7.3. *Instrument Control*

As is state-of-the-art, instrument control for COSIMA is provided by a microprocessor-based system (see below). Two categories of control are implemented, a digital subsystem transferring information on the system bus and an analog subsystem serving individual control lines. The dedicated, more complex units like COSISCOPE, and, to a lesser degree, the Target Manipulator Unit, and the Primary Ion Beam System are globally controlled, as they have some of the control functions residing within them. A general overview of the state of the instrument is maintained by continuous monitoring of the standard housekeeping values. The functions of PIBS and TOF are controlled by 20 adjustable high voltages. Apart from a collective 'disable' of all high voltage generators, these can be controlled by variable analog voltages in the range 0...10 V. (For all high voltages the voltage is controlled, except for one case: the extraction electrode of the primary ion source, where the emission current is monitored.) The high voltage settings need a resolution of 12 bits and very good stability over temperature and time. Generating these by 20 individual digital-to-analog converter ICs would have required a large amount of hardware. Instead, a simpler solution was found: A single PGA generates twenty pulse-width modulated square wave signals with a fixed frequency of 9 kHz. The duty cycles of the square waves are set under processor control between

0% and 100% with 12 bit resolution, where the LSB is generated by noise-shaping. The constant amplitude of the square waves is precisely given by a stable reference voltage source. The DC levels, which are proportional to the respective duty-cycle, are built by lowpass filtering of the individual square waves. Besides the values of the high voltages, their polarity in the TOF section and actual values in the PIBS need individual adjustment for either positive or negative secondary ions. Special precautions are needed when altering the polarity. This is done through the use of bistable relays. The control of the high voltage polarity lines has to be consistent with the control of the bistable relays, which switch between HV cascades for the positive and the negative case. Further more, these switching operations are only safe while there is no high voltage present, otherwise high voltage discharges could result in contact damage. Therefore, the control was set up in a hardware state machine, which also forces the relay coil drives to be consistent with the high voltage polarity control line setting before the high voltage generators can be enabled. It further sequentializes driving of the bistable relay coils to reduce the total coil current.

3.7.4. *Data Collection*

Two types of data are collected within COSIMA and both are needed to properly interpret the measured time-of-flight data: slow, housekeeping-like data such as settings of the actual voltages for the PIBS and the TOF section, positions of the targets and features thereon, and the fast arriving time-of-flight data for the secondary ions after a primary ion pulse. As discussed above, the fast data are accumulated at instrument speed in a FIFO, from where they are read at processor speed. The detailed timing is executed from hardware registers. Conflict may arise, when after 1000 (tbd) primary ion pulses the arrival data are assigned to their respective time bins. During this process the timing performance is verified by checking the position and width of the hydrogen ion peak (for both positive or negative ions), as well as for another (yet to be determined) mass line. Deviations above a certain limit will lead to the readjustment of operational voltages to keep the mass lines in the same bins throughout an entire analysis, which may last for several hours (rather than to use extensive recalculation of mass values to the time bins). During such phases of intense calculations, the instrument may continue to measure for the next 1000 primary shots, or its operation is halted and the primary ion emission is reduced until the end of the calculations. This task can be scheduled in flight taking into account actual performance and temperature change rates.

Once there are enough data of non-hydrogen secondary ions accumulated (typically a few thousands), the quality of the respective site is analyzed using code derived from chemometric methods (see 3.8 below). The data and the results of the analyses are then packed into an experiment data frame and sent to telemetry for transmission to ground.

3.7.5. *The Instrument Processor System and Latch-up Control*

The COSIMA instrument is entirely under the control of its processing unit. The CPU board is built to accommodate the instrument's computational and memory requirements. The board is built around a floating-point digital signal processor (DSP), type ADSP 21020 from Analog Devices, in a radiation-hard version built by Lockheed Martin Federal Systems running at 16 MHz. This signal processor has a Harvard architecture, with a 48 bit program-data bus and a 32 bit data-data bus.

The experiment software is stored in two EEPROMs of 128 kByte each. During the power-up procedure the program code is copied by the boot-loader, residing in three radhard 8 kByte PROMs from Harris, into the program RAM of six radiation tolerant 512 kByte CMOS SRAMs, from where it is later executed. The data memory is built from another four 512 kByte SRAMs, which allow processor operation with 32 bit IEEE floating-point numbers.

For permanent storage of the experiment setup and status information during times, when COSIMA is not powered, a 128 kByte SRAM is constantly supplied by a separate DC line from the S/C. This 'keep alive' memory allows quick reconfiguration of COSIMA after, e.g., a power drop or software stall.

The CPU board controls the COSIMA electronic boards through a synchronous 16 bit wide I/O bus with 256 possible addresses. The bus control by the CPU board is achieved through a combination of 'valid-memory-address', 'read', and 'write' signals. High bus reliability is obtained by synchronous timing circuits on the CPU board, which insert wait-states on the I/O bus to give long data hold times during write.

Since the memories on the CPU board are rad-tolerant but not single-event latch-up proof, a latch-up protection circuit is on the CPU board. The board is subdivided into areas, for which the individual supply currents are monitored. If a latch-up condition occurs, the supply current increase in one board area is immediately limited by an on-board current limiter, which protects the memory ICs from destruction. At the same time the power supply of the CPU board is completely switched off, so that the latch-up condition dies out. After a delay of a second, the CPU board is powered up again, and the boot-up procedure starts. The occurrence of a latch-up condition can then be deduced from the last experiment status stored within the keep alive memory.

3.7.6. *On-Board Data Handling and Telemetry*

The COSIMA software consists of two distinct parts: the boot-ROM code and operational code. The boot-ROM resident code provides for the following tasks:

- appropriate instrument setup at power up
- handling of all the ROSETTA S/C telecommand and telemetry services
- loading the operational code from the EEPROM or from the S/C.
- safe mode operation and recovery, if the operational code fails
- basic instrument housekeeping

The operational code provides all the functionality of the instrument. Individual operations are handled through interpreted code (like in the FORTH-language), which in turn calls compiled and optimized lower level subroutines.

The use of an interpreter gives more flexibility to both, updates of the software during the long mission, and it also provides a simple multitasking environment.

All of the operational code is written in relocatable modules. Should one part of the memory fail, the code can be transferred into another section. In addition, the modules can be updated individually. The interpreter calls the subroutines through jump tables so that individual tasks can be arranged by simply composing the proper jump addresses.

3.8. On-Board Pre-Evaluation

Basically COSIMA produces time-of-flight spectra. The data for each primary ion pulse are added into time bins. After about 1000 shots the data should be significant for a first evaluation to characterize the site under analysis. For this purpose the time bins are scanned for peaks at the known locations of mass lines of interest. With the expected mass resolution of $m/\Delta m > 2000$ (FWHM), several peaks may appear for each integer mass number, representing atomic and molecular ions (e.g., K^+ and $C_3H_3^+$ for mass number 39). Since cometary grains are a complex mixture of inorganic and organic compounds, this high-resolution data treatment is essential. Two peak lists are generated containing the absolute peak intensities (number of ions) per integer mass for both, inorganic and organic ions. These lists are used for further data evaluation. Although the mass resolution is not sufficient to determine the sum formula of an ion by discriminating isobars (e.g., triazine $C_3N_3H_4^+$ at 82.03997 amu from pentdienimine $C_5NH_8^+$ at 82.06513 amu), the dominating ion type can be determined by line position analysis (i.e., at which exact mass value most of the ions are found). An automatic comparison of peak list tables is necessary for the detection of cometary grains (target vs. grain signals) or to decide whether a newly measured site differs from those already analyzed. The strategy for comparison of organic spectra is as follows: Several similarity criteria will be used, and transformation of data (prior to comparison) will be applied. The aim of transforming the original data into a set of features is to achieve a better representation of the chemical structure in the mass data. A spectral feature is a numerical variable that characterizes a spectrum; it is a linear or nonlinear function of all or selected peak intensities. Varmuza *et al*. (1999, 2001) and Werther *et al.* (2002) have tested different types of spectral features using data that are similar to TOF-SIMS data. They found that promising concepts for feature generation for organic compunds are (1) intensities at selected masses, (2) intensities averaged in selected mass intervals, (3) logarithmic ratios of selected intensities, (4) summation of intensities at fixed mass differences (e.g., 14: modulo-14), and (5) autocorrelation.

Let $x(i, A)$ and $x(i, B)$ be spectral feature i for mass spectrum A and B, respectively, scaled to the range 0 to 100. Similarity criteria can be defined for instance

as following (summation over all n selected features):

$$S_1 = \sum [x(i, A) * x(i, B)] / \left\{ \sum [x(i, A)^2 * \sum [x(i, B)]^2 \right\}^{0.5}$$

correlation coefficient [0 . . . 1] (2)

$$S_2 = [1/n] \sum [x(i, A) - x(i, B)]^2 \quad \text{mean squared error [0 . . . 100]} \tag{3}$$

$$S_3 = \left\{ \sum [x(i, A) - x(i, B)]^2 \right\}^{0.5} \quad \text{Euclidean distance [0 . . .]} \tag{4}$$

Promising concepts for feature generation with mineral spectra are: (1) intensities of the major isotopes of atomic ions (which may turn out to be not so simple as they can be masked by molecular ions as, e.g., $m = 24$ amu can be superimposed by Mg and C_2), (2) intensities averaged over all isotopic contributions of atomic and molecular ions (again with the ambiguity that several isobars may additionally contribute in these mass intervals), (3) linear and logarithmic ratios of intensities (mainly for isotopic and for some crystal order analysis), (4a) modulo-4-summation (total contribution of the main isotope ions from minerals), (4b) modulo-12-summation (for subtraction of the contributions of carbon clusters), and (5) autocorrelation.

3.8.1. *Classification of Organic Mass Spectra*

A spectral classifier is a linear or non-linear algorithm where the values of spectral features are input and the output is a numerical response. In the best case the output estimates a structural property or indicates a compound class. A classifier output can also be used as a (complex) spectral feature. A classifier is defined by the features used and by a set of parameters. For instance a linear classifier with output y is given by

$$y = \sum [x(i) - a(i)] * b(i) \tag{5}$$

with $a(i)$ being the scaling bias for mean centering and $b(i)$ the loading factor for feature i. The classifier parameters are estimated from reference data and may be re-estimated when COSIMA data are available.

3.8.2. *Comparison and Classification of Mass Spectra from Minerals*

The inorganic contribution to the mass spectra exhibits the mineral constituents of the grains. Apart from established methods as laid out by Stephan (2001), we will follow up on a concept, in which the analysis is based in a first step on the average solar system isotopic ratios of the main rock forming elements (Mg, Si, S, K, Ca, Fe). Classifiers for mineral ions are ratios and ratios of ratios of intensities of atomic ions and a variety of molecular ions (each summed up over their isotopic varieties). In a next step, a more detailed analysis implying mathematical perturbation methods will then help to determine deviations in the cometary matter from the average solar system isotopic ratios. Engrand *et al*. (2005) have shown that the minerals enstatite,

olivine, serpentine, and talc can be well discriminated by applying multivariate data analysis to TOF-SIMS data.

3.8.3. *Detection of Cometary Grains*
Once a target has been exposed to cometary dust, and retrieved, and has been checked by COSISCOPE, a site identified is scanned by the ion beam in order to localize the area, which is different from the plain target. The test will start with a rather low mass resolution and a low lateral resolution. Depending on the results, the mass resolution is increased and the focus of the ion beam is reduced. These tests are repeated until a grain is identified or until stopped for other reasons. This search for a cometary grain is performed automatically. At the end, the grain is characterized using classifiers as described above.

3.8.4. *Comparison of Individual Sites*
The experience from the analysis of the Halley data suggests that cometary matter is rather similar in composition: most particles were an intimate mixture of mineral grains and an organic coating. The ratio of both components varied in the ions (!) over 8 orders of magnitude, while the variation within each component was quite small. There were, however, a few particles, the spectra of which were dominated by Fe and S ions or showed an unusual $^{12}C/^{13}C$ ion ratio (Jessberger and Kissel, 1991). With this in mind, it is the task of site comparison to point to such sites, which seem to have an unusual composition. The actual comparison is done with the use of the classifiers described above.

3.8.5. *Software*
This chapter covers the software for the control of the COSIMA ground support equipment and the in-flight software onboard the COSIMA flight instrument.

3.9. The Ground Support Equipment (GSE) for COSIMA

The GSE consists of a Pentium-based industrial PC with a visual display unit or a laptop used as such. Inside the PC's case is a dedicated power supply used to power the instrument. The operating system of the GSE is DEBIAN LINUX.

The GSE has several modes of operation:

- direct instrument control: In this mode the GSE is connected directly to the instrument. It is equipped with an interface card acting like the spacecraft's interface. The GSE also provides the power to the instrument and emulates the spacecraft functions of telecommanding and receiving telemetry.
- instrument control via the Rosetta Spacecraft Interface Simulator (SIS): The GSE controls the spacecraft simulator which in turn emulates the spacecraft functions of telecommanding, and receiving telemetry.

- telemetry interpretation when connected to the Central Checkout System or ground data segment: the GSE passively receives the COSIMA data and uses dedicated software to interpret them. The GSE can start the COSIMA instrument residing test and forward the test result as 'COSIMA OK' or 'COSIMA NOT OK' to the Central Checkout System.

In all of the above modes, GSE-residing, dedicated software is used to interpret the COSIMA telemetry data received from the instrument directly or via a network. Housekeeping data, events, and science data are saved and can be viewed at any time. The GSE displays in near real time the instrument's state in graphical format according to the housekeeping values and events sent by the instrument. The instrument can be commanded via graphical or command-line based user-interfaces.

During flight, the GSE is used to compose and check telecommands before they are sent as request to the operations center.

4. In-Flight Operation

For a versatile instrument like COSIMA the operational concept turns out to be highly complex. Several aspects have to be accommodated:

- instrument safety
- instrument maintenance
- instrument autonomy
- efficient data generation
- efficient indium usage
- dust sample temperature history
- accommodate software revisions, especially the final version after hibernation
- on board power constraints
- on board temperature constraints
- unexpected turnoff

Since there is a unique instrument usage profile on ROSETTA, only part of the operational software was on board when COSIMA was launched. Except for short time periods of maintenance, the instrument is 'OFF' from 2004 through 2012. Maintenance operation is needed to stimulate the liquid indium ion emitter, to avoid the formation of a crust, which would hinder the flow of the metal, and also for the motors in the Target Manipulator Unit, in order for the moving parts to stay lubricated. Later, around 2014, it is 'ON' sporadically for dust collection and initial test runs. For the last 6 months (or 4400 hours) of the mission, when dust will be most abundant, it should be running almost continuously. During this time period, all of the instruments would want to be turned on, and consequently the spacecraft would become too hot. Therefore time, or better, power constraints have to be expected. The signal round trip time of about 1/2 hour requires the instrument to run with a large degree of autonomy.

4.1. The Concept

The COSIMA operational concept is based on a maximum of independence of its subunits from one another and on the pre-definition of individual tasks and rules, upon which the on board system can schedule its activities. Of course, spacecraft orders and ground commands always have higher priority. When after launch the instrument is turned on, it will first of all conduct a self-test during which it checks all of its components, which have an interface to the microprocessor system, as well as all independent subsystems, TMU, COSISCOPE, and PIBS. After this autonomous test has been completed, which takes a few minutes, it will wait for another 5 minutes for instructions either stored on board the spacecraft or received directly from ground. Once this waiting period is expired, the instrument will resume from the activity list stored on board (should there be none, it will continue to wait). In doing so, it relies heavily on lookup tables or formulas to configure the functional elements into their operational modes, mostly into the measuring mode for positive or negative secondary ions. While the indium reservoir of the ion emitter is heated up, all of the high voltage converters have to be fed with their actual values, and the values for the deflection plates have to be set, and the timing of the primary ion source, i.e., for chopper and the three bunchers, has to be established. In a quick check, using H^+ or H^- ions, the pulse width of the primary ion beam is measured and adjusted if needed. The next step is to optimize the ion transmission by scanning the primary and secondary deflection plate voltages. Finally, the mass resolution is checked (using, e.g., Ag related ions) and adjusted if needed, before nominal operation is started. In another scenario, a target unit may have to be exposed or be retrieved after exposure. In yet another mode, a series of COSISCOPE images may have to be taken, the locations of collected dust particles have to be calculated and be transmitted to the main processor system. All these activities would require a huge amount of telecommands, all of them to be issued and controlled by ground operations. Many of these commands have therefore been combined into functional groups, which can be called upon at the appropriate times.

4.2. The Command Structure

For the proper operation of COSIMA, three levels of commands are implemented:

1. The *low level* commands, which write directly to the hardware cards controlling the instrument. Examples of the low level commands are: 'sub-unit power on', 'sub-unit power off', 'set one specific voltage', etc. The low level commands are primarily meant to be used during development and testing of the instrument. However, they can be used during the mission for detailed control of the instrument if needed.
2. The *middle-level* commands are useful combinations of several of the low level commands. Examples are: 'move target # to dust collection', 'setup PIBS operation', etc. These commands can be used during the mission to simplify 'manual' type operation.
3. The *high-level* commands combine several *middle-level* commands. They instruct the instrument what analysis program it shall perform, but hides the actual implementation level which is handled by lower level commands. Examples of the high level commands are: 'search a target for features', 'clean feature #', 'analyze feature #', etc. This is the nominal case for instrument operation during the mission.
4. Tasks are sequences of *high-level* commands, loaded into COSIMA via software commands. 128 tasks are available.

It is intended to sequence several types of such analyses of different features, as the results need assessment and decision on ground on how to proceed with the treatment of individual features. From data taken from laboratory tests during the development phase, the instrument can calculate the power profile for certain operations. Through specific commands, it can be instructed to schedule operations to stay within a given power level, if needed. Using this information, the instrument can operate autonomously for several days.

Command execution available at a specific moment is determined by the state of the instrument. High voltages, e.g., cannot be 'ON' while the target manipulator is in the process of moving targets. Each operational mode and sub-mode of the instrument has its own subset of *high-level*, *middle-level*, and of *low-level* commands which can be executed during that mode.

4.3. Post Launch ± Pre Arrival Activities

The use of microprocessor systems in space instrumentation allows much more sophistication and optimization. Part of this in turn requires a very detailed knowledge of the properties of the hardware actually flying and of the general type of such an instrument. On the other hand, it leaves many chances to modify the operational software according to new results in the laboratory or from the actual space instrument. Used properly, this is a very powerful tool for the success of an investigation. In the case of ROSETTA, where there is a long time between delivery of the instrument to the project and the actual measuring phase, there is an important opportunity to update COSIMA's operational software. This includes only the science related part and not the sections, which control the communications between the spacecraft and the instrument.

4.3.1. *Maintenance and In-Flight Operation During Commissioning*

Among the subsystems of COSIMA, there are two that need special attention and care between launch and arrival at the comet: The liquid indium ion emitters and the target manipulator. While for the emitter it is the contamination of the metal surface and a consequent deterioration of the flux properties of the metal, it is the

lubrication of the moving parts, which has to be assured in the target manipulator. Fortunately, action for both can be accommodated in a small routine, which is run every 9–13 months, starting with the initial in-orbit checkout of COSIMA. The following actions will be started:

- heat the indium reservoir of emitter 1
- move motor 1 for a number of steps
- move motor 2 for a number of steps
- make emitter 1 emit for up to 10 minutes
- cool emitter 1
- heat the indium reservoir of emitter 2
- move motor 3 for a number of steps
- move motor 4 for a number of steps
- make emitter 2 emit for up to 10 minutes
- cool emitter 2

As the increasing experience suggests, refined versions of these actions can and will be implemented in the instrument's operational software, and the duration and the power consumption will be documented.

Rosetta commissioning was carried out in 2004, the COSIMA instrument was operated in-flight after nearly a decade of development and tests on the ground. Positive and negative SIMS ion mass spectra were taken of one of the Ag metal targets, the resulting spectra are shown in Figure 18a and b, respectively. The inorganic and organic ions and molecules show up in separable and well resolved mass peaks, such as Si and C_2H_4 or Fe and C_4H_8. Small amounts of organic molecules being known to be present in cometary dust such as CN are adsorbed on the blank metal target and reveal themselves in the SIMS mass spectra. Since COSIMA carries also a heating station for the target, the level of volatile contamination can be further decreased before exposure of the target to the cometary dust. Comparison with mass spectra taken of the same target in 2002 before launch already shows a slight decrease of volatiles such as hydrocarbons absorbed on the target surface after residing only about 6 months in space. This contamination by organic molecules was, in part, released from the insulation material of the electrical harness and from boxes used for ground transportation. Note that the Ag peaks are caused by ions released from the target and the In peak is due to primary ions from the ion source. For high secondary ion rates, the mass spectra show saturation effects due to dead-times inherent in the ion detector counting electronics, best visible adjacent to each of the intense Ag isotope peaks.

4.3.2. *The Ground Laboratory Program*

During the cruise phase to the comet as well as while the probe is actually analyzing cometary dust; an active laboratory program will be maintained. While the SIMS method is routinely applied for relevant geological and planetological studies, the TOF-SIMS technique will benefit from this terrestrial work with the COSIMA RM

reference model. Additionally, growing experimental and methodological expertise comes from the day-to-day work with relevant samples at the TOF-SIMS laboratory instrument currently in use at the University of Münster. The complex mixture of organic and inorganic material, expected to make up the comet, will result in equally

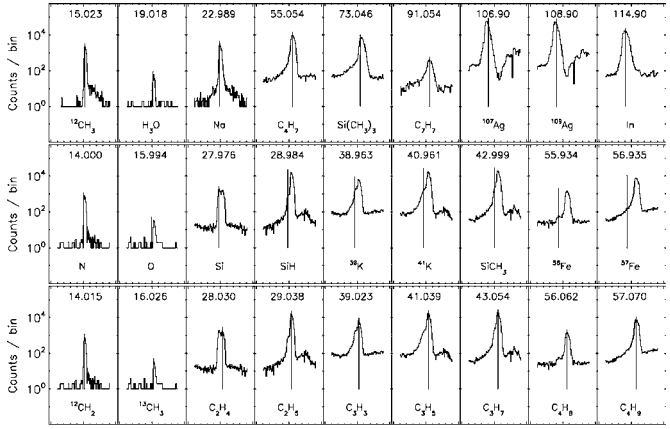

(a)

Figure 18. (a) First COSIMA in-flight positive secondary ion mass spectrum (SIMS). Each window is centered on examples of mass peaks of the COSIMA time-of-flight mass spectra. The mass range is +/− 0.5 amu and the number of secondary ions is given in counts/mass bin. The potential identification of atoms or molecules and their mass are labeled in each window, the position of the mass is indicated by a vertical line. For the same integer mass number, organic molecule peaks are located to some extent to the right, while the inorganic ion peak is located to the left of the integer mass number. The top panel refers to mass peaks with an unique atom or molecule identification. The center panel refers to mass peaks with potentially both organic and in-organic atoms or molecules within the same mass range of +/− 0.5 amu. Inorganic elements or molecules containing inorganic elements are labeled in each window. The bottom panel refers to the organic molecules, mainly hydrocarbons, identified in the ion spectrum. Comparison of the center and bottom panel reveals the mass resolution of the COSIMA instrument, sufficient to resolve e.g. Si and C_2H_4 (b) First COSIMA in-flight negative secondary ion mass spectrum (SIMS). Each window is centered on examples of mass peaks of the COSIMA time-of-flight mass spectra. The mass range is +/− 0.5 amu and the number of secondary ions is measured in counts/mass bin. The potential identification of atoms or molecules and their mass are labeled in each window, the position of the mass is indicated by a vertical line. For the same integer mass number, organic molecule peaks are located to some extent to the right, while the inorganic ions peak is located to the left of the integer mass number. Electronegative elements such as O, F or Cl and I clearly show up in the negative ion spectrum. The negative ion spectrum also shows electrons sputtered off the grids within the reflectron. The electron peaks are shifted by a defined time lag from the main ion peak. (*Continued on next page*)

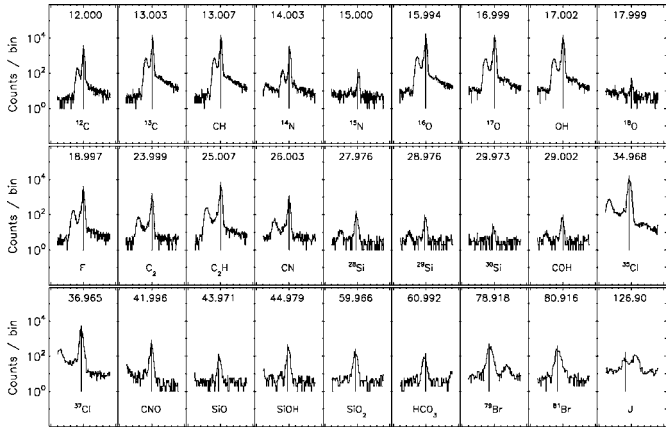

(b)

Figure 18. (*Continued*)

complex mass spectra. They have to be disentangled to provide information on the chemical, isotopic, and molecular composition of the particles that reflect the origin, history, and present state of cometary matter. The particle-to-particle variation will testify to its diversity, i.e., to the extent of the pristine nature of these materials, and to its stellar sources. Interpreting the mass spectra requires calibration. Calibration here is not meant to mimic the experiment in a one-to-one scale in the laboratory, but rather to understand the processes, which control ion formation with complex samples, as well as the instrumental parameters of mass separation and ion detection. To that end, state-of-the-art laboratory TOF-SIMS analyses with utmost lateral and mass resolution of various materials available on Earth will be performed, which include, but are not limited to:

- Interplanetary dust particles (IDPs). Some of these small and difficult-to-analyze particles actually may stem from comets. It is an active research topic to sort these out and distinguish them from asteroidal IDPs. IDPs of a certain class are mixtures of inorganic and organic matter and as such represent the best analog material for the COSIMA case.
- Carbonaceous chondrites: They are mechanical mixtures of fine-grained low-temperature matrix and carbon-rich phases (kerogen) with high-temperature clasts, single minerals, and chondrules. Their overall chemical composition is solar as far as the condensable elements are concerned. They most closely represent

and witness the Early Solar System materials and processes. They are regarded as the base line material in planetology.
- Certain IDPs and chondrites contain particles with non-standard isotopic composition of a number of elements that point towards their nucleosynthetic stellar sources. These particles (stardust or presolar particles) will serve to learn how to obtain the relevant information from cometary matter.

The extraterrestrial materials mentioned above are not as pristine as we expect cometary dust to be. IDPs are altered to an unknown extent during passage through the atmosphere, deceleration processes and residence in the stratosphere; carbonaceous chondrites were subject to metamorphism and aqueous alteration on their parent bodies. Consequently, for the analysis of organic (and icy) components anticipated in cometary particles artificial analogs are needed. They are siliceous vaporization deposits contaminated with organic substances. Certainly not all possible organic substances can be analyzed, but rather we will perform TOF-SIMS measurements of relevant substance classes.

As mentioned above, these analyses are performed with the highest possible mass and (where appropriate) lateral resolution. In addition, the temporal evolution of the mass spectra is evaluated by using the data from all primary ion pulses. This will give hints to a possible layering within the material and/or validate influences, which the TOF-SIMS method may cause in the material (by, e.g., 'radiation damage'). New statistical and chemometric methods and procedures, now under test, will be further developed and applied.

The laboratory program will benefit from and be adjusted to new insights, which will come from the analysis of the samples returned by Stardust in 2006.

5. Anticipated Results

5.1. The Mineral Phase

The anticipated results of the investigation of the mineral phase of the cometary dust are manifold:

- First, we shall establish the mean composition of the main elements, and then check whether this varies from grain to grain, either within the statistical variance or beyond that. In the latter case we'll be able to identify various classes of minerals.
- Second, the distribution of molecular ions should be sensitive to the order structure of the minerals, may they be in an amorphous or in one of several crystalline states. This would give an important clue to the thermal and radiation history of the dust.
- Third, once an elemental and molecular distribution of the main isotopic contribution is established, the contribution of the minor isotopes can be measured

from grain to grain, needed for the question whether various stellar sources have played a role to form the dust.

- Fourth (last but not least), a cross-correlation of the types of organics sitting upon the same grain will give insight into aspects of the real grain forming process as well as to possible catalytic interferences between each phase. This is important for the 'Origin of Life' topic and its relation to nano-systems.

5.2. The Organic Phase

The refractory organic phase will most probably be an intimate mixture of a lot of individual species. But still, the history of grain formation and the incorporation of them into cometary nuclei is reflected – at least partially – in the distribution of the organic species. Substance class analysis will provide clues to whether the organic phase is mainly produced by condensation of vapors and subsequent radiation processing with polycondensation and oligomerization, etc., or, if it is mainly produced by condensation of larger molecules and aggregation of small refractory particles.

Another important question is, whether the organic material in comets is suitable to start the onset of life on earth. In this case, the analysis will show that the precursors of such molecules needed for life's self-organization by exenthalpic reactions with liquid water are present.

As water usually shows up in different ways in the mass-spectra, clues to the source of water in the comet may be found, too: is it just a condensation of water ice in the grains, or, is it the result of long-term radiation induced processes, such as polycondensation or Born-Haber-type processes, or is perhaps a fraction of the water in a comet produced by thermally induced reactions, when the comet approaches the sun?

COSIMA results thus address the main questions concerning the origin of the hydrosphere, and further on, the biosphere on earth.

6. Conclusions

Writing up this paper was an opportunity to review the general concept of COSIMA. It seems that the hardware is very well suited to perform the measurements on cometary dust. As mentioned earlier, at the time of writing, the software was still in a rudimentary state awaiting all the model specific values and the definition of individual tasks. Since no instrument hardware was available at this time, those inputs still had to wait. In this sense, the description is somewhat incomplete, since it is the software that ultimately defines the 'personality' of an instrument. Fortunately, progress on the subsystem level was good enough to assure that the overall performance of COSIMA will meet the scientific objectives. COSIMA's

hardware is very well suited to perform in-situ measurements on cometary dust (in almost a decade from now). The flight software will be adapted to the experience gained with the COSIMA laboratory model, and the onboard data analysis will be updated according to the results from cometary analog material. SIMS is a very sensitive analysis method, not only for the bulk composition, but also for the surface layers of the collected cometary dust. Unlike previous measurements with impact dust mass spectrometers, COSIMA is capable to analyze the composition as a function of the stratification within the dust grains and layers of ultrafine dust or even attogram dust grains, provided that the cometary flux of these particles is sufficient. Therefore, COSIMA constitutes the next generation dust analysis instrumentation and will provide valuable insight into the cometary dust building blocks, restraining models of comet history, morphology, organic and inorganic chemistry, mineralogy, and petrology. The data from COSIMA and its operation will be the reward for the many fights against technical and bureaucratic problems.

Acknowledgements

One of us (J. K.) wants to mention that COSIMA would not have happened without the continuous support of G. Haerendel, director at the Max-Planck-Institut für extraterrestrische Physik in Garching, B. Feuerbacher, director of the Institut für Raumsimulation of the DLR, the funding agencies DARA and later DLR (grant number 50 QP 9711 3) with G. Hartmann, E. Lorenz, W. Kempe, and M. Otterbein, and last not least, H. von Hoerner, director of the contractor vH&S GmbH, who also serves as Co-PI and has conceived ever cheaper ways to build COSIMA. Substantial hardware and software contributions, without which COSIMA could not work, were contributed by COSIMA Co-Is from France, Finland, and Austria.

References

Dahl, D. A.: 1997, INEEL, Idaho Falls, Idaho 83415, DHL@inel.gov: The SIMION software manual (and later versions).

Engrand, C., Kissel, J., Krueger, F. R., Martin, P., Silén, J., Thirkell, L., et al.: *Rapid Commun. Mass Spectrom.* **20**, 1361.

Jessberger, E. K., and Kissel, J.: 1991, In: R. Newburn, M. Neugebauer, and J. Rahe (eds.), *Comets in the Post-Halley Era*, Springer Verlag, Heidelberg, pp. 1075–1092.

Kissel, J., Sagdeev, R. Z., Bertaux, J. L., Angarov, V. N., Audouze, J., Blamont, J. E., et al.: 1986, *NATURE* **321**(6067), 280.

Kissel, J., Brownlee, D. E., Büchler, K., Clark, B. C., Fechtig, H., Grün, E., et al.: 1986, *NATURE (Encounters with Comet Halley – The First Results)* **321**(6067), 336.

Kissel, J., and Krueger, F. R.: 1987, *NATURE* **326**, 755.

Krueger, F. R.: A Feasibility Study for CoMA, part 1, Aug. 1988, part 2, Jan. 1989, and part 3, Sept. 1989.

Krueger, F. R., Korth, A., and Kissel, J.: 1991, *Space Sci. Rev.* **56**, 167.

Mamyrin, B. A., Karatyev, V. I., Shmikk, D. V., and Zagulin, V. A.: 1973, *Zh Eksp. i Teor. Fiz*. **64**, 82 or: *Sov. Phys. JETP* **37**(1), July 1973.
Mazets, E. P., Sagdeev, R. Z., Aptekar, R. L., Golenetskii, S. V., Guryan, Yu. A., Dyachkov, A. V., et al.: 1987, *Astronomy Astrophys.* **187**, 699.
McDonnell, J. A. M., Green, S. F., Grün, E., Kissel, J., Nappo, S., Pankiewicz, G. S., et al.: 1989, *Adv. Space Res.* **9**(3), 277.
Schwab, M.: 1998, CEMEC GmbH, Obererlbach, FRG: Design of the COSIMA Target Manipulator, (private communication), 1998.
Stephan, T.: 2001, *Planet. Space Sci.* **49**, 859.
Varmuza, K., Werther, W., Krueger, F. R., Kissel, J., and Schmid, E. R.: 1999, *Int. J. Mass Spectrom.* **189**, 79.
Varmuza, K., Kissel, J., Krueger, F. R., and Schmid, E. R.: 2001, In E. Gelpi (Ed.), *Advances in Mass Spectrometry*, vol. 15 (Wiley & Sons, Chichester), p. 229–246.
Werther, W., Demuth, W., Krueger, F. R., Kissel, J., Schmid, E. R., and Varmuza, K.: 2002, *J. Chemom.* **16**, 99.
Zscheeg, H., Kissel, J., Natour, Gh., and Vollmer, E.: 1992, *Astrophs. Space Sci.* **195**, 447.

Article 15

KÜPPERS M., KELLER H. U., KÜHRT E., A'HEARN M. F., ALTWEGG K., BERTRAND R., BUSEMANN H., CAPRIA M. T., COLANGELI L., DAVIDSSON B., EHRENFREUND P., KNOLLENBERG J., MOTTOLA S., RATHKE A., WEISS P., ZOLENSKY M., AKIM E., BASILEVSKIJ A., GALIMOV E., GERASIMOV M., KORABLEV O., LOMAKIN I., MAROV M., MARTYNOV M., NAZAROV M., ZAKHAROV A., ZELENYI L., ARONICA A., BALL A. J., BARBIERI C., BAR-NUN A., BENKHOFF J., BIELE J., BIVER N., BLUM J., BOCKELÉE-MORVAN D., BOTTA O., BREDEHÖFT J.-H., CAPACCIONI F., CHARNLEY S., CLOUTIS E., COTTIN H., CREMONESE G., CROVISIER J., CROWTHER S., EPIFANI E. M., ESPOSITO F., FERRARI A. C., FERRI F., FULLE M., GILMOUR J., GOESMANN F., GORTSAS N., GRADY M., GREEN S. F., GROUSSIN O., GRÜN E., GUTIÉRREZ P. J., HARTOGH P., HENKEL T., HILCHENBACH M., HO T.-M., HORNECK G., HVIID S. F., IP W.-H., JÄCKEL A., JESSBERGER E., KALLENBACH R., KARGL G., KÖMLE N. I., KORTH A., KOSSACKI K., KRAUSE C., KRÜGER H., LI Z.-Y., LICANDRO J., LOPEZ-MORENO J. J., LOWRY S. C., LYON I., MAGNI G., MALL U., MANN I., MARKIEWICZ W., MARTINS Z., MAURETTE M., MEIERHENRICH U., MENNELLA V., NG T. C., NITTLER L., PALUMBO P., PÄTZOLD M., PRIALNIK D., RENGEL M., RICKMAN H., RODRIGUEZ J., ROLL R., ROST D., ROTUNDI A., SANDFORD S., SCHOENBAECHLER M., et al. (In press) Triple F - A Comet Nucleus Sample Return Mission. Experimental Astronomy.

Exp Astron
DOI 10.1007/s10686-008-9115-8

ORIGINAL ARTICLE

Triple F—a comet nucleus sample return mission

Michael Küppers · H. U. Keller · E. Kührt · M. F. A'Hearn · K. Altwegg · R. Bertrand · H. Busemann · M. T. Capria · L. Colangeli · B. Davidsson · P. Ehrenfreund · J. Knollenberg · S. Mottola · A. Rathke · P. Weiss · M. Zolensky · E. Akim · A. Basilevsky · E. Galimov · M. Gerasimov · O. Korablev · I. Lomakin · M. Marov · M. Martynov · M. Nazarov · A. Zakharov · L. Zelenyi · A. Aronica · A. J. Ball · C. Barbieri · A. Bar-Nun · J. Benkhoff · J. Biele · N. Biver · J. Blum · D. Bockelée-Morvan · O. Botta · J.-H. Bredehöft · F. Capaccioni · S. Charnley · E. Cloutis · H. Cottin · G. Cremonese · J. Crovisier · S. A. Crowther · E. M. Epifani · F. Esposito · A. C. Ferrari · F. Ferri · M. Fulle · J. Gilmour · F. Goesmann · N. Gortsas · S. F. Green · O. Groussin · E. Grün · P. J. Gutiérrez · P. Hartogh · T. Henkel · M. Hilchenbach · T.-M. Ho · G. Horneck · S. F. Hviid · W.-H. Ip · A. Jäckel · E. Jessberger · R. Kallenbach · G. Kargl · N. I. Kömle · A. Korth · K. Kossacki · C. Krause · H. Krüger · Z.-Y. Li · J. Licandro · J. J. Lopez-Moreno · S. C. Lowry · I. Lyon · G. Magni · U. Mall · I. Mann · W. Markiewicz · Z. Martins · M. Maurette · U. Meierhenrich · V. Mennella · T. C. Ng · L. R. Nittler · P. Palumbo · M. Pätzold · D. Prialnik · M. Rengel · H. Rickman · J. Rodriguez · R. Roll · D. Rost · A. Rotundi · S. Sandford · M. Schönbächler · H. Sierks · R. Srama · R. M. Stroud · S. Szutowicz · C. Tornow · S. Ulamec · M. Wallis · W. Waniak · P. Weissman · R. Wieler · P. Wurz · K. L. Yung · J. C. Zarnecki

Received: 1 February 2008 / Accepted: 14 July 2008

Abstract The *Triple F* (**F**resh **F**rom the **F**ridge) mission, a Comet Nucleus Sample Return, has been proposed to ESA's Cosmic Vision program. A sample return from a comet enables us to reach the ultimate goal of cometary research. Since comets are the least processed bodies in the solar system, the proposal goes far beyond cometary science topics (like the explanation of cometary activity) and delivers invaluable information about the formation of the solar system and the interstellar molecular cloud from which it formed. The proposed mission would extract three sample cores of the upper 50 cm from three locations on a cometary nucleus and return them cooled to Earth for analysis in the laboratory. The simple mission concept with a touch-and-go sampling by a single spacecraft was proposed as an M-class mission in collaboration with the Russian space agency ROSCOSMOS.

Keywords Comets · Cosmogony · Sample return · Space mission

M. Küppers (✉) · H. U. Keller · F. Goesmann · P. Hartogh · M. Hilchenbach · S. F. Hviid · R. Kallenbach · A. Korth · H. Krüger · U. Mall · W. Markiewicz · M. Rengel · R. Roll · H. Sierks
Max-Planck-Institute for Solar System Research,
Max-Planck-Str. 2, 37191 Katlenburg-Lindau, Germany
e-mail: Michael.Kueppers@sciops.esa.int

1 Introduction

At the first stage of the formation of the solar system there was the solar/protoplanetary nebula collapsing from a molecular cloud. The central star—our Sun—formed and started to heat the dust/gas mixture. Dust particles sank to the mid-plane, accreted, and agglomerated to planetesimals and cometesimals, the building blocks of the planets. At the outer fringes of the nebula the temperatures were cold enough that ices persisted and volatiles condensed before the comets were formed. Investigating the chemical and physical properties of this primordial mixture is a key to understanding how our solar system formed—and ultimately how life has started.

The primordial mixture has been preserved—almost unaltered from further processing due to high speed impacts, gravitational compression and

M. Küppers
European Space Astronomy Centre, P.O. Box 78,
28691 Villanueva de la Cañada, Madrid, Spain

E. Kührt · J. Knollenberg · S. Mottola · J. Benkhoff · J. Biele · N. Gortsas · G. Horneck · C. Krause · C. Tornow
German Aerospace Center (DLR), Berlin, Germany

M. F. A'Hearn
University of Maryland, College Park, MD, USA

K. Altwegg · A. Jäckel · P. Wurz
University of Berne, Berne, Switzerland

R. Bertrand
CNES, Toulouse, France

H. Busemann · A. J. Ball · S. F. Green · J. C. Zarnecki
Open University, Milton Keynes, UK

M. T. Capria · F. Capaccioni · G. Magni
IASF/INAF, Rome, Italy

L. Colangeli · E. M. Epifani · F. Esposito · V. Mennella
INAF—Osservatorio Astronomico di Capodimonte, Naples, Italy

B. Davidsson · H. Rickman
University of Uppsala, Uppsala, Sweden

heating—in low density cometary nuclei whose temperature did not exceed 50 K. Sophisticated analyses of this material in our laboratories will allow us to determine the ratio of processed to original interstellar material, and to determine the time scales of grain formation. Key questions like 'How important was ^{26}Al for heating even small bodies in the first millions of years?' can be assessed by determining the time scale for accretion of cometesimals as well as the structure of the cometesimals. Investigation of cometary material provides information about the original (primordial) mixture out of which the planetesimals and hence planets formed before they were altered in this formation process. The proposed *Triple F* (**F**resh **F**rom the **F**ridge), a Comet Nucleus Sample Return (CNSR) mission, concentrates on retrieving samples of this original mixture to bring them back for analyses that can only be undertaken in terrestrial laboratories. There the detailed chemical and isotopic composition and the internal structure of ice-mineral cometary grains will be measured as well as the granulation of the volatile material.

The relevance of cometary research goes far beyond the investigation of minor bodies, of their physical and chemical properties or even of how they came about. The driving quest has always been to learn about the composition of the primordial nebula mixture and the formation of our solar system. Now is the time to achieve this ultimate goal of the European space programme that started more than 20 years ago with ESA's first planetary mission to fly-by comet Halley. The stepwise preparation by cometary fly-bys (*VEGAs*, *Giotto*, *Sakigake*, and *Suisei* fly-bys of 1P/Halley [53], *Deep Space*

P. Ehrenfreund
University of Leiden, Leiden, Netherlands

A. Rathke
EADS Astrium, Friedrichshafen, Germany

P. Weiss · T. C. Ng · K. L. Yung
The Hongkong Polytechnic University, Hong Kong, China

M. Zolensky
NASA Johnson Space Center, Houston, USA

E. Akim · M. Marov
Keldysh Institute, Moscow, Russia

A. Basilevsky · E. Galimov · M. Nazarov
Vernadskij Institute, Moscow, Russia

M. Gerasimov · O. Korablev · A. Zakharov · L. Zelenyi
Space Research Institute, Moscow, Russia

I. Lomakin · M. Martynov
Lavochkin Association, Moscow, Russia

A. Aronica · P. Palumbo · A. Rotundi
University of Naples, Naples, Italy

1 fly-by of 19P/Borrelly [46]), impacts (*Deep Impact* on 9P/Tempel 1, [2]), collection of dust (Stardust at 81P/Wild 2, [10]), and a rendezvous (*Rosetta* with 67P/Churyumov–Gerasimenko, [27]) leads to an understanding of comets and their spectacular activity. This knowledge now provides a firm basis for the design and successful execution of a sample return mission.

The Rosetta mission will investigate the cometary nucleus from orbit and also by instruments placed onto the surface of comet 67P/Churyumov–Gerasimenko (CG) by a lander. These investigations will take place in the year 2014. The physical characteristics of the nucleus of CG will be investigated in detail, its coarse chemical composition will be analysed, and the physics of its activity examined—a very major step forward in our understanding of the chemistry and physics of cometary nuclei. However, many questions about the formation of the planetary system will not be answered. How was the interstellar (molecular cloud) material metamorphosed into solar system compounds, organics and minerals? Did comets contribute to the development of life on Earth? Investigations to reveal the physical and chemical processes and their time scales during the early stages of planetary formation need analyses on ppb levels that cannot be realized by *Rosetta*. Addressing such questions has successfully been demonstrated on meteoritic samples from various types of asteroids, the Moon, and Mars. The recent analysis of non-volatile material collected during the *Stardust* fly-by of comet 81P/Wild 2 shows that microscopic high temperature material formed near the early Sun can be found in cometary nuclei that formed at low temperatures, possibly

C. Barbieri · G. Cremonese · F. Ferri
University of Padova, Padova, Italy

A. Bar-Nun · D. Prialnik
University of Tel-Aviv, Tel Aviv, Israel

N. Biver · D. Bockelée-Morvan · J. Crovisier
Paris Observatory, Meudon, France

J. Blum
Technical University Braunschweig, Braunschweig, Germany

O. Botta
International Space Science Institute, Berne, Switzerland

J.-H. Bredehöft
University of Bremen, Bremen, Germany

S. Charnley
NASA Ames Research Center, Mountain View, USA

E. Cloutis
University of Winnipeg, Winnipeg, Canada

H. Cottin
University of Paris, Paris, France

as low as 30 K, in the outer reaches of the solar system [42]. Although an evolutionary explanation has not yet been ruled out, the structure and the chemical heterogeneity of 9P/Tempel 1 as observed by *Deep Impact* suggest that large cometesimals may contain materials from different parts of the protoplanetary disk [6]. How well, on what time scales, and how far out was the solar nebula mixed before the building blocks of the planets have accreted and agglomerated? Many of these physical and chemical processes have been revealed by the interpretation of the extremely sophisticated analyses of the diverse meteoritic materials. However, a global and conclusive picture and time line for the formation process of our solar system has not yet been developed. Bringing back a sample from a body that formed on the fringes of the planetary system, the temperature of which was always low enough to trap compounds as volatile as CO or CH_4 will allow us to investigate an end member of the minor bodies of the planetary system. Here we have the best chance to understand the relationship between the original interstellar material of the collapsing molecular cloud and the processed end-products found in the meteoritic samples. The high content of volatiles in cometary nuclei shows that little processing occurred during the formation of the comet or of the parent body it broke up from.

The scientific rationale for the *Triple F* mission is outlined in Section 2 on the basis of recent results from the cometary missions *Deep Impact* and *Stardust*. Cometary nucleus properties will be very well understood from investigations by *Rosetta*'s Lander. The months spent near the nucleus from the onset of its

S. A. Crowther · J. Gilmour · T. Henkel · I. Lyon · D. Rost
University of Manchester, Manchester, UK

A. C. Ferrari
University of Cambridge, Cambridge, UK

M. Fulle
Trieste Observatory, Trieste, Italy

O. Groussin
LAM, Marseille, France

E. Grün · R. Srama
MPIfK, Heidelberg, Germany

P. J. Gutiérrez · J. J. Lopez-Moreno · J. Rodriguez
IAA–CSIC, Granada, Spain

T.-M. Ho
ESA–ESTEC, Noordwijk, Netherlands

W.-H. Ip · Z.-Y. Li
National Central University, Taipei, Taiwan

E. Jessberger
University of Münster, Münster, Germany

activity to the perihelion of comet CG will provide extensive experience on operating inside the coma. The risks of operations in the vicinity of a cometary nucleus will be fully understood and can be minimised during sampling. Adequate knowledge to provide samples from scientifically significant locations will be available.

Section 3 demonstrates that a sample from a short period (Jupiter-Family) comet can be returned by a spacecraft that is considerably smaller than *Rosetta*. The length of the mission is typically 10 years. A spacecraft launched in April 2018 by a Soyuz launcher to comet 79P/du Toit–Hartley will return 1.5 kg of cooled cometary material in April 2028. We chose a conservative approach using systems relying on technologies that are either existing or to be developed for approved missions like *BepiColombo*. The same holds true for the trajectory calculations of the Solar-Electric Propulsion (SEP) driven spacecraft. The *Triple F* mission is proposed in collaboration with ROSCOSMOS (Russian Space Agency) and the total budget is 600 M€, equally shared between ESA and ROSCOSMOS.

2 Scientific goals of a CNSR mission

2.1 Relevance of comets for solar system formation

The scientific questions to be addressed in this mission have been raised by past space missions to comets, particularly to Halley (*Giotto*, *Vega*), Tempel 1

G. Kargl · N. I. Kömle
IWF, Graz, Austria

K. Kossacki
University of Warsaw, Warsaw, Poland

J. Licandro
IAC, Tenerife, Spain

S. C. Lowry
University of Belfast, Belfast, UK

I. Mann
University of Kobe, Kobe, Japan

Z. Martins · M. Schönbächler
Imperial College, London, UK

M. Maurette
CNRS, Orsay, France

U. Meierhenrich
University of Nice, Nice, France

L. R. Nittler
Carnegie Institution, Washington, USA

(*Deep Impact*) and Wild 2 (*Stardust*), but also by observations made with space telescopes (HST, ISO, SST), and extensive ground-based observing campaigns. What is the complement of pristine interstellar organic material in comets? Is it possible to reconstruct the physical and chemical history of interstellar material in the nebula from observations of its state in comets? Does the chemical composition of a comet reflect its formation zone in the nebula? Do different cometary materials (dust, ices, organic compounds) originate from markedly different environments? If so, what are its implications for the physical conditions (temperature, density) of nebular evolution? The scientific returns from this mission will allow these questions to be answered and permit fundamental progress to be made in advancing knowledge of the origin of our Solar System.

2.1.1 Formation of the solar system from the protosolar cloud

About 4.6 billion years ago the Solar Nebula formed from a collapsing fragment of a molecular cloud (MC). Isotopic evidence associates the collapse with explosive injection of possibly at least two pulses of material from a nearby supernova [7]. In the first phase of this process, which lasted about 10^5 years, a protostar with a surrounding thick disk formed, deeply embedded in its parental MC. During the second phase this disk became thinner and reached a size of 100 AU or more in a time of less than 3×10^6 years. At the end of this phase the solar nebula consisted of a viscous gas–dust mixture. Due to

M. Pätzold
University of Cologne, Cologne, Germany

S. Sandford
NASA Ames Research Center, Moffett Field, USA

R. M. Stroud
Naval Research Laboratory, Washington, USA

S. Szutowicz
Space Research Center of PAS, Warsaw, Poland

S. Ulamec
German Aerospace Center (DLR), Cologne, Germany

M. Wallis
University of Cardiff, Cardiff, UK

W. Waniak
University of Krakow, Krakow, Poland

P. Weissman
JPL, Pasadena, USA

R. Wieler
ETH, Zürich, Switzerland

the gas–dust interaction the coagulating grains settled to the mid-plane of the disk. Contemporaneously, the stellar accretion rate decreased and the proto-Sun reached its T Tauri state. Analogues of this ancient star forming process are observable in our galaxy today, e.g., in the Orion or Taurus Molecular Cloud. In contrast to the Taurus region, the star formation in the Orion MC is influenced by intense radiation in the far UV and by external shocks. Currently, we do not know whether our Sun has formed in a MC more similar to Orion or to Taurus. However, the different conditions prevailing during the formation of the solar system have left traces that can be found today in cometary material, such as the structure (amorphous or crystallized) and composition of the ice and dust fractions as well as pre-solar grains (identified by anomalous isotopes) and deuterated compounds or particular substances (e.g., PAHs). The Stardust mission recovered a few, probably pre-solar grains from comet Wild 2 [57], but the abundance of these grains in comets is as yet very uncertain. In the third phase, the dust grains decoupled from the gas, with the latter eventually being blown off from the disk. The solar nebula evolved to a planet-forming debris disk. This evolution took $(3–10) \times 10^7$ years and it is not yet fully understood. Planetesimals accreted to planets with fundamental difference inside and outside the snowline. The material that accreted beyond this snowline can be found in comets. The composition of comets, as well as the differences between comets and the different types of asteroids, provides constraints on the solar nebula evolution in phase three. As a prerequisite, one needs to distinguish between the influence of the evolving solar nebula on the forming comets and their potential subsequent processing.

2.1.2 Comets as remnants of solar system formation

As witnessed by the high abundance of volatile ices such as CO in cometary nuclei, comets formed and spent most of their lifetime in a cold environment. Due to their origin in the coldest part of the solar nebula, comets are the solar system objects that underwent the least processing since the formation of the solar system from the pre-solar cloud.

While it is evident that comets consist of the best preserved material from the solar nebula, it is a longstanding question to what extent material from short period comets evolved since its formation. New results, from the *Deep Impact* mission as well as from laboratory experiments and modeling efforts, suggest that we can rule out previous suggestions that cometary materials were highly processed to great depths below the surface.

An aging process operating on a short period comet is collisional processing in the Kuiper belt [19]. While such a process would hardly affect the chemical and mineralogical properties of the comet, it can be expected to change physical properties like strength and density [8]. Recent results suggest that the history of short period comets may be less violent than suggested previously. For example, it is suggested that the origin of many short period comets is the scattered disk, a collisionally much more benign environment than the classical Kuiper belt [17]. Also, *Deep Impact* has shown evidence for primordial

layering in comet Tempel 1 [6], suggesting that at least this comet is not a collisional fragment.

After injection into the inner solar system the surface layers of a comet are processed by solar heating and sublimation of volatiles. Models of the evolution of cometary surface layers disagree about the depth of the surface layer that was processed by sunlight. *Deep Impact* measurements [29, 60] of Comet Tempel 1 suggest that the thermal inertia of the surface layer of a comet is so low that, in an active area, the timescale of the penetration of the solar heat wave is comparable to that of removal of surface material by sublimation. A sample of an active region obtained around or shortly after perihelion will therefore be largely unaltered by solar heating even near the surface.

A cometary sample provides the unique opportunity to return pristine material to Earth. After the return of a small sample of the refractory component of a comet by Stardust and the upcoming in-depth investigation of a cometary surface by *Rosetta*, the return of a sample of largely unprocessed primordial material is the logical next step.

2.1.3 Potential of Triple F

The Wild 2 material in the *Stardust* sample was predominantly fine dust from our solar nebula, and not preserved isotopically anomalous pre-solar material (e.g., based upon the oxygen isotopic compositions [42]). The dust was mostly crystalline, not amorphous, and at least 10% of these crystalline materials appear to have originated in the inner solar system, not in the region where the Kuiper belt objects were assembled. A cometary sample analyzed with the powerful techniques available on Earth will shed more light into the composition of a comet and the origin of its components. It would also contain much coarser-grained materials and ices and, contrary to the aerogel capture of the *Stardust* samples, the sampled material will suffer little modification. Therefore, it will provide a much more complete picture of the processes operating in the early solar system.

Kuiper belt comets carry unique information on materials and processes across the entire solar nebula disk. For this reason direct comparison with undifferentiated asteroids (formed in the inner part of the disk) is important. Kuiper belt comets will also provide new information on the first generation planetesimals that formed the primitive asteroids, since in the comets these primordial materials are packed in ice and not heated as they were in many asteroids. However, to extract such information large returned sample masses will be required (hundreds of grams). Stardust collected <1 mg of very fine, refractory dust and only traces of volatiles [41, 54]. Large sample masses will permit radiometric dating even of minor cometary components, which are inherited from many different bodies, including broken up large Kuiper belt objects (see [9]). Only large sample masses will permit detailed studies of minor, unaltered organic components, including amino acids, and will provide sufficiently large quantities of unaltered presolar grains for detailed studies of nucleosynthesis and processing in the insterstellar medium.

2.2 Comets and life on Earth

In the endeavor to understand the different steps towards the origin of life on Earth and in a wider context in the Universe, one of the prerequisites is to identify the premises of emerging life. It is suggested that life emerged in water and that the first self-replicating molecules and their precursors were organic molecules of growing complexity. It is still an open question, however, whether the organic starting material relevant to the origin of life was produced in-situ on the primitive Earth or whether it was delivered from space. These two processes may not be exclusive but may rather represent complementary contributions towards the origin of life.

Comets represent the most accessible target for acquiring materials formed in the outer part of the solar system. How well has this material been preserved since the formation of our solar system? What is their inventory of complex organic molecules and what was their role in the processes leading to the emergence of life on Earth? Answers to these basic questions will also provide essential complementary information to the European science-driven aspects of the space exploration program with the overarching scientific goal to reach a better understanding of the emergence and co-evolution of life with its planetary environments. However, it must be stressed that the absence of liquid water in comets over long periods of time greatly diminishes, if not completely eliminates, the possibility of the existence of living organisms in or on comets.

2.2.1 Organics and prebiotic molecules

Comets probably contributed part of the carbonaceous compounds during the heavy bombardment phase in the inner solar system including the Earth 4.5–4 billion years ago [18]. Material arriving from outside may have been crucial for the evolution of carbon chemistry and subsequently life, since the atmosphere and surface of the early Earth were likely not favorable to organic syntheses. The terrestrial accretion process itself and the subsequent core differentiation as well as the impact events, are important energy sources which kept the surface of the early Earth fairly hot [40] and covered with volcanoes. Amino acids—the building blocks of proteins—and nucleic acids have been found in several carbonaceous chondrites. The small L-enantiomeric excess of amino acids measured in those meteorites indicates that the origin of asymmetric amino acid formation is not yet well understood.

Whereas the organic inventory of meteorites can be investigated in the laboratory by use of sophisticated analytical techniques, cometary nuclei—so far—evade our direct access. Our current knowledge is based on data from the different fly-by missions, and from the Stardust probe that brought back cometary grains from the coma of comet Wild 2. An organic component was identified in the Stardust samples which is richer in oxygen and nitrogen than organic compounds found in carbonaceous meteorites and Halley dust, indicating a different chemical composition and thus different chemical pathways

to its formation [54]. Polycyclic aromatic hydrocarbons (PAHs) have been observed in the *Stardust* samples, such as naphthalene ($C_{10}H_8$), phenanthrene ($C_{14}H_{10}$) and pyrene ($C_{16}H_{10}$). From laboratory simulation experiments, the existence of more complex molecular structures in comet nuclei is inferred. However, so far, we have not yet succeeded in a direct identification of complex organic molecules in cometary nuclei. One goal of the *Triple F* mission is to study the ratio of simple to complex organic molecules in the cometary nucleus. For instance, so far it is not known [21] whether H_2CO is an original nucleus molecule or rather a daughter molecule of POM (polyoxymethylene). The same is true for monomeric or polymeric HCN [25].

There is strong evidence that amorphous carbon and similar macromolecular material account for most of the carbon in the interstellar medium [43]. The same trend is observed in meteorites, where macromolecular material accounts for more than 80% of the carbon [23]. The link between macromolecular carbon in the solar system and the interstellar macromolecular carbon is yet to be understood, but it is tempting to assume that such a material is also present in comets. Apart from a major fraction of aromatic solid carbon, minor abundances of many organic molecules, probably including prebiotic ones, will be present in the cometary nucleus.

Living organisms are based on (a) left-handed amino acids that form proteins (biocatalysts, enzymes); and (b) nucleotide bases, phosphoric acid and right-handed ribose (sugar, carbohydrate) that form the genetic material DNA and RNA. The detection of life's precursor molecules in comets would provide important constraints for the origin of life on Earth and possibly elsewhere. The exact determination of enantiomeric ratios (and isotopic compositions) of prebiotic molecules in a sample returned from a comet will provide invaluable insights into the place and means of origin of the molecules important to the development of living systems.

2.2.2 Hydrosphere and atmosphere

Two sources of water on Earth are commonly envisioned: Adsorption of water by grains in the accretion disk [16] or delivery by comets and asteroids [15, 45]. The D/H ratio of SMOW (Standard Mean Ocean Water) is only half the D/H ratio of cometary water, and hence the suggestion that comets are a major source of terrestrial water is questionable. So far the cometary D/H ratio is estimated from the coma of three long-period and Halley-type comets: Halley, Hale–Bopp, and Hyakutake. It is unclear if the ratio is the same in short-period comets. Since comets formed from components that were created over a wide range of heliocentric distances, the D/H ratio may also vary between different ice crystals in the same comet, providing information about the variation of D/H in the solar nebula. Therefore, we need to determine the D/H ratio in various water ice aggregates and its variation within the comet.

A further question is related to the formation of the terrestrial atmosphere. Preferred gas components used to investigate this question are the isotopes of the noble gases and nitrogen. The former are chemically inert and the

latter corresponds to the major part of the current atmosphere. We know that the composition of the terrestrial atmosphere is not solar. Consequently, any realistic formation concept has to consider an evolutionary process starting from a primordial atmosphere. The evolution itself is caused by [51]:

- gravitational escape, probably driven by the Moon-forming impact and by the adsorption of intense ultraviolet radiation from the young Sun and
- planetary degassing.

Various scenarios describe how Earth could have acquired its primordial atmosphere. The primordial atmosphere could have been captured gravitationally from the gas of the surrounding solar nebula [52], or the atmospheric volatiles resulted from gases adsorbed on the infalling planetesimals during the accretion phase. The abundances of Ar, Kr and Xe on Mars, Earth and Venus suggest that comets could have delivered considerable amounts of these gases, along with other volatiles, to these planets at the end of the late bombardment period [49]. If one measures the elemental and isotopic noble gas ratios (e.g., $^4He/^{20}Ne$, $^4He/^{36}Ar$, $^{20}Ne/^{22}Ne$, $^{21}Ne/^{22}Ne$, $^{136}Xe/^{130}Xe$, $^{129}Xe/^{130}Xe$) and $^{15}N/^{14}N$ of the material provided by the *Triple F* mission, the potential cometary source, and hence the various scenarios, can be evaluated.

2.2.3 Potential of Triple F

A cometary nucleus sample return mission will be a crucial step in the investigation of the organic component and isotopic ratios of a cometary nucleus. The investigation of large samples with sophisticated analytical instruments in specialized laboratories will allow us to study in detail the variety of organic compounds including both large and small organic molecules, complex carbonaceous material, the organic-mineral connections in comets, and isotopic ratios.

The *Rosetta* mission on the way to Comet 67P/Churyumov–Gerasimenko carries instruments that will study the in-situ chemical composition of the comet nucleus. However, *Rosetta* is limited in the analysis of complex organics. The instrument COSAC [28] on the *Rosetta* Lander *Philae* will methylize non-volatile compounds such as carboxylic acids as well as amino acids to make them visible for gas chromatographic analyses. However, many of the larger organic molecules cannot be analyzed with *Rosetta*'s in-situ instrumentation. One important analysis that is not covered is sugar chemistry. Amino acids and their polymers are possibly accessible by derivatisation and GC–MS, but sugars and their polymers need methods too sophisticated for the kind of space instrumentation used on Rosetta's lander Philae. Similarly, the analyses of isotopic ratios is restricted to light elements and limited by sample size.

2.3 The mystery of cometary activity

In spite of substantial observational, experimental, and theoretical efforts, cometary activity is far from being understood. However, knowing how activity

works is vital for assessing how the pristine material from which comets formed has been processed and possibly altered over time. An answer may be found by combining data from the ESA mission *Rosetta* and the currently proposed mission. The latter will deliver complementary, unique, and extremely important information regarding a number of basic questions, discussed below. Some questions will be answered by conducting direct measurements on the retrieved material; others can be derived from these measurements in combination with modeling. However, there is no obvious way to settle the issue without bringing a sufficiently large and relatively unaltered sample of cometary material to Earth for analysis.

2.3.1 Heterogeneous distribution of active areas across the surface

The asymmetric shapes of the cometary gas production curves relative to perihelion as well as the asymmetric non-gravitational forces perturbing the cometary orbits are indirect evidence of discrete outgassing regions on the nuclei. More directly, the existence of jets, fans, shells and other structures in comae indicate an anisotropic emission of gases and possible "active areas" on the surface of the nucleus. The ESA Giotto mission to Comet 1P/Halley in 1986 provided the first close-up imaging of a cometary nucleus that turned out to have complex surface structures with dust emission restricted to a few "active regions" covering about 20% of the sunlit side of the nucleus [32, 33]. The close encounter with 19P/Borrelly (NASA Deep Space 1 mission, 2001) revealed narrow, highly collimated structures similar to those already seen in 1P/Halley [55]. Analysis of the surface morphology and albedo variations suggests that some landforms (e.g. mottled terrain) represent surface subjected to extensive sublimation-driven erosion in the past, while other features (e.g. bright-appearing slopes of mesas) are probably freshly exposed sources of some of the active jets [34]. Observations of Comet 9P/Tempel 1 by the NASA Deep Impact mission show differing coma distribution patterns of water and carbon dioxide with a high degree of spatial asymmetry [20]. Therefore, the mixture of active and inactive areas appears to be common, but the intrinsic differences between such surface types are unknown.

2.3.2 Depth of the water sublimation front in active areas

It is unclear if coma gas primarily originates from exposed surface ice, or from shallow sub-surface regions, but various arguments suggest that in an active area we find volatile material within a few cm of the surface. There certainly is water ice on the surface of Comet 9P/Tempel 1, as shown by spectral absorptions at 1.5 and 2.0 μm [59]. However, the estimated active area fraction [14] is at odds with the area fraction actually showing water absorption features. Furthermore, the distribution of water just above the surface strongly suggests that the bulk of the outgassing takes place along the noon meridian, which is on the visible side of the nucleus in a region that must have less than

1% surface ice coverage [20]. This implies subsurface sources, unless the far (unimaged) side of the nucleus is richer in ice, and/or additional (undetected) ice is present on the imaged side. If subsurface sources of ice indeed dominate cometary outgassing, chances are still excellent to find sublimation fronts well within the sampled 50 cm depth. Laboratory work [30] shows that a thin refractory mantle of some cm would strongly quench the outgassing, much below the level observed at comets. Both the analysis of the Hale–Bopp data [36] and the Deep Impact measurements of surface temperatures on Tempel 1 [29] show that the thermal conductivity of the surface material must be very low ($\leq$0.01 W/m K). This also implies that potential dust mantles in active areas must be very thin (mm to cm range), otherwise it would not be possible to transport enough heat to sublimate the water ice below [35].

An inactive area is probably characterized by a deeper refractory–volatile boundary. The absence of water absorption features in up range rays of Deep Impact ejecta and strong water ice absorption at 3.0 μm in the remaining ejecta indicate a stratified surface at the most likely inactive impact site, with an ice-rich interior covered by an ~1 m thick layer of dry material [60].

2.3.3 Physical, chemical, structural, and mechanical properties of near-surface material on a microscopic scale

The short- and long-term evolution of cometary material depends on its microphysical properties and the illumination conditions. To understand the outgassing processes and the physical properties that distinguish an active from an inactive region, thermal models must be supplied with physical, structural and mechanical parameters, such as heat conductivity, heat capacity, porosity, size distributions of grains and pores, pore connectivity, tensile strength, chemical composition et cetera. Such parameters change with surface location, depth, time, and in some cases, temperature. They can only be measured accurately and systematically in a sample of sufficient size in well-equipped laboratories. Such detailed information on microphysics is vital for explaining phenomena occurring on a global scale, over extended periods of time.

2.3.4 Conditions for dust mantle formation

Activity of comets at the same heliocentric distance of succeeding orbits is relatively constant. However, laboratory work on comet analog material has shown that ice and dust mixtures irradiated by solar light are quickly depleted in their water content at the surface by forming an insulating dust mantle, and activity drops quickly. Even taking into consideration that the presence of Earth's much higher gravity may cause results not directly applicable to comets, it remains true that the gas pressure of the volatiles is much lower than the Van der Waals forces between particles [37]. How then is activity maintained over time?

2.3.5 Intrinsic exothermal processes

Cometary outbursts and distant activity are common phenomena. Exothermic reactions, such as crystallization of amorphous ice [5, 38], are perhaps the strongest candidate for delivering energy for driving outbursts and dust blow-off. While it is difficult to avoid crystallization of amorphous ice during the transport from the comet to Earth, amorphous ice may be detected indirectly by a temperature increase in the sample during crystallization.

2.3.6 Potential of Triple F

Rosetta with its 21 experiments will provide important input to solve the questions listed above by investigations of Comet 67P/Churyumov–Gerasimenko. However, there are some limitations that will be overcome by the proposed mission:

- Laboratory measurements of microphysical parameters can be made in substantially larger detail and more systematically than in situ.
- The Lander Philae will go down to only one (probably inactive) area. *Triple F* will visit several regions with different morphologies and outgassing levels, exploring the reasons for diversity.
- The size of samples investigated with Philae (10 to 40 mm^3) is limited. The volume of samples returned will be orders of magnitudes larger and the samples will cover a wider depth range.
- The sample analysis is not limited by the technology and resources at the time the spacecraft is developed—analyses can be made using the full capability of terrestrial laboratories and new analyses can be made of curated samples as questions and techniques evolve.

3 The mission concept

3.1 Overview

The baseline mission foresees a launch in April 2018. The spacecraft driven by Solar-Electric Propulsion (SEP) will fly-by Earth in 2019 and arrive at the target comet 79P/du Toit–Hartley in mid-2023. During approximately 6 months of operations at the comet the spacecraft will get samples from three surface locations of the cometary nucleus by touch-and-go sampling. To prepare sampling and to enhance the scientific return, the comet will be investigated by remote sensing instruments and in situ dust and gas measurements. The sampling devices are corers that will be driven into the cometary surface once the spacecraft touches the ground. Ground contact will be for a few seconds only. After retrieving the samples, return travel to Earth will begin in early 2024. The samples are cooled down to 133 K during the complete return travel, except for 2 h at re-entry into Earth's atmosphere when the temperature will

increase to 163 K. The spacecraft will return to Earth and deliver the re-entry capsule in April 2028, after a total mission duration of 10 years.

3.2 The target comet: 79P/duToit-Hartley

A mission to Comet 79P/du Toit–Hartley (hereafter 79P) was selected as the baseline because of the relatively low ΔV of approximately 10.3 km/s required for the round trip and because it offers a launch opportunity at the beginning of the Cosmic Vision timeframe. Five other comets with ΔV between 10.0 km/s and 11.3 km/s were identified.

Comet 79P was detected by D. du Toit from South Africa in 1945. After its first observed perihelion passage it was lost for several decades. Finally it was recovered by M. Hartley in 1982, after a probable splitting event in 1976. 79P was observed again by professional astronomers during its last two orbits in 1995 and 2003. From observations of its inactive nucleus at large distance from the Sun the radius of 79P is estimated to be 1.4 ± 0.3 km [39].

The perihelion distance of 79P is currently 1.23 AU, but it will decrease to 1.12 AU by its perihelion in 2023 when it will be visited by *Triple F*. Its aphelion distance of 4.8 AU and orbital inclination of 3° are both relatively low, making 79P a good target for a sample return mission.

3.3 Launcher

For the *Triple F* mission a Soyuz launch from Kourou is considered. For Soyuz both, direct escape and escape from Geostationary Transfer Orbit (GTO) using a propulsion module are attractive. Various escape scenarios are possible. As the baseline, we consider use of a propulsion module and a lunar gravity assist which results in an escape mass of 2,000 kg and an excess velocity at escape of 1,100 m/s.

3.4 The interplanetary trajectory

The baseline trajectory for the *Triple F* mission is outlined in Fig. 1. An optimal solution was found for a launch date in April 2018. The round trip mission duration for this option is 10 years. The stay time at the comet is 7 months which provides sufficient time for a characterization of the comet and the sampling.

3.4.1 Transfer

Even with a state of the art electric propulsion system a direct transfer to Jupiter-family comets such as 79/P is not possible within reasonable time. A generically applicable strategy to reduce the ΔV for the transfer to a comet is

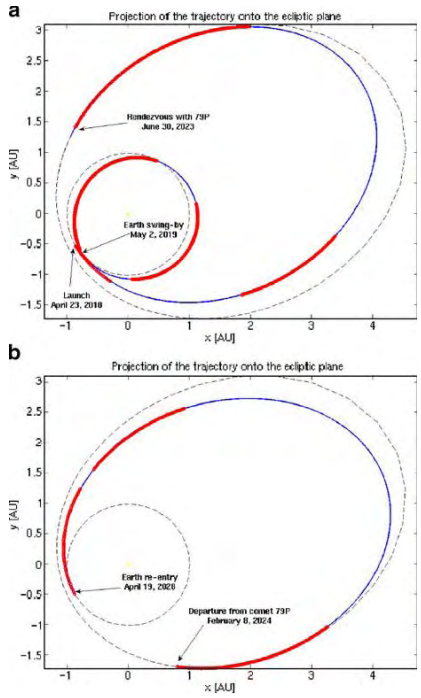

Fig. 1 Transfer (**a**) and return (**b**) trajectories to comet 79P/du Toit–Hartley (dimensions in AU). Thrusting periods are shown *in red*

the return to Earth for a gravity assist. The basic sequence for the transfer to the comet is the following:

- Launch into GTO
- Raise apogee to lunar crossing orbit by chemical propulsion stage (requires ~700 m/s from GTO)
- Perform a Lunar Gravity Assist
- Leave Earth and thrust for increasing eccentricity of heliocentric orbit and for targeting Earth
- Come back to Earth after little more than 1 year and perform an Earth Gravity Assist.

For the return trajectory it needs to be taken into account that the re-entry velocity into the Earths atmosphere shall not exceed a certain value. For the proposal a maximum reentry velocity of 13 km/s is chosen that lies within the range that was already demonstrated by previous missions (e.g. *Stardust, Genesis*). Hence the re-entry velocity is limited to 13 km/s. In order to comply with this limit, the return trajectory requires a braking maneuver that adds to the roundtrip ΔV.

3.4.2 Comet approach

Due to the low-thrust transfer the spacecraft will approach the comet at a very low relative velocity. The rendezvous will be achieved by a series of small maneuvers. In order to ensure collision avoidance during this phase (with the comet's gravity field still badly known), the maneuvers will never directly target the comet but always some point outside of its cross section. This strategy is also foreseen for *Rosetta*. However, the rendezvous maneuver sequence for *Triple F* is less risky due to the much lower relative velocity.

3.4.3 Re-entry

For the re-entry the *Triple F* spacecraft targets a hyperbola with its perigee at the Earth's surface. Approximately 5 h before the perigee the re-entry capsule is deployed.

The re-entry capsule will follow the desired re-entry trajectory entirely passively and without maneuver capability. After the deployment of the re-entry capsule the spacecraft conducts an orbit maneuver that puts itself on an Earth fly-by trajectory in order to avoid destruction.

3.5 Spacecraft

The basic concept of *Triple F* is simple: A single spacecraft will be sent to the comet, acquire the sample, and return. Due to the low gravity environment, the propellant penalty for this concept compared to a mothercraft–lander system is minimal and one can avoid the complexity of having to rendezvous the mothercraft with the lander in order to transfer the sample. The preferred sampling concept is that of a touch-and-go sampling. The whole maneuver will typically take about 1 h. Limiting factors are the rotational period of the comet and the need that the whole approach sampling and take-off sequence has to be carried out in daylight. The conclusion that touch-and-go sampling with the whole spacecraft is the preferred operational scenario had already been reached for the Hayabusa asteroid sample return mission [22] and also during the Asteroid Sample Return Technology Reference Study [1] for ESA. A major advantage is that the thermal control of the spacecraft does not have to be adjusted to the "hot" surface and that all resources of the main spacecraft are available.

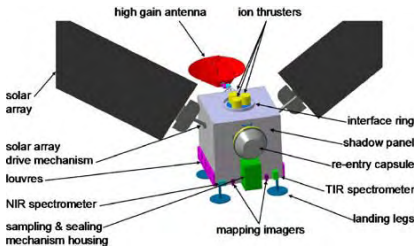

Fig. 2 *Triple F* spacecraft configuration concept

A major challenge is to reconcile the large wingspan of the solar arrays of approximately 15 m each, that is required by the electric propulsion system, with the need to avoid simultaneous ground contact of both solar panels (with the spacecraft continuing to move downwards) when landing. Our concept uses a 1 degrees-of-freedom (DOF) rotational mechanism so that when moving, the solar array follows an imaginary cone. To maximize ground clearance, the solar array will have to be turned in the morning/evening orientation when landing which is compatible with the desired landing scenario. The option yields optimal ground clearance and makes use of an existing solar array drive mechanism. The disadvantage of the concept is the motion of the centre of mass of the spacecraft introduced by the solar panel movement. However, this appears not critical, since it will be compensated by the thruster pointing mechanism of the electric propulsion system.

This thruster pointing mechanism is mandatory anyway in order to minimize the angular momentum build-up that would otherwise result from shifts in the spacecraft's center of mass due to fuel consumption and antenna pointing. Landing legs are foreseen to guarantee clearance of the attitude control thrusters from the ground.

A 2 DOF articulated high gain antenna (HGA) is proposed to ensure permanent radio link to the spacecraft during thrust phases and to allow simultaneous remote observations and data downlink at the comet.

The re-entry capsule needs to be placed on a panel of the spacecraft that is permanently in shadow. This panel also accommodates the sampling mechanism. The resulting spacecraft configuration is shown in Fig. 2.

3.5.1 Solar electric propulsion

The mission is based on the simultaneous operation of two RIT22 or T6 thrusters. The total thrust time of nearly 20,000 h per thruster is well within the 25,000 h expected lifetime capability of the *BepiColombo* thruster. In addition a third thruster is foreseen for redundancy. The architecture of the propulsion system corresponds to that of *BepiColombo* hence extensive use of the *BepiColombo* heritage could be made.

3.5.2 Power, telecommunications and data handling

For the *Triple F* mission a solar array with an area of 60 m^2 is foreseen. Considering aging and losses in the power processing units this corresponds to an available power of approximately 12,650 W at 1 AU. Of this power typically 500 W (+100 W margin) will be required for the bus leaving approximately 12,050 W to the electric propulsion system enabling a thrust level of 350 mN at 1 AU. The available power will decay with heliocentric distance, R, roughly as $R^{-1.7}$ due to the improved solar cell efficiency at lower temperatures. Ample power is available during coast phases of the transfer and during the comet proximity operations. In particular, an off-pointing of the solar arrays from the Sun direction that may be necessary to achieve sufficient ground clearance of the solar array during the touch-and-go operations is fully compatible with the available power. The minimal thrust level of the RIT22 and T6 ion engines of 30 mN is reached at 3.2 AU heliocentric distance. Beyond this distance the electric propulsion system needs to be switched off.

The solar array sizing is entirely driven by the power demand of the electric propulsion system. Also the power system design is determined by the requirements of the electric propulsion system: A 50 V bus is needed for the propulsion system while the rest of the spacecraft is powered by a 28 V bus derived from the 50 V bus. The power system architecture can be based on the concept of *BepiColombo*.

An X-band telecommunication system based on *BepiColombo* with a transmit power of 27.5 W is foreseen for telemetry, tracking and telecommand and science data downlink. An additional Ka-band link for Doppler measurements is proposed in order to allow a precise determination of the comet's gravity field even at low angles between the Earth and the Sun as seen from the spacecraft. For the HGA a design similar to that of *Mars Express* and *Rosetta* with a diameter of 1.6 m is foreseen. This system will provide a data rate of 2 kbps over a distance of 5 AU.

The two drivers for the data handling system are on the one hand the Guidance, Navigation and Control (GNC) during the touch-and-go sequence and on the other hand the demands of the remote sensing instruments, e.g. data compression. For the GNC the requirements are reduced by the fact that the gravitational acceleration due to the comet is small, and hence, the approach will be slow. Consequently processors like the LEON III that will be available in the Cosmic Vision timeframe will be more than sufficient for the GNC. Probably even a current ERC32 with 14 Mips would fulfill the requirements. The requirements for the handling of the instrument data will depend on the processing capabilities that are already incorporated within the instruments.

3.5.3 Guidance, navigation and control

Three-axis stabilisation is the only viable control concept in order to fulfill the pointing needs during thrust phases and proximity operations. The attitude

control system consists of sensors and actuators. A sun sensor is foreseen for initial attitude acquisition after launch and safe mode. Star trackers and an inertial measurement unit are used for attitude determination. Standard reaction wheels of 12 Nms capacity and a set of 12 (+12 redundant) 10 N thrusters are foreseen as actuators. In all nominal modes the attitude control of *Triple F* relies on reaction wheels. For safe mode the attitude control will rely on the thrusters. The thrusters are also used for wheel desaturation and orbit control.

The major challenge for the guidance navigation and control (GNC) are the comet proximity operations, including the touch-and-go on the comet. Years before the launch of the *Triple F* mission, extended experience of operating in the near nucleus cometary environment will have been accumulated by *Rosetta*.

The rendezvous with the comet takes place at heliocentric distances below 2 AU. Hence, the spacecraft will be confronted with significant outgassing from the comet during its proximity operations. Due to the gas and dust flux from the comet, stable orbits may not exist and a different strategy must be devised. Attractive options are hovering, which was the nominal mode of Hayabusa, or an eclipse-free terminator orbit (low cometary activity), the latter being the baseline in Agnolon [1]. For the terminator orbit, regular eccentricity control must be conducted in order to compensate disturbances by the cometary environment. These correction maneuvers will have to rely on optical navigation based on landmark tracking or limb recognition. Due to the high operational effort of a ground controlled GNC during proximity operations, the implementation of autonomous GNC seems preferable. Also for the hovering strategy, a certain level of autonomous GNC for the spacecraft is required in order to avoid a strong deviation from the nominal position due to changes in the cometary environment.

Hazards due to the activity of the comet need to be considered. The gas streaming from the nucleus exerts a pressure on the solar panels that pushes the spacecraft away from the comet. However, even for active Jupiter-family comets the average gas pressure at heliocentric distances larger than 1 AU is of the order of the gravity attraction. When the samples will be collected at a heliocentric distance of about 2 AU it will be considerably less. This can easily be compensated by the SEP. The second hazard is fine dust leaving the nucleus; the importance of that hazard depends on the sticking properties of the dust particles and the ill-constrained dust size distribution. Our strategy to avoid high dust fluxes on the solar panels is twofold. Firstly, the solar panels will be directed in a way that the area pointing towards the comet is minimized (orbit near terminator). Secondly, when operating close to the comet, times (local noon) and regions of high dust activity will be avoided. The dust flux will be continuously monitored by the cameras and the in-situ dust instrument. Due to the experience from *Rosetta* we will have a good understanding of the expected dust environment and the knowledge how to operate close to a comet. There is ample time (7 months) to characterize the inhomogeneous activity of 79P and to devise a safe strategy before touch down.

Ballistic descent from a low orbit is our baseline strategy for the GNC during the touch and go, following the conclusion of Agnolon [1]. He proposes to have the comet detection as well as the approach and orbit capture controlled by the ground, using radio navigation. The spacecraft would autonomously control the orbit and perform the landing and ascent maneuver, based on visual navigation with wide angle cameras. The duration of descent is estimated to range between 30 and 90 min, the landing precision on the order of 10 m.

The only major difference between the study by Agnolon [1] and *Triple F* as proposed here is the much larger size of the solar array due to the electric propulsion system. Avoiding the danger of ground contact with the solar arrays has already been discussed above. With this issue under control the GNC of *Triple F* can be based on the findings of Agnolon [1] and does not pose challenges beyond those identified there.

3.5.4 Thermal control

The *Rosetta* spacecraft is currently demonstrating the thermal control of a spacecraft over a range of heliocentric distances from 1 to approximately 6 AU. The thermal control of *Rosetta* is achieved by louvers which open at high temperatures and close at low temperatures. This simple concept is also applicable to the *Triple F* mission. More refined concepts could allow mass savings in the thermal control subsystems if required. In particular the louvers could be replaced by radiators and heat switches, which are currently being developed for the *Exomars* Rover in ESA's Aurora Programme.

A particular challenge of the *Triple F* thermal control is to ensure a cryogenic temperature of the sample. In Section 3.6.1 it is argued that a temperature of at most 135 K during transfer and 170 K for the reentry is desirable to maximize the science return. We designed a simple thermal control that will perform reliably during the 4 years return transfer and keeps the temperature below 133 K in interplanetary space and 163 K during re-entry.

The sample container will be transferred to the reentry capsule soon after sample acquisition. The re-entry capsule will be kept in the shadow of the spacecraft during the complete return transfer. The capsule will have three zones at different temperatures which are well thermally decoupled from each other.

The desired temperature of the sample container can be maintained with a modest radiator size of $0.4 \times 0.4\ m^2$ and a conductivity coefficient between the cold and the intermediate zone of 0.03 W/K. This is challenging due to the requirement to have a safe mechanical interface between the zones, but well within reach.

After the detachment of the re-entry capsule from the spacecraft the cooling of the sample container can no longer rely on the radiator of the return capsule because it may be exposed to sunlight due to the approach trajectory of the capsule towards Earth. Hence, during the final approach, the reentry and on ground before recovery of the capsule the sample container will be cooled from

the heat capacitor to which it is coupled. This concept is feasible because the temperature on the backside of the ablative heat shield will be quite modest. For a preliminary assessment a conservative value of 523 K was assumed taking into account the values for *Stardust*. Allowing for a temperature rise of the sample container of 30 K to 163 K and assuming a re-entry duration of 15 min (14 min for *Stardust*), followed by 2 h on ground before recovery, a heat capacitor of 5 kg water and a conductivity coefficient of 0.26 W/K between the backside of the heat shield and the cold zone is sufficient. Hence, the cooling of the sample during reentry is well compatible with the structural requirement of the re-entry capsule.

3.5.5 Re-entry capsule

There is a trade-off between the re-entry velocity of the return capsule and the braking ΔV of the *Triple F* spacecraft on its return transfer. We have taken a conservative approach in limiting the entry velocity to 13 km/s. A detailed analysis may well reveal that a higher re-entry velocity is feasible and more mass efficient and could hence lead to a better overall system performance. In any case an ablative heat shield is considered mandatory. It is the most lightweight option and it facilitates the cooling of the sample because it leads to a rather low temperature of the backside of the heat shield. For the final stage of the descent a parachute is foreseen in order to avoid high mechanical loads on the sample at touchdown.

3.5.6 Operations concept

The mission operations concept for *Triple F* shall ensure that the long mission duration of 10 years does not become a driver for the operational cost. Hence, a minimal number of ground contacts and a high level of spacecraft autonomy during transfer are desirable. For the mission the operational experience of the *BepiColombo* electric propulsion system will be available and hence it is assumed that also during thrust phase the spacecraft operations can be largely autonomous and ground contact can be reduced to once every week.

During the coast arcs of the transfer, ground contact will be infrequent—typically once per fortnight—because no specific telecommand or navigation needs arise during this phase. For the period around the Earth gravity assist and before the Earth re-entry permanent ground coverage and the use of delta-differential one-way ranging is desirable to achieve the best possible targeting accuracy.

For the comet rendezvous one ground station is sufficient and no large baseline tracking techniques are required. This low level of operational activity is possible due to the low approach velocity relative to the comet.

During the comet proximity operations the use of two or three ground stations is desirable in order to maximize the science return of this phase. However, the GNC strategy will be used to ensure safe operations of the

spacecraft when no ground contact is possible and hence a permanent operational attention during the comet proximity phase is not mandatory.

The mission will use ESA 15 m ground stations for launch and early orbit operations as well as for apogee raising sequence for escape from GTO. ESA 35 m ground stations will be used for deep space communications during all other phases of the mission.

3.6 Sampling, storage and analysis of samples

3.6.1 Requirements on sampling

Number of samples and sampling locations on the comet The purpose of the mission is to return at least three samples from different locations on the surface of the comet. Samples will be taken from places with different levels of activity and at different "geographical" locations (with respect to the spin axis and, therefore, insolation), as surveyed by the payload instruments. Highest priority will be given to a sample from an area where ice is visible, or where activity has been observed. Then, an inactive area will be sampled, to compare active versus inactive regions. Finally, one sample will be taken from a (polar) region that sees little sunlight and therefore has experienced relatively little heating since the comet reached the inner solar system. Once the topography of the comet is known from the monitoring phase, additional criteria for the choice of the sampling site may become important. For example, it would be interesting to have a sample from a smooth area similar to the ones imaged on Tempel 1 [61], because there is the possibility that this material could have erupted from the subsurface.

Dimensions of the sample container As discussed in Section 2.3, a sample depth of 50 cm will be sufficient to find water ice in an active region. The diameter of the sample container is driven by the desired sample mass and by the requirement that sampling change the sample properties as little as possible. Determination of the formation history of the comet by radiometric dating requires several hundred grams of material (Section 2.1). For a density of 500 kg/m^3, a cylinder with a length of 50 cm and a diameter of 5 cm can collect 500 g of cometary material.

Any volatiles (including organic and inorganic molecules) that are present in the subsurface should be sampled in such a way as to avoid structural or compositional changes. Therefore, non-destructive sampling is important for the further analysis of the cometary material. The maximum allowed stress during sampling must not exceed the tensile, compressive, and shear strength of most of the sample. As we expect the cometary surface material to be extremely fragile, care must be taken to ensure that the sampler will not compress or otherwise alter the sample. We consider a sampling tube with a thin wall as the best non-invasive means to fulfill this criterion. Figure 3 shows an x-ray image of a cylindrical specimen of high-porosity (85% porosity) non-volatile cometary analogue [8] which was sampled from a 2.5 cm diameter body

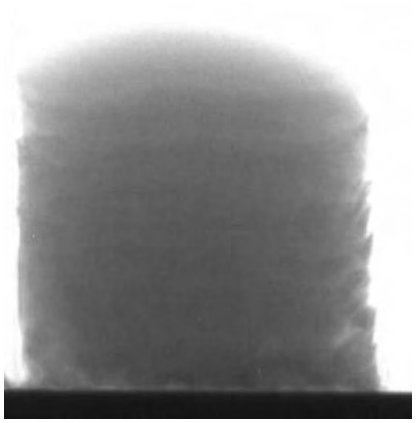

Fig. 3 X-ray image of a sample taken from a 2.5 cm diameter high-porosity dust agglomerate by means of a tube sampler. The diameter of the sample is 7.5 mm. Although the compressive strength of the sample is as low as 500 Pa, the sample structure is preserved at distances ≥1 mm from the sampler wall

by means of a plastic tube (inner diameter 7.5 mm, wall thickness 0.25 mm). Although the outer edge shows a sawtooth shape, which stems from the manual operation of the sampler, the overall morphology of the sample is unaltered. In particular, the porosity of the sample is unchanged at distances ≥1 mm from the sampler wall. The sample itself is extremely fragile with a compressive strength of 500 Pa and a tensile strength of 1,000 Pa. For a sample diameter of 5 cm, only a small fraction of the sample will be altered by interaction with the walls of the sampling tool.

Temperature of the sample during return to Earth The preservation of the sample micro-structure during sampling, cruising phase, re-entry into Earth's atmosphere and landing is vitally important for part of the mission science. The storage temperature of the samples is driven by the requirement that (at least) the most abundant volatile species, i.e. water ice, will be preserved in solid form. The relation between the gas mass and the initial solid phase mass as a function of the reservoir temperature T_R is:

$$m/M_{ice} = \Psi/(\Psi - 1) * (P_V m_g)/(\rho_{ice} k_B T_R)$$

In the above equation Ψ is the fraction of the probe volume filled by solid material, P_V is the vapour pressure, m_g the mass of a water molecule, and ρ_{ice} the density of the ice. We used the Goff Gratch equation (Smithsonian Met. Tables, 5th ed., pp. 350, 1984) to calculate $P_V(T)$. The calculations show that up to a temperature of 190 K and a porosity of 0.7, the fraction m/M_{ice} is always below $2 * 10^{-7}$. A temperature $T \leq 200$ K will guarantee that the ice

will stay in cubic form (if cubic ice is present close to a cometary surface) and that sintering will be inefficient in solidifying ice–ice contacts.

The equilibrium calculation shows that during the whole return trip only a negligible fraction of the water ice will be in gaseous form. However, equilibrium is maintained by a large number of sublimations and recondensations. In the porous cometary material the gas molecules may move before recondensation, resulting in structural changes. As a worst case scenario, we assume that sublimation and subsequent recondensation always cause modification to the sample. In this case, the requirement is that the sublimation timescale (into vacuum) is larger than the travel time from the comet to Earth.

Figure 4 shows that a temperature of 135 K is sufficient to preserve the ice quantitatively (at the 90% level) in solid form over a mission time of 5 years. A temperature increase to 170 K during 2 h of atmospheric re-entry is acceptable.

The sample temperatures fulfill the requirement of preservation of the micro-structure of the sample. This does not necessarily mean (and it is not required for the scientific goals of the mission) that the sample remains completely unchanged. For example, due to the much higher vapour pressures of other cometary volatiles, a quantitative retention of minor ice species in solid form may require still lower temperatures. Also, should amorphous ice be present in the samples, the temperatures may not be sufficiently low to avoid its transformation into crystalline ice. However, maintaining substantially lower temperatures would be technically challenging. Therefore, we decided to identify volatile ices and amorphous water ice without trying to maintain them in their original state. Since the sampling device is sealed, a mass-spectroscopic analysis of the gas composition will unambiguously determine the total contents of all volatile species. Thermal probes on the sampling device will detect the temperature increase associated with the exothermal transformation of amorphous ice into crystalline ice.

Strength of the sampled material Unfortunately neither Deep Impact nor other comet observations measured the strength of cometary material. Various

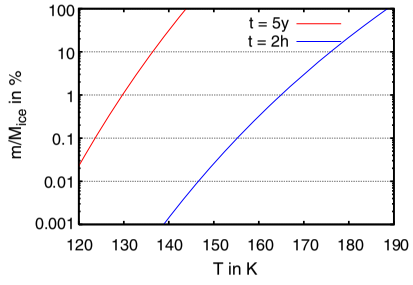

Fig. 4 The percentage of sublimated water ice molecules is shown for a time span of 5 years (*red curve*) and of 2 h (*blue curve*)

analyses of the impact cloud created by Deep Impact resulted in different upper limits for the strength of Comet Tempel 1 on scales of meters. The highest upper limit is 65 kPa [31]. The few observational constraints we have for comets and cometary meteoroids as well as theoretical considerations and laboratory measurements [8] for weakly bound aggregates lead us to estimate the quasi-static tensile (or shear) strength of cometary material in the dm- to m-range to be on the order of 1–10 kPa, while the compressive strength is estimated to be on the order of 10–100 kPa. We require the sampling mechanism to be able to sample materials with strength of up to 1 MPa. This corresponds to the highest values measured for sintered water ice.

3.6.2 Concept of the sampling mechanism

Several methods of sampling material from a small body have been discussed in Agnolon [1]. Here we show the preliminary design of a simple mechanism that allows rapid touch-and-go sampling (duration $\leq$2 s) for the expected conditions of low or moderate surface strength of a comet. It was developed at the Polytechnic University of Hong Kong based on heritage from Beagle 2 [47].

A sampling mechanism with three corers is foreseen that can be activated separately in three different regions of the nucleus (Fig. 5). The device will use a tubular coring system with a length of 50 cm and a diameter of 50 mm that is propelled by a spring mechanism into the cometary surface. Since the bottom of the sampling cylinder is open during sampling, a shutter mechanism is needed that keeps the sample in the corer during its transport from the cometary surface to the spacecraft.

The acquired sample is directly delivered into a cooled transport container inside the re-entry capsule. Cross-contamination can be avoided by

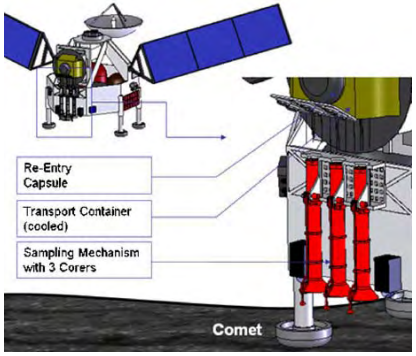

Fig. 5 Global architecture of the sampling mechanism

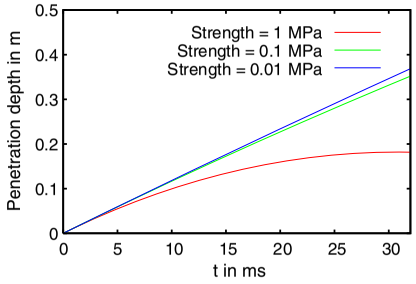

Fig. 6 Penetration depth plotted as a function of time for three different cohesive compression strengths. A friction constant of 0.1 N/m is assumed

the complete separation of the samples in the cooling compartment. The shutter mechanism is activated by the same cable mechanism that retrieves the coring tube.

The suggested sampling tube will be a Titanium cylinder with a wall thickness of 0.5 mm. Its total weight is about 200 g. Such a cylinder can be accelerated by the springs to a velocity of approximately 12 m/s (spring system has flight heritage from the *Rosetta* lander eject system). Calculations show that the device can penetrate into material of strength of up to approximately 1 MPa (see Fig. 6). The penetration depth is calculated from the linear momentum balance equation taking into account the cohesive force of the material, friction along the surface of the cylinder, gravitational force, and the increase of the moving mass due to shoved material. The calculations represent a lower limit to the actual penetration depth because the cutting force of the sharp edge of the cylinder is not considered. Should the need arise to sample still stronger materials, a projectile gas generator (flight heritage from the *Rosetta* lander anchor subsystem) could accelerate the same tube to more than 90 m/s, allowing sampling even of compact water ice.

3.6.3 Sample analysis strategy

Handling of samples on Earth, distribution and preservation The future return of extraterrestrial materials by ESA requires a European repository facility. In the present case, it will perform sample separation of gaseous volatiles, ices (including their trapped gases), organics and solid minerals. The gases in the sample containers would be transferred into reservoirs for further analyses. Organics will be present in icy and solid fractions. New techniques are required for separation of these phases under conditions similar to those on the comet. The facility will also coordinate the sample distribution. It will store the major part of the material for posterity, in anticipation of improved future analysis techniques. This facility might be associated with a scientific institution that already has required analytical techniques, experience in micro-sample

handling including microtome and in situ focused-ion-beam lift-out, as well as the preparation of thin sections. Opening of the containers, sampling and storing of the different phases will be performed in a clean environment, with the sample in vacuum to avoid adsorption of terrestrial atmospheric contaminants.

Examination of the samples with state-of-the-art analytical techniques is necessary to accomplish the major mission goals outlined in Section 2. To maximise scientific output and minimise sample consumption, many techniques will be applied to the same material. Sample requests and allocation (a few percent of the recovered material within the first 5 years after return) should be controlled by a standing committee (similar to NASA's "CAPTEM" committee or its "Meteorite Working Group"). For a fast publication of scientific results, a small fraction (<1%) of the returned material will be distributed rapidly to pre-selected research institutions.

Analyses The amount of material returned with *Triple F* (100 s of grams) will exceed by far that returned with *Stardust* (~mg). Moreover, the sampling technique (Section 3.6.2) will not mix the material intimately with any collector material. These unique mission elements will allow a large number of examinations that were not possible with the Stardust samples.

Initial non-invasive sample inspection could be achieved with x-ray tomography, providing sub-micrometer resolution and full 3D structural information. The measurements will reveal information about porosity, grain size, pore size, stratigraphy and (to some extent) elemental distribution within the sample. Initial mineralogical and petrologic analysis of most of the mineral grains should entail Scanning Electron Microscope (SEM) imaging and Energy Dispersive X-ray (EDX) analyses on all particles, enabling sample requestors to analyse the most suitable samples. Quantitative x-ray spectrometric elemental analyses should be performed on each grain to establish a library of compositions, done by the repository facility for consistency in data. Large particles (>10 μm) should be analyzed with synchrotron X-Ray Diffraction (XRD). For smaller particles, microtome slices could be prepared for TEM analysis. Relatively non-destructive spectroscopic analyses including IR, Resonant Raman and UV spectroscopy will follow, prior to further analyses by more or completely destructive techniques, such as, e.g., Secondary Ion Mass Spectroscopy (SIMS) or conventional mass spectrometry.

A major goal of all mineralogical analyses will be the search for high temperature phases and hydrated minerals. The presence of the former would add to the evidence of large scale mixing in the nebula [10, 63], whereas the latter would potentially indicate extended warm periods on the comet in the past. Moreover, as yet unknown or fragile minerals might be present that were not preserved in primitive meteorites or Wild 2 particles due to sampling technique or more severe heating on the asteroidal parent bodies.

High-precision mass spectrometric analyses of all fractions of returned cometary material will have highest priority. Deuterium enrichments will unequivocally prove the extraterrestrial origin of the material [44]. H, C, and

N isotopic anomalies in the organic fraction will localise interstellar material [11] that has survived the formation of the solar system. The O isotopic compositions in various extraterrestrial materials exhibit heterogeneities [12], implying spatial or temporal variations during the condensation of the first solar system material. Large samples to be returned with this mission will allow the investigation of refractory elements such as Mo, Zr and platinum group elements, which are important to assess heterogeneity and degree of large-scale mixing in the solar system. These analyses require high-precision isotopic measurements, obtainable with MC–ICPMS or TIMS. The samples will also be investigated for stable isotope fractionation effects, e.g. in Mg and Fe., which will provide information on the conditions during which cometary material formed.

The isotopic compositions of presolar stardust grains indicate that they formed in the dust ejecta of previous star generations [62]. Their abundances in extraterrestrial matter reflect thermal processing in the early solar system and on parent bodies. Thus, the abundance of presolar stardust in returned comet samples, identified by SIMS isotopic mapping, could be a sensitive probe of cometary thermal history. Only a few grains have been identified in comet Wild 2 dust [57], suggesting a lower abundance than in cometary IDPs [48]. However, sampling might have introduced severe bias. The more gentle collection method of this mission will allow presolar grains to be more readily preserved, providing better estimates of the presolar grain abundance in comets. Presolar grains might retain coatings acquired while present in the ISM, but that would not have survived the heating that other extraterrestrial material has experienced.

All cometary matter (ices, organics and minerals) is exposed at various times to irradiation. As the cometary surface will continuously be renewed, the most recent effects of space weathering and the production of cosmogenic nuclides can be examined. Structural changes due to such irradiation, e.g., amorphisation of ices, minerals and carbonaceous matter might be visible. For these studies, noble gases in various grains will be studied, the depth profiles of various elements, as well as the response to irradiation of carbonaceous material with Resonant Raman and IR spectroscopy. The latter techniques will also be used to find evidence for the irradiation of carbonaceous matter in interstellar space *prior* to its incorporation into the comet. Chemically, isotopically or structurally distinct rims around cometary grains would help to assess the conditions prevailing in the protosolar cloud. The composition of micron-sized grains will be measured, e.g., with the Time of Flight SIMS [58] technique, which provides high sensitivity at a very small scale. This technique also detects organic compounds in situ and provides information about the elemental distributions in mantles around cometary grains.

The volatile (noble gases, H, C, N, O, S) content of cometary ice is controlled by the conditions prevailing during its formation, either in the dense interstellar cloud or in the outer solar nebula [50]. Hence, it is of high priority to determine the relative volatile abundances in the various cometary ice grains. Moreover, the isotopic compositions of noble gases, especially Xe,

should be determined, both in solid grains and in icy agglomerates, which requires particular, highly sensitive techniques including resonance ionization [26]. Gas abundances of CH_4, CO, CO_2, N_2, NH_3, etc. are extremely important, e.g., in order to assess the form in which N has been trapped in the ice, and for comparison with spectroscopic results.

Analyses of organic matter found in ice and associated with mineral grains will provide insights on the early history of our solar system and the extraterrestrial delivery of organic compounds that occurred on early Earth (see Section 2.2). Hence, most important is the search for biologically relevant compounds, such as amino acids or nucleobases, which have been detected in meteorites. In addition, the detection of chiral excesses in these compounds will be essential, as will the comparison with meteoritic organics. Analytical techniques include liquid chromatography with fluorescence detection (HPLC–FD), liquid chromatography–mass spectrometry (LC–MS), gas chromatography–mass spectroscopy (GC–MS) and ionization techniques such as Matrix Assisted Laser Desorption Ionization (MALDI), solid state ^{13}C NMR (Nuclear Magnetic Resonance), XANES (X-ray Absorption Near-Edge Structure) and EPR (Electron Paramagnetic Resonance).

3.7 Payload

Overview

Apart from the sampling device, the mission requires a basic payload to fulfill the following objectives:

1. Characterize the comet, mainly its activity level and topography, with sufficient spatial resolution to identify appropriate sampling sites
2. Mapping of the nucleus to derive important chemical and physical properties that provide the context for the samples
3. Monitor the environment of the spacecraft to avoid hazards, mainly due to cometary dust

An overview of the payload is given in Table 1. The total mass of that payload is less than 20 kg.

Cameras

Triple F will carry a complement of four camera systems, designed to address different scientific requirements of the mission. For increased reliability, except for the high resolution camera each of the cameras consists of two identical, cold redundant units, for a total of seven camera heads. The first camera (high resolution imager, HI) provides the global monitoring of the nucleus during comet approach and during phases when the spacecraft is further than several tens of km from the nucleus. The second camera (the Mapping Imager—MI) will consist of a moderate angular resolution framing imager. This instrument will be responsible for global mapping from distances between 5 and 20 km, corresponding to a resolution between 0.5 m and 2 m.

Table 1 Summary of the payload (objective as defined in the text)

Instrument	Objective	Mass (kg)	Power (W)	Remarks
Cameras	1,2,3	4.2	10	
Near-IR imager or spectrometer	1,2,3	2.0	10	
Thermal IR instrument	1,2	3.5	7	
Mass spectrometer	2	4.0	10	Will also examine small sample
Dust in-situ monitoring experiment	3	< 5.0	20	
Radio science investigation	2			
Penetrometer	2	0.1		
Permittivity probe	2	< 0.3	< 1	On sampling device
Thermal probe	2	< 0.1	< 0.2	On sampling device

The third imager is a miniature wide-angle Fast-Framing Camera (FFC) which will be active during the descent, and ascent phases. This instrument, by acquiring image sequences at a rate in excess of 5 Hz, will document (and possibly guide) the descent of the orbiter with increasing accuracy. In this way the FFC will also provide local context by imaging the neighborhood of the sampling site with a resolution up to about 1 mm. The fourth camera will be a Close-Up Imager (CUI) which will monitor the complete sample acquisition and storage sequence during touch-down. In order to be able to observe the sample in the shadow of the S/C, the CUI will be equipped with a miniature LED illumination device.

The field of view of the HI will be 1.5°, imaged on a 2,048 × 2,048 APS array. The specifications of MI, FFC, and CUI follow those of the cameras in Agnolon [1].

Near-IR imaging spectrometer

The main scientific objectives of the infrared spectrometer are the following:

- to support the selection of the sampling sites by searching for surface ice and monitoring the gaseous activity on the nucleus and its spatial distribution
- to determine the nature of the solids on the nucleus surface (composition and structure of ices, dust and characterisation of organic compounds)
- to identify the gaseous species in the coma

While it is highly probable that the design of the near-IR instrument will benefit from the technological progress of the future years, we can refer to heritage from instruments already existing or in development.

The proposed instrument could be a simplified version of VIHI, a hyperspectral imager being developed to fly on ESA's *BepiColombo*. The VIHI channel concept is based on a collecting telescope and a diffraction grating spectrometer ideally joined at the telescope focal plane where the spectrometer entrance slit is located. The image of the slit is dispersed by the diffraction grating onto a two-dimensional detector. A single 256 × 256 thinned infrared array detector shall be used which can achieve high quantum efficiency even in the visible domain. The instantaneous acquisition on the two-dimensional

detector consists of the slit image diffracted by the grating over the selected spectral range (1–3.5 μm). The complete image is built in time by subsequent acquisitions (push broom mode). The final result is a three dimensional data set, in which each pixel has a spectrum associated with it. The instantaneous field of view will be 250 μrad and the field of view 3.7°. The instrument is housed in a single box that contains the optical system (Telescope plus Spectrometer), the calibration unit, shutter, Focal Plane Assembly (housing the detector and the TE Cooler) and proximity electronics. The operating temperature will be 170 K.

Thermal IR imaging spectrometer/radiometer

Measuring the thermal emission from the cometary surface would support the selection of the sampling site and provide valuable information about physical and mineralogical characteristics of the target. The temperature of sublimating water ice on the surface is about 200 K near perihelion. A thermal infrared radiometer (TIR) could be very useful in detecting possible locations of surface ice (and therefore activity) by their low temperature. Furthermore, the TIR spectral range provides a further excellent opportunity to characterize the mineralogical state of the cometary surface.

From the discussion above we propose an integrated imaging TIR spectrometer/radiometer, which works in the 5–40 μm range, be included in the payload of the *Triple F* mission, an instrument similar to MERTIS on *BepiColombo* but with a larger FOV (11.5°) and covering a broader wavelength range for the spectrometer part. Because of the sensitivity limitations of thermal detectors, the spectrometer is designed to provide spectra in 240 spectral channels with good S/N mainly for surface temperatures above 300 K whereas the radiometer is optimized for accurate measurements of the emitted flux in two broadband channels to cover the whole range of relevant temperatures from 100–400 K.

The focal length of the instrument will be around 5 cm. The spatial resolution will be 0.7 mrad for the spectrometer (7 m from a distance of 10 km) and 5 mrad (50 m from 10 km) for the radiometer. A bolometer and a thermopile will be the detectors for the spectrometer and radiometer, respectively. The total dimension of the instrument will be about 14 × 16 × 12 cm.

Mass spectrometer

It is well known that comets contain a wealth of volatile and super-volatile material including radicals like CO, CH_2, and CH_4 (e.g., [3, 24]). The goal of the mission is to bring back original, unprocessed material. However, taking a sample from the comet and bringing it back to the Earth cannot be done without some disturbance to the material, in particular sublimation of volatiles. Therefore, it is mandatory to have a mass spectrometer on board, which can analyze the most volatile or reactive compounds in situ in order to get the starting condition of the sample. The measurement would be twofold: the mass spectrometer would analyze the natural outgassing of the comet in the approach and prelanding phase. When acquiring the main sample a second much smaller sample will be acquired and placed in front of the mass

spectrometer. The mass spectrometer can then analyze the composition of this second sample during the journey back to the Earth over a long time (until the sample has fully evaporated). This will require two separate inlets to the ion source which can easily be achieved because the direction of the neutral gas flow is not critical. The mass spectrometer will not have the same resolution and sensitivity as laboratory mass spectrometers, but it will allow us to assess the initial condition of the sample and to deduce the chemical alterations the material has undergone from the comet to the laboratories on Earth.

We foresee using a time of flight mass spectrometer with an electron bombardment ion source. Such an instrument can easily reach a mass resolution m/dm of 1,500, high sensitivity and mass ranges up to >300 amu. The design could be based on the heritage of *Rosetta*-ROSINA/RTOF [4].

However, RTOF is too heavy to be included in the present mission. This can easily be solved by omitting the requirement that the mass spectrometer has to be built with an ultra-high vacuum enclosure and be launched sealed under vacuum as was done for ROSINA/RTOF. This requirement was necessary in the case of the *Rosetta* mission to study the comet far away from the Sun when cometary activity is minimal. RTOF has two independent channels (ion sources and detectors) that can be reduced to one for the present mission, thus saving not only detector and ion source but also electronics. Therefore, it would be possible, with current technology, to build a reflectron-time of flight instrument with a mass budget of 4 kg. The dimensions of the instrument will be about 20 × 20 × 50 cm.

Dust in-situ monitoring experiment

The S/C will have to operate deep inside the comet coma, both during the monitoring phase and during the descent for sampling. Therefore, it is important to characterize the dust distribution in the coma in order to control and guarantee safety for mission operation and S/C health. Therefore, an in situ dust instrument is essential as a “security device” to measure the dust flux on the S/C.

The GIADA experiment on board *Rosetta* will study the cometary dust environment of 67P and will accomplish unprecedented in situ primary scientific measurements [13]. A similar experiment on board the *Triple F* mission will fulfill the aforementioned security requirements and will in addition provide scientific data as it shall provide *real time* data on dust flux of “direct” and “reflected” grains, dust velocity distribution, dust evolution in the coma, dust changes vs. nucleus evolution and emission anisotropy, determination of dust-to-gas ratio, and identification of non homogeneous dust emission features from the surface (active areas, jets).

The instrument is designed to measure momentum, scalar velocity and mass of single grains. From the detection of particles vs. time information about dust abundance and spatial distribution vs. physical and dynamic properties is derived. Its two stages of detection form a cascade: an Optical Detection

System (ODS) and an Impact Sensor (IS). When a grain crosses the ODS, it is optically (scattered/reflected signal) detected, and its physical (shape and size, mainly) and chemical (through the optical constants) properties are measured. For each grain impacting onto the IS, the momentum of the incident grain is measured. With this system it is possible to measure abundance and dynamic properties of grains present in the comet coma. The ODS gives a first estimate of the speed of each crossing grain, and the speed of the grain is measured again, but with more accuracy, from the time-of-flight between ODS and IS. In this way for each detected grain, speed, time-of-flight, momentum and, therefore, mass are measured. The field of view of the ODS + IS system is about 40°. In addition, a network of microbalances (MBSs), with field of view of about 40° each, point in different directions to monitor flux of submicron and micron particles from 10^{-10} to 10^{-4} g. The instrument is equipped with controlling electronics to drive the sensors and to transmit telecommunication to and from the spacecraft. The size of the instrument is about $23 \times 25 \times 30$ cm.

Radio science investigation

The Radio Science Experiment RSE will use the radio signals transmitted from the onboard radio subsystem at the carrier frequencies X-band and Ka-band in the two-way radio mode (X-band uplink). The goal is to derive perturbing forces acting on the spacecraft by measuring the Doppler shift of the carrier signals caused by additional changes in relative velocity. Perturbing forces of interest may be:

- the gravity acceleration of the cometary nucleus which would reveal mass, bulk density (together with a volume estimate from the camera)
- the outgassing from the cometary nucleus which would reveal the combined gas and dust production rate (although the major contribution will come from the gas).

The measurements require a highly stable two-way link where the stability of the X-band uplink is derived from the ground station's hydrogen maser. The spacecraft receives the X-band uplink and transponds it back to Earth phase-coherently at two simultaneous downlink frequencies at X-band and Ka-band. Although the Ka-band downlink seems to be much noisier than the X-band downlink, it is possible to correct for the plasma noise in order to achieve a clear and four times stronger Doppler signal at Ka-band than at X-band. This allows us the detection of very small perturbations in the <10 μm/s range. X/X and X/Ka transponders are available on the market and have been flown on ESA missions (SMART-1).

These measurements require that the spacecraft performs attitude changes using the reaction wheels only during the gravity observations. Any attitude changes by thruster firing would destroy the observations.

The mass determination shall be an iterative process starting during the approach phase. Each mass determination at a certain error level will allow manoeuvring the spacecraft closer to the nucleus.

Comet Penetrometry Experiment (CPEx)

Penetrometry is the use of a penetrating probe to measure mechanical properties of the target material. A comet nucleus sample return mission offers a rare opportunity to make contact with undisturbed cometary subsurface material. Compared with previous missions, *Triple F* will provide measurements at multiple locations on the target comet. Penetrometry at the sampling locations will be useful for two main reasons:

Firstly, it can support sample collection by means of dynamics measurements performed during sampling. Questions that may be addressed include: Where did the material actually come from? What was its undisturbed volume? What is the strength and texture of the undisturbed material? To what extent was it disturbed, crushed and mixed during sampling? Secondly, penetrometry can generate unique ground-truth science. The penetration resistance of cometary material is sensitive to its origin and modification. Furthermore, measurements with depth can detect layering, e.g. the presence of low-cohesion material overlying a sintered layer at the water ice sublimation front. European heritage in this technique is strong, including sensors flown on *Huygens* and *Philae*.

Although the primary requirement for sampling limits the possibilities for dedicated geotechnical measurements, a great deal may still be learned from a set of simple measurements. The solution we propose for *Triple F* is to incorporate small sensors to monitor dynamics during touchdown and sampling. Assuming a short-duration (few s) touchdown and a coring tube driven quickly (10 m/s initial speed) into the ground, we propose the following:

- Displacement sensor to monitor the relative position of the sampling tube and spacecraft. This could be implemented by means of an optical bar-code technique. Stripes affixed to the core tube would be interrogated by a small light source and photodiode. Mass: ~5 g. Data: 1 bit at 50 kHz during sampling, i.e. 50 kbit/s. Heritage: HP^3 DACTIL tether length sensor.
- Microphone-acoustic vibrations in the sampling mechanism should be sensitive to the texture of the sampled material and its variation with depth. A small piezoelectric or strain gauge sensor mounted on the sampling system at a location affording good acoustic coupling could fulfill this role. Mass: ~2 g. Data: 12 bits at 50 kHz during sampling, i.e. 600 kbit/s. Heritage: COTS aerospace components.
- If possible, a single-axis accelerometer mounted near the upper end of the coring tube. This would measure the deceleration, and thus force, encountered by the sampling tube. Mass ~2 g. Data: 12 bits at 50 kHz during sampling, i.e. 600 kbit/s. Heritage: COTS aerospace components, *Philae* MUPUS ANC-M, *Huygens* SSP ACC-I, *Huygens* HASI ACC, HP^3 DACTIL.

- Harness and electronics: 100 g for the displacement, microphone and accelerometer sensors.

Permittivity probe

A permittivity probe measuring the electric properties of the sample between 0.1 Hz and 10 kHz is well suited to monitor changes in internal structure of the sample which are associated with sublimation processes of H_2O. The electrical permittivity of ice is unique amongst the rock forming minerals in the low frequency range, as the dielectric constant is of the order of 100 under static conditions, thus, more than an order of magnitude higher than for rocky materials, and decreases with increasing frequency to a value of 3.1 for infinite frequency.

The permittivity probe used to monitor the sample closely follows the design of a mutual impedance probe. Ringsector-like electrodes printed onto a Kapton foil are attached at different depths to the inner wall of the sample container. A current generator is connected to two selectable transmitter electrodes, and the generated voltage is sensed as a function of frequency by a number of receiver electrodes. By using different transmitter/receiver geometries across the sample an electrical "image" of the sample can be created. The total mass of the permittivity probe including electronics and harness is estimated to be less than 300 g and the average power consumption during operation is less than 1 W.

Thermal probe on sampling device

The knowledge of the original cometary temperature profile at the time of sampling measured as a function of depth would be of considerable value for the interpretation of the sample measurements. Because the titanium sample container has a several orders of magnitude higher thermal conductivity than the cometary soil, contact measurements cannot easily be used for that purpose. A possible solution is, therefore, based on the use of radiometric sensors (e.g. thermopiles as will be used for measuring the surface temperature at the *Rosetta* PHILAE landing site of comet 67P/Churyumov–Gerasimenko, [56]) which are mounted in different depths at the inner wall of the sample container. The short time constant of these sensors of about 200 ms makes the measurement of the temperature profile during the first seconds after insertion of the sampling device possible. This is before the temperature of the low conductivity cometary material can effectively adjust to the wall temperature. In addition, continuing the measurements after sampling would allow inferring thermal properties of the fresh sample. Furthermore, in case that a significant amount of heat is released inside the sample in the process of crystallization of originally amorphous ice, monitoring of the sample temperature as a function of depth could prove the existence of this process. Assuming 25% amorphous ice in the lower parts of the sample, the crystallization heat would increase the temperature by approximately 20 K, which is easily detectable by the sensors.

For the reasons described above the implementation of several (around 8–16) thermopile sensors into the sampling device could provide valuable

information about the initial temperature profile of the sample. The resources needed by this instrumentation are minor, basically an electronics comprising of multiplexer, amplifier and ADC (assuming that another DPU controls the data acquisition) with a mass of about 100 g (including harness) and a power consumption of less than 200 mW.

4 Summary

A Comet nucleus sample return mission is a unique means to provide valuable information about

- The formation of the solar system from the protosolar nebula
- The role comets played for the development of the hydrosphere and life on Earth
- The way cometary activity works

Recent results from the Deep Impact mission show that the cometary surface is of low strength and that cold, relatively unprocessed material can be found at shallow depths of a few tens of cms. Therefore, the return of a cooled sample from an active Jupiter-family comet is possible as a medium-sized mission with a total duration of approximately 10 years.

The *Triple F* mission has not been chosen for the first cycle of Cosmic Vision. Nevertheless, we believe that it is a compelling mission concept that should be considered for future space exploration programs.

References

1. Agnolon, D.: ESA Technology Reference study report SCI-PA/2007/004/DA (2007)
2. A'Hearn, M.F., et al.: Science **310**, 258 (2005)
3. Altwegg, K., Balsiger, H., Geiss, J.: Astron. Astrophys. **290**, 318 (1994)
4. Balsiger, H., et al.: Space Sci. Rev. **128**, 745 (2007)
5. Bar-Nun, A., Laufer, D.: Icarus **161**, 157 (2003)
6. Belton, M.J.S., et al.: Icarus **187**, 332 (2007)
7. Bizzarro, M., et al.: Science **316**, 1178 (2007)
8. Blum, J., et al.: Astrophys. J. **652**, 1768 (2006)
9. Brown, M.E., et al.: Nature **446**, 294 (2007)
10. Brownlee, D.E., et al.: Science **314**, 1711 (2006)
11. Busemann, H., et al.: Science **312**, 727 (2006)
12. Clayton, D.: In: Davies, A.M. (ed.) Treatise on Geochemistry—Meteorites, comets, and planets, vol. 1, pp. 269. Elsevier (2003)
13. Colangeli, L., et al.: Space Sci. Rev. **128**, 803 (2007)
14. Davidsson, B.J.R., Gutiérrez, P.J., Rickman, H.: Icarus **187**, 306 (2007)
15. Delsemme, A.H.: American Scientist. **89**, 432 (2001)
16. Drake, M.J.: Meteorit. Planet. Sci. **40**, 519 (2005)
17. Duncan, M., Levison, H., Dones, L.: In: Comets, II, Festou, M.C., Keller, H.U., Weaver, H.A. (eds.) The Univ. of Arizona Press (Tucson), pp. 193 (2004)

18. Ehrenfreund, P., et al.: Rep. Prog. Phys. **65**, 1427 (2002)
19. Farinella, P., Davis, D.R.: Science **273**, 5277 (1996)
20. Feaga, L.M., et al.: Icarus **190**, 345 (2007)
21. Fray, N., et al.: Icarus **184**, 239 (2006)
22. Fujiware, A., Mukai, T., Kawaguchi, J., Uesugi, K.T.: Adv. Space Res. **25**, 231 (2000)
23. Gardinier, A., et al.: Earth Planet Sci. Lett. **184**, 9 (2000)
24. Geiss, J., et al.: Space Sci. Rev. **90**, 253 (1999)
25. Gerakines, P.A., Moore, M.H., Hudson, R.: Icarus **170**, 202 (2004)
26. Gilmour, J.D., et al.: Rev. Sc. Instrum. **65**, 617 (1994)
27. Glassmeier, K.-H., et al.: Space Sci. Rev. **128**, 1 (2007)
28. Goesmann, F., et al.: Space Sci. Rev. **128**, 257 (2007)
29. Groussin, O., et al.: Icarus **187**, 16 (2007)
30. Grün, E., et al.: J. Geophys. Res. **98**, 15091 (1993)
31. Holsapple, K.A., Housen, K.R.: Icarus **187**, 345 (2007)
32. Keller, H.U., et al.: Nature **321**, 320 (1986)
33. Keller, H.U., et al.: Astron. Astrophys. **187**, 807 (1987)
34. Keller, H.U., Britt, D., Buratti, B.J., Thomas, N.: In: Comets II, Festou, M.C., Keller, H.U., Weaver, H.A. (eds.) The Univ. of Arizona Press (Tucson), pp. 211 (2004)
35. Kossacki, K., Szutowicz, S.: Icarus **1995**, 705 (2008)
36. Kührt, E.: Earth Moon, Planets **90**, 61 (2002)
37. Kührt, E., Keller, H.U.: Icarus **109**, 121 (1994)
38. Laufer, D., Pat-El, I., Bar-Nun, A.: Icarus **178**, 248 (2005)
39. Lowry, S.C., et al.: Astron. Astrophys. **349**, 649 (1999)
40. Marcano, V., Benitez, P., Palacios-Prü, E.: Planet. Space Sci. **51**, 159 (2003)
41. Marty, B., et al.: Science **319**, 75 (2008)
42. McKeegan, K.D., et al.: Science **314**, 1724 (2006)
43. Mennella, V., et al.: Astrophys. J. **507**, L177 (1998)
44. Messenger, S.: Nature **404**, 968 (2000)
45. Morbidelli, A., et al.: Meteorit. Planet Sci. **35**, 1309 (2000)
46. Nelson, R.M., Rayman, M.D., Weaver, H.A.: Icarus **167**, 1 (2004)
47. Ng, T.C., et al.: Lunar Planetary Sci. Conf. 34, abstract #1002 (2003)
48. Nguyen, A.N., Busemann, H., Nittler, L.R.: Lunar Planetary Sci. Conf. 38, abstract #2332 (2007)
49. Owen, T.C., Bar-Nun, A.: Orig. Life Evol. Biosph. **31**, 435 (2001)
50. Owen, T.C.: Space Sci. Rev. (2008, in press). doi:10.1007/s11214-008-9306-7
51. Pepin, R.O.: Earth Planet. Sci. Lett. **252**, 1 (2006)
52. Porcelli, D., Woolum, D., Cassen, P.: Earth Planet. Sci. Lett. **193**, 237 (2001)
53. Reinhard, R., Battrick, B. (eds.): Space Missions to Halley's Comet, ESA-SP 1066 (1986)
54. Sandford, S.A., et al.: Science **314**, 1720 (2006)
55. Soderblom, L.A., et al.: Science **296**, 1087 (2002)
56. Spohn, T., et al.: Space Sci. Rev. **128**, 339 (2007)
57. Stadermann, F.J., Floss, C.: Lunar Planet. Sc. Conf., abstract #1889 (2008)
58. Stephan, T.: Planet. Space Sci. **49**, 859 (2001)
59. Sunshine, J.M., et al.: Science **311**, 1453 (2006)
60. Sunshine, J.M., et al.: Icarus **190**, 284 (2007)
61. Thomas, P.C., et al.: Icarus **187**, 4 (2007)
62. Zinner, E.: In: Davies, A.M. (ed.) Treatise on Geochemistry—Meteorites, comets, and planets, vol. 1, p. 17. Elsevier (2003)
63. Zolensky, M.E., et al.: Science **314**, 1735 (2006)

Article 16

COTTIN H., BRIOIS C., ENGRAND C., THIRKELL L., GRAND N., TAJMAR M., GLASMACHERS A., ALIMAN M. and ILMA-TEAM (2008) ILMA (Ion Laser Mass Analyser). In Declaration of interest in science instrumentation for the MARCO POLO Cosmic Vision mission candidate.

Call for declarations of interest in Science Instrumentation For the Marco Polo Cosmic Vision mission candidate

Instrument Name	Instrument Description
ILMA	Ion Laser Mass Analyzer

Team Members	Institutions
Hervé Cottin (Team Coordinator)	LISA - Laboratoire Interuniversitaire des Systèmes Atmosphériques (F)
Christelle Briois (Deputy T. C. & Instrument Scientist)	LPCE - Laboratoire de Physique et Chimie de l'Environnement (F)
Cécile Engrand (Deputy T.C.)	CSNSM - Centre de Spectrométrie Nucléaire et de Spectrométrie de Masse (F)
Laurent Thirkell (Ion Gun/Laser Project Manager)	LPCE - Laboratoire de Physique et Chimie de l'Environnement (F)
Noël Grand (General P.M.)	LISA - Laboratoire Interuniversitaire des Systèmes Atmosphériques (F)
Martin Tajmar (Ion Source P.M.)	ARC Seiberdorsf- Austrian Research Center (A)
Albrecht Glasmachers (Ion Trap P.M.)	Bergische Universität Wuppertal (D)
Michel Aliman	Zeiss GmbH (D)
Dominique Bockelée-Morvan	LESIA - Laboratoire d'Etudes Spatiales et d'Instrumentation en Astrophysique, Observatoire de Paris (F)
John-Robert Brucato	INAF - Osservatorio Astrofisico di Arcetri, Firenze (I)
Marc Chaussidon	CRPG – Centre de Recherches Pétrographiques et Géochimiques (F)
Sylvie Derenne	BioEMCo - Biogéochimie et Ecologie des Milieux Continentaux, Paris (F)
Stéphane Erard	LESIA - Laboratoire d'Etudes Spatiales et d'Instrumentation en Astrophysique, Observatoire de Paris (F)
Marcello Fulchignoni	LESIA - Laboratoire d'Etudes Spatiales et d'Instrumentation en Astrophysique, Observatoire de Paris (F)
Martin Hilchenbach	MPS – Max Planck Institut für Sonnensystemforschung, Katlenburg-Lindau (D)
Harald Krüger	MPS – Max Planck Institut für Sonnensystemforschung, Katlenburg-Lindau (D)
Patrick Michel	Observatoire de la Côte d'Azur (F)
Eric Quirico	LPG - Laboratoire de Planétologie de Grenoble (F)
Sarah S. Russell	NHM London – the Natural History Museum of London (UK)
Giovanni Strazzulla	INAF – Osservatorio Astrofisico di Catania (I)
Wölfgang Steiger	ARC Seibersdorf- Austrian Research Center (A)
Cyril Szopa	SA, Service d'Aéronomie (F)
Roland Thissen	LPG - Laboratoire de Planétologie de Grenoble (F)

TABLE OF CONTENT

Executive Summary

This document is an answer to the call for declaration of interest in science instrumentation for the MARCO POLO Cosmic Vision mission candidate, released by the European Space Agency. We are proposing a Mass Spectrometer to be part of the MARCO POLO science payload.

Like other small bodies of the Solar System, asteroids are the remnants of planet formation. Their compositions are inherited from the Solar Nebula at the time of planetesimal accretion into planets, 4.5 billion years ago. They are valuable objects to assess the physicochemical conditions prevailing at the time and place of their formation in the Solar Nebula. Among them, some are known to be rich in carbon and volatile species (including water), which suggests that they never underwent major heating and differentiation events. Their organic content is also of prime interest because the chemical evolution leading to life on Earth may have been initiated by the delivery of extraterrestrial organic compounds into primitive oceans. For these reasons, a sample return from a primitive Near Earth Object (NEO), which is the main objective of the MARCO POLO mission, would contribute to fulfil the top-level science topics of the mission: a better understanding of (1) the origin of the Solar System and planets, (2) the formation and evolution of NEOs and (3) the origin of life (Astrobiology).

In the present payload definition of the mission for *in situ* characterization, **no instrument is addressing Astrobiology questions.** This aspect, classified as one of the top-level science topic priority of the mission, relies only on the safe return of the samples to Earth, with the inherent risk of a sample return, and with the issue of having to deal with samples which could be contaminated by terrestrial organic matter after their return to the ground.

ILMA (Ion Laser Mass Analyser) is a new generation high resolution SIMS (Secondary Ion Mass Spectrometer) and/or LIMS (Laser Ionisation Mass Spectrometry) instrument, initially proposed to address **Astrobiology** issues in the MARCO POLO proposal in response to the Cosmic Vision program. As part of the scientific payload of MARCO POLO, ILMA would be a unique tool to fulfil **two out of three priorities of the mission objectives**[1]:

1- Place the samples in their local context (science requirement SC-030: the bulk rock-forming elemental composition of the sampling area should be determined with 10^{-2} amu resolution). ILMA will set a first assessment of the collecting site, and characterise the astrobiological relevance of the returned samples.

2- Provide complementary science results not achievable from the samples themselves. Indeed, ILMA will be able to perform unique measurements of prime astrobiological importance, on site, free of any potential contamination after return to Earth.

No mass spectrometer is included in the current Payload Definition Document. **ILMA can measure the composition of solid and volatile samples: elements, molecules (mineral and organic) and isotopes.** In an optimized configuration, ILMA should be integrated in the Lander, which was part of the initial configuration of the MARCO POLO mission in the Cosmic Vision proposal. ILMA could also be integrated in the Mother Spacecraft and analyse the samples before their storage in the Earth Re-entry Capsule.

A team of 23 scientists, belonging to 16 institutions and 5 European countries has been set up to support this instrument, to ensure a high science return and contribute to the success of MARCO POLO. CNES, DLR, CNRS, MPI and several European Research Institutions and Universities would be the major contributor in the funding scheme of the present proposal.

[1] As presented in Science Requirements Document (Sci-RD – ref MP-RSSD-RD-001)

Detailed Coordinates of Team Members

Hervé Cottin
LISA
61 avenue du Général de Gaulle
94010 Créteil Cedex, France
Tel: +33 1 45 17 15 63
Fax: +33 1 45 17 15 64
E-mail : cottin@lisa.univ-paris12.fr

Christelle Briois
LPCE
3A, avenue de la recherche scientifique
45071 Orléans cedex 2, France
Tel: +33 2 38 25 53 03
Fax: + 33 2 38 49 46 72
E-mail : christelle.briois@cnrs-orleans.fr

Cécile Engrand
CSNSM Bâtiment 104
91405 ORSAY Campus, France
Tel: +33 (0)1 69 15 52 95
Fax: + 33 (0)1 69 15 50 08
E-mail : Cecile.Engrand@csnsm.in2p3.fr

Laurent Thirkell
LPCE
3A, avenue de la recherche scientifique
45071 Orléans cedex 2, France
Tel: +33 2 38 25 53 03
Fax: + 33 2 38 49 46 72
E-mail : Laurent.thirkell@cnrs-orleans.fr

Noël Grand
LISA
61 avenue du Général de Gaulle
94010 Créteil Cedex, France
Tel: +33 1 45 17 15 53
Fax: +33 1 45 17 15 64
E-mail : grand@lisa.univ-paris12.fr

Martin Tajmar
Austrian Research Centers GmbH - ARC
Space Propulsion & Advanced Concepts,
A-2444 Seibersdorf, Austria
Tel: +43-50550-3142
Fax: +43-50550-3366
E-mail : martin.tajmar@arcs.ac.at

Albrecht Glasmachers
Bergische Universität Wuppertal
FB-E Messtechnik
Rainer-Gruenter-Strasse 21
D-42119 Wuppertal, Germany
Tel: +49 (0)202 439 1814
Fax: +49 (0) 202 439 1932
E-mail: glasmachers@uni-wuppertal.de

Michel Aliman
Carl Zeiss NTS GmbH
Carl Zeiss Strasse 56
D - 73447 Oberkochen
Tel: +49 73 64 20-9397
Fax: +49 73 64 20-9624

Dominique Bockelée-Morvan
LESIA - Observatoire de Paris
5 place Jules Janssen,
F92195, Meudon, France
Tel: 33 1 45 07 76 05
Fax: 33 1 45 07 71 44
E-mail : dominique.bockelee@obspm.fr

John Robert Brucato
INAF - Osservatorio Astrofisico di Arcetri
L.go E. Fermi 5
50125 Firenze, Italy
Phone: +39 055 2752 254
Fax: + 39 055 220039
Email: jbrucato@arcetri.astro.it

Marc Chaussidon
CRPG
15, rue Notre-Dame des Pauvres
54501 Vandoeuvre-les-Nancy France
Tél: 33 3 83 59 42 25
Fax: 33 3 83 51 17 98
E-mail:chocho@crpg.cnrs-nancy.fr

Sylvie Derenne
BioEMCo
11 rue P. M. Curie
75231 Paris cedex 05, France
Tel: 33 1 44 27 67 16
Fax: 33 1 43 29 51 02
E-mail: sylvie-derenne@enscp.fr

Stéphane Erard
LESIA, Observatoire de Paris
5 place Jules Janssen
F-92195 Meudon cedex, France
tel : 33 1 45 07 78 19
fax : 33 1 45 34 76 83
E-mail: stephane.erard@obspm.fr

Marcello Fulchignoni
LESIA, Observatoire de Paris
5 place Jules Janssen
F-92195 Meudon cedex, France
tel : 33 1 45 07 75 39
fax : 33 1 45 07 71 44
E-mail: marcello.fulchignoni@obspm.fr

Martin Hilchenbach
Max-Planck-Institut für Sonnensystemforschung,
Max Planck Str. 2,
D-37191 Katlenburg-Lindau, Germany
Tel: +49 5556 979 162
Fax: +49 5556 979 240
E-mail: hilchenbach@mps.mpg.de

Harald Krüger
Max-Planck-Institut für Sonnensystemforschung
Max-Planck-Strasse 2
D-37191 Katlenburg-Lindau, Germany
Tel. +49-5556-979-234
Fax. +49-5556-979-240
E-mail: krueger@linmpi.mpg.de

Patrick Michel
UMR 6202 Cassiopée/CNRS
Observatoire de la Côte d'Azur, B.P. 4229
06304 Nice Cedex 4, France
Tel: +33 4 92 00 30 55
Fax : +33 4 92 00 30 58
E-mail: michel@oca.eu

Eric Quirico
Laboratoire de Planétologie de Grenoble
Bâtiment D de Physique
BP 53 38041 Grenoble Cedex 9, France
Tel: 33 4 76 51 41 56
Fax: 33 4 76 41 41 46
E-mail: eric.quirico@obs.ujf-grenoble.fr

Sara Russell
Laboratory: Natural History Museum, London
Department of Mineralogy, the Natural History Museum, Cromwell Road, London SW7 5BD, UK
Phone: +44 207 942 5074
Fax: +44 207 942 5537
E-mail: sarr@nhm.ac.uk

Giovanni Strazzulla
INAF-Osservatorio Astrofisico di Catania (INAF-OACT)
Via S. Sofia 78, 95123 Catania, Italy
Tel: +39-0957332222
Fax: +39-095330592
E-mail: gianni@oact.inaf.it

Wolfgang Steiger
Austrian Research Centers GmbH - ARC
Space Propulsion & Advanced Concepts,
A-2444 Seibersdorf, Austria
Tel : +43 (0) 505 50 - 3141
Fax : +43 (0) 505 50 -3366
E-mail: Wolfgang.Steiger@arcs.ac.at

Cyril Szopa
Service d'Aéronomie UMR CNRS 7620
Reduit de Verrières, Route des Gâtines, 91370
Verrières le Buisson, France
Tel: 33 1 64 47 43 01
Fax: 33 1 69 20 29 99
E-mail : cyril.szopa@aerov.jussieu.fr

Roland Thissen
Laboratoire de Planétologie de Grenoble
Bâtiment D de Physique
BP 53 38041 Grenoble Cedex 9, France
Tel: +33 4 76514173
Fax: +33 4 76514146
E-mail : Roland.thissen@obs.ujf-grenoble.fr

Contribution of Each Team Member to the Project

Hervé Cottin

LISA – Laboratoire Interuniversitaire des Systèmes Atmosphériques

Hervé Cottin is an assistant professor in Astrochemistry and Astrobiology at the science faculty of Paris 12 University. He is specialized in studying the organic chemistry of comets, the production and evolution of complex organic matter in small bodies of the Solar System, and its relevance to the origin of life.

He is a CoI of the COSIMA instrument (Time Of Flight Secondary Ion Mass Spectrometer) onboard the ROSETTA spacecraft. He is the PI of several experiments of astrobiology-related photochemistry experiments on organic matter implemented outside the International Space Station (PROCESS and AMINO in facilities EXPOSE-E & -R / 2008-2010) and the Russian automatic capsule FOTON (UVolution in BIOPAN 6 / 2007). He is the Team Coordinator of the ILMA instrument and will coordinate joined scientific and technical effort of the team to ensure a full science return of ILMA measurements.

Christelle Briois

LPCE – Laboratoire de Physique et Chimie de l'Environnement

Christelle Briois is an assistant professor in physical chemistry at the University of Orléans. Her research interests involve the study of the chemistry of the small bodies of the Solar System.

Since early 2008, she is CoI of ROSINA and CoPI of the COSIMA, both experiments onboard the orbiter of ESA mission Rosetta. ROSINA consists of three separate subsystems (pressure gauges, and two kind of mass spectrometer analysers) which will determine the composition of the comet's atmosphere and ionosphere, the velocities of electrified gas particles, and reactions in which they take part. COSIMA is a Time-Of-Flight Secondary Ion Mass Analyser dedicated to measure elemental, molecular and isotopic compounds of cometary grains, and whether they are organic or inorganic. One of the two Deputy Team Coordinator of ILMA, she will also have the role of Instrument Scientist.

Cécile Engrand

CSNSM – Centre de Spectrométrie Nucléaire et de Spectrométrie de Masse

Cecile Engrand is CNRS researcher at the University of Orsay. Her expertise lies in the study of early Solar System processes by analysing cosmic dust collected in Antarctica by her research group. These studies also have implications for the origin of life on Earth, as prebiotic chemistry on Earth may have required an extraterrestrial input of carbonaceous matter and volatiles (such as water), brought by primitive Solar System matter (cosmic dust and/or carbonaceous chondrites). She is CoI of the COSIMA instrument on ROSETTA and participates in the STARDUST consortium in France. She is one of the two Deputy Team Coordinators of ILMA and will use her background in cosmochemistry in the definition and interpretation of the analyses.

Laurent Thirkell

LPCE – Laboratoire de Physique et Chimie de l'Environnement

Laurent Thirkell is a research engineer at CNRS/LPCE space laboratory and Co Investigator of the COSIMA TOF-SIMS instrument onboard the ESA mission ROSETTA. He has developed experience in management and realisation of ion gun for the COSIMA instrument. He manages the development of new projects of spatial instrument (mass spectrometer and cathodoluminescence) funded by the French national space agency (CNES). He will have the responsibility of developing the ion gun and coupling with the mass spectrometer of ILMA.

Noël Grand

LISA – Laboratoire Interuniversitaire des Systèmes Atmosphériques

Noël Grand is head of Technical Department of the LISA. His main skill is real-time data acquisition and command of instrument. He has been project manager and system engineer for scientific aircraft's instruments (lidar, radar).

Since 2007, he is the project manager of MOMA-GC on the Pasteur Payload of the ExoMars mission. MOMA is an international instrument developed in cooperation between MPS-Germany, LISA/SA-France and JPL-US. It is a GC-MS dedicated to the analysis of organic compounds and traces of life on the surface, in the ground and in the atmosphere of Mars. The GC and the MS can work independently (with a laser head for the MS when alone) or together. He is the project manager of ILMA.

Martin Tajmar

ARC-Austrian Research Centers

Martin Tajmar is head of the space propulsion & advanced concepts department at ARC and therefore responsible for all ion emitter developments. The ARC ion emitters have been successfully flown on a number of missions including COSIMA/ROSETTA and MIGMAS (both for a mass spectrometer) as well as on CLUSTER-II, DOUBLESTAR and GEOTAIL (for spacecraft potential control) accumulating more than 12,000 h of space experience. He will be responsible for the ion emitter development for the ILMA mass spectrometer.

Albrecht Glasmachers

BUW – Bergische Universität Wuppertal

Albecht Glasmachers is a professor for electrical metrology at the University of Wuppertal. His research activities cover space instrumentation and mass spectrometry. He is Co-Investigator of the COSIMA TOF-SIMS instrument onboard the ESA mission ROSETTA and involved in the design of the electronic measuring systems for more than 10 spatial instruments He will contribute to the design of the electrical ion trap mass spectrometer and the measuring electronics for ILMA.

Dominique Bockelée-Morvan

LESIA-Observatoire de Paris

Dominique Bockelée-Morvan is a CNRS researcher at LESIA, Observatory of Paris. Her expertise is in the study of the molecular and isotopic composition of comets using infrared and millimeter spectroscopy from ground-based and space telescopes. She has been involved in several projects aimed at constraining the early phases of solar system formation from the composition of comets and planets. She is Co-investigator of the VIRTIS and MIRO experiments on Rosetta. She will use her background on comets and small bodies in the interpretation of the analyses.

John Robert Brucato

INAF – Astrophysical Observatory of Arcetri (Italy).

Researcher astronomer. Space mission instrument involvement: Co-I of DUSTER (Balloon), Co-I HRIC (BepiColombo); Co-I of MEDUSA (ExoMars); Associate Scientist of CIRS (Cassini-Huygens); Co-I of DARLING (International Space Station). Main relevant expertise: spectroscopy, organic chemistry, small bodies, origin and evolution of Solar System, astrobiology. Involved in laboratory analyses of IDPs, meteorites and comet Wild 2 dust grains captured by the NASA Stardust mission. 50 refereed papers published.

Marc Chaussidon

Centre de Recherches Pétrographiques et Géochimiques

Marc Chaussidon is CNRS senior researcher (Directeur de Recherche) at CRPG-CNRS. His main research interests focus on deciphering geochemical processes on Earth and getting insights in the formation of the Solar System using stable isotopes with secondary ion mass spectrometry (SIMS). He will use his expertise in cosmochemistry to contribute to the interpretation of the ILMA measurements.

Sylvie Derenne

BioEMCo - Biogéochimie et Ecologie des Milieux Continentaux

Sylvie Derenne is a CNRS senior scientist (Directeur de Recherche) at the University Pierre and Marie Curie in Paris. She has a recognized expertise in deciphering the chemical structure of complex organic matter from various natural environments. For more than 10 years, she has been investigating the structure and formation pathway of the insoluble organic matter of carbonaceous chondrites using a combination of analytical tools including pyrolysis coupled with gas chromatography and mass spectrometry. She will therefore help in data interpretation through comparison with carbonaceous chondrites.

Stéphane Erard

LESIA-Observatoire de Paris

Stéphane Erard is an Astronomer at Observatory of Paris. He has expertise in infrared spectroscopy in relation with planetary surfaces composition and evolution, both observational and in the laboratory (mineralogical samples). He is also involved in planetary photometry and data processing.

He is currently involved as a co-I on VIRTIS (Rosetta, VenusExpress [archive manager]), AMIE (Smart-1), SIMBIO-SYS, MERTIS and PHOEBUS (BepiColombo).

Marcello Fulchignoni
LESIA, Observatoire de Paris
With my experience acquired analyzing the Moon samples from all the Apollo missions, and the data on Mercury, Mars, Jupiter system, Titan obtained with remote and "in situ" measurements, I would like to use the ILMA results to contribute to the knowledge of the origin of the small bodies and their chemico-physical evolution as a clock for the understanding of the growth of planetary embryos.

Martin Hilchenbach
Max-Planck-Institut für Sonnensystemforschung
L-CoI SOHO CELIAS (high energy ion and neutral particle instrument), Co-I ROMAP Rosetta Lander Philae (ion and electron instrument), PI Rosetta COSIMA (secondary ion mass spectrometer for cometary dust analysis), CoI BepiColombo BELA (Laseraltimeter instrument), CoI BepiColombo MIXS (x-ray fluorescence instrument), CoI ExoMars MOMA (GC/MS coupled with ALDI laser desorption), more than 50 referred papers and 35 non-referred contributions.

Harald Krüger
Max-Planck-Institut für Sonnensystemforschung (MPS)
Harald Krüger is a researcher at MPS. He is a co-investigator of the COSIMA TOF-SIMS instrument onboard the Rosetta mission, he has been principal investigator for the impact-ionization dust detectors onboard Galileo and Ulysses spaceprobes, and he is co-investigator for the Cosmic Dust Analyzer on board the Cassini mission. His expertise lies in the field of cosmic dust research, covering interplanetary, circumplanetary, cometary and interstellar dust. He is the project manager for the Laser contribution to ILMA.

Patrick Michel
Observatoire de la Côte d'Azur
Patrick Michel is CNRS researcher at the Côte d'Azur Observatory where he leads the group of planetology of the laboratory UMR Cassiopée. He is an expert of the dynamics and physical properties of asteroids, and on the collisional process between the small bodies of our Solar System. His study of the impact disruption of asteroids by means of numerical simulations provided constraints on the likely physical (internal and surface) structures of these small bodies. To validate the numerical codes at small scale, he participates to impact experiments in Japan and to the measurements of material properties (e.g. compressive strength, porosity ...) of the targets. Determining such properties for a wide range of materials and understanding their behavior under stress can be useful to make reasonable guess of the possible surface structure of a space mission target. Finally, he was the first core member of the proposal of the Marco Polo mission to the ESA Cosmic Vision program and now belongs to the Science Study Team solicited by ESA. For ILMA, he will use his knowledge on small bodies and material properties in the definition and interpretation of the analyses.

Eric Quirico

Eric Quirico is an assistant professor in Planetary Sciences at Université Jospeh Fourier (Grenoble - France). His research field covers the study of molecular solids at the surface of small bodies in the Solar System and the origin and evolution of organic matter recovered from cosmomaterials (chondrites, cometary grains). His studies are mostly experimental, as experimental simulations on ices and refractory organics, and the characterization of organics in cosmomaterials by micro-spectroscopic techniques. He is a Team Member of the VIRTIS instrument onboard the ROSETTA spacecraft.

Sara Russell

Natural History Museum in London

Sara Russell is Head of the Division of Meteoritics and Cosmic Mineralogy at the Natural History Museum in London. Her research interests are the study of the mineralogy, geochemistry and isotope chemistry of meteorites, particularly those whose parents are primitive asteroids. Her work to date has involved the measurement of C, N and O isotopes in meteorites in order to determine the origin of components that formed in the early solar system and also in a presolar environment. She is also a co-investigator on the C1XS x ray spectrometry on board the lunar mission Chandrayaan-1.

Giovanni Strazzulla

INAF-Osservatorio Astrofisico di Catania (INAF-OACT)

Giovanni Strazzulla is a full astronomer and director of the INAF-Osservatorio Astrofisico di Catania. His research activity of has been mainly devoted to experimental studies of the chemical and physical modifications induced by fast ions on targets of astrophysical relevance (frozen gases, silicates, carbonaceous materials). Among the induced effects particular relevance have the chemical modifications that, when targets contain carbon atoms, drive the formation of organic refractory residues, sub-oxides and oxides. The relevance those results have to the physics of solid surfaces in the Solar System and to Astrobiology have been outlined in several papers.

Cyril Szopa

Service d'Aéronomie UMR CNRS 7620

Cyril Szopa is an assistant professor in astronomy and astrophysics at the science faculty of Paris 6 University. His field of researches includes the characterization of organic materials present on Mars, Titan and comets, and the processes linked to this matter. He is both a space and laboratory experimentalist involved in several space and ground projects. He is the instrument scientist for the french hardware contribution to the SAM instrument (Gas Chromatograph Mass Spectrometer) onboard the NASA/MSL Mars probe and the GAP instrument (GCMS) onboard the Roscomos/Phobos-Grunt probe to Phobos. He is the CoPI for the french hardware contribution to the MOMA instrument (GCMS) onboard the ESA/Pasteur probe to Mars.

Roland Thissen

LPG – Laboratoire de Planétologie de Grenoble

Roland Thissen is a CNRS researcher at the University of Grenoble. His expertise lies in the study of gas phase ionospheric chemistry processes by measuring the ion molecule rate constants for individual reactions, in order to feed model's chemistry databases. These studies have implications for the interpretation of the Cassini data (INMS instrument) collected in the ionosphere of Titan. He is associate scientist to the INMS team, in charge of collecting lab data for specific ion molecule reactions, in support to interpretation. He also recently proposed to develop a new design of mass spectrometer analyser, based on pure electrostatic analyser, with ultra high mass resolution capabilities.

Organization chart of the project

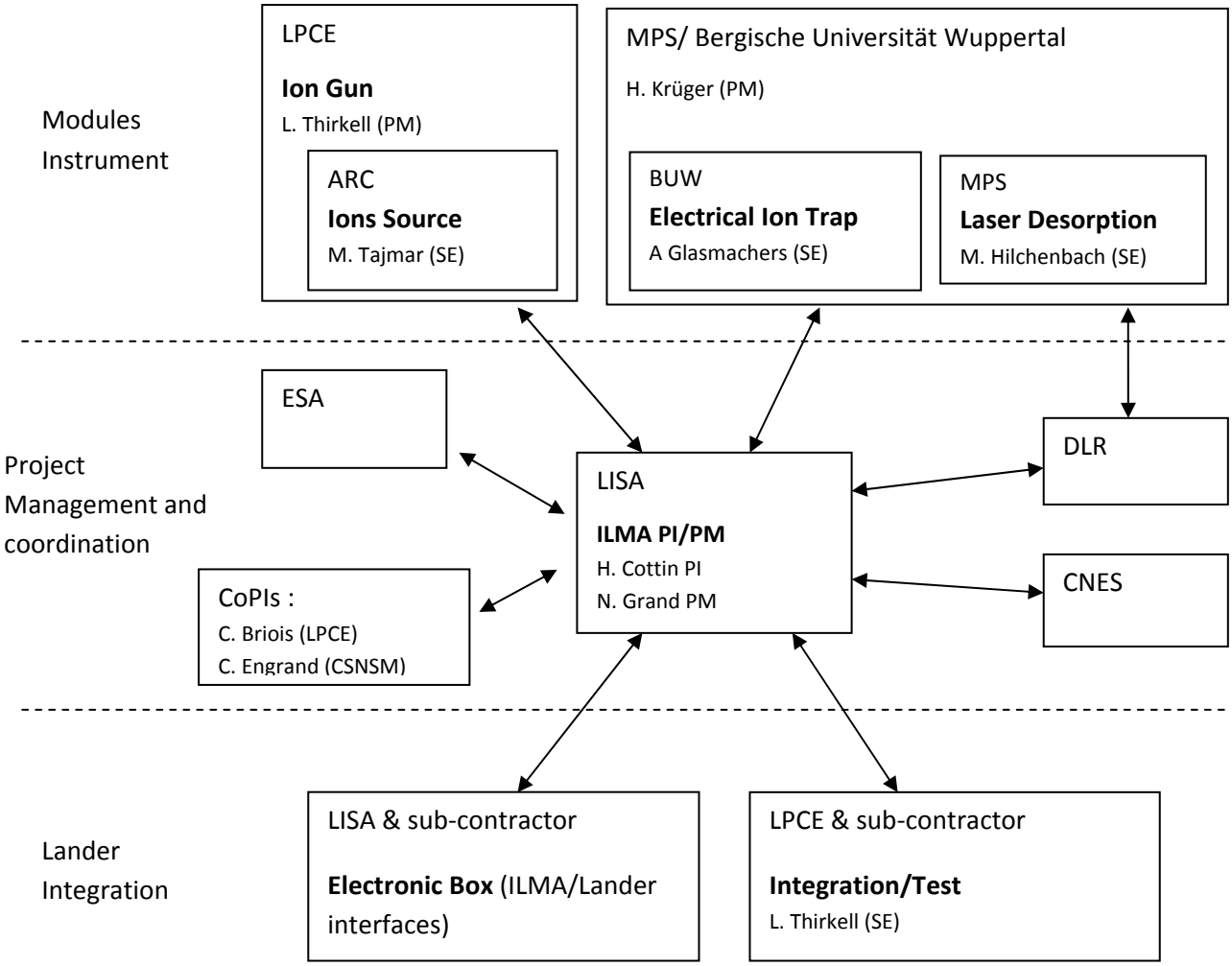

PI: Principal Investigator (Team Coordinator), PM: Project Manager, SE: System Engineer

Co-Investigators -
M. Aliman (Zeiss GmbH.), **D. Bockelée-Morvan** (Obs. Paris), **J.R. Brucato** (Florence Obs.), **M. Chaussidon** (CRPG), **S. Derenne** (Paris), **S. Erard** (Obs. Paris), **M. Fulchignoni** (Obs. Paris), **M. Hilchenbach** (MPS Katlenburg-Lindau), **H. Krueger** (MPS Katlenburg-Lindau), **P. Michel** (Obs. Côte d'Azur), **E. Quirico** (LPG), **S. Russell** (NHM London), **G. Strazzulla** (Catania Obs.), C. Szopa (S.A.), **W. Steiger** (ARC), **R. Thissen** (LPG).

Scientific Background

The MARCO POLO mission will investigate a primitive (carbonaceous) asteroid, and bring back samples to Earth. The science objectives of MARCO POLO encompass a better understanding of the processes occurring in **the primitive Solar System** and accompanying the planetary formation. They are also aiming at placing constraints on the **origin of life** in the Solar System. The **Mass Spectrometer** that is proposed, **ILMA – Ion Laser Mass Analyzer**, will be able to analyse and qualify the chemical and isotopic composition of samples from the asteroid's surface in order to contribute in these two scientific directions.

ILMA and the formation of the Solar System

What is the most abundant matter in the interplanetary medium? Are meteorites representative of that matter? What are the processes that formed the asteroids and how did they evolve? What was the astrophysical setting of the formation of the Solar System?

As the first straightforward approach, ILMA analyses will allow a comparison of the asteroid's *in situ* composition with that of meteorites recovered on Earth. Except for Lunar and Martian stones, the meteorites originate from asteroid belt. It is widely believed that the primitive meteorites 'carbonaceous chondrites' originate from C-type asteroids, and that D-type asteroids have no representative in meteorite collections, with the possible exception of the Tagish Lake meteorite [1]. Such connections are however difficult to assess, as they are based on spectroscopic properties of asteroids (that undergo space weathering) compared to the one of meteorites, which lose ~ 90% of their mass (and their outer surface) during atmospheric entry. Cosmic dust falling on Earth, which currently represents the dominant input of extraterrestrial matter (about 1000 times that of meteorites), is typically related to the relatively rare 'carbonaceous chondrite' meteorite class that represents less than 5% of the meteorite falls [e.g. 2]. This apparent discrepancy between cosmic dust and meteorite types (> 80% of the meteorites are so-called 'ordinary chondrites') could however be reconciled by the observed predominance of C-type asteroids with regard to S-type bodies in interplanetary space, and by assuming that sub-millimetre samples (dust) would then be more representative of interplanetary matter than rock sized samples found in meteorite collections. Only the characterisation of an asteroid in interplanetary space will better constrain the genetic link between asteroid types, meteorite classes and cosmic dust. Recent analyses of cometary samples returned by the STARDUST mission [e.g. 3], as well as astronomical observations of objects presenting a cometary activity in the outer asteroid belt (e.g. Phaeton) also suggest the possibility of a continuum between asteroidal and cometary material. In situ analyses performed on a carbonaceous asteroid would lead to a better understanding of the structure and repartition of interplanetary material nowadays, helping retracing the formation and early evolution of the protosolar disk formation and the Solar System 4.5 billion years ago.

A wide range of different presolar interstellar grains are also found in minute amounts (<1%) in primitive meteorites (mostly unaltered carbonaceous chondrites). The studies of these presolar grains have given an insight into a wide variety of nucleosynthetic processes predating the formation of the Solar System. ILMA isotopic analyses could identify material of possible presolar interstellar origin in the asteroid. The nature and abundance of such presolar interstellar material in a carbonaceous asteroid could help to better understand the composition and astrophysical setting of the molecular cloud that gave birth to our solar system.

ILMA and the origin of life in the Solar System

What are the nature and origin of organic compounds on an asteroid? How can asteroid organics shine a light on the origin of molecules necessary for life? What is the role of asteroid impacts for the origin of life?

Type-C asteroids are widely believed to be related to the carbonaceous chondrites (CCs), which are among the best preserved witnesses on Earth of early Solar System formation. Carbonaceous chondrites are a physical mixing of chondrules and isolated minerals formed at high temperatures embedded in a low-temperature matrix mainly composed of hydrated minerals mixed with carbonaceous matter. Carbonaceous chondrites in general, and type 2 CCs (CM2) in particular, contain a few weight percents of carbon (~ 2wt% for CM2 meteorites). The major part of this carbon (~80%) is in the form of insoluble organic matter (IOM) [e.g. 4]. Lower molecular mass organic compounds like amino acids – or their precursors – are also found in smaller amounts in carbonaceous chondrites (~100 ppm), and especially in CM2 meteorites like Murchison [e.g 5].

Current Astrobiology scenarios for the origin of life on Earth invoke an exogenous delivery of organic matter to the early Earth. It has been proposed that carbonaceous chondrite matter (in the form of planetesimals or cosmic dust) could have brought these complex organic molecules capable of triggering the prebiotic syntheses of biochemical compounds on the early Earth [e.g. 6 and references therein]. In the context of exclusive one-handedness of terrestrial amino acids and sugars, it is interesting to note that in some cases, abiotically-formed amino acids found in meteorites show significant L-enantiomeric excesses (up to ~15%) [e.g. 7].

For the first time, we will try to establish a link between an asteroid and a class of carbonaceous chondrites by *in situ* analysis, to better constrain the nature of the organic matter delivered to the early Earth for prebiotic chemistry. As the asteroid's surface was exposed for several million (or billion) years to vacuum and cosmic rays, with temperatures possibly reaching ~ 150°C, we do not expect to find volatile organic compounds on the surface. The key measurements for exobiology in the frame of the MARCO POLO mission would be to relate the C-type asteroid to a given meteorite class. Using spectroscopic classes of asteroids we could then assess the proportion of asteroids which could have brought carbonaceous matter on the early Earth and better constrain the scenarios for the origin of life.

References:

1. Hiroi T., Zolensky M.E. and Pieters C.M. (2001) The Tagish Lake meteorite : a possible sample from a D-type asteroid. *Science* **293**, 2234-2236.
2. Engrand C. and Maurette M. (1998) Carbonaceous micrometeorites from Antarctica. *Meteoritics Planet. Sci.* **33**, 565-580.
3. Brownlee D., et al. (2006) Comet 81P/Wild 2 under a microscope. *Science* **314**, 1711-1716.
4. Remusat L., Palhol F., Robert F., Derenne S. and France-Lanord C. (2006) Enrichment of deuterium in insoluble organic matter from primitive meteorites: A solar system origin? *Earth Planet. Sci. Lett.* **243**, 15-25.
5. Botta O. and Bada J.L. (2002) Extraterrestrial organic compounds in meteorites. *Surveys in Geophysics* **23**, 411-467.
6. Maurette M. (2006) *Micrometeorites and the mysteries of our origins*. Springer, Berlin Heidelberg New York. pp. 330.
7. Pizzarello S., Zolensky M. and Turk K.A. (2003) Nonracemic isovaline in the Murchison meteorite: chiral distribution and mineral association. *Geochim. Cosmochim. Acta* **67**, 1589-1595.

Instrument Measurement Objectives

ILMA is a new generation high resolution mass spectrometer, proposed to be part of the lander payload of MARCO POLO mission. MARCO POLO is a joint European-Japanese **SAMPLE RETURN** mission to a primitive carbonaceous Near-Earth Object (NEO). But the goal of MARCO POLO is also to characterize a NEO at multiple scales via ***in situ*** **measurements** by a science payload onboard an **orbiter** and a **lander**, before bringing samples back to Earth.

The current ILMA prototype has a mass resolution power > 10,000 at masses < 130 amu and can scan masses from 1 to 300 amu. ILMA would therefore be a key element to the mission and contribute to the prime objective of MARCO POLO: a better understanding of the origin and evolution of the Solar System, the Earth, and Life.

One of the science objectives of MARCO POLO is to understand the processes occurring in the **primitive Solar System** and accompanying the planetary formation. Key analyses in this context will include measurements of the chemical composition of the asteroid, as well as light element isotopic compositions (H, C, N, O, Si …). This *in situ* characterisation of a primitive asteroid in interplanetary space will better constrain the genetic link between asteroid types and meteorite classes and place constraints on the early evolution of the protosolar disk. ILMA could also identify possible presolar interstellar material to better characterize the composition and astrophysical setting of the molecular cloud that gave birth to our Solar System.

As far as **Astrobiology** is concerned, ILMA will be the only instrument of the mission to contribute to this issue. We propose to achieve this goal by the following measurements with ILMA:

- assess the carbon and water contents of the asteroid surface and at a few millimetres depth (using scratching with a robotic arm if possible);
- determine of the nature of the molecules desorbed by a Laser source coupled with the mass spectrometer;
- measure of the light element isotopic composition (H, C, N, O) of the organic material desorbed from the asteroid surface;

These analyses, in association with the measurements of the mineralogical and chemical compositions (with ILMA and by complementary IR analyses and analytical electron microscopy provided from other instruments on the lander) should allow us to better characterize the matter that could have brought organic matter to the early Earth, and relate it to a given class of meteorites. Measuring the isotopic compositions of H, C, N and O would also give strong constraints on the nature and origin of the carbonaceous matter

Science Implementation

Instrument Description

ILMA is a Fourier Transform ion trap mass spectrometer using either Secondary Ion Mass Spectrometry (SIMS, mostly for inorganic species) or Laser Desorption Mass Spectrometry (LDMS, to analyse large organic molecules) under a single platform. To this end, the mass analyser is coupled respectively to a primary ion beam and/or a laser beam. The sample exposed to the ion and/or Laser beam, produces sputtered ionized ions which are collected into a Radio frequency ion trap. Ions are stabilized in the trap by hyperbolic electrical fields and the detection is undertaken by a non destructive measurement of the ion oscillation frequency inside the trap. The electrical field is created by applying radio-frequency (Vrf) potential on a ring electrode. The trapped ions induce a periodic signal on end-cap electrodes. This signal is a sum of sinusoidal signals where each single frequency is associated to an ion mass. Deconvolution of this signal via Fourier Transformation (FT) results in a frequency spectrum which is converted into a high mass resolution spectrum (> 10,000 up to *m/z* =130 amu). Moreover, ILMA is the lightest (2.5 kg), smallest (15x17x5 cm^3) and most power efficient (1.5 Watts) mass spectrometer ever achieved for space. Therefore ILMA will constitute a significant progress compared to previous mass spectrometer in space. The geometry of ILMA is shown in Figure 1.

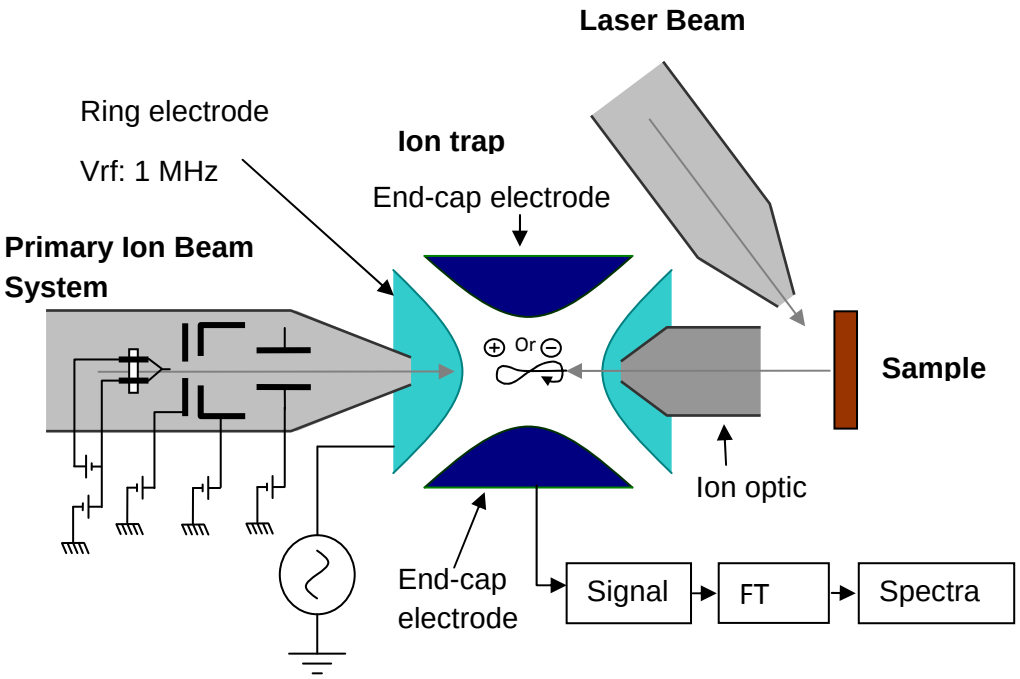

Figure 1. Global schematic diagram of ILMA

SIMS and LDMS are complementary. With the ion gun, only small molecules will be injected in the trap (SIMS is known as a very high sensitive chemical surface analytical technique) whereas the Laser desorption can produce larger molecules that will be of Astrobiology interest.

The mechanistic diagram of the primary ion beam system that will be used as one of the ILMA ion source is shown in Figure 2. Positive and negative SIMS measurements can be performed. The sample is bombarded with a continuous primary Indium ion beam over a 200 to 300 µm spot diameter. With a current of 2µA applied on the target, the particle beam will sputter approximately 10 atomic layers per second.

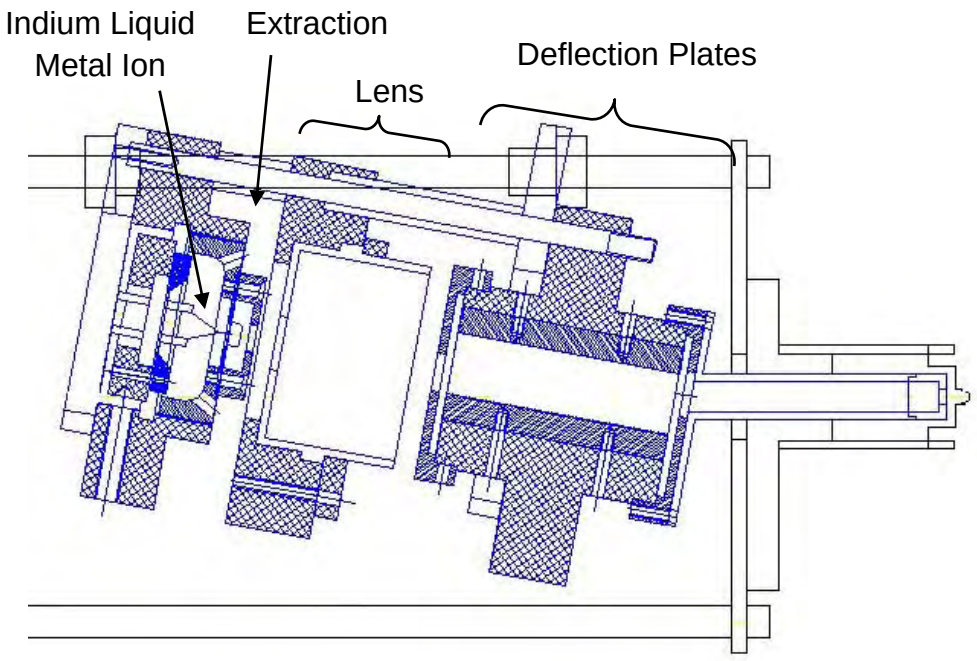

Figure 2. Mechanic diagram of the Primary Ion Beam System (COSIMA/Rosetta heritage)

The other ILMA ion source, the Laser system is shown in Figure 3. This short Laser wavelength of 266 nm should ionise most organic molecules. The advantage of the laser is that it could probe the "whole" regolith grain. The baseline for the diameter of the laser beam on the sample range between 30 to 400 µm (400 µm is the MOMA specification, 30 µm is expected to be achieved for ILMA). Within a single shot, the depth is a function of the absorption of the regolith/rock surface for the given laser wavelength, resulting into a layer of < 1 µm for a 266 nm absorbing regolith grain. The ILMA laser is specified for the highest pulse energy (i.e. < 0.25 mJ). Note that the power could be increased to achieve ablation (“drilling” into the subsurface) and perform surface cleaning process.

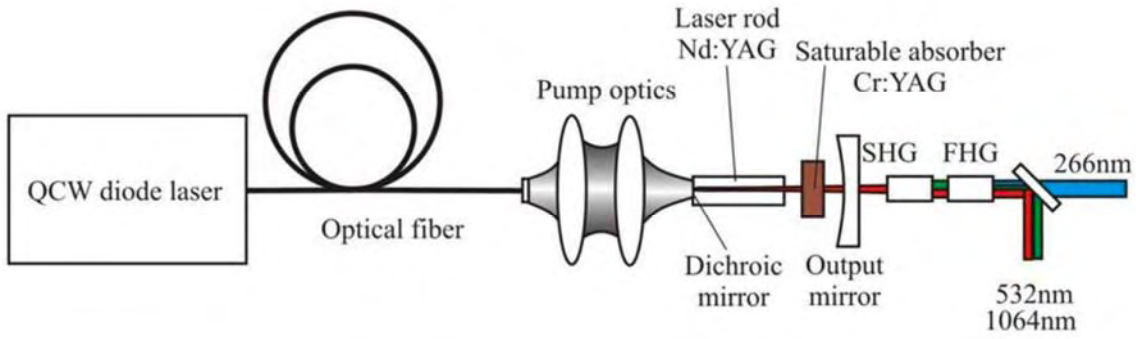

QCW - Quasi Continues Wave, **Nd:YAG -** neodymium-doped yttrium aluminium garnet, **Cr:YAG -** chromium-doped yttrium aluminium garnet, **SHG** - Second Harmonic Generation, **FHG** - Fourth Harmonic Generation

Figure 3. Schematic diagram of the Laser Desorption system (MOMA/ExoMars heritage)

The system has the flexibility of carrying out surface characterization and chemical measurements. It offers other practical uses such as laser cleaning of the surface of the sample, and laser-induced enhancement of secondary ion emission. The later could be achieved by utilizing both the SIMS and LDMS techniques: a short laser pulse would bring the sample surface just under laser desorption/ionization threshold by means of local heating and/or photochemical processes, while a focused In^+ beam would be well synchronized with the laser pulse. As a result, the sample's surface would be furthered energized, yielding additional molecular fragments from the same surface area. Complementary information from the same area of the sample at the same time could then be revealed.

Measurement Strategy

ILMA can be accommodated either in the lander for surface analysis, or in the mother spacecraft to analyze the composition of the samples collected before their return to Earth. This analysis would ensure astrobiological analyses free of any Earth contamination.

In the lander, two cases are possible:

- If the lander is equipped with a sample collection device (e.g. a robotic arm) to distribute samples to the different instruments, then the sample must be positioned at an appropriate distance relative to the inlet of the ILMA ion trap (1 mm TBD).

- If no sample collection device is available, then ILMA must be positioned at an appropriate distance to the ground (1 mm TBD).

In the mother spacecraft:

The sample must be positioned at an appropriate position relative to the inlet ion trap of ILMA (1 mm TBD).

Then, an automated analysis sequence is started on the sample:

- Production of ions (2 options):

Option 1 (in two steps). Step 1: Ion gun bombardment, and analysis of secondary ions in the trap. Step 2: Laser bombardment to generate larger molecular ions, and analysis in the trap. If needed, cleaning of the surface can be achieved with the laser before any measurement.

Option 2. Synchronised laser pulse and ion gun bombardment, which results in an enhanced emission of SIMS ions for analysis in the ion trap.

-After each sampling, data are sent to the lander (or mother spacecraft) before or after Fourier Transform computing, depending on where is the FPGA (*Field-Programmable Gate Array*) dedicated to that. Between two samplings, either the sample is moved, or the ion gun is adjusted to a different location (a few mm away) for another analysis.

Requirements for the Lander or Mother Spacecraft

ILMA must be positioned on the lander so that it can be easily moved close to the ground surfaces with precision, or samples collected with an appropriated interface of the Lander must be brought close to ILMA. Movement accuracy must be of about 1mm (TBD).

If ILMA is accommodated in the Mother Spacecraft, it must be in a position where samples can be placed at an appropriate position relatively to the inlet ion trap. Movement accuracy must be of about 1 mm.

Instrument Performance and Expected Results

The mass analyser has been developed by the Bergische Universität Wuppertal for gas analysis. It can presently provide spectra with a high mass resolution (about 10000) (see Figure 4). A SIMS prototype is under development at LPCE (Figure 5), for analysis of gas and *solid* samples. The LIMS prototype is under development in Wuppertal.

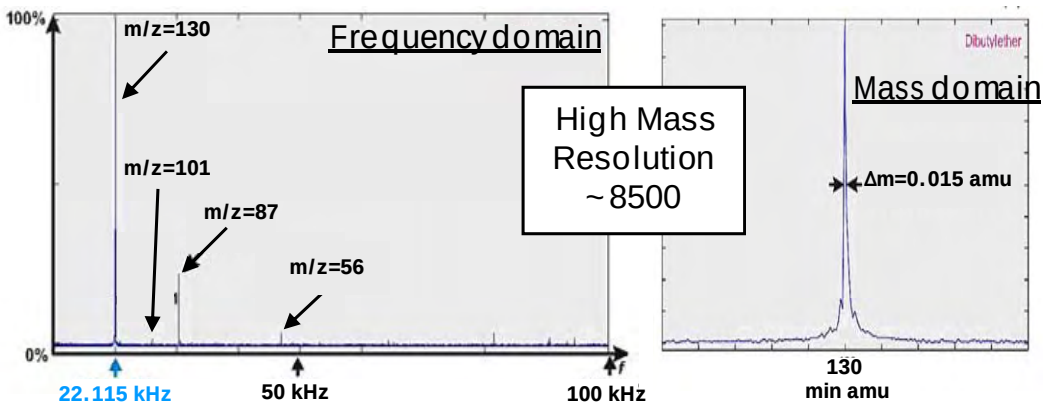

Figure 4. Gas analysis spectrum (Dibutylether)

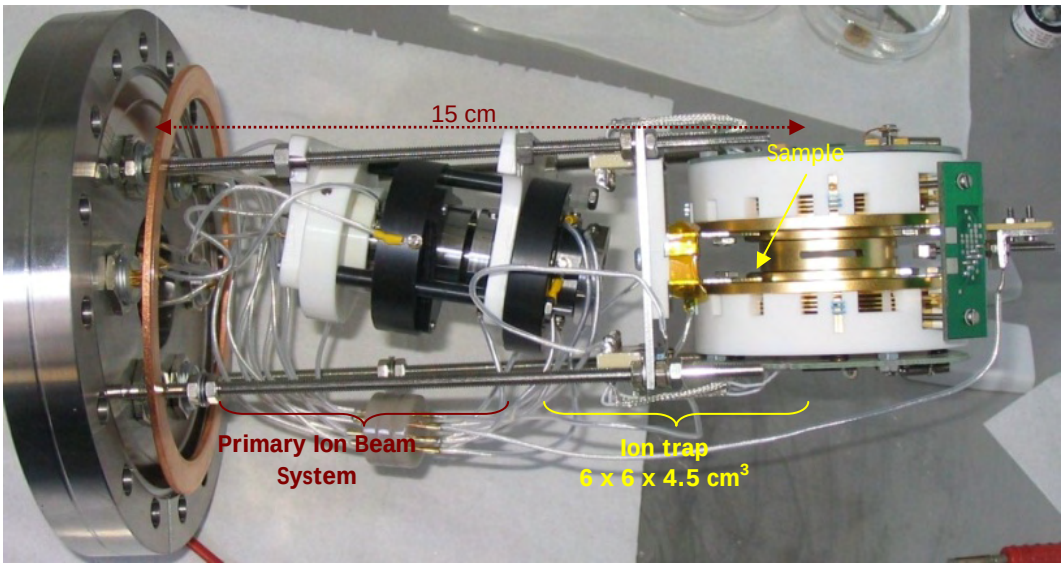

Figure 5. SIMS prototype picture (laboratory model)

Instrument Integration

Mass Properties and Budget

Ion trap + Ion Gun + Laser:

The overall instrument mass including 20% margin is 3200 g including electronics and thermal control.

Mass without laser (ion trap + ion gun only): 2500 g

Mass of the laser: 700 g

Power and Energy Budgets

The maximum instrument power consumption is 3.5 W including 20% margin.

Laser power consumption: 0.7 W.

Power conditioning is assumed to be done at Lander or Mother Spacecraft level.

Data Budget

Representative data budget for ILMA sequences is TBD (should be of the order of 1Mo/minute over a few hours).

Thermal Budget

Heat dissipation during ILMA analysis will be on average 2W when switched on.

Only a few hours of use of ILMA over the total duration of the mission.

Accommodation

Several cases are possible:

- In the lander, with sample collection (robotic arm): ILMA will be accommodated in order to allow positioning the inlet ions trap at 1mm (TBD) of sample surface.
- In the lander, with no sample collection: ILMA will be accommodated in the lander in order to allow positioning the inlet ions trap at 1mm (TBD) of ground surface.
- In the mother spacecraft: ILMA will be accommodated to allow positioning the inlet ions trap at 1mm (TBD) of sample surface.

Mechanical Interfaces

The mechanical Interfaces between ILMA and the lander (or mother spacecraft) are TBD depending on the mechanical design needed to obtain 1mm (TBD) positioning ground surface or samples.

Thermal Interfaces

Instrument	Minimum non-op	Minimum operative	Maximum operative	Maximum non-op	Dry-heat sterilization
ILMA	TBD	-10°C	+40°C	TBD	YES Same strategy as for the Moma laser on Exomars shall be applied

Electrical Interfaces

Power

ILMA requires Ground, 28 V, 12 V & 5 V supplies for the sensor and associated electronics.

Data

ILMA will use the data bus available on the lander (or mother spacecraft). The type and pin allocation of the data connectors are TBD.

Software Interfaces

ILMA will use the communication protocol corresponding to the data bus which will be implemented on the lander (or mother spacecraft).

ILMA is controlled by a command frame (TBD). It will control operations, sampling, data formatting and data transmission to the Lander's (or mother spacecraft) electronics. ILMA needs data processing with FFT facilities. Whether ILMA or an external module (Lander or mother spacecraft) is in charge of this data processing has to be defined.

Feasibility and Critical Issues

Laboratory's development has already been made for ILMA. A laboratory prototype is available and operational. The mechanical design has to be improved for QM and FM model but LPCE, LISA, MPS and ARC are involved in other space instruments and have proven capacities to manage such developments.

For these reasons, there is no specific issue considered critical to the ILMA development.

Instrument Operations

Ground Operations

Ions source should be kept in inert atmosphere (no O_2 and no H_2O).

Launch

No operation during launch.

Cruise

Ions sources should be activated once or twice a year, for a few minutes. Calibration tests can be performed during cruise phase.

NEO Surface Operations

The inlet of ILMA has to be moved at the right position from the NEO surface (1mm TBD), or samples have to be brought in order to allow positioning the inlet ions trap at 1mm (TBD) of sample surface.

Sequences are initialized and data transmitted (1 second per analysis, and about 50 sequences).

With the ion gun, more than one position can be analyzed without moving the instrument or the sample (few millimetres horizontal move adjusting the ion beam).

Instrument's Reference Operational Scenario

Timeline

Activation of ILMA

Heating of Ions Sources and electronics (about an hour) 0.5W.

ILMA is placed in the right position on the ground surface, or samples have to be brought in order to allow positioning the inlet ions trap at 1mm (TBD) of sample surface.

Analysis Sequences (a few hours depending on the number of sequences and number of analysis positions). One spectrum takes only a few seconds to acquire, and covers a mass range from 1 to 300 amu. We estimate that about 100 spectra will be needed to achieve our scientific goals.

ILMA is turned off

Heritage

Ion sources/Ion gun: COSIMA (Rosetta)
Laser: MOMA (ExoMars)
Ion trap : Ions traps have already been accommodated in space missions (e.g. PTOLEMY/Rosetta).

Funding Scheme

National Space Agencies: CNES & DLR for hardware and contractual positions

CNRS, MPI & universities for permanent staff

R&T funding in progress by CNES for LPCE

Ion sources: 1.5 M€ (10 sources) – From Austria (ARC)

Ion gun: ~ 700 k€ (including add. manpower listed below)

Laser: ~ 350 k€ (including add. manpower listed below)

Ion Trap: ~ 320 k€ (including add. manpower listed below)

Additional manpower

MPS: 1.5 man-year

BUW: 1 man-year

France (LPCE+LISA): 4 men-year

Industry Partnership

vH&S Schwetzingen & Laser Zentrum Hannover have been contacted and agree to be listed in the present document as potential industrial partners, as they have the technical and logistical capabilities to handle such a project.

Article 17

COTTIN H., SZOPA C. and MOORE M. H. (2001) Production of hexamethylenetetramine in photolyzed and irradiated interstellar cometary ice analogs. The Astrophysical Journal Letters 561(1), L139-L142.

THE ASTROPHYSICAL JOURNAL, 561:L139–L142, 2001 November 1

PRODUCTION OF HEXAMETHYLENETETRAMINE IN PHOTOLYZED AND IRRADIATED INTERSTELLAR COMETARY ICE ANALOGS

H. COTTIN,[1] C. SZOPA,[2] AND M. H. MOORE[1]
Received 2001 August 30; accepted 2001 September 26; published 2001 October 15

ABSTRACT

We report hexamethylenetetramine (HMT) detection in organic residues resulting from $H_2O : CO : CH_3OH : NH_3$ ices submitted to UV photolysis or proton irradiation. This is the first time HMT is detected after proton irradiation of an interstellar or cometary ice analog, whereas this molecule was suspected to be a characteristic signature of UV versus ion processing. This result strengthens the probability of HMT presence in the interstellar medium and in comets, where it may eventually be detected with the COSAC (COmetary Sampling And Composition) experiment on board the upcoming *Rosetta* mission.

Subject headings: astrochemistry — comets: general — ISM: molecules — methods: laboratory — space vehicles: instruments

1. INTRODUCTION

Unraveling the nature of the organic components of interstellar dust and comets is critical to understanding the chemical evolution of materials from the interstellar medium to the solar system. A classic laboratory approach to this problem is to start with various ice mixtures at ~10 K and photolyze with vacuum ultraviolet, irradiate with charged particles, or simply warm the ices, simulating the processing of ice-mantled dust in molecular clouds or the solar system. When warmed to room temperature, these processed icy mixtures leave a residue, which is generally presumed to be a close analog of the organic mantles of dust in molecular clouds (see, for instance, Greenberg 1982, Allamandola, Sandford, & Valero 1988, or Cottin, Gazeau, & Raulin 1999 for reviews on that subject).

Three kinds of energetic processing occur on icy coated dust grains in interstellar clouds or in the outer layers of comet ices in the solar system. In interstellar clouds, icy coated dust particles are subjected to processing by

1. Charged particles: Galactic cosmic rays.
2. UV photons: Lyα photons from neighboring stars in the diffuse outer regions or UV photons induced by Galactic cosmic rays in the inner regions of dense clouds.
3. Thermal processes: cycling between the cold dense cloud center and warmer diffuse regions.

In the solar system, the outer layers of comets undergo the same processes:

1. Charged particles: Galactic cosmic rays, mainly in the Kuiper belt and the Oort clouds. This process has the largest effect on the outer few meters of the nucleus.
2. UV photons: solar UV, mainly in the inner solar system when the comet is close to the Sun. This process would affect the outer few micrometers of the nucleus.
3. Thermal processes: during the formation of the solar system (depending on the region in which the comet accretes) and in the inner Solar system (when the comet approaches perihelion).

As a result of the diversity of environments involved, constraining the degrees to which different processes affect cosmic ices is a highly convoluted problem. Differences between the products synthesized during processing, according to the energy sources, could give information on the history of comets. So far the laboratory experiments have emphasized the analytical method (infrared spectroscopy, liquid and gas chromatography, mass spectroscopy, etc.) to detect the widest range of synthesized molecules rather than the form of the deposited energy (Cottin et al. 1999).

The facilities at NASA's Goddard Cosmic Ice Laboratory are equipped with a Van de Graaff accelerator and a UV lamp system so that ices can be processed using both protons and UV photons. Results can be compared using the same analytical method. Thus, a direct comparison of synthesized compounds is possible, with the aim of finding if the production of a molecule can be an indicator of the processing history of ices. The first set of data comparing UV photolysis and ion irradiation of ices at Goddard showed that the yield of major products was similar for a simple ice containing H_2O and CO_2 (Gerakines, Moore, & Hudson 2000) but different for pure CO (Gerakines & Moore 2001).

Among the complex organic refractory molecules that have been synthesized during cometary and interstellar ice analog experiments, polyoxymethylene [POM; $(CH_2-O)_n$] and hexamethylenetetramine (HMT; $C_6H_{12}N_4$) seem to be of prime interest. POM and polymers of the same family have been detected when ice mixtures containing formaldehyde and ammonia are slowly warmed to room temperature, without any photolysis or ion irradiation processing (Schutte, Allamandola, & Sandford 1993a, 1993b). After UV photolysis of ices such as $H_2O : CH_3OH : CO : NH_3$ (10 : 5 : 1 : 1), POM-like polymers have also been detected, but HMT represents ~60% of the organic residue at 300 K (Bernstein et al. 1995). Thus, it looks like POM is a good indicator for thermal processing of ices, while HMT plays the same role concerning UV photolysis. HMT is of particular interest since it forms amino acids when acid-hydrolyzed (Wolman et al. 1971).

Bernstein et al. (1995) suggested that ion irradiation of a mixture of $H_2O : CH_3OH : CO : NH_3$ would not lead to the production of HMT. Rather than a conversion of CH_3OH into H_2CO, which is the first step toward HMT formation during photolysis, acetone would form, leading to the production of linear molecules such as polyamino-dimethyl-methylene

[1] Astrochemistry Branch, Code 691, NASA Goddard Space Flight Center, Greenbelt, MD 20771; hcottin@lepvax.gsfc.nasa.gov, ummhm@lepvax.gsfc.nasa.gov.
[2] Laboratoire Interuniversitaire des Systèmes Atmosphériques, UMR 7583 CNRS, Universités Paris VII–Paris XII, 94010 Créteil Cedex, France; szopa@lisa.univ-paris12.fr.

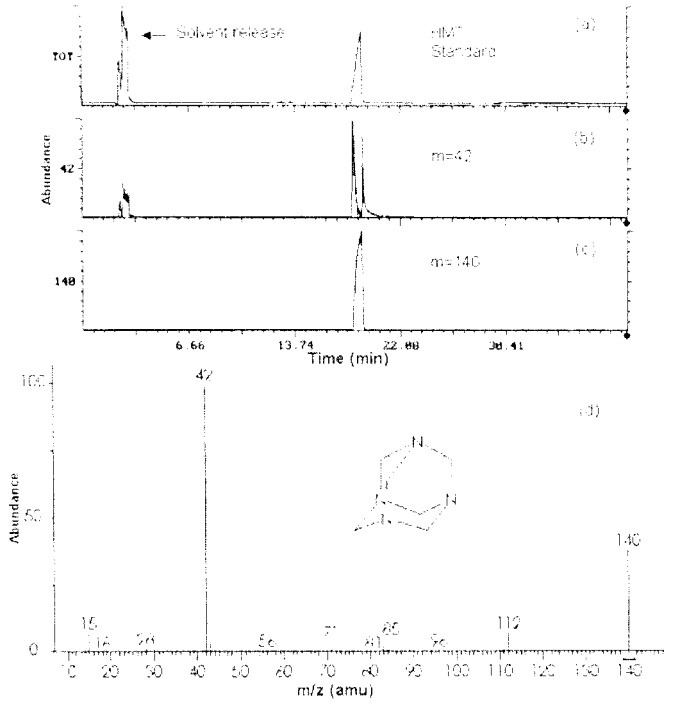

FIG. 1.—Chromatogram of HMT injected in an MXT-1 column (see text for details). (*a*) Total chromatogram. It shows the sample is released 19 minutes after injection. The same retention time for mass 42 is shown in (*b*) and for mass 140 in (*c*). (*d*) Mass spectrum of HMT (from the National Institute of Standards and Technology Mass Spectral Database). Characteristic peaks for HMT are 42 and 140 amu.

(PADMM; $[-C(CH_3)_2-NH-]_n$). HMT would then be a signature of UV processing, and PADMM a signature of proton processing. This hypothesis originated with a tentative infrared identification of acetone in irradiated water ice containing methanol by Baratta et al. (1994), which was repeated by Moore, Ferrante, & Nuth (1996) and Palumbo, Castorina, & Strazzulla (1999). However, Hudson & Moore (2000), recently showed that there is no evidence of acetone formation in proton-irradiated methanol ices. Instead, H_2CO has now been identified in both $H_2O : CH_3OH$ and $H_2O : CO$ ices. Therefore, HMT formation in proton-irradiated ices was expected in irradiated $H_2O : CH_3OH : CO : NH_3$ ices and has been confirmed by the results reported in this Letter.

For the first time, we present the analysis of two organic residues originating from the same ice composition. One residue was from UV-photolyzed $H_2O : CH_3OH : CO : NH_3$ ice and the second residue from the same ice after ion irradiation. This Letter focuses specifically on HMT formation, in order to check the hypothesis that HMT is a specific signature of UV-processed ice. Analysis of other organic compounds will require new analytical developments and is in progress.

2. EXPERIMENT

The experimental setup has been described in detail by Hudson & Moore (1995) and Moore & Hudson (1998, 2000). A gas mixture is condensed onto an aluminum cold mirror ($T <$ 20 K) in a vacuum chamber ($P \sim 10^{-8}$ torr). Gases are mixed in a glass bulb, and the concentration of each is determined by its partial pressure. The resulting ice is assumed to have the same composition as the gas phase. The ice thickness is determined by measuring laser interference fringes during deposition. The typical rate is 3–5 μm hr^{-1}. Ice can be photolyzed with a UV lamp (average energy: 7.4 eV; flux: $\sim 3 \times 10^{14}$ photons cm^{-2} s^{-1}) or irradiated with 0.8 MeV protons from a Van de Graaff accelerator. Source and purity of used compounds are the following: triply distilled H_2O with a resistance greater than 10^7 ohms cm; CO, Matheson research grade, 99.99%; CH_4, Matheson research grade, 99.999%; NH_3, Matheson anhydrous, 99.99%; CH_3OH, Sigma-Aldrich HPLC grade, 99.9%; HMT, Fluka, greater than 99.5%.

Two sets of experiments have been performed with the same ice composition: $H_2O : CH_3OH : CO : NH_3$ (10 : 5 : 1 : 1). This composition was chosen to be the same as the one studied in Bernstein et al. (1995) and includes the most abundant interstellar and cometary molecules with the exception of CO_2 and H_2 (Ehrenfreund & Charnley 2000). During the first set of experiments, two successive $\sim$0.5 μm ice layers were photolyzed each during 9 hr, in order to repeat Bernstein et al. experiment. Ices where very thin to ensure UV processing throughout the whole ice depth. The second experimental set consists of an $\sim$10 μm ice sample, irradiated with 0.8 MeV protons. This energy has a penetration range of $\sim$20 μm and will process the whole ice depth. Irradiation processing therefore is more efficient than UV processing at producing a larger amount of organic residue. Dose estimates for UV photons are described in Gerakines et al. (2000) and for protons in Moore & Hudson (1998). The proton irradiation dose has been set to be equivalent to the UV energy deposited, i.e., roughly 25 eV molecule^{-1}.

Organic residues were recovered from the aluminum mirror with methanol. Analyses were performed using a Varian Saturn II gas chromatograph–mass spectrometer (GC-MS). GC separations were performed on an MXT-1 (Restek) capillary column (length = 30 m, internal diameter = 0.18 mm, inner coating = 0.6 μm). Analysis settings were: column inlet pressure = 17 psi (relative to the atmospheric pressure), $T_{\rm column}$ = 60°C (0–5 minutes) and then 20°C minute^{-1} until 160°C, $T_{\rm injection}$ = 300°C, $T_{\rm transfer\ to\ MS}$ = 200°C. This column and settings were chosen specifically for the detection of HMT. Detection was performed with a Finnigan-Varian mass spectrometer, with an ion trap (1–650 amu; resolution: 1 amu). Secure GC-MS identification of HMT is achieved by comparing the retention time of standard HMT with the retention time of peaks resulting from the organic residue injected with the same analysis settings and by matching the mass spectrum with the HMT reference mass spectrum (Fig. 1). Blank experiments are performed before each organic sample injection in order to check the contamination level of the column.

3. RESULTS AND DISCUSSION

GC-MS analyses of residues from both UV-photolyzed and ion-irradiated $H_2O : CH_3OH : CO : NH_3$ ices are shown in Figure 2. Concerning the UV sample, there is no clear indication of HMT in the total chromatogram (Fig. 2*a*). This is due to the very low amount of residue recovered after the photolysis experiment. Nevertheless, its presence is clearly revealed on the specific plots (Figs. 2*b* and 2*c*) for masses 42 and 140 (main HMT MS fragments), both of which show a peak at the same retention time as measured for the HMT standard. The peculiar shape of the peaks is not clearly understood. It is probably due to the high polarity of amino groups such as in HMT, which interact badly with stationary phases of GC columns. Identification of HMT is confirmed by the mass spectrum sampled on peaks 42 and 140 attributed to HMT (Fig. 2*d*). Masses detected with amu > 140 are due to recombination in the ion

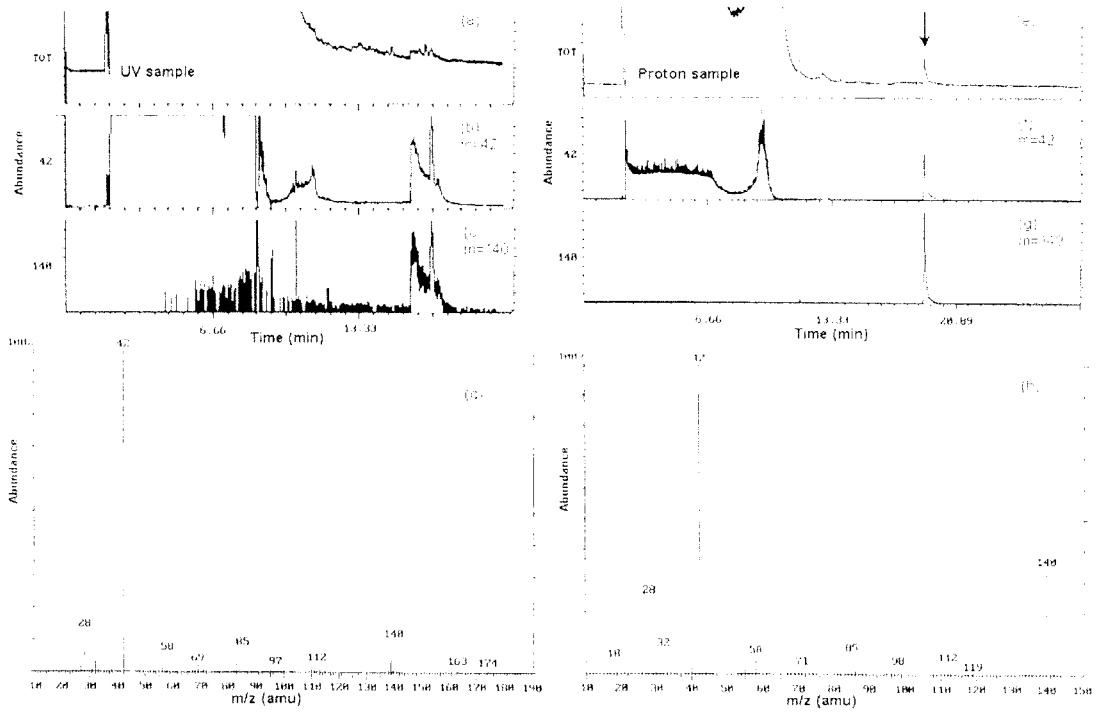

FIG. 2.—Chromatograms collected during analysis of UV-processed residue (*left panels*) and proton-processed residue (*right panels*). Upper panels are the total chromatogram compared to the two characteristic masses of HMT 42 and 140. Lower panels show the mass spectra corresponding to the peaks associated to HMT.

trap of the spectrometer. This detection is consistent with Bernstein et al. (1995).

The proton-processed ice was much thicker than the UV one; therefore, the amount of residue is larger, ensuring a better signal, as shown in the right panels of Figure 2. HMT is clearly detected in the total chromatogram thanks to its retention time, 19 minutes (Fig. 2*e*). This detection is confirmed by specific plots for masses 42 and 140 (Figs. 2*f* and 2*g*) and by the mass spectrum sampled on the peak attributed to HMT (Fig. 2*h*). No trace of substituted HMT (HMT skeleton with a CH_3, OH, CHO, or COOH group instead of one H, which should result in a parent mass of 154, 156, 168, and 184, respectively) has been so far detected in our samples (spectra not shown).

Thus, HMT is detected in both samples and should henceforth not be considered as a characteristic signature of a specific process. According to the mechanism described in Bernstein et al. (1995), the first stage toward its synthesis is the production of H_2CO by oxidation of CH_3OH. This can be achieved by UV photolysis (Allamandola et al. 1988) or proton irradiation (Hudson & Moore 2000). But CO in water also produces formaldehyde by UV (Allamandola et al. 1988) or proton processes (Moore, Khanna, & Donn 1991). Experiments starting with ^{13}C-labeled methanol reported in Bernstein et al. indicated that the carbon in HMT originated from methanol rather than from CO. But this is certainly due to a more efficient conversion rate of methanol into formaldehyde than CO into formaldehyde. Then ices containing only one carbon source (CO or CH_3OH) should yield production of HMT but with a higher efficiency with CH_3OH. Addition of CO_2 in the initial ice mixture should not induce any effect regarding HMT production as no detectable amount of H_2CO is reported after UV (Gerakines et al. 1999) or proton (Moore et al. 1991; Brucato, Palumbo, & Stazzulla 1997) irradiation of $H_2O : CO_2$ ices.

Our results strengthen the probability for the presence of HMT in the interstellar medium as being one product of radiation chemistry (UV and charged particles) between the most abundant interstellar molecules detected so far. But its actual IR detection is jeopardized since its strongest infrared bands at $\sim$10 μm overlap the Si$-$O silicate band (Bernstein et al. 1994, 1995). Its detection on comets from remote sensing has the same difficulties. Bernstein et al. (1995) suggested that the degradation of HMT on cometary grains ejected from the nucleus could possibly be responsible for the extended source of the CN radical observed in comet Halley (Klavetter & A'Hearn 1994). This could be an interesting indirect detection of HMT. But Cottin et al. (2001) have tested this hypothesis regarding the photostability of HMT and its photodegradation products and concluded that the photolysis of HMT is very unlikely to account for the amount of extended CN in comets. Nevertheless, the idea of thermal degradation of HMT on very hot cometary grains remains to be investigated in the laboratory. Indeed, HMT is known to decompose into amines and nitriles at temperatures as low as 500 K (Iwakami, Takazono, & Tsuchiya 1968), a temperature that could easily be reached by small grains in cometary comae (Crifo 1988; Greenberg & Li 1998).

The coming in situ investigation of a cometary nucleus (46P/Wirtanen) with the ESA *Rosetta* mission will search for complex organics. The COSAC (COmetary Sampling And Composition) experiment (Rosenbauer et al. 2001) on board the *Rosetta* lander includes a gas chromatography system devoted to the analysis of the nucleus molecular composition (Szopa et al. 2000). One of the columns selected to be used in the experiment is an MXT-1, similar to the one we used for our laboratory analysis of HMT, with some differences: length = 10 m, internal diameter = 0.18 mm, and inner coating = 0.1 μm. If present on P/Wirtanen in sufficient amounts, HMT should then be detected, as shown in Figure 3.

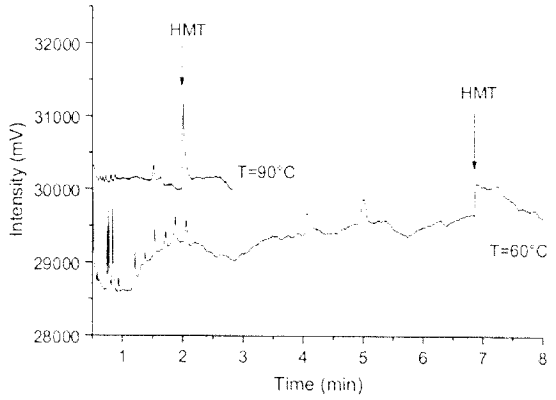

FIG. 3.—HMT injected along with other organic compounds expected to be present on a cometary nucleus (including benzene, toluene, pyridine, octane, nonane, decane, pentanol, xylene, naphtalene, indene, and trioxane). The top chromatogram was collected at $T = 90$°C and the bottom one at 60°C, on the same MXT-1 column as the one selected to be part of the COSAC experiment on board the *Rosetta* lander. Length = 10 m, internal diameter = 0.18 mm, and inner coating = 0.1 μm. The analysis has been performed within the spatial requirement of the mission (T between 30°C and 90°C).

If not, a compound such as HMT, likely to be synthesized by proton and UV irradiations in the interstellar medium, might have been destroyed during the collapse of the presolar cloud or in the early turbulent nebula. Indeed, temperatures above 800 K are necessary to produce the crystalline phase silicates observed in comet Hale-Bopp (Crovisier et al. 1997). Temperature $T > 800$ K is consistent with estimations of conditions in the inner presolar nebula (Mousis et al. 2000). They are sufficient to destroy HMT (Iwakami et al. 1968). The nondetection of HMT could therefore be an indication that most of the interstellar material has been reprocessed at high temperature before the accretion of the comet and that mainly thermal processes dominated comet P/Wirtanen ices history.

This work was performed while H. C. held an NRC-NASA/GSFC Associateship. This work was supported by NASA through RTOP 344-02-57 and 344-33-01 and the French Space Agency (CNES). Claude Smith and Steve Brown of the NASA/Goddard Radiation Facility are thanked for assistance with the proton irradiation.

REFERENCES

Allamandola, L. J., Sandford, S. A., & Valero, G. J. 1988, Icarus, 76, 225
Baratta, G. A., Castorina, A. C., Leto, G., Palumbo, M. E., Spinella, F., & Strazzulla, G. 1994, Planet. Space Sci., 42, 759
Bernstein, M. P., Sandford, S. A., Allamandola, L. J., & Chang, S. 1994, J. Phys. Chem., 98, 12,206
Bernstein, M. P., Sandford, S. A., Allamandola, L. J., Chang, S., & Scharberg, M. A. 1995, ApJ, 454, 327
Brucato, J. R., Palumbo, M. E., & Strazzulla, G. 1997, Icarus, 125, 135
Cottin, H., Bachir, S., Raulin, F., & Gazeau, M. C. 2001, Adv. Space Res., in press
Cottin, H., Gazeau, M. C., & Raulin, F. 1999, Planet. Space Sci., 47, 1141
Crifo, J. F. 1988, Part. Part. Syst. Charact., 5, 38
Crovisier, J., et al. 1997, Science, 275, 1904
Ehrenfreund, P., & Charnley, S. B. 2000, ARA&A, 38, 427
Gerakines, P. A., & Moore, M. H. 2001, Icarus, in press
Gerakines, P. A., Moore, M. H., & Hudson, R. L. 2000, A&A, 357, 793
Gerakines, P. A., et al. 1999, ApJ, 522, 357
Greenberg, J. M. 1982, in Comets, ed. L. L. Wilkening (Tucson: Univ. Arizona Press), 131
Greenberg, J. M., & Li, A. 1998, A&A, 332, 374
Hudson, R. L., & Moore, M. H. 1995, Radiat. Phys. Chem., 45, 779
———. 2000, Icarus, 145, 661
Iwakami, Y., Takazono, M., & Tsuchiya, T. 1968, Bull. Chem. Soc. Japan, 41, 813
Klavetter, J. J., & A'Hearn, M. F. 1994, Icarus, 107, 322
Moore, M. H., Ferrante, R. F., & Nuth, J. A. I. 1996, Planet. Space Sci., 44, 927
Moore, M. H., & Hudson, R. L. 1998, Icarus, 135, 518
———. 2000, Icarus, 145, 282
Moore, M. H., Khanna, R., & Donn, B. 1991, J. Geophys. Res., 96, 17,541
Mousis, O., Gautier, D., Bockelée-Morvan, D., Robert, F., Dubrulle, B., & Drouart, A. 2000, Icarus, 148, 513
Palumbo, M. E., Castorina, A. C., & Strazzulla, G. 1999, A&A, 342, 551
Rosenbauer, H., et al. 2001, ESA SP-1165 (Noordwijk: ESA), in press
Schutte, W. A., Allamandola, L. J., & Sandford, S. A. 1993a, Icarus, 104, 118
———. 1993b, Science, 259, 1143
Szopa, C., Sternberg, R., Coscia, D., & Raulin, F. 2000, BAAS, 32, 37.12
Wolman, Y., Miller, S. L., Ibañez, J., & Oro, J. 1971, Science, 174, 1039

Article 18

COTTIN H., MOORE M. H. and BÉNILAN Y. (2003) Photodestruction of relevant interstellar molecules in ice mixtures. The Astrophysical Journal 590, 874-881.

The Astrophysical Journal, 590:874–881, 2003 June 20

PHOTODESTRUCTION OF RELEVANT INTERSTELLAR MOLECULES IN ICE MIXTURES

Hervé Cottin
Laboratoire Interuniversitaire des Systèmes Atmosphériques, Universités Paris VII-Paris XII, Créteil, France; cottin@lisa.univ-paris12.fr

Marla H. Moore
Astrochemistry Branch, Code 691, NASA Goddard Space Flight Center, Greenbelt, MD 20771; marla.h.moore@nasa.gov

and

Yves Bénilan
Laboratoire Interuniversitaire des Systèmes Atmosphériques, Universités Paris VII-Paris XII, Créteil, France;
benilan@lisa.univ-paris12.fr
Received 2002 December 23; accepted 2003 March 3

ABSTRACT

UV photodestruction of some interstellar molecules is studied in different kinds of ices. CH_4, CH_3OH, NH_3, CO_2, CO, and HNCO are photolyzed as pure ices, or mixed with water or molecular nitrogen, at about 10 K. The destruction cross sections of these molecules are estimated for use in photochemical models of interstellar ices. We show that the destruction rate depends on the ice in which the studied compound is embedded.

Subject Headings: astrochemistry — ISM: molecules — methods: laboratory — molecular processes — ultraviolet: ISM

1. INTRODUCTION

Laboratory studies attempting to mimic interstellar ices, through the irradiation of low-temperature ice mixtures, have mainly been devoted to the study of complex organic molecules synthesized from a simple starting material, and contained in the refractory residue resulting from samples warmed to room temperature (see, e.g., Allamandola, Sandford, & Valero 1988; Schutte, Allamandola, & Sandford 1993; Bernstein et al. 1995; Dworkin et al. 2001; Cottin, Gazeau, & Raulin 1999 for a review of those experiments). But little is known about intrinsic chemical mechanisms dominating the evolution of simple ice mixtures, or about kinetic constants that are necessary to extrapolate laboratory simulations to interstellar environments. First steps toward a systematic approach have been published by Gerakines, Schutte, & Ehrenfreund (1996), who studied UV processing of pure ices and gave an exhaustive list of photoproducts and photodestruction cross sections. A comparison of UV photolysis and ion irradiation of CH_4 and CH_3OH is reported by Baratta, Leto, & Palumbo (2002), and CO is discussed by Gerakines & Moore (2001). Concerning binary mixtures, which are the next stage for understanding the ice chemistry, systematic studies have been performed on $H_2O + CO_2$ mixtures (Gerakines, Moore, & Hudson 2000), where the influence of photons versus protons is compared. Products, *G* values, and chemical mechanisms have been published for proton-irradiated mixtures such as $H_2O + CH_4$, $H_2O + C_2H_2$ (Moore & Hudson 1998), $H_2O + CO$, and $H_2O + H_2CO$ (Hudson & Moore 1999). More recently, Ehrenfreund et al. (2001) published the UV photodestruction rate of amino acids in H_2O, N_2, and Ar matrices, and Watanabe et al. (2002) measured the conversion rate of CO to CO_2 in H_2O ice.

The present paper focuses on the photodestruction rates of some of the most abundant molecules detected in interstellar medium ices: CO (Ehrenfreund et al. 1997), CO_2 (Gerakines et al. 1999), NH_3 (Lacy et al. 1998), CH_4 (Boogert et al. 1998), and CH_3OH (Gibb et al. 2000). HNCO is also included in our study. Although not detected directly in interstellar ices, this molecule is present in the gas phase (Snyder & Buhl 1972; Jackson, Armstrong, & Barrett 1984) and in comets (Lis et al. 1997a, 1997b). HNCO is the simplest molecule containing all four atoms, H, N, C, and O. This paper contains the photodestruction of these six molecules as single-component ices, and also in polar (H_2O) and apolar (N_2) matrices.

In the first section, we present our experimental setup, with a focus on the estimation of the UV lamp flux, a critical parameter to derive quantitative photolysis data. Then we discuss some theoretical aspects of photolysis in ices, how it can be modeled, and how results such as the ones we present in this paper can be interpreted. Then we present our results, showing that the photodestruction rate may depend on the molecule's direct environment, i.e., the dominant ice molecule.

2. EXPERIMENTAL

2.1. *Ice Preparation and Analysis*

The experimental setup has been described in detail by Hudson & Moore (1995) and Moore & Hudson (1998, 2000). Basically, a gas mixture is condensed at a rate of ~3–5 μm hr^{-1} onto an aluminum cold mirror ($T < 20$ K) in a vacuum chamber ($P \sim 10^{-8}$ torr). The ice thickness is determined by measuring laser interference fringes during deposition. Ice films can be photolyzed with a UV lamp (described in the next section) and analyzed by infrared spectroscopy (each spectrum collected had 60 scans at 4 cm^{-1} between 4000 and 400 cm^{-1}). The photolysis of CH_4, CH_3OH, NH_3, CO_2, CO, and HNCO have been studied in pure form, and as a binary mixture dominated by N_2 or H_2O with a 10 : 1 ratio.

Gas-phase mixtures are made in a glass bulb in which the concentration of each component is determined by its partial pressure. The sources and purities of the compounds used are: triply distilled H_2O with a resistance greater than 10^7 ohm cm; N_2, Matheson research grade, 99.995%; CO, Matheson research grade, 99.99%; CO_2, Matheson research grade, 99.995%; CH_4, Matheson research grade, 99.999%; NH_3, Matheson anhydrous, 99.99%; CH_3OH, Sigma-Aldrich HPLC grade, 99.9%. HNCO is synthesized by a reaction of NaOCN powder (Aldrich Chemical 96%) with HCl gas (Aldrich Chemical 99+%), and purified with an ethanol/liquid nitrogen slush bath.

2.2. *UV Lamp Spectrum and Flux*

UV photons are provided by a microwave-powered (Opthos) hydrogen flow lamp. This is the same lamp used in Gerakines et al. (2000), and is similar to ones used in Allamandola et al. (1988), Gerakines et al. (1996), Ehrenfreund et al. (2001), and Baratta et al. (2002). The lamp is separated from the vacuum system by a lithium fluoride (LiF) window, transmitting $\lambda > 104$ nm. Lamp settings during irradiation are $P_{H_2} = 1000$ torr, microwave forward power 50%, reflected power less than 5%.

The UV spectrum of the lamp transmitted through the LiF window has been measured (with vacuum-pumped spectrometer Acton VM-502; detector Acton DA781) and is shown in Figure 1. This allows us to estimate that the average energy deposited during ice photolysis is $E = 7.41 \pm 0.23$ eV (average and uncertainty estimated from four successive spectra of the lamp emission). Lyα emission at 121.6 nm accounts for at most 5% of the total intensity between 100 and 200 nm.

The lamp flux has been measured using a calibrated NIST silicon photodiode. These flux measurements are compared to estimates of the flux obtained by measuring the $O_2 \rightarrow O_3$ conversion rate during the photolysis of a pure O_2 ice at 18 K.

2.2.1. *Photodiode Flux Measurements*

Silicon photodiodes are broadband detectors that provide an absolute quantification of the flux emitted by the UV lamp. The photodiode is placed in the vacuum system at the location of the cold mirror, collecting exactly the same UV flux that would be received by an ice sample. The photon flux is calculated from the current produced by the photodiode, such as flux $= i/e$QE, where i is the current intensity, $e = 1.6 \times 10^{-19}$ coulomb electron^{-1}, and QE is the quantum efficiency of the photodiode in the 116–254 nm range. To estimate the evolution of the lamp flux as a function of time, two measurements have been performed separated by ~60 hr of lamp utilization (times $t = 25$ and 88 hr with the same window). In addition, flux measurements have been performed for several microwave output powers; these fluxes are compared with oxygen ice actinometry.

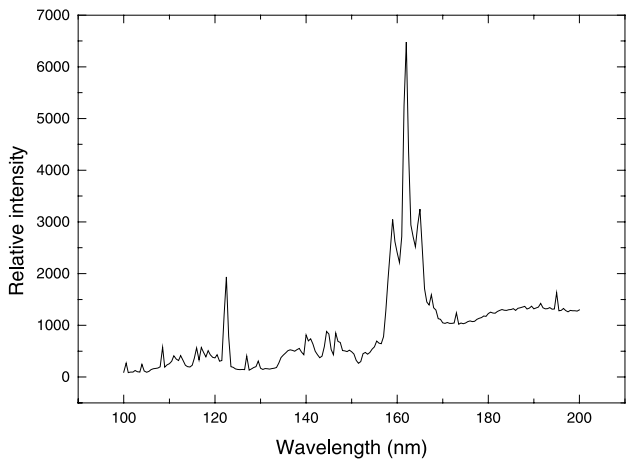

FIG. 1.—UV lamp spectrum, collected for $P_{H_2} = 1000$ torr, microwave forward power 50%, reflected power <4% (LiF window).

2.2.2. *Oxygen Photolysis*

The actinometry method using O_2 ice photolysis to form O_3 is described in Gerakines et al. (2000). It is a well-documented method for gas-phase O_3 production (e.g., Warneck 1962). However, because of a lack of solid-phase data, gas-phase O_3 values are usually used, i.e., quantum yield of O_3 from O_2, QE = 1.92 (Groth 1937), and the strength of the O_3 stretching mode at 1040 cm^{-1}, $A = 1.4 \times 10^{-17}$ cm molecule^{-1} (Smith et al. 1985, p. 111). In our laboratory a pure O_2 ice is deposited. Its thickness is roughly 1.75 μm, which should allow a total absorption of the UV flux throughout the ice. But again, this estimation is based on a gas-phase absorption cross section (Okabe 1978) because of the lack of solid-phase data for O_2 in the vacuum UV. Therefore, we have checked that this method is not thickness dependent by comparing results obtained from both a 1.75 and a 3.25 μm ice. O_3 production is measured as a function of the time of photolysis, and the flux is derived from those measurements such as flux = [(Area under the 1040 cm^{-1} feature)/(photolysis time × QE × A)]. Actinometry experiments using these methods have been done for $t = 64$, 88, and 115 hr of lamp utilization. For $t = 88$ hr, measurements have been performed for several microwave output powers to be correlated with the photodiode results.

2.2.3. *Photodiode Flux Results Compared with Actinometry*

Table 1 shows the lamp flux, F, measured using the photodiode for different setting of the microwave generator compared to the flux obtained within the same conditions by O_2 photolysis. The use of gas-phase values for the QE and A-value do not give a flux equal to the calibrated value.

TABLE 1

LAMP FLUX, F, MEASURED BY A PHOTODIODE AND BY $O_2 \rightarrow O_3$ ACTINOMETRY

MICROWAVE SETTINGS FORWARD/ REFLECTED	F (photons s^{-1} cm^{-2})		
	Photodiode	Actinometry[a] QE × A = 2.69 × 10^{-17} cm photon^{-1}	Actinometry QE × A = 8.4 × 10^{-18} cm photon^{-1}
30/0	1.70×10^{14}	6.20×10^{13}	1.98×10^{14}
50/1	3.09×10^{14}	8.99×10^{13}	2.88×10^{14}
70/6	4.17×10^{14}	1.26×10^{14}	4.05×10^{14}
80/6	4.78×10^{14}	1.52×10^{14}	4.88×10^{14}

[a] $A = 1.4 \times 10^{-17}$ cm molecule^{-1}, QE = 1.92 molecule photon^{-1}

TABLE 2
LAMP FLUX FROM $O_2 \rightarrow O_3$ ACTINOMETRY FOR TWO ICE THICKNESS

Ice thickness (μm)	F (photons s^{-1} cm^{-2})
1.75	$3.5 \pm 0.8 \times 10^{14}$
3.25	$3.4 \pm 0.8 \times 10^{14}$

NOTE.—We assumed QE $\times$ $A = 8.4 \times 10^{-18}$ cm photon^{-1}. These experiments were not performed at the same time as the results presented in Table 1, which explains the difference between the fluxes. The forward/reflected setting was 50/2.

However, one must keep in mind that both the QE and A-value are subject to variations as a function of temperature and phase. Therefore, we propose to use a corrected value for QE $\times$ A, which has been calculated in order to minimize $\Sigma(F_{O_2}^{\text{actinometry}} - F_{\text{photodiode}}^{\text{measured}})^2$: QE $\times$ $A = 8.4 \times 10^{-18}$ cm photon^{-1}. This is nothing but a working value for actinometry measurements, which can be used in laboratories where a calibrated photodiode is not available, or for routine checks of the flux as photodiode measurements are more tedious to implement. The estimated uncertainty of the photon flux by O_2 photolysis is calculated by a least-square regression on $F_{\text{photodiode}}^{\text{measured}} = F_{O_2}^{\text{actinometry}}$ is $\pm 25\%$. Table 2 is a comparison of results for two ice thickness (1.75 and 3.25 μm), showing that O_2 results are not thickness dependent.

Figure 2 presents the evolution of the lamp flux as function of time. The decay is due to decreased transmission of the LiF window from the formation of yellow color centers. Those color centers can be removed by baking the window at about 300°C for a few hours. In this paper, photodestruction cross sections are calculated with a lamp flux estimated at the time of the experiment, from our measured linear regression of the actual flux due to the window's decreasing transmission. Again, uncertainty can be estimated to be $\pm 25\%$.

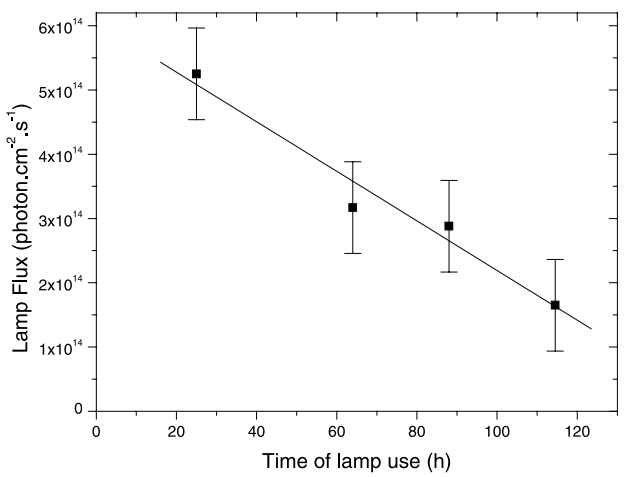

FIG. 2.—Evolution of the lamp flux as a function of time due to decreased transmittance of the LiF window.

3. SOME THEORETICAL ASPECTS OF ICE PHOTOLYSIS

The photodestruction of a molecule can be written as

$$AB \xrightarrow{h\nu} A^0 + B^0 ,$$

where AB is a molecule, and A^0 and B^0 are the resulting fragments. If N is the number density of AB (cm^{-3}), the photolysis rate is usually described by

$$\frac{dN}{dt} = -JN , \quad (1)$$

where $J = \int_\lambda \sigma_\lambda I_\lambda \, d\lambda$, σ_λ being the destruction cross section of the molecule (cm^2), which is actually the product of the cross section of the molecule and the quantum yield of the photolysis reaction, and I_λ is the UV flux (photons s^{-1} cm^{-2}). Both σ and I are a function of the wavelength λ. If the ice is optically thin, then a first-order decay can be assumed and the value of J measured experimentally, as it is in Gerakines et al. (1996) and Ehrenfreund et al. (2001). The integrated form of equation (1) is

$$N(t) = N_0 \exp(-Jt) . \quad (2)$$

Then the half-life, $t_{1/2}$, of the molecule [time for which $N(t) = N_0/2$] is written

$$t_{1/2} = \ln 2 / J \quad (3)$$

and does not depend on N_0. Here J is experimentally determined from the slope of a plot of $\ln N$ versus t for

$$\ln N = -Jt + \ln N_0 . \quad (4)$$

Gerakines et al. (2000) assumed zeroth-order kinetics to calculate the destruction rate of CO_2 in H_2O ices and the production rate of CO and H_2CO_3. This is another analysis method for dealing with chemical reaction rates in which N is assumed to be constant and equal to N_0. The zeroth-order differential equation is

$$dN/dt = -JN_0 , \quad (5)$$

and the integrated form is

$$N = N_0 - JN_0 t . \quad (6)$$

Both equations (2) and (6) are equivalent, since as $t \rightarrow 0$ then $\exp(-Jt) \rightarrow (1 - Jt)$.

Equations (2) and (6) are no longer valid if the ice cannot be considered as optically thin, and thus the photon flux is not constant throughout the ice. In this case J is a function of the ice depth, as shown in Figure 3. Then, according to the Beer-Lambert law, neglecting diffusion within the ice,

$$J(z) = J_0 \exp(-Kz) , \quad (7)$$

where J_0 is the J value at the top of the ice, z is the depth from the ice surface, and K is the absorption coefficient of the ice in cm^{-1}, assumed to be constant with depth and time.

Let us consider the ice sample as a succession of n layers in which J can be assumed to be constant (Fig. 3). Here N_1 to N_n are molecular number densities that are photolyzed at rates J_1 to J_n according to a first-order decay for each n layers; N_0 is the initial density of that molecule, and N is the average density in the ice for a time t of photolysis, as it would be measured, for example, by a spectrometer. The

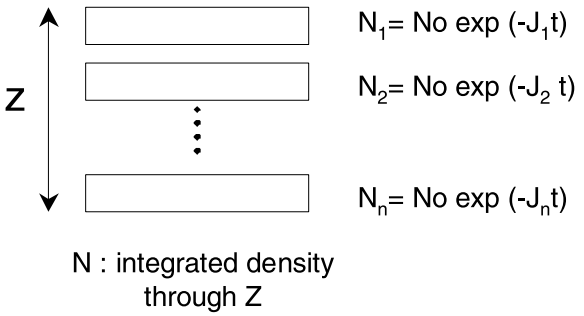

FIG. 3.—Schematic of ice sample seen as a succession of layers in which J can be assumed to be constant. Here N_1 to N_n are molecular number densities that are photolyzed at rates J_1 to J_n according to a first-order decay, N_0 is the initial density of that molecule, and N is the average density in the ice, as it would be measured, for example, by a spectrometer.

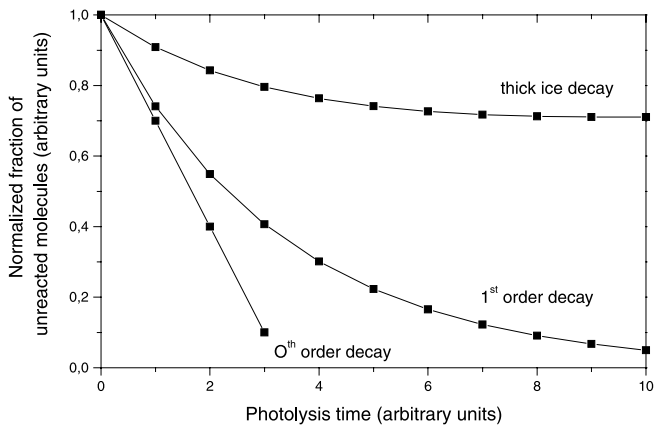

FIG. 4.—Comparison of the photodestruction rate of a molecule assuming zeroth or first-order kinetics in thin ice, and a first-order decay in thick ice. Densities are calculated from eqs. (2), (6), and (13) with the same J_0 absolute value.

average density N of a molecule AB being photolyzed in the ice can then be written

$$N = \frac{1}{n}\sum_{i=1}^{n} N_0 e^{-J_i t} \ , \tag{8}$$

which yields, with Z being the ice thickness,

$$N = \frac{N_0}{Z}\int_0^Z e^{-J(Z)t}\, dz \ , \tag{9}$$

and finally from equation (7),

$$N = \frac{N_0}{Z}\int_0^Z e^{-tJ_0 \exp(-Kz)}\, dz \ . \tag{10}$$

If we write $A = tJ_0$ and $Y = \exp(-Kz)$, then equation (10) can be rewritten as

$$N = -\frac{N_0}{KZ}\int_1^{\exp(-Kz)} e^{-AY}\, \frac{dY}{Y} \ , \tag{11}$$

where such an integration can be achieved knowing that

$$\int e^{ax}\frac{dx}{x} = \ln x + \frac{a\,x}{1!} + \frac{a^2x^2}{2(2!)} + \frac{a^3x^3}{3(3!)} + \dots \ , \tag{12}$$

which yields

$$N = N_0\left\{1 + \frac{tJ_0}{KZ}\left[\sum_{i=1}^{n}\frac{(-tJ_0)^{i-1}}{i(i!)}(e^{-KZ}-1)\right]\right\} . \tag{13}$$

From this equation, it appears necessary to quantitatively know both the ice thickness (Z) and absorption coefficient (K) to derive the actual photolysis rate J_0 and eventually the destruction cross section, σ, of the studied molecule. Figure 4 compares the normalized density decay rate for the three different equations according to zeroth- and first-order kinetics (eqs. [6] and [2]), and according to equation (13), for the same J_0 value.

One has to keep in mind that the absorption coefficient is a function of the wavelength, and that so far no ice photolysis experiments (including those presented in this paper) have been performed with a monochromatic UV lamp. This means that photons of different wavelengths reach different depths (Fig. 5) and that the J_0 and σ values derived from such experiments cover a range of wavelengths. Therefore, extrapolation to interstellar environments must be done with caution.

Gerakines et al. (2000) calculated that the depth at which the UV transmission drops to 37% is 0.15 μm in water ice, based on a gas-phase water UV absorption cross section of 2×10^{-18} cm^2 (Okabe 1978). If one refers to Warren (1984) for hexagonal ice at 80 K and assumes $\rho = 1$ g cm^{-3}, the water ice absorption cross section is about 8×10^{-18} cm^2 between 115 and 155 nm, but drops down for higher wavelengths (see Fig. 5). (We have already shown that the UV lamp used for our experiments delivers photons ranging mainly from 120 to 180 nm.) For amorphous ice, such as the one we use in our experiments, the absorption cross section seems to be slightly lower than for hexagonal ice, but still within the same order of magnitude (Warren 1984, Fig. 1). Hence, for pure water ice, 10% of the UV flux below 155 nm is absorbed within the first 10^{-2} μm of the ice (Fig. 5) and 90% within 0.1 μm. Based on these data, H_2O ices 0.1–1 μm thick cannot be considered optically thin for Lyα, and instead of first-order fits, the more complicated analysis represented by equation (13) is required. Preparation of optically thin ice would experimentally be very difficult to

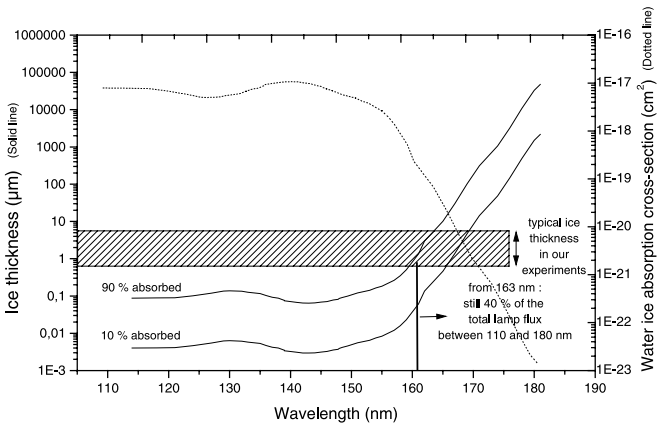

FIG. 5.—Ice thickness to which 10% and 90% of the UV flux is absorbed as a function of the wavelength (*solid line*). The absorption cross section of water ice calculated from Warren (1984) is also plotted (*dotted line*) as a function of wavelength.

achieve, and would result in weak spectral signatures which may not be sufficient for quantitative studies of photodestruction by infrared spectroscopy. Photons with lower energy than Lyα are nevertheless transmitted throughout the 0.1–1 μm thick laboratory ice (Fig. 5).

Photolysis experiments are performed on different kinds of ices (pure, mixed with water, N_2, or rare gas matrices); however, little is known about the optical properties of these ices or icy mixtures as a function of the wavelength in the far-UV. Baratta et al. (2002) measured some absorption coefficients at Lyα (but this is more likely an average value over the whole UV range of their lamp) at 12.5 K: H_2O (28×10^4 cm^{-1}), CH_4 (19×10^4 cm^{-1}), CH_3OH (12×10^4 cm^{-1}), or 8.4×10^{-18}, 5.7×10^{-18}, and 3.6×10^{-18} cm^2 molecule^{-1}, respectively, assuming an ice molecular density of 3.34×10^{22} molecules cm^{-3}. These coefficients are of the same order of magnitude, which means that our previous discussion about water ice can probably be extended to the other ices we have investigated, pure and mixed with water. In the gas phase, the N_2 absorption cross section is about 2×10^{-21} cm^2 in the far-UV (116–145 nm) (Okabe 1978), and if we assume the same order of magnitude in the solid phase, N_2 ices are transparent to UV photons above 116 nm, up to about 15 μm thickness. Thus, the molecules embedded in nitrogen ices are the main absorbers during photolysis, and compared to pure ices, the UV penetration depth in N_2 mixtures is enhanced by a factor equal to the dilution ratio of those molecules in nitrogen.

Yet, despite our discussion, we will see that results presented in this paper were fitted with first-order decay, as is the case for Gerakines et al. (1996, Fig. 13) and Ehrenfreund et al. (2001, Fig. 2). This can be explained by the fact that the microwave-powered hydrogen lamps used in such experiments produce a nonnegligible fraction of Lyα (121.6 nm) photons, and a large amount of photons at wavelengths above 160 nm (Fig. 1), for which ices can be considered as optically thin (Fig. 5). This might explain the first-order kinetics observed, and validate the reported J, σ, or half-life as long as one considers that values are integrated over the whole UV lamp emission spectrum, and not only at Lyα.

4. RESULTS AND DISCUSSION

The photostability of CH_4, CH_3OH, NH_3, CO_2, CO, and HNCO and mixtures of these molecules in N_2- and H_2O-rich ices were recorded using infrared spectra as a function of UV processing. The area of one of the dominant infrared peaks of each molecule was measured as a function of the processing time. The following bands were used: (C—H bend) CH_4 1300 cm^{-1}, (C—O st) CH_3OH 1017 cm^{-1}, (N—H bend) NH_3 1110 cm^{-1}, (C═O strecht) CO_2 2342 cm^{-1}, (C≡O strecht) CO 2137 cm^{-1}, and (C–N, C═O strecht) HNCO 2250 cm^{-1} (the actual position of the band may vary by a few cm^{-1} with the composition of the ice). No fit can be obtained between our experimental results and equation (13) by adjusting J_0, nor by adjusting Z or K within an order of magnitude around the value at which they are estimated. But as shown in Figure 6, plotting the logarithm of the normalized peak area as a function of time results in a linear decay, which shows that our ices are thin enough to be considered optically thin for most of the UV photons delivered by our lamp, as discussed in the previous section. This allows us to derive J according to equation (4) (the area being proportional to the number density of reactant molecules in the ice), and the resulting destruction cross section $\sigma = J/I$ (I = lamp flux). This destruction cross section depends on the UV lamp emission spectrum, and is therefore an average value for photons ranging from 120 to 200 nm, with an average energy of 7.4 eV.

Figure 6 shows a linear first-order decay for roughly the first hour of photolysis, after which a non–first-order behavior sets in. This is most probably due to two main factors:

1. Further reactions occur in the ice including reproduction of the initial compound from reactions between its photoproducts.
2. Changes of the optical properties of the ice occur, because of the production of new compounds that enhance absorption of the lamp flux, leading to a decrease in photolysis efficiency with time. Such a phenomenon is reported in Khriachtchev, Pettersson, & Räsänen (1998).

The destruction cross section uncertainties are calculated as the sum of the relative uncertainty on J (estimated with a least-square regression on the experimental results) and the 25% uncertainty on the lamp flux.

A summary of our results is given in Table 3. For pure ices, our results are of the same order of magnitude as those published by Gerakines et al. (1996), except that ours are systematically lower by a factor of 2–7. A consistent explanation for this trend would be that the UV flux used in the Gerakines paper was underestimated (actually, the flux was not exactly known but was assumed to be 10^{15} photons s^{-1} cm^{-2}), or if the emission spectrum of the lamp was slightly different from ours in the far-UV.

For each molecule, a half-lifetime can then be estimated in the diffuse interstellar medium (assuming an interstellar flux of 10^8 photon cm^{-2} s^{-1} for photons greater than 6 eV; Mathis, Mezger, & Panagia 1983), and in dense molecular clouds (assuming a cosmic-ray–induced UV flux of 10^3 photons cm^{-2} s^{-1}; Prasad & Tarafdar 1983). These half-lives, such as the ones presented in this paper or in Ehrenfreund et al. (2001), should be considered as kinetic values related *only* to photodestruction sinks for the molecules in simple ice mixtures. For example, one should not assume that in the diffuse ISM, the number density of CH_4 in H_2O ice is divided by 2 within 1471 yr. In the presence of other reactants representing a more relevant complex interstellar-type mixture, CH_4 is also produced (for example from photolyzed $H_2O + CH_3OH$ ices [Allamandola et al. 1988; Bernstein et al. 1995], or from ion-irradiated $H_2O + CO$ ices [Moore, Khanna, & Donn 1991]), and its concentration results from the balance between sinks and sources.

During photolysis, the intensity of the CO absorption does not measurably decrease if it is in pure form or mixed with nitrogen, e.g., $N_2 + CO$ (10 : 1). For those two experiments we have derived an upper limit for the half-life. One of the most interesting points is that CO is clearly destroyed when mixed with H_2O. By itself, CO is not photodissociated for wavelengths above 112 nm (Okabe 1978). Nevertheless, as already reported by Gerakines et al. (1996), some CO_2 or other products are synthesized in reactions of its excited state,

$$\mathrm{CO} + h\nu \rightarrow \mathrm{CO}^* \ ,$$

$$\mathrm{CO}^* + \mathrm{CO} \rightarrow \mathrm{CO}_2 + \mathrm{C} \ .$$

The fact that no significant CO_2 production is observed in the $N_2 + CO$ (10 : 1) experiment is consistent with this mechanism, since CO is isolated in this N_2 matrix.

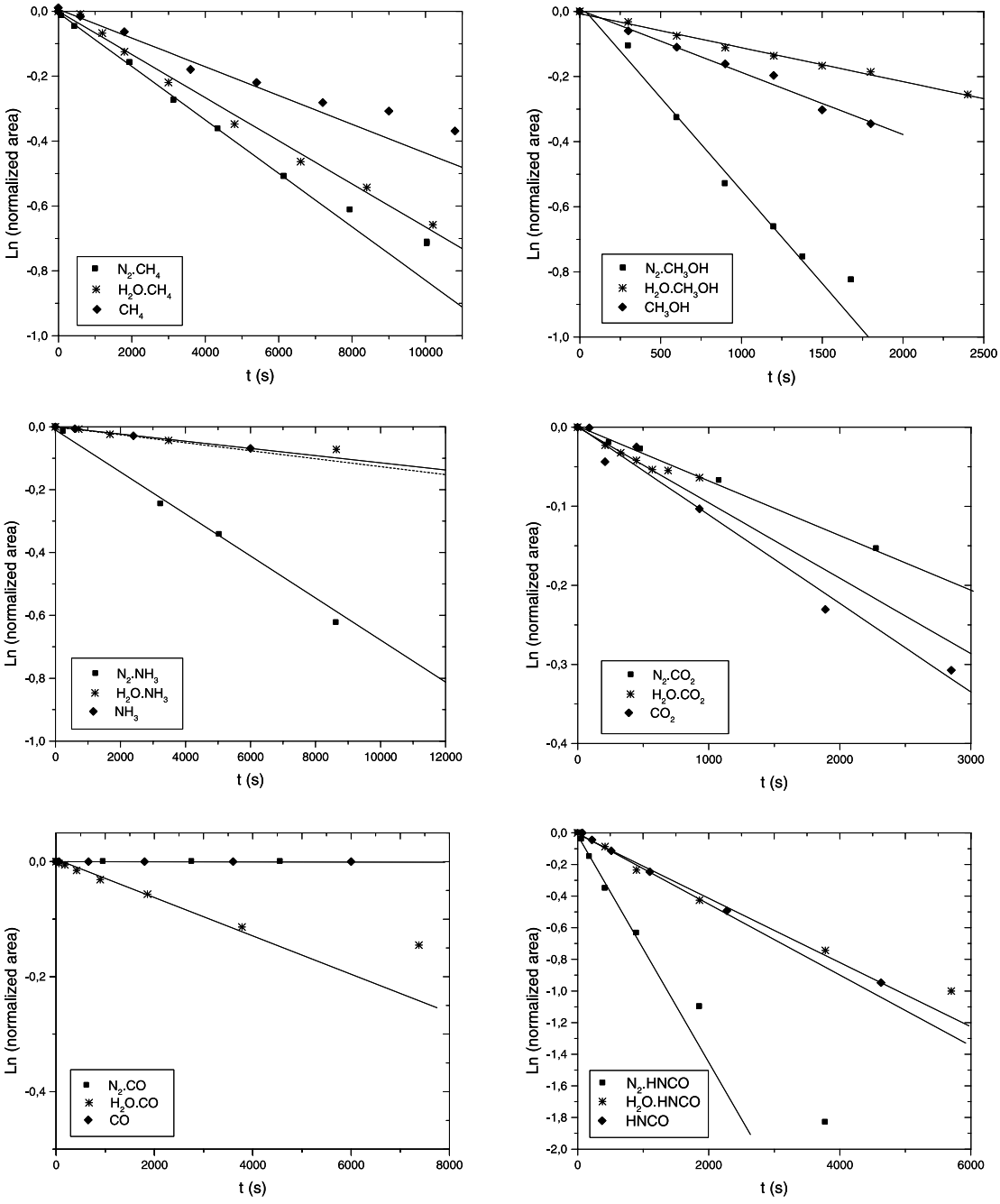

FIG. 6.—Experimental results show decreases in normalized IR band area as a function of photolysis time. Results for CH_4, CH_3OH, NH_3, CO_2, CO, and HNCO, as pure ices and mixed with H_2O or N_2, assume first-order decay kinetics. The following IR bands were used: CH_4 1300 cm^{-1}, CH_3OH 1017 cm^{-1}, NH_3 1100 cm^{-1}, CO_2 2342 cm^{-1}, CO 2137 cm^{-1}, and HNCO 2250 cm^{-1}.

When mixed with H_2O, if one refers to the gas-phase chemistry, CO can react with OH, a product of water photolysis (Atkinson et al. 1997),

$$H_2O + h\nu \rightarrow OH + H \ ,$$
$$OH + CO \rightarrow CO_2 + H \ .$$

This explains the dramatic change observed in CO, in the presence or absence of H_2O. Hence, σ depends not only on the photodestruction cross section of CO, but also on its reactivity with other photolysis products.

A similar increase in destruction rates in H_2O is not observed for the other molecules studied, even though gas-phase reactions with OH are reported for CH_4, CH_3OH, NH_3 (Atkinson et al. 1997), and HNCO (Wooldridge, Hanson, & Bowman 1996), leading to the abstraction of an H. Such reactions do not appear to be as significant, compared to direct photodissociation.

For CH_4, CH_3OH, NH_3, and HNCO, destruction is faster in N_2. In such ices, only pure photodissociation processes are likely to happen, since molecules are isolated from each other in the N_2 matrix (N_2 is not dissociated and is transparent at our wavelengths). The slower decay of pure ices or water-dominated ices could be due to competition between the actual molecule photolysis, such as observed in nitrogen, with other reactions in a more complex chemical

TABLE 3

Destruction Cross Section of Molecules Measured in This Work Compared to Previously Published Values

Ice	Ice Mixture Ratio	σ (This Work) (cm^2)	Relative Uncertainty (This Work) (%)	σ (Gerakines et al. 1996) (cm^2)	Half-life (y) Diffuse ISM	Half-life (10^6 years) Dense IS Cloud
CH_4	pure	9.1×10^{-20}	31	7.2×10^{-19}	2407	241
$CH_4 : N_2$	1 : 10	1.8×10^{-19}	29		1218	122
$CH_4 : H_2O$	1 : 10	1.5×10^{-19}	33		1471	147
CH_3OH	pure	5.0×10^{-19}	39	1.6×10^{-18}	442	44
$CH_3OH : N_2$	1 : 10	1.5×10^{-18}	38		148	15
$CH_3OH : H_2O$	1 : 10	2.7×10^{-19}	33		807	81
NH_3	pure	3.2×10^{-20}	32		6952	695
$NH_3 : N_2$	1 : 10	2.3×10^{-19}	35		937	94
$NH_3 : H_2O$	1 : 10	4.8×10^{-20}	54		4531	453
CO_2	pure	3.8×10^{-19}	41	5.6×10^{-19}	584	58
$CO_2 : N_2$	1 : 10	2.6×10^{-19}	29		845	85
$CO_2 : H_2O$	1 : 10	3.3×10^{-19}	35		657	66
CO	pure	$<1 \times 10^{-21}$	...	$<8 \times 10^{-20}$	>220,000	∞
$CO : N_2$	1 : 10	$<1 \times 10^{-21}$	...		>220,000	∞
$CO : H_2O$	1 : 10	1.2×10^{-19}	30		1894	189
HNCO	pure	6.9×10^{-19}	30		318	32
$HNCO : N_2$	1 : 10	2.5×10^{-18}	42		87	9
$HNCO : H_2O$	1 : 10	7.1×10^{-19}	39		312	31

Note.—Prediction of photodestruction half-life in both diffuse interstellar medium, and dense interstellar clouds based on our work.

system. For CO_2, no significant difference can be noted between the three experiments, which provides good information on its destruction cross section regardless of the composition of the bulk of the ice in which it is embedded.

Baratta et al. (2002) state that the destruction rate in such experiments cannot be extrapolated for a high-energy dose. We think that even if the observed destruction rate changes with time, σ is constant and a pertinent parameter to derive from such experiments. The change in an ice's absorption coefficient should be taken into account when modeling the composition of a photolyzed ice, since the photolysis rate, J, is the product of σ (constant) and I (UV flux, which may change with depth and time as the ice composition changes). For high-energy doses, sources and sinks have to be taken into account. Data derived from the linear section of our results are only related to sinks of the studied molecules, which might also be regenerated through reactions of their products.

Our results are a step toward a compilation of photochemical data that should allow modeling of the composition of interstellar ices over long periods of time. An interesting result of our work is the destruction rate dependence on ice environment. As discussed earlier in this paper, more work is still needed, and particularly work concerning knowledge of the ice absorption coefficient in the far-UV and its dependence with wavelength. Moreover, the σ values estimated from our work cover a large wavelength range, and further work should now focus on monochromatic studies. For example, 122 nm dominant emission can be achieved with a microwave-powered lamp using an H_2-He mixture, 147 nm with xenon, etc. (Cottin et al. 2000; Okabe 1978). Such data will be necessary for an accurate description of interstellar ice chemistry.

Most of this work was performed while H. C. held an NRC Research Associateship at NASA/Goddard Space Flight Center. This work was supported by NASA funding through NRA 344-33-01 and 344-01-57. We thank Reggie L. Hudson, Perry A. Gerakines, and Mark S. Lowenthal for assistance, and Ricardo Vidal and Raul Barigiola at University of Virginia for characterizing our UV lamp spectrum.

REFERENCES

Allamandola, L. J., Sandford, S. A., & Valero, G. J. 1988, Icarus, 76, 225
Atkinson, R., Baulch, D. L., Cox, R. A., Hampson, R. F., Jr., Kerr, J. A., Rossi, M. J., & Troe, J. 1997, J. Phys. Chem. Ref. Data, 26, 1329
Baratta, G. A., Leto, G., & Palumbo, M. E. 2002, A&A, 384, 343
Bernstein, M. P., Sandford, S. A., Allamandola, L. J., Chang, S., & Scharberg, M. A. 1995, ApJ, 454, 327
Boogert, A. C. A., Helmich, F. P., van Dishoeck, E. F., Schutte, W. A., Tielens, A. G. G. M., & Whittet, D. C. B. 1998, A&A, 336, 352
Cottin, H., Gazeau, M. C., Doussin, J. F., & Raulin, F. 2000, J. Photochem. Photobiol., 135, 53
Cottin, H., Gazeau, M. C., & Raulin, F. 1999, Planet. Space Sci., 47, 1141
Dworkin, J. P., Deamer, D. W., Sandford, S. A., & Allamandola, L. J. 2001, Proc. Natl. Acad. Sci., 98, 815
Ehrenfreund, P., Bernstein, M. P., Dworkin, J. P., Sandford, S. A., & Allamandola, L. J. 2001, ApJ, 550, L95
Ehrenfreund, P., d'Hendecourt, L., Dartois, E., de Muizon, M. J., Breitfellner, M., Puget J. L., & Habing, H. J. 1997, Icarus, 130, 1
Gerakines, P. A., & Moore, M. H. 2001, Icarus, 154, 372
Gerakines, P. A., Moore, M. H., & Hudson, R. L. 2000, A&A, 357, 793
Gerakines, P. A., Schutte, W. A., & Ehrenfreund, P. 1996, A&A, 312, 289
Gerakines, P. A., et al. 1999, ApJ, 522, 357
Gibb, E. L., et al. 2000, ApJ, 536, 347
Groth, W. 1937, Zeitschr. Phys. Chemie, 37, 307
Hudson, R. L., & Moore, M. H. 1995, Radiat. Phys. Chem., 45, 779
———. 1999, Icarus, 140, 451
Jackson, J. M., Armstrong, J. T., & Barrett, A. H. 1984, ApJ, 280, 608
Khriachtchev, L., Pettersson, M., & Räsänen, M. 1998, Chem. Phys. Lett., 299, 727
Lacy, J. H., Faraji, H., Sandford, S. A., & Allamandola, L. J. 1998, ApJ, 501, L105
Lis, D. C., et al. 1997a, Icarus, 130, 355
———. 1997b, Earth Moon Planets, 78, 13
Mathis, J. S., Mezger, P. G., & Panagia, N. 1983, A&A, 128, 212
Moore, M. H., & Hudson, R. L. 1998, Icarus, 135, 518
———. 2000, Icarus, 145, 282
Moore, M. H., Khanna, R., & Donn, B. 1991, J. Geophys. Res., 96, 17541

Okabe, H. 1978, Photochemistry of Small Molecules (New York: Wiley-Interscience)
Prasad, S. S., & Tarafdar, S. P. 1983, ApJ, 267, 603
Schutte, W. A., Allamandola, L. J., & Sandford, S. A. 1993, Icarus, 104, 118
Smith, M. A. H., Rinsland, C. P., Fridovich, B., & Rao, K. N. 1985, Molecular Spectroscopy: Modern Research, Volume 3 (London: Academic Press)
Snyder, L. E., & Buhl, D. 1972, ApJ, 177, 619
Warneck, P. 1962, Appl. Opt., 1, 721
Warren, S. G. 1984, Appl. Opt., 23, 1206
Watanabe, N., & Kouchi, A. 2002, ApJ, 567, 651
Wooldridge, M. S., Hanson, R. K., & Bowman, C. T. 1996, Int. J. Chem. Kinetics, 28, 361

Article 19

COTTIN H., COLL P., COSCIA D., FRAY N., GUAN Y. Y., MACARI F., RAULIN F., RIVRON C., STALPORT F., SZOPA C., CHAPUT D., VISO M., BERTRAND M., CHABIN A., THIRKELL L., WESTALL F. and BRACK A. (In Press) Heterogeneous solid/gas chemistry of organic compounds related to comets, meteorites, Titan and Mars: in laboratory and in lower Earth orbit experiments. Advances in Space Research.

Available online at www.sciencedirect.com
ScienceDirect
Advances in Space Research xxx (2007) xxx–xxx
ADVANCES IN SPACE RESEARCH (a COSPAR publication)
www.elsevier.com/locate/asr

Heterogeneous solid/gas chemistry of organic compounds related to comets, meteorites, Titan, and Mars: Laboratory and in lower Earth orbit experiments

H. Cottin [a,*], P. Coll [a], D. Coscia [a], N. Fray [a], Y.Y. Guan [a], F. Macari [a], F. Raulin [a], C. Rivron [a], F. Stalport [a], C. Szopa [b], D. Chaput [c], M. Viso [d], M. Bertrand [e], A. Chabin [e], L. Thirkell [f], F. Westall [e], A. Brack [e]

[a] *LISA, Université Paris 12 et Paris 7, CNRS, 61 Av. du Général de Gaulle, 94010, Créteil, France*
[b] *Service d'aéronomie, UMR 7620 CNRS, Réduit de Verrières – BP 3, Route des Gatines, 91371 Verrières le Buisson Cedex, France*
[c] *CNES, Centre spatial de Toulouse, 18 Avenue Edouard Belin, 31401 Toulouse Cedex 9, France*
[d] *CNES, 2 Place Maurice Quentin, 75039 Paris Cedex 01, France*
[e] *CBM, CNRS, Rue Charles-Sadron, 45071 Orleans Cedex 2, France*
[f] *LPCE, CNRS, Avenue de la Recherche Scientifique, 45071 Orleans Cedex 2, France*

Received 31 October 2006; received in revised form 22 August 2007; accepted 10 September 2007

Abstract

To understand the evolution of organic molecules involved in extraterrestrial environments and with exobiological implications, many experimental programs in the laboratory are devoted to photochemical studies in the gaseous phase as well as in the solid state. The validity of such studies and their applications to extraterrestrial environments can be questioned as long as experiments conducted in space conditions, with the full solar spectrum, especially in the short wavelength domain, have not been implemented. The experiments that are described here will be carried out on a FOTON capsule, using the BIOPAN facility, and on the International Space Station, using the EXPOSE facility. Vented and sealed exposition cells will be used, which will allow us to study the chemical evolution in the gaseous phase as well as heterogeneous processes, such as the degradation of solid compounds and the release of gaseous fragments.

Four kinds of experiments will be carried out. The first deal with comets and are related to the Rosetta mission, the second with Titan and are related to the Cassini–Huygens mission, the third with the search for life-related organic compounds on Mars and, finally, the fourth are a continuation of previous studies concerning the behavior of amino acids in space.

Keywords: Astrochemistry; Photolysis; Exo-astrobiology; Comet; Titan; Mars; Meteorite; International Space Station; FOTON; EXPOSE; BIOPAN

1. Introduction

Solar UV radiation is a major source of energy to initiate chemical evolution towards complex organic structures, but it can also photodissociate the most elaborate molecules. Thus, Solar UV can erase the organic traces of past life on the surface of planets, such as Mars (Oro and Holzer, 1979), destroy organic molecules present on meteorites (Barbier et al., 1998), influence the production of extended sources in comets[1] (Cottin et al., 2004), or initiate chemistry in Titan's atmosphere (Sagan and Thompson, 1984).

[1] The spatial distribution in the coma of some molecules is not compatible with an emission from the nucleus only or photolysis of a gaseous known parent compound. This supports the hypothesis that there is an (at least one) additional source which produces the observed molecule as it spreads outwards the nucleus. This is what is called an *extended source*.

* Corresponding author.
E-mail address: cottin@lisa.univ-paris12.fr (H. Cottin).

0273-1177/$30 © 2007 COSPAR. Published by Elsevier Ltd. All rights reserved.
doi:10.1016/j.asr.2007.09.017

AMINO, PROCESS, and UV-olution are three experiments selected to be flown on the EXPOSE facility on the International Space Station, or on the BIOPAN facility during the FOTON M3 space capsule mission. The goal of our experiments is to improve our knowledge of the chemical nature and evolution of organic molecules involved in extraterrestrial environments with astrobiological implications. Most of the previous experiments implemented in space so far were carried out in vented cells exposed to Solar UV radiation (Barbier et al., 1998, 2002b; Boillot et al., 2002). In such cases, solid organic samples are deposited behind a window transparent to UV, and exposed to the solar flux. If the studied molecule is sensitive to energetic photons, its photodestruction can be quantified after the experiment when sample are brought back to Earth for analysis. However, gaseous products resulting photolysis are lost in space. A first use of sealed cells is reported in Ehrenfreund et al. (2007). This allows studying chemical evolution in the gaseous phase as well as heterogeneous processes (degradation of solid compounds and release of gaseous fragments). In our case, both vented and sealed exposition cells will be used. Four kinds of experiments will be carried out. The first deal with comets and are related to the Rosetta mission; the second deal with Titan and are related to the Cassini–Huygens mission; the third are related to the search for organic compounds on Mars within the framework of the preparation of MSL 2009 instrument SAM (Cabane et al., 2004), while the fourth are a continuation of previous studies about the behavior of amino acids in space (Barbier et al., 1998).

2. Astrobiological relevance: organic molecules in the Solar System and the origins of life

These experiments, through the choice of the targeted Solar System environment and targeted compounds, are closely linked to the field of exo-astrobiology. Primitive terrestrial life emerged with the first aqueous chemical systems able to transfer their molecular information and to evolve. Unfortunately, the direct clues which may help chemists to identify the molecules that participated in the emergence of life on Earth about 4 billion years ago have been erased. It is generally believed that primitive life originated from the processing of organic molecules by liquid water. Oparin (1924) suggested that the small organic molecules needed for primitive life were formed in a primitive atmosphere dominated by methane. The idea was tested in the laboratory by Miller (1953) when he exposed a mixture of methane, ammonia, hydrogen, and water to electric discharges. In his initial experiment, he obtained a great diversity of organic molecules, some of which, like amino acids, are key ingredients to life as we know it on Earth. Miller's laboratory synthesis of amino acids occurs efficiently when a reducing gas mixture containing significant amounts of hydrogen is used. Similar results are observed if the same kinds of experiments are conducted under UV photolysis. However, the actual composition of the primitive Earth's atmosphere is still unknown. Nowadays, most geochemists favor a neutral or weakly reducing atmosphere dominated by carbon dioxide (Kasting, 1993). Under such conditions, chemical evolution and the production of the building blocks of life appear to be very limited if only endogenous syntheses in primitive Earth atmosphere are considered (Schlesinger and Miller, 1983). Even if the H_2 content of early atmosphere is still under discussion and model dependant (Tian et al., 2005, 2006; Catling, 2006), other sources have to be investigated. Nowadays, the origin of the first ingredients in the recipe for life between exogenous delivery and endogenous syntheses is debated, and in both cases, photolysis plays a central part in initiating the first steps of chemical evolution.

Moreover, the question of the origin of life on Earth is tightly related to the possibility that life may also have arisen on our neighbor planet, Mars. It is now established that more than 4 billion years ago, Mars environment was similar to that of the early Earth (Bibring et al., 2006), with a dense atmosphere and liquid water. If life developed on Mars, independently of the Earth, this could mean that the jump from chemistry to biology is written in the laws of the "natural" evolution of organic matter each time the requirements "organic matter + liquid water" on a rocky planet are fulfilled. Therefore, the search for organic material at the Martian surface is critical. (Water and organic molecules are not enough – the silicates and other minerals are also important – providers of energy from chemical reactions going on at the surfaces; stable surfaces upon which organic molecules can achieve the necessary conformation; once life starts, providers of energy and carbon. . ..)

2.1. Exogenous delivery

Among the hypotheses investigated to explain the origin of the biological building blocks, the seeding of the primitive Earth by molecules from outer space is of growing interest. Each year more and more molecules are detected in the interstellar medium (see for instance Ehrenfreund and Charnley (2000), for a review on this topic). Most of these compounds are based on C, H, O, N, and reveal a complex organic chemistry in molecular clouds, in contrast with the poor complexity of the chemical processes on the primitive Earth environment if the H_2 content of the atmosphere was low. Comets and primitive meteorites may have kept the memory of the composition of the organic rich interstellar medium or presolar nebula, which gave birth to our Solar System. The study of meteorites, particularly carbonaceous chondrites that contain up to 5% by weight of organic matter, has allowed a close examination of extraterrestrial organic material in the laboratory. Analysis of the Murchison meteorite, whose formation is contemporary with the birth of the Solar System, has revealed more than 500 organic compounds and among them, several nucleic bases and 74 amino acids, 8 of these being used by contemporary proteins (Cronin et al. (1988) or Botta

and Bada (2002), for a recent review). Comets are another source of interesting organics for the primitive Earth. To date, more than 20 gaseous molecules have been detected in the atmosphere (including H_2O, CO, CO_2, CH_3OH, H_2CO, HCN, NH_3) (Biver et al., 2002). However, until the in situ analysis of comet 67P/Churyumov–Gerasimenko in 2014 by the Rosetta mission, we have no direct information about the molecular composition of the nucleus, which is suspected to be extremely rich in organic compounds of high molecular weight. The presence of such complex refractory material is inferred from in situ analysis of cometary grains (Kissel and Krueger, 1987; Kissel et al., 2004), from the observation of the density distribution of molecules such as H_2CO, CN or CO, which can only be explained by the slow degradation of "unseen" complex refractory material (such a phenomenon is usually referred as an "extended source" (Cottin et al., 2004; Fray et al., 2006), and from laboratory simulation of cometary ice analogues (for reviews see Cottin et al. (1999); Despois and Cottin (2005)). The large range of chemicals observed or strongly suspected to be present in comets suggests that comets may have played a key role in the chemical evolution leading to the emergence of life on Earth (Oro and Cosmovici, 1997). Chemical evolution in comets and meteorites, production of extended sources, and the residual organic component that can be imported to planets, are strongly dependent of photochemical processes that need to be documented (Fig. 1).

2.2. Endogenous synthesis

Unlike the primitive Earth, the composition of Titan's atmosphere (N_2 and CH_4 at a few percent level) implies that it is an extremely efficient "chemical factory". The simplest molecules such as molecular nitrogen and methane, submitted to Solar UV photolysis and the impacts of electrons trapped in the magnetosphere of Saturn, evolves towards complex organic hazes hiding the surface of this satellite of Saturn (Sagan and Thompson, 1984). Most probably, the lack of liquid water on Titan prevents the chemical evolution towards life. However, this planet offers an unique opportunity to study endogenous syntheses of exobiological interest since it has been shown that the hydrolysis of laboratory analogues of Titan's organic haze (Tholins) release amino acids (Khare et al., 1986). Therefore, considering the lack of direct traces from Earth's primitive environment about 4 billions years ago or more, when prebiotic chemistry gave birth to the first living systems, it is of prime interest to study extraterrestrial environments in which prebiotic syntheses may occur. Titan's case will tell us how far chemical evolution can go with a chemically favorable atmospheric composition but in the absence of liquid water.

Moreover, recent data from the Cassini–Huygens spacecraft, orbiting the Saturnian's system have raised new questions regarding the photochemistry of Titan's atmosphere: where in the atmosphere is the origin of this organic photochemistry located? In the stratosphere or in the ionosphere, where evidence of exceptional activity was revealed by Cassini–Huygens? What is the chemical nature of the solid end product of methane photochemistry? Is it a PAH-like material or high molecular weight polyynes? What are the possible photoproducts of Titan's haze particles? Just as for comets, Solar UV driven photochemistry, plays a key role in the evolution of organic chemistry of Titan.

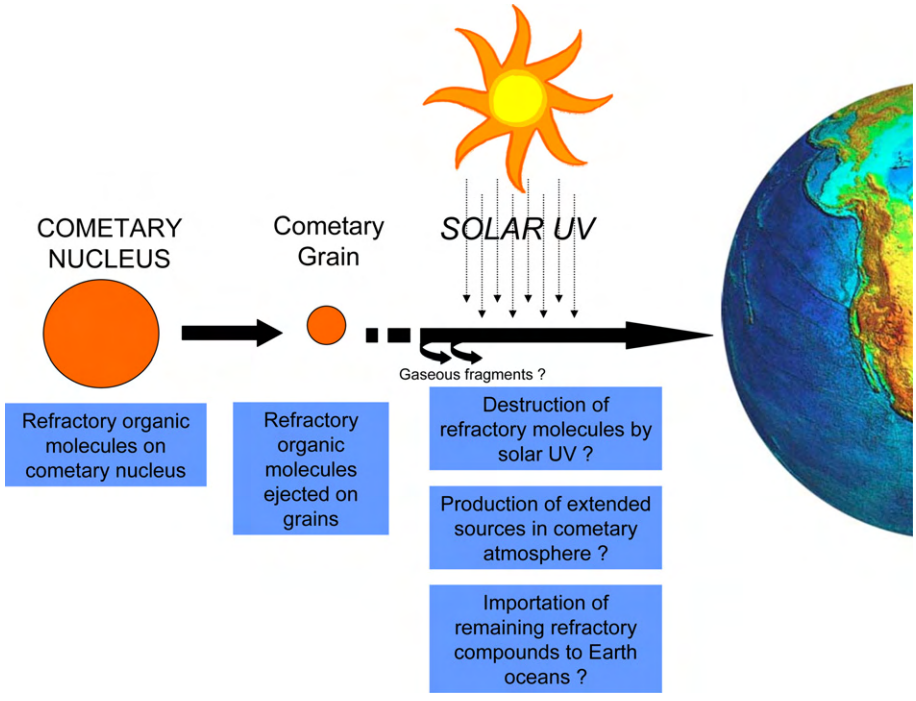

Fig. 1. History of a complex organic molecule from a cometary nucleus to potential importation to Earth on grains.

2.3. Life on another planet?

One of the main goals of astrobiology is the search for and the study of extraterrestrial life. This has important implications for our understanding of the origins of life on Earth which remains, so far, the only planetary body where we are sure that life is present.

Mars is certainly the best target in the Solar System to search for past and even for present extraterrestrial life. Indeed it is now more and more obvious that the red planet has seen liquid water for a long period of time and in particular more than 4 billion years ago (Bibring et al., 2006), when life was probably already present on the Earth, and when environments on both planets were very similar (Westall, 2005), contrary to what they are today.

Hence, it is reasonable to assume that the same processes of chemical evolution, which allowed the emergence of life on Earth, through prebiotic chemistry and the increasing complexity of organic matter in liquid water towards self-replicating systems, also occurred on Mars. Since the degradation of surface conditions on Mars (3.8–3.5 Ga), both planets have followed different evolutions and life may have disappeared from the red planet, or, if it has survived it may be now located in the subsurface of the planet, protected from the hostile surface.

However, in both cases, past or present biological activities should feed the Martian environment with many organic and inorganic compounds, including important and specific biomarkers. If life never arose on Mars, in spite of a noticeable prebiotic chemistry, there is a good probability that traces of the prebiotic processes should still be present after 4 billion years of evolution of the red planet, since the tectonic activity that has eliminated all rocks older than about 4 Gy on Earth was of extremely limited extent on Mars. Prebiotic signatures should therefore be detectable near the surface or in the surface rocks. In addition, since Mars is still experiencing a noticeable bombardment of meteoritic and cometary material, its surface should also include organic matter imported through these processes. To date, such compounds have never been detected on Mars. Photolysis of organic molecules at the surface of Mars is a key factor determining their evolution and interest to be searched for with the next Martian rovers.

3. Some basics of photochemistry in Earth laboratories and in Space

Earth orbit is subjected to intense radiation of both solar and galactic origin. Cosmic radiation entering the Solar System is composed of protons, electrons, α-particles and heavy ions. Solar particle radiation is emitted as solar wind during chromospheric eruptions. It is composed of up to 95% of protons, α-particles, and heavy ions. Protons and electrons do not reach the Earth because they are trapped by the geomagnetic field. On the other hand, the solar electromagnetic radiation above the Earth's atmosphere is composed of 45% infrared radiation, 48% visible light, and only 7% UV light (Horneck et al., 2002). But the latter photons are the most energetic, and at sufficient levels can induce photochemical evolution.

Experiments to irradiate organic compounds can easily be implemented on Earth with specific sources, such as ion or electron guns, or UV lamps. However, it is very difficult to combine all the energetic sources occurring in space to their full extent. For example, in the laboratory, we can either choose to irradiate a molecule at 122 nm (H_2/He lamp – with MgF_2 window) or 147 nm (Xe lamp – with MgF_2 window) or 193 nm (CH_4/He lamp – with quartz window). Fig. 2 is a comparison of the spectrum of Solar UV emitted by the Sun between 100 and 200 nm, with typical spectra UV lamps used in the laboratory for photochemical studies in this UV domain.

Our goal is to improve our knowledge of the chemical nature and evolution of organic molecules involved in extraterrestrial environments and/or with exobiological implications. Many experimental programs are devoted to photochemical studies of molecules in the gaseous phase as well as in the solid state. Ground laboratory experiments have been (or will be) implemented on the target compounds that we have selected for this program. However, the validity of such studies and their application to extraterrestrial environments can be questioned as long as experiments conducted in space conditions, with the full solar spectra especially in the short wavelength domain, have not been implemented.

Moreover, compared to ground experiments, space is a unique laboratory allowing the exposure of samples to all space parameters simultaneously and irradiating many samples simultaneously under strictly identical conditions.

Therefore, Earth orbit provides a unique opportunity to study the effects of UV radiation on organic molecules.

Solar energy is the main "engine" for chemical evolution in the Solar System.

The photodestruction of a molecule can be written:

$$A \xrightarrow{h\nu} \text{products}$$

with A being a molecule, and products the resulting fragments. This photochemical reaction is fully understood with the knowledge of the photodestruction rate of A, and the nature of the products. If $[A]$ is the number density of A (cm^{-3}), the photolysis rate is usually described by:

$$\frac{d[A]}{dt} = -J.[A] \quad (1)$$

with $J = \int_\lambda \sigma_\lambda I_\lambda \, d\lambda$, σ_λ being the destruction cross-section of the molecule (cm^2), which is actually the product of the cross-section of the molecule and the quantum yield of the photolysis reaction, and I_λ is the UV flux (photons s^{-1} cm^{-2}). Both σ and I are a function of the wavelength λ.

The integrated form of Eq. (1) is:

$$[A](t) = [A]_0 \exp(-Jt). \quad (2)$$

J is then experimentally determined through the measurement of A from the slope of a plot of $\ln([A])$ vs. t:

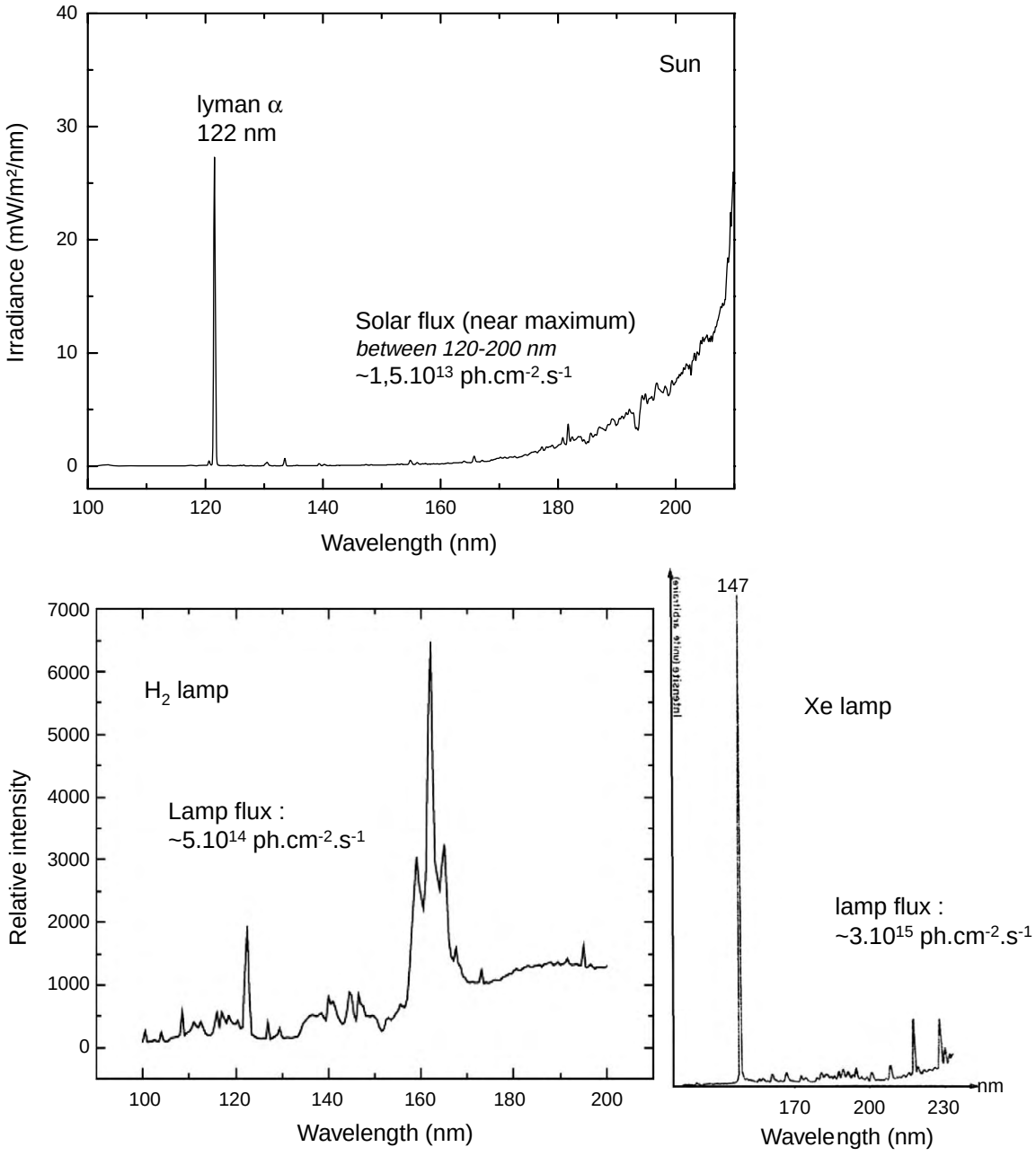

Fig. 2. Comparison of the solar spectrum between 100 and 200 nm (Thuillier et al., 2004) with two laboratory UV lamps (H_2 and Xe lamps) (Bossard, 1979; Cottin et al., 2003).

$$\ln([A]) = -Jt + \ln([A]_0). \quad (4)$$

Such a study is quite simple to implement in the laboratory, when in situ measurement of A is feasible, or if the experiment can be repeated for different times of photolysis (Gerakines et al., 1996; Cottin et al., 2003). Products can be analyzed with different analysis tools, such as infrared spectrometry, gas chromatography, etc.

However, for experiments conducted in space, only two points are available to plot Eq. (4): $t = 0$ (preparation of sample before launch) and $t =$ total time of exposition in orbit, which makes the estimation of J quite inaccurate.

Therefore, instead of plotting Eq. (4) as a function of time, J can be derived if several samples with different $[A]_0$ are exposed for the same duration, plotting $\ln[A]_t$ as a function of $\ln[A]_0$. Thus, for the same total time of exposition, with different initial abundances in several exposed samples, J can be measured as shown in Fig. 3.

4. Experimental procedure

4.1. Ground experiments

Experiments in space are associated with a ground support experimental program already in progress. At the

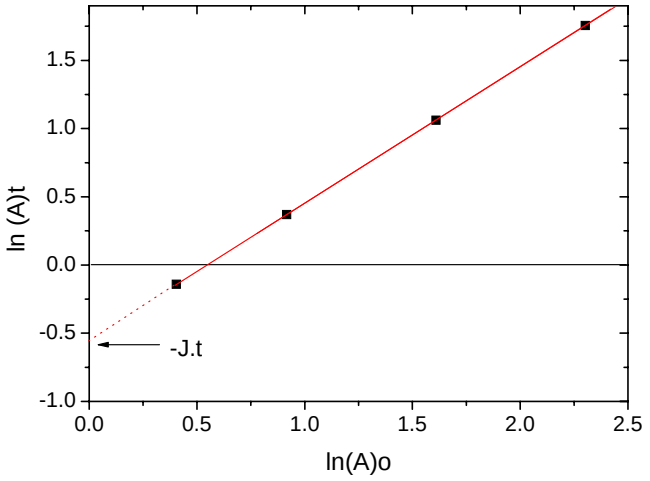

Fig. 3. Measurement of J in space experiments plotting $\ln[A]_t$ as a function of $\ln[A]_0$.

Laboratoire Interuniversitaire des Systèmes Atmosphériques (LISA), Service d'Aéronomie (SA), and Centre de Biophysique Moléculaire (CBM) we have access to:

- a full potential for photolysis experiments at different wavelengths in far UV,
- synthesis facilities for tholins, and other non-commercial organic products,
- a large range of analysis tools: IRTF, UV, GC–MS, HPLC.

LISA has already developed the tools to study the effect of photolysis on gaseous mixtures or solid molecules. In the framework of cometary study, the SEMAPHORE cométaire experiment (Fig. 4) already yielded quantitative results concerning the photodegradation of polyoxymethylene: POM (–(CH_2–O)$_n$–, polymer of formaldehyde) (Cottin et al., 2000), hexamethylenetetramine: HMT ($C_6N_4H_{12}$) (Cottin et al., 2002) and HCN polymers (Fray et al., 2004). As shown in Fig. 4, the compounds can be irradiated at different wavelengths. Destruction of the initial material can be studied, as well as, the simultaneous formation of gaseous photolysis products. Successful results have already been derived from laboratory work concerning POM, allowing one step further into understanding H_2CO extended source in comets (Cottin et al., 2004; Fray et al., 2006). It has been shown that a few percent of POM in mass on grains can explain the observed distribution of formaldehyde in comets P/Halley and Hale–Bopp (C/1995 O1). It is now crucial that such laboratory results be validated by space experiments. Concerning other cometary or meteoritic molecules, or Titan program with Tholins or gas mixtures, they can also be irradiated with the same setup.

But as already mentioned above, the full solar spectrum cannot be reproduced with such an apparatus. Therefore, we can only access wavelength dependant results with an extrapolation to other wavelengths, whose reliability is limited by the few UV lines we can access with the setup (122, 147, and 193 nm in our case).

A larger range in wavelengths (112–370 nm) is achieved in the CBM simulation chamber presented in Fig. 4b. However, with this chamber, the gaseous photoproducts cannot be analyzed during the photolysis.

Concerning organics on Mars, a new experimental device has been devised, MOMIE (Martian Organic Material Irradiation and Evolution) (Fig. 5). Its principle is relatively simple: to stimulate the evolution of target molecules either on their own or in a mineral matrix (Mars regolith analogues) under various forms of energy (UV lamp, laser...). Spectroscopic (in situ) and chemical (in situ or a posteriori) analyses allow qualification/quantification of the degradation of the target molecules. Since most of the energetic range of Solar UVs is filtered by the Martian atmosphere, in this case, a high pressure Xenon lamp provides a rather satisfactory simulation of the solar flux reaching the Martian soil, i.e. for wavelength above 190 nm (Fig. 6).

4.2. Space laboratories

The experiment series presented in this paper is built upon the results of a previous set of experiments already implemented in space. The latter were mainly devoted to the exposition of amino acids to space conditions (solar light, galactic cosmic rays (GCR), temperature, and vacuum).

DUST experiment on BIOPAN-1 in 1994: (Barbier et al., 1998).
DUST experiment on BIOPAN-2 in 1997: (Barbier et al., 2002b).
PERSEUS-EXOBIOLOGIE experiment on MIR in 1999: (Boillot et al., 2002).

These successful experiments have shown that amino acids are readily destroyed in space unless they are protected in a mineral matrix.

The new experiments are summarized in Table 1, and described in the next sections of this paper. International Space Station average altitude is about 340 km, and FOTON altitude ranges between 250 and 300 km.

For AMINO, PROCESS, and UV-olution, the procedure followed is:

For one molecule studied at a specific $[A]_0$, then two samples are exposed in space (influence of UV, GCR, and T), two samples are exposed as dark controls (influence of GCR and T), two ground controls are kept in the dark for the same duration as the space exposition and with a similar temperature history (influence of T), and two ground controls are kept in the dark at constant T (273 K).

4.2.1. AMINO (EXPOSE-R/International Space Station)

The AMINO experiment has been accepted to be part of the first wave of experiments that will be implemented on the EXPOSE-R facility (Fig. 7a) on the Russian module of the International Space Station. Along with amino

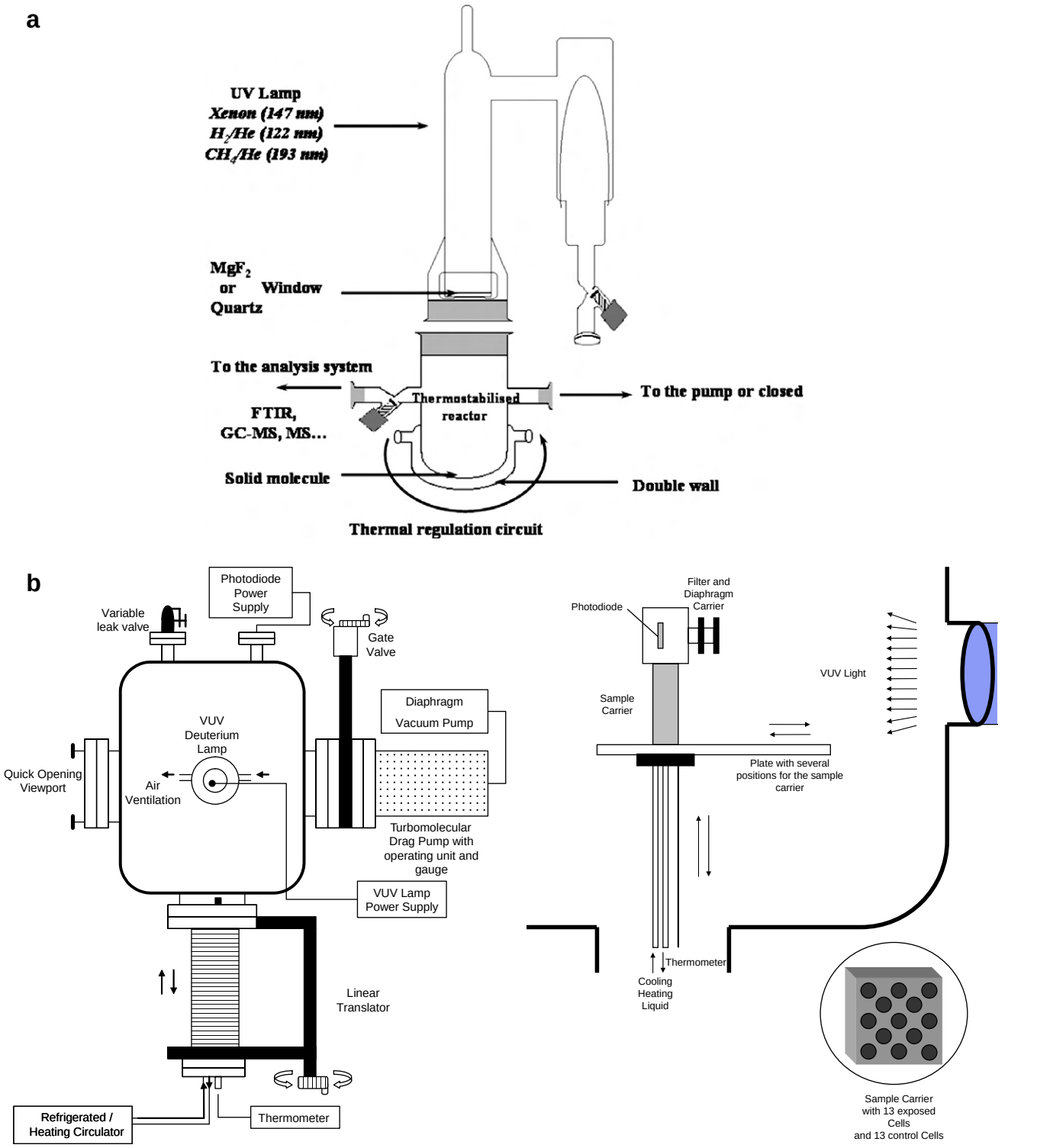

Fig. 4. (a) Experimental setup for laboratory experiments supporting space irradiation experiments. Solid molecules are deposited at the bottom of a Pyrex reactor and placed under vacuum. The solid compound can be photolyzed at different wavelengths and at a controlled temperature. The UV lamp is a Pyrex bulb filled with an appropriate gas or gas mixture according to the emitted wavelength: H_2 (2%) in He for a 122 nm emission (Lyman α), Xe for 147 nm, or CH_4 (1%) in He for 193 nm. Discharge in the lamp is initiated with a Tesla coil and the gas is excited by a microwave generator at 2450 MHz. (b) Left: Irradiation chamber at the Centre de Biophysique Moléculaire in Orléans (volume about 20 l, deuterium lamp irradiation: 112–370 nm, temperature range: −50 C to +200 C). Right: Enlarged views of the sample holder inside the chamber.

acids, samples relevant to cometary or Titan's chemistry will be exposed, and for the first time gaseous mixtures will be submitted to photolysis in space thanks to closed cells specifically designed for those new generation experiments. Other experiments, beyond the scope of this paper since they deal with biology, are also included in AMINO (Bar-

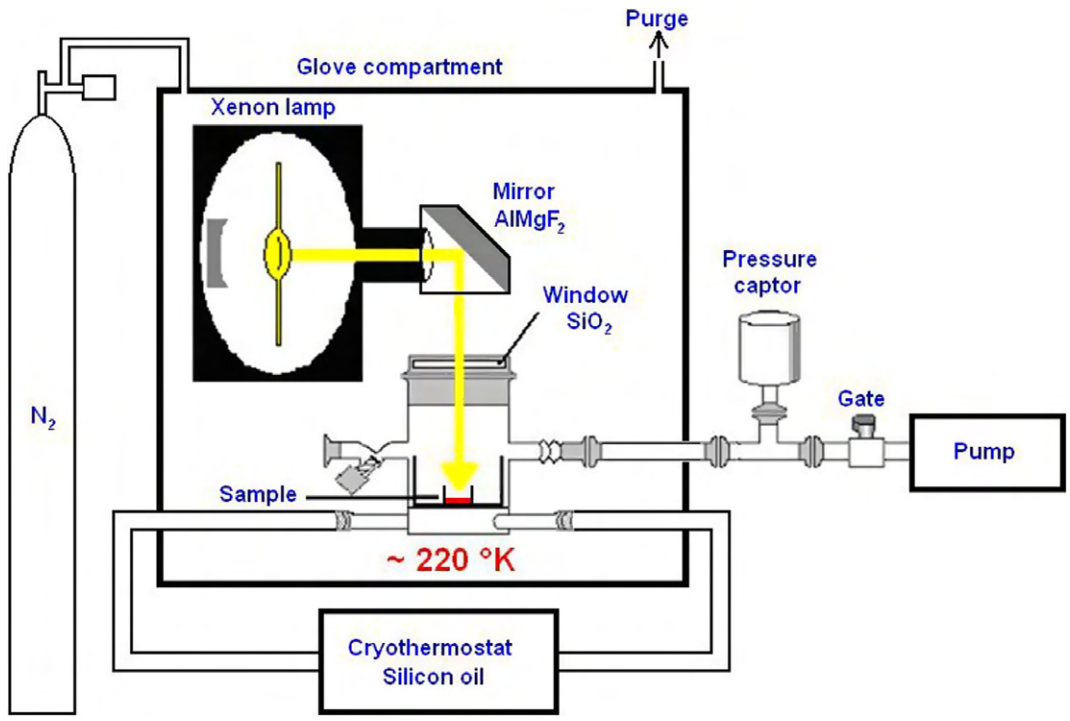

Fig. 5. The MOMIE experiment is composed of a glass reactor in which organic molecules are introduced. This reactor is pumped to vacuum ($\sim 10^{-2}$ mbar) and cooled down to a temperature of approximately −55 °C with a cryothermostat (KRYOMAT RUL 80, LAUDA). The irradiation source is a Xenon lamp (Arc Source "Research" 50–200 W Xe and Hg(Xe), LOT ORIEL) (for more details see Stalport et al., submitted for publication).

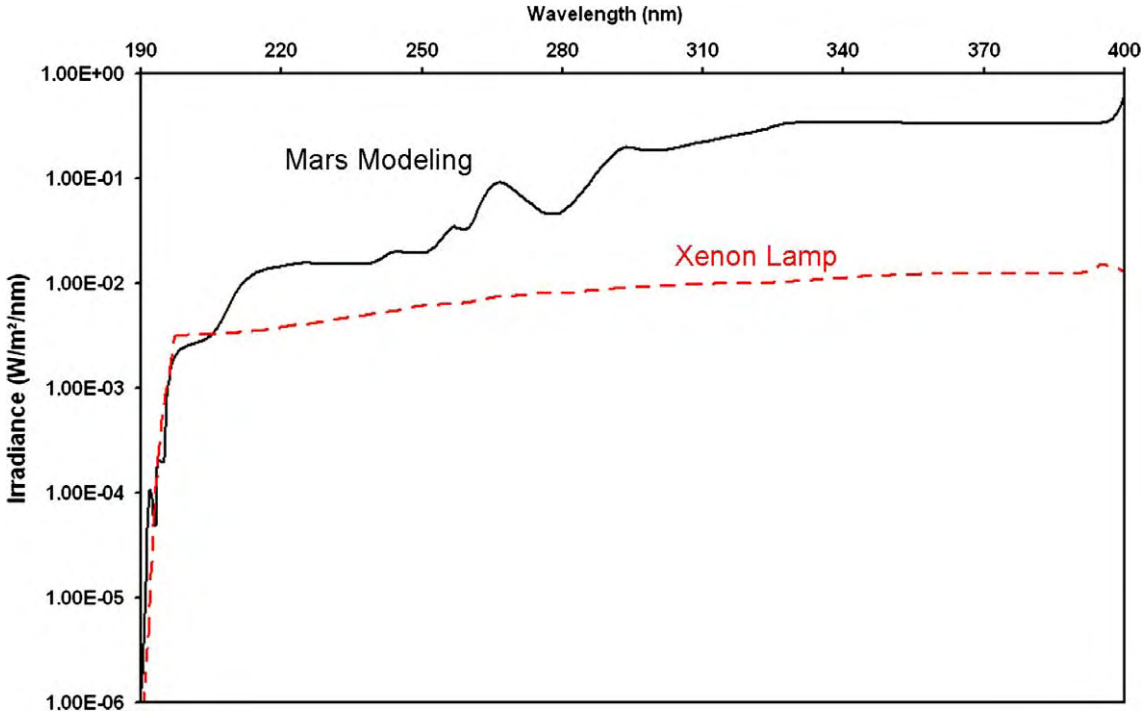

Fig. 6. Spectrum of the Xenon lamp (dotted line) in the MOMIE reactor compared to the Mars modelling spectrum (Patel et al., 2002). Both spectra are very close and cross each other at approximately 190 nm.

bier et al., 2002a). Two sample holders, similar to the one shown in Fig. 6b, are devoted to AMINO, with the following distribution of samples: 1/4 – amino acids, 1/4 – comet related experiment, 1/8 – Titan related experiments, the remaining being biology related material. Each sample holder can receive 20 samples exposed to the Sun, and 20

Table 1
List of experiments dedicated to astrochemistry using the EXPOSE and BIOPAN facilities

Name	Space facility	Space vehicle	Launch	Duration	Principal investigator	Related solar system objects
AMINO	EXPOSE-R	ISS (Russian module)	2008 (1st semester)	1 year	A. BRACK (→ end of 2006) then H. COTTIN	Comets, Meteorites, Titan
PROCESS	EXPOSE-EuTEF	ISS (European module: Colombus)	2008 (1st semester)	1.5 year	H. COTTIN	Comets, Meteorites, Titan, Mars
UV-olution	BIOPAN	FOTON	September 14th, 2007	11.8 Days	H. COTTIN	Comets, Titan, Mars

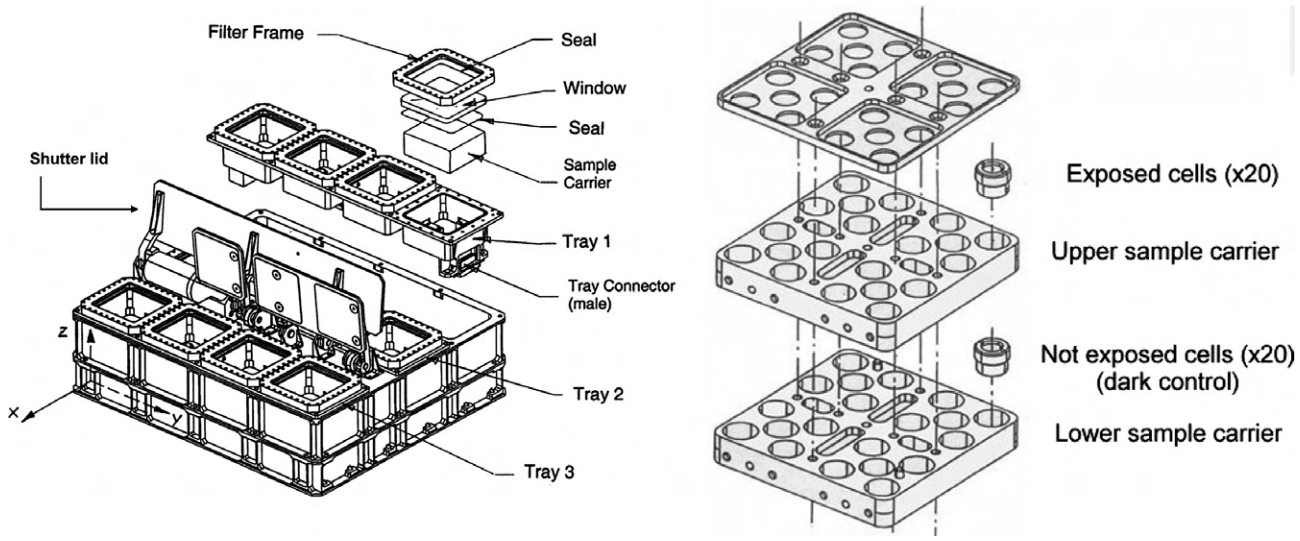

Fig. 7. The EXPOSE facility (480 × 520 × 327,5 mm) is made of three experiment trays into which four square sample carriers (77 × 77 × 26 mm) are fitted (left). For AMINO and PROCESS, each sample carrier is designed to receive up to 20 exposition cells (right). Shutter lids will be open during the whole flight. *Pictures courtesy of Kayser-Threde GmbH.*

dark in-flight controls. With the closed cells, AMINO allows us to study chemical evolution in the gaseous phase, and to collect the gaseous fragments produced when refractory compounds are irradiated. Those cells are presented in Section 4.2.4 of this paper. To date, the launch of the AMINO experiments is scheduled for the end of the first semester of 2008 for and exposition duration of one year. After exposition, the samples will be delivered back to Earth via a US Space Shuttle or a Russian PROGRESS capsule.

Due to the rotation of the International Space Station around the Earth and upon itself, it is important to note that for duration of one year in space, the integrated time of full exposure of the cells to the Sun is only approximately 10 days.

André Brack (CBM, Orléans, France) was the PI of this experiment until the end of 2006. Hervé Cottin (LISA, Créteil, France), took charge of the experiment since then.

4.2.2. PROCESS (EXPOSE-EuTEF/International Space Station)

PROCESS is a second experiment, similar to AMINO, that will be set outside the European module Columbus on the International Space Station. A second EXPOSE facility, called EXPOSE-EuTEF (European Technology Exposure Facility) will be flown on Columbus at the beginning of 2008. PROCESS is dedicated to the study of photochemical processes relevant to comets (1/4), meteorites (1/4), Mars (1/4), and Titan (1/4). Two sample holders (with a total of 40 exposed samples, and 40 in-flight dark controls) are attributed to PROCESS. The duration of the experiment in space is about 1.5 year, but may vary depending on future Space Station extravehicular activities. As for EXPOSE-R, after exposition, the samples will be delivered back to Earth via a US Space Shuttle or a Russian PROGRESS capsule.

Hervé Cottin (LISA, Créteil, France) is the PI of this experiment.

4.2.3. UV-olution (BIOPAN/FOTON M3)

BIOPAN is an ESA multi-user space exposure facility, designed for exobiology, radiation biology, radiation dosimetry, and material science investigations in space (Demets et al., 2005). It carries its payload experiments on the inner side of two 38 cm circular plates (one lid and one bottom plate) facing each other at launch and recovery. After orbit insertion, the lid is opened to expose the package to space conditions, until it is closed and sealed

Please cite this article in press as: Cottin, H. et al., Heterogeneous solid/gas chemistry of organic compounds related ..., J. Adv. Space Res. (2007), doi:10.1016/j.asr.2007.09.017

before the recovery of the capsule. BIOPAN is attached to the outer shield of a FOTON Russian capsule. UV-olution will be flown on BIOPAN 6, on the capsule FOTON M3. Launch is scheduled on September 14th 2007, for an 11.8-day duration in orbit (Fig. 8).

UV-olution is split into two parts and fits onto the lid of BIOPAN (Fig. 9). A 140 cm^2 surface is allocated to the experiment, for a total surface area of 1080 cm^2 for all the BIOPAN experiments on the bottom plate and lid. The UV-olution surface allows the exposition of 60 cells (vented or closed). The sample holders have been designed by Didier Chaput (CNES) and manufactured by COMAT Aerospace (Toulouse, France).

Hervé Cottin (LISA, Créteil, France) is the PI of this experiment.

4.2.4. Experiment cells

Two kinds of cells are used in the three experimental programs: vented and sealed cells. In the vented cells, gaseous fragments resulting from the photolytic processes on the exposed samples are released into space and lost for analysis. In this case, those volatile molecules cannot further interact with the solid phase sample deposited on the window.

Vented cells are shown in Fig. 10. They are made of a cylindrical aluminum body onto which a 9 mm (diameter) by 1 mm (thickness) MgF_2 or quartz window is glued (epoxy glue). The walls of the cell are treated with Alodine®. The sample is deposited on the inner side of the window (see Section 4.3). The refractory sample can be analyzed before and after exposition via infrared measurements. After exposition, it can be recovered with a solvent for further analyses with HPLC or gas chromatography coupled to a mass spectrometer.

Sealed cells (Fig. 11) are made of two cylindrical aluminium bodies which can be screwed one into the other. An O-ring (Viton®) prevents leaks between the two parts. The volume inside the cell is approximately 275 mm^3. Sealed cells can be used to study the photolysis of a 100% gaseous starting mixture, or for the same kind of solid materials as those deposited in the vented cells. In this case, gaseous fragments resulting from photolytic processes on the solid exposed samples are kept inside the cell and can be analyzed after the recovery of the experiment. The walls of the two parts are treated with Alodine®. Two MgF_2 or quartz windows are glued at both ends of the cell, allowing (1) photolysis of the sample from the top window and (2) in situ UV or infrared analysis of the sample. However, infrared analysis inside the cell is limited by the infrared cutoff of the windows ($\sim$1000 cm^{-1} for MgF_2 and $\sim$3000 cm^{-1} for quartz). Moreover, the optical path length inside the cell is only 4.3 mm, limiting the sensitivity for spectroscopic detection. Analysis for lower wavelengths and with a larger path length is aided by the use of an analytical cell (see Section 4.2.5). The deposition of a solid sample can be done when the two parts are separated using the same procedure as that used for a vented cell. After the deposition of the solid sample, an inert gas (Ar) is introduced using the analytical cell. If the starting material inside the cell is made only of gaseous compounds, then the preparation of the cell proceeds only through the analytical cell. In each case, the total pressure inside the cell before launch is adjusted with Ar to 1.5 bar. This pressure allows avoiding contamination from Earth's atmosphere before launch. The sealed cells are conceived to leak at a maximum level of about 1×10^{-9} mb l s^{-1} when placed in vacuum, which allows experiment durations of a few years.

4.2.5. Analytical cell

The analytical cell is shown in Figs. 12 and 13. Although called "analytical", it is used for both filling and sampling the sealed cells with gas, and for infrared analysis of the

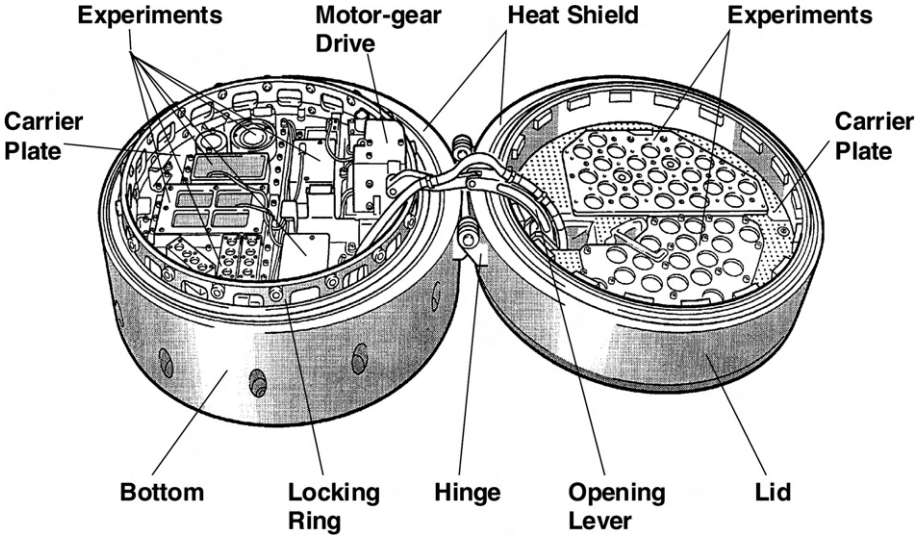

Fig. 8. The BIOPAN facility with the lid open. The bottom part is at left and the lid part, at right, can be opened and closed by telecommand from ground. The diameter of the facility is 38 cm. *Picture courtesy of Kayser-Threde GmbH.*

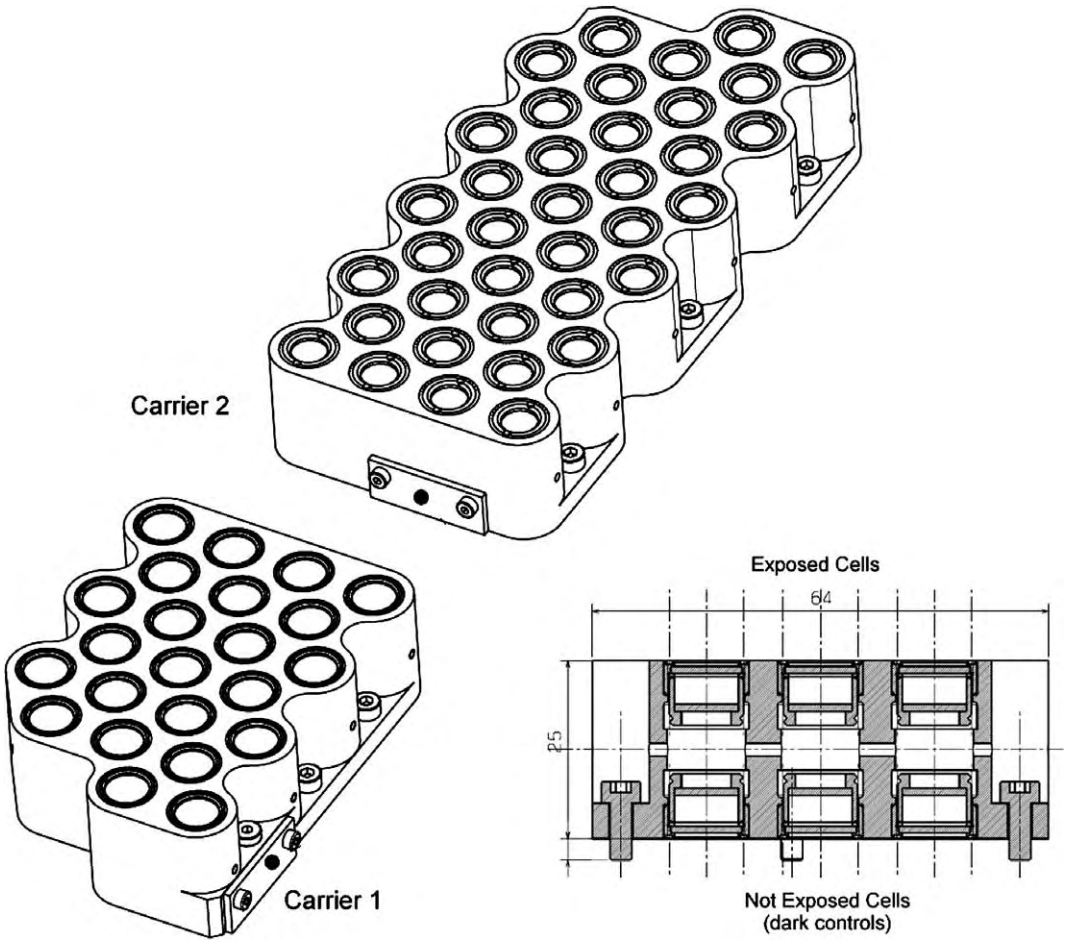

Fig. 9. UV-olution aluminum sample holders ($134 \times 64 \times 25$ mm and $88 \times 64 \times 25$ mm). The two carriers are designed to receive 33 and 27 exposed samples. In each case, both exposed cells and in-flight controls are screwed onto the sample holder. *Picture courtesy of COMAT aerospace.*

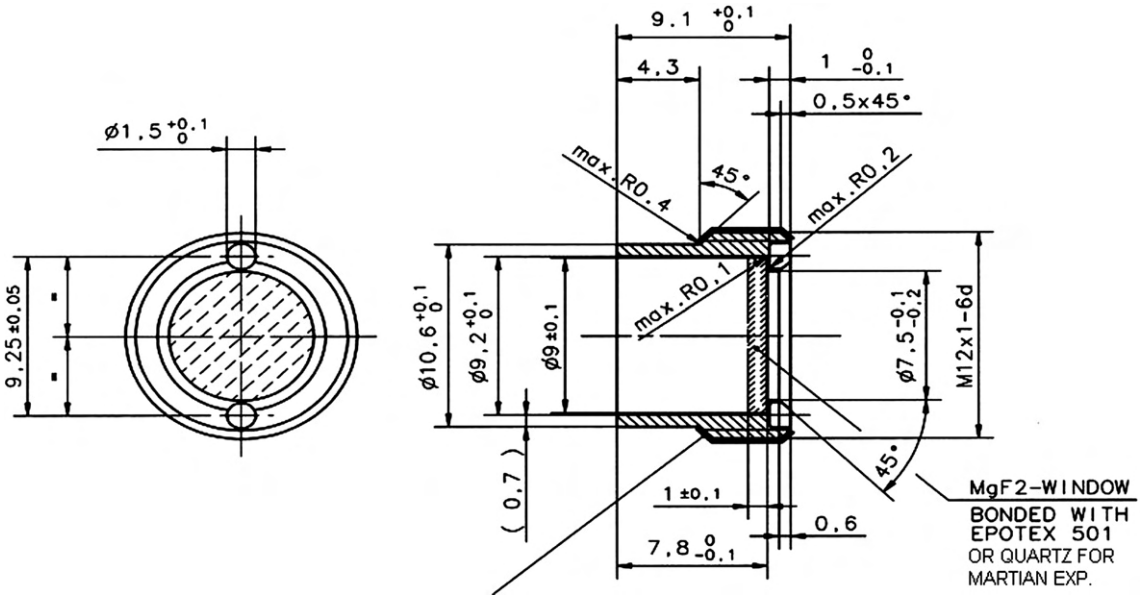

Fig. 10. Design of a vented cell made of an aluminium cylinder on top of which a MgF_2 or quartz window is glued. The organic molecule is deposited onto the inside face of the window. *Picture courtesy of COMAT aerospace.*

gaseous content of the sealed cells. It is basically made of two main Inox parts on the inside of which both parts of a sealed cell are separately fitted. The two analytical cell parts are then adjusted and sealed with a Viton® O-ring.

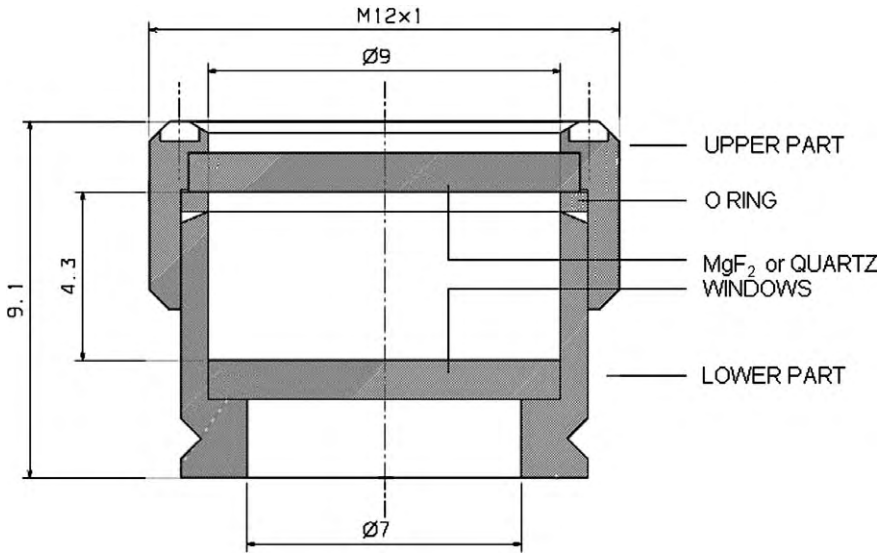

Fig. 11. Design of a sealed cell. Two aluminium cylinders are screwed into each other. Two MgF_2 or quartz windows at both ends allow the analysis of molecules inside the cell by spectroscopy. Sealing (relative to lab atmosphere or vacuum in space) is ensured by a Viton® O-ring. *Picture courtesy of COMAT aerospace.*

The gaseous component of the experiment can then be introduced inside the analytical cell before screwing the two parts of the sealed cell one into the other, using a screw connecting one part of the sealed cell to the outside of the analytical cell, enclosing the gases inside the sealed cell. The sealed cell can then be removed from the analytical cell and placed on a sample holder for the experiment in space.

After exposition in space, the content of the sealed cell can be analysed in situ by infrared spectroscopy, within the limitation of the wavelength range previously mentioned. Subsequently the two parts of the exposed cell can be unscrewed inside the analytical cell to release gases that will fill an infrared compartment embedded inside the analytical cell. KBr or CsI windows enable infrared analysis over a wider wavelength range (respectively, 400 and 200 cm^{-1}) with a 2-cm optical path length. Sampling of the gas in the analytical cell can also be made to perform gas chromatography/mass spectrometry analysis. When the two parts of the sealed cell are separated, and when the analysis of the gases has been made, study of the refractory component can be achieved in the same way as done for the open cells. Sealed and analytical cell have been designed and manufactured by COMAT Aerospace (Toulouse, France).

4.3. Deposition procedure

Films of organic samples can be obtained on the windows as described in Barbier et al. (2002b) and Boillot et al. (2002), as evaporation residues of a solution in which the molecules are previously solubilized, alone or with a suspension of minerals for organo-mineral mixtures. The thickness of the film is estimated from the initial concentration and molecular volume of each species loaded. Organic films can also be obtained by sublimation of the compounds and condensation onto the cell window. The thickness of the film can be estimated in situ from interference measurements, previously calibrated with atomic force or confocal microscopy. A sublimation chamber similar to ours is presented in Ten Kate et al. (2005).

5. Target molecules

In this section, the molecules selected to be exposed during one (or more) of the space experiment and their astrochemical relevance are presented.

5.1. Comets

Laboratory experiments conducted on interstellar and cometary ice analogues have shown that high molecular weight organic molecules are synthesized from mixtures of simple compounds detected in the cometary atmosphere (see a review in Cottin et al. (1999)). Among those complex compounds, polyoxymethylene (POM: $-(CH_2-O)_n-$ polymer of formaldehyde); hexamethylenetetramine (HMT: $C_6N_4H_{12}$), HCN polymers and carbon suboxide polymers ($(C_3O_2)_n$) are of prime interest (Schutte et al., 1993; Bernstein et al., 1995; Cottin et al., 2001; Gerakines and Moore, 2001), and their presence on the cometary nucleus could allow an interpretation of the extended source phenomena detected in the cometary atmosphere. As an example, the presence of polyoxymethylene at a mass level of a few percent is, to date, the best explanation for the origin of the puzzling occurrence of extended sources of formaldehyde in comet Halley (Cottin et al., 2004) and comet Hale–Bopp (Fray et al., 2006). On the other hand, HCN polymers could be a source for the

Please cite this article in press as: Cottin, H. et al., Heterogeneous solid/gas chemistry of organic compounds related ..., J. Adv. Space Res. (2007), doi:10.1016/j.asr.2007.09.017

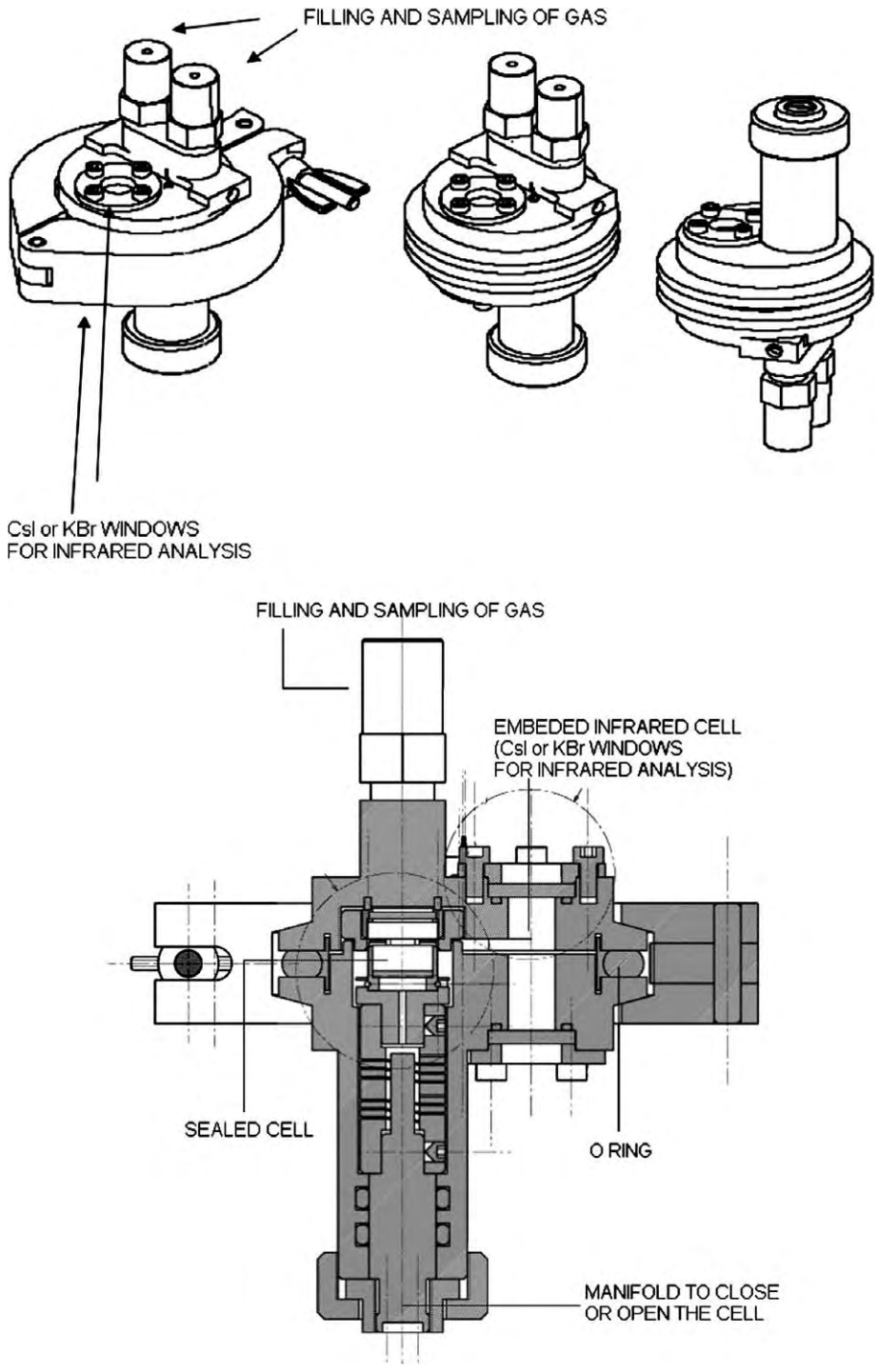

Fig. 12. Design of the analytical cell. It allows the filling or sampling of gases inside a sealed cell which can be fitted inside. An embedded infrared cell can be used for the analysis of gases in the infrared range. *Picture courtesy of COMAT aerospace.*

observed CN extended sources in comets (Fray et al., 2005) as it contains C–N bonds which can be released from the polymer by photolysis, whereas carbon suboxide polymers could explain the CO extended source (DiSanti et al., 1999, 2003). Moreover, these compounds may have strong exobiological implications. In Earth's primitive oceans, POM could have been a source of concentrated formaldehyde, a key compound involved in the synthesis of sugars (Shapiro, 1988), although this is still debated. On the other hand, hydrolysis of HMT and HCN polymer releases amino acids (Matthews and Moser, 1967; Wolman et al., 1971). Therefore, experiments related to POM, HMT, HCN, and carbon suboxide polymers are scheduled for AMINO, PROCESS, and UV-olution. The photostability of these compounds will be studied if the molecules are exposed as pure deposits, or embedded

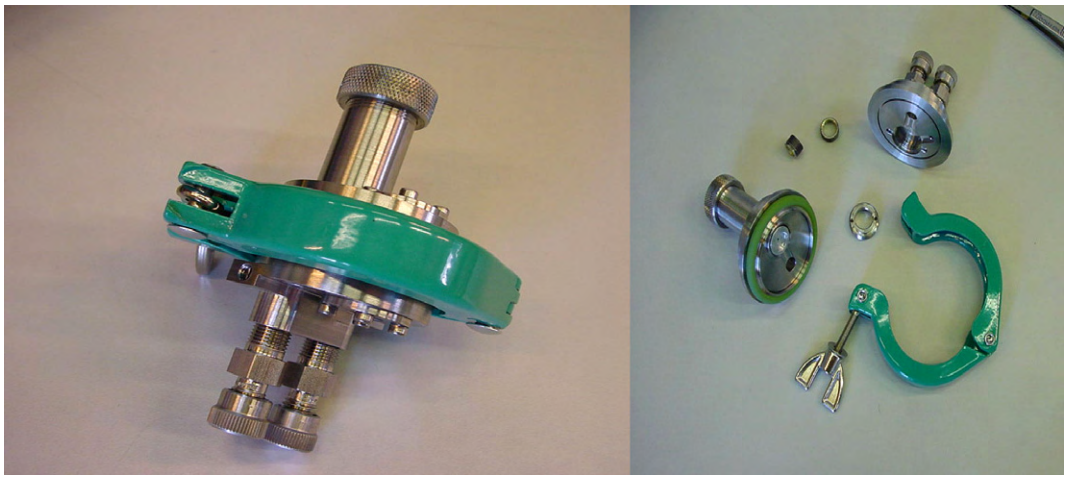

Fig. 13. Views of the analytical cell. It can be split in two for installation or to extract a sealed cell before or after closing.

in a mineral or organic matrix closely related to their actual space environment.

5.2. Meteorites

Another example of the complexity of organic chemistry occurring in space is documented by studies of carbonaceous chondrites that contain up to 5% by weight of organic matter. The Murchison meteorite has numerous organic compounds, including nucleic bases and amino acids. An excess of about 9% of the L-form for isovaline and α-methyl-isoleucine, non-protein C_α di-substituted amino acids, was found in the Murchison meteorite (Cronin and Pizzarello, 1997). These amino acids do not result from biological contamination and do not racemize easily. On the other hand, norvaline and α-amino-*n*-butyric acid, their C_α-monosubstituted analogues which can easily racemize, were found as racemic mixtures (equal mixture of L and D enantiomers) (Cronin and Pizzarello, 1997). This supports a possible asymmetric synthesis in space followed by a progressive racemization. This excess of left-handed amino acids could be an explanation for the emergence of a primitive one-handed life.

Micrometeorites (size < 1 mm), which represent more than 99% of the exogenous materials arriving on Earth (Maurette, 1998, 2006), could also have safely carried organic molecules to the primitive Earth. The study of micrometeorites extracted from old Antarctica blue ice shows that about 80% of the carbonaceous ones in the 50–100 μm size range are not melted after crossing the terrestrial atmosphere (Maurette, 1998, 2006). Analyses of such micrometeorites have shown traces of amino acids such as α-amino butyric acid (Brinton et al., 1998). Recent sample exposition to space conditions, onboard the MIR Station, has demonstrated that a 5 μm thick film of meteorite powder was able to efficiently protect associated amino acids against solar radiation (Boillot et al., 2002).

Experiments involving amino acids will therefore be implemented on AMINO and UV-olution, and will focus on degradation and racemization processes. They will be more specifically dedicated to the following materials: protein amino acids (glycine), non-protein amino acids (D-alanine, D-aspartic acid, α-amino isobutyric acid, D-amino butyric acid) and a small peptide (dileucine) to compare the chemical stability of proteinaceous and non-proteinaceous amino acids and peptide in space. Special attention will be devoted to decarboxylation reactions and racemization, i.e. the transformation of one enantiomer into its mirror image. All the amino acid related experiments will be implemented in vented cells. In some experiments, the organic material will be embedded in a mineral matrix (Allende meteorite powder).

5.3. Titan

Titan's aerosol analogues (Tholins) have been produced for years in laboratories with a wide range of experimental conditions (Coll et al., 1999). We plan to expose the main gaseous compounds of Titan's atmosphere ($N_2 + CH_4$) to the full solar spectrum, with known isotopic ratios in N or C. Indeed, in the case of nitrogen, Titan presents a $^{14}N/^{15}N$ value which is 1.5 times less than that for the primordial N, suggesting that the present mass of the atmosphere was lost several times (Niemann et al., 2005). It could also be interpreted as an isotopic fractionation during N integration in aerosols. If not, this implies that ^{14}N escapes preferentially into the Interplanetary Medium. A similar discussion can be developed for the $^{13}C/^{14}C$ ratio: its determination in the solid products can provide information on the chemical pathways involved in their synthesis (Nguyen et al., in press). We will also compare the products of our space experiments with the well characterized laboratory products (gaseous and solid) collected so far (Coll et al., 1999).

On the other hand, exposition to the solar spectrum of laboratory made, Titan aerosol analogues (Tholins) will

Please cite this article in press as: Cottin, H. et al., Heterogeneous solid/gas chemistry of organic compounds related ..., J. Adv. Space Res. (2007), doi:10.1016/j.asr.2007.09.017

help us to understand the evolution and the degradation of such a chemical structure, and therefore understand the transformation of the aerosols during their sedimentation in the atmosphere of Titan. These results have direct application to the understanding of the nitrogen cycle on Titan. This is also important to predict the nature of molecules that can condense onto the aerosols, since the nature of the aerosols is of prime importance for the nucleation process (Guez et al., 1997).

5.4. Mars

Martian irradiance at the surface has a shape close to the solar spectrum except for wavelengths shorter than 190–200 nm. Indeed, the Martian CO_2 atmosphere stops these short wavelengths. Using a quartz window, an irradiance representative of the Martian surface condition is obtained inside. For each compound, we plan to distinguish the evolution of the molecule on its own as well as associated with an analogue of the Martian soil (Feldspar and Ti-magnetite, along with minor olivine, pyroxene, and glass), in order to predict which are the resulting products.

Although numerous experiments relating to the survival and evolution of different forms of bacteria at the Martian surface have been carried out (Green et al., 1971; Mancinelli and Rocco, 1989; Horneck, 1993; Mancinelli and Klovstad, 2000), few have studied the same phenomena in the case of organics (Oro and Holzer, 1979; Stoker and Bullock, 1997; Ten Kate et al., 2005, 2006).

As a reference, we plan to study the only organic molecule already studied in space (Stoker and Bullock, 1997): glycine. We also plan to study the evolution under solar irradiation of molecules of biotic origin that are very resistant in the terrestrial environment, which is much more aggressive than the Martian one (fluid circulation, tectonics, etc.): 2-methylhopane and 3-methylhopane (oldest hopane molecular fossils found on Earth = 2.7 Gy-old, Brocks et al., 1999). In addition, benzoic acid will be studied. It is proposed as a terminal molecule resulting from the potential oxidation of organics at Mars surface and presented as a molecule resistant to the surface conditions of Mars (Benner et al., 2000). This hypothesis has to be checked experimentally due to the fact that no benzoic acid has been yet detected on Mars.

Martian related experiments will be carried out in both vented and sealed sampled. In sealed samples, experiments will be conducted under a CO_2 Martian analogous atmosphere.

6. Conclusions

The AMINO, PROCESS, and UV-olution experimental programs will address the main aspects of photochemistry related to astrobiology in the Solar System. However, even if these space laboratories offer an environment impossible to accurately reproduce in the laboratory; ground experiments are still necessary in preparation and in support of these experiments.

With respect to comets, we may be able to answer the following questions: (1) What is the stability of refractory molecules once synthesized in cometary and/or interstellar ices, and what are the chances for their actual presence on comets and cometary dust, and subsequent importation to Earth's ocean? (2) What kinds of shielding effect can we expect from the mineral and organic matrix in which they are embedded? (3) What are the gaseous photodegradation products of the target molecules, and are they related to the extended sources?

With respect to meteorites: (1) What is the stability of amino acids and small peptides in space, and their history before being imported to Earth via meteorites and micrometeorites? (2) To what extent does Solar UV radiation affect any enantiomeric excess of compounds with an asymmetric carbon?

Regarding Titan: (1) Could the isotopic integration of C and N in Titan's aerosols explain the isotopic ratios in Titan's atmosphere measured by Cassini–Huygens? (2) In the case that no direct role can be demonstrated, what will be the implications of these results on Titan's environment: isotopic fractionation during the escape from Titan's atmosphere, internal source of methane? (3) Are aerosols a final sink for nitrogen, or is any nitrogen released from the aerosols when they are exposed to photons?

With respect to Mars: (1) Which molecules are formed as a result of the irradiation of the target molecules, in terms of gaseous molecules or solid products (degradation/evolution/reaction of the original solid products)? (2) Are they likely to be detectable in the next future missions to Mars (future in situ NASA/ESA missions...)?

Space laboratories such as BIOPAN and EXPOSE offer great opportunities to perform photochemistry experiments with a "perfect" UV source for astrochemistry: the Sun. In such experiments however, the total exposition time to photons is a key parameter if one wishes to extrapolate results over relevant astrophysical time scale. The duration of the effective exposition to Solar UVs is difficult to estimate before the mission. One of the issues for such calculation is uncertainty in what pointing mode the International Space Station will be in during the exposure period. Also, shadowing and reflections from the structure further complicate the issue. Therefore, the exact exposition time is measured during the actual experiment. Next generations for such experiments should address this issue, optimizing the photolysis time using a sun pointing device. Similar experiments could also be implemented at the surface of the Moon for extra-long exposure duration. Another flaw, addressed in this paper, is that it not possible to acquire data during the experiment. In the future, onboard spectrometers and transmission of data to Earth could allow measuring the destruction of exposed compounds with their degradation products while the experiment is still in space.

References

Barbier, B., Chabin, A., Chaput, D., et al. Photochemical processing of amino acids in Earth orbit. Planet. Space Sci. 46 (4), 391–398, 1998.

Barbier, B., Coll, P., Cottin, H., et al. The ''Amino'' experiment on Expose. Proc. 2d European Workshop on Exo-/Astro-Biology ESA-SP 518, 59–62, 2002a.

Barbier, B., Henin, O., Boillot, F., et al. Exposure of amino acids and derivatives in the Earth orbit. Planet. Space Sci. 50, 353–359, 2002b.

Benner, S.A., Devine, K.G., Matveeva, L.N., Powell, D.H. The missing organic molecules on Mars. Proc. Natl. Acad. Sci. USA 97 (6), 2425–2430, 2000.

Bernstein, M.P., Sandford, S.A., Allamandola, L.J., et al. Organic compounds produced by photolysis of realistic interstellar and cometary ice analogs containing methanol. Astrophys. J. 454, 327–344, 1995.

Bibring, J.P., Langevin, Y., Mustard, J.F., et al. Global mineralogical and aqueous mars history derived from OMEGA/Mars express data. Science 312 (5772), 400–404, 2006.

Biver, N., Bockelée-Morvan, D., Crovisier, J., et al. Chemical composition diversity among 24 comets observed at radio wavelengths. Earth Moon Planets 90 (1), 323–333, 2002.

Boillot, F., Chabin, A., Buré, C., et al. The perseus exobiology mission on MIR: behaviour of amino acids and peptides in Earth orbit. Orig. Life Evol. Biosph. 32, 359–385, 2002.

Bossard, A. Rôle du Rayonnement Ultraviolet dans les Synthèses Prébiologiques. PhD, Université Paris VI, 1979.

Botta, O., Bada, J.L. Extraterrestrial organic compounds in meteorites. Surv. Geophys. 23, 411–467, 2002.

Brinton, K.L.F., Engrand, C., Glavin, D.P., et al. A search for extraterrestrial amino acids in carbonaceous antarctic micrometeorites. Orig. Life Evol. Biosph. 28, 413–424, 1998.

Brocks, J.J., Logan, G.A., Buick, R., Summons, R.E. Archean molecular fossils and the early rise of eukaryotes. Science 285, 1033–1036, 1999.

Cabane, M., Coll, P., Szopa, C., et al. Did life exist on Mars? Search for organic and inorganic signatures, one of the goals for ''SAM'' (sample analysis at Mars). Adv. Space Res. 33, 2240–2245, 2004.

Catling, D.C. Comment on ''A hydrogen-rich early Earth atmosphere''. Science 311, 5757, 2006.

Coll, P., Coscia, D., Smith, N., et al. Experimental laboratory simulation of Titan's atmosphere (aerosols and gas phase). Planet. Space Sci. 47 (10–11), 1331–1340, 1999.

Cottin, H., Bachir, S., Raulin, F., et al. Photodegradation of hexamethylenetetramine by VUV and its relevance for CN and HCN extended sources in comets. Adv. Space Res. 30 (6), 1481–1488, 2002.

Cottin, H., Bénilan, Y., Gazeau, M.-C., et al. Origin of cometary extended sources from degradation of refractory organics on grains: polyoxymethylene as formaldehyde parent molecule. Icarus 167, 397–416, 2004.

Cottin, H., Gazeau, M.C., Doussin, J.F., et al. An experimental study of the photodegradation of polyoxymethylene at 122, 147 and 193 nm. J. Photochem. Photobiol. A: Chemistry 135, 53–64, 2000.

Cottin, H., Gazeau, M.C., Raulin, F. Cometary organic chemistry: a review from observations, numerical and experimental simulations. Planet. Space Sci. 47 (8–9), 1141–1162, 1999.

Cottin, H., Moore, M.H., Bénilan, Y. Photodestruction of relevant interstellar molecules in ice mixtures. Astrophys. J. 590, 874–881, 2003.

Cottin, H., Szopa, C., Moore, M.H. Production of hexamethylenetetramine in photolyzed and irradiated interstellar cometary ice analogs. Astrophys. J. Lett. 561 (1), L139–L142, 2001.

Cronin, J.R., Pizarello, S., Cruikshank, D.P. Organic matter in carbonaceous chondrites, planetary satellites, asteroids, and comets, in: Kerridge, J.F., Matthews, M.S. (Eds.), Meteorites and the Early Solar System. University of Arizona Press, pp. 819–857, 1988.

Cronin, J.R., Pizzarello, S. Enatiomeric excesses in meteoritic amino acids. Science 275, 951–955, 1997.

Demets, R., Schulte, W., Baglioni, P. The past, present and future of BIOPAN. Adv. Space Res. 36, 311–316, 2005.

Despois, D., Cottin, H. Comets: potential sources of prebiotic molecules for the early Earth, in: Gargaud, M., Barbier, B., Martin, H., Reisse, J. (Eds.), Lectures in Astrobiology, vol. 1. Springer Verlag, pp. 289–352, 2005.

DiSanti, M.A., Mumma, M.J., DelloRusso, N., et al. Evidence for a dominant native source of carbon monoxide in Comet C/1996 B2 (Hyakatake). J. Geophys. Res. (Planets) 108 (E6), 15, 2003.

DiSanti, M.A., Mumma, M.J., DelloRusso, N., et al. Identification of two sources of carbon monoxide in comet Hale–Bopp. Nature 399, 662–665, 1999.

Ehrenfreund, P., Charnley, S.B. Organic molecules in the interstellar medium, comets and meteorites: a voyage from dark clouds to the early earth. Annu. Rev. Astron. Astrophys. 38, 427–483, 2000.

Ehrenfreund, P., Ruiterkamp, R., Peeters, Z., et al. The ORGANICS experiment on BIOPAN V: UV and space exposure of aromatic compounds. Planet. Space Sci. 55 (4), 383–400, 2007.

Fray, N., Bénilan, Y., Biver, N., et al. Heliocentric evolution of the degradation of polyoxylmethylene. Application to the origin of the formaldehyde (H2CO) extended source in comet C/1995 O1 (Hale–Bopp). Icarus 184 (1), 239–254, 2006.

Fray, N., Bénilan, Y., Cottin, H., et al. The origin of the CN radical in comets: a review from observations and models. Planet. Space Sci. 53 (12), 1243–1262, 2005.

Fray, N., Bénilan, Y., Cottin, H., et al. Experimental study of the degradation of polymers. Application to the origin of extended sources in cometary atmospheres. Meteorit. Planet. Sci. 39 (4), 2004.

Gerakines, P.A., Moore, M.H. Carbon suboxide in astrophysical ice analogs. Icarus 154 (2), 372–380, 2001.

Gerakines, P.A., Schutte, W.A., Ehrenfreund, P. Ultraviolet processing of interstellar ice analogs. I. Pure ices. Astron. Astrophys. 312, 289–305, 1996.

Green, R.H., Taylor, D.M., Gustan, E.A., et al. Survival of microorganisms in a simulated Martian environment. Space Life Sci. 3, 12–24, 1971.

Guez, L., Bruston, P., Raulin, F., et al. Importance of phase changes in Titan's lower atmosphere. Tools for the study of nucleation. Planet. Space Sci. 45, 611–625, 1997.

Horneck, G. Responses of Bacillus subtilis spores to space environment: results from experiments in space. Orig. Life Evol. Biosph. 23 (1), 37–52, 1993.

Horneck, G., Mileikowsky, C., Melosh, H.J., et al. Viable transfer of microorganisms in the solar system and beyond, in: Horneck, G., Baumstark-Khan, C. (Eds.), Astrobiology. The quest for the conditions of life. Springer, pp. 57–76, 2002.

Kasting, J.F. Earth's early atmosphere. Science 259, 920–926, 1993.

Khare, B.N., Sagan, C., Ogino, H., et al. Amino acids derived from Titan Tholins. Icarus 68, 176–184, 1986.

Kissel, J., Krueger, F.R. The organic component in dust from comet Halley as measured by the PUMA mass spectrometer on board Vega 1. Nature 326, 755–760, 1987.

Kissel, J., Krueger, F.R., Silén, J., et al. The cometary and interstellar dust analyzer at comet 81P/Wild 2. Science 304, 1774–1776, 2004.

Mancinelli, R.L., Klovstad, M. Martian soil and UV radiation: microbial viability assessment on spacecraft surfaces. Planet. Space Sci. 48 (11), 1093–1097, 2000.

Mancinelli, R.L., Rocco, L. Peroxides and the survivability of microorganisms on the surface of Mars. Adv. Space Res. 9 (6), 191–195, 1989.

Matthews, C.N., Moser, R.E. Peptide synthesis from hydrogen cyanide and water. Nature 215, 1230–1234, 1967.

Maurette, M. Carbonaceous micrometeorites and the origin of life. Orig. Life Evol. Biosph. 28, 385–412, 1998.

Maurette, M. Micrometeorites and the Mysteries of our Origins. Springer-Verlag, 2006.

Miller, S.L. The production of amino acids under possible primitive Earth conditions. Science 117, 528–529, 1953.

Nguyen, M.-J., Raulin, F., Coll, P., Derenne, S., Szopa, C., Cernogora, G., Israël, G., and Bernard, J.-M., Carbon isotopic enrichment in

Titan's tholins? Implications for Titan's aerosols. Planet. Space Sci., in press.

Niemann, H.B., Atreya, S.K., Bauer, S.J., et al. The abundances of constituents of Titan's atmosphere from the GCMS instrument on the Huygens probe. Nature 438, 779–784, 2005.

Oparin, A.I. Proikhozndenie Zhizni. Moskovskii Rabochi, 1924

Oro, J., Cosmovici, C.B. Comets and Life on the primitive Earth. In: Cosmovici, C.B., Bowyer, S., Werthimer, D. (Eds.), Astronomical and Biochemical Origins and the Search for Life in the Universe, Proceedings of the 5th International Conference on Bioastronomy; Editrice Compositori, 97–120.

Oro, J., Holzer, G. The photolytic degradation and oxidation of organic compounds under simulated Martian conditions. J. Mol. Evol. 14, 153–160, 1979.

Patel, M.R., Zarnecki, J.C., Catling, D.C. Ultraviolet radiation on the surface of Mars and the Beagle 2 UV sensor. Planet. Space Sci. 50 (9), 915–927, 2002.

Sagan, C., Thompson, W.R. Production and condensation of organic gases in the atmosphere of Titan. Icarus 59, 133–161, 1984.

Schlesinger, G., Miller, S.L. Prebiotic syntheses in atmospheres containing CH4, CO and CO2. I. Amino acids. J. Mol. Evol. 19, 376–382, 1983.

Schutte, W.A., Allamandola, L.J., Sandford, S.A. An experimental study of the organic molecules produced in cometary and interstellar ice analogs by thermal formaldehyde reactions. Icarus 104, 118–137, 1993.

Shapiro, R. Prebiotic ribose synthesis: a critical analysis. Orig. Life Evol. Biosph. 18, 71–85, 1988.

Stalport, F., Coll, P., Szopa, C., and Raulin, F., Search for life on Mars, studies of organics clues: the MOMIE project. Adv. Space Res., in press, doi:10.1016/j.asr.2007.07.004.

Stoker, C.R., Bullock, M.A. Organic degradation under simulated Martian conditions. J. Geophys. Res. 102 (E5), 10881–10888, 1997.

Ten Kate, I.L., Garry, J.R.C., Peeters, Z., et al. The effects of Martian near surface conditions on the photochemistry of amino acids. Planet. Space Sci. 54, 296–302, 2006.

Ten Kate, I.L., Garry, J.R.C., Peeters, Z., et al. Amino acid photostability on the Martian surface. Meteorit. Planet. Sci. 40, 1185, 2005.

Thuillier, G., Floyd, L., Woods, T., et al. Solar Irradiance Reference Spectra. In: Pap, J.M., Fox, P. (Eds.), Solar variability and its effects on climate, AGU Geophys. Monogr. 141, 2004.

Tian, F., Toon, O.B., Pavlov, A.A. Response to comment on "A hydrogen-rich early Earth atmosphere". Science 311 (5757), 2006.

Tian, F., Toon, O.B., Pavlov, A.A., et al. A hydrogen-rich early Earth atmosphere. Science 308 (5724), 1014–1017, 2005.

Westall, F., Early life on earth and analogies to Mars. In: T. Tokano (Ed.), Water on Mars and Life. Adv. Astrobiol. Biogeophys., 45–64, 2005.

Wolman, Y., Miller, S.L., Ibanez, J., et al. Science 174, 1039–1040, 1971.

Article 20

COCKELL C. S., LEGER A., FRIDLUND M., HERBST T., KALTENEGGER L., ABSIL O., BEICHMAN C., BENZ W., BLANC M., BRACK A., CHELLI A., COLANGELI L., COTTIN H., COUDE DU FORESTO V., DANCHI W., DEFRERE D., DEN HERDER J.-W., EIROA C., GREAVES J., HENNING T., JOHNSTON K., JONES H., LABADIE L., LAMMER H., LAUNHARDT R., LAWSON P., LAY O. P., LEDUIGOU J.-M., LISEAU R., MALBET F., MARTIN S. R., MAWET D., MOURARD D., MOUTOU C., MUGNIER L., PARESCE F., QUIRRENBACH A., RABBIA Y., RAVEN J. A., ROTTGERING H. J. A., ROUAN D., SANTOS N., SELSIS F., SERABYN E., SHIBAI H., TAMURA M., THIEBAUT E., WESTALL F., WHITE and GLENN J. (In Press) DARWIN - A Mission to Detect, and Search for Life on, Extrasolar Planets. Astrobiology.

Darwin – A Mission to Detect, and Search for Life on, Extrasolar Planets

Charles S Cockell[1]
CEPSAR, The Open University, Milton Keynes, MK7 6AA, UK.
Tel : 01908 652588. Email: c.s.cockell@open.ac.uk

Tom Herbst
Max-Planck-Institut fuer Astronomie, Koenigstuhl 17, 69117 Heidelberg, Germany

Alain Leger
IAS, bat 121, Universite Paris-Sud, F-91405, Paris, France

Lisa Kaltenegger
Harvard-Smithsonian Center for Astrophysics. 60 Garden St. MS20, Cambridge , MA 02138, USA

Olivier Absil
Laboratoire d'Astrophysique de Grenoble, CNRS, Université Joseph Fourier, UMR 5571, BP53, F-38041 Grenoble, France

Charles Beichman
Michelson Science Center, California Inst. Of Technology, Pasedena, CA 91125, USA

Willy Benz
Physikalisches Institut, University of Berne, Switzerland

Andre Brack
Centre de Biophysique Moleculaire, CNPS, Rue Charles Sadron, 45071 Orleans cedex 2, France

Alain Chelli
Laboratoire d'Astrophysique de Grenoble, CNRS, Université Joseph Fourier, UMR 5571, BP53, F-38041 Grenoble, France

Luigi Colangeli
INAF - Osservatorio Astronoomico di Capodimonte, Via Moiariello 16, 80131 Napoli, Italy

Hervé Cottin
Laboratoire Interuniversitaire des Systèmes Atmosphériques Universités Paris 12, Paris 7, CNRS UMR 7583 91, av. Di Général de Gaulle, 94010 Créteil Cedex, France

Vincent Coudé du Foresto
LESIA - Observatoire de Paris, 5 place Jules Janssen, F-92190 Meudon, France

William Danchi
Astrophysics Science Division, NASA Goddard Space Flight Center, Greenbelt, MD 20771, USA

Denis Defrère
Institut d'Astrophysique et de Géophysique de Liège, 17 Allée du 6 Août, 4000 Liège, Belgium

Jan-Willem den Herder
SRON Netherlands Institute for Space Research, Sorbonnelaan 2, 3584 CA Utrecht, Netherlands

Carlos Eiroa
Dpto Fisica Toerica C-XI, Facultad de Ciencas, Universidad Autonoma de Madrid, Cantoblanco, 28049 Madrid, Spain

Malcolm Fridlund
Astrophysics Mission Division, European Space Agency, ESTEC, SCI-SA PO Box 299, Keplerlaan 1 NL 2200AG, Noordwijk, Netherlands.

Jane Greaves
University of St Andrews - Physics & Astronomy, North Haugh, St Andrews, Fife KY16 9SS, UK

Thomas Henning
Max-Planck-Institut fuer Astronomie, Koenigstuhl 17, 69117 Heidelberg, Germany

Kenneth Johnston
United States Naval Observatory, 3450 Massachusetts Avenue NW, Washington. D.C. 20392, USA

Hugh Jones
Centre for Astrophysics Research, University of Hertfordshire, College Lane, Hatfield AL10 9AB, UK

Lucas Labadie
Max Planck Institute fur Astronomie, Konigstuhl,17, 69117 Heidelberg, Germany

Helmut Lammer
Space Research Institute, Austrian Academy of Sciences, Schmiedlstr. 6, A-8042, Graz, Austria

Ralf Launhardt
Max-Planck-Institut fuer Astronomie, Koenigstuhl 17, 69117 Heidelberg, Germany

Peter Lawson
Jet Propulsion Laboratory, California Institute of Technology, 4800 Oak Grove Drive, Pasadena 91109, USA

Oliver P. Lay
Jet Propulsion Laboratory, California Institute of Technology, 4800 Oak Grove Drive, Pasedena 91109, USA

Jean-Michel LeDuigou
Centre National d'Etudes Spatiales, optical department,18 av. E. Belin, 31401 Toulouse cedex 9, France

René Liseau
Onsala Space Observatory, Chalmers University of Technology, SE-439 92 Onsala, Sweden

Fabien Malbet
Laboratoire d'Astrophysique de Grenoble, CNRS, Université Joseph Fourier, UMR 5571, BP53, F-38041 Grenoble, France

Stefan R. Martin
Jet Propulsion Laboratory, California Institute of Technology, 4800 Oak Grove Drive, Pasadena CA 91109, USA

Dimitri Mawet
Jet Propulsion Laboratory, California Institute of Technology, 4800 Oak Grove Drive, Pasadena CA91109, USA

Denis Mourard
Observatoire de la Côte d'Azur, Avenue Copernic, 06130 Grasse, France

Claire Moutou
Laboratoire d'Astrophysique de Marseille (LAM), CNRS, Traverse du Siphon, BP 8, Les Trois Lucs, 13376 Marseille cedex 12, France

Laurent Mugnier
ONERA/DOTA, B.P. 72, F-92322 Châtillon cedex, France

Francesco Paresce
IASF-Bologna, INAF, Italy

Andreas Quirrenbach
ZAH, Landerssternwarte, Koenigstuhl, D-69117 Heidelberg, Germany

Yves Rabbia
Observatoire de la Cote d'Azur, Dpt GEMINI UMR CNRS 6203, Av Copernic, 06130 Grasse, France

John Raven
Division of Plant Sciences, University of Dundee at SCRI, Scottish Crop Research Institute, Invergowrie, Dundee DD2 5DA, UK

Huub J.A. Rottgering
Leiden Observatory, Leiden University, PO Box 9513, 2300 RA Leiden, The Netherlands

Daniel Rouan
LESIA - PHASE - Observatoire de Paris, 5 place Jules Janssen, F-92190 Meudon, France

Nuno Santos

Centro de Astrofisica, Universidade do Porto, Rua das Estrelas, 4150-762 Porto, Portugal

Franck Selsis
CRAL (CNRS UMR 5574), Université de Lyon, Ecole Supérieure de Lyon, 46 Allée d'Italie F-69007 Lyon, France

Eugene Serabyn
Jet Propulsion Laboratory, California Institute of Technology, 4800 Oak Grove Drive, Pasadena CA 91109, USA

Hiroshi Shibai
Graduate School of Science, Nagoya University, Furo-cho, Chikusa-ku, Nagoya 464-8602, Japan

Motohide Tamura
National Astronomical Observatory, Osawa 2-43-5, Mitaka, Tokyo 181-8588, Japan

Eric Thiébaut
Université Lyon 1, Villeurbanne, Centre de Recherche Astronomique de Lyon, Observatoire de Lyon, CNRS/UMR-5574, Ecole Normale Supérieure de Lyon, France

Frances Westall
Centre de Biophysique Moléculaire, CNRS, Rue Charles Sadron, 45071 Orléans cedex 2, France

Glenn White
Dept of Physics and Astronomy, The Open University, Walton Hall, Milton Keynes, MK7 6AA, UK
and Space Science and Technology Department, CCLRC Rutherford Appleton Laboratory, Chilton, Didcot, Oxfordshire, OX11 0QX, UK

ABSTRACT - The discovery of extra-solar planets is one of the greatest achievements of modern astronomy. The detection of planets with a wide range of masses demonstrates that extra-solar planets of low mass exist. In this paper we describe a mission, called *Darwin*, whose primary goal is the search for, and characterization of, terrestrial extrasolar planets and the search for life. Accomplishing the mission objectives will require collaborative science across disciplines including astrophysics, planetary sciences, chemistry and microbiology. *Darwin* is designed to detect and perform spectroscopic analysis of rocky planets similar to the Earth at mid-infrared wavelengths (6 to 20 μm), where the most advantageous contrast ratio between star and planet occurs. The baseline mission lasts 5 years and consists of approximately 200 individual target stars. Among these, 25 to 50 planetary systems can be studied spectroscopically, searching for gases such as CO_2, H_2O, CH_4 and O_3. Many of the key technologies required for the construction of *Darwin* have already been demonstrated and the remaining are estimated to be mature in the near future. *Darwin* is a mission that will ignite intense interest in both the research community and the wider public.

INTRODUCTION

Imaginative thoughts of worlds other than our own, perhaps inhabited by exotic creatures, have been an integral part of our history and culture. Some of the great intellects of classic civilization, such as Democritos of Abdera (460-371 BC), Epicurus of Samos (341-270 BC) and the medieval philosopher and theologian Giordano Bruno (1548-1600 AD) imagined habitable worlds around other stars than our sun (Crowe, 1986). These thinkers were following an ancient philosophical and theological tradition, but their ideas that we are not alone in the universe have had to wait for more than two thousand years for the possibility of observational or experimental evidence.

Our understanding of our place in the Universe changed dramatically in 1995, when Michel Mayor and Didier Queloz of Geneva Observatory announced the discovery of an extra-solar planet around a star similar to our Sun (Mayor and Queloz, 1995). Geoff Marcy and Paul Butler (2005) soon confirmed their discovery, and the science of observational extrasolar planetology was born. The field has exploded in the last dozen years, resulting in a large number of published planetary systems (see http://exoplanet.eu/ for an up-to-date list).

Many of these systems contain one or more gas giant planets very close to their parent star (0.02-0.1AU), and thus do not resemble our Solar System. Although very interesting, they do not directly address the possibility of other worlds like our own. Observational techniques continue to mature, however, and planets with a size and mass similar to the Earth may soon be within reach. “Super-Earths” are several times more massive than our planet and some might have life-supporting atmospheres (Lovis *et al*., 2006; Selsis *et al*., 2007a, Tinetti *et al*., 2007, Kaltenegger *et al*., 2008b). Recent examples of super-Earths are Gl 581c, GL 581d (Udry *et al*., 2007, Selsis *et al*., 2007c) and GJ 436b (Butler *et al.* 2004).

Finding Earth analogues in terms of mass and size will be the focus of many ground and space-based research programmes in the coming decade. Finding evidence of habitability and life represents an even more exciting challenge. Semi-empirical estimates exist of the abundance of terrestrial planets, including the frequency of life and technologically advanced civilizations. Some of these assessments are based on the Drake equation. Unfortunately, they are only educated guesses, not because the equation *per se* is incorrect, but rather because nearly all of its factors are essentially undetermined due to the lack of observational tests. Thus, the basic questions remain open: “Are there planets like our Earth out there?” and “Do any of them harbour life?”. In a recent article, G. Bignami (2007) stated: "Finding signatures of life on another (unreachable) planet will be the most important scientific discovery of all times, and a philosophical turning point. It will make clear to everyone that science and exploration eventually pay off, that it is only through the intuition of science (and its associated pigheadedness) that we understand our place among the stars."

To characterize terrestrial exoplanets, we need to detect their light and analyse it by spectroscopy. In two spectral domains, the star to planet contrast ratio is most favourable for an Earth-like planet - in the visible where the planet reflects stellar light, and the thermal infra-red (IR) where the planet emits thermal radiation. To extract the faint signal of a terrestrial planet from the associated large flux from its star the planet must be spatially resolved. Considering this constraint in the thermal IR, an interferometer with collectors carried by formation flying spacecraft with baselines adjustable from 20 m to ~ 200 m has been identified as the best suited instrument. The need to carry out these observations from space results from many factors, including the opacity of our atmosphere in several of the key spectral bands where one would want to observe gases as H_2O, O_3 and CO_2. Building on the

pioneering efforts of Bracewell (1978) and Angel (1990), a team of European researchers proposed the *Darwin* concept to ESA in 1993 (Léger *et al*.,1996) and it has been studying it since. NASA has been advancing a similar concept, the Terrestrial Planet Finder Interferometer (TPF-I), since 1996 (Beichman *et al*., 1999). The present *Darwin* concept represents the cumulative effort and synthesis of these studies.

This paper describes the science programme and some of the technological requirements for an ambitious space mission to discover and characterize Earth-like planets and to search for evidence of life on them. The *Darwin* mission will address one of the most fundamental questions: humankind’s origin and place in the Universe.

THE *DARWIN* SCIENCE PROGRAM

Searching for a phenomenon as subtle as life across parsecs of empty space may look hopeless at first glance, but considerable observational, laboratory, and theoretical effort over the past two decades is leading to the consensus that this is feasible in the near future.

To approach the observational challenge of searching for life we must first address the question, ‘what is life?’ A living being is a system that contains information and is able to replicate and evolve through random mutation and natural (*Darwin*ian) selection (Brack, 2007). Although this definition appears overly generic (for example, it includes some computer viruses), consideration of possible storage media for life’s information leads to a number of specific conclusions.

Macromolecules appear to be an excellent choice for information storage, replication, and evolution in a natural environment. Specifically, carbon chemistry is by far the richest and most flexible chemistry. The need for rapid reaction rates between macromolecules argues for a liquid solution medium. Based on physical and chemical properties as well as abundances in the universe, the most favourable, although not necessary unique, path for life to take is carbon chemistry in water solution (Owen, 1980). Our search for signs of life is therefore based on the assumption that extraterrestrial life shares fundamental characteristics with life on Earth, in that it requires liquid water as a solvent and has a carbon-based chemistry (Owen, 1980; Des Marais *et al*., 2002). Such chemistry produces a number of detectable gaseous biological indicators in the planet's atmosphere. We assume that extraterrestrial life is similar to life on Earth in its use of the same input and output gases, that it exists out of thermodynamic equilibrium, and that it has analogs to microorganisms on Earth (Lovelock, 1975, 2000). This assumption is currently necessary because we have no test cases for entirely novel types of life, although any gases out of geochemical equilibrium in a planetary atmosphere might suggest the presence of life.

The logic of the *Darwin* science program follows directly: to search for habitable planets – those where liquid water can exist – and investigate their atmospheres for biosignatures, the gas products known to be produced by the carbon macromolecule chemistry we call life.

The scientific context

Since the discovery of a planet orbiting the star 51 Pegasi (Mayor and Queloz, 1995), many planets outside our own Solar System have been discovered. These planets are found in a variety of environments. The majority of these have gas giant masses that cover masses in the

range 20 – 3 000 $M_{\oplus}$. Many of them are either in highly eccentric or very small (0.1 - 0.02 AU) orbits (Udry and Santos, 2007). The latter have surface temperatures up to 2 000 K, and are hence known as "Hot Jupiters".

The existence of Hot Jupiters can be explained by inward migration of planets formed at larger distances from their star, most likely due to tidal interactions with the circumstellar disk. We have also learned that giant planets preferentially form around higher metallicity stars: almost 15% of solar-type stars with metallicity greater than 1/3 that of the Sun possess at least one planet of Saturn mass or larger (Santos *et al.*, 2004; Fischer and Valenti, 2005).

Despite best efforts, no Earth-mass planet around a normal star has yet been found because of biases towards high mass planets and sensitivity limitations for planet searches from the ground; the lowest mass exoplanets range from 5 to 7 $M_{\oplus}$.

Planets form within disks of dust and gas orbiting newly born stars. Even though not all aspects are yet understood, growth from micrometer dust grains to planetary embryos through collisions is believed to be the key mechanism leading to the formation of at least terrestrial planets, and possibly the cores of gas giants (Wetherill and Stewart, 1989; Pollack *et al.*, 1996).

As these cores grow, they eventually become massive enough to gravitationally bind nebular gas. While this gas accretion proceeds slowly in the early phases, it eventually leads to a runaway buildup of material, once a critical mass has been reached (~10 M_{Earth}), allowing the formation of a gas giant within the lifetime of the gaseous disk (Pollack *et al.*, 1996). Terrestrial embryos, being closer to the star, have less material available and hence they

empty their feeding zone before growing massive. They must then rely on distant gravitational perturbations to induce further collisions. As a result, the growth of terrestrial planets occurs on longer timescales than for the giants.

Extended core-accretion models (Alibert *et al.*, 2005) can now be used to compute synthetic planet populations, allowing a statistical comparison with observations (see Fig. 1; Ida and Lin, 2004; Benz *et al.*, 2007). While these models are not specific to terrestrial planets (they are initialized with a seed of 0.6 $M_{\oplus}$), they demonstrate that if planetary embryos can form, only a small fraction of them will grow fast enough and big enough to eventually become giant planets. Given that we detect gas giants orbiting about 7% of the stars surveyed, *Darwin*'s harvest of terrestrial planets should be very significant.

Habitability

The circumstellar Habitable Zone (HZ) (Kasting *et al.*, 1993) is defined as the annulus around the star within which starlight is sufficiently intense to maintain liquid water at the surface of the planet (here we do consider liquid water outside this classical habitable zone, such as on Europa-like moons, as these would not be detected by Darwin. Nevertheless one should note here the potential for liquid water on planetary bodies outside this classical definition of the habitable zone). The inside boundary of the habitable zone is generally set by the location where a runaway greenhouse condition causes dissociation of water and sustains the loss of hydrogen to space and the outer zone is where a maximum greenhouse effect keeps the surface of the planet above the freezing point on the outer edge. In this paper, this inner zone is taken to be 0.84 AU as a conservative estimate, although clouds and water vapour could extent the habitable zone further in. The defined HZ around a certain star

implicitly assumes that habitability requires planets of the size and mass similar to the Earth, with large amounts of liquid water on the surfaces, and having CO_2 reservoirs with CO_2-H_2O-N_2 atmospheres (Selsis *et al.*, 2007b). The Continuously HZ is the region that remains habitable for durations longer than 1 Gyr. Fig. 2. shows the limits of the HZ as a function of the stellar mass.

Planets inside the HZ are not necessarily habitable. They can be too small, like Mars, to maintain active geology and to limit the gravitational escape of their atmospheres. They can be too massive, like HD69830d, and have accreted a thick H_2-He envelope below which water cannot be liquid. However, planet formation models predict abundant Earth-like planets with the right range of masses (0.5 - 8 $M_{\oplus}$) and water abundances (0.01-10% by mass) (Raymond *et al.*, 2006, 2007a).

To know whether a planet in the HZ is actually inhabited, we need to search for biosignatures, features that are specific to biological activities and can be detected by remote sensing. An example is O_2-producing photosynthesis. Owen (1980) suggested searching for O_2 as a tracer of life. In the particular case of Earth, most O_2 is produced by the biosphere. Less than 1 ppm comes from abiotic processes (Walker, 1977). Cyanobacteria, algae and plants are responsible for this production by using solar photons to drive the electron transport chain using water as an electron donor resulting in the production of oxygen (and generating organic molecules from CO_2 in associated dark reactions). This metabolism is called oxygenic photosynthesis. The reverse reaction, using O_2 to oxidize the organics produced by photosynthesis, can occur abiotically when organics are exposed to free oxygen, or biologically by respiration consuming organics. Because of this balance, the net release of O_2 in the atmosphere is due to the burial of organics in sediments. Each reduced carbon

buried frees an O_2 molecule in the atmosphere. This net release rate is also balanced by weathering of fossilized carbon when exposed to the surface. The oxidation of reduced volcanic gasses such as H_2, H_2S also accounts for a significant fraction of the oxygen losses. The atmospheric oxygen is recycled through respiration and photosynthesis in less than 10,000 yrs. In the case of a total extinction of Earth biosphere, the atmospheric O_2 would disappear in a few million years.

Chemolithotrophic life, thriving in the interior of the planet without using stellar light, can still exist outside (as well as inside) the HZ. The associated metabolisms – at least the ones we know on Earth – do not produce oxygen. By comparison, the energy and electron donors for photosynthesis, sunlight and water respectively, are widely distributed, yield larger biological productivity and can modify a whole planetary environment in a detectable way (Léger *et al.*, 1993; Wolstencroft and Raven, 2002; Raven and Wolstencroft, 2004, Kiang *et al.*, 2007a,b). Light sources to sustain photosynthesis are likely to be widely available in different planetary systems (Raven and Cockell, 2006), albeit they also are associated with different and potentially more hostile ultraviolet (UV) radiation regimens (Kasting *et al.*, 1997; Cockell, 1999; Segura *et al.*, 2003). For these reasons, searching for oxygenic photosynthesis is a restricted way to search for life on planets within the HZ of their stars, but it is based on empirical free energy considerations concerning the likely impact on atmospheric composition. Most importantly, it is a search that can be done by remote sensing, looking for spectroscopic signatures of O_2 or its tracers e.g. O_3.

Search for biosignatures

The range of characteristics of planets found in the HZ of their star is likely to greatly exceed our experience with the planets and satellites in our Solar System. In order to study the habitability of the planets detected by *Darwin*, and to ascertain the biological origin of the measured atmospheric composition, we need a comprehensive picture of the observed planet and its atmosphere.

In addition to providing a more favourable planet-star contrast and potential biosignatures, the mid-IR (MIR) wavelength domain provides crucial chemical, physical and climatic diagnostics, even at moderate spectral resolution. For example, the infrared light curve, i.e. the variation of the integrated thermal emission with location on the orbit, reveals whether the detected planet possesses a dense atmosphere, suitable for life, which strongly reduces the day/night temperature difference.

A low-resolution spectrum spanning the 6-20 μm region allows us to measure the effective temperature T_{eff} of the planet, and thus derive its radius R_{pl} and albedo (see section 'Mission performance'). Low-resolution mid-IR observations will also reveal the existence of greenhouse gases, including CO_2 and H_2O.

Within the HZ, the partial pressure of CO_2 and H_2O at the surface of an Earth-analogue is a function of the distance from the star. Water vapour is a major constituent of the atmosphere for planets between 0.84 AU and 0.95 AU. Fig. 3. shows the estimated evolution of the H_2O, O_3 and CO_2 features in the spectra of an Earth-like planet as a function of its location in the HZ. Carbon dioxide is a tracer for the inner region of the HZ and becomes an abundant gas further out (Kaltenegger and Selsis, 2007, Selsis *et al.*, 2007b).

Planets such as Venus, closer to their star than the HZ, can lose their water reservoir and accumulate a thick CO_2 atmosphere. Such planets can be identified by the absence of water and by the CO_2 absorption bands between 9 and 11 μm, which only show up in the spectrum at high CO_2 mixing ratios. These conditions would suggest an uninhabitable surface.

Darwin will test the theory of habitability indicators versus orbital distance by correlating the planets' spectral signature with orbital distance and comparing the results with grids of theoretical spectra, such as those shown in Fig. 3.

Fig. 4. shows that the mid-IR spectrum of Earth displays the 9.6 μm O_3 band, the 15 μm CO_2 band, the 6.3 μm H_2O band and the H_2O rotational band that extends beyond 12 μm. The Earth's spectrum is clearly distinct from that of Mars and Venus, which display the CO_2 feature only. Fig 5. illustrates the physical basis behind the spectra shown in Fig 4.

The combined appearance of the O_3, H_2O, and CO_2 absorption bands is the most well-studied signature of biological activity (Léger *et al.*, 1993; Schindler and Kasting, 2000; Selsis *et al.*, 2002; Des Marais *et al*., 2002; Segura *et al*., 2007). Despite variations in line shape and depth, atmospheric models demonstrate that these bands could be readily detected with a spectral resolution of 10–25 in Earth analogues covering a broad range of ages and stellar hosts (Selsis, 2000; Segura *et al*., 2003; Kaltenegger *et al.*, 2007).

The ozone absorption band is observable for O_2 concentrations higher than 0.1% of the present terrestrial atmospheric level (Segura *et al*., 2003). The Earth's spectrum has displayed this feature for the past 2.5 Gyr.

Other spectral features of potential biological interest include methane (CH_4 at 7.4 μm), and species released as a consequence of biological fixation of nitrogen, such as ammonia (NH_3 at 6 and 9-11 μm) and nitrous oxide (N_2O at 7.8, 8.5 and 17 μm). The presence of these compounds would be difficult to explain in the absence of biological processes. Methane and ammonia commonly appear in cold hydrogen-rich atmospheres, but they are not expected as abiotic constituents of Earth-size planetary atmospheres at habitable orbital distances.

Methane, ammoni and nitrous oxide do not produce measurable spectral signatures at low resolution for an exact Earth analogue. Nevertheless, they may reach observable concentrations in the atmosphere of exoplanets, due either to differences in the biosphere and the planetary environment, or because the planet is observed at a different evolutionary phase, as illustrated in Fig. 6. Methane, for instance, was most likely maintained at observable concentrations for more than 2.7 Gyrs of Earth's history from about 3.5 until 0.8 Gyrs ago (Pavlov *et al*., 2003). During the 1.5 Gyrs following the rise of oxygen (2.4 Gyrs ago), the spectrum of the Earth featured deep methane absorption simultaneously with ozone. The detection of reduced species, such as CH_4 or NH_3, together with O_3, is another robust indicator of biological activity (Lovelock, 1975, 2000; Sagan *et al*., 1993).

The presence of H_2O, together with reduced species such as CH_4 or NH_3, would also be indicative of a possible biological origin. Although a purely abiotic scenario could produce this mix of gases, such a planet would represent an important astrobiological target for future study. The presence of nitrous oxide (N_2O) and, more generally, any composition that cannot be reproduced by a self-consistent abiotic atmosphere model would merit follow-up.

Finally, if biology is involved in the geochemical cycles controlling atmospheric composition, as on Earth, greenhouse gases will likely be affected and sustained at a level compatible with a habitable climate. Whatever the nature of these greenhouse gases, *Darwin* will be able to see their effect by analyzing the planet's thermal emission. This is a powerful way to give the instrument the ability to characterize unexpected worlds.

COMPARATIVE (EXO) PLANETOLOGY

Over the decade since the discovery of 51 Peg, we have grown to understand that planetary systems can be much more diverse than originally expected (Udry and Santos, 2007). It is also clear that the current group of extrasolar planets, although diverse, is incomplete: as observational techniques have improved, we have pushed the lower limit of the detected masses closer and closer to the terrestrial range. In the coming decade, this trend will continue, and our understanding of the diversity of lower mass planets will be critical to the understanding of the formation of terrestrial planets in general, and of the Earth in particular.

Growing the sample of terrestrial planets from the three in our solar system to a statistically significant sample will represent a quantum leap in knowledge. And, just as 51 Peg created the discipline of observational extrasolar planetology, this effort will encompass a new type of science: comparative exoplanetology for both the giant and terrestrial planets. It will allow for the first time a comparison of the orbital, physical and chemical characteristics of full planetary systems with our solar system and model predictions (Selsis *et al.*, 2007b).

Finally, this sample will also allow help answer one of the key questions related to *Darwin* science: How frequently are planets, which are located in or near the HZ, truly habitable?

Darwin can determine the radius, but not the mass, of planets. Ground-based radial velocity measurements can provide this information, however. The estimated error in mass determination is a function of planet mass, stellar type, visual magnitude, etc. Achieving adequate mass accuracy will be possible with instruments such as HARPS on 8-meter class telescopes for a fraction of the discovered planets (Li *et al.*, 2008). Large planets, e.g. 2 – 5 M_{Earth}, around small stars that are nearby and therefore bright – mainly M and K stars - are the best candidates.

The origin and evolution of liquid water on the Earth is an ideal example of the type of puzzle that comparative exoplanetology will address. Our planet orbits in the Habitable Zone of our star, but at least some of the water on Earth must have been delivered by primordial icy planetesimal and/or water rich chondritic meteorites.

Did the early Earth capture these objects when they wandered into the inner solar system, or did our planet itself form further out and migrate inward? The answer is not clear at this point. What is clear is that habitability cannot just be reduced to a question of present-day location. The origin and fate of the water reservoir within the proto-planetary nebula is equally important.

By necessity, we have until now addressed this question using the very restricted sample of terrestrial planets in our own solar system: Venus, Earth and Mars. What have we learned? The in situ exploration of Mars and Venus taught us that all three planets probably evolved

from relatively similar initial atmospheric conditions, most probably including a primordial liquid water reservoir. In all three cases, a thick CO_2 atmosphere and its associated greenhouse effect raised the surface temperature above the classical radiative equilibrium level associated with their distance to the Sun. This atmospheric greenhouse effect was critical for habitability on Earth at a time when the young Sun was approximately 30% fainter than it is today (Newman and Rood, 1977; Gough, 1981)

At some point in the past, the evolutionary paths of Venus, Earth, and Mars began to diverge. For Venus, the combination of the greenhouse effect and a progressively hotter Sun led to the vaporization of all liquid water into the atmosphere, assuming a similar water reservoir as Earth. After upward diffusion, H_2O was dissociated by UV radiation, causing the loss of hydrogen to space by gravitational escape and erosion.Venus is today a hot, dry, and uninhabitable planet.

In contrast, Mars apparently experienced a 500 million year episode with a warmer, wetter climate, before atmospheric loss and a steady decrease in surface temperature trapped the remaining water reservoir in the polar ice caps and subsurface permafrost. Thus, Mars retained a fraction of its water reservoir.

Earth apparently followed an intermediate and complex evolutionary path, which maintained its habitability for much of the past 4.6 Gyrs. Early on, a thick CO_2 atmosphere, possibly combined with other greenhouse gases, compensated for the young Sun's low luminosity, and, as the Sun brightened, atmospheric CO_2 was progressively segregated into carbonate rocks by the combined action of the water cycle, erosion, sedimentation of carbonate deposits on the ocean floors, and partial recycling via plate tectonics. This feedback cycle, which

appears unique in the Solar System, accounts for the preservation of Earth's oceans and habitability throughout most of its history (Kasting and Catling, 2003).

Although the general definition of the HZ can be applied to all stellar spectral types one can expect that the evolution of the atmospheres of terrestrial planets within the HZs of lower mass M and K-type stars is different. These planets have closer orbital locations and experience denser stellar plasma environments (winds, Coronal Mass Ejections) (Khodachenko *et al*., 2007; Lammer *et al*., 2007; Scalo *et al*., 2007). These stars have longer active strong X-ray and extreme UV periods compared to solar-like stars. In addition, planets in orbital locations inside the HZ of low mass stars can be partially or totally tidal-locked, which could result in different climate conditions, and weaker magnetic dynamos important for protecting the atmosphere against erosion by the stellar plasma flow. These differences compared to G-star HZ planets raise questions regarding atmospheric escape, plate tectonics, magnetic dynamo generation and the possibility of complex biospheres (Grießmeier *et al*., 2005).

Terrestrial planets with no analogue in the Solar System may exist. For example, the recently proposed Ocean-Planets, which consist of 50% silicates and 50% water in mass (Léger *et al*., 2004; Selsis *et al*., 2007a), could form further out than the distance from the star where water vapour condenses (~ 4 AU around a G dwarf) and migrate to the HZ, or closer. Such objects would be a new class of planets, the terrestrial analogues of hot Jupiters and Neptunes. If these planets happen to exist, *Darwin* will be able to characterize them in detail, e.g. determining their atmospheric compositions.

With *Darwin*, the sample of terrestrial planets will be extended to our galactic neighbourhood, allowing us to study the relationship between spectral characteristics and three families of parameters:

- Stellar characteristics, including spectral type, metallicity, and if possible, age; our Solar System illustrates the importance of understanding the co-evolution of each candidate habitable planet and its star.
- Planetary system characteristics, particularly the distribution and the orbital characteristics of terrestrial and gas giant planets.
- The atmospheric composition of planets in the HZ. Here again, the solar system sample points to the importance of ascertaining the relative abundance of the main volatile species: CO_2, CH_4, H_2O, O_3, NH_3, etc.

The strategy for comparative exoplanetology will be as follows: First, a comparison of stellar characteristics with the nature of the planetary system will capture the diversity of planetary systems. Then, *Darwin*'s spectroscopic data will reveal the range of atmospheric compositions in the Habitable Zone, a range that will be related to the initial chemical conditions in the proto-planetary nebula and, if stellar ages are available, to the effects of atmospheric evolution.

Correlating the general characteristics of the planetary system with the atmospheres of the individual planets will illuminate the interplay between gas giants and terrestrial bodies and the role of migration. For example, recent numerical simulations predict that the scattering effect of giant planets on the population of planetesimals plays a key role in the collisional

growth of terrestrial planets, their chemical composition and the build-up of their initial water reservoir (Raymond *et al.*, 2006b).

Thus, *Darwin* will allow us to address the question of habitability from the complementary perspectives of the location of Earth-like planets with respect to their HZ, and of the origin, diversity and evolution of their water reservoirs.

HIGH ANGULAR RESOLUTION ASTRONOMY WITH *DARWIN*

Darwin's long interferometric baselines and large collecting area make it a powerful instrument for general astrophysics. The mission combines the sensitivity of JWST (James Webb Space Telescope, Gardner et al. 2006) with the angular resolution of VLTI (Very Large Telescope Interferometer, Schöller *et al*., 2006) in an instrument unencumbered by atmospheric opacity and thermal background.

The baseline instrumentation in *Darwin* will be able to observe general astrophysics targets whenever there is a bright point source, e.g. a non-resolved star in the field of view. This source is necessary to cophase the input pupils. Some science programs will profit from just a few visibility measurements, while others will require numerous observations and complete aperture synthesis image reconstruction.

Taking full advantage of interferometric imaging with *Darwin* – that is observing any source on the sky – will require specialized and potentially costly add-on instrumentation to allow the cophasing of the array. General astrophysics is not the primary science mission. However, it should be remembered that general astrophysical studies can in themselves improve our

understanding of the astrobiological environment for life and the nature of stars around which life might exist. Therefore, for completeness, it is useful here to briefly summarise some of these other astrophysical goals.

Star Formation

Stars are the fundamental building blocks of the baryonic universe. They provide the stable environment needed for the formation of planetary systems and thus, for the evolution of life. *Darwin* will impact our understanding of star formation in fundamental ways, for instance the 'Jet-Disk Connection'. Forming stars launch powerful jets and bipolar outflows along the circumstellar disk rotation axis (Shu *et al*., 1987; Reipurth and Bally, 2001). The mission could reveal the nature of the driving mechanism by spatially resolving the jet-launching region. Are jets formed by ordinary stellar winds, the magnetic X-points where stellar magnetospheres interact with the circumstellar disk, or are they launched by magnetic fields entrained or dynamo-amplified in the disk itself?

Planet Formation

Theory predicts that planets form in circumstellar disks over a period of 10^6 to 10^8 years (Pollack *et al*., 1996; Boss, 1997). *Darwin* can provide detailed information about planetary systems at various stages of their evolution, revealing the origin of planetary systems such as our own, and thus helping to place our solar system into context. The mission will be unique in being able to spatially resolve structures below 1 AU in nearby star forming regions, allowing us to witness directly the formation of terrestrial planets in the thermal IR. Additional planet formation science includes:

- *Disk formation and evolution.* *Darwin* will place constraints on the overall disk structure. The mission measurements will directly constrain grain growth, settling, and

mixing processes in the planet-forming region (see for example, Hollenbach et al. 2000; Rieke *et al*., 2005).

- *Disk Gaps within the Inner Few AU.* The mid-IR spectral energy distribution of protoplanetary and debris disks points to the existence of gaps. *Darwin* will determine if this clearing is due to the influence of already-formed giant planets or if they are the result of viscous evolution, photo-evaporation, and dust grain growth (see, for example, Dominik and Decin, 2003; Throop and Bally, 2005).

Formation, Evolution, and Growth of Massive Black Holes

How do black holes (BH) form in galaxies? Do they form first, and trigger the birth of galaxies around them, or do galaxies form first and stimulate the formation of BHs? How do BHs grow? Do they grow via mergers as galaxies collide? Or do they accumulate their mass by hydrodynamic accretion from surrounding gas and stars in a single galaxy? *Darwin* could probe the immediate environments of very different BHs, ranging from very massive BHs in different types of active galactic nuclei (AGN), to the massive black hole at the centre of our own Milky Way, down to BHs associated with stellar remnants.

Darwin will be able to make exquisite maps of the distribution of silicate dust, ices, and polycyclic aromatic hydrocarbons (PAHs) in weak AGN such as NGC 1068 out to a redshift of z=1-2. Brighter AGN can be mapped to a redshift of z=10, if they exist. For the first time, we will be able to measure how the composition, heating, and dynamics of the dust disks change with redshift (Dwek, 1998; Edmunds, 2001). This will provide a clear picture of when and how these tori and their associated massive BHs grow during the epoch of galaxy formation (Granato *et al*., 1997).

The Galactic centre: The centre of our Galaxy contains the nearest massive black hole (3.6 x 10^6 M⊙)(e.g., Ghez *et al*., 2005) , a uniquely dense star cluster containing more that 10^7 stars pc^{-3}, and a remarkable group of high-mass stars (e.g., IRc7, Yusef-Zadeh and Morris, 1991). *Darwin* will be able to trace the distribution of lower mass stars and probe the distribution of dust and plasma in the immediate vicinity of the central BH.

Galaxy Formation & Evolution

Galaxy evolution is a complicated process, in which gravity, hydrodynamics, and radiative heating and cooling all play a fundamental role (Dwek, 1998; Edmunds, 2001). Measurements of the detailed spatial structure of very distant galaxies will place essential constraints on galaxy formation models. Unlike JWST, *Darwin* will be able to resolve individual OB associations, massive star clusters, and their associated giant HII regions. By carefully selecting targets of a specific type, we can trace the evolution of galaxy structure as a function of redshift and environment (Franx *et al*., 2003; Labbé *et al*., 2005). The evolution of metallicity with cosmic age and redshift can be mapped using various diagnostics, including molecular tracers, ices, PAH bands, and noble gas lines that are in the (6 – 20 μm) band (e.g. Moorwood *et al*., 1996; Soifer *et al*., 2004). Fig. 7 shows an example of the mapping power of the mission.

The First Generation of Stars

The first stars formed in the early universe are thought to be quite different from the stars present today. The absence of metals reduced the opacity, allowing the first generation of stars to accumulate more gas and hence be considerably more massive (100 to 1000 M⊙) and hotter than their modern counterparts (Brom *et al*., 1999; Tumlinson and Shull, 2000). The first stars must have had a dramatic impact on their environment, creating giant HII regions

whose red-shifted hydrogen and helium emission lines should be readily observable by *Darwin*. While JWST is expected to make the first detections of galaxies containing these "Population III" stars (e.g., Gardner *et al*., 2006), *Darwin* will be capable of resolving scales of order 10 to 100 pc at all redshifts, providing the hundred-fold gain needed to resolve these primordial HII regions. *Darwin* will also be able to test the current paradigm for the formation of the first stars. Are they truly isolated, single objects that have inhibited the formation of other stars in their vicinity, or are they surrounded by young clusters of stars?

Other Important Science

The mission general astrophysics program could include a number of additional key science programmes:

- *Our home planetary system:* *Darwin* will be able to easily measure the diameters, and properties of Kuiper Belt Objects, moons, asteroids, and cometary nuclei. Low-resolution spectro-photometry will constrain the natures of their surfaces, atmospheres, and environments.
- *AGB stars:* *Darwin* can provide detailed maps of the distribution of dust and gas within the envelopes of oxygen-rich (M-type) and carbon-rich (C-type) AGB stars, in environments as extreme as the Galactic centre.
- *Supernovae:* *Darwin* could image the formation and evolution of dust, atoms and ions in supernova ejecta, and trace the structure of the circumstellar environment into which the blast is propagating.
- *Dark matter & dark energy:* *Darwin* studies of gravitational lensing by galaxy clusters, AGN, and ordinary galaxies could place unprecedented constraints on the structure of dark matter haloes at sub-kpc scales.

SYNERGIES WITH OTHER DISCIPLINES

The primary *Darwin* science objective is inherently multi-disciplinary in character, uniting astronomy with chemistry, geology, physics and branches of biology, including microbiology. Often referred to as astrobiology, this interdisciplinary field also includes molecular biology, celestial mechanics and planetary science, including the physics and chemistry of planetary atmospheres and the characterization of exoplanetary surfaces. Climatologists and ecologists will have the opportunity to study global climate influences within the context of a statistically large number of other terrestrial planets. Of particular interest will be an understanding of the diversity of Venus-like planets undergoing runaway greenhouse changes. On the technological front, the mission will drive development in such widely differing fields as material sciences, optical design, and spacecraft Formation Flying.

THE *DARWIN* MISSION PROFILE

Baseline Mission Scope

The *Darwin* mission consists of two phases: the search for and spectral characterization of habitable planets, whose relative duration can be adjusted to optimize scientific return. During the search phase (nominally 2 yrs), the mission will examine nearby stars for evidence of terrestrial planets. An identified planet should be observed at least 3 times during the mission in order to characterize its orbit. The number of stars that can be searched depends on the level of zodiacal light in the system and the diameter of the collector telescopes. As a baseline, we estimate this number under the assumption of a mean exozodiacal density 3 times that in the Solar System and collecting diameters of 2 m. Over

200 stars can be screened under these conditions. The mission focuses on Solar type stars which are long-lived, i.e., F, G, K and some M spectral types (Kaltenegger *et al*., 2008a).

The number of expected planetary detections depends upon the mean number of terrestrial planets in the HZ per star, η_{Earth}. Our present understanding of terrestrial planet formation and our Solar System, where there are 2 such planets (Earth & Mars) and one close to the HZ (Venus), point to a fairly high abundance of terrestrial planets. We assume hereafter that $\eta_{Earth} = 1$ for simulations. The COROT mission should reveal the abundance of small hot planets, and *Kepler* will evaluate η_{Earth} as well as the size distribution of these objects several years before *Darwin* flies. These inputs will allow refinement of *Darwin*'s observing strategy well in advance of launch.

During the characterization phase of the mission (nominally 3 yrs), *Darwin* will acquire spectra of each detected planet at a nominal resolution of 25 and with sufficient signal-to-noise (~10) to measure the equivalent widths of CO_2, H_2O, and O_3 with a precision of 20% if they are in abundances similar to those in the present-day Earth atmosphere.

Spectroscopy is more time consuming than detection. Assuming $\eta_{Earth} = 1$, *Darwin* can perform spectroscopy of CO_2 and O_3 on about 50 earth-analogues and of H_2O on about 25 during the nominal 3-year characterization phase.

The general astrophysics program, if adopted, will comprise 10% to 20% of the mission time. The primary science segment would then be reduced accordingly, with limited impact on its outcome.

Extended Mission Scope

An extension of the mission to 10 years will depend on the results gathered during the first 5 years. Such an extension could be valuable to observe more M stars; only 10% of the baseline time is attributed to them currently. As they are the most stable stars, the chances for habitable planets are good (Tarter *et al.*, 2007). An extension would also allow for more observation of large planets around a significantly larger sample of stars. A major reason to extend the mission will be to make additional measurements on the most interesting targets already studied and to expand the range of masses and environments explored.

Darwin Target Catalogue.

The *Darwin* target star catalogue (Kaltenegger, 2005; Kaltenegger *et al*., 2008a) is generated from the Hipparcos catalogue by examining the distance (< 30 pc), brightness, spectral type (F, G , K, M main sequence stars), and multiplicity (no companion). The catalogue has considered different interferometer architectures, since they have different sky access. The Emma design can observe 99% of the sky (see below). The corresponding star catalogue contains 1256 single target stars within 30pc, 414 of the 1256 target stars are M stars, 515 are K stars, 218 are G stars and 109 are F stars. Of the 1256 stars, 36 are known to host exo-planets. Fig. 8 shows some features of these stars.

DARWIN MISSION DESIGN

The Darwin Concept and Its Evolution

In order to disentangle the faint emission of an Earth-like planet from the overwhelming flux of its host star, the planetary system needs to be spatially resolved. This, in turn, requires an monolithic telescope up to 100 m in diameter when operating at mid-IR wavelengths since the angular size of the Habitable Zones around *Darwin* target stars ranges between 10 and 100 milliarcseconds (mas, see Fig. 8). A telescope of this size is presently not feasible, particularly since the observatory must be space-borne and cooled to provide continuous coverage and sensitivity between 6 and 20 μm.

As a result, interferometry has been identified as the best-suited technique to achieve mid-IR spectroscopy of Earth-like planets around nearby stars. In his pioneering paper, Bracewell (1978) suggested that applying a π phase shift between the light collected by two telescopes could be used to cancel out the on-axis star, while allowing the signal from an off-axis planet to pass through (Fig. 9). This technique, referred to as *nulling interferometry*, has been at the heart of the *Darwin* concept since its origin (Léger *et al.*, 1996) and many improvements have been studied since that date.

In addition to the planetary flux, a number of spurious sources contribute to the signal at the destructive output of the Bracewell interferometer (Mennesson *et al.*, 2005; Absil *et al*., 2006):

- Residual star light, referred to as *stellar leakage*, caused by the finite size of the stellar photosphere (geometric leakage) and by the imperfect control of the interferometer (instrumental leakage);
- The *local zodiacal background*, produced by the disk of warm dust particles that surround our Sun and radiate at infrared wavelengths;
- The *exozodiacal light*, arising from the dust disk around the target star;

- The *instrumental background* produced by thermal emission within the instrument.

Bracewell's original suggestion of rotating the array of telescopes can help disentangle the various contributions. The planet signal would then be temporally modulated by alternatively crossing high and low transmission regions, while the stellar signal and the background emission remain constant (except for the exozodiacal emission). Unfortunately, this level of modulation is not sufficient to achieve *Darwin's* goals, prompting a series of improvements to the strategy, including:

- Breaking the symmetry of the array to cancel all centro-symmetric sources, including the geometric stellar leakage, the local and exozodiacal emissions;
- Performing faster modulation of the planet signal via phase modulation between the outputs of sub-interferometers.

Merging of these two ideas has led to the concept of *phase chopping* (Woolf & Angel, 1997; Mennesson *et al*., 2005) which is now regarded as a mandatory feature in space-based nulling interferometry. The simplest implementation of phase chopping is illustrated in Fig. 10: the outputs of two Bracewell interferometers are combined with opposite phase shifts ($\pm\pi/2$) to produce two "chopped states," which are mirrored with respect to the optical axis. Taking the difference of the photon rates obtained in the two chopped states gives the chopped response of the array, represented by the modulation map. This chopping process removes all centro-symmetric sources, including the geometric stellar leakage and the exozodiacal emission.

Because the modulation efficiency varies across the field-of-view, the planet can only be localised and characterised through an additional level of modulation, provided by array rotation with a typical period of one day. The collected data, consisting in time series of detected photo-electrons at the destructive and constructive outputs of the interferometer,

must be inverted to obtain the fluxes and locations of any planets that are present. The most common approach is correlation mapping, which is closely related to the Fourier transform used for standard image synthesis. The result is a correlation map, which represents the point spread function (PSF) of the array (Fig 10).

This process is repeated across the waveband, and the maps are co-added to obtain the net correlation map. The broad range of wavelengths planned for *Darwin* greatly extends the spatial frequency coverage of the array, suppressing the side lobes of the PSF.

A dozen array configurations using phase chopping have been proposed and studied during the past decade (Mennesson and Mariotti, 1997; Karlsson and Mennesson, 2000; Absil *et al.*, 2003; Karlsson *et al.*, 2004; Kaltenegger and Karlsson, 2004; Lay, 2005; Mennesson *et al.*, 2005). In 2004, the ESA and NASA agreed on common figures of merit to evaluate their performance. The most important criteria are the modulation efficiency of the beam combination scheme, the structure of the PSF and its associated ability to handle multiple planets, the overall complexity of beam routing and combination, and finally, the number of stars that can be surveyed during the mission lifetime (Lay, 2005).

Mission Architecture

The desire for maximum mission efficiency, technical simplicity, and the ability to detect multiple planets around as many stars as possible has guided the selection of mission architecture. Additional top-level requirements include:

- Placement at L2 for passive cooling and low ambient forces;
- Launch with a single Ariane 5 rocket or two Soyuz-ST/Fregat vehicles;

- The ability to search a statistically meaningful sample of nearby solar-type stars (~200) for the presence of habitable planets, assuming an exozodiacal background up to 10 zodi[1];
- The ability to detect and measure terrestrial atmosphere biosignatures for a significant fraction of the planets found during the search phase (at least 20);
- Time allocation during search phase as follows: G stars 50%, K stars 30%, F and M stars 10% each;
- Two observing modes: nulling for extrasolar planet detection and spectroscopy, and constructive imaging for general astrophysics.

The effort to turn these requirements into a workable mission culminated in 2005-2006 with two parallel assessment studies of the *Darwin* mission. Two array architectures have been thoroughly investigated during these studies: the 4-telescope X-array (Lay and Dubovitsky, 2004) and the 3-telescope TTN (Karlsson *et al*., 2004). These studies included the launch requirements, payload spacecraft, and the ground segment during which the actual mission science would be executed. Almost simultaneously, NASA/JPL initiated a similar study (Martin *et al*., 2007) in the context of the Terrestrial Planet Finder Interferometer (TPF-I).

These efforts on both sides of the Atlantic have resulted in a convergence and consensus on mission architecture. The baseline for *Darwin* is a *non-coplanar,* or *Emma*[2]-type X-array, with four Collector Spacecraft (CS) and a single Beam Combiner Spacecraft (BCS). This process also identified a back-up option, in case unforeseen technical obstacles appear: a planar X-array.

[1] A "zodi" is defined as the density of our local zodiacal dust disk and acts as a scaling factor for the integrated brightness of exozodiacal dust disks.
[2] Emma was the wife of Charles Darwin.

Fig. 11. shows the non-coplanar Emma X-array. Four simple collector spacecrafts fly in a rectangular formation and feed light to the beam combiner spacecraft located approximately 1200 m above the array. This arrangement allows baselines between 7 and 168 m for nulling measurements and up to 500 m for the general astrophysics program.

The X-array configuration separates the nulling and imaging functions (Fig 10), thus allowing independent optimal tuning of the shorter dimension of the array for starlight suppression and that of the longer dimension for resolving the planet (Lay and Dubovitsky, 2004; Lay, 2005). Most other configurations are partially degenerate for these functions. The X-array also lends itself naturally to techniques for removing instability noise, a key limit to the sensitivity of *Darwin* (Chazelas, 2006; Lay, 2004; 2006; Lane *et al*., 2006).

The assessment studies settled on an imaging to nulling baseline ratio of 3:1, based on scientific and instrument design constraints. A somewhat larger ratio of 6:1 may improve performance by simplifying noise reduction in the post-processing of science images.

Each of the Collector Spacecraft (CS) contains a spherical mirror and no additional science-path optics (some components may be needed for configuration control). The four CS fly in formation to synthesize part of a larger paraboloid—the *Emma* configuration is a single, sparsely filled aperture. Flexing of the CS primary mirrors or deformable optics within the beam combiner spacecraft will conform the individual spheres to the larger paraboloid.

The Beam Combiner Spacecraft (BCS) flies near the focal point of this synthesized paraboloid. Beam combination takes place on a series of optical benches arranged within the BCS envelope. The necessary optical processing includes:

- Transfer optics and BCS/CS metrology;
- Correction and modulation, including optical delay lines, tip-tilt, deformable mirrors;
- Mirrors, wavefront sensors, and beam switching;
- Spectral separation to feed the science photons into 2 separate channels;
- Phase shifting, beam mixing;
- Recombination, spectral dispersion and detection.

The collector and beam combiner spacecrafts use sunshades for passive cooling to < 50 K. An additional refrigerator within the BCS cools the detector assembly to below 10 K.

Due to the configuration of the array and the need for solar avoidance, the instantaneous sky access is limited to an annulus with inner and outer half-angles of 46° and 83° centred on the anti-sun vector. This annulus transits the entire ecliptic circle during one year, hence giving access to almost the entire sky.

For launch, the collector and beam-combiner spacecraft are stacked within the fairing of an Ariane 5 ECA vehicle. Total mass is significantly less than 6.6 tons, the launcher capability. Table 1 lists key parameters of the *Darwin Emma* X-array. These values represent the results of the various assessment and system level studies conducted by ESA and NASA.

TABLE 1. KEY *DARWIN* PARAMETERS

Item	Value or Comment
Collector Spacecraft (CS)	4 free-flyers, passively cooled to <50K
CS Optics	Lightweight spherical mirrors, diameter *ca*. 2.0 m, no deployables
CS Array Configuration	X-array with aspect ratio 3:1 – 6:1 (to be optimized)
Available Baselines	7 m to 168 m Nulling (20 m to 500 m Imaging option)
Beam Combiner (BCS)	1 free flying spacecraft, passively cooled to <50K
Beam Combiner Optics	Transfer, modulation, beam-mixing, recombination, spectroscopy
Detection	Mid-IR detector ca. 500 x 8 pixels for nulling, (300 x 300 for imaging option), cooled to < 10 K
Detector Cooling	Low vibration refrigerator, e.g. absorption coolers (pulse tube coolers are also possible, e.g., from JWST)
Telemetry	Require ca. 1 GBit /s, direct downlink from BCS
Operating Wavelength	6-20 µm. Includes H_2O, O_3, CH_4, CO_2 signatures
Field of View	Typically 1 arcsec at 10 µm
Null Depth	10^{-5}, stable over ~ 5 days
Angular Resolution	5 milliarcsec at 10 µm for a 500 m baseline, scales inversely
Spectral Resolution	25 (possibly 300) for exo-planets; 300 for general astrophysics
Field of Regard	Annular region between 46° and 83° from anti-sun direction at a date, 99% over one year
Target Stars	F, G, K , M, at least 150 (10 exo-zodis) or 220 (3 exo-zodi)
Mission Duration	5 yrs baseline, extendable to 10 yrs
Mission Profile	Nominal 2 yrs detection, 3 yrs spectroscopy, flexible
Orbit	L2 halo orbit
Formation Flying	Radio Frequency and Laser controlled
Station Keeping	Field Effect Electric Propulsion (FEEP) or cold gas
Launch Vehicle	Single Ariane 5 ECA or 2 Soyuz-ST / Fregat

MISSION PERFORMANCE

Detecting Earths

Darwin's instruments will encounter a number of extraneous signals. The planetary flux must be extracted and analysed in the presence of these other components. The discrimination is

performed by maximizing starlight rejection, and by appropriate modulation that produces a zero mean value for the different background sources. Image reconstruction algorithms are then used to retrieve the actual flux and location of the planets, as illustrated in Fig. 12 (e.g. Draper *et al.*, 2006; Marsh et al., 2006; Thiébaut and Mugnier, 2006; Mugnier *et al.*, 2006). Even though modulation cannot eliminate the quantum noise (sometimes referred to as photon noise) associated with these sources, nor the instability noise related to imperfect instrumental control, these issues have been addressed by Lay (2006) and Lane *et al*. (2006).

Search Strategy and Performance

Performance simulations have been conducted for each star in the target catalogue, using both the *Darwin*Sim software developed at ESA (den Hartog, private communication) and the TPF-I star count model developed at NASA (Lay et al., 2007), to assess the required integration time to reach the required signal to noise ratio (SNR) for detection and spectroscopy. These requirements are an SNR of 5 on the whole band for imaging in nulling mode, and a SNR of 10 from 7.2 to 20 μm for H_2O, CO_2 and O_3 spectroscopy, using a spectral resolution $\lambda/\Delta\lambda \geq 20$. Under the assumption that the exozodiacal emission is symmetric around the target star, the chopping process will suppress it, and the exozodi will only contribute to the photon noise. The simulations presented below assume an exozodiacal density of 3 zodis.[3]

Using an Emma X-array (6:1 configuration) with 2-m diameter telescopes and assuming an optical throughput of 10% for the interferometer, we estimate that about 200 stars distributed among the four selected spectral types can be screened during the nominal 2-yrs survey

[3] In practice, exozodiacal densities below 10 times our local zodiacal cloud barely affect the overall shot noise level, while higher densities would significantly increase the required integration times.

(Table 2). *Darwin* will thus provide statistically meaningful results on nearby planetary systems. K and M dwarfs are the easiest targets in terms of Earth-like planet detection for a given integration time, because on the one hand, the total thermal infrared luminosity of a planet in the Habitable Zone depends only on its size – while, on the other hand, the stellar luminosity is a strong function of its spectral type, so that the star/planet decreases for later spectral types. Compared to the case of the Sun and Earth, this contrast is two times higher for F stars, a factor of three lower for K stars, and more than an order of magnitude lower for M-dwarfs (Kaltenegger, 2008a). However, a special effort is placed on observing Solar-like G type stars (50% of the observing time) and a significant number of them can be screened and possible terrestrial planets studied.

TABLE 1: EXPECTED PERFORMANCE OF THE X-ARRAY ARCHITECTURE IN TERMS OF NUMBER OF STARS SCREENED AND PLANETS CHARACTERISED FOR VARIOUS TELESCOPE DIAMETERS. ALL STARS ARE ASSUMED TO HOST AN EARTH-LIKE PLANET.

	1m diameter	2m diameter	3m diameter
Screened	76	218	405
# F stars	5	14	30
# G stars	15	53	100
# K stars	20	74	152
# M stars	36	77	123
CO_2, O_3 spectroscopy	17	49	87
# F stars	1	2	3
# G stars	4	8	15
# K stars	3	12	25
# M stars	9	27	44
H_2O spectroscopy	14	24	43
# F stars	0	1	1
# G stars	2	4	7
# K stars	1	5	10
# M stars	11	14	25

If each nearby cool dwarf is surrounded by one rocky planet of one Earth radius within its Habitable Zone, only a fraction of the detected planets – about 25 of the most interesting

planets - can be fully characterised (i.e., examined for the presence of H_2O, CO_2 and O_3) during the subsequent 3-year spectroscopic phase. This number would be doubled or quadrupled for planets with radii 1.5 and 2 times that of the Earth, respectively.

Imaging for the General Astrophysics Program

The 5σ, one hour, point source sensitivities for *Darwin* in 20% wide bands centred at 8, 10, 13 and 17 μm are approximately 0.1, 0.25, 0.5 and 0.8 μJy, respectively. These sensitivities are comparable to those of JWST. The maximum foreseen baselines are 500 metres, corresponding to a spatial resolution of 5 mas at 10 μm. Assuming a stability time scale of 10 seconds for the array, the sensitivity limit for self-fringe-tracking is about 10 mJy at 10 μm in a 0.5 arcsec aperture. This performance gives access to virtually all of the sources in the Spitzer SWIRE survey.

The importance of a bright source in the field to cophase the sub-pupils of the interferometer was mentioned earlier. The nature of the target and the science goal will determine the required instrumentation. We consider three different cases: few visibility measurements with a bright source in the Field of View, imaging with a bright source, and imaging without a bright source.

- With minimal impact on the nulling recombiner, *Darwin* can carry out visibility (V^2) science with JWST-like sensitivity, as long as there is a $K \leq 13$ magnitude source in the field of view to stabilize the array. The modulus of the visibility provides simple size information about the target, for example, its radius assuming spherical morphology. The phase of the visibility gives shape information, such as deviations

from spherical symmetry. If the target spectrum is smooth a few visibility measurements can be obtained rapidly, because *Darwin* can work simultaneously at several wavelengths. The baseline beam combiner could perform such measurements with very modest modification, and hence, with minimum impact on the cost of the mission. Therefore, a capability for basic visibility measurement should be implemented. Unfortunately, a limited number of V^2 observations provide useful information for only a limited number of targets.

- To obtain a fully reconstructed image, the (u,v) plane must be filled by moving the array. A significant gain in efficiency can be realized if the spectrum of the target is smooth over the operating band of the instrument. The shorter wavelengths sample higher spatial frequencies, and the longer wavelengths lower spatial frequencies, all at the same array spacing. A 100x100 image could be obtained with a few hundreds of positions, rather than the 10,000 positions required for a full spatial and spectral reconstruction.

- For targets with no bright source in the field, the preferred option for co-phasing is the use of a nearby off-axis bright reference star ($K \leq 13$). One way of doing this is to feed the K-band light of this star along with the 6-20 μm light of the target to the Beam Combiner Satellite, a so-called dual field configuration. Another option is to make the interferometer optically rigid using Kilometric Optical Gyros. These devices can maintain the phasing of the array between pointings at a reference star and the target field. Clearly, this additional instrumentation may be much more demanding and expensive. A decision whether or not to add this capability to *Darwin* will depend on an analysis undertaken during the study phase and also available funding.

TECHNOLOGY AND MISSION ROADMAP FOR *DARWIN*

Essential Technology Developments for Darwin

The pre-assessment study of *Darwin* by Alcatel in 2000, and the assessment study by TAS and Astrium in 2006 determined that there are no technology show stoppers for this ambitious mission. However, two key areas were identified that require focused attention and resources:

- *Formation Flying* of several spacecraft with relative position control of a few cm.
- The feasibility of *nulling interferometry* in the 6 - 20 µm range. Based on the expected star/planet contrast ($1.5x10^{-7}$ at 10 µm and 10^{-6} at 18 µm for an Sun-Earth analogue) and on evaluations of instability noise, the common conclusion is that the null depth must be 10^{-5} on average, and that it must be sufficiently stable on the timescale of days so that the signal to noise ratio improves as the square root of time. This stability requirement translates into tight instrument control specifications, which can be relaxed by means of the two instability noise mitigation techniques (Lay, 2006; Lane *et al.*, 2006). A thorough evaluation of these techniques and of the resulting instrumental stability requirements will be a key component of the technology development programme.

Current Status of Technology Development

Europe has devoted considerable resources, both intellectual and financial, to these technological issues since the initial Alcatel study (2000). ESA has invested approximately 20 M€ since 2000, with a significant increase in the last 2 years. Several tens of Technology

Research Programs (TRPs) have been issued. NASA has run a parallel program in the US. Most of the key technologies have been addressed and significant progress achieved.

In the area of Formation Flying (FF), the TRPs “Interferometer Constellation Control” (ICC1 and ICC2) have developed nonlinear, high fidelity navigation simulators (Beugnon *et al.*, 2004). Algorithms for Interferometer Constellation Deployment at L2 have also been demonstrated. In the USA, analogous simulations and a 2D robotic breadboard have shown the feasibility of formation flying (Scharf *et al.*, 2007). Finally, with the PRISMA mission being prepared for launch, major hardware and software components of formation flying technologies will soon be demonstrated in space.

The investment in nulling interferometry research over the past 7 years has allowed the concept to be validated in European and American laboratories. The flight requirement is a null depth of 10^{-5} in the 6 – 20 µm domain. Monochromatic experiments using IR lasers at near-infrared and mid-infrared wavelengths have yielded nulls equal to or significantly better than 10^{-5} (Ergenzinger *et al.*, 2004; Barillot *et al.*, 2004; Buisset *et al.*, 2006; Martin *et al.*, 2007). Broadband experiments have achieved nulls of $1.2x10^{-5}$ for 32% bandwidth at 10 µm, closely approaching the flight requirement (Peters *et al.*, 2006). At the time of writing the technology of nulling interferometry is nearing maturity, although it has not yet been demonstrated over the full *Darwin* bandwidth with the required depth and stability.

Additional key technological developments in recent years include:

- Selection of the baseline *interferometer configuration*. Significant effort in this area since 2000, backed by independent studies in the US and Europe, has identified the non-planar Emma X-Array as the optimal choice (Lay, 2005; Karlsson *et al.*, 2006);

- *Achromatic Phase Shifters (APS),* which allow broadband destructive interference between beams, have been demonstrated in the laboratory. A comparative study currently running in Europe should identify the preferred approach (Labèque *et al.*, 2004);
- *Space-qualified Delay Lines* to balance the different optical paths to nanometre accuracy have been demonstrated (Van den Dool *et al.*, 2006). A breadboard at TNO-TPD has achieved this performance at 40K and may be included as a test payload in the PROBA 3 space mission;
- *Single Mode Fibres*, or *Integrated Optics Modal Filters* that enable broadband nulling have recently been produced and tested (Labadie *et al.*, 2006; Huizot *et al.*, 2007). Chalcogenide fibres have demonstrated the required performance of 40% throughput and 30 dB rejection of higher order spatial modes. Ongoing work is emphasizing silver halide single-mode filters, which will operate in the 12-20 μm band (Lewi *et al.*, 2007). Photonic Crystal fibres that can cover the whole spectral domain in a single optical channel are considered (Flanagan *et al.*, 2006);
- *Detector Arrays* with appropriate read noise and dark current have been qualified for space-based operation (Love *et al.*, 2004). The Si:As Impurity Band Conductor (IBC) arrays developed for JWST appear to be fully compliant with *Darwin* requirements. A reduced-size version of the JWST 1024 x 1024 detector, e.g. 512 x 8 (300 x 300 for the general astrophysics program), could be read out at the required rate with a dissipation of a few tens to hundreds of μW. These devices exhibit high quantum efficiency (80%), low read noise (19 e^-), and minimal dark current (0.03 e^-/s at 6.7 K). Such performance permits sensitive observations, even at moderately high spectral resolution (R = 300);
- Low vibration *Cryo-coolers* for the detector system have been demonstrated in the laboratory. A European TRP has led to a prototype absorption cooler providing 5 mW of

cooling power at 4.5 K (Burger *et al.*, 2003). JPL scientists have demonstrated a system with 30 mW of cooling at 6 K (Ross and Johnson, 2006).

Conclusions:

We described the scientific and technological implementation of the *Darwin* space mission, whose primary goal is the search and characterization of terrestrial extrasolar planets as well as the search for life. *Darwin* is designed to detect and characterize rocky planets similar to the Earth and perform spectroscopic analysis of their atmosphere at mid-infrared wavelengths (6 to 20 μm). The baseline mission lasts 5 years and consists of approximately 200 individual target stars. Among these, 25 to 50 planetary systems can be studied spectroscopically, searching for gases such as CO_2, H_2O, CH_4 and O_3. Key technologies required for the construction of *Darwin* have already been demonstrated. This paper has described the science programme and some of the technological requirements for an ambitious space mission to discover and characterize Earth-like planets and to search for evidence of life on them. The *Darwin* mission will address one of the most fundamental questions: humankind's origin, and its place in the Universe.

REFERENCES

Absil, O., Karlsson, A., and Kaltenegger, L. (2003) Inherent modulation: a fast chopping method for nulling interferometry. *Proc SPIE* 4852, 431.

Absil, O., den Hartog, R., Gondoin, P., Fabry, P., Wilhelm, R., Gitton, P., and Puech, F. (2006) Performance study of ground-based infrared Bracewell interferometers. Application to the detection of exozodiacal dust disks with GENIE *Astronomy and Astrophysics* 448, 787-800.

Alibert, Y., Mordasini, C., Benz, W., and Winisdoerffer C. (2005) Models of giant planet formation with migration and disc evolution. *Astronomy and Astrophysics* 434, 343-353.

Angel, R. (1990) Proceedings of the NASA/STSI Workshop on *The Next Generation Space Telescope*, edited by P. Bely, C.J., Burrows, and G.D. Illingworth, Space Telescope Science Institute: Baltimore, MD, pp.13-15.

Barillot, M., Haguenauer, P., Weber, V., Kern, P., Schanen-Duport, I., Labeye, P., Pujol, L. and Sodnik, Z. (2004) MAI² nulling breadboard based on integrated optics: test results. *ESA SP* 554, 231-236.

Beichman, C. A., Woolf, N. J., and Lindensmith, C. A. (1999) *TPF: A NASA Origins Program to Search for Habitable Planets*, JPL Publication 99-3, Jet Propulsion Laboratory, Pasadena, CA.

Benz, W., Mordasini, C., Alibert, Y., and Naef, D. (2007) Giant planet population synthesis: comparing theory with observations. Nobel Symposium # 135, in press.

Beugnon, C., Calvel, B., Boulade, S., and Ankersen, F. (2004) Design and modeling of the formation-flying GNC system for the DARWIN interferometer. *Proc SPIE* 5497, 28-38.

Bignami, G. (2007) Boarding now for Mars. *International Herald Tribune*, 3 October.

Boss, A. P. (1997) Giant planet formation by gravitational instability. *Science* 276, 1836-1839.

Bracewell, R.N. (1978) Detecting non-solar planets by spinning infrared interferometry. *Nature* 274, 780-781.

Brack, A. (2007) From interstellar amino acids to prebiotic catalytic peptides: A review. *Chemistry and Biodiversity* 4, 665-679.

Buisset, C., Rejeaunier, X., Rabbia, Y., and Barillot, M. (2006) Stable deep nulling in polychromatic unpolarized light with multiaxial beam combination. *Applied Optics* 46 (32), 7817-7822.

Burger , J., Holland, H., Ter Brake, M., Venhorst, G., Hondebrink, E., Meijer, R.-J., Rogalla, H., Coesel, R., Dierssen, W., Grim, R., Lozano-Castello, D., and Sirbi, A. (2003) Vibration-free 5K sorption cooler for ESA's Darwin mission. *ESA SP* 539, 379-384.

Butler, R.P. , Vogt, S.S., Marcy, G.W., Fischer, D.A., Wright, J.T., Henry, G.W., Laughlin, G., and Lissauer, J.J. (2004) A Neptune-Mass planet orbiting the nearby M Dwarf GJ 436. *Astrophys. J.* 617, 580-588.

Bromm, V., Coppi, P.S., and Larson, R.B. (1999) Forming the first stars in the universe: The fragmentation of primordial gas. *Astrophys. J.* 527, L5-L8.

Chazelas, B. (2006) Instrumental stability requirements for exoplanet detection with a nulling interferometer: variability noise as a central issue. *Applied Optics* 45, 984-992.

Cockell, C.S. (1999) Carbon biochemistry and the ultraviolet radiation environments of F, G and K main sequence stars. *Icarus* 141, 399-407.

Crowe, M.J. (1986) The extraterrestrial life debate, 1750-1900. Dover Publications, New *York.*

D'Angelo, G., Lubow, S.H., and Bate, M.R. (2006) Evolution of giant planets in eccentric disks. *Astrophys. J.* 652, 1698-1714.

DesMarais, D.J., Harwit, M.O., Jucks, K.W., Kasting, J.F., Lin, D.N.C., Lunine, J.I., Schneider, J., Seager, S., Traub, W.A., and Woolf, N.J. (2002) Remote sensing of planetary properties and biosignatures on extrasolar terrestrial planets. *Astrobiology* 2, 153-181.

Dominik, D., and Decin, G. (2003) Age dependence of the Vega phenomenon: Theory. *Astrophys. J.* 598, 626–635.

Draper, D. W., Elias, N.M., Noecker, M.C., Dumont, P.J., Lay, O.P., and Ware, B. (2006) Planet signal extraction for the terrestrial planet finder interferometer. *Astroph. J.* 131, 1822-1836.

Dwek, E. (1998) The evolution and elemental abundances in the gas and dust phases of the Galaxy. *Astrophys. J.* 501, 643–665.

Edmunds, M. G. (2001) An elementary model for the dust cycle in galaxies. *Mon. Not. R. Astron. Soc.* 328, 223–236.

Ergenzinger, K., Flatscher, R., Johann, U., Vink, R., and Sodnik, Z. (2004) EADS Astrium Nulling Interferometer Breadboard for DARWIN and GENIE. *ESA SP* 554, 223-230.

Fischer, D.A., and Valenti J. (2005) The planet-metallicity correlation *Astrophys. J.* 622, 1102-1117

Flanagan, J.C., Richardson, D.J., Foster, M.J., and Bakalski, I. (2006) A microstructured wavefront filter for the Darwin nulling interferometer. *ESA SP* 621, 8pp.

Forget, F., and Pierrehumbert, R.T. (1997) Warming Early Mars with carbon dioxide clouds that scatter infrared radiation. *Science* 278, 1273 – 1276.

Franx, M., Labbé, I., Rudnick, G., van Dokkum, P.G., Daddi, E., Schreiber, N.M.F., Moorwood, A., Rix, H.W., Rottgering, H., van de Wel, A., van der Werf, P., and van Starkenburg, L. (2003) A significant population of red, near-infrared high-redshift galaxies. *Astrophys. J.* 587, L79–L82.

Gardner, J.P., Mather, J.C., Clampin, M., Doyon, R., Greenhouse, M.A., Hammel, H.B., Hutchings, J.B., Jakobsen, P., Lilly, S.J., Long, K.S., Lunine, J.I., McCaughrean, M.J., Mountain, M., Nella, J., Rieke, G.H., Rieke, M.J., Rix, H-W., Smith, E.P., Sonneborn, G., Stiavelli, M., Stockman, H.S., Windhorst, R.A., and Wright, G.S. (2006) The James Webb Space Telescope *Space Sciences Reviews* 123, 485-605.

Ghez, A. M., Salim, S., Hornstein, S.D., Tanner, A., Lu, J.R., Morris, M., Becklin, E.E., and Duchene, G. (2005) Stellar orbits around the Galactic central black hole. *Astrophys. J.* 620, 744–757.

Gough, D.O. (1981) Solar interior structure and luminosity variations. *Solar Phys*. 74, 21-34.

Granato, G., Danese, L., and Franceschini, A. (1997) Thick tori around active galactic nuclei: The case for extended tori and consequences for their x-ray and infrared emission. *Astrophys. J.* 486, 147–159.

Grießmeier, J.-M., Stadelmann, A., Motschmann, U., Belisheva, N.K., Lammer, H., and Biernat, H.K. (2005) Cosmic ray impact on extrasolar Earth-like planets in close-in habitable zones. *Astrobiology* 5, 587 – 603.

Hollenbach, D. J., Yorke, H. W., and Johnstone, D. (2000) Disk dispersal around young stars. In *Protostars and Planets IV*, edited by V. Mannings, A.P. Boss and S.S. Russell, University of Arizona Press: Tucson, AZ, pp. 401-428.

Huizot, P., Boussard-Plédel, C., Faber, A. J., Cheng, L. K., Bureau, B., Van Nijnatten, P. A., Gielesen, W. L. M., Pereira do Carmo, J., and Lucas, J. (2007) Infrared single mode chalcogenide glass fiber for space. *Optics Express* 15 (19), 12529-12538.

Ida, S., and Lin, D.N.C. (2004) Toward a deterministic model of planetary formation. I. A desert in the mass and semimajor axis distributions of extrasolar planets *Astrophys. J.* 604, 388-413.

Kaltenegger, L. (2005) Search for Extra-Terrestrial planets: The DARWIN mission - Target Stars and Array Architectures, astroph/0504497, PhD thesis.

Kaltenegger, L., and Karlsson, A. (2004) Requirements on the stellar rejection for the Darwin mission. *SPIE* 5491.

Kaltenegger, L., and Selsis F. (2007) Biomarkers set in context. In Extrasolar Planets: Formation, Detection and Dynamics, edited by R. Dvorak, Wiley, Weinheim, pp 79-97.

Kaltenegger, L., Traub, W. A., and Jucks, K. (2007) Spectral evolution of an Earth-like planet. *Astrophys. J.* 658, 598-616.

Kaltenegger, L., Eiroa, C., and Fridlund, M. (2008a) Target star catalogue for Darwin, Nearby Stellar sample for a search for terrestrial planets. *Astron. Astrophys.* Submitted.

Kaltenegger, L, Traub, W.A., and Kasting, J., (2008b) Spectral signatures of the first super Earths, *Astrophys. J.*, submitted.

Karlsson, A., and Mennesson, B. (2000) Robin Laurance nulling interferometers. *Proc SPIE* 4006, 871-880.

Karlsson, A., d'Arcio, L., den Hartog, R., and Fridlund, M. (2006) Darwin: a mission overview. *Proc. SPIE* 6265, 1O-1/9.

Karlsson, A., Wallner, O., Perdigues Armengol, J., and Absil, O. (2004) Three Telescope Nuller, based on multibeam injection into single-mode fibres. *Proc. SPIE* 5491, 831-841.

Kasting, J.F., and Catling, D. (2003) Evolution of a habitable planet. *Ann. Rev. Astron. Astrophys.* 41, 429-463.

Kasting, J.F., Whitmore, D.P., and Reynolds, R.T. (1993) Habitable zones around main-sequence stars. *Icarus* 101, 108-128.

Kasting, J.F., Whittet, D.C.B., and Sheldon, W.R. (1997) Ultraviolet radiation from F and K stars and implications for planetary habitability. *Origin. Life Evol. Biosph.* 27, 413-420.

Khodachenko, M. L., Ribas, I., Lammer, H., Grießmeier, J.-M., Leitner, M., Selsis, F., Eiroa, C., Hanslmeier, A., Biernat, H.K., Farrugia, C.J., and Rucker, H.O. (2007) CME activity of low mass M stars as an important factor for the habitability of terrestrial exoplanets, Part I: CME impact on expected magnetospheres of Earth-like exoplanets in close-in habitable zones. *Astrobiology* 7, 167 – 184.

Kiang, N.Y., Siefert, J., Govindjee, and Blankenship, R.E. (2007) Spectral signatures of photosynthesis. I. Review of earth organisms *Astrobiology* 7, 222-251.

Kiang, N.Y., Segura, A., Tinetti, G., Govindjee, Blankenship, R.E., Cohen, M., Siefert, J., Crisp, D., and Meadows, V.S. (2007) Spectral signatures of photosynthesis. II. Coevolution with other stars and the atmosphere on extrasolar worlds. *Astrobiology* 7, 252-274.

Labadie, L., Labeye, P., Kern, P., Schanen, I., Arezki, B., and Broquin, J.-E. (2006) Modal filtering for nulling interferometry. First single-mode conductive waveguides in the mid-infrared. *Astron. Astrophys.* 450, 1265-1275.

Labbé, I., Huang, J., Franx, M., Rudnick, G., Barmby, P., Daddi, E., van Dokkum, P.G., Fazio, G.G., Schreiber, N.M.F., Moorwood, A.F.M., Rix, H.W., Rottgering, H., Trujillo, I., and van der Werf, P. (2005) IRAC mid-infrared imaging of the Hubble Deep Field-South: Star formation histories and stellar masses of red galaxies at $z>2$. *Astrophys. J.* 624, L81–L84.

Labèque , A., Chazelas, B., Brachet, F., Commeaux, C., Blache, P., Leger, A., Ollivier, M., Lepine, T., and Valette, C.(2004) The Nulltimate project: building and testing, at low temperature achromatic phase shifters to prepare the Darwin mission. *Proc. SPIE* 5491, 999.

Lammer, H., Lichtenegger, H.I.M., Kulikov, Yu. N., Grießmeier, J.-M., Terada, N., Erkaev, N.V., Biernat, H.K., Khodachenko, M.L., Ribas, I., Penz, T., and Selsis, F. (2007) CME activity of low mass M stars as an important factor for the habitability of terrestrial exoplanets, Part II: CME induced ion pick up of Earth-like exoplanets in close-in habitable zones. *Astrobiology* 7, 185 - 207.

Lane, B. F., Muterspaugh, M. W., and Shao, M. (2006) Calibrating an interferometric null. *Astroph. J.* 648, 1276-1284.

Lay, O. P. (2004) Systematic errors in nulling interferometers. *Applied Optics* 43, 6100-6123.

Lay, O. P. (2005) Imaging properties of rotating nulling interferometers. *Applied Optics* 44, 5859-5871.

Lay, O. P. (2006) Removing instability noise in nulling interferometers. *Proc. SPIE* 6268, 62681A.

Lay, O. P., and Dubovitsky, S. (2004) Nulling interferometers: the importance of systematic errors and the X-array configuration. *Proc. SPIE* 5491, 874-885.

Lay, O. P., Martin, S. R., and Hunyadi, S. L. (2007) Planet-finding performance of the TPF-I Emma architecture. *Proc. SPIE* 6693, 66930A-1.

Léger, A., Pirre, M., and Marceau, F.J. (1993) Search for primitive life on a distant planet : relevance of O_2 and O_3 detection. *Astron. Astrophys.* 277, 309-313.

Léger, A,, Mariotti, J.M., Mennesson, B., Ollivier, M., Puget, J.L., Rouan, D., and Schneider, J. (1996) Could we search for primitive life on extrasolar planets in the near future? The *DARWIN* project. *Icarus* 123, 249-255.

Léger, A., Selsis, F., Sotin, C., Guillot, T., Despois, D., Mawet, D., Ollivier, M., Labeque, A., Valette, C., Brachet, F., Chazelas, B., and Lammer, H. (2004) A new family of planets? "Ocean-Planets". *Icarus* 169, 499-504.

Lewi, T., Shalem, S., Tsun, A., and Katzir, A. (2007) Silver halide single-mode fibers with improved properties in the middle infrared. *Applied Physics Letters* 91, 251112.

Li, C.H. et al. (2008) Laser frequency comb to enable radial velocity measurements with a precision of 1 cm s^{-1}, *Nature* (in press).

Love P. J., Hoffman, A. W., Lum, N. A., Ando, K. J., Ritchie, W. D., Therrien, N. J., Toth, A. G., and Holcombe, R. S. (2004) 1K x 1K Si:As IBC detector arrays for JWST MIRI and other applications. *Proc. SPIE* 5499, 86-96.

Lovelock, J. (1975) Thermodynamics and recognition of alien biospheres. *Proc. Royal Soc London* 189, 167-181.

Lovelock, J. (2000) The recognition of alien biospheres. *Cosmic Search* 2, 2-5.

Lovis, C., Mayor, M., Pepe, F., Alibert, Y., Benz, W., Bouchy, F., Correia, A.C.M., Laskar, J., Mordasini, C., Queloz, D., Santos, N.C., Udry, S., Bertaux, J.L, and Sivan, J.P. (2006) An extrasolar planetary system with three Neptune-mass planets. *Nature* 441, 305-309.

Marcy G. and Butler, R.P. (1995) The Planet around 51 Pegasi. AAS 187, 7004

Marsh, K., Velusmay, T., and Ware, B. (2006), Point Process Algorithm: a new baynesian approach for planet signal extraction with the Terrestrial Planet Finder-Interferometer. *Astrophys. J.* 132, 1789-1795.

Martin, S.R, Daniel Scharf, D., Wirz, R., Lay, O., McKinstry, D., Mennesson, B., Purcell, G., Rodriguez, J., Scherr, L., Smith, J.R., and Wayne, L. (2007) TPF-Emma: concept study of a planet finding space interferometer. *Proc. SPIE* 6693, 669309.

Mayor, M. and Queloz, D. (1995) A Jupiter-mass companion to a solar-type star. *Nature* 378, 355-359.

Meadows, V. S., and Crisp, D. (1996) Ground-based near-infrared observations of the Venus nightside: The thermal structure and water abundance near the surface. *J. Geophys. Res.* 101, 4595-4622.

Mennesson, B., and Mariotti, J.-M. (1997) Array configurations for a space infrared nulling interferometer dedicated to the search for earthlike extrasolar planets. *Icarus* 128, 202-212.

Mennesson, B., Leger, A., and Ollivier, M. (2005) Direct detection and characterization of extrasolar planets: The Mariotti space interferometer. *Icarus* 178, 570-588.

Moorwood, A.F.M., Lutz, D., Oliva, E., Marconi, A., Netzer, H., Genzel, R., Sturm, E., and deGraauw, T. (1996) 2.5-45 μm SWS spectroscopy of the Circinus galaxy. *Astron Astrophys.* 315, L109-L112.

Mugnier, L.M., Thiébaut, E., and Belu, A. (2006) Data processing in nulling interferometry: case of the *Darwin* mission. In *Astronomy with High Contrast Imaging III*, edited by M. Carbillet, A. Ferrari and C. Aime, EAS Publications Series, EDP Sciences, Les Ulis, France, pp 69-83.

Newman, M.J., and Rood, R.T. (1977) Implications of solar evolution for the Earth's early atmosphere. *Science* 198,1035-1037.

Owen, T. (1980) The search for early forms of life in other planetary systems: future prospects afforded by spectroscopic techniques. In *Strategies for the Search for Life in the Universe*, edited by M. Papagiannis, D. Riedel, Dordrecht, Netherlands 83, pp 177-185.

Pavlov, A., Hurtgen, M.T., Kasting, J.F., and Arthur, M.A. (2003) Methane-rich Proterozoic atmosphere? *Geology* 31, 87-90.

Peters, R D., Lay, O. P., Hirai, A., and Jeganathan, M. (2006) Adaptive nulling for the Terrestrial Planet Finder Interferometer. *Proc. SPIE* 6268, 62681C.

Pollack, J.B, Hubickyj, O, Bodenheimer, P, Lissauer, J.J, Podolak, M., and Greenzweig, Y. (1996) Formation of the giant planets by concurrent accretion of solids and gas *Icarus* 124, 62-85.

Raven, J.A. and Wolstencroft, R.D. (2004) Constraints on photosynthesis on Earth and Earth-like planets. *IAU Symposia* 213, 305-308.

Raven, J.A., and Cockell, C.S. (2006) Influence on photosynthesis of starlight, moonlight, planetlight, and light pollution (reflections on photosynthetically active radiation in the universe). *Astrobiology* 6, 668-675.

Raymond, S.N., Mandell, A.M., and Sigurdsson, S. (2006a) Exotic earths: forming habitable worlds with giant planet migration. *Science* 313, 1413-1416.

Raymond, S.N., Quinn, T., and Lunine, J.I. (2006b) High-resolution simulations of the final assembly of Earth-like planets I. Terrestrial accretion and dynamics. *Icarus* 183, 265-282.

Raymond, S., Quinn, T., and Lunine, J.I. (2007) High-resolution simulations of the final assembly of earth-like planets. 2. Water delivery and planetary habitability *Astrobiology* 7, 66-84.

Reipurth B., and Bally, J. (2001) Herbig-Haro flows: Probes of early stellar evolution. *Ann. Rev. Astron. Astrophys.* 39, 403-455.

Rieke, G. R., Su, K. Y. L., Stansberry, J. A., Trilling, D., Bryden, G., Muzerolle, J., White, B., Gorlova, N., Young, E.T., Beichman, C.A., Stapelfeldt, K.R., and Hines, D.C. (2005) Decay of planetary debris disks. *Astrophys. J.* 620, 1010–1026.

Ross. R., and Johnson, D. (2006) NASA's Advanced Cryocooler Technology Development Program (ACTDP). *Am. Inst. Phys. Conf. Ser.* 823, 607-614.

Sagan, C., Thompson, W.R., Carlson, R., Gurnett, D., and Hord, C. (1993) A search for life on Earth from the Galileo spacecraft. *Nature* 365, 715-721.

Santos, N.C., Israelian, G., and Mayor, M. (2004) Spectroscopic [Fe/H] for 98 extra-solar planet-host stars - Exploring the probability of planet formation *Astron. Astrophys.* 415, 1153-1167.

Scalo J., Kaltenegger, L., Segura, A., Fridlund, M., Ribas, I., Kulikov, Yu. N., Grenfell, J. L., Rauer, H., Odert, P., Leitzinger, M., Selsis, F., Khodachenko, M. L., Eiora, C., Kasting, J., and Lammer, H. (2007) M stars as targets for terrestrial exoplanet searches and biosignature detection. *Astrobiology* 7, 85 – 166.

Scharf, D., Hadaegh, F., Keim, J., Benowitz, E., and Lawson, P. (2007) Flight-like ground demonstration of precision formation flying spacecraft. *Proc. SPIE* 6693, 669307.

Schindler, T. L., and Kasting, J.F. (2000) Synthetic spectra of simulated terrestrial atmospheres containing possible biomarker gases, *Icarus* 145, 262-271.

Schöller, M., Argomedo, J., Bauvir, B., Blanco-Lopez, L., Bonnet, H., Brillant, S., Cantzler, M., Carstens, J., Caruso, F., Choque-Cortez, C., Derie, F., Delplancke, F., Di Lieto, N., Dimmler, M., Durand, Y., Ferrari, M., Galliano, E., Gitton, P., Gilli, B., Glindemann, A., Guniat, S., Guisard, S., Haddad, N., Haguenauer, P., Housen, N., Hudepohl, G., Hummel, C., Kaufer, A., Kiekebusch, M., Koehler, B., Le Bouquin, J-B., Leveque, S., Lidman, C., Mardones, P., Menardi, S., Morel, S., Mornhinweg, M., Nicoud, J-L., Percheron, I., Petr-Gotzens, M., Duc, T.P., Puech, F., Ramirez, A., Rantakyrö, F., Richichi, A., Rivinius, T., Sandrock, S., Somboli, F., Spyromilio, J., Stefl, S., Suc, V., Tamai, R., Tapia, M., Vannier, M., Vasisht, G., Wallander, A., Wehner, S., Wittkowski, M., and Zagal, J. (2006) Recent progress at the Very Large Telescope Interferometer. *Proc. SPIE 6268*, 62680L.

Segura, A., Krelove, K., Kastings, J.F., Sommerlatt, D., Meadows, V., Crisp, D., Cohen, M., and Mlawer, E. (2003) Ozone concentrations and ultraviolet fluxes on Earth-like planets around other stars. *Astrobiology* 3, 689-708.

Segura, A., Kasting, J.F., Meadows, V., Cohen, M., Scalo, J., Crisp, D., Butler, R. A. H., and Tinetti, G. (2005) Biosignatures from earth-like planets around M dwarfs *Astrobiology* 5, 706-725.

Segura, V., Meadows, S., Kasting, J.F., Cohen, M., and Crisp, D. (2007) Abiotic formation of O_2 and O_3 in high-CO_2 terrestrial atmospheres. *Astron. Astrophys.* 472, 665-679.

Selsis, F. (2000) Physics of planets I: Darwin and the atmospheres of terrestrial planets. ESA SP 451, 133.

Selsis, F., Despois, D., and Parisot, J.P. (2002) Signature of life on exoplanets: Can *Darwin* produce false positive detections? *Astron. Astrophys*. 388, 985-1003.

Selsis, F., Chazelas, B., Bordé, P., Ollivier, M., Brachet, F., Decaudin, M., Bouchy, F., Ehrenreich, D., Grießmeier, J.-M., Lammer, H., Sotin, C., Grasset, O., Moutou, C., Barge, P., Deleuil, M., Mawet, D., Despois, D., Kasting, J.F., and Léger, A. (2007a) Could we identify hot ocean-planets with CoRoT, Kepler and Doppler velocimetry? *Icarus* 191, 453-468.

Selsis, F, Kaltenegger, L., and Paillet, J, (2007b) Terrestrial exoplanets: diversity, habitability and characterization, *Physcia Scripta*

Selsis, F., Kasting, J.F., Levrard, B., Paillet, J., Ribas, I., and Delfosse, X. (2007c) Habitable planets around the star Gliese 58*1? Astron. Astrophys*. 476, 1373-1387.

Shu, F.H., Adams, F.C., and Lizano, S. (1987) Star formation in molecular clouds: observation and theory. *Ann. Rev. Astron. Astrophys*. 25, 23-81.

Soifer, B.T., Charmandaris, V., Brandl, B.R., Armus, L., Appleton, P.N., Burgdorf, M.J., Devost, D., Herter, T., Higdon, S.J.U., Higdon, J.L., Houck, J.R., Lawrence, C.R., Morris, P.W., Teplitz, H.I., Uchida, K.I., van Cleve, J., and Weedman, D. (2004) Spitzer Infrared Spectrograph (IRS) observations of the redshift 3.91 quasar APM 08279+5255 *Astrophys J.* 154, 151-154.

Tarter J.C. Backus, P.R., Mancinelli, R.L., Aurnou, J.M., Backman, D.E., Basri, G.S., Boss, A.P., Clarke, A., Deming, D., Doyle, L.R., Feigelson, E.D., Freund, F., Grinspoon, D.H., Haberle, R.M., Hauck, S.A., Heath, M.J., Henry, T.J., Hollingsworth, J.L., Joshi, M.M., Kilston, S., Liu, M.C., Meikle, E., Reid, I.N., Rothschild, L.J., Scalo, J., Segura, A., Tang, C.M., Tiedje, J.M., Turnbull, M.C., Walkowicz, L.M., Weber, A.L., and Young, R.E. (2007) A reappraisal of the habitability of planets around M dwarf stars. *Astrobiology* 7, 30-65

Thiébaut, E. and Mugnier., L. (2006) Maximum a posteriori planet detection and characterization with a nulling interferometer. In *IAUC 200, Direct Imaging of Exoplanets: Science & Techniques*, edited by C.Aime and F. Vakili, Cambridge University Press, Cambridge, pp. 547-552.

Throop, H. B. and Bally, J. (2005) Can photoevaporation trigger planetesimal formation? *Astrophys. J.* 623, L149–L152.

Tinetti, G., Meadows, V. S., Crisp, D., Fong ,W., Velusamy, T., and Snively, H. (2005) Disk-Averaged synthetic spectra of Mars, *Astrobiology* 5, 461-482.

Tinetti, G., Meadows, V. S., Crisp, D., Kiang, N. Y., Kahn, B. H., Fishbein, E., Velusamy, T., and Turnbull, M. (2006) Detectability of Planetary Characteristics in Disk-Averaged Spectra II: Synthetic Spectra and Light-Curves of Earth, *Astrobiology* 6, 881-900.

Tinetti , G., Cornia, A., Liang, M.C., Boccaletti, A., and Yung, Y.L. (2007) Spectral signatures from super-Earths, warm and hot-Neptunes. *Astrobiology* 7, 496-497.

Tumlinson, J., and Shull, J. M. (2000) Zero-metallicity stars and the effects of the first stars on reionization. *Astrophys. J.* 528, L65-L68.

Udry, S., and Santos, N.C. (2007) Statistical properties of exoplanets. *Ann. Rev. Astron. Astrophys.* 45, 397-439.

Udry, S., Bonfils, X., Delfosse, X., Forveille, T., Mayor, M., M., Perrier, C., Bouchy, F., Lovis, C., Pepe, F., Queloz, D., and Bertaux, J.-L. (2007) The HARPS search for southern extra-solar planets - XI. Super-Earths (5 and 8 $M_{\oplus}$) in a 3-planet system. *Astron. Astrophys.* 469, L43-L47.

Van den Dool , T. C., Kamphues, F., Gielesen, W., Benoit, J., Laurenceau, E., Poupinet, A., Sève, F., Stockman, Y., Fleury, K., Loix, N., Kooijman, P. P., de Vries, C., van Weers, H., and Velsink, G. (2006) The DARWIN breadboard optical delay line verification programme. *Proc. SPIE* 6268, 62682O.

Walker, J.C.G. (1977) Evolution of the Atmosphere. Macmillan, New York

Wetherill, G.W., and Stewart, G.R. (1989) Accumulation of a swarm of small planetesimals. *Icarus* 77, 330-357.

Wolstencroft, R.D., and Raven, J.A. (2002) Photosynthesis: Likelihood of occurrence and possibility of detection on earth-like planets. *Icarus* 157, 535-548.

Woolf, N., and Angel, R. (1997) Planet finder options I: New linear nulling array configurations. *ASP Conference Series* 119, 285.

Yusef-Zadeh, F., and Morris, M. (1991) A windswept cometary tail on the Galactic supergiant IRS 7. *Astrophys. J.* 371, L59–L62.

FIGURES

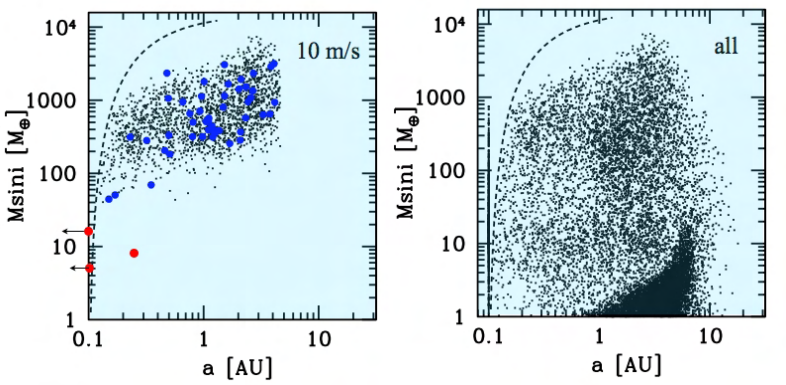

Figure 1. An example of synthetic planet populations, generated by computation, which allow a statistical comparison with observations. Left : black points are the giant planets predicted by the model, the circles are the giant planets actually detected, in reasonable agreement with predictions. Right: prediction of the same model for small planets (e.g. terrestrial) which are not yet detectable. It appears that many Earth-like or somewhat bigger planets are expected which would be interesting targets for Darwin.

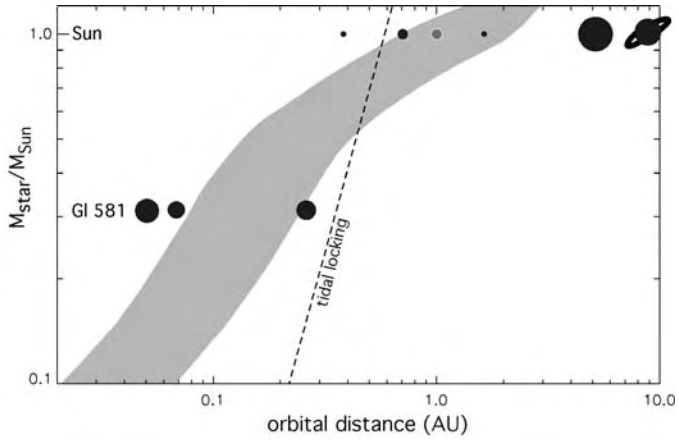

Figure 2. The limits of the Habitable Zone (grey box) as a function of the stellar mass.

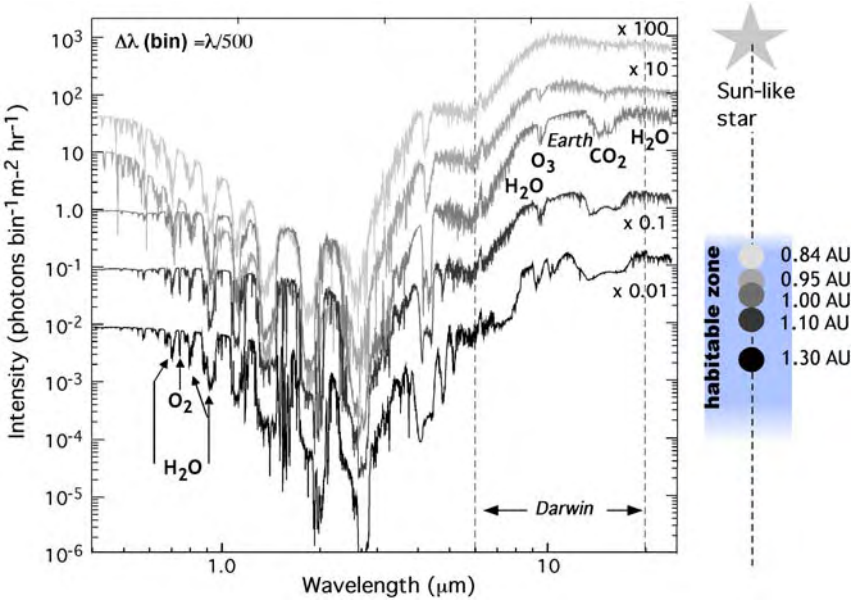

Figure 3. The estimated evolution of the H_2O, O_3 and CO_2 features in the spectra of an Earth-like planet as a function of its location in the HZ. Sun-like star refers to a 1 solar mass G star.

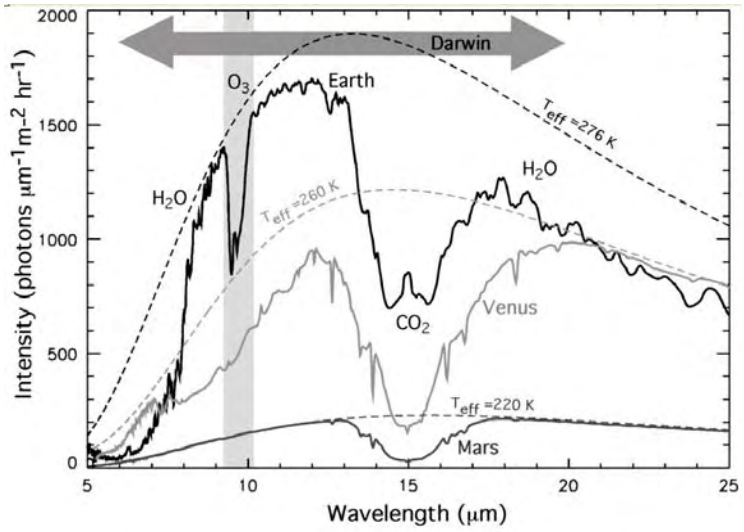

Figure 4. The mid-IR spectrum of the Earth, Venus and Mars at a low resolution (spectra are derived from a variety of published models including Meadows and Crisp, 1996; Tinetti *et al*., 2005; Tinetti *et al.*, 2006; Kaltenegger *et al*., 2007; Selsis *et al.*, 2007b).

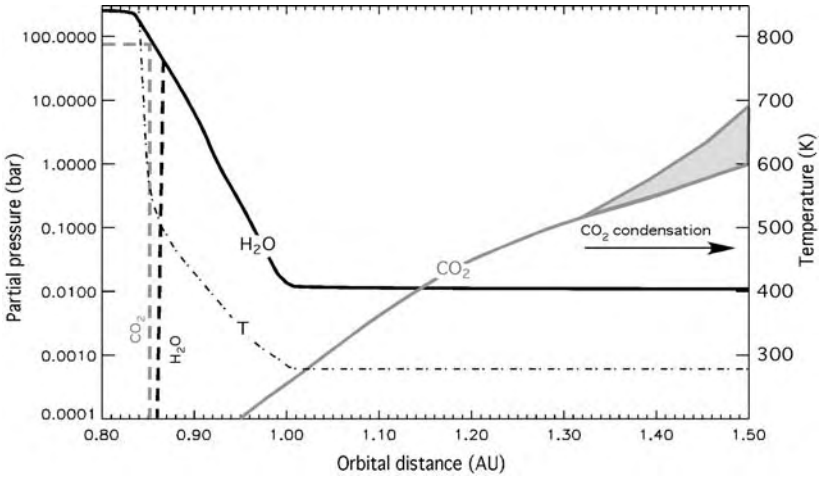

Fig. 5. Diagram illustrating the reason for the spectra shown in Figure 4. The mean surface temperature (T) and partial pressure of CO_2 and H_2O as a function of the orbital distance on a habitable planet within the habitable zone (Kaltenegger and Selsis, 2007). Data adapted from Kasting *et al.* (1993) and Forget and Pierehumbert (1997). (Partial pressure, left y-axis and Surface Temperature, right y-axis).

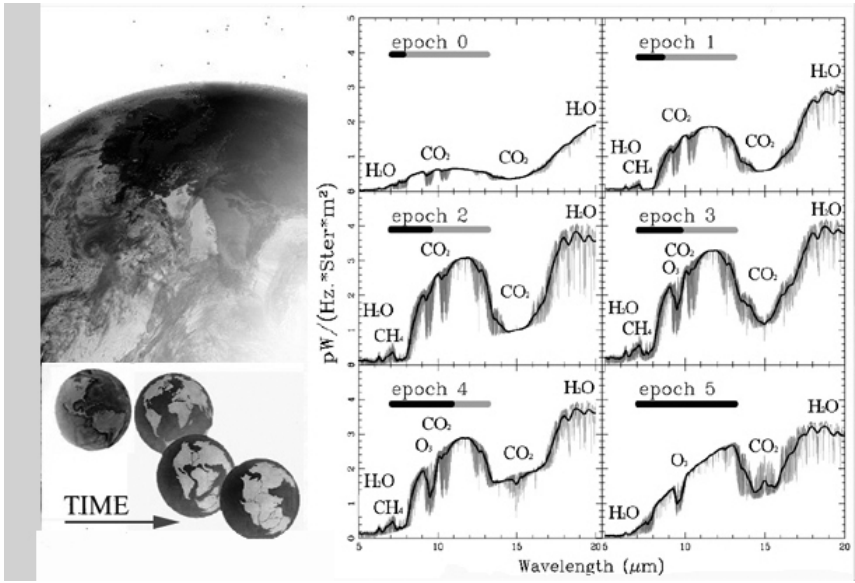

Figure 6. Mid-IR synthetic spectra of the Earth at six different stages of its evolution: 3.9 (Epoch 0), 3.0, 2.6, 2.0, 0.8 (Epoch 5) Gyrs ago and the present (figure from Kaltenegger *et al.*, 2007)

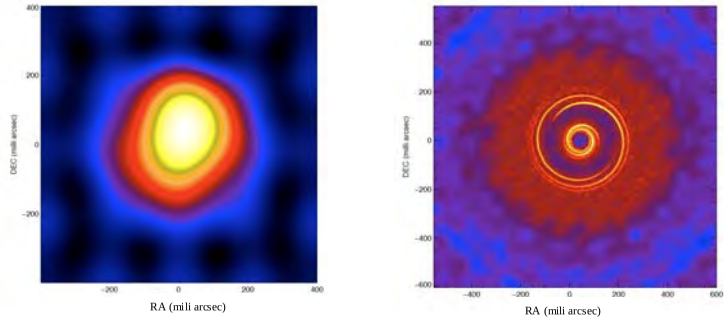

Figure 7. An illustration of the mapping power of the mission. Simulation of a hot accretion disk in the Taurus cloud (140 pc) as seen by JWST (Left) and Darwin in its imaging mode (Right). Simulated JWST and Darwin images are based on scaled models by D'Angelo et al. (2006) for the formation of a planet of one Jupiter mass at 5.2 AU, orbiting a solar type star. The most prominent feature in the model is a low-density annular region along the planet's path (known as gap) and spiral wave patterns. Total observing time is 10 h. (courtesy Cor de Vries)

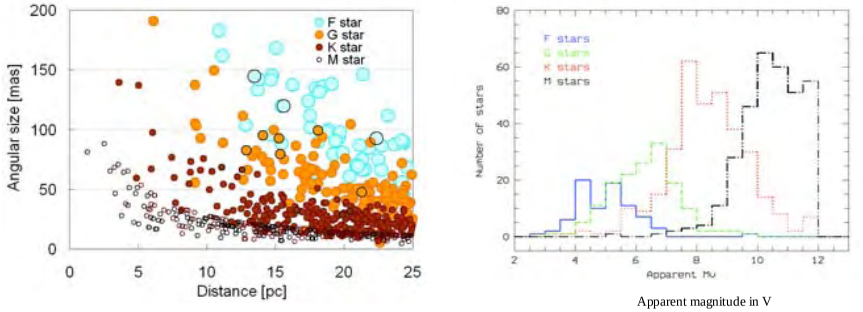

Figure 8. Some features of stars in the Darwin star catalog. Left, size of the Habitable Zone for the different spectral types of Darwin targets (Kaltenegger et al, 2008a). Right, histogram of their apparent visible magnitudes.

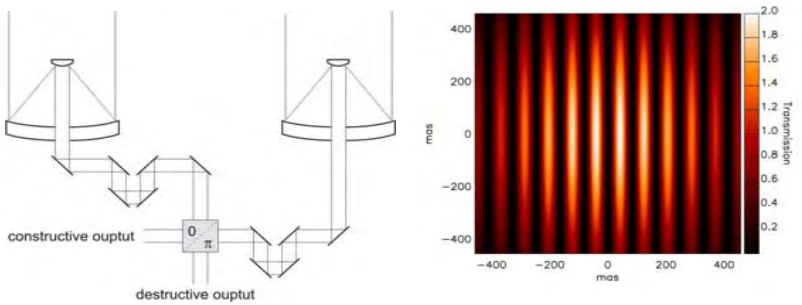

Figure 9. The concept of nulling interferometry. Left, principle of a two-telescope Bracewell nulling interferometer with its destructive (null) and constructive outputs. Right, associated transmission map, displayed for λ = 10 µm and a 25-m baseline array. This fringe pattern is effectively projected on the sky, blocking some regions, e.g. the on-axis star, while transmitting others, e.g. the off-axis planet.

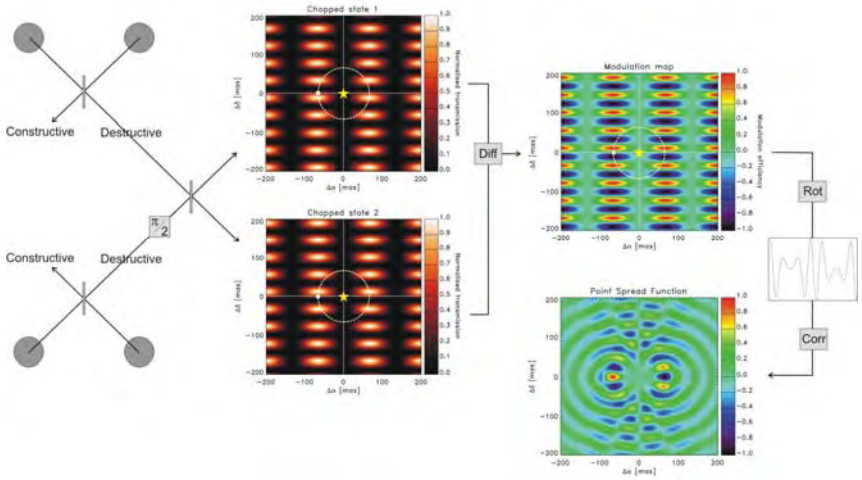

Figure 10. Phase chopping for the X-array, a four-element rectangular configuration of telescopes. Combining the beams with different phases produces two conjugated chopped states, which are used to extract the planetary signal from the background. Array rotation then locates the planet by cross-correlation of the modulated chopped signal with a template.

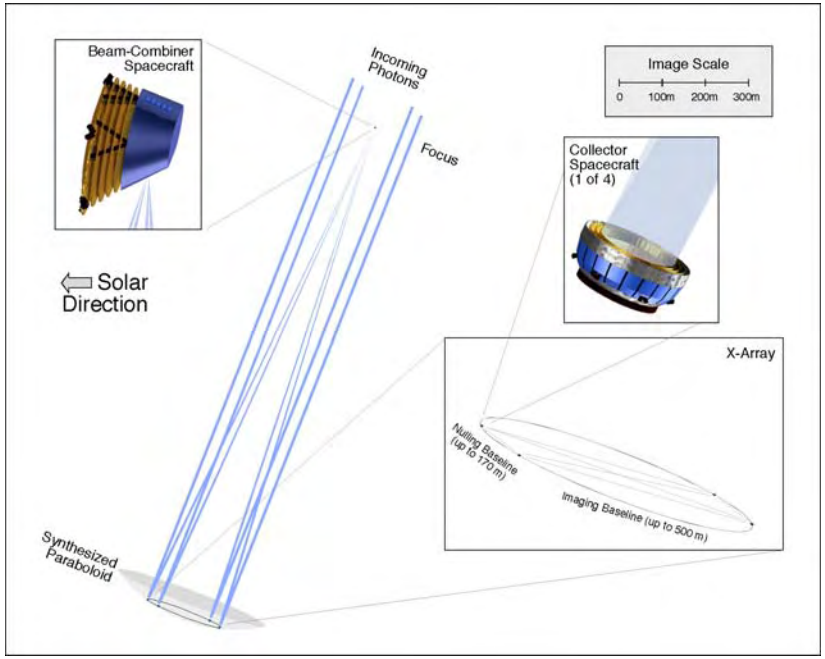

Figure 11. The non-coplanar Emma X-array configuration. It consists of 4 collector spacecrafts and a beam combiner spacecraft. Spherical mirrors in the collectors form part of a large, synthetic paraboloid, feeding light to the beam combiner at its focus.

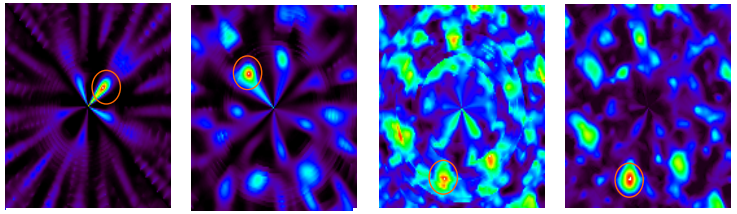

(a) Likelihood map of 1st planet - detected and positioned.

(b) Likelihood map of 2nd planet - detected and positioned.

(c) Likelihood map of 3rd planet *without* regularisation: ambiguities in position.

(d) Likelihood map of 3rd planet *with* regularisation: detected and positioned.

Figure 12. Example of the Baynesian approach to image reconstruction. Likelihood maps of the successive detection of 3 planets located at 0.64, 1.1 and 1.8 AU of a star. Red indicates a higher probability, black a lower one, white is the highest. The spectral resolution is 15 and S/N is 0.33 per spectral element. The 3rd and faintest planet is correctly detected when the so-called regulation process is used [compare (c) and (d)]